BIJOAK 348(2) 241–479 2000 • ISSN 0264-6021
Volume 348 • Part 2 • 1 June 2000

BIOCHEMICAL JOURNAL

review

Rho GTPases and their effector proteins

by A. L. Bishop and A. Hall

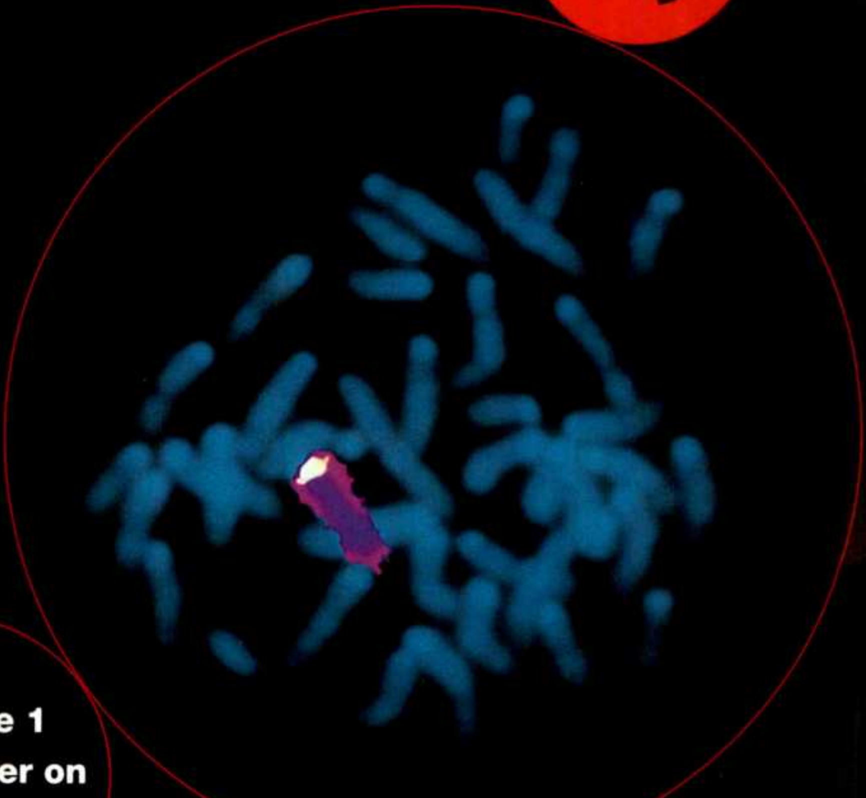

Available 1 week earlier on the Internet

The Biochemical Society, London © 2000

Cell Death Titles

from Portland Press

Portland Press

Mitochondria and Cell Death

Edited by GC Brown, University of Cambridge, UK, D Nicholls, University of Dundee, UK, and C Cooper, University of Essex, UK

This book reviews the involvement of mitochondria in cell death and disease. This is a rapidly expanding field of major importance to both basic biology and medical science. Clear and comprehensive chapters from some of the key researchers in the field cover most aspects of the subject from the molecular to the *in vivo* level. The role of mitochondria in neurodegenerative, inflammatory and ischaemic diseases, as well as necrosis, apoptosis and ageing is reviewed. Each chapter is by a different set of authors describing one aspect of the field. Researchers and postgraduates throughout biology and medical science will want to read this book.

1 85578 125 5 Hardback October 1999 240 pages £65.00

Techniques in Apoptosis: A User's Guide

Edited by TG Cotter, University College Cork, Ireland and SJ Martin, La Jolla Institute for Allergy and Immunology, USA

Cell death/apoptosis is currently an exponentially expanding field of broad research interest. The success of research projects depend on having access to detailed and clearly written accounts of techniques and methodologies used. This is particularly important in a new field. *Techniques in Apoptosis* aims to fill this niche, it differs from recent volumes on apoptosis since its focus will be purely technical in nature.

Each chapter begins with an overview of the methodology to be employed, and goes on to provide detailed experimental protocols for the identification of apoptotic cells from plants to *Drosophila* to man in an easy to-use, step-by-step format. Written by key people in the field, this book is essential reading for all researchers in cell death, from PhD students to senior scientists.

1 85578 129 8 Paperback 1997 300 pages £39.50

Nitric Oxide and the Cell: Proliferation Differentiation and Death

Edited by S Moncada, The Wolfson Institute for Biomedical Research, London, UK, G Nisticò, University of Rome, Italy, G Bagetta, University of Rome, Italy and EA Higgs, The Wolfson Institute for Biomedical Research, London, UK

Proceedings of the II International Paraelios Symosium: Nitric Oxide and the Cell: Proliferation Differentiation and Death, Baia Paraelios, Calabria, Italy, 1996

Nitric Oxide has proven to be a molecule with a wide biological significance. It is involved in myriad actions which range from physiology to pathophysiology. One of the fundamental questions in relation to its biological relevance concerns the paradoxical nature of some of its actions. There is, for example, a whole range of effects related to cytoprotection, cell proliferation, differentiation and cell death. The way in which nitric oxide becomes involved in pathophysiology is slowly being elucidated.

This volume is a summary of the discussions that took place at the Second International Paraelios Symposium on Nitric oxide research. It will make significant contribution to the clarification of this very exciting subject.

"Overall, the book is good if you want to learn details from first principals of the mechanisms of NO activity at the cellular and molecular level. It is well written, well illustrated and easy to read. I would recommend it to both the novice and the established researcher in the NO field. It is a valuable source of new information on NO action and is copiously referenced for those wishing to learn about the background of NO biology."

Immunology News

1 85578 120 4 Hardback 1998 280 pages £80.00

Orders:
www.portlandpress.com/books/orderinfo.htm

***Portland Press, Commerce Way,**
Colchester, CO2 8HP
t: 01206 796351
f: 01206 799331
e: sales@portlandpress.com

USA and Canada:
†California/Princeton
Fulfillment Services Inc.,
1445 Lower Ferry Road,
Ewing, NJ 08618, USA
t: 1 800 777 4726
f: 1 800 999 1958
e: orders@cpfs.pupress.princeton.edu

***Please add £2.50 per book to a maximum of £7.50**

†Please add US$3.75 for first book, US$1.00 for each additional book

BWY/0400/C

CUK-404424-1-P32196

Biochemical Journal

The Biochemical Society, London © 2000

Volume 348, part 2
1 June 2000

First published on the Internet
23 May 2000
http://www.BiochemJ.org

Editorial Board

Chairman
P. J. Parker • London

Deputy Chairmen
G. E. Blair • Leeds
D. N. Brindley • Edmonton
R. A. J. Challiss • Leicester
P. Ferré • Paris
J. T. Gallagher • Manchester
R. A. John • Cardiff
H. Nagase • London
J. D. Pearson • London
M. H. Rider • Bruxelles
S. B. Shears • Research Triangle Park

Reviews Editor
R. D. Burgoyne • Liverpool

Managing Editor
P. J. Starley

Deputy Managing Editor
S. E. Dilley

Senior Staff Editor
S. M. Hobday

Staff Editors
L. Johnson
W. J. Watkins
M. R. Thorne
N. B. Prowse
S. J. Cubie

Editorial Assistant
N. J. Lamb

R. L. P. Adams (Glasgow)
J. W. N. Akkerman (Utrecht)
D. R. Alessi (Dundee)
D. Attaix (Ceyrat)
S. A. Baldwin (Leeds)
F. J. Ballard (Adelaide)
G. J. Barritt (Adelaide)
N. C. Bruce (Cambridge)
A. Clerk (London)
G. M. Cohen (Leicester)
P. Crine (Montreal)
D. Cutler (London)
D. A. Day (Nedlands)
H. Deckmyn (Kortrijk)
K. Docherty (Aberdeen)
B. K. Drøbak (Norwich)
J. M. East (Southampton)
K. R. F. Elliott (Manchester)
B. Engelmann (Munich)
C. Forest (Meudon)
M. J. Fry (Reading)
A. Galione (Oxford)
D. A. F. Gillespie (Glasgow)
S. Goodbourn (London)
G. W. Gould (Glasgow)
S. V. Graham (Glasgow)
S. Gutteridge (Newark, DE)
Y. A. Hannun (Charleston)

P. I. Haris (Leicester)
M. M. Harnett (Glasgow)
J. D. Hayes (Dundee)
P. C. Heinrich (Aachen)
R. Heinrich (Berlin)
B. Henrissat (Marseille)
R. C. Hider (London)
S. High (Manchester)
M. B. Hodgins (Glasgow)
D. Hoekstra (Groningen)
N. M. Hooper (Leeds)
E. F. Hounsell (London)
W. Jessup (Sydney)
J. Johansson (Stockholm)
J. P. Kehrer (Austin)
K. I. Kivirikko (Oulu)
B. L. Knight (London)
R. G. Knowles (Stevenage)
H. Kresse (Münster)
P. W. Kuchel (Sydney)
C. MacKintosh (Dundee)
A. I. Magee (London)
T. J. Mantle (Dublin)
P. Maurel (Montpellier)
A. J. Meijer (Amsterdam)
J. E. Merritt (Welwyn Garden City)
F. Michelangeli (Birmingham)
G. Milligan (Glasgow)

B. P. Morgan (Cardiff)
J. S. Mort (Montreal)
S. E. Moss (London)
K. J. Murray (Harlow)
A. C. Newby (Bristol)
F. Paltauf (Graz)
N. J. Pyne (Glasgow)
C. I. Ragan (Windlesham)
P. R. Rich (London)
N. J. P. Ryba (Bethesda)
G. Salvesen (San Diego)
M. F. Scully (London)
S. Shenolikar (Durham, NC)
A. G. Smith (Cambridge)
M. C. Sugden (London)
P. H. Sugden (London)
R. Sundler (Lund)
J. M. Tavaré (Bristol)
K. F. Tipton (Dublin)
M. A. Titheradge (Brighton)
A. B. Tobin (Leicester)
S. A. Tooze (London)
W. J. van Blitterswijk (Amsterdam)
R. Virden (Newcastle upon Tyne)
H. M. Wallace (Aberdeen)
M. P. Walsh (Calgary)
L. A. Witters (Hanover)
S. J. Yeaman (Newcastle upon Tyne)

- The *Biochemical Journal* (ISSN 0264-6021 for print journal; ISSN 1470-8728 for online journal) is published and distributed by Portland Press Ltd on behalf of the Biochemical Society, and appears twice monthly.
- **Editorial and publishing offices:** *Biochemical Journal*, 59 Portland Place, London W1N 3AJ, U.K.
- Royal Mail International, c/o Yellowstone International, 87 Burlews Court, Hackensack, NJ 07061, U.S.A.
- **Subscriptions department:** Portland Press Ltd, P.O. Box 32, Commerce Way, Colchester CO2 8HP, U.K.

- All rights reserved. Apart from any fair dealing for the purposes of research or private study, or criticism or review, as permitted under the Copyright, Designs and Patents Act, 1988, this publication may be reproduced, stored or transmitted, in any forms or by any means, only with the prior permission in writing of the publishers, or in the case of reprographic reproduction in accordance with the terms of permissions granted by copyright clearing houses such as the Copyright Licensing Agency (U.K.) or the Copyright Clearance Center (U.S.A.). The CCC item-fee code for this publication is 0264-6021/2000/$16.00+0.00. Inquiries concerning reproduction outside those terms should be sent to the publishers at the above-mentioned address.
- Although, at the time of going to press, the information contained in this publication is believed to be correct, neither the authors nor the editors nor the publisher assume any responsibility for any errors or omissions herein contained.

- Periodicals postage paid at Rahway, NJ, and at additional mailing offices.
- **Postmaster:** send address changes to *Biochemical Journal*, c/o Mercury International, 365 Blair Road, Avenel, NJ 07001.
- **Cover illustration:** X-chromosomal location of mouse organic-anion-transporting polypeptide 1 (Oatp1) confirmed by a two-colour FISH analysis [see Hagenbuch et al. (2000) Biochem. J. **345**, 115–120].

Instructions to Authors

P32 196

General policy The *Biochemical Journal* publishes papers in English in all fields of biochemistry and cellular and molecular biology, provided that they make a sufficient contribution to biochemical knowledge Papers may include new results obtained experimentally, descriptions of new experimental methods of biochemical importance, or new interpretations of existing results Novel theoretical contributions will be considered equally with papers dealing with experimental work All work presented should have as its aim the development of biochemical concepts rather than the mere recording of facts Preliminary, confirmatory or inconclusive work will not be published The *Biochemical Journal* will not publish material that has been wholly or largely published elsewhere, even as a preliminary communication or in unrefereed symposium proceedings or on the World Wide Web (WWW), equally, fragmentation of research into the 'least publishable unit' is discouraged

Submission of a paper implies that it has been approved by all the named authors, that all persons entitled to authorship have been so named, that it reports unpublished work that is not under consideration elsewhere, and that if the paper is accepted for publication the authors will transfer to the Biochemical Society the copyright in the paper, which will then not be published elsewhere in the same form, in any language, without the consent of the Society Authors will be required to sign an undertaking to these effects

Authors may suggest potential reviewers for their papers, but the journal is under no obligation to follow such suggestions Authors may also specify the names of those they wish to be excluded from the review process, and such wishes are usually respected unless, in the opinion of the journal, such a request unreasonably excludes all the expertise available to it in that scientific area

To allow the reviewers to assess possible overlap with previous work, all submitted papers must be accompanied by duplicate copies of the author's relevant published work, including that on the WWW, and of all related papers in press or under editorial consideration in this or other journals

The paragraphs below are a summarized version of the journal's complete Instructions to Authors (see http //www BiochemJ org), copies of which are available free of charge from the editorial office

The following types of paper are included in the journal

Research Papers are the normal form of publication, and may be of any length that is justified by their content However, because of pressure for space in the journal, no paper, whatever its scientific merits, will be accepted if it exceeds the minimum length required for precision in describing the experiments and clarity in interpreting them As a guide, most Research Papers published in the *Biochemical Journal* are of between six and eight printed pages A concise well-written paper tends to be published more rapidly

Research Communications are short (maximum four printed pages) papers bringing particularly novel and significant findings to the attention of the research community. It is intended that a decision on acceptance or rejection will be made within 10 working days of receipt, and publication of accepted Communications will follow within 2 months Research Communications receive full but accelerated reviewing The criteria of 'novelty and significance' are strictly enforced, and papers may be rejected solely on the grounds of lack of novelty and significance Communications are not a path to accelerated publication of sound but non-urgent material Authors must include in their letter of submission a brief statement of why they believe their Communication merits accelerated treatment Papers reporting nucleotide sequences only are not acceptable as Research Communications One colour figure will be published free of charge in Research Communications, subsequent figures will cost £300 each

Reviews will usually be solicited, although unsolicited reviews will be considered for publication Prospective writers of reviews should first consult the Reviews Editor, via the editorial office, and should enclose a short (one typed page) summary of the area they propose to cover

Procedure for submission Before preparing papers for the journal, authors should consult a current issue to make themselves familiar with the general format, such as the use of cross-headings, layout of tables and figures and citation of references A full page of text in the *Biochemical Journal* contains approximately 1200 words, when calculating the printed length of papers, allowance must be made for the space occupied by tables and figures and the number of text words reduced accordingly

The numerical system of references must be used A reference to 'unpublished work' must be accompanied by the names of all persons concerned, a reference to a 'personal communication' must be supported by written permission for the quotation from the person or persons concerned; both of these types of citation are permitted in the text only, not in the list of references.

Three copies of the typescript (four copies for Research Communications), with a brief covering letter to which should be attached an additional copy of the synopsis, should be sent to. **The Managing Editor, *Biochemical Journal*, 59 Portland Place, London W1N 3AJ, U.K.** (telephone 020 7637 5873, fax 020 7323 1136, from overseas the international code for the U K is 44 and the leading 0 should be omitted, e-mail editorial@portlandpress com)

The typescript should indicate the name, address, telephone number, fax number and e-mail address of the person to whom all correspondence should be addressed The top copy of the typescript should be marked as such and should have attached to it the original figures, for the other copies of the typescript, glossy prints (not photocopies) of the half-tone figures should be provided, but photocopies of line drawings will suffice A short (page-heading) title of not more than 75 characters and a maximum of five key words that do not appear in the title, should be provided

Submission by fax Research Communications that do not contain half-tone or colour figures may be submitted by fax to the number above Only one copy of the typescript need be transmitted The current Instructions to Authors contains full details of this procedure

Electronic submission Manuscripts may be submitted as a **single** Adobe Acrobat PDF file either (i) as a uuencoded attachment to the e-mail address. editorial@portlandpress com; or (ii) uploaded to the ftp site ftp portlandpress com in the directory /incoming/BiochemJ [N B Authors using route (ii) are advised to alert us to any incoming documents via our regular e-mail address]

Colour figures The first colour figure is published at no charge provided that one author has been a member of the Biochemical Society for at least 2 years and that the use of colour is deemed scientifically necessary by the reviewers Subsequent colour figures in the same paper cost £300 each

Multimedia adjuncts The Biochemical Journal Online is now able to offer authors the opportunity to enhance their papers with multimedia adjuncts (e g. time-lapse movies, three-dimensional structures) These will be submitted to peer review alongside the manuscript To submit a paper with a multimedia adjunct, please contact the Managing Editor (editorial@portlandpress com) There is no extra charge associated with the publication of a multimedia adjunct online

Use of authors' diskettes Authors should submit diskettes of revised articles to the editorial office Every effort will be made to use the diskette during typesetting, but this cannot be guaranteed Authors must ensure that files have been updated to incorporate all revisions, and hence that the version on the diskette matches the revised hard copy Our preferred word-processing format is Word for Windows version 6 Submission of manuscripts in other word-processing formats may lead to delays in processing The diskette should be accompanied by a covering letter specifying manuscript number, operating system and software program. Files should be formatted double-spaced with no hyphenation and automatic wordwrap (no hard returns within paragraphs)

Other information

The *Biochemical Journal* is published and distributed by Portland Press Ltd on behalf of the Biochemical Society It is published twice monthly, in 2000 volumes 345–352 (three parts each) will appear The subscription also includes an author and key-word index

Subscription rates Institutional subscription rates for 2000 are shown below Subscribers to the *Biochemical Journal* can subscribe additionally to *Biochemical Society Transactions* and *Biotechnology and Applied Biochemistry* on a joint subscription at a reduced rate Terms are cash with order (US$ in N America, £ sterling for rest of the world, or US$ equivalent at current rate of exchange, subscribers in the EU may pay in £ sterling or Euros), or against pro forma invoice Orders should be sent to the address below, or through your usual agent

	N America	Rest of world	Euro price
One yr (8 vols)	US$1950	£1110	€1776
Single issues	US$97	£56	€90

Dollar prices include airspeeded delivery Sterling and Euro prices include airspeeded delivery in Europe and delivery by surface mail elsewhere. Airspeeded delivery is available to countries other than America and Europe at an additional cost of £50

Biochemical Journal Online Access to the Biochemical Journal Online is restricted to institutions that have a subscription to the print version It will be free to such institutions during 2000 URL. http://www BiochemJ org

Microfiche and back issues Volumes 102–296 of the *Biochemical Journal* are available on microfiche Back issues are also available Further details may be obtained from the address below

Subscription department

Portland Press Ltd
P O Box 32, Commerce Way
Colchester CO2 8HP, Essex, U K
(telephone 01206 796351, fax 01206-799331, e-mail sales@portlandpress com)

Advertising Advertising is accepted in the *Biochemical Journal* For information contact the Advertising Department, Portland Press Ltd, 59 Portland Place, London W1N 3AJ (telephone 020 7580 5530, fax 020 7323 1136, e-mail editorial@portlandpress com)

Biochemical Journal
Volume 348, part 2
1 June 2000
First published on the Internet
23 May 2000
http://www.BiochemJ.org

Review

Rho GTPases and their effector proteins **241–255**
***by* A.L. Bishop and A. Hall**

Research Papers

Proteins

Lipidation of apolipoprotein E influences its isoform-specific interaction with Alzheimer's amyloid β peptides	T. Tokuda, M. Calero, E. Matsubara, R. Vidal, A. Kumar, B. Permanne, B. Zlokovic, J.D. Smith, M.J. Ladu, A. Rostagno, B. Frangione and J. Ghiso	**359–365**
Interaction of *Bacillus subtilis* CsaA with SecA and precursor proteins	J.P. Müller, J. Ozegowski, S. Vettermann, J. Swaving, K.H.M. van Wely and A.J.M. Driessen	**367–373**
Suppression of temperature-sensitivity of a *dnaA46* mutant by excessive DNA supercoiling	T. Kondo, S. Mima, N. Fukuma, K. Sekimizu, T. Tsuchiya and T. Mizushima	**375–379**

Enzymes

Saccharomyces cerevisiae Yak1p protein kinase autophosphorylates on tyrosine residues and phosphorylates myelin basic protein on a C-terminal serine residue	S. Kassis, T. Melhuish, R.S. Annan, S.L. Chen, J.C. Lee, G.P. Livi and C.L. Creasy	**263–272**
Kinetic study of the inactivation of ascorbate peroxidase by hydrogen peroxide	A.N.P. Hiner, J.N. Rodríguez-López, M.B. Arnao, E. Lloyd Raven, F. García-Cánovas and M. Acosta	**321–328**
Positional- and stereo-selectivity of fatty acid oxygenation catalysed by mouse (12*S*)-lipoxygenase isoenzymes	F. Bürger, P. Krieg, F. Marks and G. Fürstenberger	**329–335**
Expression of an active form of recombinant Ty1 reverse transcriptase in *Escherichia coli*: a fusion protein containing the C-terminal region of the Ty1 integrase linked to the reverse transcriptase–RNase H domain exhibits polymerase and RNase H activities	M. Wilhelm, M. Boutabout and F.-X. Wilhelm	**337–342**
Purification from rat liver of a novel constitutively expressed member of the aldo-keto reductase 7 family that is widely distributed in extrahepatic tissues	V.P. Kelly, L.S. Ireland, E.M. Ellis and J.D. Hayes	**389–400**
Characterization of *N*-myristoyltransferase from *Plasmodium falciparum*	R.S. Gunaratne, M. Sajid, I.T. Ling, R. Tripathi, J.A. Pachebat and A.A. Holder	**459–463**

Carbohydrates and lipids

Phosphocholine-containing, zwitterionic glycosphingolipids of adult *Onchocerca volvulus* as highly conserved antigenic structures of parasitic nematodes	M. Wuhrer, S. Rickhoff, R.D. Dennis, G. Lochnit, P.T. Soboslay, S. Baumeister and R. Geyer	**417–423**
Action pattern and substrate specificity of the hyaluronan lyase from group B streptococci	J.R. Baker and D.G. Pritchard	**465–471**

Gene structure and expression

Inhibition of glutaminase expression by antisense mRNA decreases growth and tumourigenicity of tumour cells	C. Lobo, M.A. Ruiz-Bellido, J.C. Aledo, J. Márquez, I. Núñez de Castro and F.J. Alonso	**257–261**

Chicken Y-box proteins chk-YB-1b and chk-YB-2 repress translation by sequence-specific interaction with single-stranded RNA	S.K. Swamynathan, A. Nambiar and R.V. Guntaka	**297–305**
Zebrafish *ftz-f1* gene has two promoters, is alternatively spliced, and is expressed in digestive organs	W.-w. Lin, H.-W. Wang, C. Sum, D. Liu, C.L. Hew and B.-c. Chung	**439–446**
Expression and protein-binding studies of the *EEN* gene family, new interacting partners for dynamin, synaptojanin and huntingtin proteins	C.W. So, M.H. Sham, S.L. Chew, N. Cheung, C.K.C. So, S.K. Chung, C. Caldas, L.M. Wiedemann and L.C. Chan	**447–458**

Regulation of metabolism

Human Sug1/p45 is involved in the proteasome-dependent degradation of Sp1	K. Su, X. Yang, M.D. Roos, A.J. Paterson and J.E. Kudlow	**281–289**
Cholesterol decreases secretion of the secreted form of amyloid precursor protein by interfering with glycosylation in the protein secretory pathway	J.L. Galbete, T. Rodriguez-Martin, E. Peressini, P. Modena, R. Bianchi and G. Forloni	**307–313**
Oxalomalate, a competitive inhibitor of aconitase, modulates the RNA-binding activity of iron-regulatory proteins	M. Festa, A. Colonna, C. Pietropaolo and A. Ruffo	**315–320**
Increased translation efficiency and antizyme-dependent stabilization of ornithine decarboxylase in amino acid-supplemented human colon adenocarcinoma cells, Caco-2	H. Chabanon, L. Persson, H.M. Wallace, M. Ferrara and P. Brachet	**401–408**

Membranes and bioenergetics

CLC-Nt1, a putative chloride channel protein of tobacco, co-localizes with mitochondrial membrane markers	C. Lurin, J. Güclü, C. Cheniclet, J.-P. Carde, H. Barbier-Brygoo and C. Maurel	**291–295**
Cytochrome c release from isolated rat liver mitochondria can occur independently of outer-membrane rupture: possible role of contact sites	E. Doran and A.P. Halestrap	**343–350**

Receptors and signal transduction

Tyrosine phosphorylation of the vascular endothelial-growth-factor receptor-2 (VEGFR-2) is modulated by Rho proteins	D. Gingras, S. Lamy and R. Béliveau	**273–280**
Phosphatidylinositol 3-kinase, protein kinase B and ribosomal S6 kinases in the stimulation of thyroid epithelial cell proliferation by cAMP and growth factors in the presence of insulin	K. Coulonval, F. Vandeput, R.C. Stein, S.C. Kozma, F. Lamy and J.E. Dumont	**351–358**
The m3 muscarinic acetylcholine receptor is coupled to mitogen-activated protein kinase via protein kinase C and epidermal growth factor receptor kinase	B.E. Slack	**381–387**
Signalling pathways of insulin-like growth factor-I that are augmented by cAMP in FRTL-5 cells	M. Ariga, T. Nedachi, M. Akahori, H. Sakamoto, Y. Ito, F. Hakuno and S.-I. Takahashi	**409–416**
Perivenous localization of insulin receptor protein in rat liver, and regulation of its expression by glucose and oxygen in hepatocyte cultures	A. Krones, T. Kietzmann and K. Jungermann	**433–438**

Cell biology and development

Increase of mitochondria and mitochondrial DNA in response to oxidative stress in human cells	H.-C. Lee, P.-H. Yin, C.-Y. Lu, C.-W. Chi and Y.-H. Wei	**425–432**
Bcl-2 accelerates retinoic-acid-induced growth arrest and recovery in human gastric cancer cells	H.-K. Chou, S.-L. Chen, C.-T. Hsu, Y.-C. Chao and Y.-P. Tsao	**473–479**

Index of Authors

PAGE
Acosta, M. 321
Akahori, M. 409
Aledo, J. C 257
Alonso, F. J. 257
Annan, R. S 263
Ariga, M. 409
Arnao, M B. 321

Baker, J. R 465
Barbier-Brygoo, H. 291
Baumeister, S 417
Béliveau, R. 273
Bianchi, R. 307
Bishop, A L 241
Boutabout, M. 337
Brachet, P. 401
Burger, F. 329

Caldas, C. 447
Calero, M. 359
Carde, J.-P. 291
Chabanon, H. 401
Chan, L. C 447
Chao, Y.-C. 473
Chen, S. L 263
Chen, S.-L 473
Cheniclet, C. 291
Cheung, N 447
Chew, S. L 447
Chi, C.-W 425
Chou, H -K. 473
Chung, B.-c 439
Chung, S. K 447
Colonna, A 315
Coulonval, K 351
Creasy, C. L. 263

Dennis, R D. 417
Doran, E 343
Driessen, A. J. M 367
Dumont, J. E 351

PAGE
Ellis, E. M 389

Ferrara, M. 401
Festa, M. 315
Forloni, G 307
Franglone, B. 359
Fukuma, N 375
Furstenberger, G 329

Galbete, J L 307
García-Cánovas, F 321
Geyer, R. 417
Ghiso, J 359
Gingras, D 273
Guclu, J. 291
Gunaratne, R. S 459
Guntaka, R. V. 297

Hakuno, F 409
Halestrap, A P 343
Hall, A 241
Hayes, J D. 389
Hew, C. L 439
Hiner, A N P. 321
Holder, A A. 459
Hsu, C -T. 473

Ireland, L. S 389
Ito, Y. 409

Jungermann, K 433

Kassis, S. 263
Kelly, V. P 389
Kietzmann, T. 433
Kondo, T. 375
Kozma, S. C 351
Krieg, P 329
Krones, A. 433
Kudlow, J. E 281
Kumar, A. 359

PAGE
Ladu, M J. 359
Lamy, F 351
Lamy, S. 273
Lee, H -C. 425
Lee, J. C 263
Lin, W.-w 439
Ling, I T. 459
Liu, D 439
Livi, G. P 263
Lloyd Raven, E 321
Lobo, C 257
Lochnit, G. 417
Lu, C.-Y 425
Lurin, C. 291

Marks, F. 329
Márquez, J. 257
Matsubara, E. 359
Maurel, C 291
Melhuish, T 263
Mima, S. 375
Mizushima, T. 375
Modena, P. 307
Muller, J P 367

Nambiar, A 297
Nedachi, T. 409
Núñez de Castro, I. 257

Ozegowski, J. 367

Pachebat, J. A 459
Paterson, A. J 281
Peressini, E 307
Permanne, B 359
Persson, L 401
Pietropaolo, C. 315
Pritchard, D. G. 465

Rickhoff, S. 417
Rodríguez-López, J. N 321
Rodriguez-Martin, T. 307

PAGE
Roos, M. D 281
Rostagno, A 359
Ruffo, A. 315
Ruiz-Bellido, M. A 257

Sajid, M. 459
Sakamoto, H., 409
Sekimizu, K 375
Sham, M. H 447
Slack, B. E 381
Smith, J D. 359
So, C. K C 447
So, C. W 447
Soboslay, P. T 417
Stein, R C. 351
Su, K 281
Sum, C 439
Swamynathan, S. K 297
Swaving, J 367

Takahashi, S.-I 409
Tokuda, T. 359
Tripathi, R. 459
Tsao, Y -P. 473
Tsuchiya, T. 375

Vandeput, F. 351
van Wely, K. H M. 367
Vettermann, S 367
Vidal, R 359

Wallace, H. M 401
Wang, H.-W 439
Wei, Y.-H. 425
Wiedemann, L M 447
Wilhelm, F -X. 337
Wilhelm, M. 337
Wuhrer, M. 417

Yang, X 281
Yin, P.-H. 425

Zlokovic, B 359

Editorial Advisory Panel

C. Abell (Cambridge)
M Abrahamson (Lund)
B. A C Ackrell (San Francisco)
L. Agius (Newcastle)
L Alhonen (Kuopio)
N G Anderson (Manchester)
C Anthony (Southampton)
G J Arlaud (Grenoble)
F. A Armstrong (Oxford)
O I Aruoma (London)
B Ashby (Philadelphia)
K S. Authi (London)

A Baici (Zurich)
A J Bailey (Langford)
A J. Baines (Canterbury)
D Barford (London)
M P. Barrett (Glasgow)
K. Bartlett (Newcastle)
J F Bateman (Melbourne)
G Baverel (Lyon)
J H Beattie (Aberdeen)
C Beaumont (Paris)
D. R. Bell (Nottingham)
D. S Bendall (Cambridge)
A Benedetti (Siena)
J P Bennett (London)
M. J. Berridge (Cambridge)
A Berry (Leeds)
R. J Beynon (Liverpool)
C D Bingle (Sheffield)
I. Bjork (Uppsala)
J L. Blank (Leicester)
N Blau (Zurich)
P G Board (Canberra)
M A Bogoyevitch (Perth, West Aus)
G B Bolger (Salt Lake City)
M. Bollen (Leuven)
G. P. Bolwell (London)
A. R. Boobis (London)
K M Botham (London)
M J Brammer (London)
P Brickell (London)
K. M Brindle (Cambridge)
K. Brocklehurst (London)
E Brot-Laroche (Paris)
A J P Brown (Aberdeen)
G Brown (Birmingham)
B. Brune (Erlangen)
N. J Bulleid (Manchester)
N W Bunnett (San Francisco)
A Burchell (Dundee)
B Burchell (Dundee)
S J W. Busby (Birmingham)
P J Butterworth (London)

J J Calvete (Valencia)
M J Carden (Canterbury)
E A Carrey (London)
C Casals (Madrid)
A M. Caswell (Leeds)
A F Chaffotte (Paris)
K E Chapman (Edinburgh)
F Checler (Valbonne)
P K. Chiang (Silver Spring)
E R Chilvers (Cambridge)
M. Claret (Orsay)
P Cohen (Dundee)
J. Colyer (Leeds)
S. J Cook (Cambridge)
R. A. Cooper (Leicester)
A. P. Corfield (Bristol)
A. Cornish-Bowden (Marseille)
M W. H. Coughtrie (Dundee)
D. A Cowan (London)
C. M Cuchillo (Barcelona)
J. M Cuezva (Madrid)
P. Cullen (Bristol)
N. P. Curthoys (Fort Collins)
W Cushley (Glasgow)

R. M. Daniel (Hamilton)
M J. Davies (Sydney)
F C de Beer (Lexington)
H de Groot (Essen)
H. R. De Jonge (Rotterdam)
L Dekker (London)
P N M. Demacker (Nijmegen)
M Dickens (Leicester)
C Dingwall (Harlow)
C J. Dorman (Dublin)
R Douce (Lyon)
K T Douglas (Manchester)
C. P. Downes (Dundee)
K. Drickamer (Oxford)
M J Dufton (Glasgow)

Y. Edwards (London)
J. M Edwardson (Cambridge)
J P Eiserich (Birmingham, AL)
C Erneux (Bruxelles)
C T Evans (Melbourne, FL)
R W Evans (London)

T Feizi (London)
R C Feldhoff (Louisville, KT)
L M. Field (Harpenden)
M C Field (London)
L. M. Fisher (London)
P R. Flatt (Coleraine)
K R Fox (Southampton)
M H Fukami (Bergen)
S. J. Fuller (London)

T G Gabig (Indianapolis)
C G Gahmberg (Helsinki)
V Gerke (Munster)
C S Gillespie (Edinburgh)
D. B. Glass (Atlanta)
L Graeve (Aachen)
A Graham (London)
J. C Gray (Cambridge)
P A Grimaldi (Nice)
S Grinstein (Toronto)

H P Haagsman (Utrecht)
P A. Halban (Genève)
A Hall (London)
R A P Harrison (Cambridge)
P Hawkins (Cambridge)
F. G. Hegardt (Barcelona)
A C Herrington (Brisbane)
J Higgins (Sheffield)
A A Holder (London)
G D Holman (Bath)
M J Holness (London)
N A Hotchin (Birmingham)
M. D Houslay (Glasgow)
C Howe (Cambridge)
H Hundal (Dundee)
J C Hutton (Denver)
E Hyde (Birmingham)

Y. Ikehara (Fukuoka)
R A Iles (London)
R E Isaac (Leeds)
C M Isacke (London)
T Ishikawa (Yokohama)
P B Iynedjian (Geneva)

K H Jakobs (Essen)
S M Jarvis (Canterbury)
P Johnson (Vancouver)
N Jones (London)

M A Kaderbhai (Aberystwyth)
K E Kadler (Manchester)
H. Kanoh (Sapporo)
J H. Kaplan (Portland, OR)
P Karran (South Mimms)
D J Keeling (Molndal)
C Kennedy (Norwich)
C. M Kielty (Manchester)
T M Kitson (Palmerston North)
L Kjellen (Uppsala)
E. Knecht (Valencia)
J Knudsen (Odense)
W Kolch (Glasgow)
I M Kovach (Washington, DC)
Y Kuroki (Sapporo)
J. Kuznicki (Warsaw)

A. Lane (London)
D A. Lane (London)
P J Large (Hull)
P J Lea (Lancaster)
D S. Leake (Reading)
C C. Leslie (Denver)
R E Lewis (Omaha, NE)
J E Lillehaug (Bergen)
D M J Lilley (Dundee)
M Liscovitch (Rehovot)
J M Lord (Coventry)
M G Low (New York)
P A Lund (Birmingham)

C C Malbon (Stony Brook, NY)
W Maltese (Toledo, OH)
J P G Malthouse (Dublin)
G E Mann (London)
B Mannervik (Uppsala)
D Martin (Oslo)
G G. F Mason (Bristol)
R W Mason (Wilmington)
P. Masson (La Tronche)
B Mayer (Graz)
K H Mayo (Minneapolis)
M J. McConville (Melbourne)
A McEuen (Southampton)
J D McGivan (Bristol)
M McGrane (Storrs)
R A J McIlhinney (Oxford)
A G. McLennan (Liverpool)
L C McPhail (Winston-Salem)
P A Meacock (Leicester)
D W Meek (Dundee)
P J. Meier-Abt (Zurich)
E Melendez-Hevia (Tenerife)
H Mellor (Bristol)
A K Menon (Madison)
D J Meyer (London)
P A Millner (Leeds)
J. L A. Mitchell (DeKalb, IL)
T J Monks (Austin)
A Morgan (Liverpool)
H W Morgan (Hamilton)
I Morgan (Glasgow)
M Mori (Kumamoto)
S Morley (Brighton)
S Morris (Pittsburgh)
N Moustaid Moussa (Knoxville, TN)
M Mueckler (St Louis)
B. Mulloy (Potters Bar)
G Murphy (Cambridge)
M E Murphy (Durham, NC)

T Nagatsu (Aichi)
I. A. Nieduszynski (Lancaster)
M Nishijima (Tokyo)
R I Norman (Leicester)

S Olsnes (Oslo)
L A J. O'Neill (Dublin)

M G P Page (Basel)
M I Page (Huddersfield)
F Palmieri (Bari)
G Panayotou (Vari)
M Parenti (Milano)
M Paulsson (Koln)
T M. Penning (Philadelphia)
K C. Persaud (Manchester)
L Persson (Lund)
J M Pfeilschifter (Frankfurt)
T Pihlajaniemi (Oulu)
T S. Pillay (Nottingham)
J. Pines (Cambridge)
C Ponzetto (Torino)
F Possmayer (London, Ont)
A D Postle (Southampton)
D Poyner (Birmingham)
N C Price (Stirling)
S A Prigent (Leicester)
D Prockop (Philadelphia)
D Pruss (Salt Lake City)
M Puceat (Montpellier)
S. Pyne (Glasgow)

D. M. Raben (Baltimore)
Z Radić (La Jolla)
D P Ramji (Cardiff)
M Rattray (London)
F X. Real (Barcelona)
C C Reddy (Penn State)
C P F Redfern (Newcastle upon Tyne)
M J Reed (London)
R A. F. Reithmeier (Toronto)
P. S. Rennie (Vancouver)
C Rice-Evans (London)
P J Richardson (Cambridge)
C C Rider (London)
A Ridley (London)
H Rosen (Rahway)
G Rotilio (Roma)
F Russo-Marie (Paris)
G A Rutter (Bristol)

EDITORIAL ADVISORY PANEL (continued)

K S. Sakariassen (Uppsala)
J. P. Salier (Rouen)
J Savill (Edinburgh)
M F G Schmidt (Berlin)
N S Scrutton (Leicester)
K. Seedorf (Hamburg)
A. W Segal (London)
S D Shapiro (St Louis)
D Sheehan (Cork)
P R Shepherd (London)
Y Shimomura (Nagoya)
H Sies (Dusseldorf)
H Sjostrom (Copenhagen)
D M. Smith (London)
F. Spener (Munster)
A K Stobart (Bristol)
W Stocker (Münster)
G J Strous (Utrecht)
T W Sturgill (Charlottesville)
K Suckling (Welwyn)
B Svensson (Copenhagen)

M J A Tanner (Bristol)
C W Taylor (Cambridge)
A Tepikin (Liverpool)
M Thelen (Bellinzona)
N S. B Thomas (London)
D Thornton (Manchester)
C Tickle (Dundee)
D Tosh (Bath)
P Trayhurn (Aberdeen)
A J Trewavas (Edinburgh)
J T Triffitt (Oxford)
J Turnbull (Birmingham)
B M Turner (Birmingham)

B Ullman (Portland, OR)

G. van de Werve (Montrèal)
L M G van Golde (Utrecht)
S van Heyningen (Edinburgh)
E van Schaftingen (Bruxelles)

G. Vassart (Bruxelles)
P. F T Vaughan (Leeds)
A. Veillette (Montreal)
G Verhoeven (Leuven)
D A Vessey (San Francisco)
H. Vidal (Lyon)
J. F G Vliegenthart (Utrecht)

M J Warren (London)
N J Watmough (Norwich)
S P Watson (Oxford)
A. Watts (Oxford)
D. J Waxman (Boston)
K. G. Welinder (Copenhagen)
R E Wettenhall (Melbourne)
R Wever (Amsterdam)
M. Wheatley (Birmingham)
C Wheeler-Jones (London)
D G Wilkinson (London)
D C Wilton (Southampton)
J -O Winberg (Tromsø)
S. J Winder (Glasgow)
C. C Winterbourn
(Christchurch, NZ)
S G. Withers (Vancouver)
P. Wojtaszek (Poznan)
A Wolffe (Bethesda, MD)
J. M Woof (Dundee)
J M Wrigglesworth (London)
M C. Wright (Southampton)
S. Wright (Leeds)
G Wu (College Station)
F Wuytack (Leuven)
M P Wymann (Fribourg)

I Young (Belfast)
L S Young (Birmingham)
S P Young (Birmingham)

I. Zachary (London)
R Zamoyska (London)

Biochem. J. (2000) **348**, 241–255 (Printed in Great Britain)

REVIEW ARTICLE

Rho GTPases and their effector proteins

Anne L. BISHOP[1] and Alan HALL

MRC Laboratory for Molecular Cell Biology, University College London, Gower Street, London WC1E 6BT, U.K.

Rho GTPases are molecular switches that regulate many essential cellular processes, including actin dynamics, gene transcription, cell-cycle progression and cell adhesion. About 30 potential effector proteins have been identified that interact with members of the Rho family, but it is still unclear which of these are responsible for the diverse biological effects of Rho GTPases. This review will discuss how Rho GTPases physically interact with, and regulate the activity of, multiple effector proteins and how specific effector proteins contribute to cellular responses. To date most progress has been made in the cytoskeleton field, and several biochemical links have now been established between GTPases and the assembly of filamentous actin. The main focus of this review will be Rho, Rac and Cdc42, the three best characterized mammalian Rho GTPases, though the genetic analysis of Rho GTPases in lower eukaryotes is making increasingly important contributions to this field.

Key words: actin reorganization, autoinhibition, CRIB motif, HR1 motif.

THE RHO FAMILY

Rho GTPases are members of the Ras superfamily of monomeric 20–30 kDa GTP-binding proteins. Ten different mammalian Rho GTPases, some with multiple isoforms, have been identified to date: Rho (A, B, C isoforms), Rac (1, 2, 3 isoforms), Cdc42 (Cdc42Hs, G25K isoforms), Rnd1/Rho6, Rnd2/Rho7, Rnd3/RhoE, RhoD, RhoG, TC10 and TTF [1]. The most extensively characterized members are Rho, Rac and Cdc42. Each of these GTPases act as a molecular switch, cycling between an active GTP-bound, and an inactive GDP-bound, state. In the GTP-bound form they are able to interact with effector or target molecules to initiate a downstream response, while an intrinsic GTPase activity returns the proteins to the GDP-bound state, to complete the cycle and terminate signal transduction.

Regulation

Cycling between the GTP- and GDP-bound states is regulated by numerous cellular proteins [2]. Although still poorly characterized, over 30 guanosine nucleotide exchange factors (GEFs) have been identified that facilitate the exchange of GDP for GTP [3,4]. All Rho GEFs contain a Dbl-homology (DH) domain which encodes the catalytic activity [5,6] and an adjacent pleckstrin homology (PH) domain. The PH domain is thought to mediate membrane localization through lipid binding [7,8], but, in addition, structural and biochemical evidence suggests that it might also directly affect the activity of the DH domain. For example, a comparison of the crystal structures of the DH-PH domains of Sos GEF, in the absence of lipid ligand, and the PH domain of phospholipase Cδ bound to inositol 1,4,5-trisphosphate, suggests that a ligand binding to Sos PH domain is likely to affect the conformation of the neighbouring DH domain [9]. In Trio, a GEF with two DH-PH modules, one specific for Rac and one for Rho [10], the N-terminal DH-PH domains together have a 100-fold higher Rac GEF activity than does the DH domain alone [11]. Finally, the binding of phosphatidylinositol 4,5-bisphosphate (PIP_2) to the PH domain of Vav GEF inhibits activity, whereas phosphatidylinositol 3,4,5-triphosphate binds more strongly and stimulates Vav activity [12]. Additional domains specific to each GEF may provide variations in subcellular localization and activation mechanisms [13].

About 20 GTPase-activating proteins (GAPs) which increase the intrinsic rate of GTP hydrolysis of Rho GTPases have been identified to date [14]. The human genome sequencing project reveals that chromosome 22 alone potentially encodes eight GAPs [15]. A comparison of the crystal structures of a ground-state complex between RhoGAP and Cdc42·guanosine 5′-[β,γ-imido]triphosphate (guanosine 5′-[β,γ-imido]triphosphate, also known as 'GMPPNP', is a non-hydrolysable GTP analogue) and a transition-state-mimicking complex of RhoGAP with RhoA·GDP·AlF_4^-, along with NMR analysis of a Cdc42·RhoGAP complex, has provided insight into the mechanistic details of GAP-facilitated GTP hydrolysis [16–18]. The most striking feature is that a 20° rotation between GTPase and GAP, from ground state to transition state, allows an arginine residue in the GAP protein, the 'arginine finger', to enter the GTPase active site and participate in the stabilization of the transition state.

Rho GTPases are able to interact with membranes via a post-translational C-terminal geranylgeranyl lipid modification

---

Abbreviations used ACK, activated Cdc42-associated tyrosine kinase, GEF, guanosine nucleotide exchange factor, PH, pleckstrin homology, DH, Dbl homology, PIP_2 phosphatidylinositol 4,5-bisphosphate; GAP, GTPase-activating protein, GDI, guanosine nucleotide dissociation inhibitor; SRF, serum response factor; NF-κB, nuclear factor κB, JNK, c-*jun* N-terminal kinase, CRIB, Cdc42/Rac-interactive binding, REM, Rho effector homology, RKH, ROK–kinectin homology, MLC, myosin light chain, PI-4-P5K, phosphatidylinositol-4-phosphate 5-kinase; GTP[S], guanosine 5′-[γ-thio]triphosphate; MAP kinase, mitogen-activated protein kinase, Mlk, mixed-lineage kinase, ACC, antiparallel coiled-coil, Btk, Bruton's tyrosine kinase, MBS, myosin-binding subunit, ERM, ezrin/radixin/moesin, FH, formin-homology, WASP, Wiskott–Aldrich-syndrome protein, WAVE, WASP-like verprolin-homologous protein, LIMK, LIM kinase; EGF, epidermal growth factor, TNFα, tumour necrosis factor α, MEKK, MAP kinase kinase kinase, PAK, p21-activated kinase; PKN, protein kinase N; MRCK, myotonic dystrophy kinase-related Cdc42-binding kinase

[1] To whom correspondence should be addressed (e-mail anne bishop@ucl ac uk)

Table 1 Summary of the cellular activities which involve Rho, Rac and Cdc42

These activities refer to biological pathways which can be induced by the activated Rho GTPases indicated and/or which can be inhibited by dominant-negative constructs of the appropriate Rho GTPases SRF and NF-κB are both transcription factors, JNK and p38 are MAP kinase pathways, the NADPH oxidase complex is present only in professional phagocytic cells, secretion has only been shown to involve Rho GTPases in mast cells

	Actin	SRF	JNK/p38	NF-κB	NADPH oxidase	G_1 cell-cycle progression	Cell–cell contacts	Secretion	Cell polarity	Transformation
Rho	+	+	−	+	−	+	+	+	−	+
Rac	+	+	+	+	+	+	+	+	−	+
Cdc42	+	+	+	+	−	+	+	?	+	+

(farnesyl for RhoD and RhoE; either modification for RhoB) [19,20]. However, in the unactivated state, Rho and Rac can be isolated as a soluble complex associated with RhoGDI (guanosine nucleotide dissociation inhibitor). RhoGDI appears to sequester GDP-bound Rho GTPases in the cytoplasm and inhibit their spontaneous GDP ↔ GTP exchange activity, similar to what has been proposed for $\beta\gamma$ subunits and the α subunits of heterotrimeric G-proteins, but the precise role of GDI is still poorly understood [21]. NMR and crystal structures of GDI alone, a low-resolution crystal structure of a RhoA·GDI complex (no geranylgeranyl lipid attached to RhoA) and a recent high-resolution [0.26 nm (2.6 Å)] crystal structure of a Cdc42·GDI complex (geranylgeranyl lipid present on Cdc42) all agree that the binding of GDI to a Rho GTPase occurs through an immunoglobulin-like C-terminal domain, and that a hydrophobic pocket in this domain can accommodate the geranylgeranyl lipid, whilst a flexible N-terminal domain inhibits GDP ↔ GTP exchange [22–25]. Cerione's group reported the use of fluorescence resonance energy transfer ('FRET') to monitor the removal of Cdc42 from membranes by GDI in real time. They detected two phases which appear to represent a rapid membrane-associated GTPase–GDI binding step followed by a slow transfer of the geranylgeranyl moiety from membrane to GDI [26].

Experimental manipulation

The biological activities of individual Rho GTPases (Table 1) have been elucidated using a variety of methods, including the use of activated and dominant-negative mutants, as well as bacterial toxins. Amino acid substitutions of Val for Gly at codon 12 or of Leu for Gln at codon 61 (Rac numbering) have been extensively used to generate constitutively active Rho GTPases, since both of these mutations prevent intrinsic and GAP-induced GTP hydrolysis. The crystal structure of RhoGAP complexed with RhoA·GDP·AlF^{4-} confirms an essential role for Gln^{63} (equivalent to Gln^{61} in Rac) in stablizing the γ-phosphate during GTP hydrolysis [17]. The crystal structure of a [Val^{14}]RhoA·guanosine 5′-[γ-thio]triphosphate (GTP[S]) (equivalent to the Val^{12} mutant in Rac) (GTP[S] is a non-hydrolysable GTP analogue) shows how the larger Val side chain forces Gln^{63} away from the γ-phosphate, so preventing it from facilitating GTP hydrolysis [27]. Interestingly Rnd1-3 and TTF Rho family members do not contain Gly and Gln at positions 12 and 61 respectively and thus appear to be constitutively GTP-bound [28–30]. This raises interesting questions as to how these proteins are regulated, but so far nothing is known.

A substitution of Asn for Thr^{17} (Rac numbering) allows this mutant GTPase to compete with the corresponding endogenous GTPase for binding to cellular GEFs, but this leads to a non-productive complex unable to generate a downstream response [31]. These dominant-negative proteins appear to be rather specific for individual Rho GTPases, despite the complexity of the RhoGEF family [3].

A variety of bacterial toxins have been used to modify the activity of Rho GTPases. The exoenzyme C3 transferase, an ADP-ribosyltransferase from *Clostridium botulinum* [32], is relatively specific and inactivates only RhoA, RhoB and RhoC. *C. difficile* toxin B inactivates most, if not all, members of the Rho GTPase family and is particularly useful in assessing the involvement of a Rho GTPase in a particular biological process [33]. The prevelance of Rho GTPase modifications by bacterial toxins illustrates the fundamental importance of these proteins to cellular regulation.

Biological activities

The major function of Rho GTPases is to regulate the assembly and organization of the actin cytoskeleton [34]. The effects of Rho, Rac and Cdc42 were initially described using quiescent Swiss3T3 fibroblasts, a cell line in which serum starvation creates a very low background of organized F-actin structures. Addition of lysophosphatidic acid induces the formation of contractile actin–myosin stress fibres and associated focal adhesions, and this can be blocked by C3 transferase [35]. Growth factors, such as platelet-derived growth factor, insulin or epidermal growth factor (EGF) induce the formation of actin-rich lamellipodia and membrane ruffles associated with focal contacts and the dominant-negative [Asn^{17}]Rac specifically inhibits this response [36]. Finally bradykinin induces the formation of peripheral microspikes or filopodia, which are also associated with focal contacts, and this can be inhibited by expression of dominant-negative [Asn^{17}]Cdc42 [37]. These types of experiment have lead to the conclusion that Rho, Rac and Cdc42 regulate three signal-transduction pathways linking various membrane receptors to the assembly of actin–myosin filaments, lamellipodia and filopodia respectively. It is not surprising, therefore, that Rho GTPases have been found to play a role in a variety of cellular processes that are dependent on the actin cytoskeleton, such as cytokinesis [38–40], phagocytosis [41,42], pinocytosis [36], cell migration [43,44], morphogenesis [45] and axon guidance [46].

One of the most interesting aspects of this family of regulatory proteins is that, in addition to their effect on the actin cytoskeleton, they also regulate a variety of other biochemical pathways (see Table 1) including serum response factor (SRF) and nuclear factor κB (NF-κB) transcription factors [47,48], the c-*jun* N-terminal kinase (JNK) and p38 mitogen-activated protein kinase pathways [49,50], the phagocytic NADPH oxidase complex [51], G_1 cell-cycle progression [52], the assembly of cadherin-containing cell–cell contacts [53,54], secretion in mast cells [55], cell polarity [56] and cell transformation [3]. Therefore, although Rho GTPases are best characterized for their effects on the actin cytoskeleton, there is now much interest in their ability to affect cell proliferation and gene transcription, and the contributions of all of these activities to malignant transformation is an important field of study.

THE INTERACTION OF Rho GTPases WITH EFFECTOR PROTEINS

Given the involvement of Rho GTPases in such a wide variety of important cellular processes, it is not surprising that a great deal of effort has been put into identifying their cellular targets or effector proteins. To date 30 or so potential effectors for Rho, Rac and Cdc42 have been identified (Table 2), primarily using affinity chromatography and the yeast two-hybrid system. These proteins interact specifically with the GTP-bound form of the GTPase. A comparison of the RhoA·GDP and [Val^{14}]RhoA·GTP[S] crystal structures, reveals that the conformational differences between the GTP and GDP-bound forms are restricted primarily to two surface loops, named switch regions I and II (Cdc42/Rac amino acids 26–45 and 59–74 respectively) [27,57]. Effector proteins must, therefore, utilize these differences to discriminate between the GTP- and GDP-bound forms, though they also interact with other regions of the GTPase (see below).

Numerous point mutations have been introduced into Switch I of Rho, Rac and Cdc42, often referred to as the 'effector region', and have rather interesting effects preventing the binding of some, but not all, target proteins [58–60]. For example, the interaction of PAK (p21-activated kinase) with Cdc42/Rac is blocked by a Tyr^{40}-to-Cys mutation, but not by a Phe^{37}-to-Ala mutation [58]. Whereas the interaction of Mlk (mixed-lineage kinase) 2 and 3 with Rac is blocked by either of these mutations [61]. Substitution of different amino acids at the same position in switch I can also have varied effects upon target protein binding; for instance, [Cys^{40}]Rac can bind to p67^{phox} (a component of the NADPH oxidase complex), whereas [Lys^{40}]Rac cannot [58]. Such results suggest that different effectors interact with different residues, even within the switch I region.

Further studies using GTPase mutants and chimaeras have implicated regions outside of switch I in the binding of certain effectors. For instance, Rac–Rho chimaeras indicate that a region close to the C-terminus of Rac (amino acids 143–175) may be important for binding to p67^{phox} and for PAK activation [62]. An α-helical region present in all Rho-family GTPases (except *Drosophila* RhoL), but not in Ras, referred to as the 'insert region' (Rac amino acids 123–135), is required for Rac activation of the NADPH oxidase complex and for binding to an effector protein called IQGAP, but not for its interaction with PAK [63,64]. So far there are no known examples of Rho effectors

Table 2 Potential effector proteins for Rho, Rac and Cdc42

Proteins shown with an asterisk (*) are those which appear to be activated by GTPases in a GTP-dependent manner, but where the interaction is GTP-independent Proteins shown with a superscript plus sign ($^{+}$) are those for which a functional relationship with GTPase, but not a direct interaction, has so far been shown Note that Rho is reported to inhibit diacylglycerol kinase (DAG kinase), whereas all the other targets listed are thought to be activated by Rho GTPases Common GTPase-binding motifs, assigned according to sequence homology are CRIB, REM (also known as class-1 Rho-binding motif) and RKH (also known as class-2 Rho-binding motif) Where a function has been reported this is noted, but in many cells these are far from clear, for further discussion, see the text and key references given below Further abbreviations. PKN, protein kinase N, PLC, phospholipase C, PLD, phospholipase D, IP3, inositol trisphosphate, PA, phosphatidic acid

Potential effector protein	Type of protein	Functions	Selectivity of Rho GTPase binding			GTPase-binding motif	Key references
ROKα, ROKβ	Ser/Thr kinase	Actin/myosin	Rho			RKH	[91,128,129]
PKN/ PRK1, PRK2	Ser/Thr kinase	Unknown	Rho			REM	[90,208]
Citron kinase (citron)	Ser/Thr kinase	Cytokinesis	Rho				[102,103]
p70 S6 kinase	Ser/Thr kinase	Translation regulation		Rac	Cdc42?		[209]
Mlk2, 3	Ser/Thr kinase	JNK		Rac	Cdc42	CRIB	[61,200,201]
MEKK1, 4	Ser/Thr kinase	JNK		Rac	Cdc42	CRIB for MEKK4	[202]
PAK1, 2, 3	Ser/Thr kinase	JNK/actin		Rac	Cdc42	CRIB	[79]
PAK4	Ser/Thr kinase	Actin			Cdc42	CRIB	[81]
MRCKα, MRCKβ	Ser/Thr kinase	Actin			Cdc42	CRIB	[104]
Ack1, 2	Tyr kinase	Unknown			Cdc42	CRIB	[73,210]
MBS	Phosphatase subunit	MLC inactivation	Rho				[128]
PI-4-P5K	Lipid kinase	PIP$_2$ levels/actin	Rho^{*+}	Rac*			[144,147,169,171]
PI3K	Lipid kinase	PIP$_3$ levels		Rac	Cdc42		[211–213]
DAG kinase	Lipid kinase	PA levels	Rho^{+}	Rac*			[169,214]
PLD	Lipase	PA levels	Rho	Rac	Cdc42		[215–218]
PLC-β2	Lipase	DAG/IP$_3$ levels		Rac	Cdc42		[219]
Rhophilin	Scaffold	Unknown	Rho			REM	[76]
Rhotekin	Scaffold	Unknown	Rho			REM	[77]
Kinectin	Scaffold	Kinesin binding	Rho			RKH	[220]
Dia1, Dia2	Scaffold	Actin organization	Rho				[91,141]
WASP, N-WASP	Scaffold	Actin organization			Cdc42	CRIB	[94,96,97]
WAVE/ Scar	Scaffold	Actin organization		Rac^{+}			[94,95,172]
POSH	Scaffold	Unknown		Rac			[61]
POR-1	Scaffold	Actin organization		Rac			[166]
p140Sra-1	Scaffold	Actin organization		Rac			[168]
p67^{phox}	Scaffold	NADPH oxidase		Rac			[51,63,207]
MSE55, BORGs	Scaffold	Unknown			Cdc42	CRIB	[221,222]
IQGAP1,2	Scaffold	Actin/cell–cell contacts		Rac	Cdc42		[54,96,98,115]
CIP-4	Scaffold	Unknown			Cdc42		[223]

(a)

ACK (505–531)	L	S	A	Q	D	I	S	Q	P	L	Q	N	S	F	I	H	T	G	H	G	D	S	D	P	R	H	C
WASP (236–258)	I	S	K	A	D	I	G	A	P	.	.	S	G	F	K	H	V	S	H	V	G	W	D	P	Q	N	G
PAK1 (70–94)	K	E	R	P	E	I	S	L	P	.	.	S	D	F	E	H	T	I	H	V	G	F	D	A	V	T	G
PAK2 (71–91)	K	E	R	P	E	I	S	P	P	.	.	S	D	F	E	H	T	I	H	V	G	F	D	A	V	T	G
PAK4 (6–30)	K	K	R	V	E	I	S	A	P	.	.	S	N	F	E	H	R	V	H	T	G	F	D	Q	H	E	Q
CRIB consensus					*	I	S	*	P			S	*	F	*	H	*	*	H	*	G	*	D				

(b)

PKN/PRK1 HR1a (34–63)	Q	L	E	L	E	R	E	R	L	R	R	E	I	R	K	E	L	K	L	K	E	G	A	E	N	L	R	R	A	T
PRK2 HR1a (44–73)	K	L	D	D	I	K	D	R	I	K	R	E	I	R	K	E	L	K	I	K	E	G	A	E	N	L	R	K	V	T
Rhophilin (39–68)	Q	L	Q	S	H	R	A	R	L	H	Q	Q	I	S	K	E	L	R	M	R	T	G	A	E	N	L	Y	R	A	T
Rhotekin (20–49)	A	L	S	L	E	D	T	E	L	Q	R	K	L	D	H	E	I	R	M	R	Q	G	A	C	K	L	L	A	A	C
HR1 consensus		L				*		*	L		*		I		*	E	L	*	*	*		G	A	*	*	L		*	A	*

PKN/PRK1 HR1a (64–93)	T	D	L	G	K	S	L	G	P	V	E	L	L	L	R	G	S	S	R	K	L	D	L	L	H	Q	Q	L	Q	E
PRK2 HR1a (74–102)	T	D	K	.	K	S	L	A	Y	V	D	N	I	L	K	K	S	N	K	K	L	E	E	L	H	H	K	L	Q	E
Rhophilin (69–97)	S	N	.	T	W	V	R	E	T	V	A	L	E	L	S	Y	V	N	S	N	L	Q	L	L	K	E	E	L	A	E
Rhotekin (50–79)	S	Q	R	E	Q	A	L	E	A	T	K	S	L	L	V	C	N	S	R	I	L	S	Y	M	G	E	L	Q	R	R
HR1 consensus							*			*			*	L							L			L				*		*

PKN/PRK1 HR1a (94–103)	L	H	A	H	V	V	L	P	D	P
PRK2 HR1a (103–112)	L	H	A	H	I	V	V	S	D	P
Rhophilin (98–107)	L	S	T	S	V	D	V	D	Q	P
Rhotekin (80–89)	K	E	A	Q	V	L	E	K	T	G
HR1 consensus	*				V				*	*

Figure 1 Sequence comparisons for (a) the CRIB motifs from ACK, WASP and three PAKs and (b) the HR1 motifs from PKN/ PRK1 (HR1a), PRK2 (HR1a), rhophilin and rhotekin, which are the essential Rho-binding regions within the REM domain of each protein (see the text)

(**a**) Other mammalian GTPase effectors which contain CRIB motifs are listed in Table 2. Conserved CRIB consensus residues are shown in red; * indicates less conserved residues within the CRIB motif. (**b**) Conserved HR1 motif consensus residues are shown in red; * indicates important HR1 motif residues that are less conserved. Charged amino acids which are particularly important for PKN binding to Rho, according to structural data, and are less conserved in the other two PKN HR1 motifs (HR1b and HR1c) are underlined (see the text for discussion).

requiring this insert region for binding. Two amino acids in loop 6 (just C-terminal to switch II) of Rho are acidic (Asp^{87} and Asp^{90}), but are hydrophobic (Val and Ala) in Rac, and these appear to be important for Rho binding to two effectors PRK2 and ROK [65]. This same region of Rac (amino acids 74–90), on the other hand, has been implicated in the binding of GAPs [62] and an overlapping region of Cdc42 (amino acids 84–120) appears to be involved in binding to Wiskott–Aldrich-syndrome protein (WASP) and IQGAP, but not to PAK1 [66]. These mutational studies indicate that distinct regions of Rac, Cdc42 and Rho outside of switch I are required to make essential contacts with effector proteins.

The data obtained from the many mutational studies that have been undertaken have lead to a complex, and sometimes contradictory, picture of the mechanisms of Rho GTPase–effector interactions. However, the recently reported NMR structures of Cdc42 bound to **a**ctivated **C**dc42-associated tyrosine **k**inase (ACK) (amino acids 504–545) and WASP (amino acids 230–288) have provided much clarification [67,68]. ACK and WASP both contain the conserved GTPase-binding consensus site, the CRIB (**C**dc42/**R**ac-**i**nteractive **b**inding) motif, which is present in many, though not all, Rac- and Cdc42-binding proteins (see Table 2) [69]. The CRIB sequences for ACK and WASP, and a consensus sequence, are shown in Figure 1(a). This motif is necessary, but not sufficient, for strong binding to the GTPase, as shown by binding studies for Cdc42 with different WASP fragments [70]. The NMR structures of ACK and WASP CRIB-containing peptides bound to Cdc42 show that Asp^{38} in Switch I interacts with the two His residues conserved in all CRIB proteins (Figure 1a). Interestingly Switch I and II are almost identical in Rho, Rac and Cdc42, except for position 38 which is Asp in Rac/Cdc42 and Glu in Rho. Mutation of Cdc42 Asp^{38} to Glu decreases the affinity for PAK3 (a CRIB protein which binds to both Rac and Cdc42) by 50-fold [71], and it seems likely that all CRIB proteins may use Asp^{38} to distinguish Rac/Cdc42 from Rho.

Whereas PAK1 binds with similar affinity to Rac and Cdc42 [72], ACK and WASP are relatively selective for Cdc42 [73,74]. To achieve this selective binding, ACK and WASP must interact with amino acids that differ between Cdc42 and Rac, and these contacts have been revealed in the NMR studies [67,68]. [Leu^{174}]Cdc42, for instance, forms a strong hydrophobic contact with both ACK and WASP, but in Rac residue 174 is Arg, which would weaken this interaction. The ACK CRIB residue which interacts with Leu^{174} is Leu^{505}, but the equivalent residue in PAK is Lys, which would not pack well against Leu^{174} and is, presumably, therefore, not involved in the interaction (see Figure 1a). The equivalent residue in WASP is Ile, which should pack almost as well as Leu (see Figure 1a). Thus, a picture of how different effector proteins recognize different combinations of Rho GTPases emerges. However, while ACK and WASP are clearly Cdc42 targets, it is not clear whether, *in vivo* and under physiological conditions, PAKs 1–3 are targets for Cdc42 or Rac or both.

A further insight gained from these NMR structures is that the GTPase induces significant conformational changes in ACK and WASP. The CRIB-containing fragments of ACK and WASP used in these experiments (amino acids 504–545 and 230–288 respectively) have no discernable structure in solution, but when bound to Cdc42 they form a tight intermolecular β-sheet across the GTPase switch regions. Presumably Cdc42 stabilizes this key conformation, which is only one of many that the free peptide can adopt in solution. WASP sequences C-terminal to the core CRIB motif form an anti-parallel β-hairpin and a short α-helix only when bound to Cdc42. Equally, the switch regions of free Cdc42 in solution are flexible, but become rigid when bound to an effector.

These NMR data have certainly provided much insight into how CRIB motif-containing proteins, in general, may interact with Rac and Cdc42. However, one must remember that not all Rac/Cdc42 effector proteins contain a CRIB domain (see Table 2), so cannot be assumed to bind to GTPases in the same way. IQGAP, for instance, appears to require the insert region for binding to Rac and Cdc42 (see above) which has not been shown to be required for the binding of any of the known CRIB-containing proteins. Such observations imply that a very different set of interactions may be formed between Rac and Cdc42 and their numerous effectors.

Rho binding to its effector proteins also appears, from mutational studies, to require quite different GTPase regions compared with Rac and Cdc42 (see above). Rho effectors protein kinase N (PKN)/PRK1 and PRK2 bind to Rho via an N-terminal Rho effector homology (REM) region which contains three repeats of a leucine-zipper-like motif named HR1 (amino acids 40–91, 129–184 and 216–271). The first two HR1 repeats (HR1a and HR1b) can each independently bind to Rho, but only HR1a binding is GTP-dependent (Figure 1b shows PKN HR1a sequence and the HR1 motif consensus sequence) [75]. The scaffold-like Rho effectors rhophilin and rhotekin also contain one N-terminal HR1 motif, very similar to PKN HR1a, which is required for their GTPase binding (see Figure 1b) [76,77]. Recently the crystal structure of PKN amino acids 7–155 (HR1a and half of HR1b) bound to RhoA·GTP[S] has been solved [78]. When bound to Rho the HR1a region of PKN forms an antiparallel coiled-coil (ACC) finger fold, a very different conformation to the CRIB peptides of ACK and WASP bound to Cdc42. Rho residues within switch I, particularly Lys^{27} and Gln^{29}, make strong contacts with PKN, and allow the effector to specifically recognize the GTP-bound form of Rho; Lys^{27} in particular is inaccesible in the GDP–Rho structure. These are switch I residues different from those which appear to be important for Cdc42 recognition by ACK and WASP (see above) [67,68]. A hydrophobic patch at the end of the PKN HR1a ACC finger, plus hydrogen-bond contacts from PKN Lys^{51}, Lys^{53}, Arg^{81} and Asp^{85} (see Figure 1b), form important contacts with Rho switch I, the C-terminal end of switch II (amino acids 66–76) and some adjacent amino acids. The polar residues are less conserved in PKN HR1b and HR1c, and the hydrophobic patch is partially replaced by charged residues in HR1c, which may explain why HR1b has low affinity for Rho and why HR1c does not bind to Rho at all, despite their similar overall sequences. Sequence analysis suggests that similar ACC finger folds will be present in other REM proteins, such as rhopilin and rhotekin, and also perhaps in non-REM Rho effectors such as ROK and kinectin [78].

THE ACTIVATION OF EFFECTORS BY Rho GTPases

The structural analysis of Rho GTPase–effector interactions has so far made use of discrete binding domains derived from effectors. When considering how a GTPase might regulate the activity of a target protein, and how these proteins subsequently transduce signals to the cell, the whole effector protein must be considered.

The most common mechanism of effector activation by Rho GTPases appears to be the disruption of intramolecular autoinhibitory interactions, to expose functional domains within the effector protein (see the general model in Figure 2). For example the Rac/Cdc42 targets PAK1–3 and Ser/Thr kinases, have an intramolecular regulatory domain that inhibits kinase activity. Upon GTPase binding, the inhibitory sequence is displaced, leaving the kinase domain free to bind to substrates [79,80]. Interestingly, a more distantly related PAK family member recently cloned, PAK4, does not contain an autoinhibitory domain, and this PAK is not significantly stimulated by GTPase binding [81]. In agreement with the model a peptide from the PAK1 regulatory region (amino acids 83–149) can be used as a dominant-negative inhibitor of PAK activity both *in vitro* and *in vivo* [82], and mutants of the PAK inhibitory domain are found to have constitutive kinase activity [82,83]. Equally, cleavage of PAK-2 (and of PKN, see below) by caspases, which occurs during apoptosis, also removes its regulatory domain and creates a constitutively active protein [84,85].

Two kinases which are Rho effectors have also been reported to contain autoinhibitory domains, ROK and PKN. A region of the ROKα autoinhibitory domain (amino acids 941–1388) includes the GTPase-binding and PH domains, and when mutated so as to disrupt binding to Rho, will inhibit endogenous ROK [86]. In the case of PKN the binding of Rho–GTP appears to co-operate with binding of lipids such as arachidonic acid and with autophosphorylation to remove an autoinhibitory interaction and to fully activate its protein kinase C-like kinase domain [87–90].

A similar principal may also apply to activation of the many scaffold-like targets of GTPases (see Figure 2). Dia is thought to act as a scaffold protein that can be activated by Rho and then interacts with profilin/actin. Recent work has revealed that the N-terminal 389 amino acids interacts with a region at the C-terminus (amino acids 1116–1255), which makes full-length Dia inactive. Binding of Rho to the N-terminal sequence releaves this inhibition and, in agreement with the model, Dia becomes constitutively active when the N-terminal inhibitory region is removed [91]. Interestingly a human genetic disease, non-syndromic deafness, results from amino acid substitutions in the C-terminal 52 amino acids of human Dia1, and the experimental work suggests that this might create constitutively active protein [92]. WASP and N-WASP, two related Cdc42 targets, also appear to be regulated by an intramolecular interaction. The regions of WASP which bind to each other have recently been identified, using a tryptophan-fluorescence-quenching assay, as the N-terminal GTPase-binding domain (amino acids 230–310) and a cofilin-homology region at the C-terminus (amino acids 461–492) [93]. Cdc42–GTP competes with WASP C-terminus for binding to the N-terminus and, according to NMR data, induces a conformational change in the WASP N-terminus quite different from its conformation when autoinhibited [93]. Owing to autoinhibitory interactions, full-length N-WASP has decreased ac-

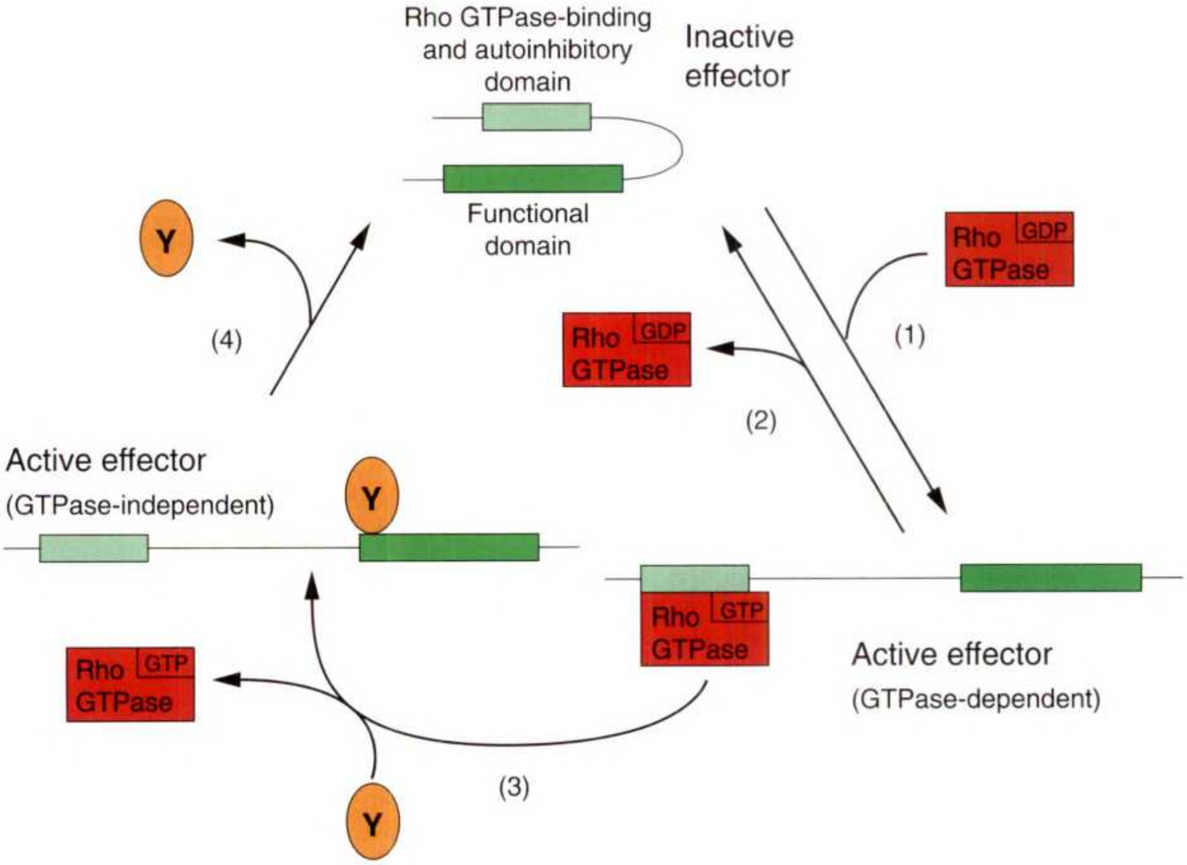

Figure 2 General model for activation of effector proteins

(1) Binding of Rho GTPase to effector relieves an antoinhibitory intramolecular interaction (this is clearly the case for the kinase PAK [80] and for the scaffold proteins Dia [91] and WASP [93], and maybe also for other effectors which contain autoinhibitory domains; see the text). (2) The effector remains active until GTP hydrolysis takes place. (3) Alternatively a modification of the effector (Y, orange ellipses) (e.g. autophosphorylation, as is the case for PAK [72], phosphorylation by a separate kinase or binding to a different activating protein) may maintain activity even after dissociation of the GTPase. (4) Inactivation of the effector occurs though removal of modification Y (e.g. dephosphorylation or removal of a bound activating protein), allowing the effector to re-enter its inactive conformation.

tivity compared with the functionally important C-terminal acidic region alone, and Cdc42-GTP can activate N-WASP by releasing intramolecular interactions [94–97]. A variation on this mode of effector activation has been suggested for the Cdc42-binding protein IQGAP. In this case a seperate protein, calmodulin-Ca^{2+}, binds to IQGAP (via its IQ motif) and inhibits its binding to actin and Cdc42 [98,99]. This might provide a calcium-sensitive regulatory mechanism for controlling the activation of IQGAP [56].

Almost all Rho GTPase effectors have multiple domains, and some of these might regulate their activity. For example, the PH domains present in WASP and N-WASP are thought to promote association with membrane, through lipid binding, where they may encounter activated Rho GTPases [100]. The Rho effectors ROK and citron/citron kinase and the Cdc42 effectors MRCKα/β also contain PH domains [101–104] (MRCKs are myotonic dystrophy kinase-related cdc42-binding kinases). Protein–protein, as well as protein–lipid, interactions can regulate the subcellular localization of GTPase effectors. For example, PRK2 (though not the related PKN/PRK1), WASP and PAK all contain Pro-Xaa-Xaa-Pro (Xaa is any amino acid) classic proline-rich SH3-binding motifs which have been reported to bind to the adaptor Nck [105–108]. Since Nck also has an SH2 domain, it could recruit these effectors to activated receptor tyrosine kinases. PAK also interacts with another SH3-containing protein, αPIX (also known as Cool-2), though this interaction is via a non-classical SH3 domain-binding region of PAK (amino acids 175–206) [109,110]. αPIX, which is a Cdc42/Rac GEF, can potentially activate PAK, and can also localize the kinase to specific sites within the cell ([79,110,111], but see [111a]); for example, paxillin recruits Cat/Git/Pkl to focal contacts which, in turn, binds to PIX [112], while free $G\beta\gamma$ subunits released by activated G-protein-coupled receptors bind to G protein-coupled receptor kinases, which can also recruit Cat/Git/Pkl and therefore PIX [113]. Interestingly, another member of the PIX family, p50Cool-1, inhibits PAK, while p85Cool-1/βPIX appears neither to inhibit nor activate PAK [114]. Exactly how the PIX–PAK interaction contributes to Rac/Cdc42 activity requires further investigation.

It is noteworthy that many of the Rho GTPase effector proteins contain coiled-coil regions (ROK, citron, IQGAP, Dia) which in some proteins have been shown to facilitate oligomerization, and indeed there is evidence that this is the case for IQGAP [115–117]. Effector oligomerization could add yet another level of complexity to target activation by Rho GTPases.

Once PAK has been activated by its interaction with Rac/Cdc42, it then autophosphorylates, which both decreases its affinity for GTPase (freeing the GTPase to bind to more effectors or to be inactivated by GAPs) and also maintains PAK in an open, activated conformation even when dissociated from the GTPase [72]. Similar mechanisms may exist for scaffold proteins, though in this case a separate kinase activity would obviously be needed to phosphorylate the effector (see Figure 2). WASP may be an example of this; it is a substrate for two tyrosine kinases found in lymphocytes, Lyn and Bruton's tyrosine kinase (Btk) [118,119]. WASP shows increased Tyr phosphorylation in the presence of constitutively active Cdc42, indicating that Cdc42 may recruit WASP to the site of Lyn and Btk activity [118]. The tyrosine residue phosphorylated by Btk (Tyr^{291}) [119] is predicted to disrupt the autoinhibited fold of WASP N-terminus, so may stabilize WASP in an active conformation even in the absence of Cdc42 [93]. The presence, or not, of kinases which phosphorylate scaffold-like effectors, and the activity of phosphatases (such as protein phosphatase 2A which co-precipitates with PAK1 [120]) which dephosphorylate effectors which are held in an active conformation, may prove to be a general mechanism for regulating the kinetics of effector activity (see Figure 2). Also, in keeping with the model, binding of other proteins to an activated effector, in addition to or instead of phosphorylation, could stabilize effectors in an active conformation after GTPase dissociation (see Figure 2), although no clear example of an effector utilizing such a mechanism has yet been identified.

EFFECTORS WHICH MEDIATE Rho GTPase FUNCTIONS

Along with an understanding of how Rho GTPases interact with, and are activated by, effector proteins, there has been much interest in identifying the contributions of specific effectors to different GTPase functions. So far significant progress has only been made in identifying effectors involved in actin reorganization.

Rho-induced actin reorganization

At least two effectors, ROK and Dia, appear to be required for Rho-induced assembly of stress fibres and focal adhesions (Figure 3). p164ROKα (also known as Rho-associated kinase) and p160ROKβ (also known as Rho-associated coiled-coil-containing protein kinase or ROCK) are Ser/Thr kinases, whose kinase domains resemble that of myotonic dystropy kinase (52% identity). They also contain a coiled-coil region, a ROK–kinectin homology (RKH) Rho-binding domain, a PH domain and a Cys-rich region. ROKs are activated by binding to Rho–GTP [121,122]. Expression of the constitutively active catalytic domain of ROKα induces stellate actin-myosin filaments in HeLa and Swiss3T3 cells [101,123]. Inhibition of ROK, on the other hand, using a pharmacological inhibitor (Y-27632) causes loss of serum and [Val^{14}]Rho-induced stress fibres [124]. These results indicate that ROK is necessary, but not sufficient, for Rho-induced stress-fibre assembly.

Two substrates of ROK which are likely to be key players in actin–myosin filament assembly are myosin light chain (MLC) [125] and the myosin-binding subunit (MBS) of MLC phosphatase [126]. MLC phosphatase is inhibited by phosphorylation, indirectly leading to an increase in MLC phosphorylation (see Figure 3). Phosphorylation of MLC occurs at Ser^{19}, which stimulates the actin-activated ATPase activity of myosin II and promotes the assembly of actomyosin filaments [125–127]. Interestingly Rho-GTP also binds directly to the MBS of MLC phosphatase, but why Rho should bind to both kinase and substrate is unclear at present [128].

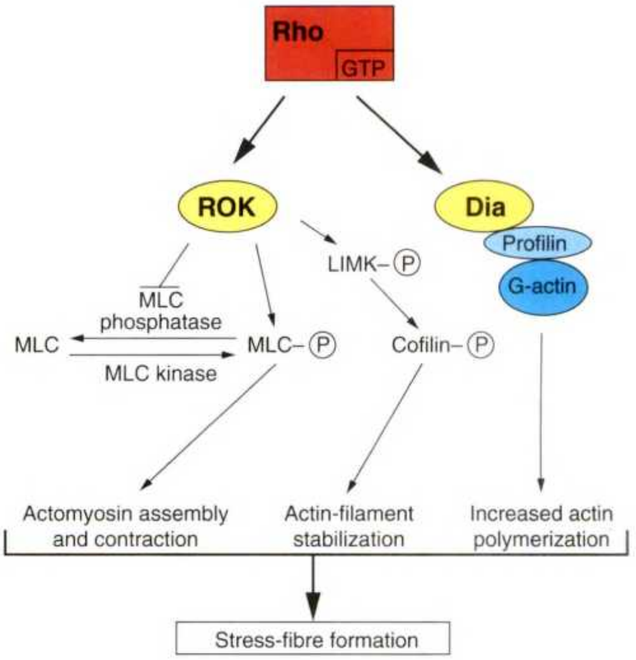

Figure 3 Signal-transduction pathways involved in Rho-induced stress-fibre assembly (see the text for details)

Another ROK target is LIM kinase (LIMK), which when phosphorylated is able to inhibit (by phosphorylation) cofilin, leading to stabilization of filamentous actin structures (Figure 3) [129,130]. ROK has also been reported to activate a ubiquitous Na^{+}/H^{+} exchange protein (NHE1) and this contributes, via an unknown mechanism, to stress fibre and focal adhesion formation [131–134]. Other substrates for ROK which could contribute to actin assembly are adducin, which is phosphorylated by ROK both *in vitro* and *in vivo*, causing it to bind more strongly to F-actin [135,136], and the ERM (ezrin/radixin/moesin) family of proteins, which link actin to the membrane [137,138]. However, recent data has questioned whether ROK is in fact an *in vivo* ERM-activating kinase [139].

While the catalytic domain of ROK alone does not induce correctly organized stress fibres, it has been reported that, when combined with an activated (N-terminal truncation) version of Dia, stress fibres are induced [91,140,141]. This has lead to the idea that activation of both Dia and ROK by Rho are required in order to induce stress fibres. Dia (Dia1 and 2 in mammals) is a member of the formin-homology (FH) family of proteins and contains two FH domains [142]. The FH1 sequence contains multiple proline-rich motifs which bind to the G-actin-binding protein, profilin. This interaction somehow allows Dia to contribute to actin polymerization and F-actin organization into stress fibres [91,142].

Many observations point to a role for lipids, particularly PIP$_2$, in actin cytoskeleton rearrangements. For instance, the binding of PIP$_2$ to capping proteins such as gelsolin can induce their release from actin-filament barbed ends, providing a mechanism whereby PIP$_2$ could increase actin polymerization [143]. There are some data to suggest that PIP$_2$ is involved in Rho effects. Injection of antibodies against PIP$_2$, for example, has been reported to inhibit serum-induced assembly of stress fibres [144]. Furthermore, overexpression of phosphatidylinositol-4-phosphate 5-kinase (PI-4-P5K) (to produce PIP$_2$) induces massive actin polymerization in COS-7 cells [145]. It is noteworthy that mutation of the gene for a yeast PI-4-P5K, *mss4*, results in defects in the formation of actin cables, which can be repressed by overexpression of Rho2p, a Rho-like GTPase [146]. A physical association between Rho and a type I (PI-activated) PI-4-P5K activity has been detected in Swiss-3T3-cell lysates, though this interaction is not GTP-dependent and may not be direct [147]. PIP_2 also binds to vinculin, increasing its talin-binding ability; therefore PIP_2 synthesis could also help to induce focal adhesion formation [144]. PI-4-P5K could, therefore, provide a link between Rho and the stimulation of both new actin polymerization and of focal adhesions assembly. Additionally, [Val^{14}]Rho and PI-4-P5K both induce ERM phosphorylation when overexpressed in fibroblasts, suggesting that Rho activation of PI-4-P5K may also be a mechanism by which Rho activates ERM proteins [139].

Cytokinesis also depends on the assembly of contractile actin–myosin filaments and has been shown to be Rho-dependent in *Xenopus* and sand-dollar (flat sea-urchin) embryos [38,39]. Rho is recruited to the cleavage furrow of Swiss3T3 cells during cytokinesis [148] and may utilize some of the same effector proteins required for stress-fibre formation. ROK, for example, phosphorylates and disassembles the intermediate filament protein glial fibrillary acidic protein to allow cleavage to occur [149], and a dominant-negative ROK construct (containing a mutant Rho-binding domain fused to the PH domain) inhibits cytokinesis when injected into *Xenopus* embryos and mammalian cells [150].

Mammalian Dia may be involved in cytokinesis, since it has been detected at the cleavage furrow in mitotic Swiss3T3 cells [141], and, in lower eukaryotes, FH-domain proteins are commonly involved in cytokinesis. For example, the *Drosophila* homologue, diaphanous, is essential for cytokinesis [151], and two yeast formin-family proteins, Bni1p and Bnr1, are both required downstream of Rho GTPases for bud formation and *bni1 bnr1* double mutants are often multinucleate [152].

Citron kinase, which appears not to play a role in stress-fibre assembly, has been localized to the cleavage furrow in HeLa cells [103]. Citron kinase, like ROK, contains an N-terminal myotonic dystrophy kinase-like kinase domain (46 % identity with ROKα), a central coiled-coil region, a Rho-binding domain (with no homology with ROK), a Cys-rich region, a PH domain and, unlike ROK, a Pro-rich SH3 domain-binding region [102,103]. Truncations of citron kinase lacking the Rho-binding domain inhibit cytokinesis in HeLa cells, producing multinucleate cells [103], suggesting that this kinase acts downstream of Rho specifically at the cleavage furrow. Whether citron phosphorylates a distinct subset of proteins from ROK, in order to fulfil its role in cytokinesis, is unknown.

Cdc42 effectors implicated in actin reorganization

WASP is expressed in haematopoetic cells, and is the product of the X-linked immunodefficiency gene found in Wiskott–Aldrich syndrome ([153,154], but see [153a]). The more ubiquitously expressed (neuronally enriched) N-WASP, like WASP, also binds to Cdc42 [100,155,156]. WASP and N-WASP each contain an N-terminal PH domain, followed by WASP-homology domain 1 (WH1), a CRIB domain, an SH3-binding proline-rich sequence, a WH2 domain containing verprolin-like sequences and an acidic C-terminus to which Arp2/3 binds (see below). It was observed that overexpression of N-WASP plus Cdc42 induces very long microspikes, like an exaggeration of Cdc42 activity [97], suggesting that these proteins may be involved in the formation of filopodia downstream of Cdc42. N-WASP binds to profilin, and WASP and N-WASP bind directly to actin monomers through their verprolin-like WH2 domains [94,157,158]. A WASP binding partner, WASP-interacting protein ('WIP'), which also binds to profilin and causes actin polymerization in BJAB cells may also be involved [159]. Recently it has been found that WASP/N-WASP, the yeast homologue Bee1p and the WASP-like Scar proteins (which do not contain a Cdc42-binding domain), bind directly to, and activate, the Arp2/3 complex via their acidic C-terminus [94,95,160]. The Arp2/3 complex binds to actin monomers and acts as a nucleation site for new actin polymerization [161,162]. Furthermore, Cdc42-GTP has been shown to induce actin polymerization *in vitro*, in extracts from *Xenopus*, the cellular slime mould *Dictostelium discoideum* or polymorphonuclear leucocytes [163,164], and biochemical disection of this process has revealed that the Arp2/3 complex and N-WASP are required [96]. Thus, WASP/N-WASP is activated by Cdc42 (plus lipids) and can then act as a scaffold to recruit the machinery required for new actin polymerization, actin monomers/profilin, and the Arp2/3 complex (Figure 4).

Cdc42 also interacts with two Ser/Thr kinases that are thought to be involved in actin reorganization and filopodia formation, MRCKs α and β. MRCKs are Cdc42-specific effector proteins which contain a PH domain and a ROK-like kinase domain which can phosphorylate MLC. Kinase-dead MRCKα inhibits Cdc42-induced filopodia, and overexpression of MRCKα synergizes with Cdc42 to induce large filopodia in HeLa cells [104]. The *Drosophila* homologue of MRCK, Genghis Khan ('GEK') is known to be required for cytoskeletal regulation during oogenesis [165]. Another protein that is able to synergize with Cdc42 to produce large filopodia-like structures is the new PAK family member PAK4 [81]. PAK4 has a CRIB motif (see Figure 1a) and a kinase domain similar to PAKs 1–3, but its sequence is divergent outside of these regions. PAK4 acts quite differently to PAKs 1–3, in that it binds to Cdc42 and not to Rac, and it is not activated by GTPase binding.

Rac effectors implicated in actin reorganization

To date there are few examples of unique Rac effectors that have been implicated in actin reorganization. POR-1 (Partner of Rac) has been implicated in Rac-induced lamellipodia formation, since truncations act as dominant negative constructs [166,167], and p140Sra-1 (Specific Rac1-associated protein) co-sediments with F-actin, implying a role in Rac-induced actin reorganization [168]. However, little more is known about the cellular functions of these two proteins. A better characterized target of Rac is PI-4-P5K. Rac interacts directly with PI-4-P5K, though this interaction is not GTP-dependent [169]. It has been established, using permeabilized platelets, that thrombin-induced actin-filament assembly requires actin-filament uncapping, which is absolutely dependent upon an increase in PIP_2 levels, and that this is mediated by Rac activation of a type I PI-4-P5K [170,171].

Interestingly a WASP-like Verprolin-homologous protein (WAVE, also known as Scar) can be precipitated with Rac, though it is not known if this is through a direct interaction. WAVE localizes to membrane ruffles, and its overexpression causes actin clusters, an activity which requires the profilin-binding and verprolin-homology (actin-binding) domains. A verprolin-homology-domain mutant of WAVE inhibits Rac-induced ruffling, further suggesting an *in vivo* link between Rac and WAVE [172]. WAVE, like WASP/N-WASP, has been shown to interact with, and activate, the Arp2/3 complex through its C-terminal acidic domain (see Figure 4) [94,95], but so far it

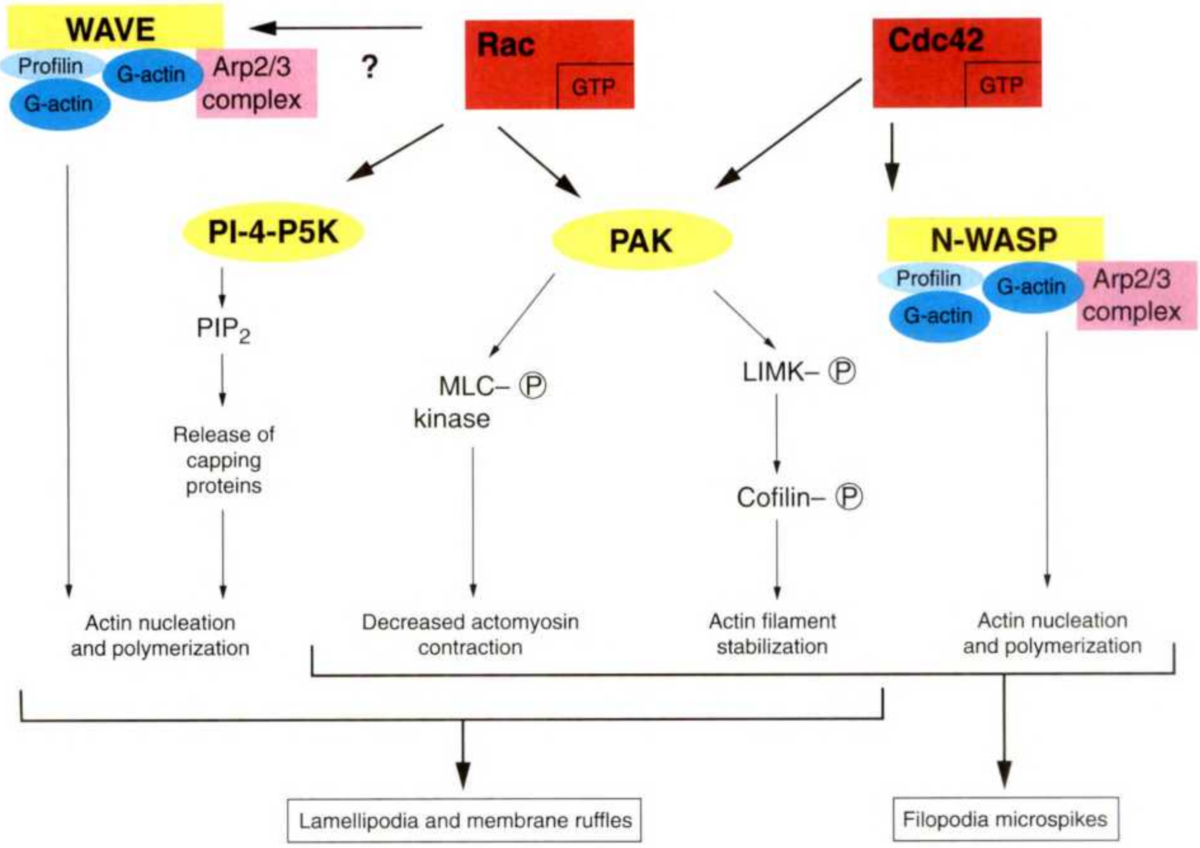
WAVE
Profilin
G-actin
G-actin
Arp2/3 complex
?
Rac
GTP
Cdc42
GTP
PI-4-P5K
PAK
N-WASP
Profilin
G-actin
G-actin
Arp2/3 complex
PIP₂
Release of capping proteins
MLC– Ⓟ kinase
LIMK– Ⓟ
Cofilin– Ⓟ
Actin nucleation and polymerization
Decreased actomyosin contraction
Actin filament stabilization
Actin nucleation and polymerization
Lamellipodia and membrane ruffles
Filopodia microspikes

Figure 4 Signal-transduction pathways induced by Rac and Cdc42 (shown in red), which are thought to contribute to the formation of actin-containing lamellipodia and filopodia respectively (see the text for details)

has not proved possible to induce actin polymerization in cell-free extracts with Rac, as has been done with Cdc42 [164].

Rac and Cdc42 effectors implicated in actin reorganization

Some common target proteins appear to be utilized by both Rac and Cdc42 in the induction of lamellipodia and filopodia respectively. PAK1,2,3 are Ser/Thr kinases, related to yeast Ste20, which have received a great deal of detailed attention [72,173,174]. *In vitro*, PAK1 and 3 bind equally well to Cdc42 and Rac, though Cdc42 simulates PAK1 activity more strongly than does Rac [173]. PAK2 only inhibits the intrinsic GTPase activity of Rac, and not Cdc42, suggesting that it may be a Rac target [175]. However, it is difficult to decide whether PAK1,2,3 are targets for Rac, Cdc42 or both *in vivo* from these *in vitro* interactions. There have been conflicting reports linking PAKs to actin changes. Activated mutants of PAK1 have been reported to induce both filopodia and membrane ruffles in Swiss3T3 cells and to cause neurite outgrowth in PC12 cells, similar to the effects of constitutively active Cdc42 and Rac [176,177]. PAK1 has been seen to localize to membrane ruffles, as well as phagocytic actin-containing cups, in *N*-formylmethionyl-leucyl-phenylalanine-stimulated neutrophils [178]. Interestingly, PAK-induced cytoskeletal changes are partly independent of its kinase activity, but require membrane targetting [176,177,179]. Other groups, however, have failed to find any effects of PAK over-expression on the actin cytoskeleton ([58,59], but see [59a]), and, taken together, these results suggest that PAKs are capable of affecting the actin cytoskeleton but that they only do so in co-operation with other signals that may or may not be present in the cell lines tested.

A variety of substrates for PAKs have been identified that could affect the actin cytoskeleton. Rac, like Rho, induces phosphorylation of LIMK [180], and PAK1 has been shown to phosphorylate LIMK *in vitro* [181]. Also, an inactive form of LIMK has been shown to inhibit both Cdc42 and Rac induced actin changes [182], suggesting that cofilin phosphorylation may be a general requirement in Rho GTPase pathways (Figures 3 and 4). PAK has been reported to phosphorylate and inactivate MLC kinase, decreasing MLC phosphorylation and reducing actomyosin assembly (Figure 4) [183]. There has also been a report of Rac-induced phosphorylation of myosin II heavy chain, which potentially would also lead to loss of actomyosin filaments [127]. Dominant-negative PAK inhibits this phosphorylation, but active PAK does not reconstitute the effect, suggesting that multiple effectors may mediate this activity [184].

IQGAP1 and 2 (named GAPs because of some homology with Ras GAP) are effectors for Rac and Cdc42 and may be involved in actin polymerization [63,185,186]. IQGAP has been detected in a complex with F-actin and Cdc42, which is enhanced by EGF and disrupted by dominant-negative Cdc42 [99]. IQGAP is able to oligomerize and to cross-link F-actin *in vitro*, an activity which is enhanced by GTP[S]–Cdc42 [115]. It has, therefore, been suggested that IQGAP oligomers may form upon binding to GTPase after dissociation of calmodulin, and that somehow this facilitates cross-linking of F-actin. In yeast an IQGAP homologue, Iqg1/Cyk1p, is involved in actin recruitment to the bud neck [187], and in *Dictyostelium* DdGAP1, also IQGAP-like, regulates cytokinesis [188]. Whether IQGAP is involved in cytokinesis in mammalian cells is unknown [189].

Effectors involved in actin-independent activities of Rho GTPases

Overexpression of activated Rac and Cdc42 leads to activation of the JNK and p38 MAP kinase pathways in a variety of cell types [49,50,190]. JNK activation by certain growth factors and cytokines [e.g. EGF, tumour necrosis factor α (TNFα) and transforming growth factor β] has been reported to be inhibited by dominant-negative Rac and Cdc42 [49,191], but it is still not clear how general the role of Rac/Cdc42 is in JNK activation. In Swiss3T3 cells, for example, TNFα induction of JNK is not dependent on Cdc42 [192]. Which Cdc42/Rac effectors mediate JNK activation in mammalian cells is still unclear. In *Drosophila* there is good genetic evidence for a link from DRac1 and DCdc42, via mis-shapen (PAK-like), to hemipterous (a JNK kinase), a pathway that is essential for dorsal closure [193,194]. Also, in yeast, a PAK-like kinase, Ste20, acts downstream of Cdc42 and is required for activation of the Kss1p/Fus3p MAP kinase cascade in the mating-pheromone response [195,196]. While mammalian PAK1 has been observed to enhance p38 activation when co-expressed with Rac and Cdc42, and constitutively active PAK1 and PAK3 has been reported to activate JNK in COS cells [197,198], many other groups have failed to find PAK activation of JNK or p38 ([57,59,61,199], but see [59a]).

Additional Rac/Cdc42 targets which may mediate JNK activation are: (1) Mlks 1, 2 and 3, which contain CRIB motifs and act as MAP kinase kinase kinases (MEKKs) [60,69,200,201]; (2) MEKK1 and MEKK4, which also interact with Rac and Cdc42 (MEKK4 has a CRIB domain). All are strong activators of JNK when overexpressed, and inhibitory-kinase-dead MEKK1 or MEKK4 mutants block Rac/Cdc42-induced JNK [202]. However, to date no physiological link has been made between Rac/Cdc42 and Mlk1, Mlk2 and Mlk3 or MEKK1 and MEKK4.

All three Rho GTPases have been implicated in the assembly and/or maintenance of cell–cell contacts [53]. In general the mechanisms mediating these effects are unknown; however, a recent report suggests that IQGAP1 may be involved [54]. IQGAP1 appears to interact with β-catenin, preventing its association with α-catenin; free IQGAP (i.e. not bound to Cdc42 or Rac) could, therefore destabilize cell–cell contacts [203,204].

Finally, Rac is known to be a regulator of the NADPH oxidase complex, a specialized enzyme of phagocytic cells that generates oxygen radicals to kill internalized micro-organisms [51,205,206]. A cytoplasm-derived component of the oxidase complex, p67^{phox}, binds directly to Rac [207]. Data suggest that the role of Rac is not to promote relocalization of this cytoplasmic protein to the membrane-bound catalytic components, as was first thought, but rather to act as an allosteric regulator by inducing a conformational change in the preformed complex to promote catalytic activity [63].

Conclusions

In conclusion, the wide range of Rho GTPase activities identified to date (see above and Table 1) is reflected in the large number of cellular targets with which they interact. Over 30 have now been identified (see Table 2), and it is likely that the list is not complete. The three-dimensional analysis of GTPase-effector complexes has increased our understanding of how a Rho GTPase can interact with many different effector proteins in a specific manner. However, to date only three effectors, PKN, WASP and ACK, have been analysed in this way, and these studies have all used isolated GTPase-binding domains and not full-length effector proteins. An emerging theme is that effectors can be activated by Rho GTPases through the relief of auto-inhibitory sequences. Clearly an analysis of the full-length effector proteins, carried out in solution, will be required to fully characterize the consequences of GTPases binding to their targets. Another potentially common feature, already demonstrated for PAK, is that additional cellular activities, such as kinases or other protein–protein interactions, can influence effector activity (see Figure 2). Progress has been made in identifying the cellular contributions of a handful of effectors. The clearest links downstream of Rho GTPases are in the area of cytoskeletal reorganization, where some targets appear to be essential (see Figures 3 and 4), while others have been shown to have the potential to be involved (see above). Another interesting possibility is that a Rho GTPase might interact with different subsets of effectors depending upon the cellular context and possibly upon the mechanism of activation; the large family of Rho GEFs could possibly contribute to such variations. A future challenge, so far not really addressed, will be to understand the spatial and temporal control of GTPase activity and the co-operation of Rho GTPases with other signalling networks. Finally, added to this complexity it should be remembered that Rho, Rac and Cdc42 are only three members of the Rho GTPase family: the functions of the seven other members awaits serious investigation.

REFERENCES

1 Ridley, A J (2000) Rho In GTPases (Hall, A, ed), pp 89–136, Oxford University Press, Oxford

2 Boguski, M S and McCormick, F (1993) Proteins regulating Ras and its relatives. Nature (London) **366**, 643–654

3 Van Aelst, L and D'Souza-Schorey, C (1997) Rho GTPases and signaling networks Genes Dev **11**, 2295–2322

4 Kjoller, L and Hall, A (1999) Signaling to Rho GTPases Exp Cell Res. **253**, 166–179

5 Cherfils, J and Chardin, P (1999) GEFs structural basis for their activation of small GTP-binding proteins. Trends Biochem Sci **24**, 306–311

6 Hart, M. J., Eva, A., Zangrilli, D, Aaronson, S A, Evans, T, Cerione, R A and Zheng, Y (1994) Cellular transformation and guanine nucleotide exchange activity are catalyzed by a common domain on the dbl oncogene product J Biol Chem **269**, 62–65

7 Rameh, L E., Arvidsson, A, Carraway, K L R, Couvillon, A D, Rathbun, G, Crompton, A, VanRenterghem, B., Czech, M. P., Ravichandran, K S, Burakoff, S J et al (1997) A comparative analysis of the phosphoinositide binding specificity of pleckstrin homology domains J Biol Chem **272**, 22059–22066

8 Zheng, Y, Zangrilli, D, Cerione, R. A and Eva, A (1996) The pleckstrin homology domain mediates transformation by oncogenic dbl through specific intracellular targeting J Biol. Chem **271**, 19017–19020

9 Soisson, S M, Nimnual, A. S., Uy, M, Bar-Sagi, D and Kuriyan, J (1998) Crystal structure of the Dbl and pleckstrin homology domains from the human Son of sevenless protein Cell **95**, 259–268

10 Debant, A, Serra-Pages, C, Seipel, K, O'Brien, S, Tang, M, Park, S H and Streuli, M (1996) The multidomain protein Trio binds the LAR transmembrane tyrosine phosphatase, contains a protein kinase domain, and has separate rac-specific and rho-specific guanine nucleotide exchange factor domains. Proc Natl. Acad Sci U S A **93**, 5466–5471

11 Liu, X, Wang, H, Eberstadt, M., Schnuchel, A, Olejniczak, E T, Meadows, R. P, Schkeryantz, J M, Janowick, D A, Harlan, J E, Harris, E A et al. (1998) NMR structure and mutagenesis of the N-terminal Dbl homology domain of the nucleotide exchange factor Trio Cell **95**, 269–277

12 Han, J, Luby-Phelps, K, Das, B, Shu, X, Xia, Y, Mosteller, R D, Krishna, U M, Falck, J R, White, M A and Broek, D (1998) Role of substrates and products of PI 3-kinase in regulating activation of Rac-related guanosine triphosphatases by Vav. Science **279**, 558–560

13 Cerione, R A and Zheng, Y. (1996) The Dbl family of oncogenes. Curr. Opin. Cell Biol **8**, 216–222

14 Lamarche, N and Hall, A (1994) GAPs for rho-related GTPases Trends Genet **10**, 436–440

15 Dunham, I., Shimizu, N, Roe, B A, Chissoe, S, Hunt, A R, Collins, J E, Bruskiewich, R, Beare, D M., Clamp, M., Smink, L J et al (1999) The DNA sequence of human chromosome 22 Nature (London) **402**, 489–495

16 Rittinger, K., Walker, P A, Eccleston, J F, Nurmahomed, K, Owen, D, Laue, E, Gamblin, S J and Smerdon, S J (1997) Crystal structure of a small G protein in complex with the GTPase- activating protein rhoGAP Nature (London) **388**, 693–697

17 Rittinger, K, Walker, P A, Eccleston, J F, Smerdon, S J and Gamblin, S. J. (1997) Structure at 1 65 Å of RhoA and its GTPase-activating protein in complex with a transition-state analogue Nature (London) **389**, 758–762

18 Nassar, N., Hoffman, G R, Manor, D, Clardy, J C. and Cerione, R A (1998) Structures of Cdc42 bound to the active and catalytically compromised forms of Cdc42GAP Nat Struct Biol **5**, 1047–1052

19 Adamson, P, Marshall, C J., Hall, A and Tilbrook, P A (1992) Post-translational modifications of p21rho proteins J Biol Chem **267**, 20033–20038

20 Cox, A D and Der, C J (1992) Protein prenylation more than just glue? Curr. Opin. Cell Biol **4**, 1008–1016

21 Olofsson, B (1999) Rho guanine dissociation inhibitors· pivotal molecules in cellular signalling Cell Signalling **11**, 545–554

22 Keep, N. H, Barnes, M, Barsukov, I, Badii, R, Lian, L Y, Segal, A W, Moody, P C. and Roberts, G C (1997) A modulator of rho family G proteins, rhoGDI, binds these G proteins via an immunoglobulin-like domain and a flexible N-terminal arm Structure **5**, 623–633

23 Gosser, Y Q, Nomanbhoy, T. K, Aghazadeh, B, Manor, D, Combs, C, Cerione, R A and Rosen, M K (1997) C-terminal binding domain of Rho GDP-dissociation inhibitor directs N-terminal inhibitory peptide to GTPases Nature (London) **387**, 814–819

24 Longenecker, K, Read, P, Derewenda, U, Dauter, Z, Liu, X, Garrard, S, Walker, L, Somlyo, A V, Nakamoto, R K., Somlyo, A P and Derewenda, Z S. (1999) How RhoGDI binds Rho Acta Crystallogr. D Biol Crystallogr **55**, 1503–1515

25 Hoffman, G R., Nassar, N. and Cerione, R A (2000) Structure of the Rho family GTP-binding protein Cdc42 in complex with the multifunctional regulator RhoGDI. Cell **100**, 345–356

26 Nomanbhoy, T. K, Erickson, J W and Cerione, R A (1999) Kinetics of Cdc42 membrane extraction by Rho-GDI monitored by real-time fluorescence resonance energy transfer. Biochemistry **38**, 1744–1750

27 Ihara, K, Muraguchi, S, Kato, M, Shimizu, T, Shirakawa, M, Kuroda, S, Kaibuchi, K. and Hakoshima, T (1998) Crystal structure of human RhoA in a dominantly active form complexed with a GTP analogue. J. Biol Chem **273**, 9656–9666

28 Dallery, E, Gallegue-Zouitina, S, Collyn-d'Hooghe, M, Quief, S., Denis, C, Hildebrand, M. P, Lantoine, D, Deweindt, C, Tilly, H., Bastard, C and et al (1995) TTF, a gene encoding a novel small G protein, fuses to the lymphoma- associated LAZ3 gene by t(3,4) chromosomal translocation Oncogene **10**, 2171–2178

29 Foster, R, Hu, K Q, Lu, Y., Nolan, K M, Thissen, J and Settleman, J (1996) Identification of a novel human Rho protein with unusual properties: GTPase deficiency and *in vivo* farnesylation Mol Cell Biol. **16**, 2689–2699

30 Nobes, C. D, Lauritzen, I, Mattei, M. G, Paris, S, Hall, A and Chardin, P. (1998) A new member of the Rho family, Rnd1, promotes disassembly of actin filament structures and loss of cell adhesion J Cell Biol **141**, 187–197

31 Feig, L A (1999) Tools of the trade use of dominant-inhibitory mutants of Ras-family GTPases Nat Cell Biol **1**, E25–E27

32 Aktories, K a. K, G (1997) *Clostridium botulinum* ADP-ribosyltransferase C3 In Bacterial Toxins Tools in Cell Biology and Pharmacology (Aktories, K, ed.), pp 61, Chapman and Hall, Weinheim

33 Aktories, K., Schmidt, G and Hofmann, F. (2000) GTPases targetted by bacterial toxins In GTPases (Hall, A, ed), pp 311–331, Oxford University Press, Oxford

34 Hall, A (1998) Rho GTPases and the actin cytoskeleton. Science **279**, 509–514

35 Ridley, A J and Hall, A (1992) The small GTP-binding protein rho regulates the assembly of focal adhesions and actin stress fibers in response to growth factors Cell **70**, 389–399

36 Ridley, A J, Paterson, H. F., Johnston, C L, Diekmann, D. and Hall, A (1992) The small GTP-binding protein rac regulates growth factor-induced membrane ruffling Cell **70**, 401–410

37 Kozma, R, Ahmed, S, Best, A and Lim, L (1995) The Ras-related protein Cdc42Hs and bradykinin promote formation of peripheral actin microspikes and filopodia in Swiss 3T3 fibroblasts Mol. Cell Biol **15**, 1942–1952

38 Mabuchi, I, Hamaguchi, Y, Fujimoto, H, Morii, N., Mishima, M and Narumiya, S (1993) A rho-like protein is involved in the organisation of the contractile ring in dividing sand dollar eggs Zygote **1**, 325–331

39 Drechsel, D N., Hyman, A A, Hall, A and Glotzer, M (1997) A requirement for Rho and Cdc42 during cytokinesis in *Xenopus* embryos Curr Biol **7**, 12–23

40 Prokopenko, S. N, Saint, R and Bellen, H. J (2000) Untying the gordian knot of cytokinesis role of small g proteins and their regulators J Cell Biol **148**, 843–848

41 Cox, D., Chang, P, Zhang, Q, Reddy, P. G, Bokoch, G M and Greenberg, S (1997) Requirements for both Rac1 and Cdc42 in membrane ruffling and phagocytosis in leukocytes J Exp Med **186**, 1487–1494

42 Caron, E and Hall, A (1998) Identification of two distinct mechanisms of phagocytosis controlled by different Rho GTPases. Science **282**, 1717–1721

43 Nobes, C. D and Hall, A (1999) Rho GTPases control polarity, protrusion, and adhesion during cell movement J Cell Biol. **144**, 1235–1244

44 Allen, W E, Zicha, D, Ridley, A J and Jones, G. E (1998) A role for Cdc42 in macrophage chemotaxis J Cell Biol **141**, 1147–1157

45 Settleman, J (1999) Rho GTPases in development Prog Mol Subcell Biol **22**, 201–229

46 Luo, L, Jan, L Y and Jan, Y. N. (1997) Rho family GTP-binding proteins in growth cone signalling Curr Opin Neurobiol **7**, 81–86

47 Hill, C. S, Wynne, J. and Treisman, R (1995) The Rho family GTPases RhoA, Rac1, and CDC42Hs regulate transcriptional activation by SRF Cell **81**, 1159–1170

48 Perona, R, Montaner, S, Saniger, L., Sanchez-Perez, I, Bravo, R and Lacal, J. C (1997) Activation of the nuclear factor-κB by Rho, CDC42, and Rac-1 proteins. Genes Dev. **11**, 463–475

49 Coso, O A, Chiariello, M, Yu, J C, Teramoto, H, Crespo, P, Xu, N, Miki, T and Gutkind, J S (1995) The small GTP-binding proteins Rac1 and Cdc42 regulate the activity of the JNK/SAPK signaling pathway Cell **81**, 1137–1146

50 Minden, A, Lin, A, Claret, F X, Abo, A and Karin, M. (1995) Selective activation of the JNK signaling cascade and c-Jun transcriptional activity by the small GTPases Rac and Cdc42Hs. Cell **81**, 1147–1157

51 Abo, A., Pick, E., Hall, A, Totty, N, Teahan, C. G and Segal, A W (1991) Activation of the NADPH oxidase involves the small GTP-binding protein p21rac1 Nature (London) **353**, 668–670

52 Olson, M F, Ashworth, A and Hall, A (1995) An essential role for Rho, Rac, and Cdc42 GTPases in cell cycle progression through G1. Science **269**, 1270–1272

53 Braga, V M M (1999) Small GTPases and regulation of cadherin dependent cell–cell adhesion Mol Pathol **52**, 197–202

54 Kaibuchi, K, Kuroda, S, Fukata, M and Nakagawa, M (1999) Regulation of cadherin-mediated cell–cell adhesion by the Rho family GTPases Curr Opin Cell Biol **11**, 591–596

55 Norman, J C, Price, L S, Ridley, A J and Koffer, A (1996) The small GTP-binding proteins, Rac and Rho, regulate cytoskeletal organization and exocytosis in mast cells by parallel pathways Mol Biol. Cell **7**, 1429–1442

56 Johnson, D I (1999) Cdc42· An essential Rho-type GTPase controlling eukaryotic cell polarity Microbiol Mol Biol. Rev. **63**, 54–105

57 Wei, Y., Zhang, Y, Derewenda, U., Liu, X, Minor, W, Nakamoto, R K, Somlyo, A. V, Somlyo, A P and Derewenda, Z S (1997) Crystal structure of RhoA-GDP and its functional implications. Nat. Struct Biol **4**, 699–703

58 Lamarche, N, Tapon, N, Stowers, L, Burbelo, P D, Aspenstrom, P, Bridges, T, Chant, J. and Hall, A (1996) Rac and Cdc42 induce actin polymerization and G1 cell cycle progression independently of p65PAK and the JNK/SAPK MAP kinase cascade Cell **87**, 519–529

59 Joneson, T, McDonough, M., Bar-Sagi, D and Van Aelst, L (1996) RAC regulation of actin polymerization and proliferation by a pathway distinct from Jun kinase Science **274**, 1374–1376

59a Erratum (1997) Science **276**, 5310

60 Sahai, E, Alberts, A. S and Treisman, R (1998) RhoA effector mutants reveal distinct effector pathways for cytoskeletal reorganization, SRF activation and transformation. EMBO J **17**, 1350–1361

61 Tapon, N, Nagata, K, Lamarche, N. and Hall, A (1998) A new rac target POSH is an SH3-containing scaffold protein involved in the JNK and NF-κB signalling pathways. EMBO J **17**, 1395–1404

62 Diekmann, D, Nobes, C D, Burbelo, P. D, Abo, A and Hall, A (1995) Rac GTPase interacts with GAPs and target proteins through multiple effector sites EMBO J **14**, 5297–5305

63 Nisimoto, Y, Freeman, J L R, Motalebi, S A, Hirshberg, M and Lambeth, J D (1997) Rac binding to p67(phox) Structural basis for interactions of the Rac1 effector region and insert region with components of the respiratory burst oxidase J Biol Chem **272**, 18834–18841

64 McCallum, S J., Wu, W J and Cerione, R A (1996) Identification of a putative effector for Cdc42Hs with high sequence similarity to the RasGAP-related protein IQGAP1 and a Cdc42Hs binding partner with similarity to IQGAP2 J Biol Chem **271**, 21732–21737

65 Zong, H, Raman, N., Mickelson-Young, L A., Atkinson, S J. and Quilliam, L A (1999) Loop 6 of RhoA confers specificity for effector binding, stress fiber formation, and cellular transformation J. Biol Chem **274**, 4551–4560

66 Li, R., Debreceni, B, Jia, B, Gao, Y, Tigyi, G and Zheng, Y (1999) Localization of the PAK1-, WASP-, and IQGAP1-specifying regions of Cdc42 J Biol. Chem **274**, 29648–29654

67 Mott, H. R, Owen, D, Nietlispach, D, Lowe, P N, Manser, E, Lim, L and Laue, E D (1999) Structure of the small G protein Cdc42 bound to the GTPase-binding domain of ACK. Nature (London) **399**, 384–388

68 Abdul-Manan, N , Aghazadeh, B , Liu, G A , Majumdar, A , Ouerfelli, O , Siminovitch, K A and Rosen, M K (1999) Structure of Cdc42 in complex with the GTPase-binding domain of the 'Wiskott-Aldrich syndrome' protein Nature (London) **399**, 379–383

69 Burbelo, P D , Drechsel, D and Hall, A (1995) A conserved binding motif defines numerous candidate target proteins for both Cdc42 and Rac GTPases. J. Biol Chem **270**, 29071–29074

70 Rudolph, M G , Bayer, P , Abo, A , Kuhlmann, J , Vetter, I R and Wittinghofer, A (1998) The Cdc42/Rac interactive binding region motif of the Wiskott–Aldrich syndrome protein (WASP) is necessary but not sufficient for tight binding to Cdc42 and structure formation J Biol Chem **273**, 18067–18076

71 Leonard, D A , Satoskar, R S , Wu, W J., Bagrodia, S , Cerione, R A and Manor, D (1997) Use of a fluorescence spectroscopic readout to characterize the interactions of Cdc42Hs with its target/effector, mPAK-3 Biochemistry **36**, 1173–1180

72 Manser, E , Leung, T , Salihuddin, H , Zhao, Z S. and Lim, L (1994) A brain serine/threonine protein kinase activated by Cdc42 and Rac1 Nature (London) **367**, 40–46

73 Manser, E , Leung, T , Salihuddin, H , Tan, L and Lim, L (1993) A non-receptor tyrosine kinase that inhibits the GTPase activity of p21cdc42 Nature (London) **363**, 364–367

74 Symons, M , Derry, J M , Karlak, B , Jiang, S , Lemahieu, V , McCormick, F , Francke, U and Abo, A (1996) Wiskott–Aldrich syndrome protein, a novel effector for the GTPase CDC42Hs, is implicated in actin polymerization Cell **84**, 723–734

75 Flynn, P., Mellor, H , Palmer, R., Panayotou, G and Parker, P J (1998) Multiple interactions of PRK1 with RhoA Functional assignment of the Hr1 repeat motif J Biol Chem **273**, 2698–2705

76 Watanabe, G , Saito, Y., Madaule, P , Ishizaki, T , Fujisawa, K , Morii, N., Mukai, H , Ono, Y , Kakizuka, A. and Narumiya, S (1996) Protein kinase N (PKN) and PKN-related protein rhophilin as targets of small GTPase Rho Science **271**, 645–648

77 Reid, T , Furuyashiki, T , Ishizaki, T , Watanabe, G , Watanabe, N , Fujisawa, K , Morii, N , Madaule, P and Narumiya, S (1996) Rhotekin, a new putative target for Rho bearing homology to a serine/threonine kinase, PKN, and rhophilin in the rho-binding domain J Biol Chem. **271**, 13556–13560

78 Maesaki, R , Ihara, K , Shimizu, T , Kuroda, S , Kaibuchi, K and Hakoshima, T. (1999) The structural basis of Rho effector recognition revealed by the crystal structure of human RhoA complexed with the effector domain of PKN/PRK1 Mol Cell **4**, 793–803

79 Bagrodia, S and Cerione, R A (1999) Pak to the future Trends Cell Biol **9**, 350–355

80 Tu, H and Wigler, M (1999) Genetic evidence for Pak1 autoinhibition and its release by Cdc42 Mol Cell Biol. **19**, 602–611

81 Abo, A., Qu, J , Cammarano, M S , Dan, C , Fritsch, A , Baud, V , Belisle, B. and Minden, A (1998) PAK4, a novel effector for Cdc42Hs, is implicated in the reorganization of the actin cytoskeleton and in the formation of filopodia. EMBO J **17**, 6527–6540

82 Zhao, Z S , Manser, E , Chen, X Q , Chong, C , Leung, T. and Lim, L (1998) A conserved negative regulatory region in alphaPAK: inhibition of PAK kinases reveals their morphological roles downstream of Cdc42 and Rac1 Mol. Cell Biol **18**, 2153–2163

83 Frost, J A , Khokhlatchev, A , Stippec, S., White, M A and Cobb, M. H. (1998) Differential effects of PAK1-activating mutations reveal activity-dependent and -independent effects on cytoskeletal regulation. J Biol Chem **273**, 28191–28198

84 Tang, T K , Chang, W. C., Chan, W H , Yang, S D , Ni, M H and Yu, J S (1998) Proteolytic cleavage and activation of PAK2 during UV irradiation-induced apoptosis in A431 cells J Cell Biochem **70**, 442–454

85 Takahashi, M., Mukai, H , Toshimori, M , Miyamoto, M and Ono, Y. (1998) Proteolytic activation of PKN by caspase-3 or related protease during apoptosis Proc Natl. Acad Sci U S A **95**, 11566–11571

86 Amano, M , Chihara, K., Nakamura, N , Kaneko, T , Matsuura, Y and Kaibuchi, K (1999) The COOH terminus of Rho-kinase negatively regulates rho-kinase activity J Biol Chem **274**, 32418–32424

87 Kitagawa, M., Shibata, H , Toshimori, M , Mukai, H. and Ono, Y (1996) The role of the unique motifs in the amino-terminal region of PKN on its enzymatic activity Biochem Biophys Res Commun **220**, 963–968

88 Yoshinaga, C , Mukai, H , Toshimori, M., Miyamoto, M and Ono, Y (1999) Mutational analysis of the regulatory mechanism of PKN the regulatory region of PKN contains an arachidonic acid-sensitive autoinhibitory domain J Biochem. (Tokyo) **126**, 475–484

89 Palmer, R H , Dekker, L V , Woscholski, R , Le Good, J. A , Gigg, R and Parker, P. J (1995) Activation of PRK1 by phosphatidylinositol 4,5-bisphosphate and phosphatidylinositol 3,4,5-trisphosphate A comparison with protein kinase C isotypes J Biol Chem. **270**, 22412–22416

90 Amano, M , Mukai, H., Ono, Y , Chihara, K , Matsui, T , Hamajima, Y , Okawa, K , Iwamatsu, A and Kaibuchi, K (1996) Identification of a putative target for Rho as the serine-threonine kinase protein kinase N Science **271**, 648–650

91 Watanabe, N , Kato, T , Fujita, A , Ishizaki, T and Narumiya, S (1999) Cooperation between mDia1 and ROCK in Rho-induced actin reorganization Nat Cell Biol **1**, 136–143

92 Lynch, E D , Lee, M K , Morrow, J E , Welcsh, P L , Leon, P E and King, M C (1997) Nonsyndromic deafness DFNA1 associated with mutation of a human homolog of the *Drosophila* gene diaphanous Science **278**, 1315–1318

93 Kim, A S , Kakalis, L T , Abdul-Manan, N , Liu, G A and Rosen, M K (2000) Autoinhibition and activation mechanisms of the Wiskott–Aldrich syndrome protein. Nature (London) **404**, 151–158

94 Machesky, L M and Insall, R H (1998) Scar1 and the related Wiskott–Aldrich syndrome protein, WASP, regulate the actin cytoskeleton through the Arp2/3 complex Curr. Biol **8**, 1347–1356

95 Machesky, L M , Mullins, R D , Higgs, H N , Kaiser, D A , Blanchoin, L , May, R C., Hall, M E and Pollard, T. D (1999) Scar, a WASP-related protein, activates nucleation of actin filaments by the Arp2/3 complex Proc Natl Acad. Sci U S A **96**, 3739–3744

96 Rohatgi, R , Ma, L , Miki, H., Lopez, M , Kirchhausen, T , Takenawa, T and Kirschner, M W (1999) The interaction between N-WASP and the Arp2/3 complex links Cdc42-dependent signals to actin assembly Cell **97**, 221–231

97 Miki, H , Sasaki, T , Takai, Y and Takenawa, T. (1998) Induction of filopodium formation by a WASP-related actin-depolymerizing protein N-WASP Nature (London) **391**, 93–96

98 Joyal, J L , Annan, R. S., Ho, Y D , Huddleston, M E., Carr, S A , Hart, M J and Sacks, D B. (1997) Calmodulin modulates the interaction between IQGAP1 and Cdc42 Identification of IQGAP1 by nanoelectrospray tandem mass spectrometry J Biol Chem. **272**, 15419–15425

99 Erickson, J W , Cerione, R A and Hart, M J (1997) Identification of an actin cytoskeletal complex that includes IQGAP and the Cdc42 GTPase J Biol Chem **272**, 24443–24447

100 Miki, H , Miura, K. and Takenawa, T (1996) N-WASP, a novel actin-depolymerizing protein, regulates the cortical cytoskeletal rearrangement in a PIP2-dependent manner downstream of tyrosine kinases EMBO J. **15**, 5326–5335

101 Leung, T , Chen, X Q , Manser, E and Lim, L (1996) The p160 RhoA-binding kinase ROK alpha is a member of a kinase family and is involved in the reorganization of the cytoskeleton Mol Cell Biol. **16**, 5313–5327

102 Madaule, P , Furuyashiki, T , Reid, T , Ishizaki, T , Watanabe, G , Morii, N and Narumiya, S (1995) A novel partner for the GTP-bound forms of rho and rac. FEBS Lett **377**, 243–248

103 Madaule, P., Eda, M , Watanabe, N , Fujisawa, K , Matsuoka, T , Bito, H., Ishizaki, T. and Narumiya, S (1998) Role of citron kinase as a target of the small GTPase Rho in cytokinesis Nature (London) **394**, 491–494

104 Leung, T , Chen, X Q , Tan, I , Manser, E and Lim, L (1998) Myotonic dystrophy kinase-related Cdc42-binding kinase acts as a Cdc42 effector in promoting cytoskeletal reorganization Mol. Cell Biol **18**, 130–140

105 Quilliam, L A , Lambert, Q T , Mickelson-Young, L A , Westwick, J K , Sparks, A B , Kay, B K., Jenkins, N A , Gilbert, D J , Copeland, N G and Der, C J (1996) Isolation of a NCK-associated kinase, PRK2, an SH3-binding protein and potential effector of Rho protein signaling J Biol Chem **271**, 28772–28776

106 Rivero-Lezcano, O. M., Marcilla, A , Sameshima, J H. and Robbins, K C (1995) Wiskott–Aldrich syndrome protein physically associates with Nck through Src homology 3 domains Mol Cell Biol. **15**, 5725–5731

107 Galisteo, M L , Chernoff, J , Su, Y. C , Skolnik, E Y and Schlessinger, J (1996) The adaptor protein Nck links receptor tyrosine kinases with the serine- threonine kinase Pak1 J Biol. Chem **271**, 20997–21000

108 Bokoch, G M , Wang, Y , Bohl, B P , Sells, M A , Quilliam, L A and Knaus, U. G. (1996) Interaction of the Nck adapter protein with p21-activated kinase (PAK1) J Biol Chem **271**, 25746–25749

109 Obermeier, A , Ahmed, S , Manser, E , Yen, S C , Hall, C. and Lim, L (1998) PAK promotes morphological changes by acting upstream of Rac EMBO J **17**, 4328–4339

110 Manser, E , Loo, T H , Koh, C G , Zhao, Z S , Chen, X Q , Tan, L , Tan, I , Leung, T and Lim, L (1998) PAK kinases are directly coupled to the PIX family of nucleotide exchange factors Mol Cell **1**, 183–192

111 Daniels, R H , Zenke, F T and Bokoch, G M (1999) alphaPix stimulates p21-activated kinase activity through exchange factor-dependent and -independent mechanisms. J Biol Chem **274**, 6047–6050

111a Erratum (1999) J Biol Chem **274**, 15292

112 Turner, C E , Brown, M. C., Perrotta, J. A , Riedy, M C , Nikolopoulos, S N , McDonald, A R , Bagrodia, S , Thomas, S and Leventhal, P S (1999) Paxillin LD4 motif binds PAK and PIX through a novel 95-kD ankyrin repeat, ARF-GAP protein A role in cytoskeletal remodeling. J. Cell Biol **145**, 851–863

113 Bagrodia, S , Bailey, D., Lenard, Z , Hart, M , Guan, J L , Premont, R T , Taylor, S J. and Cerione, R A (1999) A tyrosine-phosphorylated protein that binds to an important regulatory region on the cool family of p21-activated kinase-binding proteins J Biol Chem **274**, 22393–22400

114 Bagrodia, S, Taylor, S J, Jordon, K A, Van Aelst, L and Cerione, R A (1998) A novel regulator of p21-activated kinases J Biol Chem **273**, 23633–23636

115 Fukata, M, Kuroda, S, Fujii, K, Nakamura, T, Shoji, I, Matsuura, Y, Okawa, K, Iwamatsu, A, Kikuchi, A and Kaibuchi, K (1997) Regulation of cross-linking of actin filament by IQGAP1, a target for Cdc42 J Biol Chem **272**, 29579–29583

116 Kammerer, R. A. (1997) Alpha-helical coiled-coil oligomerization domains in extracellular proteins Matrix Biol **15**, 555–565 (and discussion 567–568)

117 Lupas, A (1996) Coiled coils new structures and new functions. Trends Biochem Sci **21**, 375–382

118 Guinamard, R, Aspenstrom, P, Fougereau, M, Chavrier, P and Guillemot, J C (1998) Tyrosine phosphorylation of the Wiskott–Aldrich syndrome protein by Lyn and Btk is regulated by CDC42 FEBS Lett **434**, 431–436

119 Baba, Y, Nonoyama, S, Matsushita, M, Yamadori, T, Hashimoto, S, Imai, K, Arai, S., Kunikata, T., Kurimoto, M, Kurosaki, T, Ochs, H D, Yata, J, Kishimoto, T and Tsukada, S (1999) Involvement of Wiskott–Aldrich syndrome protein in B-cell cytoplasmic tyrosine kinase pathway. Blood **93**, 2003–2012

120 Westphal, R S, Coffee, Jr, R L, Marotta, A, Pelech, S L and Wadzinski, B. E (1999) Identification of kinase-phosphatase signaling modules composed of p70 S6 kinase-protein phosphatase 2A (PP2A) and p21-activated kinase-PP2A J Biol Chem **274**, 687–692

121 Ishizaki, T, Maekawa, M, Fujisawa, K, Okawa, K, Iwamatsu, A, Fujita, A, Watanabe, N, Saito, Y, Kakizuka, A, Morii, N and Narumiya, S (1996) The small GTP-binding protein Rho binds to and activates a 160 kDa Ser/Thr protein kinase homologous to myotonic dystrophy kinase. EMBO J. **15**, 1885–1893

122 Matsui, T, Amano, M, Yamamoto, T, Chihara, K, Nakafuku, M., Ito, M, Nakano, T, Okawa, K, Iwamatsu, A and Kaibuchi, K (1996) Rho-associated kinase, a novel serine/threonine kinase, as a putative target for small GTP binding protein Rho. EMBO J **15**, 2208–2216

123 Ishizaki, T, Naito, M, Fujisawa, K, Maekawa, M, Watanabe, N, Saito, Y and Narumiya, S. (1997) p160ROCK, a Rho-associated coiled-coil forming protein kinase, works downstream of Rho and induces focal adhesions FEBS Lett **404**, 118–124

124 Uehata, M, Ishizaki, T, Satoh, H, Ono, T, Kawahara, T, Morishita, T, Tamakawa, H, Yamagami, K, Inui, J, Maekawa, M and Narumiya, S (1997) Calcium sensitization of smooth muscle mediated by a Rho-associated protein kinase in hypertension Nature (London) **389**, 990–994

125 Amano, M., Ito, M, Kimura, K, Fukata, Y, Chihara, K, Nakano, T, Matsuura, Y and Kaibuchi, K. (1996) Phosphorylation and activation of myosin by Rho-associated kinase (Rho-kinase) J Biol Chem **271**, 20246–20249

126 Kawano, Y, Fukata, Y, Oshiro, N, Amano, M, Nakamura, T, Ito, M., Matsumura, F, Inagaki, M. and Kaibuchi, K (1999) Phosphorylation of myosin-binding subunit (MBS) of myosin phosphatase by Rho-kinase in vivo J Cell Biol **147**, 1023–1038

127 Bresnick, A R (1999) Molecular mechanisms of nonmuscle myosin-II regulation Curr Opin. Cell. Biol **11**, 26–33

128 Kimura, K, Ito, M., Amano, M, Chihara, K, Fukata, Y, Nakafuku, M, Yamamori, B., Feng, J, Nakano, T, Okawa, K, Iwamatsu, A and Kaibuchi, K (1996) Regulation of myosin phosphatase by Rho and Rho-associated kinase (Rho-kinase) Science **273**, 245–248

129 Maekawa, M, Ishizaki, T., Boku, S., Watanabe, N, Fujita, A, Iwamatsu, A, Obinata, T, Ohashi, K, Mizuno, K and Narumiya, S (1999) Signaling from Rho to the actin cytoskeleton through protein kinases ROCK and LIM-kinase Science **285**, 895–898

130 Bamburg, J R, McGough, A and Ono, S (1999) Putting a new twist on actin ADF/cofilins modulate actin dynamics. Trends Cell Biol **9**, 364–370

131 Hooley, R., Yu, C Y, Symons, M and Barber, D L (1996) G alpha 13 stimulates Na+-H+ exchange through distinct Cdc42-dependent and RhoA-dependent pathways J Biol Chem **271**, 6152–6158

132 Vexler, Z S, Symons, M. and Barber, D. L (1996) Activation of Na^+/H^+ exchange is necessary for RhoA-induced stress fiber formation J Biol Chem **271**, 22281–22284

133 Tominaga, T, Ishizaki, T, Narumiya, S and Barber, D L (1998) p160ROCK mediates RhoA activation of Na-H exchange EMBO J **17**, 4712–4722

134 Tominaga, T. and Barber, D L (1998) Na–H exchange acts downstream of RhoA to regulate integrin-induced cell adhesion and spreading Mol Biol Cell **9**, 2287–2303

135 Kimura, K, Fukata, Y, Matsuoka, Y, Bennett, V, Matsuura, Y, Okawa, K, Iwamatsu, A and Kaibuchi, K (1998) Regulation of the association of adducin with actin filaments by Rho-associated kinase (Rho-kinase) and myosin phosphatase J Biol Chem. **273**, 5542–5548

136 Fukata, Y, Oshiro, N, Kinoshita, N., Kawano, Y, Matsuoka, Y, Bennett, V, Matsuura, Y and Kaibuchi, K (1999) Phosphorylation of adducin by Rho-kinase plays a crucial role in cell motility J Cell Biol **145**, 347–361

137 Bretscher, A (1999) Regulation of cortical structure by the ezrin–radixin–moesin protein family. Curr Opin Cell Biol **11**, 109–116

138 Matsui, T, Maeda, M, Doi, Y, Yonemura, S, Amano, M, Kaibuchi, K, Tsukita, S and Tsukita, S (1998) Rho-kinase phosphorylates COOH-terminal threonines of ezrin/radixin/moesin (ERM) proteins and regulates their head-to-tail association. J. Cell Biol **140**, 647–657

139 Matsui, T, Yonemura, S, Tsukita, S and Tsukita, S (1999) Activation of ERM proteins in vivo by Rho involves phosphatidylinositol-4-phosphate 5-kinase and not ROCK kinases Curr. Biol **9**, 1259–1262

140 Nakano, K, Takaishi, K, Kodama, A, Mammoto, A, Shiozaki, H, Monden, M. and Takai, Y (1999) Distinct actions and cooperative roles of ROCK and mDia in Rho small G protein-induced reorganization of the actin cytoskeleton in Madin–Darby canine kidney cells. Mol Biol. Cell **10**, 2481–2491

141 Watanabe, N, Madaule, P, Reid, T, Ishizaki, T, Watanabe, G, Kakizuka, A, Saito, Y, Nakao, K, Jockusch, B M and Narumiya, S (1997) p140mDia, a mammalian homolog of *Drosophila* diaphanous, is a target protein for Rho small GTPase and is a ligand for profilin EMBO J. **16**, 3044–3056

142 Wasserman, S. (1998) FH proteins as cytoskeletal organizers Trends Cell Biol **8**, 111–115

143 Janmey, P A and Stossel, T. P. (1987) Modulation of gelsolin function by phosphatidylinositol 4,5-bisphosphate Nature (London) **325**, 362–364

144 Gilmore, A P and Burridge, K (1996) Regulation of vinculin binding to talin and actin by phosphatidylinositol 4,5-bisphosphate Nature (London) **381**, 531–535

145 Shibasaki, Y., Ishihara, H., Kizuki, N, Asano, T, Oka, Y and Yazaki, Y. (1997) Massive actin polymerization induced by phosphatidylinositol-4-phosphate 5-kinase *in vivo* J Biol. Chem **272**, 7578–7581

146 Desrivieres, S, Cooke, F T, Parker, P J and Hall, M. N. (1998) MSS4, a phosphatidylinositol-4-phosphate 5-kinase required for organization of the actin cytoskeleton in *Saccharomyces cerevisiae* J Biol Chem. **273**, 15787–15793

147 Ren, X. D, Bokoch, G M, Traynor-Kaplan, A, Jenkins, G H, Anderson, R A and Schwartz, M A. (1996) Physical association of the small GTPase Rho with a 68-kDa phosphatidylinositol-4-phosphate 5-kinase in Swiss 3T3 cells Mol Biol Cell **7**, 435–442

148 Takaishi, K, Sasaki, T, Kameyama, T, Tsukita, S, Tsukita, S and Takai, Y (1995) Translocation of activated Rho from the cytoplasm to membrane ruffling area, cell–cell adhesion sites and cleavage furrows Oncogene **11**, 39–48

149 Kosako, H, Amano, M, Yanagida, M, Tanabe, K, Nishi, Y, Kaibuchi, K and Inagaki, M (1997) Phosphorylation of glial fibrillary acidic protein at the same sites by cleavage furrow kinase and Rho-associated kinase. J Biol Chem **272**, 10333–10336

150 Yasui, Y, Amano, M, Nagata, K, Inagaki, N, Nakamura, H, Saya, H., Kaibuchi, K and Inagaki, M (1998) Roles of Rho-associated kinase in cytokinesis, mutations in Rho-associated kinase phosphorylation sites impair cytokinetic segregation of glial filaments J Cell Biol **143**, 1249–1258

151 Castrillon, D H and Wasserman, S A (1994) Diaphanous is required for cytokinesis in *Drosophila* and shares domains of similarity with the products of the limb deformity gene Development **120**, 3367–3377

152 Imamura, H, Tanaka, K, Hihara, T, Umikawa, M, Kamei, T, Takahashi, K, Sasaki, T and Takai, Y. (1997) Bni1p and Bnr1p downstream targets of the Rho family small G-proteins which interact with profilin and regulate actin cytoskeleton in *Saccharomyces cerevisiae* EMBO J **16**, 2745–2755

153 Derry, J. M, Ochs, H D and Francke, U (1994) Isolation of a novel gene mutated in Wiskott–Aldrich syndrome Cell **78**, 635–644

153a Erratum (1994) Cell **79**, following 922

154 Kirchhausen, T and Rosen, F S (1996) Disease mechanism. unravelling Wiskott–Aldrich syndrome Curr Biol **6**, 676–678

155 Aspenstrom, P, Lindberg, U and Hall, A (1996) Two GTPases, Cdc42 and Rac, bind directly to a protein implicated in the immunodeficiency disorder Wiskott–Aldrich syndrome Curr. Biol **6**, 70–75

156 Kolluri, R, Tolias, K F, Carpenter, C L, Rosen, F S and Kirchhausen, T (1996) Direct interaction of the Wiskott–Aldrich syndrome protein with the GTPase Cdc42 Proc Natl Acad Sci U S A **93**, 5615–5618

157 Miki, H and Takenawa, T (1998) Direct binding of the verprolin-homology domain in N-WASP to actin is essential for cytoskeletal reorganization Biochem Biophys Res. Commun **243**, 73–78

158 Suetsugu, S, Miki, H and Takenawa, T. (1998) The essential role of profilin in the assembly of actin for microspike formation EMBO J **17**, 6516–6526

159 Ramesh, N, Anton, I. M, Hartwig, J H and Geha, R S (1997) WIP, a protein associated with Wiskott–Aldrich syndrome protein, induces actin polymerization and redistribution in lymphoid cells. Proc Natl Acad Sci U S A **94**, 14671–14676

160 Winter, D, Lechler, T and Li, R (1999) Activation of the yeast Arp2/3 complex by Bee1p, a WASP-family protein. Curr Biol **9**, 501–504

161 Machesky, L M and Gould, K L (1999) The Arp2/3 complex a multifunctional actin organizer Curr Opin Cell Biol **11**, 117–121

162 Welch, M D (1999) The world according to Arp regulation of actin nucleation by the Arp2/3 complex Trends Cell Biol. **9**, 423–427

163 Ma, L, Cantley, L C, Janmey, P A and Kirschner, M W (1998) Corequirement of specific phosphoinositides and small GTP-binding protein Cdc42 in inducing actin assembly in *Xenopus* egg extracts J Cell Biol **140**, 1125–1136

164 Zigmond, S. H., Joyce, M, Borleis, J., Bokoch, G M and Devreotes, P N. (1997) Regulation of actin polymerization in cell-free systems by GTPγS and Cdc42 J Cell Biol **138**, 363–374

165 Luo, L, Lee, T., Tsai, L, Tang, G, Jan, L Y and Jan, Y N (1997) Genghis Khan (Gek) as a putative effector for *Drosophila* Cdc42 and regulator of actin polymerization Proc. Natl Acad Sci U S A **94**, 12963–12968

166 Van Aelst, L, Joneson, T and Bar-Sagi, D (1996) Identification of a novel Rac1-interacting protein involved in membrane ruffling EMBO J **15**, 3778–3786

167 D'Souza-Schorey, C, Boshans, R L, McDonough, M, Stahl, P. D. and Van Aelst, L (1997) A role for POR1, a Rac1-interacting protein, in ARF6-mediated cytoskeletal rearrangements EMBO J **16**, 5445–5454

168 Kobayashi, K, Kuroda, S., Fukata, M, Nakamura, T, Nagase, T., Nomura, N., Matsuura, Y, Yoshida-Kubomura, N, Iwamatsu, A and Kaibuchi, K. (1998) p140Sra-1 (specifically Rac1-associated protein) is a novel specific target for Rac1 small GTPase J Biol Chem **273**, 291–295

169 Tolias, K F, Couvillon, A. D., Cantley, L C and Carpenter, C L (1998) Characterization of a Rac1- and RhoGDI-associated lipid kinase signaling complex Mol Cell Biol **18**, 762–770

170 Hartwig, J H, Bokoch, G M, Carpenter, C L, Janmey, P A, Taylor, L A, Toker, A and Stossel, T P (1995) Thrombin receptor ligation and activated Rac uncap actin filament barbed ends through phosphoinositide synthesis in permeabilized human platelets. Cell **82**, 643–653

171 Tolias, K. F., Hartwig, J H, Ishihara, H, Shibasaki, Y, Cantley, L C and Carpenter, C L (2000) Type Ialpha phosphatidylinositol-4-phosphate 5-kinase mediates rac-dependent actin assembly. Curr Biol. **10**, 153–156

172 Miki, H, Suetsugu, S and Takenawa, T (1998) WAVE, a novel WASP-family protein involved in actin reorganization induced by Rac EMBO J. **17**, 6932–6941

173 Manser, E., Chong, C, Zhao, Z S, Leung, T, Michael, G, Hall, C. and Lim, L (1995) Molecular cloning of a new member of the p21–Cdc42/Rac-activated kinase (PAK) family J. Biol Chem **270**, 25070–25078

174 Bagrodia, S, Taylor, S J, Creasy, C L; Chernoff, J and Cerione, R. A. (1995) Identification of a mouse p21Cdc42/Rac activated kinase J Biol Chem **270**, 22731–22737

175 Zhang, B, Chernoff, J and Zheng, Y (1998) Interaction of Rac1 with GTPase-activating proteins and putative effectors A comparison with Cdc42 and RhoA. J Biol Chem **273**, 8776–8782

176 Sells, M A, Knaus, U. G., Bagrodia, S, Ambrose, D M, Bokoch, G M and Chernoff, J (1997) Human p21-activated kinase (Pak1) regulates actin organization in mammalian cells Curr Biol **7**, 202–210

177 Daniels, R H., Hall, P. S. and Bokoch, G. M (1998) Membrane targeting of p21-activated kinase 1 (PAK1) induces neurite outgrowth from PC12 cells EMBO J **17**, 754–764

178 Dharmawardhane, S, Sanders, L C, Martin, S S, Daniels, R. H and Bokoch, G M (1997) Localization of p21-activated kinase 1 (PAK1) to pinocytic vesicles and cortical actin structures in stimulated cells J Cell Biol **138**, 1265–1278

179 Lu, W, Katz, S, Gupta, R and Mayer, B J (1997) Activation of Pak by membrane localization mediated by an SH3 domain from the adaptor protein Nck Curr Biol **7**, 85–94

180 Arber, S, Barbayannis, F. A, Hanser, H., Schneider, C, Stanyon, C A, Bernard, O and Caroni, P. (1998) Regulation of actin dynamics through phosphorylation of cofilin by LIM-kinase Nature (London) **393**, 805–809

181 Edwards, D C, Sanders, L C, Bokoch, G M and Gill, G N (1999) Activation of LIM-kinase by Pak1 couples Rac/Cdc42 GTPase signalling to actin cytoskeletal dynamics Nat Cell Biol. **1**, 253–259

182 Yang, N, Higuchi, O, Ohashi, K, Nagata, K, Wada, A, Kangawa, K, Nishida, E and Mizuno, K (1998) Cofilin phosphorylation by LIM-kinase 1 and its role in Rac-mediated actin reorganization Nature (London) **393**, 809–812

183 Sanders, L C., Matsumura, F, Bokoch, G M and de Lanerolle, P (1999) Inhibition of myosin light chain kinase by p21-activated kinase Science **283**, 2083–2085

184 van Leeuwen, F N, van Delft, S, Kain, H E, van der Kammen, R A and Collard, J G (1999) Rac regulates phosphorylation of the myosin-II heavy chain, actinomyosin disassembly and cell spreading Nat. Cell Biol. **1**, 242–248

185 Hart, M J, Callow, M. G., Souza, B. and Polakis, P (1996) IQGAP1, a calmodulin-binding protein with a rasGAP-related domain, is a potential effector for cdc42Hs EMBO J **15**, 2997–3005

186 Brill, S, Li, S., Lyman, C W, Church, D. M, Wasmuth, J J, Weissbach, L, Bernards, A and Snijders, A. J (1996) The ras GTPase-activating-protein-related human protein IQGAP2 harbors a potential actin binding domain and interacts with calmodulin and rho family GTPases. Mol. Cell Biol **16**, 4869–4878

187 Osman, M. A and Cerione, R A (1998) Iqg1p, a yeast homologue of the mammalian IQGAPs, mediates cdc42p effects on the actin cytoskeleton J Cell Biol **142**, 443–455

188 Faix, J and Dittrich, W (1996) DGAP1, a homologue of rasGTPase activating proteins that controls growth, cytokinesis, and development in Dictyostelium discoideum FEBS Lett **394**, 251–257

189 Machesky, L M (1998) Cytokinesis IQGAPs find a function Curr Biol **8**, R202-R205

190 Bagrodia, S, Derijard, B., Davis, R J and Cerione, R A (1995) Cdc42 and PAK-mediated signaling leads to Jun kinase and p38 mitogen-activated protein kinase activation J Biol Chem. **270**, 27995–27998

191 Atfi, A, Djelloul, S, Chastre, E, Davis, R. and Gespach, C (1997) Evidence for a role of Rho-like GTPases and stress-activated protein kinase/c-Jun N-terminal kinase (SAPK/JNK) in transforming growth factor beta-mediated signaling J Biol Chem **272**, 1429–1432

192 Puls, A, Eliopoulos, A G, Nobes, C D, Bridges, T., Young, L S and Hall, A (1999) Activation of the small GTPase Cdc42 by the inflammatory cytokines TNF(alpha) and IL-1, and by the Epstein-Barr virus transforming protein LMP1 J Cell Sci **112**, 2983–2992

193 Su, Y C, Treisman, J E and Skolnik, E Y (1998) The Drosophila Ste20-related kinase misshapen is required for embryonic dorsal closure and acts through a JNK MAPK module on an evolutionarily conserved signaling pathway Genes Dev **12**, 2371–2380

194 Glise, B. and Noselli, S (1997) Coupling of Jun amino-terminal kinase and Decapentaplegic signaling pathways in Drosophila morphogenesis Genes Dev **11**, 1738–1747

195 Leberer, E, Dignard, D, Harcus, D, Thomas, D Y and Whiteway, M (1992) The protein kinase homologue Ste20p is required to link the yeast pheromone response G-protein $\beta\gamma$ subunits to downstream signalling components EMBO J **11**, 4815–4824

196 Peter, M, Neiman, A M, Park, H O, van Lohuizen, M and Herskowitz, I (1996) Functional analysis of the interaction between the small GTP binding protein Cdc42 and the Ste20 protein kinase in yeast EMBO J **15**, 7046–7059

197 Zhang, S, Han, J, Sells, M. A., Chernoff, J., Knaus, U G, Ulevitch, R J and Bokoch, G M (1995) Rho family GTPases regulate p38 mitogen-activated protein kinase through the downstream mediator Pak1 J Biol. Chem **270**, 23934–23936

198 Brown, J L, Stowers, L, Baer, M, Trejo, J, Coughlin, S and Chant, J (1996) Human Ste20 homologue hPAK1 links GTPases to the JNK MAP kinase pathway. Curr. Biol **6**, 598–605

199 Westwick, J K, Lambert, Q T., Clark, G. J, Symons, M., Van Aelst, L, Pestell, R G and Der, C J (1997) Rac regulation of transformation, gene expression, and actin organization by multiple, PAK-independent pathways Mol Cell Biol **17**, 1324–1335

200 Nagata, K, Puls, A, Futter, C, Aspenstrom, P, Schaefer, E, Nakata, T., Hirokawa, N and Hall, A (1998) The MAP kinase kinase kinase MLK2 co-localizes with activated JNK along microtubules and associates with kinesin superfamily motor KIF3 EMBO J **17**, 149–158

201 Teramoto, H, Coso, O A, Miyata, H, Igishi, T, Miki, T and Gutkind, J S (1996) Signaling from the small GTP-binding proteins Rac1 and Cdc42 to the c- Jun N-terminal kinase/stress-activated protein kinase pathway A role for mixed lineage kinase 3/protein-tyrosine kinase 1, a novel member of the mixed lineage kinase family J Biol Chem **271**, 27225–27228

202 Fanger, G R, Johnson, N L and Johnson, G L (1997) MEK kinases are regulated by EGF and selectively interact with Rac/Cdc42 EMBO J **16**, 4961–4972

203 Kuroda, S, Fukata, M, Kobayashi, K, Nakafuku, M, Nomura, N, Iwamatsu, A and Kaibuchi, K (1996) Identification of IQGAP as a putative target for the small GTPases, Cdc42 and Rac1 J Biol Chem **271**, 23363–23367

204 Kuroda, S, Fukata, M., Nakagawa, M and Kaibuchi, K (1999) Cdc42, Rac1, and their effector IQGAP1 as molecular switches for cadherin-mediated cell-cell adhesion Biochem Biophys Res Commun **262**, 1–6

205 Chanock, S J, el, B J, Smith, R M and Babior, B M (1994) The respiratory burst oxidase J Biol Chem **269**, 24519–24522

206 Knaus, U G, Heyworth, P G, Evans, T, Curnutte, J T and Bokoch, G M (1991) Regulation of phagocyte oxygen radical production by the GTP-binding protein Rac 2 Science **254**, 1512–1515

207 Diekmann, D, Abo, A, Johnston, C, Segal, A W and Hall, A (1994) Interaction of Rac with p67phox and regulation of phagocytic NADPH oxidase activity Science **265**, 531–533

208 Vincent, S and Settleman, J (1997) The PRK2 kinase is a potential effector target of both Rho and Rac GTPases and regulates actin cytoskeletal organization Mol. Cell Biol **17**, 2247–2256

209 Chou, M M. and Blenis, J (1996) The 70 kDa S6 kinase complexes with and is activated by the Rho family G proteins Cdc42 and Rac1 Cell **85**, 573–583

210 Yang, W and Cerione, R A (1997) Cloning and characterization of a novel Cdc42-associated tyrosine kinase, ACK-2, from bovine brain J. Biol Chem **272**, 24819–24824

211 Tolias, K F, Cantley, L C and Carpenter, C L (1995) Rho family GTPases bind to phosphoinositide kinases J Biol Chem **270**, 17656–17659

212 Bokoch, G. M., Vlahos, C J, Wang, Y., Knaus, U G and Traynor-Kaplan, A. E (1996) Rac GTPase interacts specifically with phosphatidylinositol 3-kinase Biochem J **315**, 775–779

213 Zheng, Y, Bagrodia, S and Cerione, R A (1994) Activation of phosphoinositide 3-kinase activity by Cdc42Hs binding to p85. J. Biol Chem **269**, 18727–18730

214 Houssa, B, de Widt, J., Kranenburg, O, Moolenaar, W. H, and van Blitterswijk, W. J (1999) Diacylglycerol kinase theta binds to and is negatively regulated by active RhoA J Biol Chem. **274**, 6820–6822

215 Malcolm, K. C, Elliott, C M and Exton, J. H (1996) Evidence for Rho-mediated agonist stimulation of phospholipase D in rat1 fibroblasts Effects of Clostridium botulinum C3 exoenzyme J Biol Chem **271**, 13135–13139

216 Hess, J A, Ross, A H, Qiu, R G, Symons, M and Exton, J H (1997) Role of Rho family proteins in phospholipase D activation by growth factors J Biol Chem **272**, 1615–1620

217 Han, J S., Kim, H C, Chung, J K, Kang, H S, Donaldson, J and Koh, J K (1998) The potential role for CDC42 protein from rat brain cytosol in phospholipase D activation Biochem Mol Biol Int **45**, 1089–1103

218 Bae, C D, Min, D S, Fleming, I. N. and Exton, J H (1998) Determination of interaction sites on the small G protein RhoA for phospholipase D. J Biol Chem **273**, 11596–11604

219 Illenberger, D, Schwald, F, Pimmer, D, Binder, W., Maier, G, Dietrich, A and Gierschik, P (1998) Stimulation of phospholipase C-beta2 by the Rho GTPases Cdc42Hs and Rac1 EMBO J. **17**, 6241–6249

220 Hotta, K, Tanaka, K, Mino, A., Kohno, H and Takai, Y (1996) Interaction of the Rho family small G proteins with kinectin, an anchoring protein of kinesin motor Biochem Biophys. Res. Commun **225**, 69–74

221 Burbelo, P D, Snow, D M, Bahou, W and Spiegel, S (1999) MSE55, a Cdc42 effector protein, induces long cellular extensions in fibroblasts Proc Natl Acad Sci U.S.A. **96**, 9083–9088

222 Joberty, G, Perlungher, R R and Macara, I G (1999) The Borgs, a New Family of Cdc42 and TC10 GTPase-Interacting Proteins. Mol. Cell Biol **19**, 6585–6597

223 Aspenstrom, P (1997) A Cdc42 target protein with homology to the non-kinase domain of FER has a potential role in regulating the actin cytoskeleton Curr Biol **7**, 479–487

Inhibition of glutaminase expression by antisense mRNA decreases growth and tumourigenicity of tumour cells

Carolina LOBO, Miguel A. RUIZ-BELLIDO, Juan C. ALEDO, Javier MÁRQUEZ, Ignacio NÚÑEZ DE CASTRO and Francisco J. ALONSO[1]
Departamento de Biología Molecular y Bioquímica, Facultad de Ciencias, Campus de Teatinos, Universidad de Málaga, 29071 Málaga, Spain

Phosphate-activated glutaminase has a critical role in tumours and rapidly dividing cells and its activity is correlated with malignancy. Ehrlich ascites tumour cells transfected with the pcDNA3 vector containing an antisense segment (0.28 kb) of rat kidney glutaminase showed impairment in the growth rate and plating efficiency, as well as a shortage in the glutaminase protein and activity. The C-terminal segment used is well conserved in all glutaminase sequences known. The transfected cells, named 0.28AS-2, displayed remarkable changes in their morphology compared with the parental cell line. The 0.28AS-2 cells also lost their tumourigenic capacity *in vivo*. Control mice developed an ascitic tumour, with a lifespan of 16 ± 1 days, when inoculated with 10^7 cells/mouse; on the contrary, animals inoculated with transfected cells up to 2.5 times the cell numbers of control mice did not develop tumours and behaved as healthy animals. The ability to revert the transformed phenotype of antisense-transfected cells confirms the relevance of glutaminase in the transformation process and could provide new ways for the study of gene therapy.

Key words: cancer, cell proliferation, gene expression blockage, glutamine therapy.

INTRODUCTION

Tumour cells need a constant supply of both energy and nitrogen substrates. Glutamine, the most abundant amino acid in the plasma, is described as the main physiological nitrogen vehicle between different mammalian tissues [1]. The presence of a tumour produces great changes in the host glutamine metabolism a few days after tumour transplantation, resulting in an increase in the circulating glutamine [2]. Before being metabolized, glutamine must be transported across both the plasma membrane [3] and the inner mitochondrial membrane [4], since phosphate-activated glutaminase, the first step in the glutaminolytic process, is loosely anchored to the inner leaflet (on the matrix side) of the mitochondria [5]. Malignant cells transport glutamine at a faster rate than non-malignant cells across their plasmatic membranes by means of Na^+-dependent A and ASC amino acid-transport systems [3], and across the inner mitochondrial membrane by a carrier-mediated system [4].

Many experimental data provide evidence that phosphate-activated glutaminase (EC 3.5.1.2) is correlated with malignancy in tumours [6,7]. The enzyme is differentially expressed; its activity reaches a maximum during exponential growth phase, and the relative abundance of glutaminase mRNA significantly increases as compared with the stationary growth phase [8,9]. Thus glutaminase activity parallels the levels of poly(A)$^+$ RNAs encoding for mitochondrial glutaminase. The enzyme has been isolated to homogeneity from Ehrlich ascites carcinoma; the tumour enzyme shows kinetic behaviour that resembles kidney-type glutaminase [10,11].

The presence of high levels of glutaminase seems to be a common feature of rapidly dividing cells. Nevertheless, neither energy nor biosynthetic requirements can totally explain the very high glutaminolytic flux found in tumours and rapidly dividing cells (see [12,13] for reviews). Crabtree and Newsholme [14] suggest that active glutaminolysis is needed for preparing cells to supply energy or metabolic precursors when required, and consequently cells behave as dissipative systems. In spite of the relevance of glutaminase in cancer growth, studies on this enzyme are scarce.

The present study was undertaken to gain direct evidence on the role of glutaminase in tumour growth and proliferation. Ehrlich ascites carcinoma cells cultured *in vitro* have been transfected by lipofection with the plasmid pcDNA3 containing an antisense 3′-cDNA segment of rat glutaminase that is well conserved in all known glutaminase sequences. If our working hypothesis is correct, that is, that glutaminase is essential for cell-transformed phenotype sustenance, the inhibition of glutaminase by producing a glutaminase antisense RNA must result in a decrease in the proliferation rate and other characteristics of the transformed phenotype. The presented results confirm this hypothesis and the relevance of glutaminase in maintaining the malignant phenotype of tumour cells. Furthermore, transfected cells lost their tumourigenic capacity *in vivo* when inoculated in isologous mice.

MATERIALS AND METHODS

Construction of plasmids expressing antisense-RNA glutaminase

Two partial-length rat kidney glutaminase cDNA segments, *Hin*dIII (1893)–*Eco*RI (1614) and *Eco*RI (3314)–*Eco*RI (1614), obtained from the pGA104 recombinant plasmid [15], were subcloned in their antisense orientations behind the cytomegalovirus promoter of the pcDNA3 vector from Invitrogen (San Diego, CA, U.S.A.) by standard recombinant techniques. The resulting constructions were designated pcDNA3-0.28 and pcDNA3-1.7, respectively. The structures of the recombinants were verified by restriction-enzyme digestion of isolated DNA. The 3′-end sequences of 1.7 and 0.28 kb were selected because of the high sequence similarity found amongst cDNAs coding for C-terminal ends of known glutaminases [9,15–17]. The antibodies

---

Abbreviations used: EATC, Ehrlich ascites tumour cell; MTT, 3-(4,5-dimethylthiazol-2-yl)-2,5-diphenyl tetrazolium bromide.

[1] To whom correspondence should be addressed (e-mail fcarrion@uma.es).

against renal glutaminase and the pGA104 plasmid were kindly supplied by Professor N. P. Curthoys (Colorado State University, Fort Collins, CO, U.S.A.).

Cell culture and transfection procedure

The Ehrlich ascites tumour cell (EATC) line from the American Type Culture Collection, CCL-77, and its derivatives after transfection were grown in adherent cultures in RPMI-1640 medium (Sigma, St. Louis, MO, U.S.A.) supplemented with 10 % fetal calf serum and antibiotics. The cultures were incubated in a humidified atmosphere at 37 °C with 5 % CO_2/95 % air. The culture medium for cell lines containing the neomycin-resistance gene was supplemented with 600 μg/ml G418. The plasmids or the vector control pcDNA3 were transfected in EATCs by lipofection using the lipid Dosper (Boehringer Mannheim, Mannheim, Germany). Cells were selected after growing in complete RPMI-1640 medium containing 600 μg/ml G418 for 2–3 weeks Following G418 selection, 12 drug-resistant (neo$^+$) clones (six from each construction transfected) were picked randomly from different plates and studied after expansion. As a control, six neo$^+$ clones were picked from EATCs transfected with the pcDNA3 vector lacking the antisense sequences (vector-control cells).

Growth rates

Cells (10^4 cells/3 ml of medium) were seeded in each well of a six-well plate and allowed to grow for different times. The trypsin-treated cells were counted on a haemocytometer or using a Coulter counter (Coulter, Luton, Beds., U.K.). Cell lines expressing the antisense glutaminase RNA segments, cells transfected with the empty vector, and the parental EATC line were studied. Growth assays were determined by cell enumeration in triplicate for each cell line on every day of culture up to the seventh day. Doubling times and saturation densities were calculated by standard methods. All experiments were repeated at least three times and gave similar results. Cell growth rates were also determined by the MTT [3-(4,5-dimethylthiazol-2-yl)-2,5-diphenyl tetrazolium bromide] method described by Mossman with slight modification [18].

Colony-forming assays

Cells were seeded in triplicate with 250 cells/10-cm dish in complete medium. After 15 days of growth, the cells were fixed and stained with 5 % Giemsa stain, and the grossly visible colonies were counted All experiments were repeated at least three times and gave similar results

Blotting assays

Glutaminase protein in total cell extracts of transfected and non-transfected EATCs were subjected to Western-blot analyses. Exponentially growing cells (60–80 % confluence) were pelleted by centrifugation, washed twice with ice-cold PBS, and lysed on ice in RIPA buffer, pH 7.6 [30 mM Hepes, 150 mM NaCl, 1.0 % (v/v) Triton X-100, 0.1 % (w/v) SDS and 1.0 % (w/v) deoxycholic acid], with added proteinase inhibitors, pepstatin A (1.0 μg/ml), leupeptin (10 μg/ml) and 0.2 mM PMSF. Lysates were clarified by centrifugation at 10^4 g for 10 min at 4 °C. Cell protein (25 μg/lane) was electrophoresed on 10 % SDS/polyacrylamide gels and transferred to nitrocellulose membranes. The membranes were first incubated with a rabbit anti-rat renal glutaminase polyclonal antibody and then with a goat anti-rabbit IgG–biotin and avidin–peroxidase antibody; the anti-rat glutaminase polyclonal antibodies recognize Ehrlich ascites cell glutaminase [10]. Glutaminase bands were detected using diaminobenzidine as a substrate (Sigma).

Northern-blot analyses were performed as described elsewhere [8] using the 0.28 kb rat kidney cDNA segment, mentioned above, as a probe.

Glutaminase assay

Phosphate-activated glutaminase activities were determined as follows: harvested cells were washed three times with 0.1 M Tris/HCl, pH 8.0, and suspended in the same buffer for 3 h in order to deplete endogenous substrates. The reaction medium was 0.1 M phosphate, 20 mM glutamine, 20 μg/ml oligomycin and 1.2 μg/ml antimycin A, to prevent mitochondrial glutamate oxidation. Under these conditions glutamine and phosphate are at saturating concentrations [19]. For each assay 0.2 ml of cell suspension was used, equivalent to 10^6 cells; after 6 min of incubation at 37 °C the reaction was stopped by the addition of 0.5 ml of 0.4 M HCl. The KOH-neutralized mixture was centrifuged at 16000 g for 5 min. Finally, the glutamate formed was determined by the method according to Lund [20]. To be sure that glutaminase was indeed the assayed enzyme, the results obtained using controls without phosphate were always subtracted. Blanks with samples omitted were also run in parallel.

Tumourigenicity assay

To assess tumourigenic capacity, the transfected cDNA glutaminase antisense 0.28AS-2 line was intraperitoneally inoculated in isologous Swiss albino female mice of approx. 25 g in weight. Tumour growth was followed by the daily weighing of each animal [1]. The mice were housed in a controlled-environment animal facility and allowed free access to food and water.

RESULTS

Growth characteristics and morphology of the glutaminase-antisense-RNA-expressing cells

Transfection with an antisense glutaminase cDNA allows the blockage of gene expression [21]. Ehrlich ascites carcinoma cells growing *in vitro* have been transfected by lipofection, with two different genetic constructions (pcDNA3-1.7 and pcDNA3-0.28), as described in the Materials and methods section. After transfection, 12 different cell clones were selected (six from each construction transfected), and their cell-proliferation rates were determined for each clone by cell enumeration in a Coulter counter. EATC line and cell clones transfected with the pcDNA3 vector without any insert were used as controls. All transfected clones with the antisense glutaminase cDNA segments (1.7 and 0.28 kb) showed a decrease in growth rate. This decrease was more pronounced in cell lines transfected with the shorter 0 28 kb segment of glutaminase antisense cDNA (0.28AS cells). Figure 1 shows the average growth curve of 0.28AS cells, which had a growth rate approx. 50 % less than that of the controls. Colorimetric analyses of tetrazolium-stained cells provide a reliable approximation of cell-proliferation capacity [22,23]; the data obtained using the MTT test confirmed the above-expressed results by cell enumeration.

For the following growth-related experiments one of the 0.28AS cell lines, named 0.28AS-2, was selected. The main growth parameters of the 0.28AS-2 line are displayed in Table 1. The decrease in both proliferation and plating efficiency is noteworthy. This clone displayed a remarkable change in mor-

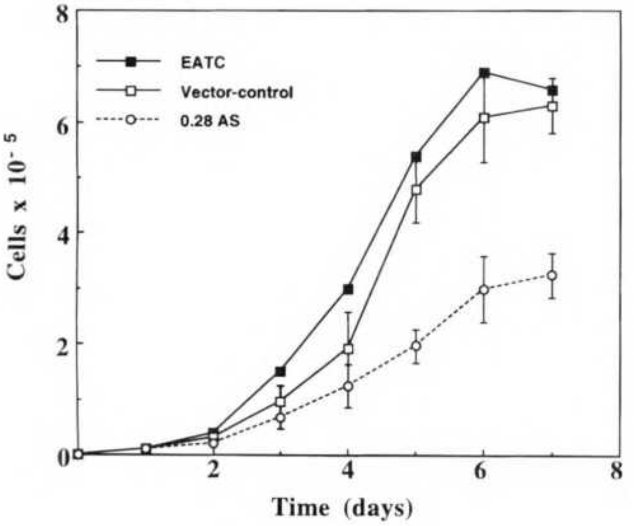

Figure 1 Growth curves of the 0.28AS clones expressing an antisense rat kidney RNA glutaminase segment compared with controls

EATC indicates the parental cell line; vector-control indicate cells transfected with the pcDNA3 vector without insert. Each point in the parental line is the mean of three different experiments; S.D. bar sizes are smaller than the symbols. Each point for vector-control and 0.28AS cells is the mean ± S.D. of six different lines; all experiments were carried out in triplicate.

Table 1 Growth characteristics of cDNA antisense glutaminase 0.28AS-2 transfected cells

EATC, parental cell line; vector-control, EATC line transfected with pcDNA3 vector without insert; 0.28AS-2, EATC line transfected with pcDNA3-0.28 construction. Saturation density represents the number of cells at saturation density per 35-mm diameter plate. Values shown are means ± S.D. Experimental differences between 0.28AS-2 cells and the two controls were analysed by the Mann–Witney U test; $^{*}P < 0.05$.

Characteristics	EATC	Vector-control	0.28AS-2
Doubling time (h)	28.5 ± 1.5	28.9 ± 2.0	35.4 ± 0.8*
Saturation density ($\times 10^6$)	2.7 ± 0.1	2.7 ± 0.1	2.3 ± 0.1*
Plating efficiency (%)	44 ± 1.0	38 ± 2.0	26 ± 2.0*

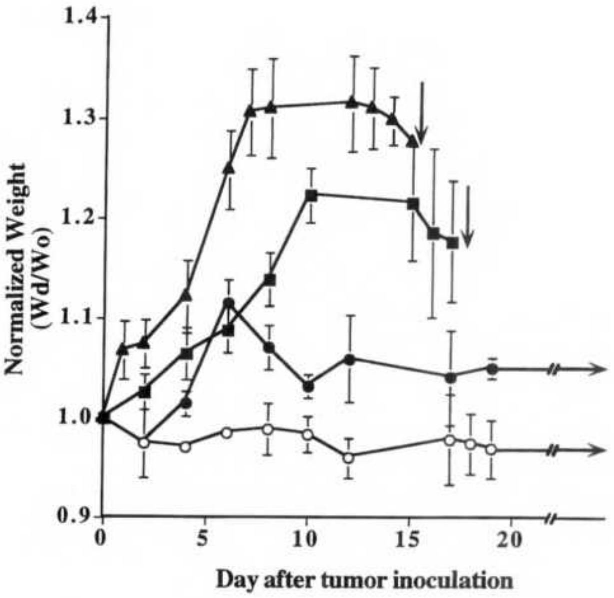

Figure 3 Tumour growth *in vivo*

Tumour growth was determined by normalized weights of inoculated animals. Normalized weights are displayed as W_d/W_0 (W_d, weight at day d; W_0, weight at day 0). ▲, Mice inoculated with 10^7 EATC parental cells. ■, Mice inoculated with 10^7 vector-control-transfected cells. ○, Mice inoculated with 10^7 0.28AS-2 antisense-glutaminase-transfected cells. ●, Mice inoculated with 2.5×10^7 0.28AS-2 antisense-glutaminase-transfected cells. Each point is the mean ± S.D. for six animals. Vertical arrows indicate the day on which all the animals in that particular cohort died; horizontal arrows indicate that animals survived. Similar results were obtained with animals inoculated with up to 4-fold antisense-glutaminase-transfected cells.

phology, compared with control cell lines (Figure 2): cells became polygonal and formed adherent clumps, in contrast with the random growth pattern of the controls. The 0.28AS-2 line also showed a significant decrease, about 40 %, in its cloning efficiency, and the duplication time was greater than the controls, the EATC parental line and the cells transfected with the pcDNA3 empty vector.

Figure 3 displays the results of experiments on tumourigenicity *in vivo* using the 0.28AS-2 cells, compared with the control lines.

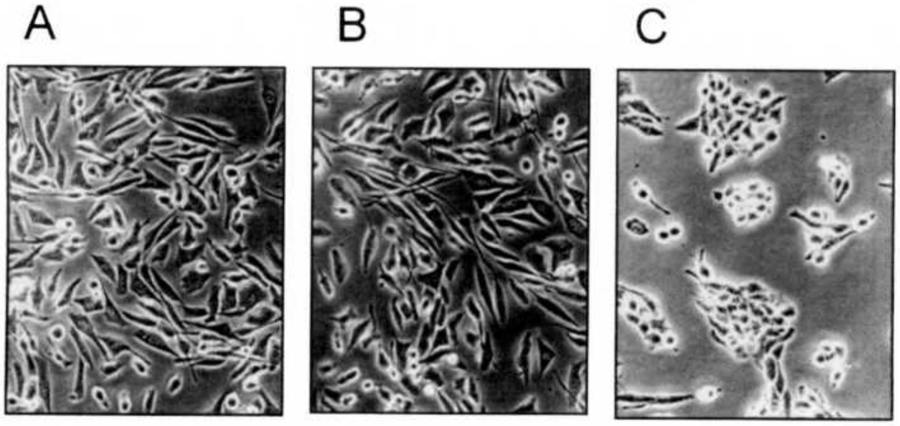

Figure 2 Optical microscopy

EATC parental cell line (**A**); vector-control (**B**) and 0.28AS-2 antisense glutaminase-transfected cell line (**C**). Identical magnifications were used for each line.

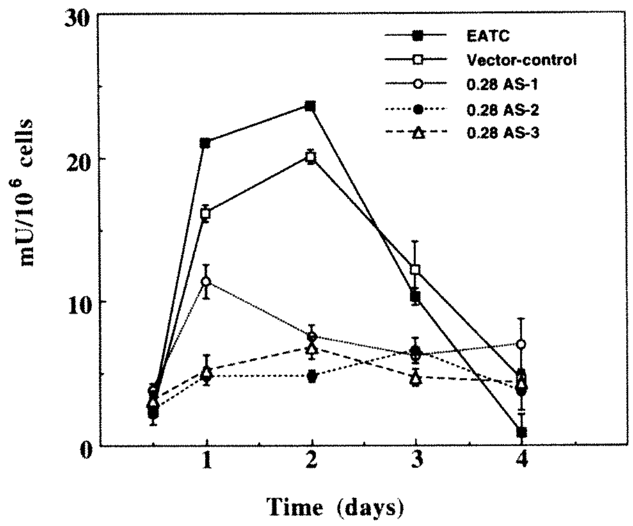

Figure 4 Glutaminase activity versus growth time of three different 0.28AS clones expressing antisense rat kidney glutaminase segment compared with controls

Each point is the mean ± S.D. for three different experiments. mU, m-units.

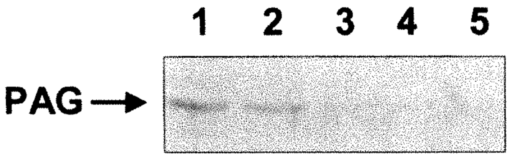

Figure 5 Western-blot analyses showing the decrease in glutaminase protein after expression of antisense 0.28 kb cDNA glutaminase segment

Lane 1, EATC parental cell line; lane 2, vector-control cell line; lane 3, 0.28AS-1 antisense-transfected cell line; lane 4, 0.28AS-2 antisense-transfected cell line; and lane 5, 0.28AS-3 antisense-transfected cell line. PAG, phosphate-activated glutaminase.

Mice inoculated with 10^7 control-line cells developed ascitic tumours and died after 16 ± 1 days; on the contrary, mice inoculated with the same number of antisense-expressing cells did not develop any tumours. Tumour growth *in vivo* was estimated by following the increase in total animal weight daily [1]. When animals were inoculated with a higher number of antisense-glutaminase-transfected cells, they only showed an increase in total weight in the first few days after inoculation due to the presence of ascitic fluid, but no cellular growth was observed. Several days later the ascitic fluid disappeared and the animals recovered their normal weight. None of the animals inoculated with antisense-glutaminase-transfected 0.28AS-2 cells showed any tumours, and they survived for several months.

Phosphate-activated glutaminase activity in antisense-transfected cells

Phosphate-activated glutaminase activities were determined in transfected and non-transfected cells during cell growth. The glutaminase activity profiles versus time obtained for cultured cells *in vitro* were similar to those obtained *in vivo* in intact ascites carcinoma cells growing in mice [8]. Glutaminase activity reached its maximum during the exponential phase of growth, with a subsequent decrease at the stationary phase of growth. Figure 4 shows the glutaminase activities versus time of three 0.28AS lines compared with the controls. The activities were similar in both controls used, but all transfected cells with the 0.28 kb antisense-cDNA glutaminase insert showed significant decreases in glutaminase activities. Western-blot analyses of these three 0.28AS lines, using polyclonal anti-rat renal glutaminase antibodies, showed a clear shortage of the glutaminase protein (Figure 5), consistent with the shortage in glutaminase activity. Non-significant changes were observed in glutaminase mRNA levels in Northern-blot experiments.

DISCUSSION

The scope of the present work was to confirm the critical role played by phosphate-activated glutaminase in the growth and proliferation of tumour cells [12,13]. The results presented here demonstrate that the stable expression of heterologous, but highly conserved [16,17], rat glutaminase cDNA antisense segments in mouse EATCs leads to a decrease in the proliferation capacity *in vitro*. After screening the behaviour of different stably transfected cell clones, the one named 0.28AS-2 was selected for the most characteristic growth experiments. As a consequence of transfection with cDNA antisense glutaminase, the cells are impaired markedly in their growth and proliferation capacity, since they show a longer doubling time and a decrease in their saturation density and plating efficiency, parameters that are correlated with malignancy. Cells also show marked changes in their morphology.

The transfected cells also display a decrease in the levels of glutaminase protein and activity; as mentioned above, many experimental data support a direct correlation between glutaminase activity and malignancy in tumours [6,7].

These results, taken together, provide evidence that the inhibition of the expression of glutaminase in tumour cells tends to revert their transformed phenotype towards normality. Furthermore, they confirm the relevance of glutamine and phosphate-activated glutaminase, the first step in the glutaminolytic process, which is essential for maintaining the energy and nitrogen metabolism of tumour cells [24]. Recently Spittler et al. [25] have reported similar results using an opposite strategy; in fact, they have communicated that low glutamine concentrations in the culture medium induce phenotypic and functional differentiation of U937 myelocytic cells.

But, what is perhaps most remarkable is that the 0.28AS-2 cells, which are able to grow *in vitro*, lose their tumourigenic capacity when they are intraperitoneally inoculated into isologous mice. The antisense derivative cells inoculated do not develop any tumours, as the controls do. Control mice (inoculated with parental and vector-control-transfected cells) die 16 ± 1 days after inoculation; the animals inoculated with cell numbers up to 2.5-fold greater than the controls survive after several months without any apparent disease. These results indicate that phosphate-activated glutaminase is not only essential for tumour growth and progression, but that this enzyme also seems to play a critical role in maintaining the tumourigenic capacity. Furthermore, the present studies provide evidence that the inhibition of glutaminase expression in tumour cells reverts the transformed phenotype *in vitro*, and inhibits their tumourigenicity *in vivo*.

Many attempts have been made in the use of glutamine-related chemotherapy in experimental oncology and in human patients [26,27]. The usefulness of glutamine analogues [azaserine, azotomycin, DON (6-diazo-5-oxo-L-norleucine) and acivicin] is very limited [28] in anti-tumour therapy because of their toxicity and the undesirable collateral effects. The use of glutamine clearance by exogenous glutaminase has been utilized in lymphoblastic leukaemia [29], but it is also limited. These findings open up the possibility of new approaches for the clinical use of glutamine-related therapy.

This work was supported by the grants PB-94-1471 from Dirección General de Investigación Cientifica y Tecníca and SAF 98-0153 from the Comisión Interministerial de Ciencia y Tecnología, and the Fundación Ramón Areces. C. L. is a scholarship holder supported by research group CVI 179 of the Junta de Andalucía.

REFERENCES

1 Carrascosa, J. M., Martínez, P. and Núñez de Castro, I. (1984) Cancer Res. **44**, 3831–3835

2 Quesada, A. R., Medina, M. A., Márquez, J., Sánchez-Jiménez, F. and Núñez de Castro, I. (1988) Cancer Res. **48**, 1551–1553

3 Medina, M. A., Quesada, A. R. and Núñez de Castro, I. (1991) J. Bioenerg. Biomembr. **23**, 689–697

4 Molina, M., Segura, J. A., Aledo, J. C., Medina, M. A., Núñez de Castro, I. and Márquez, J. (1995) Biochem. J. **308**, 629–633

5 Aledo, J. C., de Pedro, E., Gómez-Fabre, P. M., Núñez de Castro, I. and Márquez, J. (1997) Biochim. Biophys. Acta **1323**, 173–184

6 Weber, G., Lui, M. S., Sebodlt, J. and Faderan, M. A. (1984) in Glutamine Metabolism in Mammalian Tissues (Häussinger, D., ed.), pp. 278–291, Springer-Verlag, Berlin

7 Matsuno, T. and Hirai, H. (1989) Biochem. Int. **19**, 219–225

8 Aledo, J. C., Segura, J. A., Medina, M. A., Alonso, F. J., Núñez de Castro, I. and Márquez, J. (1994) FEBS Lett. **341**, 39–42

9 Gómez-Fabre, P., Aledo, J. C., Castillo-Olivares, A., Alonso, F. J., Núñez de Castro, I., Campos, J. A. and Márquez, J. (2000) Biochem. J. **345**, 365–375

10 Segura, J. A., Aledo, J. C., Gómez-Biedma, S., Núñez de Castro, I. and Márquez, J. (1995) Protein Express. Purif. **6**, 343–351

11 Aledo, J. C., Gómez-Biedma, S., Segura, J. A., Molina, M., Núñez de Castro, I. and Márquez, J. (1993) Electrophoresis **14**, 88–93

12 Medina, M. A., Sánchez-Jiménez, F., Márquez, J., Quesada, A. R. and Núñez de Castro, I. (1992) Mol. Cell. Biochem. **113**, 1–15

13 Souba, W. W. (1993) Ann. Surg. **218**, 715–728

14 Crabtree, B. and Newsholme, E. A. (1985) Curr. Top. Cell. Regul. **25**, 21–76

15 Shapiro, R. A., Farrell, L., Srinivasan, M. and Curthoys, N. P. (1991) J. Biol. Chem. **266**, 18792–18796

16 Watford, M. (1993) FASEB J. **7**, 1468–1474

17 Chung-Bok, M., Vincent, N., Jhala, U. and Watford, M. (1997) Biochem. J. **324**, 193–200

18 Mossman, T. (1983) J. Immunol. Methods **65**, 55–63

19 Quesada, A. R., Sánchez-Jiménez, F., Pérez-Rodríguez, J., Márquez, J. and Medina, M. A. (1988) Biochem. J. **255**, 1031–1036

20 Lund, P. (1985) in Methods of Enzymatic Analysis, vol. 8 (Bergmeyer, H. U., ed.), pp. 357–363, Verlag-Chemie, Weinheim

21 Murray, J. A. H. and Crockett, N. (1992) in Antisense RNA and DNA (Murray, H., ed.), pp. 1–49, Wiley–Liss, New York

22 Pagé, M. (1997) in Anticancer Drug Development Guide: Preclinical Screening, Clinical Trials and Approval (Teicher, B. A., ed.), pp. 3–21, Humana Press, Totowa

23 Greider, C. W. (1996) Annu. Rev. Biochem. **65**, 337–365

24 McKeehan, W. L. (1982) Cell Biol. Int. Rep. **6**, 635–650

25 Spittler, A., Oehler, R., Goetzinger, P., Holzer, S., Reissner, C. M., Leutmezer, F., Rath, V., Wrba, F., Fuegger, R., Boltz-Nitulescu, G. and Roth, E. (1997) J. Nutr. **127**, 2151–2157

26 Prajda, N. (1985) Adv. Enzyme Regul. **24**, 207–223

27 Chance, W. T., Cao, L., Kim, M. W., Nelson, J. L. and Fischer, J. E. (1988) Life Sci. **42**, 87–94

28 Earhart, R. H., Amato, D. J., Chang, A. Y., Borden, E. C., Shiraki, M., Dowd, M. E., Comis, R. L., Davis, T. E. and Smith, T. J. (1990) Invest. New Drugs **8**, 113–119

29 Gallagher, M. P., Marshall, R. D. and Wilson, R. (1989) Essays in Biochemistry, vol. 24 (Marshall, R. D. and Tipton, K. F., eds.), pp. 1–40, Academic Press, London

---

Received 4 January 2000/14 February 2000; accepted 7 March 2000

P 32,196

Saccharomyces cerevisiae Yak1p protein kinase autophosphorylates on tyrosine residues and phosphorylates myelin basic protein on a C-terminal serine residue

Shouki KASSIS*[1], Tiffany MELHUISH*, Roland S. ANNAN†, Susan L. CHEN†, John C. LEE*, George P. LIVI‡ and Caretha L. CREASY‡

*Department of Bone and Cartilage Biology, SmithKline Beecham Pharmaceuticals, King of Prussia, PA 19406-0939, U.S.A., †Department of Physical and Structural Chemistry, SmithKline Beecham Pharmaceuticals, King of Prussia, PA 19406-0939, U.S.A., and ‡Department of Comparative Genetics, SmithKline Beecham Pharmaceuticals, King of Prussia, PA 19406-0939, U.S.A.

The serine/threonine protein kinase, Yak1p, functions as a negative regulator of the cell cycle in *Saccharomyces cerevisiae*, acting downstream of the cAMP-dependent protein kinase. In the present work we report that overexpression of haemagglutinin-tagged full-lengthYak1p and an N-terminally truncated form (residues 148–807) lead to growth arrest in PKA compromised *yak1* null yeast cells. Both forms of recombinant Yak1p kinase were catalytically active and preferred myelin basic protein (MBP) as a substrate over several other proteins. Phosphopeptide analysis of bovine MBP by tandem MS revealed two major Yak1p phosphorylation sites, Thr-97 and Ser-164. Peptides containing each site were obtained and tested as Yak1p substrates. Both forms of Yak1p phosphorylated a peptide containing the Ser-164 residue with far more efficient kinetics than MBP. The maximal velocity (V_{max}) values of the full-length Yak1p reaction were 110±21 (Ser-164) and 8.7±1.7 (MBP), and those of N-terminally truncated Yak1p were 560.7±74.8 (Ser-164) and 34.4±2.2 (MBP) pmol/min per mg of protein. Although neither form of Yak1p was able to phosphorylate two generic protein tyrosine kinase substrates, both were phosphorylated on tyrosine residues *in vivo* and underwent tyrosine autophosphorylation when reacted with ATP *in vitro*. Tandem MS showed that Tyr-530 was phosphorylated both *in vivo* and *in vitro* after reaction with ATP. Pre-treatment with protein tyrosine phosphatase 1B removed all of Yak1p phosphotyrosine content and drastically reduced Yak1p activity against exogenous substrates, suggesting that the phosphotyrosine content of the enzyme is essential for its catalytic activity. Although the N-terminally truncated Yak1p was expressed at a lower level than the full-length protein, its catalytic activity and phosphotyrosine content were significantly higher than those of the full-length enzyme. Taken together, our results suggest that Yak1p is a dual specificity protein kinase which autophosphorylates on Tyr-530 and phosphorylates exogenous substrates on Ser/Thr residues.

Key words: dual-specificity protein kinases, protein phosphorylation, Yak1p.

INTRODUCTION

Functional modification of cellular proteins by reversible phosphorylation represents a major signalling mechanism in eukaryotic cells [1,2]. It is catalysed by a large family of protein kinases [3] that share structural similarities within a catalytic domain of about 300 amino acids encompassing 11 kinase subdomains [4]. Most protein kinases also contain regulatory domains on their N- and C-termini, which regulate the catalytic activity of the kinase, its sub-cellular localization and its interactions with cellular substrates and other proteins (see [4] for a review).

The family of protein kinases can be divided based on functional and structural parameters into three major subfamilies: (a) the protein tyrosine kinases phosphorylating the phenolic hydroxy group of tyrosine, (b) the protein Ser/Thr kinases phosphorylating the hydroxy group on the β-carbon of serine and threonine, and (c) the dual specificity protein kinases which catalyse phosphorylation of exogenous substrates and/or autophosphorylation on both tyrosine and serine/threonine residues [2,5–11]. The best characterized kinases of the dual-specificity class are the mitogen-activated protein (MAP) kinase kinases (for example mammalian MEK1 and MKK4 and yeast Ste7p), which activate the MAP kinases, extracellular signal-regulated protein kinase (ERK)2, SAPK and Fus3p/Kss1p respectively by phosphorylating on both threonine and tyrosine residues [5,6,12,13]. Several dual-specificity kinases have been identified which autophosphorylate on tyrosine and serine/threonine residues but do not appear to phosphorylate exogenous substrates on tyrosine. These include transforming growth factor ('TGF')β receptor, and Mck1p and Hrr25p from *Saccharomyces cerevisiae* [14–16]. Recently, a new subfamily of dual specificity protein kinases which autophosphorylate on tyrosine and serine/threonine, but do not appear to phosphorylate exogenous substrates on tyrosine was identified. Members of this subfamily include mammalian DYRK1A/B/C, DYRK2 and DYRK3, *Drosophila minibrain* (mnb), *S. cerevisiae* Yak1p, *Dictyostelium* YakA and, as yet, uncharacterized kinases from *Schizosaccharomyces pombe* (Z50142) and *Caenorhabditis elegans* (Z70308) [17–21]. The regions conserved amongst all members of this subfamily are restricted to the catalytic core. These features include an Ser-Ser-Cys motif following subdomain VII, and the con-

---

Abbreviations used. GST, glutathione S-transferase, MAP, mitogen-activated protein, ERK, extracellular signal-regulated protein kinase, HA, haemagglutinin, mAb, monoclonal antibody, MBP, myelin basic protein; PKA, cAMP-dependent protein kinase; PTP, protein tyrosine phosphatase, Sc-His, minimal medium lacking histidine, PSD, post-source-decay; MALDI, matrix-assisted laser-desorption ionization, TOF, time-of-flight

[1] To whom correspondence should be addressed (e-mail Shouki_Kassis-1@sbphrd com)

served sequences HCDLKPEN and YXYIQSRFYR(S/A)PE in subdomains VI and VIII respectively [20]. Full-length DYRKs and mnb, as well as a fragment of the *YAK1* gene encoding the catalytic domain (amino acids 338–713), appear to autophosphorylate on tyrosine *in vitro* when expressed as glutathione S-transferase (GST) fusion proteins in *Escherichia coli* [20].

Yak1p functions as an antagonist of the Ras/cAMP-dependent protein kinase (PKA) pathway acting as a negative regulator of cell growth [17,22]. Recent data indicate that Yak1p functions downstream of PKA [23]. In the current model, active PKA down-regulates the activity of the transcriptional activators, Msn2p and Msn4p, leading to a decrease in expression of *YAK1* and other genes containing stress response element (STRE) sites [23] Yak1p appears to be functionally similar to the *Dictyostelium* YakA, which is essential for starvation-induced development and growth arrest [21]. Overexpression of either Yak1p or YakA in a *cdc25* (temperature sensitive) yeast strain leads to G$_1$ arrest at the permissive temperature [21,22]. In addition, the sequence similarity between the two kinases extends beyond the catalytic core. Yak1p and YakA both contain poly-Gln and poly-Asn stretches, as well as conserved sequences immediately N-terminal to the kinase domain and between subdomains X and XI [21].

In contrast to Yak1p and YakA, mnb and DYRK1 may be acting as positive regulators of cell growth. In the absence of *mnb*, *Drosophila* lacks proper neuroblast cell formation and maintenance, furthermore, *DYRK1*, the closest known *mnb* homologue, has been mapped to the region of chromosome 21, which is triplicated in Down's syndrome, suggesting that mnb and DYRK1 function as positive mediators of cell growth [18,19]. However, Souza et al. [21], suggest that the loss of neurons in *mnb* mutant flies may not be due to a lack of cell maintenance or formation, but rather the absence of a signal to arrest growth and induce differentiation of neuroblasts.

Although the Yak1p protein kinase was shown to phosphorylate casein and to exhibit cell-cycle related changes in activity and protein expression, little is known about its enzymic properties and precise biological role In the present study we report the characterization of several unique enzymic features of Yak1p kinase. Our data indicate that Yak1p is a dual specificity protein kinase, which is phosphorylated *in vivo* and autophosphorylates *in vitro* on Tyr-530, but phosphorylates exogenous substrates on serine and threonine residues. We have also demonstrated that tyrosine phosphorylation is required for Yak1p catalytic activity.

EXPERIMENTAL

Materials

Anti-haemagglutinin (HA) monoclonal antibody (mAb), clone 12CA5, was obtained from Boehringer Mannheim (Indianapolis, IN, U.S.A). Detergents, electrophoresis reagents and protein determination reagents were obtained from Bio-Rad Laboratories (Hercules, CA, U.S.A.). Bovine myelin basic protein (MBP) and Protein A–agarose were obtained from Gibco–BRL (Gaithersburg, MD, U.S.A.). Protein tyrosine phosphatase (PTP) 1B (catalogue number 14-109), and the anti-phosphotyrosine mAb, 4G10, were obtained from Upstate Biotechnology Inc. (Lake Placid, NY, U.S.A.). $[\gamma\text{-}^{32}\text{P}]$ATP and chemiluminscent reagent were obtained from Amersham Pharmacia Biotechnology Inc. (Piscataway, NJ, U.S.A.). The sources of peptides used in this study are shown in the Table captions. Other reagents were obtained from Sigma Chemical Co. (St. Louis, MO, U.S.A.).

Construction of expression vectors

Oligonucleotide pairs, 5′-GCC-ACT-AGT-GCC-ATG-TAC-CCA-TAC-GAT-GTT-CCA-GAT-TAC-GCT-ATG-AAC-TCA-TCC-AAT-AAT-3′ and 5′-GCC-ATC-GAT-TTA-TTC-TTC-GAC-AAT-GTG-3′, and 5′-GCC-ACT-AGT-GCC-ATG-TAC-CCA-TAC-GAT-GTT-CCA-GAT-TAC-GCT-CCC-GCT-TAC-ACC-AGC-TCT-3′ and 5′-GCC-ATC-GAT-TTA-TTC-TTC-GAC-AAT-GTG-3′, were used to amplify full-length *YAK1* [17] and an N-terminal deletion (amino acids 148–807) respectively, using standard PCR conditions. In both cases, the 5′ oligonucleotide contained a *Spe*I site and nucleotides encoding the HA epitope, and the 3′ primer contained a *Cla*I site. Following T/A cloning and sequence confirmation of the cloned products, full length and N-terminally truncated *YAK1* were subcloned as a *Spe*I–*Cla*I fragment into p423GAL1, a high-copy yeast expression vector containing the *GAL1* promoter and *HIS3* as the selectable marker [24] The resulting plasmids were termed p423GAL1-HA-YAK1 and p423GAL1-HA-ΔNYAK1, respectively.

Growth of yeast and preparation of cellular extracts

All media for growth were prepared as described previously, unless otherwise indicated [25]. Yeast strain SGY470 [*MATa ura3 leu2 trp1 his3 lys2 ade8 tpk1::URA3 tpk2-63(ts) tpk3::TRP1 yak1::ADE8*; a gift from S Garrett, University of Medicine and Dentistry of New Jersey] was transformed by the lithium acetate procedure [26] with p423GAL1, p423GAL1-HA-YAK1, or p423GAL-HA-ΔNYAK1. Transformants were selected for growth on minimal medium lacking histidine (Sc-His). To perform spot assays, cells were grown in Sc-His overnight, cultures were normalized to similar D_{600}, serially diluted and spotted on to either Sc-His or Sc-His containing 2% galactose and 1% raffinose. Cultures for experiments were grown in liquid Sc-His to a D_{600} of at least 1.0, washed with Sc-His containing 2% galactose and 1% raffinose and resuspended in this medium to twice the original volume. The cells were then grown for 16–24 h at room temperature, washed once with water and, after centrifugation at 3200 *g* for 5 min at room temperature, the pellets were stored at −80 °C until use. To prepare lysates, cell pellets were thawed and resuspended at 1 ml/100 ml of original culture in lysis buffer [50 mM Tris/HCl, pH 7.5, 150 mM NaCl containing 10 μg/ml each of aprotinin, leupeptin and tosyl-lysylchloromethane (Tos-Lys-CH$_2$Cl, 'TLCK'), 0.1 mM PMSF, 50 mM NaF, 0.2 mM Na$_3$VO$_4$ and 10 mM 2-glycerophosphate]. Sterile acid-washed glass beads (0.5 ml) were added and cells were disrupted with ten 30 s intervals of vortex mixing. Nonidet P-40 was added to a final concentration of 2% and the mixtures were rocked at 4 °C for 30–50 min. Lysates were clarified by centrifugation at 20000 *g* for 10 min at 4 °C, and the supernatants were stored at −80 °C until use.

Immune-complex protein kinase assay

Equal amount of proteins (50 μg, unless stated otherwise) from detergent extracts of yeast cells expressing full-length Yak1p, N-terminally truncated Yak1p or vector alone were immunoprecipitated by rocking overnight at 4 °C with 4 μg of the anti-HA mAb and 100 μl of a 20% suspension of Protein A–agarose in lysis buffer containing 1% Nonidet P-40. Under these conditions, maximal immunoprecipitation of both forms of the enzyme was achieved. Samples were then washed twice with lysis buffer, once with kinase assay buffer [25 mM Hepes, pH 7.5, 10 mM 2-glycerol phosphate, 0.2 mM Na$_3$VO$_4$) and suspended in 20 μl of kinase assay buffer containing (unless stated otherwise) 0.1 mM (3 μCi) of [γ-^{32}P]ATP, 10 mM $MgCl_2$ and the protein or peptide substrate at the concentrations indicated in Table captions and Figure legends. After incubation for 10 min at 30 °C, the reactions were stopped by adding either 5 μl of 5 × SDS sample buffer or 20 μl of 0.15 M H_3PO_4. The SDS-containing solutions were boiled and centrifuged at 20000 *g* for 5 min at room temperature. The supernatant proteins were resolved by SDS/PAGE on 14% polyacrylamide gels and the phosphorylated products were detected by autoradiography. Reactions stopped with H_3PO_4 were centrifuged and the phosphorylated products were isolated by spotting 20 μl of the supernatant on to phosphocellulose (p81) filters. The filters were washed three times with 75 mM H_3PO_4, three times with water and ^{32}P-labelling was monitored by scintillation spectroscopy. Kinase specific activity is expressed as pmol of P_i transferred from ATP to the phosphate acceptor/min per mg of protein present in the extract used for immunoprecipitation after subtraction of the blank values generated in the absence of substrate or in reactions using extracts from yeast transfected with empty vector. In either case, blanks were < 5% of total activity values. Protein concentration was determined using Bio-Rad reagent with BSA as a standard.

Mapping of substrate phosphorylation sites

MBP was phosphorylated by incubation with Yak1p and Mg^{2+}ATP and digested with endoproteinase Lys-C for 2 h at 38 °C in 50 mM Tris/HCl, pH 8.8. An aliquot of the unfractionated protein digest was analysed by matrix-assisted laser-desorption ionization–time-of-flight (MALDI–TOF) MS for the presence of phosphorylated peptides. Potential phosphopeptide precursor ions were selected for post-source-decay (PSD) analysis using a Bradbury–Nielsen ion gate. Phosphopeptides were isolated by reverse-phase HPLC using a 1-mm i.d. C_{18} column. Peptides, in solution A, were eluted with a 5-50% gradient of solution B (solution A: 2% acetonitrile containing 0.1% trifluoroacetic acid in water; solution B: 95% acetonitrile containing 0.1% trifluoroacetic acid in water) at 50 μl/min. The column eluate was split after passing through the UV detector, so that 5 μl/min was sent to a QTOF mass spectrometer and 45 μl/min went to a fraction collector, where fractions were collected at 1 min intervals. Phosphopeptides were sequenced by nano-electrospray tandem MS (QTOF spectrometer)

Autophosphorylation and determination of phosphotyrosine content

To determine total autophosphorylation of Yak1p, washed immune complexes were suspended in 20 μl kinase assay buffer containing 50 μM (5 μCi) of [γ-^{32}P]ATP and 10 mM $MgCl_2$, and incubated for 10 min at 30 °C. Reactions were stopped by adding 5 μl of 5 × SDS sample buffer, and the proteins were resolved by SDS/PAGE (10% polyacrylamide gels). Phosphorylated Yak1p was revealed by autoradiography. To determine phosphotyrosine content *in vivo* and tyrosine autophosphorylation of Yak1p, washed immune complexes were suspended in 20 μl of kinase assay buffer with or without the addition of 50 μM unlabelled ATP and 10 mM $MgCl_2$. Samples without ATP were kept on ice, and those containing ATP were incubated for 10 min at 30 °C. All samples were resolved by SDS/PAGE (10% polyacrylamide), transferred to nitrocellulose, blocked in PBS/Tween-20 containing 5% (w/v) non-fat powdered milk for 1 h, and incubated for 1 h with anti-phosphotyrosine mAb (4G10). After three washes in PBS/Tween-20, membranes were incubated with horseradish-peroxidase-conjugated goat anti-mouse IgG for 45 min and washed three times in PBS/Tween-20. The secondary antibody was detected by enhanced chemiluminescence.

To determine the sites of phosphorylation *in vivo* and *in vitro*, Yak1p immunoprecipitated from 1 mg of yeast protein was incubated without or with Mg^{2+}ATP, purified by SDS/PAGE, as above, and stained with Coomassie Blue. Bands representing Yak1p were excised from the gel and digested with trypsin *in situ* as described previously [27]. The peptide mixture was desalted using a ZipTip (Millipore) according to the manufacturer's directions and enriched for phosphopeptides using immobilized metal-chelate affinity chromatography on a disposable micro-column [28]. The phosphopeptide mixture was again desalted on a ZipTip and an aliquot of the sample was analysed by MALDI–TOF to determine the molecular masses of the phosphorylated peptides. MALDI mass spectra [29] were recorded on a reflectron TOF mass spectrometer (Micromass TofSpec SE) equipped with a time-lag focusing source Samples were prepared by mixing with an equal volume of matrix solution, which contained two internal mass standards at a concentration of 200 fmol/μl. A 0.5 μl aliquot of the sample/matrix solution was applied to the MALDI target. The matrix solution was 10 μg/ml α-cyano-4-hydroxycinnamic acid in ethanol/acetonitrile (50:50, v/v). Samples were then irradiated with 337 nm photons from a pulsed nitrogen laser (Laser Science) operating at 5 Hz. Phosphopeptides were sequenced by tandem MS [30] using a quadrupole TOF mass spectrometer (QTOF, Micromass) equipped with a nano-electrospray source [31].

RESULTS

Expression and activity of Yak1p in *S. cerevisiae*

YAK1 was engineered for expression in yeast under the control of the *GAL1* promoter as both an N-terminally HA-tagged full-length form and an N-terminally truncated form (amino acid residues 148–807) (Figure 1A) Overexpression of either protein in a strain compromised for PKA and lacking Yak1p (SGY470) caused growth arrest at 30 °C (Figure 1C) and slower growth at 23 °C (Figure 1B), indicating that both forms of the enzyme were functional. However, the expression level of the full-length protein was 2–3-fold higher than that of the N-terminally truncated (ΔN) form (Figure 2). The slow growth observed at 23 °C was not due to general toxicity caused by overexpression, since neither construct caused growth arrest in a wild-type strain at either temperature (results not shown).

Cells expressing the full-length or N-terminally truncated forms, or containing vector alone were lysed in a buffer containing 2% Nonidet P-40, and an anti-HA mAb immune-complex kinase assay was performed using bovine MBP as substrate. Both full-length and N-terminally truncated forms of the enzyme were able to catalyse phosphate transfer from ATP to MBP (Figure 2). MBP phosphorylation was compared with that of other protein substrates, each used at 10 μg/reaction mixture. A much lower level of phosphorylation by either form of Yak1p was observed when casein was used as a substrate, and no phosphorylation of enolase, heat shock protein 27 (hsp27), histone or poly-Gly/Tyr was observed (results not shown). It was determined in preliminary experiments that the two forms of Yak1p were equally precipitated, since an anti-HA mAb immunoblot of the precipitated material indicated the ratio between the two forms was similar to that observed in the direct immunoblot shown in Figure 2. MBP phosphorylation, catalysed by either form of Yak1p, was better with Mg^{2+} than Mn^{2+} as the cation, was inhibited by 1 mM $CaCl_2$, was linear with time up to 15 min and was similar when incubation was at 30 °C or 37 °C (results not

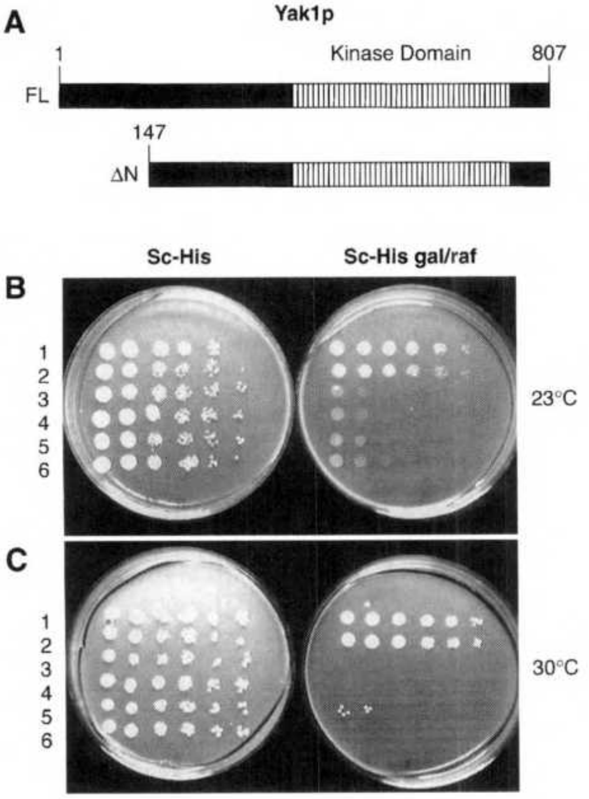

Figure 1 Overexpression of Yak1p complements a *yak1* deletion in a PKA compromised strain of *S. cerevisiae*

(**A**) Schematic diagram of full-length (FL) and N-terminally truncated (ΔN, amino acids 148–807) Yak1p. (**B**, **C**) Yeast strain SGY470 [*yak1*Δ, tpk1Δ, tpk3Δ, tpk2(ts)] was engineered to express two independent isolates of N-terminally HA-tagged Yak1p (full-length, rows 3 and 4; N-terminally truncated, rows 5 and 6) or vector alone (rows 1 and 2) under control of the *GAL1* promoter. Serial dilutions of normalized cultures were plated on to Sc-His (left) or Sc-His galactose/raffinose (Sc-His gal/raf) (right) and grown at either 23 °C (**B**) or 30 °C (**C**) for 7 days.

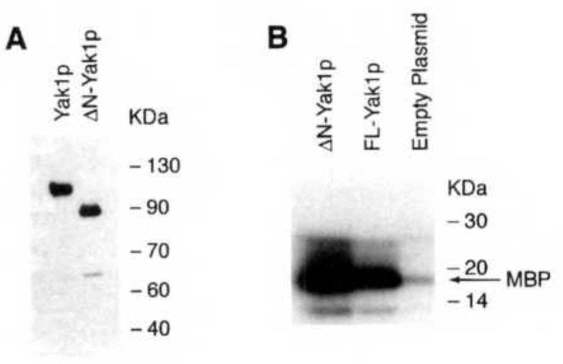

Figure 2 Protein expression of full-length and N-terminally truncated Yak1p and kinase activity with MBP

Yeast strain SGY470 was engineered to express either full-length Yak1p or an N-terminally truncated Yak1p (ΔN), and lysates were prepared as described in the Experimental section. (**A**) Total protein (30 μg) was resolved by SDS/PAGE (10% polyacrylamide), transferred to nitrocellulose and immunoblotted with anti-HA mAb as described in the Experimental section. (**B**) Total protein (50 μg) was immunoprecipitated with the anti-HA mAb and analysed for phosphorylation of bovine MBP (10 μg) as described in the Experimental section. Reactions were analysed using SDS/PAGE (14% polyacrylamide) and phosphorylated bands were revealed by autoradiography (exposure for 20 min at −80 °C).

shown). Interestingly, although expressed at a lower level, the N-terminally truncated form of Yak1p was 3- to 5-fold more active against MBP than the full-length enzyme (Figure 2). The higher activity of N-terminally truncated enzyme against MBP was observed at all concentrations of MBP tested. Although the level of expression and kinase-specific activity varied between different yeast cultures, the enzymic properties and the activity/expression ratio of each form were similar in the different cultures.

Yak1p-catalysed phosphorylation sites in bovine MBP

HA-tagged Yak1p (50 μg) was immunoprecipitated with the anti-HA mAb and incubated with 10 μg of bovine MBP in the presence or absence of Mg^{2+}ATP. MALDI–TOF analysis of 5 % of the unfractionated endoproteinase Lys-C digests from the phosphorylated (with Mg^{2+}ATP) and the non-phosphorylated (without Mg^{2+}ATP) MBP revealed two apparent phosphate-containing peptides at m/z 1571.78 (M^{+}+H) and 1682.80 (M^{+}+H) in the phosphorylated sample (Figure 3A), corresponding to peptides of molecular mass 1570.77 and 1681.79, respectively. The 1570 Da species was consistent with the mass of a peptide containing residues 91–104 from MBP and one molecule of phosphate (calculated mass 1570.78 Da), whereas the 1681 Da peptide was consistent with the mass of the C-terminal Lys-C fragment from MBP incorporating residues 155–169 plus one molecule of phosphate (calculated mass 1681.78). Further support for the incorporation of phosphate into the 1570 and 1682 Da peptides is the presence of broad peaks (marked with an asterisk in Figure 3A) which arise by metastable loss of H_3PO_4 from the intact phosphopeptide molecular ion. These metastable peaks were not present in the spectrum of a non phosphorylated sample. However, to rule out any possibility that they arose by the loss of water from the phosphorylated peptide, we isolated the phosphopeptide molecular ions using an ion gate and performed MALDI–PSD analysis. Observation of the characteristic loss of H_3PO_4 (98 Da) from both peptides upon subsequent PSD analysis [27] confirmed that these peptides were, in fact, phosphorylated (results not shown).

The Lys-C digests were fractionated by reverse phase HPLC and the fractions were subjected to MS to provide an on-line read-out of the products. Fractions containing the two putative phosphopeptides were analysed by nano-electrospray MS, and the appropriate precursor ions were sequenced by collision-induced dissociation tandem MS. The spectrum obtained for the 1570.9 peptide (Figure 3B) is consistent with two phosphorylated forms of the sequence NIVTPRTPPPSQGK, which corresponds to residues 91–104 of bovine MBP. The major phosphorylation site was found to be Thr-97. The 181.04 Da mass difference between the b_6 and b_7 ions indicated the presence of phosphothreonine at this position. A very small amount of phosphate was also found at Thr-94. The evidence for phosphorylation at this second site was a low abundance series of b_n-H_3PO_4 ions starting at b_4 and ending at b_6 (results not shown). The evidence for phosphorylation at either site converges at the b_7 ion.

The tandem mass spectrum of the 1681 peptide (Figure 3C) is consistent with a monophosphorylated form of LGGRDSRSGSPMARR, corresponding to the C-terminal residues 155–169 of bovine MBP. Although the tandem MS data clearly indicated that Ser-160 was not phosphorylated, it was not possible to distinguish between Ser-162 and Ser-164 as the sole site of phosphorylation in this peptide. However, results from a Yak1p kinase assay using synthetic peptides with Ser → Ala substitutions at position 164 or 162 as substrates supported the notion that Ser-164, not Ser-162, is the site of phosphorylation by Yak1p. As seen in Table 1, both forms of Yak1p phosphorylated the

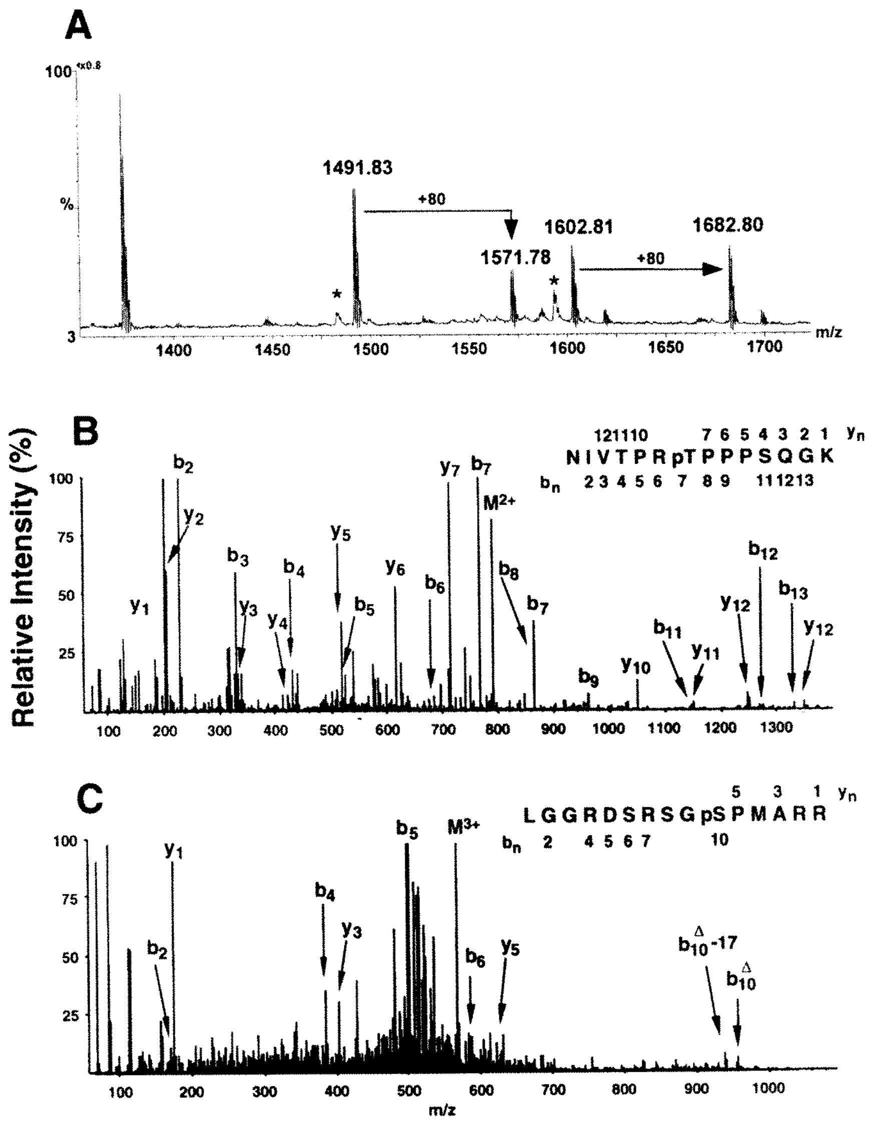

Figure 3 Determination of Yak1p-induced phosphorylation sites on MBP

(**A**) Partial MALDI mass spectrum of an unfractionated Lys-C digest of MBP phosphorylated *in vitro*. Peptides modified by a single molecule of phosphate show an increase in mass of 80 Da. Peaks marked with an asterisk (*) arise from the metastable loss of H_3PO_4 from the corresponding phosphopeptide molecular ion. (**B**) Electrospray–chromatogram-ion-detection tandem mass spectrum of the [M^{2+}] ion (*m/z* 786.4) from the 1570 Da phosphorylated peptide shown above. The mass difference between adjacent ions of the same series (i.e. b_5 and b_6) corresponds to the in-chain mass of an amino acid residue. Ions marked b_n^{Δ} have the structure b_n-H_3PO_4. (**C**) Electrospray–chromatogram-ion-detection tandem mass spectrum of the [M^{3+}] ion (*m/z* 561.6) from the 1681 Da phosphorylated peptide shown above.

LGGRDSRAGSPMARR (Ser-162 → Ala) but not the LGGRDSRSGAPMARR (Ser-164 → Ala) peptide. Phosphorylation of Ser-164, which exists as an S/TP motif, is consistent with the Yak1p-induced phosphorylation of Thr-97, which also exists in a S/TP consensus sequence. Replacement of Pro-165 with alanine resulted in $> 70\%$ loss of activity of Yak1p (Table 1). In addition, replacing the S/TP consensus sequence of Ser-164 with an S/TP for Ser-162 did not allow Ser-162 to become an efficient phospho-acceptor, as Yak1p poorly phosphorylated the Gly-163 → Pro/Pro-165 → Ala peptide (Table 1).

Phosphorylation of bovine MBP on Thr-97 by MAP kinases has been reported previously [32,33]. However, we are not aware of any kinase that phosphorylates bovine MBP on Ser-164. Therefore the phosphorylation pattern of MBP by Yak1p appears to be unique.

Several other selected peptides were obtained from commercial sources and used as substrates in the Yak1p kinase assay alongside MBP and the Ser-164 peptide (LGGRDSRSGSPMARR). As shown in Table 2, the specific activity of either full-length or N-terminally truncated Yak1p with the Ser-164 peptide (1 mM) was about 9-fold higher than the specific activity with MBP (60 μM). A peptide (termed Thr-97 in Table 2), with the PRTP motif found in the NIVTPRTPPPSQGK tryptic fragment of MBP, was poorly phosphorylated by Yak1p (Table 2). Although the MS data showed that the NIVTPRTPPPSQGK tryptic fragment of MBP was phosphorylated mainly on Thr-97, with little phosphorylation of Thr-94, the low activity of Yak1p with the synthetic Thr-97 peptide (Table 2) may be due to sequence differences, particularly the lack of a residue corresponding to Thr-94 in MBP. Two additional peptides, GS1–10

Table 1 Phosphorylation of the Ser-164 peptide and its analogues by Yak1p

Anti-HA immune-complex Yak1p kinase assay of 50 μg of protein from yeast expressing either full length or N-terminally truncated Yak1p was performed as described in the Experimental section All peptides used in this study were from California Peptide Research Inc, Napa, CA, U S A Protein substrates (1 mM) were incubated with the immunoprecipitated enzyme for 10 min at 30°C Phosphorylated substrates were isolated on phosphocellulose filters Kinase activity using the Ser-164 peptide as substrate was 894 ± 28 (full length) and 3447 ± 69 (N-terminally truncated form) pmol per mg of protein The values are the percentage kinase activity compared with that of the Ser-164 peptide as substrate, means ± S D of triplicate determinations Similar results were obtained in one additional experiment

		Yak1p activity	
Peptide	Sequence	Full-length enzyme	N-terminally truncated form
Ser-164	LGGRDSRSGSPMARR	100±3	100±2
Ser-164 → Ala	LGGRDSRSGAPMARR	7±2	4±3
Ser-162 → Ala	LGGRDSRAGSPMARR	93±5	100±2
Pro-165 → Ala	LGGRDSRSGSAMARR	20±2	28±4
Ser-164 → Thr	LGGRDSRSGTPMARR	99±7	81±2
Gly-163 → Pro	LGGRDSRSPSPMARR	90±2	95±2
Gly-163 → Pro/Pro-165 → Ala	LGGRDSRSPSAMARR	25±2	18±1

Table 2 Phosphorylation of peptides by full-length and N-terminally truncated Yak1p

Experimental details are as described in Table 1 All peptides were used at 1 mM, MBP was 30 μM The Ser-164 peptide was purchased from California Peptide Research Inc, Napa, CA, U S A Thr-669 peptide was from Amersham Pharmacia Biotech Inc, Piscataway, NJ, U S A, all other peptides were purchased from BACHEM Bioscience Inc, King of Prussia, PA, U S A The Thr-97 peptide contains the 95–98 sequence (PRTP) of bovine MBP In the peptide sequences shown, the N-terminus is on the left Results are representative of two experiments with the N-terminally truncated) enzyme or three with the full-length form

		Yak1p activity (pmol/10 min per mg of protein)	
Peptide	Sequence	Full-length enzyme	N-terminally truncated enzyme
Ser-164	LGGRDSRSGSPMARR	478	1809
Thr-97	APRTPGGRR	3	15
MBP4–14	EKRPSERSKYL	< 1	< 1
MBP68–82	YGSLPQKSQRSQDGN	< 1	< 1
GS1–10	PLSRTLSVAAKK	13	57
Thr-669	KRELVEPLTPSGEAPNQALLR	6	21
Tyr-418	RRLIEDNEYTARG	< 1	< 1
MBP		61	212

Table 3 Kinetic constants of the Yak1p kinase reaction

The anti-HA mAb immune-complex Yak1p kinase assay was performed as described in the Experimental section. Values for Michaelis–Menten kinetics (K_m and V_{max}) were calculated from double reciprocal plots of initial velocity of the enzyme versus substrate concentration, with at least nine different concentrations of a given substrate The concentrations of ATP used were 1–1000 μM, those of MBP were 1–150 μM, and peptide concentrations were 25–2500 μM The incubation time (10 min) was within the linear range of the reaction, and concentrations of enzyme and substrates were chosen so that not more than 10% of the substrate would be converted. Results are the means ± S E M of three to five independent determinations

	K_m (μM)		V_{max} (pmol/min per mg of protein)	
Substrates	Full-length	N-terminally truncated	Full-length	N-terminally truncated
ATP with MBP	48±7	36±10		
ATP with Ser-164	72±19	67±7		
MBP	31±8	34±11	8.7±1.7	34.4±2.2
Ser-164	403±56	393±102	110.3±21.1	560.7±74.8
Thr-97	1213±164	1166±92	27.1±0.9	13.2±1.9

and Thr-669, were also poorly phosphorylated by Yak1p (Table 2). The GS1–10 peptide is derived from the first ten residues of glycogen synthase, where the Ser-7 residue is a site of protein kinase C phosphorylation, and is also phosphorylated by PKA [34,35]. The Thr-669 peptide is derived from the epidermal growth factor ('EGF') receptor cytoplasmic tail, with Thr-669 (in a S/TP motif) as the site phosphorylated by ERK2 and p38 MAP kinases [33,36]. The specific activity of N-terminally truncated Yak1p towards each of the four peptide substrates was 4–5-fold higher than that of the full-length enzyme. Yak1p phosphorylated neither the two MBP-derived peptides (MBP4–14 and MBP86–82; Table 2) nor a tyrosine-containing peptide (Tyr-418, Table 2) derived from residues 412–422 of $pp60^{c\text{-}src}$, which is phosphorylated by tyrosine kinases [37].

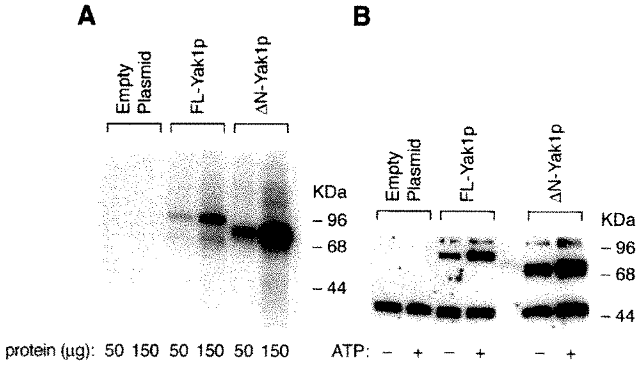

Figure 4 Total [^{32}P]ATP and tyrosine autophosphorylation of Yak1p

(**A**) The indicated amount of protein from yeast cells expressing either full-length (FL) or N-terminally truncated (ΔN) Yak1p was immunoprecipitated, assayed for Yak1p kinase activity without exogenous substrate and resolved by SDS/PAGE. Phosphorylated bands were revealed by autoradiography (exposure for 45 min at −80 °C). (**B**) Anti-phosphotyrosine mAb immunoblot of 150 µg of full-length (FL) and N-terminally truncated (ΔN) Yak1p before and after autophosphorylation. Immunoprecipitated samples were incubated in the absence or presence of Mg^{2+}ATP, resolved by SDS/PAGE and blotted with anti-phosphotyrosine mAb as described in the Experimental section.

Kinetic constants of the Yak1p kinase reaction

Since relatively high Yak1p specific activity towards the Ser-164 peptide was observed, we determined the kinetic constants of Yak1p for ATP, MBP, the Ser-164 peptide and the Thr-97 peptide using immune-complex kinase assays. The Michaelis constant (K_m) and maximum velocity (V_{max}) of the kinase reaction with each substrate were determined under conditions where the rate of phosphorylation was linear with respect to time and the concentration of the other substrate was not limiting. From double-reciprocal plots of initial velocity versus substrate concentration the apparent K_m and V_{max} with ATP, MBP, Ser-164 or Thr-97 as substrates were calculated. Values in Table 3 show that the Ser-164 peptide was a better substrate for both forms of Yak1p than MBP, with a 9-fold higher V_{max} of phosphorylation. Yak1p exhibited a single affinity for ATP regardless of the protein/peptide substrate used, giving apparent K_m [ATP] values around 40 µM. The apparent K_m value for phosphorylating any of the three phosphate acceptors was similar between full-length and N-terminally truncated forms of Yak1p, and both forms phosphorylated the Ser-164 peptide with an apparent K_m (approximately 0.4 mM) 3-fold lower and a V_{max} 50-fold higher than the corresponding values for the Thr-97 peptide (Table 3). The V_{max} value for Thr-97 phosphorylation was lower than that for MBP phosphorylation, and the apparent K_m value for this peptide was approximately 1.2 mM, which is comparable to its reported K_m value for the meiosis-activated MBP kinase (p44^{mpk}) from sea star oocytes [33,38]. Taken together, these results demonstrate that the truncated form of Yak1p exhibits higher catalytic activity than the full-length enzyme, and that both forms of the enzyme have far more efficient kinetics for Ser-164 phosphorylation than for MBP.

Phosphorylation *in vivo* and autophosphorylation *in vitro*

To determine if Yak1p autophosphorylates *in vitro*, equal amounts of yeast cell lysates were immunoprecipitated with anti-HA mAb and reacted with Mg^{2+}[^{32}P]ATP. Samples were then resolved on SDS/PAGE and incorporation of ^{32}P was revealed

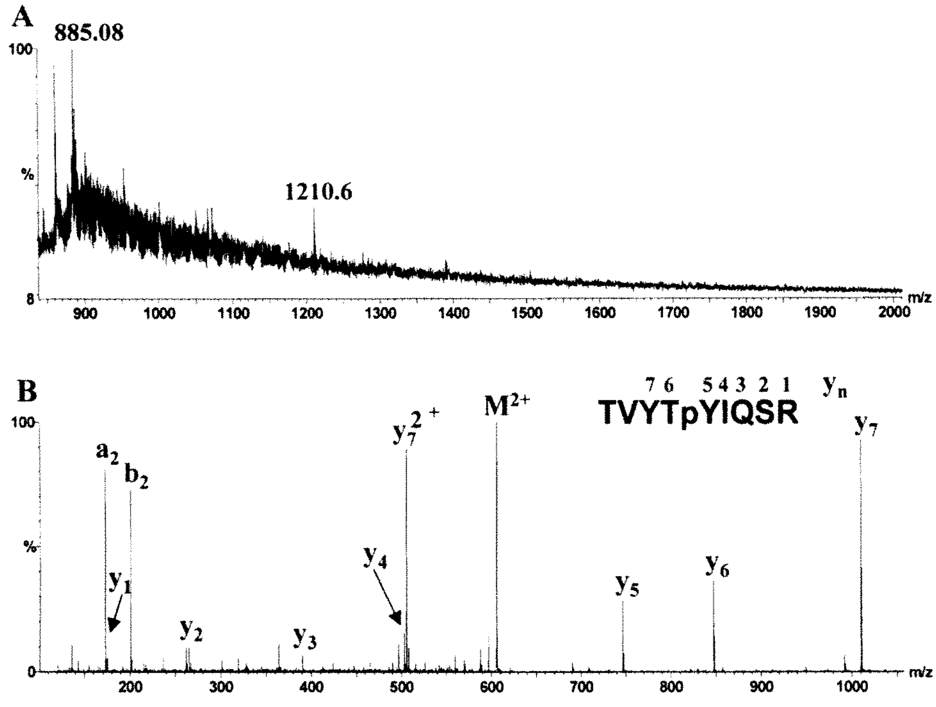

Figure 5 Determination of autophosphorylation sites on Yak1p *in vitro*

(**A**) Partial MALDI mass spectrum of the Ga^+-immobilized metal-affinity chromatography enriched fraction from a tryptic digest of Yak1p phosphorylated *in vitro*. (**B**) Electrospray–chromatogram-ion-detection tandem mass spectrum of the [M^{2+}] ion (*m/z* 605.8) from the 1210.6 Da phosphorylated peptide shown above.

by autoradiography. Both forms of Yak1p underwent autophosphorylation *in vitro*, which was significantly higher in the truncated protein (ΔN) than in the full-length enzyme (Figure 4A). To determine if Yak1p in *S. cerevisiae* was tyrosine phosphorylated *in vivo*, and if the observed autophosphorylation *in vitro* involved tyrosine residues, anti-HA mAb Yak1p immune complexes were either kept on ice or reacted with Mg^{2+}ATP to allow for autophosphorylation, resolved by SDS/PAGE and blotted with anti-phosphotyrosine mAb. Figure 4(B) shows that Yak1p was tyrosine phosphorylated *in vivo* and that the level of phosphotyrosine increased after incubation with Mg^{2+}ATP, indicating clearly that Yak1p autophosphorylates on tyrosine residues *in vitro*. It is also evident from the data shown in Figure 4 that the phosphotyrosine content *in vivo* and the level of tyrosine autophosphorylation *in vitro* were significantly higher in N-terminally truncated compared with full-length Yak1p. An ATP binding site mutant of Yak1p, in which the lysine residue at position 398 was replaced with alanine, was inactive against exogenous substrates and did not autophosphorylate *in vitro* (results not shown), indicating that the incorporation of phosphate into Yak1p (Figure 4) is most likely due to autophosphorylation of the kinase, not to other co-immunoprecipitating protein kinase activity.

To determine the *in vivo* and *in vitro* site(s) of phosphorylation, equal amounts of yeast cell lysates expressing full-length Yak1p were immunoprecipitated with anti-HA mAb, and either kept on ice or reacted with Mg^{2+}ATP to allow for autophosphorylation. The reaction mixtures were then resolved by SDS/PAGE and stained with Coomassie Blue. Yak1p appeared as a single band migrating at about 102 kDa, which was absent from samples from yeast cells transfected with vector alone (results not shown). The bands from both untreated and autophosphorylated proteins were excised and digested *in situ* with trypsin [27]. Phosphopeptides from the respective tryptic digests were isolated using microcolumn Ga^{+}-ion immobilized metal-affinity chromatography ('IMAC') [28] and analysed by MALDI MS. Mass spectra from the autophosphorylated (Figure 5A) and the unphosphorylated (results not shown) samples showed an ion at $[M^{+}+H]$ 1210.60, which corresponds to residues 526–534 of the Yak1p sequence with the addition of one molecule of phosphate (calculated $[M^{+}+H]$ 1210.55). Figure 5(B) shows the tandem MS spectrum of the 1210 Da peptide from the autophosphorylated sample. A mass difference of 243 Da between the y_4 and y_5 ions indicated phosphotyrosine in the 5 position. Sequencing of the 1210 Da peptide from each sample by tandem MS showed unambiguously that the sequence 526–534 is phosphorylated *in vivo* and *in vitro* exclusively on Tyr-530, which is the second tyrosine residue in the YTY motif of Yak1p.

To determine if the phosphotyrosine content of Yak1p *in vivo* affects its activity, immunoprecipitated Yak1p was first reacted with PTP1B [39,40] to dephosphorylate the tyrosine residues and then assayed for substrate phosphorylation. To allow proper comparison of the treatments, Yak1p was treated with PTP1B in the presence (for untreated control) or absence (treated) of 0.5 mM Na_3VO_4. In preliminary experiments it was determined that 0.5 mM Na_3VO_4 was sufficient to almost inactivate PTP1B. Whereas Yak1p treated with the phosphatase in the absence of vanadate lost most of its phosphotyrosine content, the presence of 0.5 mM vanadate provided complete protection from dephosphorylation, resulting in a phosphotyrosine content comparable with that observed in samples kept on ice (Figure 6B). Variability in the amount of immunoprecipitated material was minimal, as indicated by Western blotting with the anti-HA mAb (Figure 6A). As shown in Figure 6(C), removal of the phosphate groups from Yak1p tyrosine residues resulted in > 85% loss of both full-length and N-terminally truncated kinase activity with the Ser-164 peptide, indicating that tyrosine phosphorylation of Yak1p is required for its catalytic activity against exogenous substrates. Similar reduction in kinase activity was observed when MBP was used as substrate (results not shown).

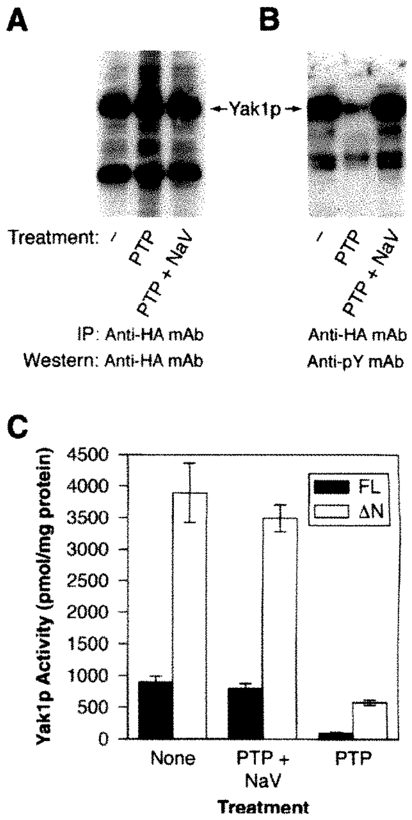

Figure 6 Effect of treatment of Yak1p with PTP1B on its phosphotyrosine content and substrate phosphorylation

Full-length (FL) and N-terminally truncated Yak1p (Δ) (100 μg each, in triplicate) were immunoprecipitated (IP) with anti-HA mAb and washed as described in the Experimental section. One set was kept on ice (None), another set was incubated for 30 min at 30 °C in 20 μl of Hepes buffer (pH 7.0) containing 1 μg (activity of 2 nmol/min) GST-fusion full-length PTP1B (PTP), and the third set was incubated as above with PTP1B and 0.5 mM Na_3VO_4 (PTP + NaV). Samples were washed three times with kinase assay buffer containing 0.5 mM Na_3VO_4, immunoblotted with anti-HA mAb (**A**) or anti-phosphotyrosine (Anti-pY) mAb (**B**) or assayed for kinase activity using 1 mM Ser-164 peptide (**C**), as described in the Experimental section. Results with full-length Yak1p only are shown in (**A**) and (**B**). Similar results were obtained in two independent experiments.

DISCUSSION

In the present study, we observed that expression of either full-length or an N-terminally truncated form of Yak1p kinase (residues 148–807) in a *S. cerevisiae* strain lacking Yak1p and compromised for PKA (*tpk1*Δ, tpk2Δ, tpk3 (ts)) complemented the *yak1* deletion phenotype by causing cell arrest at 30 °C and slow growth at the permissive temperature (23 °C). This confirms earlier observations that Yak1p serves as negative regulator of the cell cycle in yeast [17,22]. Although a phenotypic difference between full-length and N-terminally truncated Yak1p was not observed in yeast, activity of the latter was 4–5 fold greater than the full-length enzyme, suggesting that an inhibitory element may be located within the first 147 amino acid residues of the protein. This region is rich in serine residues (24/147 residues) and contains two putative PKA phosphorylation sites (residues 127 and 128; [17]). As Yak1p functions downstream of PKA [23] and was shown to be phosphorylated *in vitro* by PKA [22], it is tempting to speculate that phosphorylation of Yak1p on N-terminal serine residues (by PKA or another upstream kinase) serves to inhibit its activity. Loss of these sites in the truncated form would result in increased kinase activity as compared with the full-length enzyme.

Yak1p was previously reported to phosphorylate casein [22]. In the present study, we have shown that Yak1p prefers MBP as a substrate over casein and several other proteins, and that it is capable of phosphorylating the Ser-164 and Thr-97 residues of bovine MBP. Both forms of Yak1p phosphorylated a synthetic peptide (LGGRDSRSGSPMARR), corresponding to residues 155–169 of bovine MBP, with far more efficient kinetics than phosphorylation of native MBP. Although we were unable to distinguish between Ser-162 and Ser-164 as the sole site of phosphorylation using the tandem MS data, data generated using synthetic peptides with Ser → Ala substitutions demonstrated that Ser-164 is the phosphate acceptor for Yak1p. To our knowledge, no other kinase has been reported to phosphorylate the Ser-164 residue of bovine MBP.

Previously, it was shown that the catalytic portion of Yak1p alone autophosphorylates on tyrosine when expressed in *E. coli* as a GST fusion, however, catalytic activity was not demonstrated [20]. In the present work, we show that recombinant Yak1p kinase expressed in *S. cerevisiae* phosphorylates exogenous substrates on Ser/Thr residues, is tyrosine phosphorylated *in vivo* and undergoes tyrosine autophosphorylation *in vitro*, suggesting it is a dual specificity protein kinase. Yak1p contains a YTY motif in its activation loop (positions 528–530) [17], which is conserved in DYRK2 and DYRK3 [20], whereas a YQY motif is found in DYRK1 [19]. This is distinct from the TXY consensus sequence found in the activation loop of the Ser/Thr MAP kinases [12]. We have shown by MS-based microsequencing, that the second tyrosine (Tyr-530) in this motif was phosphorylated both *in vivo* and, after autophosphorylation, *in vitro*.

We were unable to demonstrate Yak1p-catalysed phosphorylation of either two generic tyrosine kinase substrates, enolase and poly-Gly/Tyr (results not shown), or a full-length peptide substrate (Table 2). In addition, anti-phosphotyrosine mAb immunoblots failed to detect tyrosine phosphorylation of histone (results not shown), which was weakly phosphorylated by Yak1p. Like Yak1p, four other members of this kinase family (DYRK1, DYRK2, DYRK3 and mnb) were reported to autophosphorylate on tyrosine, but from the limited reported phosphorylation studies, do not readily phosphorylate exogenous substrates on tyrosine [20]. Hence, Yak1p and members of this family may not be classical dual specificity protein kinases like GSK3, MEK1 and ESK [5,6,12,13], but rather evolutionary intermediates between Ser/Thr protein kinases and dual specificity protein kinases. Alternatively, the inability of Yak1p to phosphorylate exogenous substrates on tyrosine may simply be due to the lack of the appropriate recognition site within the selected substrates. The identification of Yak1p cellular substrates will supply direct evidence for the dual specific nature of the kinase.

Another important finding of this study is that tyrosine phosphorylation of Yak1p is required to maintain its catalytic activity towards exogenous substrates. Preincubation of Yak1p with PTP1B drastically reduced the phosphotyrosine content and the catalytic activity of the kinase when compared with samples incubated with inactive PTP1B (Figure 6). PTP1B had been successfully used to dephosphorylate tyrosine residues of various proteins *in vitro* to allow study of the function of the phosphotyrosine in these proteins [41–43]. Our observation that removal of phosphate from tyrosine residues of Yak1p suppresses its catalytic activity further supports the unique dual-specific nature of this enzyme. In comparison, classic dual specificity protein kinases, such as the various isoforms of MEK, are activated by Ser/Thr (not tyrosine) phosphorylation catalysed by an upstream MEK kinase, thereby activating the p38 and ERK MAP kinases by dual threonine and tyrosine phosphorylation. The MAP kinases themselves are specific for Ser/Thr residues, but require phosphorylation on tyrosine and threonine residues for their activity. Conversely, Yak1p is a dual specificity protein kinase (autophosphorylates on tyrosine) in which the catalytic activity is highly dependent on its phosphotyrosine content, but phosphorylates exogenous substrates on Ser/Thr residues.

In summary, the present study demonstrates that the *S. cerevisiae* Yak1p is a unique dual specificity protein kinase which autophosphorylates on Tyr-530, requires phosphorylation on tyrosine for its catalytic activity and phosphorylates exogenous substrates on Ser/Thr residues.

We are grateful to Mr Michael Huddleston for help in sequencing the MBP phosphopeptides, Ms Joanne Takata for performing quality control testing of the peptides used in this study, Dr S. Garrett, UMDNJ, for providing the yeast strains, and Dr Maxine Gowen for a critical reading of the manuscript

REFERENCES

1 Edelman, A M, Blumenthal, D K and Krebs, E G (1987) Annu Rev Biochem. **56**, 567–613
2 Hunter, T (1991) Methods Enzymol **200**, 3–37
3 Hunter, T (1987) Cell **50**, 823–829
4 Hanks, S K, Quinn, A M and Hunter, T (1988) Science **241**, 42–52
5 Lindberg, R A, Quinn, A M and Hunter, T (1992) Trends Biochem Sci **17**, 114–119
6 Posada, J and Cooper, J A (1992) Mol Biol Cell **3**, 583–592
7 Gomez, N and Cohen, P (1991) Nature (London) **353**, 170–173
8 Crews, C. M, Alessandrini, A. and Erickson, R L (1992) Science **258**, 478–480
9 Wu, J, Harrison, J K, Vincent, L A, Haystead, C, Haystead, T A J, Michel, B, Hunt, D F, Lynch, K R and Sturgill, T W (1993) Proc Natl. Acad Sci U S A **90**, 173–177
10 Zheng, C.-F and Guan, K-L (1993) J Biol Chem **268**, 11435–11439
11 Wang, Q. M, Fiol, C F, DePaoli-Roach, A and Roach, P J (1994) J Biol Chem **269**, 14566–14574
12 Payne, D M, Rossomando, A J, Martino, P, Erickson, A, Her, J H., Shabanowitz, J, Hunt, D F, Weber, M J and Sturgill, T W. (1991) EMBO J **10**, 885–892
13 Lundgren, K, Walworth, N., Booher, R, Dempski, M., Kirschner, M and Beach, D (1991) Cell **64**, 1111–1122
14 Lin, H Y, Wang, X F, Ng-Eaton, E, Weinberg, R A and Lodish, H. F (1992) Cell **68**, 775–785
15 Lawler, S, Feng, X H, Chen, R H, Maruoka, E M, Turck, C W, Griswold-Prenner, I. and Derynck, R (1997) J Biol. Chem 272, 14850–14859
16 Hoekstra, M F, Dhillon, N, Carmel, G, DeMaggio, A J, Lindberg, R. A., Hunter, T and Kuret, J. (1994) Mol Biol Cell **5**, 877–886
17 Garrett, S. and Broach, J (1989) Genes Dev **3**, 1336–1348
18 Tejedor, F, Zhu, X. R, Kaltenbach, E, Ackermann, A, Baumann, A., Canal, I, Heisenberg, M, Fischbach, K. F and Pongs, O (1995) Neuron **14**, 287–301
19 Kentrup, H, Becker, W, Heukelbach, J, Wilmes, A, Schurmann, A, Huppertz, C, Kainulainen, H and Joost, H-G (1996) J Biol Chem. **271**, 3488–3495
20 Becker, W, Weber, Y, Wetzel, K, Eirmbter, K, Tejedor, F J and Joost, H-G (1998) J Biol Chem **273**, 25893–25902
21 Souza, G M, Lu, S and Kuspa, A (1998) Development **125**, 2291–2302
22 Garrett, S., Menold, M M and Broach, J R (1991) Mol Cell. Biol **11**, 4045–4052
23 Smith, A, Ward, M. P and Garrett, S (1998) EMBO J **17**, 3556–3564
24 Mumberg, D, Muller, R and Funk, M (1994) Nucleic Acids Res **22**, 5767–5768
25 Sherman, F. (1991) Methods Enzymol **194**, 3–21
26 Gietz, D, St Jean, A, Woods, R A and Schiestl, R M (1992) Nucleic Acids Res **20**, 1425–1431
27 Joyal, J L, Annan, R S, Huddleston, M J, Carr, S A, Hart, M. J and Sacks, D B (1997) J. Biol Chem **272**, 15419–15425
28 Posewitz, M C and Tempst, P (1999) Anal Chem **71**, 2883–2892
29 Annan, R S and Carr, S. A (1996) Anal Chem **68**, 3413–3421
30 Verma, R, Annan, R S, Huddleston, M J, Carr, S. A, Reynard, G and Deshaies, R J (1997) Science, **278**, 455–560

Biochem. J. (2000) **348**, 273–280 (Printed in Great Britain)

Tyrosine phosphorylation of the vascular endothelial-growth-factor receptor-2 (VEGFR-2) is modulated by Rho proteins

Denis GINGRAS[1], Sylvie LAMY[1] and Richard BÉLIVEAU[2]

Laboratoire de Médecine Moléculaire Hôpital Sainte-Justine-UQAM, C.P. 8888, Succ. Centre-ville, Montréal, Québec, Canada H3C 3P8

The effects of Rho-specific modifying toxins on the tyrosine phosphorylation of endothelial cell proteins were investigated. Incubation of the cells with the Rho-activating toxin cytotoxic necrotizing factor 1 (CNF1) induced a marked increase in the tyrosine phosphorylation of a number of signalling intermediates of the vascular endothelial growth factor (VEGF)-mediated cascade, including focal adhesion kinase, paxillin, phospholipase Cγ1 and a Shc-associated protein of 195 kDa. Both CNF1- and VEGF-dependent tyrosine phosphorylation of these proteins were significantly reduced by prior incubation with C3 transferase, a known inhibitor of RhoA function, suggesting a Rho-dependent mechanism. The stimulation of endothelial cells with CNF1 resulted in a marked increase in the tyrosine phosphorylation of the VEGF receptor (VEGFR)-2, which was correlated with a stimulation of its kinase activity and with its association with downstream tyrosine phosphorylated proteins. The stimulatory effect of CNF1 was specific for VEGFR-2 since the phosphotyrosine content of VEGFR-1 was not affected by the toxin. Transient overexpression of a dominant-active RhoA mutant also induced an increase in the tyrosine phosphorylation of the VEGFR-2, whereas overexpression of a dominant-inactive form of the protein was without effect. Taken together, these results indicate that Rho proteins may play an important role in angiogenesis by modulating the tyrosine phosphorylation levels of VEGFR-2.

Key words: angiogenesis, signal transduction, VEGF

INTRODUCTION

Angiogenesis, the formation of new capillary blood vessels from pre-existing vessels, is a tightly regulated phenomenon that plays essential roles in reproductive functions, wound healing and embryonic development [1]. However, angiogenesis may become pathological when capillary growth is uncontrolled and the resulting excessive neovascularization may then sustain the development of a number of pathologies including retinopathies, haemangiomas, rheumatoid arthritis, psoriasis and tumour growth [1]. In the latter, it is now clearly established that the aggressive growth of tumours and of their metastases is strictly dependent on angiogenesis [2], suggesting that the inhibition of angiogenesis may represent an effective approach for blocking tumour progression. This hypothesis has been strengthened by the recent demonstration that administration of angiogenesis inhibitors to mice bearing human tumours results in tumour regression [3].

The vascular endothelial growth factor (VEGF) is an endothelial-specific mitogen that is often associated with the activation of tumour-induced angiogenesis. In tumours, VEGF secretion is upregulated by hypoxia [4] and by oncogenes such as *ras* and *src* [5]. At the endothelial cell surface, the secreted protein binds with high affinity to at least two distinct vascular endothelial growth factor receptors (VEGFRs), VEGFR-1, also known as *fms*-like tyrosine kinase (Flt-1) and VEGFR-2, also known as fetal liver kinase (Flk-1) [6]. VEGFR-2 expression in adult endothelial cells appears to account for most of the mitogenic and chemotactic effects of VEGF [7]. At the post-receptor level, activation of endothelial cells by VEGF leads to the autophosphorylation of VEGFR-2 and the subsequent tyrosine phosphorylation of numerous downstream targets, including the second messenger-producing enzymes phospholipase Cγ and phosphoinositide 3-kinase [8,9], p120GAP [8], the adaptor proteins Nck, Grb2 and Shc [8,10], the growth-factor receptor-associated tyrosine phosphatases SHP1 and SHP2 [10], as well as the cytoskeleton-associated proteins $p125^{FAK}$ (where FAK is focal adhesion kinase) and paxillin [11]. The factors involved in the regulation of this VEGF-induced signalling cascade and its overall significance in the numerous biological functions associated with the stimulation of endothelial cells by VEGF, however, remain obscure and additional proteins involved in this signal transduction pathway are likely to exist.

Rho proteins represent a family of monomeric GTPases that play essential roles in all eukaryotic cells studied to date. These proteins act as molecular switches by cycling between active, GTP-bound, and inactive, GDP-bound, states; the cycling between these two states being controlled by a complex network of regulatory proteins [12]. In their active state, Rho proteins interact with a number of downstream targets, leading to the reorganization of the actin cytoskeleton and to cell-cycle progression [13]. The control of these cellular pathways by Rho is of crucial importance for cell adhesion, movement and for a number of morphogenetic processes [12,13].

In the present study, we provide evidence that Rho proteins may also play an important role in other aspects of the signalling pathways triggered by growth factor receptors. We show that in bovine aortic endothelial cells (BAEC), activation of RhoA is both necessary and sufficient to induce the VEGF signalling cascade, possibly by increasing the tyrosine phosphorylation

---

Abbreviations used: BAEC, bovine aortic endothelial cells; CNF1, cytotoxic necrotizing factor 1 from *Escherichia coli*; DMEM, Dulbecco's modified Eagle's medium; FAK, focal adhesion kinase; Tyr(P), phosphotyrosine; VEGF, vascular endothelial growth factor; VEGFR, vascular endothelial growth factor receptor; RhoAQ63L, RhoA mutant with glutamine-63 substituted with leucine; PDGF, platelet-derived growth factor.

[1] These authors contributed equally to this work.

[2] To whom correspondence should be addressed (e-mail molmed@justine.umontreal.ca).

levels and kinase activity of the VEGFR-2. These results may have important implications for our understanding of the regulatory mechanisms underlying tumour angiogenesis.

EXPERIMENTAL

Materials

The commercial sources of antibodies used in this study are as follows: agarose-conjugated and unconjugated anti-phosphotyrosine [Tyr(P)] PY20 and anti-paxillin were from Transduction Laboratories; anti-p125^{FAK}, anti-VEGFR-2 (C-terminal), anti-VEGFR-1 and anti-c-Myc (9E10) were from Santa Cruz Biotechnology; anti-phospholipase Cγ and anti-Shc were from Upstate Biotechnology. Human recombinant VEGF was obtained from R&D Systems. The VEGFR-2 tyrosine kinase inhibitor, SU1498, was purchased from Calbiochem.

Cell culture

BAEC were kindly provided by Dr R. Sauvé (University of Montréal, Montreal, Canada). The cells were maintained in Dulbecco's modified Eagle's medium (DMEM) containing 10 % (v/v) bovine fetal serum (HyClone Laboratories), 100 units/ml penicillin, 100 μg/ml streptomycin and were used between passages 17–21. For experimental purposes, cells were plated on Nunc 33-mm 6-well plastic dishes at 10^6 cells/dish and grown to confluence in a humidified atmosphere of 5 % CO_2 and 90 % air at 37 °C. COS-7 and U-87 cell lines were purchased from the American Tissue Culture Collection and were maintained in minimal essential medium (MEM) containing 10 % (v/v) fetal bovine serum.

Purification of recombinant bacterial toxins

The prokaryotic expression vector pGEX-2T containing the cDNA encoding C3 transferase from *Clostridium botulinum* (gift of Dr A. Hall, University College London, London, U.K.) and the pQE-30 vector containing the cDNA encoding the cytotoxic necrotinizing factor (CNF) 1 from *Escherichia coli* (gift of Dr H. Lockman, Uniformed Services University, Bethesda, MD, U.S.A.) were inserted into *E. coli* strain BL21, and fusion proteins were purified from isopropyl-β-D-thiogalactopyranoside-induced exponential-phase bacterial cultures by standard procedures. For C3 transferase, the glutathione *S*-transferase moiety of the fusion protein was removed by incubating the glutathione–Sepharose beads (1 ml) overnight at room temperature with 50 units of thrombin protease (Pharmacia). Contaminating thrombin that was eluted with the recombinant C3 protein was removed by a 1-h incubation of the eluate with 5 μl of *p*-aminobenzamidine-linked agarose beads (Sigma). CNF1 was purified to apparent homogeneity by affinity chromatography on Ni-NTA–Sepharose beads (Qiagen).

VEGF stimulation of BAEC

BAEC grown to confluence were rendered quiescent by a 24-h incubation in serum-free DMEM. The cultures were washed twice with the same medium and incubated for 1 min at 37 °C in 2 ml of serum-free DMEM containing 1 nM of human recombinant VEGF (R&D Systems). After VEGF treatment, cells were washed once with PBS containing 1 mM vanadate and incubated in the same medium for 1 h at 4 °C. The cells were solubilized on ice in lysis buffer [150 mM NaCl, 10 mM Tris/HCl, pH 7.5, 1 mM EDTA, 0.5 % (v/v) Nonidet P40, 1 % (v/v) Triton X-100] containing 1 mM vanadate. The cells were then scraped from the culture dishes and the resulting lysates were clarified by centrifugation at 10000 ***g*** for 10 min. Protein concentrations were determined by the bicinchoninic acid (BCA) method (Pierce).

Toxin treatments

For incubation of the cells with CNF1, confluent BAEC cultures were washed twice with serum-free DMEM and incubated in 2 ml of DMEM containing 1 μg/ml of purified CNF1. The cells were incubated at 37 °C for 6 h in the presence of the toxin and subsequently solubilized in lysis buffer as described above. To study the effect of SU1498 on the CNF1-induced tyrosine phosphorylation, the inhibitor was added to the cells 1 h before the toxin. For pretreatment of the cells with C3 transferase, confluent cells were washed twice with serum-free DMEM and incubated for 24 h in 2 ml of the same medium containing 50 μg/ml of purified C3 transferase. The medium was aspirated and the cells were processed for VEGF stimulation as described above. The efficiency of ADP-ribosylation of RhoA by C3 transferase in these conditions was determined by monitoring the *in vitro* C3 transferase-catalysed [^{32}P]NAD incorporation into the protein, as described previously [14]. Briefly, lysates (15 μg) were incubated in a mixture containing 100 mM Tris/HCl, pH 8.0, 10 mM thymidine, 5 mM $MgCl_2$, 10 μM [^{32}P]NAD (2 μCi) (Dupont NEN) and 5 μg/ml of C3 transferase. The mixture was incubated at 30 °C for 1 h and the reaction was terminated by the addition of 5-fold concentrated Laemmli sample buffer. The samples were subjected to SDS/PAGE on a 12.5 % polyacrylamide gel and the incorporated radioactivity was revealed by autoradiography. The efficiency of the CNF1-catalysed deamidation of RhoA was estimated by the observation of a slight shift in its electrophoretic migration on a 15 % polyacrylamide gel [15].

Immunoprecipitation and immunoblotting procedures

For the immunoprecipitation studies, similar amounts of proteins from each sample (usually 50 μg) were clarified by a 1 h incubation at 4 °C with a mixture of Protein A/Protein G–Sepharose beads. Following the removal of the Sepharose beads by low-speed centrifugation, the supernatants were transferred to fresh tubes and incubated in lysis buffer overnight at 4 °C in the presence of 1–4 μg/ml of specific antibodies. With the exception of the agarose-conjugated anti-Tyr(P) monoclonal antibody, the immune complexes were collected by incubating the mixtures with 25 μl (50 % suspension) of either Protein A–Sepharose beads (for rabbit polyclonal antibodies) or Protein G–Sepharose beads (for mouse IgG_1 monoclonal antibodies). Non-specific bound proteins were removed by washing the beads three times in 1 ml of lysis buffer, and bound material was solubilized in 25 μl of 2-fold concentrated Laemmli sample buffer, boiled for 4 min and analysed by Western blotting, as described below.

Samples were separated by SDS/PAGE (7.5 % gel) and electroblotted on to PVDF membranes using standard procedures. The membranes were blocked overnight in Tris-buffered saline (147 mM NaCl, 20 mM Tris/HCl, pH 7 5) containing 2 % (w/v) BSA and probed with primary antibodies for 2 h at room temperature. Immunoreactive bands were visualized after a 1-h incubation with horseradish-peroxidase-conjugated anti-mouse or anti-rabbit antibodies (Jackson Immunoresearch Laboratories), followed by enhanced chemiluminescence (Amersham). In some cases, the immunoreactive bands were quantified by scanning densitometry (Molecular Dynamics).

Immune complex kinase assay *in vitro*

Precleared cell lysates (100 μg) were incubated overnight with anti-VEGFR-2 antibodies and the resulting immune complexes were collected using Protein A–Sepharose beads as described above. The beads were washed three times with lysis buffer, followed by two additional washes with kinase buffer (50 mM Hepes, pH 7.5, 10 mM $MnCl_2$, 1 mM dithiothreitol). The beads were then incubated for 5 min at room temperature in 25 μl of kinase buffer containing 5 μCi of [γ-^{32}P]ATP (ICN Biochemicals) and the reactions were stopped by the addition of 5-fold concentrated Laemmli sample buffer. After electrophoresis on 7.5 % polyacrylamide gels, the gels were incubated for 30 min in 2.5 % glutaraldehyde and incubated at 55 °C for 1 h in 1 M KOH to remove serine-bound phosphate. The resulting gels were washed extensively in methanol/acetic acid (4:1, v/v) and exposed to Fuji films.

Overexpression of RhoA mutants

BAEC (70 % confluent) were transfected with 1 μg of insertless vector (pcDNA3), pcDNA3–c-Myc–RhoAQ63L (dominant-active RhoA mutant where Gln-63 is substituted with Leu) or pcDNA3–c-Myc–RhoAQ63LC190R (dominant-active but non-isoprenylable RhoA mutant) (gifts from W. Moolenaar) using the Fugene6 transfection reagent (Roche Molecular Biochemicals). After 24 h of transfection, cells were lysed as described above and the Tyr(P) content of the VEGFR was determined by immunoprecipitation with anti-VEGFR-2 antibodies followed by immunodetection with the anti-Tyr(P) monoclonal antibody. The levels of overexpressed RhoA mutants in the transfected cells were determined in parallel experiments by immunoblotting the cell lysates with an anti-Myc epitope monoclonal antibody (9E10).

RESULTS

Rho-modifying toxins modulate tyrosine phosphorylation of endothelial cell proteins

VEGF is an endothelial-cell-specific mitogen which is known to induce an increase in the tyrosine phosphorylation of a number of endothelial cell proteins [7–11]. Under our experimental conditions, the addition of VEGF (1 nM) to quiescent BAEC promoted a rapid but transient increase in the tyrosine phosphorylation of a number of endothelial cell proteins, as detected by immunoblotting of anti-Tyr(P) immunoprecipitates (Figure 1A). The tyrosine phosphorylation was maximal at 1 min and rapidly returned to basal levels at longer incubation times. The induction of tyrosine phosphorylation by VEGF, measured under these conditions, was highly reproducible but the extent of stimulation was variable, ranging from 2- to 5-fold.

The effect of the Rho-specific activating toxin, CNF1, on the pattern of tyrosine phosphorylation of these endothelial cell proteins was examined. Quiescent cultures of BAEC were incubated with 1 μg/ml of the recombinant protein for various periods of time and the resulting increase in the amount of tyrosine phosphorylated proteins was monitored, as described in the Experimental section. As shown in Figure 1(B), incubation of the cells in the presence of CNF1 markedly stimulated the tyrosine phosphorylation of cellular proteins in a time-dependent manner. The stimulatory action of CNF1 was preceded by a 2 h-lag period, possibly reflecting its uptake and activation by the endothelial cells [16], and was maximal at 4–8 h and progressively declined at longer incubation times. A similar bell-shaped activation of the tyrosine phosphorylation of fibroblast proteins by CNF1 has been reported [16], and possibly represents an intrinsic feature of the toxin. This CNF1-induced tyrosine phosphorylation was correlated with a decrease in the electrophoretic mobility of RhoA, but not of Cdc42, suggesting the specific modification of RhoA by the toxin (Figure 1C) [15]. Moreover, the endogenous amount of Rho was not altered by CNF1, eliminating the possibility that the stimulatory effect of the toxin was related to an upregulation of RhoA in the cells. Interestingly, this stimulatory effect of CNF1 was several fold higher in endothelial cells than in other cell types. For example, incubation of either COS-7 or glioblastoma U87 cells with CNF1 under conditions resulting in maximal phosphorylation of endothelial cell proteins (6 h) had negligeable effect on the tyrosine phosphorylation of cellular proteins (Figure 1D). Overall, these results suggest that CNF1 is a very potent and specific inducer of tyrosine phosphorylation of endothelial cell proteins.

We next examined whether the inhibition of Rho by C3 transferase could affect the stimulation of tyrosine phosphorylation triggered by VEGF and CNF1. By contrast with CNF1, C3 does not readily enter into cells [17], and we first determined the C3 concentration that would result in a significant modification of endogenous Rho proteins. Quiescent BAEC were starved for 24 h in the presence of increasing concentrations of C3 transferase (0–50 μg/ml) and the resulting cell lysates were subjected to ADP-ribosylation *in vitro* using [^{32}P]NAD as the ribose donor. As shown in Figure 2(A), lysates from cells cultured in the presence of the toxin showed a concentration-dependent decrease in the level of [^{32}P]-labelled Rho (80 % inhibition at 50 μg/ml), indicating prior endogenous ADP-ribosylation.

Incubation of the cells with C3 transferase had a moderate effect on the basal Tyr(P) content of endothelial cell proteins, with the notable exception of a 68-kDa protein, the phosphorylation of which was sensitive to the toxin (Figure 2B). The addition of VEGF or CNF1 to BAEC promoted an increase (2-fold) in the tyrosine phosphorylation of endothelial cell proteins but their stimulatory effects were significantly reduced by prior incubation of the cells with C3 transferase (Figure 2B). Densitometric scanning of a number of gels from different cell preparations indicated that the inhibitory effect of C3 on both CNF1- and VEGF-induced tyrosine phosphorylation was 60 ± 9 % ($n = 8$). These results suggest that the stimulation of tyrosine phosphorylation of endothelial cell proteins by VEGF and CNF1 involves Rho proteins.

CNF1 stimulates the tyrosine phosphorylation of signalling intermediates

VEGF has been shown to stimulate the tyrosine phosphorylation of a number of signalling intermediates [7–11]. To determine whether the substrates phosphorylated, following stimulation of the cells with VEGF, were the same as those in which phosphorylation was increased by CNF1 or decreased following C3 treatment, lysates from cells stimulated with VEGF or from cells preincubated in the presence of the toxins were immunoprecipitated with antibodies directed against proteins that were previously reported to be tyrosine phosphorylated upon stimulation of endothelial cells with VEGF. Using this procedure, p125^{FAK}, paxillin, phospholipase Cγ and a Shc-associated protein of 195 kDa were identified as major substrates phosphorylated in response to VEGF (Figure 3, left and middle panels). Pretreatment of the cells with C3 abolished the VEGF-induced increase of tyrosine phosphorylation of these proteins, with the notable exception of phospholipase Cγ, in which tyrosine phosphorylation was less sensitive to C3 treatment. Interestingly, incubation of the cells with CNF1 stimulated the tyrosine

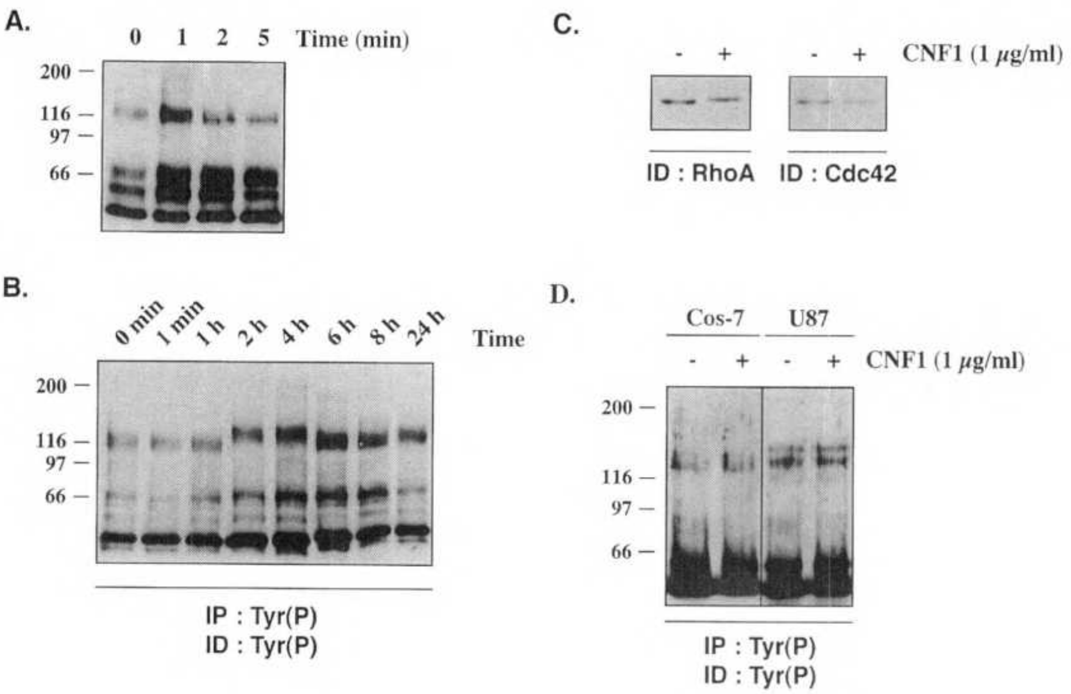

Figure 1 VEGF and CNF1 induce tyrosine phosphorylation of endothelial cell proteins

(**A**) Time course of VEGF-induced tyrosine phosphorylation. Serum-starved quiescent BAEC were incubated in serum-free medium in the presence of 1 nM of recombinant VEGF for the indicated times, and the extent of tyrosine phosphorylation was determined by immunoprecipitation with anti-Tyr(P) followed by immunoblotting with the same antibody. The results are representative of five experiments performed on different cell preparations. Molecular-mass markers (kDa) are shown on the left. (**B**) Effect of CNF1 on the tyrosine phosphorylation of BAEC proteins. Quiescent BAEC were incubated in serum-free medium with 1 μg/ml of recombinant CNF1 for the indicated times. Tyrosine phosphorylated proteins were identified by immunoprecipitation and immunoblotting with the anti-Tyr(P) monoclonal antibody. The results are representative of three experiments performed on different cell preparations. Molecular-mass markers (kDa) are shown on the left. (**C**) Modification of endogenous RhoA by CNF1. Lysate proteins from control cells and from cells incubated for 6 h in the presence of 1 μg/ml of CNF1 were separated on 12.5% polyacrylamide gels and electroblotted on to PVDF membranes. The resulting membranes were probed with anti-RhoA or anti-Cdc42 antibodies. The results are representative of two experiments performed on different cell preparations. (**D**) Specificity of CNF1 action. COS-7 and U87 glioblastoma cells were serum-starved and incubated for 6 h with 1 μg/ml of CNF1. The extent of tyrosine phosphorylation was monitored as described above. The results are representative of two experiments performed on different cell preparations. Molecular-mass markers (kDa) are shown on the left. ID, immunodetection; IP, immunoprecipitation.

phosphorylation of the same proteins (Figure 3, right and middle panels). These results strongly support the notion that Rho proteins play a major role in the tyrosine phosphorylation events triggered by VEGF.

Involvement of VEGFR-2 in CNF1-induced tyrosine phosphorylation

It is now clearly established that the mitogenic effects of VEGF on endothelial cells are related to its specific binding to the Flk receptor tyrosine kinase, VEGFR-2 [6,7,18]. By analogy with other growth factor receptors with intrinsic tyrosine kinase activities, stimulation of VEGFR-2 induces intramolecular tyrosine autophosphorylation of the receptor and subsequent association of the receptor with downstream signalling proteins [6,7,18]. We thus examined if the Rho-specific toxins could exert their effect by directly modulating the Tyr(P) content of the VEGFR-2. Lysates from treated BAEC were immunoprecipitated with anti-VEGFR-2 antibodies and the tyrosine phosphorylation of the receptor and its associated tyrosine phosphorylated proteins was examined by immunoblotting with anti-Tyr(P) antibodies. As expected, stimulation of the cells with VEGF markedly increased the amount of Tyr(P) associated with the 205-kDa VEGFR-2 protein as well as that of several tyrosine phosphorylated proteins that co-immunoprecipitated with the receptor (Figure 4A, left panel). This VEGF-dependent tyrosine phosphorylation of the receptor and of its associated proteins was, however, significantly decreased by preincubation of the cells with C3 transferase prior to stimulation with VEGF. By contrast, immunoprecipitation of VEGFR-2 from cells incubated in the presence of CNF1 showed that the toxin promoted a major increase in the Tyr(P) content of the receptor as well as its association with a number of tyrosine phosphorylated proteins (Figure 4A, left panel). The pattern of tyrosine phosphorylated proteins associated with VEGFR-2 immunoprecipitated from VEGF- and CNF1-stimulated cells was strikingly similar, with the notable exception of a 130-kDa phosphoprotein that appeared to be preferentially associated with VEGFR-2 in CNF1-treated cells.

To determine whether the increase in the phosphorylation of VEGFR-2 induced by CNF1 resulted in a stimulation of its kinase activity, anti-VEGFR-2 immunoprecipitates from control and treated cells were subjected to *in vitro* kinase assays. As shown in Figure 4(A) (right panel), immunoprecipitates from both CNF1- and VEGF-stimulated cells showed a marked increase in the radiolabelling of VEGFR-2 and its associated proteins, indicating that both treatments increased the kinase activity of the receptor. The increase in kinase activity of VEGFR-2 induced by VEGF was however significantly less in immunoprecipitates from C3-treated cells.

We next compared the stimulatory effect of CNF1 on the Tyr(P) content of VEGFR-2 with that of another VEGF receptor,

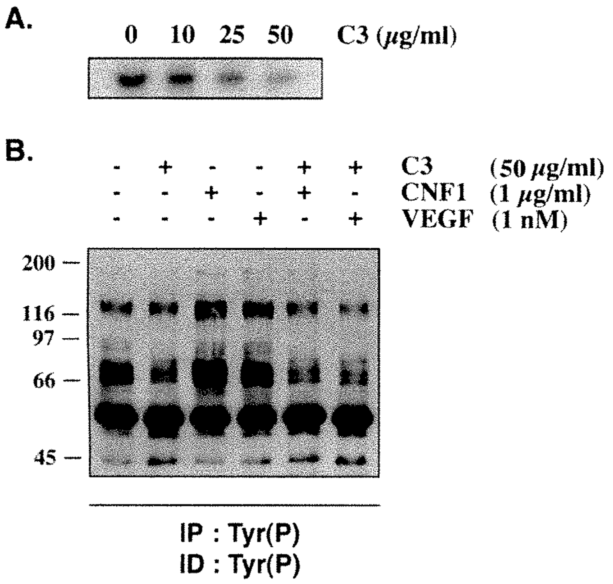

Figure 2 Effect of C3 transferase on the VEGF- and CNF1-induced tyrosine phosphorylation of BAEC proteins

(**A**) ADP-ribosylation of Rho. BAEC were incubated for 24 h in serum-free medium in the absence or in the presence of the indicated concentrations of C3 transferase (C3). The resulting cell lysates were ADP-ribosylated *in vitro*, separated by SDS/PAGE and the incorporated radioactivity was revealed by autoradiography. (**B**) BAEC were serum-starved in the absence or in the presence of 50 µg/ml of purified C3 transferase, followed by incubation of the cells with 1 nM VEGF or 1 µg/ml of CNF1. The resulting tyrosine phosphorylation of endothelial cell proteins was determined as described in the legend to Figure 1. The results are representative of five experiments performed on different cell preparations. ID, immunodetection; IP, immunoprecipitation.

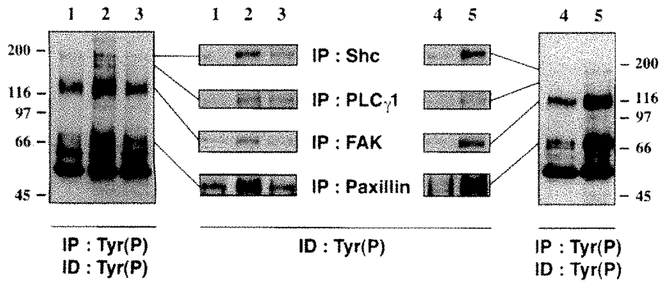

Figure 3 Identification of tyrosine-phosphorylated proteins following treatment of BAEC with VEGF and CNF1

Quiescent BAEC were serum-starved for 24 h in the absence (lanes 1 and 2) or in the presence of C3 transferase (lane 3), followed by a 1-min incubation in the absence (lane 1) or in the presence of 1 nM of VEGF (lanes 2 and 3). In parallel experiments, BAEC were serum-starved for 6 h in the absence (lane 4) or in the presence (lane 5) of 1 µg/ml of CNF1. The corresponding cell lysates were subjected to immunoprecipitation (IP) with agarose-conjugated anti-Tyr(P) (left and right panels) or with the indicated antibodies (middle panel). The immune complexes were resolved by SDS/PAGE and immunodetected with the anti-Tyr(P) monoclonal antibody. The results are representative of two experiments performed on different cell preparations. ID, immunodetection; IP, immunoprecipitation; PLC, phospholipase C.

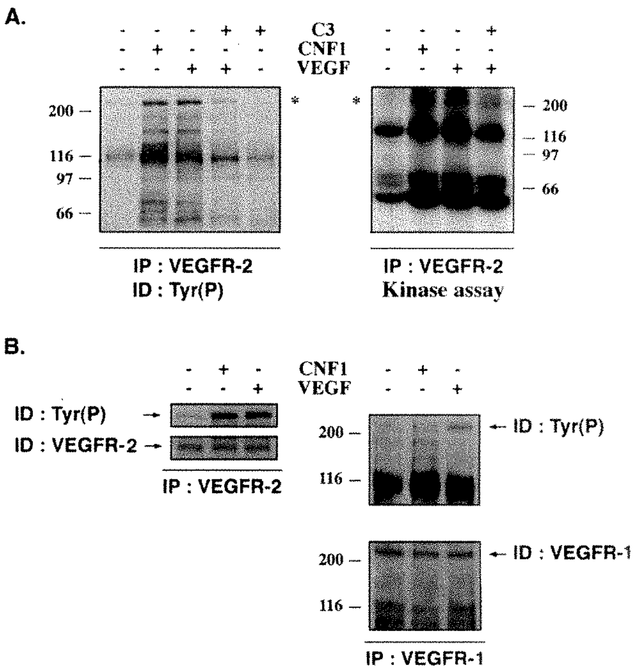

Figure 4 Effect of Rho-specific toxins on the Tyr(P) content of the VEGFR-2 and its associated proteins

(**A**) Left panel: BAEC were incubated with the Rho-specific toxins and VEGF as described in the legends to Figures 1 and 2. The resulting lysates were incubated with polyclonal antibodies raised against the VEGFR-2 and the immune complexes were subjected to SDS/PAGE, followed by immunoblotting with anti-Tyr(P) monoclonal antibody. The results are representative of three experiments performed on different cell preparations. Right panel: anti-VEGFR-2 immunoprecipitates (IP) from control and treated cells were subjected to an *in vitro* kinase assay. Samples were separated by SDS/PAGE, followed by treatment with KOH and autoradiography. The position of VEGFR-2 is indicated by asterisks. The results are representative of two experiments performed on different cell preparations. (**B**) Lysates from control and VEGF- and CNF1-treated cells were immunoprecipitated (IP) with antibodies against (ID) VEGFR-2 (upper panels) or VEGFR-1 (lower panel). The Tyr(P) content of the resulting immune complexes was monitored using the anti-Tyr(P) antibody. The results are representative of two experiments performed on different cell preparations. ID, immunodetection; IP, immunoprecipitation.

VEGFR-1. Lysates from CNF1- and VEGF-stimulated cells were subjected to immunoprecipitation with anti-VEGFR-2 or anti-VEGFR-1 antibodies and the Tyr(P) content of the receptors was revealed by immunoblotting with the anti-Tyr(P) antibody. As expected, VEGF promoted a marked increase in the tyrosine phosphorylation of both receptors, with 7- and 2.5-fold increases for VEGFR-2 and VEGFR-1 respectively (Figure 4B), in agreement with the higher stimulatory effect of VEGF on VEGFR-2 activity reported previously [7]. Interestingly, CNF1 also induced a 7-fold stimulation of the tyrosine phosphorylation of VEGFR-2, whereas it failed to significantly increase the Tyr(P) content of VEGFR-1 (1.1-fold stimulation) and of its associated proteins (Figure 4B, lower panel). The amounts of VEGFR-1 and VEGFR-2 in the immunoprecipitates were constant in all conditions, eliminating the possibility that changes in receptor levels could account for the observed effects. These data thus indicate that modulation of Rho activity by CNF1 triggers a specific modification of the Tyr(P) content of the VEGFR-2 protein that is correlated with an increase in its activity and with its association with downstream tyrosine phosphorylated proteins.

The participation of VEGFR-2 in the increase of tyrosine phosphorylation induced by CNF1 was further investigated by monitoring the effect of a rather specific VEGFR-2 kinase inhibitor, SU1498 [19], on the tyrosine phosphorylation of endothelial cell proteins. Cells were pretreated for 1 h in the presence of low concentrations of SU1498, followed by a 6-h incubation with CNF1. The resulting tyrosine phosphorylation of endothelial cell proteins was monitored by immuno-

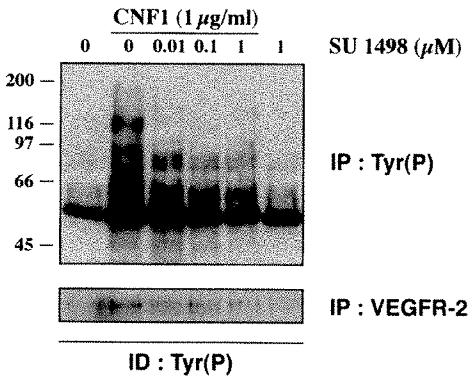

Figure 5 Inhibition of the CNF1-induced tyrosine phosphorylation by the VEGFR-2 inhibitor, SU1498

Quiescent BAEC were preincubated in serum-free medium for 1 h in the presence of vehicle (0) or of increasing concentrations of SU1498. The cells were subsequently incubated for 6 h with 1 μg/ml of CNF1 and the extent of tyrosine phosphorylation was determined following immunoprecipitation (IP) of the cell lysates with anti-Tyr(P) (upper panel) or anti-VEGFR-2 antibodies (lower panel). The results are representative of three experiments performed on different cell preparations. ID, immunodetection; IP, immunoprecipitation.

precipitation with the anti-Tyr(P) monoclonal antibody and with the anti-VEGFR-2 antibodies, as described above. As shown in Figure 5 (upper panel), preincubation of the cells with SU1498 resulted in a dose-dependent inhibition of the CNF1-induced tyrosine phosphorylation of BAEC proteins, but had no significant effect on the basal Tyr(P) content of the proteins, up to 1 μM. In these conditions, half-maximal inhibition of the CNF1-induced tyrosine phosphorylation was achieved at a concentration of approx. 0.1 μM, similar to that reported for the inhibition of the VEGF-dependent autophosphorylation of VEGFR-2 [19]. Moreover, the tyrosine phosphorylation of VEGFR-2 induced by CNF1 was inhibited to the same extent by this concentration of SU1498 (Figure 5, lower panel). These results thus strongly support the notion that the CNF1-induced stimulation of the tyrosine phosphorylation of endothelial cell proteins is related to an increase in the VEGFR-2 kinase activity.

The CNF1 toxin has been reported to act as an activator of RhoA, abolishing its GTPase activity by selective deamidation of glutamine-63 of the protein [15,20,21]. This residue is pivotal for Rho deactivation, since it is implicated in the binding of a water molecule required for hydrolysis of the GTP γ-phosphate, a process that is considerably accelerated by rhoGAP [22]. We thus examined whether overexpression of a dominant-active RhoA mutant (RhoAQ63L) could also affect the phosphorylation status of VEGFR-2. As shown in Figure 6(A), BAEC overexpressing RhoAQ63L showed an increase in tyrosine phosphorylation of the VEGFR when compared with cells transfected with the vector alone. This stimulatory effect of the RhoA mutant was much lower than that achieved using CNF1, possibly reflecting the low efficiency of gene transfection in endothelial cells [23]. Nevertheless, RhoAQ63L induced a 2-fold increase in the phosphorylation of the receptor and its association with phosphorylated proteins of 195 and 125 kDa (Figure 6A). Interestingly, the stimulatory effect of the overexpressed protein on the VEGFR-2 Tyr(P) content was abolished in cells overexpressing comparable levels of a non-isoprenylable homologue of RhoAQ63L, RhoAQ63LC190R. These results thus indicate that the stimulatory effect of CNF1 most likely occurs through its activation of RhoA GTPase, and that effective stimulation of the VEGFR-2 tyrosine phosphorylation requires the membrane localization of the protein.

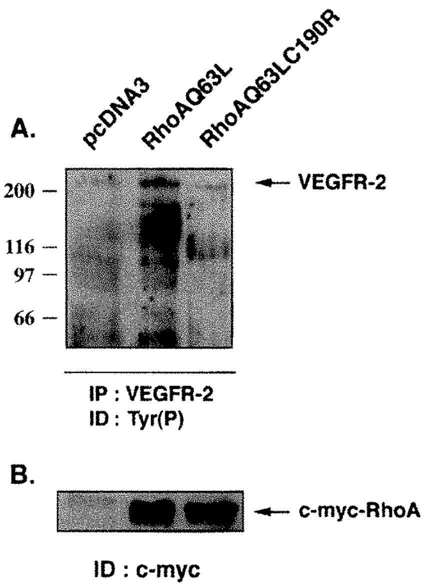

Figure 6 Effect of overexpressed RhoA mutants on the tyrosine phosphorylation of VEGFR-2

(**A**) Subconfluent BAEC were transfected with vector alone (pcDNA3) or vectors encoding the RhoAQ63L and RhoAQ63LC190R mutants. Following transfection, cells were lysed and the Tyr(P) content of the VEGFR-2 was monitored by immunoprecipitation (IP) with anti-VEGFR-2 polyclonal antibodies followed by immunoblotting (ID) with an anti-Tyr(P) monoclonal antibody. The results are representative of two experiments performed on different cell preparations. (**B**) Lysates from transfected cells (10 μg) were separated on 12% polyacrylamide gels and the levels of overexpressed RhoA mutants were determined by immunoblotting (ID) with a monoclonal antibody raised against the c-Myc epitope tag (9E10). ID, immunodetection; IP, immunoprecipitation.

DISCUSSION

The use of bacterial toxins that specifically target Rho proteins has been of crucial importance to our understanding of the key regulatory roles played by these proteins in cellular processes [24]. The recently identified CNF1 toxin is of particular interest since it specifically activates RhoA by the selective deamidation of glutamine-63 (RhoQ63) in the switch 2 domain of the protein [15,20,21]. This modification of RhoQ63 to RhoE63 by CNF1 blocks the intrinsic and GAP-stimulated hydrolysis of GTP [22], and thus results in the constitutive activation of Rho [20,21]. In addition, CNF1 readily enters cultured cells and, following its activation in the cytosol, induces changes in cell architecture that are indistinguishable from those observed following overexpression of the constitutively active form of this protein [15,17,20,21].

In the present work, we observed that the incubation of cultured BAEC with CNF1 markedly increased the tyrosine phosphorylation of a wide variety of endothelial cell proteins. An increase in the tyrosine phosphorylation of $p125^{FAK}$ and paxillin following treatment of fibroblasts and Chinese-hamster ovary cells with CNF1 has been reported [16,25], but to our knowledge our results using BAEC as a model represent the first evidence that CNF1 can stimulate the tyrosine phosphorylation of other key intermediates of growth factor-induced signalling cascades.

This CNF1-dependent increase in tyrosine phosphorylation is mediated by Rho proteins, since it was correlated with the modification of endogenous RhoA and was completely abolished by prior incubation of the cells with C3 transferase, a well-characterized inhibitor of Rho function. Moreover, immunoprecipitation experiments indicated that CNF1 stimulated the tyrosine phosphorylation of substrates of the VEGF-mediated signalling cascade, such as phospholipase $C\gamma$, $p125^{FAK}$, paxillin and a previously unidentified 195-kDa Shc-associated protein. The observation that CNF1 induced an increase in the tyrosine phosphorylation of these proteins, and C3 inhibited the VEGF-dependent phosphorylation of these substrates, strongly suggests that Rho proteins play a role in the endothelial cell response to VEGF.

We were interested to determine whether the increase in tyrosine phosphorylation induced by CNF1 could be related to activation of VEGFR-2 kinase activity, since it is well-established that autophosphorylation of VEGFR-2 on tyrosine residues represents the initial step of the VEGF-induced signalling cascade [7,18]. In this respect, we observed that the stimulation of BAEC with VEGF resulted in a marked increase in the tyrosine phosphorylation of VEGFR-2 and of a number of receptor-associated phosphorylated proteins, whereas phosphorylation of VEGFR-1 was stimulated to a much lesser extent by VEGF. Perhaps surprisingly, CNF1 induced an increase in the Tyr(P) content of VEGFR-2 and of its associated tyrosine phosphorylated proteins, which showed a striking similarity to that induced by VEGF, but pretreatment of the cells with C3 transferase inhibited the VEGF-dependent tyrosine phosphorylation of VEGFR-2. Furthermore, this increase in VEGFR-2 Tyr(P) content was correlated with an increase in kinase activity towards its associated proteins. The stimulatory effect of CNF1 on VEGFR phosphorylation was specific for VEGFR-2, as treatment of the cells with the toxin failed to increase the VEGFR-1 Tyr(P) content. The involvement of Rho proteins in the regulation of the VEGFR-2 tyrosine phosphorylation levels was also strengthened by the observation that the overexpression of a dominant-active RhoA mutant (RhoAQ63L) resulted in a similar increase in the VEGFR-2 tyrosine phosphorylation. Taken together, these results suggest that Rho proteins may represent a key intermediate in the signal transduction pathways involved in the response of endothelial cells to VEGF by modulating the activity of the most upstream component of this pathway.

Although receptor tyrosine kinase phosphorylation has been associated with ligand-induced dimerization and auto- or trans-phosphorylation of the receptors [26], other evidence has pointed to the existence of an equilibrium between monomeric and dimeric receptors in the absence of ligand [27]. In the case of VEGFR-2, monomeric forms of the extracellular domain of the receptor bind VEGF 100 times more weakly than its dimeric forms, suggesting a component with strong avidity for binding VEGF to predimerized forms of the receptor [28]. Moreover, NIH 3T3 cells overexpressing VEGFR-2 showed a higher proliferation rate in the absence of VEGF, suggesting that receptors have an intrinsic ability to dimerize in the absence of ligand [28]. It is thus possible that an unliganded but predimerized pool of VEGFR-2 is activated in a Rho-dependent manner, leading to the increase in phosphorylation of the receptor and the concomitant recruitment of tyrosine phosphorylated proteins observed in the present study.

The Rho-dependent pathways leading to VEGFR-2 phosphorylation and stimulation of its kinase activity remain to be characterized. The involvement of geranylgeranylated proteins in the modulation of growth-factor-receptor tyrosine phosphorylation activities has recently been suggested, based on the selective inhibition of the ligand-dependent tyrosine phosphorylation of both platelet-derived growth factor (PDGF) and epidermal growth factor ('EGF') receptors by inhibitors of isoprenylation [29] Since post-translational modification of Rho proteins by geranylgeranylation is essential for their association with cellular membranes and biological activities [12], the present results suggest that RhoA could represent the geranylgeranylated protein responsible for the control of the tyrosine phosphorylation activities of these receptors. This hypothesis is supported by our observation that the overexpression of a dominant-active but non-isoprenylable mutant of RhoA (RhoAQ63LC190R) failed to stimulate the tyrosine phosphorylation of VEGFR-2.

It has been demonstrated that RhoA associates physically with the PDGF receptor upon stimulation of the cells with PDGF [30], but we have been unable to detect a similar recruitment of RhoA to VEGFR-2 upon stimulation of endothelial cells with VEGF or CNF1 (D. Gingras and R. Béliveau, unpublished work). This suggests that additional proteins might induce the activation of the receptor either by inducing conformational changes in the protein or by directly phosphorylating specific tyrosine residues within the cytoplasmic tail of the receptor. In this context, it is noteworthy that recent studies have suggested that full activation of the VEGFR-2 and PDGF receptors involves the phosphorylation of multiple tyrosine residues within the receptors, possibly by other protein kinases [31,32].

In summary, our results suggest that Rho proteins play an important role in VEGFR-2 function by modulating the Tyr(P) content and kinase activity of the receptor. Further studies aimed at the identification of the Rho-dependent signalling pathways leading to the activation of VEGFR-2, and their involvement in the signalling cascade triggered by this angiogenic cytokine, may be of significant importance in the understanding of the mechanisms involved in tumour angiogenesis.

We are grateful to Dr A Hall, Dr H. Lockman and Dr W Moolenaar for their gifts of expression plasmids We thank Dr L Tremblay for her critical reading of the manuscript. This work was supported by grants from the Fondation Charles-Bruneau and from the Medical Research Council of Canada

REFERENCES

1 Folkman, J (1995) Angiogenesis in cancer, vascular, rheumatoid and other disease Nature Med **1**, 149–153

2 Hanahan, D and Folkman, J (1996) Patterns and emerging mechanisms of the angiogenic switch during tumorigenesis Cell **86**, 353–364

3 Boehm, T, Folkman, J., Browder, T and O'Reilly, M S (1997) Antiangiogenic therapy of experimental cancer does not induce acquired drug resistance Nature (London) **390**, 404–407

4 Levy, A P, Levy, N S and Goldberg, M A (1996) Post-transcriptional regulation of vascular endothelial growth factor by hypoxia J Biol Chem **271**, 2746–2753

5 Rak, J W, St Croix, B D and Kerbel, R S (1995) Consequences of angiogenesis for tumor progression, metastasis and cancer therapy Anti-Cancer Drugs **6**, 3–18

6 Thomas, K A (1996) Vascular endothelial growth factor, a potent and selective angiogenic agent J. Biol. Chem **271**, 603–606

7 Waltenberger, J, Claesson-Welsh, L, Siegbahn, A., Shibuya, M and Heldin, C.-H (1994) Different signal transduction properties of KDR and Flt1, two receptors for vascular endothelial growth factor J Biol Chem. **269**, 26988–26995

8 Guo, D, Jia, Q, Song, H-Y, Warren, R S and Donner, D B (1995) Vascular endothelial cell growth factor promotes tyrosine phosphorylation of mediators of signal transduction that contain SH2 domains Association with endothelial cell proliferation J Biol Chem **270**, 6729–6733

9 Xia, P, Aiello, L P., Ishii, H., Jiang, Z Y, Park, D J, Robinson, G S, Takagi, H., Newsome, W P, Jirousek, M R and King, G. L. (1996) Characterization of vascular endothelial growth factor's effect on the activation of protein kinase C, its isoforms, and endothelial cell growth J Clin Invest **98**, 2018–2026

10 Kroll, J. and Waltenberger, J. (1997) The vascular endothelial growth factor receptor KDR activates multiple signal transduction pathways in porcine aortic endothelial cells J Biol Chem **272**, 32521–32527

11 Abedi, H and Zachary, I (1997) Vascular endothelial growth factor stimulates tyrosine phosphorylation and recruitment to new focal adhesions of focal adhesion kinase and paxillin in endothelial cells J Biol Chem **272**, 15442–15451

12 Mackay, D J G and Hall, A (1998) Rho GTPases J Biol Chem **273**, 20685–20688

13 Hall, A (1998) Rho GTPases and the actin cytoskeleton. Science **279**, 509–514

14 Udagawa, T and McIntyre, B W (1996) ADP-ribosylation of the G protein Rho inhibits integrin regulation of tumor cell growth J Biol Chem. **271**, 12542–12548

15 Fiorentini, C , Fabbri, A., Flatau, G , Donelli, G , Matarrese, P , Lemichez, E., Falzano, L and Boquet, P (1997) *Escherichia coli* cytotoxic necrotizing factor 1 (CNF1), a toxin that activates the Rho GTPase J Biol Chem **272**, 19532–19537

16 Lacerda, H M , Pullinger, G D , Lax, A J and Rozengurt, E (1997) Cytotoxic necrotizing factor 1 from *Escherichia coli* and dermonecrotic toxin from *Bordetella bronchiseptica* induce p21(rho)-dependent tyrosine phosphorylation of focal adhesion kinase and paxillin in Swiss 3T3 cells J Biol Chem **272**, 9587–9596

17 Aktories, K (1997) Bacterial toxins that target Rho proteins J Clin Invest. **99**, 827–829

18 Neufeld, G , Cohen, T , Gengrinovitch, S and Poltorak, Z (1999) Vascular endothelial growth factor (VEGF) and its receptors FASEB J **13**, 9–22

19 Strawn, L M., McMahon, G., App, H , Schreck, R., Kuchler, W R , Longhi, M. P , Hui, T H , Tang, C , Levitzki, A , Gazit, A et al (1996) Flk-1 as a target for tumor growth inhibition Cancer Res **56**, 3540–3545

20 Schmidt, G , Sehr, P , Wilm, M , Selzer, J , Mann, M and Aktories, K (1997) Gln 63 of Rho is deamidated by *Escherichia coli* cytotoxic necrotizing factor-1 Nature (London) **387**, 725–729

21 Flatau, G , Lemichez, E , Gauthier, M , Chardin, P , Paris, S , Fiorentini, C. and Boquet, P (1997) Toxin-induced activation of the G protein p21 Rho by deamidation of glutamine Nature (London) **387**, 729–733

22 Rittinger, K , Walker, P A , Eccleston, J. F , Smerdon, S J and Gamblin, S J (1997) Crystal structure of a small G protein in complex with the GTPase-activating protein rhoGAP Nature (London) **388**, 693–698

23 Edgell, C. T , Curiel, D T , Hu, P C and Marr, H S (1998) Efficient gene transfer to human endothelial cells using DNA complexed to adenovirus particles BioTechniques **25**, 264–268

24 Fiorentini, C , Gauthier, M., Donelli, G and Boquet, P (1998) Bacterial toxins and the Rho GTP-binding protein what microbes teach us about cell regulation Cell Death Diff. **5**, 720–728

25 Defilippi, P , Venturino, M , Gulino, D , Duperray, A., Boquet, P , Fiorentini, C , Volpe, G , Palmieri, M , Silengo, L and Tarone, G (1997) Dissection of pathways implicated in integrin-mediated actin cytoskeleton assembly Involvement of protein kinase C, Rho GTPase, and tyrosine phosphorylation J Biol Chem **272**, 21726–21734

26 Klemm, J D , Schreiber, S L and Crabtree, G R (1998) Dimerization as a regulatory mechanism in signal transduction Annu Rev Immunol **16**, 569–592

27 Omura, T., Heldin, C-H and Ostman, A (1997) Immunoglobulin-like domain 4-mediated receptor-receptor interactions contribute to platelet-derived growth factor-induced receptor dimerization J Biol Chem **272**, 12676–12682

28 Fuh, G., Li, B , Crowley, C , Cunningham, B and Wells, J A (1998) Requirements for binding and signalling of the kinase domain receptor for vascular endothelial growth factor J Biol Chem **273**, 11197–11204

29 McGuire, T F , Qian, Y., Vogt, A , Hamilton, A D and Sebti, S M (1996) Platelet-derived growth factor receptor tyrosine phosphorylation requires protein geranylgeranylation but not farnesylation J Biol Chem **271**, 27402–27407

30 Zubiaur, M , Sancho, J , Terhorst, C and Faller, D. V (1995) A small GTP-binding protein, Rho, associates with the platelet-derived growth factor type-beta receptor upon ligand binding J Biol Chem **270**, 17221–17228

31 Baxter, R M , Secrist, J P , Vaillancourt, R. R. and Kazlauskas, A (1998) Full activation of the platelet-derived growth factor beta-receptor kinase involves multiple events J Biol Chem. **273**, 17050–17055

32 Kendall, R L., Rutledge, R Z , Mao, X , Tebben, A J , Hungate, R W and Thomas, K A (1999) Vascular endothelial growth factor receptor KDR tyrosine kinase activity is increased by autophosphorylation of two activation loop tyrosine residues J Biol Chem **274**, 6453–6460

Received 7 December 1999/10 February 2000; accepted 27 March 2000

Human Sug1/p45 is involved in the proteasome-dependent degradation of Sp1

Kaihong SU*, Xiaoyong YANG*, Mark D. ROOS*, Andrew J. PATERSON† and Jeffrey E. KUDLOW*†[1]
*Department of Cell Biology, University of Alabama at Birmingham, Birmingham, AL 35294, U.S.A., and †Department of Medicine, Division of Endocrinology and Metabolism, University of Alabama at Birmingham, Birmingham, AL 35294, U.S.A.

The transcription factor Sp1 was previously shown to undergo proteasome-dependent degradation when cells were glucose-starved and stimulated with the adenylate cyclase inducer, forskolin. However, the control of the Sp1 degradation process is largely unknown. Using *in vitro* and *in vivo* interaction studies, we show in the present study that Sp1 interacts with human Sug1 [hSug1, also known as p45 or thyroid-hormone-receptor interacting protein ('TRIP1')], an ATPase subunit of the 26 S proteasome and a putative transcriptional modulator. This interaction with Sp1 occurs through the C-terminus of hSug1, the region that contains the conserved ATPase domain in this protein. Both *in vitro* studies, in reconstituted degradation assays, and *in vivo* experiments, in which hSug1 is overexpressed in normal rat kidney cells, show that full-length hSug1 is able to stimulate the proteasome-dependent degradation of Sp1. However, hSug1 truncations that lack either the N- or C-terminal domain of hSug1 act as dominant negatives, inhibiting Sp1 degradation *in vitro*. Also, an ATPase mutant of hSug1, while still able to bind Sp1, acts as a dominant negative, blocking Sp1 degradation both *in vitro* and *in vivo*. These results demonstrate that hSug1 is involved in the degradation of Sp1 and that ATP hydrolysis by hSug1 is necessary for this process. Our findings indicate that hSug1 is an exchangeable proteasomal component that plays a critical regulatory role in the proteasome-dependent degradation of Sp1. However, hSug1 is not the factor limiting Sp1 degradation in the cells treated with glucosamine. This and other considerations suggest that hSug1 co-operation with other molecules is necessary to target Sp1 for proteasome degradation.

Key words: diabetes, glucosamine, glycosylation, O-GlcNAc, transcription.

INTRODUCTION

The transcription factor Sp1 is important for the expression of many cellular genes, particularly housekeeping genes [1]. Although Sp1 has generally been considered to constitutively regulate gene expression, its activity and cellular content have been shown to be regulated during a variety of cellular processes [2,3]. We have previously shown that Sp1 is rapidly degraded by the proteasome in cells that are both glucose-starved and stimulated with cAMP [4]. Under these conditions, protein modification of Sp1 and other cellular proteins by O-linked *N*-acetylglucosamine (O-GlcNAc) is markedly reduced. Conversely, treatment of cells with glucose or glucosamine results in increased levels of O-GlcNAc and blocks the cAMP-mediated degradation of Sp1. We have postulated that Sp1 degradation by the proteasome might be part of the cellular response to nutrient deprivation and stress. The loss of Sp1 would down-regulate general gene transcription to conserve nutrients.

The 26 S proteasome is a complex organelle that degrades certain proteins via an ATP-dependent proteolytic pathway [5–7]. There is considerable evidence that the proteasome plays an important role in the regulation of diverse cellular processes, such as gene transcription, cell cycle progression and metabolism [5]. The 26 S complex is composed of a 20 S proteolytically active core and a 19 S regulatory complex [8–10]. The 19 S complex is located at the end(s) of the 20 S core and provides the components necessary for selective degradation of proteins and regulation of the activity of 20 S proteases [11,12]. The ATP-dependence for proteolysis by the 26 S proteasome derives from the ATPase subunits in the 19 S complex. Thus far at least six distinct, but related, ATPases have been found in the 19 S complex of mammalian proteasomes: human Sug1 [hSug1, also known as p45 or thyroid-hormone-receptor interacting protein ('TRIP1')], S4 (also known as p56), MSS1, TBP1, TBP7, and p42 [13–18]. It is thought that ATP hydrolysis by these ATPases provides energy for the unfolding and translocation of the substrates to the lumen of the 20 S core and for the assembly of the 26 S proteasome [19]. It is not clear why proteasomes have multiple ATPases and whether there is functional specificity among them. However, in yeast, it has been shown that different proteasomal ATPases have well-differentiated functions [20,21], and mutations in individual ATPases can markedly reduce the degradation of some substrates, while not affecting others [22]. Thus the ATPases in the proteasome might participate in the recognition of distinct substrates [5].

hSug1, one of the six known mammalian proteasomal ATPases, is the human homologue of yeast Sug1 [23]. Sug1 has been identified as an integral component of the 26 S proteasome in that it co-purifies with the proteasome in both conventional and nickel-chelate affinity chromatography [18]. In yeast, mutations in Sug1 cause the accumulation of mitotic cyclins and cell cycle arrest in G2/metaphase [22]. The processing of nuclear factor-κB via the ubiquitin–proteasome pathway is inhibited when this protein is expressed in yeast with Sug1 mutations [24].

Abbreviations used: AAA, ATPase associated with a variety of cellular activities; C.Sug1, C-terminal domain of human Sug1; DMEM, Dulbecco's modified Eagle's medium; DTT, dithiothreitol; FBS, fetal bovine serum; GST, glutathione S-transferase; hSug1, human Sug1; hSug1mk, ATPase mutant of hSug1; LLnL, *N*-acetyl-Leu-Leu-norLeu-al; N.Sug1, N-terminal domain of hSug1; NRK, normal rat kidney; O-GlcNAc, O-linked *N*-acetylglucosamine; RT, reverse transcription; Stat3, signal transducer and activator of transcription 3.

[1] To whom correspondence should be addressed (e-mail kudlow@endo.dom.uab.edu)

Besides being a proteasome component, Sug1 has also been shown to interact with transcription factors and to be involved in the regulation of transcription. A yeast two-hybrid screen indicated that transcription factor c-Fos, also a known proteasome substrate, interacts with mammalian Sug1 [25]. Sug1 has been reported to mediate the association of transcriptional activators with the RNA polymerase II holoenzyme and to interact with the family members of nuclear receptors [26–29]. Recent evidence that Sug1 is a DNA helicase and that its ATPase activity is stimulated by RNAs supports the idea that Sug1 is involved in gene transcription [30,31]. How the activities of Sug1 as a transcriptional modulator and as a proteasome component can be reconciled is not clear. The observation that Sug1 is predominantly located in the nucleus implies a possible role for Sug1 in the degradation of transcription factors [25,32].

In the present study we report that hSug1 interacts with Sp1 protein both *in vitro* and *in vivo*. The C-terminal domain (amino acids 173–405) of hSug1 (C.Sug1) confers this interaction. Using an *in vitro* reconstituted degradation assay and an *in vivo* expression system, we show that wild-type hSug1 accelerates the proteasome degradation of Sp1, while inactivated mutant forms of hSug1 inhibit this Sp1 degradation. Our results provide direct evidence that hSug1 is involved in the degradation of at least one transcription factor, Sp1.

MATERIALS AND METHODS

Cell culture

Normal rat kidney (NRK) cells were grown in Dulbecco's modified Eagle's medium (DMEM) with 10 % (v/v) fetal bovine serum (FBS) with non-essential amino acids (Gibco BRL, Grand Island, NY, U.S.A.), 100 μg/ml penicillin (Sigma, St Louis, MO, U.S.A.) and 50 μg/ml gentamicin (Sigma), at 37 °C in air/CO_2 (93:7). For stimulation of the cells, exponentially growing cells were seeded at 2.5×10^6 cells/100 mm diameter dish. After overnight incubation, the cell culture medium was changed to glucose-free DMEM containing 10 % FBS, and the cells were incubated for an additional 20 h. The cells were then stimulated with vehicle alone, 100 μM forskolin or 5 mM glucosamine (Sigma) in glucose-free DMEM containing 10 % FBS, and incubation was continued for an additional 24 h before cells were harvested.

DNA constructs

The hSug1 cDNA was cloned and amplified by reverse-transcription (RT)-PCR from human breast cancer cell line MDA 468 mRNA using high-fidelity *Pfu* DNA polymerase (Stratagene, La Jolla, CA, U.S.A.). The PCR primers used to clone hSug1 cDNA were designed according to the hSug1 cDNA sequence. They were: 5′-primer, 5′-CGCGGATCCCCGATGGCGCTTG-ACGGACC-3′ and 3′-primer, 5′-CATAGGCCTTCACTTCCA-TAATTTCTTGATGG-3′. The N-terminal domain (amino acids 1–176) of hSug1 (N.Sug1) cDNA and C.Sug1 cDNA were cloned and amplified using the same strategy as that used for hSug1 full-length cDNA. The PCR primers used for N.Sug1 were: 5′-primer, 5′-CATGAATTCATGGCGCTTGACGGACCAG-3′ and 3′-primer, 5′-ATGCTCTAGACTTCGAAGAGCTCAGG-ATGC-3′. The PCR primers used for C.Sug1 were: 5′-primer, 5′-ATGCTCTAGAGAGCTCTTCGAAGCACTGG-3′ and the 3′-primer was the same as that used for cloning the full-length hSug1. The lysine residue at position 196 in hSug1 was converted to a methionine by site-directed mutagenesis to generate an ATPase mutant of hSug1 (hSug1mk). All the above constructs were confirmed by DNA sequencing.

Expression and purification of glutathione S-transferase (GST) fusion proteins in *Escherichia coli* and vaccinia virus

The GST fusion proteins were expressed in *E. coli* and purified on glutathione–Sepharose beads (Pharmacia, Piscataway, NJ, U.S.A.) according to Pharmacia's pGEX protocol. The GST fusion proteins expressed using recombinant vaccinia viruses were purified as described previously [33].

In vitro protein interaction assay

Equal quantities of the GST fusion proteins immobilized on glutathione–Sepharose affinity beads were washed extensively with binding buffer [50 mM KH_2PO_4 (pH 6.0), 100 mM KCl, 10 mM $MgCl_2$, 10 % (v/v) glycerol and 1 % (v/v) Tween-20]. The Promega *in vitro* transcription and translation ('TNT') kit from reticulocyte lysate was used as directed by the manufacturer to synthetically label Sp1 protein with [^{35}S]methionine. The labelled Sp1 (in 5 μl of reticulocyte lysate) was added to 5 μg of GST fusion proteins, immobilized on the glutathione beads. After incubation for 1 h at 4 °C the beads were washed extensively with the binding buffer and boiled in SDS/PAGE sample buffer. The proteins bound to the beads were then separated by SDS/PAGE. The ^{35}S-labelled proteins that had bound to the beads were visualized by fluorography, while the unlabelled GST fusion proteins were visualized following Coomassie Brilliant Blue staining of the gel.

The reconstituted degradation assay

Nuclear extract from differently treated NRK cells was prepared using the high salt extraction method described previously [33]. Vaccinia virus-expressed GST–hSug1, GST–hSug1mk, GST–N.Sug1, GST–C.Sug1 or GST were purified and eluted with 20 mM free glutathione. These GST proteins were preincubated with 50 μg of NRK nuclear extract at room temperature for 15 min in ATPase assay buffer containing 20 mM Tris/HCl (pH 7.5), 70 mM KCl, 1.5 mM $MgCl_2$ and 1.5 mM dithiothreitol (DTT). Vaccinia virus-expressed GST–Sp1 protein (10 ng) and 2 mM ATP were then added into the reaction mixture. Following incubation at 37 °C for 30 min, the reaction mixture was separated by SDS/PAGE and subjected to Western-blot analysis using anti-GST antibodies.

In vivo protein interaction assay

NRK cells were cultured in 5 mM glucose medium to 90 % confluency. The cells were infected with recombinant vaccinia viruses that allowed expression of the GST fusion proteins. After infection of NRK cells with recombinant viruses for 16–23 h, the cells were collected and resuspended in the whole-cell lysate buffer containing 20 mM Hepes (pH 7.9), 0.4 M NaCl, 3 mM $MgCl_2$, 0.5 % Nonidet P40, 0.2 mM EDTA, 0.2 mM EGTA, 10 % glycerol, 1 mM DTT, 1 mM PMSF, 5 μg/ml leupeptin and 5 μg/ml aprotinin. After incubation on ice for 10 min the cells were gently vortex-mixed for 10 s and centrifuged for 15 min at 16000 *g* at 4 °C. The supernatant was collected and designated as whole-cell lysate. Glutathione–Sepharose affinity beads were incubated with the whole-cell lysate for 2 h at 4 °C in the same buffer as above except that the concentration of NaCl was 150 mM. The beads were then collected and washed 4 times with the incubation buffer. The proteins bound to the beads were then separated by SDS/PAGE followed by Western-blot analysis.

RESULTS

Protein structure of hSug1 and the expression of hSug1 in *E. coli* and vaccinia virus

Structural analysis has identified hSug1 as a member of the AAA (ATPase associated with a variety of cellular activities) superfamily of putative ATPases [34]. As shown in Figure 1(A) the C-terminus of hSug1 contains a highly conserved ATPase domain ('CAD' or AAA domain). The N-terminus of hSug1 contains a putative coiled-coil structure whose function is still unknown. Recent evidence has shown that yeast and mammalian Sug1 are ATPases, and mutation of the lysine residue at position 196 eliminates their ATPase activity [30]. The lower panel in Figure 1(A) is a diagram showing the N-terminal domain (amino acids 1–176) and the C-terminal domain (amino acids 173–406) of hSug1 used in the present study. We cloned the cDNA of hSug1 by RT-PCR and expressed hSug1 as a GST fusion protein. As shown in Figure 1(B) GST–hSug1 was expressed with the correct molecular mass in mammalian cells using vaccinia virus (Figure 1B, lane 1) and in *E. coli* (Figure 1B, lane 2). GST expressed in *E. coli* is shown in Figure 1(B), lane 3.

hSug1 protein interacts with Sp1 *in vitro*

As an initial step to investigate whether hSug1 is involved in the degradation of Sp1, we first examined the potential for direct interaction between the hSug1 protein and the Sp1 protein. We performed *in vitro* binding studies using a GST pull-down assay. GST and GST–hSug1 fusion proteins were expressed in *E. coli* (Figure 2A). Equal amounts of GST or GST–hSug1 were immobilized on glutathione–Sepharose beads and incubated with *in vitro*-translated, [^{35}S]methionine-labelled human Sp1 (full-length Sp1). As shown in Figure 2(B), GST–hSug1 pulled down Sp1 (lane 2), while GST alone did not pull down Sp1 (lane 1). We observed the same results with vaccinia virus-expressed GST fusion proteins (results not shown). These results show that hSug1 specifically interacts with Sp1 *in vitro*.

C.Sug1 and hSug1mk interact with Sp1 efficiently *in vitro*

To determine which domain of hSug1 interacts with Sp1 we expressed C.Sug1 and N.Sug1 as GST fusion proteins in *E. coli* and tested their abilities to interact with Sp1 by *in vitro* protein-

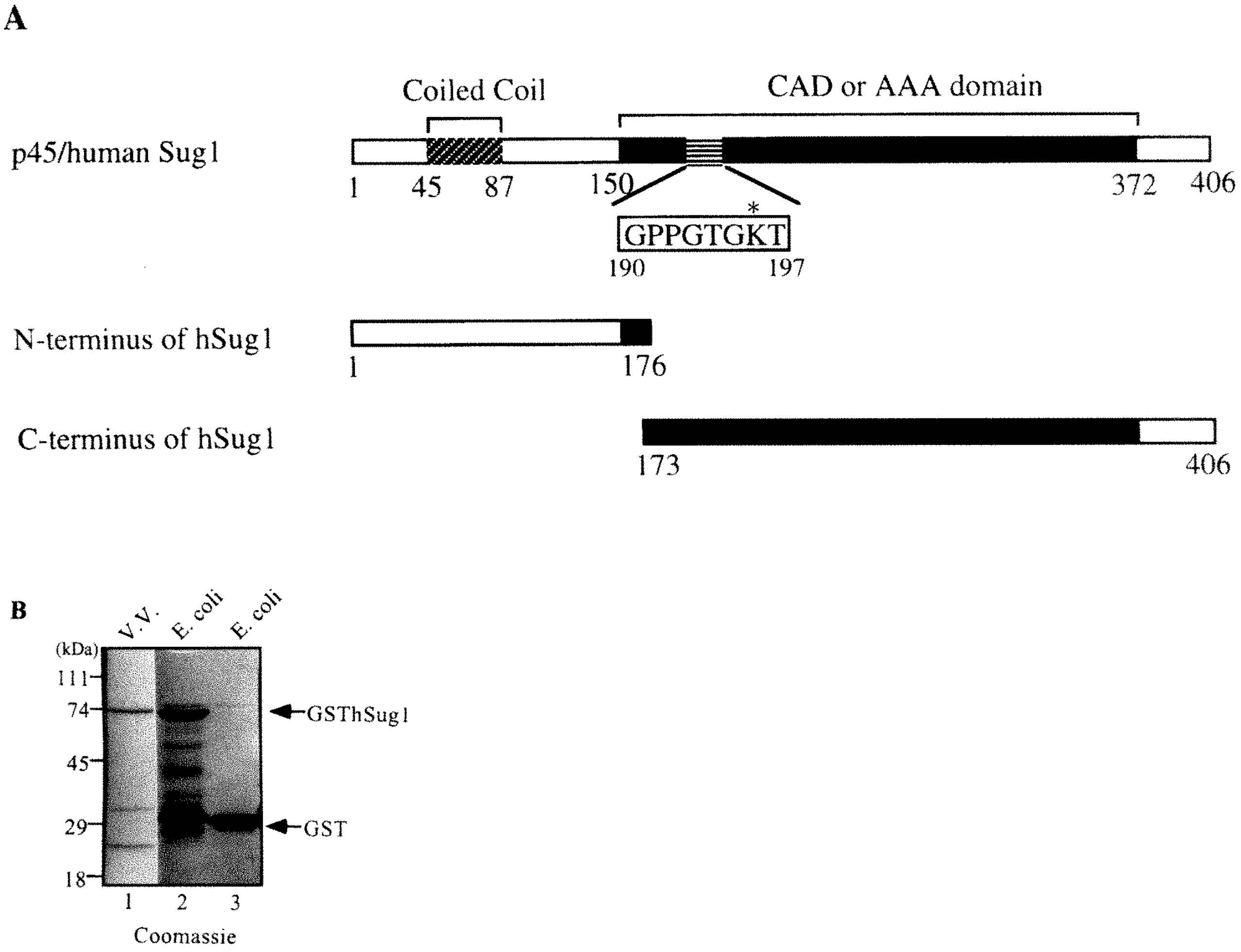

Figure 1 hSug1 protein structure and expression of hSug1 in *E. coli* and vaccinia virus

(**A**) hSug1 protein structure. The putative coiled-coil structure and the conserved ATPase domain are represented. The consensus ATP-binding motif is shown in the box. The lysine residue which is critical for ATP binding is indicated by the asterisk. The N- and C-terminal domains of hSug1 used in the present study are also shown. (**B**) The expression of hSug1 as GST fusion protein in *E. coli* and vaccinia virus (V.V.).

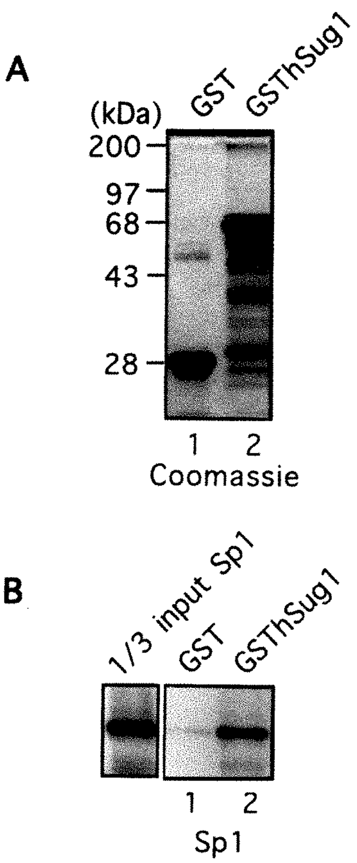

Figure 2 hSug1 protein interacts with Sp1 *in vitro*

In vitro-translated, [^{35}S]methionine-labelled human Sp1 (amino acids 1–778) was incubated with GST–hSug1 (amino acids 1–406 of hSug1) or GST protein immobilized on glutathione–Sepharose beads. After the beads were washed, bound proteins were eluted and resolved by SDS/PAGE. Coomassie Brilliant Blue staining of the gel confirmed equivalency of loading (**A**). Fluorography shows the bound ^{35}S-labelled proteins (**B**). The signals from one-third of the labelled input proteins are indicated in the left panel of (**B**).

interaction studies. Equal amounts of GST, GST–hSug1 (full-length hSug1), GST–C.Sug1 and GST–N.Sug1 were applied in each reaction (Figure 3A). As shown in Figure 3(B) C.Sug1 bound Sp1 to approximately the same extent as the full-length hSug1 (lanes 2 and 3), while N.Sug1 bound Sp1 at a near background level, as indicated by the GST control (lanes 1 and 4). These results demonstrate that the C-terminal ATPase domain of hSug1 interacts with Sp1 efficiently *in vitro*.

The assembly of the 19 S complex and the 20 S catalytic core of the proteasome is ATP-dependent, suggesting that the interactions between the subunit proteins require ATP-binding [35]. To test if the ATPase activity of hSug1 is required for its interaction with Sp1, we used site-directed mutagenesis to replace lysine^{196} with a methionine residue, thereby creating an ATPase mutant of hSug1, hSug1mk. We expressed hSug1mk as a GST fusion protein in *E. coli* and tested if this mutant hSug1 could interact with Sp1 using the *in vitro* interaction assay. Figure 3(C) shows that equal quantities of GST, GST–hSug1 or GST–hSug1mk proteins were applied in each reaction and Figure 3(D) shows that the mutant hSug1mk bound Sp1 to the same extent as the wild-type hSug1 (lanes 2 and 3). Our results show that the ATPase mutation of hSug1 does not detectably affect its binding affinity with Sp1.

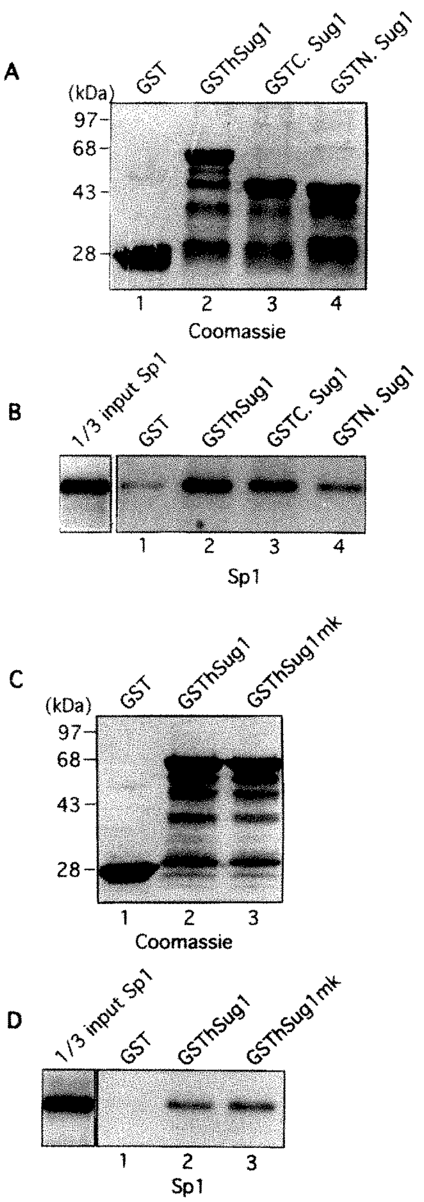

Figure 3 C.hSug1 and hSug1mk interact with Sp1 efficiently *in vitro*

In vitro-translated [^{35}S]methionine-labelled human Sp1 was incubated with GST–hSug1 (amino acids 1–406 of hSug1), GST–C.hSug1 (amino acids 173–406), GST–N.hSug1 (amino acids 1–176), GST–hSug1mk (ATPase mutant) or GST immobilized on glutathione–Sepharose beads. After the beads were washed, bound proteins were eluted and resolved by SDS/PAGE. Coomassie Brilliant Blue staining of the gel confirmed equivalency of loading (**A** and **C**). Fluorography shows the bound ^{35}S-labelled proteins (**B** and **D**). The signals from one-third of the labelled input proteins are indicated in the left panels of (**B**) and (**D**).

hSug1 interacts with Sp1 *in vivo*

To determine if the interaction of hSug1 and Sp1 can occur in living cells, we used vaccinia virus to express GST, GST–hSug1, GST–hSug1mk, GST–N.Sug1 and GST–C.hSug1 in NRK cells. The cells were cultured in 5 mM glucose medium in the presence of the proteasome inhibitor, *N*-acetyl-Leu-Leu-norLeu-al (LLnL), to prevent Sp1 degradation. The expressed GST fusion proteins were purified on glutathione–Sepharose beads and the endogenous Sp1 in the cells that co-purified with the indicated

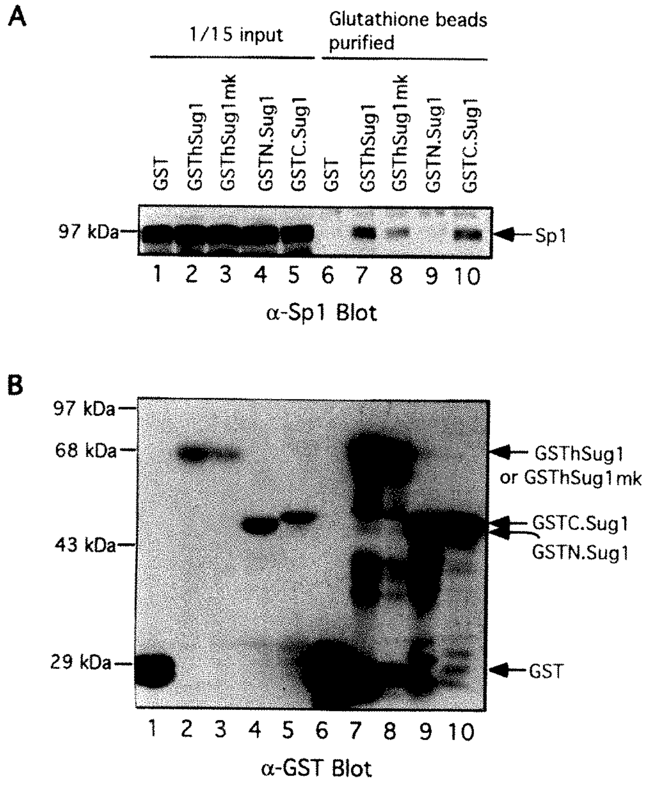

Figure 4 hSug1 interacts with Sp1 *in vivo*

(**A**) NRK cells cultured in 5 mM glucose medium were infected with vaccinia virus expressing GST, GST–hSug1, GST–hSug1mk, GST–N.Sug1 or GST–C.Sug1 for 22 h in the presence of the proteasome inhibitor LLnL. The whole-cell lysate was prepared and the expressed GST fusion proteins were purified on glutathione–Sepharose beads. The glutathione beads were extensively washed and the proteins bound on the beads were separated by SDS/PAGE followed by Western-blot analysis using an anti-Sp1 antibody (lanes 6–10). Lanes 1–5 were loaded with the whole-cell lysate before glutathione bead purification. It represents one-fifteenth of the input whole-cell lysate for glutathione bead purification. (**B**) The membrane from (**A**) was stripped and reprobed with an anti-GST antibody.

GST fusion proteins was examined by Western-blot analysis using Sp1 antiserum. Figure 4(A) shows that the endogenous Sp1 did not co-purify with GST alone or with N.Sug1 (lanes 6 and 9), but did co-purify with the wild-type hSug1, hSug1mk and C.Sug1 (lanes 7, 8 and 10). The expression levels of the GST fusion proteins in the NRK cells are shown in Figure 4(B). Although the mutant hSug1mk appears to have pulled down less Sp1 than wild-type hSug1, the level of expression of GST–hSug1mk was less in this experiment than the level of expression of the wild-type form (Figure 4B, lanes 7 and 8). These results demonstrate that *in vivo*, hSug1 through its C-terminal domain can interact with Sp1 in an ATPase-independent fashion. These *in vivo* results are in general agreement with those of the *in vitro* studies.

Wild-type hSug1 stimulates Sp1 degradation while hSug1mk, N.Sug1 and C.Sug1 inhibit Sp1 degradation *in vitro*

To determine if hSug1 is involved in the proteasome-dependent degradation of Sp1, we tested the effect of hSug1 proteins and its mutant forms on the degradation of Sp1 using an *in vitro* reconstituted assay. We have previously established this reconstituted degradation assay to map the domain in Sp1 that targets its proteasome-dependent degradation [33]. We have shown that recombinant GST–Sp1 protein is degraded *in vitro* in a proteasome-dependent manner in a two-step process by an activated nuclear extract made from glucose-starved and forskolin-stimulated NRK cells. Affinity-purified vaccinia virus-expressed GST–hSug1 was preincubated with the activated NRK nuclear extract. Then the substrate, GST–Sp1, and 2 mM ATP were added to the mixture and incubated at 37 °C for 30 min. The reaction mixture was separated by SDS/PAGE and subjected to Western-blot analysis using anti-GST antibodies. GST–Sp1 was not degraded when it was mixed with inactive nuclear extract from glucosamine-treated NRK cells (Figure 5, lane 1). GST–Sp1 was degraded when it was mixed with the activated nuclear extract from glucose-starved and forskolin-stimulated NRK cells and the usual degradation product, GST–SpX, was generated (lane 2). The addition of increasing amounts of GST–hSug1 protein resulted in further degradation of GST–Sp1, with the generation of more GST–SpX (Figure 5, lanes 3–5), while GST–hSug1 itself was not degraded. As a negative control GST alone had no effect on the GST–Sp1 degradation process (Figure 5, lanes 11 and 12). These results indicate that wild-type hSug1 augments the proteasome-dependent degradation of Sp1.

The ATPase subunits of the 26 S proteasome play important roles in the degradation of the substrates [36]. We therefore tested if the ATPase activity of hSug1 is required for Sp1 degradation. We performed the reconstituted degradation assay as described above. The addition of increasing amounts of GST–hSug1mk to activated extract resulted in progressively less GST–Sp1 degradation and less generation of GST–SpX (Figure 5, lanes 8–10). Thus not only is the ATPase activity of hSug1 necessary for its activity in the augmentation of Sp1 degradation, but also the ATPase mutant of hSug1 acts as a dominant negative, thereby inhibiting the proteasome-dependent processing of Sp1. Similarly, GST–N.Sug1 and GST–C.Sug1 also inhibited Sp1 degradation in a dose-dependent manner (Figure 5, lanes 13–18). In this experiment GST–hSug1mk, GST–N.Sug1 and GST–C.Sug1 themselves were not degraded. Taken together, while hSug1 stimulates Sp1 degradation in this *in vitro* system, both the N- and C-terminal domains of hSug1 are necessary for this function, and the ATPase activity of hSug1 is required in the degradation process of Sp1. The ability of mutant forms of Sug1 to act as dominant negatives and the ability of the wild-type form to augment processing suggest that hSug1 is at least one of the ATPases involved in the proteasome-dependent degradation of Sp1.

Wild-type hSug1 stimulates Sp1 degradation, while hSug1mk inhibits Sp1 degradation, *in vivo*

To determine if the effects of hSug1 seen *in vitro* can occur *in vivo* on native Sp1, we again used vaccinia virus to drive expression of GST–hSug1 or GST–hSug1mk in NRK cells stressed with glucose starvation and forskolin stimulation. After glucose starvation NRK cells were stimulated with forskolin in glucose-free medium for 5 h, before the cells were infected with vaccinia virus. The cells were then incubated in glucose-free medium in the presence of forskolin for an additional 16 h before cells were harvested. The whole-cell lysate was prepared and the levels of endogenous Sp1 were examined by Western-blot analysis using an anti-Sp1 antibody. As shown in Figure 6(A) the content of endogenous Sp1 was lower in the cells expressing GST–hSug1 than that in the cells expressing GST alone (lanes 1 and 2), suggesting that the expression of wild-type hSug1 in stressed NRK cells further stimulated Sp1 degradation. However, the expression of hSug1mk did not affect the levels of Sp1 in this experiment (Figure 6A, lane 3). The same blot in Figure 6(A) was stripped and reprobed with anti-[signal transducer and activator

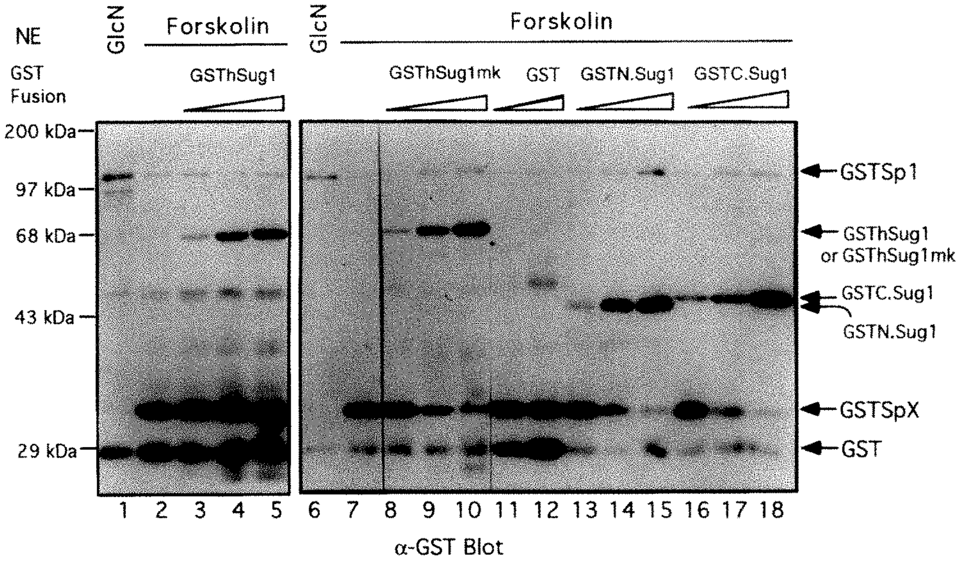

Figure 5 Wild-type hSug1 stimulates Sp1 degradation while hSug1mk, N.Sug1 and C.Sug1 inhibit Sp1 degradation *in vitro*

Nuclear extract (NE) from the NRK cells that had been glucosamine-treated (GlcN) or glucose-starved and forskolin-treated was preincubated with purified proteins GST–hSug1, GST–hSug1mk, GST–N.hSug1, GST–C.hSug1 (for each fusion protein, approx. 4 ng, 12 ng and 24 ng of protein was used in the first, second and third doses respectively), GST (approximately 12 ng and 25 ng was used in the first and second doses, respectively) or buffer alone as a control. Recombinant GST–Sp1 protein was then added to the preincubation mixture. After incubation, the reaction mixture was resolved by SDS/PAGE and subjected to Western-blot analysis using an anti-GST antibody.

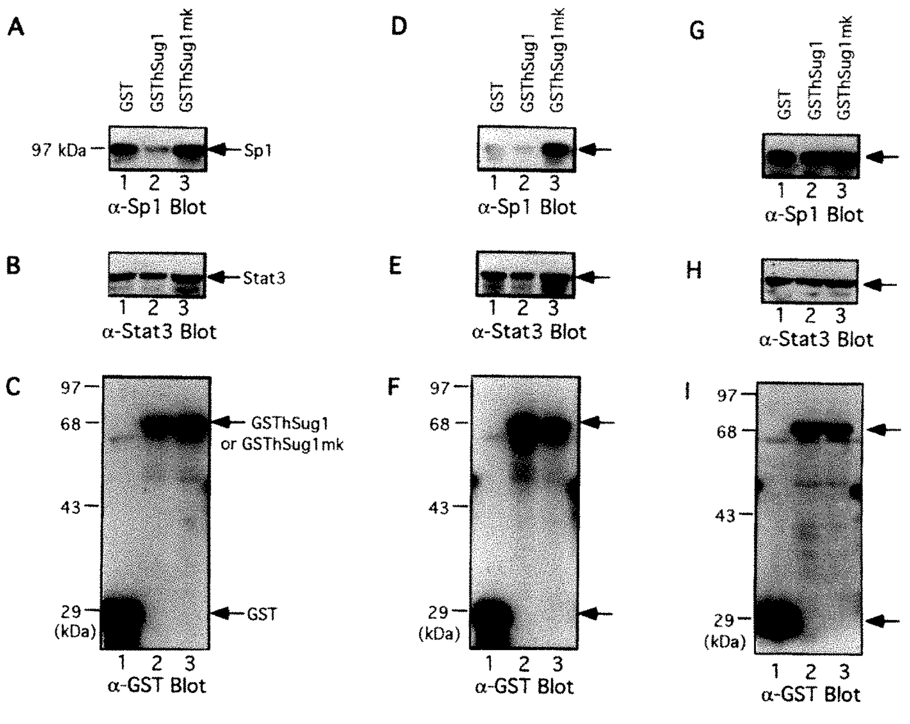

Figure 6 Wild-type hSug1 stimulates Sp1 degradation while hSug1mk inhibits Sp1 degradation *in vivo*

After 24 h of glucose starvation NRK cells were stimulated with 100 μM forskolin (**A**–**F**) or 5 mM glucosamine (**G**–**I**) in glucose-free medium for 5 h. The cells were then infected with recombinant virus expressing GST, GST–hSug1 or GST–hSug1mk for 16 h (**A**–**C**) or 23 h (**D**–**F**) in glucose-free medium with 100 μM forskolin, or for 16 h in glucose-free medium with 5 mM glucosamine (**G**–**I**). The whole-cell lysate was prepared and separated by SDS/PAGE followed by Western-blot analysis using anti-Sp1 antibody (**A**, **D** and **G**). The membranes from (**A**), (**D**) and (**G**) were stripped and reprobed with an anti-Stat3 antibody as a protein loading control (**B**, **E** and **H**). The same membranes were stripped and reprobed with anti-GST antibody to show the levels of GST fusion proteins expressed in those cells (**C**, **F** and **I**).

of transcription 3 (Stat3)] antibody to confirm the known specificity of this proteasome response and to assess equal loading of proteins in each lane (Figure 6B). As shown in Figure 6(C), approximately similar amounts of GST fusion proteins were expressed in the cells.

In a separate experiment the NRK cells were incubated in glucose-free medium in the presence of forskolin for 23 h, rather than 16 h, after vaccinia virus infection. The cells were then harvested and lysed. In this case basal degradation of Sp1 was nearly complete in the cells expressing GST (Figure 6D, lane 1). In contrast, this degradation was effectively blocked in the cells expressing GST–hSug1mk (Figure 6D, lane 3). Since Sp1 degradation was nearly complete under the basal conditions of this experiment, the augmentation of degradation by wild-type hSug1 was not clearly appreciable (Figure 6D, lane 2). The specificity/loading control with Stat3 is shown in Figure 6(E) and the expression level of the GST fusion proteins is shown in Figure 6(F). Taken together these results suggest that the expression of hSug1 in stressed NRK cells is able to stimulate the degradation of endogenous Sp1, while the expression of hSug1mk is able to inhibit Sp1 degradation.

While nutritional stress stimulates the proteasome-dependent degradation of Sp1 in NRK cells, glucosamine treatment of these cells blocks this process. Since hSug1 augments Sp1 degradation in stressed cells, we next determined whether hSug1 could stimulate this degradation in glucosamine-treated cells. After glucose starvation, NRK cells were stimulated with glucosamine for 5 h before the cells were infected with the vaccinia viruses that drive expression of either GST–hSug1 or GST–hSug1mk. The cells were incubated in the presence of glucosamine for an additional 16 h before cells were harvested. The content of Sp1 in the whole-cell lysate was examined by Western-blot analysis using an anti-Sp1 antibody. The levels of Sp1 remained constant in the cells expressing GST, GST–hSug1 or GST–hSug1mk (Figure 6G, lanes 1–3). The protein loading (Figure 6H) and GST-fusion protein expression (Figure 6I) were confirmed as above. These results show that the expression of hSug1 cannot stimulate Sp1 degradation in glucosamine-treated cells. Similar results were obtained using the *in vitro* reconstituted degradation assay. The addition of GST–hSug1 protein to an extract from glucosamine-treated NRK cells was unable to restore the proteasome-dependent degradation of Sp1 (results not shown).

hSug1 protein is not modified by O-GlcNAc

The inability of hSug1 to stimulate Sp1 degradation in glucosamine-treated cells could result from the modification of this protein by O-GlcNAc and an alteration in its ability to function in the degradation process. To determine if GST–hSug1 synthesized in glucosamine-treated NRK cells is modified by O-GlcNAc, we purified the protein from the cells and attempted to measure the O-GlcNAc content of the protein using the galactosyl-transferase method [37]. Recombinant proteins GST, GST–hSug1 and GST–SpE (SpE contains domain B, a glutamine-rich activation domain of Sp1 [37]) were expressed and purified from glucosamine or forskolin-treated cells as described above Approximately 50 ng of these proteins was labelled with [^{3}H]galactose using galactosyltransferase. Our results show that GST–hSug1, prepared from either glucosamine- or forskolin-treated cells, was not labelled by [^{3}H]galactose, suggesting that GST–hSug1 was not modified by O-GlcNAc (results not shown). However, we readily detected the glycosylation of the Sp1 peptide, SpE, prepared from glucosamine-treated cells (results not shown). As a negative control, GST alone was not modified by O-GlcNAc (results not shown). We also performed Western-blot analysis using a GlcNAc-specific monoclonal antibody, RL-2, to attempt to detect O-GlcNAc modification of hSug1 under denaturing conditions [38]. Recombinant protein GST–hSug1 prepared from glucosamine-treated cells was not recognized by the RL-2 antibody (results not shown). Our results suggest that no O-GlcNAc modification of hSug1 protein is detectable under native or denaturing conditions.

DISCUSSION

Previous studies have shown that Sp1 is rapidly degraded by the proteasome under the conditions of glucose-starvation and stimulation by cAMP [4]. However, the control of this degradation process is largely unknown. The accurate and specific selection of substrates for proteasome degradation may depend upon the signals in the substrates and also upon the proteasome itself. We have previously identified the N-terminal 54 amino acids of Sp1 as the major domain that targets Sp1 for proteasome-dependent degradation [33]. In the present study we further dissected the molecular basis for the control of Sp1 degradation.

Our results demonstrated that the proteasomal ATPase hSug1 is involved in the degradation of Sp1. Through its C-terminal domain, hSug1 interacts with Sp1 both *in vitro* and *in vivo*. While the interaction between these molecules does not depend on the ATPase activity of hSug1, in a reconstituted degradation assay and in the living cells, wild-type hSug1 stimulates Sp1 degradation, whereas the ATPase mutant hSug1mk and the N-and C-terminal domains of hSug1 block this Sp1 degradation. These results suggest that the recombinant hSug1 can exchange with the endogenous hSug1 in the degradation assay. Furthermore, full-length hSug1 with intact ATPase activity is both sufficient and necessary for the proteasome degradation of Sp1 under the experimental conditions. Like the ATPase mutant, the N- and C-terminal fragments of hSug1 both block Sp1 degradation possibly by perturbing the function of endogenous wild-type hSug1. There are two possible mechanisms to account for the observation that the N-terminal fragment of hSug1 inhibits full-length hSug1 function. The N-terminal Sug1 moiety encompasses a putative coiled-coil structure, which has been proposed to be involved in protein–protein interactions. Furthermore, previous evidence indicates that mammalian Sug1 can dimerize or oligomerize and that the N-terminus is required for Sug1 oligomerization [26]. If the activity of hSug1 depends on dimer formation, then the N-terminal hSug1 fragment could compete for dimerization with the full-length hSug1 and act as a dominant negative, thereby inhibiting the activity of this molecule in the Sp1 degradation process. The other possibility relates to the mechanism by which Sug1 is recruited to the 19 S complex of the proteasome. It has been determined that the coiled-coils in the N-terminal region of proteasomal ATPases probably direct the placement of these proteins within the proteasome [39]. Thus the truncated hSug1 N-terminal domain could inhibit the recruitment of full-length hSug1 to the proteasome by occupying the available docking sites on this organelle. Similarly the C-terminal fragment of hSug1 could compete with wild-type hSug1 for interaction with Sp1. Failure of the C-terminal fragment to dimerize or interact with the proteasome could account for the inhibitory properties of this Sug1 fragment on Sp1 degradation by the proteasome. Since there is high sequence similarity among the six proteasomal ATPases [34], our evidence does not exclude the possibility that other proteasomal ATPases may also be involved in the degradation of Sp1. However, the fact that the N-terminal domain of hSug1 has only about 18 % sequence similarity with other family members and yet inhibits Sp1 degradation argues that hSug1 is the predominant proteasomal ATPase responsible for Sp1 degradation.

Regulation of transcription factor abundance by proteasome-dependent degradation is important in the control of transcription and has been shown to play a role in the regulation of transcription factors that include c-Fos, c-Jun and p53 [40–42]. However, the controlling mechanism for the proteasome recognition of transcription factors and the proteins involved in this recognition are not totally clear. Among the six ATPases in the 26 S proteasome Sug1 has been most extensively shown to interact with transcription factors, although the functional role of this interaction has not been definitively elucidated. An intriguing possibility is that hSug1 might co-operate in the targeting of certain types of transcription factors for proteasome degradation. There is precedence for this idea in *E. coli.* The 26 S proteasome resembles the *E. coli* protease ClpAP (also known as Ti) in its general organization and structure [5]. The ClpP protease cylinder is capped at both ends by a large regulatory ATPase complex, ClpA/ClpX. Interestingly, it has been shown that the ATPases ClpA and ClpX direct the substrate specificity for the ClpP protease to different proteins [43–45]. In yeast, mutations in the different regulatory ATPases of the proteasomes result in different phenotypes [21] and alter the degradation of different substrates [46]. This result has suggested that the ATPases co-operate in the degradation of individual substrates [21]. Similarly, the different ATPases in the mammalian 26 S proteasome may direct substrate recognition thereby providing an additional means of control of substrate specificity for the proteasome. There is some evidence supporting this idea. Human proteasomal S6 ATPase (and MS73 ATPase in *Manduca Sexta*) binds the ankyrin repeats present in a set of proteasome substrates and this interaction may complement ubiquitination as recognition signal by the 26 S proteasome [47]. For Sug1 it has been shown that this proteasomal ATPase is predominantly located in the nucleus, while the proteasome is distributed in both the cytoplasm and the nucleus [32,48]. Sug1 interacts with c-Fos [25] and also appears to be involved in the degradation of the vitamin D nuclear receptor [49]. The present study clearly shows that hSug1 is also required for the proteasomal degradation of another transcription factor, Sp1. However, whether hSug1 participates in the recognition of certain types of transcription factors by the proteasome and whether there is a common structural motif in these proteins recognized by hSug1 remains to be elucidated.

Previously we have identified an N-terminal domain of Sp1 that targets its proteasome-dependent degradation. Elimination of this target domain impairs Sp1 degradation and stabilizes the protein Our preliminary results indicate that hSug1 does not interact with this target domain of Sp1 (results not shown). We have also shown that increased modification of proteins by O-GlcNAc is associated with Sp1 stabilization [4] and that nuclear extract from glucosamine-treated cells fails to degrade recombinant Sp1 [33]. However, hSug1 is not modified by O-GlcNAc even in cells that had been treated with glucosamine, and hSug1 cannot restore the activity of the proteasomes derived from glucosamine-treated cells. This evidence suggests that hSug1 is not the unique factor that links the O-GlcNAc state of the cell with Sp1 stability and targets Sp1 for degradation. Rather, it appears that Sp1 degradation results from the co-operation of other proteasome factors that require Sug1. We propose that this other factor directly recognizes the N-terminal target of Sp1 in an O-GlcNAc-dependent fashion and co-operates with Sug1 in the proteasomal degradation process. Collectively our results show that hSug1 interacts with Sp1 through a region in the C-terminal half of hSug1 and this interaction is required for the proteasome-dependent degradation of Sp1. These findings provide more detail concerning the molecular interactions involved in the proteasomal degradation of Sp1 and shed light on the function of hSug1 as a proteasomal component.

This work was supported by a program grant from the Juvenile Diabetes Foundation International

REFERENCES

1 Kadonaga, J T, Jones, K A and Tjian, R (1986) Promoter specific activation of RNA polymerase II by Sp1 Trends Biochem Sci **11**, 20–23

2 Mortensen, E R, Marks, P A, Shiotani, A and Merchant, J L (1997) Epidermal Growth Factor and Okadaic Acid Stimulate Sp1 Proteolysis J Biol. Chem **272**, 16540–16547

3 Shin, T H, Paterson, A J, Grant, III, J H, Meluch, A A and Kudlow, J. E (1992) 5-Azacytidine Treatment of HA-A Melanoma Cells Induces Sp1 Activity and Concomitant Transforming Growth Factor a Expression Mol Cell. Biol **12**, 3998–4006

4 Han, I and Kudlow, J E (1997) Reduced O Glycosylation of Sp1 Is Associated with Increased Proteasome Susceptibility Mol. Cell Biol **17**, 2550–2558

5 Coux, O, Tanaka, K and Goldberg, A L (1996) Structure and Functions of the 20S and 26S Proteasomes Annu Rev Biochem **65**, 801–847

6 Driscoll, J and Goldberg, A L (1990) The Proteasome (Multicatalytic Protease) Is a Component of the 1500-kDa Proteolytic Complex Which Degrades Ubiquitin-conjugated Proteins J Biol Chem **265**, 4789–4792

7 Laney, J. D. and Hochstrasser, M (1999) Substrate targeting in the ubiquitin system Cell **97**, 246–251

8 Arrigo, A. P., Tanaka, K, Goldberg, A L and Welch, W. J. (1988) Identity of the 19S 'prosome' particle with the large multifunctional protease complex of mammalian cells (the proteasome). Nature (London) **331**, 192–194

9 Larsen, C N. and Finley, D (1997) Protein translocation channels in the proteasome and other proteases Cell **91**, 431–434

10 Tanaka, K, Yoshimura, T, Kumatori, A, Ichihara, A, Ikai, A and Nishigai, M (1988) Proteasomes (Multi-protease Complexes) as 20S Ring-Shaped Particles In a Variety of Eukaryotic Cells. J Biol Chem **263**, 16209–16217

11 Deveraux, Q, Ustrell, V, Pickart, C and Rechsteiner, M. (1994) A 26S protease subunit that binds ubiquitin conjugates J Biol Chem **269**, 7059–7061

12 van Nocker, S, Deveraux, Q, Rechsteiner, M and Vierstra, R D (1996) Arabidopsis MBP1 gene encodes a conserved ubiquitin recognition component of the 26S proteasome. Proc Natl Acad Sci USA **93**, 856–860

13 DeMartino, G N, Moomaw, C R, Zagnitko, O P, Proske, R. J, Ma, C P, Afendis, S J, Swaffield, J C and Slaughter, C A (1994) PA700, an ATP-dependent activator of the 20S proteasome, is an ATPase containing multiple members of a nucleotide binding protein family J Biol Chem **269**, 20878–20884

14 Dubiel, W, Ferrell, K, Pratt, G and Rechsteiner, M (1992) Subunit 4 of the 26S protease is a member of a novel eukaryotic ATPase family J Biol. Chem **267**, 22699–22702

15 Dubiel, W, Ferrell, K and Rechsteiner, M (1993) Peptide sequencing identifies MSS1, a modulator of HIV Tat-mediated transactivation, as subunit 7 of the 26S proteasome FEBS Lett **323**, 276–278

16 Glickman, M H, Rubin, D M., Fried, V A and Finley, D. (1998) The regulatory particle of the *S cerevisiae* proteasome Mol Cell Biol **18**, 3149–3162

17 Richmond, C, Gorbea, C and Rechsteiner, M (1997) Specific Interactions between ATPase subunits of the 26S proteasome J Biol. Chem **272**, 13403–13411

18 Rubin, D M, Coux, O., Wefes, I, Hengartner, C, Young, R A, Goldberg, A L and Finley, D (1996) Identification of the gal4 suppressor Sug1 as a subunit of the yeast 26S proteasome Nature (London) **379**, 655–657

19 Armon, T., Ganoth, D and Hershko, A (1990) Assembly of the 26S complex that degrades proteins ligated to ubiquitin is accompanied by the formation of ATPase activity J Biol Chem. **265**, 20723–20726

20 Glickman, M H, Rubin, D. M., Fu, H, Larsen, C. N., Coux, O, Wefes, I, Pfeifer, G, Cjeka, Z, Vierstra, R, Baumeister, W et al (1999) Function analysis of the proteasome regulatory particle. Mol Biol Rep **26**, 21–28

21 Rubin, D M., Glickman, M H, Larsen, C N, Dhruvakumar, S and Finley, D. (1998) Active site mutants in the six regulatory particle ATPases reveal multiple roles for ATP in the proteasome. EMBO J **17**, 4909–4919

22 Ghislain, M, Udvardy, A and Mann, C (1993) S. cerevisiae 26S protease mutants arrest cell division in G2/metaphase. Nature (London) **366**, 358–362

23 Akiyama, K, Yokota, K, Kagawa, S, Shimbara, N, DeMartino, G N, Slaughter, C A, Noda, C and Tanaka, K (1995) cDNA cloning of a new putative ATPase subunit p45 of the human 26S proteasome, a homolog of yeast transcription factor Sug1p FEBS Lett **363**, 151–156

24 Sears, C., Olesen, J, Rubin, D., Finley, D and Maniatis, T (1998) NF-kB p105 Processing via the Ubiquitin-Proteasome Pathway J Biol Chem **273**, 1409–1419

25 Wang, W, Chevray, P M. and Nathans, D (1996) Mammalian Sug1 and c-Fos in the nuclear 26S proteasome. Proc Natl. Acad Sci U S A **93**, 8236–8240

26 Baur, E V, Zechel, C., Heery, D, Heine, M J S, Garnier, J M, Vivat, V, Douarin, B L, Gronemeyer, H, Chambon, P and Losson, R (1996) Differential ligand-dependent interactions between the AF-2 activating domain of nuclear receptors and the putative transcriptional intermediary factors mSUG1 and TIF1. EMBO J **15**, 110–124

27 Lee, J W, Ryan, F, Swaffield, J C, Johnston, S A and Moore, D D (1995) Interaction of thyroid-hormone receptor with a conserved transcriptional mediator Nature (London) **374**, 91–94

28 Swaffield, J C, Melcher, K and Johnston, S A (1995) A Highly conserved ATPase protein as a mediator between acidic activation domains and the TATA-binding protein. Nature (London) **374**, 88–91

29 Weeda, G, Rossignol, M, Fraser, R A, Winkler, G S, Vermeulen, W, Veer, L J, Ma, L, Hoeijmakers, J H J and Egly, J. M (1997) The XPB subunit of repair/transcription factor TFIIH directly interacts with SUG1, a subunit of the 26S proteasome and putative transcription factor. Nucleic Acids Res **25**, 2274–2283

30 Fraser, R. A, Rossignol, M, Heard, D J, Egly, J.-M and Chambon, P M (1997) SUG1, a putative transcriptional mediator and subunit of the PA 700 proteasome regulatory complex, is a DNA helicase J Biol Chem. **272**, 7122–7126

31 Makino, Y, Yamano, K., Kanemaki, M, Morikawa, K, Kishimoto, T., Shimbara, N., Tanaka, K and Tamura, T (1997) SUG1, a component of the 26S Proteasome, is an ATPase Stimulated by Specific RNAs J Biol Chem **272**, 23201–23205

32 Russell, S J, Steger, K A. and Johnston, S A (1999) Subcellular localization, stoichiometry, and protein levels of 26S proteasome subunits in yeast. J Biol Chem **274**, 21943–21952

33 Su, K, Roos, M. D, Yang, X, Han, I, Paterson, A. J. and Kudlow, J E (1999) An N-terminal region of Sp1 targets its proteasome-dependent degradation in vitro J Biol. Chem **274**, 15194–15202

34 Makino, Y, Yogosawa, S, Kanemaki, M, Yoshida, T, Yamano, K., Kishimoto, T, Moncollin, V, Egly, J, Maramatsu, M and Tamura, T. (1996) Structures of the Rat Proteasomal ATPases Determination of Highly Conserved Structural Motifs and Rules for Their Spacing. Biochem Biophys Res Commun **229**, 1049–1054

35 Orino, E, Tanaka, K, Tamura, T, Sone, S., Ogura, T. and Ichihara, A (1991) ATP-dependent reversible association of proteasomes with multiple protein components to form 26S complexes that degrade ubiquitinated proteins in human HL-60 cells. FEBS Lett. **284**, 206–210

36 Hoffman, L and Rechsteiner, M (1994) Activation of the multicatalytic protease J Biol Chem **269**, 16890–16895

37 Roos, M D, Su, K, Baker, J R and Kudlow, J E. (1997) O Glycosylation of an Sp1-Derived Peptide Blocks Known Sp1 Protein Interactions Mol Cell. Biol **17**, 6472–6480

38 Sayeski, P P and Kudlow, J. E. (1996) Glucose Metabolism to Glucosamine is Necessary for Glucose Stimulation of Transforming Growth Factor-a Gene Transcription J Biol Chem **271**, 15237–15243

39 Gorbea, C, Taillandier, D and Rechsteiner, M (1999) Assembly of the regulatory complex of the 26S proteasome. Mol Biol. Rep **26**, 15–19

40 Rolfe, M., Beer-Romero, P, Glass, S, Eckstein, J, Berdo, I, Theodoras, A, Pagano, M and Draetta, G. (1995) Reconstitution of p53-ubiquitinylation reactions from purified components the role of human ubiquitin-conjugating enzyme UBC4 and E6-associated protein (E6AP) Proc Natl Acad Sci. U S A. **92**, 3264–3268

41 Stancovski, I, Gonen, H, Orian, A, Schwartz, A L and Ciechanover, A (1995) Degradation of the Proto-Oncogene Product c-Fos by the Ubiquitin Proteolytic System In Vivo and In Vitro. Identification and Characterization of the Conjugating Enzymes Mol Cell Biol **15**, 7106–7116

42 Treier, M, Staszewski, L M and Bohmann, D (1994) Ubiquitin-Dependent c-Jun Degradation In Vivo Is Mediated by the d Domain Cell **78**, 787–798

43 Pak, M and Wickner, S (1997) Mechanism of protein remodeling by ClpA chaperone Proc Natl. Acad Sci. U S A **94**, 4901–4906

44 Schweder, T, Lee, K H, Lomovskaya, O and Matin, A (1996) Regulation of Escherichia coli starvation sigma (sigma s) by ClpXP protease J Bacteriol **178**, 470–476

45 Wawrzynow, A, Wojtkowiak, D., Marszalek, J, Banecki, B, Jonsen, M, Graves, B, Georgopoulos, C and Zylicz, M (1995) The ClpX heat-shock protein of Escherichia coli, the ATP-dependent substrate specificity component of the ClpP-ClpX protease, is a novel molecular chaperone EMBO J **14**, 1867–1877

46 Javerzat, J P, McGurk, G, Cranston, G, Barreau, C, Bernard, P, Gordon, C and Allshire, R (1999) Defects in components of the proteasome enhance transcriptional silencing at fission yeast centromeres and impair chromosome segregation Mol Cell Biol **19**, 5155–5165

47 Dawson, S, Hastings, R, Takayanagi, K, Reynolds, S, Low, P, Billett, M. and Mayer, R. J. (1997) The 26S-proteasome regulation and substrate recognition. Mol Biol. Rep **24**, 39–44

48 Peters, J M, Franke, W W and Kleinschmidt, J A (1994) Distinct 19S and 20S subcomplexes of the 26S proteasome and their distribution in the nucleus and the cytoplasm J Biol. Chem. **269**, 7709–7718

49 Masuyama, H and MacDonald, P N (1998) Proteasome-mediated degradation of the vitamin D receptor (VDR) and a putative role for SUG1 interaction with the AF2 domain of VDR J Cell Biochem. **71**, 429–440

Received 5 January 2000/29 February 2000, accepted 23 March 2000

Biochem J (2000) 348, 291–295 (Printed in Great Britain)

CLC-Nt1, a putative chloride channel protein of tobacco, co-localizes with mitochondrial membrane markers

Claire LURIN*[1], Josette GÜCLÜ*, Catherine CHENICLET†, Jean-Pierre CARDE†, Hélène BARBIER-BRYGOO*
and Christophe MAUREL*[2]
*Institut des Sciences Végétales, UPR 40, CNRS, Avenue de la Terrasse, F-91198 Gif-sur-Yvette Cedex, France, and
†Biologie Cellulaire et Moléculaire du Développement des Plantes, Université Bordeaux 1, Avenue des Facultés, F-33405 Talence, France

The voltage-dependent chloride channel (CLC) family of membrane proteins has cognates in animals, yeast, bacteria and plants, and chloride-channel activity has been assigned to most of the animal homologues. Lack of evidence of CLC functions in plants prompted us to characterize the cellular localization of the tobacco CLC-Nt1 protein. Specific polyclonal antibodies were raised against an N-terminal polypeptide of CLC-Nt1. These antibodies were used to probe membrane proteins prepared by various cell-fractionation methods. These included aqueous two-phase partitioning (for plasma membranes), free-flow electrophoresis (for vacuolar and plasma membranes), intact vacuole isolation, Percoll-gradient centrifugation (for plastids and mitochondria) and stepped, linear, sucrose-density-gradient centrifugation (for mitochondria). Each purified membrane fraction was characterized with specific marker enzyme activities or antibodies. Our studies ruled out the possibility that the major cell localization of CLC-Nt1 was the vacuolar or plasma membranes, the endoplasmic reticulum, the Golgi apparatus or the plastids. In contrast, we showed that the tobacco CLC-Nt1 specifically co-localized with the markers of the mitochondrial inner membrane, cytochrome *c* oxidase and NAD9 protein CLC-Nt1 may correspond to the inner membrane anion channel ('IMAC') described previously in animal and plant mitochondria.

Key words: anion transport, membranes, mitochondria, plant cell, voltage-dependent chloride channels.

INTRODUCTION

The voltage-dependent chloride channel (CLC) family, with members in bacteria, yeast, animals and plants, defines a large class of structurally related membrane proteins with putative chloride channel activities [1]. Eukaryotic CLCs can be distributed into three homology subfamilies, with mammalian CLC-0, CLC-1, CLC-2, CLC-K1 and CLC-K2 defining the first branch. All five of these proteins have been shown to function as plasma membrane chloride channels and participate in distinct cellular functions, such as membrane excitability, regulation of cell volume and epithelial transport [1]. Animal CLC-3, CLC-4 and CLC-5, together with yeast Gef1p, define the second branch of the CLC family. Whereas CLC-3 encodes a plasma membrane volume-regulated chloride channel [2], CLC-5 and Gef1p have been recently localized in intracellular membranes [3–5]. Gef1p may provide an electrical shunt for H$^+$-ATPase in acidic vesicles of the late Golgi apparatus and thus participate in anion and cation homoeostasis in this compartment [3,6]. CLC-5 is predominantly localized in endocytotic membranes, where it might play a role similar to that of Gef1p [4]. The two putative chloride channels, CLC-6 and CLC-7, from mammals, together with all the plant CLCs define the last branch of the family. The function of these putative chloride channels remains unknown, but CLC-6 was recently localized in the endoplasmic reticulum [7].

Whereas, in animals, several types of molecular chloride channels different from CLCs have been recognized, the *CLC* genes from tobacco (*Nicotiana tabacum*) [8] and *Arabidopsis thaliana* [9] represent the only known putative anion channel genes of plants. Heterologous expression of tobacco CLC-Nt1 in *Xenopus* oocytes elicited inward chloride currents upon membrane hyperpolarization [8]. However, evidence for chloride-channel activity of plant CLCs in the native membrane is still lacking. These proteins may encode some of the various voltage-dependent anion channel activities which have been established in plant cell membranes [10,11]. Because of its critical physiological role and because it is easily amenable to patch-clamp analysis, the plant plasma membrane has been the object of most studies. However, anion channels have also been reported in internal membranes, such as the tonoplast, which delimits the large central vacuole, and in mitochondrial and plastid membranes [10,11].

Lack of evidence of CLC functions in plants prompted us to characterize the cellular localization of the tobacco CLC-Nt1 protein. Specific antibodies were raised against the protein and used to probe membrane fractions purified using various cell-fractionation methods. These studies showed that CLC-Nt1 co-localized with markers of the mitochondrial membrane.

EXPERIMENTAL

Plant materials

Tobacco (*Nicotiana tabacum* cv. Xanthi; wild-type clone XHFD8) plants were grown in a greenhouse at 22 °C with a

---

Abbreviations used: CLC, voltage-dependent chloride channel, DHFR, dihydrofolate reductase; IMAC, inner membrane anion channel, N1, 53-amino-acid N-terminal polypeptide of CLC-Nt1

[1] Present address Department of Biology, University of Pennsylvania, 415 South University Avenue, Philadelphia, PA 19104-6018, U S A.

[2] To whom correspondence should be addressed. Present address. Biochimie et Physiologie Moléculaire des Plantes, ENSA-M/INRA/CNRS, 2 Place Viala, F-34 060 Montpellier, France (e-mail maurel@ensam inra fr).

photoperiod of 9 h of light/day for vegetative development and of 16 h for flowering induction. Tobacco (*N. tabacum* cv. Xanthi) suspension-cultured cells were maintained in B5 Gamborg medium containing 1 μM 2,4-dichlorophenoxyacetic acid and 60 nM kinetin in the light at 26 °C, and were transferred to fresh medium every 7 days. Exponentially growing cells were used 4–5 days after transfer

Protein expression in *Escherichia coli* and antibody production

A fusion protein between the rat dihydrofolate reductase (DHFR) and a 53-amino-acid N-terminal polypeptide of CLC-Nt1 (Met^1–Gln^{53}) (N1) was produced using a Qiagen expression system (Les Ulis, France). Briefly, a DNA fragment encoding N1 was generated by PCR with appropriate oligonucleotides as primers and CLC-Nt1 cDNA as template. This fragment was cloned in a pQE30 plasmid (Qiagen), downstream and in-frame of the His$_6$ motif. A 561-bp cDNA fragment encoding rat DHFR was then inserted in-frame between the His$_6$ motif and the CLC fragment of the plasmid. M15 (pREP4) bacteria were transformed with the resulting pQE30-DHFR-N1 plasmid. For production of the fusion protein, bacteria were grown to a D_{600} of 0 8 and induced by 2 mM isopropyl β-D-thiogalactopyranoside for 5 h. Proteins were then extracted and purified by affinity chromatography on a metal-chelation resin charged with Ni^{2+} under denaturing conditions, as described in the Qiagen instruction manual. Approx. 20 mg of fusion protein per litre of culture was usually obtained.

Two rabbits were immunized with 1 mg of fusion protein in complete Freund's adjuvant, injected subcutaneously Three booster injections were administered at 4-week intervals with the same amount of protein but in incomplete Freund's adjuvant. Blood samples were collected 10 days after each boost, kept at room temperature for 8 h and then centrifuged at 1000 *g* for 15 min. The serum was collected and stored at −80 °C. For immunopurification of antibodies, the antigenic fusion protein was coupled in anhydrous conditions to Affi-Gel 10 beads (Bio-Rad, Hercules, CA, U.S.A.). Briefly, 500 μg of DHFR fusion protein solubilized in DMSO was added to 0.5 ml of activated beads and reaction was carried out for 2 h at room temperature. Unreacted groups were blocked with 50 μl of 1 M ethanolamine, pH 8, and the beads were washed and equilibrated with 10 mM Tris/HCl, pH 7.5. Antiserum (1 ml) was heated at 56 °C for 30 min and cleared by centrifugation at 10000 *g* for 5 min The serum was then diluted 5-fold in 10 mM Tris/HCl, pH 7.5, and added to the pre-equilibrated affinity beads. The beads were maintained for 1 h at room temperature to allow binding of the antibodies. The beads were then transferred to a chromatography column and washed successively with 10 mM Tris/HCl, pH 7.5, and with 500 mM NaCl/10 mM Tris/HCl, pH 7.5. The specific antibodies were eluted first with 100 mM glycine buffer, pH 2.5, followed by 100 mM triethylamine buffer, pH 11.5. The eluted antibody fractions were combined and dialysed against PBS.

Membrane purification

A microsomal membrane fraction was prepared from suspension cells or leaves, as described by Mathieu et al. [12]. Membranes from suspension cells were further separated by free-flow electrophoresis as described previously [13]. A plasma-membrane-enriched fraction was purified from leaf microsomes by aqueous two-phase partitioning as described by Ephritikhine et al. [14]. Vacuoles were purified according to Höfte et al. [15] from tobacco mesophyll protoplasts [16]. Plastids were isolated from tobacco leaves by a three-step Percoll gradient according to the method of Douce and Joyard [17]. Mitochondria were isolated from tobacco leaves on a self-generating gradient of Percoll (28 %) in combination with a linear gradient of polyvinylpyrrolidone (0–10 %) and a linear gradient of raffinose (0–300 mM) according to Douce et al [18]. For organelle membrane purification, vacuoles, plastids and mitochondria were lysed by a hypo-osmotic treatment, collected by centrifugation at 100000 *g* for 30 min and resuspended in 300 mM sucrose, 9 mM KCl, 5 mM dithiothreitol, 10 mM Mes/Tris, pH 6. Marker enzyme assays were performed as described previously [19].

A fractionation procedure for tobacco leaf membranes by linear sucrose gradient centrifugation was adapted from that of Chaumont et al. [20], and is briefly described. Leaves (30 g) were homogenized in a blender in 150 ml of 330 mM sucrose, 50 mM Tris/HCl, 0.2 % (w/v) BSA, 0.04 % (v/v) 2-mercaptoethanol, pH 8.0, filtered through sieves (pore sizes 500 μm and 56 μm) and the homogenate was centrifuged at 3000 *g* for 5 min The supernatant was then centrifuged for 25 min at 25000 *g* and the pellet was resuspended in 1 ml of 400 mM mannitol, 10 mM potassium phosphate buffer, pH 7.2. The suspension was layered on to a linear sucrose gradient [25–50 % (w/w) sucrose in 50 mM KCl, 10 mM Tris/HCl, pH 7.5] and centrifuged for 16 h at 30000 *g*. Membrane fractions of 500 μl were removed, washed in 50 mM KCl, 10 mM Tris/HCl, pH 7.5, and centrifuged at 100000 *g* for 30 min.

Immunoblot analysis

Proteins were resolved by SDS/PAGE (10 % gel) and blotted on to PVDF membranes (Millipore, Bedford, MA, U.S.A.). The membranes, blocked with TBST [250 mM NaCl, 0.1 % (v/v) Tween 20, 50 mM Tris/HCl, pH 7.6] containing 7.5 % (w/v) fat-free milk powder, were incubated overnight at room temperature in TBST, with the appropriate dilutions of serum or purified antibodies. After two washes with TBST, secondary antibodies (goat anti-rabbit IgGs coupled to alkaline phosphatase conjugate, BioRad) (1:2000 dilution in TBST) were added and the membrane was incubated for 1 h at room temperature. After washing, the antigen–antibody complex was detected by colour development with 5-bromo-4-chloro-3-indolyl phosphate (2.5 %, w/v) and Nitro Blue Tetrazolium (5 %, w/v). Rabbit antisera anti-NAD9 (mitochondrial marker) and anti-E37 (plastid marker) were kindly provided by Dr J.-M. Grienenberger (CNRS, Strasbourg, France) and Dr J. Joyard (CEA, Grenoble, France) respectively. The polyclonal antibodies directed against a tobacco plasma membrane H^+-ATPase and the E subunit of a barley vacuolar H^+-ATPase were a gift from Professor Marc Boutry (University of Louvain-la-Neuve, Belgium) and Dr K.-J Dietz (University of Würzburg, Germany) respectively.

RESULTS

Production and characterization of the antiserum

Antibodies were raised against a fusion protein between rat DHFR and N1. To reduce the background signal observed with both preimmune and immune sera (results not shown), antibodies were affinity-purified using the DHFR–N1 fusion. As shown in Figure 1(A), the purified antibodies recognized a single band at 70 kDa, whereas the preimmune purified serum did not react with any microsomal protein. This indicates that the 70-kDa signal was specifically related to the DHFR–N1 antigens.

The antibodies, however, may recognize a plant protein immunologically related to rat DHFR. To check for this possibility, the antibodies were pretreated with an excess of recombinant DHFR protein. As shown in Figure 1(B), DHFR preadsorption completely abolished the reactivity of the DHFR–N1

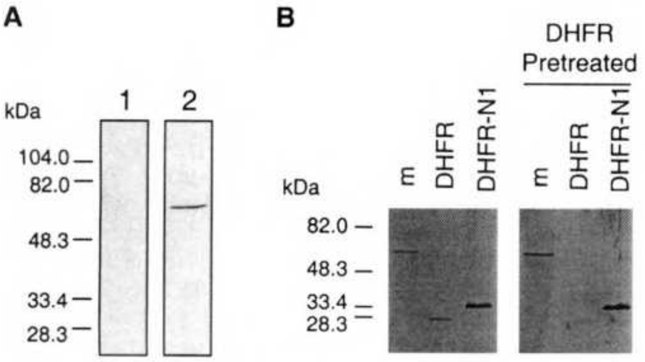

Figure 1 Specificity of polyclonal antibodies raised against CLC-Nt1 polypeptide

(**A**) Immunoblot analysis of microsomal membrane proteins (10 μg) from suspension cells using an affinity-purified preimmune (1) or immune (2) serum raised against CLC-Nt1. (**B**) Immunoblot analysis of microsomal membrane proteins (m) (20 μg), DHFR–N1 (10 ng) or DHFR (10 ng) using affinity-purified antibodies raised against CLC-Nt1. Where indicated, antibodies preabsorbed with 10 μg of DHFR were used as primary antibodies (DHFR Pretreated).

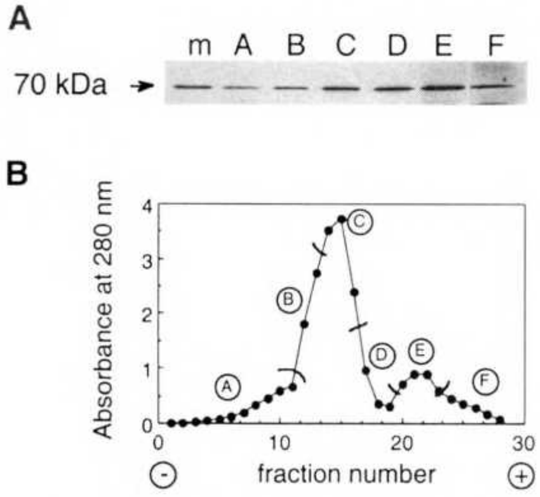

Figure 2 Immunoblot analysis of free-flow electrophoresis membrane fractions

(**A**) Microsomal proteins (m) and pooled membrane fractions (A–F) purified from tobacco cells by free-flow electrophoresis (10 μg of protein per lane) were probed with affinity-purified antibodies raised against CLC-Nt1. (**B**) Corresponding free-flow electrophoresis profile, as determined by absorbance at 280 nm. The letters A–F indicate the positions of the pooled fractions.

antibodies to DHFR protein, whereas the reactivity to the DHFR–N1 fusion protein and to the 70-kDa microsomal protein was unchanged. This result indicates that antibodies to DHFR–N1 detected a membrane protein immunologically related to the N1 fragment of CLC-Nt1, and that the 70-kDa protein revealed in immunoblot experiments is very likely to be the tobacco CLC-Nt1 protein. A signal at 70 kDa did not exactly match the calculated molecular mass of CLC-Nt1 (84.7 kDa), but abnormal electrophoretic mobility of many membrane proteins, for example renal CLC-K1 [21] has been reported.

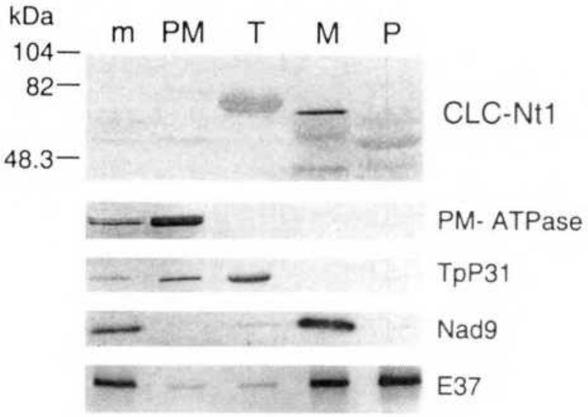

Figure 3 Immunoblot analysis of fractions enriched in tonoplast, mitochondrial, plastidial and plasma membranes

Microsomal proteins (m), plasma membrane (PM), tonoplast (T), mitochondrial membrane (M) and plastid membrane (P) fractions were probed with affinity-purified antibodies raised against CLC-Nt1. Equal amounts of proteins (10 μg) were loaded on to each lane. The proteins were also probed with antibodies raised against a *N. plumbaginifolia* plasma membrane H^+-ATPase (PM-ATPase), the subunit E of barley vacuolar H^+-ATPase (TpP31), the wheat mitochondrial protein Nad9 (Nad9) and the spinach chloroplast protein E37 (E37). The large signal with a weak intensity, observed in the tonoplast, is not specific and corresponds to the major protein of this extract, as observed after Coomassie Blue staining (results not shown).

Biochemical subcellular localization of CLC-Nt1 proteins

In plants, the activity of voltage-dependent anion channels has been generally characterized in the vacuolar (tonoplast) and plasma membranes. Because CLCs are obvious candidates for these activities, we first searched for a putative localization of CLC-Nt1 in these two membranes. Membrane vesicles from tobacco suspension cells were fractionated by free-flow electrophoresis and characterized using the antibodies raised against CLC-Nt1. Figure 2 shows that the signals specific for the protein were reduced in the least and most electronegative membrane fractions. These fractions have been shown to be being specifically enriched in plasma membrane and tonoplast respectively [13]. In contrast, strong signals were detected in the central fractions, which contained most of the internal cellular membranes. Plasma membrane and tonoplast were also prepared from tobacco leaves by two independent procedures, aqueous two-phase partitioning and intact vacuole purification. As shown in Figure 3, a faint signal was obtained with CLC-Nt1 antibodies in a crude microsomal fraction, but no specific signal could be detected in the corresponding plasma membrane and tonoplast fractions. Yet, the enhancement of signals obtained in the plasma membrane and the tonoplast fractions with antibodies raised to a tobacco plasma membrane H^+-ATPase [22] or the subunit E of a barley vacuolar H^+-ATPase [23] demonstrates the efficiency of our purification procedures. Altogether, these data indicate that CLC-Nt1 proteins are most likely not localized in the plasma membrane or in the tonoplast of tobacco cells.

In preliminary experiments, we observed that the immunodetection of the CLC-Nt1 signal was very pronounced in a 1000–10000 ***g*** fraction (results not shown). This fraction is typically enriched in mitochondria and plastids and, indeed, anion channels have been reported in these two organelles [10]. To investigate these findings, mitochondria and plastids were prepared from tobacco leaves by centrifugation on Percoll gradients. To evaluate the efficiency of Percoll-gradient separation, the mitochondria- and plastid-enriched fractions were

Table 1 Purity of mitochondria purified from tobacco leaves by Percoll centrifugation

A 1000–10000 ***g*** fraction was prepared from a tobacco leaf homogenate, as described in the Experimental section, and was used to isolate mitochondria by Percoll centrifugation. Enzyme marker activities (means ± S.E.M.) specific for mitochondria (cytochrome *c* oxidase; μmol/min per mg of protein), endoplasmic reticulum (NADH cytochrome *c* reductase; μmol/min per mg of protein) and Golgi apparatus (latent UDPase and latent IDPase; μmol/h per mg of protein) were measured at each step of the purification procedure. Numbers of replicates are shown in parentheses. ND, not detected. The enrichment in enzyme marker activities obtained after Percoll centrifugation (purified mitochondria/1000–10000 ***g*** fraction) is indicated in the last column.

	Cell fraction			
Enzyme marker	Homogenate	1000–10000 ***g***	Purified mitochondria	Fold increase
Cytochrome *c* oxidase	0.27 ± 0.08 (3)	3.71 ± 0.33 (6)	27.75 ± 0.59 (3)	7.5
NADH cytochrome *c* reductase	0.89 ± 0.15 (2)	0.25 ± 0.01 (3)	0.15 ± 0.01 (3)	0.6
Latent UDPase	0.97 ± 2.92 (5)	3.91 ± 1.60 (5)	ND	–
Latent IDPase	1.27 ± 0.96 (5)	3.63 ± 1.03 (5)	ND	–

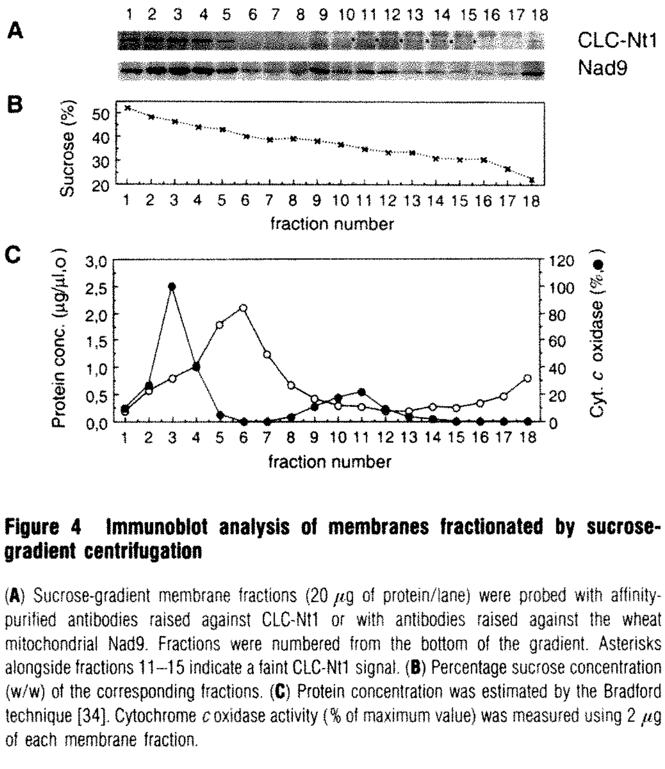

Figure 4 Immunoblot analysis of membranes fractionated by sucrose-gradient centrifugation

(**A**) Sucrose-gradient membrane fractions (20 μg of protein/lane) were probed with affinity-purified antibodies raised against CLC-Nt1 or with antibodies raised against the wheat mitochondrial Nad9. Fractions were numbered from the bottom of the gradient. Asterisks alongside fractions 11–15 indicate a faint CLC-Nt1 signal. (**B**) Percentage sucrose concentration (w/w) of the corresponding fractions. (**C**) Protein concentration was estimated by the Bradford technique [34]. Cytochrome *c* oxidase activity (% of maximum value) was measured using 2 μg of each membrane fraction.

characterized by marker antibodies, which included antibodies raised against spinach chloroplast protein E37 [24] and wheat mitochondrial protein Nad9 [25]. The purity of the mitochondrial fraction was also estimated using enzyme markers specific for the inner mitochondrial membrane (cytochrome *c* oxidase), the endoplasmic reticulum (cytochrome *c* reductase) and the Golgi apparatus (latent UDPase and IDPase) (Table 1). As shown in Figure 3, no signal was observed after immunoblot analysis of the plastid fraction with the CLC-Nt1 antibodies. In contrast, the mitochondrial fraction was strongly enriched in proteins immunologically related to CLC-Nt1. Consistent with our purification procedure, we found that the mitochondrial fraction was strongly enriched in Nad9 marker (Figure 3) and cytochrome *c* oxidase activity (Table 1). A 6- to 7-fold increase in the latter activity during mitochondrial purification was consistently paralleled by a 8- to 11-fold increase in the CLC-Nt1 immunoblot signal. The contamination of the mitochondrial fraction by plasma membrane, tonoplast (Figure 3) or Golgi membranes (Table 1) was very low and was barely detectable. In contrast, a significant level of cytochrome *c* reductase was measured in the mitochondrial fraction. However, this endoplasmic reticulum marker was depleted nearly 2-fold after Percoll centrifugation, whereas the immunodetection of CLC-Nt1 was enhanced. The mitochondrial fraction was also labelled by the chloroplast marker antibodies. However, the CLC-Nt1 antibodies gave a strong signal in the mitochondrial fraction but not in the plastid fraction, indicating that the channel protein was not localized in this fraction. Altogether, these results support the idea that, in tobacco leaves, CLC-Nt1 is not localized in plastids or in any compartment of the secretory pathway, but rather in mitochondria.

To ensure that the signal for CLC-Nt1 in purified mitochondria was not due to a contamination by yet another cellular membrane, we used equilibrium linear sucrose-gradient centrifugation (25–50 %, w/w) as a distinct method for fractionation of tobacco leaf membranes. The antibodies raised against CLC-Nt1 showed a typical signal at 70 kDa, with a major peak in fractions 1–5 (50–42 % sucrose) and a minor peak in less dense fractions 11–15 (36–32 % sucrose) (Figure 4). Cytochrome *c* oxidase activity and Nad9 protein, two markers of the inner mitochondrial membrane, also exhibited a consistent bimodal separation profile. These two peaks are characteristic of mitochondrial membranes [20]. Precise comparison of CLC-Nt1, cytochrome *c* oxidase and Nad9 showed slight differences between the three profiles, in particular in the position and intensity of the second peak. This result might indicate small differences in the populations of vesicles harbouring the three proteins.

The localization of CLC-Nt1 in tobacco cells was also investigated by immunogold electron microscopy. The number of gold particles remained very low, because of the low abundance of the CLC-Nt1 proteins and/or a loss of antigenicity after chemical fixation. Nevertheless, CLC-Nt1 antibodies specifically labelled mitochondria in suspension cells and in a crude 1000–10000 ***g*** leaf fraction (results not shown). This result confirms that the signal obtained in the immunoblot analyses of mitochondria-enriched fractions was indeed associated with mitochondrial membranes.

DISCUSSION

In contrast with their animal counterparts, little is known about the functions of plant CLCs. The anion currents observed after expression of CLC-Nt1 in *Xenopus* oocytes did not provide any obvious parallel to the various anion channels described in the plasma membrane and internal membranes of plant cells [8]. Also, it has been suggested that these currents may reflect activation of endogenous currents [8,26]. Yeast has a unique CLC homologue (Gef1p), and functional complementation of a Gef1p null strain (*gef1*) has been used to evaluate the function of *Arabidopsis* CLCs (AtCLCs) [9]. However, the *gef1* phenotype is multifactorial and could be rescued to various extents by distinct AtCLCs. For example, AtCLC-d complemented both the iron-dependent respiratory and pH-sensitive growth phenotypes of *gef1*, whereas AtCLC-c rescued only the latter deficiency [3]. CLC-0, a *Torpedo* plasma membrane channel involved in the electric organ excitability, also complemented Gef1p function in the Golgi apparatus [3]. These results show that the yeast complementation assay does not allow a definitive conclusion on the cellular localization and function of animal and plant CLCs.

To determine the cellular localization of CLC-Nt1, and thus get some idea of its function, we raised antibodies against an N-terminal polypeptide of the protein. The antibodies were used to probe various plant membrane fractions and consistently identified a 70-kDa protein immunologically related to CLC-Nt1 antigens. The use of independent membrane purification procedures allowed us to establish that CLC-Nt1 was not localized in the plasma membrane or in the tonoplast. These data are consistent with the report by Hechenberger et al. [9], who showed that the staining patterns of AtCLC-GFP (green fluorescent protein) chimeric constructs in yeast were intracellular and did not match the position of the vacuole. In the present work, we show more specifically that the CLC-Nt1 protein co-localizes with two mitochondrial membrane markers, the Nad9 protein and cytochrome *c* oxidase activity. This conclusion is reliant on the preparation of highly purified mitochondria by Percoll centrifugation. The extensive characterization of this preparation showed that the enhanced CLC-Nt1 signal observed in this fraction cannot be explained by contamination with plasma, vacuolar, plastid, endoplasmic reticulum or Golgi membranes. Similarly to the two mitochondrial markers, CLC-Nt1 also exhibited a typical bimodal separation profile after sucrose-gradient centrifugation. The localization of CLC-Nt1 was confirmed in suspension cells and in a crude leaf fraction by faint but specific immunogold labelling of mitochondria with the CLC-Nt1 antibodies.

The localization and/or function of CLCs in the intracellular membranes of yeast or animal cells has been unambiguously established by several groups [3–5,7]. Yet, the localization of tobacco CLC-Nt1 in the mitochondrial fraction remains unique, because this compartment does not directly derive from the cell secretory pathway. Similar cases have been reported for Shaker-like K^+ channels and porin-like voltage-dependent anion channels, where members of the same molecular family show very distinct cellular distributions with some members in the secretory pathway and others in mitochondria [27,28]. The unexpected localization of CLC-Nt1 in mitochondria now raises specific questions concerning the post-translational import of the protein into this compartment. The N-terminal region of CLC-Nt1 does not show any transit-peptide signature, but several inner membrane proteins, including the recently identified plant uncoupling proteins [29], do not contain any cleavable peptide extension.

The outer mitochondrial membrane harbours large conductance voltage-dependent anion channels (VDAC) encoded by porin-like channel proteins [30]. Anion transport in mitochondria is thus primarily limited by a specific pathway in the inner membrane, referred to as the inner membrane anion channel (IMAC) [31]. This pathway has been detected in the mitochondria of animals [31] and plant species, such as potato [32] and tobacco (C. Lurin and C. Maurel, unpublished work), by means of a classical mitochondrial-swelling assay. Patch-clamp experiments also revealed a voltage-gated 108-pS chloride channel in the inner mitochondrial membrane of several animal cell types, and this activity has been tentatively associated with IMAC permeability [33]. The molecular identity and the cellular functions of these channels remains unknown and the results of the present study lead to the idea that CLC-Nt1 maybe a candidate for these activities in tobacco. The *CLC-Nt1* gene may thus provide a unique molecular tool to study the putative role of mitochondrial anion transport in the regulation of mitochondrial volume and in the control of membrane electrical potential.

We thank our colleagues Dr Danny Geelen for fruitful discussions during this work and Sophie Deniau for help in some of the experiments The help of Dr M Neuberger in setting up Percoll-gradient purification procedures is gratefully acknowledged We thank Dr M Boutry, Dr K.-J Dietz, Dr J Joyard and Dr J-M. Grienenberger for providing marker antibodies.

REFERENCES

1 Jentsch, T J, Friedrich, T, Schriever, A and Yamada, H (1999) Pflugers Arch **437**, 783–795
2 Duan, D, Winter, C, Cowley, S., Hume, J R and Horowitz, B (1997) Nature (London) **390**, 417–421
3 Gaxiola, R. A, Yuan, D S, Klausner, R D and Fink, G. R (1998) Proc. Natl Acad Sci U S A. **95**, 4046–4050
4 Gunther, W, Luchow, A, Cluzeaud, F, Vandewalle, A and Jentsch, T. J (1998) Proc Natl Acad Sci U S A **95**, 8075–8080
5 Schwappach, B, Stobrawa, S, Hechenberger, M., Steinmeyer, K and Jentsch, T J. (1998) J Biol. Chem. **273**, 15110–15118
6 Davis-Kaplan, S R, Askwith, C. C, Bengtzen, A C, Radisky, D and Kaplan, J (1998) Proc. Natl Acad Sci U.S A **95**, 13641–13645
7 Buyse, G, Trouet, D, Voets, T, Missiaen, L, Droogmans, G, Nilius, B and Eggermont, J (1998) Biochem J. **330**, 1015–1021
8 Lurin, C, Geelen, D, Barbier-Brygoo, H, Guern, J and Maurel, C (1996) Plant Cell **8**, 701–711
9 Hechenberger, M, Schwappach, B, Fischer, W N, Frommer, W B, Jentsch, T J and Steinmeyer, K. (1996) J Biol Chem **271**, 33632–33638
10 Barbier-Brygoo, H, Vinauger, M, Colcombet, J, Ephritikhine, G, Frachisse, J-M and Maurel, C (2000) Biochim Biophys Acta, in the press
11 Hedrich, R and Becker, D (1994) Plant Mol Biol **26**, 1637–1650
12 Mathieu, Y, Sanchez, F. J, Droillard, M-J, Lapous, D, Laurière, C. and Guern, J (1996) Plant Physiol Biochem **34**, 399–408
13 Maurel, C, Tacnet, F, Guclu, J., Guern, J and Ripoche, P. (1997) Proc Natl. Acad Sci U S A **94**, 7103–7108
14 Ephritikhine, G, Pradier, J.-M and Guern, J. (1993) Plant Physiol Biochem **31**, 573–584
15 Hofte, H., Faye, L, Dickinson, C, Herman, E M and Chrispeels, M J (1991) Planta **184**, 431–437
16 Caboche, M (1980) Planta **149**, 7–18
17 Douce, R and Joyard, J (1982) in Methods in Chloroplast Molecular Biology (Edelman, M, Hallick, R. and Chua, N H, eds), pp 239–256, Elsevier, Amsterdam
18 Douce, R, Bourguignon, J., Brouquisse, R and Neuburger, M (1987) Methods Enzymol **148**, 403–415
19 Briskin, D. P, Leonard, R T. and Hodges, T K (1987) Methods Enzymol **148**, 542–558
20 Chaumont, F, Bernier, B, Buxant, R, Williams, M E, Levings, C. S and Boutry, M. (1995) Proc Natl Acad Sci U S A **92**, 1167–1171
21 Uchida, S, Sasaki, S., Nitta, K., Uchida, K, Horita, S, Nihei, H and Marumo, F (1995) J Clin Invest **95**, 104–113
22 de Kerchove d'Exaerde, A, Supply, P, Dufour, J-P, Bogaerts, P, Thinès, D, Goffeau, A and Boutry, M. (1995) J. Biol Chem **270**, 23828–23837
23 Dietz, K-J, Rudloff, S, Ageorges, A., Eckerskorn, C, Fischer, K and Arbinger, B (1995) Plant J **8**, 521–529
24 Teyssier, E, Block, M., Douce, R. and Joyard, J (1996) Plant J **10**, 903–912
25 Lamattina, L, Gonzalez, D, Gualberto, J and Grienenberger, J-M (1993) Eur J Biochem **217**, 831–838
26 Shimbo, K, Brassard, D L, Lamb, R A and Pinto, L H (1995) Biophys. J **69**, 1819–1829
27 Suzuki, M, Kotake, K, Fujikura, K, Inagaki, N, Suzuki, T., Gonoi, T, Seino, S. and Takata, K. (1997) Biochem. Biophys. Res Commun **241**, 693–697
28 Reymann, S, Haase, W, Krick, W, Burckhardt, G. and Thinnes, F (1998) Pflugers Arch **436**, 478–480
29 Laloi, M, Klein, M, Riesmeier, J W, Muller-Röbert, B, Fleury, C, Boulliaud, F and Ricquier, D (1997) Nature (London) **389**, 135–136
30 Sorgato, M. C and Moran, O. (1993) Crit Rev Biochem Mol Biol **28**, 127–171
31 Beavis, A D (1992) J Bioenerg Biomembr **24**, 77–90
32 Beavis, A D and Vercesi, A E (1992) J Biol. Chem **267**, 3079–3087
33 Borecky, J, Jezek, P. and Siemen, D (1997) J Biol Chem. **272**, 19282–19289
34 Bradford, M M (1976) Anal Biochem **72**, 248–254

Received 23 July 1999/17 February 2000, accepted 16 March 2000

Biochem J (2000) 348, 297–305 (Printed in Great Britain)

Chicken Y-box proteins chk-YB-1b and chk-YB-2 repress translation by sequence-specific interaction with single-stranded RNA

Shivalingappa K. SWAMYNATHAN, Ashok NAMBIAR[1] and Ramareddy V. GUNTAKA[2]
Department of Molecular Microbiology and Immunology, School of Medicine, University of Missouri-Columbia, Columbia, MO 65212, U.S.A.

Y-Box proteins comprise a large family of multifunctional proteins with a wide spectrum of activities in both transcription and translational regulation of gene expression. Earlier, we have reported on the involvement of chk-YB-2 in transcriptional regulation of Rous sarcoma virus long terminal repeats and the involvement of chk-YB-1b in transcriptional regulation of alpha1(I) collagen genes. Here, we have investigated the potential role of chk-YB-2 and chk-YB-1b in RNA metabolism. We report that chk-YB-2 and chk-YB-1b are localized predominantly in the cytoplasm and that they both can bind single-stranded RNA in a sequence-specific and reversible manner. Well-conserved cold-shock domain, N-terminal proline-rich domain and the alternating clusters of acidic and basic amino acids located in the C-terminal ends of these two proteins were all found to be necessary for their RNA-binding ability. Further, we demonstrate that these two proteins inhibit translation *in vitro* and that binding to RNA is required for this inhibition. The significance of these results is discussed.

Key words: cold-shock domain, RNA-binding proteins, Rous sarcoma virus.

INTRODUCTION

Several proteins are known to bind RNA in a non-specific and/or highly sequence-specific manner and influence properties such as stability and availability of RNA for translation in the cytoplasm [1–7]. These RNA-binding proteins belong to several different multigene families. Among them, Y-box proteins have emerged recently as an important family of multifunctional proteins. They are involved in regulation of transcription of a number of genes in several systems [8] and also in the regulation of stability and translatability of specific transcripts [1,6,9–16]. Y-Box proteins have been shown to be predominantly cytoplasmic and are usually complexed with different mRNA molecules as 50–60 S messenger ribonucleoprotein (mRNP) particles [16]. Repression of translation seems to be the most common effect of over-expression of Y-box proteins in the cytoplasm [1,17,18]. In one report, however, Y-box proteins have been shown to be necessary for translation [19]. Recently, a Y-box protein called *unr*, which contains five repeats of cold-shock domain (CSD), was shown to be required for internal initiation of translation of human rhinovirus RNA [20]. In *Xenopus* oocytes, spermatocytes and early embryos, two Y-box proteins (FRGY1 and FRGY2) have been demonstrated to bind specific mRNA sequences and mask their translation [21]. However, these RNAs are released during the development of the embryo in a regulated manner in a later stage when there is a need for these proteins but active transcription has not yet begun [22]. A mouse Y-box protein, MSY-1, is known to be associated with paternal RNA in spermatocytes [23].

Sequence comparison of RNA-binding proteins has revealed well-conserved domains that are required for RNA binding. The X-ray crystal structures of some of these domains have been worked out [24]. One such domain is the RNP1 motif, a relatively short stretch of about eight amino acids buried in the middle of the well-conserved CSD found in Y-box proteins [9,25]. Other motifs which can confer RNA-binding ability are (i) the arginine-rich motif found in the HIV Rev and Tat proteins and (ii) the RGG box, closely spaced repeats of arginine and glycine interspersed with aromatic residues. Interestingly, most Y-box proteins also have these motifs. In addition to an RNP1 motif within the N-terminal CSD, they contain alternating clusters of acidic and basic amino acids at their C-terminal ends. The relative contributions of these different domains to RNA-binding ability of many different Y-box proteins is less understood. Only in the case of *Xenopus* Y-box protein FRGY-2 it is proposed that the C-terminal charge zippers confer non-specific RNA binding while the CSD confers sequence specificity [13,26].

Previously, we have shown that an avian Y-box protein chk-YB-2 is important for transcription from the highly potent promoter of Rous sarcoma virus (RSV) long-terminal repeats (LTR) in avian cells [27,28]. In addition, we characterized the DNA-binding domain of chk-YB-2 [29]. We also have presented evidence showing that another Y-box protein, chk-YB-1b, is involved in regulating the transcription of type-I collagen genes in several species [30,31]. Apart from the RNP1 motif found in the middle of the CSD, chk-YB-1b and chk-YB-2 also have well-conserved arginine-rich motifs and the RGG repeats in the C-terminal charge zipper region [27,30], suggesting that these two proteins may also bind to RNA. In this report, we show that (i) chk-YB-1b and chk-YB-2 are localized predominantly in the cytoplasm of chicken embryo fibroblasts (CEFs), (ii) chk-YB-1b and chk-YB-2 are capable of binding to single-stranded RNA oligonucleotides in a sequence-specific and reversible manner, (iii) both CSD and the C-terminal charge zippers are required for

---

Abbreviations used. RSV, Rous sarcoma virus, LTR, long terminal repeats, CSD, cold-shock domain, mRNP, messenger ribonucleoprotein; CEF, chicken embryo fibroblast, EMSA, electrophoretic mobility shift assay, GFP, green fluorescent protein, TNT, coupled transcription and translation, MBP, maltose-binding protein

[1] Present address Department of Pathology, A614, Scaife Hall, University of Pittsburgh Medical Center, Pittsburgh, PA, U S A

[2] To whom correspondence should be addressed (e-mail guntakar@health missouri.edu).

this RNA-binding activity of chk-YB-2; and (iv) binding inhibits translation of the bound RNA.

MATERIALS AND METHODS

Cell culture, preparation of proteins and electrophoretic mobility shift assays (EMSAs)

CEF cells or RSV-infected CEF cells were grown as described previously [28]. Nuclear extracts and cytoplasmic extracts were prepared as described [32]. Each of these extracts (15 μg) was used in EMSAs. Fusion proteins maltose-binding protein (MBP)-chk-YB-1b or MBP-chk-YB-2, or their deletion mutants, were expressed in *Escherichia coli* and partially purified using amylose columns as described in [28]. These proteins were run on SDS/PAGE gels to confirm their size.

The sequences of oligonucleotides used in this study are presented in Table 1. All the oligonucleotides used were phosphodiester oligonucleotides with no modifications Double-stranded oligonucoeotides were prepared in the following way. Equimolar amounts of the constituent single-stranded oligonucleotide were mixed in 300 mM NaCl/10 mM Tris/1.0 mM EDTA (pH 8.0). This mix was heated to 95 °C and cooled down gradually to room temperature. The annealing mix was then run on a 6% acrylamide preparative gel in TBE buffer (45 mM Tris/borate/1 mM EDTA) and the double-stranded oligonucleotides were eluted from the gel. Oligodeoxyribonucleotides and oligoribonucleotides (Table 1) were obtained from commerical sources (Oligos, etc., Wilsonville, OR, U.S.A.) and radiolabelled on their 5′ termini using polynucleotide kinase. EMSAs were performed as described previously [28]. Briefly, bacterially expressed proteins or nuclear extracts were incubated with approximately 50000 c.p.m. ($\approx$ 0.5 ng) of DNA or RNA oligonucleotides in a buffer containing 20 mM Hepes (pH 7.9), 3 mM $MgCl_2$, 50 mM NaCl, 1 mM dithiothreitol, 2 μg of poly(dI-dC) and 10% glycerol for 20 min and then run on 6% polyacrylamide gels in Tris/glycine/EDTA buffer to separate the bound complex from the free oligonucleotides. Gels were dried and exposed to X-ray film for about 18 h. Competition assays were performed by incubating the proteins with the cold competitor oligonucleotides for 15 min before the addition of radiolabelled probe.

Polyclonal antibodies against chk-YB-1b and chk-YB-2 were raised in mice, using bacterially expressed chk-YB-1b or chk-YB-2, which were purified as before [28]. We have tested them and found that anti-chk-YB-1b and anti-chk-YB-2 antibodies do not cross-react with each other (S. K. Swamynathan and R. V. Guntaka, unpublished work). Super-shift assays were performed by incubating the proteins with respective antibodies for 15 min at room temperature before addition of the radiolabelled probe.

Table 1 Sequences of different oligonucleotides used

Oligonucleotide	Sequence
E4C-1 DNA	5′-GGCACGATCGTACCACCTTAC-3′
E4C-1 RNA	5′-GGCACGAUCGUACCACCUUAC-3′
E4C-1-Mut RNA	5′-GGCACGAUCGGACCGCCUUAC-3′
E4-1 RNA	5′-GUAAGGUGGUACGAUCGUGGC-3′
E4-1 RNA–E4C-1 DNA heteroduplex	5′-GUAAGGUGGUACGAUCGUGCC-3′ 3′-CATTCCACCATGCTAGCACGG-5′
E4-1 DNA–E4C-1 RNA heteroduplex	5′-GTAAGGTGGTACGATCGTGCC-3′ 3′-CAUUCCACCAUGCUAGCACGG-5′
RSV Ψ RNA	5′-ACGACUGAGCAGUCCACCCCAGGCGUGAUU-3′

Construction of green fluorescent protein (GFP)-Y-box-protein fusion proteins and transfection

Vectors expressing fusion proteins of chk-YB-1b and chk-YB-2 with GFP under the influence of the RSV LTR promoter/enhancer were constructed following standard methods [33]. They were constructed such that the coding sequences of chk-YB-1 or chk-YB-2 were inserted in-frame, in the *Bsr*GI site at the 3′-end of the *EGFP* (enhanced GFP) gene (the plasmid pEGFP containing *EGFP* was from Clontech, Palo Alto, CA, U.S.A.). Equal amounts (1.0 μg) of these plasmid DNAs were transfected into CEFs in the log phase of growth using lipofectAMINE, following the protocol suggested by the manufacturers (Gibco-BRL, Grand Island, NY, U.S.A.), as described previously [28]. After transfection (24 h), cells were observed under a fluorescence microscope and photographed.

Coupled transcription and translation (TNT) reactions

Translation reactions *in vitro* coupled to T7 polymerase-mediated transcription reactions (TNT reactions) were performed using the rabbit reticulocyte lysate TNT kit following the protocol suggested by the manufacturer (Promega, Madison, WI, U S.A.). The plasmid expressing p19 Gag protein of RSV under the influence of T7 promoter was constructed by directional cloning of the PCR-amplified fragment of RSV genome encompassing nucleotides 1–844 in pBSSK+. TNT reactions were performed using ^{35}S-methionine, following the manufacturer's protocol in a 25-μl volume. Fusion proteins MBP-chk-YB-1b or MBP-chk-YB-2 were included in the reactions at the concentrations indicated in the Figure legends. Following incubation for 2 h at 30 °C, the reactions were stopped by boiling in 1 × SDS/PAGE sample buffer and the reaction products were separated on SDS/PAGE. The gels were dried and exposed to X-ray film for 20 h.

RESULTS

Both chk-YB-1b and chk-YB-2 bind RNA in a sequence-specific manner

Earlier, we studied in detail the interaction of chk-YB-1b and chk-YB-2 with single-stranded E4C-1 DNA having the sequence 5′-GTACCACC-3′. Here, we report the results of our experiments with chk-YB-1b and chk-YB-2 proteins for their ability to interact with single-stranded RNA oligoribonucleotides in a sequence-specific manner. We performed EMSAs with ^{32}P-labelled E4C-1 RNA and chk-YB-2 or chk-YB-1b, as described in the Materials and methods section. The sequence of E4C-1 RNA is shown in Table 1. This sequence is the same as that of E4C-1 DNA on the negative strand of RSV LTR (to which we have previously demonstrated a high-affinity binding of both chk-YB-2 and chk-YB-1b), except that ribonucleotides were used. We found that chk-YB-2 bound E4C-1 RNA with high affinity in a Mg^{2+}-dependent manner (Figure 1, top panel). Inclusion of 3 mM Mg^{2+} stimulated RNA binding by chk-YB-2. There was no further stimulation or inhibition in binding upon increasing the Mg^{2+} concentration up to 10 mM in the binding reaction (Figure 1, top panel). We obtained similar results with chk-YB-1b also (results not shown).

chk-YB-2 and chk-YB-1b bind to RSV RNA within the leader region

RSV is a simple retrovirus which expresses Gag, Pol, Env and Src proteins. As the relevance of the above-demonstrated binding of chk-YB-1b and chk-YB-2 to E4C-1 RNA (which represents the

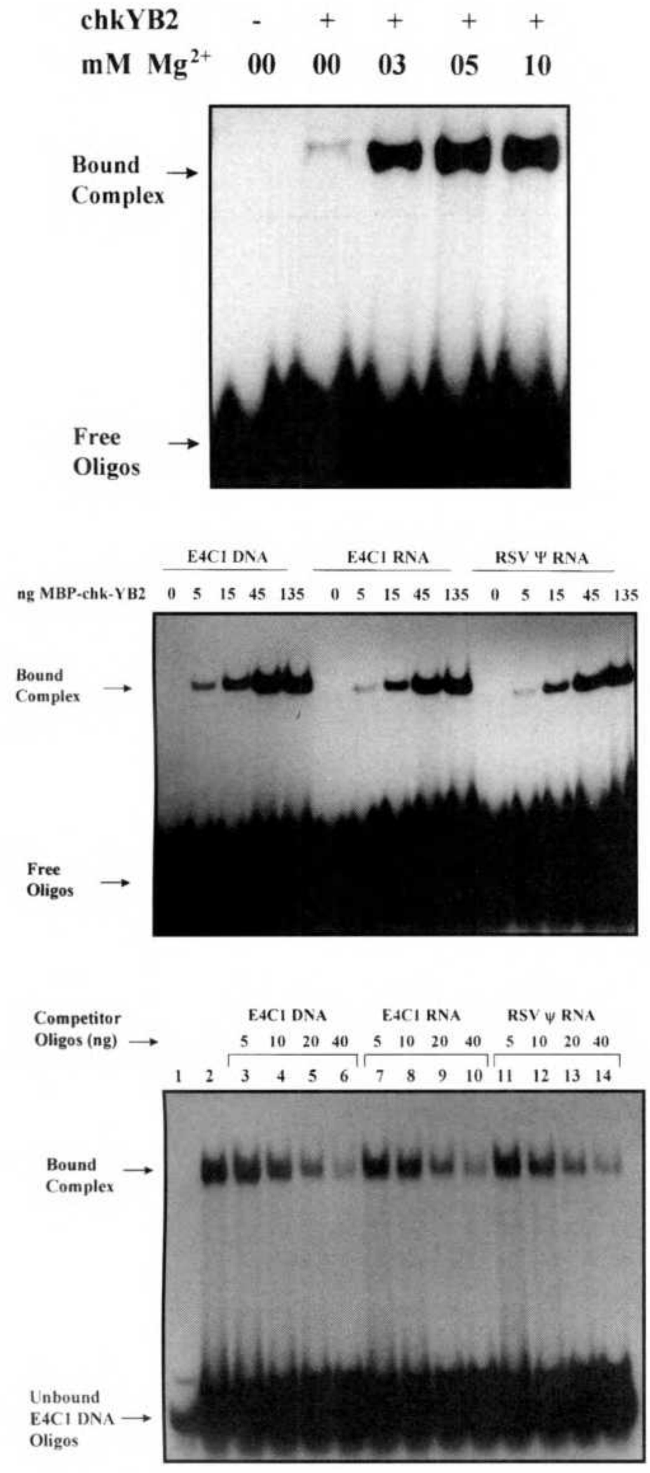

Figure 1 chk-YB-2 binds E4C-1 DNA, E4C-1 RNA and RSV Ψ RNA with equal affinity, in a Mg^{2+}-dependent manner

(Top panel) Equal amounts (10 ng) of bacterially expressed chk-YB-2 were incubated with E4C-1 RNA in the absence or presence of increasing amounts of Mg^{2+} in the reaction, and EMSAs were performed as described. Note that bound complex formation is extremely dependent on the presence of Mg^{2+} in the reaction. Similar results were obtained with chk-YB-1b (results not shown). (Middle panel) Increasing amounts of bacterially expressed MBP-chk-YB-2 fusion protein were incubated with E4C-1 DNA, E4C-1 RNA or RSV Ψ RNA labelled to the same specific activity as described in the Materials and methods section. Note that the intensity of the bound complex is roughly the same in the three different kinds of probe, at any given concentration of chk-YB-2. (Bottom panel) Increasing amounts of unlabelled E4C-1 DNA, E4C-1 RNA or RSV Ψ RNA as shown were used to compete with labelled E4C-1 DNA for binding the same amount of chk-YB-2 (50 ng). Lane 1, free (unbound) E4C-1 DNA; lane 2, E4C-1 DNA bound with 50 ng of chk-YB-2. As can be seen, E4C-1 DNA, E4C-1 RNA and RSV Ψ RNA competed equally efficiently, indicating that the affinity of chk-YB-2 for the three competitors was the same.

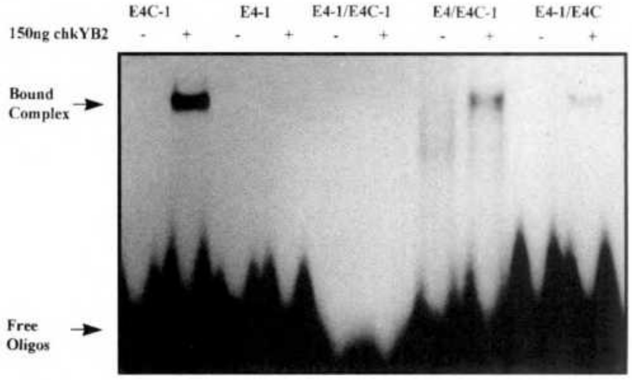

Figure 2 Sequence specificity of interaction of chk-YB-2 with E4C-1 RNA

Similar amounts of chk-YB-2 were incubated with (reading left to right on the Figure) single-stranded E4C-1 RNA, single-stranded E4-1 RNA, double-stranded E4-1/E4C-1 RNA, double-stranded heteroduplex E4-1 DNA/E4C-1 RNA or double-stranded heteroduplex E4-1 RNA/E4C-1 DNA and the EMSAs were performed as described. Note that only single-stranded E4C-1 RNA was bound well by chk-YB-2. See Table 1 for the sequences of oligonucleotides used.

sequence on the non-coding strand of RSV LTR) is questionable, a search was made for similar sequence motifs in the RSV genomic RNA that would serve as a potential binding site for chk-YB-1b and chk-YB-2. We found that a site present within the RSV leader RNA (nucleotide positions 328–357, see Table 1) closely resembled the canonical single-stranded DNA sequence 5′-GTACCACC-3′ present in the RSV LTR, with which both chk-YB-1b and chk-YB-2 interact [27–30]. We synthesized an oligoribonucleotide RSV Ψ RNA representing the sequence of RSV leader RNA, between nucleotides 328 and 357 and used in EMSAs with chk-YB-1b or chk-YB-2. We carried out EMSAs in which increasing amounts of chk-YB-2 were incubated with E4C-1 DNA, E4C-1 RNA or RSV Ψ RNA, which were labelled to the same specific activity (see Table 1 for sequences). As shown, chk-YB-2 bound these three different oligonucleotides with equal affinity (Figure 1, middle panel).

These results were confirmed further by competition experiments. Non-labelled E4C-1 DNA, E4C-1 RNA or RSV Ψ RNA oligonucleotides competed with equal efficiency with the labelled E4C-1 DNA oligonucleotides for binding to chk-YB-2 (Figure 1, bottom panel). Similar results were obtained with chk-YB-1b (results not shown).

In order to find out if this interaction of chk-YB-2 and/or chk-YB-1b with RNA is sequence-specific, we investigated if chk-YB-2 can interact with the purine-rich RNA sequence complementary to E4C-1 (5′-GGTGGTAC-3′) or the double-stranded RNA sequence representing this region. As shown in Figure 2, chk-YB-2 binds only to the pyrimidine-rich single-stranded E4C-1 RNA and not the purine-rich complementary strand E4-1 RNA or the double-stranded RNA E4-1/E4C-1. Since the genome of RSV goes through a stage of RNA–DNA duplex in the host cell during its life cycle, it was important to test if chk-YB-2 is capable of binding different RNA–DNA heteroduplexes which, if found, will be of potential significance. However, we found that chk-YB-2 bound RNA–DNA heteroduplexes with very low

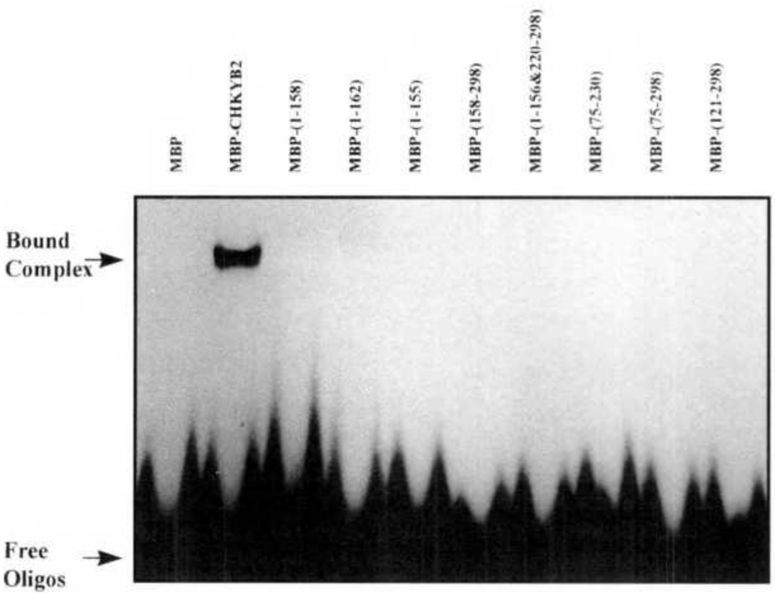

165	**R** Y A A D **R** **R** **R** Y	174
175	**R** G Y F G **R** **R** **R** G	184
210	**R** N P T Y **R** P **R** Y	218
219	**R** R G P L **R** P **R** P	227
254	**R** P Y N Y **R** **R** **R** P	265

Figure 3 CSD is essential but not sufficient for RNA-binding activity of chk-YB-2

(Top panel) Equimolar amounts of bacterially expressed MBP fusion proteins of various deletion mutants of chk-YB-2 were incubated with same amounts of radiolabelled E4C-1 RNA and EMSAs performed as described. Note that only MBP-chk-YB-2 showed an ability to bind the E4C-1 RNA under the conditions used. None of its deletion mutants could bind the E4C-1 RNA, indicating that essentially all of the full-length chk-YB-2 protein contributes to RNA binding. (Bottom panel) Presence of five repeats of eight amino acids in the C-terminus of chk-YB-2. Note that the position of arginine moieties is fairly well conserved within these repeats.

affinity (Figure 2, lanes marked E4/E4C-1 and E4-1/E4C; see Table 1 for sequence) in contrast to its high-affinity binding with the single-stranded RNA (E4C-1 RNA, Figure 2). These results suggest that chk-YB-2 binds with high affinity, only to single-stranded RNA or DNA in a sequence-specific manner but not to double-stranded DNA or double-stranded RNA or to RNA–DNA heteroduplexes.

CSD is necessary but not sufficient for conferring RNA-binding ability on chk-YB-2

We have shown previously that the CSD is necessary but not sufficient for conferring DNA-binding ability on chk-YB-2 [29]. In this report, we have used the deletion mutants of chk-YB-2 described earlier [29] to locate the RNA-binding domain in chk-YB-2. As can be seen, none of these mutant proteins was capable of binding to E4C-1 RNA, while the wild-type protein bound efficiently (Figure 3, top panel). It is interesting that the mutant containing the N-terminal 162 amino acids, which we have shown to be capable of interacting with DNA [29], fails to bind RNA [MBP-(1-162); Figure 3, top panel]. This suggests that the domain required for binding RNA extends beyond the region required for interaction with DNA. Our results also show that the CSD is necessary but not sufficient for conferring RNA-binding ability on chk-YB-2 (Figure 3, top panel). An analysis of the amino acid sequence of chk-YB-2 revealed the presence of five arginine-rich repeats, each containing eight amino acids, in the C-terminal half of the protein (Figure 3, bottom panel). Our results suggest that, in addition to the CSD, the presence of all of these repeats in the charge zipper is necessary for chk-YB-2 to exhibit RNA-binding ability.

The host factor interacting with E4C-1 RNA and RSV Ψ RNA is chk-YB-2 and is cytoplasmic

All of the above experiments were performed with bacterially expressed, partially purified Y-box proteins. It was therefore important to demonstrate the corresponding activities in either the cytoplasm or the nucleus of the avian fibroblasts. Therefore we carried out EMSAs with cytoplasmic or nuclear extracts from CEF and radiolabelled RSV Ψ RNA. As expected, a complex was detected when cytoplasmic extract was used with radiolabelled RSV Ψ RNA (Figure 4, top panel, lane 1), which could be competed out with 30-fold molar excess of unlabelled RSV Ψ RNA (Figure 4, top panel, lane 2). Higher amounts of non-specific RNA were required to compete out binding (Figure 4, top panel, lane 3). We did not observe the formation of any complex when similar amounts of nuclear extracts were used. This indicates that the complex seen in lane 1 (Figure 4, top panel) is the result of sequence-specific interaction of a cytoplasmic factor with RSV Ψ RNA.

We then performed super-shift assays, using anti-chk-YB-1b or anti-chk-YB-2 antibodies to identify the cytoplasmic factor binding to the E4C-1 RNA. Our results show that anti-chk-YB-2 antibodies either abolished the formation of the complex or caused a super-shift of the complex (Figure 4, bottom panel, lane 3). Anti-chk-YB-1b antibodies did not have a similar effect on the complex formation (Figure 4, bottom panel, lane 4). These results therefore suggest that the cytoplasmic factor binding to the E4C-1 RNA is predominantly chk-YB-2. We then confirmed the sequence specificity of this interaction by using a mutant E4C-1 RNA having changes, which when introduced in the E4C-1 DNA had abolished binding [29]. Our results show that the cytoplasmic factor fails to bind the mutant E4C-1 RNA (Figure 4, bottom panel, lanes 5–8). When RSV Ψ RNA was used in the binding reactions, we obtained essentially the same results as with E4C-1 RNA, again confirming that the cellular factor which interacts with the RSV Ψ region is predominantly chk-YB-2 (Figure 4, bottom panel, lanes 9–12).

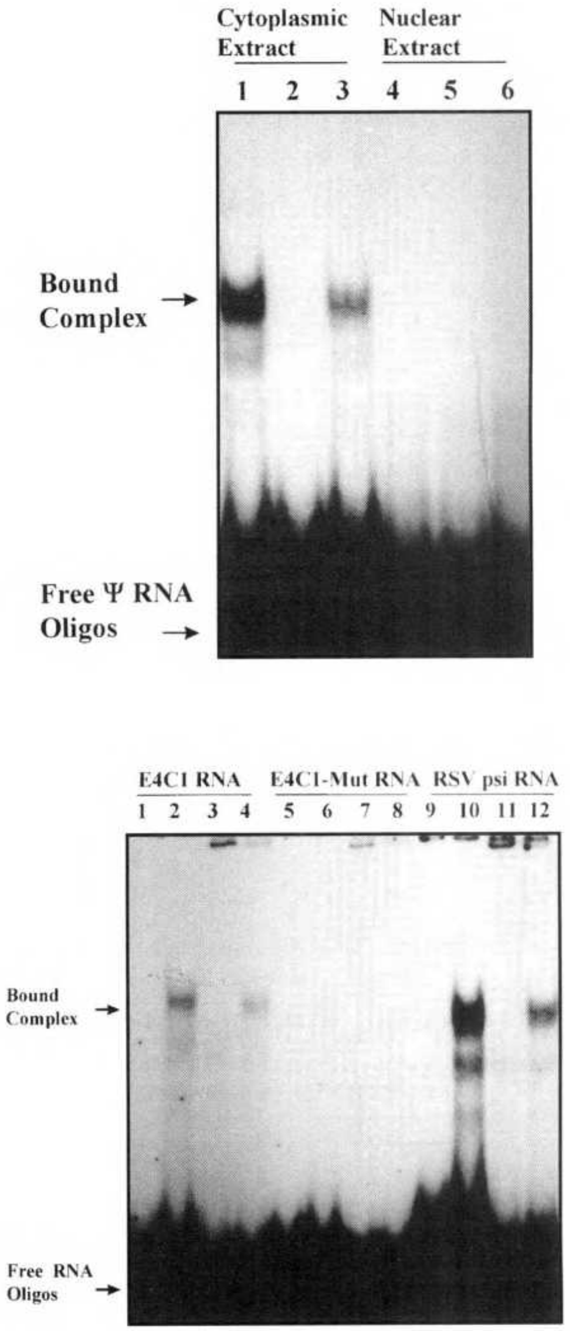

Figure 4 Sequence-specific binding of RSV Ψ RNA by the cytoplasmic factor chk-YB-2

(Top panel) The cellular factor interacting with the RNA is cytoplasmic and the nature of interaction is sequence-specific. Lane 1, 15 μg of CEF cytoplasmic extract bound with radiolabelled RSV Ψ RNA. Lane 2, as lane 1, but with 30-fold molar excess of unlabelled RSV Ψ RNA as specific competitors. Lane 3, as lane 1, but with 30-fold molar excess of a E4C-1 mutant RNA competitor. Lanes 4–6 are the same as lanes 1–3 respectively; however, in these reactions, CEF nuclear extracts were used. (Bottom panel) Super-shift experiments demonstrate that the cytoplasmic factor interacting with the RNA is chk-YB-2. Lanes 1, 5 and 9, free, unbound RNA as indicated at the top of the Figure. Lanes 2, 6 and 10, respective oligoribonucleotides bound with 15 μg of CEF cytoplasmic extracts. Lanes 3, 7 and 11, similar to lanes 2, 6 and 10, but with anti-chk-YB-2 polyclonal antibodies (1:30 final dilution). Lanes 4, 8 and 12, similar to lanes 2, 6 and 10, but with anti-chk-YB-1b polyclonal antibodies (1:30 final dilution). Note that the bound complex formation is observed only with either E4C-1 RNA (lane 2) or RSV Ψ RNA (lane 10) but not with E4C-1-Mut RNA (lane 6). Also, only the anti-chk-YB-2 antibodies could super-shift or abolish the formation of the bound complex (lanes 3 and 11), whereas anti-chk-YB-1b antibodies failed to demonstrate a similar effect (lanes 4 and 12).

GFP-chk-YB-1b and GFP-chk-YB-2 fusion proteins are localized to the cytoplasm

In order to confirm the cytoplasmic location of chk-YB-2 and chk-YB-1b, we constructed fusion proteins of chk-YB-2 or chk-YB-1b with GFP and expressed them under the influence of the RSV LTR in avian fibroblasts, by transient transfection. Fluorescence microscopic analysis indicated that GFP was present all over the cell in a diffuse manner (Figure 5A). In contrast, GFP-chk-YB-2 fusion protein was localized predominantly in the cytoplasm (Figure 5B) with very little in the nucleus. GFP-chk-YB-1b was also localized in the cytoplasm, but its appearance is quite different from chk-YB-2, as it is mainly found in discrete particles or in punctate form (Figure 5C). This punctate appearance of GFP-chk-YB-1b suggests that it probably is part of a large particulate complex, such as the 50–60 S mRNP storage particles that were documented earlier as containing homologues of YB1 proteins [16,23]. In order to find out whether infection by RSV causes any changes in the distribution of these proteins, we repeated the same experiments with CEF cells transformed by the Prague A strain of RSV (gift of Dr. Martin Stoltzfus, University of Iowa, Iowa City, IA, U.S.A.). We did not see any significant differences in the patterns of subcellular localization of these Y-box proteins in RSV-transformed CEFs (Figures 5D–5F). We have since confirmed the validity of using GFP fusion proteins to study subcellular localization of Y-box proteins by performing immunocytochemistry on CEFs and Prague A RSV-transformed CEFs using anti-chk-YB-1b and anti-chk-YB-2 antibodies (S. K. Swamynathan and R. V. Guntaka, unpublished work).

chk-YB-1b and chk-YB-2 repress translation

Our results showed that both chk-YB-1b and chk-YB-2 can interact with single-stranded RNA in a sequence-specific manner, so we were interested in understanding the functional significance of this interaction. Therefore, we performed translation reactions *in vitro* using the construct RSV 1-844, which produces the p19

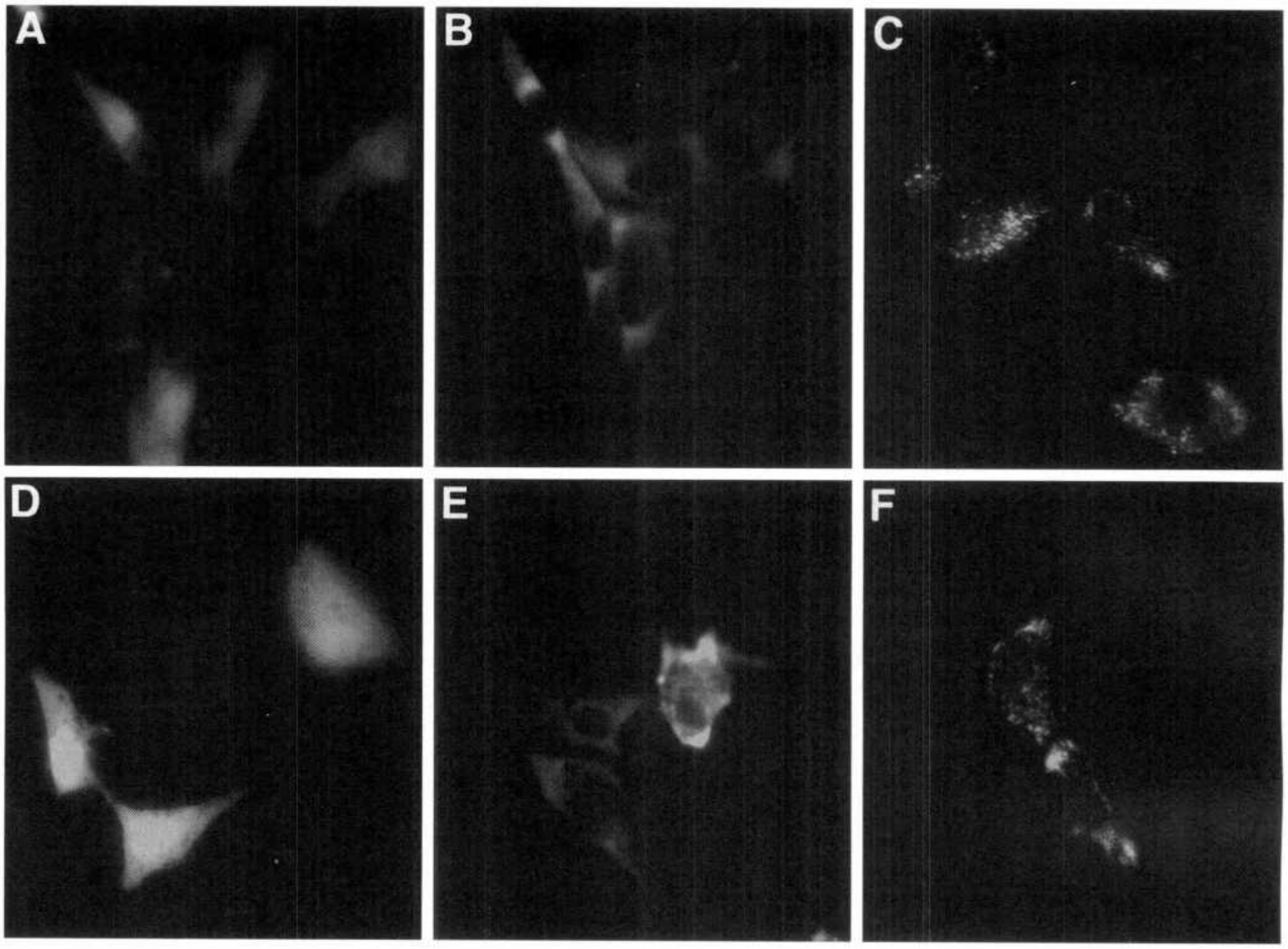

Figure 5 Subcellular localization of chk-YB-1b and chk-YB-2

Recombinant vectors expressing (i) GFP, (ii) GFP-chk-YB-2 fusion protein or (iii) GFP-chk-YB-1b fusion protein were constructed and transfected into CEF cells or RSV-transformed CEF cells. Localization of these proteins was visualized using a fluorescence microscope after 48 h of recovery from transfection. (**A**) GFP in CEF cells, (**B**) GFP-chk-YB-2 in CEF cells, (**C**) GFP-chk-YB-1b in CEF cells, (**D**) GFP in RSV-transformed CEF cells, (**E**) GFP-chk-YB-2 in RSV-transformed CEF cells and (**F**) GFP-chk-YB-1b in RSV-transformed CEF cells.

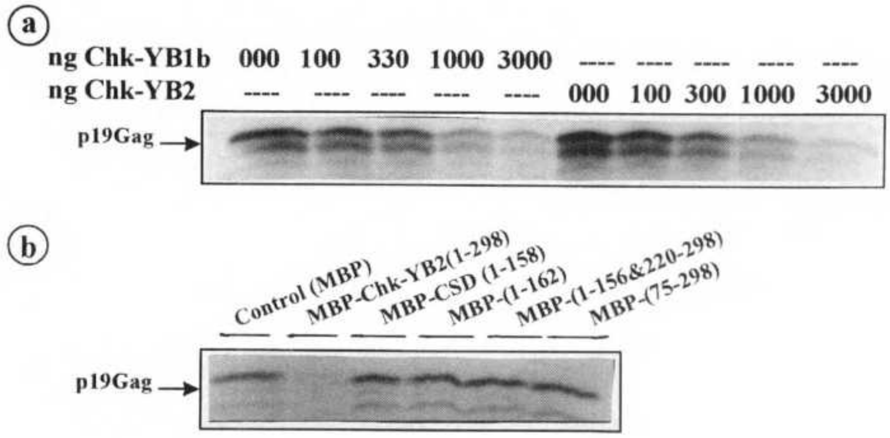
a
ng Chk-YB1b 000 100 330 1000 3000 ---- ---- ---- ---- ----
ng Chk-YB2 ---- ---- ---- ---- ---- 000 100 300 1000 3000
p19Gag
b
Control (MBP)
MBP-Chk-YB2(1-298)
MBP-CSD (1-158)
MBP-(1-162)
MBP-(1-156&220-298)
MBP-(75-298)
p19Gag

Figure 6 Both chk-YB-2 and chk-YB-1b are inhibitors of translation *in vitro*

(**a**) *In vitro* TNT reactions using T7 RNA polymerase and rabbit reticulocyte lysate were performed in either the absence or presence of increasing amounts of chk-YB-2 or chk-YB-1b, as described in the Materials and methods section. Note that both chk-YB-2 and chk-YB-1b inhibit translation *in vitro* of p19 Gag in a concentration-dependent manner. (**b**) RNA-binding ability is a prerequisite for the ability to repress translation. Only the full-length wild-type chk-YB-2 was found to be capable of repressing translation in TNT reactions (second lane from left). All the deletion mutants of chk-YB-2, which we have shown to be incapable of binding RNA (Figure 3), are also incapable of repressing translation (right-hand three lanes).

Gag protein of RSV when transcribed by T7 polymerase and translated *in vitro* using a rabbit reticulocyte extract system. This construct also contains the RSV Ψ sequence with which both chk-YB-1b and chk-YB-2 interact. TNT reactions *in vitro* in rabbit reticulocyte lysates showed a dose-dependent reduction in the amount of p19 Gag with either chk-YB-1b or chk-YB-2 (Figure 6).

We then asked whether binding to RNA is a prerequisite for repression of translation by Y-box proteins. We performed TNT reactions with different deletion mutants of chk-YB-2, which we have shown to be incapable of binding RNA. As shown in Figure 6(b), all the deletion mutants of chk-YB-2, which are unable to bind RNA, are also incapable of repressing translation of p19 Gag. Hence there is a perfect correlation between the ability of the Y-box proteins to bind RNA and their ability to repress translation. Therefore, this suggests that RNA binding is a prerequisite for Y-box-protein-mediated repression of translation.

Since transcription and translation reactions were coupled in the above experiments, we needed to ascertain that the observed reduction was due only to a reduced translation and not due to any reduction in the T7 polymerase-mediated transcription. Towards this, we performed transcription reactions *in vitro* using T7 RNA polymerase, in either the presence or absence of chk-YB-2 or chk-YB-1b. In these control reactions, no inhibitory effect of the Y-box proteins on T7 polymerase-mediated transcription was observed (results not shown). To confirm further the specificity of repression of translation by these Y-box proteins, we performed translations *in vitro* of total RNA from CEFs using rabbit reticulocyte lysates, either in the absence or presence of increasing amounts of chk-YB-2 or chk-YB-1b. We did not observe any general repression of translation in these reactions, as a result of inclusion of either chk-YB-1b or chk-YB-2 (results not shown). These results therefore suggest that chk-YB-1b and chk-YB-2 are not general repressors of translation.

DISCUSSION

In this report, we have shown that (i) bacterially expressed chk-YB-1b and chk-YB-2 are capable of interacting with single-stranded RNA in a sequence-specific and Mg^{2+}-dependent manner, (ii) CSD is necessary but not sufficient for imparting RNA-binding ability to chk-YB-2, (iii) both chk-YB-1b and chk-YB-2 are localized in the cytoplasm, (iv) in the cytoplasmic extracts from CEFs, chk-YB-2 is the predominant component of the E4C-1 RNA or RSV Ψ RNA-binding activity and (v) chk-YB-1b and chk-YB-2 inhibit translation *in vitro* in an RNA-binding-dependent manner. It is interesting to note that even though these two factors share a lot of homology and are both capable of binding E4C-1 and RSV Ψ RNA sequences in their bacterially expressed form, only chk-YB-2 demonstrated binding RNA in the cytoplasmic extracts from CEFs. Further, even though the two proteins are localized in the cytoplasm, chk-YB-1b is punctate in nature while chk-YB-2 is diffusely distributed all over the cytoplasm.

Results presented in this report show that both chk-YB-2 and chk-YB-1b are capable of interacting with single-stranded RNA in a sequence-specific manner. The sequence specificity of this interaction is proved by the fact that these proteins fail to bind to the complementary purine-rich single-stranded RNA or the double-stranded RNA having the same sequence. A comparison of the RSV Ψ sequence and the E4C-1 sequence shows that the sequence 5′-GTACCACC-3′ is conserved among them. Previously, we have shown this sequence to be the primary recognition motif for these Y-box proteins on the RSV LTR [28,29]. Interestingly, we found no difference in the affinity of interaction of these proteins with either RNA or DNA, although there was a difference in the chk-YB-2 domain required for binding RNA as compared with DNA.

EMSAs performed with the mutant proteins and E4C-1 RNA indicate that all the essential features of the protein chk-YB-2, like the proline-rich N-terminal domain, the CSD and the C-terminal charge zipper, are required for a high-affinity binding of E4C-1 RNA. This contrasts with the requirement of only the N-terminal 162 amino acids of chk-YB-2 for binding E4C-1 DNA [29]. An analysis of the structure of chk-YB-2 revealed the presence of five repeats of an eight-amino acid motif rich in arginine (Figure 3, bottom panel). Therefore, it appears as though these arginine-rich motifs and the RNP1 motif in the CSD co-operate to impart RNA-binding ability to chk-YB-2. Earlier it was suggested that the charge zippers in the C-terminal domain provide for non-specific interactions while the RNP1 and the amino acids surrounding that domain impart a sequence-specific interaction with the RNA [13]. However, in the case of chk-YB-2, both these domains are required for the ability to bind RNA in a sequence-specific manner. Further, we do not see any non-specific RNA binding by the full-length wild-type chk-YB-2, in contrast to FRGY2 [13].

It is believed that the translation-initiation sites in eukaryotic mRNAs are reached via a scanning mechanism by the ribosomes, which bind the mRNA at the 5′ end [34]. In the genome of RSV, the sequence bound by Y-box proteins (nucleotides 328–357 in the leader) is located just upstream of the translation-initiation site at nucleotide 380. Therefore, it is possible that the Y-box proteins bound in this region pose a steric hindrance to the scanning of RNA for the initiation codon, by the bound ribosomes. However, we do not have direct evidence demonstrating this. We should, however, emphasize that inhibition of translation may not be mediated only through the RSV Ψ sequence described here. It is probable that additional sites such as the polypyrimidine motif at nucleotides 430–450 of RSV also may be bound by Y-box proteins. Therefore, different Y-box-protein-binding sites in this 1–844 RSV RNA have to be precisely mapped. These experiments are in progress.

Several proteins are known to be multifunctional, influencing both transcription and translation [10,25,35]. One such example is *Drosophila* sex lethal (SXL), which is known to regulate both splicing and translation [36]. TFIIIA is another protein which can bind both DNA and RNA, and can influence both transcription and translation of 5 S rRNA gene. Our results support the contention that Y-box proteins are multifunctional proteins and that the same regulatory protein can serve to control the expression of a protein at either the transcriptional or post-transcriptional stages, or both. This multifunctional capacity of Y-box proteins has been explained as an outcome of their variable distribution between nuclear and cytoplasmic compartments, as well as their ability to bind and stabilize or destabilize either single-stranded or double-stranded RNA and DNA [25].

The ability of chk-YB-1 and chk-YB-2 to bind RSV Ψ RNA raises important questions and interesting possibilities. In any retrovirus-infected cell, a fraction of the RNA transcripts is transported out of the nucleus in an unspliced form. The unspliced RNA in the cytoplasm is translated into Gag and Gag–Pol polyproteins. Further, a fraction of the unspliced RNA is encapsidated into virions [37,38]. In HIV, *rev* gene product is known to bind specific viral RNA sequence and help in stabilizing and export of the non-spliced RNA into the cytoplasm [39,40], inhibiting its splicing [41] and translation [42].

Tat is another HIV-encoded multifunctional protein that acts as an activator of transcription from the HIV LTR [43]. This protein (Tat) is also known to bind the HIV leader RNA, TAR [44]. Recently, it has been shown that the human YB1 interacts with TAR RNA as well as the viral protein Tat [45]. Simpler retroviruses such as RSV lack these accessory proteins and therefore need to rely on the cellular machinery for performing similar events in their life cycle. Results presented in this report have brought out a candidate protein in the host cell for such functions. Interestingly in this regard, a strong homology is known to exist between the HIV Tat protein RNA-binding domain and the YB1 homologous Y-box protein dbpB [46].

In summary, we have shown here that the two chicken Y-box proteins we have studied are both localized predominantly in the cytoplasm, are capable of binding single-stranded RNA in a sequence-specific manner and inhibiting translation, and that the domains required for RNA binding include the CSD and the C-terminal charge zipper region. Taken together with our earlier report on the involvement of chk-YB-2 in transcriptional activation of RSV LTR [28], these results suggest that the Y-box proteins are involved in more than one stage of the life cycle of RSV in the host cells. How they achieve a balance between the two seemingly opposite functions of transcriptional activation and translational repression is still not clear and it should be intellectually rewarding to find out.

We thank Dr David Pintel and Dr James Schwartz for a critical review of the manuscript and Karen Ehlert for excellent secretarial assistance. This work was supported by National Institutes of Health grant 1 R01 CA54192.

REFERENCES

1 Sommerville, J. and Ladomery, M (1996) Masking of mRNA by Y-box proteins FASEB J **10**, 435–443

2 Sachs, A. B (1993) Messenger RNA degradation in eukaryotes Cell **74**, 413–421

3 Ross, J (1995) mRNA stability in mammalian cells. Microbiol Rev **59**, 423–450

4 Jacobson, A and Peltz, S W (1996) Interrelationships of the pathways of mRNA decay and translation in eukaryotic cells Annu Rev Biochem **65**, 693–739

5 Paynton, B V (1998) RNA-binding proteins in mouse oocytes and embryos expression of genes encoding Y box, DEAD box RNA helicase, and polyA binding proteins Dev Genet **23**, 285–298

6 Sommerville, J (1999) Activities of cold-shock domain proteins in translation control. Bioessays **21**, 319–325

7 Venables, J P and Eperon, I C (1999) The roles of RNA-binding proteins in spermatogenesis and male infertility Curr Opin Genet Dev. **9**, 346–354

8 Swamynathan, S. K, Nambiar, A and Guntaka, R V. (1998) Role of single-stranded DNA regions and Y-box proteins in the transcriptional regulation of viral and cellular genes FASEB J **12**, 515–522

9 Wolffe, A P (1994) Structural and functional properties of the evolutionarily ancient Y-box family of nucleic acid binding proteins Bioessays **16**, 245–251

10 Wolffe, A P and Meric, F (1996) Coupling transcription to translation – a novel site for the regulation of eukaryotic gene expression Int J Biochem Cell Biol **28**, 247–257

11 Evdokimova, V M and Ovchinnikov, L P (1999) Translational regulation by Y-box transcription factor involvement of the major mRNA-associated protein, p50. Int J Biochem Cell Biol **31**, 139–149

12 Ranjan, M, Tafuri, S and Wolffe, A P (1993) Masking mRNA from translation in somatic cells Genes Dev **7**, 1725–1736

13 Bouvet, P, Matsumoto, K. and Wolffe, A. P (1995) Sequence-specific RNA recognition by the *Xenopus* Y-box proteins J Biol Chem **270**, 28297–28303

14 Murray, M T, Krohne, G and Franke, W W (1991) Different forms of soluble cytoplasmic mRNA binding proteins and particles in *Xenopus laevis* oocytes and embryos J Cell Biol **112**, 1–11

15 Deschamps, S, Viel, A, Garrigos, M, Denis, H and le Maire, M (1992) mRNP4, a major mRNA-binding protein from *Xenopus* oocytes is identical to transcription factor FRG Y2* J Biol Chem **267**, 13799–13802

16 Evdokimova, V. M., Wei, C. L., Sitikov, A. S., Simonenko, P N., Lazarev, O A., Vasilenko, K S, Ustinov, V A, Hershey, J. W and Ovchinnikov, L P (1995) The major protein of messenger ribonucleoprotein particles in somatic cells is a member of the Y-box binding transcription factor family J Biol Chem **270**, 3186–3192

17 Davydova, E. K, Evdokimova, V. M, Ovchinnikov, L P and Hershey, J W. B (1997) Overexpression in cos cells of P50, the major core protein associated with mRNA, results in translation inhibition Nucleic Acids Res **25**, 2911–2916

18 Yurkova, M S. and Murray, M T (1997) A translation regulatory particle containing the *Xenopus* oocyte Y box protein MRNP3+4. J Biol Chem **272**, 10870–10876

19 Evdokimova, V, Kovrigina, E A., Nashchekin, D V., Davydova, E K, Hershey, J W B and Ovchinnikov, L O (1998) The major core protein of messenger ribonucleoprotein particles (p50) promotes initiation of biosynthesis *in vitro* J Biol. Chem **273**, 3574–3581

20 Hunt, S L, Hsuan, J J, Totty, N and Jackson, R J (1999) unr, a cellular cytoplasmic RNA-binding protein with five cold-shock domains, is required for internal initiation of translation of human rhinovirus RNA Genes Dev **13**, 437–448

21 Cohen, I and Reynolds, W F (1991) The *Xenopus* YB3 protein binds the B-box element of the class III promoter Nucleic Acids Res **19**, 4753–4759

22 Tafuri, S T and Wolffe, A P (1993) Selective recruitment of masked maternal mRNA from messenger ribonucleoprotein particles containing FRGY2 (mRNP4) J Biol Chem **268**, 24255–24261

23 Tafuri, S R, Familari, M and Wolffe, A P (1993) A mouse Y-box protein, MSY-1 is associated with paternal mRNA in spermatocytes J Biol Chem **268**, 12213–12220

24 Burd, C G and Dreyfuss, G (1994) Conserved structures and diversity of functions of RNA binding proteins Science **265**, 615–621

25 Matsumoto, K and Wolffe, A P (1998) Gene regulation by Y-box proteins. coupling control of transcription and translation Trends Cell Biol. **8**, 318–323

26 Ladomery, M and Sommerville, J (1994) Binding of Y-box proteins to RNA involvement of different protein domains Nucleic Acids Res **22**, 5582–5589

27 Cleavinger, P. J, Shin, B A, Kandala, J C, Nambiar, A, Swamynathan, S K and Guntaka, R. V (1996) Cloning of Rous Sarcoma virus enhancer factor genes II. RSV-EF-II, abundantly expressed in fibroblasts and muscle tissue, binds to an octamer sequence, 5′-GTACCACC-3′ in the noncoding strand of RSV enhancer Virology **222**, 133–143

28 Swamynathan, S K, Nambiar, A and Guntaka, R V (1997) Chicken YB-2, a Y-box protein, is a potent activator of Rous sarcoma virus long terminal repeat-driven transcription in avian fibroblasts J Virol **71**, 2873–2880

29 Nambiar, A, Swamynathan, S K, Kandala, J C and Guntaka, R V (1998) Characterization of the DNA-binding domain of the avian Y-box protein, chkYB-2, and mutational analysis of its single-strand binding motif in the RSV enhancer J Virol **72**, 900–909

30 Kandala, J C and Guntaka, R V (1994) Cloning of Rous Sarcoma Virus enhancer factor genes. 1 Evidence that RSV-EF-I is related to Y-box (inverted CCAAT) binding proteins and binds to multiple motifs in the RSV enhancer Virology **198**, 514–523

31 Dhalla, A, Rine, S, Swamynathan, S K, Weber, K T. and Guntaka, R V (1998) Chk-YB-1b, a Y-box binding protein activates transcription from rat $\alpha 1$(I) procollagen gene promoter Biochem J. **336**, 373–379

32 Dignam, J D., Martin, P L, Shastry, B S and Roeder, R G (1983) Eukaryotic gene transcription with purified components Methods Enzymol **101**, 582–598

33 Sambrook, J, Fritsch, E F and Maniatis, T (1989) Molecular Cloning a Laboratory Manual, Cold Spring Harbor Press, Cold Spring Harbor

34 Kozak, M (1999) Initiation of translation in prokaryotes and eukaryotes Gene **234**, 187–208

35 Ladomery, M. (1997) Multifunctional proteins suggest connections between transcriptional and post-transcriptional processes. Bioessays **19**, 903–909

36 Gebauer, F, Merendino, L, Hentze, M W and Valcarcel, J (1997) Novel functions for nuclear factors in the cytoplasm – the sex-lethal paradigm Semin Cell Dev Biol. **8**, 561–566

37 Banks, J D, Beemon, K and Linial, M (1997) RNA regulatory elements in the genomes of simple retroviruses. Semin Virol **8**, 194–204

38 Whittaker, G R. and Helenius, A (1998) Nuclear import and export of viruses and virus genomes Virology **246**, 1–23

39 Fischer, U, Huber, J, Boelens, W C., Mattaj, I W and Luhrmann, R. (1995) The HIV-1 Rev activation domain is a nuclear export signal that accesses an export pathway used by specific cellular RNAs Cell **82**, 475–483

40 Malim, M H., Hauber, J, Le, S V, Maizel, J V and Cullen, B R (1989) The HIV-1 *rev trans*-activator acts through a structured target sequence to activate nuclear export of unspliced viral mRNA Nature (London) **338**, 254–275

41 Kjems, J and Sharp, P A (1993) The basic domain of Rev from human immunodeficiency virus type 1 specifically blocks the entry of U4U6–U5 small nuclear ribonucleoprotein in spliceosome assembly J Virol **67**, 4769–4776

42 Cochrane, A, Jones, W K S, Beidas, S, Dillon, P J., Skalka, A M and Rosen, C A. (1991) Identification and characterization of intragenic sequences which repress human immunodeficiency virus structural gene expression J Virol **65**, 5305–5313

43 Jeang, K T, Chang, Y, Berkhout, B, Hammarskjold, M. L and Rekosh, D (1991) Regulation of HIV expression mechanisms of action of Tat and Rev AIDS **5**, S3–S14

44 Churcher, M J, Lamont, C, Hamy, F, Dingwall, C, Green, S M., Lowe, A D, Butler, J G, Gait, M J and Karn, J (1993) High affinity binding of TAR RNA by the human immunodeficiency virus type-1 tat protein requires base-pairs in the RNA stem and amino acid residues flanking the basic region J Mol Biol **230**, 90–110

45 Ansari, S A, Safak, M, Gallia, G L, Sawaya, B E, Amini, S and Khalili, K (1999) Interaction of YB-1 with human immunodeficiency virus type 1 Tat and TAR RNA modulates viral promoter activity J Gen Virol **80**, 2629–2638

46 Shen, Q. C, Wu, R, Leonard, J L and Newburger, P D (1998) Identification and molecular cloning of a human selenocysteine insertion sequence-binding protein a bifunctional role for DNA-binding protein B. J. Biol Chem **273**, 5443–5446

Received 13 December 1999/7 March 2000, accepted 20 March 2000

Biochem J (2000) 348, 307–313 (Printed in Great Britain)

Cholesterol decreases secretion of the secreted form of amyloid precursor protein by interfering with glycosylation in the protein secretory pathway

José Luis GALBETE, Teresa RODRIGUEZ-MARTIN, Elisa PERESSINI, Piergiorgio MODENA, Roberto BIANCHI and Gianluigi FORLONI[1]

Laboratory of Biology of Neurodegenerative Disorders, Istituto di Ricerche Farmacologiche 'Mario Negri', 20157 Milano, Italy

Cerebral deposits of β-amyloid (βA) are a major feature in Alzheimer's disease. βA is derived from amyloid precursor protein (APP). APP is subject to N- and O-glycosylation and undergoes a series of proteolytic cleavages that lead to the release of βA or of a non-amyloidogenic secreted form of APP (APPs). We used primary neuronal and glial cultures to investigate how cholesterol affects the production and secretion of APPs. Exposure to cholesterol for 2 h did not change the neuronal release of APPs; after 6 h APPs release was slightly lower, whereas 24 h of exposure decreased APPs in the medium by approx. 60 %. The time courses were similar in astrocytes and microglia preparations. To verify whether the effect of cholesterol was a consequence of membrane rigidification we tested the activity of ganglioside GM1 and prion protein fragment PrP 106–126, which affect membrane fluidity similarly to cholesterol, on APPs secretion. Neither altered the production of APPs APP mRNA and the total amount of APP in the cells were slightly decreased by cholesterol after 2 and 24 h respectively. Immunoblot analysis of APP associated with neuronal cells and astrocytes indicated that cholesterol progressively decreased the glycosylated forms of the protein; a similar tendency was noted in cells treated with brefeldin A and monensin, two substances that interfere with protein glycosylation. The cell-surface biotinylation method showed that in cholesterol-treated cells APP reached the plasma membrane. Our results indicate that cholesterol decreases the secretion of APPs by interfering with APP maturation and inhibiting glycosylation of the protein; although APP is inserted in the membrane it is not cleaved by α-secretase.

Key words: β-amyloid, Alzheimer's disease, primary tissue cultures.

INTRODUCTION

β-Amyloid (βA) is the major component of senile plaques and is deposited in cortical and meningeal blood vessels of the brain in Alzheimer's disease (AD). These features, together with tangles and cortical atrophy, are the neuropathological hallmarks of AD. βA derives from a larger transmembrane glycoprotein, the amyloid precursor protein (APP), with multiple isoforms generated by differential splicing of a gene that maps to human chromosome 21 and is highly conserved across the species [1,2]. Genetic and biochemical studies indicate a central role of βA in the pathogenesis of AD. Linkage studies have shown an association between APP gene mutations and some cases of familial early-onset AD [3], another genetic background associated with AD; mutated forms of presenilin 1 and 2 and the allele ϵ4 of apolipoprotein E resulted in the increased production of βA.

Neurotoxic effects of synthetic peptides with similar amino acid sequences as βA and its fragments have been described, and neurodegenerative transgenic mice carrying mutated human APP [4] or βA [5] have been bred. APP is subject to post-translational modifications, glycosylation, sulphation and phosphorylation along the intracellular protein secretory pathway. Cleavage of APP can occur through the amyloidogenic pathway, generating βA through β secretase cleavage, or through the non-amyloidogenic pathway, in which α-secretase cleaves the protein within the Aβ sequence (reviewed in [6]). Cleavage by α-secretase results in the release of a soluble N-terminal APP fragment [secreted form of APP (APPs)] and the retention of its C-terminus at the cell membrane [7]. βA is produced through the sequential action of β-secretase and γ-secretase in the endosomal compartment and also in the endoplasmic reticulum or Golgi complex [8]. Soluble βA and N-terminal β-APP are secreted by a variety of cells and have been found in human cerebrospinal fluid [9].

Biochemical, epidemiological and genetic aspects link cholesterol levels and AD. Cholesterol intake is considered a risk factor not only in vascular dementia but also in AD [10,11]; the cholesterol-to-phospholipid ratio was 30 % lower in the AD brain [12]. The ϵ4 allele of apolipoprotein E, which increases the risk of developing the disease, is associated with higher cholesterol levels [13].

Several studies have investigated the relationship between cholesterol and APP metabolism. High cholesterol concentrations decreased the release of APPs in HEK 293 cells transfected with APP human plasmid [14]; in fibroblasts, APPs secretion was inhibited by the application of a lower concentration of cholesterol that might act on the plasma membrane [15]. βA production in transfected hippocampal cells was decreased by lovastatin and methyl-β-cyclodextrin, treatments that deplete cholesterol [16]. We investigated the influence of cholesterol exposure on the physiological secretion of APPs in primary cultures: neurons, microglia and astrocytes. We identified the cellular mechanism responsible for the decrease in secretion of APPs caused by cholesterol in all three cell types by several approaches. We determined the total APP expression and production after exposure to cholesterol, and the influence of cholesterol on the APP secretion pathway including the insertion of APP in plasma membrane. We also analysed the role of

---

Abbreviations used βA, β-amyloid, APP, amyloid precursor protein, AD, Alzheimer's disease; APPs, secreted form of APP, DMEM, Dulbecco's modified Eagle's medium; FCS, fetal calf serum

[1] To whom correspondence should be addressed (e-mail forloni@irfmn mnegri.it)

membrane rigidification on the inhibition of APPs secretion by cholesterol. At the cellular level, we also investigated the influence of cholesterol on APP glycosylation.

MATERIALS AND METHODS

Materials

The monoclonal anti-APP antibody 22C11, protease inhibitor cocktail tablets and the glycosidases N- and O-glycosidase were obtained from Boehringer Mannheim (Mannheim, Germany). Monoclonal antibody 6E10 was from Senetek PCL (St Louis, MO, U.S.A.). Monoclonal anti-biotin antibody conjugated with agarose, anti-mouse IgG antibody conjugated with peroxidase, water-soluble β-cyclodextrin-encapsulated cholesterol, monensin, brefeldin A, tunicamycin and neuraminidase were from Sigma (St Louis, MO, U.S.A.). Sulphosuccinimidobiotin was purchased from Pierce (Rockford, IL, U.S.A.). The enhanced chemiluminescence (ECL®) detection kit was from Amersham (Little Chalfont, Bucks., U.K.). Nitrocellulose was from Schleicher and Schuell (Dassel, Germany). Protein G–Sepharose was obtained from Pharmacia Biotech.

Cell cultures

For neuron cultures, brain tissue was removed from fetal rats at embryonic day 17. Cortical cells were dissociated in serum-free medium containing 0.1 % trypsin (Difco) and 25 μg/ml deoxyribonuclease for 5 min at room temperature, plated in 24-well dishes (Falcon) precoated with poly-(D-lysine) (50 μg/ml) (Sigma) at 4×10^5 cells per dish in Eagle's minimal essential medium (Gibco) supplemented with 10 % (v/v) fetal calf serum (FCS) and 2 mM glutamine, then cultured at 37 °C in a water-saturated air/CO$_2$ (19:1) atmosphere. After 4 days *in vitro*, non-neuronal cell division was halted by exposure to 10 μM cytosine arabinoside The neuronal cell cultures are characterized elsewhere [17]

Astrocytes and microglial cells were prepared from newborn rats or mice, as described previously [18]. Cells were grown in poly-(D-lysine)-coated Primaria (Falcon) dishes containing Dulbecco's modified Eagle's medium (DMEM, Sigma) supplemented with 10 % (v/v) FCS and 2 mM glutamine. Cultures were kept at 37 °C in a humidified air/CO$_2$ (19:1) atmosphere. The medium was changed every 2 days. Astrocytes were harvested from primary mixed cultures by the method of Yao et al. [19]. After 10 days of culture, flasks containing mixed glial cultures were given fresh medium and placed on a shaker at 37 °C for 12–16 h. After 30–60 min the medium was aspirated and replaced with fresh DMEM. The adherent cells (astrocytes) were then exposed for 5 min to 0.25 % trypsin, followed by the addition of an equal volume of DMEM/10 % (v/v) FCS. The suspension was centrifuged and the pellet was resuspended in medium containing 10 % (v/v) FCS Cells were plated in 24-well dishes. The application of the complex of methyl-β-cyclodextrin and cholesterol as well as the other treatments with the various drugs were performed after 7 days of culturing of cells in a serum-free medium.

Northern blot analysis

Total cellular RNA was isolated according to the acid guanidinium/phenol/chloroform method [20]. RNA was separated on 1.2 % agarose/formaldehyde gels and transferred to Nylon 66 filters (Gene Screen Plus; Dupont). The total APP mRNA probe was a 1.0 kb *Eco*RI fragment of a mouse cDNA clone representing the βA and proximal 3′-untranslocated portions of the APP mRNA. cDNA probes were labelled with a randomly primed DNA labelling kit from Amersham and [^{32}P]dCTP. The labelled probes were purified through a Sephadex 650 column (Pharmacia). The membranes were hybridized to ^{32}P-labelled specific probes. After exposure of blots to X-ray films at −80 °C for the appropriate duration, densitometric analysis of autoradiograms was performed with an IBAS 2 image analyser (Zeiss) [21]. β-Actin mRNA was used as an internal standard to normalize the expression of APP.

Gel electrophoresis and immunoblotting

Cells were lysed in SDS/PAGE sample buffer. The cell lysates were centrifuged for 5 min at 10000 *g* and the supernatants were boiled at 95 °C. Extracellular medium was centrifuged at 15000 *g* for 15 min to remove the cellular debris. Proteins were precipitated in 50 % (w/v) trichloroacetic acid and sodium deoxycholate (2 mg/ml), washed with acetone and solubilized in sample buffer, as described previously [22]. Equal amounts of protein were separated on 7.5 % (w/v) polyacrylamide gels. Proteins were trasferred electrophoretically to nitrocellulose. Membranes were blocked by incubation in 5 % (w/v) non-fat dried milk in PBS for 1 h at room temperature. After being washed four times in PBS containing 0.1 % (v/v) Tween 20 for 30 min, membranes were incubated with primary antibody diluted in blocking buffer (1:100) for 1 h at room temperature. After a further wash, the membranes were incubated with secondary antibody diluted in blocking buffer (1:500 anti-mouse IgG peroxidase conjugate, Sigma) for 1 h at room temperature, washed again four times for 25 min in PBS containing 0.1 % Tween 20, then detected with the enhanced chemiluminescence system. The densitometric analysis of bands was calculated with an IBAS 2 image analyser (Zeiss).

Immunoprecipitation was performed with monoclonal antibodies 6E10 and 22C11. Antibody 6E10 recognizes an epitope between residues 1 and 17 of βA sequence [23] and was used to precipitate α-APPs. Antibody 22C11 recognizes a region between residues 66 and 81 of APP [24]. In brief, after harvesting, samples of medium supplemented with a proteinase inhibitor cocktail were centrifuged for 1 min at 1000 *g* to remove non-adherent cells and then at 15000 *g* for 10 min to remove other cell debris. Samples were preadsorbed on Protein G–Sepharose for 30 min at 4 °C and immunoprecipitated overnight at 4 °C in the presence of specific antibody and Protein G–Sepharose. Precipitates were washed four times with PBS, boiled in Laemmli sample buffer and separated by SDS/PAGE [7.5 % (w/v) gel].

Digestion with endoglycosidase and treatment with tunicamycin

After removal of the culture medium, the cells were washed with PBS and lysed in PBS/0.5 % (v/v) Triton-100 for 30 min at 4 °C in the presence of an EDTA-free protease inhibitor cocktail. Detergent-insoluble proteins were removed by centrifugation. Cell extracts (20 μl) were incubated at 37 °C for 18 h with 10 m-units/ml N- or O-glycosidase and 0.1 m-unit/ml neuraminidase. To control for non-specific degradation, parallel samples were incubated in the absence of enzymes. Samples were resuspended in 2 × Laemmli buffer, then boiled and analysed by SDS/PAGE [25]. Tunicamycin, which prevents the N-glycosylation of glycoproteins, was added directly to the neurons overnight.

Cell-surface biotinylation and detection of biotinylated APP

Cortical neurons (10^6, 5 days old) were cell-surface-biotinylated by incubation with 0.4 mg/ml sulphosuccinimidobiotin as described [26]. The reaction was stopped by washing the cells twice with Hepes buffer. Cells were harvested and lysed. Biotinylated proteins were precipitated with monoclonal anti-biotin–agarose; samples were boiled in 25 µl of sample buffer. Immunoprecipitates were subjected to SDS/PAGE [7.5 % (w/v) gel] and electrotransferred to nitrocellulose. Biotinylated APP was detected with monoclonal antibody 22C11 by enhanced chemiluminescence detection.

RESULTS

We evaluated the effect of cholesterol on the metabolism of APP by measuring APPs by immunoblotting in the media of rat neuronal, microglial and astroglial primary cultures. To favour the delivery of cholesterol to the cells, the compound was applied to the cultures in a complex with methyl-β-cyclodextrin, as described previously [14]. Figure 1(A) illustrates the dose–response pattern of the effect of cholesterol on APPs in neurons after 24 h of exposure. APPs progressively decreased with cholesterol dosage, from 40 % at 50 µg/ml to 70 % at 1 mg/ml; at the latter concentration, neuronal viability was affected. A similar dose–response pattern occurred in astrocyte medium (Figure 1B), although at 50 µg/ml the decrease did not reach statistical significance.

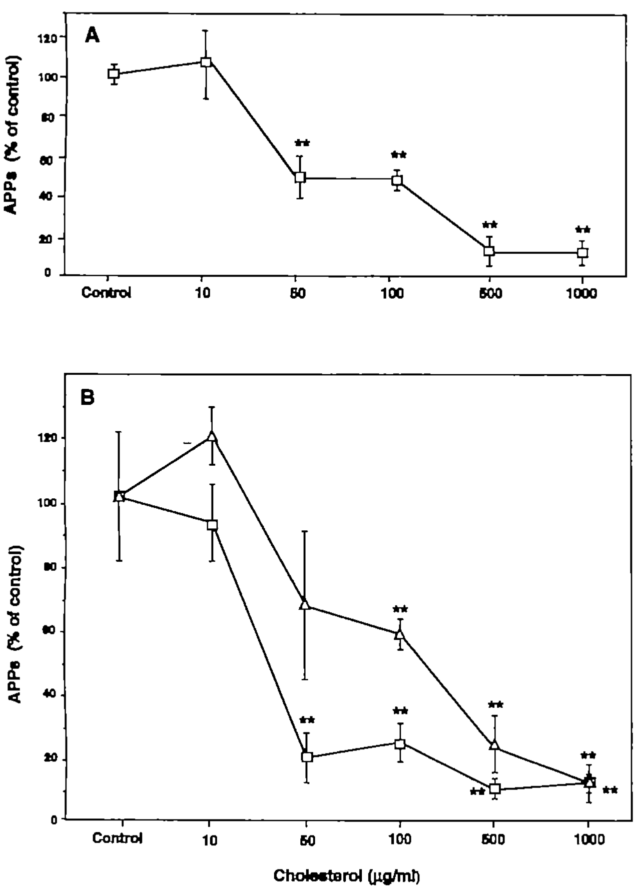

Figure 1 Dose–response pattern of the effect of cholesterol on APPs secretion in neurons and glial cells

(A) Neuronal and (B) microglial (□) and astroglial (△) cells were exposed to cholesterol for 24 h in serum-free medium. Cholesterol was complexed with cyclodextrin. APPs was determined in the culture medium by immunoblotting, the bands were quantified by densitometric analysis and expressed as percentages of the control group. Results are means ± S.E.M. for eight determinations. *$P < 0.01$ compared with control group (Dunnett's test)

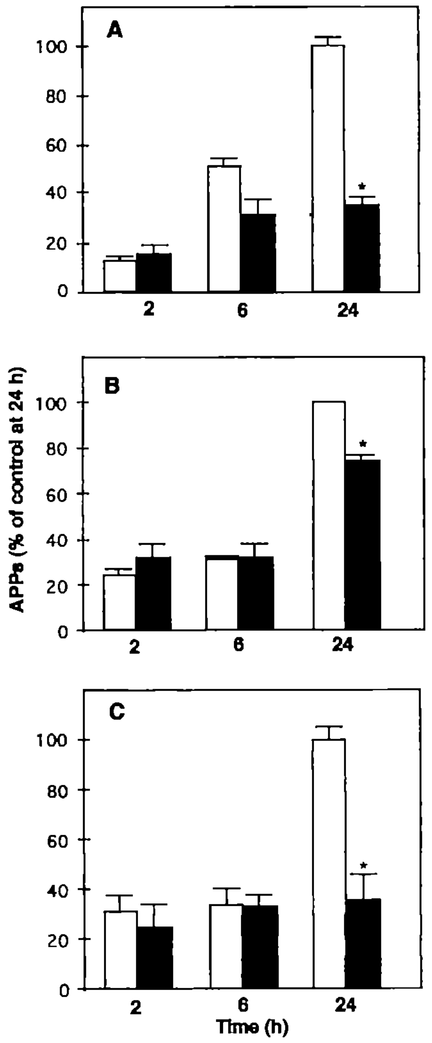

Figure 2 Time course of the effect of cholesterol on APPs secretion

Neuronal (A), astroglial (B) and microglial (C) cells were exposed to cholesterol (50 µg/ml) (filled bars) for different durations in serum-free medium. Cholesterol was complexed with cyclodextrin. APPs was determined in the culture medium by immunoblotting, the bands were quantified by densitometric analysis and are expressed as percentages of the control group at 24 h (open bars). Results are means ± S.E.M. for eight determinations. *$P < 0.01$ compared with control group (Dunnett's test)

Exposure of microglia to cholesterol markedly reduced APPs (80 %) in the medium, starting from 50 µg/ml cholesterol (Figure 1B). At this dosage the effect was already at its plateau. We used 50 µg/ml cholesterol for subsequent studies, because this concentration was close to the physiological amount of free cholesterol in interstitial fluid [27].

The time course of the effect of cholesterol (50 µg/ml) on APPs secretion in neuronal, microglial and astroglial cultures is shown in Figure 2. In the control condition the amount of APPs in the medium of neuronal cultures rose progressively with time. When the neurons were exposed to cholesterol, APPs in the medium started to decrease from 6 h; however, this became statistically significant only after 24 h of exposure (control 100±3.3 %; cholesterol 35.2±4.1 %; Figure 2A). The levels of APPs in the medium of astrocytes and microglia after 2 and 6 h of exposure to cholesterol did not differ from controls, but in both conditions APPs secretion was significantly decreased after 24 h (Figures 2B and 2C). However, in the microglial cultures

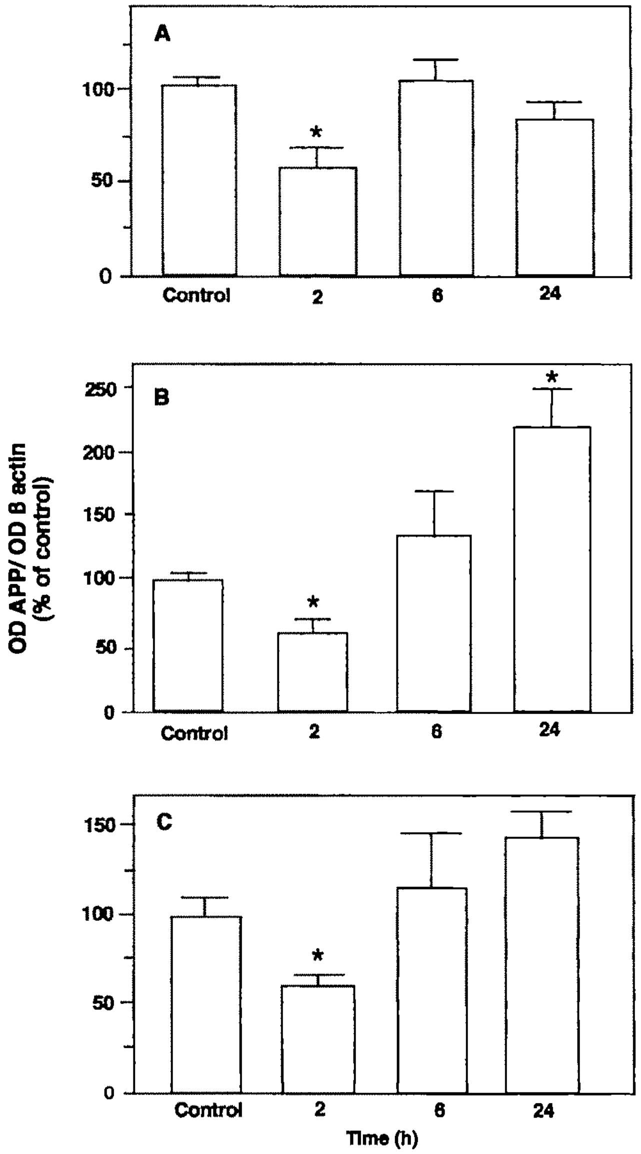

Figure 3 Effect of cholesterol on APP mRNA expression in neurons and glial cells

Neuronal (**A**), astroglial (**B**) and microglial (**C**) cells were exposed to cholesterol (50 μg/ml) for different durations in a serum-free medium Cholesterol was complexed with cyclodextrin Total RNA was extracted from the cells and APP mRNA was determined by Northern blot analysis, β-actin mRNA was measured as an internal standard The autoradiographic signal was quantified by densitometric analysis (OD, attenuance) and normalized to the β-actin mRNA signal Results are means ± S E M for four determinations $^*P < 0.01$ compared with control group (Dunnett's test).

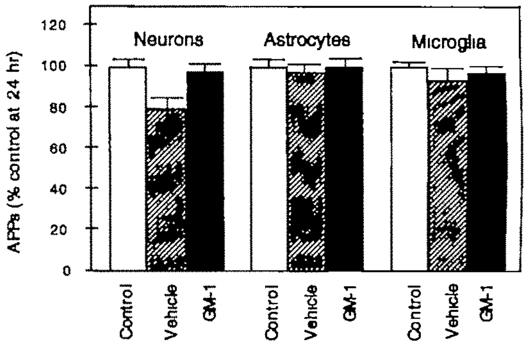

Figure 4 Effect of GM-1 on APPs secretion in neurons and glial cells

Neuronal, microglial and astroglial cells were exposed to the ganglioside GM-1 (100 μg/ml) for 24 h in a serum-free medium APPs was determined in the culture medium by immunoblotting, the bands were quantified by densitometric analysis and are expressed as percentages of the controls Results are means ± S E.M. for four or five determinations

this inhibition was similar to that in the neurons (65 %), whereas in the astrocytes the effect was less intense (25 %; Figure 1B) To verify the influence of cholesterol on APP synthesis we used Northern blot analysis to determine the expression of APP mRNA after exposure of the cells to cholesterol for different periods (Figure 3). Cholesterol significantly decreased APP mRNA levels after 2 h of exposure in all three cell types. However, at 6 and 24 h the APP mRNA in the cells was similar to that in controls, except for the 24 h treatment in astrocytes, in which APP mRNA was significantly increased (Figure 3B).

Because cholesterol decreases membrane fluidity [28], it has been hypothesized that in other cell types [14,15] the inhibition of APPs secretion by cholesterol was due to membrane rigidification. We investigated this possibility by using two substances that strongly decrease membrane fluidity. First, the cells were treated with GM-1 (100 μg/ml), a ganglioside that efficiently decreases the membrane microviscosity [29], for 24 h; APPs was measured in the culture media. No significant change in APPs secretion was observed in the media of the cells (Figure 4). Similar results were obtained with prion protein fragment PrP 106–126, which also induces a marked decrease in cellular membrane microviscosity in glial and neuronal cells [30] (results not shown). It is therefore unlikely that the inhibition of APPs secretion induced by cholesterol is a consequence of membrane rigidification.

To evaluate the effect of cholesterol on total APP production we determined the intraneuronal content of APP by immunoblot, in comparison with APPs secreted into the medium. Figure 5(A) shows examples of immunoblots from media and neurons exposed to cholesterol for different durations. As in Figure 2(A), in the control medium the level of APPs increased progressively with time. No significant difference was observed between the cholesterol-treated cultures at 2 and 6 h whereas at 24 h the APPs signal was much weaker than in control or vehicle-treated (methyl-β-cyclodextrin) cells. Three bands characterized neuronal APP: the lower band, at approx. 100 kDa, was identified as the immature form of the protein; the other two, at 110 and 125 kDa, were the mature forms. After 2 h of exposure to cholesterol, the neuronal APP pattern was not altered but at 6 h the higher-molecular-mass bands decreased and by 24 h they had almost completely disappeared.

There was a significant decrease in APPs with brefeldin A (10 μg/ml) and monesin (10 μM), two treatments that prevent the proteins from maturing in the Golgi complex and endoplasmic reticulum [31,32]. With these treatments the bands for the mature forms of neuronal APP were strongly decreased after 16 h exposure. These results were obtained with the antibody 22C11, which does not distinguish between α- and β-secretase product [24], therefore to verify the separate contributions of α- and β-APPs under our conditions, we used a specific antibody, 6E10, that recognized only the α-secretase product [23]. The media of neurons treated with vehicle or cholesterol (50 μg/ml) for 24 h were immunoprecipitated with 6E10, to separate the α-APPs, and then with antibody 22C11 to identify the β-APPs. An example of immunoblots with these preparations is shown in Figure 5(B): cholesterol strongly decreased the α-APPs signal

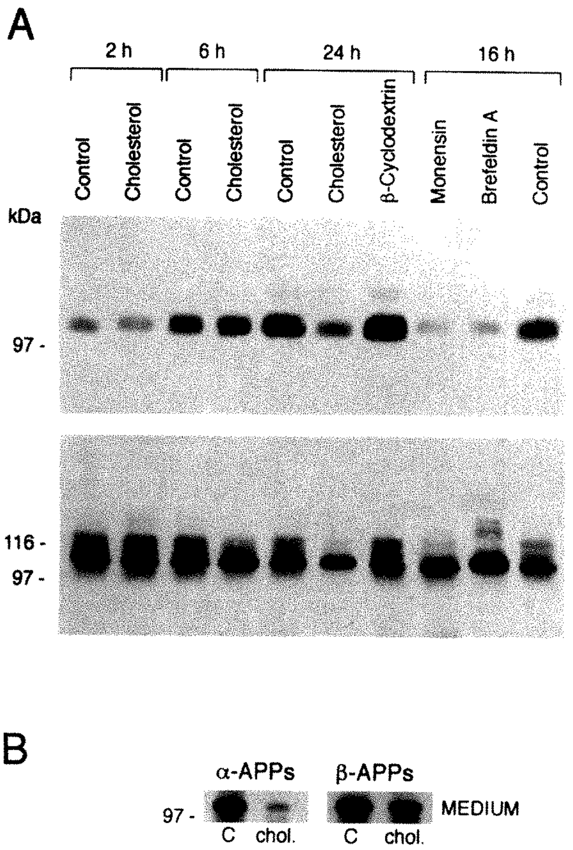

Figure 5 APP immunoblots of medium and cellular extracts from neurons

(**A**) Neuronal cells were exposed to cholesterol (50 μg/ml), β-cyclodextrin (1 mg/ml), brefeldin A (10 μg/ml) and monensin (10 μM) for different durations in a serum-free medium. Cell lysates (lower panel) and media (upper panel) were analysed by immunoblotting and APP was determined with antibody 22C11. A clear decrease in APPs (108 kDa) was evident in the medium of cells treated with cholesterol for 24 h and with brefeldin A and monesin for 16 h whereas β-cyclodextrin did not change the secretion of APPs in comparison with the control. In the cell lysates, three bands corresponding to the different maturation states of APP (100, 110 and 125 kDa) appeared in the control. At 6 h the treatment with cholesterol decreased, and at 24 h almost abolished, the signals corresponding to the glycosylated forms of APP, similar results were obtained with brefeldin A and monesin. (**B**) Immunoblots from media of neurons exposed for 24 h to cholesterol (50 μg/ml) immunoprecipitated with antibody 6E10, which recognizes only α-APPs. A subsequent immunoprecipitation was performed with antibody 22C11 to determine the β-APPs form in the cell media. Cholesterol strongly decreased the α-APPs signal, whereas β-APPs was only partly attenuated. The positions of molecular mass markers are indicated at the left.

but only slightly attenuated the β-APPs band. Thus the decrease in APPs induced by cholesterol was due almost completely to the α-secretase metabolism. Because APP is a highly glycosylated membrane glycoprotein containing both N- and O-glycans, we evaluated the influence of digestion with N and O-endoglycosidase, and the influence of neuraminidase, for comparison of these results with the effect of cholesterol. An example of an immunoblot from neuronal lysate treated for 18 h with neuraminidase (0.1 unit/ml), N-glycanase or O-glycanase (10 m-units/ml) is shown in Figure 6(A). Neuraminidase completely abolished the higher-molecular-mass APP band, whereas there was an increase in the signal intensity of the 110 kDa band. A different APP pattern was induced by N-glycanase, which also abolished the 125 kDa band but increased the intensity of the APP at the lowest molecular mass. An APP pattern similar to that observed with cholesterol treatment of the cells was found with the combination of neuraminidase and O-glycanase, which induced a complete shift of the APP signals to a single intense band at the lower molecular mass. As expected, the treatment with O-glycanase alone did not change the pattern of APP because its activity was inhibited by the presence of sialic acid groups. In addition, the treatment of the neurons overnight with tunicamycin, a classical inhibitor of N-glycosylation, induced an APP pattern similar to that observed with the cell lysate treated with N-glycase (Figure 6B). Thus the post-translational modification of APP under our conditions was essentially due to the glycosylation of the protein that was inhibited by cholesterol exposure.

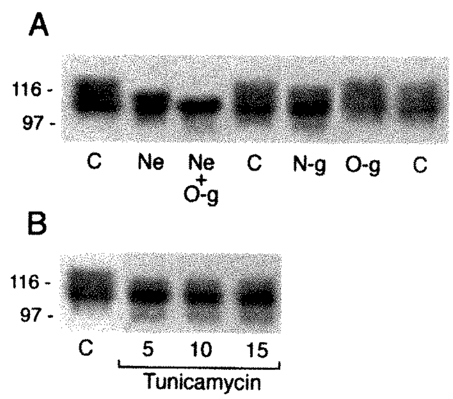

Figure 6 Digestion of APP with endoglycosidase and treatment with tunicamycin

(**A**) Immunoblot from neuronal extracts treated overnight with neuraminidase (Ne, 0.1 unit/ml), N-glycosidase (N-g, 10 m-units/ml) and/or O-glycosidase (O-g, 10 m-units/ml). The endoglycosidase digestion significantly changed the APP pattern; in particular, the combination of O-glycosidase and neuraminidase decreased APP to a single band. (**B**) Immunoblot from neurons treated overnight with tunicamycin (5–15 μg/ml), a N-glycosylation inhibitor, which induced a APP pattern similar to that induced by N-glycosidase applied directly to the cellular extract. The positions of molecular mass markers are indicated at the left.

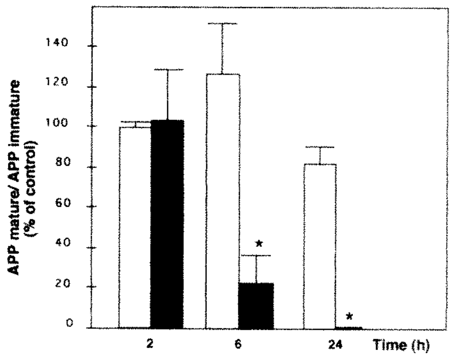

Figure 7 Ratio of mature to immature APP in neuronal cells exposed to cholesterol for different durations

Cell lysates from neuronal cells exposed to cholesterol (50 μg/ml) (filled bars) for different durations were analysed by immunoblotting; APP was determined with antibody 22C11. The signals corresponding to the different bands (see Figure 5) were quantified by densitometric analysis and the ratios of the mature (110 and 125 kDa) to the immature (100 kDa) APP were calculated. *$P < 0.01$ compared with control group at 2 h (open bars) (Dunnett's test).

The effect of cholesterol on the ratio between the signals of mature and immature APP in neuronal cells is quantified in Figure 7. After 2 h of exposure the ratio was unchanged, but

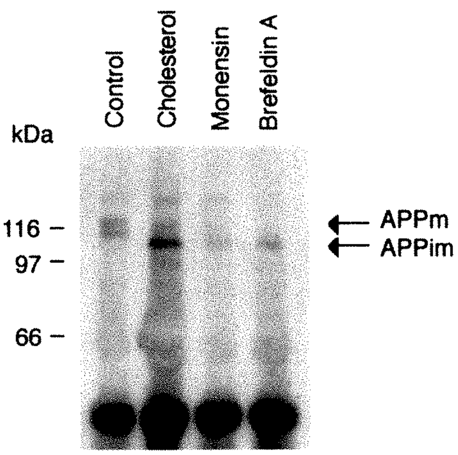

Figure 8 Cell-surface expression of APP in neuronal cells

Neuronal cells were exposed to 50 μg/ml cholesterol, 10 μg/ml brefeldin A and 10 μM monensin. Cells were labelled with sulphosuccinimidobiotin as described in the Materials and methods section. The biotinylated proteins were immunoprecipitated with anti-biotin antibody. The precipitated APP proteins were subjected to SDS/PAGE and detected with antibody 22C11. Abbreviations: APPm, mature APP; APPim, immature APP. The positions of molecular mass markers are indicated at the left.

after 6 and 24 h it decreased markedly. Similar results were obtained in astrocytes (results not shown). Thus the inhibition of APPs secretion by cholesterol seemed to be the consequence of an intracellular effect on APP maturation.

To verify whether the immature form of APP reached the membrane compartment, we measured APP inside the membrane by using the protein biotinylation technique. As shown in Figure 8, biotinylation of cellular surface proteins identified the APP associated with the membrane. In the control condition the two post-translationally modified forms of APP reached the membrane, whereas only the immature form was found in the cholesterol-treated neurons. Interestingly, after treatment with brefeldine or monensin, no more mature APP reached the membrane but a small amount of immature APP was detected.

DISCUSSION

The influence of cholesterol on APP metabolism and βA production has been investigated in various experimental models [14–16,33–35]. Here we have shown that in primary cultures of neurons, astrocytes and microglia, exposure to cholesterol markedly decreased APPs, this regulation appearing mainly at the post-translational level.

Low concentrations of cholesterol significantly decreased the secretion of APPs, with an identical time course in all three cell types. Similar results were obtained by Racchi et al. [15] in COS cells; they showed a 75% decrease in APPs secretion within 2 h of exposure to low doses of cholesterol. The inhibition of APPs production was also observed by Bodovitz and Klein [14] in an HEK 293 cell line stably transfected with APP 770, although in that case extremely high cholesterol concentrations were used (0.6–2.4 mg/ml). These authors proposed that the inhibition of APPs secretion by cholesterol was due to a change in membrane fluidity that decreased the interaction of α-secretase with APP and consequently the α-secretase cleavage. At variance with previous data [15], in the primary cultures cholesterol had a significant effect on APPs secretion only after 24 h of exposure and in the range of concentrations (50–100 μg/ml) found in human interstitial fluid [27].

To verify the influence of membrane fluidity on α-secretase cleavage we measured APPs secretion after exposing the cells to substances that induce membrane rigidification. PrP 106–126 and GM1, both of which induce robust membrane rigidification, did not alter the APPs secretion. Our data therefore indicate that the influence of cholesterol on α-secretase cleavage is unlikely to be a consequence of changes in cell membrane fluidity. In agreement with this, cholesterol's effect on APPs was significant only after 24 h exposure, whereas the alteration of membrane fluidity was seen immediately. We used antibody 22C11, which recognizes the N-terminal portion of APP [24] and does not distinguish between the α- and β-secretase products. However, by using a different, specific, antibody we determined α- and β-APPs separately: the influence of cholesterol was essentially on α-secretase metabolism.

We found that cholesterol inhibited the APP mRNA expression in all three cell types, although the effect was restricted to the first 2 h of exposure, which might partly account for the decrease in APPs production. However, because the protein has a short half-life (20–30 min), the consequence of the decrease in mRNA levels on APP synthesis is presumably small, as confirmed by an immunoblotting analysis of total APP, which showed a slight decrease.

APP maturation occurs through the Golgi complex and endoplasmic reticulum, where APP is N- and O-glycosylated [7], as confirmed under our conditions with the digestion of APP with neuraminidase, N-glycase and O-glycase and the treatment with tunicamycin. By immunoblot analysis of the immature and mature forms of APP in the neurons (and astrocytes) after exposure to cholesterol, we have shown that cholesterol progressively abolished APP maturation within 24 h. The APP pattern after the exposure of the neurons to cholesterol was similar to that obtained by digestion with endoglycosidase; the decrease in APPs secretion by cholesterol is probably due to the effect on APP glycosylation. We used two substances to test this, monensin and brefeldin A, that act with different mechanisms on the Golgi complex and endoplasmic reticulum, interfering with protein maturation. Like cholesterol, both substances inhibited APP maturation and decreased APPs secretion.

These results therefore confirmed that primary post-translational modifications of APP might cause the decrease in APPs. This is particularly interesting because it has been demonstrated that in neuronal cells a large percentage of intracellular Aβ is produced from immature APP [36–38]. Furthermore, post-translational changes in APP studied in platelets have been correlated with the severity of AD [39].

The molecular mechanism implicated in this effect is not known but, from previous investigations [40,41], a direct interaction is possible between cholesterol and APP at the endoplasmic reticulum or Golgi complex. In neurons these organelles are the site of the generation of βA 1–40 and 1–42 [38]. Furthermore, we show that, unlike with monensin and brefeldin A, most of the neuronal immature APP after treatment with cholesterol reached the cell membrane. Thus the non-glycosylated form of APP is inserted into the membrane but is not available for α-secretase cleavage. This is consistent with the observation that the principal determinants of α-secretase cleavage seem to be the conformation around the cleavage site [42], which is influenced by the state of maturation of APP.

A decrease in APP secretion without changes in the cell-associated full-length APP was observed in the brain of APP transgenic mice treated with dietary cholesterol [33]. In contrast, Simons et al. [16] showed that cholesterol depletion decreased βA generation in hippocampal neurons infected with recombinant virus carrying APP. In this case the secretion of APPs was not modified. In the latter study, human APP processing was analysed in rat cells with only some hours of survival after infection [16]. Thus the genetic manipulation and the overexpression of APP might have caused some alterations in APP metabolism. Our results are based on a more 'physiological' approach, determining the endogenous neuronal APP processing affected by low concentrations of cholesterol. Under similar conditions, Racchi et al. [15], using non-neuronal cells, obtained results similar to ours.

In conclusion, we have shown that cholesterol decreased the secretion of APPs in glial and neuronal cells. In neurons this effect was associated with a slight decrease in APP mRNA expression and a substantial effect on protein maturation. As a consequence of exposure to cholesterol, a large amount of immature APP reached the cell membrane but was not available for cleavage, decreasing the production of APPs. Thus cholesterol affects APP processing and potentially increases the amyloidogenic pathway producing $A\beta$ peptide. This mechanism might involve cholesterol in the pathogenesis of AD, explaining the clinical evidence that high levels of cholesterol are also a risk factor in non-vascular dementia.

This work was partly supported by the Italian Ministry of Scientific Research (P N R Farmaci 4/1 3.3.2 1).

REFERENCES

1 Selkoe, D. J (1998) Trends Cell Biol **8**, 447–453
2 Forloni, G, Bugiani, O, Tagliavini, F and Salmona, M (1996) Prog Neurobiol. **49**, 287–315
3 Goate, A, Chartie-Harlin, M C, Mullan, M, Brown, J, Crawford, F, Fidani, L, Giuffra, L, Haynes, A, Irving, N, James, L et al (1991) Nature (London) **349**, 704–706
4 Games, D, Adams, D, Alessandrini, R., Barbour, R, Berthelette, P., Blackwell, C., Carr, T, Clemens, J, Donaldson, T, Gillespie, F et al (1995) Nature (London) **373**, 523–527
5 LaFerla, F M, Tinkle, B T, Bierberich, C J, Haudenschild, C C and Jay, G (1995) Nat. Genet. **9**, 21–30
6 Mills, J and Reiner, P B (1999) J Neurochem **72**, 443–460
7 Weidemann, A, Koning, G, Bunke, D., Fischer, P, Salbaum, J M., Masters, C L and Beyreuther, C. (1989) Cell **57**, 115–126
8 Haass, C and Selkoe, D J (1993) Cell **75**, 1039–1042
9 Haass, C., Schlossmacher, M. G, Hung, A. Y, Vigo-Pelfrey, C, Mellon, A, Lieberburg, I, Koo, E H, Schenk, D., Teplow, D B and Selkoe, D J (1992) Nature (London) **359**, 322–325
10 Hardy, J (1998) Trends Neurosci **20**, 154–159
11 Hoshino, S, Tamaoka, A, Takahashi, M., Kobayashi, S., Furukawa, T., Oaki, Y, Mori, O., Matsuno, S, Shoji, S, Inomata, M and Teramoto, A (1998) NeuroReport **9**, 1879–1883
12 Funato, H, Yoshimura, M, Kusui, K, Tamaoka, A., Ishikawa, K, Ohkoshi, N., Namekata, K, Okeda, R and Ihara, Y (1998) Am. J Pathol **152**, 1633–1640
13 Rhee, S K, Quist, A P. and Lal, R. (1998) J Biol Chem **273**, 13379–13382
14 Bodovitz, S and Klein, W L (1996) J Biol Chem **271**, 4436–4400
15 Racchi, M, Baetta, R, Salvietti, N., Ianna, P, Franceschini, G, Paoletti, R, Fumagalli, R, Govoni, S., Trabucchi, M. and Soma, M (1997) Biochem J **322**, 893–898
16 Simons, M, Keller, P, De Strooper, B, Beyreuther, K, Dotti, C and Simons, K. (1998) Proc Natl Acad Sci U S A **95**, 6460–6464
17 Forloni, G, Angeretti, N., Chiesa, R, Monzani, E, Salmona, M, Bugiani, O and Tagliavini, F. (1993) Nature (London) **362**, 543–545
18 Chiesa, R, Angeretti, N, Lucca, E, Salmona, M, Tagliavini, F, Bugiani, O. and Forloni, G (1996) Eur J Neurosci **8**, 589–597
19 Yao, J, Keri, J, Taffs, R and Colton, C (1992) Brain Res **591**, 88–93
20 Chomczynski, P and Sacchi, N (1987) Anal. Biochem. **162**, 156–159
21 Masseroli, M, Messori, A, Bendotti, C., Ponti, M. and Forloni, G (1993) Life Sci **53**, 331–336
22 Bergamaschi, S; Binetti, G, Govoni, S, Wetsel, W C, Battaini, F, Trabucchi, M, Bianchetti, A and Racchi, M (1995) Neurosci Lett **201**, 1–4
23 Kim, K S, Wen, G Y, Bancher, C, Chen, C J M, Sapienza, V J, Hong, H and Wisniewski, H M. (1990) Neurosci Res. Commun **7**, 113–122
24 Hilbich, C, Monning, U., Grund, C., Masters, C L and Beyreuther, K (1993) J Biol Chem **268**, 26571–26577
25 Garlanda, C, Berthier, R, Garin, J, Stoppacciaro, A, Ruco, L, Vittet, D, Gulino, D, Matteucci, C, Mantovani, A, Vecchi, A. and Dejana, E (1997) Eur J. Cell Biol. **73**, 368–377
26 Usami, M, Yamao-Harigaya, W and Maruyama, K (1993) J Neurochem **61**, 239–246
27 Wong, L., Curtiss, L K, Huang, J., Mann, C. J., Maldonado, B and Roheim, P S (1992) J Clin Invest **90**, 2370–2375
28 Heron, D. S., Shinitzky, M., Hershkowitz, M. and Samuel, D. (1980) Proc. Natl. Acad Sci U S A **77**, 7463–7467
29 Mohand-Said, S, Weber, M, Hicks, D, Dreyfus, H and Sahel, J A (1997) Stroke **28**, 617–621
30 Salmona, M., Forloni, G., Diomede, L., Algeri, M., De Giogia, L, Angeretti, N., Giaccone, G, Tagliavini, F and Bugiani, O (1997) Neurobiol Dis **4**, 47–57
31 Hugh, R and Pelham, B (1999) Cell **67**, 449–451
32 Caporaso, G. L, Gandy, S. E., Buxbaum, J. D and Greengard, P (1992) Proc Natl Acad. Sci U.S.A. **89**, 2252–2256
33 Howland, D S, Trusco, S P., Savage, M J., Reaume, A. G., Lang, D. M., Hirsch, J D, Maeda, N, Siman, R, Greenberg, B D, Scott, R W and Flood, D G (1998) J Biol Chem **273**, 16576–16582
34 Mizuno, T, Haass, C., Michikawa, M. and Yanagisawa, K. (1998) Biochim Biophys Acta **1373**, 119–130
35 Mizuno, T, Nakata, M, Naiki, H, Michikawa, M., Wang, R, Haass, C and Yanagisawa, K (1999) J Biol Chem **274**, 15110–15114
36 De Strooper, B, Simons, M, Multhaup, G, Leuven, F V, Beyreuther, K and Dotti, C. G (1995) EMBO J. **14**, 4932–4938
37 Hartmann, T, Bieger, S. C, Bruhl, B, Tienari, N., Ida, N, Allsop, D., Roberts, G W., Masters, C L, Dotti, C G, Unsicker, K and Beyreuther, K (1997) Nat Med (N Y) **3**, 1016–1020
38 Wild-Bode, C., Yamazaki, T., Capell, A, Leimer, U, Steiner, H, Ihara, Y and Haass, C. (1997) J Biol. Chem **272**, 16085–16088
39 Di Luca, M, Pastorino, L, Bianchetti, A, Perez, J, Vignolo, L, Lenzi, G, Trabucchi, M, Cattabeni, A and Padovani, A (1998) Arch Neurol **55**, 1195–1200
40 Underwood, K W, Jacobs, N L, Howley, A and Liscum, L (1998) J Biol Chem **273**, 4266–4274
41 Bretscher, M. and Munro, S. (1993) Science **261**, 1280–1281
42 Sisodia, S S (1992) Proc Natl Acad Sci U S A **89**, 6075–6079

Received 5 October 1999/25 February 2000, accepted 15 March 2000

Oxalomalate, a competitive inhibitor of aconitase, modulates the RNA-binding activity of iron-regulatory proteins

Michela FESTA*, Alfredo COLONNA*, Concetta PIETROPAOLO† and Alfredo RUFFO‡[1]

*Dipartimento di Farmacologia Sperimentale, Università di Napoli 'Federico II', Via Domenico Montesano 49, I-80131 Napoli, Italy,
†Dipartimento di Biochimica e Biotecnologie Mediche, Università di Napoli 'Federico II', Via Sergio Pansini 5, I-80131 Napoli, Italy, and
‡Dipartimento di Chimica delle Sostanze Naturali, Università di Napoli 'Federico II', Via Domenico Montesano 49, I-80131 Napoli, Italy

We investigated the effect of oxalomalate (OMA, α-hydroxy-β-oxalosuccinic acid), a competitive inhibitor of aconitase, on the RNA-binding activity of the iron-regulatory proteins (IRP1 and IRP2) that control the post-transcriptional expression of various proteins involved in iron metabolism. The RNA-binding activity of IRP was evaluated by electrophoretic mobility-shift assay of cell lysates from 3T3-L1 mouse fibroblasts, SH-SY5Y human cells and mouse livers incubated *in vitro* with OMA, with and without 2-mercaptoethanol (2-ME). Analogous experiments were performed *in vivo* by prolonged incubation (72 h) of 3T3-L1 cells with OMA, and by injecting young mice with equimolar concentrations of oxaloacetate and glyoxylate, which are the precursors of OMA synthesis. OMA remarkably decreased the binding activity of IRP1 and, when present, of IRP2, in all samples analysed. In addition, the recovery of IRP1 by 2-ME in the presence of OMA was constantly lower versus control values. These findings suggest that the severe decrease in IRP1 RNA-binding activity depends on: (i) linking of OMA to the active site of aconitase, which prevents the switch to IRP1 and explains resistance to the reducing agents, and (ii) possible interaction of OMA with some functional amino acid residues in IRP that are responsible for binding to the specific mRNA sequences involved in the regulation of iron metabolism.

Key words: α-hydroxy-β-oxalosuccinic acid, iron metabolism, RNA-binding protein.

INTRODUCTION

Oxalomalate (OMA), a tricarboxylic acid (α-hydroxy-β-oxalosuccinic acid) formed *in vitro* and *in vivo* by condensation of oxaloacetate with glyoxylate, has long been known to be a powerful competitive inhibitor of aconitase [1–7]. This enzyme, which is required for the first step of the citric acid cycle, attracted renewed attention with the discovery of the structural identity between cytosolic aconitase and the iron-regulatory protein (IRP) 1. IRP1 and a structurally related protein, IRP2, are RNA-binding proteins that, by binding to a different site of a stem-loop region of the iron-responsive element (IRE), control the post-transcriptional expression of proteins involved in iron metabolism (see [8–13] for reviews).

Because OMA inhibits cytosolic aconitase, it is feasible that it also affects the IRE-binding activity of IRP1. A preliminary study showed that OMA added *in vitro* to lysates of a confluent culture of 3T3-L1 fibroblasts reduced the RNA-binding capacity of IRP1 [14]. This finding suggested that OMA plays a role in the regulation of iron metabolism and raised questions about the mechanisms by which OMA could modify the IRE-binding activity of IRP1. In an attempt to clarify these issues, we have analysed *in vitro* the IRE-binding activity of IRP1 in cell lysates of 3T3-L1 mouse fibroblasts, of SH-SY5Y cells derived from human nervous tissue and of mouse liver, with and without OMA, under reducing and non-reducing conditions. We also performed experiments *in vivo* on 3T3-L1 fibroblasts cultured with OMA for different times, and on young mice treated with equimolar concentrations of oxaloacetate and glyoxylate, known to be precursors of OMA synthesis. OMA caused a remarkable decrease in the IRE-binding activity of IRP1 and, when present, of IRP2, which is reported to lack aconitase activity [15].

EXPERIMENTAL

Cell cultures and treatment

Low-passage-number mouse 3T3-L1 fibroblasts were grown in Dulbecco's modified Eagle's medium supplemented with 10% foetal bovine serum, penicillin (50 units/ml), streptomycin (50 μg/ml) and L-glutamine (2 mM). SH-SY5Y human neuroblastoma cells were grown in Ham's F12 nutrient mixture/Eagle's minimal essential medium (1:1) supplemented with 10% foetal bovine serum, 1% non-essential amino acids, penicillin (50 units/ml), streptomycin (50 μg/ml) and L-glutamine (1 mM). The cells were grown at 37 °C in a 5% CO_2 atmosphere.

For studies on iron-repleted cells, confluent cultures of 3T3-L1 cells were treated for 18 h with 20 μg/ml of ferric ammonium citrate. The chelation of intracellular iron was achieved on 18-h treatment with 100 μM desferrioxamine mesylate (Desferal; Ciba-Geigy, Varese, Italy). Oxalomalic acid trisodium salt was prepared as described in [2] or purchased from Sigma (St. Louis, MO, U.S.A.). Oxaloacetic acid and glyoxylic acid sodium salt were produced by Fluka Chemika (Buchs, Switzerland).

For experiments *in vivo*, confluent cultures of 3T3-L1 cells were incubated at 37 °C with 5 mM OMA for 24, 48 and 72 h, after which RNA–protein complexes were evaluated by electrophoretic mobility-shift assay (see below).

Abbreviations used: OMA, oxalomalic acid; IRP, iron-regulatory protein; IRE, iron-responsive element; Desferal, desferrioxamine mesylate; 2-ME, 2-mercaptoethanol

[1] To whom correspondence should be addressed (e-mail alfcolon@unina.it)

Preparation of cytosolic extracts

3T3-L1 and SH-SY5Y cells were washed and scraped off with PBS containing 1 mM EDTA. To obtain cytosolic extracts, cells were lysed at 4 °C in lysis buffer containing 10 mM Hepes, pH 7.5, 3 mM $MgCl_2$, 40 mM KCl, 5 % glycerol, 1 mM dithiothreitol and 0.2 % Nonidet P-40. After lysis, samples were diluted 3-fold with lysis buffer without Nonidet P-40. Nuclei and mitochondria were removed by centrifugation for 30 min at 100000 *g* in a Beckman L8-70 ultracentrifuge, and the supernatants were frozen in small aliquots at −80 °C. The protein concentration was determined by a Bio-Rad protein assay used according to the supplier's manual (Bio-Rad Laboratories, Milan, Italy).

OMA treatment *in vitro*

Cytosolic lysates (5 μg) from 3T3-L1 and SH-SY5Y cells and from mouse liver (see below) were incubated with various concentrations of OMA (0.5, 1, 2.5 and 5 mM) at the times indicated in each experiment. The reaction volume was adjusted to about 19 μl with lysis buffer with Nonidet P-40 diluted to 0.07 %. In alternative reaction mixtures 2 % 2-mercaptoethanol (2-ME) was added 10 min after incubation with OMA. In all samples the binding reaction was started by the addition of 0.2 ng of radiolabelled RNA, giving a final volume of 20 μl, and left for 30 min at room temperature (for further details see the section on electrophoretic mobility-shift assay, below).

Treatment *in vivo* of mice and preparation of liver extracts

Male Swiss mice (Mario Negri Sud, Chieti, Italy) weighing about 30–40 g were used. The mice were starved for 20 h (water *ad libitum*) and then injected subcutaneously with aliquots of a solution that yielded 92.6 mg of neutralized oxaloacetic acid and 50.3 mg of sodium glyoxylate per 100 g of body weight. Other mice were injected with a half dose and the controls were injected with physiological solution. After 1 h all the mice were killed by CO_2 and the livers were removed, washed in physiological solution and 500 mg were homogenized at 4 °C in 2 ml of lysis buffer supplemented with 350 mM sucrose, 2.5 μg/ml leupeptin and 0.5 mM PMSF. The homogenates were centrifuged at 100000 *g* for 30 min at 4 °C in a Beckman L8-70 ultracentrifuge and the supernatants were frozen in small aliquots at −80 °C. The protein concentration was determined by the Bio-Rad protein assay used according to the supplier's manual.

Electrophoretic mobility-shift assay

Plasmid pSPT-fer, containing the sequence corresponding to the IRE of the H-chain of human ferritin mRNA, was kindly provided by Professor G. Cairo (University of Milan, Milan, Italy). This plasmid was linearized at the *Bam*H1 site and transcribed *in vitro* with T7 RNA polymerase (Promega, Madison, WI, U.S.A.). The transcription reaction was performed at 38.5 °C for 1 h with 200 ng of plasmid DNA in the presence of 50 μCi of [α-^{32}P]CTP (800 Ci/mmol; Amersham Corporation, Milan, Italy) and 0.5 mM ATP, GTP and UTP (Promega) in a 20-μl reaction volume. The DNA template was digested with 10 units of RNase-free DNase 1 for 10 min at 37 °C. Free nucleotides were removed on a Sephadex G-50 column (Boehringer-Mannheim, Milan, Italy).

For electrophoretic mobility-shift analysis, 5 μg of protein extracts were mixed with 0.2 ng of *in vitro*-transcribed ^{32}P-labelled IRE RNA with or without unlabelled competitor RNA. The reaction was performed, as reported above, in lysis buffer with Nonidet P-40 adjusted to 0.07 %, in a final volume of 20 μl for 30 min at room temperature. Then, to degrade unbound probe, the reaction mixture was incubated with 1 unit of RNase T1 (Calbiochem, La Jolla, CA, U.S.A.) for 10 min, and non-specific RNA–protein interaction was displaced by the addition of 5 mg/ml heparin for 10 min. A 6 % non-denaturing polyacrylamide gel was pre-electrophoresed for 20 min at 200 V. Then, after the addition of 10 μl of loading buffer containing 30 mM Tris/HCl, pH 7.5, 40 % sucrose and 0.2 % Bromophenol Blue, the reaction mixtures were electrophoresed for 2 h at the same voltage. The dried gel was autoradiographed at −80 °C. The IRP–IRE complexes were quantified with a GS-700 imaging densitometer (Bio-Rad Laboratories).

Cytosolic aconitase assay

Cytosolic aconitase activity was determined on the liver lysates used for the mobility-shift assay, by monitoring the disappearance of *cis*-aconitate at 240 nm for 10 min [6,7] from a sample containing 0.2 mM *cis*-aconitate and 100 μg of protein in 10 mM Hepes buffer, pH 7.5, in a final volume of 1 ml.

RESULTS

OMA modulates the IRE-binding activities of IRP1 in 3T3-L1 and SH-SY5Y cell lines and in mouse liver

IRP1, a 98-kDa protein, possesses structural identity with 4Fe-4S cytosolic aconitase [16,17], and the mechanism of the switch from aconitase to IRP1 was clarified by experiments of site-directed mutagenesis that revealed the disassembling steps of the [4Fe-4S] cluster of cytosolic aconitase [18,19]. Consequently, it was found that the addition of iron to IRP1 restores aconitase activity, thus preventing RNA-binding, which implies that IRP1/aconitase plays a bifunctional role [20,21]. IRP2 shares 61 % amino acid identity with IRP1, a major difference being a 73-amino acid insertion rich in cysteine residues [22,23], and it has a different pattern of tissue specificity and expression level [24].

Because OMA acts as an efficient competitive inhibitor of liver cytosolic aconitase [6], we predicted that OMA linked to the active site can affect the RNA-binding capacity of IRP1 by preventing the aconitase/IRP1 switch [14]. To verify this hypothesis, we investigated the effect *in vitro* of OMA on lysates obtained from mouse 3T3-L1 fibroblasts, from cells of human neural origin and from mouse livers. We also investigated the effect *in vivo* both by incubating 3T3-L1 fibroblasts with OMA for a short period, and by treating young mice with appropriate doses of OMA precursors (see the Experimental section). Because the addition of high concentrations of reducing agents to cell extracts enhances IRP1 RNA-binding activity, thereby revealing the total 'activatable' amounts of IRP1 [25], we compared the effect of OMA with and without 2 % 2-ME. In all samples tested, OMA greatly decreased the amount of IRP1 available for RNA binding (Figure 1). The experiments in which 2-ME was added after incubation with OMA showed that the recovered 'activatable' RNA-binding activity was always less than that recovered without the inhibitor. This finding indicates that a fraction of the OMA added was tightly bound to the active site of aconitase and consequently less IRP1 was recovered by reduction. Finally, in the presence of OMA, 3T3-L1 cells unexpectedly showed a remarkable decrease in the signal corresponding to the RNA-binding activity of IRP2.

The effect of OMA on IRP1 activity is dose- and time-dependent

Because the results shown in Figure 1 demonstrated that the fraction of aconitase in which OMA is bound to the active site

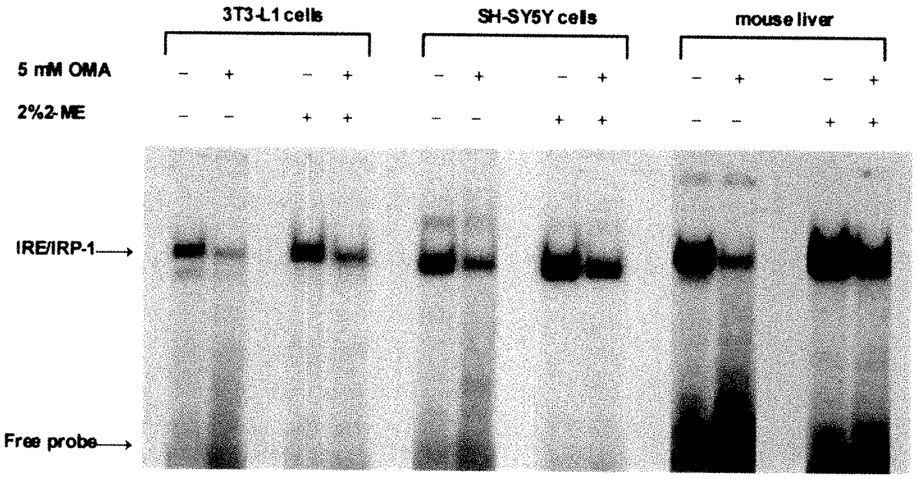

Figure 1 Effect of OMA on the RNA-binding capacity of IRP1 in different experimental systems

Protein extracts (5 μg) were incubated with 5 mM OMA for 10 min, then the RNA–protein binding reaction was started by the addition of 0.2 ng of ^{32}P-labelled IRE probe (6 × 10^4 c.p.m.) with and without 2% 2-ME, as indicated. The autoradiogram shows the complexes corresponding to IRE-bound IRP1, and the residual unbound RNA probe (free probe). In 3T3-L1 cells a faster-migrating band is present corresponding to IRE-bound IRP2. These data are typical of three experiments.

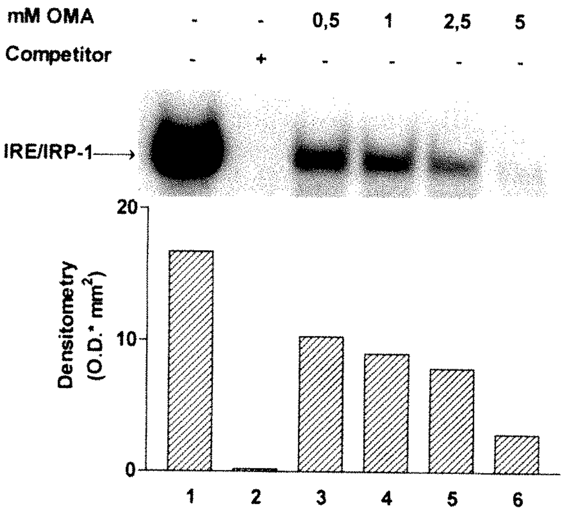

Figure 2 Dose-dependence of the effects of OMA on IRP activity

Cytosolic extracts from mouse liver were treated for 10 min with increasing concentrations of OMA before the addition of ^{32}P-labelled IRE probe. The IRE–IRP1 complexes were determined by electrophoretic mobility-shift assay and quantified with an imaging densitometer. The relative activities are plotted as arbitrary units.

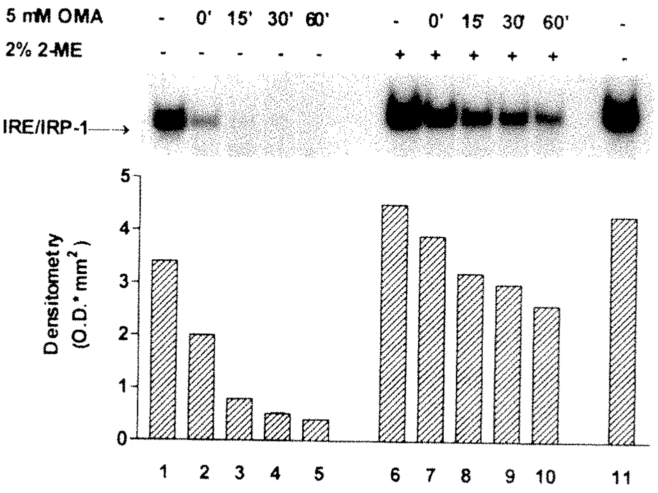

Figure 3 Time dependence of the effects of OMA on IRP activity

Cytosolic extracts from mouse liver were incubated with 5 mM OMA for the times indicated and then treated or not with 2% 2-ME before the addition of ^{32}P-labelled IRE probe. Lane 11 shows the IRE–IRP1 binding activity of the same cytosolic extract kept at room temperature for 60 min before addition of the probe. The IRE–IRP1 complexes were quantified by densitometry. The relative activities are plotted as arbitrary units.

cannot be recovered by 2-ME, we investigated the mechanism by which OMA might modify the residual '2-ME-activatable' fraction of IRP1. We first determined the dose- and time-dependence of the effects exerted by OMA on the cytosolic extract from the liver of untreated mice. As shown in Figure 2, 0.5 mM OMA significantly decreased the RNA-binding activity of IRP1 and the effect increased with concentrations up to 5 mM, at which point RNA-binding activity was negligible. Therefore, we used a 5 mM concentration of OMA in all the experiments described herein.

We next evaluated the time-dependence of the effect of OMA by incubating extracts at room temperature, with and without OMA, and by adding 2% 2-ME at the end of incubation with OMA (Figure 3). IRP1 RNA-binding activity decreased very rapidly and practically disappeared between 15 and 60 min of OMA exposure. This effect was not due to protein degradation because after 60 min (Figure 3, lane 11) the IRP1 binding capacity was not modified in the untreated sample. Moreover, the recovery of the binding activity of IRP1 by 2-ME never reached the value of the control and decreased as the incubation

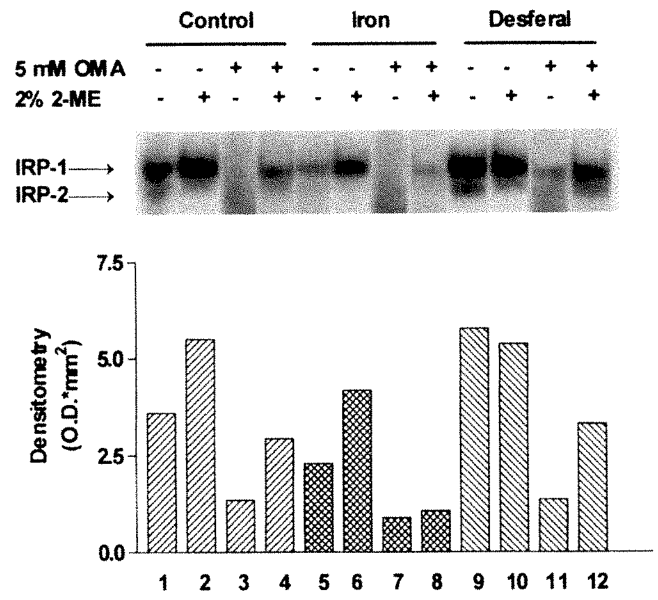

Figure 4 Effects *in vitro* of OMA on IRP from iron-repleted and -depleted cells

3T3-L1 cells were treated for 18 h with 20 μg/ml ferric ammonium citrate (lanes 5–8) or with 100 μM Desferal (lanes 9–12) in comparison with untreated cells (lanes 1–4). The obtained cytosolic extracts were incubated with and without 5 mM OMA for 30 min at room temperature. Where indicated, 2% 2-ME was added before the addition of ^{32}P-labelled IRE probe. The IRP–IRE complexes were resolved by electrophoretic mobility-shift assay and plotted as arbitrary units.

time increased. This finding shows that the formation of the inhibitor–aconitase complex was time-dependent.

OMA *in vitro* modulates the RNA-binding activity of IRP1 and of IRP2 from iron-repleted as well as from iron-depleted cells

The RNA-binding activity of IRP1 depends on the amount of iron available to the cell [8,9,21]. We analysed lysates of 3T3-L1 cells maintained in an iron-rich medium containing ferric ammonium citrate, and in an iron-depleted medium containing Desferal, a potent iron chelator. Also in the 3T3-L1 cells, iron repletion and depletion provoked a decrease and an increase, respectively, in the RNA-binding capacity of IRP1 and IRP2 (Figure 4). As expected, the effect of OMA was much more evident in the iron-repleted than in the iron-depleted cells. It is noteworthy that, in the presence of an excess of iron, 2-ME was unable to restore IRP1, a finding that reinforces the concept of stability of the association between the inhibitor and the [4Fe-4S] cluster. IRP2 was absent from lysates of iron-repleted cells because iron accelerates the turnover of the protein [26,27], but, when present as in the control and in iron-depleted cells, it decreased upon the addition of OMA. Interestingly, 2-ME restored the IRP2 activity in iron-depleted cells. Since IRP2 does not possess an [Fe-S] cluster, but has five cysteine residues in its specific 73-amino acid insertion [22,23], it is not unreasonable to predict that OMA might interfere also with IRP2 cysteine residues.

OMA synthesized *in vivo* inhibits cytosolic aconitase activity and modulates the RNA-binding activity of IRP1

Early experiments demonstrated that OMA synthesis occurs *in vivo* by the condensation of two cellular metabolites, namely oxaloacetate and glyoxylate [1,3,7]. In light of this finding, we investigated the effects of OMA *in vivo* both in the whole animal

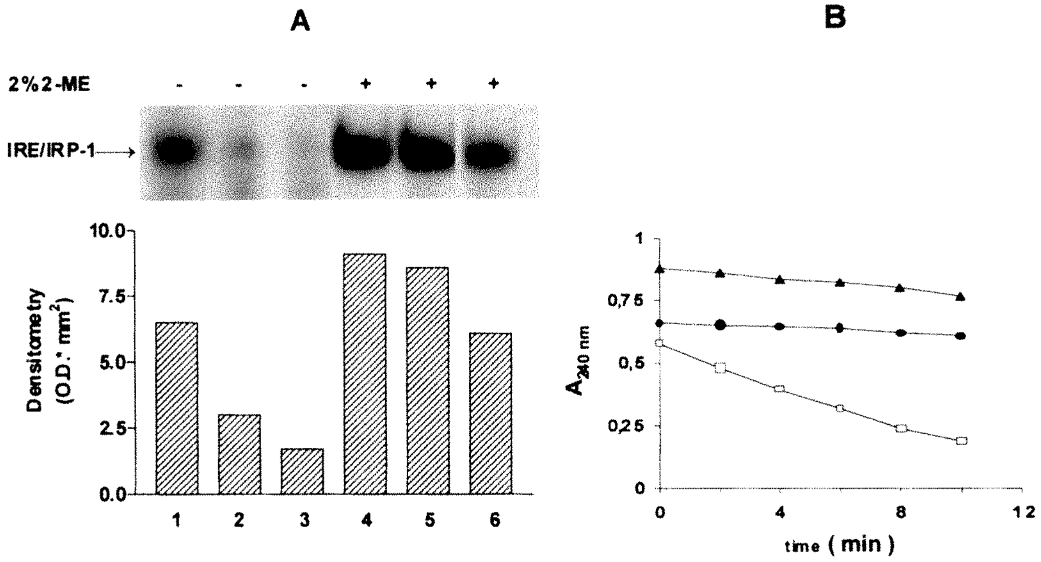

Figure 5 Effects *in vivo* of OMA

(**A**) Cytosolic extracts were prepared either from the livers of mice killed 1 h after injection of equimolar amounts of oxaloacetate plus glyoxylate (corresponding to $\approx$ 2.5 mM OMA in lanes 2 and 5, and $\approx$ 5 mM OMA in lanes 3 and 6), or from livers of mice injected with physiological solution (lanes 1 and 4). As indicated, 2% 2-ME was added before the reaction was started with the ^{32}P-labelled IRE probe. The IRE–IRP1 complexes were quantified by densitometry and reported in arbitrary units. (**B**) The aconitase assay was performed on 100 μg/ml cytosolic extract used for RNA mobility-shift assay. Aconitase activity was evaluated by monitoring the disappearance of *cis*-aconitate at 240 nm: □, control; ▲, lower dose of OMA precursors (2.5 mM); ●, higher dose of OMA precursors (5 mM).

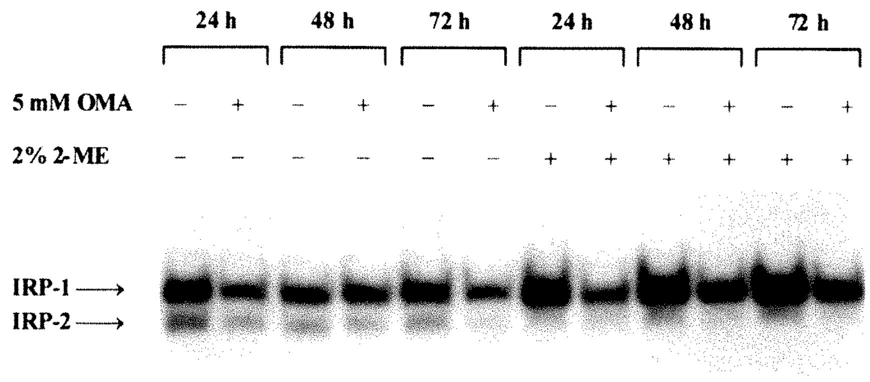
24 h
48 h
72 h
24 h
48 h
72 h
5 mM OMA – + – + – + – + – + – +
2% 2-ME – – – – – – + + + + + +
IRP-1
IRP-2

Figure 6 Effects of OMA treatment on IRP1 and IRP2 RNA-binding activity in 3T3-L1 cells

Confluent cultures of 3T3-L1 cells were grown with and without 5 mM OMA for the times indicated. Cytosolic extracts were incubated at room temperature with and without 2% 2-ME before the addition of ^{32}P-labelled IRE probe. Arrows indicate the positions of complexes IRE–IRP1 and IRE–IRP2.

and on cultured 3T3-L1 cells. In the first experiment we injected subcutaneously into young mice amounts of glyoxylate and oxaloacetate that approximately reproduced, in the whole body, the concentrations of 2.5 and 5 mM OMA used *in vitro*. Other mice injected with physiological solution served as controls. All animals were killed 1 h after the injection. Cytosolic extracts were prepared as described in the Experimental section. Aliquots of the same extracts were used to assay aconitase activity and the RNA-binding capacity of IRP1. The effect exerted by the newly synthesized OMA on IRP1 RNA binding resulted in the disappearance of IRP1 (Figure 5A). The addition of 2-ME confirmed the difference in the recovery of IRP1 activity between the control and treated mice (Figure 5A). As expected, *cis*-aconitate absorbance decreased in the liver of controls while it remained unchanged in the treated mice even in those given the lower concentration of OMA precursor (Figure 5B). This finding confirms that aconitase was completely inhibited.

In the second experiment, confluent cultures of 3T3-L1 were treated with 5 mM OMA for the times indicated in Figure 6. In mobility-shift analyses of lysates, the effect of OMA became evident after 24 h and remained almost constant up to 72 h. The 2-ME-induced recovery of IRP1 was always lower versus controls, which confirms yet again that the OMA linked to the active site cannot be removed. IRP2 binding decreased up to 72 h, more remarkably in OMA-treated cells. The addition of 2-ME did not restore IRP2 activity. These results demonstrate that OMA synthesized *in vivo*, or added to long-term cell cultures, possesses the same capacity to inhibit formation of the RNA–IRP complex as observed *in vitro*.

DISCUSSION

The results of our experiments show that the addition of OMA *in vitro* and *in vivo* to lysates from various sources leads to a constant decrease in the RNA-binding activity of IRP1 and, surprisingly, also of IRP2, when present. Experiments with the reducing agent 2-ME, which in the presence of OMA only partially restored the RNA-binding capacity of IRP, confirm that a fraction of OMA is tightly fixed to the active site of aconitase. These findings agree with previous observations that aconitase substrates prevent full recovery of the binding activity promoted by 2-ME in different cell lines [19,21]. OMA decreased the binding of IRP to practically the same extent in iron-repleted cells, which are rich in aconitase, and in iron-depleted cells, rich in IRP1 and IRP2. Interestingly, 2-ME only minimally restored IRP binding in iron-enriched cells compared with iron-depleted cells. This finding indicates that iron also increases the stability of the OMA complex with the [Fe-S] cluster. In all our experiments, OMA decreased the binding activity of IRP2; this suggests reactivity with a protein that lacks an [Fe-S] cluster. Therefore, OMA may also interact with IRP1, in which the [Fe-S] cluster of aconitase is disassembled. Consequently, OMA may prevent binding of IRP to IRE regions in two ways. One entails direct contact with the cluster; in this case OMA mimics the substrate with which it shares close structural analogy. The other is by decreasing the efficiency of the active components of IRP, i.e. the amino acid residues cysteine, arginine and/or lysine [19,28], which are involved in the interaction with the mRNA IRE regions that control iron metabolism.

We believe that, besides reacting with the [4Fe-4S] cluster, the highly negative-charged OMA might well interfere with the amino acid residues involved in IRE binding by impeding the post-transcriptional control exerted by IRP. This hypothesis is supported by the finding that the newly synthesized OMA in mouse livers, which inhibits aconitase activity *in vivo*, promotes the decrease of RNA-binding capacity of IRP1. Moreover, in 3T3-L1 cells cultured with OMA, IRP2 also had a modulating effect on RNA-binding capacity, similar to IRP1, and a response to 2-ME at all times, analysed similarly to that observed *in vitro*. These results obtained *in vivo* strongly support the earlier observation [14], obtained *in vitro*, that OMA, by modulating the activity of IRP1 and IRP2, directly participates in the complex system of iron-metabolism regulation. In addition, the results *in vivo* also support the utility of OMA synthesis in living cells because, besides regulating the flux of the citric acid cycle, OMA appears to exert another important function in the regulation of mRNA expression in iron metabolism.

In conclusion, the data presented shed new light on early reports of OMA synthesis in mammalian tissues [1,3,7]. The specific effect of OMA on the cytosolic and mitochondrial aconitase give a meaning to the presence of the cytosolic form of this enzyme, whose function in the cytoplasm is unknown. Moreover, our data suggest that OMA plays a role in the complex mechanism of iron-metabolism regulation. Since OMA precursors also lead to the synthesis of OMA in animal tissues, events occurring in mitochondria, such as interruption of the citric acid cycle, may be correlated with cytosolic events, such as translational control of specific mRNA.

This work was supported by grants from the Ministero della Università e della Ricerca Scientifica e Tecnologica (40% MURST to A C) and from the National Research Council (CNR, Rome, to A.R) We are grateful to Jean Gilder for revising the text

REFERENCES

1 Ruffo, A , Romano, M and Adinolfi, A. (1959) Inhibition of aconitase by glyoxylate plus oxaloacetate Biochem J **72**, 613–618
2 Ruffo, A , Testa, E., Adinolfi, A and Pelizza, G. (1962) Control of the citric acid cycle by glyoxylate 1. A new inhibitor of aconitase formed by the condensation of glyoxylate with oxaloacetate Biochem J **85**, 588–593
3 Ruffo, A , Adinolfi, A., Budillon, G and Capobianco, G (1962) Control of the citric acid cycle by glyoxylate 2 Mechanism of the inhibition of respiration in liver and kidney particles Biochem J. **85**, 593–596
4 Ruffo, A , Testa, E , Adinolfi, A , Pelizza, G. and Moratti, R. (1967) Control of the citric acid cycle by glyoxylate Mechanism of the inhibition by oxalomalate and γ-hydroxy-α-oxoglutarate Biochem J **103**, 19–23
5 Adinolfi, A , Moratti, R , Olezza, S and Ruffo, A (1969) Control of the citric acid cycle by glyoxylate The mechanism of inhibition of oxoglutarate dehydrogenase, isocitrate dehydrogenase and aconitate hydratase. Biochem J **114**, 513–518
6 Adinolfi, A , Guarriera-Bobyleva, V , Olezza, S and Ruffo, A (1971) Inhibition by oxalomalate of rat liver mitochondrial and extramitochondrial aconitate hydratase Biochem J **125**, 557–562
7 Adinolfi, A , Speranza, M L , Guarriera-Bobyleva, V and Ruffo, A. (1973) Citrate metabolism in liver of rats treated with glyoxylate and oxaloacetate Ital J Biochem **22**, 92–104
8 Klausner, R D , Rouault, T A and Harford, J B (1993) Regulating the fate of mRNA the control of cellular iron metabolism Cell **72**, 19–28
9 Melefors, O and Hentze, M W (1993) Iron regulatory factor – the conductor of cellular iron regulation Blood Rev **7**, 251–258
10 Hentze, M. W and Kuhn, L C (1996) Molecular control of vertebrate iron metabolism mRNA-based regulatory circuits operated by iron, nitric oxide, and oxidative stress Proc. Natl Acad Sci. U S A **93**, 8175–8182
11 Rouault, T A and Klausner, R D (1996) Iron-sulfur clusters as biosensors of oxidants and iron Trends Biochem Sci **21**, 174–177
12 Eisenstein, R S and Blemings, K P (1998) Iron regulatory proteins, iron responsive elements and iron homeostasis J Nutr **128**, 2295–2298
13 Theil, E C (1998) The iron responsive element (IRE) family of mRNA regulators In Metal Ions in Biological Systems, vol 35 (Sigel, A and Sigel, H , eds), pp 403–434, Marcel Dekker, New York
14 Festa, M , Colonna, A , Pietropaolo, C and Ruffo, A (1999) Regulation of iron metabolism by oxalomalate Rend Fis Acc Lincei s. 9, **10**, 21–24
15 Guo, B., Yu, Y and Leibold, E A. (1994) Iron regulates cytoplasmic levels of a novel iron-responsive element-binding protein without aconitase activity J Biol Chem **269**, 24252–24260
16 Paraskeva, E and Hentze, M. W (1996) Iron-sulphur clusters as genetic regulatory switches the bifunctional iron regulatory protein-1 FEBS Lett **389**, 40–43
17 Rouault, T A , Stout, C D., Kaptain, S , Harford, J. B and Klausner, R D (1991) Structural relationship between an iron-regulated RNA-binding protein (IRE-BP) and aconitase functional implications. Cell **64**, 881–883
18 Philpott, C C , Haile, D , Rouault, T A and Klausner, R D. (1993) Modification of a free Fe-S cluster cysteine residue in the active iron-responsive element-binding protein prevents RNA binding J Biol Chem **268**, 17655–17658
19 Hirling, H , Henderson, B R and Kuhn, L C (1994) Mutational analysis of the [4Fe-4S]-cluster converting iron regulatory factor from its RNA-binding form to cytoplasmic aconitase EMBO J **13**, 453–461
20 Kennedy, M C , Emptage, M. H , Dreyer, J. L and Beinert, H (1983) The role of iron in the activation-inactivation of aconitase J Biol Chem **258**, 11098–11105
21 Haile, D J , Rouault, T A , Harford, J B , Kennedy, M C , Blondin, G A , Beinert, H and Klausner, R D (1992) Cellular regulation of the iron-responsive element binding protein disassembly of the cubane iron-sulphur cluster results in high-affinity RNA binding Proc Natl Acad Sci U S A **89**, 11735–11739
22 Guo, B , Brown, F M., Phillips, J D , Yu, Y and Leibold, E A (1995) Characterization and expression of iron regulatory protein 2 (IRP2) J Biol. Chem **270**, 16529–16535
23 Iwai, K , Klausner, R D and Rouault, T. A (1995) Requirements for iron-regulated degradation of the RNA binding protein, iron regulatory protein 2. EMBO J **14**, 5350–5357
24 Recalcati, S , Conte, D and Cairo, G (1999) Preferential activation of iron regulatory protein-2 in cell lines as a result of higher sensitivity to iron Eur J Biochem **259**, 304–309
25 Hentze, M W , Rouault, T A , Harford, J B. and Klausner, R D (1989) Oxidation-reduction and the molecular mechanism of a regulatory RNA-protein interaction Science **244**, 357–359
26 Guo, B , Phillips, J D., Yu, Y and Leibold, E A (1995) Iron regulates the intracellular degradation of iron regulatory protein 2 by the proteasome J. Biol Chem **270**, 21645–21651
27 Henderson, B R and Kuhn, L C (1995) Differential modulation of the RNA-binding proteins IRP-1 and IRP-2 in response to iron J Biol. Chem **270**, 20509–20515
28 Philpott, C C , Klausner, R D. and Rouault, T. A. (1994) The bifunctional iron-responsive element binding protein/cytosolic aconitase the role of active-site residues in ligand binding and regulation Proc Natl Acad Sci U S A **91**, 7321–7325

Received 4 January 2000/29 February 2000, accepted 27 March 2000

Biochem J (2000) **348**, 321–328 (Printed in Great Britain)

Kinetic study of the inactivation of ascorbate peroxidase by hydrogen peroxide

Alexander N. P. HINER*, José Neptuno RODRÍGUEZ-LÓPEZ†, Marino B. ARNAO*, Emma LLOYD RAVEN‡, Francisco GARCÍA-CÁNOVAS† and Manuel ACOSTA*[1]

*Departamento de Biología Vegetal (Fisiología Vegetal), Universidad de Murcia, E-30100 Espinardo, Murcia, Spain,
†Departamento de Bioquímica y Biología Molecular-A, Universidad de Murcia, E-30100 Espinardo, Murcia, Spain, and
‡Department of Chemistry, University of Leicester, University Road, Leicester LE1 7RH, U.K.

The activity of ascorbate peroxidase (APX) has been studied with H_2O_2 and various reducing substrates. The activity decreased in the order pyrogallol > ascorbate > guaiacol > 2,2′-azino-bis-(3-ethylbenzthiazoline-6-sulphonic acid) (ABTS). The inactivation of APX with H_2O_2 as the sole substrate was studied. The number of H_2O_2 molecules required for maximal inactivation of the enzyme was determined as approx. 2.5. Enzymic activity of approx. 20 % of the original remained at the end of the inactivation process (i.e. approx. 20 % resistance) when ascorbate or ABTS was used as the substrate in activity assays. With pyrogallol or guaiacol no resistance was seen. Inactivation by H_2O_2 followed over time with ascorbate or pyrogallol assays exhibited single-exponential decreases in enzymic activity. Hyperbolic saturation kinetics were observed in both assay systems; a similar dissociation constant (0.8 μM) for H_2O_2 was obtained in each case. However, the maximum rate constant (λ_{max}) obtained from the plots differed depending on the assay substrate. The presence of reducing substrate in addition to H_2O_2 partly or completely protected the enzyme from inactivation, depending on how many molar equivalents of reducing substrate were added. An oxygen electrode system has been used to confirm that APX does not exhibit a catalase-like oxygen-releasing reaction. A kinetic model was developed to interpret the experimental results; both the results and the model are compared and contrasted with previously obtained results for horseradish peroxidase C. The kinetic model has led us to the conclusion that the inactivation of APX by H_2O_2 represents an unusual situation in which no enzyme turnover occurs but there is a partition of the enzyme between two forms, one inactive and the other with activity towards reducing substrates such as ascorbate and ABTS only. The partition ratio is less than 1.

Key words: catalase, mechanism-based inactivation, protection, reductants, suicide inactivation.

INTRODUCTION

The superfamily of haem peroxidases from plants, fungi and bacteria are a group of enzymes that utilize H_2O_2 to oxidize a second (reducing) substrate. These enzymes share a similar catalytic cycle in which H_2O_2 reacts with the resting ferric enzyme to form the intermediate compound I (known as compound ES in cytochrome *c* peroxidase) which carries two oxidizing equivalents. Compound I is subsequently reduced by reactions with two reducing substrate molecules. The first of these reduction steps generates the intermediate, compound II, which is then further reduced back to the ferric enzyme.

Haem peroxidases have been classified into three classes [1]: class I contains intracellular enzymes [e.g. yeast cytochrome *c* peroxidase (CcP), ascorbate peroxidase (APX) and bacterial gene-duplicated catalase-peroxidases] [2]; class II consists of secretory fungal enzymes (e.g. manganese peroxidase and lignin peroxidase); class III contains the secretory plant peroxidases [e.g. horseradish peroxidase (HRP)]. The classification is based on sequence comparisons and enzyme localization rather than on function; thus APX, which preferentially reacts with a small substrate molecule, ascorbate, is in the same class as CcP, which reacts with another protein, cytochrome *c*.

APX (EC 1.11.1.11) is located in the chloroplasts and cytosol of plants and eukaryotic algae, and has also been identified in certain cyanobacteria [3]. In the chloroplasts, thylakoid-bound ('tAPX') [4,5] and soluble stromal ('sAPX') [6,7] forms have been described. In the cytosol a single isoform was previously believed to be present [7] that exhibited slightly different characteristics from the chloroplastic enzymes [4–6]. However, by using the database of expressed sequence tags ('dbEST') from *Arabidopsis thaliana* (thale cress), seven APXs have been identified, including various soluble and membrane-bound cytosolic isoenzymes [8].

The function of all the forms of APX is thought to be the scavenging of the H_2O_2 that is continuously generated in cells [3,9]. For instance, in the chloroplasts of photosynthetic organisms superoxide ($O_2^{\bullet-}$) is formed when insufficient CO_2 is available to balance electrons being generated by the photosystems, these excess electrons then reduce O_2 to $O_2^{\bullet-}$. Additionally, in the mitochondria the electron transport chains can also produce $O_2^{\bullet-}$. In both cases superoxide dismutase converts $O_2^{\bullet-}$ into H_2O_2, which APX or catalase can then remove.

We have previously studied the mechanism-based inactivation, by H_2O_2 and *m*-chloroperoxybenzoic acid (*m*-CPBA), of various isoenzymes and mutants of HRP [10–16]. We now present a similar examination of the inactivation of APX.

For this study we used the recombinant cytosolic form of pea APX [17]. The enzyme is a homodimer with a molecular mass of 57.5 kDa [17,18]. The structure has been determined by X-ray crystallography [18] and the cDNA encoding the enzyme has been sequenced [17]. APX shares 33 % sequence identity with CcP [17]. It has been observed that Trp-191 in CcP and the equivalent residue in APX, Trp-179, are conserved in identical conformations [18]. Trp-191 forms the site of the protein cation

---

Abbreviations used. ABTS, 2,2′-azino-bis-(3-ethylbenzthiazoline-6-sulphonic acid); APX, ascorbate peroxidase; CcP, yeast cytochrome *c* peroxidase; [E], concentration of APX active sites; HR, hypersensitive response; HRP, horseradish peroxidase; *m*-CPBA, *m*-chloroperoxybenzoic acid; tAPX, thylakoid-bound APX.

[1] To whom correspondence should be addressed (e-mail macosta@fcu.um.es).

radical in CcP compound ES [19–21]. Most peroxidases, with the exception of CcP, are believed to form compound I species that possess a π-cation radical delocalized over the haem ring in addition to the oxyferryl iron centre common to all haem peroxidases [22]. However, recently evidence has emerged for the existence of a protein radical in wheat-germ peroxidase compound I [23]. In compound II the radical (whether π or protein) has been discharged by reaction with a molecule of reducing substrate to leave only the oxyferryl iron [24]. APX is generally thought to form a typical, but unstable, compound I containing a π-cation radical; this undergoes rapid conversion into another species, which exhibits a compound II-type absorption spectrum [25,26]. In our previous studies of the inactivation of HRP-C we have established that compound I has a central role in the reaction mechanism of inactivation, whereas compound II is much less important [16].

Because APX forms an important part of the defences of the cell against oxidative stress, the study of the inactivation of the enzyme by one of the major products of such stress, namely H_2O_2, provides an indication of the limitations of resistance to attack by reactive oxygen species. Examination of the class I peroxidase, APX, also provides a useful comparison with the class III peroxidase, HRP, and extends our knowledge of peroxidase inactivation, providing an additional and distinct example of the process, within the established framework.

EXPERIMENTAL

APX

Recombinant pea cytosolic APX was expressed in and purified from *Escherichia coli* [17]. The enzyme used had an RZ value (A_{403}/A_{280}) of 1.93 and was homogeneous by gel electrophoresis. No peroxidase activity with 2,2′-azino-bis-(3-ethylbenzthiazoline-6-sulphonic acid) (ABTS), ascorbate or guaiacol was detected in the sample after incubation with the specific APX inhibitor 4-chloromercuribenzoic acid [27], indicating that no guaiacol peroxidase was present. The concentration of enzyme was calculated from a molar absorption coefficient (ϵ) at 403 nm of 88 $mM^{-1}\cdot cm^{-1}$ per haem. The individual active sites of APX are referred to as E throughout. Because APX is a homodimer, [E] = 2[APX].

Chemicals

H_2O_2 (30 %, v/v) was from Aldrich, its concentration being determined spectrophotometrically from $\epsilon_{240} = 43.6\ M^{-1}\cdot cm^{-1}$. H_2O_2 concentration was additionally checked by using the HRP-catalysed reaction with ABTS, 2 mol of ABTS radical ($\epsilon_{414} = 31100\ M^{-1}\cdot cm^{-1}$) being formed from 1 mol of H_2O_2. *m*-CPBA was purchased from Aldrich and was further purified by recrystallization from light petroleum (boiling range 40–60 °C)/diethyl ether (3:1, v/v) [28], purity was estimated by NMR spectroscopy as 99 % [29]. Crystalline L-ascorbic acid was obtained from Scharlau. Pyrogallol (1,2,3-trihydroxybenzene) and guaiacol (2-methoxyphenol) were from Aldrich. ABTS as its ammonium salt was purchased from Sigma. Experiments were performed in sodium phosphate buffer (50 mM, pH 7.0). All solutions were prepared with water drawn from a Milli-Q system (Millipore).

UV/visible spectroscopy

UV/visible electronic absorption spectroscopy was performed in a Perkin-Elmer Lambda-2 spectrophotometer interfaced on-line to a compatible PC. The cuvette temperature was controlled at 25 ± 0.1 °C by a Haake D1G circulating bath with heater/cooler unit attached.

Oxygen measurements

Measurements of dissolved oxygen concentration were made with a Hansatech (Kings Lynn, Cambs., U.K.) oxygraph unit controlled from a PC. The oxygraph used a Clark-type silver/platinum electrode with a 0.0125 mm Teflon membrane. The sample was continuously stirred during experiments and its temperature was controlled at 25 °C, as above. The zero oxygen level for calibration and experiments was obtained by bubbling oxygen-free nitrogen through the sample for at least 10 min.

APX activity assays

APX activity was determined with assays containing H_2O_2 and one of the reducing substrates: ascorbate, pyrogallol, guaiacol or ABTS. For ascorbate the activity was followed as the decrease in A_{290} due to the consumption of ascorbate in an assay containing 10 mM H_2O_2 and 0.5 mM ascorbate ($\epsilon_{290} = 2800\ M^{-1}\cdot cm^{-1}$) in buffer. The activity with pyrogallol (5 mM) was determined at 430 nm ($\epsilon_{430} = 2470\ M^{-1}\cdot cm^{-1}$) and guaiacol (30 mM) at 470 nm ($\epsilon_{470} = 5570\ M^{-1}\cdot cm^{-1}$) The increases in absorbance as a result of the formation of the oxidized products were measured at these wavelengths. The assays contained 10 mM H_2O_2. The ABTS assay followed the formation of the ABTS radical at 414 nm ($\epsilon_{414} = 31100\ M^{-1}\cdot cm^{-1}$) in a solution containing 30 mM ABTS and 10 mM H_2O_2. The total volume of each assay was 1 ml in a quartz cuvette with a 1 cm path length All the assays were started by the addition of a sample of APX. The exact final concentration of E added varied for each individual experiment but a concentration between 10 and 50 nM generated a satisfactory linear absorbance change over the 2–5 min assay period (30 s for pyrogallol). Activity was calculated from the gradient of the change in absorbance with time (ΔA) divided by the molar absorption coefficient (ϵ).

Time dependence of inactivation

The inactivation of APX by H_2O_2 over time was followed by incubating APX ([E] = 80 nM) with H_2O_2 (0, 1, 2, 5, 7.5 and 10 μM) in buffer (500 μl total volume). The reaction was initiated by addition of the enzyme. At the appropriate time points 50 μl aliquots were removed and their residual enzymic activities (A_R) were determined with the ascorbate or pyrogallol assay. The A_R was taken as the activity remaining (A_t) compared to the initial activity at the beginning of the experiment (A_0) expressed as a percentage. A plot of ln A_R against time permitted the calculation of the observed rate constants of inactivation (λ, s^{-1}). The maximum apparent rate constant of inactivation (λ_{max}, s^{-1}) and the dissociation constant of H_2O_2 from APX compound I [K_I (μM), the concentration of peroxide giving $\frac{1}{2}\lambda_{max}$] [30] were obtained by non-linear regression fitting of a hyperbolic curve to a plot of λ against [H_2O_2]. Curve and line fitting was done with the program SigmaPlot for Windows (Jandel Scientific Software, San Rafael, CA, U.S.A.).

Catalase activity of APX

Possible oxygen production as a result of a catalase-like action of APX on H_2O_2 was determined with the oxygraph on a total volume of 1.0 ml of deoxygenated buffer containing nominal H_2O_2 concentrations of 0, 0 1, 0.5, 1.0, 5.0, 10.0, 25.0 and 50.0 mM. The exact concentrations of H_2O_2 were determined spectroscopically just before use. The reaction was started by the addition of APX (0.25 μM final concentration of E). The initial rate of oxygen production was calculated from the slope of the trace observed on the addition of APX after discounting the rapid rise in O_2 due to the introduction of sample containing dissolved air.

Determination of the number of equivalents of H_2O_2 required for APX inactivation

APX ([E] = 0.30–0.50 μM, depending on each experiment) was incubated with molar ratios of H_2O_2 ($[H_2O_2]$-to-[E] ratios from 0 to 1000 were used, the actual concentrations of substrate added depending on the APX concentration) in buffer (100 μl total volume for each ratio). The inactivation process was left to continue to completion. After 16–18 h the residual APX activity (A_R) at each ratio was determined with the ascorbate, pyrogallol, guaiacol or ABTS assay. From plots of A_R against $[H_2O_2]/[E]$ a fitted line extrapolated from the linear part of the data to the x-axis gave the number of equivalents of H_2O_2 required for the inactivation of each active centre of the enzyme. For comparison a similar incubation experiment was performed in the presence of *m*-CPBA rather than H_2O_2 at [*m*-CPBA]-to-[E] ratios from 0 to 100, A_R was determined with the ascorbate assay (results not shown).

Protection of APX by reducing substrate against inactivation by H_2O_2

The same protocol as in the incubation experiments above was followed (0.25 μM APX) except that the incubation medium included ascorbate or guaiacol (1, 10 and 100 μM). Residual activities were determined with the ascorbate assay. Control incubations containing reducing substrate and H_2O_2 only showed that ascorbate was very slowly decomposed by H_2O_2 (followed at 290 nm). Guaiacol (observed at 470 nm) did not seem to be similarly sensitive.

RESULTS

Relative activities of APX with different reducing substrates

The activity of APX with a selection of substrates is shown in Table 1. The activity with ascorbate is defined as 1; thus pyrogallol was oxidized 3.2-fold more rapidly than ascorbate. Guaiacol and ABTS were poorer substrates of APX with 0.38-fold and 0.15-fold the activity of ascorbate respectively. The results given are values of V_{max}; they are in good agreement with the relative activities of wild-type APX [31].

Time dependence and kinetics of APX inactivation by H_2O_2

When the decrease in residual activity due to inactivation by H_2O_2 was followed over time, with either the ascorbate or the pyrogallol assay, single-exponential curves were obtained for several hours (results for ascorbate are shown in Figure 1a). When the enzyme activity remaining was determined with the

Table 1 Relative APX enzyme activities with different reducing substrates

Enzyme activities were determined spectroscopically with the assays described in the Experimental section, the relative activity with ascorbate was defined as 1. The concentrations of reagents used were H_2O_2, 10 mM, ascorbate, 0.5 mM, ABTS, 30 mM, pyrogallol, 5 mM, guaiacol, 30 mM in 50 mM sodium phosphate buffer, pH 7 0

Reducing substrate in assay	V_{max} (M · min^{-1})	Relative activity
Ascorbate	5.3×10^{-5}	1.0
ABTS	$8\,2\times10^{-6}$	0 15
Pyrogallol	$1\,7\times10^{-4}$	3 2
Guaiacol	$2\,0\times10^{-5}$	0 38

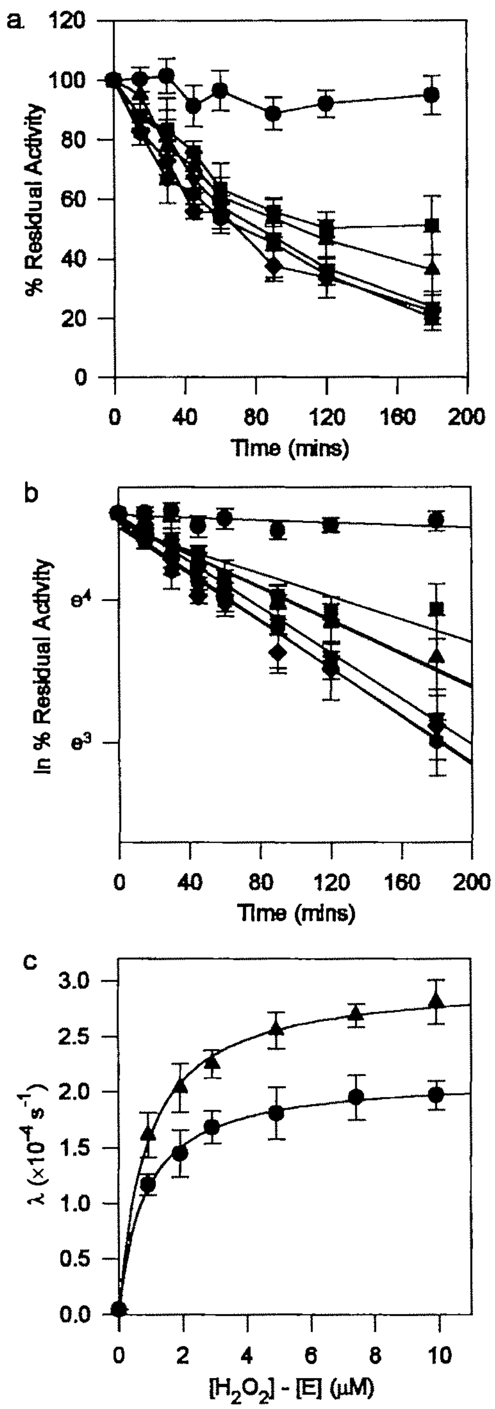

Figure 1 Time dependence and kinetics of the inactivation of APX by H_2O_2

(a) Inactivation of APX followed over time APX ([E] = 80 nM) was incubated with H_2O_2 at concentrations of 0 (●), 1 0 (■), 2 0 (▲), 5.0 (▼), 7 5 (◆) and 10.0 (⬢) μM in phosphate buffer (50 mM, pH 7 0, 25 °C) Aliquots of 50 μl were assayed at the specified times for residual activity with pyrogallol or ascorbate (b) Plot with a natural logarithmic (ln) scale showing straight-line fits to the data in (a), from which the values of λ were determined (c) Plot of λ against $[H_2O_2]-[E]$ with ascorbate (●) or pyrogallol (▲) assays. The apparent rate constants of inactivation (λ_{max}) and the dissociation constants (K_i) were obtained by using SigmaPlot for Windows.

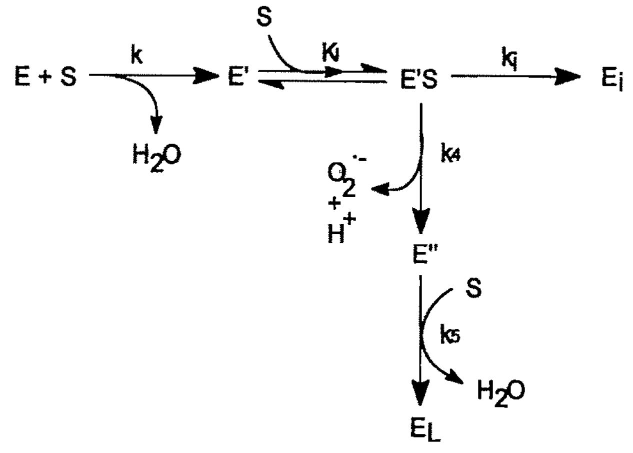

Scheme 1 Proposed mechanism of the inactivation of APX by H_2O_2

E, APX active site, S, H_2O_2, E', enzyme compound formed by reaction of E and S, E'S, complex between E' and S, E_i, inactive APX, E", intermediate formed from E'S by loss of superoxide, E_L, an APX species with modified specificity for reducing substrates (active only with ABTS and

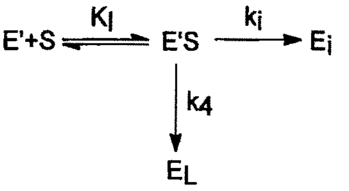

Scheme 2 Simplified model of the mechanism of APX inactivation by H_2O_2

E', APX active site that has previously undergone reaction with H_2O_2, S, H_2O_2, E'S, complex between E' and S, E_i, inactive E, E_L, E with modified reducing substrate specificity (active only with ABTS and ascorbate).
ascorbate)

pyrogallol assay, the curves obtained tended to approach 0%, but with ascorbate the curves tended to approx. 20% of the original activity (i.e. a fraction of APX seemed resistant to inactivation).

A plot of the natural logarithms of the percentage residual activities (ln A_R) against time gave straight lines (Figure 1b) with slopes equivalent to the observed rate constants of inactivation (λ) [see Appendix, eqn. (A 17)] The inactivation of APX by H_2O_2 clearly demonstrated saturation kinetics, as seen from the hyperbolic curves fitted to the plot of λ against [H_2O_2] (Figure 1c). The dissociation constant (K_I), defined as the H_2O_2 concentration giving $\frac{1}{2}\lambda_{max}$, was similar (means ± S.D.) with either the ascorbate (0.80 ± 0.12 μM) or the pyrogallol (0.86 ± 0.10 μM) assay and indicated a high affinity of APX for H_2O_2. However, the maximum apparent rate constant of inactivation (λ_{max}) [see Appendix, eqns. (A 18) and (A21)] calculated from the curve fitted to each data set was different: λ_{max} for ascorbate was $(2.13 \pm 0.08) \times 10^{-4}\ s^{-1}$, λ_{max} for pyrogallol was $(3.00 \pm 0.11) \times 10^{-4}\ s^{-1}$. This variation in the apparent rate constants and, above all, the different final activity levels observed with different reducing substrates are consequences of the kinetics describing the proposed mechanism shown in Schemes 1 and 2.

When ascorbate or ABTS (or any other substrate that reveals a resistant fraction of APX; see below) is used to determine the enzyme activity [see Appendix, eqn. (A21)], then:

$\lambda_{max} = k_i = (2.13 \pm 0.08) \times 10^{-4}\ s^{-1}$

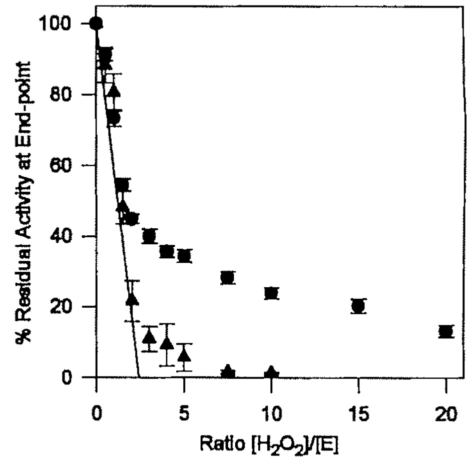

Figure 2 Sensitivity to inactivation of APX at different molar ratios of H_2O_2

APX ([E] = 0.3–0.5 μM) was incubated with molar excesses of peroxide at the ratios indicated in phosphate buffer (50 mM, pH 7.0, 100 μl total volume). When the reaction was complete (16–18 h incubation) the percentage residual activities were measured with ascorbate (●) or pyrogallol (▲). Lines were fitted by using SigmaPlot for Windows and the intercepts at the x-axis were determined

When pyrogallol or guaiacol (or any other substrate that does not reveal resistant APX) is used then [see Appendix, eqn. (A 18)]:

$\lambda_{max} = k_4 + k_i = (3.00 \pm 0.11) \times 10^{-4}\ s^{-1}$

thus:

$k_4 = (0.87 \pm 0.19) \times 10^{-4}\ s^{-1}$

and because r, the partition ratio between the formation of the enzymic forms E_i and E_L (discussed below) is:

$r = k_4/k_i$

Therefore

$r = 0.41 \pm 0.26$

(Note that in this case r does not represent a partition between catalytic and inactivatory pathways as it does for HRP-C [12].)

Catalase activity of APX

The results of oxygraph experiments showed that APX did not possess any significant catalase-like activity. Active and heat-inactivated (boiled) APX gave similar traces. This result was consistent with the single-exponential time courses observed for the reaction and the low values of r obtained in incubation experiments below.

Number of equivalents of H_2O_2 required for inactivation of APX

APX was sensitive to inactivation by H_2O_2, as demonstrated by values of 2–3 obtained for the intercepts at the x-axis in plots of residual activity (A_R) against the molar ratio of H_2O_2 to APX active sites (E), when A_R was measured with the different assays. Figure 2 shows the plots with the ascorbate and pyrogallol activity assays. When the residual activities were measured with ascorbate or ABTS the plots deviated from linearity at higher substrate-to-enzyme ratios. Activity was not fully lost even at

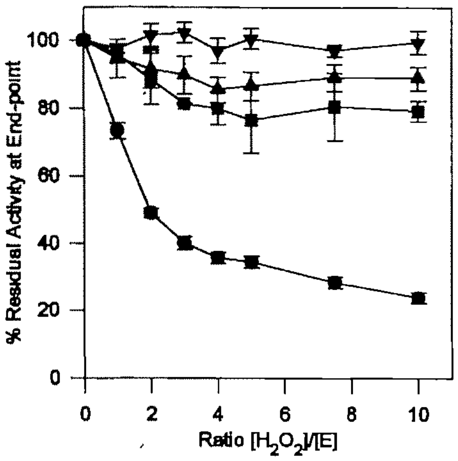

Figure 3 Protection of APX by ascorbate against inactivation by H_2O_2

APX ([E] = 0.5 μM) was incubated under the same conditions as specified in the legend to Figure 2, except that ascorbate was present in the samples at concentrations of 0 (●), 1.0 (■), 10.0 (▲) and 100.0 μM (▼). Results obtained with guaiacol instead of ascorbate were very similar

$[H_2O_2]$-to-[E] ratios as high as 1000 (results not shown); a residual activity, measured with ascorbate, of 9.6 % remained. When one of the phenolic substrates pyrogallol or guaiacol was used as the reducing substrate in the activity assays, this deviation from linearity was not observed and APX activity was decreased to immeasureably low levels by incubation with H_2O_2. When *m*-CPBA was substituted for H_2O_2 in the incubations, very similar results were obtained (results not shown).

From Scheme 1 and the stoichiometry of the reaction it can be seen that two molecules of H_2O_2 per APX active site are required to generate the inactive enzyme form, E_I, and three equivalents are required to make the enzyme form (with altered activity toward substrates), E_L [see Appendix, eqns. (A 1) and (A 2)]. Thus no enzyme turnover occurs but there is a partition ratio, *r*, obtained by the endpoint incubation method, which describes the formation of E_I and E_L with a value of $r = 0.66 \pm 0.15$ [see Appendix, eqn. (A 15), and Figure 2], in good agreement with the value obtained from the kinetic constants above.

Protection of APX by reducing substrate against inactivation by H_2O_2

The presence of ascorbate or guaiacol in the incubation medium had a strong protective effect on the enzyme (Figure 3; results for ascorbate are shown). With 10 equiv. of H_2O_2, approx. 80 % inactivation (20 % residual activity) was seen in the absence of reducing substrate (with the use of the ascorbate activity assay), whereas the addition of 2 equiv. of reducing substrate lowered the inactivation to less than 20 % (more than 80 % residual activity); 90 % residual activity was measured with 20 equiv. of reducing substrate, and 100 % protection (no measurable inactivation) was afforded by the inclusion of 200 equiv. of reducing substrate.

Kinetic model

To account for these results, a kinetic model (Schemes 1 and 2 and Appendix) has been developed that uses as its basis a previous theoretical examination of the kinetics of mechanism-based inactivation (suicide inactivation) [32].

The principal characteristics of the mechanism are as follows. A species E′ is formed by the reaction of an active site of APX (E) with H_2O_2. The identity of E′ is not clear because APX compound I (apparent rate constant of formation at pH 7.8, $k_1 = 8.0 \times 10^7\ M^{-1} \cdot s^{-1}$ [25]) is unstable and undergoes conversion into another species with a rate constant, determined by stopped-flow, of $k_2 = 0.8 \pm 0.01\ s^{-1}$, this value being independent of H_2O_2 concentration in the range 0–8 μM (E. L. Raven and L. Lad, unpublished work). This enzyme form, when generated by incubation with 1 equiv. of H_2O_2 per APX active site, exhibits approx. 80 % of the activity with reducing substrates of native APX. In the presence of additional H_2O_2, an enzyme–substrate complex, E′S, is made. There is a partition from complex E′S leading either directly to the inactive form, E_I, or, by the release of $O_2^{\cdot -}$, to the intermediate E″, which can react with a third equivalent of H_2O_2 to generate E_L. E_L possesses modified substrate specificity such that no reaction is observed with phenolics (e.g. pyrogallol, guaiacol), but approx. 20 % of the original activity of APX remains with ascorbate and ABTS. This behaviour manifests itself as the difference in the λ_{max} observed in the time courses of inactivation by using different reducing substrates in the assays and also in the divergence from linearity in incubation experiments with ascorbate or ABTS (Figure 2).

Because no enzymic turnover of H_2O_2 occurs (i.e. there is no catalytic cycle) in the absence of reducing substrate but several molecules of H_2O_2 are required to inactivate each APX active site, the partition ratio between the routes to E_I and E_L is observed to have a value of $r < 1$.

DISCUSSION

In previous work we have examined the inactivation of the class III secretory plant peroxidase HRP [10–16]. HRP clearly undergoes mechanism-based inactivation with H_2O_2 and *m*-CPBA. Time dependence and saturation kinetics have been observed, along with protection of the enzyme by the presence of a reducing substrate. The stoichiometry of inactivator to enzyme has been closely defined with *m*-CPBA. Results from steady-state and rapid kinetics are consistent, and a detailed kinetically defined model of the inactivatory process has been developed [16]. In the present study we have examined the process of inactivation of a class I peroxidase, APX, and found that it shares similarities with, but also exhibits differences from, HRP.

The inactivation of APX by H_2O_2 was time dependent and the reaction showed saturation kinetics (Figure 1). The kinetically derived affinity of APX for H_2O_2 was much higher than that of HRP [$K_I^{APX} = 0.8$ μM, $K_I^{HRP\text{-}C} = (1.3 \pm 0.2)$ mM] [13,14]. APX was also much more sensitive to H_2O_2, as shown by the requirement of each active centre of APX for only approx. 2–3 molecules of H_2O_2 to be inactivated (Figure 2). This value was much lower than the equivalent value of 625 previously measured for the principal basic isoenzyme (form C) of HRP ($r = 335$ for non-glycosylated recombinant HRP-C) under the same conditions [13]. However, the cytosolic isoform of APX with which we performed this study was still considerably more resistant to inactivation than tAPX [27]. tAPX has been observed to undergo inactivation in medium containing less than 20 μM ascorbate and even as a result of the autoxidation of nanomolar concentrations of ascorbate (leading to the formation of H_2O_2) in dilute oxygenated solutions [9]. The sensitivity of tAPX might reflect the rather high level of ascorbate (up to 50 mM) normally found in the chloroplast [33], which protects the enzyme.

Despite APX's higher affinity for and greater sensitivity to H_2O_2, its inactivation proceeded an order of magnitude more slowly than that of HRP [$k_i^{APX} = (2.13 \pm 0.08) \times 10^{-4}\ s^{-1}$, $k_i^{HRP\text{-}C}$

$= (4.6 \pm 0.2) \times 10^{-3}\ s^{-1}$] [13,14]. This was a reflection of the low values of the kinetic constants controlling the inactivation pathway in APX.

Cytosolic APX was protected against inactivation by H_2O_2 by the presence of micromolar levels of the reducing substrates ascorbate or guaiacol in addition to H_2O_2 in the incubations (Figure 3). A similar effect has also been seen with HRP [10]. In both cases the reducing substrate protects the enzyme because peroxidase compound I preferentially oxidizes the reducing substrate rather than undergoing further reaction with H_2O_2, which can lead to inactivation.

In incubations with the oxidizing substrate, *m*-CPBA, the behaviours of APX and HRP-C were much more alike. APX was as sensitive to inactivation by this peroxide as by H_2O_2. The partition ratio for HRP-C with *m*-CPBA was only 2 [16].

The much greater sensitivity of HRP-C to inactivation by *m*-CPBA than by H_2O_2 has been attributed to the lack of the protective catalase-like (releasing oxygen gas) reaction that has been observed with H_2O_2 but that cannot occur with *m*-CPBA as the substrate [34,35]. The catalase-like reaction of H_2O_2 with HRP is the dominant pathway of enzyme turnover in the absence of reducing substrate and accounts for almost all the protection of HRP against mechanism-based inactivation by H_2O_2. Oxygraph experiments with APX confirmed that the enzyme did not possess a catalase-like cycle, as would be expected from its sensitivity to inactivation. It now seems that most peroxidases possess at least some catalase activity; they can be listed in the following order of activity: true catalases $\geqslant$ bacterial catalase–peroxidases > chloroperoxidases > HRP > APX. There is presumably some reason why catalase-like activity has not evolved or has been lost in APX; this would suggest that APX's instability to peroxide might, in some way, be physiologically important.

The deviations from linearity of the plots of residual activity against the concentration ratios of APX with inactivator substrate at higher ratios (i.e. more substrate) when ascorbate and ABTS assays were used reveal that a fraction of the enzyme activity remained even at molar excesses of substrate up to 1000, despite the fact that most of the enzyme was inactivated with less than 10 equiv. of peroxide. Scheme 1 suggests that the explanation of this observation is that the enzyme does not complete a catalytic cycle (i.e. turnover) with H_2O_2. APX forms either the inactive species (E_I) or the enzyme form with changed activity (E_L), which retains approx. 20% activity with substrates like ascorbate (resistant fraction) but does not demonstrate any reaction with phenolics. E_L therefore seems to be unable to withdraw electrons from phenolic substrates but can do so to a limited extent from acids such as ascorbate. There is evidence [36] that ascorbate and phenolic substrates, such as guaiacol and pyrogallol, bind to distinct electron transfer sites in APX. Specific modification of APX Cys-32, by either Ellman's reagent [5,5′-dithiobis-(2-nitrobenzoic acid)] or mutagenesis to serine, greatly decreased APX activity with ascorbate but did not appreciably affect phenolic oxidation. In contrast, the δ-meso-haem edge is believed to be the site of reaction for phenolics. Our results are consistent with the notion that there are two separate electron transfer sites in APX for phenolics and ascorbate, and that the phenolic site is blocked by inactivation.

Our studies so far have demonstrated that APX undergoes inactivation with H_2O_2 and also *m*-CPBA, as has been observed for HRP. The inactivatory process being observed can essentially be described as irreversible mechanism-based (suicide) inactivation, using the definition of Silverman [37]. However, with APX, the unusual situation arises where no enzyme turnover occurs and $r < 1$. Inactivation of APX therefore proceeds in much the same way as irreversible inhibition ($r = 0$) but each active centre of APX requires several molecules of H_2O_2 for inactivation.

The structural changes that occur in the formation of the inactive enzyme, and the nature of this species, remain unclear. In preliminary UV/visible spectroscopic studies we have failed to identify a species similar to the inactive compound P670 verdohaemochrome seen in our previous work with HRP. However, the P670 of HRP is not particularly stable and easily decomposes; the equivalent species in APX might therefore be even less stable and harder to observe. P670 has also been observed to form in the reaction of wheat-germ peroxidase compound I, which seems to contain a protein radical, with excess H_2O_2 [23]. We did, however, notice a fall in Soret peak intensity, broadly in agreement with other studies [9] and suggesting that some haem degradation was occurring in APX. In addition, when excess ascorbate was added to the species that formed spontaneously from APX compound I (generated by the addition of 1 equiv. of H_2O_2 to the ferric enzyme), the spectrum of the original ferric species was not recovered. Similarly, the ferric spectrum was not fully recovered if the spontaneously formed species was allowed to evolve further over a period of several hours.

The sensitivity of APX to inactivation by its substrate H_2O_2 was surprising considering the enzyme's supposed role as a scavenger of this substance in cells as a protective measure against oxidative stress. Indeed, it has been shown in tobacco that, whereas APX functioned well under benign environmental conditions, under conditions of drought and bright illumination APX was completely inactivated, exposing the photosynthetic systems of the plants to severe damage. The introduction of the gene for bacterial catalase into tobacco plants allowed them to tolerate harsh environmental conditions much better than the wild-type plants [38]. In potato tubers stored at low temperature (causing oxidative stress due to the increase in dissolved O_2) APX did seem to protect the cells, at least until levels of ascorbate started to fall [39]. The same study also noted the protective effect of catalase, whose activity tended to increase as that of APX fell.

APX has been implicated in other cellular processes in plants in which its instability to H_2O_2 could be important. In response to pathogenic attack, plant cells undergo programmed cell death ('PCD'), termed the hypersensitive response (HR), to form a layer of dead cells as a barrier to the spread of disease. It is widely believed that reactive oxygen species such as H_2O_2 and $O_2^{\cdot -}$ are instrumental in mediating the HR ([40] and references therein); however, the action of APX could decrease their effectiveness. It has been shown that APX expression is suppressed at the post-transcriptional stage so that no new enzyme is produced during the HR [40]. The inactivation of APX by H_2O_2 at this stage could then further enhance the HR.

There is also evidence that H_2O_2 acts as a developmental signal in the differentiation of secondary walls in cotton fibres and other structures, such as tracheal elements, in other plants and that the scavenging of H_2O_2 can prevent such differentiation ([41] and references therein).

If we take into account observations such as those described above, it seems likely that the inactivation of APX by peroxide under certain circumstances could have important implications in plant development. The role of the different isoenzymes of APX with their specific localizations within plant cells is an area of plant biochemistry and physiology that still leaves many questions to be answered.

The purification of the APX used in this study was performed by Mr D. Turner and Mr K. Singh. This work was supported in part by a grant from the EU Training and Mobility of Researchers Programme – TMR Network, 'Peroxidases in Agriculture, the Environment and Industry' (Contract FMRX-CT98-0200), and from Comisíon Interministerial de Ciencia y Tecnología (Spain), CICYT-ALI98-0524. A N P H holds a fellowship from the EU TMR Network

REFERENCES

1 Welinder, K G (1992) Superfamily of plant, fungal and bacterial peroxidases Curr Opin Struct Biol **2**, 388–393

2 Welinder, K G (1991) Bacterial catalase–peroxidases are gene duplicated members of the plant peroxidase superfamily Biochim Biophys Acta **1080**, 215–220

3 Asada, K (1992) Ascorbate peroxidase – a hydrogen peroxide-scavenging enzyme in plants Physiol Plant **85**, 235–241

4 Miyake, C. and Asada, K (1992) Thylakoid-bound ascorbate peroxidase in spinach chloroplasts and photoreduction of its primary oxidation product monodehydroascorbate radicals in thylakoids Plant Cell Physiol **33**, 541–553

5 Miyake, C, Cao, W and Asada, K (1993) Purification and molecular properties of thylakoid-bound ascorbate peroxidase in spinach chloroplasts. Plant Cell Physiol **34**, 881–889

6 Nakano, Y and Asada, K (1987) Purification of ascorbate peroxidase in spinach chloroplasts, its inactivation in ascorbate-depleted medium and reactivation by monodehydroascorbate radical Plant Cell Physiol **28**, 131–140

7 Chen, G and Asada, K (1989) Ascorbate peroxidase in tea leaves occurrence of two isoenzymes and the differences in their enzymatic and molecular properties Plant Cell Physiol **30**, 987–998

8 Jespersen, H M, Kjærsgård, I V. H., Østergaard, L and Welinder, K G (1997) From sequence analysis of three novel ascorbate peroxidases from *Arabidopsis thaliana* to structure, function and evolution of seven types of ascorbate peroxidase Biochem J **326**, 305–310

9 Miyake, C and Asada, K (1996) Inactivation mechanism of ascorbate peroxidase at low concentrations of ascorbate, hydrogen peroxidase decomposes compound I of ascorbate peroxidase Plant Cell Physiol **37**, 423–430

10 Arnao, M. B, Acosta, M, del Rio, J A and García-Cánovas, F (1990) Inactivation of peroxidase by hydrogen peroxide and its protection by a reductant substrate Biochim Biophys Acta **1038**, 85–89

11 Acosta, M, Arnao, M B and Hernández-Ruiz, J (1993) Inactivation of peroxidase by hydroperoxides In Plant Peroxidases· Biochemistry and Physiology (Welinder, K G, Rasmussen, S K., Penel, C and Greppin, H, eds), pp 201–205, University of Geneva, Geneva

12 Arnao, M B, Acosta, M, del Rio, J A, Varón, R and García-Cánovas, F (1990) A kinetic study on the suicide inactivation of peroxidase by hydrogen peroxide Biochim. Biophys Acta **1041**, 43–47

13 Hiner, A. N P, Hernández-Ruiz, J, García-Cánovas, F, Smith, A T, Arnao, M B and Acosta, M (1995) A comparative study of the inactivation of wild-type, recombinant and two mutant horseradish peroxidase isoenzymes c by hydrogen peroxide and *m*-chloroperoxybenzoic acid Eur J Biochem **234**, 506–512

14 Hiner, A N P, Hernández-Ruiz, J, Arnao, M B, García-Cánovas, F and Acosta, M (1996) A comparative study of the purity, enzyme activity, and inactivation by hydrogen peroxide of commercially available horseradish peroxidase isoenzymes a and c Biotechnol Bioeng **50**, 655–662

15 Arnao, M. B, García-Cánovas, F and Acosta, M (1996) Role of the reductant substrates on the inactivation of horseradish peroxidase by *m*-chloroperoxybenzoic acid Biochem Mol Biol Int **39**, 97–107

16 Rodriguez-López, J N, Hernández-Ruiz, J, García-Cánovas, F, Thorneley, R N F, Acosta, M and Arnao, M B (1997) The inactivation and catalytic pathways of horseradish peroxidase with *m*-chloroperoxybenzoic acid J Biol Chem **272**, 5469–5476

17 Mittler, R and Zilinskas, B A (1991) Molecular cloning and nucleotide sequence analysis of a cDNA encoding pea cytosolic ascorbate peroxidase FEBS Lett **289**, 257–259

18 Patterson, W R. and Poulos, T L (1995) Crystal structure of recombinant pea cytosolic ascorbate peroxidase Biochemistry **34**, 4331–4341

19 Goodin, D B, Mauk, A G and Smith, M. (1987) The peroxide complex of yeast cytochrome *c* peroxidase contains two distinct radical species, neither of which resides at methionine 172 or tryptophan 51 J Biol Chem **262**, 7719–7724

20 Mauro, J M, Fishel, L A, Hazzard, J. T, Meyer, T E, Tollin, G, Cusanovich, M and Kraut, J (1988) Tryptophan-191 → phenylalanine, a proximal-side mutation in yeast cytochrome *c* peroxidase that strongly affects the kinetics of ferrocytochrome *c* oxidation Biochemistry **27**, 6243–6256

21 Erman, J E, Vitello, L B, Mauro, J M and Kraut, J (1989) Detection of an oxyferryl porphyrin π-cation-radical intermediate in the reaction between hydrogen peroxide and a mutant cytochrome *c* peroxidase Evidence for tryptophan-191 involvement in the radical site of compound I. Biochemistry **28**, 7992–7995

22 Dolphin, D, Forman, A, Borg, D C, Fajer, J and Felton, R H (1971) Compounds I of catalase and horseradish peroxidase π-cation radicals Rec Res Dev. Agr Food Chem **68**, 614–618

23 Converso, D A and Fernández, M E (1998) Evidence for an unusual electronic structure of wheat germ peroxidase compound I Arch Biochem Biophys **357**, 22–26

24 Dunford, H B and Stillman, J S (1976) On the function and mechanism of action of peroxidases Coord Chem Rev **19**, 187–251

25 Márquez, L A, Quitoriano, M, Zilinskas, B A and Dunford, H B (1996) Kinetic and spectral properties of pea cytosolic ascorbate peroxidase FEBS Lett **389**, 153–156

26 Patterson, W R, Poulos, T L and Goodin, D B (1995) Identification of a porphyrin π-cation radical in ascorbate peroxidase compound I Biochemistry **34**, 4342–4345

27 Amako, K., Chen, G and Asada, K. (1994) Separate assays specific for ascorbate peroxidase and guaiacol peroxidase and for the chloroplastic and cytosolic isozymes of ascorbate peroxidase in plants Plant Cell Physiol **35**, 497–504

28 Davies, D. M, Jones, P and Mantle, D (1976) The kinetics of formation of horseradish peroxidase compound I by reaction with peroxobenzoic acids pH and peroxo acid substituent effects Biochem J **157**, 247–253

29 Pourchert, C J and Campbell, J R (1974) The Aldrich Library of NMR spectra, vol 6, p 146, Aldrich Chemical Company, Milwaukee, WI

30 García-Cánovas, F, Tudela, J, Varón, R and Vázquez, A M. (1989) Experimental methods for kinetic study of suicide substrates J Enz Inhib **3**, 81–90

31 Mittler, R and Zilinskas, B. A (1991) Purification and characterisation of pea cytosolic ascorbate peroxidase Plant Physiol **97**, 962–968

32 Tudela, J, García-Cánovas, F, Varón, R., García-Carmona, F, Gálvez, J and Lozano, J A (1987) Transient-phase kinetics of enzyme inactivation induced by suicide substrates Biochim Biophys. Acta **912**, 408–416

33 Salin, M. L (1987) Toxic oxygen species and protective systems in the chloroplast Physiol Plant **72**, 681–689

34 Arnao, M B, Hernández-Ruiz, J, Varón, R, García-Cánovas, F and Acosta, M (1995) The inactivation of horseradish peroxidase by *m*-chloroperoxybenzoic acid, a xenobiotic hydroperoxide J Molec Cat A Chem **104**, 179–191

35 Chamulitrat, W, Takahashi, N and Mason, R P (1989) Peroxyl, alkoxyl, and carbon-centred radical formation from organic hydroperoxides by chloroperoxidase J Biol Chem **264**, 7889–7899

36 Mandelman, D, Jamal, J and Poulos, T L (1998) Identification of two electron-transfer sites in ascorbate peroxidase using chemical modification, enzyme kinetics, and crystallography Biochemistry **37**, 17610–17617

37 Silverman, R B (1995) Mechanism based enzyme inactivators Methods Enzymol **249**, 240–283

38 Shikanai, T, Takeda, T., Yamauchi, H, Sano, S, Tomizawa, K-I, Yokota, A and Shigeoka, S (1998) Inhibition of ascorbate peroxidase under oxidative stress in tobacco having bacterial catalase in chloroplasts FEBS Lett **428**, 47–51

39 Mizuno, M, Kamei, M and Tsuchida, H (1998) Ascorbate peroxidase and catalase co-operate for protection against hydrogen peroxide generated in potato tubers during low-temperature storage Biochem Molec Biol Int **44**, 717–726

40 Mittler, R, Feng, X and Cohen, M (1998) Post-transcriptional suppression of cytosolic ascorbate peroxidase expression during pathogen-induced programmed cell death in tobacco Plant Cell **10**, 461–473

41 Potikha, T S, Collins, C C, Johnson, D I, Delmer, D P and Levine, A (1999) The involvement of hydrogen peroxide in the differentiation of secondary wall in cotton fibers Plant Physiol **119**, 849–858

APPENDIX

The proposed mechanism for the reaction of APX with H_2O_2 leading to enzyme inactivation is shown in Scheme 1.

E represents the concentration of APX active sites other than the dimer.

The stoichiometry of the pathway leading to E_i is:

$$2H_2O_2 + E \rightarrow 2H_2O + E_i \qquad (A\ 1)$$

and for the generation of E_L it is:

$$3H_2O_2 + E \rightarrow 2H_2O + H^+ + O_2^{\cdot-} + E_L \qquad (A\ 2)$$

where the exact natures of E_i and E_L have not been determined.

Experiments on the end-point residual activity

The equation for partition ratio (*r*) was developed as follows.

The balance of material in the mechanism in the case of the phenolic substrates where the residual activity falls to 0 is:

$$[S_0] = 2[E_i]+3[E_L] \tag{A 3}$$

where $[S_0]$ is the initial $[H_2O_2]$

The differential equations for the partition between E_i and E_L are:

$$d[E_L]/dt = k_4[E'S] \tag{A 4}$$

$$d[E_i]/dt = k_1[E'S] \tag{A 5}$$

Removing time from eqns. (A 4) and (A 5):

$$d[E_L]/d[E_i] = k_4/k_1 \tag{A 6}$$

Integrating eqn. (A 6); $[E_L]0 \rightarrow [E_L]$ and $[E_i]0 \rightarrow [E_i]$:

$$[E_L] = [E_i]k_4/k_1 \tag{A 7}$$

Substituting eqn. (A 7) into eqn (A 3):

$$[S_0] = 2[E_i]+3([E_i]k_4/k_1) \tag{A 8}$$

Rearranging:

$$[S_0] = [E_i](2+3k_4/k_1) \tag{A 9}$$

and:

$$[E_i] = \frac{1}{2+3k_4/k_1}[S_0] \tag{A 10}$$

The balance of material with respect to E is:

$$[E_0] = [E_a]+[E_L]+[E_i] \tag{A 11}$$

where $[E_0]$ is the initial concentration of APX active sites (E) and $[E_a]$ is residual active E.

Substituting eqns. (A 7) and (A 10) into eqn. (A 11) we obtain:

$$[E_0]-[E_a] = \frac{1+k_4/k_1}{2+3k_4/k_1}[S_0] \tag{A 12}$$

Dividing by $[E_0]$ and rearranging gives:

$$A_R = \frac{[E_a]}{[E_0]} = \frac{1+k_4/k_1}{2+3k_4/k_1}\frac{[S_0]}{E_0]} \tag{A 13}$$

$[E_a]$ can be determined from the remaining APX activity after incubation (A_t) and $[E_0]$ from the original APX activity (A_0). Thus both quantities on the left of eqn. (A 13) can be observed experimentally.

From the intercept at the x-axis of a plot of A_R against $[S_0]/[E_0]$ (Figure 2) we see that, for pyrogallol and guaiacol, $A_R = 0$ when $[S_0]/[E_0] = 2.4$.

From Schemes 1 and 2 we define:

$$r = k_4/k_1 \tag{A 14}$$

Thus, by using eqns. (A 13) and (A 14):

$$r = 0.66 \pm 0.15$$

which is in good agreement with the value obtained kinetically.

Kinetics of inactivation

Under conditions where $[S_0] \geqslant 15[E_0]$ the mechanism shown in Scheme 1 can be simplified to Scheme 2.

For substrates such as pyrogallol or guaiacol, for which no enzyme resistance is observed, $[E_L] \equiv [E_i]$.

The differential rate equation that describes the disappearance of the active enzyme, E_a, is:

$$-\frac{d[E_a]}{dt} = \frac{d[E_i]}{dt} = \frac{(k_4+k_1)[E_a][S]_0}{K_I+[S]_0} \tag{A 15}$$

$$-\frac{d[E_a]}{dt} = \frac{(k_4+k_1)[S]_0}{K_I+[S]_0}dt \tag{A 16}$$

Integrating between $[E_0]$ for $t = 0$ and $[E_a]$ for $t = t$ gives:

$$\ln\frac{[E_a]}{[E_0]} = -\frac{(k_4+k_1)[S]_0}{K_I+[S]_0}t = -\lambda t \tag{A 17}$$

where λ is the observed rate constant of inactivation. Thus in a plot of λ against $[S_0]-[E_0]$ the maximum rate of inactivation (λ_{max}) and the affinity of E′ for S (K_I) can be obtained from a non-linear regression fit. In this case:

$$\lambda_{max} = k_4+k_1 \tag{A 18}$$

Note that the generation of 1 mol of E′ from E (Scheme 1) consumes 1 mol of S; therefore the plot and regression are done against $[S_0]-[E_0]$.

For ascorbate and ABTS, for which a resistant fraction of enzyme is detected, $[E_L] \neq [E_i]$.

The differential equations are:

$$-\frac{d[E_a]}{dt} = \frac{d[E_i]}{dt} = \frac{k_1[E_a][S]_0}{K_I+[S]_0} \tag{A 19}$$

yielding:

$$\ln([E_a]/[E_0]) = -\lambda' t = -k_1 t \tag{A 20}$$

Therefore in a plot of λ' against $[S_0]-[E_0]$:

$$\lambda'_{max} = k_1 \tag{A 21}$$

Thus:

$$\lambda_{max}-\lambda'_{max} = k_4 \tag{A 22}$$

and additionally:

$$r = k_4/k_1 \tag{A 23}$$

Received 17 January 2000/6 March 2000, accepted 24 March 2000

Positional- and stereo-selectivity of fatty acid oxygenation catalysed by mouse (12*S*)-lipoxygenase isoenzymes

Friederike BÜRGER, Peter KRIEG, Friedrich MARKS and Gerhard FÜRSTENBERGER[1]

Research Program Tumor Cell Regulation (B0500), Deutsches Krebsforschungszentrum, Im Neuenheimer Feld 280, 69120 Heidelberg, Germany

A quantitative stereochemical analysis of the products generated by recombinant mouse (12*S*)-lipoxygenase isoenzymes was performed with arachidonic acid and linoleic acid as substrates. The leucocyte-type (12*S*)-lipoxygenase generated, in addition to 12-hydroxyeicosatetraenoic acid (12-HETE) as the main product, 15- and 8-HETE from arachidonic acid and 13- and 9-hydroxyoctadecadienoic acid (13- and 9-HODE) from linoleic acid. The platelet-type enzyme oxygenated arachidonic acid to 12- and 8-HETE and linoleic acid to 13- and 9-HODE, whereas the epidermis-type (12*S*)-lipoxygenase reaction was essentially mono-specific with arachidonic acid but oxygenated linoleic acid to both 13- and 9-HODE. 12-HETE and 13-HODE were almost exclusively the *S* enantiomers. 8-HETE was the *R* enantiomer as a side-product of the platelet-type (12*S*)-lipoxygenase reaction but the *S* enantiomer as a side-product of the leucocyte-type reaction. 9-HODE was generated as the *R* enantiomer by the platelet-type and the epidermis-type isoenzymes and as the *S* enantiomer by the leucocyte-type (12*S*)-lipoxygenase. On the basis of published models of lipoxygenase–substrate interaction, the stereochemistry of the products generated by the platelet- and epidermis-type (12*S*)-lipoxygenases is in agreement with a fixed 'tail-to-head' orientation of the substrate fatty acid in the binding pocket of these enzymes, whereas that of the reaction products of the leucocyte-type (12*S*)-lipoxygenase can be explained only when the inverse orientation of the substrate or a rotational isomerism along the longitudinal axis of the substrate is allowed. Both the product spectra generated and the sensitivity towards the 12-lipoxygenase selective inhibitors *N*-benzyl-*N*-hydroxy-4-phenylpentanamide and cinnamyl-3,4-dihydroxy-α-cyanocinnamate indicated the platelet-type and the epidermis-type isoenzymes to be biochemically more related to each other than to the leucocyte-type (12*S*)-lipoxygenase.

Key words: arachidonic acid, dioxygenation, epidermis, linoleic acid.

INTRODUCTION

Lipoxygenases are a family of structurally related non-haem iron-containing enzymes that insert molecular oxygen into *cis,cis*-1,4-pentadiene-containing polyunsaturated fatty acids [1,2]. Depending on the position of oxygen insertion into arachidonic acid, mammalian lipoxygenases are classified as 5-, 8-, 12- and 15-lipoxygenases. Primary reaction products are 5-, 8-, 12- and 15-hydroperoxyeicosatetraenoic acids (HpETEs) which are reduced to the corresponding hydroxyeicosatetraenoic acids (HETEs) or converted into various other types of eicosanoids including leukotrienes, lipoxins and hepoxilins. Oxygen insertion occurs with high enantioselectivity in that the main reaction products possess *S*-chirality. Only recently has a (12*R*)-lipoxygenase generating enantiomeric (12*R*)-HpETE been identified in mammalian skin [3–5].

The multiplicity of lipoxygenases is further increased by the identification of individual isoenzymes with similar positional specificities: two (15*S*)-lipoxygenase isoenzymes [6,7] and three (12*S*)-lipoxygenase isoenzymes [8] have been described. We and others have cloned three cDNA species from mouse tissues, encoding the leucocyte-type, the platelet-type and the epidermis-type 12-lipoxygenases, and expressed them as recombinant proteins [9–13]. After their cloning and expression there is a need for a detailed comparison of the three recombinant mouse (12*S*)-lipoxygenase isoenzymes regarding the differences and/or similarities in catalytic activity, regioselectivity and stereoselectivity and effects of inhibitors so as to be able to distinguish between these isoenzymes *in vivo*.

Here we describe a qualitative and quantitative analysis of the reaction products obtained by the three isoenzymes with free arachidonic acid and linoleic acid as substrates.

EXPERIMENTAL

Materials

(8*S*)- and (8*R*)-hydroxyeicosa-(5*Z*,9*E*,11*Z*,15*Z*)-tetraenoic acid [(8*S*)- and (8*R*)-HETE], (12*S*)- and (12*R*)-hydroxyeicosa-(5*Z*,8*Z*,10*E*,14*Z*)-tetraenoic acid [(12*S*)- and (12*R*)-HETE], (9*S*)- and (9*R*)-hydroxyoctadeca-(10*E*,12*Z*)-dienoic acid [(9*S*)- and (9*R*)-HODE] and (13*S*)- and (13*R*)-hydroxyoctadeca-(9*Z*,11*E*)-dienoic acid [(13*S*)- and (13*R*)-HODE] standards were from Reatec (Weiterstadt, Germany). *N*-Benzyl-*N*-hydroxy-4-phenylpentanamide (BHPP) was a gift from Dr K. V. Honn (Wayne State University, Detroit, MI, U.S.A.); cinnamyl-3,4-dihydroxy-α-cyanocinnamate (CDC) was purchased from Biomol (Hamburg, Germany). All other chemicals and solvents were of analytical grade. SEP-PAK C_{18} cartridges were from ICT (Bad Homburg, Germany).

Expression of 12-lipoxygenase cDNA

For transient expression, plasmid DNA (10 μg) and vector DNA as control were introduced into HEK-293 cells (seeded at 1.5×10^6 cells per 100 mm plate) by a modified calcium phosphate transfection procedure with a mammalian transfection kit, in accordance with the manufacturer's protocol (Stratagene, La Jolla, CA, U.S.A.). Cells were harvested 48 h after transfection.

Abbreviations used: BHPP, *N*-benzyl-*N*-hydroxy-4-phenylpentanamide, CDC, cinnamyl-3,4-dihydroxy-α-cyanocinnamate, 8-, 12- and 15-HpETE, 8-, 12- and 15-hydroperoxyeicosatetraenoic acids; 8-, 12- and 15-HETE, 8-, 12- and 15-hydroxyeicosatetraenoic acids, 9- and 13-HpODE, 9- and 13-hydroperoxyoctadecadienoic acids, 9- and 13-HODE, 9- and 13-hydroxyoctadecadienoic acids

[1] To whom correspondence should be addressed (e-mail g.fuerstenberger@dkfz-heidelberg.de)

Preparation of 10000 *g* supernatants

Transfected cells were homogenized by sonication (Branson Sonifier, 10 pulses of 6 s on ice) in TEE buffer [50 mM Tris/HCl (pH 7.4)/1 mM EDTA/1 mM EGTA/10 μg/ml leupeptin]. The supernatant received after centrifugation (10000 *g* for 15 min at 4 °C) was used for the lipoxygenase assay.

Lipoxygenase assay

Aliquots of 250 μl of 10000 *g* supernatants were incubated with 100 μM arachidonic acid or linoleic acid for 12 min at 37 °C in the presence or absence of various concentrations of inhibitors dissolved in ethanol. The incubations were terminated by the addition of 40 μl of 1 M sodium formate buffer, pH 3.1. To reduce the hydroperoxy acids to hydroxy acids, 20 μl of trimethylphosphite was added and incubated at room temperature for 5 min. Samples were extracted twice by ethyl acetate. The combined organic extracts were evaporated to dryness, redissolved in 0.75 ml of ethanol and diluted to a final ethanol concentration of 15 % (v/v) by the addition of 0.1 M sodium formate buffer. An enriched HETE or HODE fraction was obtained by solid-phase extraction by the method of Powell [14].

Analysis of HETEs and HODEs

For HPLC, a Zorbax Sil column (250 mm × 4.6 mm, 5 μm particle size; Bischoff, Stuttgart, Germany) was used. HETEs and HODEs were eluted at 1 ml/min with a solvent system of n-hexane/propan-2-ol/acetic acid/water (98.5:1.5:0.1:0.025, by vol.). The eluate was monitored at 236 nm. Individual HETEs and HODEs separated by straight-phase analysis were analysed by chiral-phase chromatography with a Chiracel column (250 mm × 4.6 mm, 5 μm particle size; Baker Instruments Corp., Deerfield, IL, U.S.A.) with the solvent system n-hexane/propan-2-ol/acetic acid (99:1:0.05, by vol.) for elution of the *R* and *S* enantiomers of 15- and 12-HETE and 13-HODE, and the solvent system n-hexane/propan-2-ol/acetic acid (97.5:2.5:0.05, by vol.) for elution of the *R* and *S* enantiomers of 8-HETE and 9-HODE. The flow rate of the solvent systems was 0.5 ml/min; the eluate was monitored at 236 nm. The recovery was 57 ± 7 % for HETEs and 61 ± 11 % for HODEs (means ± S.E.M.).

GLC/MS

Derivatization of the HETEs and HODEs and qualitative GLC/MS were performed as described previously [15].

RESULTS

Determination of enzymic activity

HEK-293 cells were transiently transfected with the pcDNA3 expression vector carrying the cDNA encoding the leucocyte-type, platelet-type or epidermis-type (12*S*)-lipoxygenase. At 48 h after transfection, the cells were homogenized by ultrasonication and the enzymic activity was determined in 10000 *g* supernatants of the homogenates. When incubated with saturating concentrations of arachidonic acid for 12 min, i.e. during the linear time course of product formation, a linear relationship between the formation of 12-HETE and the sample's protein concentration of up to 0.2 mg/ml supernatant for both the leucocyte-type and the platelet-type enzyme and of 0.5–5.0 mg/ml supernatant for the epidermis-type isoenzyme was observed. The specific activities of leucocyte-type and platelet-type (12*S*)-lipoxygenases were approx. 600-fold and 300-fold that of the epidermis-type (12*S*)-lipoxygenase respectively (Table 1). With linoleic acid as a substrate, 13-HODE formation was linear up to a protein concentration of 0.2 mg/ml for the leucocyte-type lipoxygenase, up to 5 mg/ml for the platelet-type enzyme and between 4 and 5 mg/ml protein for the epidermis-type enzyme. Again, leucocyte-type 12-lipoxygenase exhibited the highest enzymic activity, being approx. 8-fold and 80-fold more efficient than the platelet-type and epidermis-type enzymes respectively (Table 2).

Table 1 Specific enzymic activities and reaction products of recombinant mouse (12*S*)-lipoxygenase isoenzymes with arachidonic acid as substrate

Supernatants (10000 *g*) from sonicated HEK-293 cells transfected with leucocyte-type (0.1 mg/ml protein), platelet-type (0.2 mg/ml protein) or epidermis-type (5 mg/ml protein) (12*S*)-lipoxygenase cDNA, or pcDNA3 vector alone (5 mg/ml protein) were incubated in TEE buffer with 100 μM arachidonic acid for 12 min at 37 °C. The hydroperoxy derivatives of the fatty acids were reduced and extracted by the method of Powell [14]; the ethyl acetate fraction was analysed by straight-phase HPLC as described in the legend to Figure 1. Activities were measured by comparison of the areas of the 8-, 12- and 15-HETE peaks with corresponding standards. The amounts of 8-, 12- and 15-HETE generated by vector-transfected cells were subtracted. Results are means ± S.D. for $3 \leqslant n \leqslant 5$ experiments. Abbreviation: n.d., not detectable.

	Reaction products (pmol/min per mg of protein)		
(12*S*)-Lipoxygenase type	12-HETE	15-HETE	8-HETE
Leucocyte	13580 ± 2250	1020 ± 105	185 ± 25
Platelet	7655 ± 950	n.d.	22 ± 9
Epidermis	23 ± 5	n.d.	n.d.

Table 2 Specific enzymic activities and reaction products of recombinant mouse (12*S*)-lipoxygenase isoenzymes with linoleic acid as substrate

Supernatants (10000 *g*) from sonicated HEK-293 cells transfected with leucocyte-type (0.15 mg/ml protein), platelet-type (1.0 mg/ml protein) or epidermis-type (5 mg/ml protein) (12*S*)-lipoxygenase cDNA, or pcDNA3 vector alone (5 mg/ml protein) were incubated in TEE buffer with 100 μM linoleic acid for 12 min at 37 °C. The hydroperoxy derivatives of the fatty acids were reduced and extracted by the method of Powell [14]; the ethyl acetate fraction was analysed by straight-phase HPLC as described in the legend to Figure 2. Activities were measured by comparison of the areas of the 9- and 13-HODE peaks with corresponding standards. The amounts of 9- and 13-HODE generated by vector-transfected cells were subtracted. Results are means ± S.D. for $3 \leqslant n \leqslant 5$ experiments.

	Reaction products (pmol/min per mg of protein)	
(12*S*)-Lipoxygenase type	13-HODE	9-HODE
Leucocyte	1420 ± 55	40 ± 5
Platelet	185 ± 60	4.4 ± 0.8
Epidermis	15 ± 5	4.2 ± 2.5

Product analysis

Although the positional specificity of oxygen insertion is thought to be a characteristic property of individual lipoxygenases, it is known from previous studies that the pig and mouse leucocyte-type (12*S*)-lipoxygenases can direct oxygen into the 12- and the 15-positions of arachidonic acid [9,10,16]. A more detailed product analysis of the mouse isoenzyme showed that, in addition to 12-HETE as the main product, 15-HETE was the predominant and 8-HETE a minor side-product (Figure 1 and Table 1). In contrast, platelet-type (12*S*)-lipoxygenase generated almost exclusively 12-HETE with very small amounts of 8-HETE as a side product; 12-HETE was the only reaction product generated by

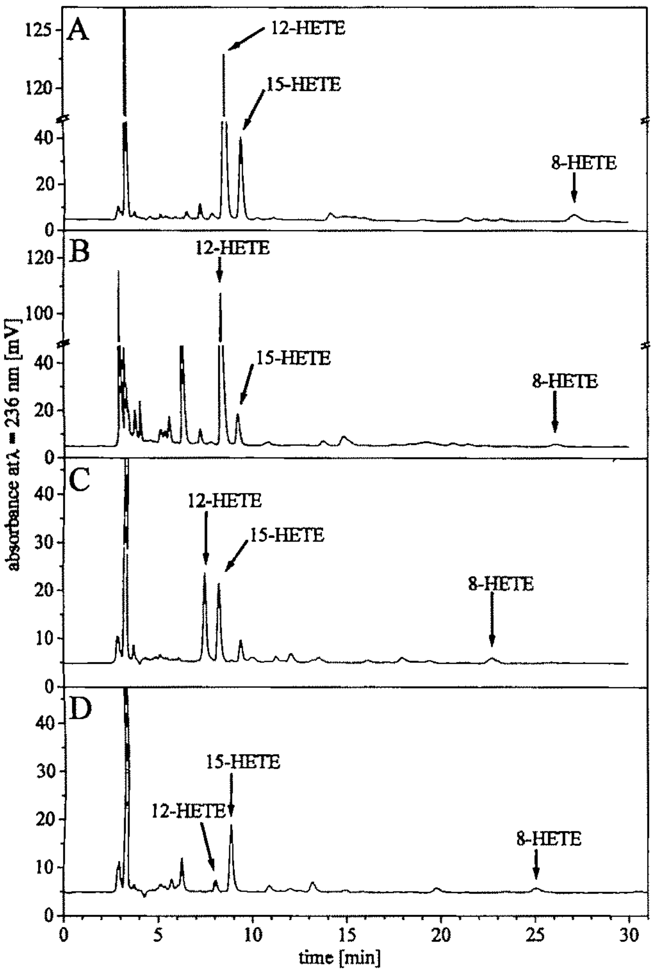

Figure 1 Straight-phase HPLC analysis of lipid extracts obtained after incubation with arachidonic acid of 10000 *g* supernatants from sonicated HEK-293 cells transiently transfected with leucocyte-type (A), platelet-type (B) or epidermis-type (C) (12*S*)-lipoxygenase expression constructs or with pcDNA vector alone (D)

Supernatants (10000 *g*) from sonicated HEK-293 cells transfected with pcDNA3 expression constructs containing epidermis-type, leucocyte-type or platelet-type (12*S*)-lipoxygenase cDNA or with pcDNA3 vector alone were incubated in TEE buffer with 100 μM arachidonic acid for 12 min at 37 °C. The protein concentration in each assay was 0.1 mg/ml protein [leucocyte-type (12*S*)-lipoxygenase], 0.2 mg/ml protein [platelet-type (12*S*)-lipoxygenase], 5 mg/ml protein [epidermis-type (12*S*)-lipoxygenase] and 5 mg/ml protein (vector). HpETEs were reduced and extracted by the method of Powell [14]. The ethyl acetate fraction was dried under vacuum, redissolved in n-hexane/propan-2-ol/acetic acid/water (98.5:1.5:0.1:0.025, by vol.), injected on a Zorbax Sil column and eluted at 1 ml/min. The eluate was monitored at 236 nm. Authentic 8-, 12- and 15-HETE and 9- and 13-HODE were used as standards. The identities of HETEs were confirmed by GC/MS.

epidermis-type (12*S*)-lipoxygenase (Figure 1 and Table 1). When linoleic acid was used as a substrate in addition to the main product 13-HODE, the isomer 9-HODE was generated as a by-product by all three isoenzymes with a ratio of 13-HODE to 9-HODE of approx. 50:1 for leucocyte- and platelet-type (12*S*)-lipoxygenase and approx. 3:1 for epidermis-type (12*S*)-lipoxygenase (Table 2 and Figure 2).

Chirality of the reaction products

The chiral analysis of the reaction products obtained after the incubation of arachidonic acid with preparations of the three

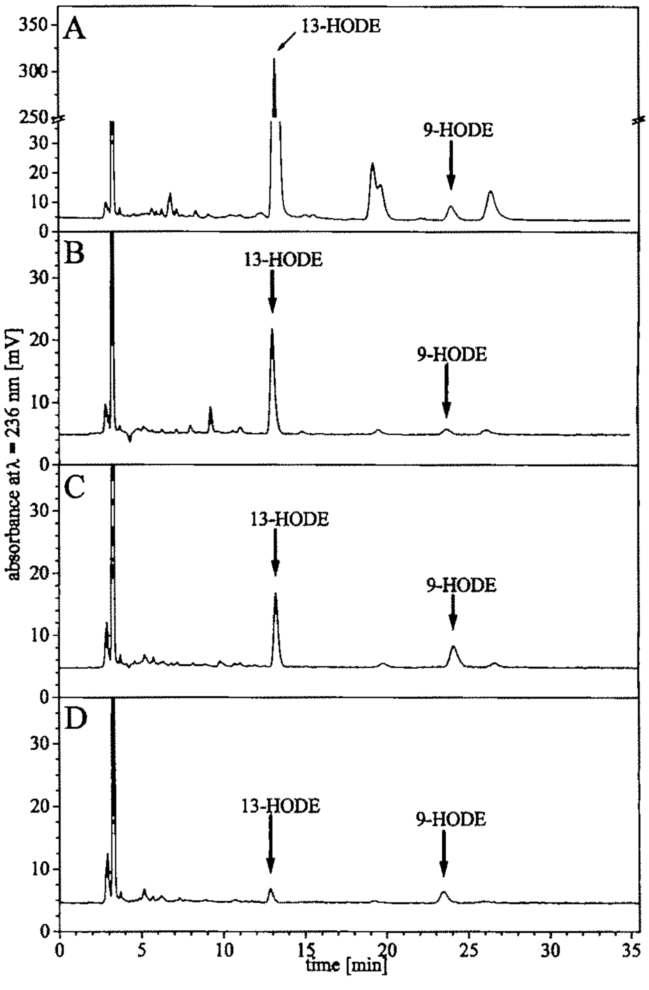

Figure 2 Straight-phase HPLC analysis of lipid extracts obtained after incubation with linoleic acid of 10000 *g* supernatants from sonicated HEK-293 cells transiently transfected with leucocyte-type (A), platelet-type (B) or epidermis-type (C) (12*S*)-lipoxygenase expression constructs or with pcDNA vector alone (D)

Supernatants (10000 *g*) were incubated with linoleic acid instead of arachidonic acid. The protein concentration in each assay was 0.15 mg/ml protein [leucocyte-type (12*S*)-lipoxygenase], 1.0 mg/ml protein [platelet-type (12*S*)-lipoxygenase], 5 mg/ml protein [epidermis-type (12*S*)-lipoxygenase] and 5 mg/ml protein (vector). For details see the legend to Figure 1.

isoenzymes showed a strict enantiomeric purity of the main product (12*S*)-HETE. In addition, the by-products 15-HETE and 8-HETE generated by leucocyte-type (12*S*)-lipoxygenase were predominantly the *S* enantiomers. However, 8-HETE generated by platelet-type (12*S*)-lipoxygenase was found to be the *R* enantiomer (Figure 3 and Table 3). All three isoenzymes oxygenated linoleic acid to (13*S*)-HODE, whereas the chirality of the by-product 9-HODE was predominantly the *S* enantiomer with leucocyte-type (12*S*)-lipoxygenase but *R* with the two other isoenzymes (Figure 4 and Table 4). HETEs and HODEs generated in 10000 *g* supernatants of vector-transfected cells were found to be racemic.

Inhibitor experiments

Two selective inhibitors of the human platelet-type (12*S*)-lipoxygenase, BHPP [17] and CDC [18], were tested for (12*S*)-lipoxygenase isoenzyme selectivity. BHPP was more efficient in

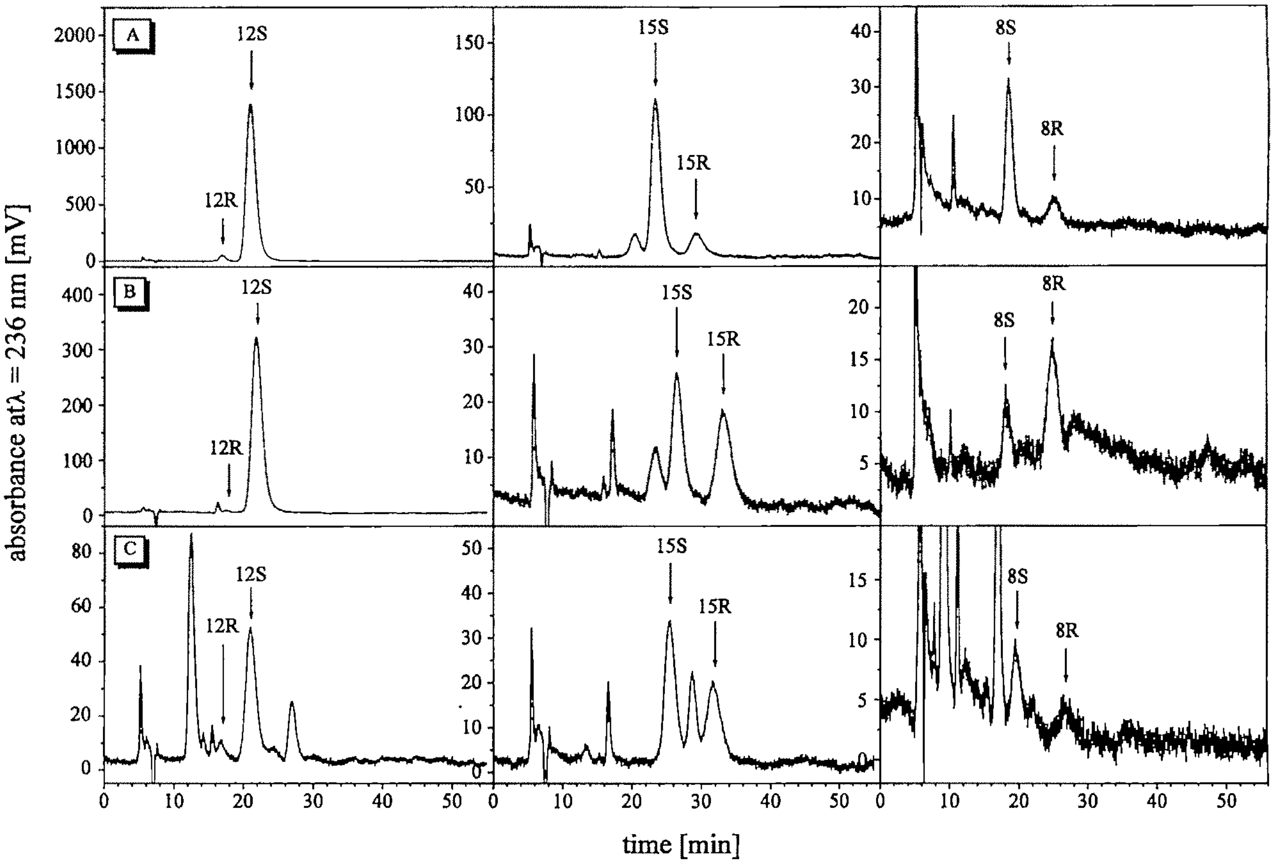

Figure 3 Chiral-phase HPLC of the regioisomeric HETEs formed by (12*S*)-lipoxygenase isoenzymes expressed in HEK-293 cells

The 8-, 12- and 15-HETE eluates were subjected to chiral-phase chromatography with a Chiracel column (250 mm × 4 6 mm, 5 μm particle size) with n-hexane/propan-2-ol/acetic acid (99.1:0 05, by vol) for the elution of the *R* and *S* enantiomers of 15- and 12-HETE and with n-hexane/propan-2-ol/acetic acid (97 5 2.5.0.05, by vol.) for the elution of the *R* and *S* enantiomers of 8-HETE Authentic (15*S*)-, (12*S*)- and (8*S*)-HETE and the corresponding *R* enantiomers were used as external standards and were eluted at a flow rate of 0 5 ml/min. (**A**) Leucocyte-type (12*S*)-lipoxygenase, (**B**) platelet-type 12(*S*)-lipoxygenase and (**C**) epidermis-type 12(*S*)-lipoxygenase.

Table 3 Chiral-phase analysis of the reaction products of (12*S*)-lipoxygenase isoenzymes with arachidonic acid as substrate

Chiral-phase analysis was done with HETE fractions obtained by straight-phase HPLC (see Figure 1) with a Chiracel column (for details see the legend to Figure 3). Authentic (12*R*)-, (12*S*)-, (15*R*)-, (15*S*)-, (8*R*)- and (8*S*)-HETE (100 ng of each) were used as external standards The concentrations of *S* and *R* enantiomers were determined from the peak areas and used to determine the ratios, the sum of which was set at 100%.

	Chirality of HETE (%)		
(12*S*)-Lipoxygenase type	12*S*:12*R*	15*S* 15*R*	8*S* 8*R*
Leucocyte	99·1	84 16	81 19
Platelet	99 1	–	30:70
Epidermis	92·8	–	–

suppressing platelet-type (12*S*)-lipoxygenase activity than epidermis-type and leucocyte-type (12*S*)-lipoxygenases, both with arachidonic acid and with linoleic acid as a substrate (Table 5). CDC almost exclusively inhibited the platelet-type enzyme with arachidonic acid as a substrate. The high selectivity was not observed with linoleic acid as substrate (Table 6).

DISCUSSION

Phylogenetically, the three mouse (12*S*)-lipoxygenase isoenzymes are found in different subgroups, sequence comparisons yield only moderate amino acid identities of between 57.0 and 60.7% [5,19]. This structural diversity is reflected by differences in catalytical activity, positional selectivity and stereoselectivity, and sensitivity to inhibitors. Although the isoenzymes oxygenated arachidonic acid predominantly to (12*S*)-HpETE and linoleic acid to (13*S*)-hydroperoxyoctadecadienoic acid [(13*S*)-HpODE], the yields varied widely. In particular, the specific activity of the epidermis-type isoenzyme was 1–2.5 orders of magnitude lower than that of leucocyte-type or platelet-type (12*S*)-lipoxygenase. Epidermis-type (12*S*)-lipoxygenase shares low catalytic efficiency with other lipoxygenases preferentially expressed in epidermis, i.e. human (15*S*)-lipoxygenase 2, human and mouse (12*R*)-lipoxygenase and mouse 8-lipoxygenase [4,5,7,12,20]. This indicates that either (1) free arachidonic acid or linoleic acid are not the appropriate substrates or (2) that epidermis-specific cofactors or post-translational modifications [21–23] are not provided on expression of the recombinant protein in HEK-293 cells. The leucocyte-type (12*S*)-lipoxygenase oxygenated linoleic acid with approx. one-tenth the efficiency of arachidonic acid. In this respect, the mouse enzyme resembled the bovine analogue, whereas the pig analogue was reported to oxygenate linoleic acid

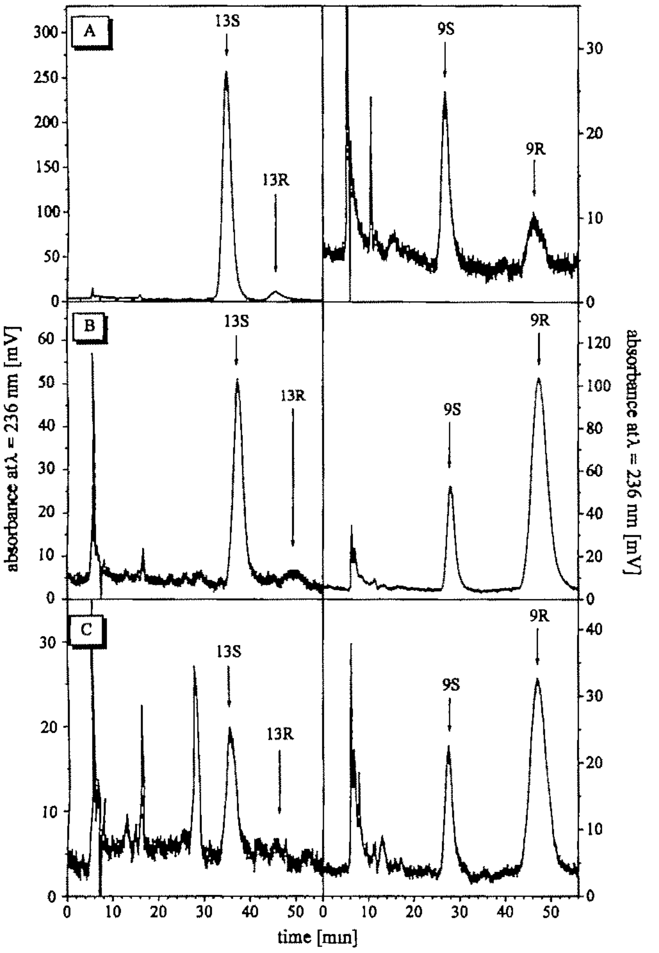

Figure 4 Chiral-phase HPLC of the regioisomeric HODEs formed by (12*S*)-lipoxygenase isoenzymes expressed in HEK-293 cells

The 9- and 13-HODE eluates were subjected to chiral-phase chromatography by using a Chiracel column (250 mm × 4 6 mm, 5 μm particle size) with n-hexane/propan-2-ol/acetic acid (99.1.0.05, by vol.) for the elution of the *R* and *S* enantiomers of 13-HODE and with n-hexane/propan-2-ol/acetic acid (97 5:2 5 0 05, by vol) for the elution of the *R* and *S* enantiomers of 9-HODE Authentic (13*S*)- and (9*S*)-HODE and the corresponding *R* enantiomers were used as external standards and were eluted at a flow rate of 0 5 ml/min For platelet-type and epidermis-type (12*S*)-lipoxygenases, the 9-HODE chromatograms were performed by pooling several 9-HODE fractions obtained by straight-phase HPLC (**A**) Leucocyte-type 12(*S*)-lipoxygenase, (**B**) platelet-type 12(*S*)-lipoxygenase and (**C**) epidermis-type 12(*S*)-lipoxygenase

Table 4 Chiral-phase analysis of the reaction products of (12*S*)-lipoxygenase isoenzymes with linoleic acid as substrate

Chiral-phase analysis was done with HODE fractions obtained by straight-phase HPLC (see Figure 4) with a Chiracel column (for details see the legend to Figure 4) (13*R*)-, (13*S*)-, (9*R*)- and (9*S*)-HODE (100 ng of each) were used as external standards The concentrations of *S* and *R* enantiomers were determined from the peak areas and used to determine the ratios, the sum of which was set at 100%

	Chirality of HODE (%)	
(12*S*)-Lipoxygenase type	13*S* 13*R*	9*S*·9*R*
Leucocyte	97 3	65·35
Platelet	95 5	25 75
Epidermis	93 7	24.76

Table 5 Inhibition by BHPP of (12*S*)-lipoxygenase isoenzymes with arachidonic acid or linoleic acid as substrate

	IC_{50} (μM)	
(12*S*)-Lipoxygenase type	Arachidonic acid	Linoleic acid
Leucocyte	20 8	2 3
Platelet	0 8	0 3
Epidermis	3 7	0 7

Table 6 Inhibition by CDC of (12*S*)-lipoxygenase isoenzymes with arachidonic acid or linoleic acid as substrate

	IC_{50} (μM)	
(12*S*)-Lipoxygenase type	Arachidonic acid	Linoleic acid
Leucocyte	> 50	2 3
Platelet	0 3	6 2
Epidermis	36	6 7

at least as efficiently as arachidonic acid [8]. The mouse platelet-type (12*S*)-lipoxygenase also showed considerable enzymic activity with linoleic acid as substrate, whereas the bovine and human analogues were reported to exhibit low and undetectable activity respectively [8].

The leucocyte-type enzyme was unique among the three (12*S*)-lipoxygenase isoenzymes in that it exhibited a promiscuous positional specificity, generating considerable quantities of 15-HETE and 8-HETE as by-products. Dual positional specificity has been previously shown for the pig and the mouse leucocyte (12*S*)-lipoxygenases [8–10,16] as well as for the rabbit and human reticulocyte-type (15*S*)-lipoxygenases [24,25], which are considered to be the corresponding orthologues of the mouse leucocyte-type (12*S*)-lipoxygenase [8]. The platelet-type (12*S*)-lipoxygenase generated only small quantities of 8-HETE as a side product. In previous studies the human platelet-type (12*S*)-lipoxygenase was shown to generate small quantities of 15-HETE, whereas the mouse analogue was reported to be monospecific [8–10]. The epidermis-type isoenzyme inserted molecular oxygen exclusively into the 12-position of arachidonic acid. With linoleic acid as substrate the leucocyte-type and platelet-type isoenzymes generated 13-HODE and 9-HODE in the ratio of approx. 50:1 and the epidermis-type (12*S*)-lipoxygenase in the ratio of approx. 3:1.

Whereas the main products, 12-HETE and 13-HODE, generated by the three (12*S*)-lipoxygenase isoenzymes were almost exclusively *S* enantiomers, the chirality of the by-products differed with the isoenzyme. Thus (15*S*)-HETE and (8*S*)-HETE were generated by leucocyte-type (12*S*)-lipoxygenase and (8*R*)-HETE by platelet-type (12*S*)-lipoxygenase; linoleic acid was oxygenated to (9*R*)-HODE by both the epidermis-type and the platelet-type (12*S*)-lipoxygenases but to the *S* enantiomer by the leucocyte-type enzyme.

The positional and enantiomeric specificity of (12*S*)-lipoxygenases might cast light on mechanisms involved in the catalytic process. On the basis of biochemical [26,27], X-ray [28–30] and spectroscopic analyses [31], models have been proposed that predict the product spectrum of lipoxygenases [32–34]. The initial, rate-limiting step of the lipoxygenase reaction

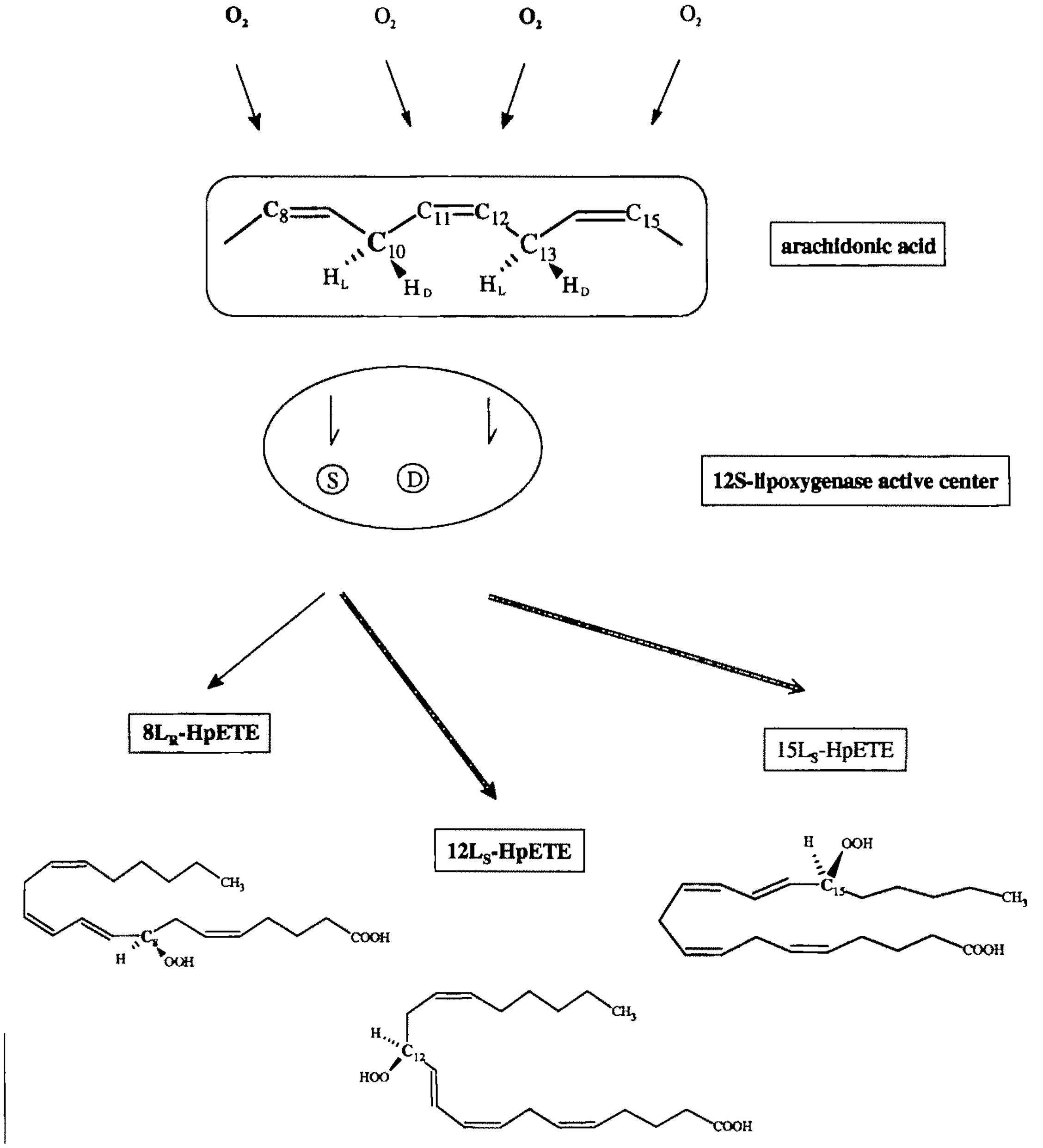

Figure 5 Positional selectivity and stereoselectivity of the (12*S*)-lipoxygenase reaction with arachidonic acid as substrate

The 1,4-*cis*-pentadiene unit with the bis-allylic C-10 binds to the active centre of the enzyme. Abstraction of hydrogen 10 with the L configuration directs oxygen insertion into the 12 L_S or 8 L_R position and the hydrogen with the 10 D configuration into the 12 D_R or 8 D_S (not shown) position of arachidonic acid. Oxygen insertion into the 15 L_S position requires the abstraction of hydrogen 13 with the L configuration.

is the abstraction of one of the two bis-allylic methylene hydrogens from one (or two different) 1,4-pentadiene structure(s) followed by a rearrangement of the intermediate pentadienyl radical driven by a *Z*,*E*-diene conjugation, and the stereospecific (antarafacial) addition of molecular oxygen to one of the two possible radical carbons. The intermediate peroxide radical is then reduced by the addition of a hydrogen atom to the corresponding hydroperoxy fatty acid.

As far as (12*S*)-lipoxygenase is concerned, isotope tracer experiments have shown that the hydrogen with the L configuration at C-10 of arachidonic acid is removed and oxygen is directed into the 12 L_S position, yielding (12*S*)-HpETE as the major primary product [26]. The generation of regioisomeric by-products can be due either to oxygen insertion into one of the mirror-image-specific carbons of the intermediary pentadienyl radical or to a double regiospecificity in that hydrogen abstraction occurs from two different bis-allylic methylene groups (Figure 5). Thus the generation of (8*R*)-HpETE by platelet-type (12*S*)-lipoxygenase might result from oxygen insertion into the 8 L_R position instead of the mirror-image-specific 12 L_S position, yielding a product with an inverse chirality (Figure 5) (see also [35]), whereas the formation of (8*S*)-HpETE by leucocyte-type (12*S*)-lipoxygenase is compatible with the removal of the 10 D hydrogen, directing oxygen to the 8 D_S position. In fact, the epidermal 8-lipoxygenase generating (8*S*)-HETE as the main product has been shown to abstract the 10 D rather than the

10 L hydrogen [36]. With linoleic acid as a substrate, leucocyte-type, platelet-type and epidermis-type (12*S*)-lipoxygenases produced (13*S*)-HpODE and (9*R*)-HpODE as by-products, most probably through abstraction of the 11 L hydrogen, which directs oxygen insertion into the 13 L_S or 9 L_R position. In contrast, the formation of (9*S*)-HpODE required the abstraction of hydrogen 11 D.

Provided that in all (12*S*)-lipoxygenase isoenzymes hydrogen abstraction is occurring at the same site of the substrate-binding cavity, the mutual removal of either the L or D hydrogen is possible only under two conditions: (1) the substrate can be twisted by 109 °, corresponding to the tetrahedral angle, thus permitting the abstraction of either the L or D hydrogen, or (2) the orientation of the fatty acid in the substrate cavity can have two orientations, i.e. a terminal methyl group ('tail-first') or a carboxy group ('head-first') towards the centre of the enzyme, a concept previously put forward by Brash et al. [35]. Thus the product spectra of the three (12*S*)-lipoxygenase isoenzymes might be explained by a 'tail-first' positioning of arachidonic acid and a binding pocket of differing volumes, permitting the regiospecific positioning of the bis-allylic methylene groups with respect to the site of hydrogen abstraction. An exception is the generation of (8*S*)-HETE and (9*S*)-HODE by the leucocyte-type (12*S*)-lipoxygenase and (8*S*)-lipoxygenase because it requires an opposite orientation ('head-first') or a twisted fixation of the substrate in the binding cavity.

We thank Ina Kutchera and Brigitte Steinbauer for excellent technical assistance This project was supported by a grant from the Deutsche Krebshilfe, Bonn, Germany

REFERENCES

1 Brash, A R (1999) Lipoxygenases occurrence, functions, catalysis, and acquisition of substrate. J. Biol Chem. **274**, 23679–23682

2 Funk, C D. (1996) The molecular biology of mammalian lipoxygenases and the request for eicosanoid functions using lipoxygenase-deficient mice Biochim Biophys Acta **1404**, 65–84

3 Krieg, P, Kinzig, A, Heidt, M, Marks, F. and Furstenberger, G (1998) cDNA cloning of a 8-lipoxygenase and a novel epidermis-type lipoxygenase from phorbol ester-treated mouse skin Biochim. Biophys Acta **1391**, 7–12

4 Boeglin, W E, Kim, R. B and Brash, A R (1998) A 12*R*-lipoxygenase in human skin mechanistic evidence, molecular cloning, and expression Proc. Natl Acad Sci. U S A **95**, 6744–6749

5 Krieg, P, Siebert, M, Kinzig, A, Bettenhausen, R, Marks, F. and Furstenberger, G (1999) Murine 12(*R*)-lipoxygenase: functional expression, genomic structure, and chromosomal localization FEBS Lett **446**, 142–148

6 Thiele, B. J, Fleming, J., Chester, J, O'Prey, J, Prehn, S, Janetzki, S, Rapoport, S M and Harrison, P R (1990) Structure of the mRNA and of the gene coding for the rabbit erythroid 15-lipoxygenase Biomed Biochim Acta **49**, 17–24

7 Brash, A. R, Boeglin, W E and Chang, M S (1997) Discovery of a second 15*S*-lipoxygenase in humans. Proc Natl Acad. Sci U S A **94**, 6148–6152

8 Yamamoto, S, Suzuki, H and Ueda, N (1997) Arachidonate 12-lipoxygenases Progr Lipid Res. **36**, 23–41

9 Chen, X S, Kurre, U, Jenkins, N A, Copeland, N G and Funk, C. D (1994) cDNA cloning, expression, mutagenesis of C-terminal isoleucine, genomic structure, and chromosomal localizations of murine 12-lipoxygenases J Biol Chem **269**, 13979–13987

10 Krieg, P., Kinzig, A, Ress-Loschke, M., Vogel, S, VanLandingham, B, Stephan, M, Lehmann, W D., Marks, F and Furstenberger, G (1995) 12-lipoxygenase isoenzymes in mouse skin tumor development Mol. Carcinogenesis **14**, 118–129

11 Van Dijk, K W., Steketee, K., Havekes, L, Frants, R and Hofker, M (1995) Genomic and cDNA cloning of a novel mouse lipoxygenase gene Biochim Biophys Acta **1259**, 4–8

12 Funk, C D, Keeney, D S, Oliw, E H, Boeglin, W E and Brash, A R (1996) Functional expression and cellular localization of mouse epidermal lipoxygenase J. Biol Chem. **271**, 23338–23344

13 Kinzig, A, Furstenberger, G, Burger, F, Vogel, S., Muller-Decker, K, Mincheva, A, Lichter, P, Marks, F and Krieg, P (1997) Murine epidermal lipoxygenase (Aloxe) encodes a 12-lipoxygenase isoform FEBS Lett **402**, 162–166

14 Powell, W S (1982) Rapid extraction of arachidonic acid metabolites from biological samples using octadecylsilica Methods Enzymol **86**, 467–477

15 Lehmann, W. D, Stephan, M and Furstenberger, G (1992) Profiling assay for lipoxygenase products of linoleic and arachidonic acid by gas chromatography–mass spectrometry. Anal Biochem **204**, 158–170

16 Yokoyama, C, Shinjo, F, Yoshimoto, T, Yamamoto, S, Oates, J A and Brash, A R (1986) Arachidonate 12-lipoxygenase purified from porcine leukocytes by immunoaffinity chromatography and its reactivity with hydroperoxyeicosatetraenoic acids. J Biol Chem **261**, 16714–16721

17 Chen, Y Q, Duniec, Z M, Liu, B, Hagmann, W, Gao, X, Shimoji, K., Marnett, L J, Johnson, C R and Honn, K V. (1994) Endogenous 12(S)-HETE production by tumor cells and its role in metastasis Cancer Res **54**, 1574–1579

18 Cho, H, Ueda, M., Tamaoka, M, Hamaguchi, M, Aisaka, K, Kiso, Y, Inoue, T., Ogino, R, Tatsuoka, T and Ishihara, T (1991) Novel caffeic acid derivatives extremely potent inhibitors of 12-lipoxygenase. J Med Chem **34**, 1503–1505

19 Kuhn, H and Thiele, B J (1999) The diversity of the lipoxygenase family FEBS Lett **449**, 7–11

20 Burger, F, Krieg, P, Kinzig, A, Schurich, B, Marks, F and Furstenberger, G (1999) Constitutive expression of 8-lipoxygenase in papillomas and clastogenic effects of lipoxygenase-derived arachidonic acid metabolites Mol Carcinogenesis **24**, 108–117

21 Lepley, R A, Muskardin, D T and Fitzpatrick, F A (1996) Tyrosine kinase activity modulates catalysis and translocation of cellular 5-lipoxygenase. J Biol Chem **271**, 6179–6184

22 Rapoport, S M, Schewe, T, Wiesner, R, Halangk, W, Ludwig, P, Jahnicke-Hohne, M, Tannert, C, Hiebsch, C and Klatt, D (1979) The lipoxygenase of reticulocytes purification, characterization, and biological dynamics of the lipoxygenase, its identity with the respiratory inhibitors of the reticulocyte Eur J. Biochem **96**, 545–561

23 Mancini, J A, Abramovitz, M., Cox, M E, Wong, E, Charleson, S, Perrier, H, Wang, Z, Prasit, P and Vickers, P J (1993) 5-lipoxygenase-activating protein is an arachidonate binding protein FEBS Lett **318**, 277–281

24 Bryant, R, Bailey, J M, Schewe, T and Rapoport, S M (1982) Positional specificity of a reticulocyte lipoxygenase. Conversion of arachidonic acid into 15-*S*-hydroperoxy-eicosatetraenoic acid J Biol Chem **257**, 6050–6055

25 Kuhn, H, Barnett, J, Grunberger, D, Baecker, P, Chow, J, Nguyen, B, Bursztyn-Pettegrew, H., Cahn, H and Sigal, E (1993) Overexpression, purification, and characterization of human recombinant 15-lipoxygenase Biochim Biophys Acta **1169**, 80–89

26 Hamberg, M and Hamberg, G (1980) On the mechanism of the oxygenation of arachidonic acid by human platelet lipoxygenase Biochem Biophys Res Commun. **95**, 1090–1097

27 Kuhn, H, Sprecher, H and Brash, A R (1990) On singular or dual positional specificity of lipoxygenases The number of chiral products varies with alignment of methylene groups at the active site of the enzyme J Biol Chem **265**, 16300–16305

28 Boyington, J. C, Gaffney, B. J and Amzel, L M (1993) The three-dimensional structure of an arachidonic acid 15-lipoxygenase Science **260**, 1482–1486

29 Minor, W, Steczko, J, Stec, B, Otwinowski, Z, Bolin, J T, Walter, R and Axelrod, B (1996) Crystal structure of soybean lipoxygenase L-1 at 1 4 Å resolution Biochemistry **35**, 10687–10701

30 Gillmor, S A, Villasenor, A, Fletterick, A, Sigal, E and Browner, M F (1997) The structure of mammalian 15-lipoxygenase reveals similarity to the lipases and the determinants of substrate specificity Nat Struct Biol. **2**, 1003–1009

31 Solomon, E I, Zhou, J, Neese, F and Pavel, E G (1997) New insights from spectroscopy into structure/function relationships of lipoxygenases Chem Biol **4**, 795–808

32 Lehmann, W D (1994) Regio- and stereochemistry of the dioxygenation reaction catalyzed by (S)-type lipoxygenases or by the cyclooxygenase activity of prostaglandin H synthases Free Radical Biol. Med **16**, 241–253

33 Nelson, M J and Seitz, S P (1994) The structure and function of lipoxygenase Curr Opin Struct Biol **4**, 878–884

34 Prigge, S T., Gaffney, B B and Amzel, L M. (1998) Relation between positional specificity and chirality in mammalian lipoxygenases. Nat Struct Biol. **5**, 178–179

35 Brash, A R, Boeglin, W A, Chang, M S and Shieh, B (1996) Purification and molecular cloning of an 8*R*-lipoxygenase from the coral *Plexaura homomalla* reveal the related primary structures of *R*- and *S*-lipoxygenases J Biol Chem **271**, 20949–20957

36 Hughes, M. A and Brash, A R (1991) Investigation of the mechanism of biosynthesis of 8-hydroxyeicosatetraenoic acid in mouse skin Biochim Biophys Acta **1081**, 347–354

Received 12 November 1999/3 March 2000; accepted 24 March 2000

Biochem J (2000) 38, 337–342 (Printed in Great Britain)

Expression of an active form of recombinant Ty1 reverse transcriptase in *Escherichia coli*: a fusion protein containing the C-terminal region of the Ty1 integrase linked to the reverse transcriptase–RNase H domain exhibits polymerase and RNase H activities

Marcelle WILHELM, Mansour BOUTABOUT and François-Xavier WILHELM[1]

Unité Propre de Recherche 9002 du Centre National de la Recherche Scientifique, Institut de Biologie Moléculaire et Cellulaire, 15 rue René Descartes, 67084 Strasbourg Cedex, France

Replication of the *Saccharomyces cerevisiae* Ty1 retrotransposon requires a reverse transcriptase capable of synthesizing Ty1 DNA. The first description of an active form of a recombinant Ty1 enzyme with polymerase and RNase H activities is reported here. The Ty1 enzyme was expressed as a hexahistidine-tagged fusion protein in *Escherichia coli* to facilitate purification of the recombinant protein by metal-chelate chromatography. Catalytic activity of the recombinant protein was detected only when amino acid residues encoded by the integrase gene were added to the N-terminus of the reverse transcriptase–RNase H domain This suggests that the integrase domain could play a role in proper folding of reverse transcriptase Several biochemical properties of the Ty1 enzyme were analysed, including the effect of $MgCl_2$, NaCl, temperature and of the chain terminator dideoxy GTP on its polymerase activity. RNase H activity was examined by monitoring the cleavage of a RNA–DNA template–primer. Our results suggest that the distance between the RNase H and polymerase active sites corresponds to the length of a 14-nucleotide RNA–DNA heteroduplex. The recombinant protein produced in *E. coli* should be useful for further biochemical and structural analyses and for a better understanding of the role of integrase in the activation of reverse transcriptase.

Key words: polymerization, retrotransposon, sequence comparison, template-primer, yeast.

INTRODUCTION

The genome of the yeast *Saccharomyces cerevisiae* contains five families of long-terminal-repeat (LTR) retrotransposons, Ty1–Ty5 [1]. They are structurally and functionally similar to eukaryotic retroviruses [2,3] The Ty1 elements have a length of 5.9 kb, and consist of a large internal domain composed of two overlapping open reading frames, TyA and TyB, analogous to the retroviral *gag* and *pol* genes, flanked on either side by direct long terminal repeats. The life cycle of Ty elements begins with transcription of the integrated retrotransposon DNA. The Ty transcript is then packaged into the intracytoplasmic virus-like particles (VLPs) where it is converted into double-stranded DNA by the process of reverse transcription [4,5]. Both strands of the retrotransposon DNA are synthesized by the retrotransposon reverse transcriptase (RT) which is able to utilize both RNA and DNA as template and requires primers to initiate DNA synthesis. A specific host tRNA is used as a primer to initiate minus-strand cDNA synthesis and an RNase H (RH)-resistant oligoribonucleotide spanning a purine-rich sequence is used to prime plus-strand-DNA synthesis. RT activity has been demonstrated in VLPs purified from cells overproducing Ty1 elements. Attempts to obtain a soluble fraction of Ty1 RT from VLPs or to clone an active recombinant enzyme have been unsuccessful until now.

In the present paper we describe the expression, purification and initial biochemical characterization of an active recombinant Ty1 RT. DNA fragments encoding the RT open reading frame were synthesized by PCR and cloned into an *Escherichia coli* expression vector. We demonstrate that a fusion protein Ty1 integrase (IN)–RT–RH with a 115-amino-acid C-terminal fragment of the Ty1 integrase fused to the N-terminus of the RT–RH domain exhibits significant polymerase and RH activities. We have compared the biochemical features of the recombinant protein with the equivalent features of the Ty1 VLP-associated enzyme.

EXPERIMENTAL

Construction of *E. coli* plasmids expressing Ty1 proteins

The *E. coli* expression vector p6H (kindly given by S. Le Grice, NCI-Frederick Cancer Research and Development Center, Frederick, MD, U.S.A.) which encodes a hexahistidine array (His-tag) at the N-terminus of the recombinant proteins was used to clone the Ty1 RT [6]. The RT–RH domain spanning nts 3946–5562 of the Ty1-H3 coding sequence [7] and the three IN–RT–RH constructs spanning nts 3868–5562 (construct 1), nts 3601–5562 (construct 2) and nts 3511–5562 (construct 3) of the Ty1-H3 were amplified by PCR and cloned into the p6H vector.

The same 3′ amplification primer was used for all constructs. It contained a *Sal*I site and was complementary to the 3′ terminal coding sequence (including the stop codon) of the TyB open reading frame (ORF) (5′-ACGCGTCGACCTAATGAATCCATTTG-3′). Different 5′ amplification primers were used to amplify the RT–RH and IN–RT–RH domains. All 5′ primers contained a *Bam*HI site. They differed by the coding sequence for the N-terminal amino acids: 5′-CGCGGATCCGCTGTAAAA-

---

Abbreviations used. RT, reverse transcriptase, RH, RNase H; LTR, long terminal repeat, VLP, virus-like particle, IN, integrase; His-tag, hexahistidine, ORF, open reading frame, PR, protease; dd, dideoxy; HTLV-1, human T-cell leukaemia virus Type 1

[1] To whom correspondence should be addressed (e-mail wilhelm@ibmc.u-strasbg.fr)

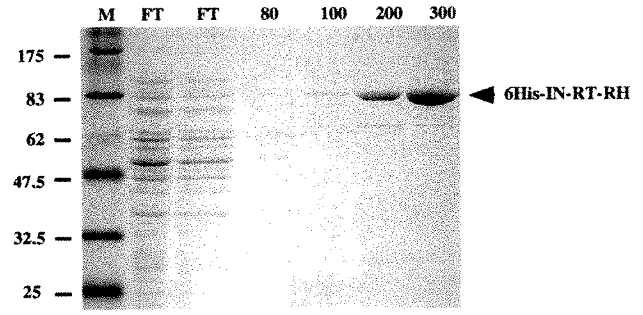

Figure 1 Purification of hexahistidine-tagged recombinant Ty1 IN-RT-RH (construct 2) by Ni^{2+}-nitrilotriacetic acid–agarose affinity chromatography

SDS/PAGE analysis of the proteins eluted from the affinity column by increasing concentrations of imidazole (80, 100, 200 and 300 mM) is shown. Lane M, molecular-mass markers (indicated in kDa on the left); lanes FT, flow-through fractions. The calculated molecular mass of the His$_6$–IN–RT–RH (construct 2) fusion protein is 76.4 kDa.

GCAGTAAAATC-3′ (RT–RH), 5′-CGCGGATCCTCACGA-GACACATGGAATACTAAG-3′ (IN–RT–RH construct 1), 5′-CGCGGATCCAATAATTCATCGCACAATATTG-3′ (IN–RT–RH construct 2) and 5′-CGCGGATCCAACAACAAAA-CTGTTCCGCAG-3′ (IN–RT–RH construct 3). The PCR amplification products were gel-purified, digested with *Bam*HI and *Sal*I and ligated into *Bam*HI–*Sal*I-digested p6H vector. Recombinant plasmids were introduced into component *E. coli* M15 cells.

Expression and purification of recombinant proteins

The Ty1 recombinant proteins containing a short array of histidine residues at their N-terminus were expressed in *E. coli* and purified by Ni^{2+} nitrilotriacetic acid–agarose (Qiagen) affinity chromatography as described by Le Grice et al. [6] (Figure 1). We did not expect that the His-tag would inhibit the activity of Ty1 RT, since, in all cases studied so far, it has been observed that inclusion of a polyhistidine extension in recombinant RTs has no deleterious effect on their polymerase or RH activities [6,8,9].

Purification of Ty1 VLPs

Ty1 VLPs were isolated from the yeast strain AGY9 (*MATa leu2Δ1 ura3-52 trp1Δ63 his4-539 lys2-801 spt3-202*) transformed with plasmid pJEF1105 [4,10]. The yeast strain and the plasmid were kindly provided by J. D. Boeke (Department of Molecular Biology and Genetics, Johns Hopkins University, Baltimore, MD, U.S.A.). Ty1 VLPs were purified by using the method described by Eichinger and Boeke [4]. RT activity was assayed in purified VLP preparations with added exogenous poly(rC)$_n$-oligo(dG)$_{12-18}$: 4 μl of purified VLPs were mixed with 16 μl of assay mix and incubated for 60 min at room temperature (22–24 °C). The standard assay mix (20 μl) contained final concentrations of 50 mM Tris/HCl, pH 7.8, 40 mM KCl, 20 mM MgCl$_2$, 0.05 % Nonidet P40, 0.15 μM dGTP, 8 mM 2-mercaptoethanol, 0.01 unit of poly(rC)$_n$–oligo(dG)$_{12-18}$ (where 1 unit of poly(rC)$_n$-oligo(dG)$_{12-18}$ is 50 μg) and 1 μCi of [α-^{32}P]dGTP. Incorporation of ^{32}P-radiolabelled dGTP into high-molecular-mass poly(dG) was determined by scintillation counting. Aliquots of the reaction mixture were spotted on to DE81 filters (Whatman). The filters were washed three times in 5 % Na$_2$HPO$_4$ to remove unincorporated [α-^{32}P]dGTP, washed once in deionized water and dried after one ethanol wash (75 % ethanol, 0.15 M NaCl).

RNA labelling, RNA template–DNA primer annealing and RH assay

A 311-nt single-stranded RNA template was prepared by T7 polymerase *in vitro* transcription of *Rsa*I-digested pJCB plasmid (kindly given by F. Brulé, Institut de Biologie Moleculaire et Cellulaire, Strasbourg, France). The transcript consists of 311 nt of the 5′ terminal region of HIV-1 RNA starting at the first nucleotide of the genomic RNA [11]. The RNA was radiolabelled by adding [α-^{32}P]UTP to the reaction mixture and purified by electrophoresis on a 8 % denaturing polyacrylamide gel. RNA was eluted from the excised gel slices with 0.5 M ammonium acetate/1 mM EDTA. The 35-nucleotide chemically synthesized RNA (kindly given by L. Jaeger, Institut de Biologie Moleculaire, Strasbourg, France) was labelled at the 5′ terminus with ^{32}P using [γ-^{32}P]ATP and T4 polynucleotide kinase. An alkaline ladder was prepared by treating the 5′-labelled RNA with sodium carbonate (0.1 M, pH 9) for 4 min at 90 °C.

To prepare the RNA template–DNA primer duplex used in RH assay, a 3 M excess of DNA primer was hybridized with the RNA template in a buffer containing 50 mM Tris/HCl, pH 7.8, 15 mM NaCl and 8 mM 2-mercaptoethanol. The mixture was heated at 90 °C for 1 min and then incubated for 5 min at 70 °C and 10 min at 42 °C. RH cleavage was initiated with MgCl$_2$ at a final concentration of 20 mM. After addition of the Ty1 or HIV-1 enzyme the samples were incubated for 10 min at 23 °C. The reaction was stopped by addition of formamide sample buffer. The products of the reaction were analysed on denaturing 8 % or 15 % (w/v) polyacrylamide gels.

RT assay of purified recombinant proteins

The purified Ty proteins were tested for RT activity by following the poly(rC)$_n$-oligo(dG)$_{12-18}$ directed incorporation of [α-^{32}P]dGTP. Unless otherwise stated, assay mix (20 μl) contained final concentrations of 50 mM Tris/HCl, pH 7.8, 15 mM NaCl, 20 mM MgCl$_2$, 0.15 μM dGTP, 8 mM 2-mercaptoethanol, 0.01 unit of poly(rC)$_n$-oligo(dG)$_{12-18}$ and 1 μCi of [α-^{32}P]dGTP. Incubation was for 30 min at 23 °C. Incorporation of ^{32}P-radiolabelled dGTP into high-molecular mass poly(dG) was determined as described above.

RESULTS AND DISCUSSION

Expression and purification of recombinant Ty1 RT

The enzymes essential for the replication and transposition of Ty1 elements are encoded by the TyB ORF (Figure 2). Coding domains for a protease (PR), an IN and RT–RH have been identified on the TyB gene. The TyB-encoded proteins are synthesized as part of a 190 kDa TYA–TYB precursor. The order of the protein domains on the TYA–TYB precursor is TYA–PR–IN–RT–RH. The TYA, PR, IN and RT–RH polypeptides are cleaved from the TYA-TYB polyprotein by the Ty1-encoded PR. The cleavage sites between TYA and PR, PR and IN, and IN and RT–RH have been characterized [12–14]. Moore and Garfinkel [15] have reported that the 5′ end of the RT–RH coding region starts at position 3946 of the transcriptionally active Ty1-H3 element [7]. The RT–RH coding region ends at the stop codon located at the 3′ end of the TyB ORF (nt 5562). Consequently we cloned the RT–RH coding region extending from nt 3946 to nt 5562 into the p6H *E. coli* expression vector. The recombinant RT–RH protein was

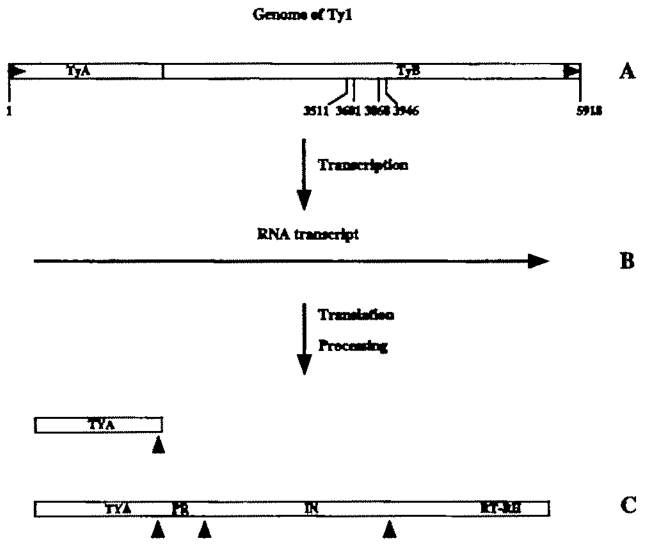

Figure 2 Map of Ty1 showing sites and co-ordinates relevant to the present study

(**A**) The Ty1 genome contains two LTRs (▶) flanking two partially overlapping open reading frames, TyA and TyB, which are analogous to the retroviral *gag* and *pol* genes. The transcriptionally active Ty1-H3 element is 5918 bp in length. The LTRs are 334 bp in length. The frameshift region separating TyA and TyB is indicated by a vertical line. The positions of the nucleotides at the 5′ end of the four constructs used in this study are indicated. (**B**) Transcription of the Ty1 element yields a major transcript of 5.7 kb. (**C**) The Ty1 RNA is translated to form two translation products, TYA and the TYA–TYB readthrough protein. The TYA–TYB protein contains TYA, a PR, an IN and a RT–RH domain. TYA and TYA–TYB are cleaved by the Ty1 PR to yield mature proteins. The cleavage sites are indicated by arrowheads (▲).

expressed, purified, and assayed for RT activity as described in the Experimental section. We found that the purified RT–RH protein encoded by nts 3946–5562 did not show any polymerase activity.

Several reports have implicated a role of the IN domain in the enzymic activity of some retroelement RTs [9,16,17]. We therefore constructed three IN–RT–RH fusion recombinant proteins containing fragments of the C-terminal region of the Ty1 IN attached to the N-terminus of the RT–RH domain: construct 1 had 26 residues from the IN C-terminal region fused to the RT–RH domain. One of the nuclear localization signals of Ty1 IN identified by Kenna et al. [18] and Moore et al. [19] was included in the N-terminal extension. Constructs 2 and 3 had 115 and 145 residues from the IN C-terminal region fused to the RT–RH domain respectively. The N-terminal region of constructs 2 and 3 ends at an NN motif, which could be a cleavage recognition site for the Ty1 PR. The three IN–RT–RH fusion proteins were expressed in *E. coli* and assayed for polymerase activity. Constructs 2 and 3 showed a high DNA polymerase activity, whereas construct 1 was inactive. In the experiments described below we used construct 2, which is the shortest protein with a high DNA polymerase activity, to characterize some biochemical features of the Ty1 RT.

Polymerase activity of the recombinant Ty1 IN–RT–RH enzyme

Four parameters of the RT polymerase activity were assessed using construct 2 of recombinant Ty1 IN–RT–RH and were compared with those of Ty1 VLP-associated enzyme. These parameters included the bivalent-cation requirement, the effects of NaCl and temperature on enzymic activity, and the sensitivity to inhibition by the chain terminator dideoxy GTP (ddGTP).

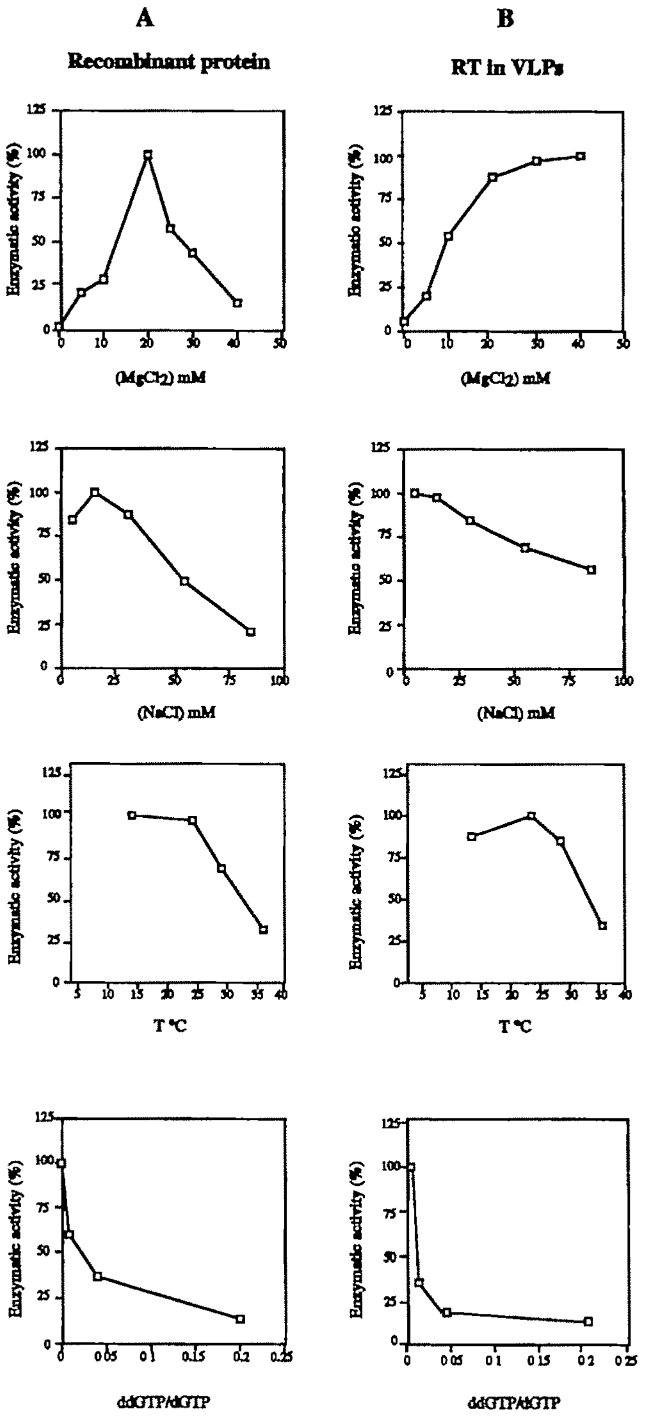

Figure 3 Effect of MgCl$_2$, NaCl, temperature and ddGTP on the polymerase activity of purified recombinant Ty1 IN–RT–RH protein and VLP-associated enzyme

Polymerase activity was measured as described in the Experimental section. For the recombinant protein, 100% activity is equal to 90 pmol of dGTP incorporated/μg in 30 min. For the VLPs, 100% activity is equal to 5 pmol of dGTP incorporated in 30 min for 4 μl of sucrose-gradient-purified VLPs.

The Ty1 RT requires bivalent cations for optimal activity. The effect of Mg^{2+} and Mn^{2+} on the activity of Ty1 RT was examined.

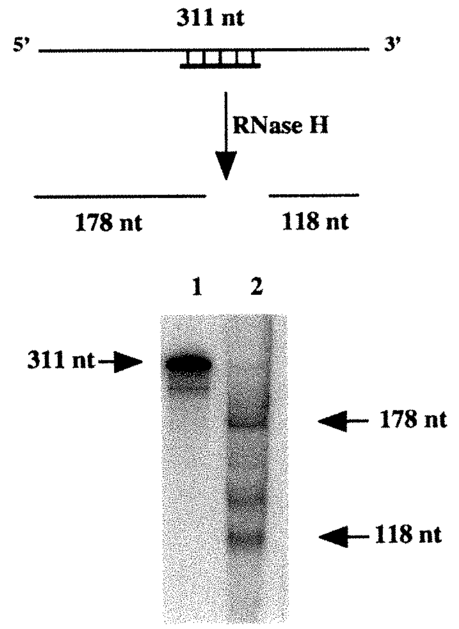

Figure 4 RH activity of the Ty1 IN–RT–RH protein

An internally ^{32}P-labelled 311 nt RNA template was hybridized with a molar excess of 18 nt DNA oligonucleotide primer and incubated with Ty1 enzyme as described in the Experimental section. The products of the reaction were analysed on a denaturing 8%-polyacrylamide gel. Polymerase-dependent cleavage by RH produced the expected 5′ fragment of 178 nt and 3′ fragment of 118 nt. Arrows indicate the positions of these fragments. A prominent polymerase-independent or non-specific cleavage product is also visible on the gel. A mock-treated RNA is shown in lane 1.

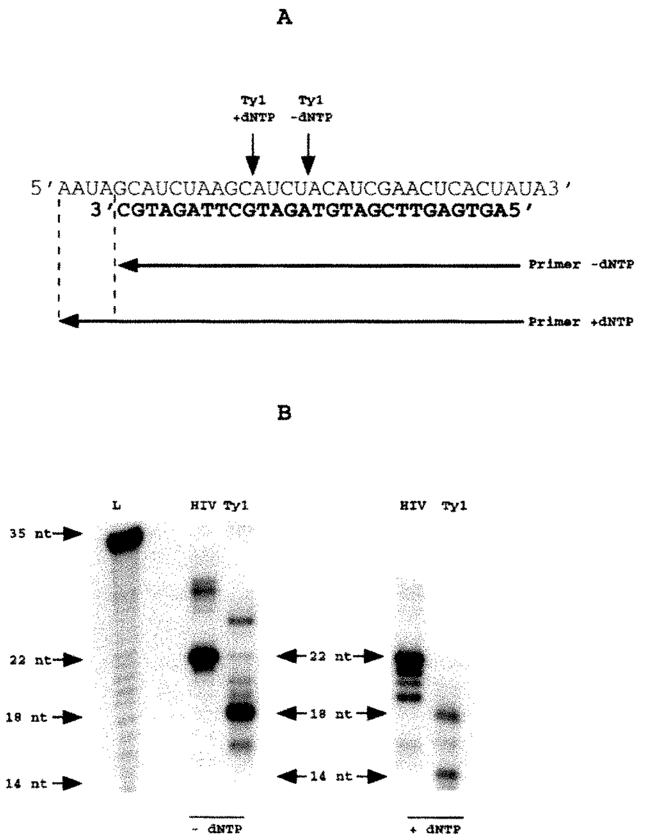

Figure 5 Interplay between the RH and polymerase active sites

A 35 nt-long RNA was annealed with a 28 nt-long complementary DNA primer; the DNA primer is shown in **bold** letters (**A**). The RNA template was radiolabelled at the 5′ end. The RNA–DNA heteroduplex and the Ty1 or HIV-1 enzyme were incubated (with or without dNTPs) to induce RH cleavage. In the presence of dATP and dTTP the primer was extended by 4 nt. The sites of cleavage by the Ty1 enzyme are indicated by arrows in (**A**). The cleavage products analysed on a denaturing 15%-polyacrylamide gel are shown in (**B**). Lane L, alkaline hydrolysis of the RNA template. HIV-1 or Ty1 enzymes were incubated with template–primer without any added dNTPs ('−dNTP'). The size of the main cleavage products are 22 nt and 18 nt for HIV-1 and Ty1 enzymes respectively. HIV-1 or Ty1 enzymes were incubated with template–primer, dATP and dTTP (+dNTP). The original 18 nt band and a 14 nt band are observed for the Ty1 enzyme. Cleavage bands at 22, 21, 20 and 19 nt are observed for the HIV-1 enzyme.

We found that the enzymic activity with Mg^{2+} was about threefold that with Mn^{2+} (results not shown). Therefore, in common with all other RTs studied, the Ty1 protein shows a preference for Mg^{2+} over Mn^{2+}. The Mg^{2+} response curve illustrated in Figure 3 demonstrates that the recombinant and VLP-associated enzymes have an absolute requirement for a bivalent cation. The recombinant enzyme exhibited a maximal activity at 20 mM Mg^{2+}, which decreased rapidly at higher Mg^{2+} concentrations. The activity of the VLP-associated enzyme was almost maximum at 20 mM Mg^{2+}, but did not decrease when the Mg^{2+} concentration was increased to 30 or 40 mM.

The effect of NaCl on the polymerase activity of recombinant and VLP-associated enzyme is shown in Figure 3. Both enzymes were inhibited by increasing concentrations of NaCl, but the VLP-associated enzyme was not inhibited to the same extent as the recombinant enzyme.

The polymerase activity of the recombinant enzyme was optimum at temperatures between 15 °C and 25 °C. The same temperature optimum was observed for the polymerase activity in VLPs (Figure 3). The low temperature optimum of the Ty1 enzyme can probably be correlated to the temperature-sensitivity of the Ty1 transposition process.

RTs are known to be sensitive to ddNTPs, which act as chain terminators. The effect of increasing concentrations of ddGTP on $poly(rC)_n$-$oligo(dG)_{12-18}$-directed polymerization of ^{32}P-labelled dGTP was tested. The titration curves shown in Figure 3 demonstrate that ddGTP is a strong inhibitor of Ty1 RT. In common with RTs from other eukaryotes, both recombinant and VLP-associated RTs were inhibited at low ddGTP concentration.

RH activity of the recombinant Ty1 IN–RT–RH enzyme

The RH activity of Ty1 enzyme was examined by monitoring the cleavage of an internally labelled 311 nt RNA transcript annealed to a complementary 18 nt oligodeoxyribonucleotide. The template–primer and the Ty1 enzyme were incubated to induce RH cleavage, as described in the Experimental section. Analysis of the RNA cleavage products on a denaturing gel showed that efficient cleavage was obtained with the recombinant Ty1 IN–RT–RH enzyme (Figure 4).

Next we analysed the interdependence between the RH and polymerase active sites of the Ty1 enzyme. To this end we used a 35 nt RNA template–28 nt DNA primer as substrate (Figure 5). The resulting complex contained a recessed 3′-terminus of DNA primer and four single-stranded RNA template bases. The 5′ end of the RNA was radiolabelled to allow one to reveal the RH cleavage products by gel electrophoresis. As shown in Figure 5(B) ('−dNTP'), RH cleavage of the Ty1 enzyme was specific for the RNA phosphodiester bond between nts 14 and 15 downstream from the nucleotide complementary to the 3′ ter-

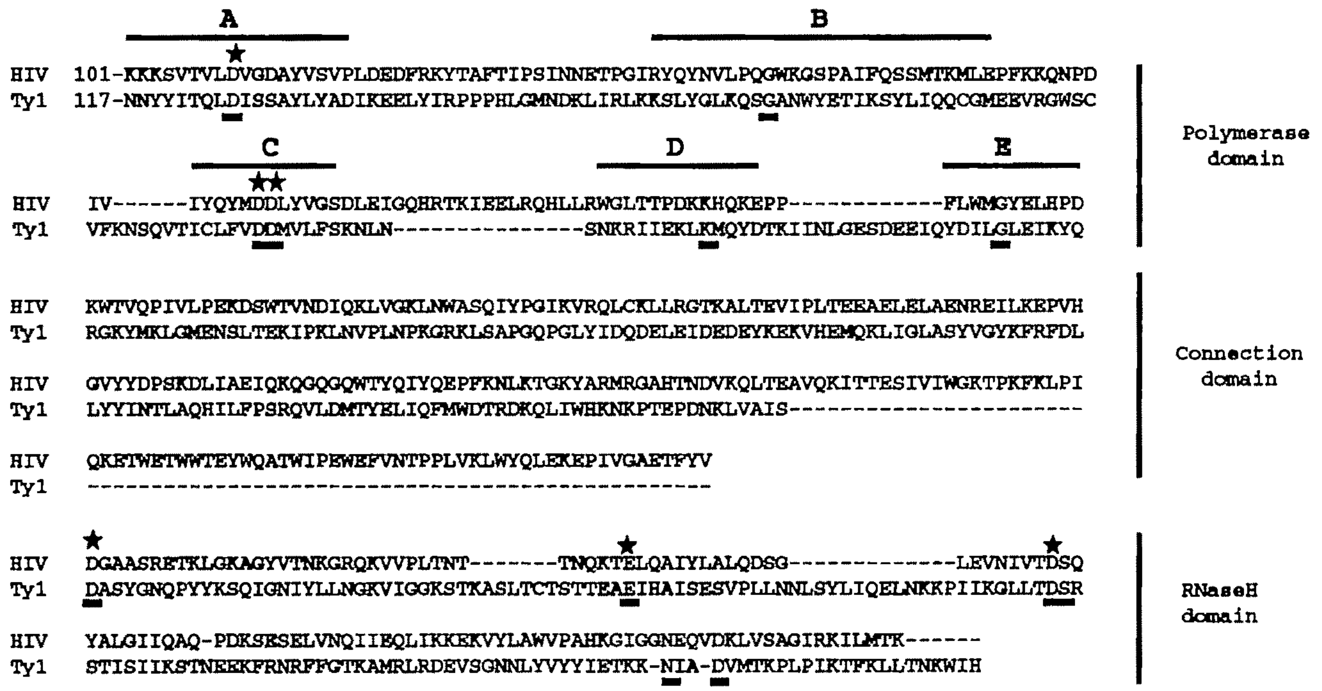
A
B
HIV 101-KKKSVTVLDVGDAYVSVPLDEDFRKYTAFTIPSINNETPGIRYQYNVLPQGWKGSPAIFQSSMTKMLEPFKKQNPD
Ty1 117-NNYYITQLDISSAYLYADIKEELYIRPPPHLGMNDKLIRLKKSLYGLKQSGANWYETIKSYLIQQCGMEEVRGWSC
C
D
E
HIV IV------IYQYMDDLYVGSDLEIGQHRTKIEELRQHLLRWGLTTPDKKHQKEPP------------FLWMGYELHPD
Ty1 VFKNSQVTICLFVDDMVLFSKNLN---------------SNKRIIEKLKMQYDTKIINLGESDEEIQYDILGLEIKYQ
Polymerase domain
HIV KWTVQPIVLPEKDSWTVNDIQKLVGKLNWASQIYPGIKVRQLCKLLRGTKALTEVIPLTEEAELELAENREILKEPVH
Ty1 RGKYMKLGMENSLTEKIPKLNVPLNPKGRKLSAPGQPGLYIDQDELEIDEDEYKEKVHEMQKLIGLASYVGYKFRFDL
HIV GVYYDPSKDLIAEIQKQGQGQWTYQIYQEPFKNLKTGKYARMRGAHTNDVKQLTEAVQKITTESIVIWGKTPKFKLPI
Ty1 LYYINTLAQHILFPSRQVLDMTYELIQFMWDTRDKQLIWHKNKPTEPDNKLVAIS----------------------
HIV QKETWETWWTEYWQATWIPEWEFVNTPPLVKLWYQLEKEPIVGAETFYV
Ty1 ---
Connection domain
HIV DGAASRETKLGKAGYVTNKGRQKVVPLTNT-------TNQKTELQAIYLALQDSG-------------LEVNIVTDSQ
Ty1 DASYGNQPYYKSQIGNIYLLNGKVIGGKSTKASLTCTSTTEAEIHAISESVPLLNNLSYLIQELNKKPIIKGLLTDSR
HIV YALGIIQAQ-PDKSESELVNQIIEQLIKKEKVYLAWVPAHKGIGGNEQVDKLVSAGIRKILMTK------
Ty1 STISIIKSTNEEKFRNRFFGTKAMRLRDEVSGNNLYVYYIETKK-NIA-DVMTKPLPIKTFKLLTNKWIH
RNaseH domain

Figure 6 Sequence alignment of Ty1 and HIV-1 RTs

Three domains have been identified the polymerase domain, the connection domain and the RH domain Alignment of the five conserved motifs (A to E, indicated by black bars above the alignment) within the polymerase domain was as described by Poch et al. [29] The nearly invariant amino acid residues found in all RNA-dependent polymerases are underlined. The three catalytically essential D residues are highlighted by stars The connection domain extends from the last residue in the conserved motif E to the first invariant residue of the RH domain [31] The connection domains of HIV-1 and Ty1 contain 205 and 133 residues respectively Alignment of the RH domains was as described by McClure [31] The catalytically essential residues are indicated by stars The nearly invariant amino acid residues found in all RH domains are underlined The numbers at the beginning of the sequences indicate the number of residues from the N-terminus of the RT–RH omitted from the Figure

minal nucleotide of the primer (the cleaved labelled RNA fragment has a length of 18 nt) In comparison, HIV-1 enzyme cleaved the RNA between positions 18 and 19, in keeping with biochemical and crystallographic data, indicating that, in HIV-1 RT, the distance between the positions of RH cleavage and DNA polymerase active sites is 18–20 bp [20–27]. The effect of primer extension on RH cleavage was examined (Figure 5B, '+dNTP'). When dATP and dTTP were present in the reaction mixture, the primer was extended by four nucleotides. Interestingly, for the Ty1 enzyme, both the originally observed RH-cleavage band and a new band four nucleotides shorter were obtained. This new band results from RH cleavage of the RNA between nts 14 and 15 from the nucleotide complementary to the 3′ terminus of the extended primer. It is a polymerase-dependent cleavage site, as defined by Furfine and Reardon [28], since it is advanced upon primer extension and remains at a fixed distance from the extended primer terminus. In the case of HIV-1, the originally observed RH cleavage and three additional sites of RNA hydrolysis were observed when the primer was extended by four nucleotides. The specific cleavage site between nts 18 and 19 from the nucleotide complementary to the 3′ end of the elongated primer was not observed. This is in line with results of Furfine and Reardon [28], showing that the RH of HIV-1 does not always make all the cleavages upon primer extension.

Our results have shown that the distance between the RH and polymerase active sites of the Ty1 enzyme is 14 nucleotides. It is four nucleotides shorter than the distance measured for HIV-1 RT. We suggest that this difference can be explained by a difference of structure of the two enzymes. The crystal structure of the p66 subunit of HIV-1 RT has shown that the polymerase domain is separated from the RH domain by a connection subdomain which forms a groove between the two active sites and plays a role in binding of the primer–template [22]. Sequence comparison of Ty1 and HIV-1 RTs [29–31] shows that the connection domain of the Ty1 enzyme is shorter than the connection domain of the HIV-1 RT (Figure 6). This difference could explain the difference of length of primer–template which can be accommodated between the active sites of the two enzymes. Crystallization of Ty1 RT will allow this suggestion to be directly tested.

Concluding remarks

Replication of retrotransposons and retroviruses requires an RT capable of reverse-transcribing the RNA genomes into double-stranded DNA. Here we have reported on the expression and the purification of Ty1 RT with polymerase and RH activities. An active recombinant protein could be obtained only after adding amino acid residues encoded by the IN gene to the N-terminus of the RT–RH domain. This suggests that the interaction between the C-terminal region of the IN and the RT–RH domain is important for the function of RT. It has been previously reported that a 140 kDa IN–RT–RH intermediate was observed during maturation of the TYA–TYB precursor. Thus it is possible that an interaction between the RT–RH and IN is also necessary for the activity of RT in VLPs. A mature 60 kDa protein encoded by the RT–RH ORF co-fractionates with Ty1 VLPs. The possibility that an interaction in *trans* between this protein and IN is necessary for its activity cannot be excluded. Interestingly a role for the IN domain in RT activity has been demonstrated by

Kirchner and Sandmeyer [16] for *S. cerevisiae* Ty3 retrotransposon; it is noteworthy that a decreased RT activity of Ty3 mutant VLPs relative to wild-type was observed for IN C-terminal deletion mutants, despite a different TyB gene organization (in Ty3 the order of RT–RH and IN domains is RT–RH–IN, whereas it is IN–RT–RH in Ty1). There are precedents in retroviral systems for RT–RH–IN intermediates in the maturation of *pol* gene products and for the role of integrase in RT activity. For example, Trentin et al. [9] have reported that the Human-T-cell-leukaemia-virus-Type 1 (HTLV-1) RT requires the presence of both RT–RH (α-subunit) and RT–RH–IN (β-subunit) for its activity. Since the HTLV-1 RT is not active in the absence of the β subunit, the RT–RH–IN can be viewed as an integrant part of RT transcriptase. The active reverse transcriptase of Rous sarcoma virus, an avian retrovirus, is also composed of α- and β-subunits [17]. These results suggest that interaction of the RT–RH and IN domains is functionally significant and that the IN domain could play a role in the proper folding of RT. This could be achieved in *cis* when the IN domain is attached to the RT–RH domain or in *trans* as part of heterodimeric RTs containing α- and β-subunits or by direct interaction between the mature IN and RT–RH proteins. Ongoing efforts to crystallize the Ty1 RT, in addition to biochemical and genetic analyses, will help us to understand how the polymerase domain of Ty1 RT is affected by its interaction with the IN domain.

We thank T. Heyman for support and helpful advice. This work was supported in part by grant 9589 from the Association pour la Recherche contre le Cancer (ARC)

REFERENCES

1 Boeke, J D. and Sandmeyer, S (1991) Yeast transposable elements In The Molecular and Cellular Biology of the Yeast *Saccharomyces cerevisiae* (Broach, J. R., Jones, E. W. and Pringle, J., ed.), pp 193–261, Cold Spring Harbor Laboratory Press, New York

2 Varmus, H (1988) Retroviruses Science **240**, 1427–1435

3 Boeke, J. D , Garfinkel, D. J., Styles, C A and Fink, G R (1985) Ty elements transpose through an RNA intermediate. Cell **40**, 491–500

4 Eichinger, D. J. and Boeke, J. D (1988) The DNA intermediate in yeast Ty1 element transposition copurifies with virus-like particles cell-free Ty1 transposition. Cell **54**, 955–966

5 Mellor, J , Fulton, S M., Dobson, M J , Wilson, W , Kingsman, S. M and Kingsman, A J (1985) A retrovirus-like strategy for expression of a fusion protein encoded by yeast transposon Ty1. Nature (London) **313**, 243–246

6 Le Grice, S F , Cameron, C E. and Benkovic, S J (1995) Purification and characterization of human immunodeficiency virus type 1 reverse transcriptase Methods Enzymol **262**, 130–144

7 Boeke, J D , Eichinger, D., Castrillon, D and Fink, G R (1988) The *Saccharomyces cerevisiae* genome contains functional and nonfunctional copies of transposon Mol Cell Biol **8**, 1432–1442

8 Taube, R , Loya, S , Avidan, O , Perach, M and Hizi, A (1998) Reverse transcriptase of mouse mammary tumour virus expression in bacteria, purification and biochemical characterization Biochem J **329**, 579–587

9 Trentin, B , Rebeyrotte, N. and Mamoun, R Z (1998) Human T-cell leukemia virus type 1 reverse transcriptase (RT) originates from the *pro* and *pol* open reading frames and requires the presence of RT-RNase H (RH) and RT–RH–Integrase proteins for its activity J Virol **72**, 6504–6510

10 Mathias, S L , Scott, A. F., Kazazian, H. J., Boeke, J D. and Gabriel, A (1991) Reverse transcriptase encoded by a human transposable element Science **254**, 1808–1810

11 Baudin, F , Marquet, R , Isel, C , Darlix, J L., Ehresmann, B and Ehresmann, C (1993) Functional sites in the 5′ region of human immunodeficiency virus type 1 RNA form defined structural domains J. Mol. Biol **229**, 382–397

12 Garfinkel, D J , Hedge, A M , Youngren, S D and Copeland, T. D (1991) Proteolytic processing of pol-TYB proteins from the yeast retrotransposon Ty1 J. Virol **65**, 4573–4581

13 Martin-Rendon, E , Hurd, D. W , Marfany, G , Kingsman, S. M and Kingsman, A J (1996) Identification of proteolytic cleavage sites within the gag-analogue protein of Ty1 virus-like particles Mol Microbiol. **22**, 1035–1043

14 Merkulov, G V , Swiderek, K M , Brachmann, C B and Boeke, J D. (1996) A critical proteolytic cleavage site near the C terminus of the yeast retrotransposon Ty1 Gag protein J Virol **70**, 5548–5556

15 Moore, S P and Garfinkel, D J (1994) Expression and partial purification of enzymatically active recombinant Ty1 integrase in *Saccharomyces cerevisiae* Proc. Natl. Acad. Sci U S A **91**, 1843–1847

16 Kirchner, J and Sandmeyer, S B (1996) Ty3 integrase mutants defective in reverse transcription or 3′-end processing of extrachromosomal Ty3 DNA J Virol. **70**, 4737–4747

17 Hippenmeyer, P J and Grandgenett, D P. (1984) Requirement of the avian retrovirus pp32 DNA binding protein domain for replication Virology **137**, 358–370

18 Kenna, M A , Brachmann, C B , Devine, S E and Boeke, J. D. (1998) Invading the yeast nucleus: a nuclear localization signal at the C terminus of Ty1 integrase is required for transposition *in vivo* Mol Cell. Biol **18**, 1115–1124

19 Moore, S P , Rinckel, L A and Garfinkel, D J (1998) A Ty1 integrase nuclear localization signal required for retrotransposition Mol. Cell. Biol **18**, 1105–1114

20 Jacobo-Molina, A , Ding, J , Nanni, R G , Clark, A D., Lu, X , Tantillo, C., Williams, R L , Kamer, G , Ferris, A. L., Clark, P et al. (1993) Crystal structure of human immunodeficiency virus type 1 reverse transcriptase complexed with double-stranded DNA at 3.0 Å resolution shows bent DNA Proc Natl. Acad Sci U.S.A. **90**, 6320–6324

21 Kohlstaedt, L A , Wang, J., Friedman, J M., Rice, P. A. and Steitz, T. A (1992) Crystal structure at 3.5 Å resolution of HIV-1 reverse transcriptase complexed with an inhibitor Science **256**, 1783–1790

22 Huang, H., Chopra, R , Verdine, G L and Harrison, S C (1998) Structure of covalently trapped catalytic complex of HIV-1 reverse transcriptase: implications for drug resistance Science **282**, 1669–1675

23 Wohrl, B M and Moelling, K (1990) Interaction of HIV-1 ribonuclease H with polypurine tract containing RNA–DNA hybrids Biochemistry **29**, 10141–10147

24 Gopalakrishnan, V , Peliska, J. A and Benkovic, S J (1992) Human immunodeficiency virus type 1 reverse transcriptase spatial and temporal relationship between the polymerase and RNase H activities Proc. Natl Acad Sci. U S A **89**, 10763–10767

25 Kati, M. W., Johnson, K A., Jerva, L F and Anderson, K S (1992) Mechanism and fidelity of HIV Reverse transcriptase J Biol. Chem **267**, 25988–25997

26 Gotte, M , Fackler, S , Hermann, T., Perola, E , Cellai, L , Gross, H J , Le Grice, S F J and Heumann, H (1995) HIV-1 reverse transcriptase-associated RNase H cleaves RNA/RNA in arrested complexes implications for the mechanism by which RNase H discriminates between RNA/RNA and RNA/DNA EMBO J **14**, 833–841

27 Gotte, M , Maier, G , Onori, A. M., Cellai, L , Wainberg, M A and Heumann, H (1999) Temporal coordination between initiation of HIV(+)-strand DNA synthesis and primer removal J Biol Chem **274**, 11159–11169

28 Furfine, E S and Reardon, J. E (1991) Reverse transcriptase-RNase H from the human immunodeficiency virus J Biol. Chem **266**, 406–412

29 Poch, O , Sauvaget, I , Delarue, M. and Tordo, N (1989) Identification of four conserved motifs among the RNA-dependent polymerase encoding elements EMBO J **8**, 3867–3874

30 Xiong, Y and Eickbush, T H (1990) Origin and evolution of retroelements based upon their reverse transcriptase sequences EMBO J **9**, 3353–3362

31 McClure, M A (1993) Evolutionary history of reverse transcriptase. In Reverse Transcriptase (Skalka, A M and Goff, S. P , ed), pp 425–444, Cold Spring Harbor Laboratory Press, Cold Spring Harbor, New York

Received 13 January 2000/1 March 2000; accepted 15 March 2000

Biochem J (2000) 348, 343–350 (Printed in Great Britain)

Cytochrome *c* release from isolated rat liver mitochondria can occur independently of outer-membrane rupture: possible role of contact sites

Elena DORAN and Andrew P. HALESTRAP[1]

Department of Biochemistry, School of Medical Sciences, University of Bristol, Bristol BS8 1TD, U.K.

Percoll-purified rat liver mitochondria were shown to contain BAX dimer and rapidly (< 2 min) release 5–10 % of their cytochrome *c* when incubated in a standard KCl incubation medium under energized conditions. This release was not accompanied by release of adenylate kinase (AK), another intermembrane protein, and was not inhibited by Mg^{2+}, dATP, inhibitors of the permeability transition or ligands of the peripheral benzodiazepine receptor. However, release was greatly reduced by the presence of 5 % (w/v) dextran (40 kDa), which caused a decrease in the light scattering (A_{520}) of mitochondrial suspensions. Dextran also inhibited both mitochondrial oxidation of exogenous ferrocytochrome *c* in the presence of rotenone and antimycin, and respiratory-chain-driven reduction of exogenous ferricytochrome *c*. Hypo-osmotic medium or digitonin treatment of mitochondria caused a large additional release of both cytochrome *c* and AK that was not blocked by dextran. Polyaspartate, which stabilizes the low conductance state of the voltage-dependent anion channel (VDAC), increased cytochrome *c* release. VDAC and BAX are both found at the contact sites between the inner and outer membranes and dextran is known to stabilize these contact sites in isolated mitochondria. Thus our data suggest that regulation of a specific permeability pathway for cytochrome *c* may be mediated by changes in protein–protein interactions within contact sites. The adenine nucleotide translocase is known to bind to VDAC and thus provides an additional link between the specific cytochrome *c* release pathway and the permeability transition.

Key words: adenylate kinase, apoptosis, BAX, mitochondrial permeability transition, VDAC.

INTRODUCTION

Mitochondria are now known to play a central role in both necrotic and apoptotic cell death (see [1–3]). In necrosis, the opening of the mitochondrial permeability transition (MTP) pore (MPTP) may well be the point of no return for the cell, since once mitochondria have undergone the permeability transition they become uncoupled. Not only are they unable to synthesize ATP, they actively hydrolyse it, thus preventing glycolysis from maintaining ATP supplies [3]. Since ATP is required to maintain cellular integrity and repair damage, the cell can no longer control its fate and dies by necrosis. In contrast, apoptosis is a controlled form of cell death that requires maintenance of cellular ATP and mitochondrial function, at least in the early stages [4]. The role of the mitochondria here appears to be in the release of cytochrome *c*, and probably other apoptosis-inducing factors, which initiate or amplify the apoptotic cascade [1,5]. In the presence of dATP, the released cytochrome *c* binds with APAF-1 (apoptosis-activating factor 1) and pro-caspase 9 to form a complex that leads to the proteolytic activation of pro-caspase 9 to active caspase 9. This then cleaves pro-caspase 3 to caspase 3, which directly or indirectly activates a range of enzymes critical for the rearrangement of the nucleus, cytoskeleton and plasma membrane that are characteristic of apoptosis [1,2].

The release of cytochrome *c* involves the pro-apoptotic members of the Bcl-2 family, such as BAX, BAD and BID, whose effects are antagonized by the anti-apoptotic members of the family such as Bcl-2 and Bcl-X_L [1,2]. It is unclear how these proteins interact in order to maintain the required balance between cell survival and proliferation on the one hand and apoptosis on the other. Proteolytic modifications and phosphorylations of the different Bcl-2 family members have been suggested to provide the link between cell-surface receptors and stimulation of cytochrome *c* release (see [2]). In particular, activation of members of the tumour-necrosis-factor receptor family leads to death-domain-dependent activation of caspase 8 and it has recently been shown that caspase 8 can proteolytically cleave a BID precursor to form active BID, which migrates to the mitochondria where it interacts with BAX to cause cytochrome *c* release. This then activates caspase 9 and hence caspase 3, which then sets in motion the apoptotic cascade [2]. What is still unresolved is the mechanism by which BID in association with BAX causes the release of cytochrome *c* from the intermembrane space. Two possibilities have been proposed. One is outer-membrane rupture caused by either the MPT or some other mechanism such as increased mitochondrial potassium uptake [6,7]. The second involves BAX, alone or in combination with other proteins, forming a specific pathway (channel) for cytochrome *c* transport [8–10]. The former mechanism would be associated with release of other intermembrane proteins such as adenylate kinase (AK), and there are data to suggest that for some toxins that induce apoptosis, such as etoposide and staurosporin, this may be the case [7,11]. However, breakage of the outer mitochondrial membrane is not a very precise mechanism for regulating a sophisticated process such as apoptosis and a more specific cytochrome *c* release mechanism might be expected. Indeed, it has been shown that cytochrome *c* release can occur without any sign of mitochondrial swelling and outer-membrane breakage; rather mitochondrial shrinkage may be observed [12–14].

In this paper we investigate the release of cytochrome *c* by a well-characterized liver mitochondrial preparation and dem-

---

Abbreviations used: ANT, adenine nucleotide translocase, AK, adenylate kinase, CsA, cyclosporin A, MPT, mitochondrial permeability transition, MPTP, MPT pore, TMPD, *N,N,N',N'*-tetramethyl-*p*-phenylenediamine, VDAC, voltage-dependent anion channel

[1] To whom correspondence should be addressed (e-mail A.Halestrap@Bristol.ac.uk).

onstrate that cytochrome *c* can be released rapidly without the concomitant loss of AK. This process is reduced greatly in the presence of dextran, which maintains inner- and outer-membrane interactions at contact sites, and is enhanced by polyaspartate, which binds to the voltage-dependent anion channel (VDAC) and favours its low conductance state. Since Bcl-2 and VDAC are associated with contact sites, these data suggest that a specific permeability pathway for cytochrome *c* can open when contact sites are disrupted.

MATERIALS AND METHODS

Mitochondria

Male Wistar rats (225–250 g in weight and allowed free access to food and water) were used for the preparation of liver mitochondria as described previously [15]. The isolation medium was 300 mM sucrose/2 mM EGTA/10 mM Tris/HCl/0.5 % BSA, pH 7.4, and the mitochondria were subjected to Percoll-gradient centrifugation to remove microsomal and plasma-membrane contamination. Mitochondria were washed in media without added BSA and stored on ice in this medium at about 30 mg of protein/ml Unless otherwise stated, all subsequent experiments were performed within 2 h of isolation. Mitoplasts were prepared from mitochondria by removal of the outer membrane by digitonin treatment [16].

Chemicals

Leupeptin, antipain, diazepam, protoporphyrin IX and poly-L-aspartate were from Sigma-Aldrich (Poole, Dorset, U.K.), Z-VAD-FMK (benzyloxycarbonyl-Val-Ala-DL-Asp-fluoromethylketone) was from Calbiochem-Novabiochem UK (Nottingham, U.K.) and Dextran FP40 (pyrogen-free) and all enzymes and cofactors were from Boehringer Mannheim UK (Lewes, East Sussex, U K.). Purified mouse monoclonal antibodies against cytochrome *c* and BAX were obtained from PharMingen International (Beckton Dickinson UK, Oxford, U.K.) and Santa Cruz Biotechnology (Santa Cruz, CA, U.S.A.) respectively. All other chemicals were of the highest purity commercially available.

Determination of cytochrome *c* and AK release from mitochondria

The standard incubation medium (pH 7.2) contained 25 mM KCl, 20 mM Mops, 10 mM Tris, 2 mM EGTA, 0.2 μM rotenone, 1 mM succinate and either sucrose or additional KCl to give the desired osmolarity. For iso-osmotic media (300 mosmol/l), additional KCl (100 mM) or sucrose (200 mM) were added. Mitochondria (1 mg of protein) were incubated in 1 ml of medium for 1 min at 25 °C in the presence or absence of 5 % (w/v) dextran (40 kDa) and other additions as indicated. After incubation mitochondria were placed on ice and then pelleted by centrifugation. The supernatant and pellet fractions were subjected to SDS/PAGE and analysed by Western blotting using purified mouse anti-cytochrome *c* monoclonal antibody with enhanced chemiluminescence detection. Quantification was by densitometry using a commercial scanner and ImageQuant software (Molecular Dynamics, Sunnyvale, CA, U S.A.). Various film exposures were employed to ensure determinations were made under conditions in which the response of the film was linear with respect to loading AK activity in the same samples (20 μl) was determined spectrophotometrically at 25 °C in 1 ml of medium (pH 7.5) containing 130 mM KCl, 6 mM $MgSO_4$, 100 mM Tris/HCl, 0.2 mM NADH, 0.5 mM ATP, 0.5 mM phosphoenolpyruvate, 0.5 μM rotenone, 7.5 μM oligomycin, 20 units/ml pyruvate kinase and 20 units/ml lactate dehydrogenase. The reaction was started by adding 0.75 mM AMP and followed by the decrease in A_{340}.

Polarographic and spectrophotometric determination of cytochrome *c* permeation across the outer membrane

NADH-cytochrome b_5-dependent oxidation of exogenous cytochrome *c* was determined polarographically using a Clarke-type oxygen electrode at 30 °C. Mitochondria (4 mg of protein) were suspended in 1 ml of standard KCl or sucrose incubation medium without succinate but supplemented with 0.25 mM NADH, 0.5 μM antimycin A and, when required, 5 % (w/v) dextran (40 kDa). After a basal rate of oxygen consumption was obtained (1 min), 10 μM cytochrome *c* was added and the new rate determined. For the spectrophotometric determination of exogenous cytochrome *c* reduction, mitochondria (2 mg of protein) were suspended in 7 ml of iso-osmotic KCl incubation medium without succinate but supplemented with 6 μM cytochrome *c* and, when required, 5 % (w/v) dextran (40 kDa). The suspension was divided between two cuvettes and incubated at 25 °C in a split-beam spectrophotometer with continuous monitoring of A_{550}. At the required time 1 mM succinate, 1 mM KCN and 0.12 mM *N,N,N′,N′*-tetramethyl-*p*-phenylenediamine (TMPD) were added to the sample cuvette only.

Measurement of the permeability transition and changes in mitochondrial conformation

Mitochondria (1 mg of protein) were incubated at 25 °C in 3.5 ml of standard iso-osmotic KCl medium but containing only 0.5 mM EGTA, which was absent for MPT assays, and other additions as required. Light scattering (A_{520}) was used to monitor changes in mitochondrial volume or conformation as described previously [15].

Protein assay

Protein was determined by the Bradford method using BSA as a standard.

Statistics

Results are expressed as means ± S.E.M. and statistical significance calculated using a two-tailed Student's *t* test.

RESULTS

In the absence of a colloidal osmotic support, isolated mitochondria rapidly release cytochrome *c*

Isolated rat liver mitochondria were incubated at 25 °C under energized conditions in a standard iso-osmotic medium containing physiological concentrations of K^+ (125 mM KCl) designed to mimic conditions *in vivo*. Following the required period of incubation the release of cytochrome *c* was determined by sedimentation of the mitochondria and analysis of the cytochrome *c* content of the supernatant and pellet by SDS/PAGE and Western blotting. In Figure 1(A) we show that after 2 min in KCl medium (300 mosmol/l) about 5–6 % of the total mitochondrial cytochrome *c* was detectable in the supernatant. This increased to about 20 % in hypotonic medium (50 mosmol/l), which would be expected to cause mitochondrial swelling and outer-membrane rupture. In Figure 1(B) we show that a similar amount of cytochrome *c* was released by disruption of the outer membrane by digitonin treatment. In these experiments the release of AK was determined enzymically and this

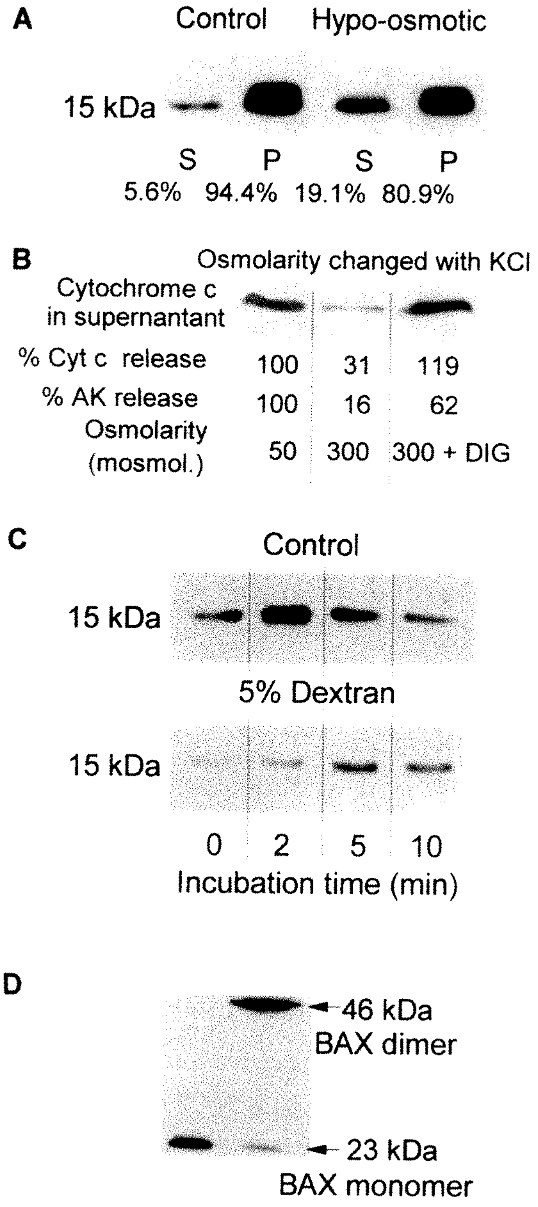

Figure 1 Release of cytochrome *c* by isolated rat liver mitochondria incubated in KCl medium

Mitochondria (1 h post-isolation) were incubated at 25 °C in KCl medium for the times indicated before sedimentation of mitochondria by centrifugation, as described in the Materials and methods section. Where indicated the medium also contained 0.12 mg/ml digitonin (DIG) and 5% (w/v) dextran (40 kDa). The cytochrome *c* content of the supernatant (S) and (in **A**) mitochondrial pellet (P) was determined by Western blotting following SDS/PAGE. The percentages shown below (**A**) represent the percentage of the total mitochondrial cytochrome *c* found in the pellet and supernatant fractions. In (**D**) cytosol (post-mitochondrial supernatant clarified by centrifugation at 100000 ***g*** for 15 min) and mitochondria (15 μg of protein per track) were separated by SDS/PAGE and the presence of BAX revealed by Western blotting.

also was increased substantially by both hypo-osmotic and digitonin treatments. These experiments also suggested that relatively more cytochrome *c* was released in normal KCl medium than was AK. In Figure 1(C) we show the time course of cytochrome *c* appearance in the supernatant, which was found to be maximal within 2 min and thereafter declined. This decline might have been due to proteolysis, although in three separate experiments addition of the proteinase inhibitors leupeptin and antipain (both at 4 μg/ml) to the incubation medium gave little reduction in the loss of cytochrome *c*.

Cytochrome *c* release is not accompanied by outer-membrane rupture

The rapid release of mitochondrial cytochrome *c* could reflect a specific release mechanism involving pro-apoptotic members of the Bcl-2 family known to stimulate cytochrome *c* release such as BAX. Indeed, using anti-BAX antibodies we were able to demonstrate the presence of the dimeric (active) form of the protein (46 kDa) in mitochondria, as illustrated in Figure 1(D). Relatively little of the monomeric form of BAX (23 kDa) was detected in mitochondria, although this form of BAX was present in the cytosol. The stability of the dimeric form of BAX during SDS/PAGE despite the denaturing conditions has been observed by others [17,18] and is not uncommon for proteins with hydrophobic membrane-spanning domains [19]. However, it might appear more likely that the cytochrome *c* release we observed was due merely to the instability of the outer membrane in our incubation medium. This possibility was investigated by comparing the release of cytochrome *c* and AK from mitochondria incubated in both KCl and sucrose media of varying osmolarity. Since cytochrome *c* binding to the inner membrane is known to decrease at higher ionic strengths, the use of both media was important to discriminate between the potential effects of decreasing ionic strength and osmolarity. In addition, we also investigated the effects of 5% (w/v) 40 kDa dextran on cytochrome *c* release in order to mimic the colloidal osmotic pressure by cytosolic proteins. The media routinely employed for incubating mitochondria *in vitro* usually lack such colloidal osmotic support, which may be important to prevent osmotic swelling of the intermembrane space.

The data of Figure 1(C) demonstrate that 5% (w/v) dextran (40 kDa) does indeed cause a substantial inhibition of cytochrome *c* release when mitochondria were incubated in KCl (125 mM) medium. However, the data of Figure 2(A) and Table 1 suggest that this effect does not merely reflect a reduction in the swelling of the intermembrane space and outer-membrane rupture since the release of AK remains unaffected by the presence of dextran. In contrast, when mitochondria were swollen by progressively decreasing the osmolarity of the incubation medium, AK was released, whether or not dextran was present, and was accompanied by additional release of cytochrome *c* (Figure 2). As noted in Figure 1(B), similar data were obtained with digitonin treatment, which specifically permeabilizes the outer membrane. Very much less cytochrome *c* release was observed when mitochondria were incubated in iso-osmotic medium containing only 25 mM KCl (with sucrose providing the remainder of the osmotic support), although AK release was similar to that observed in KCl medium (see Figure 2B). However, extensive release of both cytochrome *c* and AK was still obtained in this medium when swelling was induced by reducing the sucrose concentration. These data imply that the greater release of cytochrome *c* observed in iso-osmotic KCl medium than sucrose medium does not merely reflect less tight binding of cytochrome *c* to the inner membrane. The release of cytochrome *c* from mitochondria was slightly greater when mitochondria were stored on ice for longer periods. Thus after 2 h on ice, subsequent incubation of mitochondria for 2 min in KCl medium caused a $58\pm12\%$ (mean ± S.E.M. of nine different mitochondrial preparations) greater increase in cytochrome *c* release than after 1 h on ice. However, AK release was also increased by $31\pm7\%$ under the same conditions, suggesting that some damage to the outer membrane may also be occurring with time. The ability of

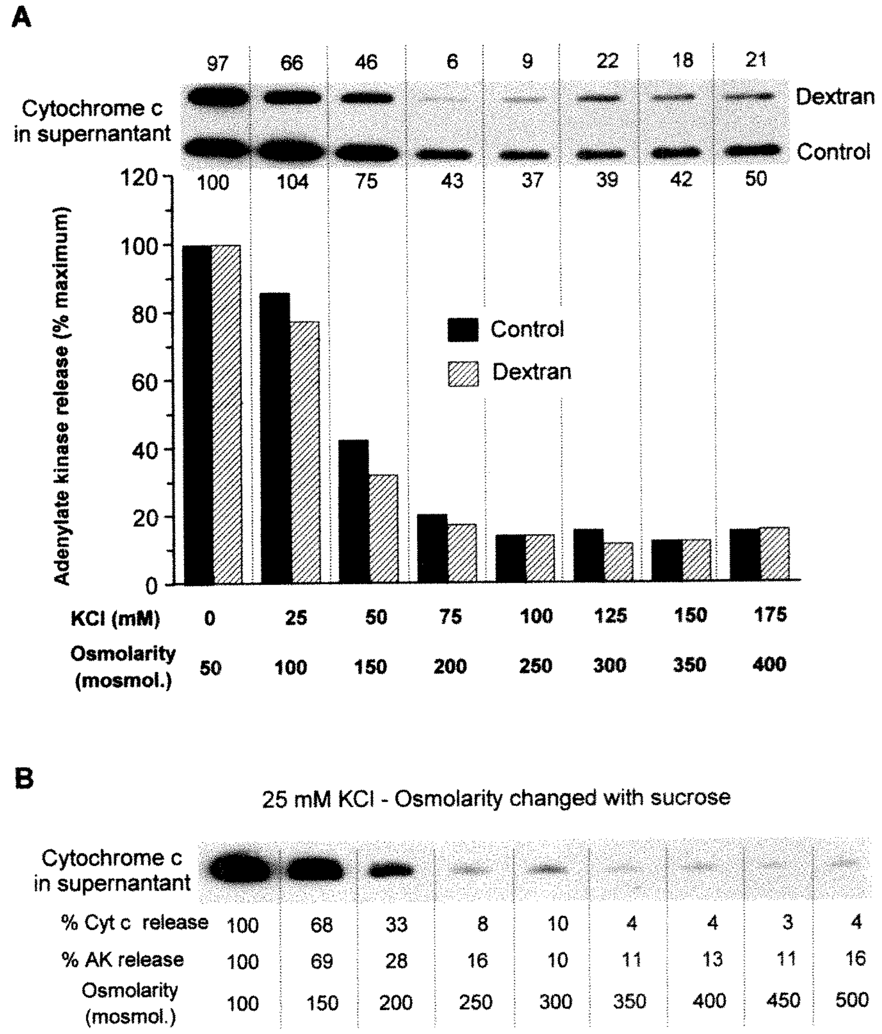

Figure 2 The effect of osmolarity on cytochrome *c* and AK release from isolated mitochondria in the presence or absence of dextran

Isolated mitochondria (1 mg of protein) were incubated for 1 min at 25 °C in standard medium containing 25mM KCl (see the Materials and methods section) in the presence or absence of 5% (w/v) dextran and increasing amounts of KCl (**A**) or sucrose (**B**) to vary the osmolarity as indicated. After incubation mitochondria were sedimented by centrifugation and cytochrome *c* content and AK activity of supernatants were assayed by Western blotting and enzymic assay respectively. The blots were quantified by scanning and band intensities expressed as a percentage of the value determined for 50 (**A**) or 100 mosM (**B**) medium without added dextran. Data for the AK activity determined enzymically are expressed similarly. The experiment shown is representative of two experiments showing similar results.

Table 1 Effect of dextran and other factors on the release of cytochrome *c* and AK from isolated rat liver mitochondria

Mitochondria were stored on ice for 1 or 2 h after isolation before incubation for 2 min at 25 °C in KCl medium with additions as indicated. After sedimentation of mitochondria by centrifugation the cytochrome *c* and AK contents of the supernatant were measured as described in the Materials and methods section. Data are expressed as a percentage of the corresponding control and as means ± S.E.M. for three separate mitochondrial preparations for dextran, carbonyl cyanide-*p*-trifluormethoxyphenylhydrazone (FCCP) and cyclosporin A, and for four preparations for polyaspartate (37 kDa). The release of cytochrome *c* and AK 2 h after isolation were 158 ± 12% and 131 ± 7% of that at 1 h post-isolation, respectively ($n = 9$). Statistically significant differences are indicated as follows: *$P < 0.05$, **$P < 0.001$.

	Cytochrome *c*		AK	
Time post-isolation...	1 h	2 h	1 h	2 h
Control	100	100	100	100
5% Dextran	65 ± 5*	34 ± 1**	94 ± 8	80 ± 9
54 μM Polyaspartate	318 ± 134	172 ± 17*	124 ± 13	110 ± 8
3 μM FCCP	174 ± 23	108 ± 23	117 ± 4	117 ± 11
0.2 μM Cyclosporin A	131 ± 15	102 ± 12	100 ± 1	105 ± 3

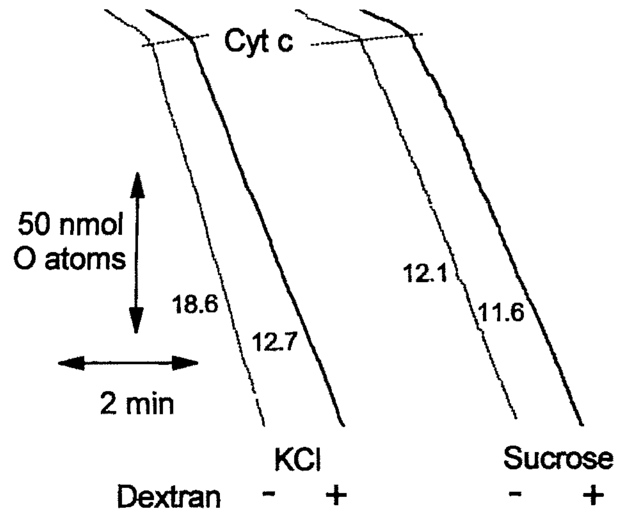

Figure 3 Dextran inhibits oxidation of exogenous cytochrome *c* by mitochondria in KCl medium

NADH-cytochrome b_5-dependent oxidation of exogenous cytochrome *c* was determined polarographically using a Clarke-type oxygen electrode at 30 °C as described in the Materials and methods section Mitochondria (4 mg of protein) were suspended in 1 ml of KCl or sucrose medium containing 0 25 mM NADH, 0 5 μM antimycin A and, where indicated, 5% (w/v) dextran (40 kDa). Cytochrome *c* (10 μM) was added where indicated Rates of oxygen consumption in nmol of O/min per mg of protein are given alongside each trace Data are representative of several similar experiments whose results are summarized in the text

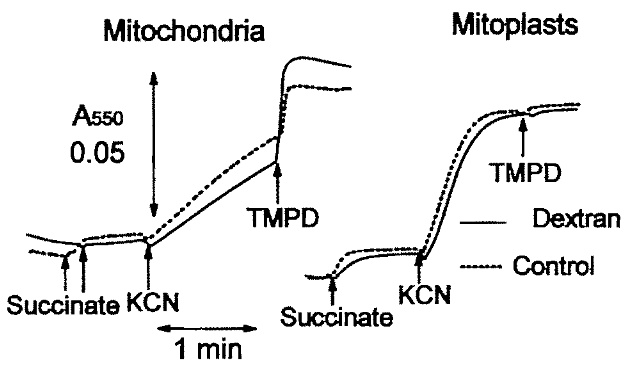

Figure 4 The effects of dextran and outer-membrane removal on the succinate-driven reduction of extramitochondrial cytochrome *c*

Mitochondria or mitoplasts (1 mg of protein/ml) were incubated in a split-beam spectrophotometer at 25 °C in standard KCl buffer (see the Materials and methods section) containing 6 μM cytochrome *c* and, when required, 5% (w/v) dextran, but no succinate A_{550} was monitored continuously, and additions of 1 mM succinate, 1 mM KCN and 0 15 mM TMPD were made as indicated The data shown are typical of three separate mitochondrial preparations for which 5% dextran inhibited the rate of cyanide-induced cytochrome *c* reduction by 23 ± 1 7% (mean ± S E M., $P < 0\,01$).

dextran to inhibit cytochrome *c* release was unaffected by storage on ice (see Table 1).

Cytochrome *c* can move in both directions across the mitochondrial outer membrane

In order to establish whether the release of cytochrome *c* from mitochondria was a bidirectional process involving a pore, rather than a unidirectional transport process, we studied the respiratory-chain-dependent oxidation of externally added ferrocytochrome *c*, as shown in Figure 3. In these experiments endogenous substrate oxidation is prevented by the presence of rotenone and antimycin and added oxidized cytochrome *c* is reduced to ferrocytochrome *c* through the action of NADH-cytochrome b_5 reductase on the outer-mitochondrial membrane [20]. In sucrose medium, cytochrome *c*-dependent oxidation of NADH consumed oxygen at the rate of about 12 nmol of O atoms/min per mg of protein whether or not dextran was present. However, in KCl medium without added dextran, the rate of oxygen uptake was about 50% greater but was decreased significantly by the presence of dextran. In the experiment shown involving mitochondria isolated from two rats, four separate determinations of oxygen uptake in the presence and absence of dextran were made over a 4 h period. No significant changes in the inhibition caused by dextran were observed over this time period, during which the mitochondria were stored at 0 °C. The mean inhibition (±S.E.M.) caused by dextran was 22±4.5%. With a second mitochondrial preparation the inhibition caused by dextran was 26% after 1 h at 0 °C and 32% after 5 h. These data suggest that the NADH/cytochrome *c*-dependent oxygen uptake observed in sucrose medium represents the contribution by mitochondria with ruptured outer membranes that allow cytochrome *c* free access to cytochrome oxidase. The additional oxidation observed in KCl medium that is largely prevented by dextran correlates with the additional release of cytochrome *c* (but not AK) observed in this medium (Figure 2) and appears to reflect a specific dextran-sensitive cytochrome *c*-transport mechanism across the outer membrane.

This conclusion was further strengthened by studying the reduction of exogenous ferricytochrome *c* by electrons donated from the cyanide-inhibited respiratory chain. Under these conditions, electrons from succinate oxidation are passed to complex III, which then donates electrons to exogenous cytochrome *c*. This is only possible if the outer membrane is broken or if there is a bidirectional cytochrome *c* transport mechanism. It may also be mediated by addition of TMPD, which is lipid soluble and hence can shuttle electrons across the outer membrane. The data of Figure 4 show that reduction of external cytochrome *c* can occur under such conditions, but is greatly stimulated by the addition of 0.15 mM TMPD or when the outer membrane is removed by digitonin treatment. The rate of cytochrome *c* reduction seen in the absence of TMPD could reflect only the small fraction of mitochondria with damaged outer membranes. However, addition of 5% dextran caused a 23±1.7% inhibition in the rate of cytochrome *c* reduction (mean±S.E.M. of three separate mitochondrial preparations; $P < 0.01$), implying that some of the cytochrome *c* was being reduced through the operation of the same mechanism that caused the cytochrome *c* release. The similarity of this dextran-mediated inhibition to that observed on NADH/cytochrome *c* oxidation described above increases confidence that this is the correct interpretation. Using these two methods we were able to screen a variety of potential effectors of the cytochrome *c* permeability pathway. No effects of ATP, ADP (+oligomycin), dATP, Mg^{2+}, bongkrekic acid or cyclosporin A (CsA) were observed.

VDAC but not the peripheral benzodiazepine receptor or MPTP may be involved in cytochrome *c* release

It has been suggested that the MPT may be involved in cytochrome *c* release, but this should be calcium-dependent, whereas we observe cytochrome *c* release in the presence of EGTA. Furthermore, we have been unable to detect any effect of CsA on the release of cytochrome *c* (Table 1). Nor was dextran able to inhibit the rate of the light-scattering change induced by

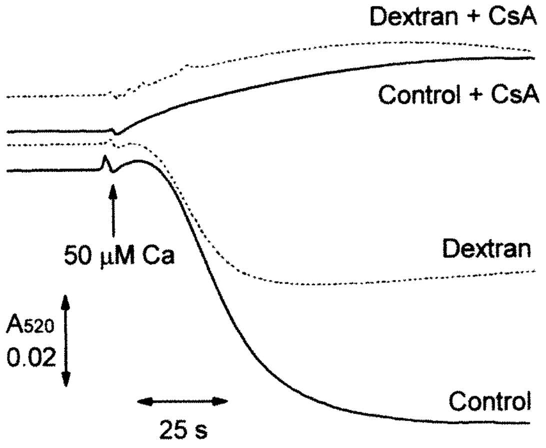

Figure 5 The effects of 5% dextran on the MPT of isolated liver mitochondria

Mitochondria were incubated under energized conditions in a split-beam spectrophotometer before addition of 50 μM Ca^{2+} at the time shown. Further details are given in the Materials and methods section. The experiment shown is typical of three similar experiments on separate mitochondrial preparations.

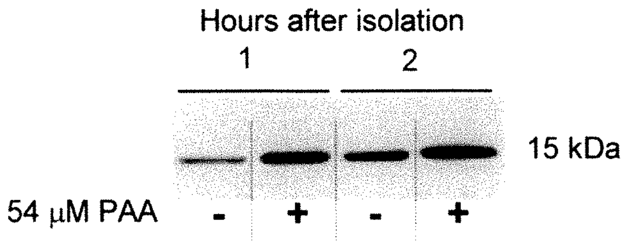

Figure 6 Effect of polyaspartate on mitochondrial cytochrome *c* release

After isolation (1 or 2 h), mitochondria were incubated in the presence or absence of 54 μM polyaspartate (PAA; 37 kDa) and pelleted by centrifugation as described in the Materials and methods section. The cytochrome *c* content of the supernatant was determined by Western blotting following SDS/PAGE. The data shown are typical of three independent experiments for which quantitative analysis is given in Table 1.

calcium overload under energized conditions (Figure 5), which suggests that the MPT is not inhibited by dextran. This is not surprising since the MPT involves a change in the inner- rather than outer-membrane permeability, most probably mediated by a calcium-triggered, cyclophilin-dependent conformational change of the adenine nucleotide translocase (ANT) [21,22]. However, it has been proposed that the ANT may interact with VDAC and possibly the peripheral benzodiazepine receptor in the outer membrane [23,24]. We have been unable to detect any effect of a range of concentrations of either protoporphyrin IX or diazepam (both ligands of the benzodiazepine receptor) on cytochrome *c* release (results not shown). This suggests that the benzodiazepine receptor is not involved in the release mechanism. Nor did de-energization of mitochondria with uncoupler (3 μM carbonyl cyanide-*p*-trifluormethoxyphenylhydrazone, FCCP) have a significant effect on cytochrome *c* release (Table 1). However, the addition of 54 μM polyaspartate (37 kDa), which causes VDAC to take up its low conductance state for anions [25], caused a significant increase in cytochrome *c* release (Figure 6 and Table 1).

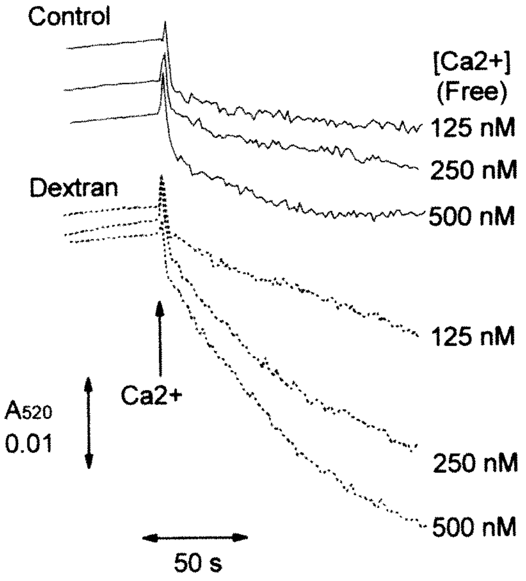

Figure 7 The effects of 5% dextran on the conformational changes induced in isolated energized liver mitochondria by sub-micromolar [Ca^{2+}]

The experimental protocol was as described in the Materials and methods section. After 1 min of incubation in the spectrophotometer, $CaCl_2$ was added to the sample cuvette alone to give the calculated free [Ca^{2+}] indicated [27]. The experiment shown is typical of three similar experiments on separate mitochondrial preparations.

The potential role of contact sites in cytochrome *c* release

The inner and outer mitochondrial membranes are closely apposed at various points known as contact sites, which are believed to be associated with an interaction between the ANT and VDAC. Dextran has been shown to increase the number of such contact sites in isolated mitochondria [26], and thus the ability of dextran to inhibit cytochrome *c* release is consistent with their disruption being associated with the unmasking of a cytochrome *c*-release pathway. One potential indicator of the effect of dextran on the contact sites may be the light scattering of the mitochondrial suspension. Indeed, we observed that the initial light scattering of liver mitochondria suspended in energized KCl medium was significantly less in the presence of 5% dextran, the A_{520} values at 1 and 2 h post-isolation (as means ± S.E.M. of four separate preparations) being 74.3 ± 7.6% ($P < 0.05$) and 64.6 ± 9.0% ($P < 0.02$) of control values respectively. Furthermore, although dextran had no effect on the rate of the light-scattering change occurring during the MPT induced by calcium overload, the maximum extent of the light-scattering change observed was diminished (Figure 5). These data are consistent with the formation of contact sites changing the conformation of mitochondria and leading to a decrease in their light scattering.

During the course of the latter experiments we observed that, in the presence of dextran, the exposure of energized mitochondria to sub-micromolar concentrations of Ca^{2+} (buffered with EGTA) caused a rapid decrease in light scattering, which was barely visible in the absence of dextran (Figure 7). The effect, which we have observed previously in heart mitochondria [15,27], was not inhibited by CsA and was quite distinct from the MPT, which required much greater loading of mitochondria with Ca^{2+}. Calcium has been demonstrated to increase contact-site formation in the perfused heart [28] and thus these data are also consistent with decreased light scattering detecting a conformational change that reflects greater contact-site formation.

DISCUSSION

The data we present in this paper demonstrate that Percoll-purified isolated rat liver mitochondria contain BAX dimer and can release cytochrome *c* independently of AK, and thus by implication without outer-membrane rupture. The ability of dextran to inhibit this process may reflect its ability to maintain the structure of contact sites between the inner and outer membrane [26]. Such contact sites are thought to involve an interaction between the ANT and VDAC that allows the communication between the inner and outer membranes [29–31] and our data suggest that their disruption may unmask a latent pathway for cytochrome *c* release In this context it may be significant that both BAX and Bcl-2 have been shown to be concentrated at the contact sites [32,33]. Evidence for a role of VDAC in the cytochrome *c*-release mechanism comes from the ability of polyaspartate to enhance cytochrome *c* release. Polyaspartate binds to VDAC and induces the low anion-conductance state [25], and it is known that when VDAC changes from the high- to the low-conductance conformation there is a large-scale rearrangement of protein domains [34]. Thus it is possible that the low-conductance conformation of VDAC may activate a cytochrome *c*-release pathway by some protein–protein interaction within the contact sites. A role for the low-conductance conformation of VDAC in cytochrome *c* release is supported by the observation that apoptosis induced by growth-factor withdrawal is associated with impaired ATP/ADP exchange into mitochondria [35]. The low anion-conductance state of VDAC is known to greatly inhibit ATP/ADP transport into mitochondria [36]. In contrast, Bcl-X_L over-expression facilitates mitochondrial ATP/ADP exchange and inhibits cytochrome *c* release [35], suggesting that it stabilizes the high-conductance state of VDAC associated with low cytochrome *c* permeability. In contrast, it would be envisaged that BAX might interact with VDAC to favour the low-conductance conformation and so enhance cytochrome *c* release. It may also be significant that VDAC possesses a tight binding site for cytochrome *c* on its intermembrane surface [34].

Recently Shimizu et al. [10] have reported that when VDAC is reconstituted into proteoliposomes, the addition of either BAX or BAK enables permeation by cytochrome *c*, which was blocked by Bcl-X_L. VDAC alone did not allow cytochrome *c* permeation, suggesting that BAX and BAK cause a conformational change in VDAC that allows it to transport cytochrome *c*, while Bcl-X_L antagonizes this effect. At first glance, our data might appear compatible with this hypothesis, if it is assumed that a VDAC interaction with the ANT at contact sites might prevent the cytochrome *c* translocation. However, closer examination of the data of Shimizu et al. [10] reveals discrepancies between their data and those of others, including ourselves. First, Shimizu et al. suggest that it is the high-conductance conformation of VDAC that allows cytochrome *c* permeation, yet our own data and those of Vander Heiden et al. [35] suggest that cytochrome *c* release and apoptosis are associated with the low-conductance conformation of VDAC. Second, Priault et al. [37] have demonstrated that BAX can induce cytochrome *c* release in VDAC-deficient yeast Shimizu et al. used proteoliposomes containing VDAC reconstituted from Triton-solubilized protein to demonstrate cytochrome *c* release. Since even very low concentrations of Triton X-100 can exert profound effects on both the inhibitor sensitivity of VDAC [38] and on the general permeability of liposomes [39], results obtained in this way must be treated with caution.

If VDAC present at the contact sites does participate directly or indirectly in the cytochrome *c*-release mechanism, there is the possibility that the conformation of the MPTP in the inner membrane may communicate directly with the cytochrome *c*-release mechanism independently of outer-membrane rupture. The MPTP is thought to be associated with contact sites and to be formed by a conformational change in the ANT, possibly in association with VDAC [1,2,15,40,41]. This may provide an explanation of how Bcl-2 may inhibit both the specific (MPTP-independent) cytochrome *c*-release mechanism and the MPTP-dependent mechanism. The latter is most likely to operate under conditions of oxidative stress and calcium overload, which are known to stimulate the opening of the MPTP. Examples include reperfusion of tissues following a period of ischaemia or the addition of chemical toxins where MPTP opening has been shown directly and treatment with CsA or over-expression of Bcl-2 may offer protection (see [2,41–43]). However, cell death is often necrotic under such circumstances unless MPTP opening is transient (see for example [44,45]), since mitochondria will be uncoupled and not maintain sufficient ATP concentrations to support apoptosis [2,4,41].

Our results also suggest the presence of a mechanism for the removal of released cytochrome *c* (Figure 1C). The mechanism of this is unknown but it was insensitive to standard protease inhibitors. If such a mechanism also exists within the cell, it provides a means by which apoptosis could be prevented or reversed if the apoptotic signal is weak or transient. This would ensure that cells do not enter apoptosis too readily. It might also explain how cells that have released cytochrome *c* following growth-factor withdrawal can be rescued from apoptosis by re-administration of growth factors and re-establish their normal compartmentation of cytochrome *c* within the mitochondria [13].

This work was supported by the Medical Research Council and a Royal Society/NATO Fellowship to E.D

REFERENCES

1 Green, D R. and Reed, J C (1998) Mitochondria and apoptosis Science **281**, 1309–1312

2 Li, H. L and Yuan, J Y. (1999) Deciphering the pathways of life and death Curr Opin Cell Biol **11**, 261–266

3 Halestrap, A. P (1999) The mitochondrial permeability transition its molecular mechanism and role in reperfusion injury. In Mitochondria and Cell Death, Biochemical Society Symposium no 66 (Brown, G C., Nicholls, D G and Cooper, C. E, eds.), pp 181–203, Portland Press, London

4 Nicotera, P, Leist, M. and Ferrando May, E (1998) Intracellular ATP, a switch in the decision between apoptosis and necrosis Toxicol Lett **103**, 139–142

5 Susin, S A, Lorenzo, H K., Zamzami, N, Marzo, I, Snow, B E, Brothers, G M, Mangion, J, Jacotot, E, Costantini, P, Loeffler, M et al (1999) Molecular characterization of mitochondrial apoptosis-inducing factor Nature (London) **397**, 441–446

6 Vander Heiden, M G, Chandel, N. S, Williamson, E K., Schumacker, P T and Thompson, C B (1997) Bcl-x(L) regulates the membrane potential and volume homeostasis of mitochondria Cell **91**, 627–637

7 Marzo, I, Brenner, C, Zamzami, N, Jurgensmeier, J M, Susin, S A, Vieira, H L A, Prevost, M C, Xie, Z H, Matsuyama, S, Reed, J C and Kroemer, G (1998) Bax and adenine nucleotide translocator cooperate in the mitochondrial control of apoptosis Science **281**, 2027–2031

8 Eskes, R, Antonsson, B, OsenSand, A, Montessuit, S, Richter, C, Sadoul, R, Mazzei, G, Nichols, A and Martinou, J C (1998) Bax-induced cytochrome *c* release from mitochondria is independent of the permeability transition pore but highly dependent on Mg^{2+} ions J Cell Biol **143**, 217–224

9 Desagher, S, OsenSand, A, Nichols, A, Eskes, R, Montessuit, S, Lauper, S, Maundrell, K, Antonsson, B and Martinou, J C (1999) Bid-induced conformational change of Bax is responsible for mitochondrial cytochrome *c* release during apoptosis J Cell Biol **144**, 891–901

10 Shimizu, S, Narita, M and Tsujimoto, Y (1999) Bcl-2 family proteins regulate the release of apoptogenic cytochrome *c* by the mitochondrial channel VDAC Nature (London) **399**, 483–487

11 Kohler, C, Gahm, A, Noma, T, Nakazawa, A, Orrenius, S and Zhivotovsky, B (1999) Release of adenylate kinase 2 from the mitochondrial intermembrane space during apoptosis FEBS Lett **447**, 10–12

12 Finucane, D M, BossyWetzel, E, Waterhouse, N J, Cotter, T G and Green, D R (1999) Bax-induced caspase activation and apoptosis via cytochrome *c* release from mitochondria is inhibitable by Bcl-xL J Biol Chem. **274**, 2225–2233

13 Martinou, I, Desagher, S, Eskes, R., Antonsson, B., Andre, E, Fakan, S and Martinou, J. C. (1999) The release of cytochrome *c* from mitochondria during apoptosis of NGF-deprived sympathetic neurons is a reversible event J Cell Biol **144**, 883–889

14 Zhuang, J G and Cohen, G M (1998) Release of mitochondrial cytochrome *c* is upstream of caspase activation in chemical-induced apoptosis in human monocytic tumour cells Toxicol Lett **103**, 121–129

15 Halestrap, A P and Davidson, A M. (1990) Inhibition of Ca^{2+}-induced large amplitude swelling of liver and heart mitochondria by cyclosporin A is probably caused by the inhibitor binding to mitochondrial matrix peptidyl-prolyl cis-trans isomerase and preventing it interacting with the adenine nucleotide translocase. Biochem J. **268**, 153–160

16 Greenawalt, J W (1979) Survey and update of outer and inner mitochondrial membrane separation Methods Enzymol **55**, 88–98

17 Zhang, H, Heim, J and Meyhack, B (1998) Redistribution of Bax from cytosol to membranes is induced by apoptotic stimuli and is an early step in the apoptotic pathway Biochem Biophys Res Commun **251**, 454–459

18 Antonsson, B, Montessuit, S, Lauper, S, Eskes, R and Martinou, J. C (2000) Bax oligomerization is required for channel-forming activity in liposomes and to trigger cytochrome *c* release from mitochondria. Biochem J **345**, 271–278

19 Poole, R C, Sansom, C E and Halestrap, A P (1996) Studies of the membrane topology of the rat erythrocyte H^+/lactate cotransporter (MCT1) Biochem. J **320**, 817–824

20 Marzulli, D, La Piana, G, Cafagno, L, Fransvea, E and Lofrumento, N E (1995) Proton translocation linked to the activity of the bi-trans-membrane electron transport chain Arch Biochem Biophys **319**, 36–48

21 Halestrap, A P, Woodfield, K. Y and Connern, C. P. (1997) Oxidative stress, thiol reagents, and membrane potential modulate the mitochondrial permeability transition by affecting nucleotide binding to the adenine nucleotide translocase J Biol Chem **272**, 3346–3354

22 Woodfield, K, Ruck, A., Brdiczka, D and Halestrap, A P (1998) Direct demonstration of a specific interaction between cyclophilin-D and the adenine nucleotide translocase confirms their role in the mitochondrial permeability transition Biochem J **336**, 287–290

23 Kroemer, G, Dallaporta, B and Resche Rigon, M (1998) The mitochondrial death/life regulator in apoptosis and necrosis. Annu Rev Physiol **60**, 619–642

24 Crompton, M., Virji, S and Ward, J M (1998) Cyclophilin-D binds strongly to complexes of the voltage-dependent anion channel and the adenine nucleotide translocase to form the permeability transition pore Eur J Biochem **258**, 729–735

25 Mangan, P. S. and Colombini, M (1987) Ultrasteep voltage dependence in a membrane channel Proc Natl Acad Sci U S A **84**, 4896–4900

26 Wicker, U, Bucheler, K, Gellerich, F N, Wagner, M., Kapischke, M. and Brdiczka, D (1993) Effect of macromolecules on the structure of the mitochondrial inter-membrane space and the regulation of hexokinase Biochim Biophys Acta **1142**, 228–239

27 Halestrap, A. P. (1987) The regulation of the oxidation of fatty acids and other substrates in rat heart mitochondria by changes in matrix volume induced by osmotic strength, valinomycin and Ca^{2+} Biochem J **244**, 159–164

28 Bakker, A, Bernaert, I, Deble, M, Ravingerova, T, Ziegelhoffer, A, Vanbelle, H and Jacob, W (1994) The effect of calcium on mitochondrial contact sites a study on isolated rat hearts. Biochim Biophys Acta **1224**, 583–588

29 Bucheler, K, Adams, V and Brdiczka, D (1991) Localization of the ATP/ADP translocator in the inner membrane and regulation of contact sites between mitochondrial envelope membranes by ADP - a study on freeze-fractured isolated liver mitochondria Biochim Biophys Acta **1056**, 233–242

30 Mcenery, M. W, Snowman, A. M, Trifiletti, R R and Snyder, S. H (1992) Isolation of the mitochondrial benzodiazepine receptor - association with the voltage-dependent anion channel and the adenine nucleotide carrier Proc Natl Acad Sci. U S A **89**, 3170–3174

31 Beutner, G, Ruck, A, Riede, B and Brdiczka, D (1998) Complexes between porin, hexokinase, mitochondrial creatine kinase and adenylate translocator display properties of the permeability transition pore. Implication for regulation of permeability transition by the kinases Biochim Biophys Acta **1368**, 7–18

32 Dejong, D, Prins, F. A, Mason, D Y, Reed, J C, Vanommen, G B. and Kluin, P. M (1994) Subcellular localization of the Bcl-2 protein in malignant and normal lymphoid cells Cancer Res **54**, 256–260

33 Marzo, I, Brenner, C and Kroemer, G (1998) The central role of the mitochondrial megachannel in apoptosis evidence obtained with intact cells, isolated mitochondria, and purified protein complexes Biomed Pharmacother **52**, 248–251

34 Mannella, C A (1998) Conformational changes in the mitochondrial channel protein, VDAC, and their functional implications. J Struct Biol **121**, 207–218

35 Vander Heiden, M G, Chandel, N S, Schumacker, P T and Thompson, C B (1999) Bcl-x(L) prevents cell death following growth factor withdrawal by facilitating mitochondrial ATP/ADP exchange Mol Cell **3**, 159–167

36 Rostovtseva, T and Colombini, M. (1996) ATP flux is controlled by a voltage-gated channel from the mitochondrial outer membrane J Biol. Chem **271**, 28006–28008

37 Priault, M, Chaudhuri, B, Clow, A, Camougrand, N and Manon, S (1999) Investigation of bar-induced release of cytochrome *c* from yeast mitochondria - permeability of mitochondrial membranes, role of VDAC and ATP requirement Eur. J Biochem **260**, 684–691

38 Bathori, G, Fonyo, A and Ligeti, E (1995) Trace amounts of Triton X-100 modify the inhibitor sensitivity of the mitochondrial porin Biochim. Biophys Acta **1234**, 249–254

39 Alder, G M, Arnold, W. M, Bashford, C L, Drake, A F, Pasternak, C A and Zimmermann, U (1991) Divalent cation-sensitive pores formed by natural and synthetic melittin and Triton X-100 Biochim Biophys Acta **1061**, 111–120

40 Crompton, M (1999) The mitochondrial permeability transition pore and its role in cell death Biochem J **341**, 233–249

41 Halestrap, A P, Kerr, P M, Javadov, S. and Woodfield, K Y (1998) Elucidating the molecular mechanism of the permeability transition pore and its role in reperfusion injury of the heart. Biochim Biophys Acta **1366**, 79–94

42 Lemasters, J J, Nieminen, A L, Qian, T, Trost, L C, Elmore, S P, Nishimura, Y, Crowe, R A, Cascio, W E, Bradham, C A, Brenner, D A and Herman, B (1998) The mitochondrial permeability transition in cell death: a common mechanism in necrosis, apoptosis and autophagy. Biochim Biophys Acta **1366**, 177–196

43 Halestrap, A P, Kerr, P J, Javadov, S and Suleiman, S (1998) The mitochondrial permeability transition role in ischemia/reperfusion injury Sepsis **2**, 313–325

44 Kerr, P. M, Suleiman, M S. and Halestrap, A P. (1999) Reversal of permeability transition during recovery of hearts from ischemia and its enhancement by pyruvate Am. J Physiol **276**, H496–H502

45 Minamikawa, T, Williams, D. A, Bowser, D N and Nagley, P (1999) Mitochondrial permeability transition and swelling can occur reversibly without inducing cell death in intact human cells. Exp Cell Res **246**, 26–37

Received 24 June 1999/29 February 2000, accepted 28 March 2000

Phosphatidylinositol 3-kinase, protein kinase B and ribosomal S6 kinases in the stimulation of thyroid epithelial cell proliferation by cAMP and growth factors in the presence of insulin

Katia COULONVAL*[1,2], Fabrice VANDEPUT†[2], Rob C. STEIN†, Sara C. KOZMA‡, Françoise LAMY* and Jacques E. DUMONT*

*Institute of Interdisciplinary Research, Free University of Brussels, Campus Erasme, Route de Lennik 808, B-1070 Brussels, Belgium,
†Ludwig Institute for Cancer Research and Department of Oncology, University College London, 91 Riding House Street,
London WIP 8BT, U.K., and ‡Friedrich Miescher Institute, Maulbeerstrasse 66, CH-4058, Basel, Switzerland

The proliferation of most normal cells depends on the co-operation of several growth factors and hormones, each with a specific role, but the key events involved in the action of each necessary stimulant remain largely uncharacterized. In the present study, the pathways involved in the mechanism(s) of co-operation have been investigated in primary cultures of dog thyroid epithelial cells. In this physiologically relevant system, thyroid stimulating hormone (TSH) acting through cAMP, epidermal growth factor (EGF) and phorbol esters (such as PMA) induce DNA synthesis. Their effect requires stimulation of the insulin-like growth factor-1 (IGF-1) receptor by either IGF-1 or insulin, which are not themselves mitogenic agents. In contrast, hepatocyte growth factor (HGF) is itself fully mitogenic. The results of the study demonstrate that cAMP, EGF, HGF and PMA stimulate p70 ribosomal S6 kinase (p70 S6 kinase). However, insulin/IGF-1 also stimulate p70 S6 kinase. Thus stimulation of p70 S6 kinase might be necessary, but is certainly not sufficient, for the induction of DNA synthesis and is not specific for any stimulated pathway. In contrast, phosphatidylinositol 3-kinase (PI 3-kinase) and protein kinase B (PKB) activation by insulin and HGF is strong and sustained, whereas it is weak and transient with EGF and absent in the presence of TSH or PMA. These findings suggest that: (i) stimulation of PI 3-kinases and/or PKB is not involved in the cAMP-dependent pathways leading to thyrocyte proliferation, or in the action of PMA, (ii) the stimulation of the PI 3-kinase/PKB pathway may account for the permissive action of insulin/IGF-1 in the proliferation of these cells, and (iii) the stimulation of this pathway by HGF may explain why this agent does not require insulin or IGF-1 for its mitogenic action.

Key words: DNA synthesis, hepatocyte growth factor, rapamycin, thyrotropin, wortmannin.

INTRODUCTION

The regulation of cell proliferation has been much studied in cell lines. Such models are only distantly related to normal cells. Moreover, the roles of the various pathways studied have been found to be different, or even the converse, in one cell type and another. In the study of physiological control it is, therefore, essential to establish the regulatory network of each normal cell type. Some form of co-operation is generally needed between different growth factors in order to achieve the stimulation of division of normal cells. In particular, the almost ubiquitous activity of insulin-like growth factor 1 (IGF-1) in supporting cell proliferation triggered by growth factors is illustrated by the almost universal requirement of IGF-1 or high concentrations of insulin [1] as a supplement in serum-free culture media for most normal cell types [1–3]. The positive role of cAMP in cell cycle progression provides interesting examples of such a co-operation in many different epithelial cells [4]. The mechanism(s) of this co-operation is unclear, mainly because the key events involved in each signalling cascade have not been delineated. In this study, we have investigated the role of phosphatidylinositol 3-kinase (PI 3-kinase), protein kinase B (PKB) and p70 ribosomal protein S6 kinase (p70 S6 kinase) in this regard. Activation of p70 S6 kinase is involved in the regulation of both protein and DNA synthesis. p70 S6 kinase was identified on the basis of its ability to phosphorylate the 40 S ribosomal protein S6 *in vitro* [5]. A number of other kinases, including the growth-regulated 90 kDa ribosomal S6 kinase (p90 S6 kinase), which is phosphorylated and activated by the p42/p44 mitogen-activated protein kinases (MAPKs), can also phosphorylate S6 in *in vitro* systems, but it has been shown that, in the cell, this function is mostly performed by p70 S6 kinase [5,6]. S6 phosphorylation is thought to increase the rate of synthesis of certain proteins which are required for efficient G_1 progression and whose mRNAs contain a polypyrimidine tract at the 5′ end [5]. p70 S6 kinase has been suggested to play an essential role throughout G_1, as its inhibition by microinjection of neutralizing antibodies [5] or by the immunosuppressant rapamycin severely compromised the ability of various types of cells to progress through the G_1 phase of the cell cycle [7]. Complexed to FK506-binding-protein ('FKBP'), rapamycin interacts with the mammalian target of rapamycin (mTOR) and blocks the activation of p70 S6 kinase in response to all stimuli so far studied [7,8]. p70 S6 kinase activation in response to stimuli requires a hierarchical phosphorylation at multiple serine/threonine sites [8,9]. A role for PI 3-kinase and protein kinase B (PKB) in this activation has been suggested but remains controversial and probably depends on the nature of the agonist and of the cell type [8,10–12]. PKB itself is a direct target of PI 3-kinase although it can also be activated by PI 3-kinase independent pathways [13,14].

Abbreviations used: IGF-1, insulin-like growth factor 1; PI 3-kinase, phosphatidylinositol 3-kinase; PKB, protein kinase B; p70 S6 kinase, p70 ribosomal S6 kinase; p90 S6 kinase, p90 ribosomal S6 kinase; MAPK, mitogen-activated protein kinase; TSH, thyroid stimulating hormone; PKA, protein kinase A; EGF, epidermal growth factor; HGF, hepatocyte growth factor; mTOR, mammalian target of rapamycin.

[1] To whom correspondence should be addressed (e-mail kcoulonv@ulb.ac.be).

[2] These authors made equal contributions to this study.

Dog thyroid follicular cells (thyrocytes) in primary culture are representative of their *in vivo* counterpart [15]. In these cells, cAMP, as a second messenger for thyrotropin (thyroid stimulating hormone; TSH), positively controls proliferation and differentiation through pathways that require protein kinase A (PKA) activity and other mechanisms [15,16]. DNA synthesis can also be induced through cAMP-independent mechanisms, in response to epidermal growth factor (EGF), hepatocyte growth factor (HGF) and phorbol esters, coinciding with an inhibition of differentiation [15]. The mitogenic effects of TSH, EGF and PMA, but not those of HGF, require IGF-1 receptor stimulation by IGF-1 or high concentrations of insulin [17,18]. In themselves, IGF-1 and insulin have little mitogenic action As the real physiological stimulator of thyroid cells is TSH, the role of insulin/IGF-1 is described as permissive for TSH and thus, by extension, for EGF and PMA action. Until now the mechanism of the permissive effect of insulin/IGF-1 has been little studied.

Whereas signalling pathways stimulated by growth factors acting on receptor tyrosine kinases or on protein kinase C have been relatively well delineated, little is known about those stimulated by cAMP. In an earlier study we have shown that stimulation of dog thyrocytes by TSH did not result in the activation of any member of the MAPK family ([19,20]; F. Vandeput, unpublished work), suggesting a distinct signalling pathway. Recent studies using cell lines demonstrated stimulation of PKB by cAMP [13,21].

In the present work, in order to unravel the mechanism(s) of co-operation leading to cell proliferation, we have studied the effect of TSH acting through cAMP and of growth factors acting through receptor tyrosine kinases (insulin/IGF-1, EGF, HGF) or through protein kinase C (PMA) on the activities of p70 and p90 S6 kinases, PKB and PI 3-kinase in primary cultures of dog thyroid cells.

EXPERIMENTAL

Materials

Dulbecco's modified Eagle's medium (DMEM), Ham's F12 medium, MCBD104 medium, penicillin, streptomycin and amphotericin B (Fungizone) were obtained from GIBCO (Paisley, Scotland, U.K.) Bovine insulin, PMA, murine EGF and bovine TSH were purchased from Sigma Chemical Co. (St Louis, MO, U.S.A). Forskolin was from Calbiochem (La Jolla, CA, U.S.A.). Human recombinant HGF (hrHGF) was a gift from T. Nakamura and K. Matsuto (Osaka University Medical School, Osaka, Japan). Rapamycin and wortmannin were gifts from Wyeth-Ayerst Research (Princeton, CN, U.S.A.) and Sandoz Pharma Ltd. (Basel, Switzerland) respectively. Wortmannin was also purchased from Sigma, as well as LY294002 and PtdIns. The p70 S6 kinase antibodies used were raised against the N-terminal (amino acids 1–31) [22] or the C-terminal peptide sequence specific for p70 S6 kinase (amino acids 485–502) (C-18; Santa Cruz Biotechnology, Santa Cruz, CA, U.S.A.) of rat p70 S6 kinase. Polyclonal antibodies to p90 S6 kinase (C-21), pRb (C-15), p107 (C-18) and p130 (C-20) were purchased from Santa Cruz Biotechnology, polyclonal antibodies to PKB were from Upstate Biotechnology (Lake Placid, NY, U.S.A.), and anti-phosphotyrosine monoclonal antibody (PY20) from Transduction Laboratories (Lexington, KY, U.S.A.). The S6 substrate and PKA inhibitor peptides were supplied by Santa Cruz Biotechnology, the crosstide peptide by Upstate Biotechnology. Secondary antibodies, enhanced chemiluminescence reagents, [^{32}P]P$_i$, [γ-^{32}P]ATP and [^{3}H]thymidine were from Amersham International (Little Chalfont, Bucks., U.K.). Protein A–Sepharose CL4B and Protein G were purchased from Pharmacia, and phosphocellulose (Whatman P-81) was from Whatman (Maidstone, Kent, U.K.). Silica gel 60 aluminium TLC plates were obtained from Merck.

Primary culture

Cells were obtained from dog thyroid tissue as detailed previously [15]. Thyrocytes were cultured in monolayer (2×10^4 cells/cm^2) in the following medium · Dulbecco's modified Eagle's medium/Ham's F12 medium/MCBD 104 medium (2:1:1, by vol.) supplemented with 40 μg/ml ascorbic acid, antibiotics, and with or without insulin (5 μg/ml). After culture for 4 days, the cells were stimulated for various periods of time by different agents. In some cases, cells were treated with rapamycin (2 mM stock in ethanol), wortmannin (10 μM stock in DMSO) or LY294002 (5 M stock in DMSO) for 30 min before activation.

DNA synthesis

After 4 days of culture in the absence or presence of insulin (5 μg/ml), dog thyroid cells were incubated for 48 h with the mitogenic agents and with [^{3}H]thymidine (10 μCi/ml, 3×10^{-6} M) and deoxycytidine (10^{-4} M) for the final 24 h. The number of cells entering into DNA synthesis was estimated by the frequency of [^{3}H]thymidine-labelled nuclei, as revealed by autoradiography. In each duplicate dish, at least 1000 nuclei chosen at random in different fields were counted blind [15].

S6 kinases assay

p70 S6 kinase and p90 S6 kinase activities were measured as described previously [22], except that 100 μM RRRLSSLRA peptide was used as substrate [23], and the reaction was terminated by the addition of acetic acid to a final concentration of 30%. The amount of ^{32}P-label incorporated into the peptide substrate was determined by scintillation spectroscopy [24]. Controls were processed similarly in the absence of protein kinase. Protein determinations were performed as described previously [25] with BSA as standard.

PKB assay

After stimulation, the cells were solubilized in a buffer composed of 120 mM NaCl, 25 mM Tris/HCl (pH 7.6), 50 mM NaF, 1 mM benzamidine, 1mM EDTA, 15 mM sodium pyrophosphate, 1 mM EGTA, 20 mM 2-glycerophosphate, 2 mM Na_3VO_4, 0.5% sodium deoxycholate, 1% (v/v) Nonidet P-40, 60 μg/ml Pefabloc, 100 mM okadaic acid and 10 μg/ml each of leupeptin and pepstatin. Samples containing 200 μg protein were subjected to immunoprecipitation using a polyclonal antibody against PKB coupled to Protein G–Sepharose. After washing the immunoprecipitates four times with 50 mM Tris/HCl (pH 7.5), 50 mM NaF, 1 mM EDTA, 5 mM sodium pyrophosphate, 1 mM EGTA, 10 mM 2-glycerophosphate, 1 mM Na_3VO_4, 0.1% (v/v) Triton X-100, and twice with kinase buffer [20 mM Mops (pH 7.2), 5 mM EGTA, 25 mM 2-glycerophosphate, 1 mM dithiothreitol, 1 mM Na_3VO_4], kinase activity was assayed in a final volume of 30 μl kinase buffer containing 50 μM ATP, 75 mM $MgCl_2$, 30 μM crosstide peptide, 17 μM protein kinase A inhibitor and 3 μCi [γ-^{32}P]ATP. The phosphorylation reaction was allowed to proceed for 15 min at 30 °C The amount of ^{32}P incorporated into the peptide substrate was determined by scintillation spectroscopy as described previously.

PI 3-kinase assay

PI 3-kinase activity was measured on anti-phosphotyrosine immune complexes essentially as described previously [26]. The reactions were initiated by the addition of 50 μM ATP, 5 mM $MgCl_2$ and 2 μCi [γ-^{32}P]ATP (final concentrations) and stopped after 20 min at 30 °C with 15 μl of 4 M HCl and 250 μl of chloroform/methanol (1:1, v/v). The lower organic phase was washed with 150 μl of methanol/1 M HCl (1:1, v/v) and dried. Phospholipids were resuspended in 10 μl of chloroform, separated by TLC on aluminium-backed silica gel 60 plates pretreated with 1 % potassium oxalate in the solvent system chloroform/methanol/acetone/acetic acid/water (60:20:23:18:11, by vol.) and detected by autoradiography.

Gel electrophoresis and immunodetection of proteins

At the end of the culture period, total cellular proteins were separated according to molecular mass by SDS/PAGE (6.5 % gel) and immunodetected after Western blotting as described previously [25]. Immunoblots were developed using ^{125}I-labelled Protein A or the ECL® kit (Amersham) and subjected to autoradiography.

Analysis of intracellular levels of 3-phosphorylated phosphoinositides

Production of 3-phosphorylated lipids *in vivo* was determined essentially as described previously [27,28]. Briefly, thyroid cells were prelabelled with [^{32}P]P_i (0.3 mCi/ml) for 3 h and then stimulated for various periods of time with the appropriate agents. Cells were scraped into 1 M HCl and phospholipids were extracted into HCl/methanol/chloroform (47:48:3, by vol.) in the presence of 25 mM EDTA, butylated hydroxytoluene antioxidant and 30 μg of a mixture of brain phosphoinositides. The phospholipids were then converted to water-soluble deacylated derivatives [28], separated on a Partisphere SAX (Whatman) HPLC column and the radioactivity was estimated [29].

RESULTS

Rapamycin and wortmannin inhibit DNA synthesis

To investigate the role of mTOR/p70 S6 kinase and PI 3-kinase activation in the pathways leading to thyroid cell proliferation, the effect of inhibitors of these enzymes on DNA synthesis has been studied. Table 1 shows that rapamycin and wortmannin substantially reduced DNA synthesis in cells stimulated by TSH, forskolin, EGF, HGF or PMA in the presence of insulin, as in control cells. Figure 1 represents an experiment in which both rapamycin and wortmannin strongly decreased mitogen-induced proliferation of dog thyrocytes, coincident with the prevention of the hyperphosphorylation of pRb, p107 and p130, as demonstrated by the lack of appearance of the slower migrating form(s) of the proteins. This finding is in agreement with our previous study where we showed that the extent of hyperphosphorylation of these proteins correlated well with the actual induction of DNA synthesis by the mitogenic agents tested [25]. This inhibition is not a consequence of an up-regulation of the cyclin dependent kinase (cdk)-inhibitor p27^{kip1} as no change in its level of expression was observed after treatment of the cells with wortmannin or rapamycin (not shown). Table 1 also shows that wortmannin provoked a strong inhibition of the DNA synthesis induced by HGF in the absence of insulin in the culture medium. Table 2 shows that the inhibition by rapamycin or wortmannin of DNA synthesis was still present when these inhibitors were added 12 h after the stimulatory agents, i.e. during the second part of the prereplicative phase (DNA synthesis starts after 16 to 18 h) [30].

Table 1 Inhibition of DNA synthesis in thyrocytes by rapamycin and wortmannin

After 4 days of culture in medium supplemented with or without (*) 5 μg/ml insulin, the cells were untreated or preincubated with 20 nM rapamycin or 100 nM wortmannin for 30 min before the addition of the various reagents for 48 h. During this time, because of the transient effect of wortmannin, 100 nM was added every 12 h up to 400 nM [48,49]. [^{3}H]Thymidine was present for the last 24 h. Results are means ± S.D. of at least three different experiments performed in duplicate with similar results.

	Labelled nuclei (%)		
Reagent	No pretreatment	Repamycin	Wortmannin
Control	11.3 ± 4.4	0.8 ± 0.5	0.3 ± 0.3
TSH (1 m-unit/ml)	52.4 ± 15.9	23.4 ± 9.5	13.1 ± 5.2
Forskolin (10^{-5} M)	63.4 ± 7.5	25.6 ± 6.7	11.9 ± 3.8
EGF (25 ng/ml)	51.2 ± 2.5	12.7 ± 2.0	28.0 ± 10.3
PMA (10 ng/ml)	41.2 ± 6.1	3.2 ± 3.1	7.3 ± 3.1
HGF (50 ng/ml)	69.9 ± 3.4	21.9 ± 2.5	23.4 ± 1.4
*Control	1.2 ± 0.6	–	0.2 ± 0.3
*HGF (50 ng/ml)	33.5 ± 4.5	–	1.4 ± 0.5

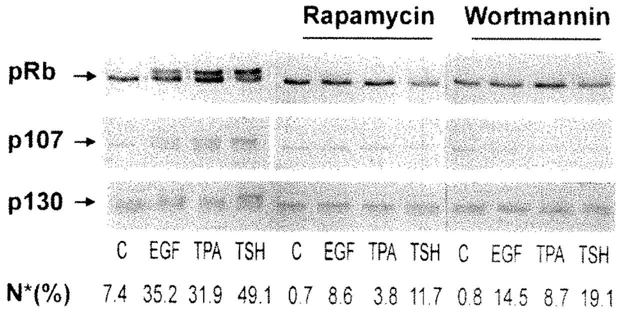
Rapamycin
Wortmannin
pRb →
p107 →
p130 →
C EGF TPA TSH C EGF TPA TSH C EGF TPA TSH
N*(%) 7.4 35.2 31.9 49.1 0.7 8.6 3.8 11.7 0.8 14.5 8.7 19.1

Figure 1 Inhibition of pRb, p107 and p130 phosphorylation by rapamycin and wortmannin

Anti-pRb, -p107, -p130 immunoblots of whole cell extracts. Dog thyrocytes were cultured for 4 days in basal medium supplemented with 5 μg/ml insulin. They were then pretreated with 20 nM rapamycin or 100 nM wortmannin for 30 min prior to stimulation by EGF (25 ng/ml), PMA (TPA; 10 ng/ml) or TSH (1 m-unit/ml) for 24h or remained in control condition (C). A second addition of wortmannin was made 12 h later. A 40 μg sample of total cellular proteins was loaded per lane. Arrows indicate the position of the hypophosphorylated form of pRb and p107, and of the faster migrating hypophosphorylated form of p130. In the same representative experiment, the proportion (%) of [^{3}H]thymidine labelled nuclei was determined in duplicate with similar results for each experimental condition (N*).

Table 2 Inhibition of DNA synthesis in dog thyrocytes by later addition of rapamycin and wortmannin

After 4 days of culture in medium supplemented with 5 μg/ml insulin, thyrocytes were stimulated by various reagents for 48 h with or without 20 nM rapamycin or 400 nM wortmannin, which were added 12 h later. [^{3}H]Thymidine was present for the final 24 h. The results are the means ± S.D. of at least three different experiments performed in duplicate with similar results.

	Labelled nuclei (%)		
	No pretreatment	Rapamycin	Wortmannin
Control	9.9 ± 2.5	0.8 ± 0.4	0.9 ± 0.7
EGF (25 ng/ml)	36.2 ± 1.0	11.7 ± 3.3	12.8 ± 0.4
PMA (10 ng/ml)	28.7 ± 3.2	4.8 ± 2.5	6.1 ± 1.8
TSH (1 m-unit/ml)	47.9 ± 1.1	14.4 ± 4.1	18.4 ± 0.4

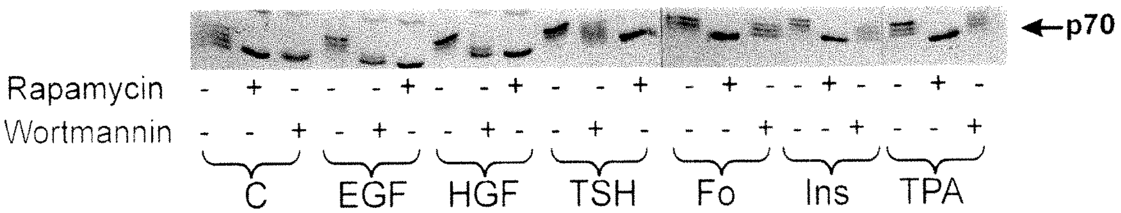
p70
Rapamycin - + - - - + - - + - - + - + - - + - - + -
Wortmannin - - + - + - - + - - + - - - + - - + - - +
C
EGF
HGF
TSH
Fo
Ins
TPA

Figure 2 Increase of p70 S6 kinase electrophoretic mobility by rapamycin and wortmannin

Anti-p70 S6 kinase immunoblots of whole cell extracts. After 4 days of culture in the absence of insulin, the thyrocytes were pretreated or not with 20 nM rapamycin or 100 nM wortmannin for 30 min prior to exposure to EGF (25 ng/ml), PMA (TPA; 10 ng/ml), TSH (1 m-unit/ml), forskolin (Fo) (10^{-5} M), HGF (50 ng/ml) or insulin (5 μg/ml) for 30 min or remained in control condition (C). A 50 μg sample of total cellular proteins was loaded per lane. The arrow indicate the position of the hypophosphorylated form of p70 S6 kinase.

Table 3 Incorporation of [^{3}H]thymidine into the nuclei of thyrocytes cultured in the absence of insulin

After 4 days of culture in medium lacking insulin, thyrocytes were preincubated with 100 nM wortmannin or 15 μM LY294002 for 30 min before the incubation with various agents for 48 h. During this time, because of the transient effect of wortmannin, 100 nM was added every 12 h, up to 400 nM. [^{3}]Thymidine was present for the final 24 h. The results are the means ± S.D. of data from at least three independent experiments performed in duplicate with similar results.

Reagent	Labelled nuclei (%)
Control	3.6 ± 3.1
Insulin (5 μg/ml)	13.3 ± 4.1
TSH (1 m-unit/ml)	13.9 ± 5.3
Forskolin (10^{-5} M)	8.7 ± 1.8
PMA (10 ng/ml)	3.9 ± 3.6
EGF (25 ng/ml)	5.7 ± 4.5
HGF (50 ng/ml)	32.9 ± 11.2
TSH + insulin	45.0 ± 9.5

Table 4 Effect of various reagents, and influence of rapamycin, wortmannin and LY294002 on p70 S6 kinase activity

After 4 days of culture in the absence of insulin, dog thyrocytes were preincubated with 20 nM rapamycin, 100 nM wortmannin or 15 μM LY294002 for 30 min before incubation with various reagents for 30 min. The results of p70 S6 kinase assays are presented as fold stimulation above control and are means ± S.E.M. of three independent experiments. p70 S6 kinase activity in control cells was 4.41 ± 0.70 units/mg of protein when an S6 peptide was used as substrate.

	p70 S6 kinase activity			
Reagent	No pretreatment	Rapamycin	Wortmannin	LY294002
Control	1.00	0.01 ± 0.01	0.11 ± 0.06	0.16 ± 0.09
Insulin (5 μg/ml)	3.62 ± 0.17	–	0.25 ± 0.07	1.52 ± 0.19
TSH (1 m-unit/ml)	2.29 ± 0.14	0.05 ± 0.06	0.67 ± 0.05	0.19 ± 0.03
Insulin + TSH	3.54 ± 0.22	–	0.63 ± 0.29	1.01 ± 0.21
Forskolin (10^{-5} M)	2.28 ± 0.22	–	1.03 ± 0.24	0.30 ± 0.05
EGF (25 ng/ml)	2.65 ± 0.15	0.14 ± 0.01	0.30 ± 0.09	0.60 ± 0.16
PMA (10 ng/ml)	2.58 ± 0.24	0.01 ± 0.01	1.06 ± 0.09	0.92 ± 0.22
HGF (50 ng/ml)	3.37 ± 0.30	–	–	–

Effect of different agents on p70 and p90 S6 kinase activities

Dog thyrocytes in culture require a high insulin concentration for most mitogens to induce DNA synthesis [15]. The effect of these agents acting alone on p70 S6 kinase activation was assessed from p70 S6 kinase immunoblots of total cell lysates, by the relative mobility of this protein following SDS/PAGE (Figure 2), reflecting different degrees of p70 S6 kinase phosphorylation [9]. Before stimulation, thyrocytes were cultured for 4 days in the absence of insulin. In these culture conditions, the agents have little to no mitogenic effect, except HGF whose action on proliferation does not require the presence of insulin (Table 3). Figure 2 shows that in control cells four forms of p70 S6 kinase can already be distinguished, the faster migrating one being the most abundant. Both cAMP-independent agents (EGF, HGF, insulin and PMA) and cAMP-dependent agents provoked a retardation in the migration of p70 S6 kinase, the slowest migrating band corresponding to the catalytically active enzyme [9]. The presence of a small amount of fully phosphorylated p70 S6 kinase in control cells could result from a small activation of this enzyme following attachment and spreading of thyroid cells on Petri dishes [31]. Inhibition of p70 S6 kinase phosphorylation by rapamycin or wortmannin was reflected by the decreased intensity of the slower electrophoretic mobility band of the kinase and by the corresponding increase of intensity of the faster migrating band (Figure 2).

In order to assess the potency of the different agents studied on p70 or p90 S6 kinase activity, *in vitro* kinase assays were performed using immunoprecipitates of these enzymes from control or stimulated cells. Table 4 shows that (i) insulin and HGF are the most potent activators of p70 S6 kinase activity in these cells (3.62 and 3.37 fold respectively); (ii) TSH, EGF and PMA stimulate p70 S6 kinase activity to about the same extent (2.29, 2.65 and 2.58 fold respectively); (iii) stimulation by TSH of p70 S6 kinase activity is reproduced by forskolin, a general activator of adenylate cyclase; (iv) simultaneous addition of TSH and insulin resulted in a comparable activation to that obtained with insulin alone (3.54 fold). This is in contrast with the results of Withers et al. [32] who observed, in Swiss 3T3 cells, that the mitogenic combination of forskolin and insulin induced an additive stimulation of p70 S6 kinase activity. Time course experiments revealed that TSH or EGF induced a biphasic activation of p70 S6 kinase, peaking after about 30 and 120 min (not shown). The enzyme activity was already increased after 5 min and remained over control for at least 8 h (not shown). On the other hand, in accordance with our results on MAPK phosphorylation [18,20,33] all these agents except TSH and forskolin stimulate p90 S6 kinase activity, EGF, HGF and PMA having about the same potency, insulin being the weakest stimulator (Table 5). Moreover, TSH did not affect the stimulation, by insulin, of the p90 S6 kinase activity (Table 5). These results thus confirm that in dog thyroid cells, in contrast to many other cell types [34,35], cAMP had no inhibitory or stimulatory effect on the MAPK/p90 S6 kinase pathway. Rapamycin (20nM) lowered the basal level of p70 S6 kinase activity in control cells and almost totally abolished p70 S6 kinase activation by TSH,

Table 6 Effect of various reagents on p90 S6 kinase activity

After 4 days of culture in the absence of insulin, thyrocytes were stimulated with various reagents for 20 min. The results of p90 S6 kinase assays are presented as fold stimulation above control and are means ± S.E.M. of three independent experiments. p90 S6 kinase activity in control cells was 7.82 ± 0.92 units/mg of protein when an S6 peptide was used as substrate.

Reagent	p90 S6 kinase activity
Control	1.00
TSH (1 m-unit/ml)	0.88 ± 0.05
Forskolin (10^{-5} M)	0.82 ± 0.12
EGF (25 ng/ml)	2.99 ± 0.76
HGF (50 ng/ml)	2.54 ± 0.50
PMA (10 ng/ml)	2.36 ± 0.51
Insulin (5 μg/ml)	2.06 ± 0.12
Insulin + TSH	2.16 ± 0.12

EGF or PMA (Table 4). The effect of wortmannin and of LY294002, was also investigated on p70 S6 kinase activity. Although treatment of the cells with LY294002 (15 μM) resulted, as with wortmannin (100 nM), in the inhibition of p70 S6 kinase activity in control cells as well as in cells stimulated by the different agents, LY294002 seemed to be a more potent inhibitor than wortmannin of the cAMP dependent activation of p70 S6 kinase and a lesser one of the insulin activation of this kinase (Table 4). These observations have still no explanation. In any case these inhibitions suggest the implication of PI 3-kinase upstream of p70 S6 kinase. It is worth noting that there are some discrepancies between our data and those obtained by Cass and Meinkoth [36] and Cass et al. [37] in the WRT cell line as, in these cells, inhibition of the cAMP dependent p70 S6 kinase was obtained with 15 μM LY294002 but not with 200 nM wortmannin.

Agents acting through receptor tyrosine kinases, but not TSH or PMA, stimulate PKB activity

As it is generally accepted that PKB is a primary downstream target of the different isoforms of PI 3-kinase [10,38], we investigated the activity of this kinase in dog thyrocytes. The cells were cultivated for 4 days without insulin before the addition of the different stimulating agents. PKB activity was measured in immune-complex assays using the crosstide peptide as substrate. Figure 3(A) showed that after 8 min of stimulation, PKB activity was increased by insulin, HGF and EGF. Insulin and HGF were the most potent stimulating agents (respectively 7.5 and 6.9 fold), followed by EGF (3.5 fold), while PMA and forskolin were without effect. The very small stimulation of PKB activity observed in the presence of TSH (1.2 fold) did not depend upon the intracellular increase in cAMP as forskolin, a general activator of adenylate cyclase, had no effect on the activity of this enzyme. Treatment of thyrocytes with wortmannin (100 nM), added to the culture medium prior to stimulation of the cells by insulin, EGF or HGF, inhibited the activity induced by these agents. As expected, rapamycin (20 nM) was without effect on PKB activation. Stimulation, by insulin, EGF and HGF, of PKB activity was rapid as it was already noticed at the first time point studied (2 min), but the duration of the EGF action was much more transient than that of insulin and HGF, which induced PKB activation for at least 4 h (Figure 3B). The kinetic analysis also showed that TSH or forskolin did not enhance PKB activity at any time point studied from 2 min to 4 h. There was a good correlation between these results and the effect of the different agents on PKB mobility observed in immunoblotting experiments (not shown).

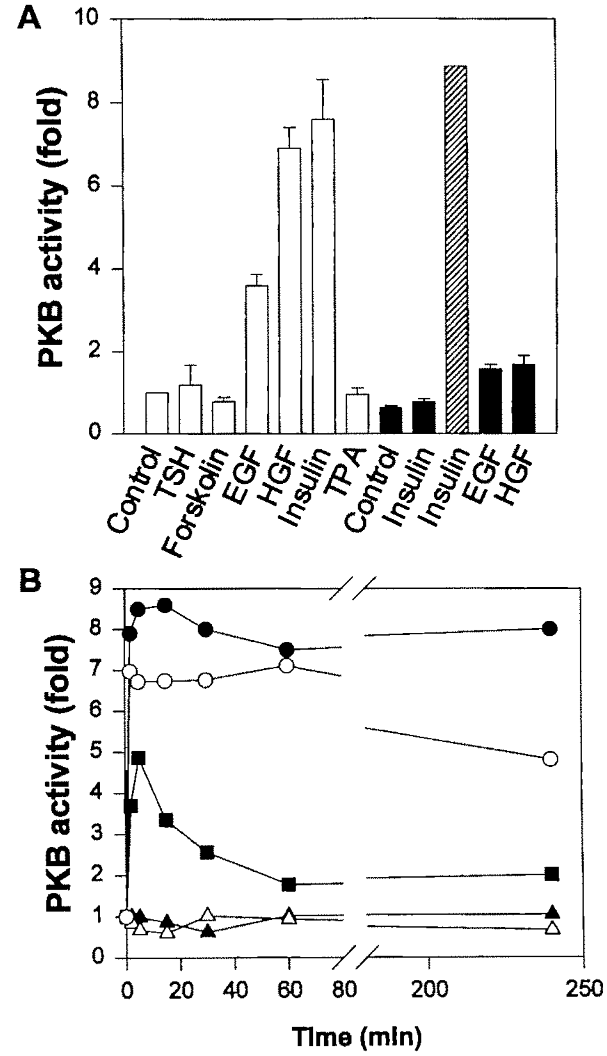

Figure 3 Agents acting through receptor tyrosine kinases but not TSH or PMA stimulate PKB activity

After 4 days of culture in the absence of insulin, dog thyroid cells were stimulated (**A**) for 8 min with insulin (5 μg/ml), TSH (1 mU/ml), forskolin (10^{-5} M), EGF (25 ng/ml), HGF (50 ng/ml) or PMA (TPA, 10 ng/ml) or (**B**) for the indicated times with insulin, ●, HGF, ○, EGF, ■, TSH, ▲, or forskolin, △. Where indicated in (**A**), the cells were pretreated with 100 nM wortmannin (filled bars) or 20 nM rapamycin (hatched bar) for 30 min. PKB activity was determined in an *in vitro* kinase assay as described in the Experimental section using crosstide as a substrate. Results are presented as fold stimulation above control, and are a representative (**B**) or means ± S.D. of at least three independent experiments (**A**).

Evaluation of PI 3-kinase activity *in vitro*

The PI 3-kinase activity was assayed by the capacity of the enzyme found in anti-phosphotyrosine immunoprecipitates to phosphorylate PtdIns (Figure 4). Its activity was significantly increased in the anti-phosphotyrosine immunoprecipitates from thyrocytes treated for 5 min with either insulin, HGF or EGF (Figure 4A). The effect of EGF on this activity was much weaker than that of insulin or HGF. All three agents were also shown to

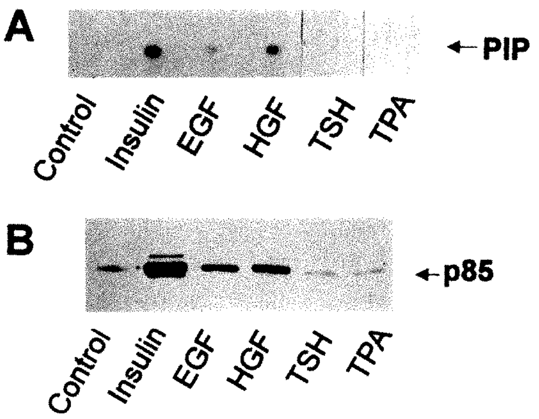

Figure 4 Agents acting through receptor tyrosine kinases but not TSH or PMA stimulate PI 3-kinase activity

After 4 days of culture in the absence of insulin, dog thyroid cells were stimulated for 5 min with insulin (5 μg/ml), EGF (25 ng/ml), TSH (1 m-unit/ml) or PMA (10 ng/ml) (TPA). Cells lysed using 1% (v/v) Nonidet-P40 were immunoprecipitated with an anti-phosphotyrosine antibody. (**A**) Precipitates were assayed for PI 3-kinase activity (see the Experimental section) and the ^{32}P-labelled lipid products were separated by TLC. PIP, PtdIns3*P*. (**B**) Precipitates were subjected to Western-blot analysis to determine the relative amount of p85α.

Table 6 Abundance of PtdIns(3,4,5)P_3 in thyroid cells stimulated by various reagents

After 4 days of culture in the absence of insulin, dog thyroid cells were prelabelled with [^{32}P]P$_i$ (0.3 mCi/ml) for 3 h and stimulated for various periods of time with the appropriate reagents. Lipids were extracted and analysed as described in the Experimental section. The results are means of duplicate determinations in one representative experiment, and are expressed as a percentage of the total radioactivity. Similar results were obtained in one other experiment. N.D., below the limit of detection.

Reagent	Time	PtdIns(3,4,5)P_3
Control	–	0.064 ± 0.006
TSH (1 m-unit/ml)	2 min	0.032
	8 min	0.017
	30 min	0.030
Forskolin (10^{-5} M)	2 min	N.D.
	8 min	N.D.
Insulin (5 μg/ml)	2 min	0.245 ± 0.004
	8 min	0.180 ± 0.014
EGF (25 ng/ml)	2 min	0.131 ± 0.018
	8 min	0.070 ± 0.009
HGF (50 ng/ml)	2 min	0.161 ± 0.019
	8 min	0.158
PMA (10 ng/ml)	2 min	0.078 ± 0.016
	8 min	0.055 ± 0.007

increase the amount of p85α on Western blots of anti-phosphotyrosine immunoprecipitated material (Figure 4B), insulin being the most potent agent, followed by HGF, EGF being the weakest one. These results are consistent with the magnitude of the effect of these agents on PKB activity, and suggest that PI 3-kinase plays a minor role in EGF receptor-mediated signal transduction in dog thyrocytes. Figures 4(A) and 4(B) also show that we were unable to detect any PI 3-kinase activity or the presence of p85α in anti-phosphotyrosine immunocomplexes from cells treated with TSH or PMA. This is in agreement with the absence of PKB stimulation by these agents (Figure 3).

Agents acting through receptor tyrosine kinases but not TSH or PMA stimulate the production of 3-phosphoinositides *in vivo*

To establish with certainty the lack of effect of TSH or PMA on the activity of any isoform of PI 3-kinase, intracellular levels of 3-phosphorylated phosphoinositides were analysed. This approach does not rely on any assumptions about how receptors may cause the increased formation of 3-phosphorylated phosphoinositides. Thyroid cells were prelabelled with [^{32}P]P$_i$ for 3 h and then stimulated with the different agents for 2 or 8 min. In the case of TSH, an additional time point (30 min) has been investigated as the increase in intracellular cAMP caused by this agent is maximal after about 30 min (results not shown). At the end of the culture, ^{32}P-labelled lipids were extracted, converted to water-soluble deacylated derivatives and quantified by HPLC. As generally accepted, we make the assumption that changes in the ^{32}P content of the ^{32}P-labelled phosphoinositides reflect changes in their concentrations. Table 6 shows that insulin and HGF are very good stimuli of PI 3-kinase and that EGF is a weaker one. The increases in the level of [^{32}P]PtdIns(3,4,5)P_3 in response to both insulin and HGF were observed after 2 min and were still present after 8 min of action of these agents, whereas the effect of EGF appeared quite transient, with PtdIns(3,4,5)P_3 levels almost returning to those of the control by 8 min. Insulin also provoked a measurable accumulation of [^{32}P]PtdIns(3,4)P_2 observed after 2 as well as after 8 min of action of the hormone (not shown). By contrast, PMA, TSH and forskolin did not increase the level of [^{32}P]PtdIns(3,4,5)P_3. TSH and forskolin seemed to even reduce its basal formation.

DISCUSSION

The aim of our work was to delineate the steps of the cascades leading to thyroid cell proliferation. In our study we show that in dog thyrocytes, p90 S6 kinase is only stimulated by cAMP-independent agents. This pattern of stimulation of p90 S6 kinase is similar to the one observed for MAPK activation [18,20,33] which agrees with and supports, in the case of the thyroid cell, the concept that p90 S6 kinase participates in Ras/MAPK-mediated signal transduction [6]. The absence of stimulation of this pathway by the cAMP cascade shows that such a stimulation is not necessary for mitogenicity.

cAMP-induced stimulation of p70 S6 kinase activity has been previously reported by Withers et al. [32] in the Swiss 3T3 cell line and by Cass et al. [36,37] in the WRT cell line. In this work, we show by mobility shift and immune-complex kinase assays that, in primary cultures of dog thyroid cells, which represent the best studied physiological model of the cAMP pathway, p70 S6 kinase is indeed phosphorylated and activated by the cAMP-dependent agents, TSH and forskolin, and also by the cAMP-independent agents, EGF, HGF, PMA or insulin, although among them only HGF is mitogenic by itself. In dog thyroid cells, p70 S6 kinase activation thus represents the first common step of all the signalling pathways involved in proliferation: the mitogenic pathways which require insulin action (TSH, forskolin, EGF, PMA), the permissive but non-mitogenic insulin pathway, and the fully mitogenic pathway (HGF).

The first approach to identify participants in the mTOR/p70 S6 kinase pathway was to use the inhibitors rapamycin and wortmannin or LY294002 which have been reported to be specific inhibitors of mTOR [7] and of PI 3-kinase [39] respectively. In agreement with the results obtained in other cell types [7], we have found that rapamycin almost completely blocked the basal phosphorylation and activity of p70 S6 kinase as well as its stimulation by the different agents acting on dog thyroid cells. Wortmannin and LY294002 also decreased cAMP-independent and cAMP-dependent phosphorylation and activation of p70 S6 kinase in these cells, although the cAMP-dependent p70 S6 kinase activity was only partially reduced by wortmannin in the WRT cell line [37]. The inhibition by wortmannin, LY294002 and rapamycin of p70 S6 kinase activity stimulated by TSH, forskolin, EGF, HGF and PMA suggested that PI 3-kinase(s) and mTOR reside in the pathways controlled by all these agents leading to p70 S6 kinase stimulation. Moreover, mTOR and PI 3-kinase seem to be necessary to induce the transition of quiescent cells through G_1 into S phase as rapamycin and wortmannin, even added late in G_1, induced a marked decrease of the [^{3}H]thymidine incorporation into nuclei and the prevention of the hyperphosphorylation of pRb and its related family members p107 and p130. As mTOR has been shown to have other substrates than p70 S6 kinase [40,41], we cannot confirm that p70 S6 kinase plays a necessary role in the proliferation of dog thyrocytes, but our results are compatible with this idea. On the other hand, as neither insulin, nor TSH, forskolin, EGF or PMA is mitogenic *per se*, activation of p70 S6 kinase alone is certainly not sufficient to trigger DNA synthesis

In order to investigate the role of PI 3-kinase(s) in the activation of p70 S6 kinase and/or DNA synthesis by the different mitogens acting on thyrocytes, we have studied the effect of these agents on the formation of 3-phosphoinositides products and on the activity of PI 3-kinase and of PKB. As already suggested by its mechanism of activation [10], PKB has been shown to be a target not only for the much studied PI 3-kinases α and β but also for PI 3-kinase γ [42]. Its activation is therefore a good marker of the activation of any known isoform of PI 3-kinase [10]. In our work, we show that all of the growth factors tested which stimulate cells via receptor tyrosine kinases (insulin/IGF-1, HGF and EGF) were able to provoke the appearance of 3-phosphorylated inositol lipids in intact cells, the association of a PI 3-kinase with anti-phosphotyrosine antibodies and the phosphorylation and activation of PKB. Moreover there is a parallelism in the efficacy of these different agents to stimulate PI 3-kinase and PKB, insulin and HGF causing a strong and sustained activation of these enzymes whereas the effect of EGF on these activities was weak and transient. The inability of TSH, forskolin or PMA to cause the formation of PtdIns(3,4,5)P_3 in intact cells and the activation of its direct target PKB strongly suggest that, in dog thyroid cells, TSH and cAMP as well as protein kinase C are not coupled to the formation of 3-phosphoinositides. Thus in dog thyrocytes, the events leading to p70 S6 kinase activation following exposure of the cells to TSH or PMA participate in pathways which do not include PI 3-kinase and which are still unknown.

The inhibition by wortmannin and LY294002 of the TSH (or forskolin) or PMA stimulated p70 S6 kinase activity is intriguing. It may suggest a lack of specificity in the action of these drugs. Indeed wortmannin and LY294002 have been shown to suppress the kinase activity of mTOR *in vitro* [43] and the former to inhibit stimulated phospholipase A_2 activity in Swiss 3T3 cells [44].

A lack of PI 3-kinase/PKB activation by phorbol esters has already been shown in other systems [42,45], while there are only few data concerning the regulation of these kinases by G-protein-coupled receptors. Recently Murga et al. [42] have reported that the pathway connecting G proteins to PI 3-kinase and PKB implicates a signal emanating from $G\alpha_q$, $G\alpha_i$, and $\beta\gamma$ dimers, but not from $G\alpha_{12}$ or $G\alpha_s$. This is in agreement with the fact that TSH and its receptor which act, in dog thyroid cells, mostly through $G\alpha_s$ [46] is without effect on these enzymes. However in the WRT cell line, TSH and cAMP-elevating agents were reported to stimulate PKB through a PI 3-kinase dependent pathway [37], while in COS cells, cAMP-elevating agents stimulate PKB through a PI 3-kinase independent one [13]. Obviously, as for other characteristics, the pathways stimulated by cAMP are different in these cell lines [15].

The fact that EGF, which strongly stimulates p70 S6 kinase, had only a weak and transient effect on PKB and on PI 3-kinase activities, is in agreement with the results obtained in skeletal muscle and adipose tissue [47]. It suggests the implication of other pathways in the action of this agent on p70 S6 kinase activity.

In contrast, we found a perfect correlation between the effect of insulin on PI 3-kinase, PKB and p70 S6 kinase activities which were all strongly stimulated by this agent. These observations are in agreement with numerous reports which implicate PI 3-kinase and PKB in the activation of p70 S6 kinase by insulin [10]; they do not shed light on the exact architecture of the pathway leading to p70 S6 kinase activation which is still unknown. HGF, the only growth factor acting on thyroid cells which does not require the presence of insulin to induce DNA synthesis, also strongly stimulates PI 3-kinase/PKB and p70 S6 kinase activities. Unlike the activation of p70 S6 kinase, the activation of the PI 3-kinase/PKB pathway thus represents the first effect of insulin not reproduced by the mitogenic agents which require insulin action. It is an obvious candidate to explain the permissive role of this hormone in the mitogenic effect of TSH, PMA and perhaps EGF in dog thyroid cells. Several facts support this hypothesis: (i) HGF, the only mitogenic agent which does not require insulin for its action, strongly activates PI 3-kinase and PKB, (ii) DNA synthesis induced by HGF in the absence of insulin is strongly inhibited by wortmannin, (iii) PMA and EGF, which as insulin activate the MAPK/p90 S6 kinase pathway but do not or weakly activate PI 3-kinase, are not permissive agents for TSH or forskolin [17]. However in the case of the mitogenesis induced by TSH or forskolin we cannot exclude a complementary contribution of the p42/p44 MAPK pathway in the permissive effect of insulin. As insulin is routinely added to many cell culture media, this permissive mechanism may in fact apply to other cell types. Moreover, contrary to what was reported in the WRT cell line [37], we demonstrate in the physiologically relevant system of primary cultures of dog thyroid cells, that as PI 3-kinase/PKB activity is not enhanced by the physiological stimulus of thyroid cells cAMP, the PI 3-kinase/PKB pathway cannot account either for the PKA-dependent mitogenic pathway(s) or for the PKA-independent one(s). Finally, as insulin/IGF-1 greatly activates the PI 3-kinase/PKB pathway but does not by itself induce mitogenesis or dedifferentiation, the activation of this pathway *per se* is not sufficient to elicit these processes in thyroid cells.

We thank P P Roger and G Thomas for a critical reading of the manuscript and Dr T. Nakamura for providing HGF This work was supported by the Belgian Program on Interuniversity Poles of Attraction initiated by the Belgian State, Prime Minister's Office, Science Policy Programming. It was also supported by the Fonds de la Recherche Scientifique Médicale, Télévie, the Association Contre le Cancer, the Fonds Cancérologique de la CGER, and the Association Sportive Contre le Cancer K C was a fellow of the Fondation Rose et Jean Hoguet and the Télévie. F.V. was a fellow of the Fondation Van Buuren and the Fonds pour la formation à la Recherche dans l'Industrie et l'Agriculture

REFERENCES

1 Baserga, R., Sell, C, Porcu, P and Rubini, M (1994) The role of the IGF-1 receptor in the growth and transformation of mammalian cells. Cell Proliferation **27**, 63–71

2 Barnes, D and Sato, G (1980) Serum-free culture a unifying approach Cell **22**, 649–655

3 Werner, H, Adamo, M, Roberts, Jr, C T and LeRoith, D (1994) Molecular and cellular aspects of insulin-like growth factor action Vitam Horm **48**, 1–58

4 Roger, P. P., Reuse, S., Maenhaut, C. and Dumont, J. E. (1995) Multiple facets of the modulation of growth by cAMP. Vitam. Horm. **51**, 59–191

5 Kozma, S. C. and Thomas, G. (1994) p70s6k/p85s6k: mechanism of activation and role in mitogenesis. Semin. Cancer Biol. **5**, 255–260

6 Frodin, M. and Gammeltoft, S. (1999) Role and regulation of 90 kDa ribosomal S6 kinase (RSK) in signal transduction. Mol. Cell. Endocrinol. **151**, 65–77

7 Dumont, F. J. and Su, Q. (1996) Mechanism of action of the immunosuppressant rapamycin. Life Sci. **58**, 373–395

8 Pullen, N. and Thomas, G. (1997) The modular phosphorylation and activation of p70s6k. FEBS Lett. **410**, 78–82

9 Weng, Q., Kozlowski, M., Belham, C., Zhang, A., Comb, M. J. and Avruch, J. (1998) Regulation of the p70 S6 kinase by phosphorylation *in vivo*. J. Biol. Chem. **273**, 16621–16629

10 Shepherd, P. R., Withers, D. and Siddle, K. (1998) Phosphoinositide 3-kinase: the key switch mechanism in insulin signalling. Biochem. J. **333**, 471–490

11 Kanda, S., Hodgkin, M. N., Woodfield, R. J., Wakelam, M. J., Thomas, G. and Claesson Welsh, L. (1997) Phosphatidylinositol 3′-kinase-independent p70 S6 kinase activation by fibroblast growth factor receptor-1 is important for proliferation but not differentiation of endothelial cells. J. Biol. Chem. **272**, 23347–23353

12 Marmy Conus, N., Hemmings, B. A. and Pearson, R. B. (1998) Differential regulation by calcium reveals distinct signaling requirements for the activation of Akt and $p70^{s6k}$. J. Biol. Chem. **273**, 4776–4782

13 Filippa, N., Sable, C. L., Filloux, C., Hemmings, B. and Van Obberghen, E. (1999) Mechanism of protein kinase B activation by cAMP-dependent protein kinase. Mol. Cell. Biol. **19**, 4989–5000

14 Konishi, H., Matsuzaki, H., Tanaka, M., Takemura, Y., Kuroda, S., Ono, Y. and Kikkawa, U. (1997) Activation of protein kinase B (Akt/RAC-protein kinase) by cellular stress and its association with heat shock protein Hsp27. FEBS Lett. **410**, 493–498

15 Roger, P. P., Christophe, D., Dumont, J. E. and Pirson, I. (1997) The dog thyroid primary culture system: a model of the regulation of function, growth and differentiation expression by cAMP and other well-defined signaling cascades. Eur. J. Endocrinol. **137**, 579–598

16 Dremier, S., Pohl, V., Poteet Smith, C., Roger, P. P., Corbin, J., Doskeland, S. O., Dumont, J. E. and Maenhaut, C. (1997) Activation of cyclic AMP-dependent kinase is required but may not be sufficient to mimic cyclic AMP-dependent DNA synthesis and thyroglobulin expression in dog thyroid cells. Mol. Cell. Biol. **17**, 6717–6726

17 Deleu, S., Pirson, I., Coulonval, K., Drouin, A., Taton, M., Clermont, F., Roger, P. P., Nakamura, T., Dumont, J. E. and Maenhaut, C. (1999) IGF-1 or insulin, and the TSH cyclic AMP cascade separately control dog and human thyroid cell growth and DNA synthesis and complement each other in inducing mitogenesis. Mol. Cell. Endocrinol. **149**, 41–51

18 Burikhanov, R., Coulonval, K., Pirson, I., Lamy, F., Dumont, J. E. and Roger, P. P. (1996) Thyrotropin via cyclic AMP induces insulin receptor expression and insulin co-stimulation of growth and amplifies insulin and insulin-like growth factor signaling pathways in dog thyroid epithelial cells. J. Biol. Chem. **271**, 29400–29406

19 Contor, L., Lamy, F., Lecocq, R., Roger, P. P. and Dumont, J. E. (1988) Differential protein phosphorylation in induction of thyroid cell proliferation by thyrotropin, epidermal growth factor, or phorbol ester. Mol. Cell. Biol. **8**, 2494–2503

20 Lamy, F., Wilkin, F., Baptist, M., Posada, J., Roger, P. P. and Dumont, J. E. (1993) Phosphorylation of mitogen-activated protein kinases is involved in the epidermal growth factor and phorbol ester, but not in the thyrotropin/cAMP, thyroid mitogenic pathway. J. Biol. Chem. **268**, 8398–8401

21 Sable, C. L., Filippa, N., Hemmings, B. and Van Obberghen, E. (1997) cAMP stimulates protein kinase B in a wortmannin-insensitive manner. FEBS Lett. **409**, 253–257

22 Lane, H. A., Morley, S. J., Doree, M., Kozma, S. C. and Thomas, G. (1992) Identification and early activation of a *Xenopus laevis* p70s6k following progesterone-induced meiotic maturation. EMBO J. **11**, 1743–1749

23 Flotow, H. and Thomas, G. (1992) Substrate recognition determinants of the mitogen-activated 70K S6 kinase from rat liver. J. Biol. Chem. **267**, 3074–3078

24 Heasley, L. E. and Johnson, G. L. (1989) Detection of nerve growth factor and epidermal growth factor-regulated protein kinases in PC12 cells with synthetic peptide substrates. Mol. Pharmacol. **35**, 331–338

25 Coulonval, K., Maenhaut, C., Dumont, J. E. and Lamy, F. (1997) Phosphorylation of the three Rb protein family members is a common step of the cAMP-, the growth factor and the phorbol ester-mitogenic cascades but is not necessary for the hypertrophy induced by insulin. Exp. Cell Res. **233**, 395–398

26 Krause, U., Rider, M. H. and Hue, L. (1996) Protein kinase signaling pathway triggered by cell swelling and involved in the activation of glycogen synthase and acetyl-CoA carboxylase in isolated rat hepatocytes. J. Biol. Chem. **271**, 16668–16673

27 Folch, J., Lees, M. and Sloane-Stanley, G. H. (1957) A simple method for the isolation and purification of total lipids from animal tissues. J. Biol. Chem. **226**, 497–509

28 Serunian, L. A., Auger, K. R. and Cantley, L. C. (1991) Identification and quantification of polyphosphoinositides produced in response to platelet-derived growth factor stimulation. Methods Enzymol. **198**, 78–87

29 Arcaro, A., Volinia, S., Zvelebil, M. J., Stein, R., Watton, S. J., Layton, M. J., Gout, I., Ahmadi, K., Downward, J. and Waterfield, M. D. (1998) Human phosphoinositide 3-kinase C2beta, the role of calcium and the C2 domain in enzyme activity. J. Biol. Chem. **273**, 33082–33090

30 Baptist, M., Dumont, J. E. and Roger, P. P. (1993) Demonstration of cell cycle kinetics in thyroid primary culture by immunostaining of proliferating cell nuclear antigen: difference in cyclic AMP-dependent and -independent mitogenic stimulations. J. Cell Sci. **105**, 69–80

31 Malik, R. K. and Parsons, J. T. (1996) Integrin-dependent activation of the p70 ribosomal S6 kinase signaling pathway. J. Biol. Chem. **271**, 29785–29791

32 Withers, D. J., Bloom, S. R. and Rozengurt, E. (1995) Dissociation of cAMP-stimulated mitogenesis from activation of the mitogen-activated protein cascade in Swiss 3T3 cells. J. Biol. Chem. **270**, 21411–21419

33 Dremier, S., Taton, M., Coulonval, K., Nakamura, T., Matsumoto, K. and Dumont, J. E. (1994) Mitogenic, dedifferentiating, and scattering effects of hepatocyte growth factor on dog thyroid cells. Endocrinology **135**, 135–140

34 Frodin, M., Peraldi, P. and Van Obberghen, E. (1994) Cyclic AMP activates the mitogen-activated protein kinase cascade in PC12 cells. J. Biol. Chem. **269**, 6207–6214

35 Miller, M. J., Prigent, S., Kupperman, E., Rioux, L., Park, S. H., Feramisco, J. R., White, M. A., Rutkowski, J. L. and Meinkoth, J. L. (1997) RalGDS functions in Ras- and cAMP-mediated growth stimulation. J. Biol. Chem. **272**, 5600–5605

36 Cass, L. A. and Meinkoth, J. L. (1998) Differential effects of cyclic adenosine 3′,5′-monophosphate on p70 ribosomal S6 kinase. Endocrinology **139**, 1991–1998

37 Cass, L. A., Summers, S. A., Prendergast, G. V., Backer, J. M., Birnbaum, M. J. and Meinkoth, J. L. (1999) Protein kinase A-dependent and -independent signaling pathways contribute to cyclic AMP-stimulated proliferation. Mol. Cell. Biol. **19**, 5882–5891

38 Vanhaesebroeck, B., Leevers, S. J., Panayotou, G. and Waterfield, M. D. (1997) Phosphoinositide 3-kinases: a conserved family of signal transducers. Trends Biochem. Sci. **22**, 267–272

39 Ui, M., Okada, T., Hazeki, K. and Hazeki, O. (1995) Wortmannin as a unique probe for an intracellular signalling protein, phosphoinositide 3-kinase. Trends Biochem. Sci. **20**, 303–307

40 von Manteuffel, S. R., Gringas, A.-C., Ming, X.-F., Sonenberg, N. and Thomas, G. (1996) 4E-BP1 phosphorylation is mediated by FRAP-$p70^{s6k}$ pathway and is independent of mitogen-activated protein kinase. Proc. Natl. Acad. Sci. U.S.A. **93**, 4076–4080

41 Parekh, D., Ziegler, W., Yonezawa, K., Hara, K. and Parker, P. J. (1999) Mammalian TOR controls one of two kinase pathways acting upon nPKCδ and nPKCε. J. Biol. Chem. **274**, 34758–34764

42 Murga, C., Laguinge, L., Wetzker, R., Cuadrado, A. and Gutkind, J. S. (1998) Activation of Akt/protein kinase B by G protein-coupled receptors. J. Biol. Chem. **273**, 19080–19085

43 Brunn, G. J., Williams, J., Sabers, C., Wiederrecht, G., Lawrence, Jr., J. C. and Abraham, R. T. (1996) Direct inhibition of the signaling functions of the mammalian target of rapamycin by the phosphoinositide 3-kinase inhibitors, wortmannin and LY294002. EMBO J. **15**, 5256–5267

44 Cross, M. J., Stewart, A., Hodgkin, M. N., Kerr, D. J. and Wakelam, M. J. (1995) Wortmannin and its analogue demethoxyviridin inhibit stimulated phospholipase A2 activity in Swiss 3T3 cells. Wortmannin is not a specific inhibitor of phosphatidylinositol 3-kinase. J. Biol. Chem. **270**, 25352–25355

45 Reif, K., Burgering, B. M. and Cantrell, D. A. (1997) Phosphatidylinositol 3-kinase links the interleukin-2 receptor to protein kinase B and p70 S6 kinase. J. Biol. Chem. **272**, 14426–14433

46 Allgeier, A., Laugwitz, K. L., Van Sande, J., Schultz, G. and Dumont, J. E. (1997) Multiple G-protein coupling of the dog thyrotropin receptor. Mol. Cell. Endocrinol. **127**, 81–90

47 Cross, D. A., Watt, P. W., Shaw, M., van der Kaay, J., Downes, C. P., Holder, J. C. and Cohen, P. (1997) Insulin activates protein kinase B, inhibits glycogen synthase kinase-3 and activates glycogen synthase by rapamycin-insensitive pathways in skeletal muscle and adipose tissue. FEBS Lett. **406**, 211–215

48 Jaster, R., Bittorf, T. and Brock, J. (1997) Involvement of phosphatidylinositol 3-kinase in the mediation of erythropoietin-induced activation of p70S6k. Cell Signal. **9**, 175–179

49 Karnitz, L. M., Burns, L. A., Sutor, S. L., Blenis, J. and Abraham, R. T. (1995) Interleukin-2 triggers a novel phosphatidylinositol 3-kinase-dependent MEK activation pathway. Mol. Cell. Biol. **15**, 3049–3057

Received 4 January 2000/9 March 2000; accepted 24 March 2000

Lipidation of apolipoprotein E influences its isoform-specific interaction with Alzheimer's amyloid β peptides

Takahiko TOKUDA*, Miguel CALERO*, Etsuro MATSUBARA†, Ruben VIDAL*, Asok KUMAR*, Bruno PERMANNE*, Berislav ZLOKOVIC‡, Jonathan D. SMITH§, Mary Jo LADU¶, Agueda ROSTAGNO*, Blas FRANGIONE* and Jorge GHISO*[1]

*Department of Pathology, New York University School of Medicine, 550 First Avenue, New York, NY 10016, U.S.A., †Department of Neurology, Gunma University School of Medicine, Maebashi, Gunma 371-8511, Japan, ‡Department of Neurological Surgery, USC School of Medicine, Los Angeles, CA 90033, U.S.A., §Laboratory of Biochemical Genetics and Metabolism, The Rockefeller University, New York, NY 10021, U.S.A., and ¶ENH Research Institute, Evanston, IL 60201, U.S.A.

The inheritance of the apolipoprotein E (apoE) ϵ4 allele is a prevailing risk factor for sporadic and familial Alzheimer's disease (AD). ApoE isoforms bind directly to Alzheimer's amyloid β (Aβ) peptides both *in vitro* and *in vivo*. Recent studies suggest that association of apoE with lipids may modulate its interaction with Aβ. We examined the binding of lipid-associated and delipidated apoE3 and apoE4 isoforms to Aβ utilizing a solid-phase binding assay and estimated the dissociation constants for the interaction of various apoE and Aβ species. Using native apoE isoforms from stably transfected RAW 264 and human embryonic kidney 293 cells, apoE3 had greater affinity than apoE4 for both Aβ1-40 and Aβ1-42. Delipidation of apoE decreased its affinity for Aβ peptides by 5–10-fold and abolished the isoform-specificity. Conversely, incorporation of apoE isoforms produced by baculovirus-infected Sf9 cells into reconstituted human high-density-lipoprotein lipoparticles restored the affinity values for Aβ peptides and resulted in preferential binding of apoE3. The data demonstrate that native lipid-associated apoE3 binds to Aβ peptides with 2–3-fold higher affinity than lipid-associated apoE4. Since the isoforms' binding efficiency correlate inversely with the risk of developing late-onset AD, the results suggest a possible involvement of apoE3 in the clearance or routing out of Aβ from the central nervous system as one of the mechanisms underlying the pathology of the disease.

Key words: Aβ, apoE isoform, dissociation constant, HDL, lipid.

INTRODUCTION

Amyloid β (Aβ) peptide is the major constituent of the fibrils deposited in senile plaques and cerebral blood vessels of patients with Alzheimer's disease (AD) and related disorders. The Aβ peptide extracted from senile plaques is mainly 42–43 amino acids long (Aβ42/43), whereas the vascular amyloid consists mainly of shorter Aβ species (39–40 amino acids, Aβ39/40). Although both the short and long species self-aggregate and form fibrils *in vitro*, biochemical and immunohistochemical studies have shown that Aβ42/43 has a higher propensity for aggregation and fibrillogenesis (reviewed in [1]). Soluble Aβ, predominantly 40 amino acids long, is also normally present in plasma, cerebrospinal fluid [2–4], urine [5] and brain parenchyma [6,7]. An increased amount of soluble Aβ in AD and Down's syndrome brains precedes the appearance of Aβ deposits [8], suggesting that soluble Aβ species may be the immediate precursors of deposited Aβ fibrils. Alternatively, a particular species of soluble Aβ may be responsible for the neurotoxic effect observed *in vitro*, as well as for the neuronal loss *in vivo* not spatially correlated with fibrillar deposits [9–11].

Apolipoprotein E (apoE) co-localizes with cerebral amyloid deposits in patients with AD [12–15]. Its three major isoforms in humans (E2, E3 and E4) are products of three alleles at a single gene locus [16]. Genetic studies have shown that inheritance of apoE4 is a significant risk factor for AD [17,18], decreasing the age of onset and duration of disease [18,19]. In addition, the extent of Aβ deposition in AD patients correlates with the doses of the *APOE4* gene [20,21]. On the contrary, the ϵ2 allele may confer lower risk for the disease than ϵ3 and ϵ4. The precise mechanisms by which the apoE isoforms are involved in the development of AD still remain unclear.

The three apoE isoforms bind Aβ peptides *in vitro*, leading to the formation of complexes [18,22,23], although it is controversial whether there are differences in the binding interaction of the different isoforms with Aβ peptides. Initially, it was shown that purified (non-lipidated) apoE4 binds Aβ to form an SDS-stable complex more rapidly than apoE3 [22], although the efficiency of binding of the two apoE isoforms seemed comparable after prolonged incubations. Subsequent studies utilizing recombinant particle-associated apoE (native apoE) from human plasma and conditioned media of transfected eukaryotic cells, showed a preferential binding of apoE3 to Aβ, suggesting that the lipid association of apoE could play a relevant role in the isoform-specific interaction, probably by inducing a conformational modification in the apolipoprotein molecule [24–28]. All these studies detected the formation of complexes by SDS/PAGE followed by Western-blot analysis. This protocol provides limited information since it only detects SDS-stable apoE–Aβ complexes and does not result in quantitative estimation of the binding data. In the present report the binding of particle-associated and purified delipidated apoE3 and apoE4 to both Aβ40 and Aβ42 species was assessed by solid-phase binding assays that allow the calculation of the corresponding dissociation constants based on saturation profiles. Our results demonstrate that the affinity of native apoE3 for Aβ peptides is 2–3-fold higher than that of apoE4 and that native apoE molecules that contain lipid-associated moieties express 5–10-fold higher Aβ-binding affinity than the delipidated isoforms.

Abbreviations used: Aβ, amyloid β; AD, Alzheimer's disease; apoE, apolipoprotein E; BS3, bis(sulphosuccinimidyl) suberate; HDL, high-density lipoprotein; rHDL, reconstituted HDL; HEK, human embryonic kidney.

[1] To whom correspondence should be addressed (e-mail ghisoj01@popmail.med.nyu.edu).

EXPERIMENTAL

Synthetic peptides and proteins

Peptides DAEFRHDSGYEVHHQKLVFFAEDVGSNKGAIIGLMVGGVV (Aβ40) and DAEFRHDSGYEVHHQKLVFFAEDVGSNKGAIIGLMVGGVVIA (Aβ42), identical to residues 672–711 and 672–713 of Aβ-precursor protein 770 respectively, were synthesized at the W. M. Keck Facility at Yale University (New Haven, CT, U.S.A.) using *N*-t-butyloxycarbonyl chemistry and purified by HPLC. Aliquots of the final products were lyophilized and stored at −20 °C until use. For preparation of aggregated peptides, 50 μg of either Aβ40 or Aβ42 were dissolved in 100 μl of PBS (0.02 M phosphate buffer, pH 7.4, containing 0.15 M NaCl) and incubated at 37 °C for 72 h. apoE3 and apoE4 produced in Sf9 insect cells by the baculovirus expression system were purchased from PanVera (Madison, WI, U.S.A.). In all cases, protein purity was corroborated by SDS/PAGE and N-terminal sequence analysis.

apoE expressed by eukaryotic cell lines

Human apoE3 or apoE4 were expressed individually in RAW 264 mouse macrophage cells (A. T. C. C. TIB71) stably transfected with genomic DNA encoding the human apoE isoforms, and in human embryonic kidney (HEK) 293 cells (A.T.C.C. CRL1573) stably transfected with cDNA encoding the human apoE isoforms, and harvested in serum-free conditioned medium for each cell line as described in [24,25,29,30]. Concentrations of secreted apoE were determined by capture-ELISA (ApoTek ApoE; PerImmune, Rockville, MD, U.S.A.) after incubating the harvested conditioned media with 0.05 % β-octyl glucopyranoside for 1 h. Aliquots of conditioned media containing apoE3 or apoE4 were stored at 4 °C and used within 2 weeks of harvesting

Purification of apoE from RAW-264-cell conditioned media

Polyclonal AB947 anti-apoE antibody (1 ml; Chemicon, Temecula, CA, U.S.A.) was coupled to 2 ml of CNBr-activated Sepharose 4B according to the manufacturer's instructions. Conditioned media containing apoE3 or apoE4 was loaded on to the AB947-affinity matrix. Bound apoE was eluted with 0.2 M acetic acid, pH 2.2, and immediately neutralized. The elution profile was monitored at 280 nm and the pertinent fractions were pooled and dialysed against 0.02 M Tris/HCl, pH 8.5, containing 0.1 M NaCl.

Isolation of apoE-containing particles from HEK-293-cell conditioned media

Aliquots of serum-free conditioned media from HEK-293 cells stably transfected with human apoE3 or apoE4 cDNA, in which the apolipoproteins constituted approx. 50 % of the total protein content, were concentrated 50-fold with Centricon-10 (Amicon; Millipore, Bedford, MA, U.S.A.) as described previously [24]. Particles that contained apoE3 or apoE4 were isolated from the corresponding concentrated conditioned media by FPLC using tandem Superose 6 HR10/30 columns (Pharmacia, Piscataway, NJ, U.S.A.) equilibrated in 0.02 M sodium phosphate, pH 7.4, containing 0.05 M NaCl, 0.03 % EDTA and 0.02 % sodium azide as described in [31].

Delipidation of apoE isoforms purified from conditioned media of eukaryotic cell lines and from baculovirus-transfected Sf9 cells

apoE isoforms from RAW-264 and HEK-293 cells, purified as described above, as well as apoE produced in Sf9 insect cells by the baculovirus expression system (PanVera), were delipidated in aqueous state using diethyl ether and ethanol as described in [32]. Briefly, the lipoprotein-containing samples were extracted with an equal volume of a 3:2 (v/v) diethyl ether/ethanol mixture, followed by four subsequent extractions of the aqueous phase with a 3:1 (v/v) diethyl ether/ethanol solution. After the final extraction, the remaining solvent was evaporated under a N_2 stream and the apoE concentration determined as described above.

Incorporation of apoE into reconstituted high-density lipoprotein (rHDL) particles

Extraction of total lipids from the human HDL fraction

Human HDL fractions were isolated by preparative gradient ultracentrifugation of plasma obtained from normal healthy subjects, ages 25–40, after a 10–12-h fast as described previously [33]. The HDL fractions were dialysed extensively at 4 °C against PBS containing 1 mM EDTA, and the total lipid fractions (HDL-lipid) were extracted with a mixture of chloroform and methanol (1:2, v/v) and centrifuged at 1700 *g* for 5 min. The supernatant was combined with chloroform and 0.88 % KCl (1:1, v/v) and centrifuged at 1700 *g* for 5 min. The bottom layer that contained the extracted lipids was collected, dried under a N_2 atmosphere, dissolved in chloroform and stored at −70 °C until use. The amount of total cholesterol, total triacylglycerols and phospholipids in the HDL and HDL-lipid fractions were determined enzymically with Sigma (St. Louis, MO, U.S.A.) diagnostic kits.

Preparation of reconstituted apoE-containing HDL particles

rHDL particles containing apoE were prepared as described in [34] using recombinant apoE expressed in baculovirus-infected Sf9 cells and the HDL-lipids extracted from human plasma HDL lipoparticles. In a typical experiment, the HDL-lipids (500 μg) were placed in a glass tube, dried under N_2 atmosphere, resuspended in 0.01 M Tris/HCl buffer, pH 8, containing 0.15 M NaCl (TBS) and 0.001 M EDTA. After the addition of 280 μg of sodium cholate, the suspension was incubated at 4 °C for 12 h. Subsequently, 500 μg of either Sf9 apoE3 or apoE4 was added to the reaction, incubated at 4 °C for another 12 h, and dialysed extensively at 4 °C against PBS containing 0.01 % EDTA. The fractions containing apoE incorporated into lipoparticles (apoE-rHDL) were separated from lipid-free apoE by gel-filtration chromatography using a Superose 12 column (Pharmacia) equilibrated in 0.02 M phosphate buffer, pH 7.4, containing 0.05 M NaCl, 0.03 % EDTA and 0.02 % sodium azide, at a flow rate of 0.8 ml/min. Collected fractions were analysed by native PAGE using 4–20 % Tris/glycine gels and Western-blot analysis employing a monoclonal anti-apoE antibody (3D12; BioDesign, Kennebunk, ME, U.S.A.). The fractions containing apoE-rHDL were pooled for solid-phase binding studies and the concentration of apoE in the lipoparticles was determined using the ApoTek ApoE system as described above.

Electron microscopy analysis of rHDL particles

rHDL particles containing either apoE3 or apoE4 were examined by transmission electron microscopy Droplets (10 μl) of each of the 5-fold-concentrated apoE-rHDL fractions were placed on a Formvar carbon-coated grid and stained with 2 % sodium phosphotungstate as described in [35,36]. The shape and diameter of the lipoparticles were evaluated from enlarged prints of photomicrographs and the mean diameter was calculated from 100 particles.

Chemical cross-linking of rHDL particles

apoE molecules reconstituted into HDL particles were cross-linked using bis(sulphosuccinimidyl) suberate (BS3) as described in [36,37]. Briefly, BS3 was added to the apoE-rHDL fraction at a concentration of 0.002 M in PBS, incubated at room temperature for 4 h, and the reaction stopped by the addition of 0.03 M Tris/HCl buffer, pH 7.4. After desalting with Microcon10 (Amicon, Millipore) and lyophilization, the cross-linked samples were separated by Tris/Tricine PAGE (10 % polyacrylamide), transferred on to an Immobilon-P membrane (Millipore) and reacted with monoclonal 3D12 anti-apoE antibody followed by horseradish-peroxidase-conjugated anti-mouse IgG. The Western blot was developed by chemiluminescence using the SuperSignal kit (Pierce, Rockford, IL, U.S.A.).

Solid-phase binding assays

The binding of apoE to Aβ species was studied by ELISA using immobilized freshly prepared (non-aggregated) or 72-h-aggregated Aβ40 and Aβ42 as described in [38] and apoE3 or apoE4 isoforms with different degrees of lipidation. Polystyrene microtitre plates (Immulon 2; Dynex Technology, Chantilly, VA, U.S.A.) were coated for 2 h at 37 °C with either fresh or aggregated Aβ40 and Aβ42 (400 ng in 100 μl of 0.1 M $NaHCO_3$, pH 9.6, per well). Under these conditions, 10 ng of fresh Aβ40, 9.6 ng of fresh Aβ42, 10.2 ng of aggregated Aβ40 and 10.9 ng of aggregated Aβ42 (representing 2.5, 2.4, 2.6 and 2.7 % of the peptide offered, respectively) were coated to the microtitre wells, as determined by a modification of the Quantigold assay (Diversified Biotech, Boston, MA, U.S.A.) for protein quantification. After blocking with Superblock (Pierce), increasing concentrations of apoE (0–150 nM in TBS; 100 μl per well) were added to the Aβ-coated wells and incubated for 3 h at 37 °C. Bound apoE was detected with monoclonal anti-apoE antibody (3D12, 1:1000) followed by alkaline-phosphatase-conjugated goat F(ab')2 anti-mouse IgG (1:3000; BioSource International, Camarillo, CA, U.S.A.). The reaction was developed for 30 min with p-nitrophenyl phosphate in diethanolamine buffer (Bio-Rad, Hercules, CA, U.S.A.), and quantified at 405 nm on a Microplate Reader (Cambridge Technology, Watertown, MA, U.S.A.). For Scatchard analysis, bound apoE values were expressed in fmol with the aid of a calibration curve in which known concentrations of apoE coated to microtitre wells (as determined by Quantigold assay) were reacted with 3D12, followed by alkaline-phosphatase-conjugated F(ab')2 anti-mouse IgG under conditions identical with those described above. Under the experimental conditions employed, an excess of apoE was reacted with solid-phase Aβ; therefore, only a small fraction of added ligand bound to the immobilized peptide and the concentration of free ligand was considered equivalent to the total apoE added. Non-linear regression analysis, Scatchard plots, estimation of dissociation constants and comparison of protein-binding data for statistical significance by calculation of the F ratios were assessed using GraphPad Prism software (GraphPad, San Diego, CA, U.S.A.).

RESULTS

apoE3 and apoE4 isoforms produced by baculovirus-infected Sf9 cells were incorporated into rHDL particles employing the lipids extracted from human plasma HDL fractions. The resulting lipoparticles were characterized in terms of molecular mass, particle size, number of apoE molecules per particle, and lipid content. As indicated in Figure 1, both apoE3- and apoE4-rHDL were eluted from the gel-filtration matrix at a retention time consistent with a molecular mass of approx. 230000 Da, which corresponds to the mass of HDL particles. apoE molecules not incorporated into the particles were recovered mostly in a second peak at a retention time corresponding to 135000–140000 Da and a minor peak at 35000 Da that consisted of apoE monomers and which represented approx. 10 % of the total apoE. Delipidated apoE preparations subjected to gel-filtration chromatography, under identical conditions, were eluted as a major peak at 135000–140000 Da, corresponding to the tetrameric form of the molecule, and a minor peak (10–20 %) that corresponded to the 35000 Da monomer (results not shown), in agreement with data reported previously [39] that demonstrated that apoE in aqueous solutions and in the absence of lipids self-associates and forms stable tetramers.

Electron microscopy studies revealed that apoE3- and apoE4-rHDL were spherical in shape and relatively homogeneous in size (Figure 2A), with a diameter that ranged from 7.1 to 17.9 nm for the apoE3-rHDL (mean, 11.8 nm) and from 7.0 to 18.1 nm for the apoE4-rHDL (mean, 11.9 nm). The number of apoE molecules incorporated per particle, assessed by covalent cross-linking followed by Western-blot analysis, was similar for both isoforms. Per particle, 1–4 molecules of apoE were incorporated (Figure 2B). The majority of the lipoparticles in both apoE3-rHDL and apoE4-rHDL preparations contained three molecules of apolipoprotein per particle. The lipid composition of rHDLs was 18.7 % total cholesterol, 9.0 % triacylglycerols and 72.3 % phospholipids, comparable with the plasma HDL fraction.

To study the effect that apoE lipidation exerts on the binding interaction with Aβ peptides the following apoE preparations were employed in the solid-phase assays: (i) apoE molecules

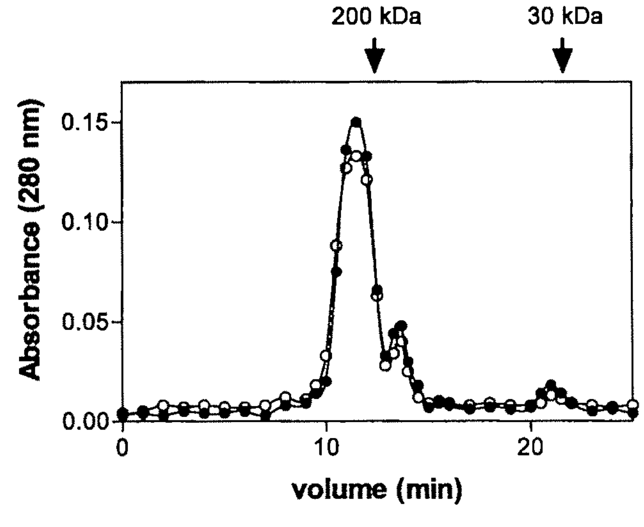

Figure 1 Purification of apoE-containing rHDL particles by gel-filtration chromatography

rHDLs were prepared by incorporating apoE3 and apoE4 produced in the baculovirus expression system into HDL particles employing the lipids extracted from human HDL fractions, as described in the Experimental section. apoE-containing rHDL particles were separated from lipid-free apoE by gel-filtration chromatography using a Superose 12 column (Pharmacia) equilibrated in 20 mM phosphate buffer, pH 7.4, containing 50 mM NaCl and 0.03 % EDTA, at a flow rate of 0.8 ml/min. The corresponding elution profiles for apoE3 (●) and apoE4 (○) were monitored by A_{280}, and the presence of apoE in the eluted fractions was corroborated by Western-blot analysis employing monoclonal anti-apoE antibody 3D12. The elution profile indicates that the apoE molecules incorporated into rHDL particles were eluted at a retention time that ranged from 9 to 12 min, corresponding to a molecular mass of 230 kDa. Lipoprotein-free apoE monomers were eluted at 22 min, a retention time that corresponded to a molecular mass of approx. 35 kDa.

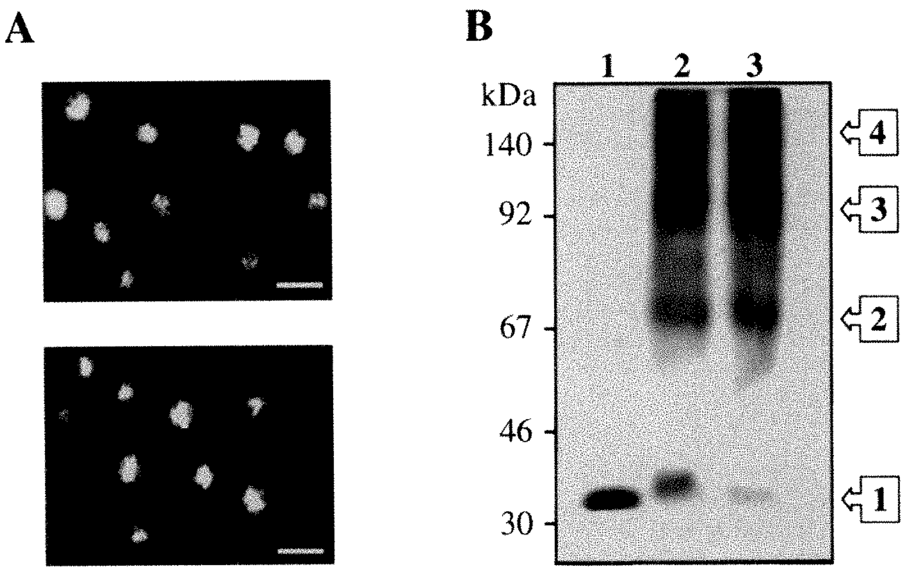

Figure 2 Biochemical characterization of apoE-containing rHDL

(**A**) Electron microscopy: rHDL particles containing apoE3 (upper panel) or apoE4 (lower panel) were placed on a Formvar carbon-coated electron microscopy grid and negatively stained with 2% sodium phosphotungstate. The lipoparticles consisted of spherical particles relatively homogeneous in size with an average diameter of 11.8 nm for apoE3, and of 11.9 nm for apoE4. The scale bar corresponds to 30 nm. (**B**) Covalent cross-linking and Western-blotting analysis of apoE molecules in rHDL particles. apoE3 or apoE4 molecules incorporated into rHDL were cross-linked for 4 h using BS3. After desalting and lyophilization, the cross-linked samples were separated by Tris/Tricine gel electrophoresis, transferred to an Immobilon P membrane and analysed by Western blotting using monoclonal 3D12 anti-apoE antibody. Visualization was carried out by chemiluminescence. Lane 1, delipidated apoE4; lane 2, apoE3 incorporated into rHDL particles; lane 3, apoE4 incorporated into rHDLs. Arrows indicate the positions of the monomers, dimers, trimers and tetramers of apoE incorporated into the lipoparticles.

produced by baculovirus-infected Sf9 insect cells, including native preparations, delipidated apoE isoforms and delipidated apoE molecules reconstituted into lipoparticles with human HDL lipids, and (ii) apoE secreted by stably transfected RAW and HEK cells, both in their native state and after removal of the lipid moieties. In all cases, increasing concentrations of the apoE3 or apoE4 isoforms with or without lipids were allowed to interact with a constant amount of immobilized $A\beta$ peptides ($A\beta40$ and $A\beta42$) at physiological pH and temperature. The binding curves were generated by determining the amount of each apoE isoform bound to the $A\beta$ peptides for each concentration of added apoE monomer. A dose–response relationship that reached saturation and fitted a rectangular hyperbola was obtained in each case. The dissociation constants were calculated as the half-maximal concentration of apoE monomer required for saturation, assuming that each monomer behaves as an independent entity and that there is no co-operative or synergistic interaction among the different molecules within the lipoparticle. In support of this assumption it is interesting to note that apoE molecules appear not to self-associate on lipid surfaces [40]. Scatchard plots were used to display the results more graphically and demonstrate the differences in affinity showed by the different apoE preparations. As indicated in Figure 3, removal of the lipid moieties from the different apoE preparations tested resulted in a lower binding activity for both $A\beta40$ and $A\beta42$. In addition, the lack of lipid-associated molecules translated into the loss of the isoform specificity for the interaction with $A\beta$ peptides. A higher binding for $A\beta$ peptides was observed for the apoE3 than for the apoE4 isoform when the lipoproteins contained lipid-associated molecules. This isoform specificity was abolished by delipidation that resulted in an overlapping of the binding curves for both apoE3 and apoE4 from stably transfected HEK (Figures 3B and 3E) and RAW cells (Figures 3C and 3F). A similar effect was observed when delipidated apoE molecules derived from Sf9 cells were used for the binding interaction (Figures 3A and 3D). Interestingly, incorporation into rHDL-like lipoparticles restored the binding activity difference between the two isoforms, with higher values obtained for apoE3. In all cases non-specific binding, determined as the binding of increasing concentrations of apoE to blocked microtitre wells that were not coated with $A\beta$ peptides, never exceeded 8% of the specific binding.

Table 1 displays the dissociation constants estimated from the corresponding saturation curves shown in Figure 3. The lipidated apoE isoforms (E3 and E4) showed, in all cases, higher affinity for $A\beta$ peptides than the delipidated molecules ($P < 0.01$). In addition, there was a statistically significant ($P < 0.01$) higher affinity of binding for the apoE3 isoform than for the apoE4 for both $A\beta$ peptides in lipidated apolipoprotein preparations (RAW- and HEK-derived) and in Sf9-derived molecules upon incorporation into rHDL particles. On the contrary, in lipid-depleted isoforms the binding of apoE3 and apoE4 to all $A\beta$ species tested did not differ significantly ($P > 0.05$), confirming that lipid association confers isoform specificity. A quantitative difference in $A\beta$ binding was also observed for nascent apoE secreted by transfected eukaryotic cells in culture compared with apoE produced by the baculovirus expression system, with a higher affinity of binding for the native lipoparticles. The K_d values obtained for Sf9-derived apoE3 for $A\beta40$ and $A\beta42$ were 9.3 ± 0.6 nM and 13.3 ± 1.3 nM, respectively, while for apoE4 binding to $A\beta40$ and $A\beta42$ the corresponding K_d values were 10.3 ± 0.9 nM and 13.9 ± 1.4 nM. These results are in agreement with previous reports that found that native apoE molecules secreted by BHK-21 transfected cells have higher tendency to form complexes with $A\beta$ than the baculovirus-generated apolipoproteins [28]. It is likely that the differences in $A\beta$-binding affinity of the apoE isoforms from various sources reflect a dissimilar degree of lipid association. In the case of BHK-21 cells, flotation

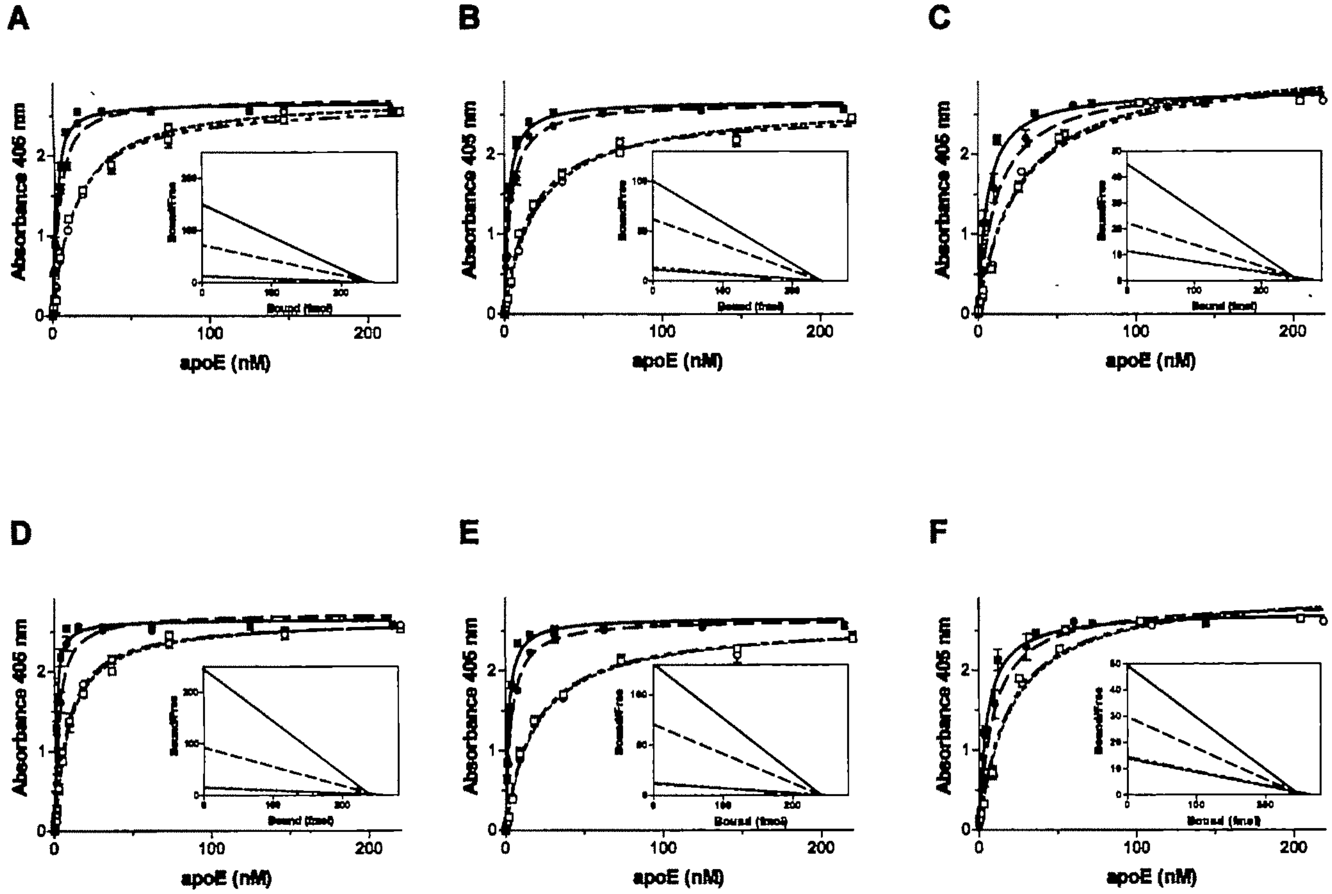

Figure 3 Binding curves for the interactions of apoE3 and apoE4 with immobilized Aβ peptides

Increasing concentrations (0–150 nM) of various apoE3 (■, □) or apoE4 (●, ○) preparations were reacted with microtitre ELISA wells coated with non-aggregated Aβ40 or Aβ42 for 3 h. Bound apoE was detected, in all cases, with monoclonal 3D12 anti-apoE antibody, followed by alkaline-phosphatase-labelled anti-mouse IgG. Insets, Scatchard transformation of the binding data. **(A, D)** Binding to Aβ40 and Aβ42, respectively, of Sf9-derived apoE3 and apoE4, both delipidated (□, ○) and upon incorporation into rHDLs (■, ●). **(B, E)** Binding to Aβ40 and Aβ42, respectively, of HEK-derived apoE3 and apoE4, both in their native HDL particles (■, ●) and following delipidation (□, ○). **(C, F)** Binding to Aβ40 and Aβ42, respectively, of RAW-derived apoE3 and apoE4, both in their native HDL particles (■, ●) and following delipidation (□, ○). In all cases, each point represents the mean ± S.D. of experiments performed in triplicate. ——, Lipidated apoE3; – – –, lipidated apoE4; – · – ·, delipidated apoE3; ----, delipidated apoE4

Table 1 Effect of lipidation in the interaction of non-aggregated Aβ40 and Aβ42 with apoE3 and apoE4

Values represent the mean dissociation constants (± S.D., expressed in nM) of triplicate experiments. Statistical significance: lipidated versus non-lipidated, $P < 0.01$; lipidated apoE3 versus lipidated apoE4, $P < 0.01$; non-lipidated apoE3 versus non-lipidated apoE4, $P > 0.05$ (all F tests).

	Dissociation constant (nM)			
	Lipidated		Non-lipidated	
apoE (source and isoform)	Aβ40	Aβ42	Aβ40	Aβ42
Sf9 cells				
apoE3	1.6 ± 0.1	1.0 ± 0.1	22.7 ± 2.7	18.6 ± 2.7
apoE4	3.3 ± 0.3	2.7 ± 0.4	23.3 ± 3.4	22.5 ± 4.1
HEK cells				
apoE3	2.4 ± 0.2	1.8 ± 0.1	17.8 ± 3.1	18.6 ± 3.6
apoE4	3.9 ± 0.4	3.4 ± 0.3	18.2 ± 3.0	19.7 ± 3.2
RAW cells				
apoE3	5.7 ± 0.9	5.0 ± 0.7	23.9 ± 3.1	19.2 ± 2.4
apoE4	11.9 ± 2.5	9.1 ± 1.2	23.2 ± 3.3	20.3 ± 3.2

analysis demonstrated that 45% of the secreted apoE is associated with HDL-like particles, 40% with lipid-poor particles, and 15% is found in the lipid-free fraction [41]. Removal of the associated lipids from Sf9-, RAW- and HEK-derived apoE molecules resulted in similar affinities for Aβ peptides (Table 1). Upon incorporation into rHDL particles the binding affinity of the Sf9-derived apoE isoforms reached values almost identical with those of the HEK-derived apolipoprotein (e.g. K_d = 1.6 nM versus 2.4 nM for the apoE3–Aβ40 and K_d = 3.3 nM versus 3.9 nM for the apoE4–Aβ40, respectively). In addition, the Sf9-derived apoE molecules reconstituted into HDL particles showed isoform-specific binding behaviour with a higher binding affinity for the apoE3 isoform. This contrasts with previous reports that baculovirus-produced apoE isoforms incorporated into lipoparticles generated with synthetic lipids (1-palmitoyl-2-oleoyl glycero-3-phosphocholine) showed a diminished efficiency to form complexes with Aβ peptides, although the preferential binding of apoE3 apoE4 was maintained [28].

Binding studies using immobilized aggregated Aβ peptides showed similar results to the non-aggregated species. A preferential binding for the apoE3 isoform derived from RAW cells was observed for both aggregated Aβ40 and Aβ42 (K_d values were 6.5 ± 1.1 nM and 6.7 ± 1 nM, respectively), with an approx. 3-fold higher affinity than the apoE4 isoform (K_d = 16.5 ± 2.7 nM for Aβ40 and K_d = 18.2 ± 2.8 nM for Aβ42). This isoform specificity disappeared following delipidation that resulted in K_d values of 30.4 ± 2.8 nM and 28.3 ± 2.8 nM for the binding to Aβ40 of apoE3 and apoE4, respectively; the corresponding constants for apoE3 and apoE4 binding to Aβ42 were 24.6 ± 3 nM and 27.6 ± 2.9 nM.

DISCUSSION

apoE is a ubiquitous protein synthesized predominantly in liver, brain, spleen, lung, adrenal gland, kidney and muscle. In the brain apoE mRNA is present mainly in astrocytes and microglia [42,43]. During synthesis, apoE is incorporated into lipoprotein particles that are involved in lipid transport and clearance through the binding to the low-density lipoprotein (LDL) and very-low-density lipoprotein (VLDL) receptors, as well as to low-density lipoprotein receptor-related protein 1, apoE receptor 2 and glycoprotein 330 (also known as megalin or low-density lipoprotein receptor-related protein 2) [44]. In the central nervous system the secretion of apoE by non-neuronal cells increases dramatically following neuronal injury, and it has been suggested that apoE participates in the growth and repair of the nervous system by providing the lipid moieties necessary for membrane synthesis.

The three apoE isoforms have been demonstrated to bind Aβ peptides, resulting in the formation of SDS-stable complexes [18,22,23]. Our results provide for the first time quantitative data clarifying the isoform-specific binding of apoE to Aβ by means of the estimation of the corresponding dissociation constants. In addition, by comparing the affinity constants for the Aβ interaction of apoE from different sources, both lipid-associated and delipidated, these results demonstrate quantitatively that lipidation of apoE molecules modifies their affinity for different species of Aβ Lipidation not only increased the affinity of both apoE3 and apoE4 for Aβ, but also accentuated the isoform differences.

Purified apoE molecules have been shown to require lipids to maintain their biological activity in most other assay systems, presumably by allowing the molecules to acquire their functional configuration in the hydrophobic lipidic environment. These apoE biological assays include such diverse functions as receptor binding, modulation of neuritic growth and antioxidant properties. It is known that association with lipids is essential for apoE binding to cellular apoE receptors [31]. Purified delipidated apoE is not a functional ligand for the apoE receptor; however, the receptor-binding activity is restored after apoE is reconstituted with phospholipid moieties [45]. Another example of lipid requirement for the expression of the biological activity of apoE is provided by primary dorsal root ganglia cultures. In this system purified apoE3 and apoE4 have no effect on neuritic growth. However, when employed in the presence of VLDLs, both apoE isoforms affect neuritic growth, with apoE3 increasing neuritic extension and decreasing branching and apoE4 decreasing both branching and extension [46]. Finally, another setting in which the lipid association affects the activity of apoE are the antioxidant and anti-cytotoxic effects indicated by apoE isoforms secreted by stably transfected RAW-246 cells that are enhanced by lipid association [30]. In summary, the association with lipid moieties seems to be a prerequisite for the expression of the diverse biological activities of apoE in their full capacity, presumably by contributing to the acquisition of an optimal three-dimensional configuration.

apoE has been related to the pathogenesis of AD. Epidemiological studies have shown that the ε4 allele is a risk factor for AD, although the mechanisms underlying this association remain to be defined. Substantial evidence suggests that the binding interactions between apoE and Aβ peptides may be critical in the pathogenesis of the disease by affecting the aggregation properties and/or the clearance of the Aβ peptide and thereby influencing Aβ deposition. Recent studies have provided compelling evidence for a role of apoE in Aβ deposition *in vivo*. In transgenic mice that over-express a mutant amyloid precursor protein and develop age-dependent Aβ deposition, breeding with apoE-knock-out animals (apoE$^{-/-}$) resulted in a significant decrease of Aβ deposition in comparison with animals expressing endogenous apoE [47]. In a strikingly contrasting result, it was found that the expression of human apoE3 and apoE4 isoforms at physiological levels, in amyloid precursor protein-transgenic mice with apoE$^{-/-}$ background, suppress early Aβ deposition [48]. This suggests that human apoEs have different binding affinities for Aβ peptides from the mouse isoforms, resulting in different clearance capabilities. Further studies will provide a better understanding of the Aβ catabolism/deposition pathways and the involvement of the apoE, and other chaperones in the biochemical mechanisms leading to AD. Systematic analysis of the interactions of Aβ peptides with different intra- and extracellular protein ligands, including apoE, as well as clarification of the effects that post-translational modifications exert on the various ligand interactions, may provide new insights into the molecular events leading to the pathogenesis of the disease.

This work was supported by National Institutes of Health grants AG05891, AG10491, NS38777, AG16233 and NS34467. M.C. is the recipient of a fellowship from the Ministerio de Educacion y Cultura, Spain J G Is the recipient of the New Investigator Development Award from the American Heart Association, New York City affiliate.

REFERENCES

1 Wisniewski, T., Ghiso, J and Frangione, B (1997) Biology of Aβ amyloid in Alzheimer's disease Neurobiol Dis **4**, 313–328

2 Seubert, P, Vigo-Pelfrey, C, Esch, F, Lee, M, Dovey, H, Davis, D, Sinha, S, Schlossmacher, M, Whaley, J, Swindlehurst, C et al (1992) Isolation and quantification of soluble Alzheimer's β-peptide from biological fluids. Nature (London) **359**, 325–327

3 Shoji, M, Golde, T E, Ghiso, J, Cheung, T T, Estus, S, Shaffer, L M., Cai, X D, McKay, D M, Tintner, R, Frangione, B and Younkin, S G (1992) Production of the Alzheimer amyloid β protein by normal proteolytic processing Science **258**, 126–129

4 Vigo-Pelfrey, C, Lee, D, Keim, P, Lieberburg, I. and Schenk, D. B. (1993) Characterization of β-amyloid peptide from human cerebrospinal fluid J. Neurochem **61**, 1965–1968

5 Ghiso, J, Calero, M, Matsubara, E, Governale, S, Chuba, J, Beavis, R, Wisniewski, T and Frangione, B. (1997) Alzheimer's soluble amyloid β is a normal component of human urine FEBS Lett **408**, 105–108

6 Naslund, J, Schierhorn, A, Hellman, U, Lannfelt, L, Roses, A D., Tjernberg, L O, Silberring, J, Gandy, S E, Winblad, B., Greengard, P et al (1994) Relative abundance of Alzheimer Aβ amyloid peptide variants in Alzheimer disease and normal aging. Proc Natl Acad Sci U S.A. **91**, 8378–8382

7 Tabaton, M., Nunzi, M G, Xue, R, Usiak, M, Autilio-Gambetti, L and Gambetti, P (1994) Soluble amyloid β-protein is a marker of Alzheimer amyloid in brain but not in cerebrospinal fluid Biochem Biophys. Res Commun **200**, 1598–1603

8 Teller, J K, Russo, C., DeBusk, L M, Angelini, G, Zaccheo, D, Dagna-Bricarelli, F, Scartezzini, S, Bertolini, S, Mann, D M. A, Tabaton, M and Gambetti, P (1996) Presence of soluble amyloid β-peptide precedes amyloid plaque formation in Down's syndrome Nat. Med **2**, 93–95

9 Oda, T, Wals, P, Osterburg, H H, Johnson, S. A, Pasinetti, G M., Morgan, T E, Rozovsky, I, Stine, W B, Snyder, S W., Holzman, T F et al. (1995) Clusterin (apoJ) alters the aggregation of amyloid β-peptide (Aβ 1-42) and forms slowly sedimenting Aβ complexes that cause oxidative stress Exp. Neurol **136**, 22–31

10 Wujek, J R, Dority, M. D, Frederickson, R C. and Brunden, K R. (1996) Deposits of Aβ fibrils are not toxic to cortical and hippocampal neurons *in vitro* Neurobiol Aging **17**, 107–113

11 Lambert, M. P., Barlow, A. K, Chromy, B. A, Edwards, C, Freed, R, Liosatos, M, Morgan, T E, Rozovsky, I, Trommer, B., Viola, K L et al (1998) Diffusible, nonfibrillar ligands derived from Aβ1-42 are potent central nervous system neurotoxins Proc Natl. Acad Sci U S A **95**, 6448–6453

12 Namba, Y, Tomonaga, M, Kawasaki, H, Otomo, E and Ikeda, K (1991) Apolipoprotein E immunoreactivity in cerebral amyloid deposits and neurofibrillary tangles in Alzheimer's disease and kuru plaque amyloid in Creutzfeldt–Jakob disease Brain Res. **541**, 163–166

13 Wisniewski, T. and Frangione, B (1992) Apolipoprotein E a pathological chaperone protein in patients with cerebral and systemic amyloid Neurosci. Lett **135**, 235–238

14 Naslund, J, Thyberg, J, Tjernberg, L O., Wernstedt, C, Karlstrom, A R., Bogdanovic, N, Gandy, S E, Lannfelt, L, Terenius, L and Nordstedt, C (1995) Characterization of stable complexes involving apolipoprotein E and the amyloid β peptide in Alzheimer's disease brain Neuron **14**, 219–228

15 Wisniewski, T, Lalowski, M, Golabek, A, Vogel, T. and Frangione, B (1995) Is Alzheimer's disease an apolipoprotein E amyloidosis? Lancet **345**, 956–958

16 Zannis, V I and Breslow, J. L (1981) Human very low density lipoprotein apolipoprotein E isoprotein polymorphism is explained by genetic variation and posttranslational modification Biochemistry **20**, 1033–1041

17 Saunders, A. M, Strittmatter, W J, Schmechel, D, George-Hyslop, P H, Pericak-Vance, M A, Joo, S H, Rosi, B L, Gusella, J F, Crapper-MacLachlan, D R., Alberts, M J et al (1993) Association of apolipoprotein E allele $\epsilon 4$ with late-onset familial and sporadic Alzheimer's disease. Neurology **43**, 1467–1472

18 Strittmatter, W J, Saunders, A M, Schmechel, D, Pericak-Vance, M, Enghild, J, Salvesen, G S. and Roses, A D (1993) Apolipoprotein E high-avidity binding to β-amyloid and increased frequency of type 4 allele in late-onset familial Alzheimer disease Proc Natl Acad Sci U S A **90**, 1977–1981

19 Corder, E H, Saunders, A M, Strittmatter, W. J, Schmechel, D E, Gaskell, P C, Small, G. W, Roses, A. D, Haines, J L and Pericak-Vance, M A (1993) Gene dose of apolipoprotein E type 4 allele and the risk of Alzheimer's disease in late onset families Science **261**, 921–923

20 Rebeck, G W, Reiter, J S, Strickland, D. K and Hyman, B T (1993) Apolipoprotein E in sporadic Alzheimer's disease: allelic variation and receptor interactions Neuron **11**, 575–580

21 Schmechel, D E, Saunders, A M, Strittmatter, W J, Crain, B J, Hulette, C M, Joo, S. H, Pericak-Vance, M A., Goldgaber, D and Roses, A D (1993) Increased amyloid β-peptide deposition in cerebral cortex as a consequence of apolipoprotein E genotype in late-onset Alzheimer disease Proc Natl Acad. Sci U S A **90**, 9649–9653

22 Strittmatter, W. J, Weisgraber, K H., Huang, D. Y, Dong, L.-M, Salvesen, G S, Pericak-Vance, M, Schmechel, D, Saunders, A M, Goldgaber, D and Roses, A D (1993) Binding of human apolipoprotein E to synthetic amyloid β peptide isoform-specific effects and implications for late-onset Alzheimer disease Proc Natl Acad Sci U S A **90**, 8098–8102

23 Wisniewski, T, Golabek, A, Matsubara, E., Ghiso, J and Frangione, B (1993)) Apolipoprotein E binding to soluble Alzheimer's β-amyloid. Biochem Biophys Res. Commun **192**, 359–365

24 LaDu, M J, Falduto, M T, Manelli, A. M, Reardon, C A., Getz, G S and Frail, D E (1994) Isoform-specific binding of apolipoprotein E to β-amyloid. J Biol. Chem **269**, 23403–23406

25 LaDu, M J., Pederson, T M, Frail, D E, Reardon, C A, Getz, G S and Falduto, M T. (1995) Purification of apolipoprotein E attenuates isoform-specific binding to β-amyloid J Biol Chem **270**, 9039–9042

26 Zhou, Z., Smith, J. D, Greengard, P and Gandy, S (1996) Alzheimer amyloid-β peptide forms denaturant-resistant complex with type $\epsilon 3$ but not type $\epsilon 4$ isoform of native apolipoprotein E Mol Med. **2**, 175–180

27 LaDu, M J, Lukens, J R, Reardon, C A and Getz, G. S (1997) Association of human, rat, and rabbit apolipoprotein E with β-amyloid J. Neurosci Res **49**, 9–18

28 Aleshkov, S., Abraham, C R and Zannis, V I (1997) Interaction of nascent ApoE2, ApoE3, and ApoE4 isoforms expressed in mammalian cells with amyloid peptide β (1-40) Relevance to Alzheimer's disease Biochemistry **36**, 10571–10580

29 Smith, J D, Melian, A, Leff, T and Breslow, J (1988) Expression of the human apolipoprotein E gene is regulated by multiple positive and negative elements J. Biol Chem **263**, 8300–8308

30 Miyata, M. and Smith, J. D (1996) Apolipoprotein E allele-specific antioxidant activity and effects on cytotoxicity by oxidative insults and beta-amyloid peptides Nat Genet **14**, 55–61

31 LaDu, M J, Gilligan, S. M, Lukens, J R, Cabana, V. G, Reardon, C A, Van Eldik, L J. and Holtzman, D M. (1998) Nascent astrocyte particles differ from lipoproteins in CSF J Neurochem **70**, 2070–2081

32 Osborne, J. R (1986) Delipidation of plasma lipoproteins. Methods Enzymol. **128**, 213–222

33 Koudinov, A, Matsubara, E., Frangione, B and Ghiso, J (1994) The soluble form of Alzheimer's amyloid β protein is complexed to high density lipoprotein 3 and very high density lipoprotein in normal human plasma Biochem Biophys Res Commun **205**, 1164–1171

34 Matz, C. E and Jonas, A (1982) Micellar complexes of human apolipoprotein A-I with phosphatidylcholines and cholesterol prepared from cholate-lipid dispersions J Biol Chem **257**, 4535–4540

35 Forte, T M and Nordhausen, R W (1986) Electron microscopy of negatively stained lipoproteins Methods Enzymol **128**, 442–457

36 Calero, M, Tokuda, T, Rostagno, A., Kumar, A, Zlokovic, B, Frangione, B and Ghiso, J (1999) Functional and structural properties of lipid-associated apolipoprotein J (clusterin) Biochem J **344**, 375–383

37 Chacko, G K., Mahlberg, F. H and Johnson, W J (1988) Cross-linking of apoproteins in high density lipoprotein by dimethylsuberimidate inhibits specific lipoprotein binding to membranes. J Lipid Res **29**, 319–324

38 Matsubara, E, Frangione, B and Ghiso, J (1995) Characterization of apolipoprotein J-Alzheimer's A beta interaction J. Biol Chem **270**, 7563–7567

39 Yokoyama, S, Kawai, Y, Tajima, S and Yamamoto, A (1985) Behavior of human apolipoprotein E in aqueous solutions and at interfaces. J Biol Chem **260**, 16375–16382

40 Yokoyama, S. (1990) Self-associated tetramer of human apolipoprotein E does not lead to its accumulation on a lipid particle. Biochim. Biophys Acta **1047**, 99–101

41 Aleskov, S. B, Lavrentiadou, Z N. and Zannis, V I (1999) Contribution of Cysteine 158, the glycosylation site Threonine 194, the amino- and carboxy-terminal domains of apolipoprotein E in the binding to amyloid peptide β (1-40) Biochemistry **38**, 8918–8925

42 Pitas, R E., Boyles, J. K, Lee, S. H., Foss, D. and Mahley, R W (1987) Astrocytes synthesize apolipoprotein E and metabolize apolipoprotein E-containing lipoproteins Biochim Biophys. Acta **917**, 148–161

43 Poirier, J, Hess, M., May, P C. and Finch, C E (1991) Astrocytic apolipoprotein E mRNA and GFAP mRNA in hippocampus after entorhinal cortex lesioning Mol Brain Res **11**, 97–106

44 Rebeck, G W and Hyman B T. (1999) Lipoprotein receptors in brain In Clusterin in Normal Brain Functions and during Neurodegeneration (Finch, C E, ed), pp. 49–59, R G. Landes Co., Austin

45 Innerarity, T L, Pitas, E and Mahley, R W (1979) Binding of arginine-rich (E) apoprotein after recombination with phospholipid vesicles to the low density lipoprotein receptors of fibroblasts J. Biol Chem **254**, 4186–4190

46 Nathan, B P, Bellosta, S., Sanan, D A, Weisgraber, K. H, Mahley, R. W and Pitas, R. E (1994). Differential effects of apolipoproteins E3 and E4 on neuronal growth *In vitro* Science **264**, 850–852

47 Bales, K. R, Verina, T, Dodel, R. C, Du, Y., Alstiel, L, Bender, M, Hyslop, P, Johnstone, E M, Little, S P, Cummins, D J et al (1997) Lack of apolipoprotein E dramatically reduces amyloid beta-peptide deposition. Nat Genet **17**, 263–264

48 Holtzman, D M, Bales, K R, Wu, S, Pnyanka, B, Parsadanian, M., Fagan, A. M., Chang, L K, Sun, Y and Paul, S M (1999) Expression of human apolipoprotein E reduces amyloid-beta deposition in a mouse model of Alzheimer's disease J Clin. Invest **103**, R15–R21

Received 6 December 1999/15 March 2000, accepted 23 March 2000

Biochem J (2000) 348, 367–373 (Printed in Great Britain)

Interaction of *Bacillus subtilis* CsaA with SecA and precursor proteins

Jörg P. MÜLLER*[1], Jörg OZEGOWSKI†, Stefan VETTERMANN‡, Jelto SWAVING§, Karel H. M. VAN WELY§ and Arnold J. M. DRIESSEN§

*Institute for Molecular Biology, Jena University, Winzerlaer Strasse 10, D-07745 Jena, Germany, †Institute of Experimental Microbiology, Jena University, Winzerlaer Str 10, D-07745 Jena, Germany, ‡ProThera GmbH, Winzerlaer Str. 10,D-07745 Jena, Germany, and §Department of Microbiology, Groningen Biomolecular Sciences and Biotechnology Institute, University of Groningen, Kerklaan 30, NL-9751 Haren, The Netherlands

CsaA from the Gram-positive bacterium *Bacillus subtilis* has been identified previously as a suppressor of the growth and protein-export defect of *Escherichia coli secA*(Ts) mutants. CsaA has chaperone-like activities *in vivo* and *in vitro*. To examine the role of CsaA in protein export in *B. subtilis*, expression of the *csaA* gene was repressed. While export of most proteins remained unaffected, export of at least two proteins was significantly reduced upon CsaA depletion. CsaA co-immunoprecipitates and co-purifies with the SecA proteins of *E. coli* and *B. subtilis*, and binds the *B. subtilis* preprotein prePhoB. Purified CsaA stimulates the translocation of prePhoB into *E. coli* membrane vesicles bearing the *B. subtilis* translocase, whereas it interferes with the SecB-mediated translocation of proOmpA into membrane vesicles of *E. coli*. The specific interaction with the SecA translocation ATPase and preproteins suggests that CsaA acts as a chaperone that promotes the export of a subset of preproteins in *B. subtilis*.

Key words: chaperone, co-immunoprecipitation, co-purification, *in vitro* translocation, protein translocation.

INTRODUCTION

In Eubacteria, proteins can be translocated across the cytoplasmic membrane and secreted into the medium. These proteins are usually synthesized as precursors with an N-terminal extension, the signal peptide (for review, see [1]), which is essential for directing them into the export pathway (for review, see [2]). Genetically and biochemically the best-characterized bacterial export system is that of *Escherichia coli* (for reviews, see [2,3]). This system, termed preprotein translocase, consists of the peripheral membrane protein SecA [4] and a multi-subunit membrane-protein complex with SecY, SecE and SecG as subunits [5]. The SecYEG complex acts as a receptor for SecA, and functions as a preprotein-conducting channel [6,7]. During or shortly after the translocation of the preprotein across the membrane, the signal peptide is removed by signal peptidase(s) (for review, see [8]), a prerequisite for the release of the mature protein from the membrane [9]. The integral membrane proteins SecD and SecF [10] are not essential for precursor protein translocation but, when overproduced, stabilize the SecYEG-bound SecA in a membrane-inserted state [11].

Whereas bacterial protein translocation is largely uncoupled from ongoing translation [12], efficient export requires chaperones to maintain preproteins in a translocation-competent state and to target them to the membrane-associated part of the translocase. In *E. coli*, SecB is an export-dedicated cytosolic chaperone that is required for efficient export of a subset of preproteins [13]. SecB stabilizes preproteins in an unfolded, non-aggregated state [14], and binds post-translationally or at the late co-translational stage to the mature region of these proteins [15]. The SecB–preprotein complex is then targeted to the SecYEG-bound SecA. The preprotein is subsequently transferred from SecB to SecA, and, upon the ATP-dependent initiation of translocation, the SecB is released into the cytosol [3]. *In vivo*, only a subset of preproteins appears to be translocated in a SecB-dependent manner [2]. A second targeting factor, consisting of the Ffh protein and the 4.5 S RNA, assists the export of SecB-independent exported proteins [16]. Other molecular chaperones, such as the heat-shock proteins DnaK/DnaJ/GrpE [17–19] and GroEL/GroES [20], appear also to be involved under specific conditions.

The central components of the protein-translocation system of *B. subtilis* are similar to those of *E. coli*. So far, homologues of Ffh, 4.5 S RNA, SecA, SecY, SecE, SecG, SecDF and several type-I signal peptidases have been identified (for review see [21]).

So far, it is unknown if chaperones are involved in protein translocation in *B. subtilis*. *B. subtilis* lacks a SecB homologue [22] and this has raised the question of whether other chaperones are involved in protein translocation. Depletion of signal-recognition-peptide (SRP) components impairs protein translocation [23,24], and the *B. subtilis* Ffh interacts directly with SecA and promotes the formation of soluble SecA–preprotein complexes [25]. This has led to the suggestion that SRP of *B. subtilis* not only acts as a targeting factor in co-translational translocation, but also stimulates post-translational translocation of preproteins [25]. The *B. subtilis* CsaA protein specifies chaperone-like activities possibly related to protein translocation [26]. The *csaA* gene was identified as a suppressor of growth and secretion defects of *E. coli secA*(Ts) strains [27]. Presence of CsaA stimulated precursor processing in *secA*, *secB*, *groEL* and *dnaJ* mutant strains of *E. coli* and it suppressed the growth defects of *dnaK*, *dnaJ* and *grpE* mutants of *E. coli*. CsaA stimulates the reactivation of heat-denatured firefly luciferase in *groEL*, *groES*, *dnaK* and *grpE* mutant strains of *E. coli*, and prevents the aggregation of heat-denatured luciferase *in vitro*. The exact mechanism by which CsaA suppresses the growth and secretion defects of *E. coli secA*(Ts) strains is unknown. CsaA may either improve the translocation-competence of exported preproteins, thereby making them better substrates for mutant SecA proteins, or stimulate the translocation activity of the

---

Abbreviations used. NaP_i, inorganic phosphate, NaH_2PO_4; His_6-CsaA, hexa-histidine-tagged CsaA; His_6-SecB, hexa-histidine-tagged SecB; His_6-prePhoB, hexa-histidine-tagged prePhoB, IPTG, isopropyl β-D-thiogalactoside, Ni-NTA, Ni^{2+}-nitrilotriacetate, SRP, signal recognition peptide

[1] To whom correspondence should be addressed (e-mail jmueller@imb-jena de)

mutant SecA proteins. Expression of CsaA in *E. coli* suppresses synthesis of SecB [26], whereas an impaired function of general chaperones causes an elevation in SecB expression [28]. These data further suggest a chaperone function of CsaA that could possibly be related to protein translocation.

In this paper we have further examined the role of CsaA in protein translocation in *B. subtilis*. CsaA affects the efficient secretion of some preproteins, and interacts specifically with SecA and preproteins. The data suggest that CsaA acts as a chaperone that promotes the export of a subset of preproteins in *B. subtilis*.

EXPERIMENTAL

Bacterial strains, plasmids and media

Bacterial strains and plasmids used in this study are listed in Table 1. Strains were grown in TY medium (Bacto Tryptone/Bacto Yeast extract) or on TY plates [28] Pulse labelling of *B. subtilis* was carried out in defined HPDM medium [29], casamino acids were replaced by amino acids (0.02 mg/ml) excluding methionine and cysteine. If required, ampicillin (80 μg/ml), erythromycin (5 μg/ml) or kanamycin (20 μg/ml) were added.

Biochemicals

B. subtilis SecA [32], *E. coli* SecA [33] and the *B. subtilis* GroELS complex [34] were isolated from overproducing strains as described. proOmpA [7] and hexa-histidine-tagged prePhoB (His$_6$-prePhoB) [35] were purified as described. Purified proOmpA, prePhoB and SecA proteins were labelled with carrier-free ^{125}I according to van Wely et al. [35]. Labelled preproteins were stored frozen in 6 M urea. Polyclonal antiserum was raised against purified hexa-histidine-tagged CsaA (His$_6$-CsaA). Antisera against SecA from *B. subtilis* were from R. Freudl (Forschungszentrum Jülich, Jülich, Germany). Membrane vesicles were prepared from *E. coli* strain SF100 [36] containing plasmid pET605 overproducing SecYEG from *E. coli* [37] or plasmid pET822 overproducing SecYEG from *B. subtilis* DB104 as described in [38]. Membrane vesicles were treated with polyclonal antibodies against *E coli* SecA to deplete and inactivate the endogenous SecA [38].

Table 1 Bacterial strains and plasmids, and their genotype/phenotypes

IPTG, isopropyl β-D-thiogalactoside, His$_6$-CsaA, hexa-histidine-tagged CsaA, His$_6$-SecB, hexa-histidine-tagged SecB

Strain/plasmid	Relevant genotype/phenotype	Reference
Strains		
B subtilis		
DB104	*his, nprE, aprE*	[30]
DB104 pMUTIN*csaA′*	DB104, allows IPTG-inducible expression of *csaA*	This study
E coli		
TG1	*hsdD5*/*F traD36, proA*$^+$*B*$^+$, Δ(*lac-pro*) *lacIQ, lacZ* ΔM15	[31]
TG1(pREP4)	Host for overexpression of His-tagged proteins	This study
TG1(pREP4, pQE9*csaA*)	TG1 derivative strain, Km^r, Ap^r, allows IPTG-inducible synthesis of His$_6$-CsaA	This study
TG1(pREP4, pQE9*secB*)	TG1 derivative strain, Km^r, Ap^r, allows IPTG-inducible synthesis of His$_6$-SecB	This study
Plasmids		
pMUTIN2	pBR322-based integration vector for *B subtilis*, containing IPTG-inducible P$_{spac}$ promoter, Ap^r, Em^r	[40]
pMUTIN*csaA′*	pMUTIN2 derivative, carries the 5′ part of *csaA*	
pREP4	plasmid, containing *lacI*^{q} repressor gene, Km^r	Qiagen
pQE9	pBR322-based vector for IPTG-inducible synthesis of His$_6$-tagged proteins, Ap^r	Qiagen
pQE9*csaA*	pQE9 derivative plasmid, Ap^r, allows IPTG-inducible synthesis of His$_6$-CsaA	This study
pQE9*secB*	TG1 derivative plasmid, Ap^r, allows IPTG-inducible synthesis of His$_6$-SecB	This study

DNA manipulation/techniques

Procedures for DNA purification, restriction, ligation, transformation of *E. coli* and agarose-gel electrophoresis were carried out as described by Sambrook et al [39] The nucleotide sequences of cloned PCR fragments were confirmed by DNA sequencing.

To amplify *csaA′*, oligonucleotides 5′-TCTCGAATTCAATAGGAGAAAAAGGAGTT^{574}-3′, localized 5′ to the ribosome-binding site of *csaA* and incorporating an *Eco*RI restriction site, and 5′-GGACCAAGGGATCCGATTTAAATCCGGCG^{805}-3′, localized within *csaA* and incorporating a *Bam*HI restriction site, were used (the numbers refer to those in Müller et al. [27]). The *csaA′* gene was amplified by PCR from *B. subtilis* chromosomal DNA. The amplified fragment was digested with *Eco*RI and *Bam*HI and cloned into pMUTIN2 [40] digested with the same enzymes. The resulting plasmid pMUTIN *csaA′* was integrated into the chromosome of *B subtilis* DB104 via Campbell-type integration.

For synthesis of His-tagged proteins *secB* and *csaA* genes were amplified excluding their ATG start codons and were inserted 3′ to the His-coding region of pQE9. Genes were amplified by PCR using oligonucleotides 5′-CACGGATCCGAACAAAACAACACTG^{103}-3′, incorporating a *Bam*HI restriction site, and 5′-CCGACTGCAGTCATTGAAGCATTACG^{558}-3′, with a *Pst*I restriction site, for *secB* (the numbers refer to those used in [41]), and oligonucleotides 5′-GGAGTTATTGGATCCGCAGTTATTGATGAC^{598}-3′, with a *Bam*HI restriction site, and 5′-GCCGATCTCTGCAGGCCTTTACGGCACACACG^{981}-3′, incorporating a *Pst*I restriction site, for *csaA* (the numbers refer to those used in [27]). PCR fragments were purified, digested with *Bam*HI and *Pst*I and inserted into pQE9 digested with the same enzymes. The resulting plasmids pQE9secB and pQE9csaA were transformed into *E. coli* TG1(pREP4).

Pulse–chase protein labelling and analysis of protein secretion

Pulse–chase protein-labelling experiments were performed as described by van Dijl et al. [42]. *B. subtilis* was grown in minimal medium to exponential growth in the absence or presence of 1 mM isopropyl β-D-thiogalactoside (IPTG), pulse labelled with [^{35}S]methionine for 1 min and subsequently chased. Samples were taken 2 and 5 min post chase time and proteins secreted into the growth medium were collected as described in [43]. SDS/PAGE was performed according to Laemmli [44] ^{14}C-Methylated proteins (Amersham International, Amersham, Bucks, U.K.) were used as molecular-size markers. Relative amounts of radioactivity were estimated by using a PhosphoImager (Fuji) and associated image-analysis software.

Purification of proteins

His$_6$-CsaA and hexa-histidine-tagged SecB (His$_6$-SecB) were prepared from IPTG-induced *E. coli* TG1(pREP4, pQE9csaA) and TG1(pREP4, pQE9secB) cultures as abundant proteins and purified by Ni^{2+}-nitrilotriacetate (Ni-NTA) agarose affinity chromatography. Purification was carried out under native conditions following standard protocols (Qiagen, Hilden, Germany). Cell lysates prepared in 50 mM NaP_i (inorganic phosphate, NaH_2PO_4), pH 8.0, and 300 mM NaCl, were supplemented with 10 mM imidazole and applied on to the Ni-NTA column. The column was washed three times with several column volumes of NaP_i buffer containing 20 mM imidazole. His-tagged proteins were eluted with NaP_i buffer containing 500 mM imidazole.

CsaA from *B. subtilis* was purified immunologically. Affinity-purified rabbit antibodies against CsaA were covalently linked to CNBr-activated Sepharose. Exponentially grown *B. subtilis* DB104 cells were harvested and extracts were prepared from lysozyme-treated cells via sonication. Cleared cell extracts were loaded on to the anti-CsaA–Sepharose column at room temperature. Anti-CsaA–Sepharose was washed with 30 ml of phosphate buffer (50 mM, pH 7.0) containing 0.5 M NaCl until no detectable protein was eluted from the column. CsaA was eluted with 0.1 M acetic acid, pH 3.0, and subsequently lyophilized. To obtain SecA-free CsaA *B. subtilis* cell extracts were purified by preparative isoelectric focusing in Sephadex gel with a pH gradient from pH 4.0 to 9.0 for 18 h. After focusing, the Sephadex gel was cleaved to fractions and CsaA-containing fractions (as determined immunologically) were analysed by thin-layer polyacrylamide gel isoelectric focusing with an ampholyte solution (pH 3.5–10.0) and SDS/PAGE. The CsaA was precipitated with ammonium sulphate to a final concentration of 80 % saturation. The precipitated protein was dissolved, dialysed against H_2O and lyophilized.

Western blotting

Proteins isolated from exponentially growing cultures were assayed by Western blotting [45]. Cell lysates were prepared by boiling (5 min) in sample buffer and subjecting to SDS/PAGE [44]. Separated proteins were transferred to a nitrocellulose membrane (Schleicher & Schüll), as described by Towbin et al. [45]. CsaA and SecA proteins were detected with specific polyclonal antibodies and alkaline phosphatase-conjugated goat anti-rabbit antibodies (Bio-Rad) according to the manufacturer's instructions. Similar amounts of total cell protein were loaded on to each lane.

Binding studies

Binding of $[^{125}I]His_6$-prePhoB or $[^{125}I]$SecA to CsaA was measured as follows: 1 μg of ^{125}I-labelled protein and 1 μg of CsaA were incubated at room temperature in 50 μl of Hepes buffer (50 mM, pH 7.6, additional buffer components as indicated). After 60 min, 5 μl of CsaA-specific antiserum precomplexed with 5 mg of Protein A–Sepharose was added and the mixture was further incubated for 60 min with regular vortexing. Subsequently, the Protein A–Sepharose beads were washed five times with 500 μl of Hepes buffer, pH 7.6. ^{125}I-Labelled proteins bound to Protein A–Sepharose beads were counted in Optima Gold scintillation liquid (Packard Instruments B.V., Groningen, The Netherlands).

Translocation assay

The efficiency of translocation *in vitro* of $[^{125}I]$proOmpA and $[^{125}I]$prePhoB into *E. coli* membrane vesicles was assayed by treatment with proteinase K [46]. When indicated, 1.0 μg of purified *E. coli* or *B. subtilis* SecA protein, 2.0 μg of *E. coli* SecB or 4 μg of purified *B. subtilis* GroESL or *B. subtilis* CsaA were added. Reactions were started by the addition of 1 μl of ^{125}I-labelled precursor protein (0.5 μg of protein). For preincubation experiments, mixtures were incubated for 30 min at 37 °C without membrane vesicles prior to the translocation reactions. After 30 min of translocation at 37 °C samples were chilled on ice, treated with proteinase K (0.5 mg/ml) for 15 min, precipitated with 7.5 % trichloroacetic acid, washed with acetone, dissolved in SDS/PAGE sample buffer, and analysed by SDS/PAGE (10 % gel) and autoradiography.

RESULTS

Repression of CsaA expression results in alteration of protein secretion

In *B. subtilis* strain DB104::pMUTIN2*csaA'*, *csaA* is localized downstream of the P_{spac} promoter, allowing the IPTG-inducible expression of the CsaA protein. Cells grown in the absence of IPTG were normally viable but Western-blotting analysis showed that they contained a dramatically reduced cellular level of CsaA. Induction of the P_{spac} promoter resulted in a production level of CsaA that was about 2-fold higher than in the wild type (Figure 1A). To study the function of CsaA in protein secretion, the pattern of proteins secreted by *B. subtilis* DB104::pMUTIN2*csaA'* grown in the absence or presence of IPTG was determined. While the pattern of secreted proteins of the strain grown in presence of IPTG was indistinguishable from that of the wild type, repression of *csaA* expression resulted in a decrease in at least two proteins with apparent molecular masses of 19 and 36 kDa (Figure 1B). In particular, the 36-kDa protein

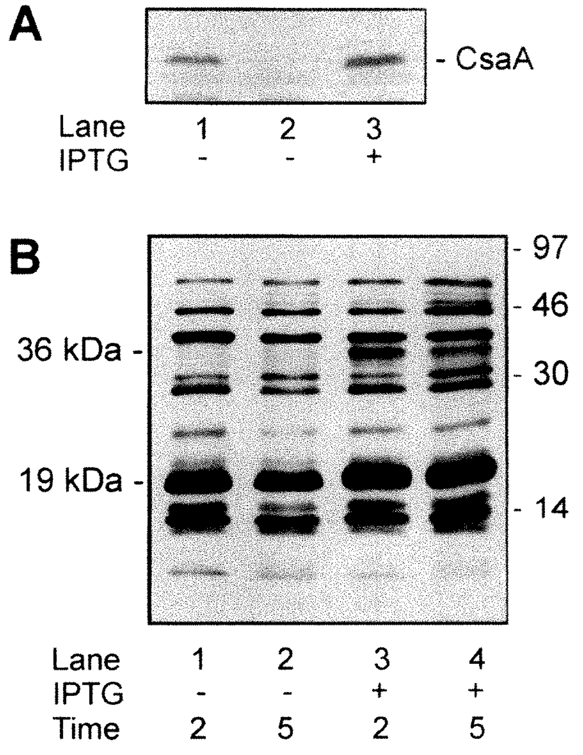

Figure 1 Repression of *csaA* in *B. subtilis* affects protein export

(**A**) *B. subtilis* strain DB104 (lane 1) and strain DB104::pMUTIN2*csaA'* (lanes 2 and 3) were grown in TY medium in the absence (lanes 1 and 2) or presence (lane 3) of 1 mM IPTG. Cell extracts were analysed by SDS/PAGE and Western blotting using CsaA-specific antibodies. (**B**) Protein secretion of *B. subtilis* DB104::pMUTIN2*csaA'* was analysed by pulse labelling of cells grown in the absence (lanes 1 and 2) or presence (lanes 3 and 4) of IPTG. Secreted proteins were collected by filtration and analysed by SDS/PAGE and autoradiography.

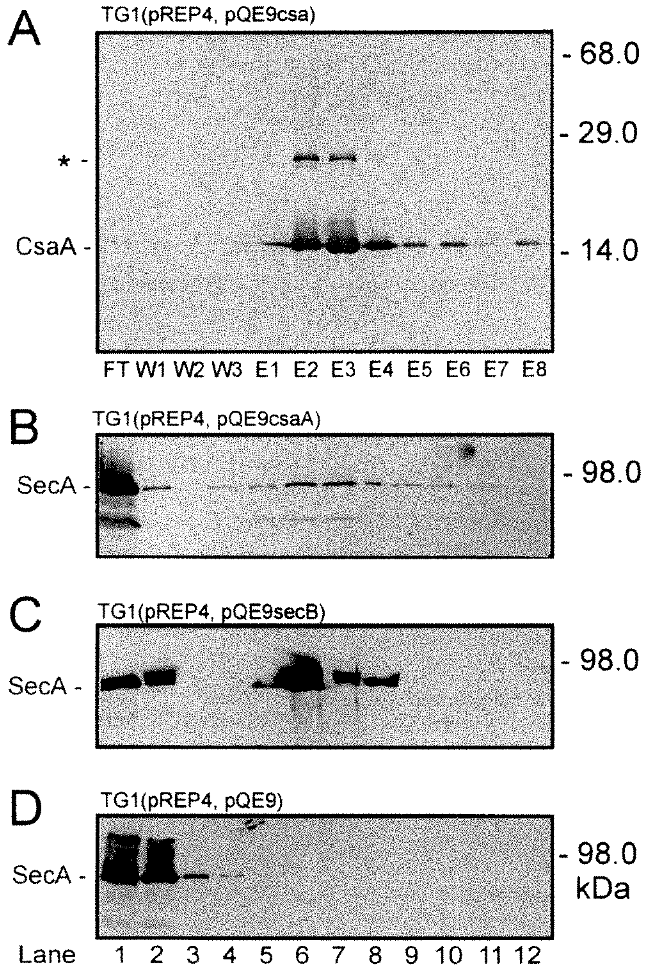

Figure 2 *E. coli* SecA interacts with His$_6$-CsaA and His$_6$-SecB

E. coli strains TG1(pREP4, pQE9csaA) (**A**, **B**), TG1(pREP4, pQE9secB) (**C**) and TG1(pREP4, pQE9) (**D**) were cultivated in TY medium to exponential growth and the phage T5 promoter was derepressed by adding IPTG (final concentration, 2 mM) to the culture medium. After 2 h, cells were harvested and lysed by sonication, and the cleared cell extracts were loaded on to Ni-NTA columns. Aliquots of non-bound fraction (FT, lane 1), wash (W1–W3, lanes 2–4) and elution fractions (E1–E8, lanes 5–12) were analysed by SDS/PAGE and Western blotting using antibodies directed against CsaA (**A**) and *E. coli* SecA (**B**–**D**). The asterisk indicates the position of dimeric CsaA.

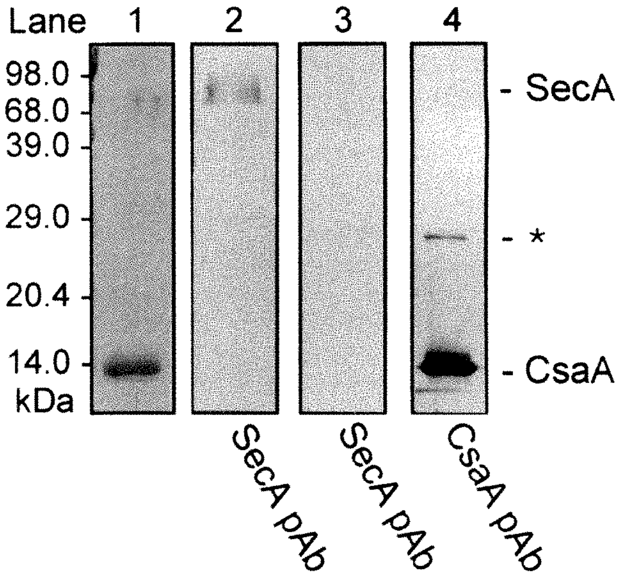

Figure 3 *B. subtilis* SecA co-purifies with CsaA

A cell lysate of *B. subtilis* DB104 was loaded on to an anti-CsaA–Sepharose column, washed with NaCl buffer (0.5 M) and the immunologically bound CsaA was eluted with 0.1 M acetic acid. The eluate was analysed by SDS/PAGE and Coomassie Brilliant Blue staining (lane 1) or Western blotting using polyclonal antibodies (pAb) directed against the *B. subtilis* SecA (lane 2) or CsaA (lane 4). The asterisk indicates the localization of dimeric CsaA. As a control, a lysate of *B. subtilis* DB104::pMUTIN2*csaA′* grown in the absence of IPTG was loaded on to the anti-CsaA–Sepharose column, and the fraction eluted with 0.1 M acetic acid was stained immunologically with antibodies directed against the *B. subtilis* SecA (lane 3).

seemed completely absent in the supernatant of CsaA-depleted cells. Both protein bands were isolated from Coomassie Brilliant Blue-strained SDS/PAGE, and N-terminally sequenced. While the N-terminus of the 36-kDa protein appeared blocked, the N-terminus of the 19-kDa protein corresponded to KENHTFSGED. This amino acid sequence matched the amino acid residues 33–42 of the precursor of YvaY, a protein with unknown function and a calculated molecular mass of 18.8 kDa.

E. coli SecA co-purifies with His$_6$-CsaA and His$_6$-SecB

His-tagged CsaA protein was overproduced in *E. coli* TG1 (pREP4, pQE9*csaA*) and purified by Ni-NTA-column chromatography. The imidazole-eluted protein fraction predominantly contained the 13-kDa CsaA protein, and a protein with an apparent molecular mass of about 30 kDa that stained with antibodies directed against CsaA (Figure 2A). The latter probably represents some dimeric CsaA. Immunodetection with SecA antibodies revealed that SecA co-eluted with CsaA from the column (Figure 2B). To exclude the possibility that SecA non-specifically binds to the Ni-NTA resin, a lysate of *E. coli* TG1(pREP4) cells that do not express the His-tagged CsaA was loaded on to an Ni-NTA column (Figure 2D). Under those conditions, no SecA was retained by the column, suggesting an interaction between CsaA and SecA. Since SecA is known to interact with SecB in *E. coli* [6,7,47], His$_6$-SecB was purified from *E. coli* TG1(pREP4,pQE9*secB*) under conditions used for purification of His$_6$-CsaA. SecA was found to co-elute with His$_6$-SecB (Figure 2C). These results indicate that SecA was retained in the Ni-NTA column via specific binding to His-tagged CsaA or SecB.

B. subtilis SecA interacts with CsaA

To establish whether the interaction of CsaA with SecA can be observed in *B. subtilis*, CsaA was purified from *B. subtilis* DB104. Cell extracts were loaded on to an anti-CsaA–Sepharose column, washed and eluted as described in the Experimental section. The eluate was analysed by SDS/PAGE and Coomassie Brilliant Blue staining (Figure 3, lane 1). In addition to CsaA, a protein co-eluted with an apparent molecular mass of about 90 kDa. The latter could be immunostained with an antibody directed against the *B. subtilis* SecA (Figure 3, lane 2), suggesting that the *B. subtilis* SecA associates with CsaA. As a control, a lysate of *B. subtilis* DB104::pMUTIN2*csaA′* grown in the absence of IPTG was used. Under those conditions, CsaA was not expressed (Figure 1A, lane 2) and no SecA was found to bind to the anti-CsaA–Sepharose column (Figure 3, lane 3).

Since the data *in vivo* suggest a specific interaction between SecA and CsaA, the interaction was examined further using

Table 2 Co-immunoprecupitation of CsaA with *E. coli* and *B. subtilis* SecA

Purified CsaA and [^{125}I]SecA proteins from *E. coli* or *B. subtilis* were mixed in 50 mM Hepes, pH 7.6, supplemented with 60 mM urea and 1.25% octylglucoside. After 60 min of incubation at room temperature, CsaA- or *E. coli* or *B. subtilis* SecA-specific antibodies pre-complexed with Protein A–Sepharose were added and the incubation was continued for another 60 min. Immunoprecipitates were collected by centrifugation and the amount of bound SecA was quantified by liquid scintillation counting. Amounts of radiolabelled SecA (means ± S.D. from two independent experiments) are shown in c.p.m. pAb, polyclonal antibody.

			Bound [^{125}I]SecA (c.p.m.)	
CsaA	CsaA pAb	SecA pAb	*E. coli*	*B. subtilis*
+	+	–	3140 ± 10	470 ± 106
+	–	–	948 ± 470	100 ± 6
–	+	–	1198 ± 75	176 ± 32
–	–	–	889 ± 3	139 ± 5
–	–	+	9724 ± 100	2170 ± 15

Table 3 Co-immunoprecupitation of CsaA with *B. subtilis* prePhoB

Purified CsaA and [^{125}I]His$_6$-prePhoB were mixed in 50 mM Hepes, pH 7.6, supplemented with 60 mM urea and 1.25% octylglucoside. After a 60-min incubation at room temperature, CsaA- or prePhoB-specific antibodies pre-complexed with Protein A–Sepharose were added and the incubation was continued for another 60 min. Immunoprecipitates were collected by centrifugation and the amount of bound prePhoB was quantified by liquid scintillation counting. pAb, polyclonal antibody.

CsaA	CsaA pAb	PhoB pAb	Bound [^{125}I]PhoB (c.p.m.)
+	+	–	1199
+	–	–	75
–	+	–	292
–	–	–	329
–	–	+	4291

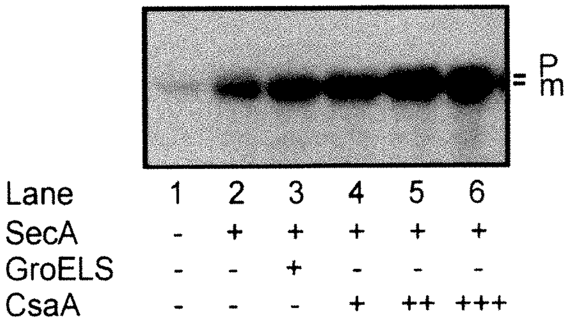

Figure 4 Effect of CsaA on the SecA-mediated translocation of prePhoB into membrane vesicles of *E. coli* containing *B. subtilis* SecYEG

Translocation of [^{125}I]His$_6$-prePhoB in membrane vesicles was carried out in the absence (lane 1) and presence (lanes 2–6) of exogenous SecA, and the presence of GroELS complex (1 μg, lane 3) or CsaA (0.5 μg, lane 4; 2 μg, lane 5; 5 μg, lane 6). After translocation, samples were treated with proteinase K and analysed by SDS/PAGE and autoradiography. p, precursor; m, mature protein.

purified proteins. CsaA was co-incubated with ^{125}I-labelled *E. coli* and *B. subtilis* SecA. Complex formation was analysed by immunoprecipitation of CsaA. To differentiate between CsaA-mediated and non-specific binding of SecA to Protein A–Sepharose, CsaA and/or antiserum against CsaA were excluded from the reaction mixture. In the presence of CsaA, both the *E. coli* and *B. subtilis* SecA proteins could be immunoprecipitated by the CsaA antibodies (Table 2). Background levels of immunoprecipitation were observed when either CsaA (Table 2) or the CsaA antibodies were excluded from the reaction mixture. These results suggest that SecA and CsaA are interacting proteins.

CsaA binds the preprotein prePhoB and stimulates its translocation *in vitro*

CsaA interacts with unfolded proteins [26]. To determine if CsaA also interacts with unfolded preproteins, urea-denatured *B. subtilis* preprotein [^{125}I]His$_6$-prePhoB at 1 mg/ml was diluted 100-fold into a buffer containing 10 μg/ml CsaA protein. Complex formation was assessed by immunoprecipitation with a CsaA antibody. A substantial amount of the His$_6$-prePhoB could be co-immunoprecipitated with CsaA (Table 3), whereas only low levels of prePhoB were immunoprecipitated when either the CsaA (Table 3) or the CsaA antibodies were excluded from the reaction mixture.

His$_6$-prePhoB was used previously to demonstrate preprotein translocation into *E. coli* membrane vesicles derived from a strain that overexpresses the SecYEG complex of *B. subtilis* [38]. The ATP-dependent translocation of urea-denatured [^{125}I]His$_6$-prePhoB by *E. coli* membrane vesicles bearing SecYEG and SecA from *B. subtilis* was examined using the proteinase digestion assay. While in the absence of SecA (Figure 4, lane 1) or ATP (results not shown) hardly any translocation of [^{125}I]His$_6$-prePhoB occurred, efficient translocation was observed when the membrane vesicles were supplemented with purified *B. subtilis* SecA (Figure 4, lane 2). Addition of *B. subtilis* GroESL complex or increasing amounts of CsaA (Figure 4, lanes 4–6) further stimulated the translocation of [^{125}I]His$_6$-prePhoB. To establish if the stimulatory effect of CsaA is related to maintenance of the translocation competence of [^{125}I]His$_6$-prePhoB, experiments were performed in which [^{125}I]His$_6$-prePhoB was diluted 50-fold into buffer in the absence and presence of CsaA, followed by a 30-min precubation at 37 °C. However, under these conditions prePhoB hardly exhibited a loss in translocation competence (results not shown), suggesting that CsaA may stimulate translocation by another mechanism.

CsaA interferes with SecB for translocation of proOmpA into *E. coli* membrane vesicles

Since CsaA interacts with preproteins and with SecA, an activity reminiscent of SecB, we determined if CsaA is able to substitute for SecB in the translocation of [^{125}I]proOmpA into *E. coli* membrane vesicles that contain elevated levels of *E. coli* SecYEG complex. Urea-denatured [^{125}I]proOmpA was preincubated in buffer for 30 min in the absence or presence of SecB or CsaA. In the absence of SecB, the translocation activity of the preincubated [^{125}I]proOmpA was largely abolished (Figure 5A, compare lanes 2 and 3). Preincubation of proOmpA with CsaA did not maintain the translocation competence of proOmpA (Figure 5A, lanes 4–6). Next, the effect of co-incubation of CsaA and SecB with proOmpA was determined (Figure 5B). The amount of translocated [^{125}I]proOmpA decreased with the concentration of CsaA present in the pre-incubation mixture (Figure 5B). When CsaA was added at the end of the SecB–proOmpA pre-incubation period, the inhibitory effect of CsaA on the translocation of [^{125}I]proOmpA was still evident (Figure 5C). The data indicate that CsaA interferes with the ability of SecB to promote proOmpA translocation.

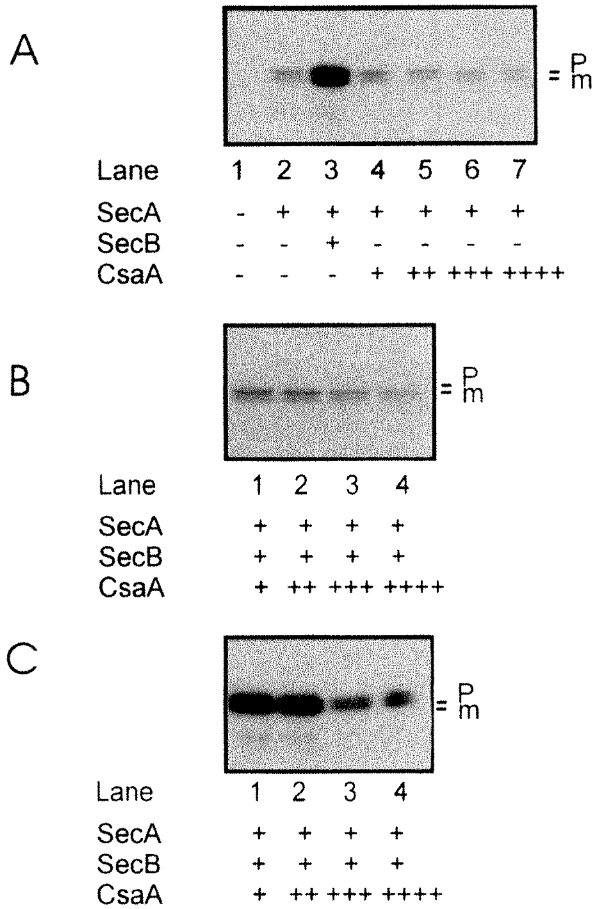

Figure 5 Translocation of proOmpA by *E. coli* membrane vesicles containing overproduced *E. coli* SecYEG

Translocation of [^{125}I]proOmpA into membrane vesicles was performed as described in the Experimental section. (**A**) proOmpA was pre-incubated for 30 min at 37 °C in the absence (lane 1), or presence of SecA (1 μg; lane 2) and SecB (1 μg; lane 3) or CsaA (0.1 μg, lane 4; 0.5 μg, lane 5; 1 μg, lane 6; 5 μg, lane 7). (**B**) proOmpA was pre-incubated for 30 min at 37 °C in the presence of SecA and SecB (1 μg each) and CsaA (0.1 μg, lane 1; 0.5 μg, lane 2; 1 μg, lane 3; 5 μg, lane 4). (**C**) as (**B**) except that CsaA was added at the end of the pre-incubation period. Translocation was assayed after the pre-incubation period by the addition of membrane vesicles, and was performed as described in the Experimental section. p, precursor; m, mature protein.

DISCUSSION

The cytosolic *B. subtilis* protein CsaA has been identified as a suppressor of *E. coli secA* mutations [26]. CsaA has chaperone-like activities both *in vivo* and *in vitro* [26]. We have now studied the role of CsaA in protein translocation in *B. subtilis* using an *in vitro* translocation system [35,38]. The data indicate that CsaA is able to interact with the *B. subtilis* preprotein prePhoB and the translocation ATPase SecA, and that this interaction results in a stimulation of prePhoB translocation. Moreover, repression of the *csaA* gene in *B. subtilis* results in a reduction of the secretion efficiency of at least two proteins. Such interactions are reminiscent of the secretion-dedicated function of the molecular chaperone SecB in *E. coli* [15]. Since *B. subtilis* lacks a protein homologous to SecB [22], CsaA may fulfil a similar function for a specific subset of preproteins to the *E. coli* SecB.

As a heterologous component, CsaA suppresses export and chaperone defects in *E. coli* [26,27]. To study the function of CsaA in protein export in *B. subtilis*, protein export was analysed in response to *csaA* suppression. Earlier extensive gene-disruption experiments failed [27], suggesting that *csaA* is an essential gene of *B. subtilis*. Therefore, *csaA* was placed under transcriptional control of the P$_{spac}$ promoter using the integrative plasmid pMUTIN2 [40]. Despite the fact that CsaA could not be detected in the absence of IPTG (Figure 1A), no alteration of growth was observed for *B. subtilis* DB104::pMUTIN2*csaA′* when grown in complex or defined medium. The possibility that minimal expression of CsaA, beyond the detection limit, suffices to sustain growth of this strain in the absence of IPTG cannot be excluded. Whereas in the presence of IPTG, protein secretion was essentially similar to the parental strain, repression of *csaA* resulted in a reduced export of at least two proteins at the end of the exponential growth phase.

An interaction between CsaA and *E. coli* or *B. subtilis* SecA could be demonstrated by various techniques. *E. coli* SecA co-purifies with His$_6$-tagged CsaA on an Ni-NTA affinity resin, while the *B. subtilis* SecA was found to specifically co-purify with CsaA by means of an immuno-purification technique. Likewise, *E. coli* SecA co-purifies with His$_6$-SecB using the Ni-NTA-affinity column-chromatography technique. Since the latter interaction has been established previously [6], it suggests that the CsaA–SecA complex is also stable. No other proteins were co-purified in detectable amounts. The markedly lower retention of SecA in the presence of His$_6$-CsaA compared with the retention by His$_6$-SecB might have been due to the heterologous character of CsaA when expressed in *E. coli*. The interaction between CsaA and SecA could be demonstrated further *in vitro* by a co-immunoprecipitation of ^{125}I-labelled purified proteins. In *E. coli*, SecB binds to a well-conserved C-terminal region of SecA [7]. When fused to glutathione S-transferase, the 20 C-terminal amino acids of *E. coli* SecA represent an authentic SecB-binding domain. This glutathione S-transferase-fusion protein, however, does not interact with CsaA (J. P. Müller, J. Swaving, K. H. M. van Wely and A. J. M. Driessen, unpublished work), indicating that other domains of SecA are involved in this binding reaction. Interaction of CsaA with unfolded preproteins could be demonstrated by co-immunoprecipitation of His$_6$-prePhoB via CsaA. Similar experiments with radiolabelled proOmpA suggest that CsaA also interacts with this precursor (J. P. Müller, J. Swaving, K. H. M. van Wely and A. J. M. Driessen, unpublished work). Interaction of CsaA with these unfolded precursors is not unexpected since CsaA can also interact with other unfolded proteins [26].

The exact mechanism of suppression of impaired activity of the temperature-sensitive SecA proteins has not yet been established. CsaA may act by improving the translocation-competence of exported preproteins, thereby making them better substrates for the malfunctioning SecA proteins, or it may act directly on the activity of SecA [25]. Our current data suggest that it may stimulate translocation by improving the targeting to SecA as it binds SecA specifically.

In *E. coli*, chaperones are needed to support translocation of preproteins *in vitro*. SecB is required for a subset of preproteins [14,48], while other chaperones such as GroES/GroEL or DnaK/DnaJ/GrpE support translocation under certain conditions only [49]. In *B. subtilis*, no chaperones have thus far been found that stimulate preprotein translocation, although this function may be fulfilled by SRP, which has been shown to interact with SecA, thereby promoting the formation of soluble SecA–preprotein complexes [24]. Here we have shown that CsaA stimulates the translocation *in vitro* of prePhoB into membrane vesicles by about 2–3-fold. It is important to note that prePhoB only slowly loses its translocation competence when diluted from urea, suggesting that the stimulation is due to targeting. More striking is the observation that CsaA competes with SecB for proOmpA translocation. When proOmpA is preincubated with a mixture of SecB and CsaA, SecB is no longer able to stimulate the translocation of proOmpA. In this context, it is important to note that CsaA itself does not stimulate the translocation of proOmpA, nor is it able to maintain the translocation competence of proOmpA. Since the inhibitory effect of CsaA is less pronounced when proOmpA is first pre-incubated with SecB, it seems that competition is mainly at the level of binding of the precursor, thus preventing SecB to target proOmpA to the translocation sites while maintaining its translocation competence. Elucidation of the mechanism of inhibition may provide further insight into the function of CsaA.

Taken together, the results *in vivo* and *in vitro* indicate that CsaA is able to bind to both *B. subtilis* preproteins and the SecA translocation ATPase, suggesting an export-related function of CsaA in *B. subtilis*. Depletion of CsaA in *B. subtilis* gives rise to an export defect of a set of proteins. Analysis of the translocation of these proteins in *B. subtilis* will further define the function of CsaA in protein secretion.

These investigations were supported by a short-term EMBO fellowship to J P.M., by grants from the Deutsche Forschungsgemeinschaft, and by grants to A.J M D from CEC Biotech nos. BIO2 CT 930254 and BIO4 CT 960097.

REFERENCES

1 Von Heijne, G. (1990) J. Membrane Biol **115**, 195–201
2 Wickner, W, Driessen, A J. M. and Hartl, F-U (1991) Annu Rev. Biochem **60**, 101–124
3 Fekkes, P and Driessen, A. J. M (1999) Microbiol Mol Biol. Rev **63**, 161–173
4 Oliver, D B and Beckwith, J. (1982) Cell **330**, 311–319
5 Douville, K, Price, A, Eichler, J, Economou, A and Wickner, W (1995) J. Biol Chem **270**, 20106–20111
6 Hartl, F.-U, Lecker, S, Schiebel, E, Hendrick, J P. and Wickner, W (1990) Cell **63**, 269–279
7 Fekkes, P, van der Does, C and Driessen, A. J M (1997) EMBO J **16**, 6105–6113
8 Dalbey, R E, Lively, M O, Bron, S and van Dijl, J M (1997) Protein Sci **6**, 1129–1138
9 Dalbey, R E and Wickner, W (1985) J. Biol Chem. **260**, 15925–15931
10 Gardel, C., Johnson, K, Jacq, A and Beckwith, J (1990) EMBO J **10**, 3209–3216
11 Economou, A, Pogliano, J A, Beckwith, J, Oliver, D B. and Wickner, W (1995) Cell **83**, 1171–1181
12 Randall, L L and Hardy, S J S (1995) Trends Biochem Sci. **20**, 65–69
13 Kumamoto, C A and Beckwith, J (1985) J Bacteriol **163**, 267–274
14 Lecker, S, Lill, R, Ziegelhofer, T, Georgopoulos, C, Bassford, P J, Kumamoto, C A and Wickner, W. (1989) EMBO J. **8**, 2703–2709
15 Kumamoto, C. A and Francetic, O. (1993) J Bacteriol **175**, 2184–2188
16 Phillips, G. J. and Silhavy, T J (1992) Nature (London) **359**, 744–746
17 Wild, J, Altman, E, Yura, T and Gross, C A (1992) Genes Dev **6**, 1165–1172
18 Wild, J., Rossmeissl, P, Walter, W A and Gross, C. A. (1996) J. Bacteriol. **178**, 3608–3616
19 Wild, J, Walter, W A, Gross, C A and Altman, E (1993) J. Bacteriol. **175**, 3992–3997
20 Kusukawa, N., Yura, T, Ueguchi, C, Akiyama, Y and Ito, K (1989) EMBO J. **8**, 3517–3521
21 Braun, P., Gerritse, G., van Dijl, J. M and Quax, W J (1999) Curr Opin Biotechnol **10**, 376–381
22 Kunst, F, Ogasawara, N, Moszer, I, Albertini, A M, Alloni, G, Azevedo, V., Bertero, M. G, Bessieres, P, Bolotin, A, Borchert S. et al (1997) Nature (London) **390**, 249–256
23 Nakamura, K, Imai, Y., Nakamura, A and Yamane, K (1992) J Bacteriol **174**, 2185–2192
24 Honda, K., Nakamura, K., Nishiguchi, M. and Yamane, K (1993) J. Bacteriol **175**, 4885–4894
25 Bunai, K., Yamada, K., Hayashi, K., Nakamura, K. and Yamane, K (1999) J. Biochem. (Tokyo) **125**, 151–159
26 Muller, J., Bron, S, Venema, G and van Dijl, J M. (2000) Microbiology **146**, 77–88
27 Muller, J., Walter, F, van Dijl, J M and Behnke, D. (1992) Mol. Gen. Genet **235**, 89–96
28 Muller, J. (1996) J. Bacteriol **178**, 6097–6104
29 Hulett, F. M., Bookstein, C. and Jensen, K. (1990) J. Bacteriol **172**, 735–740
30 Kawamura, F. and Doi, R H (1984) J Bacteriol **160**, 442–434
31 Carter, P., Bedouelle, H. and Winter, G. (1985) Nucleic Acids Res **13**, 4431–4443
32 van der Wolk, J., Klose, M, Breukink, E, Demel, R A, de Kruijff, B., Freudl, R and Driessen, A J M. (1993) Mol Microbiol **8**, 31–42
33 Cabelli, R J, Chen, L, Tai, P. C and Oliver, D B (1988) Cell **55**, 683–692
34 Schon, U. and Schumann, W (1995) FEMS Microbiol. Lett **134**, 183–188
35 van Wely, K H., Swaving, J. and Driessen, A J. M (1998) Eur J Biochem **255**, 690–697
36 Baneyx, F and Georgiou, G (1990) J. Bacteriol **172**, 491–494
37 van der Does, C, Manting, E H, Kaufmann, A, Lutz, M and Driessen, A J M (1998) Biochemistry **37**, 201–210
38 Swaving, J, van Wely, K H and Driessen, A J. M (1999) J Bacteriol **181**, 7021–7027
39 Sambrook, J., Fritsch, E F. and Maniatis, T. (1989) Molecular Cloning. a Laboratory Manual, Cold Spring Harbor Press, Cold Spring Harbor
40 Vagner, V, Dervyn, E. and Ehrlich, S D (1998) Microbiology **144**, 3097–3104
41 Kumamoto, C. A and Nault, A K (1989) Gene **75**, 167–175
42 van Dijl, J M., de Jong, A, Smith, H, Bron, S and Venema, G (1991) Mol Gen Genet **227**, 40–48
43 Muller, J and Harwood, C. R (1998) Appl. Microbiol Biotechnol **49**, 321–327
44 Laemmli, U K. (1970) Nature (London) **227**, 680–685
45 Towbin, H, Staehelin, T and Gordon, J (1979) Proc Natl Acad Sci U S A **76**, 4350–4354
46 Hoffschulte, H K, Drees, B and Muller, M (1994) J. Biol Chem **269**, 12833–12839
47 van der Does, C, den Blaauwen, T., de Wit, J. G., Manting, E H, Groot, N. A., Fekkes, P and Driessen, A J (1996) Mol Microbiol. **22**, 619–629
48 Weiss, J B., Ray, P H. and Bassford, Jr, P J (1988) Proc Natl Acad Sci U S A **85**, 8978–8982
49 Altman, E., Kumamoto, C A and Emr, S D (1991) EMBO J **10**, 239–245

Received 4 January 2000/6 March 2000, accepted 27 March 2000

Suppression of temperature-sensitivity of a *dnaA46* mutant by excessive DNA supercoiling

Taemi KONDO*, Shinji MIMA*, Nobuko FUKUMA†, Kasuhisa SEKIMIZU†, Tomofusa TSUCHIYA* and Tohru MIZUSHIMA*‡[1]

*Faculty of Pharmaceutical Sciences, Okayama University, Okayama 700-8530, Japan, †Faculty of Pharmaceutical Sciences, Kyushu University, Fukuoka 812-8581, Japan, and ‡PRESTO, Japan Science and Technology Corporation, Okayama 700-8530, Japan

We report here that the high-temperature sensitivity of a *dnaA46* mutant was suppressed by addition of high concentrations of NaCl into the culture medium. This suppression was also observed with other high-temperature-sensitive *dnaA* mutants, except *dnaA167* and *dnaA508* mutants, which have mutations in the N-terminal region of DnaA protein. Since high concentrations of NaCl in the medium increased negative DNA supercoiling in a *dnaA46* mutant, we hypothesized that the increase in DNA supercoiling is involved in the suppression of the temperature-sensitivity of the *dnaA46* mutant by high concentrations of NaCl. This hypothesis was supported by *in vitro* and *in vivo* results as follows. A low DNA replication activity of purified DnaA46 protein at high temperatures was increased in line with an increase in DNA supercoiling of template DNA. The *dnaA46* mutant showed higher sensitivity to nalidixic acid, a DNA-relaxing drug, than did the wild-type cells under the conditions of high temperatures and high concentrations of NaCl

Key words: DNA replication, DnaA protein, *Escherichia coli*, linking number, nalidixic acid.

INTRODUCTION

Initiation of chromosomal DNA replication is regulated by various mechanisms, including the control of the activity of initiator proteins. In *Escherichia coli*, control of the activity of DnaA protein (the initiator of chromosomal DNA replication) by its adenine-nucleotide binding seems to play an important role in the regulation of the initiation of DNA replication [1]. DnaA protein has high affinities for ATP and ADP, and the ATP-binding form is the active form for DNA replication [2]. Recent genetic and biochemical studies strongly suggest that adenine-nucleotide binding to DnaA protein regulates the initiation of chromosomal DNA replication in *E. coli* cells [3–10]. However, some other mechanisms should be investigated in order to understand completely the regulation of DNA replication. To identify such a novel mechanism, one approach would be to identify conditions under which temperature-sensitivity of a *dnaA* mutant is suppressed.

In cells, chromosomal DNA is negatively supercoiled. The extent of DNA supercoiling is altered according to changes in intracellular or extracellular conditions, resulting in changes in various DNA transactions, such as transcription and recombination [11–13]. Recent genetic and biochemical studies strongly suggest that changes in DNA supercoiling affect the initiation of DNA replication in cells, as follows. *In vitro*, the DNA replication reaction requires the negative supercoiling of template DNA [14]. *In vivo*, various environmental stresses, which decreased DNA supercoiling, inhibited DNA replication [15]. We suggested a close relationship between DnaA protein and DNA supercoiling, as follows. Some *dnaA* mutants show much higher DNA supercoiling than do the wild-type cells [16]. DnaA protein itself has an ability to change DNA supercoiling *in vitro* [17].

DnaA protein specifically binds to the origin of DNA replication and forms oligomers [1]. ATP binding to DnaA protein is required for the oligomerization [2,6]. The torsional stress on DNA caused by this oligomerization is thought to open up the duplex DNA at *oriC* (the origin of chromosomal DNA replication) to initiate DNA replication. An increase in negative DNA supercoiling also put a torsional stress on DNA, which may open up duplex DNA. Thus we considered that excessive DNA supercoiling assists DnaA protein to open up the duplex DNA at the origin. In other words, inhibition of initiation of DNA replication caused by a low duplex-opening activity of DnaA proteins (such as in some high-temperature-sensitive *dnaA* mutants at high temperatures) may be suppressed by an increase in DNA supercoiling of chromosomal DNA. In the present study we showed that addition of high concentrations of NaCl in the medium caused suppression of the high-temperature-sensitivity of a *dnaA46* mutant and excessive DNA supercoiling in cells. Our genetic and biochemical results suggest that excessive DNA supercoiling by high concentrations of NaCl causes this suppression in cells.

MATERIALS AND METHODS

Materials

A crude extract for an *oriC* complementation assay was prepared from the WM433 strain of *E. coli* as previously described [18]. The wild-type DnaA and DnaA46 proteins were purified as described [19]. KS1001 (W3110 *dnaA*$^+$ *tnaA*::Tn*10* *lac*$^-$), KS1002 (W3110 *dnaA5*), KS1003 (W3110 *dnaA46*), KS1004 (W3110 *dnaA167*), KS1006(W3110 *dnaA205*), KS1007 (W3110 *dnaA508*), KS1008 (W3110 *dnaA601*), and KS1009 (W3110 *dnaA604*) were from our laboratory stocks [20–22].

Luria-broth (LB) medium [1% tryptone and 0.5% yeast extract (both from Difco)] was used for all experiments. In the present paper, the concentration of salt stated is the total concentration, not that added.

oriC DNA replication in a crude extract

Replication of minichromosomes in a crude extract (Fraction II) was assayed as described in [18] with some modifications.

Abbreviation used LB, Luria broth

[1] To whom correspondence should be addressed (e-mail mizushima@pheasant.pharm.okayama-u.ac.jp).

Template DNA (pTB101) [23] (600 pmol as nucleotides), 240 μg of Fraction II from WM433 (*dnaA204*) and DnaA protein were mixed with reaction cocktails [18] and incubated for replication at 40 °C for 10 min. The reaction was terminated by chilling on ice and adding 10 % trichloroacetic acid. Samples were passed through Whatman GF/C glass-fibre filters. The amount of radioactivity on the filters was measured in a liquid-scintillation counter, and the amount of DNA synthesized (pmol of nucleotides) was calculated [18].

Analysis of supercoiling of plasmid DNA in cells

Supercoiling of plasmid DNA in cells was measured by an agarose-gel-electrophoresis method [24,25]. Briefly, *E. coli* cells harbooring the plasmid pBR322 were harvested by centrifugation at 4 °C for 5 min, followed by washing with 0.9 % NaCl. Plasmid DNA was extracted and purified by the alkaline method. The samples were analysed by 1 %-agarose-gel electrophoresis in the presence of chloroquine. Electrophoresis was carried out in TBE buffer [0.089 M Tris/borate (pH8.0)/2 mM EDTA] at 60 V for 16 h. Gels were rinsed in deionized water for 5 h to remove chloroquine, and DNA was stained with 1 μg/ml ethidium bromide. DNA bands were revealed under a UV illuminator, and photographs were taken with a Polaroid apparatus.

RESULTS AND DISCUSSION

Suppression of a high-temperature-sensitivity of a *dnaA46* mutant

In order to test the hypothesis that excessive DNA supercoiling suppresses a low activity of DnaA protein for the duplex DNA opening, we used a temperature-sensitive *dnaA46* mutant and a culture medium containing high concentrations of NaCl. DnaA46 protein has mutations in the ATP-binding site, and ATP binding to DnaA protein is essential for the duplex opening at the origin [1,2,6]. High concentrations of NaCl in the medium were shown to induce excessive DNA supercoiling in wild-type cells [26]. The colony-formation abilities of the wild-type (KS1001) and the *dnaA46* (KS1003) strains were examined at 30 or 40 °C in the presence of various concentrations of NaCl. As shown in Figure 1, the colony-formation ability of the *dnaA46* mutant at 40 °C was increased depending on the concentration of NaCl in the medium. In the presence of 0.68 M NaCl, the colony-formation ability was almost indistinguishable between the *dnaA46* and the wild-type strains. The colony-formation abilities of the *danA46* mutant at 30 °C and of the wild-type cells both at 30 °C and 40 °C were not affected by the presence of NaCl in the medium (Figure 1). Suppression was also observed at 39 °C and 41 °C in the *dnaA46* mutant (results not shown). These results indicate that the temperature-sensitivity of the *dnaA46* mutant is suppressed by high concentrations of NaCl.

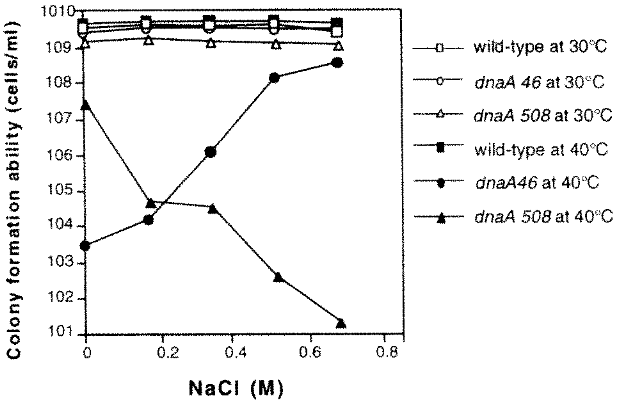

Figure 1 Suppression of the temperature-sensitivity of the *dnaA46* mutant by high concentrations of NaCl

KS1001 (*dnaA*$^+$), KS1003 (*dnaA46*), and KS1008 (*dnaA508*) strains were grown to the stationary phase at 30 °C in LB medium without NaCl. The suspension was diluted with the same medium and spread on LB agar plates containing the indicated concentrations of NaCl and incubated at 30 or 40 °C for 24 h. The number of viable cells per ml of original culture suspension was calculated and is shown as the colony-formation ability (101 = 10^1 etc.).

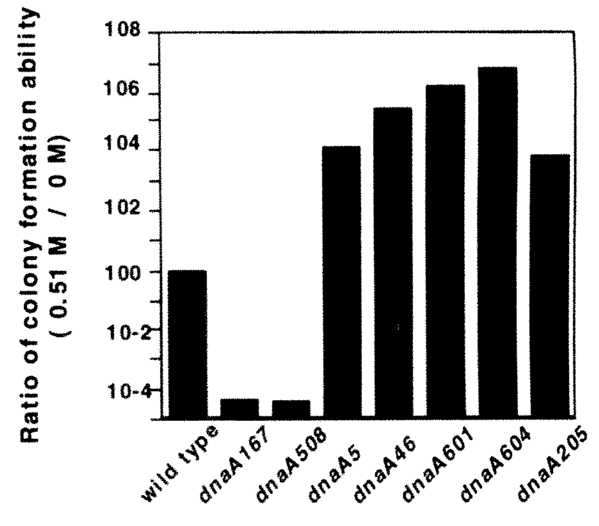

Figure 2 Effect of high concentrations of NaCl on the temperature-sensitivities of various *dnaA* mutants

The colony-formation ability of each *dnaA* mutant was examined on LB agar plates with or without 0.51 M NaCl at 40 °C as described in the legend to Figure 1. The ratio of the colony-formation ability (with 0.51–0 M NaCl) is shown as the relative colony-formation ability (10 − 4 = 10^{-4} etc.). Mutants were arranged in order of their mutation positions (left, N-terminal; right, C-terminal).

We next asked whether the suppression of the temperature-sensitivity of the *dnaA46* mutant is specific for NaCl. The change in DNA supercoiling by high concentrations of NaCl is due to the alteration in osmotic pressure in the medium, because the alteration in osmotic pressure by other reagents (such as glucose) also caused a change in DNA supercoiling in cells [26]. We examined the effect of KCl, ammonium sulphate and glucose on the colony-formation ability of the *dnaA46* mutant at 40 °C and found that they all could suppress the temperature-sensitivity of the *dnaA46* mutant to much the same extent as NaCl (results not shown). These results suggest that a change in osmotic pressure in the medium suppresses the temperature-sensitivity of the *dnaA46* mutant by these chemicals and thus that the suppression is due to the increase in DNA supercoiling in cells.

Effect of high concentrations of NaCl on the temperature-sensitivity of other *dnaA* mutants

A number of temperature-sensitive *dnaA* mutants have been isolated and the mutations have been identified [1]. In order to examine the allele specificity of the suppression of temperature-sensitivity of *dnaA* mutants by high concentrations of NaCl, we investigated the effect of high concentrations of NaCl on the temperature-sensitivities of various *dnaA* mutants (Figure 2). Temperature-sensitivities of mutants with mutations in the ATP-binding site (*dnaA5*, *dnaA601* and *dnaA604*) were suppressed by

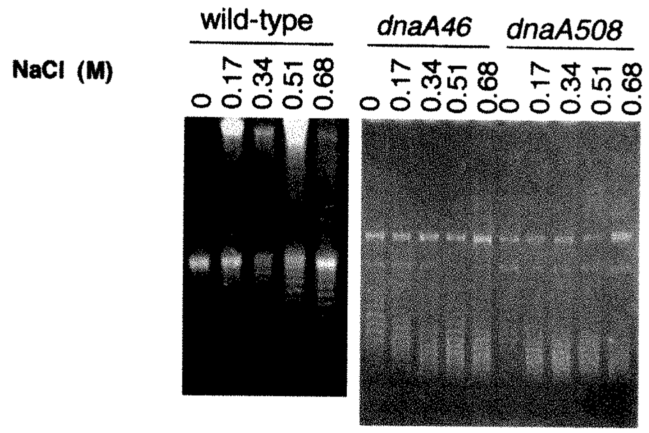

Figure 3 DNA supercoiling by high concentrations of NaCl in cells

KS1001 (*dnaA*⁺), KS1003 (*dnaA46*), and KS1008 (*dnaA508*) strains harbouring the pBR322 plasmid were grown at 40 °C in LB medium containing the indicated concentrations of NaCl until the A_{600} reached 1.0. Cells were collected by centrifugation and plasmid DNA was extracted and analysed by agarose-gel electrophoresis in the presence of 3 μg/ml chloroquine as described in the Materials and methods section.

0.51 M NaCl as much as was the *dnaA46* mutant, which also has mutations in this region. The temperature-sensitivity of the *dnaA205* mutant, which has a mutation in the DNA-binding domain (C-terminal region), was partly suppressed. In contrast, the *dnaA508* and *dnaA167* mutants, which have mutations in the N-terminal region of DnaA protein, showed the opposite results. The colony-formation abilities of these mutants were decreased in the presence 0.51 M NaCl (Figure 2). The decrease in the colony-formation ability of the *dnaA508* mutant is dependent on the concentration of NaCl and was not observed at 30 °C (Figure 1). These results clearly show the allele specificity of *dnaA* mutants for the suppression by high concentrations of NaCl. High concentrations of NaCl may affect the function of DnaA protein, which is related to the ATP-binding activity of this protein (such as the duplex DNA opening).

Effect of high concentrations of NaCl on DNA supercoiling in the *dnaA46* and *dnaA508* mutants

As mentioned above, we consider that excessive DNA supercoiling suppresses the temperature-sensitivities of *dnaA* mutants by high concentrations of NaCl. Thus we tried to confirm that the extent of DNA supercoiling is increased by high concentrations of NaCl in the *dnaA46* mutant at high temperatures. To determine why NaCl did not suppress the temperature-sensitivity of the *dnaA508* mutant, we also examined DNA supercoiling in this mutant. The wild-type, *dnaA46* and *dnaA508* cells harbouring pBR322 (a reporter plasmid for DNA supercoiling in cells) were incubated with various concentrations of NaCl at 40 °C for 4 h. The extent of DNA supercoiling of plasmids prepared from these cells was analysed by agarose-gel electrophoresis in the presence of 3 μg/ml chloroquine. Under these conditions, more negatively supercoiled DNA migrates more rapidly [27]. To an extent depending on the concentration of NaCl, DNA in the *dnaA46* mutant became more negatively supercoiled, as is the case in the wild-type cells (Figure 3). The extent of change in DNA supercoiling in the wild-type cells was consistent with a previous paper [26]. Even in the *dnaA508* mutant, NaCl increased DNA supercoiling in a dose-dependent manner (Figure 3), suggesting that the inability of NaCl to suppress the temperature-sensitivity of *dnaA508* is not due to its inability to increase DNA supercoiling. DNA in *dnaA46* and *dnaA508* mutants in the absence of NaCl was more negatively supercoiled than in the wild-type cells, which is consistent with our previous results [16]. The results in Figures 1 and 2 were reproduced with *dnaA* mutants harbouring pBR322 (results not shown).

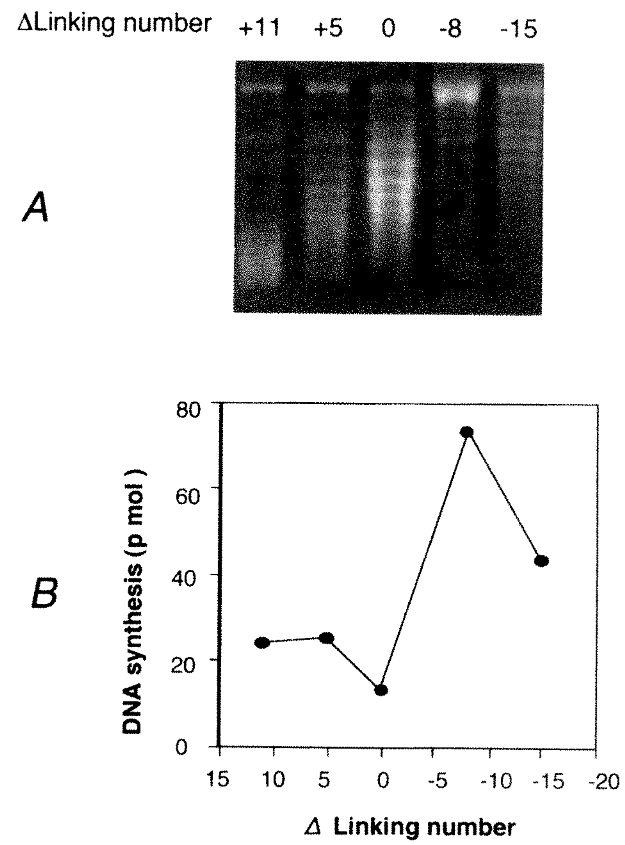

Figure 4 Effect of excessive DNA supercoiling of template DNA on the replication activity of DnaA46 protein *in vitro*

pTB101, a plasmid with *oriC*, was constructed as described in [23]. Plasmids with various extents of DNA supercoiling were prepared as described in [33]. The linking number of each plasmid was determined on the basis of the results of agarose-gel electrophoresis with various concentrations of chloroquine (one of them is shown as Figure 4A, 1.5 μg/ml). Δ Linking number shows the difference in the linking number of each plasmid in comparison with that of the normal plasmid (plasmid extracted from cells, without topoisomerase I treatment). The plasmids of + values of Δlinking number are more relaxed and those of − values are more negatively supercoiled compared with the normal plasmid. All plasmids are negatively supercoiled in the absence of chloroquine. DNA replication with each plasmid as a template was done in the presence of 100 ng of DnaA46 as described in the Materials and methods section.

Effect of excessive DNA supercoiling of template DNA on the replication activity of DnaA46 *in vitro*

We next tested our hypothesis using an *in vitro* DNA replication system. Since high-temperature-dependent inhibition of DNA replication with DnaA46 was reproduced in an *in vitro oriC* complementation assay using a crude extract, but not in a system reconstituted from purified proteins [3], we used a system consisting of a crude extract. A problem with this system is that the extent of DNA supercoiling changed upon incubation at high temperatures even without dNTP (without DNA replication reaction), which is due to the presence of DNA topoisomerases (results not shown). We solved this problem by shortening the

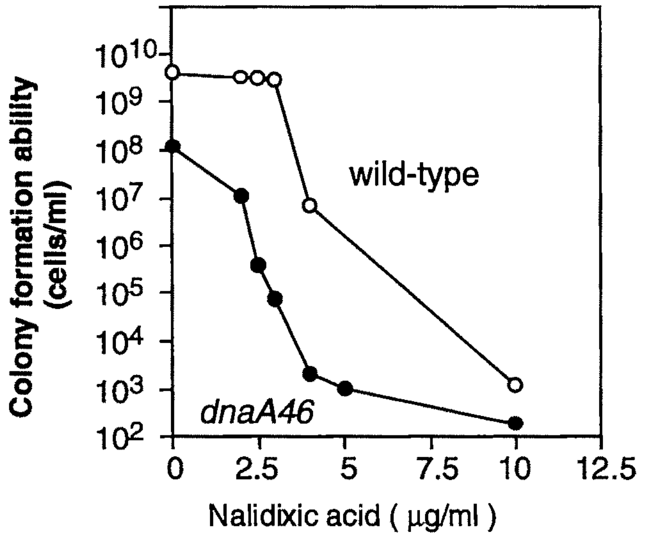

Figure 5 A phenotype of the *dnaA46* mutant sensitive to nalidixic acid.

The colony-formation abilities at 40 °C of the *dnaA46* and the wild-type strains on LB agar plates with 0.51 M NaCl and the indicated concentrations of nalidixic acid were examined as described in the legend to Figure 1

reaction period of DNA replication. Under the conditions of an *in vitro oriC* DNA replication system in a crude extract (but without dNTP), we found the extent of DNA supercoiling of plasmid DNA was maintained up to 10 min at 40 °C (results not shown) Thus we examined the effect of the extent of DNA supercoiling of template DNA on DNA replication with purified DnaA46 protein by incubating at 40 °C for 10 min. As shown in Figure 4(A), we prepared *oriC* plasmids with various extents of DNA supercoiling. The DNA-replication reaction rate with DnaA46 protein at 40 °C was higher when the more negatively supercoiled DNA was used as a template (Figure 4B). The DNA-replication activities of DnaA46 at 30 °C or of the wild-type DnaA protein both at 30 °C and 40 °C were not affected by an increase in DNA supercoiling above the normal level of DNA supercoiling (DNA extracted from cells), whereas a decrease in DNA supercoiling inhibited the DNA replication reaction (results not shown), which is consistent with previous results [14]. Since the extent of change in DNA supercoiling by addition of 0.51 M NaCl in the *dnaA46* mutant cells was about −6 of the Δlinking number (see the legend to Figure 4), the results shown in Figure 4 suggest that the increase in DNA supercoiling by high concentrations of NaCl can increase the activity of Dna46 for DNA replication in cells.

A phenotype of the *dnaA46* mutant sensitive to nalidixic acid

On the basis of the notion that DNA replication in the *dnaA46* mutant, but not in the wild-type cells at 40 °C in the presence of high concentrations of NaCl, is maintained by excessive DNA supercoiling, we predicted that, under these conditions, the *dnaA46* mutant would show a higher sensitivity to DNA relaxation. We used nalidixic acid, which is known to relax DNA in cells [15]. Full-growth suspensions of the wild-type and the *dnaA46* mutant were spread on LB agar plates containing 0.51 M NaCl and various concentrations of nalidixic acid and incubated at 40 °C. As shown in Figure 5, the *dnaA46* mutant showed a phenotype that was more sensitive to nalidixic acid than the wild-type cells at all the concentrations tested. The *dnaA46* mutant showed a phenotype that was more sensitive to nalidixic acid, even at 30 °C, although the difference in the sensitivity between the wild-type and the mutant was not as apparent as it was at 40 °C (results not shown). These data suggest that excessive DNA supercoiling is required to maintain DNA replication in the *dnaA46* mutant.

In the present study we tested the hypothesis that excessive DNA supercoiling suppresses a low activity of DnaA protein and obtained supporting evidence as follows. High concentrations of NaCl suppressed the temperature-sensitivity of the *dnaA46* mutant (Figure 1), in which DNA supercoiling in cells increased (Figure 3). The low DNA-replication activity of DnaA46 protein was stimulated by increasing the DNA supercoiling of template DNA *in vitro* (Figure 4). The *dnaA46* mutant showed a greater sensitivity to nalidixic acid, a DNA-relaxing drug, than did the wild-type cells under the conditions of high temperature and high concentrations of NaCl (Figure 5). It would be very noteworthy if *E. coli* cells were to change the extent of DNA supercoiling to maintain the proper frequency of DNA replication. Our previous finding, that DNA in temperature-sensitive *dnaA* mutants was more negatively supercoiled at semi-permissive temperature than was the DNA in the wild-type cells [16], suggest such a mechanism.

It was reported that genetic inactivation of topoisomerase I suppresses the temperature-sensitivity of the *dnaA46* mutant [28]. Since topoisomerase I relaxes DNA, mutations in the *topA* gene cause an increase in DNA supercoiling in cells [27,29]. Thus this previous observation supports the notion that the increase in DNA supercoiling by high concentrations of salts is involved in the suppression of the temperature-sensitivity of the *dnaA46* mutant.

The suppression of temperature-sensitivity by high concentrations of NaCl showed an allele specificity of *dnaA* mutants (Figure 2). The temperature-sensitivities of *dnaA* mutants with mutations in the ATP-binding site or DNA-binding sites, but not in the N-terminal region, were suppressed by high concentrations of NaCl. The function of DnaA protein can be divided into two categories. One is duplex opening at *oriC* and the other is loading DnaB protein into the *oriC* region. Excessive DNA supercoiling may assist the former function, but not the latter one. ATP binding and DNA binding are involved in the former function. As for the N-terminal region of DnaA protein, several functions (oligomerization, loading of DnaB, and retention of DnaB) have been suggested [30–32]. DnaA508 and DnaA167 proteins may have a defect in DnaB loading and retention, which may cause the inability of excessive DNA supercoiling to suppress the temperature-sensitivity of these mutants

This work was supported in part by Grants-in-Aid for Scientific Research from the Ministry of Education, Science, Sports, and Culture, Japan, the Naito Foundation, the Nissan Foundation, and 'Ground Research Announcement for Space Utilization' promoted by the Japan Space Forum

REFERENCES

1 Skarstad, K and Boye, E (1994) The initiator protein DnaA evolution, properties and function Biochim Biophys Acta **1217**, 111–130
2 Sekimizu, K, Bramhill, D and Kornberg, A. (1987) ATP activates dnaA protein in initiating replication of plasmids bearing the origin of the *E. coli* chromosome Cell **50**, 259–265
3 Hwang, D S and Kaguni, J M (1988) Interaction of dnaA46 protein with a stimulatory protein in replication from the *Escherichia coli* chromosomal origin J Biol Chem **263**, 10633–10640
4 Hupp, T R and Kaguni, J M (1993) Activation of mutant forms of DnaA protein of *Escherichia coli* by DnaK and GrpE proteins occurs prior to DNA replication J Biol Chem **268**, 13143–13150
5 Katayama, T and Crooke, E (1995) DnaA protein is sensitive to a soluble factor and is specifically inactivated for initiation of *in vitro* replication of the *Escherichia coli* minichromosome J. Biol Chem **270**, 9265–9271

6 Mizushima, T, Sasaki, S, Ohshu, H, Kobayashi, M., Katayama, T., Miki, T., Maeda, M. and Sekimizu, K. (1996) Molecular design of inhibitors of *in vitro oriC* DNA replication based on the potential to block the ATP binding of DnaA protein. J Biol. Chem **271**, 25178–25183

7 Carr, K. M and Kaguni, J. M (1996) The A184V missense mutation of the *dnaA* 5 and *dnaA* 46 alleles confers a defect in ATP binding and thermolability in initiation of *Escherichia coli* DNA replication Mol.Microbiol **20**, 1307–1318

8 Mizushima, T, Nishida, S, Kurokawa, K, Katayama, T, Miki, T and Sekimizu, K (1997) Negative control of DNA replication by hydrolysis of ATP bound to DnaA protein, the initiator of chromosomal DNA replication in *Escherichia coli.* EMBO J **16**, 3724–3730

9 Mizushima, T, Takaki, T., Kubota, T, Tsuchiya, T., Miki, T., Katayama, T. and Sekimizu, K. (1998) Site-directed mutational analysis for the ATP binding of DnaA protein Functions of two conserved amino acids (Lys-178 and Asp-235) located in the ATP-binding domain of DnaA protein *in vitro* and *in vivo* J. Biol Chem **273**, 20847–20851

10 Katayama, T., Kubota, T, Kurokawa, K, Crooke, E. and Sekimizu, K (1998) The initiator function of DnaA protein is negatively regulated by the sliding clamp of the *E coli* chromosomal replicase. Cell **94**, 61–71

11 Drlica, K (1984) Biology of bacterial deoxyribonucleic acid topoisomerases Microbiol Rev **48**, 273–289

12 Drlica, K (1992) Control of bacterial DNA supercoiling Mol Microbiol. **6**, 425–433

13 Luttinger, A. (1995) The twisted 'life' of DNA in the cell bacterial topoisomerases Mol Microbiol. **16**, 601–606

14 Baker, T. A and Kornberg, A (1988) Transcriptional activation of initiation of replication from the *E coli* chromosomal origin an RNA–DNA hybrid near *oriC* Cell **55**, 113–123

15 Mizushima, T, Natori, S and Sekimizu, K (1993) Relaxation of supercoiled DNA associated with induction of heat shock proteins in *Escherichia coli* Mol Gen Genet **238**, 1–5

16 Mizushima, T, Tanino, J, Miki, T. and Sekimizu, K (1996) Decrease in the linking number of plasmid DNA in *dnaA* mutants of *Escherichia coli* Biochem Biophys Res Commun **218**, 137–141

17 Mizushima, T, Katayama, T and Sekimizu, K (1996) Effect on DNA topology by DnaA protein, the initiation factor of chromosomal DNA replication in *Escherichia coli* Biochemistry **35**, 11512–11516

18 Fuller, R S., Kaguni, J M. and Kornberg, A. (1981) Enzymatic replication of the origin of the *Escherichia coli* chromosome Proc Natl Acad. Sci U S.A **78**, 7370–7374

19 Kubota, T., Katayama, T, Ito, Y, Mizushima, T and Sekimizu, K (1997) Conformational transition of DnaA protein by ATP structural analysis of DnaA protein, the initiator of *Escherichia coli* chromosome replication Biochem Biophys Res Commun **232**, 130–135

20 Shinpuku, T, Mizushima, T, Guo, L, Miki, T. and Sekimizu, K. (1995) Phenotypes of *dnaA* mutants of *Escherichia coli* sensitive to detergents and organic solvents Biochem. Biophys Res Commun. **212**, 84–89

21 Mizushima, T, Shinpuku, T, Katayama, H, Kataoka, K., Guo, L, Miki, T and Sekimizu, K. (1996) Phenotypes of *dnaA* mutants of *Escherichia coli* sensitive to phenothiazine derivatives Mol Gen Genet **252**, 212–215

22 Mizushima, T, Yokoyama, K, Mima, S, Tsuchiya, T. and Sekimizu, K (1997) Inhibition of thymidine transport in *dnaA* mutants of *Escherichia coli* J Biol. Chem 272, 21195–21200

23 Wold, S, Boye, E, Slater, S., Kleckner, N and Skarstad, K. (1998) Effects of purified SeqA protein on *oriC*-dependent DNA replication *in vitro* EMBO J. **17**, 4158–4165

24 Kataoka, K, Mizushima, T, Ogata, Y, Miki, T and Sekimizu, K (1996) Heat shock-induced DNA relaxation *in vitro* by DNA gyrase of *Escherichia coli* in the presence of ATP J Biol Chem **271**, 24806–24810

25 Ogata, Y, Mizushima, T, Kataoka, K, Kita, K, Miki, T and Sekimizu, K (1996) DnaK heat shock protein of *Escherichia coli* maintains the negative supercoiling of DNA against thermal stress J Biol Chem **271**, 29407–29414

26 Higgins, C F, Dorman, C J., Stirling, D A., Waddell, L, Booth, I. R, May, G and Bremer, E (1988) A physiological role for DNA supercoiling in the osmotic regulation of gene expression in *S typhimurium* and *E coli* Cell **52**, 569–584

27 Ogata, Y., Mizushima, T, Kataoka, K, Miki, T and Sekimizu, K (1994) Identification of DNA topoisomerases involved in immediate and transient DNA relaxation induced by heat shock in *Escherichia coli.* Mol Gen Genet **244**, 451–455

28 Louarn, J, Bouche, J P, Patte, J. and Louarn, J. M (1984) Genetic inactivation of topoisomerase I suppresses a defect in initiation of chromosome replication in *Escherichia coli.* Mol Gen Genet. **195**, 170–174

29 Mizushima, T., Natori, S and Sekimizu, K (1992) Inhibition of *Escherichia coli* DNA topoisomerase I activity by phospholipids Biochem J **285**, 503–506

30 Mima, S, Yamagachi, Y, Kondo, T, Tsuchiya, T and Mizushima, T (1999) Role of the amino-terminal region of the DnaA protein in opening of the duplex DNA at the *oriC* region. FEMS. Microbiol. Lett. **176**, 163–167

31 Sutton, M D., Carr, K. M, Vicente, M and Kaguni, J. M (1998) *Escherichia coli* DnaA protein The N-terminal domain and loading of DnaB helicase at the *E coli* chromosomal origin. J Biol. Chem **273**, 34255–34262

32 Marszalek, J, Zhang, W, Hupp, T R, Margulies, C, Carr, K M, Cherry, S and Kaguni, J. M (1996) Domains of DnaA protein involved in interaction with DnaB protein and in unwinding the *Escherichia coli* chromosomal origin. J. Biol. Chem. **271**, 18535–18542

33 Kurokawa, K, Mizushima, T., Miki, T. and Sekimizu, K (1996) Influence of the linking number of template DNA on σ^{32}-dependent transcription initiation *in vitro* of the *Escherichia coli groE* gene. Biol Pharm Bull **19**, 922–925

Received 7 February 2000/10 March 2000, accepted 29 March 2000

Biochem J (2000) 348, 381–387 (Printed in Great Britain)

The m3 muscarinic acetylcholine receptor is coupled to mitogen-activated protein kinase via protein kinase C and epidermal growth factor receptor kinase

Barbara E. SLACK[1]

Boston University School of Medicine, Department of Pathology and Laboratory Medicine, 85 East Newton Street, Room M1007, Boston, MA 02118, U.S.A.

The acetylcholine analogue carbachol rapidly activated mitogen-activated protein kinase (MAPK), and caused tyrosine phosphorylation of the adapter protein p52 Shc and the epidermal growth factor (EGF) receptor, in human embryonic kidney cells stably expressing m3 muscarinic receptors. The protein kinase C (PKC) inhibitor GF109203X caused a significant partial inhibition of m3 receptor-mediated activation of MAPK. The PKC-independent MAPK activity elicited by carbachol in the presence of GF109203X was reproducibly abolished by AG1478, an inhibitor of EGF-receptor tyrosine kinase activity, and by the Src tyrosine kinase inhibitor PP1. In a subset of these experiments, GF109203X concomitantly increased carbachol-induced tyrosine phosphorylation of p52 Shc and the EGF receptor. In co-stimulation experiments, carbachol and EGF activated MAPK in a non-additive fashion; moreover, EGF-induced association of Shc with the phosphorylated EGF receptor was inhibited by carbachol. This effect of carbachol was blocked by GF109203X. The results indicate that MAPK activation by m3 receptor stimulation is regulated by two pathways; one dependent on PKC, and the other mediated via the EGF receptor and Src. Moreover, the EGF-receptor-dependent pathway may be subject to negative-feedback regulation via m3 receptor-coupled activation of PKC.

Key words: bisindolylmaleimide, carbachol, Shc, Src, transactivation.

INTRODUCTION

Activation of the mitogen-activated protein kinase (MAPK)/extracellular signal-regulated kinase (ERK) cascade is an important consequence of cell stimulation by growth factors, by ligands for receptors coupled to G-proteins and by extracellular matrix proteins that are ligands for integrins [1–3]. The MAPK family members p42 MAPK (ERK 2) and p44 MAPK (ERK 1) are key regulators of cell proliferation, migration, differentiation, transformation and survival [4–8]. The canonical MAPK-activation pathway initiated by growth factors involves recruitment of the adapter protein Grb2 in association with the Ras guanine nucleotide-exchange protein mSos to the activated, autophosphorylated growth factor receptor, with subsequent sequential activation of Ras, Raf, MAPK kinase (MEK 1/2) and MAPK [9].

It was recognized subsequently that G-protein-coupled receptors (GPCRs), including members of the muscarinic acetylcholine receptor family, are functionally linked to the MAPK cascade via several distinct pathways. Of the five muscarinic receptor subtypes that have been cloned, only m1, m3 and m5 receptors are coupled efficiently to phosphatidylinositol 4,5-bisphosphate hydrolysis [10,11]. Muscarinic m1 receptors have been reported to activate MAPK via a pathway that involves pertussis toxin-insensitive $G_{q/11}$, or pertussis toxin-sensitive G_o G-proteins, protein kinase C (PKC) and Raf, but which is independent of Ras [12,13]. Others describe a pathway that, while dependent on Raf, and independent of Ras, is only partially PKC-dependent [14]. Some reports have implicated $\beta\gamma$ subunits in Ras-dependent activation of MAPKs by m1 receptors [15,16], whereas other investigators have found that the response to m1 receptor stimulation is not affected by inhibitors of $\beta\gamma$ signalling [12]. Activation of MAPKs by m2 muscarinic receptors is also reportedly dependent on release of $\beta\gamma$ subunits from pertussis toxin-sensitive G-proteins, with subsequent tyrosine phosphorylation of Shc, which in turn associates with Grb2–mSos, leading to Ras activation [17–19]. The link between $G_{\beta\gamma}$ release and Shc phosphorylation may involve sequential activation of phosphatidylinositol 3-kinase γ and a Src-like tyrosine kinase [19–21].

Typically, activation of MAPK by GPCRs involves tyrosine phosphorylation of one or more proteins that act as scaffolds, forming complexes with Grb2–mSos, and thereby promoting the activation of the Ras-MAPK cascade [22]. One such scaffolding protein is the epidermal growth factor (EGF) receptor. EGF-independent activation of this receptor by GPCRs, a phenomenon referred to as 'transactivation' [21,23–28], results in the formation of a complex composed of the phosphorylated EGF receptor and the adapter proteins Shc and Grb2 [23,26,27]. The adapter proteins mediate the recruitment of mSos to the complex, thus recapitulating the sequence of events set into motion by direct activation of growth factors by their ligands. Other evidence implicates the focal adhesion-associated protein focal adhesion kinase (FAK) [22], and another member of this family, PYK2 [29–33], as additional scaffolds for the assembly of a Ras activation complex, and activation of MAPK, in response to GPCR ligands. More information about these signalling mechanisms may be found in two recent reviews [34,35].

Abbreviations used. DMEM, Dulbecco's modified Eagle's medium, EGF, epidermal growth factor, ERK, extracellular signal-related kinase, GPCR, G-protein-coupled receptor, HEK, human embryonic kidney, MAPK, mitogen-activated protein kinase, PKC, protein kinase C, PP1, 4-amino-5-(4-methylphenyl)-7-(t-butyl)pyrazolo-D-3,4-pyrimidine

[1] E-mail bslack@bu.edu.

In the present study the regulation of MAPK by muscarinic m3 receptors was examined in human embryonic kidney (HEK) cells stably expressing m3 receptors. The results indicate that the m3 receptor is coupled to MAPK via both PKC-dependent and EGF receptor-dependent pathways.

EXPERIMENTAL

Materials

Antibodies and other reagents were obtained from the following sources. Anti-paxillin, anti-phosphotyrosine (clone PY20), monoclonal anti-Shc and goat peroxidase-linked anti-mouse IgG were from Transduction Laboratories (Lexington, KY, U.S.A.). Monoclonal peroxidase-linked anti-phosphotyrosine clone PY99 was obtained from Santa Cruz Biotechnology (Santa Cruz, CA, U.S.A.). Polyclonal anti-Shc and anti-EGF-receptor antibodies were purchased from Upstate Biotechnology (Lake Placid, NY, U.S.A.). A polyclonal antibody specific for the activated form of MAPK was obtained from New England Biolabs (Beverly, MA, U.S.A.). Protein G agarose was purchased from Oncogene Science (Cambridge, MA, U.S.A.). Protein A–Sepharose was obtained from Pharmacia (Piscataway, NJ, U.S.A.). Reagents, equipment and mini-gels for electrophoresis were supplied by Bio-Rad Laboratories (Hercules, CA, U.S.A.). Carbamylcholine chloride (carbachol), PMA and mouse EGF were obtained from Sigma (St. Louis, MO, U.S.A.). The tyrphostin AG1478, bisindolylmaleimide I (GF109203X), bisindolylmaleimide IX (Ro 31-8220) and the Src inhibitor PP1 [4-amino-5-(4-methylphenyl)-7-(t-butyl)pyrazolo-D-3,4-pyrimidine] were purchased from Alexis Biochemicals (San Diego, CA, U.S.A.). The indolocarbazole Gö6976 was obtained from Calbiochem (San Diego, CA, U.S.A.). Other reagents were obtained from Sigma or from Fisher Scientific (Pittsburgh, PA, U.S.A.).

Cell culture

HEK cells stably transfected with muscarinic m3 receptors were maintained in Dulbecco's modified Eagle's medium (DMEM) supplemented with 10 % fetal bovine serum [36]. These cells were shown previously to express approx. 200000 m3 receptors per cell [11]. Cells were grown on 60- or 100-mm culture dishes (Falcon; Becton Dickinson Labware, Bedford, MA, U.S.A.) coated with poly-D-lysine for 3–4 days prior to an experiment. Cultures were maintained in growth medium until the day of the experiment. All pharmacological treatments were carried out in serum-free DMEM. Stock solutions of inhibitors and PMA were dissolved in DMSO, and diluted with culture medium prior to treatment of cells.

Immunoprecipitation and determination of tyrosine-phosphorylated proteins

Following incubation, test media were aspirated and cells were collected in 1 ml of lysis buffer containing 1 % Nonidet P-40, 0.1 % SDS, 0.5 % deoxycholate, 50 mM Tris, pH 7.5, 150 mM NaCl, 1 mM sodium orthovanadate, 25 mM NaF, 2 mM 4-(2-aminoethyl)benzenesulphonyl fluoride (AEBSF), 1 μg/ml leupeptin and 2 μg/ml aprotinin. Lysates were centrifuged to remove insoluble material, normalized for protein content, and incubated overnight with immunoprecipitating antibodies, usually at concentrations of 2–4 μg/500 μg of protein, and with Protein A–Sepharose or Protein G agarose (3.5 mg per sample). Immunoprecipitates were centrifuged and washed three times in a washing buffer containing 0.1 % Triton X-100, 25 mM Tris, pH 7.5, 250 mM NaCl and 1 mM sodium orthovanadate. Immunoprecipitates were size-fractionated by SDS/PAGE, and the proteins were transferred on to PVDF membranes. The membranes were blocked with 3 % gelatin or 5 % milk in Tris-buffered saline containing 0.15 % Tween-20. Tyrosine-phosphorylated proteins were immunoprecipitated with anti-phosphotyrosine antibodies (clone PY20). Immunoblots were probed with recombinant peroxidase-linked anti-phosphotyrosine (PY99) antibodies, or antibodies to paxillin or Shc. Activated MAPK was detected in cell lysates by immunoblotting with a phosphorylation-specific antibody (New England Biolabs). Approximate molecular masses were estimated using calibrated prestained standards (Bio-Rad Laboratories).

Statistical analysis

Comparisons based on immunoblotting data were derived from samples processed on the same blot. The statistical significance of differences was estimated by analysis of variance followed by Fisher's least-significant-difference (LSD) test. Differences were taken to be significant at $P < 0.05$.

RESULTS

MAPK is activated by carbachol and EGF in HEK cells expressing m3 receptors

In HEK cells expressing muscarinic m3 receptors, carbachol caused a concentration-dependent increase in MAPK activity. The response was detected using an antibody specific for the activated, tyrosine- and threonine-phosphorylated form of the enzyme (Figure 1A). The activation was apparent within 2 min, and reached a maximum value by 5 min (Figure 1B). EGF at a concentration of 50 ng/ml, acting on endogenous EGF receptors, stimulated MAPK as effectively as carbachol (Figure 1A).

PKC inhibitors reduce m3 receptor-mediated MAPK activation

A number of different mechanisms regulate MAPK activation by GPCR ligands. The response in some cell types is dependent on

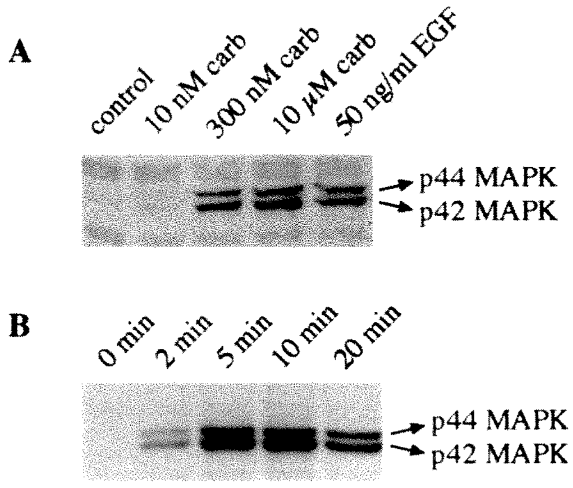

Figure 1 Stimulation of m3 muscarinic receptors increases MAPK activity

(**A**) HEK cells stably expressing the m3 muscarinic receptor were treated for 10 min with various concentrations of carbachol (carb), or with 300 ng/ml EGF. (**B**) Cells were treated with 100 μM carbachol for various periods of time. Cell lysates were immunoblotted with polyclonal antibodies specific for phosphorylated, activated MAPK.

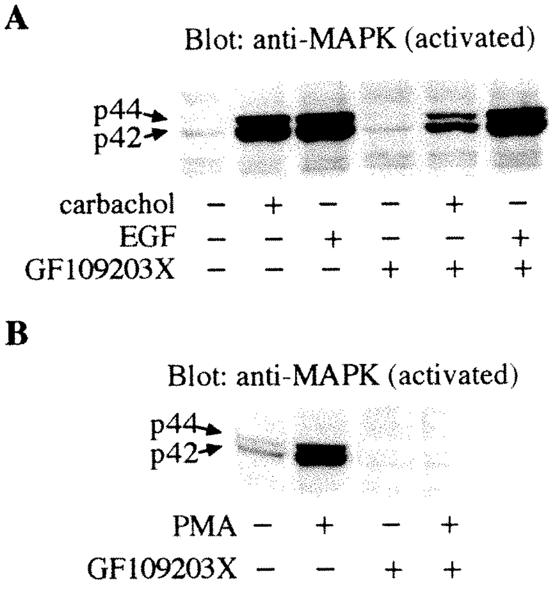

Figure 2 PKC inhibition reduces m3 receptor-coupled MAPK activation

(**A**) Cells were pretreated for 30 min with serum-free medium containing GF109203X (2.5 μM) or the vehicle DMSO. Cells were then incubated for 10 min in fresh medium containing GF109203X or DMSO with or without carbachol (100 μM) or EGF (50 ng/ml). Phosphorylated MAPK was detected in cell lysates by immunoblot analysis. (**B**) Cells were pretreated with DMSO or GF109203X for 30 min, then incubated for 10 min in fresh medium containing DMSO or the inhibitor with or without PMA (1 μM).

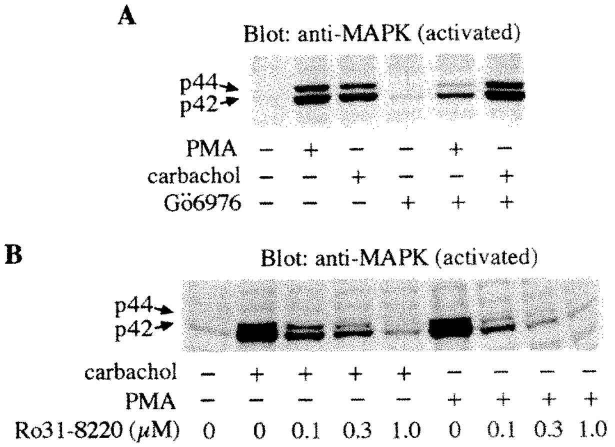
A
Blot: anti-MAPK (activated)
p44
p42
PMA − + − − + −
carbachol − − + − − +
Gö6976 − − − + + +
B
Blot: anti-MAPK (activated)
p44
p42
carbachol − + + + + − − − −
PMA − − − − − + + + +
Ro31-8220 (μM) 0 0 0.1 0.3 1.0 0 0.1 0.3 1.0

Figure 3 Effects of Ro31-8220 and Gö6976 on stimulation of MAPK by carbachol

(**A**) Cells were pretreated with DMSO or Gö6976 (5 μM) for 30 min, then treated for 10 min with fresh medium containing DMSO or the inhibitor, alone or with carbachol (100 μM), or PMA (1 μM). (**B**) Cells were pretreated with DMSO or various concentrations of Ro31-8220 for 30 min, then treated for 10 min with fresh medium containing carbachol (100 μM) or PMA (1 μM) in the presence of DMSO and/or the inhibitor. Final DMSO concentrations were the same in all test solutions. The control received DMSO alone. Phosphorylated MAPK was detected in cell lysates by immunoblot analysis.

PKC [12,13]. When the PKC inhibitor GF109203X (bisindolylmaleimide I) was tested in our model, a partial reduction in carbachol-induced MAPK activation was observed. Although the degree of inhibition observed was variable (ranging from 9 to 96 %), an average reduction of 65 ± 5 % (mean ± S.E.M., $n = 21$) was induced by a concentration of GF109203X (2.5 μM) that abolished the response to the PMA (Figures 2 and 6A, see below). In contrast, EGF-induced MAPK activation was consistently resistant to this inhibitor (Figures 2A and 6B). Two additional PKC inhibitors were also tested; the indolocarbazole Gö6976 and the bisindolylmaleimide Ro31-8220. Gö6976, a selective inhibitor of the calcium-dependent PKC isozymes α and β1 [37], inhibited PMA- but not carbachol-induced MAPK activation (Figure 3A). Ro31-8220, which inhibits both calcium-dependent and calcium-independent PKC subtypes [38], as well as the atypical subtype PKCζ [39], markedly inhibited carbachol-induced MAPK activation at a concentration (0.3 μM) that abolished the response to PMA (Figure 3B).

PKC-independent MAPK activation by carbachol depends on transactivation of the EGF receptor

It has been reported that stimulation of certain GPCRs transactivates the EGF receptor, leading to stimulation of MAPK, apparently via recruitment of Shc, which couples the activated receptor to mSos [23–28,33,40]. The possibility that this mechanism might account for the PKC-independent stimulation of MAPK by carbachol was addressed using a specific inhibitor of EGF receptor tyrosine kinase activity, AG1478 [41]. This inhibitor abolished MAPK activation by EGF, as expected (Figure 4A), but did not significantly inhibit carbachol-mediated tyrosine phosphorylation of paxillin, a substrate of Src [42,43] (results not shown), supporting the selectivity of AG1478 for the EGF receptor tyrosine kinase. AG1478 alone caused a consistent partial inhibition (of approx. 35 %) of MAPK activation by carbachol. Notably, GF109203X and AG1478 in combination virtually abolished the activation of MAPK by muscarinic receptor stimulation (Figure 4B). The results suggest that the MAPK activity remaining in the presence of carbachol and GF109203X might be due to the activity of a second pathway dependent upon EGF receptor activation.

The adapter protein Shc has been implicated in the activation of MAPK following EGF receptor activation by its cognate ligand EGF or by GPCRs [34,44]. Although three isoforms of Shc have been described, only two of these, p46 and p52 Shc, were detectable in HEK cells expressing m3 receptors. The p46 isoform was tyrosine phosphorylated under basal conditions, and did not exhibit any consistent change in phosphorylation with exposure to carbachol. In contrast, tyrosine phosphorylation of p52 Shc was increased 3.6 ± 0.7-fold by carbachol (mean ± S.E.M., $n = 10$; Figure 4C). An increase in tyrosine phosphorylation of the EGF receptor was also observed (Figure 4C). In a subset of these experiments, carbachol-induced tyrosine phosphorylation of p52 Shc and the EGF receptor was increased further in the presence of GF109203X (Figure 4D). These effects were abolished by AG1478 (Figure 4D). In other experiments, GF109203X instead caused a partial inhibition of Shc and EGF receptor tyrosine phosphorylation. The reasons for this inconsistency have not been determined; however, it was noted that GF109203X tended to increase carbachol-mediated Shc tyrosine phosphorylation in those experiments in which it was comparatively less effective as an inhibitor of MAPK activation.

Src is a mediator of PKC-independent MAPK activation by carbachol

Src has been implicated in the activation of MAPK by certain GPCRs [22,24]. In the present study, the Src inhibitor PP1 reduced carbachol-evoked MAPK activation by approx. 50 %

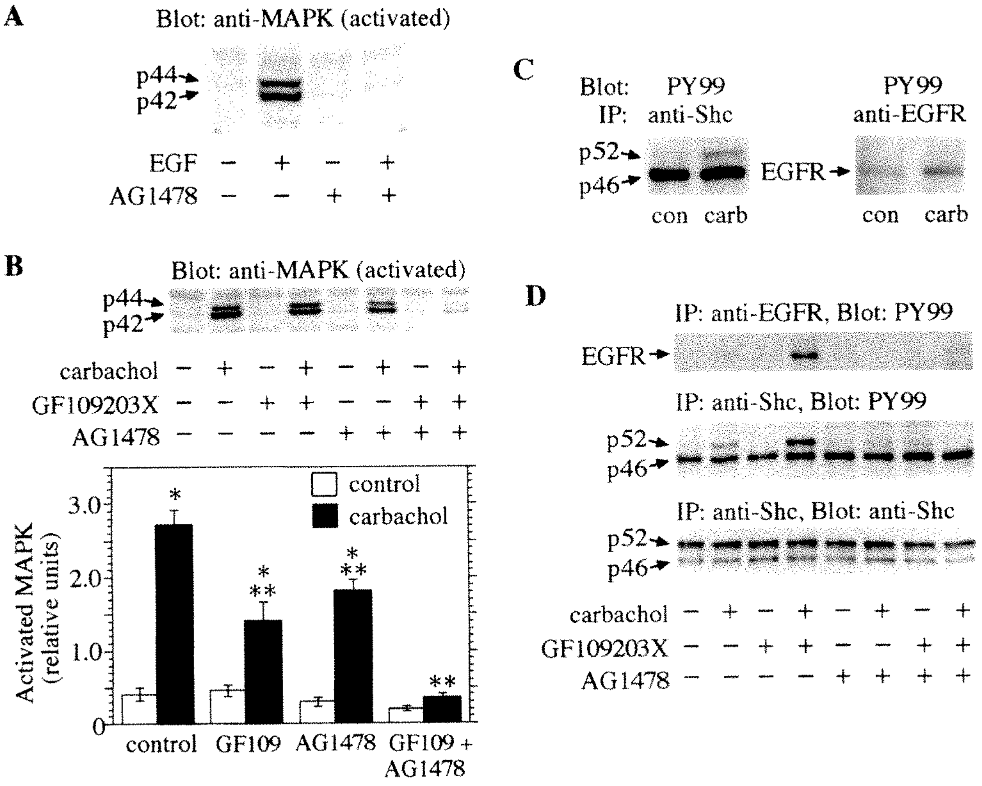

Figure 4 Activation of MAPK by m3-receptor stimulation is dependent on PKC and EGF-receptor transactivation

(**A**) Cells were pretreated for 30 min in serum-free medium containing AG1478 (250 nM) or DMSO, then treated for 10 min in fresh medium containing DMSO or the inhibitor, with or without EGF (50 ng/ml). (**B**) Cells were pretreated for 30 min with serum-free medium containing GF109203X (GF109; 2.5 μM) or AG1478 (250 nM) alone or in combination, or the vehicle DMSO. Cells were then incubated for 10 min in fresh medium containing one or both inhibitors, or DMSO, with or without carbachol (100 μM). Phosphorylated MAPK was detected by immunoblot analysis (upper panel) and quantified by densitometry (lower panel). Results represent means ± S.E.M. from 3–9 experiments. *, Significantly different from the corresponding control group; **, significantly different from carbachol alone, $P < 0.05$. (**C**) Cells were treated with carbachol (carb; 100 μM) or control (con) medium for 10 min. Immunoprecipitates (IP) were prepared using antibodies to Shc (left panel), or the EGF receptor (EGFR; right panel), and analysed by immunoblotting with a peroxidase-linked anti-phosphotyrosine antibody (clone PY99). (**D**) Cells were treated as in (**B**). Immunoprecipitates were prepared using polyclonal antibodies to the EGF receptor (upper panel), or to Shc (middle and lower panels) and immunoblotted using anti-phosphotyrosine antibodies (clone PY99) (upper and middle panels) or monoclonal antibodies to Shc (lower panel). In the experiment shown, GF109203X reduced MAPK activation by 31%.

(Figure 5A). In the same series of experiments, GF109203X reduced the mean response to carbachol by 76%. The combined action of PP1 and GF109203X abolished MAPK stimulation by carbachol (Figure 5A). PP1 reduced the tyrosine phosphorylation of Shc elicited by EGF, and decreased the association of the tyrosine-phosphorylated EGF receptor with Shc in EGF-treated cells (Figure 5B, middle panel). PP1 also blocked the tyrosine phosphorylation of p52 Shc induced by carbachol (Figure 5C). The concentration of PP1 used in these experiments (10 μM) did not affect tyrosine phosphorylation of the EGF receptor induced by EGF (Figure 5B, upper panel), but effectively inhibited carbachol-mediated tyrosine phosphorylation of paxillin, a Src substrate (results not shown). Similar results were described by Daub and colleagues [24].

Role of PKC in suppression of EGF-mediated signalling by carbachol

The results of the experiments described in this report suggest that EGF and m3 receptors might activate MAPK by at least partially convergent pathways. Therefore an experiment was carried out to determine if carbachol and EGF exert additive effects on MAPK activity. Interestingly, the responses to the two agonists were completely non-additive (Figure 6A). The PKC inhibitor GF109203X reduced the activation of MAPK by carbachol, as shown earlier, but did not inhibit the response to EGF alone, or to EGF in combination with carbachol. The non-additive nature of MAPK stimulation by carbachol and EGF may be due to an inhibitory effect of carbachol on EGF signalling. Specifically, in the presence of carbachol, EGF-induced association of the tyrosine-phosphorylated EGF receptor with Shc was inhibited. The effect was reversed by GF109203X, suggesting that carbachol inhibits EGF signalling by activating PKC (Figure 6B).

DISCUSSION

The results described in this study demonstrate that the regulation of MAPK activity by muscarinic receptors is dependent on PKC- and EGF receptor-mediated signalling pathways. A number of studies have shown that PKC plays a role in the coupling of GPCRs, including muscarinic m1 and m3 receptors, to MAPK. PKC inhibitors, or down-regulation of PKC by long-term exposure to phorbol esters, completely inhibited MAPK activation in response to carbachol in Chinese hamster ovary cells transfected with m1 receptors [12,13], and in SH-SY5Y and SK-N-BE2(C) human neuroblastoma cells, which express endogenous m3 receptors [45,46]. However, the stimulation of MAPK by carbachol in NIH 3T3 cells transfected with m1 receptors was

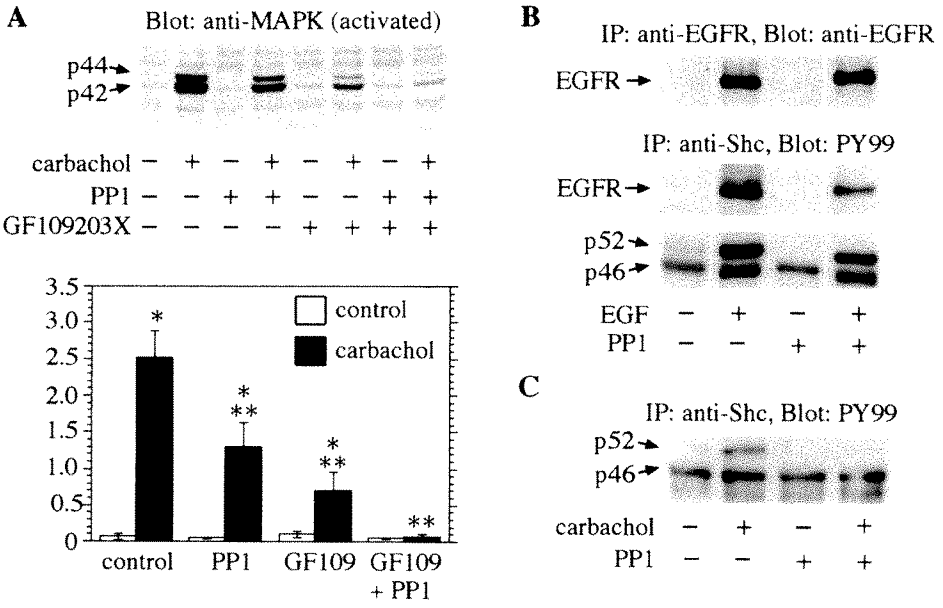

Figure 5 Src acts downstream of the EGF receptor to mediate MAPK activation by carbachol

(**A**) Cells were pretreated for 30 min with serum-free medium containing GF109203X (2.5 μM) or PP1 (10 μM), alone or in combination, or the vehicle DMSO. Cells were then incubated for 10 min in fresh medium containing one or both inhibitors, or DMSO, with or without carbachol (100 μM). Phosphorylated MAPK was detected by immunoblot analysis (upper panel) and quantified by densitometry (lower panel). Results represent means ± S.E.M. from 3 experiments. *, Significantly different from the corresponding control group; **, significantly different from carbachol alone, $P < 0.05$. (**B**) Cells were pretreated for 30 min with medium containing DMSO or PP1 (10 μM) then incubated for 10 min in fresh medium containing DMSO or PP1, with or without EGF (50 ng/ml). Immunoprecipitates (IP) of Shc proteins or the EGF receptor (EGFR) were prepared, and then immunoblotted with the anti-phosphotyrosine antibody PY99. (**C**) Cells were pretreated for 30 min with medium containing DMSO or PP1 (10 μM) then incubated for 10 min in fresh medium containing DMSO or PP1, with or without carbachol (100 μM). Immunoprecipitates of Shc proteins were prepared, and immunoblotted with the anti-phosphotyrosine antibody PY99.

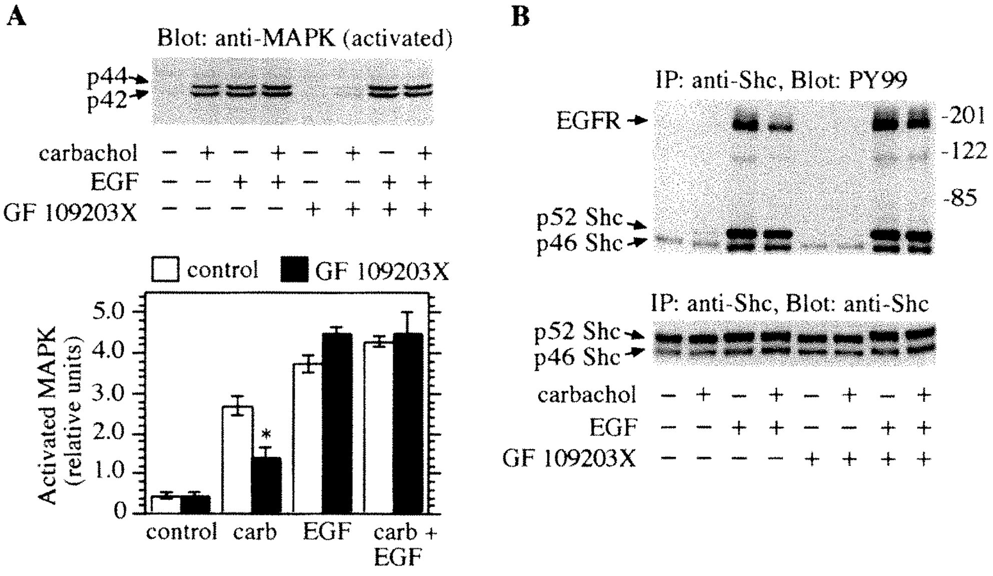

Figure 6 Carbachol and EGF exert non-additive effects on MAPK activity

(**A**) Cells were pretreated for 30 min with serum-free medium containing GF109203X (2.5 μM) or the vehicle DMSO. Cells were then incubated for 10 min in fresh medium containing GF109203X or DMSO with or without carbachol (100 μM) and/or EGF (50 ng/ml). Phosphorylated MAPK was detected in cell lysates by immunoblot analysis (upper panel). Bands of phosphorylated MAPK were quantified by densitometry (lower panel; carb, carbachol). Results are expressed as means ± S.E.M. from 3–8 experiments. *, Significantly different from carbachol alone, $P < 0.05$. (**B**) Cells were treated as in (**A**). Anti-Shc immunoprecipitates (IP) were prepared, and analysed by immunoblotting with anti-phosphotyrosine (upper panel) or anti-Shc (lower panel). The numbers to the right of the blot represent molecular masses in kDa.

only partially inhibited by GF109203X at a concentration (1 μM) that nearly abolished the response to the PMA [14], indicating that an alternate pathway may mediate the response in some cell types. In the present study, which employed as a model HEK cells stably transfected with m3 muscarinic receptors, the PKC inhibitor GF109203X caused a partial reduction in carbachol-induced MAPK activation. Another PKC inhibitor, the bisindolylmaleimide Ro31-8220, also substantially reduced MAPK activation by carbachol at a concentration that abolished the response to PMA. In contrast, the indolocarbazole Gö6976 did not affect the stimulation of MAPK by carbachol, although it too reduced the response to PMA. GF109203X and Ro31-8220 are inhibitors of both calcium-dependent and calcium-independent PKC isoforms, whereas Gö6976 inhibits only calcium-dependent isoforms [37,38]. Taken together, the results suggest that calcium-dependent and -independent PKC isoforms are both capable of regulating MAPK activity in HEK cells That Gö6976 was ineffective against carbachol implies a role for calcium-independent PKCs as mediators of MAPK activation by m3 receptors, but does not rule out the possibility that calcium-dependent isoforms are also involved, since inhibition of their effects by Gö6976 could be masked by the activity of isoforms resistant to this inhibitor. A recent study in SK-N-BE2(C) human neuroblastoma cells showed that, although these cells express multiple PKC isoforms, only PKCϵ was activated by carbachol, and was determined to mediate MAPK activation by carbachol [46]. This is surprising, since the stimulation of phosphoinositide hydrolysis by muscarinic receptor stimulation would be expected to activate calcium-dependent as well as calcium-independent PKC isoforms [47], and indeed, stimulation of m3 receptors in transfected Chinese hamster ovary cells activated PKC isoforms of both classes [48]. Additional experiments will be necessary to determine which specific PKC isoforms mediate the activation of MAPK by m3 receptor stimulation in the present model.

The PKC-independent MAPK activity elicited by carbachol in the presence of GF109203X was abolished either by an inhibitor of EGF receptor tyrosine kinase activity, or by an inhibitor of Src, suggesting the involvement of these two tyrosine kinases in this component of the response. A number of GPCRs have been shown to activate MAPK via transactivation of the EGF receptor. This conclusion is based on a series of reports demonstrating that pharmacological inhibitors of the EGF receptor kinase, or expression of dominant negative EGFreceptor mutants, prevent the activation of MAPK in response to GPCR ligands such as endothelin-1, lysophosphatidic acid, α-thrombin, angiotensin II, UTP and carbachol [23–28,33]. In most reports to date, the EGF receptor-dependent pathway is the principal route connecting GPCRs with MAPK, and inhibition of the EGF receptor activity alone is enough to interrupt the stimulation of MAPK by the GPCR ligand. In the present study, in contrast, the EGF receptor-dependent component appeared to account for only a part of the response.

Many studies of EGF receptor transactivation by GPCRs report that tyrosine phosphorylation of adapter proteins such as Shc, Cbl and Gab1 is increased by GPCR activation [23,24,27,33,40]. Consistent with these reports, stimulation of m3 receptors increased tyrosine phosphorylation of p52 Shc by 3.6-fold. The increase was blocked by the EGF receptor inhibitor AG1478, and by the Src inhibitor PP1, suggesting that Shc phosphorylation was a result of an interaction with the activated EGF receptor, and with Src. Moreover, since PP1 inhibited the association of the tyrosine-phosphorylated EGF receptor with Shc, without decreasing total EGF receptor tyrosine phosphorylation (Figure 5), it is likely that PP1 does not directly inhibit EGF receptor tyrosine kinase activity. Similar results have been reported by others [21,24], leading to the suggestion that Src may act 'downstream' of the EGF receptor to mediate tyrosine phosphorylation of Shc, possibly after the latter associates with the activated EGF receptor [34]. The results are also consistent with the possibility that tyrosine-phosphorylated Shc couples the activated EGF receptor to the MAPK cascade, presumably via recruitment of the Grb2–mSos complex [49], although the authors do not rule out the involvement of other adapter proteins in the response.

In a subset of experiments in which the response was assessed, it was noted that tyrosine phosphorylation of p52 Shc induced by carbachol was actually increased in the presence of GF109203X (Figure 4D). This was accompanied by increased tyrosine phosphorylation of the EGF receptor. These effects tended to occur in experiments in which the inhibitory effect of GF109203X on carbachol-induced MAPK activation was less than average. It is important to note that, regardless of the extent of MAPK inhibition by GF109203X, the residual, PKC-independent response was virtually abolished by AG1478 or by PP1. The results suggest that, under certain conditions that are as yet ill-defined, activation of PKC by carbachol may inhibit signalling by the EGF receptor/Src-dependent pathway. In such an instance, addition of the PKC inhibitor GF109203X unmasks, or potentiates, this secondary pathway. This hypothesis is supported by the observation that carbachol inhibited the association of tyrosine-phosphorylated EGF receptor with Shc caused by exogenous EGF, an effect that was reversed by GF109203X (Figure 6B). A similar interaction between carbachol and EGF has also been described by others [50]. The combined effect of carbachol and EGF on MAPK activation did not exceed the response to EGF alone, a result that also supports the notion that carbachol inhibits signalling by EGF (although it is also possible that the magnitude of the MAPK response is restricted by the limited availability of additional factors). A similar PKC-dependent suppression of the EGF receptor transactivation pathway was observed in GN4 rat liver epithelial cells stimulated with angiotensin II [28]. In contrast to these findings, tyrosine phosphorylation of endogenous EGF receptors by carbachol in m1 receptor-expressing HEK cells was reported to be mediated by PKC, as it was inhibited by GF109203X [40]. It is therefore possible that m1 and m3 receptors differentially modulate EGF receptor signalling pathways.

The mechanism linking activated GPCRs to the EGF receptor is unclear. Although EGF receptor transactivation by m1 or angiotensin-II receptors occurred in the absence of detectable EGF release from the cells [26,40], it was recently reported that the GPCR ligands endothelin, carbachol and lysophosphatidic acid activate the EGF receptor via metalloprotease-dependent cleavage of the transmembrane precursor of heparin-binding EGF-like growth factor [51]. It remains to be determined whether this mechanism accounts for the transactivation of the EGF receptor observed in the present study.

In summary, the results indicate that muscarinic m3 receptors regulate the activation of MAPK by two mechanisms; one dependent on PKC, and the other on sequential activation of the EGF receptor and Src tyrosine kinase. The consequences of this dual regulatory mechanism for cell signalling are currently unknown. In PC12 cells, nerve growth factor results in sustained activation of MAPK activity, and cell differentiation, whereas EGF produces a short-lived increase in MAPK, and cell proliferation ([52] and references therein). Moreover, the sustained, but not the early phase of, integrin-mediated MAPK activation is dependent on PKC [53] It is therefore plausible to propose that the duration of MAPK activation, and therefore the downstream consequences of m3 receptor stimulation, may depend on whether or not the response is mediated principally by PKC or by transactivation of the EGF receptor, or by a combination of both signals. The existence of multiple, independently regulated pathways linking GPCRs to MAPK may thus expand the repertoire of responses available to a cell exposed to a given extracellular signal.

I thank E. Peralta for the gift of the transfected HEK cells, and J. K. Blusztajn for helpful discussions. This work was supported by National Institutes of Health grants NS30791 and AG09525

REFERENCES

1 Cobb, M. H and Goldsmith, E J. (1995) J Biol Chem **270**, 14843–14846
2 Gutkind, J. S (1998) J Biol Chem **273**, 1839–1842
3 Schlaepfer, D. D and Hunter, T. (1998) Trends Cell Biol **8**, 151–157
4 Pages, G, Lenormand, P., L'Allemain, G, Chambard, J C., Meloche, S and Pouyssegur, J (1993) Proc Natl Acad. Sci U.S.A. **90**, 8319–8323
5 Mansour, S J, Matten, W. T, Hermann, A S., Candia, J M, Rong, S, Fukasawa, K, Vande Woude, G F and Ahn, N. G (1994) Science **265**, 966–970
6 Cowley, S, Paterson, H, Kemp, P and Marshall, C J (1994) Cell **77**, 841–852
7 Xia, Z G, Dickens, M., Raingeaud, J, Davis, R J and Greenberg, M E (1995) Science **270**, 1326–1331
8 Anand-Apte, B, Zetter, B R, Viswanathan, A, Qiu, R G, Chen, J, Ruggieri, R and Symons, M (1997) J Biol Chem **272**, 30688–30692
9 Seger, R and Krebs, E G (1995) FASEB J **9**, 726–735
10 Peralta, E G, Ashkenazi, A., Winslow, J W, Ramachandran, J and Capon, D J (1988) Nature (London) **334**, 434–437
11 Sandmann, J., Peralta, E G and Wurtman, R J (1991) J Biol Chem. **266**, 6031–6034
12 Hawes, B E, Van Biesen, T, Koch, W J, Luttrell, L M and Lefkowitz, R J (1995) J Biol Chem **270**, 17148–17153
13 Van Biesen, T, Hawes, B E, Raymond, J R., Luttrell, L M, Koch, W J. and Lefkowitz, R. J (1996) J Biol. Chem **271**, 1266–1269
14 Crespo, P, Xu, N., Daniotti, J L, Troppmair, J, Rapp, U R and Gutkind, J S (1994) J. Biol Chem **269**, 21103–21109
15 Crespo, P, Xu, N, Simonds, W F. and Gutkind, J S (1994) Nature (London) **369**, 418–420
16 Mattingly, R R. and Macara, I G (1996) Nature (London) **382**, 268–272
17 Winitz, S., Russell, M, Qian, N-X, Gardner, A, Dwyer, L and Johnson, G. L (1993) J Biol. Chem **268**, 19196–19199
18 Koch, W. J, Hawes, B E, Allen, L F. and Lefkowitz, R. J. (1994) Proc Natl Acad Sci. U S A. **91**, 12706–12710
19 Lopez-Ilasaca, M, Crespo, P, Pellici, P G, Gutkind, J S and Wetzker, R (1997) Science **275**, 394–397
20 Wan, Y., Kurosaki, T and Huang, X. Y (1996) Nature (London) **380**, 541–544
21 Luttrell, L M., Della Rocca, G. J., Van Biesen, T, Luttrell, D. K and Lefkowitz, R. J (1997) J Biol. Chem **272**, 4637–4644
22 Della Rocca, G. J., Maudsley, S, Daaka, Y., Lefkowitz, R. J. and Luttrell, L M. (1999) J Biol Chem **274**, 13978–13984
23 Daub, H, Weiss, F. U, Wallasch, C and Ullrich, A. (1996) Nature (London) **379**, 557–560
24 Daub, H., Wallasch, C, Lankenau, A., Herrlich, A and Ullrich, A (1997) EMBO J **16**, 7032–7044
25 Cunnick, J M., Dorsey, J F, Standley, T, Turkson, J, Kraker, A J, Fry, D W, Jove, R and Wu, J (1998) J Biol. Chem **273**, 14468–14475
26 Eguchi, S, Numaguchi, K, Iwasaki, H, Matsumoto, T, Yamakawa, T, Utsunomiya, H, Motley, E D, Kawakatsu, H, Owada, K M, Hirata, Y, Marumo, F and Inagami, T (1998) J. Biol Chem **273**, 8890–8896
27 Keely, S J, Uribe, J M and Barrett, K. E (1998) J Biol Chem. **273**, 27111–27117
28 Li, X., Lee, J W., Graves, L M. and Earp, H S (1998) EMBO J **17**, 2574–2583
29 Lev, S, Moreno, H, Martinez, R, Canoll, P., Peles, E., Musacchio, J M, Plowman, G D, Rudy, B and Schlessinger, J (1995) Nature (London) **376**, 737–745
30 Dikic, I., Tokiwa, G., Lev, S, Courtneidge, S A. and Schlessinger, J (1996) Nature (London) **383**, 547–550
31 Della Rocca, G J, Van Biesen, T, Daaka, Y., Luttrell, D. K, Luttrell, L M and Lefkowitz, R J. (1997) J. Biol Chem. **272**, 19125–19132
32 Soltoff, S P, Avraham, H, Avraham, S. and Cantley, L C (1998) J Biol. Chem **273**, 2653–2660
33 Soltoff, S. P (1998) J. Biol Chem **273**, 23110–23117
34 Zwick, E., Hackel, P O, Prenzel, N and Ullrich, A. (1999) Trends Pharmacol Sci **20**, 408–412
35 Luttrell, L M, Daaka, Y and Lefkowitz, R J (1999) Curr Opin Cell Biol **11**, 177–183
36 Petryniak, M A, Wurtman, R J and Slack, B E (1996) Biochem J. **320**, 957–963
37 Martiny-Baron, G, Kazanietz, M. G, Mischak, H, Blumberg, P. M, Kochs, G, Hug, H, Marmé, D. and Schachtele, C. (1993) J Biol Chem. **268**, 9194–9197
38 Wilkinson, S E, Parker, P. J and Nixon, J S (1993) Biochem J. **294**, 335–337
39 Limatola, C, Schaap, D, Moolenaar, W. H and Van Blitterswijk, W J (1994) Biochem. J. **304**, 1001–1008
40 Tsai, W, Monelli, A. D and Peralta, E G. (1997) EMBO J **16**, 4597–4605
41 Levitzki, A and Gazit, A (1995) Science **267**, 1782–1788
42 Burridge, K and Chrzanowska-Wodnicka, M (1996) Annu Rev Cell Dev. Biol **12**, 463–518
43 Richardson, A, Malik, R K, Hildebrand, J D and Parsons, J T. (1997) Mol. Cell Biol. **17**, 6906–6914
44 Moghal, N and Sternberg, P W (1999) Curr Opin. Cell Biol. **11**, 190–196
45 Offermanns, S, Bombien, E and Schultz, G (1993) Biochem J. **294**, 545–550
46 Kim, J Y, Yang, M. S, Oh, C. D, Kim, K T, Ha, M J, Kang, S. S and Chun, J S (1999) Biochem J **337**, 275–280
47 Ha, K.-S and Exton, J H. (1993) J Biol. Chem **268**, 10534–10539
48 Strassheim, D, May, L G, Varker, K A, Puhl, H L, Phelps, S H, Porter, R A, Aronstam, R S, Noti, J D and Williams, C L (1999) J Biol Chem **274**, 18675–18685
49 Rozakis-Adcock, M., McGlade, J, Mbamalu, G, Pelicci, G., Daly, R., Li, W, Batzer, A., Thomas, S, Brugge, J, Pelicci, P G., Schlessinger, J. and Pawson, T (1992) Nature (London) **360**, 689–692
50 Zhang, L and Jope, R. S (1999) Biochem Biophys Res Commun **255**, 774–777
51 Prenzel, N, Zwick, E, Daub, H, Leserer, M, Abraham, R, Wallasch, C and Ullrich, A. (2000) Nature (London) **402**, 884–888
52 Marshall, C J. (1995) Cell **80**, 179–185
53 Howe, A K and Juliano, R L (1998) J Biol Chem **273**, 27268–27274

Received 3 February 2000; accepted 27 March 2000

Purification from rat liver of a novel constitutively expressed member of the aldo-keto reductase 7 family that is widely distributed in extrahepatic tissues

Vincent P. KELLY, Linda S. IRELAND, Elizabeth M. ELLIS[1] and John D. HAYES[2]
Biomedical Research Centre, Ninewells Hospital and Medical School, University of Dundee, Dundee DD1 9SY, Scotland, U.K.

Antiserum raised against human aflatoxin B_1 aldehyde reductase 1 (hAFAR1) has been used to identify a previously unrecognized rat aldo-keto reductase (AKR). This novel enzyme is designated rat aflatoxin B_1 aldehyde reductase 2 (rAFAR2) and it characteristically migrates faster during SDS/PAGE than does the archetypal ethoxyquin-inducible rAFAR protein (now called rAFAR1). Significantly, rAFAR2 is essentially unreactive with polyclonal antibodies raised against rAFAR1. Besides its distinct electrophoretic and immunochemical properties, rAFAR2 appears to be regulated differently from rAFAR1 as it is expressed in most rat tissues and does not appear to be induced by ethoxyquin. Multiple forms of rAFAR2 have been identified. Anion-exchange chromatography on Q-Sepharose, followed by adsorption chromatography on columns of Matrex Orange A and Cibacron Blue, have been employed to purify rAFAR2 from rat liver cytosol. The Q-Sepharose chromatography step resulted in the resolution of rAFAR2 into three peaks of AKR activity, two of which were purified and shown to be capable of catalysing the reduction of 2-carboxybenzaldehyde, succinic semialdehyde, 4-nitrobenzaldehyde and 9,10-phenathrenequinone. The two most highly purified rAFAR2-containing preparations eluted from the Cibacron Blue column were 91 and 98 % homogeneous. Analysis of these by SDS/PAGE indicated that the least anionic (peak CBA5) comprised a polypeptide of 37.0 kDa, whereas the most anionic (peak CBA6) contained two closely migrating polypeptides of 36.8 and 37.0 kDa; by contrast, in the present study, rAFAR1 was estimated by SDS/PAGE to be composed of 38.0 kDa subunits. Final purification of the 37 kDa polypeptide in CBA5 and CBA6 was accomplished by reversed-phase HPLC. Partial proteolysis of the two preparations of the 37 kDa polypeptide with *Staphylococcus aureus* V8 protease yielded fragments of identical size, suggesting that they represent the product of a single gene. Furthermore, the peptide maps from CBA5 and CBA6 differed substantially from that yielded by rAFAR1, indicating that they are genetically distinct from the inducible reductase. A peptide generated by CNBr digestion of the 37 kDa polypeptide from CBA6 was shown by Edman degradation to share 88 % sequence identity with residues Tyr^{168}–Leu^{183} of rAFAR1. This provides evidence that the rat protein identified by its cross-reactivity with anti-hAFAR1 serum is an additional member of the AKR7 family.

Key words: carboxybenzaldehyde, γ-hydroxybutyrate, phenanthrenequinone, succinic semialdehyde, tissue-specific expression.

INTRODUCTION

The aldo-keto reductase (AKR) superfamily comprises soluble NAD(P)(H)-dependent oxidoreductases that typically catalyse the reduction of carbonyl-containing compounds and/or the oxidation of alcohols [1,2]. Endogenous substrates for AKR include monosaccharides [3,4], prostaglandins [5,6] and steroids [7], neurotransmitter aldehydes produced by monoamine oxidase [8] and reactive α,β-unsaturated carbonyls arising from lipid peroxidation [9,10]. In addition, AKR metabolizes numerous harmful compounds of foreign origin, including cytotoxic therapeutic drugs, polycyclic aromatic hydrocarbons, mycotoxins, isoflavonoid phytoalexins, herbicides and pesticides [11–14].

Amino acid sequence alignments have allowed division of AKR into seven multigene families [1,2]. The AKR1 family contains all of the better characterized mammalian isoenzymes, including aldehyde reductase, aldose reductase, chlordecone reductase, 3α-hydroxysteroid dehydrogenase (also called dihydrodiol dehydrogenase), prostaglandin F synthase, and Δ^4-3 oxosteroid 5β-reductase [15]. As indicated by their names, the AKR1 proteins exhibit diverse activities; they are widely distributed and have been identified in human, rat, mouse, cow, pig, rabbit, frog and barley. The AKR2–5 families comprise reductases from bacteria, yeast and plants, and do not appear to be represented in mammalian species [1,2]. Proteins placed in the AKR6 family are β-subunits of the *Shaker*-related voltage-gated K^+ channels isolated from human, rat and cow [1,16–18]. It has been proposed that β-subunits mediate the regulation of the K^+ channel by intracellular chemical signals, presumably carbonyl groups, though it remains to be established whether β-subunits function as enzymes. Finally, the AKR7 family has been identified in rat and human [19–22]. Whilst only distantly related to other AKR families, the mammalian AKR7 isoenzymes catalyse the reduction of many of the aromatic aldehydes and α-dicarbonyls which are metabolized by aldehyde reductase and aldose reductase [21–23].

Protein crystallography has shown that human aldose reductase (AKR1B1), rat 3α-hydroxysteroid dehydrogenase

---

Abbreviations used AFAR, aflatoxin B_1-aldehyde reductase, hAFAR, human AFAR, rAFAR, rat AFAR, AFB_1, aflatoxin B_1; AKR, aldo-keto reductase, 2-CBA, 2-carboxybenzaldehyde, CBA1–6, chromatography peaks 1–6 containing reductase activity towards 2-carboxybenzaldehyde, DTT, dithiothreitol; ECL®, enhanced chemiluminescence (Amersham), GABA, γ-aminobutyric acid, GHB, γ-hydroxybutyric acid, 4-NBA, 4-nitrobenzaldehyde, NQO1, NAD(P)H:quinone oxidoreductase 1, 9,10-PQ, 9,10-phenanthrenequinone; SSA, succinic semialdehyde, UTR, untranslated region

[1] Present address. Department of Bioscience and Biotechnology and Pharmaceutical Sciences, University of Strathclyde, Glasgow G1 1XW, Scotland, U.K.

[2] To whom correspondence should be addressed (e-mail hayes@icrf.icnet.uk).

(AKR1C9) and mouse fibroblast-growth-factor-1-induced protein (AKR1B8) are monomeric proteins and share a common $(\alpha/\beta)_8$-barrel three-dimensional fold [24–26]. Such studies have demonstrated that the active centres of the AKR1 enzymes are structurally similar. Moreover, their catalytic mechanism is distinct from that employed by either the long-chain alcohol dehydrogenase or the short-chain dehydrogenase/reductase superfamilies, some of which can metabolize compounds that are also AKR substrates [15]. The crystal structure of the rat voltage-gated K^+-channel β-subunit 2 (Kvβ2 or AKR6A2) has also been solved [27]. This has shown that, although AKR6A2 possesses a $(\alpha/\beta)_8$-barrel fold similar to that of the AKR1 family members, and can bind nicotinamide cofactor, it is capable of forming tetramers. This is an important observation, because it means that the quaternary structure of AKR proteins is variable.

The body of literature describing the biological activities of AKR7 isoenzymes is relatively small. The founding member of this family (AKR7A1) was discovered in rat liver as an aflatoxin B_1-aldehyde reductase (rAFAR1) that was induced by feeding rodents on diets containing the synthetic antioxidant 6-ethoxy-1,2-dihydro-2,2,4-trimethylquinoline (ethoxyquin) [19]. Subsequent work revealed that rAFAR1 is induced by a range of xenobiotics, including butylated hydroxyanisole, coumarin, 1,2-dithiole-3-thione, β-naphthoflavone, oltipraz and *trans*-stilbene oxide [28–30], most of which are believed to transcriptionally activate gene expression through the antioxidant responsive element [31]. Following characterization of this inducible rat AKR, two related human reductases, called hAFAR1 (or AKR7A2) [22] and hAFAR2 (or AKR7A3) [32], were isolated by molecular-cloning techniques. Functional studies of the rat and human AKR7 isoenzymes have shown that, under *in vitro* conditions, aflatoxin B_1-aldehyde is not a particularly good substrate for this family of reductases [21,22]. Both rAFAR1 and hAFAR1 have substantial activity towards succinic semialdehyde (SSA) [21,22], suggesting that this compound, which is derived from γ-aminobutyric acid, may represent an important physiological substrate for the AKR7 enzymes. In addition to exhibiting SSA reductase activity, rAFAR1 and hAFAR1 are able to metabolize 2-carboxybenzaldehyde (2-CBA) [22], a compound that is structurally related to SSA and has been shown to be reduced *in vivo* by rats and man [33]. Among aldo-keto reductases, 2-CBA appears to be a relatively specific substrate for AKR7 family members [23]

In the light of the finding that humans possesses two AFAR isoenzymes, we have been prompted to consider whether the rat also possesses multiple AFARs. In the present study polyclonal antibodies raised against hAFAR1 have been used to reveal the existence of an immunochemically related protein in numerous rat tissues, which is not induced by ethoxyquin and is not recognized by anti-rAFAR1 serum. The novel immunoreactive protein exists in several forms, and these have been purified from rat liver. As described below, the purified protein has been designated rAFAR2 because it is catalytically active with the carbonyl-containing substrates 2-CBA and SSA. Though rAFAR2 is distinct from rAFAR1, it is structurally related and is a member of the AKR7 family.

MATERIALS AND METHODS

Reagents

Chemicals were of the highest grade and were readily available commercially. Matrex Orange A chromatography gel was obtained from Amicon Ltd. (Stonehouse, Gloucestershire, U.K.). The pre-packed HiTrap Blue columns as well as the Q-Sepharose and Sephadex G-150 chromatography gels, and *Staphylococcus aureus* V8 protease, were purchased from Sigma Chemical Co (Poole, Dorset, U.K.).

Buffers

These were prepared at 20 °C, and the pH values quoted are those obtained at ambient temperature.

Animals

The initial study into possible existence of multiple AFAR proteins used as tissue source livers from 12 week old male Fischer 344 rats fed on either a control diet or on a diet containing 0.5% (w/w) ethoxyquin for the 14 days immediately before sacrifice. The Fischer rats for this analysis were purchased from Harlan Olac Ltd. (Bicester, Oxon., U.K.), and the feeding experiments performed by colleagues at the MRC Toxicology Unit, University of Leicester, Leicester, U.K. (for further details see [34]). In all other studies, 12-week-old male Sprague–Dawley rats (from Imperial Cancer Research Fund, Biological Resource, Clare Hall, Potters Bar, Herts, U.K.) were used as the tissue source. Upon removal, the organs from Fischer 344 and Sprague–Dawley rats were snap-frozen, shipped to Dundee on solid CO_2, and stored at −70 °C until use.

Human material

Several samples of normal human liver cytosol were examined during the course of the study to allow comparison of hepatic polypeptides in rat and man that cross-react with antibodies against various AFAR proteins. The liver sample examined was from patient 387 who died from a cerebral infarct; the specimen has been characterized previously [35].

Cell culture

Rat H4IIE hepatoma cells were from the European Collection of Animal Cell Cultures. The cells were seeded at a density of 2×10^4 into T-75 flasks containing minimal essential medium with Earle's salts and glutaMAX-1® (Eagle) supplemented with 1% (v/v) non-essential amino acids, 10% (v/v) foetal-bovine serum and 50 units of penicillin/streptomycin. Cells were maintained in an atmosphere of 5% CO_2 at 37 °C. Cells were harvested at 80% confluency by scraping them into a Universal sterile tube containing 10 ml of PBS.

Molecular cloning and expression of rat AKR1 family members

Complementary DNAs were amplified by reverse-transcription (RT)-PCR using total rat liver RNA as source of message for aldehyde reductase (AKR1A3), 3α-hydroxysteroid dehydrogenase (AKR1C9) and Δ^4-3-ketosteroid 5β-reductase (AKR1D2). Aldose reductase (AKR1B4) was cloned using RNA from rat kidney as template for RT-PCR. In these reactions, the oligonucleotide primers used to amplify the cDNA were designed to create an *Nde*I restriction site at the initiation codon, either a *Eco*RI or *Kpn*I restriction site in the 5′-untranslated region (UTR) and either a *Bam*HI or *Xho*I restriction site in the 3′-UTR. The primers, along with the cDNA sequences used in their design, were as follows:

AKR1A3[36]:
5′-CCGGATTCATATGACGGCCTCCAGTG-3′ (sense) and
5′-CGCGGATCCTACGGGCCTCAGTATG-3′ (antisense)

AKR1B4 [37]:
5′-CCGGATTCATATGGCTAGCCATCTGGA-3′ (sense) and
5′-CCGCTCGAGCCACAGCTTCAGACTTC-3′ (antisense)
AKR1C9 [38]:
5′-CGGGGTACCATATGGATTCCATATCTCTGC-3′ (sense)
and
5′-CGCGGATCCCACCATGTTACTATTCATC-3′ (antisense)
AKR1D2 [39]:
5′-CCGGATTCATATGAACCTCAGCACTGC-3′ (sense)
and
5′-CGCGGATCCATGTTCAGTATTCGTCATG-3′ (antisense)

The amplified cDNAs were purified from the reaction mixtures (using QIAquick PCR purification kits) before being subjected to double digestion with either *Eco*RI or *Kp*NI and either *Bam*HI or *Xho*I. The restriction-digest products were resolved by agarose-gel electrophoresis, and the fragments of interest were ligated into pTZ19r that had been treated with the same restriction enzymes using standard methods. Following propagation of these cDNA clones in pTZ19r, the coding regions for AKR1A3, AKR1C9 and AKR1D2 were excised with *Nde*I and *Bam*HI and that for AKR1B4 was excised with *Nde*I and *Xho*I to allow them to be subcloned into the pET15b expression vector. This was achieved by ligation of the cDNAs both in-frame and downstream of the region in pET15b that encodes an N-terminal polyhistidine tag. The ligation products were transformed into *Escherichia coli* BL21 pLysS cells. Recombinant rat AKR isoenzymes were purified from soluble bacterial extracts by nickel chelate chromatography as described previously [20,22].

Antibodies

These were all raised in female New Zealand White rabbits. The antiserum employed against rAFAR1 was raised previously against the native ethoxyquin-inducible reductase purified from rat liver [19]. Antiserum for hAFAR1 was raised by Ireland et al. [22] against the recombinant protein expressed in *E. coli*; the RW143 serum was used, and this displays specificity for the C-terminal portion of the protein [22]. Production of antibodies against rat NAD(P)H:quinone oxidoreductase 1 (NQO1) is described elsewhere [30]. During the present project antibodies were raised against bacterially expressed polyhistidine-tagged AKR1A3, AKR1B4, AKR1C9 and AKR1D2 using standard methods.

Biochemical analyses

Protein concentrations were measured by the method of Bradford [40].

Reductase activity was measured at 25 °C in 100 mM sodium phosphate buffer, pH 7.0, using either 2-CBA (1 mM), SSA (1 mM), 4-nitrobenzaldehyde (1 mM) or 9,10-phenanthrenequinone (0.05 mM) as substrates. Both NADPH and NADH were employed as cofactors (at a concentration of 0.2 mM) and the initial rate of reaction was monitored using a Cobas Fara centrifugal analyser (Hoffmann–La Roche Ltd., Basel, Switzerland) at 340 nm.

Discontinuous SDS/PAGE was performed by the method of Laemmli [41], and proteins were stained with Coomassie Blue. For most analyses the Bio-Rad Mini-Protean II Cell apparatus was used (Bio-Rad Laboratories, Hemel Hempstead, Herts, U.K.). However, when maximal resolution between the multiple AFAR proteins was required, electrophoresis was carried out in the larger Bio-Rad Protean II xi Cell. In many electrophoretic runs, bacterially expressed rAFAR1 was included as a purified standard to facilitate identification of proteins. For this purpose, the cDNA coding region for the reductase was subcloned into pET17b and expressed in *E. coli* as the full-length rat protein without an N-terminal polyhistidine tag. The heterologously expressed rAFAR1 was purified from bacterial lysates by Q-Sepharose chromatography, essentially as described by Ellis et al. [28].

For Western blotting, electrophoretic transfer of polypeptides from SDS/PAGE gels to nitrocellulose membranes was carried out with Bio-Rad equipment that was appropriate for the size of the PAGE gel. Protein binding sites on membranes were blocked by placing them overnight in 20 mM Tris/HCl/150 mM NaCl/0.25 % (v/v) Tween, pH 7.4, which contained 10 % (w/v) semi-skimmed milk (buffer A). The blots were then incubated for 1 h at room temperature with antisera against AKR isoenzymes (at 1:2000 dilution in buffer A). After washing, bound antibody was allowed to react for 1 h at room temperature with a horseradish peroxidase-conjugated secondary antibody (goat anti-rabbit IgG, at 1:3000 dilution) in buffer A. The antibody complexes were detected by enhanced chemiluminescence (ECL$^\bullet$, Amersham) and revealed after exposure to Blue-sensitive X-ray film (Genetic Research Instrumentation, Braintree, Essex, U.K.) [28].

Protein purification

The chromatography methods used to isolate the rat AFAR proteins were adapted from those used to purify hAFAR1 [22]. All steps were performed on ice or at 4 °C. The protocol is described fully in the Results section below. Briefly, rat liver 100000 *g* supernatant (cytosol) was prepared in 10 mM Tris/HCl, pH 8.2 (buffer B), containing 1 mM dithiothreitol (DTT) and dialysed extensively against the same buffer before being subjected to chromatography on Q-Sepharose. This anion-exchange step resulted in resolution of rAFAR1 from the additional AFAR forms in rat liver. The various AFAR-containing peaks were collected separately, and each was subjected sequentially to chromatography on columns of Matrex Orange A and HiTrap Blue (i.e. Cibacron Blue).

Protein chemistry

Portions (100 μg protein) of the AFAR preparations obtained from the HiTrap Blue step were subjected to reversed-phase HPLC on a 4.6 mm × 250 mm Brownlee C_{18} column (7 μm particle size and 300 Å pore size). This column was developed using a linear 35–70 % acetonitrile gradient which was formed in 0.1 % (v/v) trifluoroacetic acid over 90 min using two model 510 pumps from Waters Associates (Instruments), Northwich, Cheshire, U.K. The column was eluted at 1.0 ml/min, and the entire chromatography run took 100 min to complete; it included a 10 min isocratic 'loading' period during which the flow rate was increased from 0.1 to 1.0 ml/min. The protein-containing peaks were collected manually (about 1.5 ml) and freeze-dried twice to remove all traces of trifluoroacetic acid. The dried material was dissolved in about 100 μl of electrophoresis sample buffer (0.1 % (v/v) SDS in 10 mM Tris/HCl, pH 7.0) and subjected to a final SDS/PAGE purification step in 12 %-(w/v)-polyacrylamide resolving gels. Western blotting was used to confirm that the correct polypeptide had been isolated.

Peptide maps were prepared by examination of partial digestion of the AFAR preparations with *S. aureus* V8 protease. Electrophoretically purified AFAR proteins were located within PAGE gels by rinsing them briefly with ice-cold water followed by immersion in aq. 250 mM KCl containing 1 mM DTT. The polypeptide band of interest was cut out of the polyacrylamide gel using a razor blade, and the gel slice obtained was rinsed twice for a total of 10 min with 3.0 ml ice-cold aq. 1 mM DTT before being freeze-dried. A single freeze-dried gel slice was allowed to rehydrate for 5 min in the sample well of a pre-cast slab SDS/PAGE gel (comprising a 16 % polyacrylamide resolving gel). This was allowed to occur in a solution of protein elution buffer [i.e. 0.1 % (v/v) SDS/1 mM EDTA/2.5 mM DTT/125 mM Tris/HCl, pH 6.8], which was placed into the sample well immediately before the gel slice. Once rehydrated, the gel slice was overlaid with a 5 μl aliquot of protein elution buffer containing 20 % (v/v) glycerol. On top of this was layered a 5 μl aliquot of a 100 μg/ml solution of *S. aureus* V8 protease in 125 μM Tris/HCl, pH 6.8, containing 1 mM EDTA, 0.1 % (w/v) SDS, 10 % (v/v) glycerol and 0.001 % (w/v) Bromophenol Blue. Immediately following these additions, the electrophoresis run was begun. Digestion of the AFAR proteins by V8 protease was allowed to proceed within the gel by briefly stopping electrophoresis for 30 min once the sample had migrated about two-thirds the way through the 3 % polyacrylamide stacking gel, at which time the components appeared to be maximally concentrated.

CNBr digestion of AFAR was performed on material that had been purified by HPLC and SDS/PAGE, as described above. Freeze-dried polyacrylamide-gel slices, which contained about 2 μg of AFAR, were rehydrated for 10 min in ice-cold aq. 70 % (v/v) formic acid. After this period of equilibration (carried out in a microcentrifuge tube), the acid was removed, two crystals of CNBr were added along with 0.5 ml of fresh 70 % (v/v) formic acid, and the mixture was flushed with N_2 gas. The reaction was allowed to proceed in the dark for 30 min at room temperature. Digestion was stopped by removing the solution and washing the gel twice with 1 ml of ice-cold water for 5 min, followed by two changes of ice-cold 1 M Tris/HCl buffer, pH 6.8, also for 5 min. The gel slices were placed in the wells of preformed slab SDS/PAGE gels, and the cleavage products were resolved by electrophoresis in 16 %-(w/v)-polyacrylamide gels. The fragments were either stained with Coomassie Blue or transferred onto Problott® membrane for amino acid sequencing. This was performed as described previously [42].

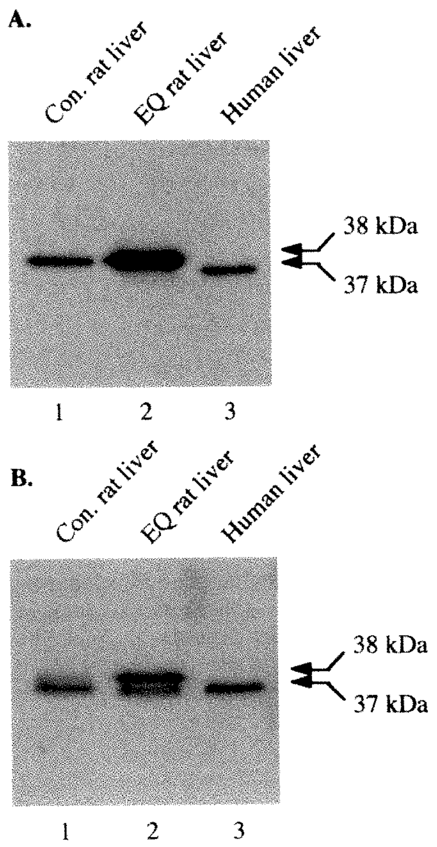

Figure 1 A novel 37 kDa polypeptide in rat liver cross-reacts with anti-hAFAR1 serum

Portions (5 μg of protein) of hepatic cytosol were subjected to Western blotting. The samples were loaded in an identical fashion on to two separate polyacrylamide-gels as follows: 1, liver from Fischer 344 rats fed on control diet; 2, liver from rats fed on an ethoxyquin-containing diet; 3, normal human liver. Once the SDS/PAGE run was complete, the proteins were transferred electrophoretically to immobilon-P membranes and probed with either anti-rAFAR1 serum (**A**) or anti-hAFAR1 serum (**B**). Cross-reacting polypeptides were revealed by ECL®. The position of mobility of 37 kDa and 38 kDa polypeptides is indicated. Abbreviations: Con., control; EQ, ethoxyquin.

RESULTS

Identification of a novel 37 kDa-AFAR protein in rat tissues and rat cell line

The molecular mass of rAFAR1, as estimated by SDS/PAGE, has been variously reported to lie between 36 and 40 kDa [19,22,28]. During the present study it was estimated by SDS/PAGE to be 38 kDa.

Western blotting with anti-rAFAR1-serum has previously shown that the reductase is present at low levels in livers of rats fed on control diet, but is induced 15-fold in the livers of rats fed on an ethoxyquin-containing diet [28]. Figure 1(A) shows that anti-rAFAR1 serum cross-reacts with a single electrophoretic band in both rat and human liver cytosol. Surprisingly, in the reverse experiment, the antibody raised against hAFAR1 detected two polypeptides in liver cytosols from rats fed on a control diet and those fed on an ethoxyquin-containing diet (Figure 1B). Among these two cross-reacting bands the polypeptide that migrated more slowly during SDS/PAGE corresponded to the inducible rat protein and was estimated to have a molecular mass of 38 kDa. The additional polypeptide with the faster electrophoretic mobility, which was not detected with anti-rAFAR1 serum, was found to co-migrate with the human AKR7A2 immunogen (L. S. Ireland and J. D. Hayes, unpublished work). In these experiments its molecular mass was estimated to be 37 kDa, and as this polypeptide did not appear to be inducible by ethoxyquin, it was thought to be distinct from rAFAR1. The fact that it cross-reacted with hAFAR1 antiserum suggests that it is likely to be a further member of the AKR7 family. It was postulated that the 37 kDa polypeptide which is immunochemically related to hAFAR1 might represent rAFAR2. However, until this hypothesis was substantiated (see below) the putative rAFAR2 isoenzyme was called 37 kDa-AFAR.

Immunoblotting of extracts prepared from rat H4IIE cells with anti-hAFAR1-serum also showed the presence of two cross-reacting polypeptides (Figure 2). The two bands observed in H4IIE-cell extracts co-migrated with those in rat liver, and the slower electrophoretic band had the same mobility as bacterially expressed rAFAR1. The 37 kDa-AFAR rat protein was not recognized with antibodies raised against rAFAR1.

The expression of 37 kDa-AFAR was examined in extrahepatic rat organs, not only to confirm that it is regulated differently from rAFAR1, but also to identify the best tissue source for the

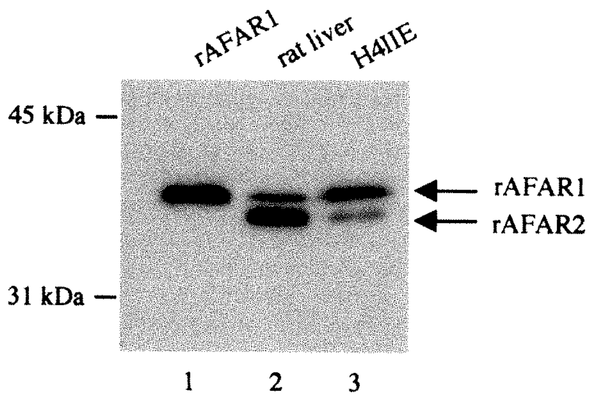

Figure 2 Identification of 37 kDa-AFAR in a rat hepatoma cell line

Portions (5 μg of protein) of postnuclear supernatants from the livers of rats fed on control diet and from H4IIE cells, along with heterologously expressed purified rAFAR1 (0.02 μg of protein), were subjected to Western blotting as described in the text. SDS/PAGE, performed in a Bio-Rad Protean II xi Cell apparatus, was loaded as follows: 1, rAFAR1; 2, Sprague–Dawley rat liver cytosol; 3, soluble extract from untreated H4IIE cells. Blots of the resolved proteins were prepared and probed with anti-hAFAR1 serum.

novel protein. Western blotting of organs from rats fed on a control diet showed that rAFAR1 has a limited tissue distribution. Among the organs studied, significant amounts of rAFAR1 were observed in only kidney, liver, testis and pancreas. By contrast, 37 kDa-AFAR was found to possess a broader tissue distribution than rAFAR1, with substantial levels being observed in kidney, vas deferens, testis, pancreas, brain, adrenal gland and lung (Figure 3). Significant amounts of this novel protein were also detected in liver, heart, skeletal muscle, epididymus, ovary, spleen and stomach. The Western blots also revealed the presence of a fast-migrating cross-reacting protein in kidney, liver and spleen that was estimated to be about 36.8 kDa.

Resolution of rat carbonyl-reducing enzymes from liver cytosol

Liver was chosen as the source of 37 kDa-AFAR because immunoblotting demonstrated it to be relatively abundant in hepatic cytosol; also the liver is a large organ and our laboratory has previous experience of analysing AKR from this tissue [28,43]. Dialysed rat liver cytosol was applied to a column of Q-Sepharose that was developed with a linear 0–250 mM NaCl gradient in buffer B containing 1 mM DTT. Monitoring the column eluate with the substrates SSA, 4-nitrobenzaldehyde (4-NBA) and 9,10-phenanthrenequinone (9,10-PQ) showed that this anion-exchange-chromatography step gave rise to seven peaks of carbonyl-reducing activity. These have been designated peaks Ia, Ib, Ic, II, III, V and VI (Figure 4a) in accordance with the nomenclature introduced by Ellis et al. [28]. The highly anionic material recovered in peak VI, which was eluted by the final 1 M NaCl step, did not possess activity towards 4-NBA and 9,10-PQ with NADPH as cofactor. Peak VI did, however, exhibit activity towards 4-NBA and 9,10-PQ with NADH as cofactor (results not shown). It should be noted that, in the present study, the use of a larger column resulted in greater resolution than was achieved previously, and as a consequence three separate activities were detected in peak I (Ia, Ib and Ic). The enzyme activity designated peak IV by Ellis et al. [28] has not been recovered as a separate entity in the present chromatographic fractionation (Figure 4a).

Examination of eluate from Q-Sepharose with 2-carboxybenzaldehyde as substrate revealed a unique set of activities which could not be readily aligned with activity for SSA, 4-NBA or 9,10-PQ. As shown in Figure 4(b), a total of six 2-CBA reductase peaks (CBA1–CBA6) were distinguished across the profile. The first of these, CBA1, did not bind the anion-exchange column and was eluted during the washing stage between fractions 27 and 35, whereas CBA2 was eluted by the salt gradient at a similar position to peak Ic. Fractions representing CBA3 correspond to peak III. The three remaining peaks of reductase activity towards 2-CBA were designated CBA4, CBA5 and CBA6 and eluted in fractions 130–142, 145–158 and 162–176 respectively. Although CBA4 appears to be eluted with peak V, neither CBA5 nor CBA6 was co-eluted with previously described AKR chromatography peaks.

The identity of some of the enzymes in the peaks from Q-Sepharose could be inferred from substrate activities. Peak Ia displays activity towards SSA, 4-NBA and 9,10-PQ, and on this basis could contain a protein related to carbonyl reductase, as carbonyl reductase itself has been found to be absent from rat liver [44]. Aldehyde reductase is likely to contribute to the enzyme activity in peak II because it exhibits significant activity towards SSA and 4-NBA. Also, the absence of NADH-dependent reductase activity in this peak (results not shown) is consistent

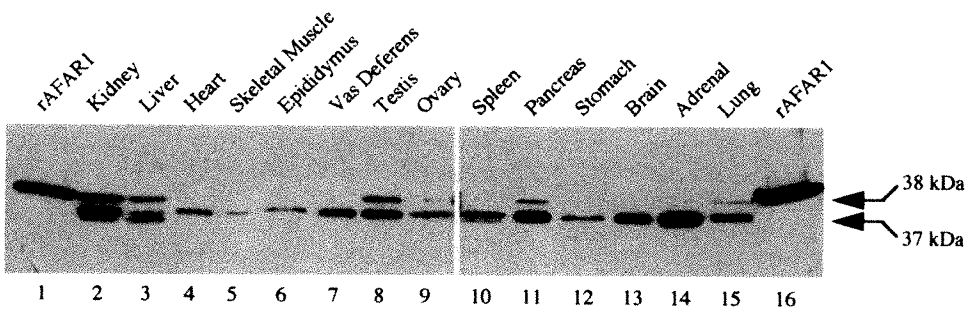

Figure 3 Tissue-specific expression of rAFAR1 and the 37 kDa-AFAR in the rat

Extracts from approx. 100 mg of fresh frozen tissue were prepared as described previously. Portions (20 μg of protein) of 12 000 ***g*** supernatants from tissues of Sprague–Dawley rats were subjected to SDS/PAGE using a Bio-Rad Protean II xi Cell to ensure complete resolution of the 37 and 38 kDa immunoreactive polypeptides. As a marker for rAFAR1, a 0.02 μg portion of the purified protein was also applied. The identity of the organs analysed is shown, and the Western blot was probed with anti-hAFAR1 serum.

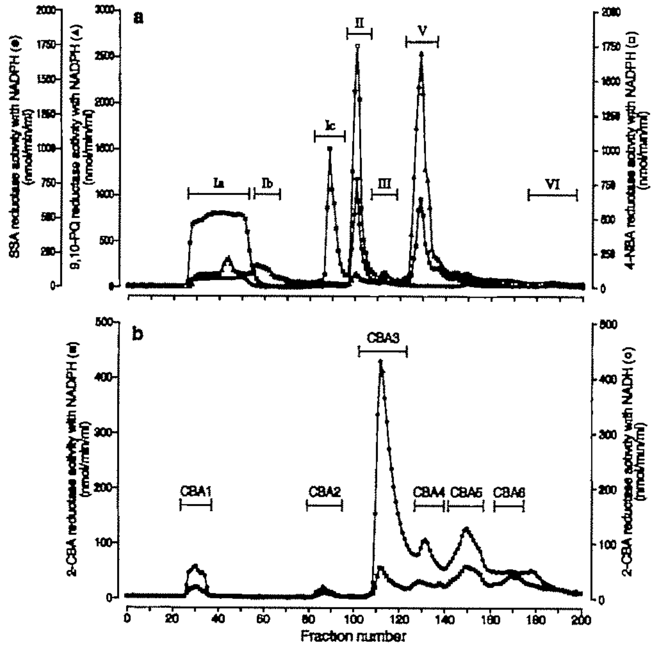

Figure 4 Resolution of AKR from rat liver by anion-exchange chromatography

Rat liver cytosol (approx. 9 g of protein) that had been dialysed against 10 mM Tris/HCl buffer, pH 8.2 (buffer B), containing 1 mM DTT, was applied to a 2.6 cm × 72 cm column of Q-Sepharose equilibrated with the same buffer. The Q-Sepharose column was eluted at 32 ml/h and fractions (8 ml each) were collected. The anion-exchanger was developed with a linear 0–250 mM NaCl gradient formed in buffer B containing 1 mM DTT that was applied to the column between fractions 35 and 185. Lastly, highly anionic proteins were recovered by elution with 1 M NaCl in buffer B containing 1 mM DTT. Reductase activity in column eluate towards SSA (●), 4-NBA (□) and 9,10-PQ (▲) with NADPH was measured, and is shown in (A). AKR activity towards 2-CBA with either NADPH (■) or NADH (○) was measured (B). Note that peak IV, as described by Ellis et al. [28], was not recovered in this chromatography step.

with this assumption. The elution position and preferential activity of peak III towards SSA and 9,10-PQ suggests it contains rAFAR1. Peak V possesses significant activity with 9,10-PQ and could therefore contain either a hydroxysteroid dehydrogenase or NQO1, or both.

The proteins eluted within the peaks of enzyme activity from Q-Sepharose were probed with antibodies to allow identification of the reductases present. Antibodies against AKR1A3, AKR1B4, AKR1C9, AKR1D2 and rat NQO1 cross-reacted with proteins in peaks Ia, II, III, and VI (Table 1). Each peak containing reductase activity towards 2-CBA was probed with antisera against rAFAR1 and hAFAR1. The two minor peaks, CBA1 and CBA2, did not contain any protein species that could be detected by these antisera. Western blotting using anti-rAFAR1 serum showed that, in addition to cross-reacting with a 38 kDa polypeptide in CBA3, the same protein was also detectable in large amounts in CBA4, and in lesser amounts in CBA5. As expected, Western blotting of column fractions with anti-hAFAR1 serum identified two polypeptides of 37 and 38 kDa. The distribution of the cross-reacting 38 kDa polypeptide among the column fractions was identical with that observed with the rAFAR1 antibodies (Table 1). By contrast with the 38 kDa protein, the cross-reacting 37 kDa polypeptide appeared to be more tightly bound by the anion-exchange column. Relatively small amounts of this polypeptide were observed in CBA3. Quantitatively, the major fraction of the immunoreactive 37 kDa protein recovered was found to be eluted equally between CBA4, CBA5 and CBA6. Thus Q-Sepharose showed that the 37 and 38 kDa polypeptides in rat liver that cross-react with anti-hAFAR1 serum are chromatographically separate, and that both exhibit activity towards 2-CBA.

Purification of 37 kDa-AFAR

Following Q-Sepharose fractionation, the peaks of reductase activity towards 2-CBA were combined as indicated in Figure 4(b) and dialysed against 10 mM sodium phosphate buffer, pH 8.0, containing 1 mM DTT. Each peak was loaded on to an identical Matrex Orange A column that was developed using a standardized procedure with a linear 0–1.5 M NaCl gradient. Succinic semialdehyde and 2-CBA were used to detect rAFAR1 and 37 kDa-AFAR. The CBA3 pool was resolved by Matrex

Table 1 Immunochemical properties of AKR chromatographic peaks obtained from Q-Sepharose

Western blotting was carried out on the fractions eluted from the Q-Sepharose anion-exchanger shown in Figure 4 as described in the text

Column fraction	Peak	Cross-reactivity with antibodies against AKR1A3	AKR1B4	AKR1C9*	AKR1D2	rAFAR1	hAFAR1†	NQO1
50	Ia	–	–	++	–	–	–	–
57	Ib	–	–	–	–	–	–	–
89	Ic/CBA2	–	–	–	–	–	–	–
101	II	+++	–	–	–	–	–	–
113	III/CBA3	++	+++	–	–	+++	+	–
129	V/CBA4	–	++	+++	–	+++	+	+++
133	CBA4	–	–	+++	+	+++	+++	–
150	CBA5	–	–	++	+++	+	+++	–
169	CBA6	–	–	–	–	–	+++	–
187	VI	–	–	–	–	–	+	–

* The protein in peak Ia which cross-reacted with anti-AKR1C9 serum was 31 kDa, whereas the cross-reacting protein in fractions 129–150 was 37 kDa, as the immunogen is 37 kDa, the polypeptide in peak Ia that cross-reacts with the antibody is not AKR1C9, but is a structurally distinct protein

† Anti-hAFAR1 serum cross-reacted with a 37 and a 38 kDa polypeptide the 37 kDa protein was detected in fractions 133–187; the 38 kDa protein was detected in fractions 113–150.

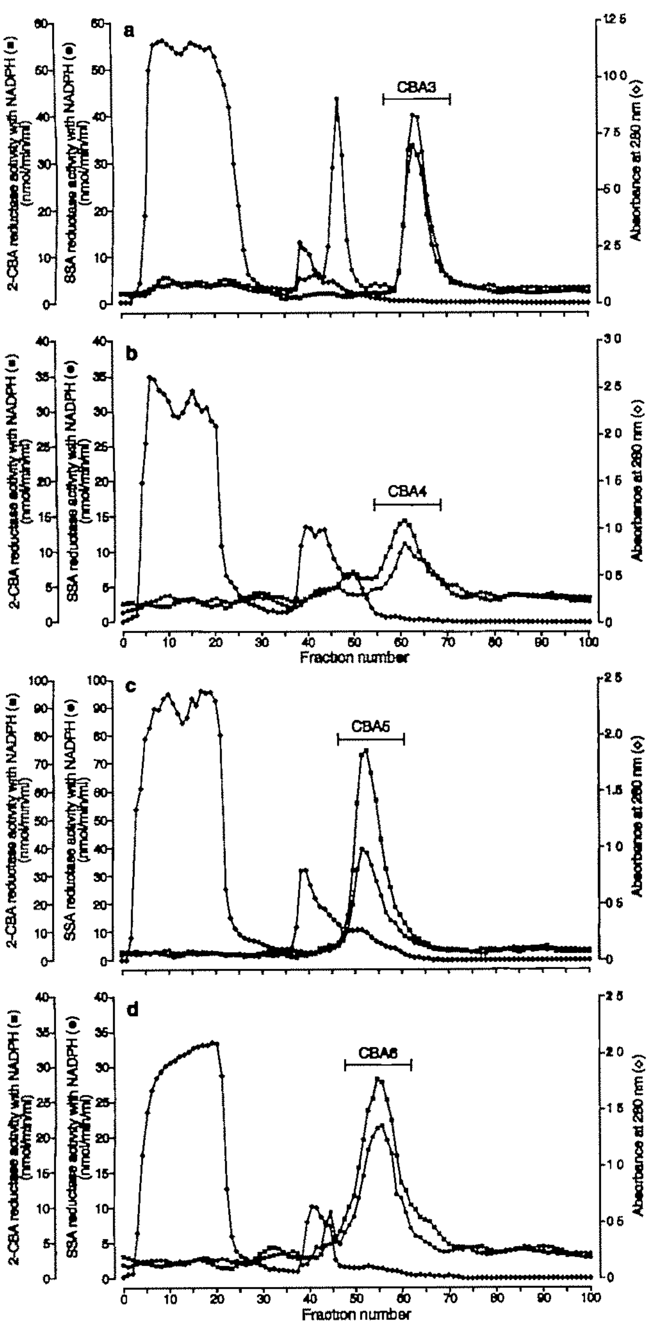

Figure 5 Fractionation of major hepatic anionic 2-CBA reductases by Matrex Orange A

The 2-CBA reductases in rat liver cytosol were resolved by anion-exchange chromatography The four major forms (CBA3–CBA6) were isolated as shown in Figure 4 and dialysed against 10 mM sodium phosphate buffer, pH 8.0 (buffer C), containing 1 mM DTT Each peak was diluted to 120 ml volume before being applied to 1.6 cm × 1.4 cm columns of Matrex Orange A The columns were eluted at 30 ml/h and developed with 400 ml linear 0–1.5 M NaCl gradients in buffer C containing 1 mM DTT The salt gradients were initiated at fraction 32, and the fraction volume was 6 ml The absorbance of the eluate at 280 nm (◇), and AKR activity towards 2-CBA (■) and SSA (●) with NADPH as cofactor was examined The elution profiles of CBA3, CBA4, CBA5 and CBA6 are shown in (**a**), (**b**), (**c**) and (**d**) respectively

Orange A into two peaks of reductase activity with SSA as substrate (Figure 5a). The first SSA reductase peak to be eluted from this column lacked reductase activity towards 2-CBA and is therefore assumed to represent AKR1A3 or AKR1B4. The second peak to be eluted exhibited activity towards 2-CBA and was therefore considered to be rAFAR1, a conclusion supported by Western-blotting data (results not shown). Furthermore, this second peak exhibited approx. 6-fold higher 2-CBA reductase activity with NADH as cofactor than with NADPH (for simplicity, only 2-CBA activity with NADPH is shown in Figure 5). The CBA4, CBA5 and CBA6 pools from Q-Sepharose were each eluted from Matrex Orange A as essentially a single peak of reductase activity towards SSA and 2-CBA (Figures 5b–5d). Furthermore, it was also noted that the CBA5 and CBA6 reductases did not bind the Matrex Orange A adsorption gel as tightly as did rAFAR1 (CBA3).

Each enzyme-containing peak eluted from Matrex Orange A was subjected to SDS/PAGE. This revealed that the CBA3 preparation was homogeneous and the single polypeptide co-migrated with the bacterially expressed rAFAR1 protein of 38 kDa molecular mass. By contrast, the reductase-containing fractions from CBA4, CBA5 and CBA6 contained multiple protein bands.

Further purification of CBA4, CBA5 and CBA6 was performed on the ADP-analogue matrix Cibacron Blue, using pre-packed HiTrap Blue columns. Fractions from Matrex Orange A were combined as shown in Figure 5, and each pool was applied directly to a HiTrap Blue column. The AKR protein in these preparations bound tightly to the Cibacron Blue matrix with insignificant quantities of the reductase activity being eluted in the flow-through fractions. Displacement of active protein from Cibacron Blue was achieved using a 1 mg/ml solution of NADPH in buffer B. The material eluted from the HiTrap Blue columns with reductase activity was examined by SDS/PAGE. This showed that the CBA4 preparation still contained significant amounts of a contaminating 58 kDa protein. However, both CBA5 and CBA6 were found to be comparatively pure, and both contained a 37 kDa protein which was demonstrated to cross-react with anti-hAFAR1 serum (results not shown). Densitometric scanning indicated that CBA5 was about 92 % pure, and Western blotting suggested that the major contaminant was rAFAR1. Although CBA6 was estimated to be 98 % pure, close examination of the electrophoresis gel indicated the presence of two partially resolved bands in the preparation.

The purification scheme resulted in excellent recovery of 2-CBA reductase activity from rat liver. Typically, from roughly 9 g of cytosolic protein, between 0.5 and 1.5 mg of purified protein was obtained in the final CBA5 and CBA6 pools eluted from HiTrap Blue. The purification method is highly efficient and allowed a total recovery of about 15 % of the total reductase activity between CBA5 and CBA6, and a further 9 % in CBA3. A summary of the purification is shown in Table 2.

The specific activities of CBA5 and CBA6 towards AKR substrates were determined. Table 3 shows that under ‘standard’ assay conditions, CBA5 exhibits activities similar to those of CBA6 towards 2-CBA and SSA. However, CBA5 possesses higher activity than CBA6 towards 4-NBA and 9,10-PQ. Furthermore, comparison of the activity of these preparations with that of rAFAR1 revealed significant differences in specificity under the conditions used. For example, rAFAR1 exhibited greater activity for both 4-NBA and 9,10-PQ than either CBA5 or CBA6. This survey also revealed that, under the assay conditions used, rAFAR1 uniquely possesses about 7-fold greater activity towards 2-CBA with NADH as cofactor than with NADPH; by contrast, with SSA, 4-NBA and 9,10-PQ as substrates, rAFAR1 shows a preference for NADPH as cofactor. Neither CBA5 nor CBA6 displayed higher activity towards 2-CBA with NADH as cofactor than with NADPH as cofactor (Table 3).

Table 2 Purification of 2-carboxybenzaldehyde reductases from rat liver

Reductase activity was monitored using 2-CBA and NADPH at 25 °C, and protein concentration was measured by the method of Bradford [40].

Fraction	Volume (ml)	Total Protein (mg)	Total activity (nmol/min)	Specific activity (nmol/min per mg)	Yield (%)	Purification (fold)
Cytosol	210	9240	34400	3.7	100	1
CBA3 Q-Sepharose	92	1060	5340	5	15	1.4
CBA3 Matrex Orange	81	8	3110	390	9	105
CBA4 Q-Sepharose	102	350	3640	10.5	11	2.8
CBA4 Matrex Orange	86	9	1270	141	4	38
CBA4 HiTrap Blue	10	0.3	710	2370	2	640
CBA5 Q-Sepharose	119	285	5300	18.6	15	5
CBA5 Matrex Orange	94	14	3980	285	12	77
CBA5 HiTrap Blue	10	1.2	3690	3075	11	830
CBA6 Q-Sepharose	128	224	4550	20	13	5.4
CBA6 Matrex Orange	92	10.1	2820	280	8	76
CBA6 HiTrap Blue	10	0.5	1850	3700	5	1000

Table 3 Specific activities of the AFAR preparations from rat liver

The enzyme assays were performed in triplicate at 25 °C Activities towards the aldehyde-containing substrates were measured at a concentration of 1 mmol/l, and activity towards 9,10-PQ was determined at 0.05 mmol/l

		Specific activity (nmol/min per mg of protein)				
	Substrate ...	2-CBA		SSA	4-NBA	9,10-PQ
Protein	Cofactor	NADH	NADPH	NADPH	NADPH	NADPH
rAFAR1		2980±42	390±25	345±20	1080±20	4520±70
CBA5		1840±20	3075±40	2245±20	890±15	3320±90
CBA6		1735±25	3700±50	2990±30	490±20	1790±70

Demonstration that rAFAR1 and 37 kDa-AFAR are structurally distinct

The two electrophoretically distinguishable rat polypeptides that cross-react with anti-hAFAR1-serum were resolved by reversed-phase HPLC on a Brownlee C_{18} column as described in the Materials and methods section. Using this method, the 37 kDa-AFAR protein was eluted from the Brownlee C_{18} column at 67 min, whereas the 38 kDa rAFAR1 was eluted at 70 min. This chromatographic approach was therefore adopted to remove traces of rAFAR1 from CBA5, and to purify CBA6 further (Figure 6). The polypeptides eluted from the reversed-phase HPLC column were freeze-dried and their identity confirmed by Western blotting with antibodies against rAFAR1 and against hAFAR1 before further analysis

Peptide fingerprinting by partial proteolysis was performed on the 37 kDa-AFAR polypeptide present in both CBA5 and CBA6 to establish whether they might be identical. The fingerprints obtained were also compared directly with that generated from a digest of rAFAR1, performed in parallel (from CBA3), to help establish their relationship. Figure 7 shows SDS/PAGE of the partial proteolysis products obtained from these proteins following digestion with *S. aureus* V8 protease. Examination of the gel shows that the 37 kDa polypeptide from CBA5 and the 37 kDa polypeptide from CBA6 yield digestion products with essentially identical electrophoretic mobilities. The gel also demonstrates that these digestion products are distinct from those obtained from rAFAR1. In particular, major proteolysis products of 21 kDa, 12 kDa and 10 kDa were recovered from the CBA5 and CBA6 protein that were not observed in digests of rAFAR1.

Evidence to support the designation of 37 kDa-AFAR as rAFAR2

The 37 kDa-AFAR obtained by reversed-phase HPLC of CBA6 was subjected to amino acid sequencing to establish its relationship with rAFAR1. Attempts to obtain sequence data by subjecting the 37 kDa AFAR directly to Edman degradation were unsuccessful, suggesting that the protein has a blocked N-terminus. However, following CNBr digestion of 37 kDa-AFAR by the 'in-gel' protocol described in the Materials and methods section, four peptide fragments were recovered. The smallest of these was about 14 kDa. Automated Edman degradation of this fragment yielded the sequence:

YNATTRQVETELLPCL

which aligned with amino acids 168 and 183 of rAFAR1 (Figure 8). Although the amino acid sequence from 37 kDa-AFAR is closely similar to that of rAFAR1, differences occur at positions equivalent to Ile^{171} and Phe^{180} of rAFAR1; at these positions the 37 kDa-AFAR protein contains threonine and leucine. These data indicate 37 kDa-AFAR has a primary structure that is distinct from that of rAFAR1. The 37 kDa protein is therefore designated rAFAR2.

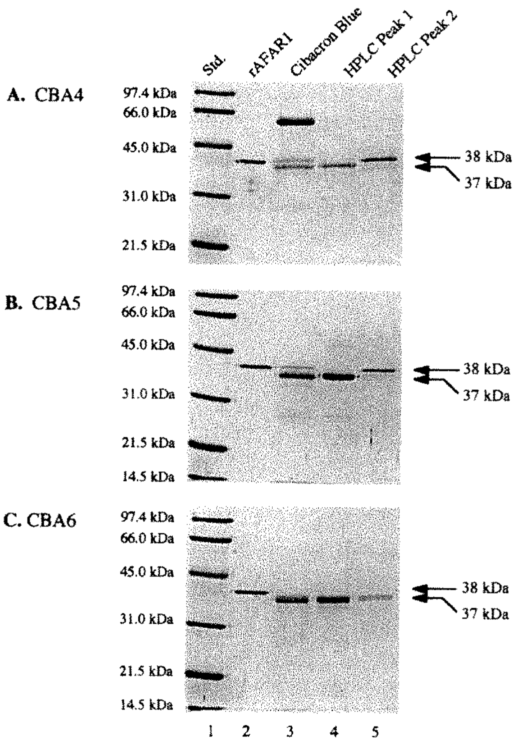

Figure 6 SDS/PAGE analysis of AFAR proteins resolved by reversed-phase HPLC

The CBA4, CBA5 and CBA6 pools of 2-CBA reductase activity were prepared by sequential chromatography on Q-Sepharose, Matrex Orange A and HiTrap Blue. Portions (100 μg of protein) of material from the HiTrap Blue column were applied to a 4.6 mm × 250 mm Brownlee C_{18} column and proteins resolved by using a 35–70% acetonitrile gradient in aq. 0.1% trifluoroacetic acid as described in the Materials and methods section. The protein-containing peaks were collected and tested for cross-reactivity towards anti-hAFAR1 serum. Those peaks which reacted with this antibody were analysed by SDS/PAGE. The gel was loaded as follows: 1, molecular-mass standards; 2, 0.2 μg of recombinant rAFAR1; 3, HiTrap Blue-purified material from CBA4 (**A**), CBA5 (**B**) and CBA6 (**C**) respectively; 4, material from CBA4, CBA5 and CBA6 that was eluted at 67 min from the reversed-phase HPLC column; 5, material from CBA4, CBA5 and CBA6 that was eluted at 70 min from the reversed-phase HPLC column.

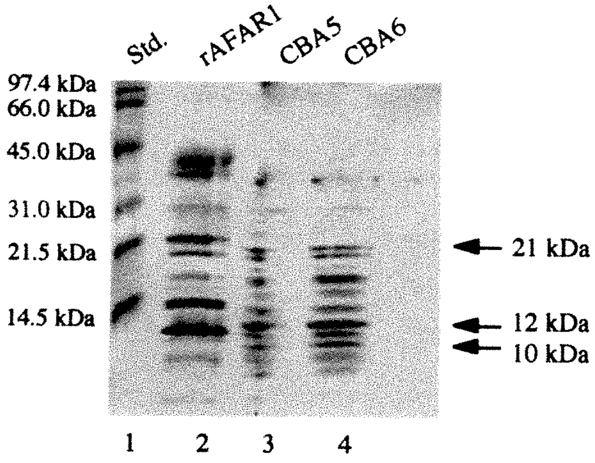

Figure 7 Peptide maps of 37 kDa-AFAR and rAFAR1 proteins

Cleavage of the 37 kDa-AFAR and rAFAR1 with *S. aureus* V8 protease was performed 'in-gel' as described in the text. The peptide products were examined by SDS/PAGE. The polyacrylamide gel was loaded as follows: 1, molecular-mass standards; 2, 2 μg rAFAR1 (from CBA3); 3, 2 μg of 37 kDa-AFAR from CBA5; 2 μg of 37 kDa-AFAR from CBA6.

rAFAR2	(M)	YNATTRQVETELLPCL
rAFAR1	M	YNAITRQVETELFPCL-183
hAFAR1	M	YNATTRQVETELFPCL-186
hAFAR2	M	YNAITRQVETELFPCL-187
AKR1A3	E	CHPYLAQNELIAHCQA-202
AKR1B4	E	CHPYLTQEKLIEYCHC-202
AKR1C9	E	CHLYLNQSKMLDYCKS-208
AKR1D2	E	CHPYFTQTKLLEVSAS-210

Figure 8 Sequence alignment of CNBr peptide from rAFAR2 with other AKRs

The alignments are based on the work of Jez et al. [1,2]. The residues in rAFAR2 that differ from those in rAFAR1 are underlined. Sequences of hAFAR1 and hAFAR2 are from [22] and [32].

DISCUSSION

Identification of AFAR proteins

The present study describes the purification of a hitherto unidentified member of the AKR7 family. The novel protein is designated rAFAR2, denoting the fact that it is the second AFAR protein to be identified in the rat. Thus the inducible rat AFAR protein described in earlier studies is now referred to as rAFAR1. The rAFAR1 isoenzyme has also been called AKR7A1 [1], but in the present paper we have chosen to retain our rAFAR nomenclature since the 'r' (rat) and 'h' (human) prefixes help to avoid confusion about the source of the immunogen used to raise antibodies.

The detection of rAFAR2 has been greatly facilitated by the use of an antibody that was raised against recombinant hAFAR1 and which cross-reacts with the rat protein. Fortunately, rAFAR2 possesses a faster mobility during SDS/PAGE than rAFAR1, and hence Western blotting using the appropriate antiserum can readily identify the 'new' isoenzyme. In addition, the task of monitoring the eluate of columns used to purify rAFAR2 was made easier by employing the substrate 2-CBA.

The aromatic aldehyde 2-CBA was originally chosen for study as a possible AFAR substrate by Ireland et al. [22] while searching for compounds with similar properties to the dialdehydic form of AFB_1-8,9-dihydrodiol. As a substrate, 2-CBA has certain of the chemical features favoured by members of the AFAR family, including an aromatic ring structure and a negatively charged group removed four carbon atoms from the carbonyl group that is catalytically reduced. The method employed to measure 2-CBA reductase activity is convenient for monitoring column eluate as it is a spectrophotometric assay and is thus easier to perform than the HPLC-based assay used to determine AFAR activity [13,45]. Recent examination of human AKRs suggests 2-CBA is not utilised as a substrate by AKR1 members [23]. It is therefore possible that this aldehyde will prove to be a useful reagent in the discovery of additional AFAR isoenzymes.

Catalytic properties of the two rat AFAR proteins

Whereas rAFAR2 utilizes some of the same substrates as rAFAR1, catalytic differences appear to exist between the two reductases. The two principal rAFAR2-containing preparations (CBA5 and CBA6) both seem to possess significantly higher SSA reductase activity than rAFAR1. The specific activity of rAFAR1 towards SSA recovered in the present study (Table 3) is lower than that we have observed previously, presumably because of differences in the method of purification employed. However, this does not alter the conclusion that rAFAR2 is probably more active than rAFAR1 towards this physiological carbonyl. Preliminary data indicate that rAFAR2 has a significantly lower K_m for SSA than rAFAR1 (V. P. Kelly and J. D. Hayes, unpublished work), but further work is required to determine precisely the kinetic properties of rAFAR2 towards SSA and cofactor. Without knowledge of K_m and V_{max}, comments about catalytic differences between the two AFAR isoenzymes should be treated with caution, because it is likely that the 'standard' assay conditions adopted in the present study do not saturate rAFAR1 and rAFAR2 to an equal extent. Unfortunately, because of paucity of material, this task will be laborious until methods are established for large-scale purification of rAFAR2.

An interesting cofactor-specific difference between the activities of the two AFAR proteins towards 2-CBA was apparent throughout the purification (see Figure 4). With NADH as cofactor, rAFAR1 displayed an approx. 7-fold higher specific activity under 'standard' assay conditions than with NADPH as cofactor. By contrast, rAFAR2 exhibited lower activity towards 2-CBA with NADH as cofactor than with NADPH. The high activity of rAFAR1 towards 2-CBA with NADH is surprising given that previous work [21] has shown that this reductase has a markedly lower K_m for NADPH than for NADH, at least with 4-NBA as substrate. The possibility that rAFAR1-catalysed reduction of 2-CBA with NADPH as cofactor is subject to product inhibition, whereas rAFAR2 is not inhibited, requires evaluation. Further investigation is required to clarify the basis for the catalytic differences between the two rat AFARs.

Biological function of rAFAR2

The rAFAR1 and rAFAR2 proteins differ markedly in their distribution in rat tissues (see Figure 3). The expression of rAFAR1 is restricted to liver, kidney, testis and pancreas, and is highly inducible in the liver by metabolizable synthetic antioxidants such as ethoxyquin. With the possible exception of expression of the reductase in the pancreas, this pattern of regulation is consistent with rAFAR1 playing a role in detoxification. By contrast, rAFAR2 is more widely distributed than rAFAR1, and is not obviously induced by ethoxyquin. The fact that rAFAR2 is present in pancreas, brain, adrenal gland, heart, stomach and skeletal muscle, organs which are not particularly associated with drug metabolism, suggests that this member of the AKR7 family performs a constitutive 'house-keeping' role. It is noteworthy that rAFAR2 has a tissue distribution that is similar to that of hAFAR1 [22,23].

The work of Ireland et al. [22] identified SSA, a metabolite of the major inhibitory neurotransmitter γ-aminobutyric acid (GABA), as a likely *in vivo* substrate of the hAFAR1 protein. Support for this suggestion has been more recently obtained by finding that purification and cloning of the major SSA reductase from human brain resulted in isolation of hAFAR1 [46]. In the present study it has been found that rAFAR2 also exhibits SSA reductase activity Thus it seems likely that a major biological function for many of the AKR7 family members is that of synthesis of γ-hydroxybutyric acid (GHB).

SSA produced catalytically from GABA by a transaminase may be catabolized by SSA dehydrogenase to succinic acid [47]. However, SSA can also be converted into GHB by SSA reductase. In many rat tissues this step could be catalysed by rAFAR2. Rather than being an unwanted metabolite, GHB has important physiological properties. At low concentrations, GHB modulates dopamine (3,4-dihydroxyphenethylamine) synthesis and release, whereas at high concentrations it binds to $GABA_B$ receptors and causes a reversal of the effects produced at low concentrations [48,49]. It has also been proposed that GHB helps protect cells against death during periods of anoxia and during periods of excessive metabolic demand [50] Thus the AFAR proteins may contribute to cell survival during physiological stress.

Multiple forms of rAFAR2

The chromatographic profiles obtained during purification of rAFAR2 suggested that the enzyme exists in several different forms. In particular, Q-Sepharose chromatography yielded three peaks of 2-CBA reductase activity which cross-reacted with hAFAR1 antibodies; these were called CBA4, CBA5 and CBA6 according to their order of elution. Lack of material prevented CBA4 from being characterized and, although the most highly purified preparation contained substantial amounts of a 37 kDa polypeptide that cross-reacted with anti-hAFAR1 serum, the relationship between CBA4 and CBA5 and between CBA4 and CBA6 has not been rigorously established. The 37 kDa-AFAR polypeptides in CBA5 and CBA6 have, however, been purified to homogeneity, and peptide mapping indicated that they represent closely similar, if not identical, proteins. The reason for resolution of the protein into several chromatographic peaks is uncertain, but it is an important issue, because the CBA5 and CBA6 preparations displayed different activities for SSA and other substrates. It appears unlikely that oxidation is responsible for the generation of three peaks, since all the buffers employed for protein purification contained DTT. It is probable that rAFAR2 is modified post-synthetically, possibly by phosphorylation, glycosylation, glutathiolation or proteolysis. Close examination of SDS/PAGE analysis of CBA6 indicated that, in addition to the major 37 kDa polypeptide, a 36.8 kDa band could also be discerned. Although it seems highly likely that a product–precursor relationship exists between the polypeptides of apparent 36.8 and 37 kDa molecular mass, this heterogeneity does not provide an explanation of why the 37 kDa-AFAR subunit is recovered in both CBA5 and CBA6.

In view of the fact that AFAR proteins are more closely related to the tetrameric voltage-gated K^+-channel β-subunits than to the monomeric AKR1 enzymes, the possibility has been considered that rAFAR2 may be capable of self-associating. This hypothesis has been tested by subjecting CBA4, CBA5 and CBA6 preparations (post Q-Sepharose fractions shown in Figure 4b) to gel-filtration chromatography on Sephadex G-150. Following calibration of the column with β-amylase, alcohol dehydrogenase, BSA, carbonic anhydrase and cytochrome *c*, it was found that CBA4, CBA5 and CBA6 were eluted from Sephadex G-150 with apparent native molecular masses of 59, 70 and 65 kDa (results not shown). Since the estimated molecular masses of the reductase in these preparations determined by gel-filtration chromatography greatly exceeds that determined by SDS/PAGE, it appears likely that rAFAR2 is engaged in some type of protein–protein interaction. Dimerization of rAFAR2 would be expected to yield a complex of 74 kDa. This value slightly exceeds that estimated by chromatography. It is therefore concluded that rAFAR2 may exist as a homodimer, but that the size of the complex is underestimated, either because the association between the subunits is reversible, or because the dimer has a propensity to interact with the column matrix.

At this stage it is unclear why rAFAR2 should exist as a dimeric protein in the cell. If the sole purpose of rAFAR2 is to act as an enzyme, it would not be required to exist as a dimer, since the AKR1 members are both monomeric and catalytically active. It is therefore possible that rAFAR2 serves an additional role besides that of reducing carbonyls. It may dimerize in order to regulate enzyme activity or intracellular localization. Our gel-filtration-chromatography experiments indicate that, in its native state, rAFAR2 does not exist as a single subunit, but that it is able to form complexes either with itself or with another protein. It requires to be established whether rAFAR2 can dimerize with rAFAR1.

Concluding comments

This paper reports the identification of a hitherto unrecognized AFAR isoenzyme in the rat, and its purification from rat liver cytosol. The first member of the AFAR family to be described was discovered because of its marked inducibility by ethoxyquin and unique catalytic activity towards aflatoxin B_1. The rAFAR2 protein is notable because of its broad distribution in rat tissues. Rather than contributing to detoxification of xenobiotics, the 'new' protein may play an important *in vivo* role in the synthesis of GHB in neural and peripheral tissues. The rAFAR2 protein appears to be able to form dimers. Its further molecular characterization will expand our knowledge of the physiological roles played by the AKR7 proteins in general.

This work was funded in part by Medical Research Council Grant G9322073PA V P K was in receipt of a Biomedical Research Centre Ph D studentship. E M E was supported by a Beit Memorial Research Fellowship The Cobas Fara centrifugal analyser was purchased with funds from the Scottish Office Home and Health Department (K/CSO/2/20/3/7)

REFERENCES

1 Jez, J M., Flynn, T G and Penning, T M. (1997) A new nomenclature for the aldo-keto reductase superfamily Biochem Pharmacol **54**, 639–647

2 Jez, J M, Bennett, M J, Schlegel, B. P, Lewis, M. and Penning, T M (1997) Comparative anatomy of the aldo-keto reductase superfamily Biochem J **326**, 625–636

3 Vander Jagt, D L, Robinson, B, Taylor, K K and Hunsaker, L A (1992) Reduction of trioses by NADPH-dependent aldo-keto reductases Aldose reductase, methylglyoxal, and diabetic complications J Biol Chem **267**, 4364–4369

4 Petrash, J M., Tarle, I, Wilson, D K and Quiocho, F A (1994) Aldose reductase catalysis and crystallography Insights from recent advances in enzyme structure and function Diabetes **43**, 955–959

5 Watanabe, K, Fujii, Y, Nakayama, K, Ohkubo, H, Kuramitsu, S., Kagamiyama, H, Nakanishi, S and Hayaishi, O (1988) Structural similarity of bovine lung prostaglandin F synthase to lens ϵ-crystallin of the European common frog Proc Natl. Acad Sci U S A **85**, 11–15

6 Ohara, H, Nakayama, T, Deyashiki, Y., Hara, A, Miyabe, Y and Tsukada, F. (1994) Reduction of prostaglandin D_2 to $9\alpha,11\beta$-prostaglandin F_2 by a human liver 3α-hydroxysteroid/dihydrodiol dehydrogenase isoenzyme Biochim Biophys Acta **1215**, 59–65

7 Penning, T M, Pawlowski, J. E, Schlegel, B. P, Jez, J M, Lin, H.-K, Hoog, S S, Bennett, M J and Lewis, M. (1996) Mammalian 3α-hydroxysteroid dehydrogenases Steroids **61**, 508–523

8 Turner, A J, Illingworth, J A and Tipton, K F (1974) Stimulation of biogenic amine metabolism in the brain. Biochem J. **144**, 353–360

9 Feather, M S, Flynn, T G, Munro, K A, Kubiseski, T. J. and Walton, D J (1995) Catalysis of reduction of carbohydrate 2-oxoaldehydes (osones) by mammalian aldose reductase and aldehyde reductase Biochim Biophys Acta **1244**, 10–16

10 Vander Jagt, D. L, Kolb, N S, Vander Jagt, T. J, Chino, J., Martinez, F. J, Hunsaker, L A. and Royer, R E (1995) Substrate specificity of human aldose reductase· identification of 4-hydroxynonenal as an endogenous substrate Biochim. Biophys Acta **1249**, 117–126

11 Molowa, D T, Shayne, A G and Guzelian, P S (1986) Purification and characterization of chlordecone reductase from human liver J Biol Chem **261**, 12624–12627

12 Welle, R, Schroder, G, Schiltz, E, Grisebach, H. and Schroder, J. (1991) Induced plant responses to pathogen attack Analysis and heterologous expression of the key enzyme in the biosynthesis of phytoalexins in soybean (*Glycine max* L Merr cv Harosoy 63) Eur J Biochem **196**, 423–430

13 Judah, D J, Hayes, J D, Yang, J-C, Lian, L.-Y, Roberts, G C K, Farmer, P B, Lamb, J H and Neal, G E (1993) A novel aldehyde reductase with activity towards a metabolite of aflatoxin B_1 is expressed in rat liver during carcinogenesis and following the administration of an antioxidant Biochem J **292**, 13–18

14 Penning, T. M., Burczynski, M E, Hung, C.-F, McCoull, K D, Palackal, N T and Tsuruda, L S. (1999) Dihydrodiol dehydrogenases and polycyclic aromatic hydrocarbon activation generation of reactive and redox active *o*-quinones Chem. Res Toxicol **12**, 1–18

15 Weiner, H, Holmes, R S and Wermuth, B (eds) (1995) Enzymology and Molecular Biology of Carbonyl Metabolism 5. Advances in Experimental Medicine and Biology, vol 372, Plenum Press, New York

16 Rettig, J, Heinemann, S. H, Wunder, F, Lorra, C, Parcej, D N, Dolly, J O and Pongs, O (1994) Inactivation properties of voltage-gated K^+ channels altered by presence of β-subunit Nature (London) **369**, 289–294

17 McCormack, T and McCormack, K (1994) *Shaker* K^+ channel β subunits belong to an NAD(P)H-dependent oxidoreductase superfamily Cell **79**, 1133–1135

18 Chouinard, S W, Wilson, G F, Schlimgen, A K and Ganetzky, B (1995) A potassium channel β subunit related to the aldo-keto reductase superfamily is encoded by the *Drosophila* hyperkinetic locus Proc Natl Acad Sci U.S A **92**, 6763–6767

19 Hayes, J D, Judah, D J and Neal, G E (1993) Resistance to aflatoxin B_1 is associated with the expression of a novel aldo-keto reductase which has catalytic activity towards a cytotoxic aldehyde-containing metabolite of the toxin Cancer Res **53**, 3887–3894

20 Ellis, E M, Judah, D J, Neal, G E and Hayes, J D (1993) An ethoxyquin-inducible aldehyde reductase from rat liver that metabolizes aflatoxin B_1 defines a sub-family of aldo-keto reductases Proc Natl Acad Sci. U S A **90**, 10350–10354

21 Ellis, E M and Hayes, J D (1995) Substrate specificity of an aflatoxin-metabolizing aldehyde reductase. Biochem. J **312**, 535–541

22 Ireland, L S, Harrison, D J, Neal, G E and Hayes, J. D (1998) Molecular cloning of a 2-carboxybenzaldehyde reductase from human liver as a homologue of the rat aflatoxin-metabolising aldehyde reductase, AFAR Biochem J. **332**, 21–34

23 O'Connor, T, Ireland, L S, Harrison, D J. and Hayes, J D (1999) Major differences in the function and tissue-specific expression of human aflatoxin B_1 aldehyde reductase (AFAR) and the principal human aldo-keto reductase AKR1 family members Biochem J **343**, 487–504

24 Wilson, D K, Bohren, K M, Gabbay, K H. and Quiocho, F A (1992) An unlikely sugar substrate site in the 1 65 Å structure of the human aldose reductase holoenzyme implicated in diabetic complications Science **257**, 81–84

25 Hoog, S S., Pawlowski, J E, Alzari, P M, Penning, T. M and Lewis, M (1994) Three-dimensional structure of rat 3α-hydroxysteroid/dihydrodiol dehydrogenase a member of the aldo-keto reductase superfamily. Proc Natl. Acad Sci. U S A **91**, 2517–2521

26 Wilson, D. K., Nakano, T, Petrash, J M and Quiocho, F A (1995) 1 7 Å structure of FR-1, a fibroblast growth factor-induced member of the aldo-keto reductase family, complexed with coenzyme and inhibitor. Biochemistry **34**, 14323–14330

27 Gulbis, J M, Mann, S. and MacKinnon, R (1999) Structure of a voltage-dependent K^+ channel β subunit Cell **97**, 943–952

28 Ellis, E M, Judah, D J, Neal, G E, O'Connor, T. and Hayes, J D (1996) Regulation of carbonyl-reducing enzymes in rat liver by chemoprotectors. Cancer Res **56**, 2758–2766

29 Primiano, T, Gastel, J A, Kensler, T W and Sutter, T R (1996) Isolation of cDNAs representing dithiolethione-responsive genes Carcinogenesis **17**, 2297–2303

30 Kelly, V P., Ellis, E M., Manson, M. M, Chanas, S A, Moffat, G J, McLeod, R, Judah, D. J, Neal, G E and Hayes, J D (2000) Chemoprevention of aflatoxin B_1 hepatocarcinogenesis by coumarin, a natural benzopyrone that is a potent inducer of AFB_1-aldehyde reductase, the glutathione S-transferase A5 and P1 subunits, and NAD(P)H quinone oxidoreductase in rat liver Cancer Res **60**, 957–969

31 Hayes, J D, Ellis, E M, Neal, G E, Harrison, D J. and Manson, M M (1999) Cellular response to cancer chemopreventive agents contribution of the antioxidant responsive element to the adaptive response to oxidative and chemical stress In Cellular Responses to Stress (Biochem Soc Symp **64**) (Downes, C P., Wolf, C. R. and Lane, D P, eds), pp 141–168, Portland Press, London

32 Knight, L P, Primiano, T., Groopman, J D, Kensler, T W. and Sutter, J. R (1999) cDNA cloning, expression and activity of a second human aflatoxin B_1-metabolizing member of the aldo-keto reductase superfamily, AKR7A3 Carcinogenesis **20**, 1215–1223

33 Shiobara, Y (1977) The effect of carboxyl substituent on the metabolism of aromatic aldehydes Xenobiotica **7**, 457–468

34 Sherratt, P J , Manson, M M , Thomson, A M , Hissink, E A M , Neal, G E , van Bladeren, P. J , Green, T and Hayes, J. D. (1998) Increased bioactivation of dihaloalkanes in rat liver due to induction of class Theta glutathione S-transferase T1-1 Biochem J. **335**, 619–630

35 Sherratt, P J , Pulford, D J , Harrison, D J , Green, T. and Hayes, J D (1997) Evidence that human class Theta glutathione S-transferase T1–1 can catalyse the activation of dichloromethane, a liver and lung carcinogen in the mouse. Comparison of the tissue distribution of GSTT1–1 with that of classes Alpha, Mu and Pi GST in human Biochem. J. **326**, 837–846

36 Takahashi, M , Fujii, J , Teshima, T , Suzuki, K , Shiba, T. and Taniguchi, N (1993) Identity of a major 3-deoxyglucosone-reducing enzyme with aldehyde reductase in rat liver established by amino acid sequencing and cDNA expression Gene **127**, 249–253

37 Carper, D , Nishimura, C , Shinohara, T , Dietzchold, B , Wistow, G , Craft, C , Kador, P and Kinoshita, J H (1987) Aldose reductase and ρ-crystallin belong to the same protein superfamily as aldehyde reductase FEBS Lett **220**, 209–213

38 Pawlowski, J E , Huizinga, M and Penning, T M (1991) Cloning and sequencing of the cDNA for rat liver 3α-hydroxysteroid/dihydrodiol dehydrogenase. J. Biol Chem **266**, 8820–8825

39 Onishi, Y , Noshiro, M., Shimosato, T and Okuda, K (1994) Molecular cloning and sequence analysis of cDNA encoding Δ^4-3-ketosteroid 5β-reductase of rat liver. FEBS Lett **283**, 215–218

40 Bradford, M M. (1976) A rapid and sensitive method for the quantitation of microgram quantities of protein utilizing the principle of protein-dye binding Anal. Biochem **72**, 248–254

41 Laemmli, U K (1970) Cleavage of structural proteins during the assembly of the head of bacteriophage T4 Nature (London) **227**, 680–685

42 Hayes, J D , Kerr, L A and Cronshaw, A D (1989) Evidence that glutathione S-transferases B_1B_1 and B_2B_2 are the products of separate genes and that their expression in human liver is subject to inter-individual variation Biochem J **264**, 437–445

43 McLeod, R , Ellis, E M , Arthur, J R , Neal, G E , Judah, D J , Manson, M M and Hayes, J D (1997) Protection conferred by selenium deficiency against aflatoxin B_1 in the rat is associated with the hepatic expression of an aldo-keto reductase and a glutathione S-transferase subunit that metabolize the mycotoxin Cancer Res , **57**, 4257–4266

44 Iwata, N , Inazu, N and Satoh, T (1990) Immunological and enzymological localization of carbonyl reductase in ovary and liver of various species J Biochem (Tokyo) **107**, 209–212

45 Hayes, J D , Judah, D J., McLellan, L I , Kerr, L A , Peacock, S D and Neal, G. E (1991) Ethoxyquin-induced resistance to aflatoxin B_1 in the rat is associated with the expression of a novel Alpha-class glutathione S-transferase subunit, Yc_2, which possesses high catalytic activity for aflatoxin B_1-8,9-epoxide Biochem J **279**, 385–398

46 Schaller, M , Schaffhauser, M., Sans, N and Wermuth, B (1999) Cloning and expression of succinic semialdehyde reductase from human brain. Identity with aflatoxin B_1 aldehyde reductase Eur J Biochem **265**, 1056–1060

47 Tillakaratne, N J K , Medina-Kauwe, L and Gibson, K M. (1995) Gamma-aminobutyric acid (GABA) metabolism in mammalian neural and nonneural tissues Comp Biochem Physiol **112A**, 247–263

48 Cash, C D (1994) Gamma-hydroxybutyrate an overview of the pros and cons for it being a neurotransmitter and/or a useful therapeutic agent Neurosci Biobehav Rev **18**, 291–304

49 Tunnicliff, G (1997) Sites of action of gamma-hydroxybutyrate (GHB) – a neuroactive drug with abuse potential Clin Toxicol **35**, 581–590

50 Mamelak, M (1989) Gammahydroxybutyrate an endogenous regulator of energy metabolism. Neurosci Biobehav Rev **13**, 187–198

Received 30 November 1999/8 February 2000; accepted 15 March 2000

Biochem. J. (2000) **348**, 401–408 (Printed in Great Britain)

Increased translation efficiency and antizyme-dependent stabilization of ornithine decarboxylase in amino acid-supplemented human colon adenocarcinoma cells, Caco-2

Hervé CHABANON*, Lo PERSSON†, Heather M. WALLACE‡, Marc FERRARA* and Patrick BRACHET*[1]

*Unité de Nutrition Cellulaire et Moléculaire, Institut National de la Recherche Agronomique, 63122-Theix, France, †Department of Physiological Sciences, University of Lund, S-223 62 Lund, Sweden, and ‡Department of Medicine and Therapeutics and Biomedical Sciences, University of Aberdeen, Institute of Medical Sciences, Aberdeen AB25 2ZD, Scotland, U.K.

The mechanisms of the response of ornithine decarboxylase (ODC), the rate-limiting enzyme in polyamine biosynthesis, to amino acid supplementation were studied in the human colon adenocarcinoma cell line, Caco-2. Supplementation of serum-deprived, subconfluent Caco-2 cells with any one of a series of amino acids (10 mM) resulted in increased ODC activity, reaching a maximum of approx. 12.5-fold after approx. 4 h, over control cells either not supplemented or supplemented with iso-osmolar D-mannitol. Glycine, L-asparagine and L-serine, as well as their D-enantiomers, were the strongest effectors and acted in a concentration-dependent manner; millimolar concentrations of most of these amino acids being sufficient to significantly increase ODC activity. In contrast, supplementation with D-methionine, L-lysine, L-aspartate or L-glutamate had little or no effect on ODC activity, whereas supplemental L-methionine, L-arginine, L-ornithine or L-cysteine was inhibitory. Polyamine assays showed that the putrescine content of cells varied in accordance with the changes in ODC activity. Western-blot and Northern-blot analyses revealed specifically increased levels of ODC protein but not mRNA, respectively, in response to supplementation with an ODC-inducing amino acid. Suppression of the increase in cycloheximide-treated cells confirmed a requirement for protein synthesis. Pulse-labelling of cells with [^{35}S]methionine showed a 3-fold increase in the synthesis of ODC protein after 4 h of supplementation with glycine or L-serine. Supplemental glycine also augmented, reversibly, the half-life of ODC by almost 4-fold and simultaneously decreased the activity of putrescine-induced free antizyme. These results suggest that translational, but not transcriptional, regulation of ODC takes part in ODC induction by amino acids in Caco-2 cells. However, it also appears to occur in concert with decreased enzyme inactivation and/or degradation.

Key words. glycine, polyamine biosynthesis, nutrient, ODC, post-translational regulation.

INTRODUCTION

Therapeutic enteral supplementation with conditionally essential amino acids has proven to be beneficial to intestinal recovery after impairment of epithelial renewal during gut injuries or disease [1]. Mammalian cell growth and tissue regeneration, in particular in the rapidly renewing intestinal epithelium, is highly dependent on the polyamines, putrescine, spermidine and spermine [2]. Moreover, the nutritional state of the organism is clearly an important factor in polyamine biosynthesis [3,4] and transport [5]. Whole-animal studies have reported that ornithine decarboxylase (ODC, EC 4.1.1.17), the first and rate-limiting enzyme in polyamine biosynthesis, is subject to regulation by food [6,7]. Attempts have been made to discriminate the components of food and/or the factors brought into play by eating that may be responsible for ODC activation. Dietary amines [7], hormones [6], proteins [3,8,9], amino acids [10–12] and sugars [8] have been reported to stimulate intestinal, renal or hepatic ODC *in vivo*.

Regarding stimulation by amino acids, strong differences were observed between tissues, e.g. the liver and the small intestine, in the animal [11]. Moreover, intraperitoneal injection of glycine could stimulate hepatic ODC, but not intestinal ODC, despite similar tissue accumulation of the amino acid. Since glycine was among the strongest inducers of ODC in the rat small intestine when administered intragastrically, it was proposed that amino acids must act on the apical surface of enterocytes to trigger ODC induction. Stimulation of the membrane Na$^+$/H$^+$ exchanger was found to be required for induction by L-asparagine and L-glutamine [13,14], and studies in cultured cell lines suggested that ODC induction by amino acids, as well as sugars, may be dependent on the coupled influx of Na$^+$ and organic solute [15–17]. However, intragastric administration of passively diffusing D-alanine or D-serine could also induce rat intestinal ODC [11,12,18], while actively transported amino acids such as L-phenylalanine, L-glutamate and α-amino isobutyric acid (α-AIB) [19] could not induce ODC in porcine jejunal epithelial cells [14]. These results, and reports of no increase in volume of rat intestinal crypt IEC-6 cells after supplementation with Na$^+$-coupled co-transported L-asparagine, [20,21] indicate that cell swelling may not be a prerequisite for ODC induction.

Marked discrepancies also exist between the reports on the respective role of the multiple regulatory steps that may control ODC activity in response to amino acid supplementation. From

---

Abbreviations used. α-AIB, α-amino isobutyric acid, DMEM, Dulbecco's modified Eagle's medium; eIF, eukaryotic initiation factor; FCS, fetal calf serum; GAPDH, glyceraldehyde-3-phosphate dehydrogenase, neAA, non-essential amino acids, ODC, ornithine decarboxylase

[1] To whom correspondence should be addressed (e-mail brachet@clermont.inra.fr)

in vivo studies in the rat, it was concluded that the translation efficiency of intestinal ODC mRNA was predominantly increased after intragastric ingestion of L-serine or L-alanine, since neither the ODC mRNA level nor its protein stability were found to vary significantly [12]. On the other hand, each D-stereoisomer of these amino acids was able to substantially augment the ODC mRNA level, however, by an unknown mechanism supposedly associated with cell stress, possibly induced by D-amino acid toxicity. Among numerous L-amino acids able to induce ODC activity in cultured cells, L-asparagine is the one that appears to display the most ubiquitous and potent effect. For that reason and since it is important in certain cancers [22], L-asparagine has been chosen as the test amino acid in most *in vitro* studies. Translational and post-translational regulation of ODC by L-asparagine was evidenced in rat primary cultured hepatocytes [23], as well as in the mouse neuroblastoma DF-40 cell line [24]. However, only the latter study demonstrated substantial post-transcriptional stabilization of ODC mRNA. Although increased amounts of ODC transcripts in response to L-asparagine were reported to be associated with transformation of mammalian cells [25], a similar regulation was also observed in normal, undifferentiated, rat intestinal crypt IEC-6 cells [20,21]. However, it was recently found that, when exposing IEC-6 cells to a salt/glucose solution, supplemented with L-asparagine, ODC activity increased through post-translational mechanism(s) without change at the protein level [26].

As a step towards the clarification of the molecular mechanisms of ODC regulation by amino acids, we re-address this issue in human colon adenocarcinoma Caco-2 cells, which are known to have the ability to differentiate as enterocyte-like cells. The present study demonstrates that, in these cells, ODC activity increases following supplementation with any one of a variety of amino acids, glycine being the most effective amino acid, as observed previously *in vivo* in rat small intestine [11,12]. Amino acid supplementation in Caco-2 cells led specifically to increased amounts of ODC protein, but not mRNA, owing to higher biosynthesis efficiency and increased half-life of ODC. Transient variations in the enzyme stability were concurrent with opposite changes in the activity of antizyme, a polyamine-inducible protein able to bind and inactivate ODC, as well as enhancing its ATP-dependent degradation by the 26 S proteasome [27]. Our data point out that Caco-2 cells constitute a valuable model for future studies on the signals triggered by amino acids to cause induction of ODC synthesis, on the one hand, and antizyme decay, on the other hand.

MATERIALS AND METHODS

Materials

D,L-[1-^{14}C]Ornithine (43.8 mCi/mmol) was purchased from Du Pont New England Nuclear (Boston, MA, U.S.A.). ^{35}S-labelled L-methionine (587 Ci/mmol) and [α-^{32}P]dCTP (3000 Ci/mmol) were obtained from Amersham Pharmacia Biotech (Orsay, France). Dulbecco's modified Eagle's medium (DMEM), non-essential amino acids (neAA), antibiotics and fetal calf serum (FCS) were purchased from Gibco-BRL (Cergy-Pontoise, France). The amino acids used were of the highest purity grade available from Sigma and, in most cases, they were cell culture tested. The antiserum to mouse ODC was obtained from Eurodiagnostica (Lund, Sweden). The Caco-2 cell line (passages 190–205) [28] and the human ODC cDNA were generously provided by Dr A. Zweibaum (INSERM U 178, Villejuif, France) and Dr O. A. Jänne (Institute of Biomedicine, University of Helsinki, Finland), respectively.

Cell culture and treatment

Cells were seeded at 12 × 10^3 cells/cm^2 and routinely grown at 37 °C under a O_2/CO_2 (19:1) atmosphere, in DMEM containing 25 mM D-glucose and supplemented with 20 % (v/v) heat-inactivated FCS, 1 % (v/v) neAA, 100 units/ml penicillin and 100 μg/ml streptomycin. The culture medium was changed 48 h after seeding, then every day. For the experiments 3-day-old cells were incubated without serum for 24 h prior to use. Then they were rinsed with PBS and exposed to serum-deprived DMEM either not supplemented (DMEM control) or supplemented with a single amino acid or iso-osmolar D-mannitol (D-mannitol control). Medium osmolarities, measured by using an osmometer (Roebling, Berlin, Germany), averaged 0.32 osmol/litre.

ODC activity assay

After rinsing twice with cold PBS cells were scraped with a cell lifter (Costar, Corning, NY, U.S.A.) and homogenized in buffer containing 125 mM Tris/HCl (pH 7.5)/200 μM pyridoxal-phosphate. The cell suspensions were then centrifuged at 38000 *g* for 20 min and the resulting supernatants, supplemented with 0.1 mM EDTA and 5 mM dithiothreitol, were stored at −80 °C until use. ODC activity was determined as reported previously [5] by measuring the release of $^{14}CO_2$ from D,L-[1-^{14}C]ornithine in the presence of 160 μM unlabelled L-ornithine and 200 μM pyridoxal-phosphate. One unit of ODC activity is defined as the amount releasing 1 nmol of CO_2 from L-ornithine/h at 37 °C.

RNA isolation and Northern-blot analysis

Total cellular RNA was isolated according to the procedure of Chomczynski and Sacchi [29], and Northern-blots were performed as described by Sambrook et al. [30]. RNA was cross-linked to the membrane (Hybond N$^+$, Amersham Pharmacia Biotech) by UV irradiation. The blot was then prehybridized for 2 h at 42 °C in 50 % (v/v) formamide/6 × SSC (where 1 × SSC is 0.015 M sodium citrate/0.15 M NaCl)/5 × Denhardt's reagent (where 1 × Denhardt's reagent is 0.02 % Ficoll 400/0.02 % polyvinylpyrrolidone/0.02 % BSA)/0.5 % SDS. Gel-purified *Eco*RI/*Cla*I fragments (1150 bp) of ODC cDNA were labelled by random priming with [α-^{32}P]dCTP using dCTP-devoid, ready-To-Go® DNA labelling beads (Amersham Pharmacia Biotech) and used as ODC probes. Hybridization was carried out overnight at 42 °C. The blots were washed at 42 °C for 15 min twice in 2 × SSC/0.1 % SDS, then once in 0.5 × SSC/0.1 % SDS and once in 0.1 × SSC/0.1 % SDS. Labelled bands were visualized and quantified using a STORM PhosphorImager (Molecular Dynamics, Sunnyvale, CA, U.S.A.) and the IMAGEQUANT software. Each blot was re-hybridized with a glyceraldehyde-3-phosphate dehydrogenase (GAPDH) cDNA probe in order to take into account variations in the amount of RNA in different samples or loading errors.

Analyses of ODC protein

Cell extracts were prepared in 125 mM Tris/HCl (pH 7.5)/200 μM pyridoxal-phosphate buffer supplemented with 1 % (v/v) Triton X-100, before centrifugation at 12000 *g* for 10 min [31]. Proteins (80 μg) from the supernatant were separated by SDS/PAGE on a 10 % (w/v) polyacrylamide gel and electrophoretically transferred on to a nitrocellulose membrane in 48 mM Tris/39 mM glycine/20 % (v/v) methanol. First, the membranes were blocked for 1 h at room temperature with 5 % (w/v) non-fat dry milk in PBS/0.1 % Triton X-100 prior to a further 3 h incubation with the anti-ODC antibody at 1:500

dilution. Secondly, the membranes were washed three times with a blocking solution of 0.5% non-fat dry milk in PBS/0.5% Triton X-100 before a 1 h incubation with horseradish peroxidase-conjugated goat anti-(rabbit IgG) at 1:5000 dilution. After three washes, the immunocomplexes were revealed using the ECF Western-blotting kit (Amersham Pharmacia Biotech). Quantification was performed after scanning of the film using the STORM PhosphorImager and IMAGEQUANT software.

ODC and total protein synthesis measurements

Cells treated with 10 mM amino acid for 3.5 h were washed with pre-warmed PBS, then exposed for 10 min to L-methionine-deprived DMEM, containing 10 mM glycine, before being pulse-labelled for 25 min with a supplement of L-[^{35}S]methionine. This was followed by extraction of the cells and immunoprecipitation of the ODC protein, which was analysed by SDS/PAGE and autoradiography as described previously [31].

For measuring total protein synthesis, cells were exposed for 3 h to DMEM, containing 10 mM glycine, then for 1 h to a similar medium depleted of unlabelled L-methionine and supplemented with 5.8 μCi/ml of L-[^{35}S]methionine. After removal of the radioactive medium the cells were processed as described in [32]. Results are given as L-[^{35}S]methionine d.p.m. incorporated/mg of cell protein per h.

Free antizyme assay

In order to determine the activity of free antizyme, 3-day-old subconfluent Caco-2 cells were deprived of serum for 24 h, while being supplemented during the last 12 h with or without 10 mM putrescine. They were subsequently exposed for various times to DMEM, containing 10 mM putrescine, that was either not supplemented (DMEM control) or supplemented with 10 mM of a single amino acid or D-mannitol (D-mannitol control). Treatments were stopped by rinsing the cells twice with PBS and homogenization in 125 mM Tris/HCl (pH 7.5)/200 μM pyridoxal-phosphate before storage at −80 °C until use.

The activity of free antizyme was determined by measuring the loss of ODC activity attributed to antizyme addition [33]. Samples of antizyme-enriched homogenates obtained from amino acid-supplemented or control cells were mixed with a constant amount (approx. 70 units) of partially purified ODC. After 10 min on ice, the mixture was assayed for ODC activity as described above. One unit of antizyme is defined as the amount inhibiting one unit of ODC activity. Inhibition of ODC activity up to 75% has previously been shown to be linear with respect to the amount of antizyme added [34].

Miscellaneous methods

For polyamine analysis cells were harvested in 0.2 M perchloric acid and the acid fraction containing the polyamines was stored at −20 °C before assays by the HPLC method described in [35]. Protein concentrations of cell extracts were measured by the bicinchoninic acid ('BCA') method [36]. When applicable, data were examined statistically by analysis of variance, with $P < 0.05$ considered significant.

RESULTS

Induction of ODC activity by a single amino acid supplementation

To determine the amino acid pattern of ODC induction in Caco-2 cells, serum-starved subconfluent cells were incubated for 4 h in DMEM either not supplemented or supplemented with 10 mM of any one of a series of amino acids or 10 mM D-mannitol, which was used as an osmolarity control. A number of these amino acids were able to increase ODC activity individually (Figure 1). Glycine was by far the most efficient amino acid, but substantial increase also resulted from supplementation with the stereoisomers of asparagine or serine, as well as with L-proline, L-threonine or the sulphonate, taurine. On the other hand,

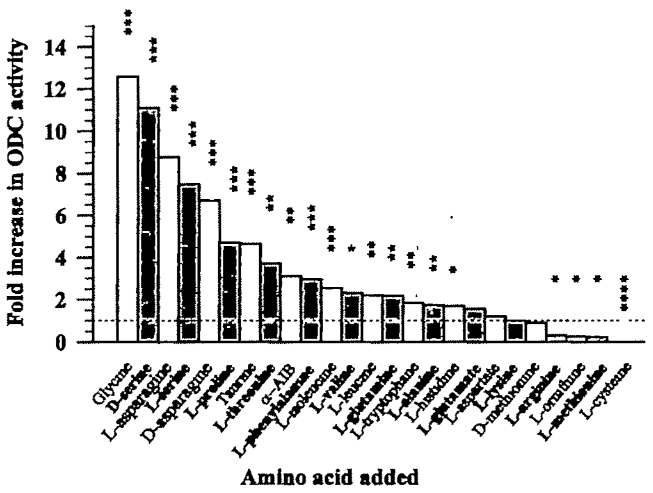

Figure 1 Effect of L-amino acids and amino acid D-isomers on ODC activity in subconfluent Caco-2 cells

Three-day-old cells were exposed for 24 h to an FCS-deprived DMEM medium, then for 4 h to DMEM supplemented with 10 mM of any one of the indicated L- or D-amino acids or D-mannitol (control) Data are expressed as the fold increase in ODC activity in amino acid-supplemented cells relative to control cells, and are means of at least three separate experiments, each done in triplicate. The dashed line (fold increase of 1) refers to the average control activity (approx 0.5 nmol/h per mg protein) ***$P < 0.001$, **$P < 0.01$ and *$P < 0.05$ compared with control

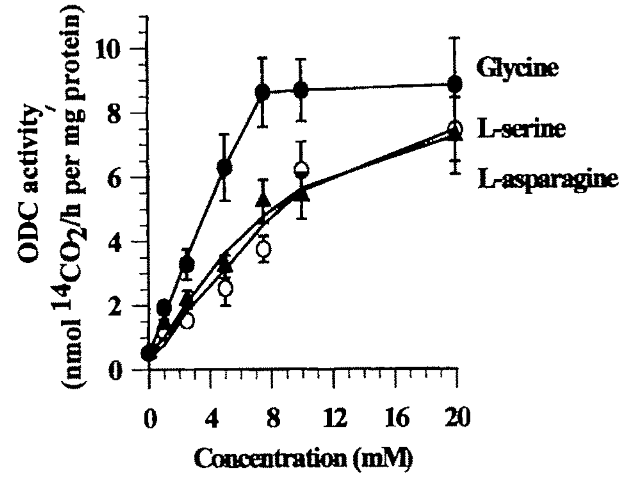

Figure 2 Amino acid concentration dependence of ODC activity in subconfluent Caco-2 cells

Three-day-old cells were exposed for 24 h to an FCS-deprived DMEM medium, then for 4 h to DMEM supplemented with increasing concentrations of glycine (●), L-serine (○) or L-asparagine (▲) Data are means±S D of at least two separate experiments, each done in triplicate Where not shown, S D were smaller than symbols As compared with D-mannitol-supplemented control cells (not illustrated), the increases in ODC activity were significant ($P < 0.05$) throughout the kinetics except at 1 mM L-asparagine and L-serine ($P = 0.08$ and 0.13, respectively)

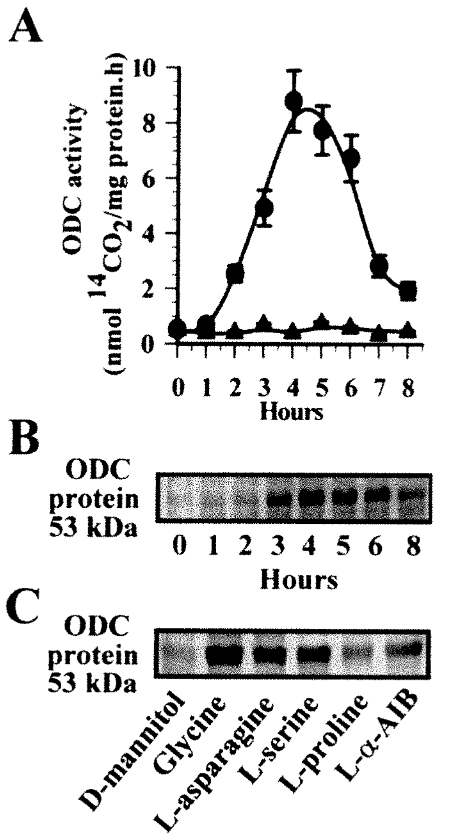

Figure 3 Changes in ODC activity and protein amount following amino acid supplementation in subconfluent Caco-2 cells

Three-day-old cells were exposed for 24 h to an FCS-deprived DMEM medium, then for various times to DMEM supplemented with 10 mM of a single amino acid or D-mannitol (control). (**A**) Time-dependent variations in ODC activity in glycine- (●) or D-mannitol- (▲) supplemented cells. Data are means ± S.D. of at least two separate experiments, each done in triplicate. (**B**) Western-blot analysis of the time course for the changes in ODC protein after glycine supplementation. (**C**) Western-blot analysis of the changes in ODC protein after 4 h of supplementation with 10 mM D-mannitol (control) or one of the indicated amino acids. In (**B**) and (**C**) three experiments were performed that showed similar results.

D-methionine, the dibasic amino acid, L-lysine, and the acidic amino acids, L-aspartate and L-glutamate, had little or no effect on ODC activity, while the polyamine precursors, L-methionine, L-arginine and L-ornithine, as well as the free thiol-containing amino acid cysteine, were inhibitory. Globally similar observations were seen in differentiated, 18-day-old Caco-2 cells (results not shown). The increase in ODC activity was dependent on the concentration of supplemental L-asparagine, L-serine or glycine (Figure 2). At 1 mM of any one of these amino acids, ODC activity was increased by more than 1.3-fold relative to the corresponding control. The increase reached its maximum level with 7.5 mM glycine and apparently with higher concentrations of L-serine or L-asparagine.

The observation that glycine is the most potent stimulator of ODC activity in Caco-2 cells is in good agreement with previous *in vivo* observations in rat intestinal ODC [11]. Glycine was therefore chosen as a model inducer in our study of the mechanism of ODC induction by amino acids. Throughout the study, glycine was compared with other ODC-inducing amino acids where appropriate.

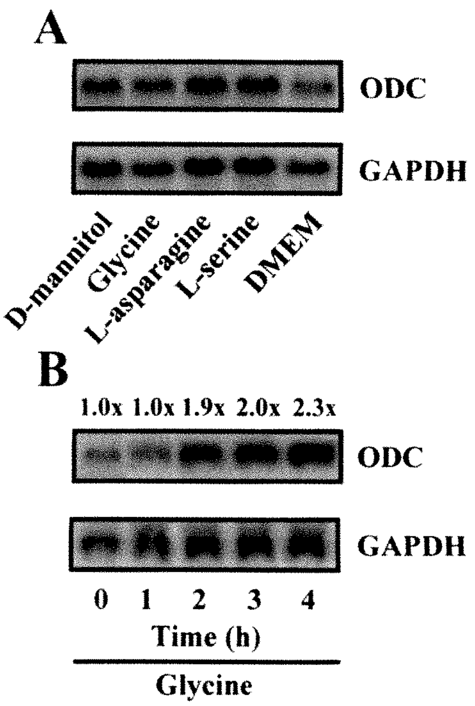

Figure 4 Effect of amino acid supplementation on ODC mRNA amount in subconfluent Caco-2 cells

Three-day-old cells were exposed for 24 h to an FCS-deprived DMEM medium, then: (**A**) for 4 h to fresh medium with 10 mM of either D-mannitol, glycine, L-asparagine or L-serine, or without any addition (DMEM); (**B**) for various times to DMEM supplemented with 10 mM glycine. The data illustrate Northern-blot analysis of ODC mRNA and GAPDH (control for RNA loading) in total RNA preparations from cells. In (**B**) values at the top indicate the fold increase of the GAPDH-normalized ODC mRNA band relative to time 0 of supplementation. Three experiments were performed that showed similar results.

Increased amount of ODC protein, but not mRNA, in amino acid-supplemented cells

The time course for ODC induction by 10 mM glycine was transient with a peak at approx. 4–5 h (Figure 3A). Similar time courses were obtained with other ODC-inducing amino acids, unlike non-metabolized α-AIB that resulted in maximal ODC activity up to at least 8 h, the longest time period examined so far (results not shown). Comparatively no significant change occurred when supplementation was carried out with 10 mM D-mannitol instead of the amino acid. In addition, data from Western-blots (Figure 3B) showed that, qualitatively, the variations in ODC activity were accompanied by parallel changes in the amount of ODC protein. Cells supplemented for 4 h with 10 mM L-asparagine or L-serine displayed almost the same increased levels of ODC protein as cells supplemented with glycine (Figure 3C). On the other hand, the increase was lower with supplemental L-proline or α-AIB, while no significant change took place after supplementation with D-mannitol.

To establish whether or not the ODC mRNA level was also increased following amino acid supplementation, Caco-2 cells were exposed for 4 h to FCS-deprived, fresh DMEM without or with 10 mM of either D-mannitol, glycine, L-asparagine or L-serine (Figure 4A). The results showed no significant differences between these various conditions. Similar observations were noted following cell exposure to D-serine or D-asparagine (results

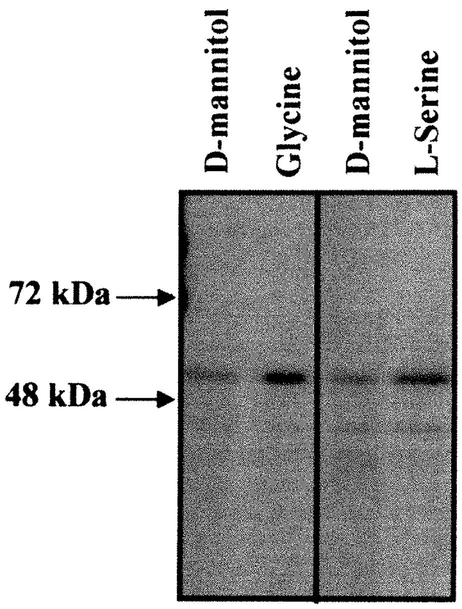

Figure 5 Effect of supplemental glycine or L-serine on the incorporation of [^{35}S]methionine into newly synthesized ODC protein

Three-day-old cells were exposed for 24 h to an FCS-deprived DMEM medium, then for 4 h to DMEM supplemented with either 10 mM glycine, L-serine or D-mannitol (control). Synthesis was determined as described in the Materials and methods section by pulse-labelling cells with [^{35}S]methionine, immunoprecipitating ODC, then analysing cytosolic extracts by SDS/PAGE and autoradiography. Two experiments, each done in duplicate, were performed that showed similar results.

not shown). However, when the ODC mRNA level was measured as a function of the duration of supplementation with glycine (Figure 4B) or D-mannitol (results not shown), it appeared that it increased rapidly up to a maximum of approx. 2-fold relative to its zero-time level.

Increased mRNA translation efficiency, and protein stabilization of ODC, after amino acid supplementation

Since amino acid supplementation, as compared with D-mannitol supplementation, led to increased amounts of ODC protein without specific variations in the ODC mRNA level, we hypothesized that the increase could result from higher efficiency of protein synthesis and/or stability. To examine whether protein synthesis was necessary for ODC induction by amino acid supplementation, we first treated Caco-2 cells with increasing concentrations of cycloheximide concomitant with glycine supplementation. The experiments showed that concentrations of 0.1 and 5 μg/ml of the protein synthesis inhibitor were sufficient to reduce ODC activity by approx. 50 and 97%, respectively (results not shown). Secondly, we compared ODC protein synthesis in cells supplemented with 10 mM D-mannitol or one of the amino acids, glycine or L-serine (Figure 5). The data showed that, after a 3.5 h incubation with 10 mM glycine or L-serine, the 25 min incorporation of radiolabelled L-methionine into ODC protein was 3–4- or 2–3-fold that measured in D-mannitol-supplemented control cells, respectively. This augmentation seemed specific for ODC since the overall protein synthesis, as measured by a 1 h incorporation of radiolabelled L-methionine in the trichloroacetic acid-precipitable cellular fraction, was similar after supplementation with any one of the above-mentioned amino acids or D-mannitol (results not shown).

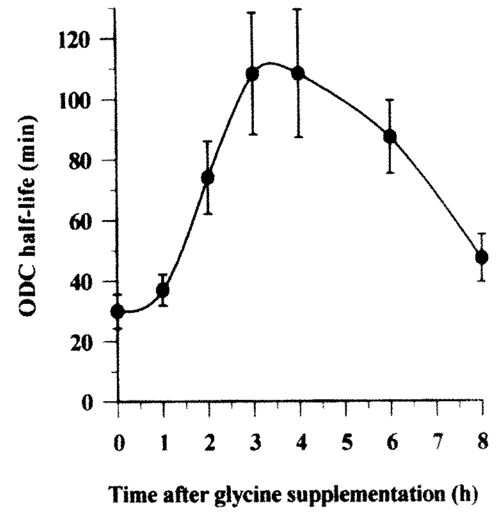

Figure 6 Time course for the effect of glycine supplementation on the stability of ODC activity

Three-day-old cells were exposed for 24 h to an FCS-deprived DMEM medium and incubated for the indicated times in DMEM supplemented with 10 mM glycine. Cells were then treated with cycloheximide (5 μg/ml) for a further 15, 30, 60, 120 or 180 min, harvested and processed as indicated in the Materials and methods section. The data are provided as ODC half-life values which were calculated by linear regression ($r \geqslant 0.93$) from semi-logarithmic plots of percentage ODC activity remaining after exposure to cycloheximide as a function of time. Data are means ± S.D. of at least two separate experiments, each done in triplicate.

Since stabilization has been shown to contribute substantially to ODC regulation in many instances, we searched for possible changes in the half-life of ODC activity throughout the time course of its response to glycine supplementation. For that purpose subconfluent Caco-2 cells were treated with 5 μg/ml cycloheximide at various times after addition of the amino acid supplement and the resulting decrease in ODC activity was measured during a further 3 h. In glycine-supplemented cells, the half-life of ODC activity augmented in a time-dependent manner (Figure 6), whereas it remained essentially steady after a 4 h supplementation with D-mannitol (results not shown). The augmentation was transient, reaching a maximal level of approx. 3.6-fold after 3–4 h. However, the ODC half-life after 8 h remained approx. 1.6-fold higher than that at zero-time of glycine supplementation.

Decreased activity of free antizyme after supplementation with an ODC-inducing amino acid

Since ODC degradation can be up-regulated specifically by antizyme [27,33,34], we investigated whether amino acid supplementation could alter the activity of this modulator protein. Assays of free antizyme, as described in the Materials and methods section, showed that a decrease in the antizyme activity was detectable as early as 1 h after exposure of putrescine-treated cells to 10 mM glycine relative to putrescine-treated control cells exposed to 10 mM D-mannitol (Figure 7). The activity of free antizyme decreased further after 2 and 4 h of glycine supplementation, especially in cells that had not been pre-treated with putrescine. In the latter case, the decrease remained substantial, although lower, afterwards, since it appeared to last at least over 9 h of supplementation with the amino acid.

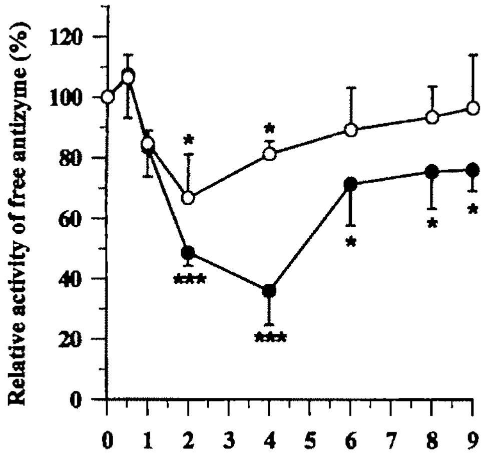

Figure 7 Time course for the effect of glycine supplementation on the activity of free antizyme

Three-day-old cells were exposed for 24 h to a DMEM medium deprived of FCS and supplemented during the last 12 h with (○) or without (●) 10 mM putrescine. They were then incubated for the indicated times in DMEM containing 10 mM putrescine and either 10 mM glycine or D-mannitol (control). The results (percentage of activity of free antizyme in the corresponding control cells) derive from linear regression analysis ($r \geqslant 0.95$) of plots of decreasing activity of an ODC source after addition of increasing amounts of antizyme preparation from glycine- or D-mannitol-supplemented cells. Data are shown as means + SD (○) and means − SD (●) of at least two separate experiments, each done in triplicate. $^{***}P < 0.001$ and $^{*}P < 0.05$ compared with the corresponding D-mannitol control.

Table 1 Effect of a 4 h supplementation with a single amino acid on polyamine levels in subconfluent Caco-2 cells

Three-day-old cells were exposed to FCS-deprived DMEM for 24 h, then to the same medium supplemented with either a single amino acid or D-mannitol (10 mM) for 4 h. Polyamines were measured as described in the Materials and methods section. Results represent means ± S.D. ($n = 3$)

	Polyamines (nmol/mg protein)			
Supplementation	Putrescine	Spermidine	Spermine	Total
D-mannitol (Control)	0.78 ± 0.01	5.92 ± 0.66	9.57 ± 1.45	16.27 ± 1.03
glycine	3.65 ± 0.66†	5.12 ± 1.38	11.05 ± 3.03	19.82 ± 5.05
L-serine	4.12 ± 0.97†	7.23 ± 1.90	11.51 ± 0.20	22.86 ± 3.03*
L-asparagine	2.73 ± 0.55†	7.23 ± 0.84	8.79 ± 2.43	18.75 ± 2.83
D-serine	2.52 ± 0.10‡	7.06 ± 1.31	10.48 ± 1.44	20.06 ± 2.80
D-asparagine	2.14 ± 0.17‡	5.56 ± 1.31	8.93 ± 2.51	16.64 ± 3.95
D-methionine	1.17 ± 0.16*	5.19 ± 0.39	10.52 ± 1.28	16.88 ± 0.95
L-arginine	N.D.	5.73 ± 0.43	10.10 ± 1.03	15.83 ± 1.44
L-methionine	N.D.	6.59 ± 0.12	10.99 ± 0.79	17.64 ± 0.91
L-cysteine	N.D.	4.88 ± 1.07	9.90 ± 2.65	14.78 ± 3.56

$^{*}P < 0.05$, $^{\dagger}P < 0.01$ and $^{\ddagger}P < 0.001$ compared with control. N.D., not detectable.

Polyamine concentrations after amino acid supplementation

We addressed whether induction of ODC evoked changes in the polyamine concentration of amino acid-supplemented cells. Polyamine assays showed essentially that the putrescine content of Caco-2 cells supplemented for 4 h with one of the ODC-inducing amino acids increased many fold as compared with that in cells exposed to D-mannitol (Table 1). Additionally, it was moderately but significantly increased after supplementation with D-methionine, in spite of the absence of augmented ODC activity (Figure 1). On the other hand, putrescine was undetectable in cells supplemented with L-methionine, L-arginine or L-cysteine, in accordance with the observed decrease in ODC activity. Despite some fluctuations, no significant differences in spermidine and spermine concentrations were measurable. Total polyamine content only varied significantly after L-serine supplementation, although the trend was for an increase after supplementation with most ODC-inducing amino acids.

DISCUSSION

In vivo rat intestinal cells respond to intragastric supplementation with a single amino acid, by increasing notably the activity and the amount, but not the mRNA level, of ODC, a key enzyme in the regulation of polyamine biosynthesis [11,12]. The data in the present study document that (1) similar variations in ODC expression took place in subconfluent cells of the human colon adenocarcinoma cell line, Caco-2, following supplementation with any one of a series of amino acids, (2) increased amounts of ODC protein resulted from both increased protein synthesis and stability, and (3) consistent with the latter finding, the antizyme activity of cells decreased following supplementation with an ODC-inducing amino acid.

Glycine, L-asparagine, L-serine and their D-stereoisomers were by far the most potent ODC-inducing amino acids in Caco-2 cells. More precisely, a maximal induction in ODC activity, averaging 12-fold, was found to occur in a transient manner 4 h after supplementing with 7.5 mM glycine. The time course of induction exhibited a roughly similar pattern to that observed after intragastric administration of glycine *in vivo* [11] or L-asparagine supplementation in cultured cells [16,20,23]. Our results also indicate that a group of L-amino acids, similar to that reported for induction of rat intestinal ODC [11], increased ODC activity in Caco-2 cells. Enzyme stimulation by the non-metabolized amino acid analogue, α-AIB, shows that the amino acids exert their effect directly without a prerequisite for processing in Caco-2 cells, as also observed in other cell lines [16,26].

ODC regulation has repeatedly been shown to involve multiple pathways and to be dependent on cell and tissue type, especially concerning its polyamine requirement for function [2,37]. The existence of discrepancies between cell lines regarding the mechanisms of ODC control by L-amino acids is therefore not surprising. We show in the present study that if the ODC mRNA level actually increased following amino acid supplementation, it also increased after D-mannitol supplementation as well as after mere substitution of 24 h-old FCS-deprived DMEM with fresh similar medium. This indicates that, in contrast with L-asparagine-supplemented rat intestinal undifferentiated IEC-6 cells [20] or mouse neuroblastoma cells [24], subconfluent Caco-2 cells respond to L-amino acid supplementation without increasing specifically their ODC mRNA content. Our data show that, in these cells, ODC induction after amino acid supplementation clearly results from regulation at both the translational and post-translational levels.

The importance of the translational regulation of ODC in mammalian cells has been well demonstrated [37,38]. It has supposedly been reported to depend on secondary structure that may form in the long 5′ untranslated region of ODC mRNA. Accordingly, ODC translation could be up-regulated by the activation of translation initiation factors, such as eukaryotic initiation factor (eIF)-4E, which are able to melt mRNA secondary structure. Several recent studies have shed some light on the mechanisms involved in the regulation of translation of such mRNAs by amino acids [39,40]. In particular, regulation by

L-leucine of ODC synthesis in L6 myoblasts was found to be associated with availability of eIF-4E and phosphorylation of ribosomal protein S6 [41]. However, the involved signalling components, as well as their relationships, remain to be identified. Furthermore, it has long been known that the cell concentration of spermidine, spermine and, to a lesser extent, putrescine down-regulates the efficiency of ODC mRNA translation [2,37]. In the present study, increased intracellular levels of putrescine may contribute to the decrease in ODC expression that took place after 4–5 h of supplementation with glycine or any ODC-inducing amino acid. However, such a decrease was not observable when supplementing cells with non-metabolized α-AIB (results not shown). This suggests that amino acid consumption during the course of incubation may also play a part in the decline of ODC activity beyond 4–5 h of amino acid supplementation. Furthermore, it is possible that, as reported previously [42], the time-dependent decrease in antizyme levels (see Figure 7) may lead to diminished degradation of nascent ODC and, consequently, be responsible for higher apparent protein biosynthesis in glycine-supplemented cells relative to control cells.

Stabilization of ODC was found *in vitro* in cultured cells following L-asparagine supplementation [20,23,24], but not *in vivo* in intestinal cells of rats given a casein, glycine or L-serine load intragastrically [11,12]. We report in the present study that glycine supplementation increased ODC half-life in a transient manner in subconfluent Caco-2 cells. This increase seems to be satisfactorily correlated with that in ODC activity (see Figures 3A and 6). However, the data indicate that, during the first 3 h of supplementation, ODC half-life rapidly reached its maximal value whereas ODC activity was still increasing. This was consistent with the observation of a rapid decrease in the activity of free antizyme, which has been reported both to inactivate ODC and to enhance its energy-dependent degradation by the 26 S proteasome [27], in putrescine-treated cells supplemented with glycine. The decrease in antizyme activity, which was also transient, was particularly dramatic when the onset of antizyme induction by putrescine coincided with the beginning of amino acid supplementation. This suggests that expression of antizyme and/or that of so far unknown regulatory protein(s) involved in antizyme expression may be highly sensitive to changes in the amino acid supply. Antizyme is expressed as two constantly produced labile proteins with half-lives estimated at approx. 24 and 83 min, and thus cells may rapidly adjust its level in response to various environmental changes or stresses [33]. Moreover, owing to its rather low physiological level antizyme would probably act as a catalytic agent in normal cells. Therefore, although evidences were obtained using putrescine-induced cells, it can be thought from the present study that slight decreases in the antizyme level could contribute to ODC induction that follows physiological increases in the amino acid supply of cells normally expressing antizyme.

Antizyme stability was reported to decrease in putrescine-stimulated rat hepatoma HTC cells exposed to hypo-osmotic medium [33]. Millimolar concentrations of actively transported amino acids can induce mammalian cell swelling secondary to their internalization and prior to an osmo-regulatory volume decrease [43]. As already sketched for ODC induction [15–17,23], a parallel might be drawn between the decreases in antizyme level after supplementation with such an amino acid and after hypotonic shock. Moreover, the mechanisms by which hypo-tonicity induces ODC activity appear to be post-transcriptional in most cells [31,44]. However, amino acid supplementation and hypotonicity may not trigger ODC induction through similar mechanisms since (1) certain D-amino acids, namely D-asparagine and D-serine, which are not taken up by Na$^+$-dependent transport systems in intestinal cells [45], seem to regulate ODC translationally and/or post-translationally, as shown in the present study; (2) conversely, no induction was observed in the present study with L-aspartate and L-glutamate, on the one hand, and L-lysine, on the other hand, although they can be taken up by the Na$^+$-dependent, acidic amino acid transport system X_{AG-} [46] and the basic amino acid transport system [47], respectively; (3) the substrate preference of the broad-specificity, Na$^+$-dependent, neutral L-amino acid transporter in Caco-2 cells [48] is not correlated with the herein reported order of potency of amino acids to induce ODC; (4) in contrast with amino acid supplementation, hypo-osmotic conditions have been found to cause a dramatic reduction in general protein synthesis in certain cell types, suggesting disruption of cell function [44]; and (5) no change in the volume of IEC-6 cells after exposure to 10 mM L-asparagine has been repeatedly reported [20,21]. Further studies, e.g. regarding the involved signalling pathway(s), are required in order to delineate the molecular basis for ODC stimulation during the cell response to amino acid supplementation, on the one hand, and to hypo-osmotic conditions, on the other hand.

In addition to L-cysteine, all amino acids that are precursors of polyamine biosynthesis, namely L-methionine, L-arginine and L-ornithine, led to a dramatic decrease in ODC activity when supplemented to subconfluent Caco-2 cells. In all cases, this decrease was followed by a depletion of intracellular putrescine. Inactivation of ODC by supplemental L-cysteine probably resulted from changes in the redox thiol status of the protein and formation of iron reactive species [49]. L-Methionine or L-arginine, as such, were unable to alter ODC activity; however, ODC inactivation after L-methionine catabolism to L-cysteine seemed plausible (results not shown). Moreover, the inhibitory effect of L-arginine might rely on intracellular biosynthesis of nitric oxide which has recently been reported to inactivate ODC *in vitro* [50].

In conclusion, the results of this and other studies [23,24,26] stress the importance of the translational and post-translational regulation of ODC by amino acids in mammalian cells. A remarkable feature of the latter regulation is the dramatic decrease in the activity of antizyme that follows exposure of subconfluent Caco-2 cells to glycine. The cell signals that trigger ODC induction and antizyme decay, as well as the resulting metabolic consequences of these changes, remain to be elucidated.

We thank Dr A Bruhat, Dr P Fafournoux and Dr S. Mordier (Unité de Nutrition Cellulaire et Moléculaire, INRA - Theix) for critical reading of the manuscript. We are grateful to Keith Thompson for help with HPLC samples H. Chabanon is a recipient of a French Ministère de l'Education Nationale, de la Recherche et de la Technologie (M E N R.T) scholarship. This work was supported by INRA, the Skogs-och Jordbrukets Forskningsråd (SJFR) and the Swedish Cancer Society.

REFERENCES

1 Griffiths, R D (1997) Outcome of critically ill patients after supplementation with glutamine Nutrition **13**, 752–754

2 Pegg, A E (1986) Recent advances in the biochemistry of polyamines in eukaryotes Biochem J **234**, 249–262

3 Farwell, D C, Miguez, J B and Herbst, E J (1977) Ornithine decarboxylase and polyamines in liver and kidneys of rats on cyclical regimen of protein-free and protein-containing diets. Relationship to deoxyribonucleic acid synthesis in liver. Biochem J **168**, 49–56

4 McAnulty, P. A and Williams, J P G (1977) Polyamines and their biosynthetic decarboxylases in various tissues of the young rat during undernutrition Br. J Nutr **38**, 73–86

5 Brachet, P, Prevoteau, H, Mathé, V and Tomé, D (1996) Modulation of putrescine transport in rat intestinal brush-border membrane vesicles by fasting and refeeding Digestion **57**, 374–381

6 Murakami, Y, Noguchi, T and Hayashi, S (1981) Role of pancreatic hormones in dietary induction of ornithine decarboxylase of rat liver J Biochem. (Tokyo) **90**, 141–147

7 Tabata, K and Johnson, L R (1986) Mechanism of induction of mucosal ornithine decarboxylase by food. Am J Physiol **251**, G370–G374

8 Moore, P and Swendseld, M E (1983) Dietary regulation of the activities of ornithine decarboxylase and S-adenosylmethionine decarboxylase in rats J Nutr **113**, 1927–1935

9 Kameji, T, Murakami, Y, Takiguchi, M, Mori, M., Tatibana, M and Hayashi, S (1987) Effect of dietary protein source on the activity of polysomal ornithine decarboxylase messenger RNA in rat liver J Nutr. **117**, 1801–1804

10 Sens, D A, Levine, J H and Buse, M G (1983) Stimulation of hepatic and renal ornithine decarboxylase activity by selected amino acids Metabolism **32**, 787–792

11 Minami, H, Miyamato, K, Fujii, Y, Nakabou, Y and Hagihira, H (1985) Induction of intestinal ornithine decarboxylase by single amino acid feeding. J. Biochem (Tokyo) **98**, 133–139

12 Miyamoto, K., Oka, T, Fujii, T, Matsubara, T, Minami, H, Nakabou, Y, Natori, Y. and Hagihira, H (1992) Differential mechanisms of induction of ornithine decarboxylase in rat intestine by L- and D-amino acids Biochim Biophys Acta **1129**, 195–198

13 Ulrich-Baker, M G, Wang, P, Fitzpatrick, L and Johnson, L R. (1988) Amiloride inhibits rat mucosal ornithine decarboxylase activity and DNA synthesis Am. J. Physiol **254**, G408–G415

14 Kandil, H M, Argenzio, R A, Chen, W, Berschneider, H M, Stiles, A D, Westwick, J K, Rippe, R. A, Brenner, D A and Rhoads, M (1995) L-glutamine and L-asparagine stimulate ODC activity and proliferation in a porcine jejunal enterocyte line Am J Physiol **269**, G591–G599

15 Chen, K Y and Canellakis, E S (1977) Enzyme regulation in neuroblastoma cells in a salts/glucose medium induction of ornithine decarboxylase by asparagine and glutamine Proc Natl Acad Sci U.S A **74**, 3791–3795

16 Rinehart, C. A., Viceps-Madore, D, Fong, W-F, Ortiz, J G and Canellakis, E S (1985) The effect of transport system A and N amino acids and of nerve and epidermal growth factors on the induction of ornithine decarboxylase activity J Cell Physiol **123**, 435–441

17 Lundgren, D W and Vacca, C V (1990) Nonmetabolizable glucose analogues and ornithine decarboxylase expression in LLC-PK1 cells Am. J. Physiol **259**, C647–C653

18 Jain, R, Eikenburg, B E and Johnson, L R (1987) Stimulation of ornithine decarboxylase activity in digestive tract mucosa Am J Physiol. **253**, G303–G307

19 Kekuda, R, Torres-Zamorano, V, Fei, Y. J., Prasad, P D, Li, H. W., Mader, L D, Leibach, F H and Ganapathy, V (1997) Molecular and functional characterization of intestinal Na(+)-dependent neutral amino acid transporter B0. Am J Physiol **272**, G1463–G1472

20 Wang, J. Y., Viar, M J, Blanner, P M. and Johnson, L R (1996) Expression of the ornithine decarboxylase gene in response to asparagine in intestinal epithelial cells Am J Physiol **271**, G164–G171

21 Wang, J Y, Li, J., Patel, A R, Summers, S, Li, L and Bass, B L (1998) Synergistic induction of ornithine decarboxylase by asparagine and gut peptides in intestinal crypt cells Am J Physiol. **274**, C1476–C1484

22 Adamson, R. H. and Fabro, S (1968) Embryotoxic effect of L-asparaginase Nature (London) **218**, 1164–1165

23 Kanamoto, R, Boyle, S M., Oka, T and Hayashi, S (1987) Molecular mechanisms of the synergistic induction of ornithine decarboxylase by asparagine and glucagon in primary cultured hepatocytes J Biol Chem **262**, 14801–14805

24 Chen, Z P. and Chen, K Y (1992) Mechanism of regulation of ornithine decarboxylase gene expression by asparagine in a variant mouse neuroblastoma cell line J Biol Chem **267**, 6946–6951

25 Chen, Z. P. and Chen, K Y (1994) Asparagine markedly induces the expression of ornithine decarboxylase gene in transformed mammalian cells but not in their untransformed counterparts Cancer Lett **86**, 97–103

26 Ray, R M, Viar, M J, Patel, T B and Johnson, L R (1999) Interaction of asparagine and EGF in the regulation of ornithine decarboxylase in IEC-6 cells. Am J Physiol. **276**, G773–G780

27 Hayashi, S, Murakami, Y and Matsufuji, S (1996) Ornithine decarboxylase antizyme a novel type of regulatory protein Trends Biochem Sci. **21**, 27–30

28 Chantret, I, Barbat, A, Dussaulx, E, Brattain, M G and Zweibaum, A (1988) Epithelial polarity, villin expression, and enterocytic differentiation of cultured human colon carcinoma cells a survey of twenty cell lines Cancer Res **48**, 1936–1942

29 Chomczynski, P and Sacchi, N (1987) Single-step method of RNA isolation by acid guanidinium thiocyanate-phenol-chloroform extraction Anal. Biochem **162**, 156–159

30 Sambrook, J, Fritsch, E F and Maniatis, T (1989) Extraction, purification and analysis of messenger RNA from eukaryotic cells In Molecular Cloning, a Laboratory Manual (Nolan, C, ed), pp 7.1–7 52, Cold Spring Harbor Press, Cold Spring Harbor

31 Lovkvist-Wallstrom, E, Stjernborg-Ulvsback, L, Scheffler, I. E and Persson, L (1995) Regulation of mammalian ornithine decarboxylase Studies on the induction of the enzyme by hypotonic stress Eur J Biochem **231**, 40–44

32 Aubel, C, Chabanon, H, Persson, L, Thiman, L, Ferrara, M and Brachet, P. (1999) Antizyme-dependent and -independent mechanisms are responsible for increased spermidine transport in amino acid-restricted human cancer cells Biochem Biophys Res Commun. **256**, 646–651

33 Mitchell, J L A, Judd, G G, Leyser, A and Choe, C Y (1998) Osmotic stress induces variation in cellular levels of ornithine decarboxylase-antizyme Biochem. J. **329**, 453–459

34 Hayashi, S-I and Fujita, K (1983) Antizyme and antizyme inhibitor of ornithine decarboxylase (rat liver) In Methods in Enzymology vol. 94, Polyamines (Tabor, H and Tabor, C W, eds), pp 185–193, Academic Press Inc., New York

35 Wallace, H M, Nuttall, M E and Robinson, F C (1988) Acetylation of spermidine and methylglyoxal bis(guanylhydrazone) in baby-hamster kidney cells (BHK-21/C13) Biochem. J **253**, 223–227

36 Smith, P K, Krohn, R I, Hermanson, G. T, Mallia, A K, Gartner, F H, Provenzano, M D, Fujimoto, E K, Goeke, N. M., Olson, B J and Klenk, D C (1985) Measurement of protein using bicinchoninic acid Anal Biochem **150**, 76–85

37 Heby, O and Persson, L (1990) Molecular genetics of polyamine synthesis in eukaryotic cells Trends Biochem Sci **15**, 153–158

38 Shantz, L M and Pegg, A E (1999) Translational regulation of ornithine decarboxylase and other enzymes of the polyamine pathway Int J Biochem Cell Biol. **31**, 107–122

39 Hara, K., Yonezawa, K, Weng, Q.-P, Kozlowski, M T., Belham, C and Avruch, J (1998) Amino acid sufficiency and mTOR regulate p70 S6 kinase and eIF-4E BP1 through a common effector mechanism. J Biol Chem **273**, 14484–14494

40 Iiboshi, Y, Papst, P J, Kawasome, H, Hosoi, H, Abraham, R T, Houghton, P. J and Terada, N (1999) Amino acid-dependent control of p70(s6k) Involvement of tRNA aminoacylation in the regulation J Biol Chem **274**, 1092–1099

41 Kimball, S R., Shantz, L M, Horetsky, R L and Jefferson, L S (1999) Leucine regulates translation of specific mRNAs in L6 myoblasts through mTOR-mediated changes in availability of eIF4E and phosphorylation of ribosomal protein S6 J Biol. Chem **274**, 11647–11652

42 Mitchell, J. L A, Choe, C Y and Judd, G G (1996) Feedback repression of ornithine decarboxylase synthesis mediated by antizyme. Biochem J **320**, 755–760

43 Kristensen, L O and Folke, M (1984) Volume-regulatory K+ efflux during concentrative uptake of alanine in isolated rat hepatocytes Biochem J **221**, 265–268

44 Poulin, R and Pegg, A E (1990) Regulation of ornithine decarboxylase expression by anisosmotic shock in alpha-difluoromethylornithine-resistant L1210 cells J Biol Chem **265**, 4025–4032

45 Daniels, V G., Newey, H and Smyth, D H. (1969) Stereochemical specificity of neutral amino acid transfer systems in rat small intestine Biochim. Biophys Acta **183**, 637–639

46 Nicklin, P L, Irwin, W J, Hassan, I F, Mackay, M and Dixon, H B (1995) The transport of acidic amino acids and their analogues across monolayers of human intestinal absorptive (Caco-2) cells in vitro Biochim Biophys Acta **1269**, 176–186

47 Harvey, C M, Muzyka, W R, Yao, S Y, Cheeseman, C I and Young, J D (1993) Expression of rat intestinal L-lysine transport systems in isolated oocytes of Xenopus laevis Am J. Physiol **265**, G99–G106

48 Pan, M and Stevens, B (1995) Protein kinase C-dependent regulation of L-arginine transport activity in Caco-2 intestinal cells J Biol Chem **270**, 3582–3587

49 Murakami, Y, Kameji, T and Hayashi, S (1984) Cysteine-dependent inactivation of hepatic ornithine decarboxylase Biochem J **217**, 573–580

50 Bauer, P. M., Fukuto, J M, Buga, G M, Pegg, A E and Ignarro, L J (1999) Nitric oxide inhibits ornithine decarboxylase by S-nitrosylation Biochem. Biophys Res Commun **262**, 355–358

Received 23 November 1999/9 March 2000, accepted 23 March 2000

Biochem J (2000) 348, 409–416 (Printed in Great Britain)

Signalling pathways of insulin-like growth factor-I that are augmented by cAMP in FRTL-5 cells

Miyako ARIGA, Taku NEDACHI, Masakazu AKAHORI, Hideki SAKAMOTO, Yoshiaki ITO, Fumihiko HAKUNO and Shin-Ichiro TAKAHASHI[1]

Departments of Animal Sciences and Applied Biological Chemistry, Graduate School of Agriculture and Life Sciences, The University of Tokyo, Tokyo 113-8657, Japan

We have reported that pretreatment of rat FRTL-5 thyroid cells with thyrotropin (TSH) markedly potentiates the mitogenic response to insulin-like growth factor-I (IGF-I). The present study was undertaken to determine whether the augmentation by cAMP of IGF-I-dependent tyrosine phosphorylation of known IGF-I receptor substrates plays an important role in the cAMP-dependent potentiation of DNA synthesis induced by IGF-I. Pretreatment with TSH or dibutyryl cAMP did not affect the IGF-I-dependent tyrosine phosphorylation of insulin receptor substrate-1 (IRS-1). In contrast, cAMP pretreatment potentiated the tyrosine phosphorylation of IRS-2 induced by IGF-I, but did not affect the amount of IRS-2. We found that the IGF-I-dependent tyrosine phosphorylation of 66 kDa Shc (Src homology collagen) was markedly increased by cAMP pretreatment, and that this change was mainly due to an increase in the levels of 66 kDa Shc protein. Under these conditions, cAMP pretreatment significantly increased binding of Grb2 (growth-factor-receptor-bound protein 2) to Shc in response to IGF-I, and activation of MAP kinase (mitogen-activated protein kinase) induced by IGF-I was also enhanced by cAMP. The presence of PD98059, an inhibitor of MEK (MAP-kinase/Erk kinase), during treatment with IGF-I partially inhibited the cAMP-dependent augmentation of DNA synthesis in response to IGF-I. On the other hand, cAMP pretreatment increased binding of the phosphoinositide 3-kinase (PI 3-kinase) p85 subunit to IRS-2, which was reflected in PI 3-kinase activity. LY294002, a PI 3-kinase inhibitor, strongly depressed IGF-I-dependent DNA synthesis after pretreatment with and without TSH or dibutyryl cAMP. Our results suggest that the interaction between cAMP-dependent and IGF-I-dependent pathways leads to an augmentation of cell proliferation, which is mediated, at least in part, through the MAP kinase and PI 3-kinase signalling pathways. These effects are mediated by changes in tyrosine phosphorylation of IGF-I receptor substrates, including IRS-2 and Shc.

Key words: IGF-I, IRS-1, IRS-2, Shc.

INTRODUCTION

Insulin-like growth factor-I (IGF-I) can stimulate both cell proliferation and differentiation in many cell types [1,2]. IGF-I by itself often has weak biological effects, which are greatly potentiated in the presence of other hormones or growth factors [3–10]. Although cAMP has been reported to antagonize tyrosine kinase receptor-activated pathways in some cells [11–19], we have shown previously that pretreatment of FRTL-5 cells with thyrotropin (TSH), which acts through a cAMP-dependent pathway, potentiates DNA synthesis induced by IGF-I [20,21]. The present studies are part of ongoing attempts to elucidate the signalling pathways through which such synergistic actions are mediated.

Pretreatment of FRTL-5 cells with TSH or other substances that increase cAMP levels enhances the IGF-I-dependent tyrosine phosphorylation of several intracellular proteins, predominantly those with molecular masses of 175–185 kDa or 90–100 kDa [21]. Under these conditions, we reported that cAMP did not increase IGF-I receptor number or kinase activity [22]. These results suggested that the interaction between cAMP-dependent and IGF-I-dependent pathways leads to an augmentation of cell proliferation through changes in IGF-I-dependent tyrosine phosphorylation at a step distal to IGF-I receptor kinase activation.

Binding of IGF-I to its specific receptor on a target cell membrane is followed by activation of tyrosine kinase in the β-subunit of the IGF-I receptor [22]. The activated IGF-I receptor in turn phosphorylates specific substrates, in particular insulin receptor substrate-1 (IRS-1), IRS-2 and Src homology collagen (Shc), as well as putative substrates such as Crk (CT10 regulator of kinase) and Jaks (Janus-activated kinases) [23–28]. Recently it has become clear that phosphorylated tyrosine residues of IRS-1, IRS-2 and Shc are recognized by various signalling molecules that contain a Src homology 2 (SH2) domain [29,30]. These include Grb2 (growth-factor-receptor-bound protein 2) and the 85 kDa regulatory subunit of phosphoinositide (phosphatidylinositol) 3-kinase (PI 3-kinase), suggesting that binding of tyrosine-phosphorylated substrates to these SH2-domain-containing proteins mediates IGF-I bioactivities. These associations are thought to stimulate the mitogen-activated protein kinase (MAP kinase) cascade or the PI 3-kinase cascade, well known signalling pathways that mediate many significant actions of growth factors [31].

The present study was undertaken to determine whether the augmentation by cAMP of IGF-I-dependent tyrosine

---

Abbreviations used. CH2 domain, collagen-homology 2 domain, Erk, extracellular-signal-regulated kinase, Grb2, growth-factor-receptor-bound protein 2, HBSS, Hanks balanced salt solution, IGF-I, insulin-like growth factor-I, IRS, insulin receptor substrate; MAP kinase, mitogen-activated protein kinase, MEK, MAP-kinase/Erk kinase, NBS, newborn bovine serum, PI 3-kinase, phosphoinositide (phosphatidylinositol) 3-kinase, SH, Src homology, Shc, Src homology collagen, TSH, thyrotropin

[1] To whom correspondence should be addressed Laboratory of Cell Regulation, Departments of Animal Sciences and Applied Biological Chemistry, Graduate School of Agriculture and Life Sciences, The University of Tokyo, 1-1-1 Yayoi, Bunkyo-ku, Tokyo 113-8657, Japan (e-mail atkshin@mail ecc u-tokyo.ac jp)

phosphorylation is specifically reflected in increased phosphorylation of the known IGF-I receptor substrates IRS-1, IRS-2 and Shc. In addition, we investigated whether potentiation of tyrosine phosphorylation causes an increase in binding of these substrates to Grb2 or to the 85 kDa regulatory subunit of PI 3-kinase, followed by activation of MAP kinase or PI 3-kinase.

EXPERIMENTAL

Materials

Coon's modified Ham's F-12 medium (Coon's F-12) was purchased from Sigma (St. Louis, MO, U.S.A.); newborn bovine serum (NBS) was from Nichirei (Tokyo, Japan); Hanks balanced salt solution (HBSS) was from Nissui (Tokyo, Japan), bovine insulin, bovine TSH and human transferrin were purchased from Sigma; penicillin was obtained from Ban-yu Pharmaceutical Co. (Tokyo, Japan), streptomycin and kanamycin were from Meiji Seika Co. (Tokyo, Japan); and amphotericin B (fungizone) was from Sankyo Pharmaceutical Co. (Tokyo, Japan). Purified bovine TSH (30 units/mg) for biological studies was generously donated by the National Hormone and Pituitary Program [National Institute of Diabetes and Digestive and Kidney Diseases (NIDDK), Bethesda, MD, U.S.A.], and recombinant human IGF-I was a gift from Dr Toshiaki Ohkuma (Fujisawa Pharmaceutical Co., Osaka, Japan). Leupeptin and pepstatin were kindly donated by Dr Takaaki Aoyagi (Institute of Microbial Chemistry, Tokyo, Japan). Anti-phosphotyrosine monoclonal antibody was kindly provided by Dr Takao Yamori (Cancer Chemotherapy Center, Japanese Foundation for Cancer Research, Tokyo, Japan). Anti-(rat IRS-1) antibody for immunoprecipitation, anti-(human Grb2) antibody (against N-terminal SH3 region), anti-p85 antibody (against N-terminal SH2 region) and anti-Shc antibody were purchased from Upstate Biotechnology Inc. (Lake Placid, NY, U.S.A.). Anti-(human IRS-1) antibody for immunoblotting and anti-(rat IRS-2) (M-19) were purchased from Santa Cruz Biotechnology Inc. (Santa Cruz, CA, U.S.A.). Anti-phosphoErk antibody (where Erk is extracellular-signal-regulated kinase) was from Transduction Laboratories (Lexington, KY, U.S.A.). Anti-IRS-3 and anti-IRS-4 antibodies were kindly donated by Dr Tomoichiro Asano (Faculty of Medicine, The University of Tokyo, Tokyo, Japan). [γ-^{32}P]ATP (> 6000 Ci / mmol) was purchased from Amersham Pharmacia Biotech (Uppsala, Sweden). Other chemicals were of reagent grade available commercially.

Cell cultures

FRTL-5 cells (A.T.C.C. no. CRL8305), a line of rat thyroid follicular cells developed by Ambesi-Impionbato et al. [31a], were generously provided by Dr Leonard Kohn (Section of Cell Regulation, NIDDK). Cells were routinely cultured in Coon's F-12 medium including three hormones (3H): TSH (1 m-unit/ml), insulin (10 μg/ml) and transferrin (5 μg/ml). Cells were cultured in 150-cm^2 flasks (IWAKI, Tokyo, Japan) at 37 °C in an atmosphere of 95 % air/5 % CO_2 in a humidified incubator [20]. All media contained penicillin (100 units/ml), streptomycin (10 μg/ml), kanamycin (1 μg/ml) and amphotericin B (0.2 μg/ml).

Cell treatments

FRTL-5 cells (1×10^6 cells/8 ml) were sparsely seeded in 100-mm dishes (IWAKI) in Coon's F-12 medium containing 5 % (v/v) NBS and 3H. For DNA synthesis assays, cells (1×10^4 cells/500 μl per well) were seeded in 48-well plates (IWAKI). After 6 days, the cells were washed twice with HBSS, and the cultures were continued for an additional 24 h in Coon's F-12 medium containing 0.1 % (w/v) BSA without NBS and 3H until cells became quiescent. The medium was then replaced with the experimental medium (Coon's F-12 medium containing 0.1 % BSA) without or with TSH (1 nM) or dibutyryl cAMP (1 mM), and the cells were pretreated for 24 h. At the end of pretreatment, the cells were washed twice with HBSS The cells were then treated with IGF-I (100 ng/ml) for periods of time specified for each experiment.

Immunoprecipitation of IRSs or Shc, followed by immunoblotting with anti-phosphotyrosine antibody or antibody against each protein

As described above, the quiescent FRTL-5 cells were pretreated without or with TSH (1 nM) or dibutyryl cAMP (1 mM) for 24 h, followed by treatment with IGF-I (100 ng/ml) for various times. The cells were then harvested at 0 °C in 400 μl of immunoprecipitation buffer containing 50 mM Tris/HCl, pH 8.0, 150 mM NaCl, 1 mM Na_3VO_4, 10 mM EDTA, 1 mM EGTA, 1.5 mM $MgCl_2$, 1 % Triton X-100, 100 kallikrein-inactivating units/ml aprotinin, 20 μg/ml PMSF, 10 μg/ml leupeptin, 5 μg/ml pepstatin and 10 mg/ml *p*-nitrophenyl phosphate. The lysates were centrifuged at 12000 ***g*** for 10 min at 4 °C. The supernatant was diluted with immunoprecipitation buffer to 1 mg of protein/ml as a final concentration. The protein assay was carried out using a protein assay kit (Bio-Rad, Hercules, CA, U.S.A.). The lysates were incubated with anti-IRS-1 antibody (10 μg), anti-IRS-2 antibody (10 μg), anti-Shc antibody (10 μg), anti-IRS-3 antibody (10 μl) or anti-IRS-4 antibody (10 μl) for 12 h at 4 C; 40 μl of Protein A–Sepharose [50 % (v/v); Pharmacia Biotech] was then added and the incubation was continued for 2 h. The immunoprecipitates were collected by centrifugation at 4 °C, washed three times with immunoprecipitation buffer containing 300 mM NaCl, and boiled for 5 min in a mixture of 60 μl of immunoprecipitation buffer and 30 μl of 3 × Laemmli sample buffer (9 % SDS, 15 % glycerol, 30 mM Tris/HCl, pH 7.8, 0.05 % Bromophenol Blue and 6 % 2-mercaptoethanol). These samples were then stored at −80 °C until electrophoresis.

Portions of each sample (containing equal amounts of protein) were run on SDS/PAGE followed by immunoblotting analysis, as described previously [32]. The transferred membrane was incubated for 2 h at room temperature in blocking buffer containing a monoclonal anti-phosphotyrosine antibody (1 : 1000 dilution) or anti-Grb2 antibody (1 : 1000), or incubated overnight at room temperature in the blocking buffer containing anti-IRS-1 antibody (1 : 200), anti-IRS-2 antibody (1 : 500), anti-Shc antibody (1 : 1000) or anti-p85 antibody (1 : 2000). The results were quantified using the NIH Image computer program (Version 1.61).

Immunoblotting of cell lysates using anti-IRS-1, anti-IRS-2 and anti-Shc antibodies

As described above, quiescent FRTL-5 cells were treated without or with TSH (1 nM) or dibutyryl cAMP (1 mM) for 24 h, and then harvested at 0 °C in 400 μl of immunoprecipitation buffer. The lysates were centrifuged at 12000 ***g*** for 10 min at 4 °C. The protein assay of the supernatants was carried out using a protein assay kit (Bio-Rad), and the protein content of the lysates was adjusted to 1 mg/ml by addition of immunoprecipitation buffer. A portion of 200 μl of concentrated 3 × Laemmli sample buffer containing 9 % SDS and 6 % 2-mercaptoethanol was added to 400 μl of supernatant, and the mixture was boiled for 5 min.

These samples were stored at −80 °C until electrophoresis. Portions of each sample containing the same amount of protein were run on SDS/PAGE, followed by immunoblotting using anti-IRS-1 antibody, anti-IRS-2 antibody or anti-Shc antibody.

MAP kinase assay by immunoblotting with anti-phosphoErk antibody

As described above, quiescent FRTL-5 cells were pretreated without or with TSH (1 nM) or dibutyryl cAMP (1 mM) for 24 h, followed by treatment with IGF-I (100 ng/ml) for 5 min. Cells were lysed and homogenized at 4 °C in 400 μl of buffer containing 80 mM β-glycerophosphate, pH 7.4, 15 mM $MgCl_2$, 20 mM EGTA, 1 mM Na_3VO_4, 20 μg/ml PMSF, 10 μg/ml leupeptin, 5 μg/ml pepstatin and 1 mM benzamidine. The lysates were centrifuged at 12000 ***g*** for 15 min at 4 °C. The supernatants were recovered and the concentration of protein was measured using a protein assay kit. Portions of each sample containing the same amount of protein were run on SDS/12.5 %-PAGE and immunoblotting was performed as described above, but using anti-phosphoErk polyclonal antibody (1:1000). The amounts of phosphorylated Erk1 (lower mobility) and Erk2 (higher mobility) were taken to represent activated Erk1 and Erk2 respectively.

PI 3-kinase activity assay

As described above, quiescent FRTL-5 cells were pretreated without or with TSH (1 nM) or dibutyryl cAMP (1 mM) for 24 h, followed by treatment with IGF-I (100 ng/ml) for 2 min. Cells were lysed at 4 °C in 300 μl of Nonidet P-40 buffer (10 mM Tris/HCl, pH 7.5, 150 mM NaCl, 0.5 mM Na_3VO_4, 1 mM EDTA, 1 % Nonidet P-40, 100 kallikrein-inactivating units/ml aprotinin, 20 μg/ml PMSF, 10 μg/ml leupeptin, 5 μg/ml pepstatin and 10 mg/ml *p*-nitrophenyl phosphate). The lysates were centrifuged at 12000 ***g*** for 10 min at 4 °C. The supernatant was incubated with anti-IRS-1 antibody (10 μg), anti-IRS-2 antibody (10 μg) or anti-phosphotyrosine antibody (20 μl) for 12 h at 4 °C; 10 μl of Protein A–Sepharose (50 %, v/v) was then added and the incubation was continued for 2 h. The immunoprecipitates were collected by centrifugation at 4 °C, washed once each with Nonidet P-40 buffer, LiCl buffer (100 mM Tris/HCl, pH 7.5, and 500 mM LiCl), distilled water and TNE buffer (10 mM Tris/HCl, pH 7.5, 150 mM NaCl and 1 mM EDTA), and finally resuspended in 45 μl of reaction buffer (20 mM Tris/HCl, pH 7.5, 100 mM NaCl and 0.5 mM EGTA).

The PI 3-kinase assay was carried out using the method of Whitman et al. [33], with slight modifications. Briefly, the PI 3-kinase assay was initiated by incubation of immunocomplex in 45 μl of reaction buffer with 5 μl of [γ-^{32}P]ATP/$MgCl_2$/phosphatidylinositol to give final concentrations of 20 μM [γ-^{32}P]ATP (4 μCi/mmol), 20 mM $MgCl_2$ and 20 μg of phosphatidylinositol (Avanti, Pharmacia Biotech) at 25 °C for 30 min. After incubation, 100 μl of chloroform/methanol/HCl (10:20:1, by vol.) was added to the reaction mixture to stop the reaction. A lipid product was extracted, spotted on to a silica gel plate and developed with chloroform/methanol/NH_4OH/water (43:38:6:6, by vol.). ^{32}P radioactivity incorporated into phosphatidylinositol was measured by autoradiography as PI 3-kinase activity. Each experimental point represents the mean from three replicate dishes.

DNA synthesis assay

Determination of [*methyl*-^{3}H]thymidine incorporation into DNA was performed as described previously [20]. In all experiments, each experimental point represents the mean from three replicate wells.

RESULTS

Effects of cAMP pretreatment on tyrosine phosphorylation of IRSs stimulated by IGF-I

To test the effects of pretreatment with TSH or dibutyryl cAMP (cAMP pretreatment) on tyrosine phosphorylation of IGF-I receptor substrates, such as IRS-1 and IRS-2, FRTL-5 cells were preincubated without or with TSH or dibutyryl cAMP for 24 h. We then analysed the tyrosine phosphorylation of each substrate by immunoprecipitation using an antibody against each protein, followed by immunoblotting with an anti-phosphotyrosine antibody. The tyrosine phosphorylation of IRS-1 increased after IGF-I treatment, and this increase was not affected by cAMP pretreatment (Figures 1A and 1B). In the case of IRS-2, tyrosine phosphorylation in response to IGF-I was clearly potentiated by pretreatment with cAMP (Figures 2A and 2B). However, under

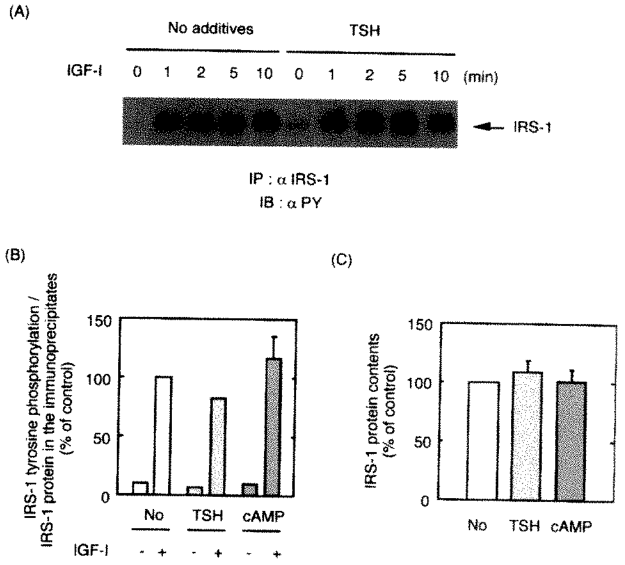

Figure 1 Effects of TSH and dibutyryl cAMP on tyrosine phosphorylation of IRS-1 stimulated by IGF-I

(**A**) Quiescent FRTL-5 cells were pretreated without (No additives) or with TSH (1 nM) for 24 h, washed twice with HBSS and incubated with 100 ng/ml IGF-I for various time (0, 1, 2, 5 and 10 min). After treatment, cells were harvested and the cell lysate was subjected to immunoprecipitation (IP) with anti-IRS-1 antibody, followed by SDS/8%-PAGE and immunoblotting (IB) with anti-phosphotyrosine antibody (αPY), as described in the Experimental section. These experiments were performed on three independent occasions, and a representative blot is presented. (**B**) Quiescent FRTL-5 cells were pretreated without (No) or with TSH (1 nM) or dibutyryl cAMP (cAMP; 1 mM) for 24 h, washed twice with HBSS and incubated without or with 100 ng/ml IGF-I for 2 min. After treatment, cells were harvested and the cell lysate was subjected to immunoprecipitation with anti-IRS-1 antibody, followed by SDS/8%-PAGE and immunoblotting with anti-phosphotyrosine antibody and anti-IRS-1 antibody, as described in the Experimental section. IRS-1 tyrosine phosphorylation and IRS-1 protein content were quantified by NIH Image software. IRS-1 tyrosine phosphorylation corrected for its protein content is expressed as a percentage of IGF-I-dependent tyrosine phosphorylation in cells pretreated with no additives, and results represent means ± S.E.M. of three independent experiments. (**C**) Quiescent FRTL-5 cells were treated without (No) or with TSH (1 nM) or dibutyryl cAMP (cAMP; 1 mM) for 24 h. Cells were harvested without exposure to IGF-I, and the cell lysate was subjected to immunoblotting with anti-IRS-1 antibody as described in the Experimental section. The amount of IRS-1 in cells treated with no additives, TSH or cAMP was quantified by NIH Image software. The amount of IRS-1 is expressed as a percentage of the IRS-1 content in cells treated with no additives, and the results represent means ± S.E.M. of three independent experiments.

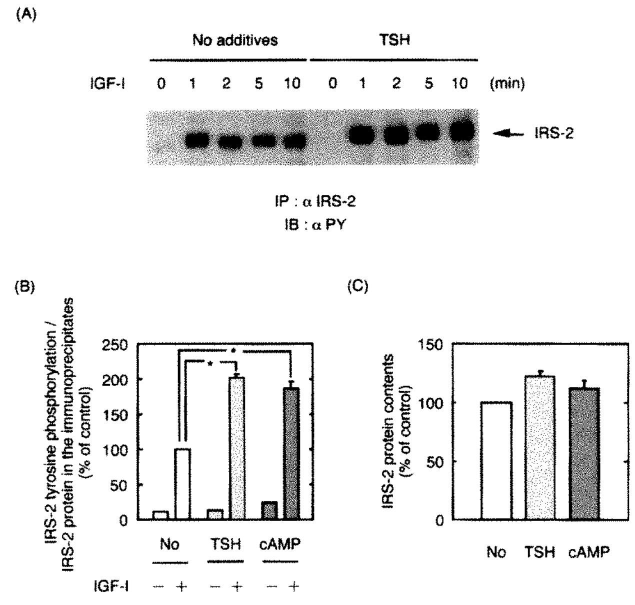

Figure 2 Effects of TSH and dibutyryl cAMP on tyrosine phosphorylation of IRS-2 stimulated by IGF-I

(**A**) Quiescent FRTL-5 cells were pretreated without (No additives) or with TSH (1 nM) for 24 h, washed twice with HBSS and incubated with 100 ng/ml IGF-I for various times (0, 1, 2, 5 and 10 min). After treatment, cells were harvested and the cell lysate was subjected to immunoprecipitation (IP) with anti-IRS-2 antibody, followed by SDS/8%-PAGE and immunoblotting (IB) with anti-phosphotyrosine antibody (αPY), as described in the Experimental section. These experiments were performed on three independent occasions, and a representative blot is presented. (**B**) Quiescent FRTL-5 cells were pretreated without (No) or with TSH (1 nM) or dibutyryl cAMP (cAMP; 1 mM) for 24 h, washed twice with HBSS and incubated without or with 100 ng/ml IGF-I for 2 min. After treatment, cells were harvested and the cell lysate was subjected to immunoprecipitation with anti-IRS-2 antibody, followed by SDS/8%-PAGE and immunoblotting with anti-phosphotyrosine antibody and anti-IRS-2 antibody, as described in the Experimental section. The quantitative analysis was performed as described for Figure 1(B); * indicates a significant difference ($P < 0.05$) between values obtained in cells pretreated with no additives and those pretreated with TSH or cAMP, followed by IGF-I treatment in all cases (unpaired *t*-test). (**C**) Quiescent FRTL-5 cells were treated without (No) or with TSH (1 nM) or dibutyryl cAMP (cAMP; 1 mM) for 24 h. Cells were harvested without exposure to IGF-I and the cell lysate was subjected to immunoblotting with anti-IRS-2 antibody, as described in the Experimental section. These experiments were performed on three independent occasions. Densitometric analysis of the blot was performed as described for Figure 1(C).

these conditions cAMP did not affect the amounts of these proteins, as assessed by analysing the lysates by immunoblotting with antibodies against IRS-1 and IRS-2 (Figures 1C and 2C). We could not detect tyrosine phosphorylation of IRS-3 and IRS-4 in this cell line (results not shown).

Effects of cAMP pretreatment on tyrosine phosphorylation of Shc stimulated by IGF-I

We next studied the tyrosine phosphorylation of Shc in response to IGF-I. In FRTL-5 cells we observed the tyrosine phosphorylation of three isoforms of Shc, with molecular masses of 46 kDa, 52 kDa and 66 kDa, and an IGF-I-dependent increase in tyrosine phosphorylation was observed in each case (Figure 3A). Of these three proteins, cAMP pretreatment significantly potentiated the tyrosine phosphorylation of 66 kDa Shc induced by IGF-I (Figure 3B). In Figure 3(C) the degree of tyrosine phosphorylation of 66 kDa Shc induced by IGF-I is related to the amount of 66 kDa Shc protein in the immunoprecipitates. The ratio was not significantly changed by cAMP pretreatment, suggesting that an increase in the phosphorylation of 66 kDa Shc was mainly due to an increase in its amount. Figures 3(D) and 3(E) also show that cAMP treatment caused a marked increase in the amount of 66 kDa Shc.

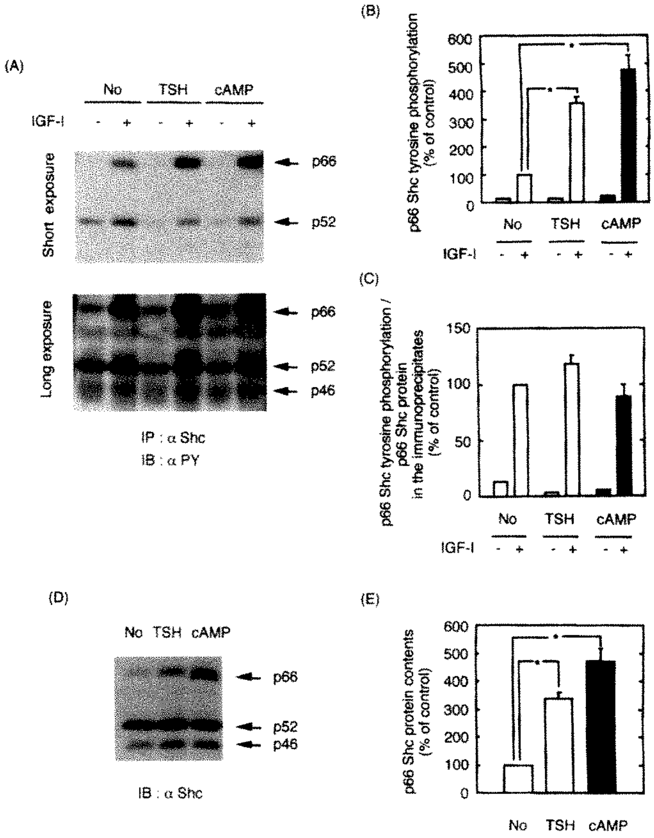

Figure 3 Effects of TSH and dibutyryl cAMP on tyrosine phosphorylation of Shc stimulated by IGF-I

(**A**)–(**C**) Quiescent FRTL-5 cells were pretreated without (No) or with TSH (1 nM) or dibutyryl cAMP (cAMP; 1 mM) for 24 h, washed twice with HBSS and incubated without or with 100 ng/ml IGF-I for 5 min. After treatment, cells were harvested and the cell lysate was subjected to immunoprecipitation (IP) with anti-Shc antibody, followed by SDS/10%-PAGE and immunoblotting (IB) with anti-phosphotyrosine antibody or anti-Shc antibody, as described in the Experimental section. These experiments were performed on three independent occasions, and a representative blot is shown (**A**). The quantitative analysis of tyrosine phosphorylation of 66 kDa Shc (p66 Shc) (**B**) was performed as described for Figure 1(B); * indicates a significant difference ($P < 0.05$) between values obtained in cells pretreated with no additives and those pretreated with TSH or cAMP, followed by IGF-I treatment in all cases (unpaired *t*-test). Panel (**C**) shows the degree of tyrosine phosphorylation of p66 Shc corrected for the amount of protein. (**D**)–(**E**) Quiescent FRTL-5 cells were treated without (No) or with TSH (1 nM) or dibutyryl cAMP (cAMP; 1 mM) for 24 h. Cells were harvested without exposure to IGF-I and the cell lysate was subjected to immunoblotting (IB) with anti-Shc antibody, as described in the Experimental section. These experiments were performed on three independent occasions and a representative blot is shown (**D**). The densitometric analysis of the amount of 66 kDa Shc (**E**) was performed as described for Figure 1(C); * indicates a significant difference ($P < 0.05$) between values obtained in cells treated with no additives and those treated with TSH or cAMP (unpaired *t*-test).

Effects of cAMP pretreatment on the association of tyrosine-phosphorylated IRS-1, IRS-2 or Shc with Grb2, followed by activation of MAP kinase

We then examined whether TSH or dibutyryl cAMP pretreatment affected binding of tyrosine-phosphorylated substrates to Grb2, using co-immunoprecipitation with an antibody against IRS-1, IRS-2 or Shc. Association of Grb2 with IRS-2 or Shc was

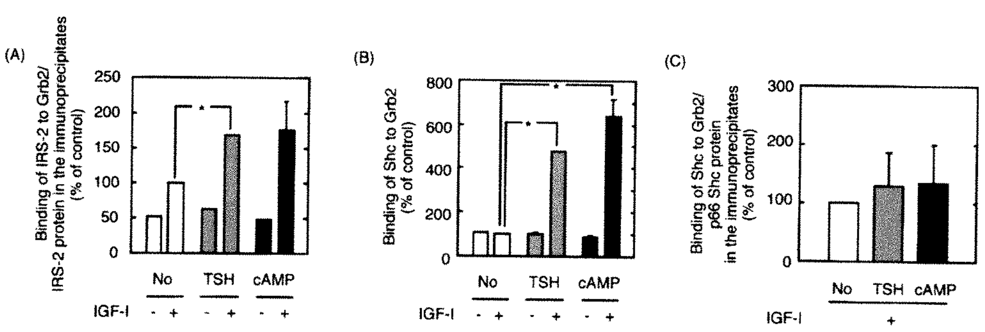

Figure 4 Effects of pretreatment with TSH or dibutyryl cAMP on binding of Grb2 to tyrosine-phosphorylated substrates stimulated by IGF-I

Quiescent FRTL-5 cells were pretreated without (No) or with TSH (1 nM) or dibutyryl cAMP (cAMP; 1 mM) for 24 h, washed twice with HBSS and incubated without or with 100 ng/ml IGF-I, for 2 min in the case of IRS-2 and for 5 min in the case of Shc. After treatment, cells were harvested and the cell lysate was subjected to immunoprecipitation with anti-IRS-2 antibody (**A**) or anti-Shc antibody (**B** and **C**), followed by SDS/12.5%-PAGE and immunoblotting with anti-Grb2 antibody plus anti-IRS-2 antibody or anti-Shc antibody, as described in the Experimental section. These experiments were performed on three independent occasions. The amounts of Grb2 and IRS-2 or Shc were quantified using NIH Image software. The extent of interaction between Grb2 and IRS-2 corrected for the amount of IRS-2 (**A**), the amount of Grb2 bound to Shc (**B**), and the extent of the interaction between Grb2 and Shc corrected for the amount of 66 kDa Shc (p66 Shc) (**C**) are presented as described for Figure 1(B); * indicates a significant difference ($P < 0.05$) between values obtained in cells pretreated with no additives and those pretreated with TSH or cAMP, followed by IGF-I treatment in all cases (unpaired *t*-test).

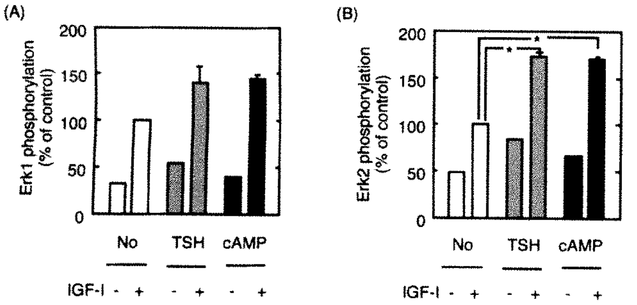

Figure 5 Effects of TSH or dibutyryl cAMP pretreatment on Erk activity stimulated by IGF-I

Quiescent FRTL-5 cells were pretreated without (No) or with TSH (1 nM) or dibutyryl cAMP (cAMP; 1 mM) for 24 h, washed twice with HBSS and incubated without or with 100 ng/ml IGF-I for 5 min. After treatment, cells were harvested and the cell lysate was subjected to immunoblotting with anti-phosphoErk antibody, as described in the Experimental section. These experiments were performed on three independent occasions. The amounts of phosphoErk1 (p44 MAP kinase) (**A**) and phosphoErk2 (p42 MAP kinase) (**B**) were quantified using NIH Image software, and are expressed as a percentage of the respective phosphoErk in cells pretreated with no additives followed by IGF-I treatment. Results represent the means ± S.E.M. of three independent experiments; * indicates a significant difference ($P < 0.05$) between values obtained in cells pretreated with no additives and those pretreated with TSH or cAMP, followed by IGF-I treatment in all cases (unpaired *t*-test).

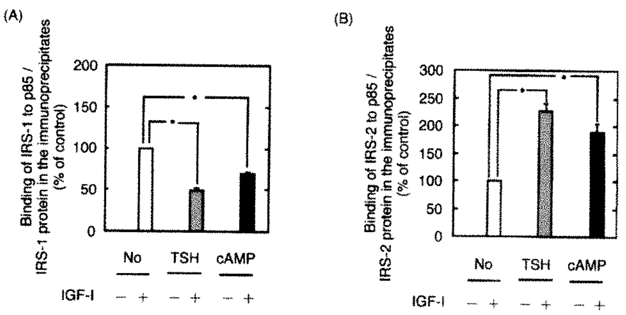

Figure 6 Effects of TSH or dibutyryl cAMP pretreatment on binding of the p85 regulatory subunit of PI 3-kinase to tyrosine-phosphorylated substrates stimulated by IGF-I

Quiescent FRTL-5 cells were pretreated without (No) or with TSH (1 nM) or dibutyryl cAMP (cAMP; 1 mM) for 24 h, washed twice with HBSS and incubated without or with 100 ng/ml IGF-I for 2 min. After treatment, cells were harvested and the cell lysate was subjected to immunoprecipitation with anti-IRS-1 antibody (**A**) or anti-IRS-2 antibody (**B**), followed by SDS/8%-PAGE and immunoblotting with anti-(p85 subunit of PI 3-kinase) antibody and an antibody against the respective IRS, as described in the Experimental section. These experiments were performed on three independent occasions. The amounts of p85 PI 3-kinase and of each IRS were quantified using NIH Image software. The extent of the interaction between the p85 subunit and IRS-1 or IRS-2, corrected for the amount of IRS, is presented as described for Figure 1(B); * indicates a significant difference ($P < 0.05$) between values obtained in cells pretreated with no additives and those pretreated with TSH or cAMP, followed by IGF-I treatment in all cases (unpaired *t*-test).

detected in response to IGF-I (Figures 4A and 4B), but association of Grb2 with IRS-1 was not observed (results not shown). cAMP pretreatment markedly increased Grb2 binding to Shc and slightly increased its binding to IRS-2 (Figures 4A and 4B). Figure 4(C) shows the extent of the interaction between Grb2 and Shc corrected for the amount of 66 kDa Shc protein, which was not affected by cAMP pretreatment.

From the results of the phosphoErk assay, cAMP increased the IGF-I-dependent phosphorylation of Erk, indicating that activation of Erk in response to IGF-I was enhanced by cAMP pretreatment (Figure 5). cAMP pretreatment was more effective in potentiating IGF-I-dependent Erk2 activation compared with that of Erk1.

Effects of cAMP pretreatment on the association of tyrosine-phosphorylated IRS-1 or IRS-2 with the p85 subunit of PI 3-kinase, followed by activation of PI 3-kinase

We also examined whether TSH or dibutyryl cAMP pretreatment affected the binding of tyrosine-phosphorylated substrates to the p85 regulatory subunit of PI 3-kinase, using co-immunoprecipitation with an antibody against IRS-1 or IRS-2. The PI 3-kinase p85 subunit was associated with tyrosine-phosphorylated IRS-1 and IRS-2 in response to IGF-I, but basal binding of p85 to IRS-1 or IRS-2 was not observed (Figures 6A and 6B). Although cAMP pretreatment decreased PI 3-kinase p85 subunit binding to IRS-1, its association with IRS-2 was increased by

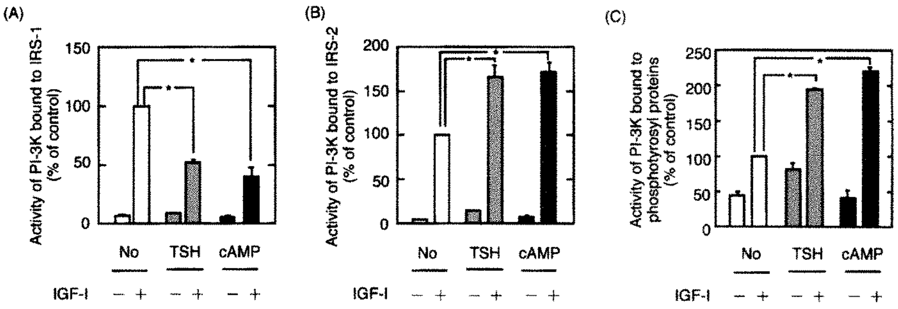

Figure 7 Effects of TSH or dibutyryl cAMP pretreatment on PI 3-kinase activity stimulated by IGF-I

Quiescent FRTL-5 cells were pretreated without (No) or with TSH (1 nM) or dibutyryl cAMP (cAMP; 1 mM) for 24 h, washed twice with HBSS and incubated with 100 ng/ml IGF-I for 2 min. PI 3-kinase activity in immunocomplexes obtained using anti-IRS-1 antibody (**A**), anti-IRS-2 antibody (**B**) or anti-phosphotyrosine antibody (**C**) was measured as described in the Experimental section. Each treatment was performed in triplicate in three independent experiments. PI 3-kinase activity is expressed as a percentage of the activity in cells pretreated with no additives followed by IGF-I treatment. Results represent means ± S.E.M. of three independent experiments; * indicates a significant difference ($P < 0.05$) between IGF-I-dependent activities in cells pretreated with no additives and those treated with TSH or cAMP (unpaired *t*-test).

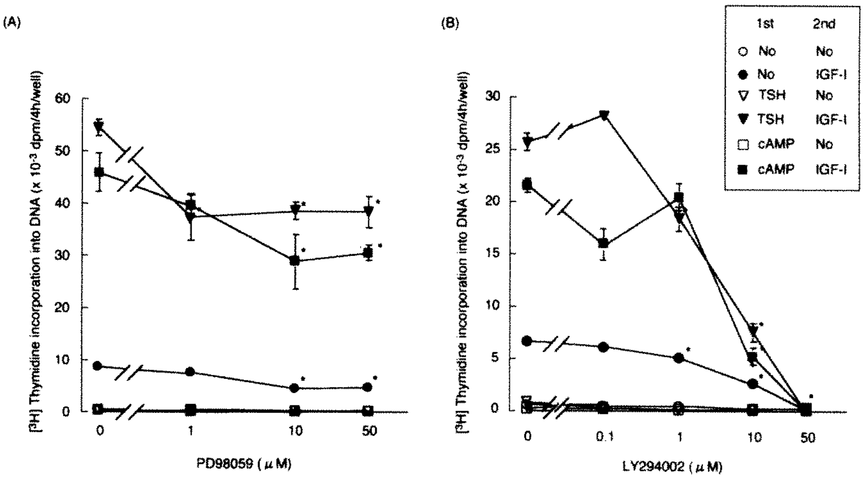

Figure 8 Effects of a MEK inhibitor or a PI 3-kinase inhibitor on DNA synthesis induced by cAMP and IGF-I

Quiescent FRTL-5 cells were pretreated with no additives (No) or with TSH (1 nM) or dibutyryl cAMP (cAMP; 1 mM) for 24 h. The cells were then washed three times with HBSS and incubated with or without IGF-I (100 ng/ml) for an additional 24 h in the absence or presence of various concentrations of PD98059 (**A**) or LY294002 (**B**). [*methyl*-^{3}H]Thymidine incorporation into DNA was measured during the final 4 h, as described in the Experimental section. Results are means ± S.E.M. of triplicate wells; * indicates a significant difference ($P < 0.05$) in thymidine incorporation in the presence of an inhibitor compared with in the absence of an inhibitor under each treatment condition.

cAMP pretreatment. Under these conditions, IGF-I-induced PI 3-kinase activity bound to IRS-2, but not that bound to IRS-1, was enhanced by cAMP pretreatment (Figures 7A and 7B). In addition, IGF-I caused PI 3-kinase activation in the immunoprecipitates, as assessed using an anti-phosphotyrosine antibody, and IGF-I-dependent PI 3-kinase activation was significantly potentiated by cAMP pretreatment (Figure 7C).

Effects of inhibition of MAP-kinase/Erk kinase (MEK) or PI 3-kinase on DNA synthesis in cells treated with cAMP and IGF-I

To study the physiological roles of the cAMP-dependent potentiation of Erk and PI 3-kinase activities stimulated by IGF-I, we measured DNA synthesis in cells pretreated with TSH or dibutyryl cAMP for 24 h, followed by IGF-I treatment for 24 h in the presence or absence of the MEK inhibitor PD98059 or the PI 3-kinase inhibitor LY294002. PD98059 partially inhibited a cAMP-dependent increase in DNA synthesis induced by IGF-I, in a concentration-dependent manner (Figure 8A). LY294002 strongly depressed IGF-I-dependent DNA synthesis after pretreatment with or without TSH or dibutyryl cAMP (Figure 8B).

DISCUSSION

We showed previously that pretreatment of FRTL-5 cells with cAMP potentiates the IGF-I-dependent tyrosine phosphorylation of various intracellular proteins, such as those of molecular mass 175–185 kDa and 90–100 kDa [21], although these proteins were not identified. These results suggested that the synergism between cAMP and IGF-I in the growth of these cells was correlated with changes in IGF-I-dependent tyrosine phosphorylation. Activation of cAMP-dependent signalling pathways has been reported to depress growth-factor-dependent signals [11–19], which are typically mediated by activation of tyrosine kinase receptors; however, especially in endocrine cells, it has become clear that cAMP may enhance IGF-I-dependent signals through novel mechanisms [34–37]. Accordingly, in the present study we investigated whether cAMP increases the tyrosine phosphorylation of known substrates of the IGF-I receptor, followed by enhancement of IGF-I-dependent signals, in FRTL-5 cells.

In FRTL-5 cells, brief treatment with cAMP has been shown to enhance insulin receptor or IGF-I receptor activation in response to the appropriate ligand; however, this enhancement vanished after a 2 h incubation with TSH [38]. In contrast, we have reported that prolonged cAMP treatment, e.g. for 24 h, decreased the IGF-I receptor number, but did not affect its affinity [21]. Our previous experiments further demonstrated that cAMP did not affect IGF-I-dependent autophosphorylation of the IGF-I receptor, or activation of its tyrosine kinase in response to IGF-I [21]. These results indicated that the long-term effects of cAMP on changes in tyrosine phosphorylation in response to IGF-I occurred at a step distal to tyrosine kinase activation of the IGF-I receptor.

In the present study, we first showed that tyrosine phosphorylation of IRS-2 stimulated by IGF-I is enhanced by cAMP pretreatment, but the IGF-I-dependent tyrosine phosphorylation IRS-1 is not (Figures 1 and 2). This enhancement requires long-term stimulation of the cAMP-dependent signalling pathway (results not shown). These results clearly indicate that tyrosine phosphorylation of each IRS is regulated in a distinct manner, even though IRS family members possess a similar structure [39], suggesting that each IRS has a different physiological role. Based on the results of immunoprecipitation with an antibody against each protein, tyrosine-phosphorylated proteins in the 175–185 kDa range include IRS-1 and IRS-2, but not IRS-4. During cAMP treatment, the amounts of IRS-1 and IRS-2 proteins, as judged by immunoblot analysis, were not changed significantly (Figures 1C and 2C), suggesting that the increase in the tyrosine phosphorylation of IRS-2 is not due to an increase in the amount of protein. It is possible to speculate that cAMP treatment modulates IRS-2 to increase the affinity of an IGF-I receptor or to decrease the affinity of a protein-tyrosine phosphatase to dephosphorylate IRS-2, depresses protein-tyrosine phosphatase activities, or changes the localization of IRS-2. Work to elucidate the mechanisms of the cAMP-dependent potentiation of tyrosine phosphorylation of IRS-2 induced by IGF-I is in progress in our laboratory.

Shc has been shown to have three protein isoforms, with molecular masses of 46 kDa, 52 kDa and 66 kDa. These isoforms are synthesized by using different translation start sites from two mRNAs produced by alternative splicing: one encodes 46 kDa and 52 kDa Shc, with the other encoding 46 kDa, 52 kDa and 66 kDa Shc [40,41]. In FRTL-5 cells, low-level tyrosine phosphorylation of 46 kDa and 52 kDa Shc was detected without IGF-I treatment. In contrast, IGF-I stimulated the tyrosine phosphorylation of 46 kDa, 52 kDa and 66 kDa Shc, and cAMP pretreatment prominently potentiated the IGF-I-dependent tyrosine phosphorylation of 66 kDa Shc (Figures 3A and 3B). In addition, cAMP treatment increased the amount of 66 kDa Shc protein (Figures 3D and 3E), and in fact the degree of IGF-I-dependent tyrosine phosphorylation of 66 kDa Shc normalized to its amount in the immunoprecipitates was not changed by cAMP pretreatment (Figure 3C), suggesting that cAMP-dependent potentiation of tyrosine phosphorylation of 66 kDa Shc induced by IGF-I is mainly due to an increase in the amount of protein. This mechanism could be an important point of interaction between the signalling pathways of cAMP and IGF-I. The expression and tyrosine phosphorylation of these three Shc isoforms in response to growth factors has been reported to be regulated differently in various cell types [41,42]. Based on these results, each isoform may have a different role in controlling cell behaviour. It has been reported that, unlike the other two isoforms, 66 kDa Shc has a collagen-homology 2 domain (CH2 domain) [41]. Studies of the physiological roles of CH2 domains are clearly required in the light of our findings and the intriguing findings of Pelicci and co-workers [41] that the CH2 domain is a negative regulator of the c-*fos* promoter.

It is well known that tyrosine-phosphorylated IRS family proteins and Shc are recognized by Grb2, one of the family of adaptor signal molecules that have SH2 and SH3 domains [43]. Grb2 associates with Sos, which is a GDP/GTP exchanger of Ras. These associations are followed by activation of the MAP kinase cascade, which is an important signal transduction pathway for cell growth and differentiation [44,45]. In FRTL-5 cells, we demonstrated that the amount of Shc–Grb2 complex formed in response to IGF-I was significantly increased by cAMP pretreatment (Figure 4B). However, the extent of the interaction between Shc and Grb2, when corrected for the amount of 66 kDa Shc protein in the immunoprecipitates, was not affected by cAMP pretreatment (Figure 4C). This suggests that the cAMP-dependent increase in binding of Grb2 to Shc induced by IGF-I was due mainly to an increase in the amount of 66 kDa Shc protein in response to cAMP treatment, as was also seen for the cAMP-dependent potentiation of 66 kDa Shc tyrosine phosphorylation induced by IGF-I. On the other hand, Grb2 binding to phosphorylated IRS-2 in response to IGF-I was slightly enhanced by cAMP pretreatment (Figure 4A), and this enhancement effect of cAMP was much smaller than its effect on Grb2 binding to Shc (Figure 4B). Since binding of Grb2 to phosphorylated IRS-1 was not detected in the present study, we assumed that the amount of Grb2 binding to IRS-1 must be very low in this cell line. These results, along with the cAMP-induced enhancement of IGF-I-dependent MAP kinase activation (Figure 5), are mainly the predicted consequence of the cAMP enhancement of IGF-I-dependent tyrosine phosphorylation of 66 kDa Shc.

Tyrosine-phosphorylated IRS-1 and IRS-2 associate with the p85 regulatory subunit of PI 3-kinase, resulting in activation of the PI 3-kinase cascade, which also controls various cell functions [31]. In the present study, pretreatment with cAMP decreased the amount of p85 subunit bound to phosphorylated IRS-1, but increased its binding to IRS-2 (Figures 6A and 6B). We could detect large amounts of PI 3-kinase p85 subunit in the supernatant after immunodepletion of IRS-1 and IRS-2 from the lysates of cells pretreated with TSH or dibutyryl cAMP (results not shown) These results indicate that the decrease in p85 subunit association with IRS-1 was not due to an increased interaction between p85 subunit and IRS-2. These changes in the amounts of the p85 subunit associated with IRS-1 or IRS-2 reflected well the PI 3-kinase activity that was bound to IRS-1 or IRS-2 (Figures 6 and 7). Furthermore, an IGF-I-dependent increase in PI 3-kinase activity in the immunoprecipitates, as detected with an anti-phosphotyrosine antibody, was amplified by cAMP pretreatment (Figure 7C), suggesting that total PI 3-kinase activity was increased through changes in IRS-2 tyrosine phosphorylation. Although the mechanisms leading to these changes remain to be elucidated, our new observations also support our hypothesis that IRS-1 and IRS-2 possess different roles in the mediation of IGF-I bioactivities in FRTL-5 cells.

Finally, we tested the effects of the presence of an inhibitor of each signalling pathway during IGF-I treatment on DNA synthesis in FRTL-5 cells pretreated with cAMP and then treated with IGF-I. cAMP-dependent potentiation of DNA synthesis induced by IGF-I was partially, but significantly, depressed by the MEK inhibitor PD98059 (Figure 8A). Thus potentiation by cAMP of the MAP kinase cascade in response to IGF-I could mediate, in part, the potentiation of cell growth stimulated by cAMP and IGF-I. In addition, LY294002, a PI 3-kinase inhibitor, completely abolished IGF-I-dependent DNA synthesis, whether or not there was cAMP pretreatment (Figure 8B). From these results, we conclude that PI 3-kinase activation is essential to mediate IGF-I-dependent cell growth in this cell line.

In the present study we have focused on the cAMP-dependent enhancement of IGF-I-dependent signals through changes in tyrosine phosphorylation, and shown this to be an important mechanism of the cross-talk between cAMP and growth factors. Other groups have shown that a cAMP stimulus changes the amount or activity of cyclin/Cdk (cyclin-dependent kinase)/Cdk inhibitor systems in FRTL-5 cells [46]. These mechanisms may be complementary in amplifying the traverse of cells through the cell cycle in response to IGF-I.

In summary, we have demonstrated that, in FRTL-5 cells, pretreatment with cAMP enhances the IGF-I-dependent tyrosine phosphorylation of IRS-2 and 66 kDa Shc. Our results suggest that the interaction between cAMP-dependent and IGF-I-dependent pathways leads to an augmentation of cell proliferation, which is mediated, at least in part, through the MAP kinase and PI 3-kinase signalling pathways. These effects are mediated by changes in the tyrosine phosphorylation of IGF-I receptor substrates, including IRS-2 and Shc.

We thank Dr Leonard Kohn (Section of Cell Regulation, NIDDK) and Interthyr Corp (Baltimore, MD, U.S.A) for the gift of FRTL-5 cells, and the National Hormone and Pituitary Program (NIDDK) for providing bovine TSH (lot #AFP-3950B) Recombinant human IGF-I was kindly donated by Dr Toshiaki Ohkuma (Fujisawa Pharmaceutical Co) We also express our appreciation to Dr Takaaki Aoyagi (Institute of Microbial Chemistry, Tokyo, Japan) for providing leupeptin and pepstatin In addition, we acknowledge Dr Takao Yamori and Dr Tomoichiro Asano for donating anti-phosphotyrosine monoclonal antibody and anti-IRS-3 and -IRS-4 antibodies respectively Finally, we acknowledge the helpful discussions during the writing of this paper with Dr Judson J. Van Wyk (University of North Carolina, Chapel Hill, NC, U S A.) and Dr Steven C. Boyages (Westmead Hospital, University of Sydney, NSW, Australia) This work was supported by a Grant-in-Aid for International Joint Research from the Ministry of Education, Science and Culture of Japan (to S-I T ; no 08044193)

REFERENCES

1 Johns, J I and Clemmons, D R (1995) Endocr Rev **16**, 3–34
2 LeRoith, D, Werner, H, Beitner-Johnson, D and Roberts, Jr, C T (1995) Endocr Rev **16**, 143–163
3 Stiles, C D, Capone, G T, Scher, C D, Antoniades, H N, Van Wyk, J J and Pledger, W J (1979) Proc Natl Acad Sci U S A **76**, 1279–1283
4 Adashi, E Y, Resnick, C E, Svoboda, M E and Van Wyk, J J (1985) Endocrinology **116**, 2135–2142
5 Kurtz, A, Hartl, W, Jelkmann, W, Zapf, J and Bauer, C. (1985) J. Clin Invest **76**, 1643–1648
6 Tramontano, D, Moses, A C, Veneziani, B M and Ingbar, S. H (1988) Endocrinology **122**, 127–132
7 Cala, J F and Rosenfield, R L (1988) Endocrinology **124**, 2365–2372
8 Friger-Gaillard, B, Hossenlopp, P, Adolphe, M and Binoux, M (1989) Endocrinology **124**, 2365–2372
9 Thorsen, T, Lahooti, H, Rasmussen, M and Aakvaag, A (1992) J Steroid Biochem Mol Biol **41**, 537–540
10 Koide, T, Ono, Y, Akahori, M, Nedachi, T, Hakuno, F, Takenaka, A, Takahashi, S-I and Noguchi, T (1998) Endocr J **45**, 151–163
11 Stadmauer, L and Rosen, O M (1986) J Biol Chem **261**, 3402–3407
12 Roth, R A and Beaudoin, J (1987) Diabetes **36**, 123–126
13 Magnaldo, I, Pouyssegur, J and Paris, S (1989) FEBS Lett **245**, 65–69
14 Grave, L M, Bornfeld, K E, Raines, E W, Potts, B C, Macdonald, S G., Ross, R and Krebs, E G (1993) Proc Natl Acad Sci U S A **90**, 10300–10304
15 Wu, J, Dent, P, Jelinek, T, Wolfman, A, Webwer, M J and Sturgill, T W (1993) Science **262**, 1069–1072
16 Cook, S J and McCormick, F (1993) Science **262**, 1069–1072
17 Burgering, B M T., Pronk, G J, Van Weeren, P C., Chardin, P and Bos, J L (1993) EMBO J **12**, 4211–4220
18 Hordijk, P L, Verlaan, I, Jalink, K, Van Corven, E J and Moolenaar, W H (1994) J Biol Chem **269**, 3534–3538
19 Calleja, V., Enriquez, P R, Filloux, C, Peraldi, P, Baron, V and Van Obberghen, E (1997) Endocrinology **138**, 1111–1120
20 Takahashi, S-I, Conti, M and Van Wyk, J J (1990) Endocrinology **126**, 736–745
21 Takahashi, S-I, Conti, M, Prokop, C, Van Wyk, J J and Earp, III, H S (1991) J Biol Chem **266**, 7834–7841
22 Grønborg, M, Wulff, B S, Rasmussen, J S, Kjeldsen, T and Gammeltoft, S (1993) J Biol Chem **268**, 23435–23440
23 Florini, J R, Ewton, D Z and Coolican, S A (1996) Endocr Rev **17**, 481–517
24 Giorgetti, S, Ballotti, R, Kowalski-Chauvel, A, Tartare, S. and Van Obberghen, E (1993) J Biol Chem. **268**, 7358–7364
25 Craparo, A A, O'Neill, T J and Gustafson, T A (1995) J Biol Chem **270**, 15639–15643
26 Sawka-Verhelle, D, Tartare-Deckert, S, White, M F and Van Obberghen, E (1996) J Biol Chem **271**, 5980–5983
27 Beitner-Johnson, D and LeRoith, D (1995) J Biol Chem **270**, 5187–5190
28 Gual, P, Baron, V, Lequoy, V and Van Obberghen, E (1998) Endocrinology **139**, 884–893
29 Sun, X J, Pons, S, Wang, L-M, Zhang, Y, Yenush, L, Burks, D, Myers, Jr, M G, Glasheen, E, Copeland, N G, Jenkins, N A et al (1997) Mol Endocrinol **11**, 251–263
30 Li, N, Batzer, A, Daly, R, Yajnik, V, Skolnik, E, Chardin, P, Bar-Sagi, D., Margolis, B and Schlessinger, J (1993) Nature (London) **363**, 85–88
31 Shepherd, P R, Withers, D J and Siddle, K (1998) Biochem J **333**, 471–490
31a Ambesi-Impiombato, F S, Parks, L A M and Coon, H G (1980) Proc Natl Acad Sci U S A **77**, 3455–3459
32 Ito, Y, Uchijima, Y, Ariga, M, Seki, T, Takenaka, A, Hakuno, F, Takahashi, S-I, Ariga, T and Noguchi, T (1997) Biochem J **324**, 379–388
33 Whitman, M, Kaplan, D R., Schaffhausen, B, Cantley, L and Roberts, T M (1985) Nature (London) **315**, 239–242
34 Lombardi, A, Veneziani, B M, Tramontano, D and Ingbar, S H (1988) Endocrinology **123**, 1544–1552
35 Dai, Z, Takahashi, S-I, Van Wyk, J J and D'Ercole, A J (1992) Endocrinology **130**, 3175–3183
36 Takano, T, Takada, K, Tada, H, Nishiyama, S and Amino, N (1994) Endocr Res **20**, 235–245
37 Talavera, F, Chen, Z and Menon, K M J (1996) Biochim Biophys Acta **1310**, 10–18
38 Condorelli, G, Formisano, P, Miele, C and Beguinot, F (1992) Endocrinology **130**, 1615–1635
39 Sun, X J, Wang, L-M, Zhang, Y, Yenush, L, Myers, Jr, M G, Glasheen, E, Lane, W S, Pierce, J H and White, M F (1995) Nature (London) **377**, 173–177
40 Pelicci, G, Lanfrancone, L, Grignani, F, McGlade, J, Cavallo, F., Forni, G, Nicoletti, I, Grignani, F, Pawson, T and Pelicci, P G (1992) Cell **70**, 93–104
41 Migliaccio, E, Mele, S, Salcini, A E, Pelicci, G, Lai, K M, Superti-Furga, G, Pawson, T, Di Fiore, P P., Lanfrancone, L and Pelicci, P G (1997) EMBO J **16**, 706–716
42 Pelicci, G, Lanfrancone, L, Salcini, A E, Romano, A, Mele, S, Borrello, M G, Segatto, O, Di Fiore, P P and Pelicci, P G (1995) Oncogene **11**, 899–907
43 Lowenstein, E J, Daly, R J, Batzer, A G., Li, W, Margolis, B, Lammers, R, Ullrich, A, Skolnik, E Y, Bar-Sagi, D and Schlessinger, J (1992) Cell **70**, 431–442
44 Pelech, S L and Sanghera, J S (1993) Trends Biochem Sci **17**, 233–238
45 Blumer, K J and Johnson, G L (1994) Trends Biochem Sci **19**, 236–240
46 Yamamoto, K, Hirai, A, Ban, T, Saito, J, Tahara, K, Terano, T, Tamura, Y, Saito, Y and Kitagawa, M (1996) Endocrinology **137**, 2036–2042

Received 12 October 1999/24 February 2000, accepted 20 March 2000

Phosphocholine-containing, zwitterionic glycosphingolipids of adult *Onchocerca volvulus* as highly conserved antigenic structures of parasitic nematodes

Manfred WUHRER*[1], Sandra RICKHOFF*[1], Roger D. DENNIS*, Günter LOCHNIT*, Peter T. SOBOSLAY†, Stefan BAUMEISTER‡ and Rudolf GEYER*[2]

*Biochemisches Institut, Justus-Liebig-Universität, Friedrichstrasse 24, D-35392 Giessen, Germany, †Institut fur Tropenmedizin, Universitat Tubingen, Tubingen, Germany, and ‡Fachbereich Biologie, Zoologie, Philipps-Universität Marburg, Marburg, Germany

Human *Onchocerca volvulus* infection sera were found to recognize zwitterionic glycolipids of *O. volvulus* and to cross-react with those of other parasitic nematodes (*Ascaris suum*, *Setaria digitata* and *Litomosoides sigmodontis*). By the use of an epitope-specific monoclonal antibody, zwitterionic glycolipids of all these nematode species were observed to contain the antigenic determinant phosphocholine. A hyperimmune serum specific for arthro-series glycolipid structures reacted with the various neutral glycolipids of all these nematodes, which demonstrated that their oligosaccharide moieties belonged to the arthro-series of protostomial glycolipids. These results indicated that arthro-series glycosphingolipids carrying, in part, phosphocholine substituents, represent highly conserved, antigenic glycolipid markers of parasitic nematodes. Three glycolipid components of the *O. volvulus* zwitterionic fraction were structurally characterized by matrix-assisted laser-desorption/ionization time-of-flight MS, methylation analysis and exoglycosidase treatment. Their chemical structures were elucidated to be phosphocholine-6GlcNAc(β1-3)Man(β1-4)Glc(1-1)ceramide, GalNAc(β1-4)-[phosphocholine-6]GlcNAc(β1-3)Man(β1-4)Glc(1-1)ceramide and Gal(α1-3)GalNAc(β1-4)[phosphocholine-6]GlcNAc(β1-3)-Man(β1-4)Glc(1-1)ceramide for the zwitterionic ceramide tri-, tetra- and penta-hexosides respectively. The ceramide composition was found to be dominated by 2-hydroxylated docosanoic ($C_{22h\ 0}$), tricosanoic ($C_{23h\ 0}$) and tetracosanoic ($C_{24h\ 0}$) acids, and C_{17} sphingosine ($C_{d17\ 1}$) (where $_h$ is hydroxylated and $_d$ is dihydroxylated).

Key words: glycolipids, phosphocholine, on-target enzymic cleavage, parasitic filarial nematodes.

INTRODUCTION

The antigenic determinant phosphocholine (PC) has been found to be the structural basis for the immunological cross-reactivity of zwitterionic glycolipids from various parasitic nematodes [1–3]. Zwitterionic glycolipids of *Litomosoides sigmodontis* (= *carinii*) and *Ascaris suum* reacted with homologous and heterologous infection sera derived from animals experimentally infected with *A. suum*, *L. sigmodontis* and *Nippostrongylus brasiliensis* [2,3]. In addition, zwitterionic glycolipids from *L. sigmodontis*, which is a rodent laboratory model for filariases, were recognized by sera from humans infected with *Onchocerca volvulus*, *Brugia malayi*, *Loa loa*, and *Strongyloides stercoralis* [3]. Detailed structural analysis of the zwitterionic glycolipid antigens of parasitic nematodes has been performed for two components bearing the PC substituent, which were derived from the porcine parasite *A. suum*, that yielded the structures Gal(α1-3)-GalNAc(β1-4)[PC-6]GlcNAc(β1-3)Man(β1-4)Glc(β1-1)Cer (component A) and Gal(α1-3)GalNAc(β1-4)[PC-6]GlcNAc(β1-3)[PE-6]Man(β1-4)Glc(β1-1)Cer [component C; containing PC and phosphoethanolamine (PE) substituents] [1]. Both components were found to be biologically active in inducing human peripheral-blood mononuclear cells to release the proinflammatory monokines tumour necrosis factor α, interleukin 1 and interleukin 6, whilst the biological activity was dependent on the presence of the PC substituent [1].

Besides these immunological, biological and structural analyses of glycolipid-conjugated PC, macromolecules containing PC have been detected using monoclonal antibodies (mAbs) in extracts of numerous species of parasitic nematodes [4–7]. They have been localized to the pseudocoelomic cavity (inner cuticular surface and intestinal lining) in adult males and the reproductive tract (uterine endothelium and embryo membranes) in adult females of the human filarial nematode *B. malayi* [4].

The excretory/secretory PC-containing protein ES-62, secreted by *Acanthocheilonema viteae*, has been structurally analysed to show PC attached to N-linked glycans [8–11], comprising substoichiometrically fucosylated, truncated, complex-type structures ($Fuc_{0-1}Man_3GlcNAc_{3-6}$; [12]). The location of the substitution is likely to be to GlcNAc residues present as either mono-, di-, tri- or tetra-antennary, monomeric stubs [12] or as up to pentameric, (β1-4)-linked, chito-oligomeric antennae [13]. Both PC-substituted, N-glycan families have been shown to be similarly conserved in the human filarial nematode *O. volvulus* and its bovine analogue *Onchocerca gibsoni* [13]. The protein-bound PC determinant is not restricted to N-linked glycans, being predominantly present on O-glycans in *O. gibsoni* [5]. The longevity of filarial nematode infections and frequently associated modulation of the host's immune response have been correlated with the release of PC-containing excretory–secretory protein products, and related to their immunomodulatory/suppressive properties, i. e., the inhibition of polyclonal activation/pro-

---

Abbreviations used CDH, ceramide dihexoside, CMH, ceramide monohexoside, CPH, ceramide pentahexoside, CTetH, ceramide tetrahexoside; CTH, ceramide trihexoside, GC–MS, gas chromatography–MS, HexNAc, *N*-acetylhexosamine, HPTLC, high-performance TLC, mAb, monoclonal antibody, Int, intensity, MALDI-TOF-MS, matrix-assisted laser-desorption/ionization time-of-flight MS, PC, phosphocholine, PE, phosphoethanolamine, TFA, trifluoroacetic acid, $_h$, $_d$ and $_t$, hydroxylated, dihydroxylated and trihydroxylated, ΔM, mass difference

[1] These authors contributed equally to this work

[2] To whom correspondence should be sent (e-mail rudolf geyer@biochemie med uni-giessen de)

liferation of human T- and murine B-lymphocytes *in vitro* [14–16]. Such PC-containing excretory–secretory products may play a role in the B- and T-lymphocyte hyporesponsiveness of human filariases. They have been implicated, following ligation, with selectively uncoupling the antigen–receptor and associated protein tyrosine kinase complex from signalling cascades responsible for the transduction of signals for activation, transcription and proliferation [17–19]. This immunomodulation of T- and B-cells has been considered to be an escape mechanism by which the filarial parasite avoids both cell-mediated and humoral immunity.

In the present study we have disclosed by immunostaining and detailed structural analysis that PC-containing glycosphingolipids are highly conserved among parasitic nematodes, which parallels the known presence of PC-containing glycoprotein glycans of different filarial nematodes [10,11,13].

Some of the results reported here have already been presented at the International GlycoBioTechnology Symposium, held in Braunschweig, Germany, on 3–8 May 1998.

EXPERIMENTAL

Isolation and purification of glycolipids

An adult *O. volvulus* worm homogenate was used for the preparation of worm-derived antigen, as described previously [20]. Freeze-dried worm pellets (350 mg) were stored at −20 °C until lipid extraction. Glycolipids were isolated by consecutive extractions as described elsewhere [21]. Raw extracts were saponified in 50 ml of methanolic 0.1 M NaOH for 2 h at 37 °C. Salts and hydrophilic contaminants were removed by reverse-phase chromatography (Chromabond $C18_{ec}$; Macherey–Nagel, Düren, Germany; [22]) and the glycolipids were fractionated on a DEAE-Sephadex column (10 mm × 50 mm, A-25, acetate form; Pharmacia, Freiburg, Germany) as outlined previously [22]. The neutral-fraction glycolipids were resolved on a silica-gel cartridge (Waters, Eschborn, Germany), as described elsewhere [2], and analysed by matrix-assisted laser-desorption/ionization time-of-flight MS (MALDI-TOF-MS), as well as high-performance TLC (HPTLC) and orcinol/H_2SO_4 staining. The fractions chloroform/methanol (19:1, v/v) to chloroform/methanol (1:1, v/v) contained neutral glycolipids and were pooled and purified by Florisil chromatography [22]. The fractions chloroform/methanol/water (60:35:8, by vol.) and (15:30:4, by vol.) contained glycolipids that migrated similarly to *A. suum* zwitterionic glycolipids on HPTLC [2] and gave similar MALDI-TOF-MS spectra [1], and were thus pooled and designated the 'zwitterionic fraction'. Glycolipids from adult *Setaria digitata* worms were extracted analogously, the crude extract was desalted by reverse-phase chromatography and used for HPTLC analyses without further purification. Glycolipids from adult *A. suum* worms, and *L. sigmodontis* microfilariae and adult females were isolated as described previously [2,3].

HPTLC

HPTLC, orcinol/H_2SO_4 staining and immunostaining were performed as described elsewhere [23]. On immunostaining, sera from four patients with an *O. volvulus* infection, an anti-arthro [30]-series rabbit hyperimmune serum (G. Lochnit, R. D. Dennis, S. Nispel and R. Geyer, unpublished work) and the PC-specific mouse mAb TEPC-15 (Sigma, Deisenhofen, Germany) were applied as primary antibodies. Goat horseradish peroxidase-conjugated anti-rabbit Ig and rabbit horseradish peroxidase-conjugated anti-mouse Ig (Dako Diagnostics, Hamburg, Germany), as well as rabbit horseradish peroxidase-conjugated anti-human Ig (Sigma), were used as secondary antibodies (diluted 1:1000). Staining was performed using a chloronaphthol/diethylphenylenediamine substrate mixture as described previously [23].

HF and exoglycosidase treatment

HF treatment of zwitterionic glycolipids from *O. volvulus* and *A. suum* was performed as described previously [1]. For exoglycosidase cleavage, HF-treated glycolipids were taken up in 50 μl of 50 mM sodium citrate buffer, pH 6.0, containing 1 g/litre sodium taurodeoxycholate and incubated at 37 °C for 24 h with 250 m-units of α-galactosidase from green coffee (*Coffea* sp.) beans (Roche Diagnostics, Mannheim, Germany). Enzyme addition was repeated after 12 h. The sample was purified by anion-exchange chromatography on a DEAE-Sephadex column [2] and the resultant neutral fraction analysed by HPTLC orcinol/H_2SO_4 staining, MALDI-TOF-MS and methylation analysis.

Carbohydrate composition and methylation analysis

Glycolipids were hydrolysed in aq. 4 M trifluoroacetic acid (TFA) for 4 h at 100 °C and analysed as their alditol acetates by gas chromatography (GC) [24]. For linkage analysis, glycolipids were permethylated, being either untreated, before or after HF treatment and hydrolysed (4 M TFA, 4 h, 100 °C). Partially methylated alditol acetates obtained after sodium borohydride reduction and peracetylation were analysed by capillary GC–MS, using the instrumentation and microtechniques described elsewhere [25].

MALDI-TOF-MS and on-target enzymatic cleavage

MALDI-TOF-MS and on-target enzymatic cleavage was performed using the instrumentation and methods described previously [26]. For on-target enzymic cleavage, α-galactosidase from green coffee beans (Roche Diagnostics), β-*N*-acetylhexosaminidase from jack beans (*Canavalia ensiformis*; Sigma) and β-mannosidase from snail acetone-dried powder (Sigma) were used.

Ceramide analysis

The zwitterionic glycolipid fractions of *O. volvulus* and *A. suum* were treated with 200 μl of anhydrous 1 M methanolic HCl for 16 h at 80 °C. The released fatty acid methyl esters were separated from the remaining sphingoid bases and saccharide residues by a three-fold phase partition against n-hexane. The pooled n-hexane partitions were dried down under N_2. Fatty acid methyl esters were analysed by GC–MS (Finnigan, Sunnyvale, CA, U.S.A., model 4500) using a fused-silica capillary column (Optima 210, 0.25 mm internal diameter, 30 m long; Macherey–Nagel). The temperature was increased from 100 °C, at 4 °C/min, to a final temperature of 280 °C. Spectra were recorded in the positive-ion mode after electron-impact ionization (70 eV; source temperature 190 °C). For sphingoid base analysis, as a modification of the method described by Zanetta et al. [27], the lower methanol partition was dried under N_2 and, after addition of 200 μl of acetonitrile and 25 μl of pentafluoropropionic anhydride (Supelco, Deisenhofen, Germany), the sample was heated for 30 min at 150 °C, dried under N_2 and taken up in acetonitrile. Samples were analysed by GC–MS using fused-silica capillary columns [Optima 5 (0.25 mm internal diameter, 30 m long) and Optima 210 (as described above; Macherey–Nagel)]. The injector temperature was 280 °C, and the column temperature was increased from 130 °C, at 6 °C per min, to a final temperature of 250 °C. GC–MS was performed in the negative-ion mode after chemical ionization with ammonia at 150 eV and in the positive-ion mode after electron-impact ionization (70 eV, source temperature 190 °C). For identification, $C_{d18:1}$, $C_{d18:0}$ and $C_{t18:0}$ (where $_t$ is trihydroxylated) standards (Sigma) were used.

RESULTS

PC and the arthro-series motif as common determinants of parasitic nematode lipid-bound carbohydrate structures

Neutral and zwitterionic glycolipids from *O. volvulus* were compared immunochemically with the corresponding glycolipid fractions from *A. suum* adults [1,21], *S. digitata* adults and *L. sigmodontis* microfilariae and adult females (Figure 1). Neutral glycolipids were revealed by HPTLC–immunostaining using an anti-arthro-series hyperimmune serum raised against *A. suum* neutral-fraction glycolipids (Figure 1A). This serum detected co-migrating ceramide trihexoside (CTH) and ceramide pentahexoside (CPH) components in all four nematode species examined. Human *O. volvulus* infection serum revealed cross-reactive zwitterionic glycolipids in all four parasitic nematode species surveyed (Figure 1B). This cross-reactivity, at least in part, would appear to be due to the common antigenic determinant PC being present on all these glycolipids, as indicated by their immunoreactivity with the PC-specific mAb TEPC-15 (Figure 1C). All four nematode species exhibited a band with migration properties similar to those of component A, which has been structurally analysed ([1]; Figure 1C, lanes 2–6). When comparing the chemical and immunological staining of *A. suum* zwitterionic glycolipids (Figures 1B and 1C), component C, which was one of the chemically dominant glycolipids, was only weakly recognized immunologically by the *O. volvulus* infection serum (Figure 1B, lane 3) and mAb TEPC 15 (Figure 1C, lane 3). In contrast, the fastest-migrating *A. suum* zwitterionic glycolipid was strongly recognized by the mAb TEPC 15 (Figure 1C, lane 3); however, chemically it was found to be a minor component (Figure 1C, lane 1). The comparative immunochemical HPTLC staining (Figure 1) indicated that arthro-series glycosphingolipids carrying, in part, PC substituents, represented highly conserved antigens among parasitic nematodes.

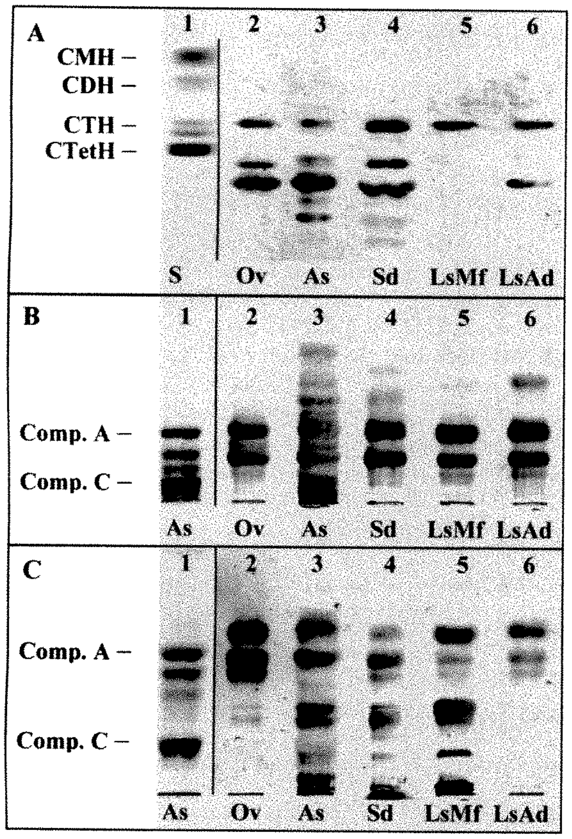

Figure 1 HPTLC–immunostaining of neutral and zwitterionic glycolipids from different, parasitic nematodes

(**A**) Neutral glycolipids were separated by HPTLC [running solvent chloroform/methanol/aq. 0.25% KCl (5:4:1, by vol.)] and revealed with anti-arthro-series hyperimmune serum (lanes 2–6; dilution 1:100). (**B**) Zwitterionic glycolipids were resolved by HPTLC (running solvent as in **A**) and revealed with a pool of four human *O. volvulus*-infection sera (lanes 2–6; dilution 1:100). (**C**) Zwitterionic glycolipids were separated by HPTLC [(running solvent chloroform/methanol/water (10:10:3, by vol.)] and revealed with the PC-specific mAb TEPC-15 (lanes 2–6; dilution 1:500). A globoside standard mixture containing CMH-CTetH (**A**, lane 1) and *A. suum* zwitterionic glycolipids (**B**, lane 1 and **C**, lane 1) were revealed by orcinol/H_2SO_4 staining. Comp. A, component A; Comp. C, component C as *A. suum* zwitterionic glycolipids of known structure. Glycolipid fractions were derived from: Ov, *O. volvulus* adults; As, *A. suum* adults; Sd, *S. digitata* adults; LsMf, *L. sigmodontis* microfilariae; LsAd, *L. sigmodontis* adult females.

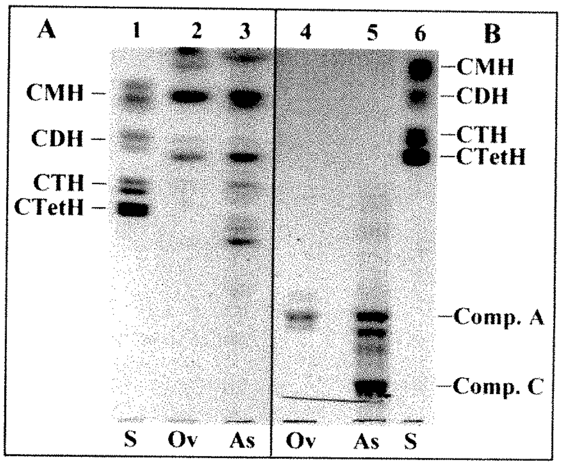

Figure 2 HPTLC–orcinol/H_2SO_4 staining of *O. volvulus* and *A. suum* neutral and zwitterionic glycolipids

(**A**) Neutral glycolipids of *O. volvulus* (lane 2) and *A. suum* (lane 3) were separated by HPTLC using the running solvent chloroform/methanol/aq. 0.25% KCl (5:4:1, by vol.). (**B**) Zwitterionic glycolipids of *O. volvulus* (lane 4) and *A. suum* (lane 5) were resolved by HPTLC using the running solvent chloroform/methanol/water (10:10:3, by vol.). Comp. A, component A; Comp. C, component C as *A. suum* zwitterionic glycolipids of known structure. The globoside standard (S) of CMH-CTetH corresponded to ceramide mono-, di-, tri- and tetra-saccharides respectively. Ov, *O. volvulus*; As, *A. suum*.

Neutral and zwitterionic glycolipids from *O. volvulus* were also compared by HPTLC and chemical staining with the equivalent fractions from *A. suum* adults. The *O. volvulus* neutral glycolipid fraction was further purified by Florisil chromatography and collated by HPTLC (Figure 2A). Both nematodes exhibited ceramide monohexoside (CMH) and ceramide dihexoside (CDH) species of identical migration properties. Although significant amounts of apparent CTH and CPH species were present in *A. suum* (Figure 2A, lane 3), for *O. volvulus* these components could not be detected (Figure 2A, lane 2). In parallel, *O. volvulus* zwitterionic glycolipids, without further purification, were collated by HPTLC (Figure 2B). The chemically predominant

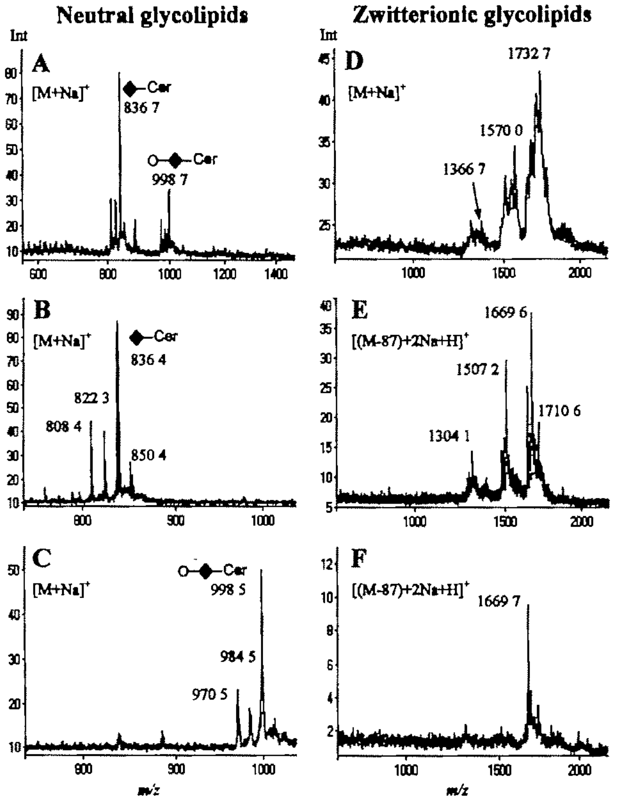

Figure 3 MALDI-TOF-MS analysis of *O. volvulus* neutral as well as *O. volvulus* and *A. suum* zwitterionic glycolipids

(**A**) *O volvulus* total neutral glycolipids; (**B** and **C**) *O volvulus* purified CMH and CDH compounds, respectively, (**D** and **E**) *O volvulus* zwitterionic glycolipids, (**F**) *A suum* zwitterionic glycolipid component A Analyses were performed in the positive-ion reflectron (**A–C**, **E** and **F**) or linear (**D**) modes Pseudomolecular ions are given in monoisotopic masses (reflectron mode) or average masses (linear mode) rounded to one decimal place ○, Man; ◆, Glc, Cer, ceramide

O. volvulus zwitterionic glycolipid component co-migrated with the *A. suum* zwitterionic glycolipid component A, whose structure has been previously elucidated [1].

Structural analysis of *O. volvulus* neutral glycolipids

MALDI-TOF-MS of the *O. volvulus* neutral glycolipid fraction (Figure 3A) revealed the pseudomolecular ions $[M+\mathrm{Na}]^+$ for CMH and CDH only. Neutral glycolipids were fractionated on a silica-gel cartridge and the purified CMH and CDH species re-analysed by MALDI-TOF-MS. The CMH mass spectrum (Figure 3B) exhibited pseudomolecular ions $[M+\mathrm{Na}]^+$ at *m/z* 808.4, 822.3, 836.4 and 850.4. The dominant Na^+ adduct at *m/z* 836.4 corresponded to a major pseudomolecular ion observed for *A. suum* CMH at *m/z* 837 [21]. The CDH mass spectrum (Figure 3C) revealed signals at *m/z* 970.5, 984.5 and 998.5. The mass difference (ΔM) between respective CMH and CDH ions of 162 Da corresponded to one hexose residue. Again, the dominant CDH pseudomolecular ion at *m/z* 998.5 coincided with the Na^+ adduct of a major *A. suum* CDH species at *m/z* 998 [21].

Methylation analysis of the total neutral glycolipid fraction revealed terminal Glc, 4-substituted Glc, terminal Man and terminal Gal in the relative amounts 1.0:0.45:0.3:0.05 respectively. Methylation analysis of isolated CDH resulted in the ratio of terminal Man to 4-substituted Glc of 0.5:1.0 respectively. On-target enzymic cleavage of CDH with β-mannosidase resulted in the loss of one hexose residue and shifted the CDH pseudomolecular ions ($[M+\mathrm{Na}]^+$) from 998.5, 984.5 and 970.5 to 837.1, 823.1 and 809.1 respectively. Hence methylation analyses and on-target enzymic cleavage indicated CDH to be Man(β-4)-Glc(1-1)Cer and CMH to be Glc(1-1)Cer.

Structural analysis of *O. volvulus* zwitterionic glycolipids

MALDI-TOF-MS of *O. volvulus* zwitterionic fraction glycolipids revealed major pseudomolecular ions of characteristic PC fragmentation at *m/z* 1669.6, 1507.2 and 1304.1 in the positive-ion reflectron mode {$[(M-87)+2\mathrm{Na}+\mathrm{H}]^+$; loss of choline; Figure 3E} and corresponding ions at *m/z* 1732.7, 1570.0 and 1366.7 in the positive-ion linear mode ($[M+\mathrm{Na}]^+$; Figure 3D). Again, the dominant ions at *m/z* 1669.6 (Figure 3E) and 1732.7 (Figure 3D) were in agreement with the *A. suum* zwitterionic glycolipid component A (Figure 3F; [1]). Carbohydrate composition analysis of the native *O. volvulus* zwitterionic glycolipid fraction revealed the monosaccharide molar ratios for Gal/Glc/Man/GalNAc to be 0.65.1.65:1.0:1.0 respectively. In order to confirm the presence of the arthro-series carbohydrate structure and to determine the position(s) of the phosphodiester sub-

Table 1 Methylation analysis of *O. volvulus* total zwitterionic glycolipid fraction

The partially methylated monosaccharide derivatives obtained after hydrolysis, reduction and peracetylation were analysed by GC–MS Results are expressed as peak ratios of the alditol acetates found on the basis of 2,4,6 ManOH = 1.0 Gal(1- as linkage corresponded to 2,3,4,6-GalOH or 2,3,4,6-tetra-*O*-methylgalactitol as alditol acetate, GalNAc(1- as linkage corresponded to 3,4,6-GalN(Me)AcOH or 2-deoxy-2-(*N*-methyl)acetamido-3,4,6-tri-*O*-methylgalactitol as alditol acetate, etc **Bold type** has been used to denote significant differences in composition after the various treatments α-Gal'ase, α-galactosidase

		Relative amount				
Linkage	Treatment	Native	Methylation preceded by HF treatment	Methylation followed by HF treatment	Methylation preceded by HF/α-Gal'ase treatments	Partially methylated alditol acetate
Gal(1-		0.5	0.3	0.65	–	2,3,4,6-GalOH
-4)Glc(1-		0.9	1.0	1.0	0.8	2,3,6-GlcOH
-3)Man(1-		1.0	1.0	1.0	1.0	2,4,6-ManOH
GlcNAc(1-		–	0.3	–	0.15	3,4,6-GlcN(Me)AcOH
GalNAc(1-		0.45	0.15	0.5	**0.80**	3,4,6-GalN(Me)AcOH
-3)GalNAc(1-		0.65	0.3	0.75	–	4,6-GalN(Me)AcOH
-4)GlcNAc(1-		–	**0.75**	–	**0.65**	3,6-GlcN(Me)AcOH
-4,6)GlcNAc(1-		–	–	**0.55**	–	3-GlcN(Me)AcOH

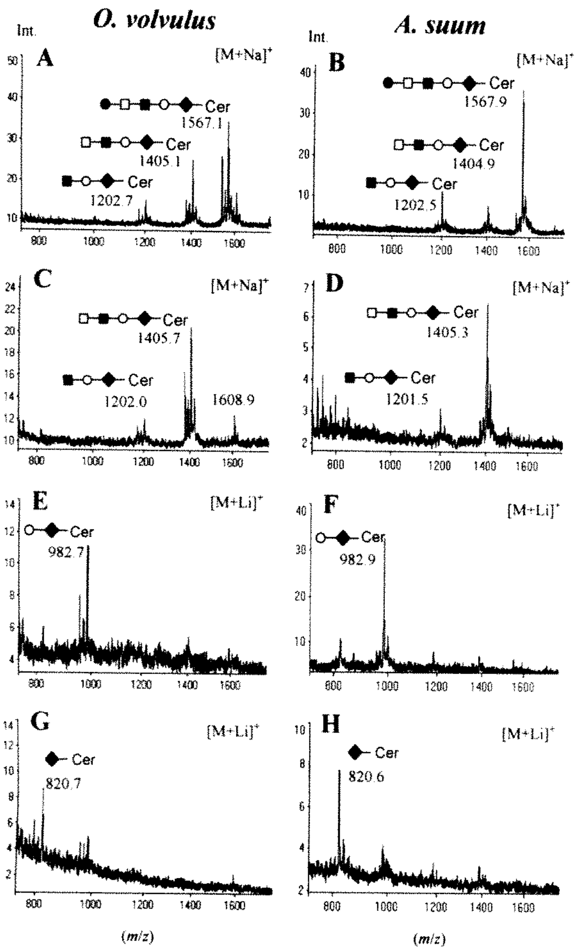

Figure 4 MALDI-TOF mass spectra of the products of on-target sequential exoglycosidase treatments of *O. volvulus* (left column) and *A. suum* (right column) HF-treated zwitterionic glycolipids

Enzymic cleavage of the glycolipids (**A** and **B**) was performed with 1.5 m-units of α-galactosidase from green coffee beans (6h; **C** and **D**), 80 m-units of β-*N*-acetylhexosaminidase from jack beans (overnight; **E** and **F**) and 3.5 m-units of β-mannosidase from snail (overnight; **G** and **H**). In some cases, 1 μl of a 4 mM LiCl solution was added to the analyte spot to produce $[M+Li]^+$ pseudomolecular ions instead of the Na^+ adducts. Pseudomolecular ions are given in accurate mass units rounded to one decimal place. Measurements were performed in the positive-ion reflectron mode. ●, Gal; □, GalNAc; ■, GlcNAc; ○, Man; ◆, Glc; Cer, ceramide.

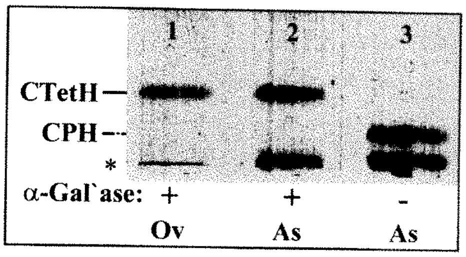

Figure 5 Cleavage of *O. volvulus* and *A. suum* HF-treated zwitterionic glycolipids with α-galactosidase

A. suum zwitterionic glycolipids yielded mainly CPH after HF treatment (lane 3). For *O. volvulus* and *A. suum* HF-treated zwitterionic glycolipids, cleavage with α-galactosidase (green coffee beans) resulted in a CTetH (lanes 1 and 2 respectively). Under the running solvent conditions employed [chloroform/methanol/water (65:25:4) by volume], more polar glycolipids of *A. suum* remained at the origin (indicated by asterisk; lanes 2 and 3). Glycolipids were revealed by orcinol/H_2SO_4 staining. Glycolipid fractions were derived from: Ov, *O. volvulus* adults; As, *A. suum* adults. α-Gal'ase, α-galactosidase treatment.

stitution, methylation analyses either without, before or after HF treatment were performed (Table 1). Native zwitterionic glycolipids yielded terminal Gal, 4-substituted Glc, 3-substituted Man, and 3-substituted and terminal GalNAc residues. HF treatment after permethylation revealed the additional presence of a 4,6-disubstituted GlcNAc residue. When HF treatment was performed before permethylation, in order to remove PC, the GlcNAc residue appeared to be 4-substituted. This indicated that PC was 6-linked to the 4,6-disubstituted GlcNAc residue. In the methylation analysis of the native zwitterionic glycolipid fraction, no GlcNAc species was observed, as PC had not been removed and the resultant derivative with PC still attached at the 6-position was not volatile and, therefore, not detected by GC–MS. In order to determine monosaccharide sequences and anomeric linkages, *O. volvulus* and *A. suum* zwitterionic glycolipids were analysed in parallel by sequential on-target enzymic cleavage with specific exoglycosidases and MALDI-TOF-MS. Following HF treatment, the mass spectra exhibited the characteristic signals for CTH, ceramide tetrahexoside (CTetH) and CPH (Figures 4A and 4B; [21]). Incubation with α-galactosidase cleaved one hexose residue from the dominant CPH components at 1567.1, 1553.1 and 1539.1 Da (ΔM = 162 Da; Figures 4C and 4D). However, an additional minor CPH component appeared to be present in the *O. volvulus* sample with a pseudomolecular ion at 1608.9, which was not cleaved by α-galactosidase treatment (Figure 4C). This CPH component exhibited a ΔM of 203 Da to the CTetH species in Figure 4(C), which indicated the presence of a terminal HexNAc. Further degradation by β-*N*-acetylhexosaminidase treatment removed two HexNAc residues consecutively (Figures 4E and 4F). The observed mass shift of 422 Da resulted from the loss of two HexNAc residues (ΔM = 406 Da) and the exchange of Na^+ by Li^+ (ΔM = 16 Da). β-Mannosidase removed one hexose residue and resulted in CMH (Figures 4G and H). In addition, the zwitterionic glycolipids of *O. volvulus* and *A. suum*, after HF treatment, were incubated with α-galactosidase and the reaction products were analysed by HPTLC; they exhibited the migration properties of CTetH (Figure 5, lanes 1 and 2). Methylation analysis of *O. volvulus* zwitterionic glycolipids after HF and α-galactosidase treatments yielded terminal GalNAc, 4-substituted and terminal GlcNAc, 3-substituted Man and 4-substituted Glc (Table 1). This revealed terminal Gal to be α-linked to the 3-position of GalNAc and yielded the sequence Gal(α1-3)GalNAc(β1-4)-GlcNAc(β1- and not Gal(α1-4)GlcNAc(β1-3)GalNAc(β1- for the carbohydrate backbone.

Fatty acids were analysed by GC–MS using electron-impact ionization (Table 2). The results demonstrated the predominance of hydroxytetracosanoic acid ($C_{24h:0}$) (where $_h$ is hydroxylated). *O. volvulus* zwitterionic glycolipids were found to contain higher relative amounts of $C_{22h:0}$ and $C_{23h:0}$ than the corresponding *A. suum* glycolipids. The obtained fragment-ion patterns showed all hydroxy fatty acids to be 2-hydroxy derivatives, which is in agreement with previous data [1,21]. Analysis of the pentafluoropropionic acid-derivatized sphingoid base fraction by GC–MS in the positive-ion mode following electron-impact ionization allowed C_{17}-sphingosine ($C_{d17:1}$) (where $_d$ is dihydroxylated) to be identified as the main compound (results not shown), which is in accordance with the data obtained for *A. suum* zwitterionic glycolipids [1]. A characteristic ion at *m/z* 395 was observed, which corresponded to a C_{17}-sphingosine fragment

Table 2 Fatty acid analysis of *O. volvulus* and *A. suum* zwitterionic glycosphingolipid fractions

Fatty acid methyl esters were analysed by capillary GC–MS and identified by their retention times and molecular ($[M]^+$) as well as fragment ions after electron-impact ionization. Relative amounts are based on peak ratios of individual fatty acid derivatives normalized to 100%. $C_{24:0}$, saturated fatty acid with 24 carbon atoms; $C_{24h:0}$, saturated hydroxy fatty acid, etc.

Fatty acid methyl ester	Molecular ion $[M]^+$	Species	Relative amount (%)	
			O. volvulus	*A. suum*
$C_{16:0}$	270		3.0	1.6
$C_{18:0}$	298		4.7	5.7
$C_{20:0}$	326		0.5	–
$C_{22:0}$	354		1.7	1.4
$C_{22h:0}$	370		22.8	7.0
$C_{23h:0}$	384		13.7	3.3
$C_{24:0}$	382		1.2	10.9
$C_{24h:0}$	398		52.4	70.1

ment with only one pentafluoropropionic acid moiety remaining. The fragmentation pattern was analogous to that observed for the $C_{d18:1}$ standard. Detection in the negative-ion mode following chemical ionization resulted in a major ion at m/z 540 which coincided with an ion at m/z 554 found for the $C_{d18:1}$ standard (loss of HF and one pentafluoropropionic acid moiety). A similar fragmentation has been described by Zanetta et al. for sphingosines derivatized with heptafluorobutyric acid [27].

Taken together, the data allowed the structures of *O. volvulus* zwitterionic CTH, CTetH and CPH to be defined as PC-6GlcNAc(β1-3)Man(β1-4)Glc(1-1)Cer, GalNAc(β1-4)[PC-6]GlcNAc(β1-3)Man(β1-4)Glc(1-1)Cer and Gal(α1-3)GalNAc(β1-4)[PC-6]-GlcNAc(β1-3)Man(β1-4)Glc(1-1)Cer respectively.

DISCUSSION

The various serological and analytical procedures performed in the present study for the characterization of *O. volvulus* neutral and zwitterionic glycosphingolipid fractions varied in their specificities and detection limits. Immunochemically, neutral fraction CTH, CTetH and CPH were strongly immunoreactive with the anti-arthro-series hyperimmune serum, but chemically, HPTLC-orcinol/H_2SO_4 staining, carbohydrate composition analysis, methylation analysis and MALDI-TOF-MS revealed these glycosphingolipids to be only minor components in comparison with CMH and CDH. Thus these findings differ from those of a previous study of *Onchocerca* spp. glycolipids, from adult worms of the bovine filarial nematode *O. gibsoni*, which suggested the presence of neutral components (orcinol/H_2SO_4-spray reagent) and acidic components (sialic acid-specific, resorcinol-spray reagent) by HPTLC [28]. Similarly, the *O. volvulus* pooled infection sera and the PC-specific mAb showed different patterns of immunoreactivity with *O. volvulus* zwitterionic glycosphingolipids, manifesting other immunologically dominant compounds besides component A, yet HPTLC-orcinol/H_2SO_4-staining and methylation analysis demonstrated component A to be chemically the dominant zwitterionic glycolipid. While PC-substituted CTH and CTetH were easily detected by MALDI-TOF-MS, they were not detected by HPTLC–orcinol/H_2SO_4 staining owing to the lower sensitivity of this method (cf. Figures 2 and 3).

The phylogenetic structural conservation between the oligosaccharide backbone of neutral and zwitterionic glycosphingolipids from the Nematoda and Arthropoda is not so surprising in the light of recent data [29] showing the nematode lineage to be nearer to that of the arthropods than the Annelida. The oligosaccharide cores are based on the prototypic, arthro-series glycosphingolipid CTetH of the blowfly *Calliphora vicina*, i.e., GalNAc(β1-4)GlcNAc(β1-3)Man(β1-4)Glc(β1-1)Cer [30]. The predominant traits of the oligosaccharide moiety of *O. volvulus* neutral and zwitterionic glycosphingolipids were: (1) the neutral glycolipid fraction was represented by the components CMH and CDH (structurally analysed) and CTH-CPH (immunochemically analysed only); (2) the zwitterionic glycolipid fraction was represented by the components CTH, CTetH and CPH with the third residue in the carbohydrate chain, GlcNAc, substituted by PC at position C-6, that extended the homology of structural conservation with the porcine parasite *A. suum* [1,21]; and (3) the zwitterionic components belonged to a biosynthetic series in which elongation proceeded by the stepwise attachment of the specified monosaccharide. The zwitterionic CPH of *O. volvulus* (the present study), *A. suum* [1] and *Caenorhabditis elegans* [31] represents a modulation of the insect-derived, arthro-series glycosphingolipid, because the prototypic CTetH can be extended in one of three ways, i.e., the addition of an α-GalNAc residue to yield component 5A, an α-Gal residue to yield component 5B or a β-Gal residue to yield component 5C [30,32,33]. Insect glycosphingolipids are elongated from CPH component 5A [30], whilst nematode glycosphingolipids utilize CPH component 5B as either a termination point [1,21] or for extension [31]. Besides the structures of *O. volvulus* PC-containing CTH, CTetH and CPH defined in the present study, pseudomolecular ions have been detected in reflectron-mode MALDI-TOF-MS of the zwitterionic glycosphingolipid fraction before and after HF treatment (see, for example, signals at m/z 1710.6 in Figure 3E and at 1608.9 in Figure 4C), which indicated the presence of a second PC-substituted CPH component with the putative composition $PCHexNAc_3Hex_2Cer$. Its resistance to α-galactosidase treatment indicated that the terminal galactose present in component A has been replaced by a HexNAc residue. The carbohydrate structure of this second CPH species may be analogous to the CPH component 5A [GalNAc(α1-4)GalNAcβ(1-4)GlcNAc(β1-3)Man(β1-4)Glc(β1-1)Cer] found in *C. vicina* [30], which has been found to occur, in part, with a PE modification [33]. However, this proposal was not examined further in the present study owing to the extremely small amounts of available material.

The structures of PC-substituted *N*-linked glycans of excreted-secreted and somatic proteins from parasitic filarial nematodes [12,13] and the PC-substituted zwitterionic glycosphingolipids of parasitic and free-living nematodes ([1,31]; the present study) are highly conserved. The function(s) of these exogenous glycoproteins of the former has been related to their immunomodulatory properties and correlated with the longevity of filarial parasitism as survival factors in subverting the immune response of the host, a characteristic trait in the microfilaraemic state of infection [34]. The resultant cellular anergy is assumed to facilitate the persistence of the parasitic infection, but at the same time may protect the host against the development of parasite-induced immunopathogenesis, e.g., inflammation. The generation and regulation of protective or pathogenic immune responses in filariases have been investigated intensively with the focus on those antigens that may elicit and confer protective immunity, whether they are known to be substituted with PC [35] or not [36,37].

The finding of PC-substituted glycosphingolipids and proteins in the free-living nematode *C. elegans* [31], however, would argue for their function as endogenous factors in the worm itself. Nothing is known as to the biological significance of free-living nematode-derived PC (macro)molecules, although, they have exhibited tissue- and stage-specific expression during ontogeny as potential markers for embryonic, hypodermal-seam cell differentiation and post-embryonic basement-membrane differentiation [31]. We have assumed that the highly conserved structures are an indication of their biological importance. The speculation is that the functional protein- and lipid-bound PC epitopes of the free-living nematode have been misappropriated by parasitic nematodes for additional roles relevant to the parasitic mode of existence, such as modulation of the host's immune response.

We acknowledge the expert technical assistance of Peter Kaese, Siegfried Kuhnhardt, Werner Mink and Markus Schwinn. This study was supported by the German Research Council (SFB 535, Projects A8 and Z1)

REFERENCES

1 Lochnit, G, Dennis, R D, Ulmer, A J and Geyer, R (1998) Structural elucidation and monokine-inducing activity of two biologically active zwitterionic glycosphingolipids derived from the porcine parasitic nematode *Ascaris suum* J Biol. Chem **278**, 466–474

2 Dennis, R D, Baumeister, S, Smuda, C, Lochnit, G, Waider, T and Geyer, E (1995) Initiation of chemical studies on the immunoreactive glycolipids of adult *Ascaris suum*. Parasitology **110**, 611–623

3 Baumeister, S, Dennis, R D, Klunder, R, Schares, G, Zahner, H and Geyer, E (1994) *Litomosoides carinii*: macrofilariae-derived glycolipids – chromatography, serology and potential in the evaluation of anthelminthic efficacy Parasite Immunol **16**, 629–641

4 Wenger, J D., Forsyth, K P and Kazura, J W (1988) Identification of phosphorylcholine epitope-containing antigens in *Brugia malayi* and relation of serum epitope levels to infection status of jirds with brugian filariasis Am. J. Trop Med Hyg. **38**, 133–141

5 MacDonald, M, Copeman, D B and Harnett, W (1996) Do excretory–secretory products of *Onchocerca gibsoni* contain phosphorylcholine attached to O-type glycans? Int J. Parasitol **26**, 1075–1080

6 Garate, T, Kliks, M M, Cabrera, Z and Parkhouse, R M (1990) Specific and cross-reacting antibodies in human responses to *Onchocerca volvulus* and *Dracunculus medinensis* infections Am J Trop Med Hyg. **42**, 140–147

7 Lal, R B. and Ottesen, E A (1989) Phosphocholine epitopes on helminth and protozoal parasites and their presence in the circulation of infected human patients Trans R Soc Trop. Med Hyg **83**, 652–655

8 Harnett, W, Worms, M J, Kapil, A, Grainger, M. and Parkhouse, R M (1989) Origin, kinetics of circulation and fate *in vivo* of the major excretory-secretory product of *Acanthocheilonema viteae* Parasitology **99**, 229–239

9 Harnett, W, Houston, K. M., Amess, R and Worms, M. J (1993) *Acanthocheilonema viteae*: phosphorylcholine is attached to the major excretory-secretory product via an N-linked glycan Exp Parasitol **77**, 498–502

10 Houston, K. M and Harnett, W (1996) Prevention of attachment of phosphorylcholine to a major excretory-secretory product of *Acanthocheilonema viteae* using tunicamycin. J Parasitol **82**, 320–324

11 Houston, K M, Cushley, W and Harnett, W (1997) Studies on the site and mechanism of attachment of phosphorylcholine to a filarial nematode secreted glycoprotein J. Biol Chem **272**, 1527–1533

12 Haslam, S M., Khoo, K-H, Houston, K M, Harnett, W, Morris, H R and Dell, A (1997) Characterisation of the phosphorylcholine-containing N-linked oligosaccharides in the excretory-secretory 62 kDa glycoprotein of *Acanthocheilonema viteae* Mol Biochem Parasitol **85**, 53–66

13 Haslam, S M, Houston, K M, Harnett, W, Reason, A J, Morris, H R and Dell, A (1999) Structural studies of N-glycans of filarial parasites. Conservation of phosphorylcholine-substituted glycans among species and discovery of novel chito-oligomers J Biol Chem **274**, 20953–20960

14 Lal, R B, Kumaraswami, V., Steel, C and Nutman, T B (1990) Phosphocholine-containing antigens of *Brugia malayi* nonspecifically suppress lymphocyte function Am J Trop. Med Hyg **42**, 56–64

15 Harnett, W and Harnett, M M (1993) Inhibition of murine B cell proliferation and down-regulation of protein kinase C levels by a phosphorylcholine-containing filarial excretory–secretory product J Immunol **151**, 4829–4837

16 Harnett, W and Harnett, M M (1999) Phosphorylcholine friend or foe of the immune system? Immunol Today **20**, 125–129

17 Deehan, M R, Harnett, M M and Harnett, W (1997) A filarial nematode-secreted product differentially modulates expression and activation of protein kinase C isoforms in B lymphocytes J Immunol **159**, 6105–6111

18 Deehan, M R, Frame, M J, Parkhouse, R. M., Seatter, S. D., Reid, S. D., Harnett, M M and Harnett, W. (1998) A phosphorylcholine-containing filarial nematode-secreted product disrupts B lymphocyte activation by targeting key proliferative signaling pathways. J Immunol **160**, 2692–2699

19 Harnett, M. M, Deehan, M R, Williams, D M. and Harnett, W (1998) Induction of signalling anergy via the T-cell receptor in cultured Jurkat T cells by pre-exposure to a filarial nematode secreted product. Parasite Immunol **20**, 551–563

20 Soboslay, P T, Luder, C G K, Riesch, S, Geiger, S M, Banla, M, Batchassi, E and Stadler, A. (1999) Regulatory effects of Th1-type (IFN-γ, IL-12) and Th2-type cytokines (IL-10, IL-13) on parasite-specific cellular responsiveness in *Onchocerca volvulus*-infected humans and exposed endemic controls. Immunology **97**, 219–225

21 Lochnit, G, Dennis, R D, Zahringer, U and Geyer, R (1997) Structural analysis of neutral glycosphingolipids from *Ascaris suum* adults (Nematoda Ascaridida). Glycoconj J **14**, 389–399

22 Dennis, R D, Lochnit, G. and Geyer, R (1998) Strategies for preliminary characterization of novel amphoteric glycosphingolipids In Glycoanalysis Protocols, vol 76 (Hounsell, E F, ed), pp 197–212, Humana Press, Totowa, NJ

23 Wuhrer, M, Dennis, R. D., Doenhoff, M J, Bickle, Q, Lochnit, G and Geyer, R. (1999) Immunochemical characterisation of *Schistosoma mansoni* glycolipid antigens Mol Biochem. Parasitol **103**, 155–169

24 Geyer, R, Geyer, H., Kuhnhardt, S., Mink, W and Stirm, S. (1982) Capillary gas-chromatography of methylhexitol acetates obtained upon methylation of *N*-glycosidically linked glycoprotein oligosaccharides Anal. Biochem **121**, 263–274

25 Geyer, R and Geyer, H (1994) Saccharide linkage analysis using methylation and other techniques Methods Enzymol **230**, 86–107

26 Geyer, H, Schmitt, S, Wuhrer, M and Geyer, R (1999) Structural analysis of glycoconjugates by on-target enzymatic digestion and MALDI-TOF-MS. Anal Chem **71**, 476–482

27 Zanetta, J P, Timmerman, P and Leroy, Y (1999) Gas-liquid chromatography of the heptafluorobutyrate derivatives of the O-methyl glycosides on capillary columns a method for the quantitative determination of the monosaccharide composition of glycoproteins and glycolipids. Glycobiology **9**, 255–266

28 Maloney, M D and Semprevivo, L H (1991) Thin-layer and liquid column chromatographic analyses of the lipids of adult *Onchocerca gibsoni* Parasitol. Res **77**, 294–300

29 Sidow, A. and Thomas, W. K (1994) A molecular evolutionary framework for eukaryotic model organisms Curr Biol. **4**, 596–603

30 Dennis, R D, Geyer, R, Egge, H., Peter-Katalinic, J, Li, S.-C, Stirm, S and Wiegandt, H (1985) Glycosphingolipids in insects Chemical structures of ceramide tetra-, penta-, hexa-, and heptasaccharides from *Calliphora vicina* pupae (Insecta: Diptera). J Biol Chem. **260**, 5370–5375

31 Gerdt, S, Dennis, R D, Borgonie, G., Schnabel, R and Geyer, R (1999) Isolation, characterization and immunolocalization of phosphorylcholine-substituted glycolipids in developmental stages of *Caenorhabditis elegans* Eur J Biochem **266**, 952–963

32 Weske, B, Dennis, R D., Helling, F, Keller, M, Nores, G A, Peter-Katalinic, J, Egge, H., Dabrowski, U. and Wiegandt, H (1990) Glycosphingolipids in insects Chemical structures of two variants of a glucuronic-acid-containing ceramide hexasaccharide from pupae of *Calliphora vicina* (Insecta Diptera), distinguished by a *N*-acetylglucosamine-bound phosphoethanolamine sidechain. Eur J Biochem **191**, 379–388

33 Helling, F, Dennis, R D, Weske, B, Nores, G, Peter-Katalinic, J, Dabrowski, U, Egge, H and Wiegandt, H (1991) Glycosphingolipids in insects. The amphoteric moiety, *N*-acetylglucosamine-linked phosphoethanolamine, distinguishes a group of ceramide oligosaccharides from the pupae of *Calliphora vicina* (Insecta. Diptera) Eur J Biochem. **200**, 409–421

34 Soboslay, P T, Dreweck, C M., Taylor, H. R., Brotman, B, Wenk, P and Greene, B M (1991) Experimental onchocerciasis in chimpanzees Cell-mediated immune responses, and production and effects of IL-1 and IL-2 with *Onchocerca volvulus* infection J Immunol **147**, 346–353

35 Lal, R B, Lynch, T J and Nutman, T B (1987) *Brugia malayi* antigens associated with lymphocyte activation in filariasis. J Immunol **139**, 1652–1657

36 Lobos, E, Ondo, A, Ottesen, E A and Nutman, T B (1992) Biochemical and immunologic characterization of a major IgE-inducing filarial antigen of *Brugia malayi* and implications for the pathogenesis of tropical pulmonary eosinophilia. J. Immunol **149**, 3029–3034

37 Luder, C G, Schulz-Key, H, Banla, M, Pritze, S. and Soboslay, P. T (1996) Immunoregulation in onchocerciasis predominance of Th1-type responsiveness to low molecular weight antigens of *Onchocerca volvulus* in exposed individuals without microfilaridermia and clinical disease Clin. Exp Immunol **105**, 245–253

Received 1 February 2000/15 March 2000, accepted 28 March 2000

Biochem J. (2000) 348, 425–432 (Printed in Great Britain)

Increase of mitochondria and mitochondrial DNA in response to oxidative stress in human cells

Hsin-Chen LEE*, Pen-Hui YIN†, Ching-You LU*, Chin-Wen CHI† and Yau-Huei WEI*[1]

*Department of Biochemistry and Center for Cellular and Molecular Biology, National Yang-Ming University, Taipei, Taiwan 112, Republic of China, and †Institute of Pharmacology, National Yang-Ming University and Department of Medical Research and Education, Taipei Veterans General Hospital, Taipei, Taiwan 112, Republic of China

Mitochondrial respiratory function is impaired in the target tissues of patients with mitochondrial diseases and declines with age in various human tissues. It is generally accepted that respiratory-chain defects result in enhanced production of reactive oxygen species and free radicals in mitochondria. Recently, we have demonstrated that the copy number of mitochondrial DNA (mtDNA) is increased in the lung tissues of elderly human subjects. The mtDNA copy number was suggested to be increased by a feedback mechanism that compensates for defects in mitochondria harbouring mutated mtDNA and a defective respiratory system. However, the detailed mechanism remains unclear. In this study, we treated a human lung fibroblast cell line, MRC-5, with H_2O_2 at concentrations of 90–360 μM. After the treatment for 24–72 h, we found that cells were arrested at G_0 and G_1 phases but that mitochondrial mass and mtDNA content were significantly increased in a concentration- and time-dependent manner. Moreover, the oxidative stress induced by buthionine sulphoximine was also found to cause an increase in mitochondrial mass of the treated cells. Increased uptake of a vital mitochondrial dye Rhodamine 123 and enhanced tetrazolium [MTT, 3-(4,5-dimethylthiazol-2-yl)-2,5-diphenyl-2*H*-tetrazolium bromide] reduction revealed that the mitochondria increased by H_2O_2 treatment were functional. In addition, the increase in the mitochondrial mass was also observed in cell-cycle-arrested cells induced by mimosine, lovastatin and genistein. Taken together, these findings suggest that the increase in mitochondrial mass and mtDNA content are the early molecular events of human cells in response to endogenous or exogenous oxidative stress through cell-cycle arrest.

Key words: aging, cell-cycle arrest, hydrogen peroxide, mtDNA copy number, reactive oxygen species.

INTRODUCTION

Mitochondria are the intracellular organelles responsible for ATP synthesis through the coupling of oxidative phosphorylation to respiration in human and animal cells. Under normal physiological conditions, a small fraction of oxygen consumed by mitochondria is converted to superoxide anions, H_2O_2 and other reactive oxygen species (ROS) [1]. Moreover, mitochondrial respiratory function has been demonstrated to decline in various human tissues during the aging process [2,3]. This is thought to be caused, at least partly, by oxidative damage and mutation of mitochondrial DNA (mtDNA) in somatic tissues of aged individuals [3].

Recently, we found that mtDNA copy number is increased in the lung tissues of elderly human subjects [4]. Moreover, we showed that mtDNA mutation, oxidative DNA damage and lipid peroxidation are increased during aging in the human lung [4–7] and other tissues [8,9]. These findings are consistent with a previous report that mtDNA contents are increased in the tissues of old rats [10] and of elderly subjects [11]. This increase in the content of mtDNA was thought to compensate for respiratory-function decline during the aging process [12]. However, the molecular mechanism underlying the increase of mtDNA associated with respiratory-function decline in human aging remains unclear.

Mitochondria are the major intracellular source and primary target of ROS, which are generated under normal conditions as by-products of aerobic metabolism in animal and human cells. It has been established that defects in the respiratory chain lead to enhanced production of ROS and free radicals in mitochondria [13–15]. Moreover, H_2O_2 has been proposed to play a role as a secondary messenger in signal-transduction pathways [16,17]. The increase of ROS and enhanced oxidative stress stimulates the expression of early growth-related genes such as c-*fos* and c-*jun* [18]. Recently, H_2O_2 was proposed to be involved in the communication between mitochondria and the nucleus [19,20]. Therefore, we hypothesized that the age-dependent increase in the production of superoxide anions and H_2O_2 from mitochondria is one of the factors involved in feedback compensation for the decline of respiratory function during the aging process [21].

To test this hypothesis, we exposed MRC-5, a human lung fibroblast cell line, to oxidative stress by treatment with low concentrations of H_2O_2 or buthionine sulphoximine (BSO). The effect of oxidative-stress treatment on the copy number of mtDNA and mitochondrial mass in the cell was investigated.

MATERIALS AND METHODS

Cell culture

Human lung fibroblasts, from the MRC-5 cell line, were cultured at 37 °C in humidified 5 % CO_2/95 % air in Dulbecco's modified Eagle's medium (Gibco/BRL, Bethesda, MD, U.S.A.) supplemented with 10 % fetal bovine serum, 50 units/ml penicillin G

Abbreviations used: mtDNA, mitochondrial DNA; ROS, reactive oxygen species; BSO, buthionine sulphoximine; NAO, 10-*n*-Nonyl-Acridine Orange; DCF, 2′,7′-dichlorofluorescein; DCFH-DA, 2′,7′-dichlorofluorescin diacetate; MTT, 3-(4,5-dimethylthiazol-2-yl)-2,5-diphenyl-2*H*-tetrazolium bromide; $DiOC_6(3)$, 3,3′-dihexyloxacarbocyanine iodide.

[1] To whom correspondence should be addressed (e-mail joeman@mailsrv.ym.edu.tw).

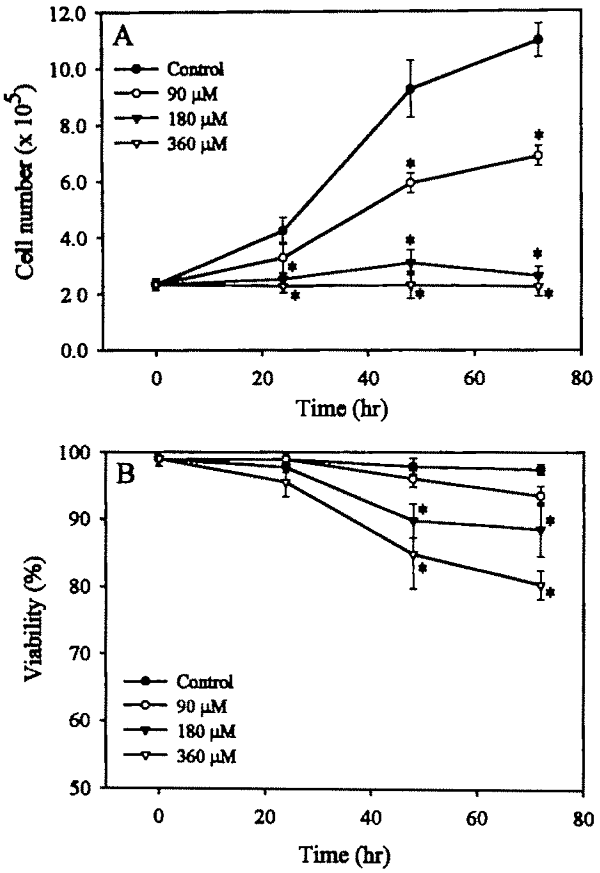

Figure 1 Cell growth and viability of MRC-5 cells treated with H_2O_2

MRC-5 cells were treated with H_2O_2 at concentrations from 90 to 360 μM. After treatment for 24–72 h, cells were enumerated using a haemocytometer (A), and the number of viable cells was determined by Trypan Blue exclusion (B). Data points represent measured values ± S.D. of two independent experiments performed on cells from three separate dishes. The differences in growth kinetics and viability between untreated and H_2O_2-treated cells were found to be statistically significant by using one-way ANOVA (*, $P < 0.05$).

and 50 mg/ml streptomycin sulphate. Cells were subjected to a 1:2 split every 4 days.

Oxidative-stress treatment

Oxidative-stress treatment was performed on cells that had all been cultured at the same density. An aliquot of 2.5 x 10^5 cells at 25–35 passages was plated in triplicate in 25-cm^2 flasks 24 h before treatment. For H_2O_2 treatment, a suitable aliquot of 30 % H_2O_2 solution was freshly diluted into the culture medium before the experiment. Cells were exposed to the indicated concentrations of H_2O_2 for a fixed period of time under normal culture conditions as described above. To deplete intracellular glutathione, cells were treated with 1 or 2 mM BSO (Sigma, St. Louis, MO, U.S.A.) for 72 h. The treated cells were then washed once with Hanks' balanced salt solution (Gibco/BRL) and were harvested by trypsinization at various time points for further analysis.

Treatment with drugs affecting the cell cycle

To arrest the cell cycle, cells were treated with 200 μM mimosine, 2.5 μM lovastatin or 50 μM genistein (Sigma) for 24 h. The treated cells were then washed once with Hanks' balanced salt solution and were harvested by trypsinization at various time points for cell-cycle analysis and mitochondrial-mass determination.

Cell growth and viability assay

Cells were harvested by trypsinization and resuspended in 1 ml of Medium 199 (Gibco/BRL). The cells were enumerated using a haemocytometer, and the number of viable cells was determined on the basis of their exclusion of 0.4 % Trypan Blue.

Cell-cycle analysis

After treatment with H_2O_2 or other chemicals, cells were trypsinized and resuspended in 70 % ethanol. The cells were incubated on ice for at least 1 h and resuspended in 1 ml of cell-cycle assay buffer (0.38 mM sodium citrate, 0.5 mg/ml RNase A and 0.01 mg/ml propidium iodide) at a concentration of 5 x 10^5 cells/ml. Samples were stored in the dark at 4 °C until cell-cycle analysis, which was carried out by use of a flow cytometer and ModFit LT 2.0 software (Verity Software, Topsham, ME, U.S.A.).

Determination of mitochondrial mass

The fluorescent dye 10-*n*-Nonyl-Acridine Orange (NAO; Molecular Probes, Eugene, OR, U.S.A.), which binds specifically to cardiolipin at the inner mitochondrial membrane independently of membrane potential ($\Delta\Psi_m$) [22,23], was used to monitor the mitochondrial mass [24]. Cells were trypsinized and resuspended in 0.5 ml of Medium 199 containing 10 μM NAO or 10 μM MitoTracker Green FM (Molecular Probes), which is preferentially accumulated in mitochondria regardless of mitochondrial membrane potential. After incubation for 10 min at 25 °C in the dark, cells were transferred immediately to a tube on ice for flow-cytometric analysis.

Dichlorofluorescin staining

H_2O_2 production by cultured cells was measured using the probe 2′,7′-dichlorofluorescin diacetate (DCFH-DA; Molecular Probes) [24–26]. This probe is accumulated by cells and hydrolysed by cytoplasmic esterases to become 2′,7′-dichlorofluorescin, which then reacts with H_2O_2 to give the fluorescent product 2′,7′-dichlorofluorescein (DCF) [25]. Cells were incubated with 5 μM DCFH-DA in culture medium for 30 min at 37 °C and then washed, resuspended in 0.5 ml of PBS, and submitted to flow-cytometric analysis.

Measurement of mitochondrial membrane potential

Cells were trypsinized and resuspended in 0.5 ml of Medium 199 containing 0.5 μg/ml Rhodamine 123 (Molecular Probes) or 3,3′-dihexyloxacarbocyanine iodide [DiOC$_6$(3); Molecular Probes]. After incubation for 30 min at 37 °C in the dark, cells were transferred immediately to a tube on ice for analysis of the fluorescence intensity by flow cytometry.

Flow-cytometric analysis

A FACScan flow cytometer (Becton Dickinson, Bedford, MA, U.S.A.) equipped with a 488-nm argon laser was used for the flow-cytometric analysis. Forward and side scatters were used to establish size gates and exclude cellular debris from the analysis.

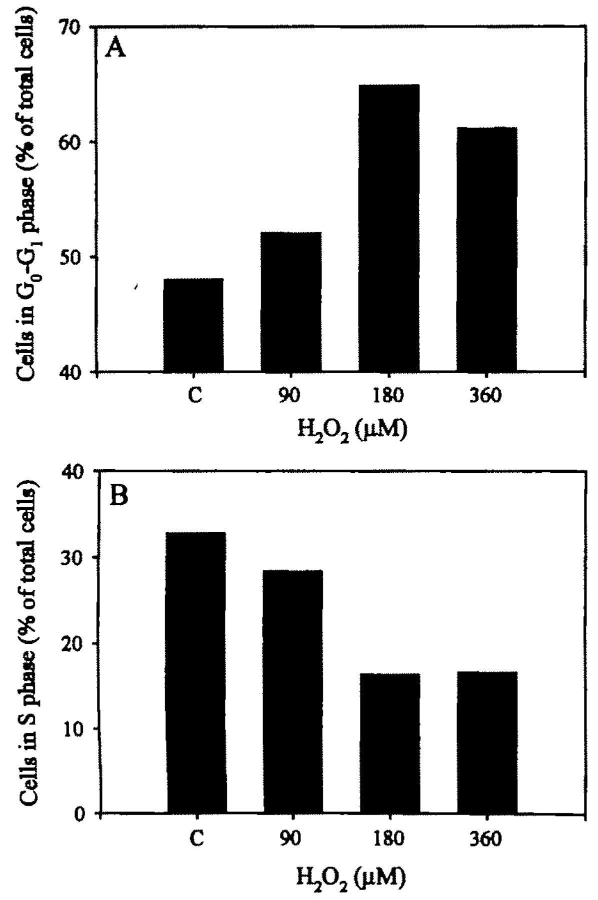

Figure 2 Cell-cycle arrest induced by H_2O_2

MRC-5 cells were treated with 90–360 μM H_2O_2. After treatment for 24 h, the percentages of cells in G_0–G_1 phase (**A**) and S phase (**B**) were analysed on a flow cytometer as described in the Materials and methods section. C, control

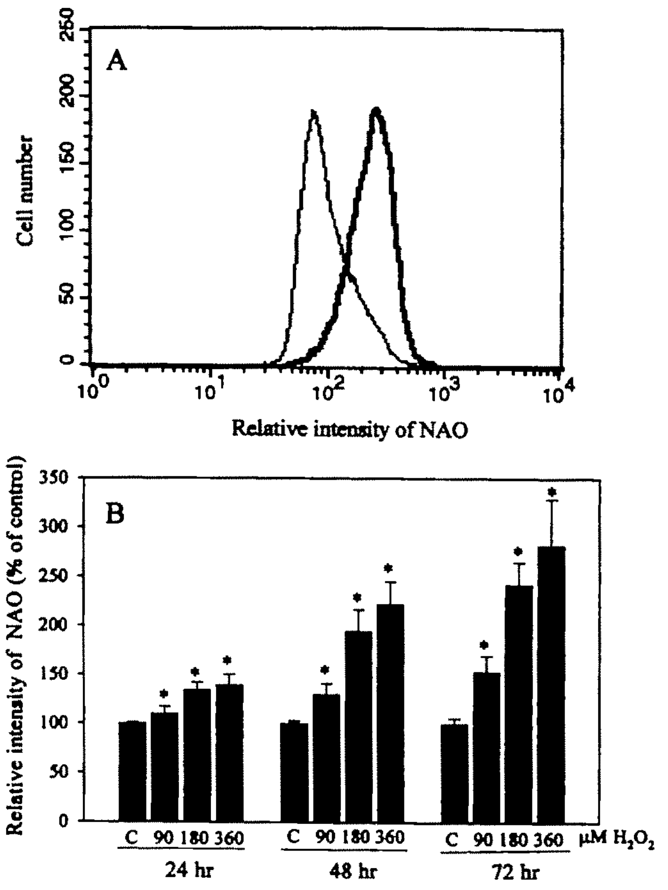

Figure 3 Increase of mitochondrial mass in MRC-5 cells treated with H_2O_2

(**A**) MRC-5 cells were treated with 180 μM H_2O_2. After 48 h of treatment, the mitochondrial mass of the cells stained with NAO was analysed by flow cytometry. The area under the thin (left-hand) curve represents the population of control cells, and the area under the thick (right-hand) curve represents the population of H_2O_2-treated cells. (**B**) MRC-5 cells were treated for 24–72 h with 90–360 μM H_2O_2, and the relative NAO intensity of treated cells was analysed by flow cytometry. Results are expressed graphically as percentages of the fluorescence intensity of the untreated control (C) cells. Values are means ± S.D. of results from six independent experiments performed in triplicate. Statistical analysis showed that the differences in the NAO intensity between the untreated and H_2O_2-treated cells were statistically significant (*, $P < 0.05$ versus control).

The excitation wavelength was set at 488 nm. The observation wavelength of 530 nm was chosen for green fluorescence and 585 nm for red fluorescence and the intensities of emitted fluorescence were collected on FL1 and FL2 channels, respectively. In each measurement, a minimum of 20000 cells were analysed. Data were acquired and analysed using the Cell Quest software (Becton Dickinson). Relative change in the mean fluorescence intensity was calculated as the ratio between mean fluorescence intensity in the channel of the treated cells and that of the control cells.

Southern-blot hybridization

For Southern-blot analysis, 5 μg of total DNA of the treated and control cells were linearized by digestion with *Bam*HI (Boehringer Mannheim, Mannheim, Germany), and the digested DNA was electrophoresed at 50 V for 12 h in a 1.0% agarose gel. DNA bands in the gel were denatured and transferred on to a Hybond N^+ nylon membrane (Amersham, Little Chalfont, Bucks., U.K.). Hybridization with a [α-^{32}P]dCTP-labelled human mtDNA probe of the D-loop region (spanning nucleotide positions 16455–1462) was carried out at 65 °C for 2 h in a rapid hybridization buffer (Amersham). The filter was washed with 2×SSC/0.1% SDS (where 1×SSC is 0.15 M NaCl/0.015 M sodium citrate) for 15 min at room temperature and then washed twice with 0.1×SSC/0.1% SDS for 15 min at 65 °C. The washed filter was wrapped with Saran Wrap ('clingfilm') and subjected to autoradiography.

MTT reduction assay

Cells were treated with H_2O_2 at the concentrations from 90 to 360 μM as described above. After 48 h of incubation, cells were harvested and cell viability was determined by the Trypan Blue-exclusion method. For determination of mitochondrial function, we incubated the cells with 3-(4,5-dimethylthiazol-2-yl)-2,5-diphenyl-2*H*-tetrazolium bromide (MTT; Sigma) at a final concentration of 2.0 μg/ml during the last 2 h of the incubation period. The cells were lysed with DMSO and the absorbance at 570 nm was measured. An MTT reduction index was calculated as the ratio between the absorbance at 570 nm and the number of viable cells [27].

Statistics

Data are presented as means ± S.D. except where indicated. Comparisons among multiple groups were made by a one-way analysis of variance (ANOVA) followed by Fisher's protected least significant difference *post hoc* test. The differences with $P <$ 0.05 were considered significant.

RESULTS

After treatment for 24–72 h with 90–360 μM H_2O_2, growth kinetics and viability of MRC-5 cells were affected in a dose-dependent manner as shown in Figure 1(A) and 1(B), respectively. We found that the untreated cells and the cells treated with 90 μM H_2O_2 kept growing steadily, but growth retardation was observed in the cells treated with 180 or 360 μM H_2O_2. Moreover, the rate of increase in the number of the cells treated with 90 or 180 μM H_2O_2 was significantly lower than that of the untreated cells ($P < 0.05$, Figure 1A). Most of the cells treated with 180 or 360 μM H_2O_2 appeared enlarged, flattened, and less spindle-shaped as compared with the control cells at the end of 24-h treatment (results not shown). We also found that the viability of the cells treated with 180 or 360 μM H_2O_2 was lower than that of the control cells ($P < 0.05$), but still remained 80% after 72-h treatment (Figure 1B). Furthermore, we found that 24 h after treatment the percentage of cells in G_0 and G_1 phases was increased (Figure 2A), and that the percentage of cells in the S phase decreased as a function of H_2O_2 concentration (Figure 2B).

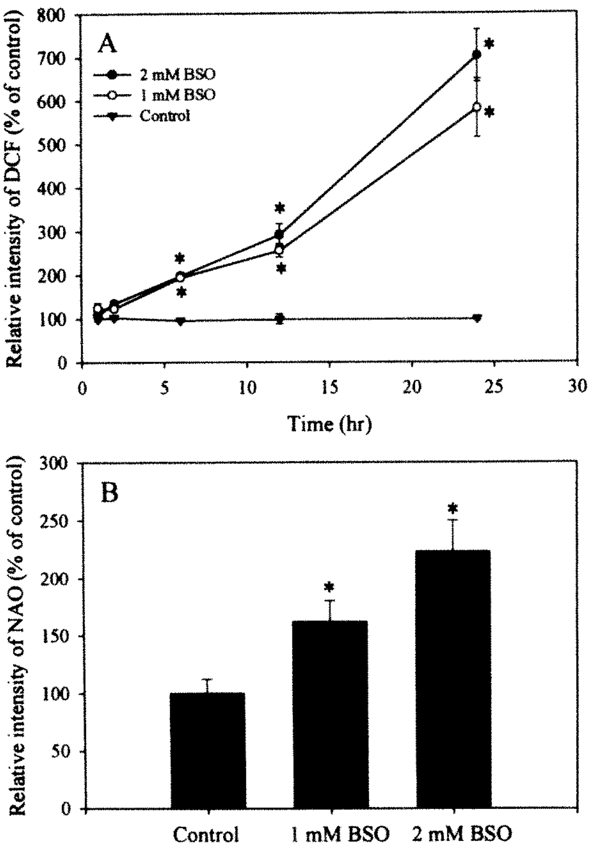

Figure 4 Increase of mitochondrial mass in MRC-5 cells treated with BSO

After treatment of MRC-5 cells with 1 or 2 mM BSO, the production of ROS in the cells, monitored by DCF fluorescence, increased with time (**A**). After 72 h of treatment, the mitochondrial mass of the cells stained with NAO was analysed by flow cytometry (**B**). Results are expressed graphically as percentages of the fluorescence intensity of the untreated (C) cells. Values are means ± S.D. of the results from two independent experiments performed in triplicate. Statistical analysis showed that the differences in the DCF or NAO intensity between the untreated and BSO-treated cells were statistically significant (*, $P < 0.05$ versus control).

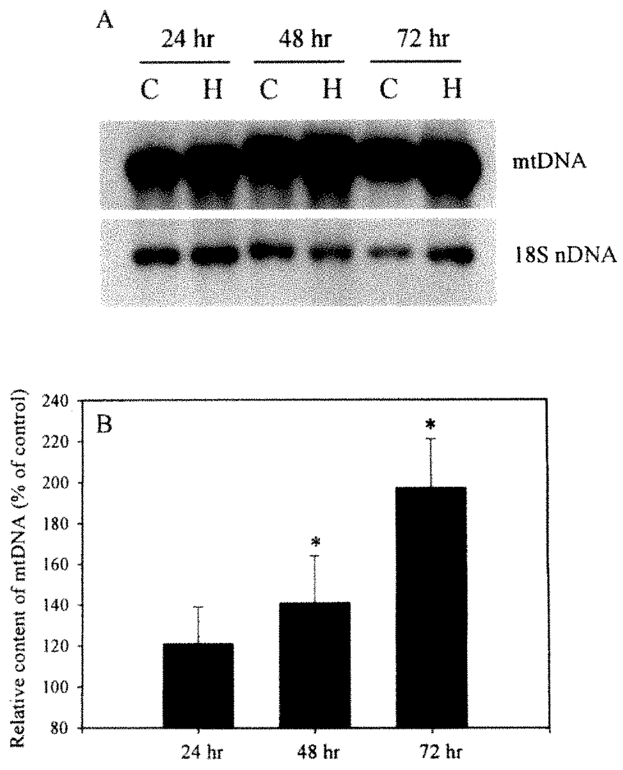

Figure 5 Increase of mtDNA content in MRC-5 cells treated with H_2O_2

After treatment of MRC-5 cells with 180 μM H_2O_2 for 24–72 h, the relative mtDNA content of the H_2O_2-treated cells (H) was determined by Southern-blot hybridization (**A**). The DNA band intensities were analysed by scanning densitometry and mtDNA content was corrected for variation in sample loading by normalization with the DNA band intensity of the 18 S rRNA gene. (**B**) Results are expressed graphically as percentages of the mtDNA band intensity of the untreated (C) cells. Values are means ± S.D. of the results from three independent experiments. Statistical analysis showed that the differences in the mtDNA band intensity between the untreated and H_2O_2-treated cells were statistically significant (*, $P < 0.05$ versus control).

In an attempt to determine whether H_2O_2 leads to the proliferation of mitochondria, we used the fluorescent dye NAO to monitor the mitochondrial mass [22–24]. After treatment for 24–72 h with the indicated concentrations of H_2O_2, the relative NAO intensity of the treated cells was found to be significantly higher than that of the untreated cells ($P < 0.05$, Figure 3). The relative NAO intensity of the treated cells was increased to 1.3–2.5-fold as compared with that of the control cells, depending on the H_2O_2 concentration and the duration of incubation (Figure 3). We observed a similar increase in the relative intensity of another fluorescent dye, MitoTracker Green FM (results not shown). These results indicate that the oxidative stress induced by H_2O_2 can lead to an increase in the number of mitochondria in MRC-5 cells in a concentration- and time-dependent manner.

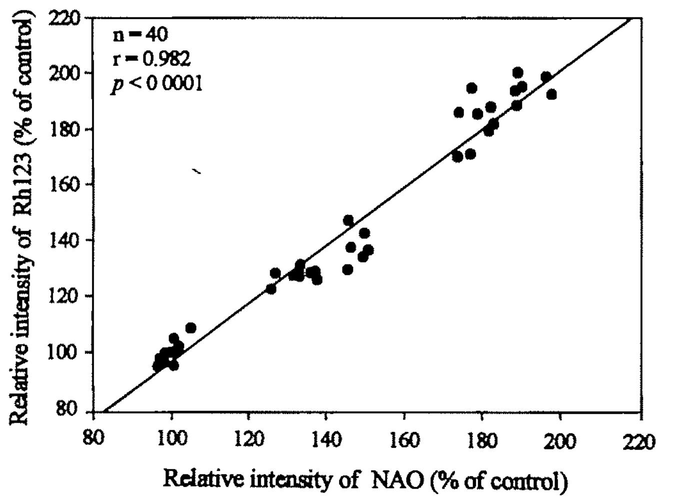

Figure 6 Membrane potential is normal in the extra mitochondria of the H_2O_2-treated cells

After treatment of MRC-5 cells with 90 or 180 μM H_2O_2 for 48 h, the mitochondrial mass and membrane potential were measured by flow cytometry after staining the cells with NAO and Rhodamine 123 (Rh123), respectively. The relative intensity is expressed graphically as a percentage of the fluorescence intensity of the untreated cells. The increase in mitochondrial membrane potential and mitochondrial mass were correlated throughout the 48-h period of the experiment ($r = 0.982$, $P < 0.0001$)

In addition to the oxidative stress induced by H_2O_2, BSO, an inhibitor of the glutathione biosynthetic pathway, was used to treat the cultured cells. After treatment with 1 or 2 mM BSO, we found that the concentration of ROS in the cells, as revealed by staining with DCFH-DA, increased with time ($P < 0.05$, Figure 4A). After treatment for 72 h with 1 or 2 mM BSO, the relative intensity of NAO of the treated cells was increased to 1.6- or 2.2-fold as compared with that of the control cells, respectively ($P < 0.05$, Figure 4B). These results indicate that not only H_2O_2 but also glutathione depletion can lead to an increase in the number of mitochondria in MRC-5 cells.

Using Southern-blot hybridization, we determined the mtDNA content of the MRC-5 cells after treatment with 180 μM H_2O_2 for 24–72 h. We found that the mtDNA content of the treated cells was higher than that of the untreated cells and increased with the duration of incubation (Figure 5). This increase of mtDNA content was consistent with the observation of proliferation of mitochondria in the H_2O_2-treated cells as revealed by NAO staining.

To analyse whether the extra mitochondria in the H_2O_2-treated cells were functional, we measured mitochondrial membrane potential of the treated cells by staining with Rhodamine 123 [25]. The relative intensity of Rhodamine 123 of the H_2O_2-treated cells was significantly higher than that of the control cells and was increased with the duration of incubation (results not shown). The increase in mitochondrial membrane potential correlated well with the increase in mitochondrial mass throughout the 48 h period of the experiment ($r = 0.982$, $P < 0.0001$, Figure 6). The mitochondrial membrane potential per unit mitochondrial mass, expressed as the ratio of fluorescence intensity of Rhodamine 123 to that of NAO, appeared to be similar throughout the 48 h of the experiment (Figure 6). Moreover, we observed similar results using another fluorescent dye, $DiOC_6(3)$, the uptake of which is sensitive to mitochondrial membrane potential (results not shown).

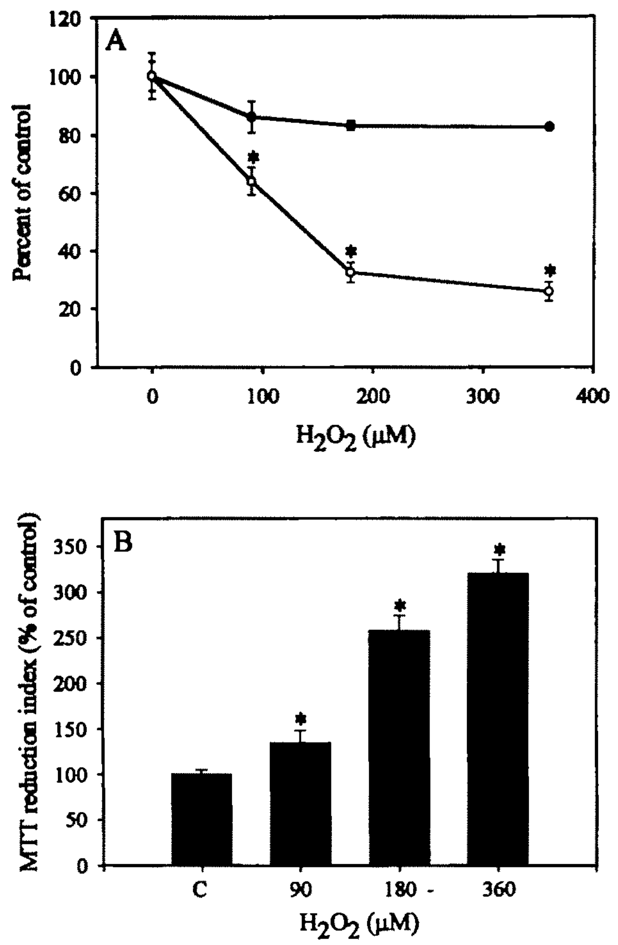

Figure 7 The increased mitochondria in the H_2O_2-treated cells are functional

Cells were treated with H_2O_2 at concentrations from 90 to 360 μM as described in the text. After 48 h of incubation, the capacity of the treated cells to reduce MTT was analysed as described in the Materials and methods section. The absorbance at 570 nm of the formosan formed in the MTT assay (●) and the number of viable cells (○) were determined concurrently after incubation of the MRC-5 cells for 48 h with the indicated concentrations of H_2O_2, and are expressed as percentages of the control (**A**). MTT reduction index was calculated as the ratio between the absorbance at 570 nm and the number of viable cells counted using a haemacytometer after 48 h of incubation with indicated concentrations of H_2O_2 (**B**). The data are expressed as the percentage of controls (C, means ± S.D.) from two independent experiments in triplicate. Statistical analysis showed that the differences in MTT reduction index between H_2O_2-treated and control cells are statistically significant (*, $P < 0.05$ versus control)

For the assessment of mitochondrial function, we analysed the capacity of H_2O_2-treated cells to reduce MTT. We found that although the number of the viable cells after H_2O_2 treatment was significantly decreased ($P < 0.05$), the absorbance at 570 nm of the remaining cells was only slightly decreased as compared with the untreated cells (Figure 7A). An arbitrary MTT reduction index, calculated as the ratio between the absorbance at 570 nm and the corresponding number of viable cells, revealed a significant increase in the relative MTT activity ($P < 0.05$, Figure 7B). These results indicate that the mitochondria increased in the H_2O_2-treated cells were functional.

To test whether the alteration of mitochondrial mass and mtDNA copy number in the cell might be uncoupled from the cell-cycle-controlled biosynthesis of chromosomal DNA, we treated MRC-5 cells with mimosine, lovastatin or genistein,

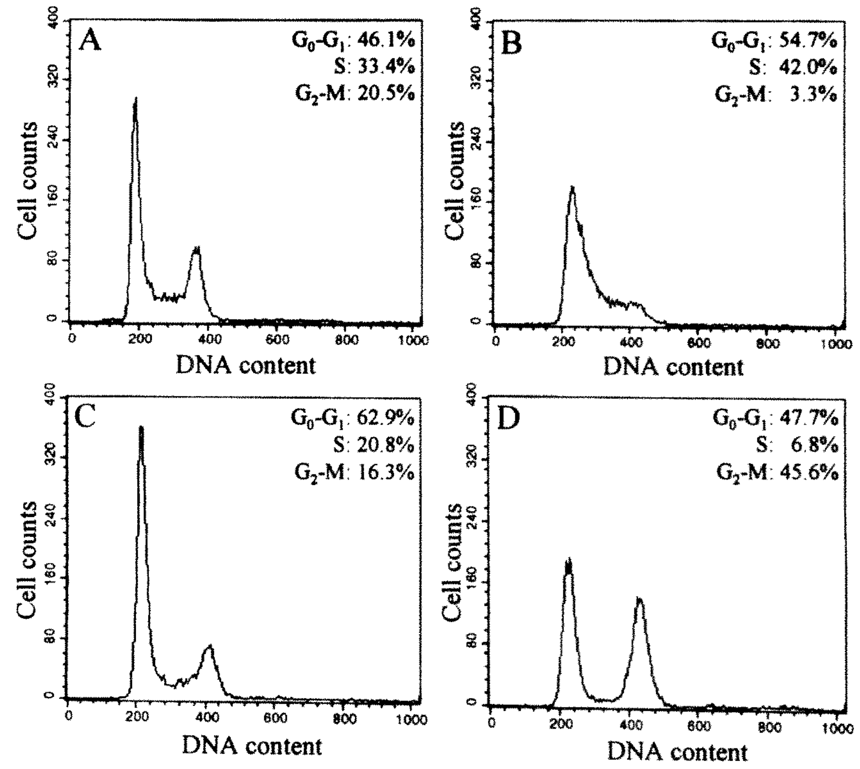

Figure 8 Cell-cycle arrest induced by mimosine, lovastatin and genistein

MRC-5 cells were treated with 200 μM mimosine, 2.5 μM lovastatin and 50 μM genistein in Dulbecco's modified Eagle's medium supplemented with 10% fetal bovine serum. After 24 h of incubation at 37 °C, the cell cycle was analysed on a flow cytometer as described in the Materials and methods section. Typical results from untreated cells (**A**) and cells treated with mimosine (**B**), lovastatin (**C**) and genistein (**D**) are presented.

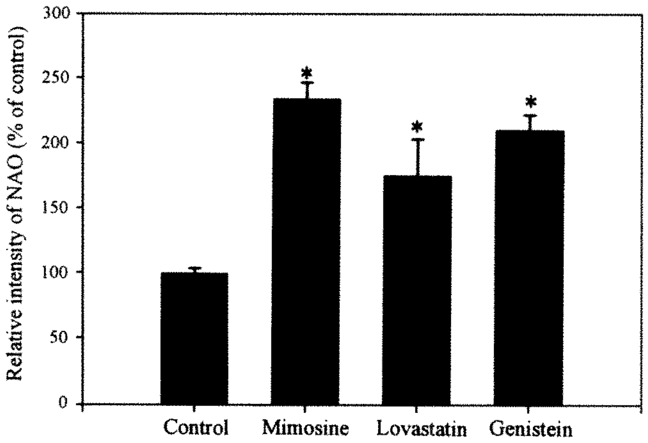

Figure 9 Increase of mitochondrial mass in MRC-5 cells treated with drugs affecting the cell cycle

MRC-5 cells were treated with 200 μM mimosine, 2.5 μM lovastatin and 50 μM genistein to cause cell-cycle arrest. After 48 h of incubation at 37 °C, the relative NAO intensity of treated cells was analysed by flow cytometry as described in the Materials and methods section. The results are expressed graphically as a percentage of the fluorescence intensity of the untreated MRC-5 cells. Values are means ± S.D. of the results obtained from three independent experiments. Statistical analysis showed that the differences in the NAO intensity between the untreated and drug-treated cells were statistically significant (*, $P < 0.05$ versus control).

which cause cell-cycle arrest. We found that after 24 h of treatment the cell cycle was arrested at the late G_1, G_0/G_1 and G_2/M phases by mimosine, lovastatin and genistein, respectively (Figure 8). Moreover, after 48 h of treatment the relative intensity of NAO of the treated cells was increased to 2.3-, 1.7- and 2.1-fold, respectively, as compared with that of the control cells ($P < 0.05$, Figure 9).

DISCUSSION

Each human and animal cell contains between several hundred and over a thousand mitochondria, each carrying 2–10 copies of mtDNA. The mitochondrial mass and mtDNA copy number of individual cells vary with the type of the cell and tissue, and are changed during cell differentiation, hormone treatment and exercise [28–31].

In the present study, we observed growth arrest in human lung fibroblasts treated with low concentrations of H_2O_2 (Figures 1 and 2). It is apparent that H_2O_2 at concentrations of between 90 and 180 μM increased the population-doubling time and that 360 μM H_2O_2 caused a permanent growth arrest. Most of the treated cells exhibited significant alterations in morphology as compared with the control cells. The results are consistent with the previous observations that H_2O_2 at sublethal concentrations can induce senescence-like growth arrest in human cells [32,33]. Moreover, we found in this study that the oxidative stress induced by sublethal concentrations of H_2O_2 caused an increase in the amount of mitochondria and mtDNA of the treated cells and that the increased mitochondria were functional. Furthermore, the oxidative stress induced by reduction of the intracellular glutathione level with BSO was also found to increase mitochondria in the treated cells (Figure 4). In a separate experiment, we exposed MRC-5 cells to 20 μM antimycin A and observed that the ROS generation in the treated cells was increased 2-fold compared with that of the untreated cells after 30 min of treatment. Moreover, after treatment for 72 h, we found that the relative intensity of NAO in the treated cells was increased to 2.6-fold compared with that of the control cells. This is consistent with the observation that by partial inhibition of respiratory function by antimycin A, the expressions of both cytochrome c_1 and cytochrome b are increased in human fibroblasts [34]. Moreover, intracellular H_2O_2 level was found to increase within 3 h prior to expression of these genes. These results indicate together that mild oxidative stress can trigger cell-cycle arrest and lead to an increase of mitochondrial mass and mtDNA in human cells.

Increases of mitochondria and mtDNA synthesis have been observed to occur in the absence of nuclear DNA replication [35]. The alteration of mitochondrial mass and mtDNA in the cell might be uncoupled from the cell-cycle-controlled biosynthesis of chromosomal DNA. To confirm this, we treated MRC-5 cells with lovastatin, genistein or mimosine and observed that these drugs caused cell-cycle arrest (Figure 8). In addition, the mitochondrial mass was increased, to a different extent, in the cells after 48 h of treatment (Figure 9). It is worth noting that the amplitude of increase of the mitochondrial mass in the cells treated with the cell-cycle-arresting drugs was similar to that in the H_2O_2-treated cells within the same treatment period. The results imply that whereas overall cell division was arrested by H_2O_2 or the drugs, mitochondrial biogenesis was unaffected and that mitochondria continued to proliferate as if the cells were going to divide. Thus, mild oxidative stress may induce an increase of mitochondria and mtDNA via a pathway that bypasses cell-cycle control.

Increase of mitochondria has also been observed in some tumour cells treated with herbimycin A and genistein [24,27]. Mancini et al. [24] found that herbimycin A, a tyrosine kinase inhibitor, induces cell-cycle arrest in G_2/M and results in a marked accumulation of mitochondria in a human colon carcinoma cell line (Colo-205). In addition, the G_2/M cell-cycle arrest and increase of mitochondrial number and/or function were also observed in three tumour cell lines (MCF-7, human breast tumour; Jurkat cells, human T-cell leukaemia; and L-929, mouse transformed fibroblasts) after treatment of genistein [27]. The results obtained in these studies are consistent with our findings and support the notion that the cell-cycle arrest induced by oxidative stress plays a critical role in the increase of mitochondria and mtDNA.

Furthermore, it has been found that the relative content of mtDNA is increased with age and that the mtDNA content is correlated with the level of oxidative damage to DNA in human lung tissues [4]. Both oxidative DNA damage and lipid peroxidation are enhanced during aging in the human lung [4–7], indicating that there is a higher oxidative stress in the tissues of aged individuals. Therefore, the endogenous and/or exogenous oxidative stress in the lung of elderly subjects may cause cell-cycle arrest and thereby increase the amount of mitochondria and mtDNA in lung tissues.

In summary, we have demonstrated clearly for the first time that oxidative stress induced by H_2O_2 leads to an increase of mitochondria and mtDNA in human lung fibroblasts Moreover, the mitochondria increased by H_2O_2-elicited oxidative stress are functional. We therefore suggest that the increase in mitochondrial mass and mtDNA content may be one of the early molecular events gearing the human cells up to respond to endogenous or exogenous oxidative stress through cell-cycle arrest.

This work was supported by a grant (NSC89-2316-B010-012) from the National Science Council and a 5-year national laboratory grant (NHRI-GT-EX89S505L) from the National Health Research Institutes, Republic of China

REFERENCES

1 Chance, B , Sies, H and Boveris, A (1979) Hydroperoxide metabolism in mammalian organs Physiol Rev **59**, 527–604
2 Papa, S. (1996) Mitochondrial oxidative phosphorylation changes in the life span Molecular aspects and physiopathological implications Biochim Biophys Acta **1276**, 87–105
3 Wei, Y H (1998) Oxidative stress and mitochondrial DNA mutations in human aging Proc Soc Exp Biol Med **217**, 53–63
4 Lee, H. C , Lu, C Y , Fahn, H J and Wei, Y H (1998) Aging- and smoking-associated alteration in the relative content of mitochondrial DNA in human lung FEBS Lett **441**, 292–296
5 Fahn, H J , Wang, L S , Hsieh, R. H , Chang, S C , Kao, S H , Huang, M H and Wei, Y H. (1996) Age-related 4,977 bp deletion in human lung mitochondrial DNA Am J Respir Crit Care Med **154**, 1141–1145
6 Fahn, H J , Wang, L S , Kao, S H , Chang, S C , Huang, M H and Wei, Y H (1998) Smoking-associated mitochondrial DNA mutations and lipid peroxidation in human lung tissues Am J Respir Cell Mol Biol **19**, 901–909
7 Lee, H. C , Lim, M L R , Lu, C Y , Liu, V W. S , Fahn, H J., Zhang, C , Nagley, P. and Wei, Y H. (1999) Concurrent increase of oxidative DNA damage and lipid peroxidation together with mitochondrial DNA mutation in human lung tissues during aging-smoking enhances oxidative stress on the aged tissues Arch Biochem Biophys **362**, 309–316
8 Wei, Y H , Kao, S H. and Lee, H C. (1996) Simultaneous increase of mitochondrial DNA deletions and lipid peroxidation in human aging Ann N Y. Acad Sci **786**, 24–43
9 Lu, C. Y , Lee, H C , Fahn, H. J and Wei, Y. H (1999) Oxidative damage elicited by imbalance of free radical scavenging enzymes is associated with large-scale mtDNA deletions in aging human skin Mutat Res **423**, 11–21
10 Gadaleta, M N , Rainaldi, G , Lezza, A. M S , Milella, F , Fracasso, F and Cantatore, P (1992) Mitochondrial DNA copy number and mitochondrial DNA deletion in adult and senescent rats Mutat Res. **275**, 181–193
11 Barrientos, A., Casademont, J., Cardellach, F , Estivill, X , Urbano-Marquez, A. and Nunes, V (1997) Reduced steady-state levels of mitochondrial RNA and increased mitochondrial DNA amount in human brain with aging Mol Brain Res **52**, 284–289
12 Ames, B N , Shigenaga, M K. and Hagen, T M (1995) Mitochondrial decay in aging. Biochim Biophys Acta **1271**, 165–170
13 Sohal, R S and Sohal, B. H (1991) Hydrogen peroxide release by mitochondria increases during aging. Mech. Ageing Dev **57**, 187–202
14 Richter, C , Gogvadze, V , Laffranchi, R , Schlapbach, R , Schnizer, M , Suter, M , Walter, P. and Yaffee, M (1995) Oxidants in mitochondria: from physiology to disease Biochim Biophys. Acta **1271**, 67–74
15 Sohal, R S , Sohal, B H and Orr, W. C (1995) Mitochondrial superoxide and hydrogen peroxide generation, protein oxidative damage and longevity in different species of flies Free Radical Biol Med **19**, 499–504
16 Sen, C. K and Packer, L (1996) Antioxidant and redox regulation of gene transcription. FASEB J **10**, 709–720
17 Lander, H M (1997) An essential role for free radicals and derived species in signal transduction. FASEB J. **11**, 118–124
18 Burdon, R. H (1995) Superoxide and hydrogen peroxide in relation to mammalian cell proliferation Free Radical Biol. Med **18**, 775–794
19 Poyton, R O and McEwen, J E. (1996) Crosstalk between nuclear and mitochondrial genomes Annu Rev Biochem **65**, 563–607
20 Scarpulla, R C (1997) Nuclear control of respiratory chain expression in mammalian cells. J. Bioenerg Biomembr **29**, 109–119
21 Lee, H C and Wei, Y H (2000) Mitochondrial role in life and death of the cell. J Biomed Sci **7**, 2–15
22 Maftah, A., Petit, J M , Ratinaud, M H and Julien, R (1989) 10-N nonyl acridine orange a fluorescent probe which stains mitochondria independently of their energetic state Biochem. Biophys. Res Commun **164**, 185–190
23 Petit, J M , Maftah, A , Ratinaud, M H and Julien, R (1992) 10-N nonyl acridine orange interacts with cardiolipin and allows the quantification of this phospholipid in isolated mitochondria Eur J Biochem **209**, 267–273
24 Mancini, M , Anderson, B O , Caldwell, E , Sedghinasab, M., Paty, P B and Hockenbery, D M (1997) Mitochondrial proliferation and paradoxical membrane depolarization during terminal differentiation and apoptosis in a human colon carcinoma cell line J Cell Biol **138**, 449–469
25 Rothe, G and Valet, G (1990) Flow cytometric analysis of respiratory burst activity in phagocytes with hydroethidine and 2′,7′-dichlorofluorescin. J Leuk Biol **47**, 440–448

26 Garcia-Ruiz, C, Colell, A, Morales, A, Kaplowitz, N and Fernandez-Checa, J C (1995) Role of oxidative stress generated from mitochondrial electron transport chain and mitochondrial glutathione status in loss of mitochondrial function and activation of transcription factor nuclear factor-κB studies with isolated mitochondria and rat hepatocytes Mol Pharmacol **48**, 825–834

27 Pagliacci, M C, Spinozzi, F, Migliorati, G, Fumi, G, Smacchia, M, Grignani, F, Riccardi, C. and Nicoletti, I (1993) Genistein inhibits tumour cell growth *in vitro* but enhances mitochondrial reduction of tetrazolium salts a further pitfall in the use of the MTT assay for evaluating cell growth and survival Eur J Cancer **29A**, 1573–1577

28 Robin, E D and Wong, R (1988) Mitochondrial DNA molecules and virtual number of mitochondria per cell in mammalian cells J Cell Physiol **136**, 507–513

29 Renis, M, Cantatore, P, Polosa, P L, Fracasso, F and Gadaleta, M N (1989) Content of mitochondrial DNA and of three mitochondrial RNAs in developing and adult cerebellum J. Neurochem **52**, 750–754

30 Shay, J W, Pierce, D J and Werbin, H (1990) Mitochondrial DNA copy number is proportional to total cell DNA under a variety of growth conditions J Biol Chem **265**, 14802–14807

31 Williams, R S, Salmons, S, Newsholme, E A, Kaufman, R E and Mellor, J (1986) Regulation of nuclear and mitochondrial gene expression by contractile activity in skeletal muscle J Biol Chem **261**, 376–380

32 Bladier, C, Wolvetang, E J., Hutchinson, P, de Haan, J B and Kola, I (1997) Response of a primary human fibroblast cell line to H_2O_2 senescence-like growth arrest or apoptosis Cell Growth Differ **8**, 589–598

33 Chen, Q M, Bartholomew, J C, Campisi, J, Acosta, M, Reagan, J D and Ames, B N (1998) Molecular analysis of H_2O_2-induced senescent-like growth arrest in normal human fibroblasts p53 and Rb control G_1 arrest but not cell replication Biochem J **332**, 43–50

34 Suzuki, H, Kumagai, T, Goto, A and Sugiura, T (1998) Increase in intracellular hydrogen peroxide and upregulation of a nuclear respiratory gene evoked by impairment of mitochondrial electron transfer in human cells Biochem Biophys Res Commun **249**, 542–545

35 Sazer, S and Sherwood, S W (1990) Mitochondrial growth and DNA synthesis occur in the absence of nuclear DNA replication in fission yeast J Cell Sci **97**, 509–516

Received 30 September 1999/8 March 2000, accepted 29 March 2000

Biochem J (2000) 348, 433–438 (Printed in Great Britain)

Perivenous localization of insulin receptor protein in rat liver, and regulation of its expression by glucose and oxygen in hepatocyte cultures

Anja KRONES, Thomas KIETZMANN[1] and Kurt JUNGERMANN

Institut für Biochemie und Molekulare Zellbiologie, Georg-August-Universität, Humboldtallee 23, D-37073 Göttingen, Germany

Insulin stimulates glucose utilization in the liver, which occurs mainly in the less aerobic, perivenous, zone. Accordingly, the insulin receptor protein was predominantly expressed in this area, although the insulin receptor mRNA was homogeneously distributed. In hepatocyte cultures venous O_2 partial pressure (pO_2) induced insulin receptor protein expression. High glucose concentrations enhanced insulin receptor protein under arterial and venous pO_2. The induction of insulin receptor protein by venous pO_2 would explain its zonated expression.

Key words: carbohydrate, hormones, hypoxia, metabolic zonation.

INTRODUCTION

Insulin, a peptide hormone composed of an A chain, with 21 amino acids, and a B chain, with 30 amino acids, linked by two disulphide bridges, activates hepatic glucose utilization via glycolysis and glycogen synthesis. Insulin acts via an ectocellular receptor, which is a transmembrane glycoprotein consisting of two α- (130 kDa) and two β- (95 kDa) chains [1] linked to each other by disulphide bridges. On binding of insulin to the two ectocellular α-chains [2] the membrane spanning β-chains of the insulin receptor are autophosphorylated [3,4]. The autophosphorylated insulin receptor is an activated protein tyrosine kinase [5] which triggers the phosphorylation of effector proteins, such as insulin receptor substrate-1 (IRS-1), at multiple tyrosine residues [6]. The phosphotyrosine residues of the IRS-1 function as docking sites for Src homology ('SH2') domains of other proteins, e.g. phospholipase Cχ and phosphatidylinositol 3-kinase [1].

The major target organ for insulin is the liver, which exhibits a heterogeneous distribution of key enzymes and subcellular structures between periportal and perivenous areas. The zonal enzyme distribution in conjunction with functional studies led to the model of metabolic zonation [7–12]. Accordingly, glucose uptake for glycogen synthesis and glycolysis occurs mainly in the perivenous area; conversely, glucose release from glycogenolysis and gluconeogenesis takes place preferentially in the periportal area. Due to metabolism, concentration gradients of substrates, such as oxygen and hormones, are formed during a single passage of blood through the liver [7,11,12]. The O_2 partial pressure (pO_2) falls from periportal values of approx. 65 mmHg (1 mmHg ≡ 133.3 Pa) to perivenous values of approx. 35 mmHg. The glucagon concentration is decreased by approx. 50 % and the insulin concentration only by approx. 15 % after meals. Thus during the absorptive phase the concentrations of oxygen and glucagon are relatively higher in the periportal area; conversely, the concentration of insulin is relatively higher in the perivenous zone. The oxygen gradient was considered to be a key regulator for the zonal expression of the genes of carbohydrate-metabolizing enzymes [7,10–12]. The zonation of key enzymes and capacities of metabolism within the liver are well understood, but little is known about the distribution of hormone receptors, except that the glucocorticoid receptor was found to be homogenously distributed [13] and that glucagon receptor mRNA was predominantly expressed periportally [14]

Since the insulin-stimulated process of glycolysis together with its rate-limiting enzyme, the insulin-dependent glucokinase, were found predominantly in the perivenous zone, the insulin receptor gene would be expected to be expressed mainly in this less aerobic area. Therefore it was the aim of the present study to investigate the zonation of insulin receptor gene expression in rat liver and to study the regulation of its expression by the substrates glucose and O_2 in rat primary hepatocyte cultures. In line with expectations the insulin receptor protein was predominantly localized perivenously and could be induced in primary hepatocyte cultures at basal glucose levels by perivenous pO_2. Since insulin and the insulin receptor are coupled to glucose utilization the induction of insulin receptor gene expression by glucose in the absorptive phase would be in line with expectations.

MATERIALS AND METHODS

All biochemicals and enzymes were of analytical grade and were purchased from commercial suppliers.

Animals

Male Wistar rats (200–260 g) were kept on a 12 h day/12 h night cycle (light from 07:00–19:00 h) with free access to water and food. Rats were anaesthetized with pentobarbital (60 mg/kg body weight) prior to preparation of hepatocytes between 08:00 h and 09:00 h.

Abbreviations used cMRP, canalicular multidrug resistance protein, DIG, digoxigenin, ECL, enhanced chemiluminescence, FCS, fetal calf serum; GS, glutamine synthetase, IRS-1, insulin receptor substrate 1; PCK1, cytosolic phosphoenolpyruvate carboxykinase 1, L-PK, pyruvate kinase L, pO_2, O_2 partial pressure (O_2 tension)

[1] To whom correspondence should be addressed (e-mail tkietzm@gwdg de)

Cell culture experiments

Liver cells were isolated by collagenase perfusion. Cells (1×10^6/dish) were maintained under standard conditions in an atmosphere of $O_2/N_2/CO_2$ (16:79:5, by vol.) in medium M 199 containing 0.5 nM insulin, added as a growth factor for culture maintenance, 100 nM dexamethasone, required as a permissive hormone, and 4% (v/v) fetal calf serum (FCS) for the initial 4 h of culture. After 4 h, cells were cultured in serum-free M 199 at 16% O_2 (mimicking arterial pO_2) or 8% O_2 (mimicking venous pO_2) with additions as described in the Figure legends. The O_2 values take into account the O_2 diffusion gradient from the media surface to the cells [15].

RNA preparation, cDNA synthesis and competitive PCR

Total RNA was prepared from 3×10^6 cells using a NucleoSpin Kit (Macherey and Nagel, Düren, Germany). For cDNA synthesis 2 μg of RNA was incubated with 500 μg/ml Oligo-dT$_{12-18}$ (Pharmacia Biotech, Freiburg, Germany) and 1 μl of 10 × hexanucleotide mix (Roche, Mannheim, Germany) in a volume of 12 μl at 68 °C for 10 min, and was subsequently chilled on ice for 10 min. To this, a total of 13 μl of cDNA synthesis mix, containing 5 μl of 5 × reaction buffer, 2.5 μl of 0.1 mM dithiothreitol, 1.5 μl of 10 mM dNTP mix, 40 units of RNasin and 200 units of Superscript® II RT (Gibco BRL, Eggenstein, Germany), was added. Incubations were carried out for 90 min at 42 °C, 30 min at 52 °C, 15 min at 95 °C and finally the mixture was cooled on ice. A 1 μl sample of this cDNA preparation was used in competitive PCR. The principle of competitve PCR is that target cDNA and a competitor DNA compete for the use of the same primers. The amount of the target cDNA can then be quantified via gel electrophoresis by comparing the intensity of the stained target PCR product with the intensity of the PCR product amplified from the known concentration of competitor DNA. The DNA competitor was prepared using a Competitive DNA Construction Kit (Takara, Heidelberg, Germany) as outlined in the manufacturer's protocol The 5′-end and the 3′-end of the competitor can bind the primers which are used to amplify the insulin receptor cDNA. The competitor PCR product was distinguishable from the insulin receptor PCR product, because the size and internal sequence were different. The competitor was constructed by using hybrid primers containing sequences of the target cDNA (insulin receptor) and sequences of the competitor DNA: sense primer, 5′-CAGGCATGCAATC-AGGACTCGTACGGTCATCATCTGACAC-3′; antisense primer 5′-AACGTATACGGAAGATGGAAAGACACTGC-GTGTTGAGCTTGA-3′ (underlining indicates the insulin receptor sequence; the rest of the sequence corresponds to the λDNA sequence). The competitor had a size of 489 bp.

This competitor DNA was added in various concentrations to the PCR, while the amount of cDNA remained constant. Competitive PCR was performed by using 1 μl of cDNA preparation, various concentrations of competitor DNA (as descibed in the Figure legends), 20 pmol of sense primer [bp 2817–2836 from rat insulin receptor cDNA (GenBank accession number M290145); 5′-CAGGCATGCAATCAGGACTC-3′], 20 pmol of antisense primer (bp 3363–3386 from rat insulin receptor cDNA; 5′-AACGTATACGGAAGATGGAAAGAC-3′), 1 μl of DMSO, 4 μl of 2.5 mM dNTP mix, 5 μl of 10 × buffer and 1 unit of *Taq* polymerase (Takara, Heidelberg, Germany) in a final volume of 50 μl. PCR reactions (35 cycles) were carried out at 95 °C for 1 min, 53 °C for 1 min and 72 °C for 2 min. A 570 bp product (insulin receptor cDNA) and a 487 bp product (competitor DNA) were expected; the PCR products were analysed by electrophoresis on a 2% agarose gel and their identities were checked by sequencing.

In situ hybridization

Liver tissue of normal fed rats was embedded in paraffin wax, 5 μm sections were prepared and paraffin wax was removed from the liver sections with xylene. The sections were then rehydrated with descending concentrations of ethanol and finally equilibrated in PBS. They were subsequently permeabilized in 0.3% Triton X-100, 10 μg/ml proteinase K and 4 mg/ml glucosidase for 15 min at 37 °C, and finally incubated in 0.1 M triethanolamine (pH 8.0) containing 0.25% acetic acid anhydride for 10 min. For hybridization, digoxigenin (DIG)-labelled antisense RNA transcripts served as hybridization probes. The cDNA of the insulin receptor (537 bp; nt 1171–1707) was cloned into pBS and transcribed into antisense RNA by using T3 RNA polymerase and DIG RNA labelling mixture (Roche). Cytosolic phosphoenolpyruvate carboxykinase 1 (PCK1) antisense RNA was synthesized from pBS-PCK containing a 1200 bp *Pst*I cDNA fragment [20] by using T3 RNA polymerase and DIG RNA labelling mixture. The DIG-labelled antisense insulin receptor RNA and PCK1 antisense RNA were hydrolysed to lengths of 200–300 bp in the presence of sodium carbonate buffer (pH 10.2). Hybridization was performed overnight with 25 ng of RNA probes at 42 °C in 100 μl of hybridization solution, containing 50% (v/v) formamide, 10% (w/v) dextran sulphate, 1 × Denhardt's solution (0.02% BSA, 0.02% polyvinylpyrrolidone and 0.02% Ficoll) and 0.5 mg/ml *Escherichia coli* DNA in 4 × SSC (where 1 × SSC is 0.15 M NaCl/0.015 M sodium citrate, pH 7.0). After hybridization, sections were washed in 4 × SSC and non-hybridized RNA was digested by incubation with RNaseA (10 μg/ml) for 30 min. Bound DIG-labelled hybrids were detected by enzyme-linked immunoassay using an anti-DIG alkaline phosphatase conjugate, and visualized via a colour reaction with Nitroblue Tetrazolium and 5-bromo-4-chloroindol-3-yl phosphate as substrates (Roche).

Western-blot analysis

Cultured primary hepatocytes in 60 mm diameter dishes were washed with 0.9% NaCl and then frozen for 10 min at −20 °C. The cells were scraped in 1 ml of boiled SDS buffer [10 mM Tris/HCl (pH 7.5)/0.1% SDS], boiled for 5 min, homogenized through a 25 G needle and centrifuged at 15800 *g* for 5 min. Protein content in the supernatant was determined using the Bradford method. Protein samples (30–50 μg), dissolved in 27 μl of SDS sample buffer [16], were loaded on to an SDS-10% polyacrylamide gel and after electrophoresis blotted on to nitrocellulose membranes. Non-specific binding sites were blocked with blocking buffer [10 mM Tris/HCl (pH 7.5), 100 mM NaCl, 0.1% Tween 20 and 10% (w/v) milk powder]. Blots were incubated with the primary polyclonal rabbit antibody against the β-chain of the human insulin receptor (Affiniti, Exeter, Devon, U.K.) at a 1:250 dilution in blocking buffer overnight at 4 °C. Washing was performed with blocking buffer without the milk powder. The secondary antibody was an anti-rabbit IgG from goat (Santa Cruz Biotechnology, Santa Cruz, CA, U.S.A.) and was used at a 1:2000 dilution for 1 h. After washing for 30 min the enhanced chemiluminescence (ECL) Western-blotting system (Amersham, Braunschweig, Germany) was used for detection. Under these conditions, the insulin receptor β-chain was visible as two bands, of 95 kDa and 69 kDa, caused by different glycosylation status.

Immunohistochemistry

Liver tissue of normal fed rats was embedded in paraffin wax, 5 μm sections were prepared and paraffin wax was removed from liver sections with xylene. The sections were then rehydrated with descending ethanol concentrations and finally equilibrated for 10 min in TBS [50 mM Tris/HCl (pH 7.5)/150 mM NaCl]. For detection of insulin receptor protein after rehydratation, the sections were washed three times with H_2O and boiled for 2.5 min in citrate buffer (1.8 mM mono-citrate and 8.2 mM tri-sodium-citrate, pH 6) at 360 W in a microwave oven. The sections were subsequently treated with 100 μl of pepsin [0.4 % (w/v) pepsin in 0.01 M HCl] for 5 min at 37 °C and were washed again in TBS for 10 min. To prevent non-specific binding of the primary antibody, the sections were blocked with 20 % (v/v) FCS in TBS for 30 min at 37 °C. The diluted primary antibody was applied in 0.1 % BSA in TBS overnight at 37 °C. The following were used as primary antibodies: insulin receptor β-chain antibody (Affiniti) at 1:100 dilution and glutamine synthetase (GS) antibody (Affiniti) at 1:100 dilution were used as perivenous markers [17,18] and EAG15 polyclonal antibody at 1:100 dilution, raised against the C-terminus of the rat canalicular multidrug resistance protein (cMRP), was used as a membrane marker [19]. The peroxidase-conjugated secondary antibodies were used at 1:100 dilution in 0.1 % BSA in TBS for 30 min at 37 °C. After washing, the sections were incubated with a 1:10 dilution of diaminobenzidine (Pierce, Rockford, IL, U.S.A.) in 1 × peroxidase buffer (Pierce) for 10 min. The reaction was stopped in TBS and the sections were covered with DePex (Serva, Heidelberg, Germany) and photographed.

RESULTS

The possible zonated insulin receptor gene expression in rat liver was studied by *in situ* hybridization and immunhistochemistry. Primary rat hepatocyte cultures were used to study the influence of the substrates glucose and oxygen as possible determinants for the zonated gene expression.

Homogeneous distribution of insulin receptor mRNA in rat liver

In situ hybridization with paraffin-embedded sections from rat liver showed that insulin receptor mRNA was equally distributed over the liver acinus (Figure 1). In parallel sections, PCK1 mRNA, which served as a periportal marker [20], was localized in the periportal area (Figure 1). GS mRNA, which is a perivenous marker [17,18], was found to be expressed in the distal perivenous area only (results not shown). Since there was no zonation of insulin receptor mRNA expression in rat liver, the regulation of a possible zonation of the insulin receptor might occur at the post-transcriptional level.

Perivenous zonation of insulin receptor protein in rat liver

The distribution of the insulin receptor protein was studied by immunhistochemistry using sections from paraffin-embedded rat liver, which were incubated with an antibody against the β-subunit of the insulin receptor. The insulin receptor protein was predominantly localized in the perivenous zone (Figure 2A), mainly in the plasma membranes (Figure 2B). In parallel sections, GS protein was detected in the distal perivenous area (Figure 2A). In contrast to the GS protein, which was expressed only in the last two cell layers around the central vein (distal perivenous zone), the insulin receptor protein was found in all zones, with a predominance in the intermediate and the distal perivenous zones. These results were identical with the results obtained with an antibody against the α-subunit of the insulin receptor (results not shown). As a positive control for the presence of the insulin receptor protein on the outer cell

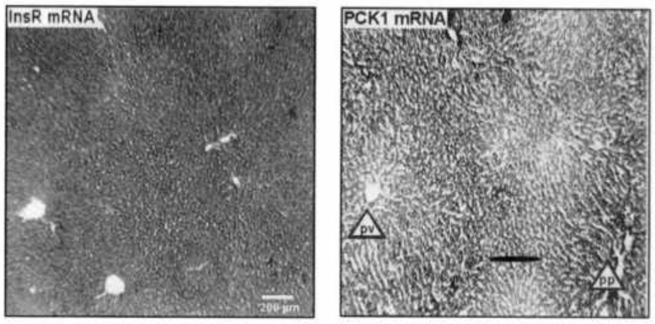

Figure 1 Homogenous distribution of insulin receptor mRNA in rat liver

Parallel sections (5 μm) were prepared at the end of the feeding period from livers of rats kept under a normal daily feeding cycle. mRNAs were localized by *in situ* hybridization using DIG-labelled insulin receptor (InsR) and PCK1 antisense RNA probes, and an alkaline phosphatase-conjugated antibody against DIG (see the Materials and methods section). Dark precipitates indicate high levels of InsR mRNA throughout the tissue, and of PCK1 mRNA in the periportal area. pp, periportal; pv, perivenous. Bar, 200 μm.

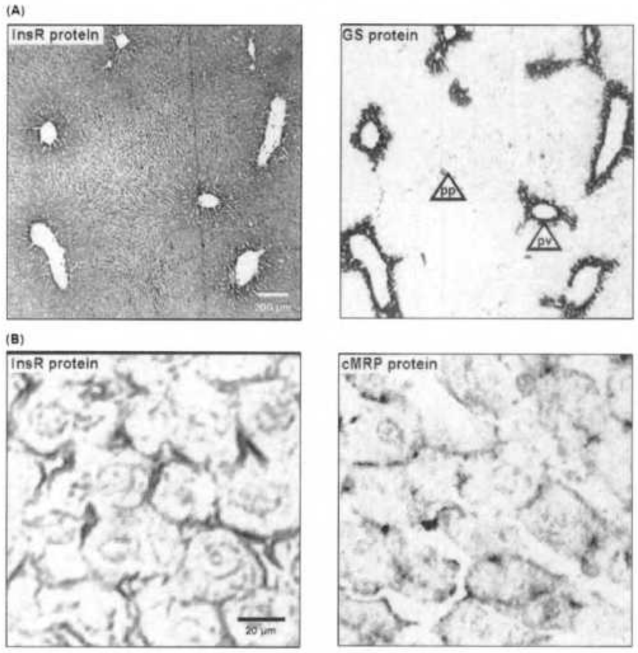

Figure 2 Perivenous zonation of insulin receptor protein in rat liver

(**A**) Localization of insulin receptor protein in the tissue. Parallel sections (5 μm) were prepared at the end of the feeding period from livers of rats kept under a normal daily feeding cycle. Proteins were localized by immunhistochemistry using a polyclonal rabbit antibody raised against the β-chain of the insulin receptor (InsR) or a mouse antibody raised against sheep GS, as primary antibodies, and a peroxidase-conjugated secondary antibody against rabbit or mouse IgG (see the Materials and methods section). Dark precipitates indicate high levels of InsR protein and GS protein. pp, periportal; pv, perivenous. Bar, 200 μm. (**B**) Localization of insulin receptor protein on the basolateral cell membrane. Immunhistochemistry was performed as described in (**A**). A polyclonal antibody against the C-terminus of the rat cMRP was used as a membrane marker [19]. Bar, 20 μm.

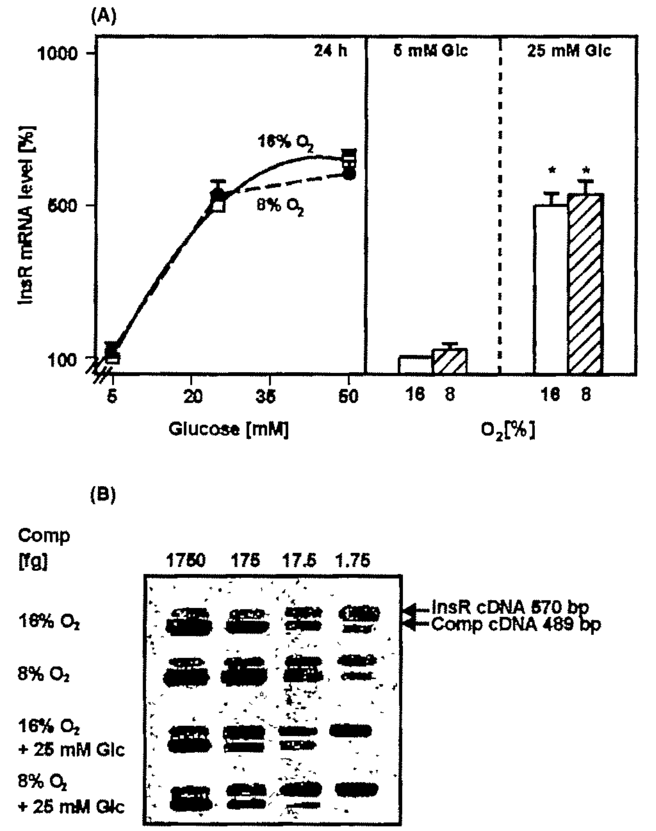

Figure 3 Induction of insulin receptor mRNA by glucose under periportal and perivenous pO_2 in rat primary hepatocyte cultures

(A) Cells were cultured for 4 h under arterial pO_2 (16% O_2) at the basal glucose levels (5 mM) of the culture medium M 199 Glucose was then added to the final indicated concentrations and the cells were cultured under arterial or venous pO_2 (8% O_2) for a further 24 h Cells were harvested and total RNA was prepared Total RNA (2 μg) was used to generate cDNA by reverse transcription, which was used with different concentrations of competitor DNA (1 75–1750 fg), sense primer and antisense primer in competitive PCR (see the Materials and methods section) In each experiment with basal glucose under arterial pO_2 the insulin receptor (InsR) mRNA levels were set to 100% when equimolar amounts of InsR cDNA and competitor DNA were present (17 5 fg = 100%) Values are means ± S E M of three independent culture experiments Statistics Student's *t* test for paired values *significant difference between basal glucose versus high glucose, $P \leq 0\ 05$ (B) Competitive PCR PCR products with a size of 570 bp (InsR) and 489 bp (Competitor DNA) were separated in a 2% agarose gel Glc, glucose, Comp, competitor

membranes, parallel sections were treated with an antibody against the isoform of the cMRP, which is localized on the canalicular membranes (Figure 2B). Thus the insulin receptor protein was predominantly expressed in the perivenous area, in which the insulin-activated pathways of glycolysis and glycogen synthesis have been localized previously [7,11].

Induction of insulin receptor mRNA by glucose in primary hepatocyte cultures

To study the influence of the substrates oxygen, as a key regulator of the zonated gene expression, and glucose, hepatocyte cultures were treated with increasing glucose levels and incubated under arterial or venous pO_2. In 4-h rat hepatocyte cultures the expression of insulin receptor mRNA was induced within 24 h by increasing glucose concentrations from 5 mM up to 50 mM to the same extent under periportal pO_2 and perivenous pO_2 (Figure 3). Glucose (25 mM) induced insulin receptor mRNA by approx. 5-fold and with 50 mM glucose it was induced by approx. 5.2-fold. The increase in insulin receptor mRNA levels by 25 mM glucose was linear with time over 24 h (results not shown) and this concentration was chosen for further experiments. As a control, the induction by glucose of pyruvate kinase L (L-PK) was studied [21]. Glucose (25 mM) increased L-PK mRNA by 2-fold within 24 h (results not shown). Thus since the difference in glucose concentration from periportal to perivenous is rather shallow, the increase in glucose concentrations, as occurs in the portal vein after a meal, enhanced insulin receptor mRNA to approx. the same levels in hepatocyte cultures under periportal and perivenous pO_2. This is in accord with the homogenous expression of insulin receptor mRNA in rat liver (Figure 1).

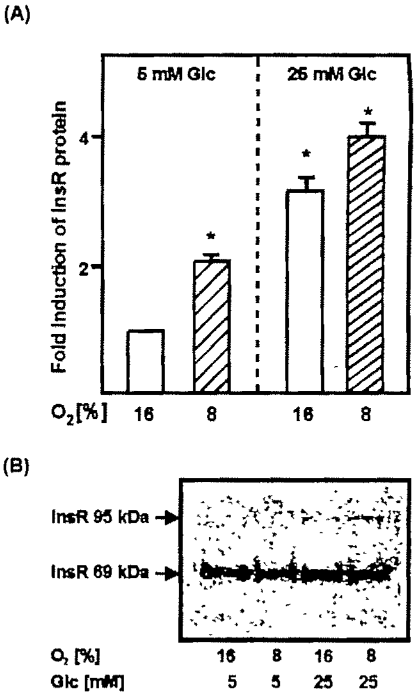

Figure 4 Induction of insulin receptor protein by perivenous pO_2 at basal glucose levels and by high glucose concentrations under periportal and perivenous pO_2 in rat primary hepatocyte cultures

(A) Cells were cultured for 4 h under arterial pO_2 (16% O_2) at the basal glucose levels (5 mM) of the culture medium M199 The cells were cultured under arterial or venous pO_2 (8% O_2) for a further 24 h with the glucose concentration being raised to 25 mM, when indicated Total protein was analysed by Western blotting using a polyclonal rabbit antibody raised against the β-chain of the insulin receptor (InsR) as primary antibody and an anti-rabbit IgG as secondary antibody (see the Materials and methods section), the immune complex was detected by ECL Blots were quantified with a videodensitometer Values are means ± S E M. of three independent experiments Statistics· Student's *t* test for paired values *significant differences between 16% O_2 basal glucose versus 8% basal glucose, 16% O_2 basal glucose versus 16% high glucose, 16% O_2 basal glucose versus 8% high glucose, $P \leq 0\ 05$ (B) Representative Western-blot, 40 μg of total protein was analysed Glc, glucose

Induction of insulin receptor protein by perivenous pO_2 at basal glucose levels and by high glucose concentrations under periportal and perivenous pO_2 in primary hepatocyte cultures

In 4-h rat hepatocyte cultures insulin receptor protein was induced at basal 5 mM glucose within 24 h by perivenous pO_2, and more strongly by 25 mM glucose under both periportal and perivenous pO_2 (Figure 4). Perivenous pO_2 induced insulin receptor protein approx. 2-fold, 25 mM glucose enhanced insulin receptor protein expression approx. 3-fold under periportal pO_2 and approx. 4-fold under perivenous pO_2 (Figure 4). Thus the zonation of insulin receptor protein appeared to be regulated mainly at the post-transcriptional level by O_2 (Figure 2).

DISCUSSION

Zonation of insulin receptor gene expression

According to the model of 'metabolic zonation' insulin-stimulated glycolysis and glycogen synthesis occur mainly in the less aerobic perivenous zone of the liver acinus [7,10–12]. Therefore it was expected that the insulin receptor would be expressed in the perivenous area. It was found that the insulin receptor mRNA was distributed homogenously and that the insulin receptor protein was predominantly localized in the perivenous zone (Figures 1 and 2). The equal expression of insulin receptor mRNA and the mainly perivenous localization of insulin receptor protein corresponds to the homogenous distribution of the insulin-inducible glucokinase mRNA [22], and the preferentially perivenous occurrence of glucokinase protein [23] in the liver of normal fed rats [24]. However, the glucagon receptor mRNA [14] and glucagon-inducible PCK1 mRNA and protein [25] were located in the more aerobic periportal zone of the liver acinus, where gluconeogenesis and glucagon-stimulated glycogenolysis mainly occur [7,11,12]. Thus the perivenous expression of the insulin receptor protein is in good agreement with the model of metabolic zonation.

Modulation of insulin receptor gene expression by oxygen and glucose

The periportal to perivenous pO_2 gradient was proposed to be a key regulator for the zonation of gene expression [7,10–12]. In rat primary hepatocyte cultures the glucose-inducible insulin receptor mRNA expression was not modulated by O_2. This pO_2-independent induction might explain the equal expression of the insulin receptor mRNA, and implies that the regulation of the zonation of insulin receptor protein might occur mainly at the post-transcriptional level. Indeed, insulin receptor protein expression was induced at basal 5 mM glucose levels by venous pO_2 (Figure 4). Insulin receptor protein was also induced by high glucose concentrations; but then the modulation by O_2 became less dominant (Figure 4). Thus the insulin receptor might be an example of a role for O_2 to modulate zonation of gene expression at the post-transcriptional level. Conversely, the modulatory role of O_2 in the zonation of gene expression was shown to occur at the transcriptional level in rat primary hepatocytes with the gluconeogenic key enzyme, PCK1, and the glucose-utilizing enzyme, glucokinase; glucagon activated the transcription of the PCK1 gene maximally under periportal pO_2 [26,27] and, reciprocally, insulin activated the transcription of the glucokinase gene maximally under perivenous pO_2 [28].

Glucose is known to induce the expression of the glycolytic enzyme gene L-PK in hepatocytes and the lipogenic enzyme genes, acetyl-CoA carboxylase and fatty acid synthase, in liver and adipose tissue [29–31]. Insulin and consequently the insulin receptor are functionally linked to glucose uptake. Therefore one would have expected an inductive effect of glucose, which was indeed the case (Figures 3 and 4). The mechanism by which glucose induced insulin receptor mRNA is not completely understood. A post-transcriptional mechanism such as stabilization of insulin receptor mRNA may be responsible in part for the glucose-induced insulin receptor mRNA increase This is indicated by a previous study with mouse embryo fibroblasts transformed with a vector containing the coding region of the human insulin receptor [31]. In these transformed cells, 25 mM glucose increased insulin receptor mRNA levels, the amount of insulin receptor protein and tyrosine kinase activity after 24–48 h. These alterations were associated with an increased half-life of insulin receptor mRNA in the presence of 25 mM glucose [32].

The positive modulation by perivenous pO_2 of the insulin receptor protein would confirm the predominant perivenous localization of the insulin receptor, which is in good agreement with the model of metabolic zonation, and is further evidence that the periportal to perivenous pO_2 gradient appears to be a major determinant in the zonation of gene expression.

This study was supported by the Deutsche Forschungsgemeinschaft SFB 402 Teilprojekt A1 We thank Professor Dr Dietrich Keppler (Deutsches Krebsforschungszentrum, Abteilung Tumorbiochemie, Heidelberg, Germany) for providing us with the EAG15 polyclonal antibody against the C-terminus of the rat cMRP.

REFERENCES

1 Lee, J and Pilch, P F (1994) The insulin receptor structure, function, and signaling Am J Physiol **266**, C319–C334

2 Schumacher, R, Soos, M A, Schlessinger, J, Brandenburg, D, Siddle, K. and Ullrich, A. (1993) Signaling-competent receptor chimeras allow mapping of major insulin receptor binding domain determinants J. Biol Chem **268**, 1087–1094

3 Rosen, O. M (1987) After insulin binds Science **237**, 1452–1458

4 White, M F and Kahn, C R. (1994) The insulin signaling system J. Biol Chem **269**, 1–4

5 Wei, L, Hubbard, S R, Hendrickson, W A and Ellis, L (1995) Expression, characterization, and crystallization of the catalytic core of the human insulin receptor protein-tyrosine kinase domain. J Biol Chem **270**, 8122–8130

6 Myers, Jr, M G, Sun, X. J and White, M F (1994) The IRS-1 signaling system. Trends Biochem Sci **19**, 289–293

7 Jungermann, K. and Katz, N. (1989) Functional specialization of different hepatocyte populations. Physiol Rev **69**, 708–764

8 Haussinger, D, Lamers, W H and Moorman, A F (1992) Hepatocyte heterogeneity in the metabolism of amino acids and ammonia Enzyme **46**, 72–93

9 Gebhardt, R, Gaunitz, F and Mecke, D (1994) Heterogeneous (positional) expression of hepatic glutamine synthetase features, regulation and implications for hepatocarcinogenesis Adv Enzyme Regul **34**, 27–56

10 Jungermann, K (1995) Zonation of metabolism and gene expression in liver Histochem Cell Biol **103**, 81–91

11 Jungermann, K and Kietzmann, T (1996) Zonation of parenchymal and nonparenchymal metabolism in liver Annu Rev Nutr **16**, 179–203

12 Kietzmann, T and Jungermann, K (1997) Modulation by oxygen of zonal gene expression in liver studied in primary rat hepatocyte cultures Cell Biol. Toxicol. **13**, 243–255

13 Antakly, T and Eisen, H J (1984) Immunocytochemical localization of glucocorticoid receptors in target cells Endocrinology **115**, 1984–1989

14 Krones, A, Kietzmann, T and Jungermann, K (1998) Periportal localization of glucagon receptor mRNA in rat liver and regulation of its expression by glucose and oxygen in hepatocyte cultures FEBS Lett **421**, 136–140

15 Nauck, M, Wolfle, D, Katz, N and Jungermann, K (1981) Modulation of the glucagon-dependent induction of phosphoenolpyruvate carboxykinase and tyrosine aminotransferase by arterial and venous oxygen concentrations in hepatocyte cultures Eur J. Biochem **119**, 657–661

16 Laemmli, U K (1970) A factor preventing the major head protein of bacteriophage T4 from random aggregation Nature **227**, 680–685

17 Gebhardt, R, Ebert, A and Bauer, G (1988) Heterogeneous expression of glutamine synthetase mRNA in rat liver parenchyma revealed by in situ hybridization and Northern blot analysis of RNA from periportal and perivenous hepatocytes. FEBS Lett **241**, 89–93

18 Moorman, A F, De, B P, Geerts, W J, van-den, Z L, Lamers, W H and Charles, R (1988) Complementary distribution of carbamoylphosphate synthetase (ammonia) and glutamine synthetase in rat liver acinus is regulated at a pretranslational level. J Histochem Cytochem **36**, 751–755

19 Buchler, M, Konig, J, Brom, M., Kartenbeck, J., Spring, H, Horie, T and Keppler, D (1996) cDNA cloning of the hepatocyte canalicular isoform of the multidrug resistance protein, cMrp, reveals a novel conjugate export pump deficient in hyperbilirubinemic mutant rats. J Biol Chem **271**, 15091–15098

20 Bartels, H, Linnemann, H and Jungermann, K (1989) Predominant localization of phosphoenolpyruvate carboxykinase mRNA in the periportal zone of rat liver parenchyma demonstrated by in situ hybridization. FEBS Lett **248**, 188–194

21 Doiron, B, Cuif, M H, Kahn, A and Diaz, G M. (1994) Respective roles of glucose, fructose, and insulin in the regulation of the liver-specific pyruvate kinase gene promoter J Biol Chem. **269**, 10213–10216

22 Eilers, F, Bartels, H and Jungermann, K (1993) Zonal expression of the glucokinase gene in rat liver Dynamics during the daily feeding rhythm and starvation-refeeding cycle demonstrated by in situ hybridization Histochemistry **99**, 133–140

23 Kirchner, G, Harbers, M., Bunsch, A, Seitz, H J. and Hoppner, W (1993) Zonation of glucokinase in rat liver changes during postnatal development FEBS Lett **328**, 119–124

24 Moorman, A F., De, B P., Charles, R and Lamers, W. H (1991) Pericentral expression pattern of glucokinase mRNA in the rat liver lobulus FEBS Lett **287**, 47–52

25 Bartels, H, Freimann, S and Jungermann, K (1993) Predominant periportal expression of the phosphoenolpyruvate carboxykinase gene in liver of fed and fasted mice, hamsters and rats studied by in situ hybridization Histochemistry **99**, 303–309

26 Hellkamp, J, Christ, B, Bastian, H and Jungermann, K (1991) Modulation by oxygen of the glucagon-dependent activation of the phosphoenolpyruvate carboxykinase gene in rat hepatocyte cultures Eur. J Biochem **198**, 635–639

27 Kletzmann, T, Freimann, S, Bratke, J. and Jungermann, K (1996) Regulation of the gluconeogenic phosphoenolpyruvate carboxykinase and glycolytic aldolase A gene expression by O_2 in rat hepatocyte cultures Involvement of hydrogen peroxide as mediator in the response to O_2 FEBS Lett **388**, 228–232

28 Kietzmann, T, Roth, U., Freimann, S and Jungermann, K (1997) Arterial oxygen partial pressures reduce the insulin-dependent induction of the perivenously located glucokinase in rat hepatocyte cultures mimicry of arterial oxygen pressures by H_2O_2 Biochem. J **321**, 17–20

29 Towle, H C (1995) Metabolic regulation of gene transcription in mammals J. Biol Chem **270**, 23235–23238

30 Kahn, A (1997) Transcriptional regulation by glucose in the liver. Biochimie **79**, 113–118

31 Girard, J, Ferre, P and Foufelle, F. (1997) Mechanisms by which carbohydrates regulate expression of genes for glycolytic and lipogenic enzymes Annu. Rev Nutr **17**, 325–352

32 Hauguel-de, M S, Mrejen, C., Alengrin, F and Van, O E (1995) Glucose-induced stimulation of human insulin-receptor mRNA and tyrosine kinase activity in cultured cells Biochem J **305**, 119–124

Received 1 March 2000/28 March 2000, accepted 30 March 2000

Zebrafish *ftz-f1* gene has two promoters, is alternatively spliced, and is expressed in digestive organs

Wen-wen LIN*, Hsin-Wei WANG*†, Cristina SUM*, Dong LIU‡, Choy L. HEW‡ and Bon-chu CHUNG*[1]

*Institute of Molecular Biology, Academia Sinica, Nankang, Taipei, Taiwan, Republic of China, †Graduate School of Zoology, National Taiwan University, Taipei, Taiwan, Republic of China, and ‡Division of Structural Biology and Biochemistry, Hospital for Sick Children, Toronto, Ontario, Canada M5G 1X8

Fushi-tarazu Factor-1 (FTZ-F1) is a family of nuclear receptors involved in various developmental processes. We have cloned a zebrafish FTZ-F1 gene, termed *ff1*, which belongs to the feto-protein transcription factor/liver receptor homologue-1 (FTF/LRH-1) subgroup of the FTZ-F1 family. Four transcripts arise as a result of differential promoter usage and alternative splicing at the 3′-most exons. The longer transcript, form A, encodes a transcriptional activator. The shorter transcript, form B, lacks the activation domain, and hence could not activate transcription. The difference in promoter usage generates FF1 proteins with different N-terminal sequences. All four transcripts appear to be expressed in most of the adult tissues, whereas, during embryo development, the IIA form is the predominant transcript. Reverse transcriptase-PCR and *in situ* hybridization experiments showed that the *ff1* transcript is expressed in the hypothalamus, spinal cord, mandibular arch and digestive organs, including pancreas, liver, and intestine. The expression of *ff1* in the digestive organs implies its function in gut development.

Key words: fetoprotein transcription factor (FTF), gut, liver receptor homologue (LRH), nuclear receptor, steroidogenic factor 1 (SF1).

INTRODUCTION

Fushi-tarazu Factor-1 (FTZ-F1) was first found to be the transcription factor that activates the *ftz* gene in *Drosophila*, and was subsequently named as such [1,2]. Many FTZ-F1 homologues have been found in mouse, human, zebrafish and *Xenopus* [3–7]. These FTZ-F1 homologues contain a conserved sequence adjacent to the C-terminal end of the zinc-finger motif, termed the FTZ-F1 box [2]. In addition, they belong to the nuclear receptor superfamily, most members of which can activate transcription when bound to their ligands [8]. FTZ-F1 belongs to the orphan receptor family, which does not have known ligands, but can activate transcription [9,10]. Unlike other members in the nuclear receptor superfamily, which often dimerize and recognize the GGTCA sequence as direct or inverted repeats, FTZ-F1 binds to the monomeric (A/T)CAAGG(A/T)C(C/G) sequence [11]. Many nuclear receptors activate transcription via an activation domain, AF-2, located at their C-terminus. Some of the FTZ-F1 members do not have this activation domain; they therefore serve as repressors of transcription [6,12]. Since these nuclear receptor proteins control many important developmental and physiological processes, it is imperative to understand their control mechanism.

Two forms of the *Drosophila ftz-f1* gene products, named α and β, have been identified. *ftz-f1*α is maternally expressed and distributed in the early embryo [1], whereas *ftz-f1*β is zygotically expressed and present in the late embryo and early pupal stages [13]. Both forms play a role in ecdysone-induced gene expression [14].

Xenopus also has two *ftz-f1* genes [3], of which the gene products, xFF1rA and xFF1rB, are probably the orthologues of mouse liver receptor homologue (LRH)-1. In addition to the full-length cDNA, another shorter gene product with a C-terminal deletion, termed 'xFF1rA-short', was also isolated [12]. xFF1A-short is present at a lower concentration, and lacks the transactivation function.

In humans, different FTZ-F1 homologues exist. One is hB1F, which is expressed in the hepatocyte and can bind and activate enhancer II of hepatitis B virus [15]. Various mouse FTZ-F1 homologues have also been reported. Among them, steroidogenic factor 1 (SF1) and embryonal long-terminal-repeat binding protein (ELP) have overlapping transcription units, which share most exons, but have their own promoters and are differentially spliced [16]. SF1 is expressed mainly in the adrenal, testis, ovary, pituitary gonadotroph and some regions of the brain [17]. It plays an important role in the development of the above cell types and transactivation of a number of genes involved in steroidogenesis and other endocrine functions. ELP is found in embryonic carcinoma cells, with an as-yet-unidentified physiological function [18].

Another FTZ-F1 homologue in the mouse is termed LRH-1 [19]. LRH-1 and SF1 are very similar in the DNA-binding domain, but more divergent in the ligand-binding domain. Therefore there are at least two different *ftz-f1* genes in the mouse. LRH-1 is expressed mainly in the liver, but its function is still not clear at present. In the rat, the LRH-1 orthologue is termed FTF (fetoprotein transcription factor), a transcription factor for the α1-fetoprotein gene [20]. Rat FTF is expressed mainly in the gut endodermal cells, including liver and pancreas [20]. On the basis of the expression pattern, it may be inferred that FTF functions during differentiation of gut endodermal cells.

Abbreviations used: FTZ-F1, Fushi-tarazu Factor-1, *ff1*, zebrafish gene homologue of the FTZ-F1 family of nuclear receptors (the corresponding protein product is FF1); FTF, fetoprotein transcription factor, LRH, liver receptor homologue, ELP, embryonal long terminal repeat-binding protein, SF1, steroidogenic factor 1; 5′-RACE, 5′-rapid amplification of cDNA ends, RT, reverse transcriptase, CAT, chloroamphenicol acetyltransferase, LG22, linkage group 22

[1] To whom correspondence should be addressed (e-mail mbchung@sinica.edu.tw).

In zebrafish, we have cloned an *ftz-f1* homologue named *ff1* [6], or NR5A2, according to the new nomenclature [21] (the protein products are designated as FF1 proteins). In the present report we describe our characterization of the zebrafish *ff1* gene. We found that the *ff1* gene is differentially spliced, resulting in an active A form and an inactive B form. In addition, it contains two separate promoters, resulting in differential utilization of exons at the 5′-region. Although both promoters are used in most of the tissues examined, the downstream promoter is preferentially used during embryonic development. *In situ* hybridization experiments showed that the *ff1* transcript was found in the brain, spinal cord, mandibular arch and digestive organs. This expression pattern implies the functional importance of *ff1* in the development of digestive organs.

MATERIALS AND METHODS

Isolation of genomic clones and DNA sequencing

Genomic clones containing the *ff1* gene were isolated from a zebrafish genomic DNA library using FF1 cDNA fragments as probes. Four clones (nos. 36, 48, 55 and 37) were further analysed. The exons and introns in these clones were identified by either PCR amplification of the λ-phage lysate with exon-specific primers or hybridization with specific end-labelled oligonucleotides. The fragments spanning exon–intron boundaries were either sequenced directly from λ-DNA or subcloned into pCRII vector (Invitrogen, San Diego, CA, U.S.A.), followed by sequencing. Introns 1, 2 and 3 were fully sequenced.

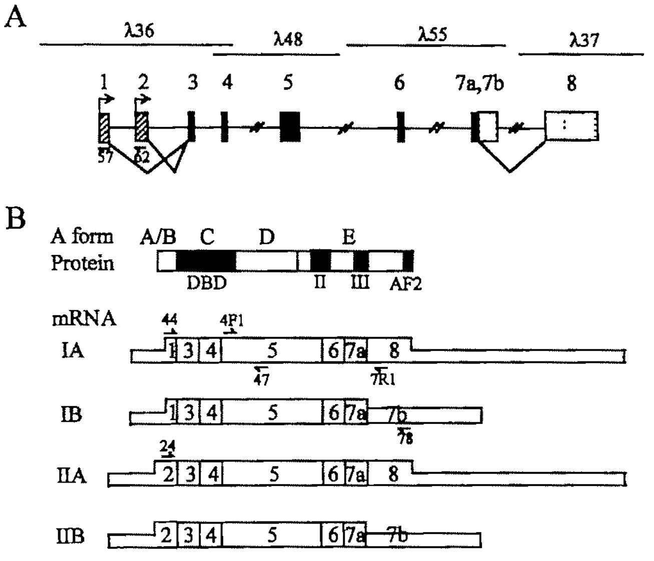

Figure 1 Organization and multiple transcripts of the zebrafish *ff1* gene

(A) Structure and alternative splicing patterns of the *ff1* gene Exons are shown by boxes and introns by intervening lines Horizontal lines above the gene structure indicate the extent of phage genomic clones Alternative splicing events at the 5′- and 3′-ends of the gene are shown below the gene structure Filled-in boxes represent exons common to all transcripts Hatched and stippled boxes are exons unique to one form of the transcripts The antisense primers 57 and 62, used in primer extensions, are shown by semi-arrows. **(B)** Diagram of four transcripts encoded by the *ff1* gene The functional domains of the FF1 protein are shown above the exons The DNA-binding domain (DBD), regions II and III and AF-2 are indicated by the filled-in boxes Numbers inside boxes represent exon numbers, and the locations of primers used in the RT-PCR analysis are also shown (by semi-arrows) The translated and untranslated regions are shown by wide and narrow rectangular boxes respectively

Primer extension and 5′-rapid amplification of cDNA ends (5′-RACE)

Antisense oligonucleotides, #57 (AGTCTTTGCAGTCAC GTTGTCCT) and #62 (GTGGTCTTTGCAGTGACTATG-ATG), were used for mapping the transcription-start sites on exon 1 and exon 2 respectively. Oligonucleotides were end-labelled with $[^{32}P]$ATP, and annealed to 50 μg of total RNA at 50 °C overnight before extension reactions, as described previously [22] The sequencing of the genomic fragment using the same primers was performed in parallel, and the reaction products were resolved by sequencing gels. Transcription-start sites were confirmed by 5′-RACE [23], followed by cloning and sequencing of the amplified fragments.

Reverse transcriptase (RT)-PCR and Southern-blot hybridization

RT-PCR and Southern-blot hybridization procedures were carried out as described previously [24]. The locations of the primer pairs 44/47, 24/47, 4F1/7R1 and 4F1/78 for the amplification of exon 1, exon 2, form A and form B cDNA respectively, are shown in Figure 1. Their sequences are as follows: 44, AGGACAACGGACTG CAAAGACT; 24, GGACGGCGTT-TTTGAGAATCTGTGGTG; 47, CATGCTGACTGGTG AATGTACGA; 4F1, AATGTGCAAGATGGCTGACCAG; 78, GATGCCAGACTAG TCACGTCT; and 7R1, CACATC-ACGTAGTCCAGCAGTG.

Computer analysis

DNA sequences were analysed with the Wisconsin Sequence Analysis Package of GCG. The BLAST program was used to compare the zebrafish FF1 amino acid sequences with GenBank® and EMBL databases [25]. Multiple sequence alignments and phylogenetic trees were generated with the UPGMA method in SeqWeb (http://www.nhri.org.tw/b5/mis/seqweb.htm). Both TESS and MatInspector programs in the BCM launcher were used to search for potential transcription-factor binding sites [26,27]. Photographs of embryos and sections were scanned and processed using the Adobe Photoshop program.

Whole-mount *in situ* hybridization and sectioning

Adult zebrafish and embryos were reared at 28.5 °C, as described previously [28]. Sense and antisense RNA probes were synthesized by *in vitro* transcription from linearized plasmids containing FF1 cDNA fragments using T7 RNA polymerase and digoxigenin/RNA-labelling mix. Whole-mount *in situ* hybridization was carried out as described previously [28]. After *in situ* hybridization, embryos were washed in 0.1 % (v/v) Tween 20, stored in 4 % (w/v) paraformaldehyde, and photographed in 80 % (v/v) glycerol. Embryos were washed in PBS and embedded in 1.2 % agarose/5 % sucrose (w/v) prior to cryosectioning, as described previously [28]. Frozen sections were stained with Nuclear Fast Red.

Analysis of the activation function of FF1

The full-length FF1A protein (amino acids 1–516) and subsequent deletion fragments were obtained by PCR based on the original FF1 cDNA plasmid [6]. Primers used for the C-terminal deletion constructs were as follows: AAGAGAATTCTCAG-GGCACGTCTCCGTTCAGGTGT(1–501); AGTGAATTCG-CCCGGATCAAGGCTTTCT (1–155). The primer used to obtain the N-terminal deletion clones (43–516 and 43–434) was GACGGATCCATGGATGAGATGTGTCC (Δ1–43). Deletion clone 1–434 was equivalent to the FF1B ORF (where ORF is open reading frame). Restriction enzyme sites at both ends were introduced, so that the resulting DNA fragments could be cloned into the pcDNA3 expression vector (Invitrogen), and stop codon sequences were located in each lower primer for PCR. HeLa cells were chosen for the transient transfection analysis, and consensus gonadotrope-specific element (GSE)-TATA-CAT (where CAT is chloramphenicol acetyltransferase) containing the FF1 recognition site was used as a reporter [6]. Expression plasmid (1 μg), 5–10 μg of CAT reporter plasmid and 1 μg of pCMVβ-LacZ plasmid (as an internal control) were included in each transfection (60-mm dish). CAT and β-galactosidase activities were determined as described previously [29].

RESULTS

Genomic organization and multiple forms of the zebrafish *ftz-f1* gene

We first isolated zebrafish *ftz-f1* A- and B-form cDNAs, which are identical in sequence in most regions, but have distinct sequences at their 3′-ends [6]. To characterize the genomic structure and splicing pattern of the *ftz-f1* (*ff1*) gene, we screened a zebrafish genomic library with FF1A cDNA fragments. Four clones (nos. 36, 37, 48 and 55) were isolated, which mutually covered the entire *ff1* gene (Figure 1A). The zebrafish *ff1* gene consists of eight exons interrupted by seven introns. All exon–intron junctions follow the 'GT...7AG' rule for the splice donor and acceptor sites (Table 1). The A- and B-form mRNAs result from alternative splicing at exon 7. In form A, exon 7a is spliced to exon 8. The form B mRNA retains exon 7b, so that the mature mRNA is terminated at exon 7b. In addition to the 3′ mRNA variants, RT-PCR and cDNA sequence analysis revealed the presence of two leader exons. Transcription starting at exon 2 is spliced to exon 3, whereas transcription starting at exon 1 skips exon 2 and is spliced directly to exon 3.

Therefore alternative promoter usage and splicing of the zebrafish *ff1* gene give rise to four mRNA variants, designated as IA, IB, IIA and IIB respectively (Figure 1B). Exons 3, 4, 5, 6 and 7a are shared by all of these mRNA variants, whereas exons 1, 2, 8 and 7b are unique to each form. Exons 1 and 2 encode the A/B domain in comparison with other nuclear receptor family members (Figure 1B). Exons 3, 4, and part of exon 5 encode the C domain, which contains two zinc-finger motifs and the FTZ-F1 box. Most of exon 5 encodes domain D (hinge region). The 3′ region of exon 5, together with exons 6, 7a and 8 encode the E domain (ligand-binding domain), which contains the AF-2 core. Exon 7b encodes only two amino acids before it runs into a stop codon. Consequently, exon 1 and exon 2 transcripts produce distinct FF1 proteins with different A/B domain sequences. The A-form transcripts produce full-length FF1, whereas the B-form transcripts produce C-terminal-truncated FF1 lacking AF-2.

The transcription-start sites for both leader exons in the liver of adult zebrafish were mapped further by primer extension and 5′-RACE. One major start site in exon 1 was found approx. 222 bp upstream from the 3′-end of exon 1 (Figures 2A and 2B). Although there were two minor bands above and below the major primer-extension product (Figure 2B), they could not be confirmed by 5′-RACE. The start site of exon 2 was mapped to 351 nt upstream from the 3′-end of exon 2 (Figures 2A and 2B). The same transcription-start sites were also identified in brain, ovary and testis RNA (results not shown). Scanning the 5′-flanking sequences for putative transcription-factor binding sites, we found sequences flanking exon 1 that will bind XFD2 (*Xenopus* fork-head domain factor 2), SN (Snail), MyoD, GATA1 and SOX5, and sequences flanking exon 2 that will bind BRN2 (Brain 2), hepatic nuclear factor-3 (HNF3) and S8 (homeoprotein S8) (Figure 2A).

Properties of different forms of the *ff1* gene products

We have shown that alternative promoter usage and splicing generate FF1 forms with different A/B domains and C-termini. To determine whether different A/B domains and C-termini could lead to differences in the transcriptional activities of various forms of FF1, a series of N-terminal and C-terminal

Table 1 Nucleotide sequences of exon/intron boundaries of the zebrafish *ff1* gene

Exon sequences are shown in uppercase letters and intron sequences in lowercase letters

Exon	Size (bp)		Exon/intron junctions Donor site	 Acceptor site
1	222	1/3	TGCAAAGACTTGGgtaagt……	tcttatgttttagCCCCACAGTTTAAA
2	351	2/3	GGAAACATGCAAGgtaagc……	tcttatgttttagCCCCACAGTTTAAA
3	119	3/4	TGAGAGCTGTAAGgtgtgt……	acctcactctgcagGGCTTCTTCAAGCG
4	142	4/5	ATGAAACTGGAGGgtaaga……	tgtccttctataagCTGTGAGAGCCGAT
5	695	5/6	CCGGGAACTAAAGgtatgt……	cactgtcccctcagGTTGACGACCAAAT
6	120	6/7	CACGGGGCAACAGgtgagt……	tgccttctcttcagGTGGATTACGCTCT
7a 7b	148 748	7a/8	CTGTTCAGCTTGGgtgagt……	tctgttttcctcagACGTGAAGAACCTG
8	1697			

A

Exon 1 and its upstream sequence

```
-520  GCCTACATTC ATCCCATTTT AATAAACGAA TACATAAAAA ATTAGATAGG
                                                   XFD2
-470  CCTATGTGCT TTTTGGACTC TGTATACAAA CATGAAAAGT ATAAACATAT

-420  ACTTTGGAGG TGTGTTTACG TGTATTTATT TCCGTCTGTA AGGTGTGACT

-370  TCATCTTGAT CCCGCAGTGA ACACGCGTGT ATATCCTGAT CCTCACACGT

-320  CCAATAAAAC CGCTCGTGTT TGGCAGAAAC TAGTTCAAAG TTTGCGGCCC
          SN                                      MyoD
-270  ACTATCAACC TGTTGTGTTC TTTTGATCTC GCATTTTACC ACCTGTCTCA

-220  TTTCCATTCA GTCATTGCCG TGGACGGTCT TGTCCGCCGG TTAATCATTC
                                 GATA1
-170  CTTCAGTACT ATCTGTCCGC TCCGGCTTAT CTGTCCGTGT GTCACTTTAT

-120  AACTGGCTCT TATCAATCTT GTCCAGCTCC ACGTGATCTG GGCAAACCTA
                               SOX5
 -70  TCAACCTCAG AAGTTTTGAA TATTGTTGAG GAGGTGAGAT ATGACTGCAG
                           +1
 -20  GTTTAGTGCA GGTCATGGCG AGGGGGGATG AGGGCTGAGA AAGTCAAGAG

  31  ATGTCAGGCG GATGGTTTGG GGCAAAAAAA CACCTCAATT TTCTATTCAA

  81  ACGACGGTGA AAGATTTGGA AAGAATGGAC GCGTTTTGTG GGATATAACT
                                                M
 131  AGCCACTCAG GTGGATCACC TGGTGTATTT CTGCACTAAA ATGTCCAGTA

 181  GTTTTGAGAG TGAATTAGGA CAACGTGACT GCAAAGACTT GG
```

Exon 2 and its upstream sequence

```
          BRN2
-480  ATTAACATGA ATAATGCATC TCCTAATTTA AATAACTATG TTTTATGTAG
                                                     HNF3
-430  CTATTTCCAC AAATTAAACT TTTAAAAATC CTTTAGCATC TTGGTGCAAA

-380  TAAGTAAGTC GCAAATATAT AAAAAACGCA ATTTTATGAG ATTATTTTAG

-330  ATCTTATATC AAATTTTATT TAGCCTGATT TTCGTCTTGC CTCCAATTCC

-280  CCCTTTCTCT ATATTTTTTA ATAGCTACAT ACAAACATTT TAACCCTCCG

-230  GTAGGCTAAA TCACCACATA CCTCCCGGTG CTCCAGTTAA CGGCGCGGCG
                    S8
-180  TGTCTCGTAA TGTTCAATTA GTTTAGTTTG TCTGTGTTTG CCGCTGCAAC

-130  TGAGGCGCTT ATTCTCGGGC CCGTTTCTGA TTGGACAAAC GCGTGACGCC

 -80  AGCGCACTGA TCCGAACGCT GATTGGTCGA CGCGGTGTCA GTGCGGCGTA
                                      +1
 -30  AACAAAGCAG CGAGGAGCCG TTTGAACTTC ACAGATAGAG CGACACGGAG

  21  CGCGCGCGGA GGAGGGGCTC GTGCCAAGTT CCTGACAGTT CGCGCACTCC

  71  GGTTTAAAGA CCAGCATCAT AGTCACTGCA AAGACCACCC GAATGAACTT

 121  ACACAGCGTG TGAAGAACTA AAAGAAAAAA GAAGGGTAGT CGAAGTCAAG

 171  CCGAGGATTT GTTTCGGACG TTTGGACGGC GTTTTTGAGA ATCTGTGGTG

 221  GCGCGCAGGC GGAGCGGCGC GCGCTCATCA TCGGCTCAGC AGAGCTGTCA
      M
 271  TGCTGCCTAA AGTCGAGTCA GAATATCTGG GACTCGCTCG ATCGCATGGG

 321  GAACAGGGGC ATATGCCTGG AAACATGCAA G
```

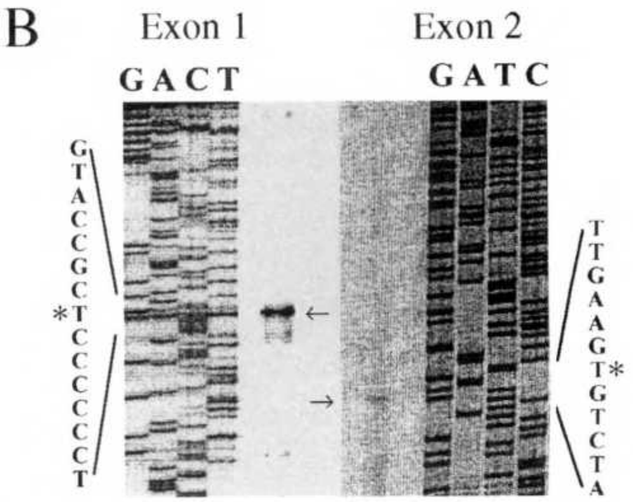

Figure 2 Zebrafish *ff1* gene has two promoters

(**A**) Sequences of the first and second exon and their respective 5′-upstream regions. Transcription-start sites and the translation initiation codon are indicated by horizontal arrows and M respectively. Potential transcription-factor binding sites located upstream of the start sites are indicated by lines above the recognition sequence. (**B**) Mapping of transcription-start sites on exon 1 and exon 2 by primer extension. A ^{32}P-labelled antisense oligonucleotide was hybridized to liver total RNA and extended with RT, as described in the Materials and methods section. The same primer was used in the dideoxynucleotide-sequencing reactions on a plasmid containing the exon 1 or exon 2 sequences. The primer extension product and the sequencing reactions were separated on a sequencing gel, and detected by autoradiography. The asterisk denotes the transcription-start nucleotide in the lower strand, and the arrows highlight the primer-extension products.

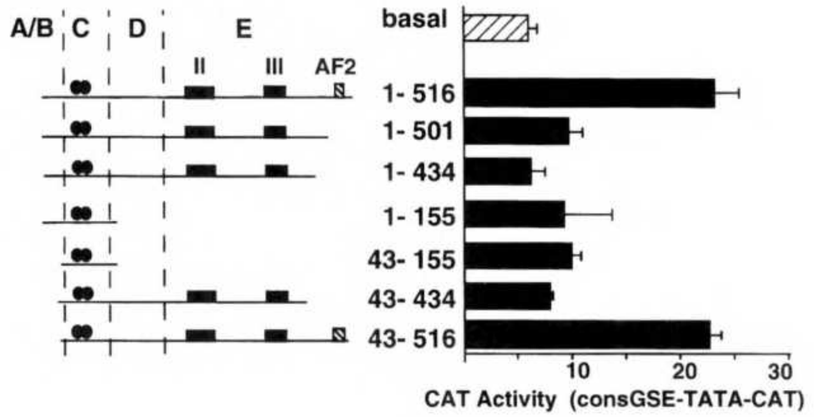

Figure 3 Analysis of FF1 domain function for transcriptional activation

The structure of the effector plasmids are shown on the left (Figure is not to scale), with the numbers indicating the beginning and end of the effector molecules. The effect of deletion clones were examined with a co-transfection study in HeLa cells. The reporter construct is a *sGTHIIβ* gene −39 basal promoter linked to the *CAT* gene, with a consensus GSE sequence 5′ upstream (consGSE-TATA-CAT). Basal value represents the activity of the consGSE-TATA promoter without transcription-factor co-transfection. All histograms represent the means ± S.E.M. of at least two independent experiments (in duplicate or triplicate).

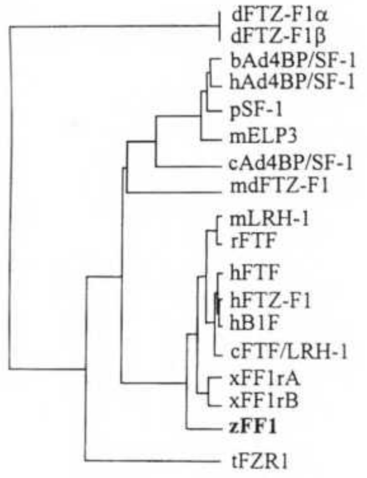

Figure 4 A phylogenetic tree of FTZ-F1-related proteins

The zebrafish FF1 protein falls into the group of FTF/LRH-1 proteins. The DDBJ/EMBL/GenBank* accession numbers of the proteins included in the tree are: dFTZ-F1 (M63711), dFTZ-F1 (M98937), bAd4BP/SF-1 (D13569), hAd4BP/SF-1 (U76388), pSF-1 (U84399), mELP3 (AB000490), cAd4BP/SF-1 (AB002404), mdFTZ-F1 (AB016834), mLRH-1 (M81385), rFTF (U47280), hFTF (U93553), hFTZ-F1 (AB019246), hB1F (U80251), cFTF/LRH-1 (AB002403), xFF1rA (U05001), xFF1rB (U05003), zFF1 (AF014926), tFZR1 (AB006153). d, *Drosophila*; b, bovine; h, human; p, pig; m, mouse; c, chicken; md, medaka; r, rat; x, *Xenopus*; z, zebrafish; t, trout.

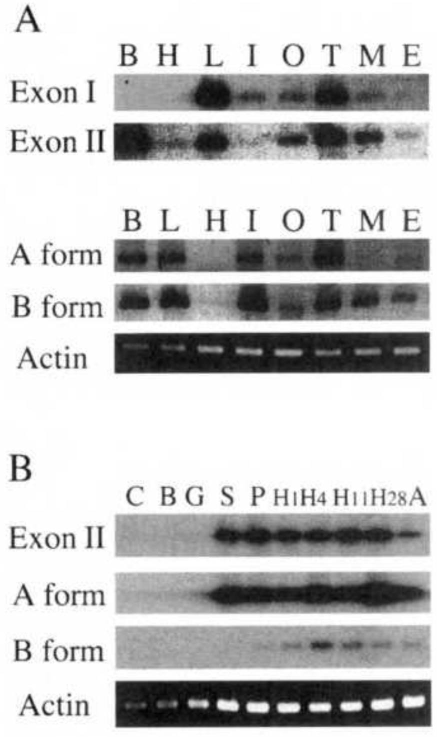

Figure 5 Tissue and developmental expression patterns for zebrafish FF1 mRNA variants

RT-PCR was performed using primers specific for different isoforms of the ff1 mRNA, followed by Southern-blot hybridization. Actin amplification was used as a reference for the amount of total RNA input in the analysis. (**A**) Expression of FF1 mRNA variants in various adult tissues. B, brain; H, heart; L, liver; I, intestine; O, ovary; T, testis; M, muscle; E, eye. (**B**) Developmental expression of *FF1* exon II, A form, and B form mRNA. C, cleavage; B, blastula; G, gastrula; S, segmentation; P, pharyngula; H1, H4, H11 and H28, 1, 4, 11 and 28 days after hatching respectively; A, adult.

deletion constructs were tested (Figure 3). In co-transfection experiments, the removal of the AF-2 region resulted in a significant loss of the transcriptional activity of FF1A (as seen in clone 1–501). Proteins with clone 1–434 (equivalent to zFF1B) and 1–155 yielded a transactivation potential similar to that of clone 1–501. These data suggest that AF-2 is critical to the activation function of FF1A, and FF1B is transcriptionally inactive. N-terminal truncation of the A/B domain of FF1A (clone 43–516) did not change the transactivity of FF1A. The activity of FF1A was drastically lowered only when the AF-2 and A/B domains were simultaneously deleted (clone 43–434). Therefore the A/B domain of FF1 is not directly involved in the transactivation of its target genes.

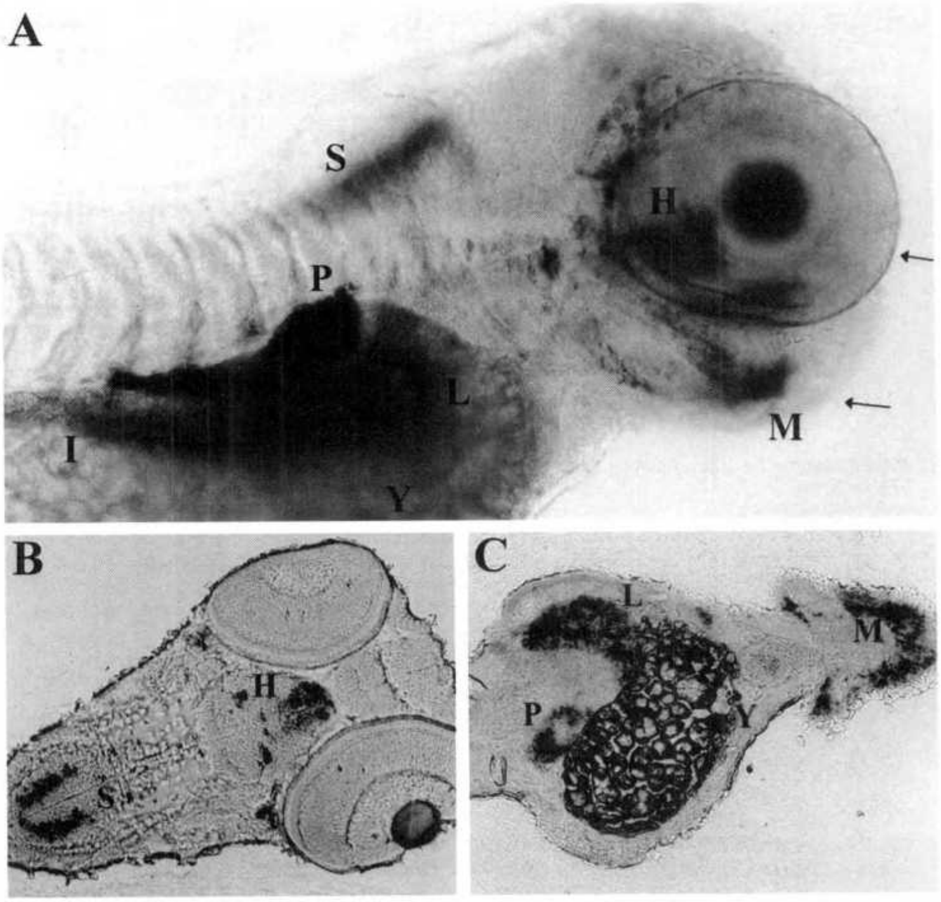

Figure 6 Expression of *ff1* in zebrafish larvae

Views are anterior right and posterior left. (**A**) Lateral view of zebrafish 96 h post-fertilization after whole-mount *in situ* hybridization. (**B** and **C**) Dorsal views of the horizontal sections of whole-mount, *in situ*-hybridized larva. Expression of *ff1* was seen in the mandibular arch (M), hypothalamic nucleus (H), spinal cord (S), pancreas (P), liver (L) and intestine (I). Y: yolk. Arrows indicate the planes of the horizontal sections shown in (**B**) and (**C**).

Zebrafish FF1 is a member of the vertebrate FTF/LRH-1 family

To understand the link between zebrafish FF1 and other FTZ-F1-related proteins, multiple-sequence alignments and phylogenetic analysis were performed. Compared with other FTZ-F1-related proteins, zebrafish FF1 shares higher identity (78–84 %) with the frog (xFF1rA, xFF1rB), chicken, murine and human FTF/LRH-1 proteins than with the chicken, murine, bovine and human Ad4BP/SF-1 (58–66 %). Phylogenetic tree analysis shows that the vertebrate FTZ-F1-related proteins can be divided into two subgroups (the Ad4BP/SF-1 and FTF/LRH-1 subgroups), where zebrafish FF1 protein falls into the subgroup of FTF/LRH-1 (Figure 4). Therefore it should be assigned with the name NR5A2, according to the new nomenclature [21].

Spatial and temporal expression of FF1 mRNA variants

To examine the expression profiles of FF1 mRNA variants, RT-PCR was performed to detect their expression in various adult tissues and developmental stages (Figure 5). *ff1* was expressed in many tissues, including brain, liver, intestine, muscle, eye and gonads. All four mRNA variants were similarly expressed in these tissues with some quantitative variation, with the exception that exon 1 transcripts appeared to be missing in the brain. During development, exon 2 and form A transcripts were first detected in the segmentation stage and expression continued through the pharyngula, larval and adult stages (Figure 5B). Form B transcripts were expressed at low levels in the embryonic and larval stages, whereas exon 1 transcripts could only be detected after amplification with more cycles (results not shown).

Whole-mount *in situ* hybridization was performed to probe further the site of *ff1* expression during early development. Strong signals were detected only when probes specific for exon 2, form A or common to all regions were used for hybridization. No signal was observed in embryos hybridized to RNA probes specific for either exon 1 or the B form transcripts (results not shown). This result was consistent with the results of RT-PCR, in which transcript IIA was the major form expressed in early zebrafish development. Whole-mount *in situ* hybridization revealed *ff1* transcripts in the developing hypothalamus, mandibular arch, spinal cord and gut derivatives, such as intestine, pancreas and liver (Figure 6A). Sectioning of whole-mount embryos confirmed further that *ff1*-expressing cells were located in the hypothalamus, neurons of spinal cord, mandibular arch, liver and exocrine cells of pancreas (Figures 6B and 6C). Zebrafish GATA-5 [30], used as a marker for liver and pancreatic exocrine cells, showed a similar expression pattern in the gut derivatives (results not shown).

DISCUSSION

In this report, we analysed the zebrafish *ftz-f1 (ff1)* gene structure and expression. We showed that the presence of two promoters and alternative splicing of the *ff1* gene results in four transcripts encoding proteins with different N- and C-terminal sequences. Alternative splicing at the 3′-end generates transcription factors with opposite functions, whereas differential promoter utilization does not produce an apparent effect on protein function in our assay system. These transcripts are similarly expressed in many adult tissues. During embryogenesis, however, there exists only a major transcript, IIA. IIA transcripts are detected mainly in brain and gut derivatives during embryonic development, thus implying that they function in the development of these cell lineages.

The zebrafish *ff1* gene belongs to the FTF/LRH-1 subgroup in the FTZ-F1 family of the nuclear receptor superfamily This conclusion is on the basis of two lines of evidence, i.e. sequence comparison studies and the pattern of gene expression. Our phylogenetic analysis studies have shown that the vertebrate FTZ-F1 family can be divided into the Ad4BP/SF-1 and FTF/LRH-1 subgroups (Figure 4). These two groups have probably arisen by gene duplication specific to the vertebrate lineage [3]. Zebrafish FF1 falls into the subgroup of vertebrate FTF/LRH-1 because its sequence in several regions, including the D box in the second zinc finger, region II, region III and helical segments H9 and H10 in the C-terminus, is more similar to that of FTF/LRH-1 than that of Ad4BP/SF-1.

The zebrafish *ff1* gene is located on linkage group 22 (LG22) [31]. The only other known gene in this linkage group is the zebrafish *SCL* gene [31]. Another human FTF/LRH-1 subgroup member, *B1F* [15], and the human *SCL* gene [32] are both located on chromosome 1. It is commonly observed that chromosome segments are conserved across species, i.e. when genes on one chromosome segment are linked, they are also often linked on the chromosome from a different species [31]. Although it may be coincidental, the linkage of these two genes on both zebrafish and human chromosomes could indicate similarity between zebrafish LG22 and human chromosome 1. To date, very few genes have been mapped to zebrafish LG22. When more genes are mapped, the possibility of conservation between LG22 and human chromosome 1 can be further evaluated.

Zebrafish *ff1* is highly expressed in many tissues, but mainly in gut derivatives such as liver and pancreas, as shown by RT-PCR and *in situ* hybridization. This strong hepatic or pancreatic expression is also found for genes of the *FTF/LRH-1* subgroup [3,15,20,33], but not for the *Ad4BP/SF-1* genes, which are expressed primarily in adrenal glands and gonads [4,16,34]. Therefore both phylogenetic and expression pattern analyses lead to the assignment of zebrafish *ff1* to the *FTF/LRH-1* subgroup.

Since most vertebrates have *ftz-f1* genes belonging to both *Ad4BP/SF-1* and *FTF/LRH-1* subgroups, zebrafish should also have its members in both subgroups. Because zebrafish chromosome segments are often duplicated [31], it is possible that the zebrafish *ftz-f1* genes are also duplicated; therefore more than two *ftz-f1* genes could be present. Consistent with our prediction, many ftz-f1 cDNA fragments have been isolated in zebrafish (D. Liu and C. L. Hew, unpublished work).

Zebrafish FF1 mRNA is expressed in the developing gut, liver and pancreas. It implies that *ff1* may function in these gut derivatives. Supporting this hypothesis, the FF1 homologue, human B1F, functions as a hepatocyte transcription factor to activate hepatitis B virus enhancer [15]. Rat FTF has been shown to activate α1-fetoprotein transcription in liver cells [20]. Furthermore, the locations of zebrafish *ff1* expression in the gut derivatives are the same as those of zebrafish GATA-5 expression ([30]; W.-w. Lin, unpublished work). Thus the co-localization with zebrafish GATA-5 suggests that the function of FF1 might be related to the action of GATA-5 in the development of gut derivatives. The mouse GATA-5 homologue, GATA-6, is required for the differentiation of visceral endoderm [35]. Consistent with the notion of expression in gut derivatives, we found sequences in the 5′-flanking region of the *ff1* gene that will bind the gut-enriched transcription factors HNF-3 (hepatic nuclear factor-3) and GKLF (gut-enriched Kruppel-like factor). In addition, consensus sequences that will bind brain transcription factor BRN2, gonad factor SOX5, and factors related to early embryogenesis, such as MyoD, XFD2 and Snail, are also present in this region. Whether these sites function in the transcription of the gene remains to be elucidated.

Apart from the gut derivatives, we also detected ff1 mRNA in the mandibular arch, and neurons in the spinal cord and hypothalamus (Figure 6). The significance of *ff1* expression in these sites is not yet clear. One possible link is that the formation of hypothalamic nuclei is known to require SF-1 [36]. It remains to be elucidated whether *ff1* plays a role similar to that of SF-1 in the development of the hypothalamus. It is also possible that other uncharacterized Ad4BP/SF-1 family members are important for the development of the hypothalamus.

To date, *ff1* is the only member of the FTF/LRH-1 subgroup for which the gene structure has been characterized. Its structure is very similar to the genes in the Ad4BP/SF-1 subgroup [5,16]. This suggests that the gene structure in the *ftz-f1* family is conserved. Multiple promoter usage and alternative splicing are common features shared by members of the *ftz-f1* family [5,16], which generate protein diversity and allow for regulation of gene expression at multiple levels. All four forms of FF1 mRNA variants are expressed similarly in the gut derivatives and gonads, except in the brain, where only exon 2 transcripts are detected (Figure 5). We also detected predominant expression of exon 2 and A form transcripts during early development. This suggests that promoter 2 is probably used preferentially, and the full-length A form receptor rather than the truncated B form prevails to exert its activation function in early development.

Exon 1 and 2 transcripts encode FF1 proteins with different A/B domains (Figure 1). The A/B domain usually contains the AF-1 function important for ligand-independent transactivation through interaction with other co-factors [8,37–39]. We show that the A/B domain does not contribute towards transcriptional activity in HeLa and COS-1 cells, both of which do not normally express FF1 (Figure 3; also D. Liu, unpublished work). However, we cannot exclude the possibility that the A/B domain may play a role in some tissues where appropriate cofactors are present Since the brain expresses only exon 2 transcripts, it might imply the existence of functions specific to the brain.

Compared with the mouse *ftz-f1* gene, there is a difference in the 3′ alternative splice site. Zebrafish *ff1* is alternatively spliced at exon 7, whereas mouse *ftz-f1* is at exon 6 [16]. This results in proteins truncated at different positions. Alternative splicing at exon 7 generates FF1A and FF1B, which function differently in their transactivation potential. FF1B retains regions II and III important for DNA binding [12], but loses the ability to transactivate. Therefore it could be a transcriptional repressor by competing for DNA binding [6]. Other 3′-splicing variants, like mELP1 and xFF1rA-short, lack region III and therefore bind

DNA at a reduced efficiency. High amounts of these short forms are required to achieve the dominant negative effect *in vitro* [12].

We thank Chi-Yao Chang, Sheng-Ping Hwang, Jye-I Wang and John Postlethwait for the zebrafish genomic DNA library, fish maintenance and helpful discussions This work was supported by grants NSC87-2311-B-001-032-B24 and NSC86-2745-B-001-001-B24 from the National Science Council, and by Academia Sinica, Republic of China to B -c.C and funding support from the Medical Research Council of Canada to C L H D L is a recipient of a Research Training Fellowship from the Hospital for Sick Children in Canada

REFERENCES

1 Lavorgna, G, Ueda, H, Clos, J and Wu, C. (1991) Science **252**, 848–851
2 Ueda, H, Sun, G C, Murata, T and Hirose, S (1992) Mol Cell Biol **12**, 5667–5672
3 Ellinger-Ziegelbauer, H, Hihi, A K., Laudet, V, Keller, H, Wahli, W and Dreyer, C. (1994) Mol Cell Biol **14**, 2786–2797
4 Ikeda, Y., Lala, D. S, Luo, X, Kim, E., Moisan, M -R and Parker, K L (1993) Mol Endocrinol **7**, 852–860
5 Wong, M, Ramayya, M. S, Chrousos, G P., Driggers, P H and Parker, K L (1996) J. Mol Endocrinol **17**, 139–147
6 Liu, D, Le Drean, Y, Ekker, M, Xiong, F and Hew, C L (1997) Mol Endocrinol **11**, 877–890
7 Lala, D. S, Rice, D A and Parker, K L (1992) Mol Endocrinol **6**, 1249–1258
8 Tsai, M -J and O'Malley, B W (1994) Annu Rev Biochem **63**, 451–486
9 Mangelsdorf, D. J. and Evans, R M. (1995) Cell **83**, 841–850
10 Enmark, E and Gustafsson, J A (1996) Mol Endocrinol **10**, 1293–1307
11 Ohno, C K, Ueda, H and Petkovich, M (1994) Mol Cell. Biol **14**, 3166–3175
12 Ellinger-Ziegelbauer, H, Glaser, B and Dreyer, C (1995) Mol Endocrinol **9**, 872–886
13 Ohno, C K. and Petkovich, M (1993) Mech. Dev **40**, 13–24
14 White, K P., Hurban, P., Watanabe, T and Hogness, D. S (1997) Science **278**, 114–117
15 Li, M, Xie, Y H, Kong, Y Y, Wu, X., Zhu, L and Wang, Y (1998) J Biol Chem **273**, 29022–29031
16 Ninomiya, Y, Okada, M, Kotomura, N, Suzuki, K, Tsukiya, T and Niwa, O (1995) J Biochem (Tokyo) **118**, 380–389
17 Parker, K L and Schimmer, B P (1993) Trends Endocrinol Metab **4**, 46–50
18 Tsukiyama, T, Ueda, H., Hirose, S and Niwa, O (1992) Mol Cell Biol. **12**, 1286–1291
19 Tugwood, J D, Issemann, I and Green, S (1991) GenBank® Nucleotide Sequence Database accession no M81385
20 Galarneau, L, Pare, J F, Allard, D, Hamel, D, Levesque, L, Tugwood, J. D, Green, S and Belanger, L (1996) Mol. Cell Biol. **16**, 3853–3865
21 Nuclear Receptors Committee (1999) Cell **97**, 1–20
22 Guo, I -C., Huang, C and Chung, B -c (1993) DNA Cell Biol. **12**, 849–860
23 Frohman, M A, Dush, M K and Martin, G R (1988) Proc Natl Acad Sci. U S A. **85**, 8998–9002
24 Lai, W W -K, Hsiao, P -H, Guiguen, Y. and Chung, B -c (1998) Endocr Res **24**, 927–931
25 Altschul, S F and Lipman, D J (1990) Proc. Natl Acad Sci U.S A **87**, 5509–5513
26 Quandt, K, Frech, K, Karas, H, Wingender, E and Werner, T (1995) Nucleic Acids Res. **23**, 4878–4884
27 Smith, R F, Wiese, B. A, Wojzynski, M. K, Davison, D B and Worley, K C (1996) Genome Res **6**, 454–462
28 Westerfield, M (1995) The Zebrafish Book A Guide for the Laboratory Use of Zebrafish (*Danio rerio*), University of Oregon Press, Eugene
29 Drean, Y L, Liu, D, Wong, A O, Xiong, F and Hew, C L (1996) Mol. Endocrinol **10**, 217–229
30 Pack, M, Solnica-Krezel, L, Malicki, J, Neuhauss, S C, Schier, A F, Stemple, D. L, Driever, W and Fishman, M C (1996) Development **123**, 321–328
31 Postlethwait, J H, Yan, Y L, Gates, M. A, Horne, S, Amores, A, Brownlie, A, Donovan, A, Egan, E S, Force, A, Gong, Z et al (1998) Nat Genet **18**, 345–349
32 Begley, C G., Aplan, P. D, Davey, M P, Nakahara, K., Tchorz, K., Kurtzberg, J, Hershfield, M S, Haynes, B. F, Cohen, D I, Waldmann, T A et al (1989) Proc Natl Acad. Sci U S A **86**, 2031–2035
33 Kudo, T and Sutou, S (1997) Gene **197**, 261–268
34 Parker, K L and Schimmer, B P (1997) Endocr Rev **18**, 361–377
35 Morrisey, E. E, Tang, Z, Sigrist, K, Lu, M M, Jiang, F, Ip, H S and Parmacek, M S (1998) Genes Dev **12**, 3579–3590
36 Ikeda, Y, Luo, X, Abbud, R, Nilson, J H and Parker, K L (1995) Mol Endocrinol **9**, 478–486
37 Hadzic, E, Desai-Yajnik, V, Helmer, E, Guo, S, Wu, S, Koudinova, N., Casanova, J, Raaka, B M and Samuels, H H (1995) Mol. Cell Biol. **15**, 4507–4517
38 Tora, L, White, J, Brou, C, Tasset, D, Webster, N, Scheer, E and Chambon, P (1989) Cell **59**, 477–487
39 Onate, S A, Boonyaratanakornkit, V, Spencer, T. E, Tsai, S Y, Tsai, M J, Edwards, D P. and O'Malley, B W (1998) J Biol Chem **273**, 12101–12108

Received 15 October 1999/11 January 2000, accepted 2 March 2000

Expression and protein-binding studies of the *EEN* gene family, new interacting partners for dynamin, synaptojanin and huntingtin proteins

Chi Wai SO*[1], Mai Har SHAM†, Sze Lun CHEW*, Ngai CHEUNG*, Cary K. C. SO*, Sookja K. CHUNG‡, Carlos CALDAS§, Leanne M. WIEDEMANN‖ and Li Chong CHAN*

*Department of Pathology, The University of Hong Kong, Hong Kong, Peoples' Republic of China, †Department of Biochemistry, The University of Hong Kong, Hong Kong, People's Republic of China, ‡Institute of Molecular Biology, The University of Hong Kong, Hong Kong, Peoples' Republic of China, §Department of Oncology, University of Cambridge, Cambridge CB2 2QQ, U.K., and ‖Leukaemia Research Fund Centre, Chester Beatty Laboratories, London SW3 6JB, U.K.

EEN, identified initially as a fusion partner to the mixed-lineage leukaemia gene in human leukaemia, and its related members, *EEN-B1* and *EEN-B2*, have recently been shown to interact with two endocytic molecules, dynamin and synaptojanin, as well as with the huntingtin protein. In the present study, we show that the expression of the *EEN* gene-family members is differentially regulated. Multiple-spliced variants were identified for *EEN-B2*. In the brain, EEN-B1 and EEN-B2 mRNA are preferentially expressed in the cerebellar Purkinje and granule cells, dentate gyrus cells, hippocampal pyramidal neurons and cerebral granule cells. The expression patterns of EEN-B1 and EEN-B2 mRNA in the brain overlap with those of dynamin-I/III, synaptojanin-I and huntingtin, whereas the ubiquitous expression of *EEN* is consistent with that of dynamin-II. In testes, members of the *EEN* family are co-expressed with testis-type dynamin and huntingtin in Sertoli cells and germ cells respectively. Our results on the overlapping expression patterns are consistent with the proposed interaction of *EEN* family members with dynamin, synaptojanin and huntingtin protein *in vivo*. Although all three *EEN* family members bind to dynamin and synaptojanin, *EEN-B1* has the highest affinity for binding, followed by *EEN* and *EEN-B2*. We also demonstrate that amphiphysin, a major synaptojanin-binding protein in brain, can compete with the *EEN* family for binding to synaptojanin and dynamin. We propose that recruitment of the *EEN* family by dynamin/synaptojanin to clathrin-coated pits can be regulated by amphiphysin.

Key words: endocytosis, endophilin family, SH3 domain.

INTRODUCTION

The EEN family [also called the endophilin/Src homology region 3 (SH3)p/SH3GL family] is a new family of SH3-domain-containing proteins that has recently been found to be involved in both normal and malignant cellular processes, including clathrin-mediated endocytosis [1,2] and chromosomal translocation in human leukaemia [3]. The *EEN* gene family consists of at least three members, *EEN*, *EEN-B1* and *EEN-B2*, which are evolutionarily conserved and show over 70 % sequence identity at the amino acid level [3–5]. Proteins of the EEN family can interact with the proline-rich domains (PRDs) of dynamin and synaptojanin via their SH3 domains [2]. These EEN proteins are also co-localized with dynamin, synaptojanin and amphiphysin in the nerve termini of rat brain, where dynamin and synaptojanin can be co-precipitated by antibodies raised against EEN family members [2].

Dynamin is a GTPase involved in synaptic vesicle recycling. It shares similarity to the product of the *Drosophila shibire* gene [6,7], and a temperature-sensitive mutation in the *shibire* gene impairs the endocytosis of synaptic vesicle membrane following exocytosis, disrupting the release of neurotransmitter [8,9]. The functional importance of dynamin in endocytosis has been illustrated further by the conformational change of the dynamin rings formed at the necks of invaginated coated pits that correlate with GTP hydrolysis, which represents a key step leading to vesicle fission from the plasmalemma [10,11]. Synaptojanin is a type II inositol 5-phosphatase containing an N-terminal SacI domain that is homologous with the cytosolic domain of the yeast SacI protein [12]. Inositol phosphate metabolism and yeast SacI protein have been implicated in a variety of membrane-trafficking events, including endocytosis [13]. The role of SacI protein in endocytosis has been supported by the findings that it can mediate ATP transport into the yeast endoplasmic reticulum [14], and a yeast mutant lacking synaptojanin-like genes (*SJL1-L3*) exhibits a severe defect in receptor-mediated and fluid-phase endocytosis [15].

Both dynamin and synaptojanin bind to the SH3 domain of amphiphysin isoforms I and II [16], proteins that were first identified in chicken synaptic fractions [17] and are concentrated in mammalian nerve termini [18]. Amphiphysin also interacts with AP2, an adaptor protein for the plasma-membrane clathrin coat [18,19]. Mutation of the yeast homologues of amphiphysin, RVS 161 and RVS 167, results in an endocytosis defect characterized, in part, by an impairment in α-factor receptor internalization [20]. The disruption of SH3 domain interaction of amphiphysin I in living nerve-termini preparations leads to incomplete synaptic-vesicle endocytosis at the stage of invaginated clathrin-coated pits [21,22], highlighting the role of SH3-domain-mediated interactions in endocytosis. Notably, the EEN family of proteins, apart from amphiphysin, are the only interacting partners containing an SH3 domain enriched in

---

Abbreviations used SH3, Src homology region 3; PRD, proline-rich domain, HD, huntingtin, poly(A)$^+$, polyadenylated, ISH, *in situ* hybridization, dpc, days post-coitum, GST, glutathione transferase, RT, reverse transcriptase, CNS, central nervous system; SLMV, synaptic-like microvesicle, LPAAT, lysophosphatidic acid acyltransferase.

[1] To whom correspondence and offprint requests should be addressed, at the present address. Department of Pathology, Stanford University Medical Center, Stanford, CA 94305, U S A (e-mail cwso@stanford edu)

The nucleotide sequence data reported in this paper have been submitted to the GenBank® and Human Gene Nomenclature Committee, with accession numbers for *EEN-B1* and *EEN-B2*-L1, -L2, -L3 and -L4 of AF036268, AF036269, AF036270, AF036271 and AF036272 respectively.

presynaptic termini [2,23,24]. The physiological significance of the EEN family in endocytosis has been strengthened further by the finding that endophilin I (the rat homologue of EEN-B1), instead of amphiphysin, is the major synaptojanin-binding protein in the rat brain [1].

Table 1 PCR primers used for amplification of *EEN-B1* and *EEN-B2* variant transcripts

Primer used	Sequences (5′ → 3′)	Purposes
EEN-B1(1f)	gtgatggaaataatgactaa	Amplification of EEN-B1 transcript
EEN-B1(1r)	tttgacctccgacagttc	
EEN-B2(1f)	gctgaagaagcagttccaca	Amplification of EEN-B2-L1 and EEN-B2-L2 transcripts
EEN-B2(2r)	agagagtctttcacctcagc	
EEN-B2(6f)	tcagaagatgaatgaatgg	Amplification of EEN-B2-L3 transcript
EEN-B2(4r)	gaagatattcagtggttt	
EEN-B2(4f)	cagttggctgtgttcataga	Amplification of EEN-B2-L4 transcript [first round, *B2*(4f) and *B2*(5r), nested, *B2*(5f) and *B2*(5r)]
EEN-B2(5f)	ctgtcgtggtctctatgac	
EEN-B2(5r)	gatgctaaacaccattattc	
EEN-B2(3f)	gaatgctgaacactgtgtcg	Amplification of all EEN-B2-L1–L4 transcripts (ALL-EEN-B2)
EEN-B2(1r)	atcttgtagtaactgaagt	
EEN-B2(2f)	gatgttaccaataaagttgttgcag	Amplification of genomic EEN-B2
EEN-B2(3r)	ccagcaagccttccgtctg	
Actin-1f	actcttccagccttccttcc	Actin PCR
Actin-1r	cgtcatactcctgcttgctg	

There is emerging evidence showing that the EEN family may also be involved in the pathogenesis of Huntington's disease [25,26]. Huntingtin (HD) protein, like EEN family members, is concentrated in the presynaptic termini, and enriched in the synaptosomal membrane fractions, together with synaptophysin, dynamin and p145, the latter of which is probably the short isoform of synaptojanin [27]. A recent yeast two-hybrid study has shown that a EEN family member interacts and co-localizes with HD protein in Huntington's disease patients [25]. SH3GL3/EEN-B2 can specifically interact with the Huntington's Disease exon 1 protein (HDex1p), which contains a glutamine repeat in the pathological range. This interaction promotes the formation of insoluble polyglutamine-containing aggregates *in vivo*, and is induced by the length of polyglutamine sequence in HDex1p. The strong and specific binding of EEN-B2 to the HD fragment with an elongated polyglutamine repeat has been suggested to promote the formation of fibrillar structures in neurons, leading to a selective neuronal degeneration in distinct regions (including the cortex and striatum) of the brain of Huntington's disease patients [25].

It has also been shown that the expression and regulation of endocytic molecules that are known at present, including dynamin, synaptojanin and amphiphysin, are very complex [16,23,28–30]. Multiple-splice-variant transcripts are differentially expressed in various tissues, and some splice variants of dynamin have different subcellular localization patterns and functions [31]. However, little is known about the expression and regulation of the EEN family and their interactions with other endocytic molecules. In the present study, we identified three novel splice variants of the *EEN-B2* gene that are differentially expressed in various tissues. We also characterized the expression domains of EEN family members in various human and mouse tissues at different developmental and adult stages, and their binding properties to dynamin and synaptojanin. Our results clearly demonstrate that the expression patterns of the EEN family in the nervous tissue overlap with those of dynamin, synaptojanin and HD, and support their interaction *in vivo*.

EXPERIMENTAL

Library screening and DNA sequencing

EEN cDNA and human expression tag (EST) clones (H50251, H20385 and H19489) encoding EEN-related sequences were labelled with ^{32}P to screen a human fetal-brain cDNA library under low-stringency hybridization and washing conditions [32]. Positive clones were isolated and converted into pBluescript phagemids for restriction mapping and DNA sequencing. All sequencing was performed using fluorescently labelled dideoxy terminators on a 377 Applied Biosystems automated sequencer. The DNA sequence was assembled and analysed, and both the nucleotide and predicted open reading frames were compared with public databases using various online and network facilities.

Amplification of EEN-B1 and EEN-B2 from brain RNA and genomic DNA

Total RNAs were extracted from normal human adult brain, 10-week fetal brain and brain medulloblastoma, and subjected to reverse transcription with random hexamers. Except for EEN-B2-L1 and EEN-B2-L2, which were amplified using the same set of primers [*EEN-B2*(1f) and *EEN-B2*(2r)], specific primers were designed for PCR amplification on random-primed cDNA for the following transcripts, as shown in Table 1; see also Figure 1. EEN-B2-L1 and EEN-B2-L2 transcripts, which differed from each other by a 7-bp deletion in EEN-B2-L2, were distinguished by their different mobility on gel electrophoresis, and confirmed by DNA sequencing. RNA quality was assessed by comparative actin PCR using actin-specific primers. Each actin PCR consisted of 62.5 fg of internal-template control, which would produce a fragment of size approx. 400 bp that was 100 bp larger than the band amplified from human actin cDNA (see Figures 3a and 3c).

A genomic fragment of *EEN-B2* flanking the 7-bp deletion found in *EEN-B2*-L2 was amplified by *EEN-B2*(2f) and *EEN-B2*(4r) from human genomic DNA. The amplified fragment was cloned into pGEM-T vector, and partially sequenced from both ends.

Gene expression studies by Northern blot hybridization and PCR analysis

Polyadenylated [poly(A)$^{+}$]-selected human and mouse RNA multiple-tissue Northern blots (Clontech, Palo Alto, CA, U.S.A.) were hybridized with a cDNA probe derived from specific coding sequence or the 3′-untranslated regions of the genes. Probes used for hybridization included: (i) a 1.6-kb *Pst*I fragment spanning part of the coding and 3′-untranslated region of *EEN*; (ii) a 2.8-kb probe covering the coding and part of the 3′-untranslated region of *EEN-B1*; and (iii) a 400-bp *EEN-B2* probe derived from the 3′-untranslated region shared by *EEN-B2*-L1, *EEN-B2*-L2 and *EEN-B2*-L3. The probes used for mouse blots were essentially the same as those used for *in situ* hybridization (ISH; see below). Hybridization was performed under standard high-stringency conditions [32]. The expression of EEN-B1 and each of the EEN-B2 transcripts was examined by PCR on a human multiple-tissue cDNA panel (Clontech). In each PCR reaction, approx. 0.4 ng of cDNA from different tissues, previously normalized with six different housekeeping genes, was amplified using 2.5 pmol of gene-specific primers. These primers were similar to those used for the amplification of EEN-B1 and EEN-B2 transcripts from brain tissues, with one exception, i.e. amplification of total EEN-B2 transcripts (ALL EEN-B2), in which primers *EEN-B2*(3f) and *EEN-B2*(1r) were designed from the common sequence shared by all four EEN-B2 transcripts (Table 1; also see Figure 1) The qualities and normalization of the cDNA panel were assessed by comparison with actin PCR.

ISH

The same murine cDNA templates (kindly given by B. Kay, University of Wisconsin–Madison, Madison, WI, U.S.A.) were used for both whole-mount and section ISH. Riboprobes used for ISH included: (i) a 2-kb fragment covering the coding sequence and both 5′- and 3′-untranslated regions of SH3p8/endophilin II (murine *EEN*); (ii) an 800-bp fragment spanning part of the coding sequence and 5′-untranslated region of SH3p4/endophilin I (murine *EEN-B1*); and (iii) a 900-bp probe covering part of the coding sequence and 3′-untranslated region of SH3p13/endophilin III (murine *EEN-B2*). Whole mount embryo ISH was performed as described previously [33] using digoxigenin-labelled UTP as a substrate for the transcription of probes *in vitro* Embryos at 8.5- and 9.5-days post-coitum (dpc) were collected from FBB mice and fixed in 4% (v/v) paraformaldehyde overnight before protease K treatment. After overnight hybridization at 65 °C, the embryos were washed three times at 65 °C with 0.2 × SSC (where 1 × SSC is 0.15 M NaCl/0.015 M sodium citrate) for 30 min each. Hybridization signals were detected by ELISA using anti-digoxigenin alkaline phosphatase and X-phosphate/Nitro Blue Tetrazolium. Section ISH was performed using ^{35}S-radiolabelled riboprobes, according to a standard protocol. Mouse embryos or tissues were snap-frozen in liquid nitrogen and then fixed in 4% (v/v) paraformaldehyde for 20 min. Overnight hybridization was performed at 55 °C with a probe concentration of 1×10^8 c.p.m./ml. Non-specific probe binding was washed off at 55 °C with 2 × and 0 2 × SSC for 60 min each. The slides were dipped into emulsion (Amersham Pharmacia Biotech, Little Chalfont, Bucks., England) and exposed for 2–4 weeks before signal development. The sections were counter-stained with haematoxylin and eosin, and silver granules were examined under both a light microscope (Axiophot; Zeiss, Cologne, Germany) and a stereomicroscope (SV11; Zeiss).

Production of glutathione S-transferase (GST) fusion protein and *in vitro*-synthesized proteins

SH3 domains of EEN family members (EEN, EEN-B1 and EEN-B2), human amphiphysin I (Genbank® accession no. U07616; 590–695 amino acids), amphiphysin II (GenBank® accession no. U87558; 496–593 amino acids), and RasGAP (GenBank® accession no. M23379; 274–347 amino acids) were amplified by PCR on appropriate cDNA templates, and cloned in-frame into pGEX vectors that express recombinant GST fusion proteins. Constructs were verified by DNA sequencing prior to the expression of the GST fusion protein in the host strain DH5α upon isopropyl β-D-thiogalactoside induction using a standard method. Various deletion constructs of EEN-B2 were also amplified and cloned into pGEM-T vectors for protein synthesis *in vitro*. Human dynamin-I and the rat synaptojanin 145-kDa isoform were kindly given by De Camilli (Yale University, New Haven, CT, U.S.A.). Following column purification (Qiagen, Hilden, Germany), 1 μg of each plasmid DNA was expressed using the TNT-coupled reticulocyte lysate system (Promega, Madison, WI, U.S.A.) according to the manufacturer's instructions. All protein products were analysed on an SDS/12% (w/v) polyacrylamide gel, and subjected to autoradiography or immunoblotting using an anti-GST antibody.

Competitive GST binding assays

GST fusion proteins (1 μg) were preincubated with glutathionine–Sepharose beads (Amersham Pharmacia Biotech) in NETN buffer [0.5% (v/v) Nonidet P-40/20 mM Tris/HCl (pH 8.0)/100 mM NaCl/1 mM EDTA] for 60 min at 4 °C, and subsequently used for protein competitive-binding assay: ^{35}S-labelled *in vitro*-synthesized dynamin/synaptojanin was added with 1, 5, 25 or 50 μg of competitor proteins to the beads. These proteins were synthesized as GST fusion proteins, except that the GST portions of the fusion proteins had been removed by factor Xa (Amersham Pharmacia Biotech) digestion according to the manufacturer's instructions, so they could not bind to the glutathionine–Sepharose bead. After a 90-min incubation at 4 °C, the beads were washed five times in buffer H [20 mM Hepes (pH 7.7)/50 mM KCl/20% (v/v) glycerol/0.1% (v/v) Nonidet P40/0.007% 2-mercaptoethanol]. Bound proteins were eluted by boiling in SDS/PAGE loading buffer, resolved by electrophoresis and detected by autoradiography. All competitive binding assays were repeated at least twice to confirm the results.

RESULTS

Cloning of the *EEN* gene family

Using *EEN*-related sequences to screen a human fetal-brain cDNA library, several overlapping clones containing *EEN* homologous sequence were identified. Sequence analysis indicated that these clones could be aligned to form five major contigs Four of these (subsequently referred to as *EEN-B2*-L1 to *EE2-B2*-L4) appeared to be derived from a single gene (*EEN-B2*) and the fifth was referred to as *EEN-B1*, on account of their preferential expression in brain (described below). The three members of the EEN protein family, EEN, EEN-B1 and EEN-B2, share over 70% amino acid sequence identity and highly homologous C-terminal SH3 domains (with 80% amino acid identity) These have also been identified by degenerative PCR amplification, and named as SH3GL1, SH3GL2 and SH3GL3 respectively [5]. BLAST homology searches revealed that EEN, EEN-B1 and EEN-B2 are the human homologues of the mouse endophilin II, endophilin I and endophilin III [4]. The identity between each of the human and mouse homologues is over 85% at the nucleic acid level, and 90% at the amino acid level.

Identification of variant transcripts of EEN-B2

During the course of cDNA library screening, four highly related cDNA clones encoding *EEN-B2* were identified. Sequence analysis and restriction mapping revealed that they represent four different types of EEN-B2 transcripts, i.e EEN-B2-L1, -L2, -L3 and -L4 (Figure 1). These transcripts could arise from the utilization of alternative transcriptional start sites and splicing variations. Compared with other transcription variants of EEN-B2, EEN-B2-L1 equivalent to EEN-B2 in Figure 1 shows highest overall sequence homology with transcripts of EEN and EEN-B1. Conceptual translation of the EEN-B2-L1 cDNA sequence revealed that the longest open reading frame codes for a 40-kDa polypeptide containing an SH3 domain at the C-terminus and several in-frame, internal methionine codons (AUG^{I-IV} in Figure 1). EEN-B2-L2 is similar to EEN-B2-L1, apart from a 7-bp deletion upstream of AUG^{II}, which could result in a frame-shifted translated protein product. (This -L2 transcript was also represented by the EST clones with accession numbers H50251, H20385 and H19489.) Interestingly, the EEN-B2-L2 transcript

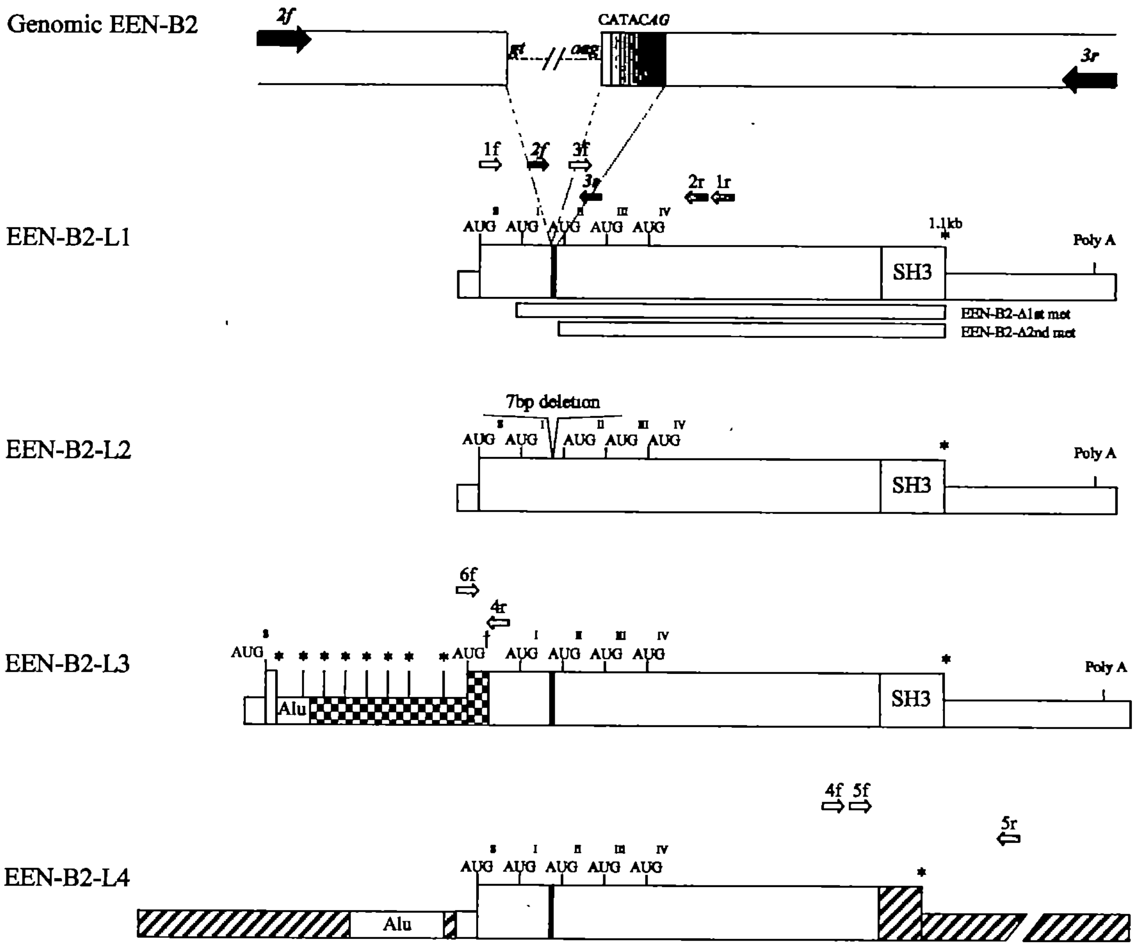

Figure 1 Schematic representation of partial genomic structure and alternatively spliced forms of *EEN-B2* identified in cDNA library screening

The putative start codon and the first four internal methionine codons identified in EEN-B2-L1 are indicated as AUG^{S}, AUG^{I}, AUG^{II}, AUG^{III} and AUG^{IV} respectively The in-frame-inserted methionine in EEN-B2-L3 is indicated as AUG† Large and small rectangular blocks represent predicted coding sequences and untranslated regions respectively The thick vertical black line and asterisks indicate the 7-bp mini-exon sequence and stop codons respectively The chequered- and hatched-shaded boxes represent sequence specific to EEN-B2-L3 and EEN-B2-L4 respectively. The 3 2-kb genomic fragment amplified by *EEN-B2*(2f) and *EEN-B2*(3r) primers is shown on the top The consensus 3′-splice site, including the 7-bp alternative splice acceptor, is written in block lettering at the top of the diagram The location of SH3 domains, *Alu* homologous sequences (Alu), polyadenylation signal sites (poly A) and the primers used for PCR analysis [arrows labelled with 1f, (forward)–6f and 1r (reverse)–5r] are also shown in the diagram

could encode an N-terminal-truncated protein retaining the functional SH3 domain if internal methionines (AUG^{II}–AUG^{IV}) downstream of the deletion were utilized as initiation codons. The EEN-B2-L3 transcript differs from EEN-B2-L1 in having a 513-bp fragment with multiple stop codons between the putative starting methionine (AUG^{S}) and the first internal methionine (AUG^{I}) of EEN-B2-L1 (Figure 1). However, the 513-bp insertion would introduce a new in-frame methionine (AUG†), which could be used to make a protein product with a new 22-amino-acid sequence which might replace the first 15 amino acids encoded in EEN-B2-L1. The EEN-B2-L4 transcript was the longest, with additional non-coding sequence at the 5′-end and an alternative 3′-sequence, which would lead to the replacement of the SH3 domain (Figure 1).

Alternative translation initiations for EEN-B2 transcripts

In order to test whether any of the internal methionine codons in EEN-B2 transcripts could be used for translation initiation, *in vitro* transcription and translation assays were performed. The EEN-B2-L1 cDNA clone yielded three protein bands (Figure 2): a faint 40 kDa band that is likely to be initiated from the putative start codon, AUG^{S} (Figure 1), and two strong but smaller protein bands, most likely resulting from initiation from the first and second internal methionine codons (AUG^{I} and AUG^{II} respectively). The use of these two internal methionines was confirmed by testing two types of EEN-B2-L1 cDNA deletion constructs in the assay. With EEN-B2-Δ1st Met (in Figure 1, the EEN-B2-L1 cDNA clone with deletion of 5′ sequence, including the AUG^{S} codon), the two smaller protein bands were produced, whereas only the smallest band was present when EEN-B2-Δ2nd Met (in Figure 1, the EEN-B2-L1 cDNA clone with both AUG^{S} and AUG^{I} deleted) was used (Figure 2). From the intensities of the bands observed, we conclude that AUG^{I} and AUG^{II} function more efficiently than the AUG^{S} codon *in vitro*. When the EEN-B2-L3 cDNA clone was tested, three protein bands of similar intensities were produced; two smaller proteins were initiated from AUG^{I} and AUG^{II}, and the third of approx. 41 kDa was possibly from the new methionine codon AUG† (Figure 1) within the unique 513-bp sequence. When the EEN-B2-L2 cDNA

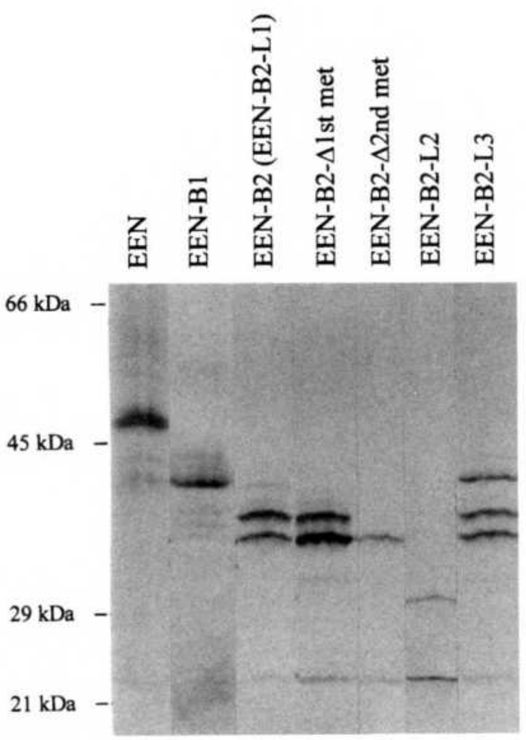

Figure 2 Analysis of protein encoded by different clones of the EEN family

Major protein products with sizes corresponding to those encoded by the longest open reading frame were generated for EEN and EEN-B1 clones. Multiple protein products were produced for EEN-B2 clones. Molecular sizes of the proteins are given in kDa to the left of the gel. The structures of EEN-B2 clones used are shown in Figure 1. EEN-B2-Δ1st met and EEN-B2-Δ2nd met, EEN-B2 with the first or first and second methionines deleted, respectively.

clone was used, a polypeptide of approx. 31 kDa was observed. On the basis of the size of the predicted protein product, this could result from the use of the fourth internal methionine, AUG$^{\text{IV}}$, as an initiation codon. We believe that the preferential use of the fourth internal methionine as the initiation codon is the result of a better match to the ACCATGG Kozak consensus sequence [34]. There is also a weak 23-kDa band from EEN-B2-derived transcripts that could be an N-terminal-truncated product upon utilization of an internal initiation codon. Together with the alternative splicing patterns of the *EEN-B2* gene, our data indicate the presence of complex regulation of the *EEN-B2* gene at the levels of both transcription and translation. In contrast, EEN and EEN-B1 cDNAs generate only a single major protein product corresponding to the longest open reading frame (Figure 2), although these four internal in-frame methionines of EEN-B2 are conserved in EEN and EEN-B1 sequences.

Amplification of EEN-B2 transcripts (-L1 to -L4) from human brain tissues

To study the expression of EEN-B2 variants in human brain, PCR amplification was performed with specific primers for each transcript in normal adult and fetal brain, and medulloblastoma (Figure 3A). Transcript-specific primer pairs for *EEN-B2*-L3 and *EEN-B1* resulted in the amplification of RNA transcripts from all three samples, but not in the control genomic DNA. The *EEN-B2*(1f) and *EEN-B2*(2r) primer pair, which flanked the 7-bp deletion identified in EEN-B2-L2, resulted in the amplification of doublets from the brain samples. Sequence analysis showed that the lower band of 372 bp was derived from the EEN-B2-L2 transcript, which had a 7-bp deletion, whereas the upper band of 379 bp was amplified from EEN-B2-L1 (Figure 3A), confirming the presence of these two transcripts. However, EEN-B2-L4-specific primers did not generate a PCR product, indicating that the cDNA clone might represent an incompletely processed form of EEN-B2.

EEN-B2-L2 is generated using an alternative 3′-splice acceptor site

In order to distinguish whether EEN-B2-L2 was derived from alternative splicing of EEN-B2-L1 or from a separate *EEN-B2*-like gene, PCR analysis was performed on human genomic DNA using another pair of transcript-specific primers, *EEN-B2*(2f) and *EEN-B2*(3r), flanking the 7-bp deletion of EEN-B2-L2 (Figure 1). A DNA fragment of 3.2 kb was amplified and sequenced. Comparison of the DNA sequences of this fragment with the EEN-B2-L1 cDNA indicated the presence of a 3.1-kb intron with perfect 5′- and 3′-splice sites at the junctions (GT-AG consensus) (Figure 1). At the 3′-splice site, the sequence was a*ag*/CATAC*AG/* (potential 3′-cryptic splice sites are shown underlined and in italics), suggesting that there are two potential alternative splice junctions (Figure 1), of which the second with a 5′ cytosine (C) could be preferred to the first one with adenosine (A) in front of the consensus AG splice sequence. This is also consistent with the scanning model of RNA splicing [35], and suggests that differential splicing at these two sites would produce two transcripts differing by 7 bp. Thus the EEN-B2-L2 transcript is likely to be an alternatively spliced form that is 7 bp shorter than EEN-B2-L1.

Expression of EEN-B1 and EEN-B2 transcripts is spatially and temporally specific

The expression of EEN, EEN-B1 and EEN-B2 was examined in Northern blots of poly(A)$^{+}$ RNA from different human and mouse tissues (Figure 3B), as well as by reverse transcriptase (RT)-PCR analysis on human multiple tissue cDNA panels (Figure 3C). In contrast with EEN mRNA, which was expressed ubiquitously in all adult tissues tested, EEN-B1 and -B2 mRNAs were preferentially expressed in brain and testis of adult mice, with higher levels of EEN-B1 mRNA expression in the brain and higher levels of EEN-B2 mRNA signal in the testis. Within the central nervous system (CNS), EEN-B2 and EEN mRNA were both expressed at a high level in most parts of the brain and spinal cord, whereas EEN-B1 mRNA is preferentially expressed in regions enriched in neurons, including cerebral and cerebellar cortex, occipital lobe, frontal lobe and temporal lobe, but only at a very low level in the spinal cord, corpus callosum and subthalamic nucleus. Using RT-PCR analysis, EEN-B1 was found to be expressed weakly in most non-neuronal tissues, but not in adult colon or leucocytes (Figure 3C).

EEN-B2 variant transcripts were differentially expressed in various tissues

To investigate whether the various EEN-B2 transcripts were differentially expressed, PCR analysis was performed using primers specific for individual EEN-B2 transcripts. When *EEN-B2*(1f) and *EEN-B2*(2r) primers were used, doublets were amplified from all the tissues in which these transcripts were expressed, including adult brain, testis and thymus. In each doublet, the intensity of the smaller band, corresponding to EEN-B2-L2, was much weaker (Figure 3C). Using EEN-B2-L3 transcript-specific primers, the tissue distribution of the EEN-B2-L3 transcript was

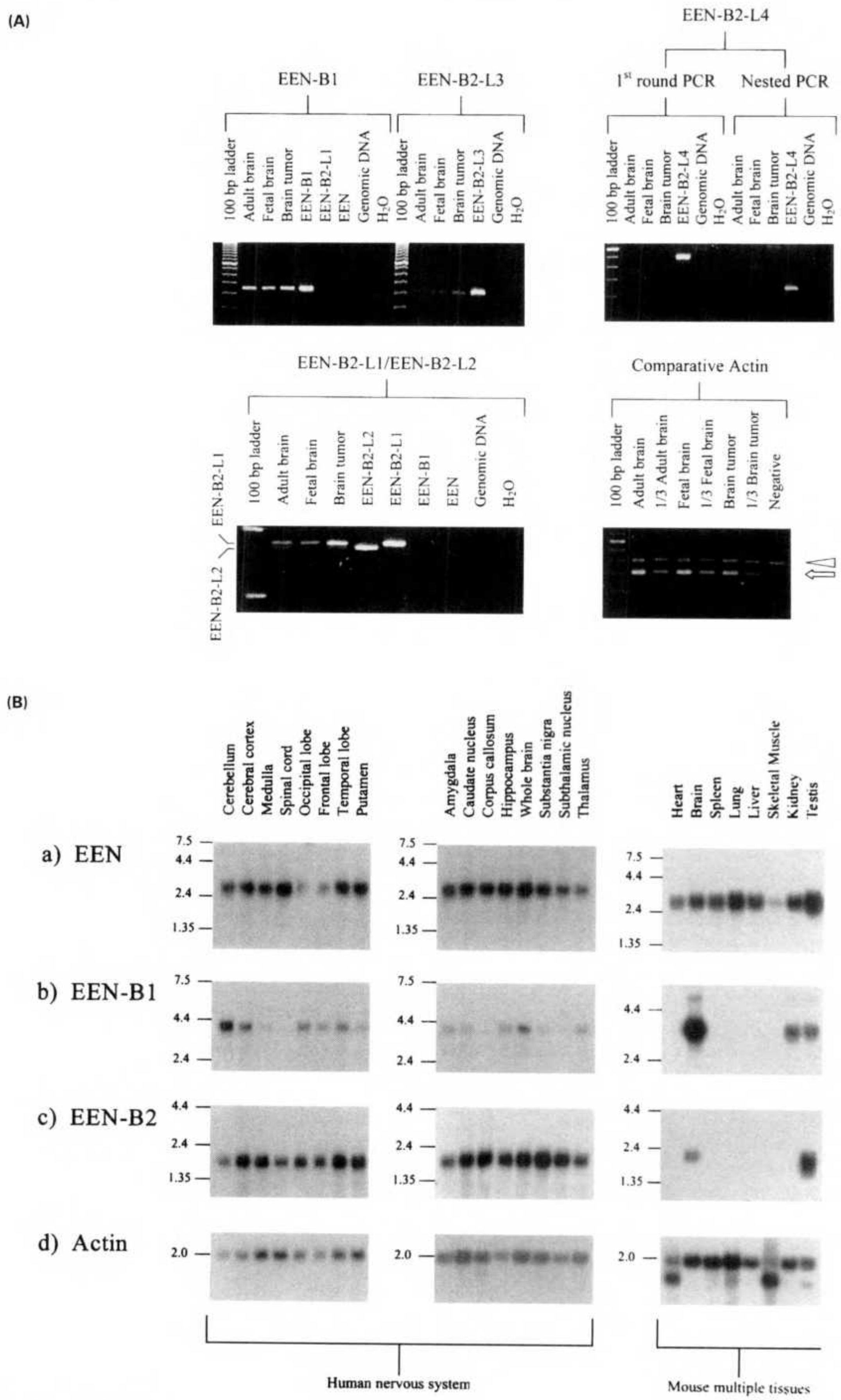

Figure 3 For legend see facing page.

(C)

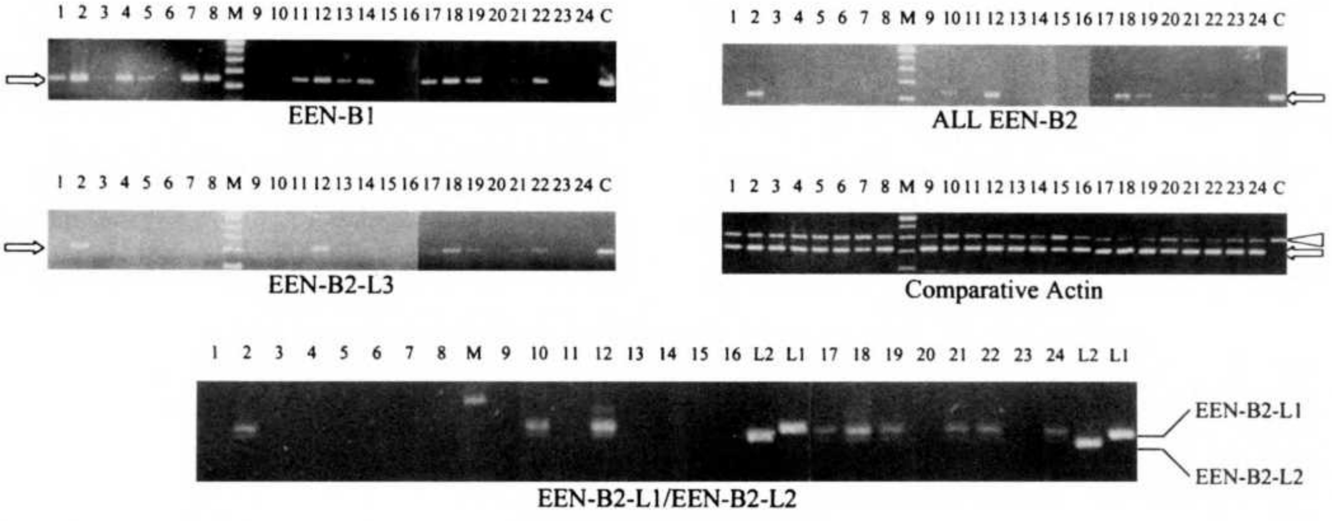
1 2 3 4 5 6 7 8 M 9 10 11 12 13 14 15 16 17 18 19 20 21 22 23 24 C
EEN-B1
ALL EEN-B2
EEN-B2-L3
Comparative Actin
1 2 3 4 5 6 7 8 M 9 10 11 12 13 14 15 16 L2 L1 17 18 19 20 21 22 23 24 L2 L1
EEN-B2-L1
EEN-B2-L2
EEN-B2-L1/EEN-B2-L2

Figure 3 Expression analysis of *EEN* family in human and mouse tissues

(**A**) PCR amplification of EEN-B1 and -B2 variant transcripts from various human brain tissues. Transcripts that were amplified are indicated above the brackets. cDNA templates (i.e. EEN, EEN-B1 and EEN-B2-L1–L4) and genomic DNA were used as positive and negative controls respectively for each amplification. The relative positions of EEN-B2-L1 and EEN-B2-L2 transcripts are indicated to the left of the bottom left gel in (**A**). In the comparative actin PCR, the arrowhead indicates the control actin band amplified from internal control plasmid DNA, whereas the arrow indicates the actin amplified from the cDNA samples. Actin PCR was also performed using a 3-fold dilution of the cDNA templates. (**B**) Northern blot analysis of the EEN family in the human nervous system (left and centre panels of gels) and mouse multiple tissues (right panel of gels). These blots were hybridized with human and mouse probe (see the Experimental section). Each blot was normalized with actin hybridization. Molecular sizes of RNA fragments are given in kb. (**C**) Differential expression of EEN-B1 and -B2 splice variants assessed by PCR analysis on multiple tissue cDNA panels. The transcripts that were amplified are indicated at the bottom of each panel. 'ALL EEN-B2' represents the amplification of EEN-B2-L1–L3 transcripts. Arrows indicate specific products amplified from the samples; the arrowhead to the right of the ALL EEN-B panel indicates the control actin band amplified from the internal control plasmid DNA, as shown in (**A**). 1, adult heart; 2, adult brain; 3, placenta; 4, adult lung; 5, adult liver; 6, adult skeletal muscle; 7, adult kidney; 8, adult pancreas; 9, adult spleen; 10, adult thymus; 11, adult prostate; 12, adult testis; 13, adult ovary; 14, adult small intestine; 15, adult colon; 16, adult peripheral blood leucocyte; 17, fetal heart; 18, fetal brain; 19, fetal lung; 20, fetal liver; 21, fetal skeletal muscle; 22, fetal kidney; 23, fetal spleen; 24, fetal thymus; c, control plasmid DNA; M, 100-bp ladder marker.

similar to the overall EEN-B2 expression pattern (Figure 3C, ALL EEN-B2), except that EEN-B2-L3 transcripts were present in neither adult nor fetal thymus. No signal could be amplified from any of the tissues using EEN-B2-L4-specific primers (results not shown), suggesting that this transcript is not normally expressed in those tissues that were tested.

Expression of the *EEN* family in mouse embryos

To examine the expression patterns of *EEN* family members during embryonic development, whole-mount and section ISHs of mouse embryos were performed using riboprobes transcribed from the murine homologues of the *EEN* family [4]. The murine *EEN* was widely distributed in 8.5 dpc mouse embryos and by 9.5 dpc, high levels of expression were detected throughout the entire embryo (Figures 4A and 4B). This expression pattern persisted in later-stage embryos (10.5, 12.5 and 14.5 dpc), as shown in Figures 4(G), 4(L) and 4(Q). Therefore the murine EEN mRNA appears to be expressed ubiquitously during embryonic development.

The expression patterns of murine EEN-B1 and EEN-B2 mRNA were very similar, and their onset of expression was much later than that of murine EEN. No expression could be detected in 8.5 or 9.5 dpc embryos by whole-mount ISH (Figures 4D and 4E). However, by 10.5 dpc, both murine EEN-B1 and EEN-B2 messages were observed, and their expression appeared to be confined to the developing CNS, including various parts of brain (throughout the telencephalon, mesencephalon, metencephalon and myelencephalon) and spinal cord (Figures 4H and 4I). The expression for these two genes at this stage appeared to be stronger in the ventral region of the CNS. In addition, vascular structures, such as dorsal aorta and the epithelial surface of the branchial arches, also expressed the EEN-B1 and -B2 mRNA. At 12.5 dpc, the signals detected in the developing CNS were uniform and stronger: almost all neurons in the spinal cord and brain expressed EEN-B1 and EEN-B2. Hybridization signals could also be found in tissues of the peripheral nervous system. High levels of EEN-B1 and EEN-B2 mRNA expression were seen in the outermost layer of the cortical plate in the telencephalon (cortical neuroepithelium), as well as spinal ganglia. At the same time, weak signals were also detected in some non-neuronal tissues, including kidney, intestine and lung (Figures 4M and 4N). At 14.5 dpc, EEN-B1 and EEN-B2 mRNAs were strongly expressed in all neurons of the CNS, including the olfactory bulb. Signals can also be seen in the cranial ganglia of the developing nervous system, and in the developing cochlea (Figures 4R and 4S). At this stage, the expression levels of EEN-B1 and EEN-B2 in non-neuronal tissues, including kidney, adrenal medulla, intestine and lung, were remarkably higher than that at 12.5 dpc.

Expression of EEN family members in mouse adult brain and testis

To examine in more detail the expression of *EEN* family members in adult tissues, ISH on mouse tissue sections revealed that EEN-B1 and EEN-B2 mRNAs were widely expressed throughout the adult brain, including the cerebral cortex, hippocampus, cer-

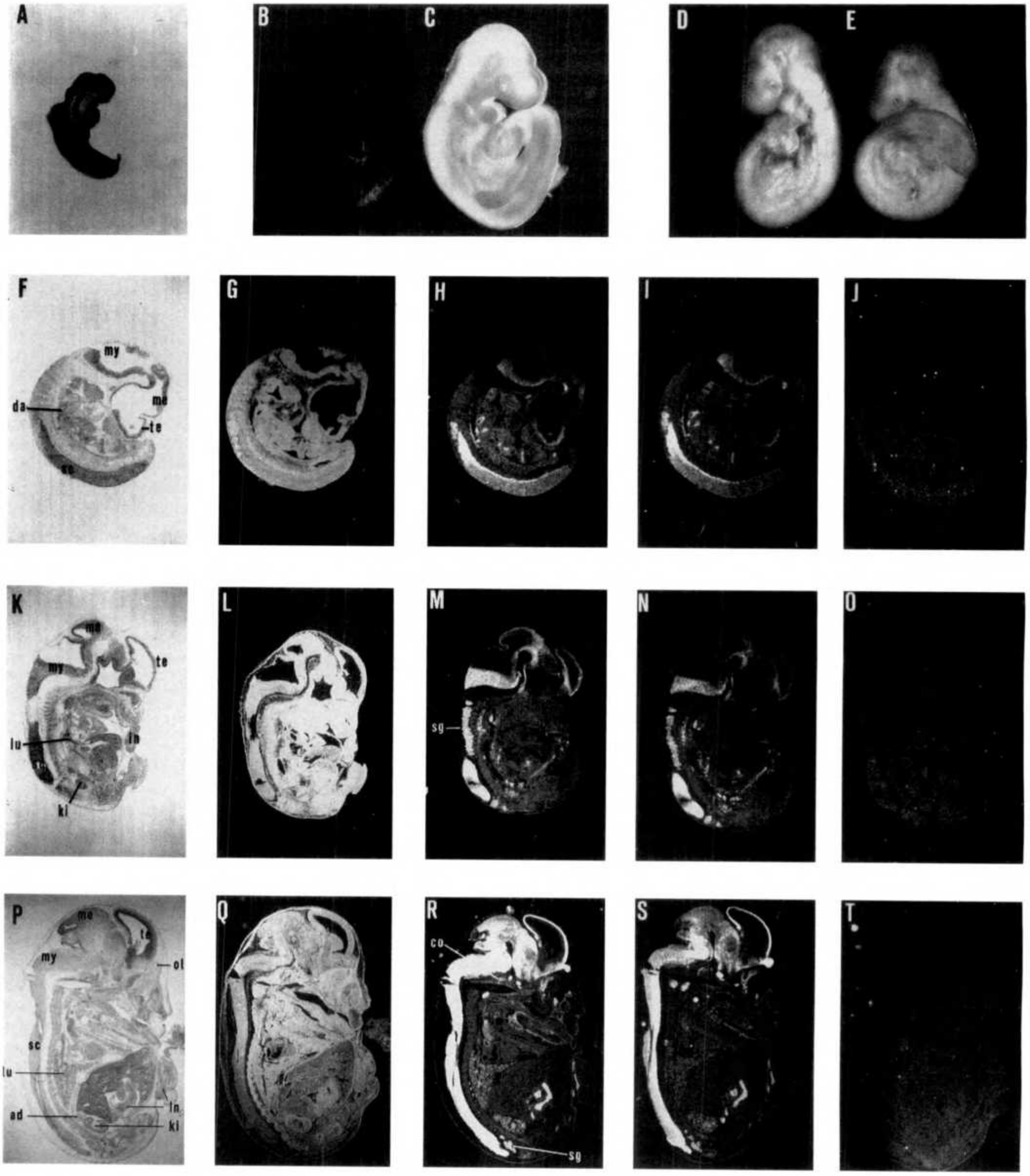

Figure 4 Temporal and spatial patterns of EEN family expression during mouse embryonic development by ISH

Whole-mount mouse embryos of 8.5 (**A**) and 9.5dpc (**B**–**E**) were hybridized with digoxigenin-labelled mouse EEN antisense probe (**A**, **B**), EEN sense probe (**C**), EEN-B1 antisense probe (**D**) and EEN-B2 antisense probe (**E**) respectively. Mouse embryos of 10.5 (**F**–**J**), 12.5 (**K**–**O**) and 14.5 dpc (**P**–**T**) were sectioned and hybridized with ^{35}S-radiolabelled mouse EEN antisense probe (**G**, **L** and **Q**), EEN-B1 antisense probe (**H**, **M** and **R**) or EEN-B2 antisense probe (**I**, **N** and **S**) respectively. All EEN, EEN-B1 and EEN-B2 probes exhibited similar results on sense probe hybridization; only the EEN sense probe (**J**, **O** and **T**) was shown. Bright fields of 10.5, 12.5 and 14.5 dpc embryos were shown as (**F**), (**K**) and (**P**) respectively. ad, adrenal medulla; co, cochlea; da, dorsal aorta; in, intestine; ki, kidney; lu, lung; me, mesencephalon; mt, metencephalon; my, myelencephalon; ol, olfactory bulb; sc, spinal cord; sg, spinal ganglia; te, telencephalon.

ebellum, brain stem, thalamus and striatum (Figures 5C and 5D). Highest levels of expression were detected in regions with high neuronal density, such as the cerebral cortex, cerebellum, the dentate gyrus and pyramidal cell layer of the hippocampal formation. Morphological appearance of cells showing hybridization signals suggested that both EEN-B1 and EEN-B2 are expressed in neurons; the expression pattern of EEN in adult brain was similar to that of EEN-B1 and EEN-B2, with expression predominantly occurring in the grey matter, except for a low level of EEN expression that was detected in the white matter and the epithelium of the choroid plexus (Figure 5B).

In the hippocampus, the expression of EEN-B1 and EEN-B2 in pyramidal cells CA3 was much stronger that in CA1, CA2, CA4 and dentate gyrus (Figures 5G and 5H); whereas EEN mRNA showed a similar level of expression in pyramidal cells of CA1 to CA4, and the dentate gyrus (Figure 5F). In the cerebral cortex, the expression of EEN family members were restricted to the neuronal cells of the granular layer, and were not found in the molecular layer (Figures 5J–5L). Similar expression patterns were also found in cerebellar cortex, with predominant expression in cerebellar granular layer and Purkinje cells and weak signals in the molecular layer (Figures 5N–5P). Although the striatum has a low neuronal density, cells in striatum with morphological characteristics consistent with neurons expressed high levels of EEN-family-member mRNAs, whereas glial cells did not (Figures 5R–5U)

Besides the adult brain, testis is the only mouse tissue where the three EEN family members are co-expressed (Figure 3B). ISH revealed that all EEN family members were highly expressed in seminiferous tubules in the testis (Figures 5V–5X). High magnification revealed that EEN-B1 and EEN-B2 were expressed in the basal lamina of the seminiferous epithelium, containing Sertoli cells and immature spermatogonia, whereas EEN was predominantly expressed in the primary and secondary spermatocytes, although weak EEN expression could also be seen in Sertoli cells and Leydig cells (Figures 5AA–5CC). The expression of EEN family members in Sertoli cells has been confirmed further by RT-PCR analysis using RNA extracted from primary Sertoli cell culture of purity > 98 %, prepared as described previously ([36], and results not shown).

EEN family members and amphiphysin compete for synaptojanin and dynamin

To assess the relative binding affinity of individual members of the EEN family to their potential interacting partners, synaptojanin and dynamin, various amounts (1–50 μg) of SH3-domain proteins derived from EEN family members (EEN and EEN-B1) were used as competitors to compete with different GST fusion proteins containing the SH3 domains of EEN family members for binding with ^{35}S-labelled synaptojanin and dynamin. Since similar results were obtained using synaptojanin or dynamin as input; we only show here the result with synaptojanin. As shown in Figure 6(a), B1-SH3 protein could readily compete with both GST–EEN-SH3 and GST–B2-SH3 fusion proteins for binding with synaptojanin, indicating that B1-SH3 protein has a higher affinity for synaptojanin and dynamin compared with EEN and EEN-B2. On the other hand, EEN-SH3 protein could compete only with GST–B2-SH3, and not with GST–B1-SH3, for binding with synaptojanin and dynamin, whereas B2-SH3 could not inhibit any binding of GST-EEN-SH3 or GST-B1-SH3 (results not shown). These inhibitions were unlikely to be due to non-specific binding, since no inhibition was found using 50 μg of RasGAP-SH3 protein, which exhibits a different binding specificity. The competition results suggested that the binding affinity of EEN family members to synaptojanin and dynamin, in order of decreasing affinity, was EEN-B1 > EEN > EEN-B2.

Since members of the EEN family, amphiphysin, synaptojanin and dynamin have overlapping domains of expression in the neural tissues, we wanted to identify whether EEN family members and amphiphysin could compete under normal circumstances for binding with synaptojanin and dynamin. Since the SH3 domains of amphiphysin I and II are known to bind to the same PRD on dynamin [37], they were used as a positive control in the protein competitive-binding assay. We showed that amphiphysin I-SH3 protein could efficiently compete with GST–amphiphysin-II-SH3 fusion protein for synaptojanin when 25 μg of competitor protein was used (Figure 6b). When amphiphysin-I-SH3 protein competed with GST–EEN family proteins, inhibition could be seen using < 50 μg of competitor protein (Figure 6b). Similar results were obtained using dynamin as the input (results not shown). Inhibition was not found using 50 μg of RasGAP-SH3 protein. Our results suggested that, in terms of binding affinity, amphiphysin could compete with EEN family members for binding with synaptojanin and dynamin.

DISCUSSION

The EEN family belongs to the group of SH3-domain-containing proteins, which have been implicated in many biochemical processes, including cell proliferation and differentiation, cell architecture, protein trafficking and subcellular localization, as well as the immune response to infection (for a review, see [38]). Studies *in vitro* and *in vivo* have shown that the EEN family is now known to interact with dynamin, synaptojanin, endocytic proteins involved in endocytosis [1,2] and leukaemia [3], as well as with HD, which is implicated in Huntington's disease [25]. There are few data, however, in existence comparing the expression of the EEN family in various mouse and human tissues with that reported for dynamin, synaptojanin and HD, or from binding studies, which may reveal further insights into how the EEN family mediates various cellular functions.

Using the combination of Northern blot analysis, RT-PCR and ISH, we have shown that the EEN family members, despite high sequence and structural similarities, have distinctive but overlapping expression domains. Our data show that EEN is ubiquitously expressed in most tissues, whereas EEN-B1 is expressed mainly in adult brain and EEN-B2 is expressed in both the brain and the testis. Within the brain, the expression of EEN-B1 and EEN-B2 in the brain is highest in the neurons of the granular layer of the cerebral cortex, the internal granules and Purkinje cells of cerebellar cortex and hippocampus; these expression patterns are parallel with those reported for dynamin-I/III [28,39] and synaptojanin-I [40]. In the testis, EEN-B1 and EEN-B2, like testis-type dynamin, i.e. dynamin-III [29,41], are preferentially expressed in the Sertoli cells, which are known to elaborate endocytic processes and nurse developing germ cells. Taken together, our results support a role for the EEN family members in endocytosis in both the brain and the testis. We also show that EEN family members are not functionally redundant, and might act in different tissues at different developmental stages. This is apparent from the expression patterns of EEN-B1 and EEN-B2, both are expressed similarly in mouse embryos, whereas in the adult stage only EEN-B1 is expressed in the mouse adult kidney.

Our detailed studies in the brain have revealed two unexpected findings. First, there is intense expression of EEN-B1 and -B2 in the CA3 area of the hippocampus; this is the same region where dynamin and synaptojanin are highly expressed. To date, very

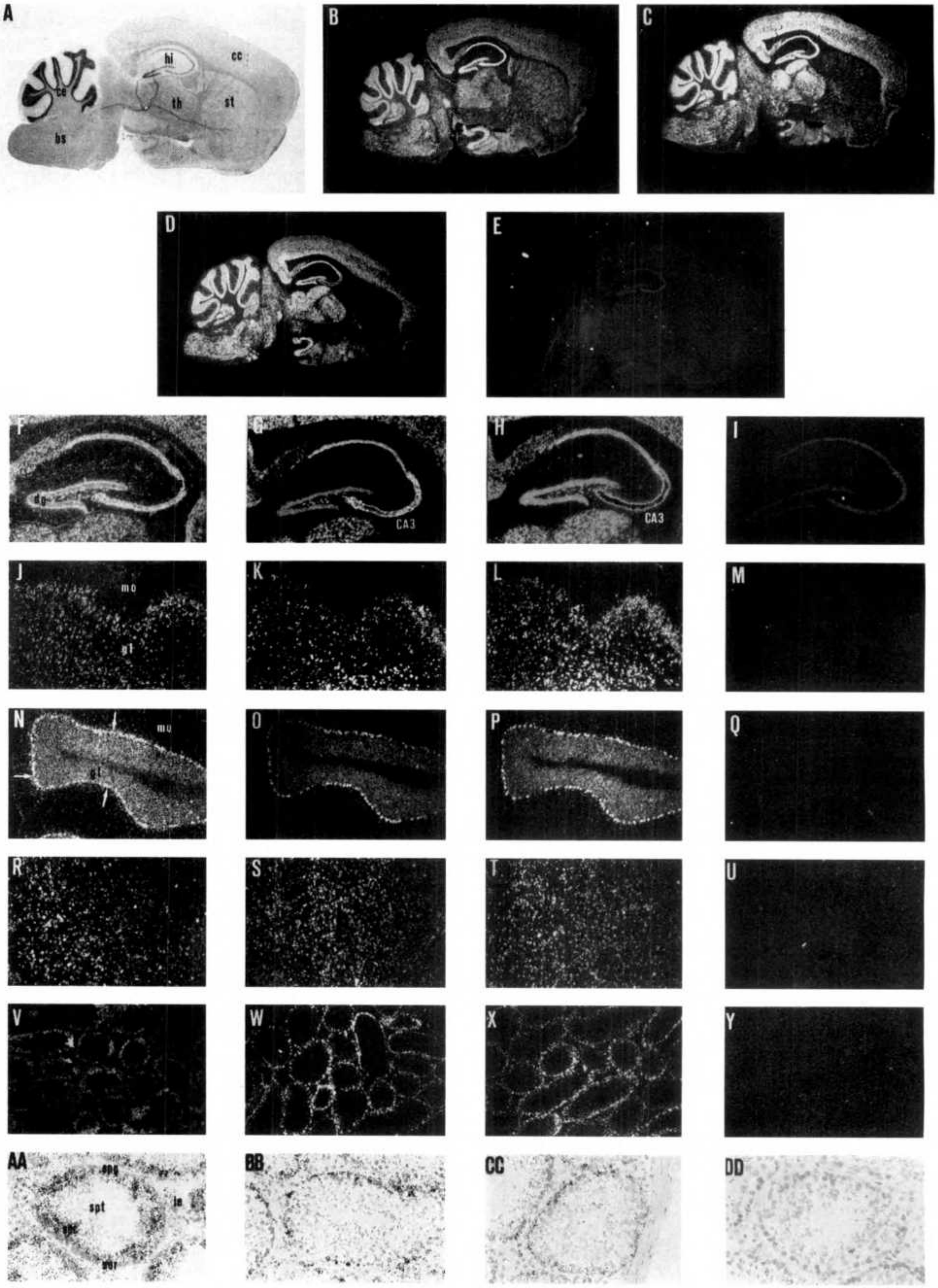

Figure 5 Expression of EEN family members in adult brain (A–U) and testis (V–Y, and AA–DD)

Sagittal sections of mouse brain (**A**–**E**) were hybridized with ^{35}S-radiolabelled mouse antisense probe of EEN (**B**), EEN-B1 (**C**), EEN-B2 (**D**) and sense probe of EEN (**E**). Photomicrographs of emulsion-dipped sections of hippocampal formation (**F**–**I**), cerebral cortex (**J**–**M**), cerebellar cortex (**N**–**Q**), striatum (**R**–**U**) and testis (**V**–**Y** and **AA**–**DD**) that were hybridized with antisense probes

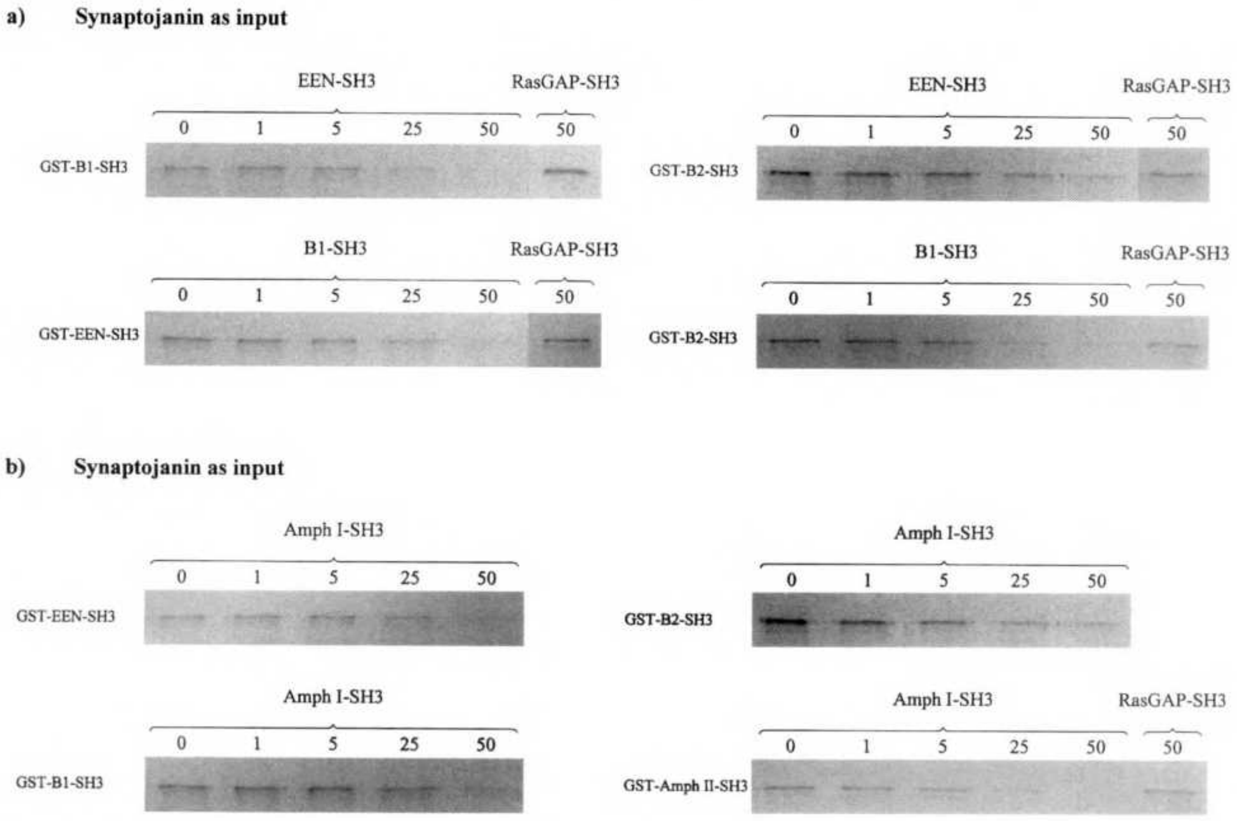

Figure 6 Competitive binding assay of synaptojanin among members of the EEN family and amphiphysin

(**a**) Top panels: immobilized GST fusion proteins of B1-SH3 (left) and B2-SH3 (right) were incubated with ^{35}S-labelled synaptojanin-145 in the presence of 0, 1, 5, 25 or 50 μg of EEN-SH3 protein respectively. Bottom panels: immobilized GST fusion proteins of EEN-SH3 (left) and B2-SH3 (right) were incubated with ^{35}S-labelled synaptojanin-145 in the presence of 0, 1, 5, 25 or 50 μg of B1-SH3 protein respectively. (**b**) Immobilized GST fusion proteins of EEN-SH3 (top left), B1-SH3 (bottom left), B2-SH3 (top right), and amphiphysin II (Amph II)-SH3 domains (bottom right) were incubated with ^{35}S-labelled synaptojanin-145 in the presence of 0, 1, 5, 25 or 50 μg of amphiphysin I (Amph I)-SH3 protein respectively. The negative controls using 50 μg RasGAP-SH3 protein are also indicated for (**a**) and (**b**). Similar results were obtained using dynamin as the input (results not shown).

few numbers of molecules that discriminate between sub-populations of hippocampal cells have been identified [42]. The significance of the finding that these four different molecules are predominantly co-expressed in the CA3 area of the hippocampus is unclear; one possibility is that they might play a role in mediating the specific synaptic functions of this discrete area in the hippocampus. Secondly, we have found that EEN-B1/-B2 and HD share similar expression patterns in both adult and fetal tissues [43–47]. Taken together with the observation that EEN-B2 has been found to interact with the glutamine expansion region of the HD protein and promotes the formation of insoluble polyglutamine-containing aggregates [25], our findings suggest a link between the pathogenesis of Huntington's disease and the association of HD with EEN family members.

In our study, we have also identified three different spliced variants of EEN-B2 (L1 to L3), which all contain a C-terminal SH3 domain. EEN-B2-L1 and EEN-B2-L2 possess identical expression patterns, whereas EEN-B2-L3 is expressed only in adult brain and testis, and not in the thymus, where L1 and L2 can be detected. Interestingly, the recent study on dynamin in rat tissues using RT-PCR has also identified multiple-spliced variants with different tissue specificity [31]. Most of these dynamin variants can be found in adult brain, but not in epithelial-based tissues, except in the testis, where over half of the splice variants of dynamin II and III can be detected. One could speculate that splice variants of the EEN family and dynamin may be targeted to different cellular compartments in order to carry out their functions. This speculation is consistent with a recent study on Intersectin, a newly identified SH3-domain-containing protein with an affinity for dynamin, in which different splice variants of Intersectin with specific tissue distribution were shown to be components of the endocytic machinery in neurons and non-neuronal cells respectively [48].

We have shown that, within the EEN family, the binding affinity of EEN-B1 to synaptojanin and dynamin is higher than that of EEN and EEN-B2. Accordingly, EEN-B1 will preferentially interact with synaptojanin in the cells (e.g. in neurons) co-expressing other EEN family members. This result is consistent with the finding of EEN-B1/endophilin I as being the major synaptojanin-binding protein in rat brain [1]. However, competition *in vitro* can only be seen with large amounts of competitor proteins (e.g. 50 μg).

---

of EEN (**F**, **J**, **N**, **R**, **V**, **AA**), EEN-B1 (**G**, **K**, **O**, **S**, **W**, **BB**) and EEN-B2 (**H**, **L**, **P**, **T**, **X**, **CC**) and EEN sense probes (**I**, **M**, **Q**, **U**, **Y**, **DD**) respectively. bs, brain stem; cc, cerebral cortex; ce, cerebellum; dg, dentate gyrus; gl, granular layer; hi, hippocampus; le, Leydig cells; mo, molecular layer; py, pyramidal cell layer of the hippocampal formation; ser, Sertoli cells; spc, spermatocytes; spg, spermatogonia; spt, spermatids; st, striatum; th, thalamus; wm, white matter. Arrows (white) indicate the Purkinje cells in (**J**). CA3, a type of pyramidal cell of the hippocampus.

The possible role of the EEN family in clathrin-mediated endocytosis has been demonstrated by the recent finding of lysophosphatidic acid acyltransferase (LPAAT) activity of EEN-B1/endophilin I [49]. The LPAAT activity of EEN-B1 converts an 'inverted-cone-shaped' lipid into a cone-shaped lipid, and induces membrane curvature, which leads to the formation of synaptic-like microvesicles (SLMVs). A C-terminal EEN-B1 mutant lacking the dynamin/synaptojanin-binding SH3 domain, but still retaining LPAAT activity, was defective in the formation of SLMVs [49,50]. These findings demonstrated that protein–protein interaction of EEN-B1 via its SH3 domain is essential for mediating the formation of SLMVs. In addition to the EEN family, the SH3 domain of amphiphysin also binds specifically to dynamin and synaptojanin in the presynaptic termini. Using peptide-competition assays, we demonstrate that amphiphysin I will prevent EEN family members from binding to synaptojanin and dynamin. This inhibition possibly resulted from the steric effect of these two proteins binding, since EEN family proteins and amphiphysin bind to two adjacent PRDs on synaptojanin ([51,52]; C. W. So and L. C. Chan, unpublished work). Previous studies *in vivo* [53] have shown that synaptojanin can form two separate and stable complexes in the nerve terminal, i.e. (i) synaptojanin with EEN-B1, and (ii) synaptojanin with amphiphysin and dynamin. Our finding of competitive binding between the EEN family members and amphiphysin suggest that amphiphysin may regulate the amount of synaptojanin and/or dynamin at the sites of endocytosis by controlling the availability of these proteins for the EEN family. Further studies *in vivo* involving the overexpression of wild-type and mutant proteins of amphiphysin and EEN family members may help to address this possibility.

We thank Brian Kay for providing murine cDNA of the EEN family, P De Camilli for providing cDNA of dynamin and synaptojanin, H. T. McMahon for GST–Grb2 fusion cDNA and constructive advice, W M. Lee for provision of cDNA from purified Sertoli cells, and Stanley Ko for technical support This work was funded by RGC grant 338-046-0009

REFERENCES

1 De Heuvel, E, Bell, A W, Ramjaun, A R, Wong, K., Sossin, W. S and McPherson, P S (1997) J Biol. Chem. **272**, 8710–8716
2 Ringstad, N, Nemoto, Y and De Camilli, P (1997) Proc Natl Acad Sci. U S A. **94**, 8569–8574
3 So, C. W, Caldas, C., Liu, M-M, Chen, S-J, Huang, Q-H, Gu, L-J, Sham, M H., Wiedemann, L M and Chan, L C (1997) Proc Natl Acad Sci U S A **94**, 2563–2568
4 Sparks, A B, Hoffman, N G., McConnell, S J, Fowlkes, D M and Kay, B K (1996) Nat Biotechnol **14**, 741–744
5 Giachino, C, Lantelme, E, Lanzetti, L, Saccone, S, Della Valle, G and Migone, N (1997) Genomics **41**, 427–434
6 Chen, M S, Obar, R A, Schroeder, C C., Austin, T W., Poodry, C A, Wadsworth, S. C and Vallee, R B (1991) Nature (London) **351**, 583–586
7 van der Bliek, A M and Meyerowitz, E M (1991) Nature (London) **351**, 411–414
8 Kosaka, T. and Ikeda, K (1983) J. Cell Biol **97**, 499–507
9 Ramaswami, M., Krishnan, K. S and Kelly, R. B (1994) Neuron **13**, 363–375
10 Hinshaw, J E and Schmid, S L (1995) Nature (London) **374**, 190–192
11 Takei, K, McPherson, P S, Schmid, S L and De Camilli, P (1995) Nature (London) **374**, 186–190
12 McPherson, P. S, Garcia, E P, Slepnev, V I, David, C, Zhang, X., Grabs, D, Sossin, W S., Bauerfeind, R, Nemoto, Y. and De Camilli, P (1996) Nature (London) **379**, 353–357
13 De Camilli, P., Emr, S. D, McPherson, P S and Novick, P. (1996) Science **271**, 1533–1539
14 Mayinger, P, Bankaitis, V A and Meyer, D I (1995) J Cell Biol **131**, 1377–1386
15 Singer-Kruger, B, Nemoto, Y., Daniell, L, Ferro-Novick, S. and De Camilli, P (1998) J Cell Sci **111**, 3347–3356
16 Wigge, P and McMahon, H. T (1998) Trends Neurosci **21**, 339–343
17 Lichte, B, Veh, R W, Meyer, H E and Kilimann, M W (1992) EMBO **11**, 2521–2530
18 David, C, McPherson, P S, Mundigl, O and De Camilli, P (1996) Proc Natl Acad Sci U S A **93**, 331–335
19 Robinson, M S. (1994) Curr Opin Cell Biol **6**, 538–544
20 Munn, A L, Stevenson, B. J, Geli, M. I and Riezman, H (1995) Mol Biol Cell **12**, 1721–1742
21 Shupliakov, O., Low, P, Grabs, D, Gad, H, Chen, H, David, C, Takei, K., De Camilli, P and Brodin, L (1997) Science **276**, 259–263
22 Wigge, P, Vallis, Y. and McMahon, H. T (1997) Curr Biol. **7**, 554–560
23 Urrutia, R., Henley, J. R, Cook, T. and McNiven, M. A (1997) Proc Natl Acad Sci U S.A **94**, 377–384
24 Schmid, S L., McNiven, M A and De Camilli, P. (1998) Curr Opin Cell Biol **10**, 504–512
25 Sittler, A, Walter, S, Wedemeyer, N, Hasenbank, R., Scherzinger, E, Eickhoff, H, Bates, G P., Lehrach, H. and Wanker, E E. (1998) Mol. Cell **2**, 427–436
26 Zechner, U., Scheel, S, Hemberger, M., Hopp, M., Haaf, T, Fundele, R, Wanker, E. E, Lehrach, H, Wedemeyer, N. and Himmelbauer, H (1998) Genomics **54**, 505–510
27 Sharp, A H., Love, S J., Schilling, G., Li, S. H, Li, X J., Bao, J, Wagster, M V., Kotzuk, J A, Steiner, J. P, Lo, A et al (1995) Neuron **14**, 1065–1074
28 Sontag, J-M, Fykse, E M, Ushkaryov, Y, Liu, J.-P., Robinson, P J and Sudhof, T. C (1994) J. Biol. Chem. **269**, 4547–4554
29 Cook, T, Mesa, K and Urrutia, R (1996) J. Neurochem. **67**, 927–931
30 Nemoto, Y, Arribas, M, Haffner, C and De Camilli, P (1997) J. Biol. Chem. **272**, 30817–30821
31 Cao, H., Garcia, F and McNiven, M A. (1998) Mol. Biol Cell **9**, 2595–2609
32 Ausubel, F M., Brent, R, Kingston, R E, Moore, D. D, Seidman, J. G, Smith, J. A and Struhl, K (1987) Current Protocols in Molecular Biology, pp 6 0.1–6 12.12 (suppl 27), John Wiley & Sons, New York
33 Sham, M H, Vesque, C, Nonchev, S, Marshall, H, Frain, M, Gupta, R D, Whiting, J, Wilkinson, D, Charnay, P and Krumlauf, R (1993) Cell **72**, 183–196
34 Kozak, M (1996) Cell **44**, 283–292
35 Sharp, P A. (1981) Cell **23**, 643–646
36 Chung, S S, Zhu, L J, Mo, M Y, Silvestrini, B, Lee, W M and Cheng, C Y (1998) J Androl **19**, 686–703
37 Owen, D. J, Wigge, P., Vallis, Y, Moore, J. D A., Evans, P R. and McMahon, H T (1998) EMBO **17**, 5273–5285
38 Pawson, T (1995) Nature (London) **373**, 573–580
39 Nakata, T, Iwamoto, A, Noda, Y, Takemura, R, Yoshikura, H. and Hirokawa, N (1991) Neuron **7**, 461–469
40 Kudo, M, Saito, S, Sakagami, H, Suzaki, H and Kondo, H (1999) Mol Brain Res **64**, 179–185
41 Nakata, T, Takemura, R and Hirokawa, N (1993) J. Cell Sci **105**, 1–5
42 Woodhams, P L, Webb, M, Atkinson, D J and Seeley, P J. (1989) J Neurosci. **9**, 2170–2181
43 Schmitt, I, Bachner, D, Megow, D, Henklein, P, Hameister, H, Epplen, J T and Riess, O (1995) Hum Mol Genet **4**, 1173–1182
44 Bhide, P G, Day, M, Sapp, E, Schwarz, C, Sheth, A, Kim, J, Young, A. B, Penney, J, Golden, J, Aronin, N and DiFiglia, M (1996) J Neurosci **16**, 5523–5535
45 Strong, T V, Tagle, D A, Valdes, J M, Elmer, L W, Boehm, K, Swaroop, M, Kaatz, K W, Collins, F S and Albin, R L (1993) Nat Genet **5**, 259–265
46 Li, S H, Schilling, G, Young, III, W S, Li, X J, Margolis, R L., Stine, O C, Wagster, M. V, Abbott, M. H, Franz, M L, Ranen, N G et al (1993) Neuron **11**, 985–993
47 Hoogeveen, A T, Willemsen, R, Meyer, N, Rooij, K E, Roos, R A C, Ommen, G J B and Galjaard, H (1993) Hum Mol Genet **2**, 2069–2073
48 Hussain, N K, Yamabhai, M., Ramjaun, A R, Guy, A M, Baranes, D., O'Bryan, J. P., Der, C J, Kay, B. K and McPherson, P S. (1999) J Biol. Chem. **274**, 15671–15677
49 Schmidt, A, Wolde, M, Thiele, C, Fest, W, Kratzin, H, Podtelejnikov, A V, Witke, W, Huttner, W B and Soling, H D (1999) Nature (London) **401**, 133–141
50 Scales, S J and Scheller, R H (1999) Nature (London) **401**, 123–124
51 Cestra, G, Castagnoli, L, Dente, L., Minenkova, O., Petrelli, A, Migone, N, Hoffmuller, U, Schneider-Mergener, J. and Cesareni, G (1999) J Biol Chem **45**, 32001–32007
52 So, C W, So, C K C, Cheung, N, Chew, S L, Sham, M H and Chan, L C (2000) Leukemia **14**, 594–601
53 Micheva, K D, Kay, B K and McPherson, P S. (1997) J Biol Chem **272**, 27239–27245

Received 26 October 1999/31 January 2000; accepted 8 March 2000

Biochem J (2000) **348**, 459–463 (Printed in Great Britain)

Characterization of *N*-myristoyltransferase from *Plasmodium falciparum*

Ruwani S. GUNARATNE[1,2], Mohammed SAJID[3], Irene T. LING, Renu TRIPATHI[4], Justin A. PACHEBAT and Anthony A. HOLDER
Division of Parasitology, The National Institute for Medical Research, The Ridgeway, Mill Hill, London NW7 1AA, U.K

The gene coding for myristoyl-CoA:protein *N*-myristoyltransferase (NMT) has been cloned from the malaria parasite *Plasmodium falciparum*. The gene appears to be single copy and mRNA is expressed in asexual blood-stage forms. Comparison of cDNA and genomic sequences identified three small introns. The open reading frame codes for a 410-amino-acid protein and no evidence of forms with an extended N-terminal coding sequence was obtained. Residues important in substrate binding and in the catalytic mechanism in other species are conserved. The protein was expressed from a plasmid in *Escherichia coli*, partially purified and shown to have enzymic activity using a synthetic peptide substrate. Comparison of the malaria parasite protein with that derived from the human gene showed a different pattern of inhibition by chemical modification. Human NMT activity was inhibited by diethylpyrocarbonate and partially inhibited by iodacetamide, whereas *P. falciparum* NMT activity was not inhibited by either pre-treatment. Since the enzyme in infectious fungi is a target for potential chemotherapeutic drugs, it should also be investigated in the context of parasitic infections such as that responsible for malaria.

Key words: malaria parasite, protein acylation, recombinant enzyme.

INTRODUCTION

Malaria is a debilitating disease transmitted by mosquitoes and caused by protozoa of the genus *Plasmodium*. *Plasmodium falciparum* causes the most serious illness and the asexual blood stage that replicates in erythrocytes may lead to coma and death within a few days. Due to emerging resistance against current anti-malarial drugs, there is an urgent need to identify new chemotherapeutic targets in malaria.

One candidate target is myristoyl-CoA:protein *N*-myristoyltransferase (NMT; EC 2.1.3.97). NMT catalyses the co-translational transfer of the $C_{14:0}$ fatty acid from myristoyl-CoA to the N-terminal glycine of a variety of cellular proteins [1]. There are several reasons why NMT may be an attractive target for chemotherapy of infectious eukaryotes, and it has been investigated in the context of fungal infections [2]. The activity of this acyltransferase is essential for fungal viability [3,4] and in *Saccharomyces cerevisiae NMT* is an essential gene [5]. Although the binding site for the acyl-CoA is highly conserved, the protein binding site is variable [6,7], and peptide binding studies suggest that the protein substrate specificity has diverged in different species [8]. Significant differences between NMT in humans and fungi have led to the design of peptidomimetic inhibitors, which are highly selective against *Candida albicans* NMT compared with the human enzyme [9,10]. These studies suggest that NMT is a potential target for chemotherapeutic drugs against fungal infections and should be investigated in the context of parasitic infections.

Recently the structure of the *C. albicans* apoenzyme [11] and a ternary complex of the *S. cerevisiae* enzyme with bound myristoyl-CoA and peptide substrate analogues [12] have been reported, allowing the identification of the residues involved in substrate binding and a proposed catalytic mechanism. It has been proposed that acyl transfer occurs through a direct nucleophilic attack of the glycine nitrogen on the carbonyl carbon of the thioester of myristoyl-CoA, following polarization of the carbonyl in an oxyanion hole and proton transfer from the glycine α-amino group to the C-terminal carboxylate of NMT [12].

The NMT enzyme activity is not dependent on its N-terminal sequence. The first 59 amino acids of the yeast enzyme appear to be unnecessary for enzymic activity [7]. In mammalian cells a number of different-sized forms have now been described, resulting from transcription from two loci [13], differential mRNA splicing [14] and proteolytic cleavage of the N-terminus [15]. The extended form of NMT appears to contain a ribosomal targeting sequence [16].

Although there have been few studies that directly demonstrate N-myristoylation of *P. falciparum* proteins, potential substrates such as the ADP-ribosylation factor 1 (ARF1) have been identified [17]. Metabolic labelling studies in pathogenic fungi have identified the ADP-ribosylation factors as major substrates for NMT [2], which require N-myristoylation for biological activity. Here we report the cloning and sequence analysis of the *P. falciparum NMT*, describe expression studies in *Escherichia coli* and carry out an initial comparison between the parasite and human enzymes.

MATERIALS AND METHODS

Preparation of *P. falciparum* parasites, and extraction of nucleic acids

P. falciparum clone T9/96 was maintained in erythrocytes in continuous culture, as described previously [18]. Infected ery-

---

Abbreviations used ARF1, ADP-ribosylation factor 1, DEPC, diethylpyrocarbonate, ORF, open reading frame, NMT, myristoyl-CoA:protein *N*-myristoyltransferase; RT-PCR, reverse transcriptase PCR, Ni^{2+}-NTA, Ni^{2+}-nitrilotriacetate

[1] Present address Department of Biochemistry, University of Cambridge, Main Building, Downing Site, Tennis Court Road, Cambridge CB2 1QW, U.K

[2] To whom correspondence should be addressed (e-mail rsg25@mole.bio.cam.ac.uk)

[3] Present address: Tropical Disease Research Unit, University of California, San Francisco, VAMC 113B, 4150 Clement St, San Francisco, CA 94121, U.S.A

[4] Present address: Central Drug Research Institute, Chatter Manzil, Post Box No 173, Lucknow-226001, India

throcytes were harvested by centrifugation at 400 *g* for 5 min, washed twice with ice-cold PBS, and then lysed by the addition of 1% (v/v) acetic acid to release the intracellular parasites. After addition of a large volume of ice-cold PBS, the parasites were harvested by centrifugation at 400 *g* for 5 min, washed twice with ice-cold PBS, and then stored at −70 °C.

Nucleic acids were prepared from the parasite material. The frozen extracts were thawed and genomic DNA prepared using the Blood and Cell Culture Genomic DNA Maxi Kit (Qiagen), according to the manufacturer's instructions. Total RNA was prepared from 3.8 × 10^9 infected red cells using the SNAP® Kit (Invitrogen) according to the manufacturer's guidelines. Approx. 200 ng of RNA was used for cDNA synthesis using the cDNA Cycle Kit for reverse transcriptase PCR (RT-PCR; Invitrogen).

PCR amplification with degenerate primers, isolation of a specific DNA fragment, analysis of products from Vectorette libraries, and assembly of the genomic sequence for *P. falciparum NMT*

In the first step to cloning *P. falciparum NMT*, degenerate oligonucleotide primers were synthesized, based on regions of amino acid sequence homology between NMT of six different organisms, and biased for *P. falciparum* codon usage. Two primers, NMT2F [CCA/T GTA/T T/CTA/T ATA/T AAA GAA A/GTA/T AC (forward PVLIKEV/IT)] and NMT3R [CC ATC A/TCC NNN A/TCC AAA TTT (reverse KFGXGDG)], produced an approx. 630 bp product by PCR amplification from genomic DNA. This was confirmed to be part of the *NMT* gene by sequence analysis.

In the second step a specific probe was used to screen a Southern blot and clone a hybridizing fragment. A 480 bp sequence was amplified by PCR from the partial *NMT* sequence, and labelled with [α-^{32}P]dATP (Amersham), using the Prime-It II Random Labelling Kit (Stratagene), according to the manufacturer's guidelines. Southern blotting was carried out using 5 μg of *P. falciparum* genomic DNA digested with several restriction enzymes. The DNA was transferred to Hybond-N+ Nylon membranes (Amersham) overnight in 20 × SSC (where 1 × SSC is 0.15 M NaCl/0.015 M sodium citrate) and immobilized by UV cross-linking. After probe addition and washing under high-stringency conditions (final wash in 0.1 × SSC/0.1% SDS at 65 °C for 15 min), hybridizing fragments were identified Based on the result of the Southern blotting, a fragment hybridizing to the probe was cloned from a library prepared in λ-ZAP II (Stratagene) from size-fractionated *Bgl*II-digested genomic DNA. This fragment was sequenced and found to extend 3′ from a *Bgl*II site within the *NMT* gene. At this stage a shotgun sequence (PF2MJ) read in The Institute for Genome Research *P. falciparum* genome database was found to overlap the sequence obtained and it was used to extend the sequence for an additional 150 bp in the 5′ direction. These preliminary sequence data were obtained from The Institute for Genomic Research website (http://www.tigr.org). This sequencing was part of the International Malaria Genome Sequencing Project.

In the final step to obtain the full sequence of *P. falciparum NMT* two rounds of Vectorette-II PCR were used to clone the remainder of the gene. Vectorette-II libraries were made according to the manufacturer's guidelines (Genosys) using 0.1 μg of T9/96 genomic DNA digested with either *Alu*I, or *Dra*I. PCR reactions were carried out in 100 μl reaction volumes, using 1 μl of each Vectorette-II library, 250 nM of Universal Vectorette Primer, 250 nM of *NMT*-specific primer, either NMTVEC2 (AAC ACA TAA AAA ATT CAC CAC AGC) or NMTVEC4 (GAT ATA AAT CCC TAC CAA CAA A), and 5 units of AmpliTaq Gold (Perkin-Elmer). Thermal cycling was as follows: 94 °C for 2 min; 94 °C for 1 min, 60 °C for 2 min, 72 °C for 3 min for 40 cycles, followed by final extension step of 72 °C for 10 min. In the first round a 984 bp fragment was produced from the *Dra*I library with the NMTVEC2 primer, cloned and sequenced; and in the second round a 702 bp fragment was produced from the *Alu*I library using the NMTVEC4 primer, cloned and sequenced.

Cloning full-length *P. falciparum NMT* from genomic DNA and cDNA and confirmation of the putative translational start site

To confirm the full-length *NMT* sequence, and to allow insertion of the DNA into an expression vector, it was amplified from both genomic DNA and cDNA using two primers, termed NMTORF1A and NMTORF2A. NMTORF1A (GGATCCCG AAT GAT GAT AAG AAA GAT TTT GTT GG) contained an artificial *Bam*H1 restriction site (underlined) and NMTORF2A (G GAATTC AAG ATG GTG GTT ATA AAC TTA TAA TAA AAC) contained an artificial *Eco*RI restriction site. PCR reactions used 100 ng of genomic DNA or 50 ng of cDNA and Klen*Taq* Polymerase (Clontech). Cycling conditions were 94 °C for 5 min for 1 cycle, 94 °C for 1 min, 64 °C for 30 s, 68 °C for 2 min, for 30 cycles, followed by a final extension step of 68 °C for 10 min. PCR products were ligated into the TA vector used to transform *E. coli* TOP10, and the sequence of chosen inserts was obtained by automatic sequencing using an ABI 377 machine.

The absence of an additional intron 5′ of the putative translational initiation site was confirmed by amplification using both genomic and cDNA as DNA templates using the primers NMTUP4 (CGT TAA AAT AAA ATA AAC C) and NMTVEC4. Products were analysed by agarose gel electrophoresis and cloned and sequenced.

Expression of *P. falciparum NMT* in *E. coli*

The *NMT* open reading frame (ORF) was ligated into the expression plasmid pTrcHis-C (a vector that directs expression of the inserted sequence as a polypeptide fused to six histidine residues and the Xpress® epitope at the N-terminus), the DNA was used to transform *E. coli* TOP10 cells, and the DNA sequence was confirmed in a chosen clone. Bacteria from a single colony were grown overnight at 37 °C in Terrific Broth, the culture was diluted 20-fold, and after a further 2 h (D_{600}, 0.6–1.0) protein expression was induced by addition of 1 mM isopropyl β-D-thiogalactoside and overnight incubation at 37 °C. Bacterial cells were harvested by centrifugation and resuspended in 1 ml of lysis buffer (50 mM sodium phosphate, pH 8.0, 300 mM NaCl, 10 mM imidazole and Complete® Protease Inhibitor Cocktail EDTA-free from Boehringer Mannheim). They were then lysed by addition of lysozyme to a final concentration of 1 mg · ml^{-1} on ice for 30 min followed by sonication in a Sonics and Materials VibraCell Sonicator, for 4 × 15 s bursts on maximum deflection. The lysate was cleared by centrifugation (147000 *g*, 1 h at 4 °C) and loaded on to a Ni^{2+}-nitrilotriacetate (Ni-NTA) column (Qiagen), equilibrated with lysis buffer. The column was washed twice with wash buffer (50 mM sodium phosphate, pH 8.0, 300 mM NaCl and 20 mM imidazole), and then the bound protein was eluted from the column using elution buffer (50 mM sodium phosphate, pH 8.0, 300 mM NaCl and 1.0 M imidazole). The expressed protein was detected by Western blotting, using the Anti-Penta His (Qiagen) or the Anti-Xpress® Antibodies (Invitrogen). The blot was developed using a secondary antibody conjugated to horseradish peroxidase and ECL® reagents (Pierce), and exposed to X-Omat film (Kodak) for 10–30 s. Protein concentration was estimated using the BCA (bicinchoninic acid) assay according to the manufacturer's guidelines and the reactions were incubated at 65 °C for 1 h.

NMT activity and inhibition assays

The assay was based on that of King and Sharma [19] that measures the ability of active NMT to transfer [^{3}H]myristate from [^{3}H]myristoyl-CoA, to the N-terminal glycine of a synthetic peptide *in vitro*. The assay was performed using human NMT (kindly provided by Dr Jeffrey McIlhinney [20]) and *P. falciparum* NMT expressed in *E. coli*. A peptide, termed *Pf*G8, was designed based on the N-terminal sequence of the *P. falciparum* ARF1 protein. This peptide contained the sequence Gly-Leu-Tyr-Val-Ser-Arg-Leu-Phe and conformed to the consensus sequence required for the N-myristoylation of proteins by NMT. The peptide sequence was verified after reversed-phase HPLC and provided as a freeze-dried powder (Peptide Synthesis Service, National Institute for Medical Research, London, U.K.), which was resuspended in DMSO to a final stock concentration of 10 mM and used subsequently in the NMT assays.

The NMT assay was carried out in a final volume of 100 μl in 30 mM Tris/HCl, pH 7.4, containing 0.5 mM EGTA, 40 nM peptide, 1 % (w/v) Triton X-100 and partially purified *P. falciparum* NMT (615 ng/assay). The reaction was initiated by the addition of 0.55 μCi of [^{3}H]myristoyl-CoA (Amersham) and incubation at 37 °C. Samples were removed at various time points and spotted on to P81 phosphocellulose paper (Whatman), which was then washed in three changes of 40 mM Tris/HCl at pH 7.3. The level of incorporation of [^{3}H]myristoyl-CoA was quantified in 5 ml of Ready Safe Liquid Scintillation mixture (Beckman), in a Liquid Scintillation Counter (Beckman LKB Wallac 1216 Rackbeta).

NMT enzyme assays were also carried out after preincubation of the partially purified enzyme (370 ng/assay) in the presence or absence of two known human-NMT inhibitors, 10 mM iodoacetamide and 10 mM diethylpyrocarbonate (DEPC), at room temperature for 15 min. The reaction was then initiated by addition of the peptide substrate and [^{3}H]myristoyl-CoA and transferred to 37 °C for a further 4 h in a reaction volume of 50 μl. The assays were carried out in parallel with human NMT (100 ng/assay) as a positive control at 37 °C for 30 min, unless otherwise stated.

RESULTS AND DISCUSSION

Isolation and sequencing of the full-length *P. falciparum NMT* gene

The full *NMT* gene sequence was amplified from both genomic and cDNA. Initially, degenerate oligonucleotide primers based on conserved sequences in NMTs of six other organisms were used to amplify a genomic DNA fragment. This fragment was used to clone a *Bgl*II fragment extending beyond the 3′ end of the ORF, and sequences extending in the 5′ direction were obtained largely from overlapping Vectorette clones. Finally the full genomic and RT-PCR gene sequences were amplified and analysed. Southern-blotting experiments suggested that *NMT* is a single-copy gene in *P. falciparum* (results not shown). The amplification of *P. falciparum NMT* as an RT-PCR product indicates that the mRNA for this protein is expressed in the asexual blood stages of the malarial parasite's life cycle.

The full-length *NMT* cDNA ORF contains 1230 bp, with the potential to encode a 48 kDa protein. The corresponding genomic DNA contains 1617 bp consisting of four exons; the first exon codes for the first five amino acids in the ORF. The three introns (all of which have the GT/AG boundary consensus) are located towards the 5′ end of the coding region and span 117, 126 and 144 bp, respectively. It has been shown that human NMT exists in two forms as a result of differential mRNA splicing, the longer form containing a lysine-rich N-terminal extension [14]. Comparison of both genomic and cDNA sequences upstream of the proposed ATG initiation codon, based on the size of amplified products and sequence analysis, provided no evidence for a similar extended form of the protein in *P. falciparum*.

An alignment of orthologous NMT sequences showed that the *P. falciparum* protein conforms to the pattern of extensive sequence conservation in the central and C-terminal regions of the protein (an alignment with three other sequences is shown in Figure 1), with most diversity at the N-terminus. The deduced *P. falciparum* NMT amino acid sequence is approx. 50 % identical to human NMT and approx. 40 % identical to the two fungal enzymes. The N-terminal sequence divergence is most evident in both the *Histoplasma capsulatum* NMT [2] and the human NMT [13,14]. *H. capsulatum* contains an apparent N-terminal extension of 71 residues and human NMT can also contain an N-terminal extension resulting from differential mRNA splicing. This N-terminal extension is postulated to direct the normally soluble enzyme to the ribosomal fraction [16]. Previous studies using *S. cerevisiae* NMT have suggested that the first 59 amino acids are not required for catalytic activity [7]. The data presented here indicate that there is no alternative start site for *P. falciparum* NMT and that the protein does not contain an N-terminal extension.

All the residues known to participate directly in the enzymic mechanism or play critical regulatory roles in yeast NMT are conserved in the *P. falciparum* enzyme with the exception of Ile^{180}, which is replaced by Val, and His^{46}, which is Tyr as in other non-yeast enzymes. A conserved cysteine residue (Cys^{229} in Figure 1) is replaced by Ala in *P. falciparum* NMT. The two PROCITE signature sequences that uniquely identify NMT proteins, (KFGXGDG) and [(E/D)(I/V)NFLC(V/I)HK], are present.

Expression of active *P. falciparum* NMT in *E. coli*

To determine whether or not the protein could be expressed in an enzymically active form, the 1230 bp *NMT* cDNA obtained by RT-PCR was cloned into the plasmid pTrcHis-C and used to transform *E. coli* TOP10 cells. *E. coli* has no endogenous NMT activity [21]. The recombinant protein was expressed as a N-terminal hexa-histidine and Xpress® epitope-tagged fusion protein and partially purified by affinity chromatography using a nickel-chelate (Ni-NTA) column. After induction of protein expression the NMT fusion protein was detectable by Western blotting using monoclonal antibodies anti-pentaHis (results not shown) and anti-Xpress® directed at the N-terminal tag coded by the expression vector (Figure 2). The fusion protein was purified partially by binding to a Ni-NTA column and eluted with 1.0 M imidazole. The antibodies recognized a 47 kDa protein, in good agreement with the predicted size, in the crude lysate of bacteria expressing *P. falciparum* NMT (Figure 2, lane 1) and material eluted from the nickel column (Figure 2, lane 3), but did not recognize proteins in the lysate of bacteria containing the expression vector alone (Figure 2, lanes 4–6).

The assay for NMT activity is based on the transfer of the [^{3}H]myristoyl group from myristoyl-CoA to a synthetic peptide and the binding of the [^{3}H]myristoylated peptide to phosphocellulose paper [19]. In the complete reaction mixture containing *P. falciparum* NMT and a peptide substrate based on the N-terminal amino acid sequence of the *P. falciparum* ARF1 protein

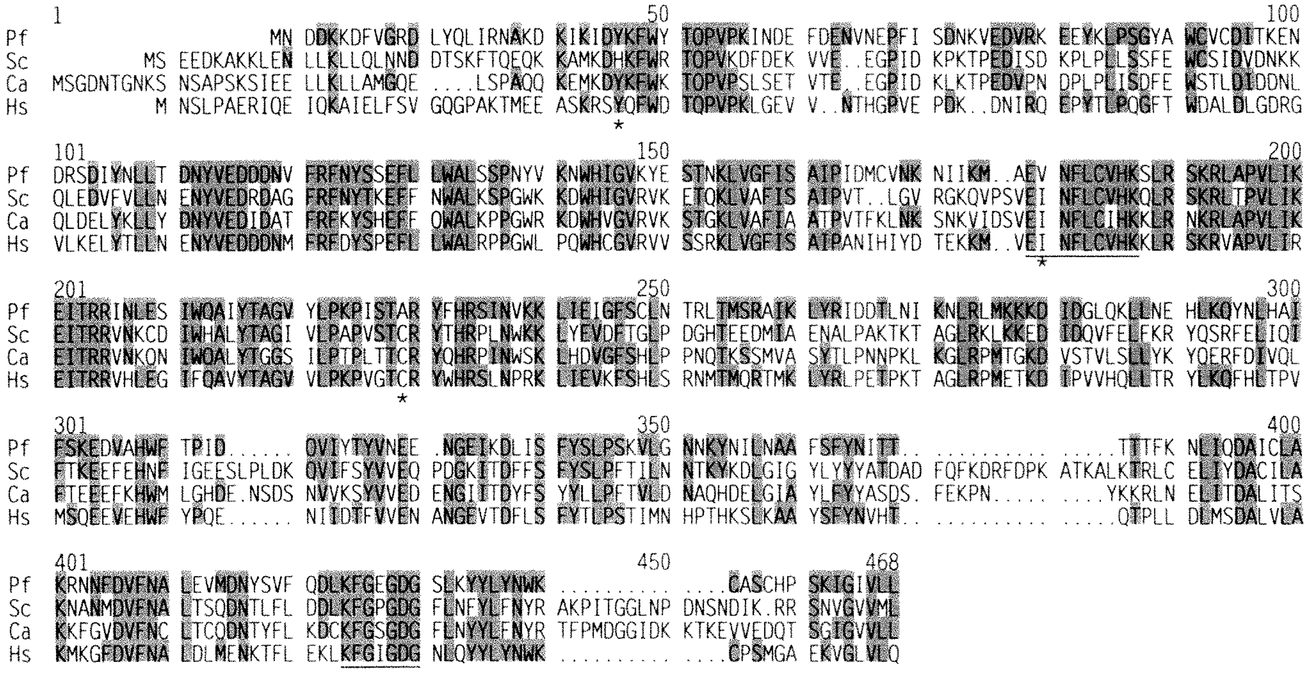

```
     1                                                 50                                                  100
Pf               MN DDKKDFVGRD LYQLIRNAKD KIKIDYKFWY TQPVPKINDE FDENVNEPFI SDNKVEDVRK EEYKLPSGYA WCVCDITKEN
Sc         MS EEDKAKKLEN LLKLLQLNND DTSKFTQEQK KAMKDHKFWR TQPVKDFDEK VVE..EGPID KPKTPEDISD KPLPLLSSFE WCSIDVDNKK
Ca MSGDNTGNKS NSAPSKSIEE LLKLLAMGQE ....LSPAQQ KEMKDYKFWK TQPVPSLSET VTE..EGPID KLKTPEDVPN DPLPLISDFE WSTLDIDDNL
Hs          M NSLPAERIQE IQKAIELFSV GQGPAKTMEE ASKRSYQFWD TQPVPKLGEV V..NTHGPVE PDK..DNIRQ EPYTLPQGFT WDALDLGDRG
                                                     *
     101                                               150                                                 200
Pf DRSDIYNLLT DNYVEDDDNV FRFNYSSEFL LWALSSPNYV KNWHIGVKYE STNKLVGFIS AIPIDMCVNK NIIKM..AEV NFLCVHKSLR SKRLAPVLIK
Sc QLEDVFVLLN ENYVEDRDAG FRFNYTKEFF NWALKSPGWK KDWHIGVRVK ETQKLVAFIS AIPVT..LGV RGKQVPSVEI NFLCVHKQLR SKRLTPVLIK
Ca QLDELYKLLY DNYVEDIDAT FRFKYSHEFF QWALKPPGWR KDWHVGVRVK STGKLVAFIA ATPVTFKLNK SNKVIDSVEI NFLCIHKKLR NKRLAPVLIK
Hs VLKELYTLLN ENYVEDDDNM FRFDYSPEFL LWALRPPGWL PQWHCGVRVV SSRKLVGFIS AIPANIHIYD TEKKM..VEI NFLCVHKKLR SKRVAPVLIR
                                                                                           *
     201                                               250                                                 300
Pf EITRRINLES IWQAIYTAGV YLPKPISTAR YFHRSINVKK LIEIGFSCLN TRLTMSRAIK LYRIDDTLNI KNLRLMKKKD IDGLQKLLNE HLKQYNLHAI
Sc EITRRVNKCD IWHALYTAGI VLPAPVSTCR YTHRPLNWKK LYEVDFTGLP DGHTEEDMIA ENALPAKTKT AGLRKLKKED IDQVFELFKR YQSRFELIQI
Ca EITRRVNKQN IWQALYTGGS ILPTPLTTCR YQHRPINWSK LHDVGFSHLP PNQTKSSMVA SYTLPNNPKL KGLRPMTGKD VSTVLSLLYK YQERFDIVQL
Hs EITRRVHLEG IFQAVYTAGV VLPKPVGTCR YWHRSLNPRK LIEVKFSHLS RNMTMQRTMK LYRLPETPKT AGLRPMETKD IPVVHQLLTR YLKQFHLTPV
                                    *
     301                                               350                                                 400
Pf FSKEDVAHWF TPID...... QVIYTYVNEE .NGEIKDLIS FYSLPSKVLG NNKYNILNAA FSFYNITT.. .......... .....TTTFK NLIQDAICLA
Sc FTKEEFEHNF IGEESLPLDK QVIFSYVVEQ PDGKITDFFS FYSLPFTILN NTKYKDLGIG YLYYYATDAD FQFKDRFDPK ATKALKTRLC ELIYDACILA
Ca FTEEEFKHWM LGHDE.NSDS NVVKSYVVED ENGIITDYFS YYLLPFTVLD NAQHDELGIA YLFYYASDS. FEKPN..... ....YKKRLN ELITDALITS
Hs MSQEEVEHWF YPQE...... NIIDTFVVEN ANGEVTDFLS FYTLPSTIMN HPTHKSLKAA YSFYNVHT.. .......... .....QTPLL DLMSDALVLA

     401                                               450                 468
Pf KRNNFDVFNA LEVMDNYSVF QDLKFGEGDG SLKYYLYNWK .......... ....CASCHP SKIGIVLL
Sc KNANMDVFNA LTSQDNTLFL DDLKFGPGDG FLNFYLFNYR AKPITGGLNP DNSNDIK.RR SNVGVVML
Ca KKFGVDVFNC LTCQDNTYFL KDCKFGSGDG FLNYYLFNYR TFPMDGGIDK KTKEVVEDQT SGIGVVLL
Hs KMKGFDVFNA LDLMENKTFL EKLKFGIGDG NLQYYLYNWK .......... ....CPSMGA EKVGLVLQ
```

Figure 1 The deduced amino acid sequence of *P. falciparum* NMT aligned with that of two fungal and a corresponding human sequence

The *P. falciparum* NMT (Pf) sequence is aligned with those of *S. cerevisiae* (Sc; accession no. M23726) and *C. albicans* (Ca; accession no. M80544), two fungal enzymes that have been used for X-ray crystallographic studies, and with the short form of human NMT1 (Hs; accession no. M86707). Residues identical in the *P. falciparum* sequence to one or more of the other three sequences are shaded; gaps inserted to improve the alignment are shown (.). Residues discussed in the text are indicated (*), together with the two PROCITE NMT signature sequences (underlined). The alignment was made using the program PileUp (Genetics Computer Group™).

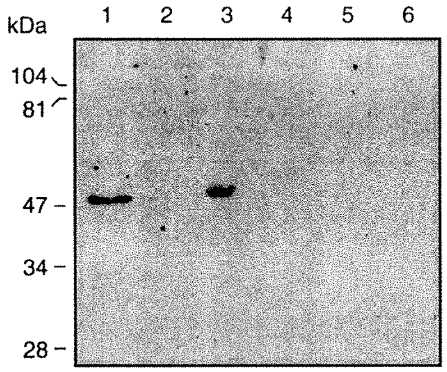

Figure 2 Expression of *P. falciparum* NMT in *E. coli* and a partial purification

A lysate was prepared from bacterial cells and the soluble fraction applied to a Ni-NTA column. After washing the column, bound material was eluted with 1.0 M imidazole. Samples of each fraction were resolved by SDS/PAGE analysis on a 12.5% gel and the proteins analysed by Western blotting using the Anti-Xpress™ monoclonal antibody. In lane 1, the total lysate from bacteria containing the *P. falciparum* NMT plasmid construct; lane 2, the proteins not bound to the column; lane 3, proteins bound to the column and eluted with imidazole; lane 4, the total lysate from control bacteria containing the plasmid without the NMT sequence; lane 5, proteins in the control lysate not bound to the column; lane 6, proteins in the control lysate bound to the column and eluted with imidazole. The mobilities of the molecular-mass markers are shown on the left. In lanes 1 and 3 a 47 kDa band corresponds to the full-length *P. falciparum* NMT fusion protein.

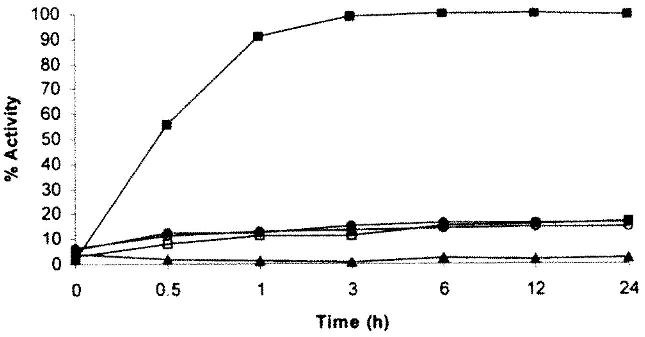

Figure 3 Recombinant *P. falciparum* NMT is enzymically active

The time course for *P. falciparum* NMT activity of protein purified from *E. coli* using the Ni-NTA column. Samples were assayed as described in the Materials and methods section. The results of a representative experiment from three performed are shown as the means of duplicate samples (which consistently differed by less than 10%). ■, *P. falciparum* NMT with synthetic peptide substrate; ○, *P. falciparum* NMT without peptide substrate; □, synthetic peptide substrate without NMT; ▲, control eluate with synthetic peptide substrate; ●, control eluate without peptide substrate; 100% activity corresponds to an incorporation of 16297 c.p.m. ^{3}H.

[17], enzyme activity was detected, whereas in the absence of either peptide or NMT expression only background levels of radiolabel incorporation were observed (Figure 3).

Although the level of expression in *E. coli* was not high (12 μg·l of bacterial culture^{-1}), the protein could be detected by Western blotting and by enzymic activity. In view of the skewed codon usage, typical of *P. falciparum* genes, it is likely that expression levels would be improved by re-synthesis of the gene using *E. coli*-preferred codons. Furthermore, additional purification steps will be required to obtain homogeneous enzyme. The sequence of the peptide used is consistent with the consensus

Table 1 A comparison of the sensitivity of the malarial and human enzymes to chemical inhibition

The inhibition of human and *P falciparum* NMT activities by treatment with 10 mM iodoacetamide or 10 mM DEPC for 20 min at 37 °C was measured Samples were assayed as described in the Materials and methods section using an incubation period of 4 h to allow maximal incorporation The results of a representative experiment are shown as the means of duplicate samples (which differed consistently by less than 10%). In this assay 100% activity corresponds to incorporations of 8645 and 6950 c p m ^{3}H for the human and *P falciparum* enzymes, respectively

Assay	Activity (%)	
	Human NMT	*P falciparum* NMT
With peptide substrate	100	100
Without peptide substrate	11.3	2.9
Iodoacetamide pre-treated	53.0	113.2
DEPC pre-treated	22.7	85.5

requirement for N-myristoylation and the specific incorporation of radiolabel due to NMT-dependent transfer of [^{3}H]myristate to the peptide indicated that *P. falciparum* NMT is expressed as an enzymically active form in *E. coli.*

Inhibition of *P. falciparum* NMT activity by chemical modification

The sensitivity of both human and *P. falciparum* NMT to inhibition by iodoacetamide and DEPC was investigated. Using these inhibitors, the recombinant *P. falciparum* NMT could be distinguished from the human enzyme. Human NMT is partially inhibited by 5 mM iodoacetamide and completely inhibited by 10 mM DEPC [20]. *P. falciparum* NMT expressed in *E. coli* was not inhibited by 10 mM iodoacetamide or 10 mM DEPC (Table 1), conditions under which human NMT activity was inhibited by 50 % and > 75 %, respectively.

Although it had been suggested previously that one or more of the conserved cysteine and histidine residues are involved directly in the catalytic transfer mechanism [22], this is now considered unlikely based on the structural studies [12]. Whether or not the replacement of the conserved cysteine residue (residue 229 in Figure 1) by Ala in *P. falciparum* NMT results in insensitivity to iodoacetamide inhibition remains to be determined. Further studies are required of the effects of other NMT inhibitors on the purified enzyme and on parasite cultures to determine whether or not anti-*N*-myristoyltransferase drugs are anti-parasitic.

We thank Dr Jeffrey McIlhinney for the generous gift of the recombinant human enzyme R G was supported by an MRC postgraduate studentship; R.T. was supported by a Royal Society-Indian National Scientific Academy Exchange Fellowship, the work undertaken by J.A.P. was in part fulfilment of an M Sc degree from the London School of Hygiene and Tropical Medicine Support from the British Council Deutsche Akademische Austauschdienst (DAAD) Academic Research Collaboration (ARC) programme is gratefully acknowledged Some preliminary sequence data were obtained from The Institute for Genomic Research website (http://www tigr org), this sequencing was part of the International Malaria Genome Sequencing Project and was supported by awards from the National Institute of Allergy and Infectious Diseases, National Institutes of Health, the Burroughs Wellcome Fund and the U S Department of Defense

REFERENCES

1 Rudnick, D. A., McWherter, C A, Gokel, G. W and Gordon, J I. (1993) Myristoyl CoA·protein N-myristoyltransferase Adv Enzymol Relat. Areas Mol Biol **67**, 375–430

2 Lodge, J K, Johnson, R L, Weinberg, R A and Gordon, J I (1994) Comparison of myristoyl-CoA protein N-myristoyltransferases from three pathogenic fungi *Cryptococcus neoformans*, *Histoplasma capsulatum*, and *Candida albicans*. J. Biol. Chem **269**, 2996–3009

3 Lodge, J K, Jackson-Machelski, E, Toffaletti, D L, Perfect, J R and Gordon, J. I (1994) Targeted gene replacement demonstrates that myristoyl-CoA.protein N-myristoyltransferase is essential for viability of *Cryptococcus neoformans* Proc Natl Acad Sci U S A **91**, 12008–12012

4 Weinberg, R A, McWherter, C A, Freeman, S K, Wood, D C, Gordon, J I and Lee, S. C (1995) Genetic studies reveal that myristoyl CoA protein N-myristoyltransferase is an essential enzyme in *Candida albicans* Mol Microbiol **16**, 241–250

5 Duronio, R J, Towler, D A, Heuckeroth, R O and Gordon, J I (1989) Disruption of the yeast N-myristoyl transferase gene causes recessive lethality Science **243**, 796–800

6 Duronio, R J, Reed, S I and Gordon, J I (1992) Mutations of human myristoyl-CoA protein N-myristoyltransferase cause temperature-sensitive myristic acid auxotrophy in *Saccharomyces cerevisiae* Proc. Natl. Acad. Sci. U S A **89**, 4129–4133

7 Rudnick, D A, Johnson, R L and Gordon, J I (1992) Studies of the catalytic activities and substrate specificities of *Saccharomyces cerevisiae* myristoyl-coenzyme A·protein N-myristoyltransferase deletion mutants and human/yeast Nmt chimeras in *Escherichia coli* and *S cerevisiae* J Biol Chem **267**, 23852–23861

8 Towler, D. A, Adams, S P, Eubanks, S R, Towery, D S, Jackson-Machelski, E, Glaser, L and Gordon, J. I. (1988) Myristoyl CoA.protein N-myristoyltransferase activities from rat liver and yeast possess overlapping yet distinct peptide substrate specificities J Biol Chem **263**, 1784–1790

9 Devadas, B, Freeman, S. K., Zupec, M. E, Lu, H F, Nagarajan, S R, Kishore, N S, Lodge, J K., Kuneman, D. W., McWherter, C A, Vinjamoori, D V et al (1997) Design and synthesis of novel imidazole-substituted dipeptide amides as potent and selective inhibitors of *Candida albicans* myristoyl-CoA protein N-myristoyltransferase and identification of related tripeptide inhibitors with mechanism-based antifungal activity. J. Med Chem **40**, 2609–2625

10 Devadas, B., Freeman, S K, McWherter, C A, Kishore, N S, Lodge, J. K., Jackson-Machelski, E, Gordon, J I and Sikorski, J. A. (1998) Novel biologically active nonpeptidic inhibitors of myristoyl CoA protein N-myristoyltransferase. J Med. Chem **41**, 996–1000

11 Weston, S A, Camble, R, Colls, J., Rosenbrock, G, Taylor, I, Egerton, M, Tucker, A D, Tunnicliffe, A, Mistry, A, Mancia, F et al (1998) Crystal structure of the anti-fungal target N-myristoyl transferase Nat Struct Biol **5**, 213–221

12 Bhatnagar, R. S, Futterer, K, Farazi, T A, Korolev, S., Murray, C L, Jackson-Machelski, E, Gokel, G W., Gordon, J I. and Waksman, G (1998) Structure of N-myristoyltransferase with bound myristoyl CoA and peptide substrate analogs. Nat Struct Biol **5**, 1091–1097

13 Giang, D. K. and Cravatt, B F (1998) A second mammalian N-myristoyltransferase J Biol Chem **273**, 6595–6598

14 McIlhinney, R A J., Young, K, Egerton, M, Camble, R, White, A and Soloviev, M (1998) Characterization of human and rat brain myristoyl-CoA protein N-myristoyltransferase evidence for an alternative splice variant of the enzyme Biochem. J **333**, 491–495

15 Glover, C J and Felsted, R. L (1995) Identification and characterization of multiple forms of bovine brain N-myristoyltransferase. J Biol Chem **270**, 23226–23233

16 Glover, C J, Hartman, K. D. and Felsted, R L (1997) Human N-myristoyltransferase amino-terminal domain involved in targeting the enzyme to the ribosomal subcellular fraction J Biol Chem **272**, 28680–28689

17 Stafford, W. H L, Stockley, R W, Ludbrook, S B and Holder, A A (1996) Isolation, expression and characterization of the gene for an ADP-ribosylation factor from the malarial parasite, *Plasmodium falciparum* Eur J Biochem **242**, 104–113

18 Blackman, M J., Chappel, J A, Shai, S and Holder, A A (1993) A conserved parasite serine protease processes the *Plasmodium falciparum* merozoite surface protein-1 (MSP1) Mol Biochem. Parasitol **62**, 103–114

19 King, M J and Sharma, R. K. (1991) N-myristoyl transferase assay using phosphocellulose paper binding. Anal. Biochem **199**, 149–153

20 McIlhinney, R A. J., Patel, P B and McGlone, K (1994) Characterization of a polyhistidine-tagged form of human myristoyl-CoA protein N-myristoyltransferase produced in *Escherichia coli*. Eur. J Biochem **222**, 137–146

21 Duronio, R J, Jackson-Machelski, E, Heuckeroth, R O, Olins, P O., Devine, C S, Yonemoto, W, Slice, L W, Taylor, S. S and Gordon, J I. (1990) Protein N-myristoylation in *Escherichia coli* reconstitution of a eukaryotic protein modification in bacteria. Proc Natl Acad Sci. U.S A **87**, 506–510

22 Peseckis, S M and Resh, M D (1994) Fatty acyl transfer by human N-myristyl transferase is dependent upon conserved cysteine and histidine residues J Biol Chem **269**, 30888–30892

Received 22 November 1999/21 February 2000, accepted 20 March 2000

Biochem. J (2000) 348, 465–471 (Printed in Great Britain)

Action pattern and substrate specificity of the hyaluronan lyase from group B streptococci

John R. BAKER[1] and David G. PRITCHARD

Department of Biochemistry and Molecular Genetics, University of Alabama at Birmingham, Birmingham, AL 35294, U.S.A

The hyaluronan lyase of group B streptococci rapidly cleaves hyaluronan by an elimination mechanism to yield the unsaturated disaccharide 2-acetamido-2-deoxy-3-*O*-(β-D-gluco-4-enepyranosyluronic acid)-D-glucose. Additionally, it has been shown that the enzyme has limited specificity for a chondroitin sulphate and cleaves the chain at unsulphated sites [Baker, Yu, Morrison, Averett and Pritchard (1997) Biochem. J. 327, 65–71]. In the present extension of that study it was found that 6-sulphated regions of chondroitin sulphate are also susceptible to cleavage by this hyaluronan lyase. Of the four 6- and/or 4-sulphated tetrasaccharides which can be isolated from testicular hyaluronidase digests of chondroitin sulphate, only those two tetrasaccharides with a 6-sulphated disaccharide at the reducing end were cleaved. From this and other data, a model is proposed for the cleavage specificity of hyaluronan lyase on a chondroitin sulphate. Evidence is presented in support of an action pattern for hyaluronan lyase which involves an initial random endolytic cleavage followed by rapid exolytic and processive release of unsaturated disaccharide. Since the only oligosaccharides which tend to accumulate in near-complete digests of hyaluronan are unsaturated, it is argued that the processive cleavage occurs from the non-reducing to the reducing end of a hyaluronan chain. This detailed knowledge of substrate specificity contributes to our understanding of the enzyme's role in Group B streptococcal pathogenesis. In addition, the hyaluronan lyase may find application in sequence studies of chondroitin sulphates.

INTRODUCTION

Group B streptococci (GBS), which are frequently present in the microflora of the human vagina, are a common cause of fatal infections of the newborn [1]. The large majority of vaginal GBS isolates secrete a hyaluronan lyase (hyase) [2]. It has been suggested that the GBS hyase facilitates bacterial invasion by degrading extracellular hyaluronan (HA) and may promote persistent colonization of the vagina by GBS (D. Pritchard, B. Lin, X. Li, J. Ware and J. Philips, unpublished work).

Studies of this enzyme during the past 4 years have included a partial definition of its substrate specificity. The activity of GBS hyase is not restricted to the cleavage of HA. It was shown that a chondroitin 4-sulphate, which contains some unsulphated disaccharide repeats, is cleaved to a limited extent [4]. Cleavage occurred between Di0S and Di0S, and between Di4S and Di0S repeats, but Di0S-Di4S and Di4S-Di4S could not be cleaved by this enzyme (for brevity the saccharides Di0S etc. are defined only in the abbreviations footnote).

When acting on HA, GBS hyase appears to make an initial random cleavage and then to rapidly and processively degrade the chains to yield unsaturated disaccharide [5]. This is the first reported example of a glycosaminoglycan lyase acting processively. Enzymes that degrade biopolymers may act in one of two ways, or, like GBS hyase, employ both pathways. A 'distributive' enzyme will bind to a biopolymer and, after a single cleavage reaction, release the two biopolymer chains. (The term 'random endolytic cleavage' also describes this kind of activity). A 'processive' enzyme acts differently [6]. Although the initial cleavage by an enzyme that acts processively may not be at one end of the chain (i.e. it may not be exolytic), subsequent cleavages while the enzyme is bound to the polymer chain are exolytic. After binding to the biopolymer, it catalyses a series of identical cleavage reactions and simultaneously releases a series of small identical products into the medium. Among the known lyases which cleave glycosaminoglycan chains, there are examples of both endolytic and exolytic modes of action [7,8].

In the present study, evidence of the direction of processive cleavage (i.e. non-reducing end to reducing end or vice versa) by GBS hyase is presented. Also, the specificity of GBS hyase towards segments of 6-sulphated chondroitin is investigated and, as a result, a more complete description of chondroitin sulphate (CS) degradation by this enzyme can be presented.

EXPERIMENTAL

Materials

Ovine testicular hyase was obtained from ICN. Hyaluronan (from human umbilical cord), chondroitinase ACII, and chondro-4- and -6-sulphatases were purchased from Sigma.

Abbreviations used: ΔDiHA, 2-acetamido-2-deoxy-3-*O*-(β-D-gluco-4-enepyranosyluronic acid)-D-glucose; DiHA, 2-acetamido-2-deoxy-3-*O*-(β-D-glucopyranosyluronic acid)-D-glucose, ΔDi0S, 2-acetamido-2-deoxy-3-*O*-(β-D-gluco-4-enepyranosyluronic acid)-D-galactose, Di0S, 2-acetamido-2-deoxy-3-*O*-(β-D-glucopyranosyluronic acid)-D-galactose, ΔDi4S, 2-acetamido-2-deoxy-3-*O*-(β-D-gluco-4-enepyranosyluronic acid)-4-*O*-sulpho-D-galactose, Di4S, 2-acetamido-2-deoxy-3-*O*-(β-D-glucopyranosyluronic acid)-4-*O*-sulpho-D-galactose, ΔDi6S, 2-acetamido-2-deoxy-3-*O*-(β-D-gluco-4-enepyranosyluronic acid)-6-*O*-sulpho-D-galactose, Di6S, 2-acetamido-2-deoxy-3-*O*-(β-D-glucopyranosyluronic acid)-6-*O*-sulpho-D-galactose, CE, capillary electrophoresis; CS, chondroitin sulphate, ESI–MS, electrospray-ionization MS, GBS hyase, hyaluronan lyase from group B streptococci, HA, hyaluronan, ΔHA_4 and ΔHA_6, unsaturated HA oligosaccharides of degree of polymerization ($\overline{DP}$) 4 and 6 respectively, HA_4–HA_{12}, HA oligosaccharides of $\overline{DP}$ 4–12

[1] To whom correspondence should be sent, at the following address. 786 BDB (Box 9), University of Alabama at Birmingham, 1530, 3rd Avenue South, Birmingham, AL 35294-0012, U S A (e-mail jrbaker@bmg bhs uab edu)

Table 1 Relative rates of release of DiHA and △DiHA during digestion of HA_{12} by GBS hyase

The percentage digestion of HA_{12} by GBS hyase was determined spectroscopically at 232 nm The methods of analyses of HA_{12} digests for DiHA and △DiHA by CE and ESI–MS are outlined in the Experimental section

		DiHA/ΔDiHA molar ratio	
Digestion of HA_{12} (%)	Analysis by ..	CE	ESI–MS
10		0.96	0.73
20		0.67	0.54
30		0.62	0.49
40		0.46	–
50		0.45	0.39
100		0.20	0.17

Sephadex G-25 (superfine grade) was obtained from Pharmacia. Standard unsaturated chondro- and hyalurono-disaccharides were from Seikagaku Kogyo, Tokyo, Japan. HA oligosaccharides, HA_4–HA_{12}, prepared by digestion of HA using testicular hyase and fractionated according to size by gel chromatography on Sephadex G-50, were a gift from Dr. Jim Christner, Environmental Test Systems Inc., Elkhart, IN, U.S.A.

CS

The disaccharide compositions of four different commercially available CSs were determined. CS A (Calbiochem), with the composition 6.3 % Di0S, 35.4 % Di6S and 58.3 % Di4S, was selected as a preparative source of CS tetrasaccharides, as its Di6S/Di4S ratio was closest to 1.0. A CS (5.3 % Di0S/13.7 % Di6S/81.0 % Di4S) isolated from bovine nasal cartilage following exhaustive proteolytic digestion [9] and a CS (3.6 % Di0S/86.6 % Di6S/9.7 % Di4S) similarly isolated from gill cartilage of the basking shark were employed for digestion by the GBS hyase.

GBS hyase

The preparation and purification of the recombinant GBS hyase have been described previously [4]. The working solution of pure enzyme (12 mg/ml in 50 mM Hepes/10 mM EDTA, pH 8.0) was stored at 4 °C.

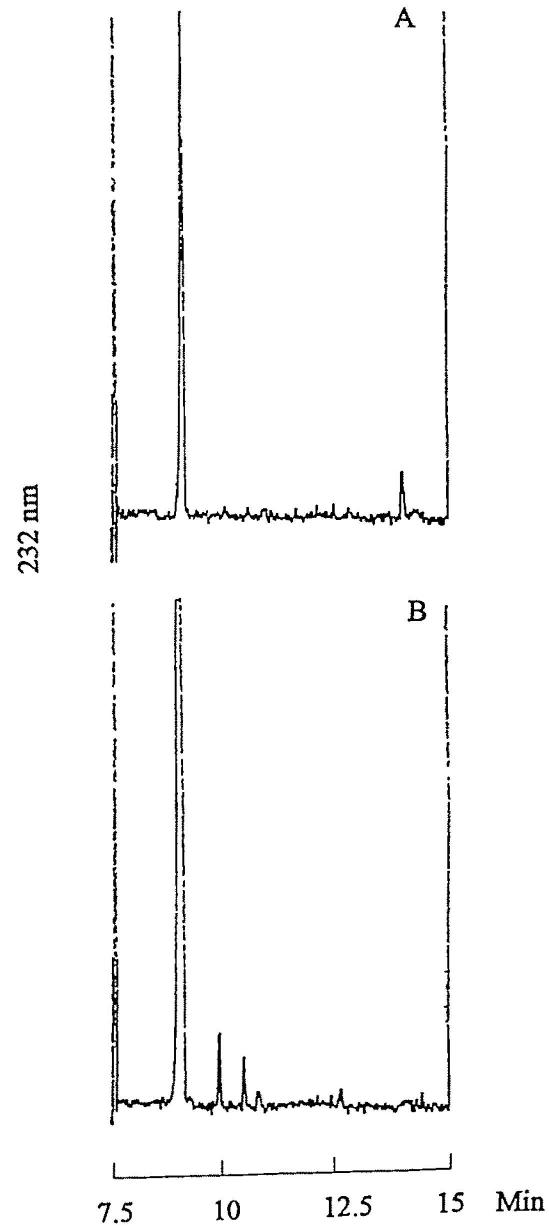

Figure 1 CE analyses of hyaluronan after partial enzymic digestion

HA was digested with (**A**) GBS hyase and (**B**) chondroitinase ACII to 10 % of completion The major peak at 9.08 min, present in (**A**) and (**B**), is of △DiHA The peak at 10.24 min, seen in (**B**) only, is of $△HA_4$

Digestion of CS using testicular hyase and recovery of di- and tetrasaccharides

CS (253 mg) was dissolved in 0.15 M NaCl/0.05 M sodium phosphate, pH 6.0 (10 ml), ovine testicular hyase (25 mg) was added and the mixture incubated at 37 °C for 27 h. A further 10 mg of enzyme was added at 22 h. At the end of the incubation, the mixture was deproteinized by addition of trichloroacetic acid at 0 °C to a final concentration of 5 %. Protein was removed by centrifugation and the supernatant brought to pH 6.2 by the gradual addition, with vigorous stirring, of 10 M NaOH. The neutralized supernatant (approx. 12 ml) was applied to a column (192 cm × 2.5 cm) of Sephadex G-25, developed in 0.5 M NaCl/aq. 10 % (v/v) methanol at a flow rate of 20 ml/h. The column effluent was monitored at 206 nm and fractions (30 min) were collected. Six peaks were detected in advance of the large salt peak (V_t). Peaks 5 and 6 were identified, using electrospray-ionization (ESI)–MS analysis, as tetra- and disaccharides from CS respectively. Fractions from both peaks were pooled separately and applied to a column (2.0 cm × 20 cm) of Sephadex G-10 developed in aq. 20 % (v/v) methanol at a flow rate of 0.5 ml/min and monitored at 200 nm. Both tetra- and disaccharide pools, separated from salt, were concentrated using a Savant SpeedVac to 1–10 mg of saccharide/ml. Yields were 43 mg of tetrasaccharide and 2.4 mg of disaccharide.

Determination of disaccharides released by enzymic digestion of HA and CS

CS or CS oligosaccharide samples (< 0.25 μg) were dried, dissolved in 0.1 M Tris/HCl, 0.03 M sodium acetate and 0.01 M EDTA, pH 7.4 (10 μl) containing chondroitinase ACII (2.5 m-units) and incubated at 37 °C for 1 h. To determine susceptibility of CS and CS oligosaccharides to digestion by GBS

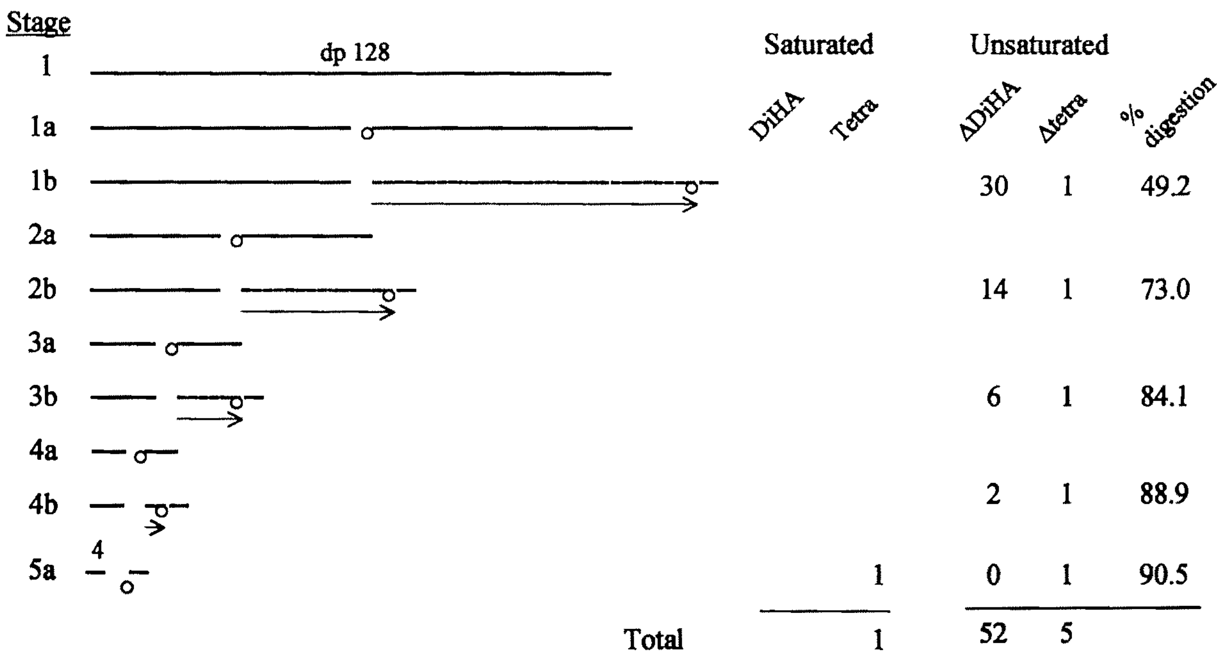

Figure 2 Proposed action pattern of GBS hyase

For convenience, the cleavage of an HA oligosaccharide of DP 128 is illustrated, and endolytic cleavages are shown as splitting a chain into equal parts, although it is understood that they occur randomly. In this model, it is assumed that processive cleavage by GBS hyase is from the non-reducing to the reducing end of an HA oligosaccharide According to this model, an enzyme molecule binds to a random position along the chain and catalyses a single endolytic cleavage (stage 1a). The enzyme remains bound to the new non-reducing end at this cleavage site and, during a rapid series of processive exolytic cleavages, remains substrate-bound (stage 1b) During this process, △DiHA alone is released When the substrate is decreased to the size of a tetra- or hexasaccharide, the enzyme disengages from the substrate. [It is suggested that the enzyme releases substrate at this stage, as only tetra- and hexa-saccharide are seen to accumulate in a partial digest (Figure 1); for simplicity, only release of tetrasaccharide is illustrated] As illustrated, 30 molecules of △DiHA, each represented by a single dash in a broken line, and a single unsaturated tetrasaccharide, represented by a double-length dash, are released at stage 1b This pattern of action repeats through stages 2–4, at each stage there is another random cleavage of the remaining HA chain and rapid processive cleavage from the new non-reducing end At stage 5, following a random cleavage, the enzyme disengages from the substrate, as the latter is too short to bind the enzyme or to permit any further processive cleavage. The tetra- and hexa-saccharides from HA appear in partial digests because they are not cleaved processively and therefore are cleaved more slowly, but they are finally cleaved. Thus, in a digest of HA by GBS hyase which has been allowed to proceed to completion, the only product which is observed is △DiHA If, as depicted in this Figure, processive cleavage proceeds from a new non-reducing end towards its reducing end, small unsaturated oligosaccharides will tend to accumulate [In this simplified example, five unsaturated tetrasaccharides per one saturated tetrasaccharide, from a much longer HA, the relative accumulation of the unsaturated small oligosaccharide(s) will be more marked] If processive cleavage occurred in the reverse direction, it would be small saturated oligosaccharide(s) that accumulate in partial digests Beginning with a longer HA chain than depicted here, many more stages or random cleavages, some occurring simultaneously, would be required, but the essential features of this model would apply

hyase, samples (< 0.25 μg) were incubated in 0.05 M ammonium acetate, 0.01 M calcium chloride, pH 6.5 (10 μl) containing GBS hyase (9 units) at 37 °C for 1 h. Both chondroitinase and hyase digests were subsequently diluted with HPLC-grade water (40 μl) and centrifugally filtered through Ultrafree-MC filter units (Millipore). Filtrates were analysed for disaccharides using capillary electrophoresis (CE) at pH 9.8 as described in [4,10]. Samples were loaded hydrostatically (2 s) at 500 mmHg (1 mmHg ≡ 133.3 Pa) and separated at pH 9.8. Detection of peaks was at 200 nm (saturated and unsaturated disaccharides) and at 232 nm (unsaturated disaccharides).

The same CE separation system gave a near-baseline separation of DiHA (8.67 min) from △DiHA (8.78 min) in GBS hyase digests of HA oligosaccharides.

MS

Samples were analysed using the ESI mode on a PE Sciex API III triple quadrupole mass spectrometer. Aqueous samples were injected into a 25 μl/min flow of aq. 1:1 (v/v) acetonitrile containing 0.1 % formic acid. A Harvard Apparatus model 22 syringe pump was used to deliver the flow to the electrospray interface.

Desulphation of CS disaccharides

The saturated disaccharides Di4S and Di6S at 13.48 min were not separated by CE at pH 9.8, although they were well resolved from their unsaturated counterparts, △Di6S and △Di4S, at 14.00 min and 14.23 min respectively. GBS hyase digests of CS oligosaccharides, which contained Di4S and/or Di6S, were dried using the Savant SpeedVac and redissolved in 0.1 M Tris/HCl, 0.03 M sodium acetate and 0.01 M EDTA, pH 7.4 (10 μl), and incubated with chondro 4- or 6-sulphatase (0.2 m-units) at 37 °C for 1 h. The digests were processed and separated by CE as described above. Under the conditions employed, the 4-sulphatase showed absolute specificity for digestion of Di4S (and △Di4S) and the 6-sulphatase was specific for the desulphation of Di6S (and △Di6S). From both Di4S and Di6S, the product of digestion, as identified by CE, was Di0S.

RESULTS AND DISCUSSION

GBS hyase can act on HA in a random endolytic manner and this can be demonstrated directly by an experiment employing HA_{12}. All disaccharide repeats, with the exception of that from the non-

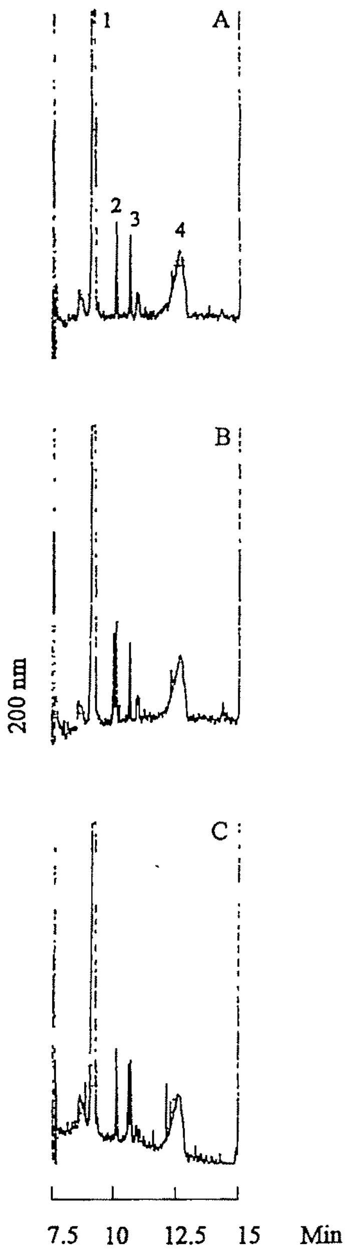

Figure 3 Analyses by CE of hyaluronan partially digested by GBS hyase

(**A**) A GBS hyase digest of HA, taken to 82.5% of completion, was analysed by CE at 200 nm. The off-scale peak at 9 min, and labelled 1, is of $\triangle$DiHA. The peaks labelled 2 and 3 have mobilities similar to those of HA_4 and HA_6 respectively. The broad peak labelled 4 is of partially digested HA. (**B**) As (**A**), plus authentic HA_4. The added HA_4 has a slightly shorter retention time than 2. (**C**) As (**A**), plus authentic HA_6. The added HA_6 has a slightly shorter retention time than 3. At 232 nm, peaks 1, 2 and 3 were detected. Peak 4, and authentic HA_4 and HA_6, added to (**B**) and (**C**), were not seen at this wavelength (not shown). Therefore the partial GBS hyase digest of HA, as observed in (**A**), does not contain HA_4 and HA_6, but does contain their unsaturated counterparts, $\triangle HA_4$ and $\triangle HA_6$

reducing end, are liberated as $\triangle$DiHA during the digestion of HA_{12} by GBS hyase. The saturated disaccharide DiHA is a marker of the non-reducing end. The rate of release of the disaccharide DiHA from the non-reducing end relative to the rate of release of other disaccharide repeats ($\triangle$DiHA) provides information about the enzyme's action pattern. Thus, if the action pattern is exclusively random endolytic, HA_{12} with five cleavage sites will give, at < 20% digestion, a DiHA/$\triangle$DiHA ratio of 1.0. This ratio would decline to 0.2 at complete digestion. By contrast, exclusively exolytic and processive action would give a constant ratio of 0.2 during digestion (assuming that the cleavage of an HA chain is extremely rapid compared with the time required for enzyme molecules to bind to another chain). The release of DiHA and $\triangle$DiHA at different times were determined by CE analysis of digests. Analyses for species of 378 *m/z* ($\triangle$DiHA) and 396 *m/z* (DiHA) were performed on the same digests by ESI–MS. The determined ratios of DiHA/$\triangle$DiHA from both analyses (Table 1) are compatible with a random endolytic mode of enzyme action.

Although, as demonstrated by the previous experiment, cleavage by GBS hyase of HA_{12} is primarily random endolytic, cleavage of a long HA chain appears to occur predominantly by other means. That the principal mode of action of GBS hyase on HA, following initial random endolytic cleavage, is exolytic is strikingly demonstrated by CE analysis of a partial digest, i.e. the only peak seen is of $\triangle$DiHA (Figure 1A). Also shown (Figure 1B) is a partial digest of HA by chondroitinase ACII, which has been reported to act in an exolytic manner [7]. Again, the predominant product is $\triangle$DiHA.

It is not known whether the exolytic and processive cleavage of HA by GBS hyase occurs from the non-reducing to the reducing end or vice versa. Unfortunately, to distinguish between these two possibilities by monitoring the rates of DiHA and $\triangle$DiHA release is not experimentally feasible, as the ratio of DiHA to $\triangle$DiHA from HA is too low (< 0.0004 in a complete digest). Instead, we have used CE analysis to determine whether small saturated or unsaturated oligosaccharides tend to accumulate during the digestion of HA by GBS hyase. As proposed in Figure 2, accumulation of small unsaturated oligosaccharides from HA is indicative of a non-reducing-to-reducing-end action pattern. In a preliminary experiment it was found that maximal accumulation of intermediate small oligosaccharides (2.0–2.5% relative to $\triangle$DiHA) occurred at 60-90% of complete digestion (results not shown). CE analysis of an 82% digest (Figure 3) revealed low levels of two small HA oligosaccharides (labelled 2 and 3 in Figure 3A) in addition to the predominant $\triangle$DiHA product (labelled 1). Both 2 and 3 could be detected at 232 nm, as well as at 200 nm, and their mobilities are similar to, but not identical with, those of HA_4 and HA_6 respectively (Figures 3B and 3C). It is evident that 2 and 3 are $\triangle HA_4$ and $\triangle HA_6$ respectively. The accumulation of these two small unsaturated, but no small saturated, HA oligosaccharides during digestion of HA by GBS hyase strongly suggests that the action of the enzyme is processive from the non-reducing to the reducing end of the chain.

Preliminary data, reported previously [4], suggests that 6-sulphated regions of a CS can be slowly cleaved by GBS hyase with the release of $\triangle$Di6S. In order to define this activity properly, we determined whether the tetrasaccharides Di6S-Di4S, Di4S-Di6S, Di6S-Di6S and Di4S-Di4S are substrates for GBS hyase. Accordingly, a hybrid chondroitin 4-/6-sulphate was digested using testicular hyase, the digest fractionated by gel chromatography on a column of Sephadex G-25 and a peak containing the tetrasaccharides was identified and recovered (pool 5), as described in the Experimental section. Analysis of pool 5 by CE (Figure 4A) revealed a peak of rapid mobility, peak 1, followed by a cluster of three peaks, numbered 2, 3 and 5. A small shoulder on peak 3 was indicative of an additional component, numbered 4. This cluster of peaks was within the range of mobilities expected for disulphated tetrasaccharides from CS. Therefore the presence of all four possible disulphated tetrasaccharides listed above could be predicted. Pool 5 was

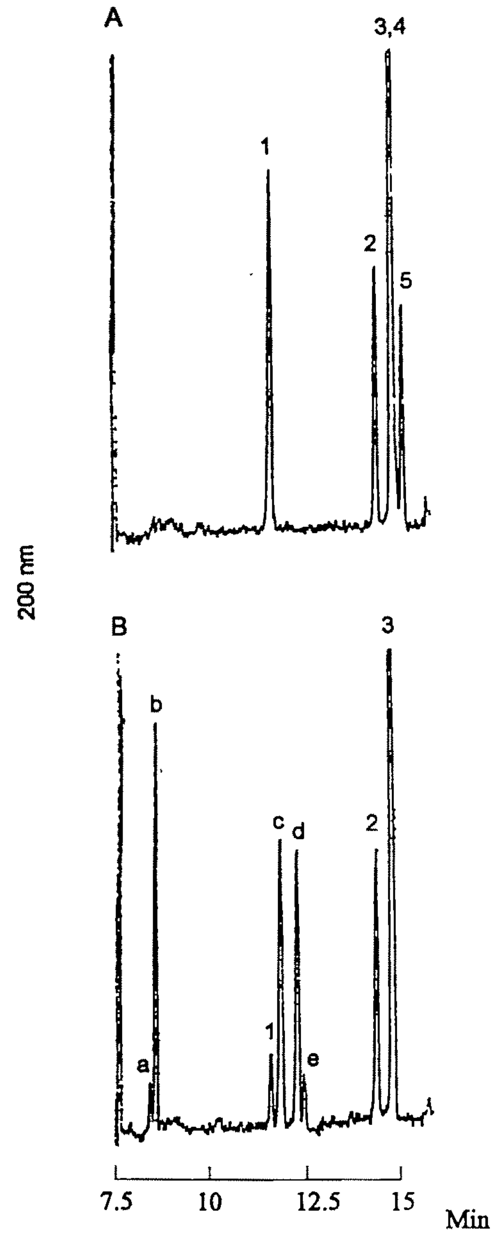

Figure 4 Analysis by CE of CS tetrasaccharides

(**A**) Pool 5, obtained by fractionation of a testicular hyase digest of CS by gel chromatography on Sephadex G-25 (see the Experimental section), was analysed by CE at pH 9.8. Observed is a peak at 12.17 min, numbered 1, and a cluster of three peaks at 15.3–16.3 min, numbered 2, 3 and 5. A shoulder, suggestive of a fourth peak and numbered 4, is seen on the down slope of peak 3. (**B**) Pool 5, after digestion using GBS hyase, was also analysed by CE at pH 9.8. Peaks 4 and 5, but not 2 and 3, disappeared as a result of the digestion. Peak 1 was largely digested. The disaccharides produced by the digestion were identified by their mobilities relative to standards as: a, Di0S, b, ΔDi0S; c, Di6S and/or Di4S, d, ΔDi6S, and e, ΔDi4S

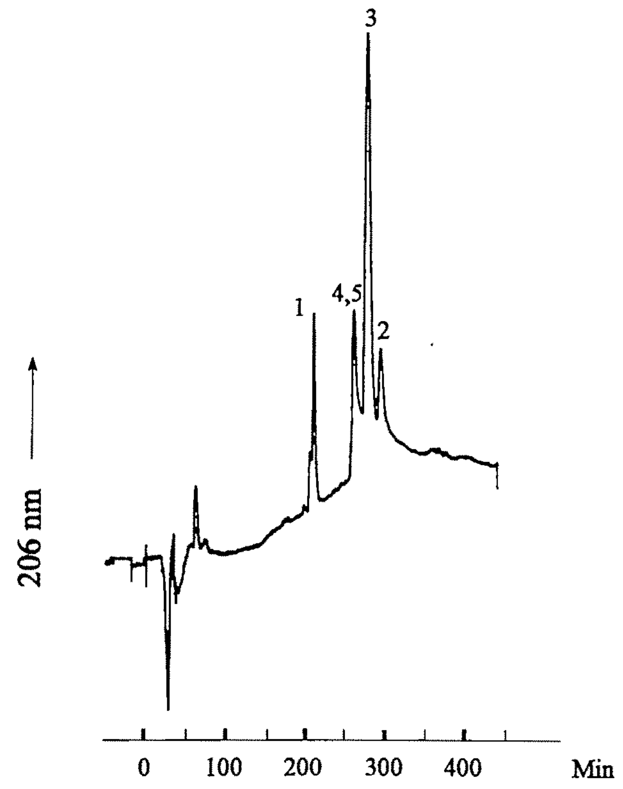

Figure 5 Fractionation of CS tetrasaccharides by anion-exchange HPLC

CS tetrasaccharides (pool 5) were applied to a Partisil-SAX column (250 mm × 4.6 mm, 10 μm particle size) and fractionated in a gradient of KH_2PO_4 (30–300 mM) in aq. 10% (v/v) methanol. The flow rate was 0.2 ml/min, and the elution of saccharides was detected at 206 nm. Fractions constituting the four peaks eluted between 200 and 300 ml were separately pooled, desalted on a column of Sephadex G-10 developed with aq. 20% (v/v) methanol [4] and dried using a Sorvall SpeedVac apparatus. CE of aliquots from each peak permitted their identification (Table 2). Each peak number represents the same tetrasaccharide as in Figure 4

Table 2 Analyses by CE of CS tetrasaccharides separated by anion-exchange HPLC

The peak numbers are identified in Figures 4 and 5. Peak 1 was seen to contain monosulphated tetrasaccharides, but was not further analysed.
Abbreviation: tr, a trace component

	Disaccharides identified in a chondroitinase ACII digest			
Peak	At 232 nm	At 200 nm		Identity of tetrasaccharide
2	ΔDi4S	ΔDi4S	Di6S	Di6S-Di4S
3	ΔDi4S	ΔDi4S	Di4S	Di4S-Di4S
4, 5	ΔDi6S (tr)	ΔDi6S (tr)	Di6S (tr)	Di6S-Di6S
	ΔDi6S	ΔDi6S	Di4S	Di4S-Di6S

digested using GBS hyase prior to separation by CE (Figure 4B). Of the clustered peaks numbered 2–5, only 4 and 5 were susceptible to digestion by the enzyme.

To separate the tetrasaccharides and allow for their identification, pool 5 was fractionated by anion-exchange HPLC on a SAX-Partisil column using a gradient of KH_2PO_4 in aq. 10% (v/v) methanol (Figure 5). Four peaks were separated, and aliquots from each were analysed by CE. Then the peaks of Figure 5 were numbered 1–5 to match, by electrophoretic mobility, the similarly numbered peaks of Figure 4. The first peak was found to contain monosulphated tetrasaccharide (Table 2) and was not further analysed. Aliquots from the other peaks were digested with chondroitinase ACII and the disaccharide products analysed by CE. Identification of the characteristic disaccharides from each tetrasaccharide permitted identification of each tetrasaccharide (Table 2). It was found that peak 2 is Di6S-Di4S, the major peak (peak 3) is Di4S-Di4S, a minor

Table 3 Unsaturated disaccharides released from bovine nasal-cartilage (BNC) and basking-shark (BS) CSs by GBS hyase

A CS (20 μg in 100 μl) was digested exhaustively with GBS hyase (12 μg) for 24 h at 30 °C or with chondroitinase AC II (12 m-units) for 2 h at 30 °C Digests, diluted five-fold with HPLC-grade water, were analysed by CE at pH 9.8 Peaks were detected at 232 nm and integrated Data given are from the average of triplicate analyses

Enzyme digestion	CS (0.2 mg/ml)	△Di0S (μg/ml)	%*	△Di6S (μg/ml)	%	△Di4S (μg/ml)	%
GBS hyase	BNC	0.74	100.7	0.77	40.7	0	0
	BS	0.58	99.1	11.44	83.3	0	0
Chondroitinase AC II	BNC	0.73		1.89		11.21	
	BS	0.58		3.73		1.55	

* The disaccharide released by GBS hyase is expressed as a percentage of the total present (i.e. that released by digestion with chondroitinase AC II)

component (peak/shoulder 4) is of Di6S-Di6S and peak 5 contains Di4S-Di6S. Therefore, as peaks 4 and 5, but not peaks 2 and 3, were absent following incubation with GBS hyase (Figure 4), it is evident that Di6S-Di6S and Di4S-Di6S are cleaved by GBS hyase, whereas Di6S-Di4S and Di4S-Di4S are not. To verify these findings, aliquots from the separately isolated peaks 2, 3 and 4/5 were incubated with GBS hyase and the digests analysed by CE. Only the constituents of peaks 4 and 5 were digested by the enzyme. Peaks 2 and 3 remained intact (results not shown). The further significance of these results is discussed below.

Two CSs from different sources and content of 6-sulphated repeats (bovine nasal cartilage and basking-shark gill cartilage, with 13.7 % and 86.6 % Di6S respectively) were digested with the GBS hyase in order to determine the proportion of their total Di6S and Di0S repeats which could be released as △Di6S and △Di0S respectively. The digestions were allowed to go to completion (i.e. the incubation time at which no further increase in A_{232} occurred). The unsaturated disaccharides released were identified and quantified by CE analyses and were compared with total disaccharide compositions of these two CSs (Table 3). A much higher proportion (83.3 %) of the Di6S content of the shark Di6S can be released by GBS hyase (cf. 40.7 % from the bovine nasal CS). Di0S was completely released, as △Di0S, by GBS hyase from both CS preparations.

Treatment of both GBS hyase digests by oxymercuration [4,11] resulted in the loss of all remaining 6-sulphated residues (results not shown). It is evident that, after hyase digestion of the CSs, any 6-sulphated residues not released as △Di6S occupy non-reducing terminal positions, making them susceptible to destruction by oxymercuration The significance of these results is discussed in greater detail below with reference to a proposed model of GBS hyase specificity towards CS.

GENERAL DISCUSSION

Previous results indicated that the initial attack on HA by GBS hyase may be random endolytic followed by processive cleavage [5]. Thus a digest of HA taken to only 5 % of completion by slow enzymic action contained not only △DiHA, but also a broad range of very large HA oligosaccharides, as determined by gel chromatography. In the present study, an HA oligosaccharide, HA_{18}, was shown to be cleaved endolytically by GBS hyase. It is reasonable to expect that GBS hyase cannot act processively on a small HA oligosaccharide. Indeed, it was found that, in digests, at 60–90 % of completion, $\triangle\mathrm{HA}_4$ and $\triangle\mathrm{HA}_6$ tend to accumulate. It would appear that cleavage by GBS hyase is initially and finally non-processive. Nevertheless, GBS hyase can rapidly cleave HA, its principal substrate, to yield unsaturated disaccharide, △DiHA, as the sole product of complete digestion. Even in partial digests, the predominant product is △DiHA, which indicates in agreement with earlier findings [5] that the enzyme's mode of action is primarily processive. Other glycosaminoglycan lyases, for example heparinase I [12], also act processively. Random endolytic cleavage followed by a series of processive cleavages provides a rapid and efficient means for the complete digestion of HA. Evidence has been presented for processive cleavage proceeding from the non-reducing to the reducing end of HA or HA oligosaccharides. This finding will aid computer-assisted studies, which are presently underway, to properly dock HA in the active-site cleft of the modelled GBS hyase molecule [13].

Our results indicate that the GBS hyase will cleave a 4-/6-sulphated chondroitin chain as illustrated below:

$$(\mathrm{Di4S})_n\text{-Di6S-}(\mathrm{Di4S})_p\text{-}(\mathrm{Di6S})_q\text{-Di0S-Di0S-U-G-G-X-S}$$

$$\big\downarrow \text{GBS hyase}$$

$$(\mathrm{Di4S})_n + \triangle\mathrm{Di6S}\text{-}(\mathrm{Di4S})_p + q\ \triangle\mathrm{Di6S} + 2\ \triangle\mathrm{Di0S} + \triangle\text{U-G-G-X-S}$$

(where the sequence U-G-G-X-S represents the linkage region of CS)

An essential feature of this model is that no Di6S repeat remains in an internal position along a CS chain following exhaustive digestion with GBS hyase. Cleavage will occur at a Di6S bounded by Di4S repeats, but the resulting residue of △Di6S will remain glycosidically linked in a non-reducing terminal position. In support of this aspect of the model, it has been found that, after exhaustive digestion of a CS with GBS hyase, although some 6-sulphated residues are not released as △Di6S, they invariably occupy non-reducing terminal positions (i.e. they are removed by oxymercuration). Where a cluster of Di6S repeats, $(\mathrm{Di6S})_q$, occurs within the chain of CS, cleavage takes place with the release of q △Di6S. The activity of GBS hyase towards 6-sulphated disaccharide repeats within a CS chain is remindful of cleavage by this enzyme at unsulphated sites [4].

In support of the model, although only 41 % of the Di6S content of bovine nasal-cartilage CS was released as △Di6S by GBS hyase, the remainder could be completely destroyed by oxymercuration (a procedure which removes non-reducing terminal unsaturated uronic acid residues). Of the total Di6S content of a CS, that part released by GBS hyase digestion is derived from 'clusters' of two or more Di6S repeats. Thus much of the Di6S of this CS is distributed in short segments throughout the chain. This result is consistent with the findings of Cheng and others [14], who reported a heterogeneous distribution of 6-sulphated repeats in the CS from bovine nasal cartilage, although in CSs from other sources (e.g. tracheal cartilage) 6-sulphated residues were clustered within a certain segment of the chain. By contrast, 81 % of the Di6S of basking-shark CS is released by GBS hyase. The Di6S of this CS is organized into longer segments, uninterrupted by Di4S repeats. Interestingly, the GBS hyase-catalysed release of all Di0S as △Di0S from the CSs suggests that the Di0S repeats are clustered and/or linked to Di6S repeats.

The glycosaminoglycan chains, whether they be chondroitin, dermatan or heparan sulphates, which are attached to certain proteoglycans, are now known to perform essential and quite specific functions. For example, the heparan sulphate chains of the basement-membrane proteoglycan perlecan act as receptors for the basic fibroblast growth factor [15]. Glycosaminoglycans have a characteristic disaccharide repeat pattern, but the extent and positions of substitutions with ester sulphate groups may vary considerably. A particular sulphation pattern may relate to a CS's specific biological activity [16], so methods for the determination of sequence of sulphated disaccharide repeats are assuming more importance. Recently, the utility of MS methods for sequencing glycosaminoglycans has gained attention [17,18]. Nevertheless, limited specific enzymic cleavage of the glycosaminoglycan, to provide oligosaccharides amenable to MS study, is a prerequisite. Detailed knowledge of the substrate specificities of glycosaminoglycan-degrading enzymes, such as the GBS lyase, is essential for their use in this important application, as well as in other studies of this ubiquitous family of biopolymers.

Support for this work from the National Institutes of Health (grant AI-41596) is gratefully acknowledged. The MS Shared Facility of the Comprehensive Cancer Center at the University of Alabama at Birmingham, supported in part by National Institutes of Health grant P30 CA-13148, provided ESI–MS services We thank Ms Anne Burrows for expert secretarial assistance

REFERENCES

1 Zangwill, K, Schuchat, A and Wenger, J. (1992) Morbid. Mortal Wkly Rep **41**, 25–32
2 Hauge, M, Jespersgaard, K, Poulsen, K and Kilian, M (1996) Infect Immun **64**, 919–925
3 Reference deleted
4 Baker, J, Yu, H, Morrison, K, Averett, W and Pritchard, D (1997) Biochem J **327**, 65–71
5 Pritchard, D, Lin, B., Willingham, T and Baker, J (1994) Arch. Biochem. Biophys **316**, 431–437
6 delCardayre, S and Raines, R (1994) Biochemistry **33**, 6031–6037
7 Jandik, K, Gu, K and Linhardt, R. (1994) Glycobiology **4**, 289–296
8 Park, Y, Cho, S and Linhardt, R (1997) Biochim. Biophys Acta **1337**, 217–226
9 Rodén, L, Baker, J, Cifonelli, J. and Mathews, M (1972) Methods Enzymol. **28**, 73–140
10 Carney, S and Osborne, D. (1991) Anal Biochem **195**, 132–140
11 Chai, W., Kogelberg, H and Lawson, A (1996) Anal. Biochem. **237**, 88–102
12 Ernst, S, Rhomberg, A., Biemann, K and Sasisekharan, R (1998) Proc Natl Acad. Sci U S A **95**, 4182–4187
13 Pritchard, D, Trent, J, Li, X, Zhang, P., Egan, M. and Baker, J (2000) Proteins, in the press
14 Cheng, F, Yoshida, K, Heinegård, D. and Fransson, L-Å. (1992) Glycobiology **2**, 553–561
15 Aviezer, D, Hecht, D., Safran, M, Eisinger, M, David, G and Yayon, A (1994) Cell **79**, 1005–1013
16 Lander, A (1999) in Guidebook to the Extracellular Matrix, Anchor, and Adhesion Proteins (Kreis, T and Vale, R., eds), pp. 351–356, Oxford University Press, New York
17 Rhomberg, A, Ernst, S, Sasisekharan, R and Biemann, K (1998) Proc. Natl Acad. Sci. U S A **95**, 4176–4181
18 Venkataraman, G, Shriver, Z, Raman, R and Sasisekharan, R (1999) Science **286**, 537–542

Received 10 January 2000, accepted 3 April 2000

Biochem J (2000) **348**, 473–479 (Printed in Great Britain)

Bcl-2 accelerates retinoic acid-induced growth arrest and recovery in human gastric cancer cells

Hua-Kang CHOU*†‡, Show-Li CHEN*, Chung-Te HSU§, You-Chen CHAO‡ and Yeou-Ping TSAO*¶[1]

*Department of Microbiology and Immunology, National Defense Medical Center, Taipei, Taiwan, Republic of China, †Graduate Institute of Medical Science, National Defense Medical Center, Taipei, Taiwan, Republic of China, ‡Division of Gastroenterology, Tri-Service General Hospital, National Defense Medical Center, Taipei, Taiwan, Republic of China, §Division of Gastroenterology, Poh Ai Hospital, I-Lan, Taiwan, Republic of China, and ¶Department of Ophthalmology, Chang Gung Memorial Hospital and Chung Gung University, Taoyuan, Taiwan, Republic of China

The role of Bcl-2 as an anti-apoptotic protein has been well documented. In the present work, we present evidence that Bcl-2 may also be involved in cell growth regulation. SC-M1 is an unique cell line which responds to retinoic acid (RA) treatment with reversible growth arrest [Shyu, Jiang, Huang, Chang, Wu, Roffler and Yeh (1995) Eur. J. Cancer **31**, 237–243]. In this study, when treated with RA, SC-M1/Bcl2 cells, which were generated by transfecting SC-M1 cells with bcl-2 DNA, were growth-arrested two days earlier than SC-M1/neo cells, which were generated by transfecting SC-M1 cells with vector DNA. This indicates that Bcl-2 accelerates RA-induced growth arrest. In addition to the accelerated growth arrest, RA-treated SC-M1/Bcl2 cells also recovered from growth arrest two days faster than SC-M1/neo cells after the removal of RA. Previously, we had identified the cyclin-dependent kinase inhibitor p21$^{(WAF1/CIP1)}$ (p21) as a mediator of RA-induced growth arrest [Tsao, Li, Kuo, Liu and Chen (1996) Biochem. J. **317**, 707–711]. In a search for the mechanism by which Bcl-2 affects growth regulation, we found that *p21* gene expression was more prominent in SC-M1/Bcl2 cells than in SC-M1/neo cells in the presence of RA, but when RA was removed, *p21* gene expression levels in SC-M1/Bcl2 cells were also reduced earlier than in SC-M1/neo cells. The present report is the first to show that Bcl-2 accelerates not only growth arrest but also recovery from growth arrest. Moreover, the close correlation between the effect of Bcl-2 on both RA-induced growth arrest and RA-induced *p21* gene expression suggests the possibility that Bcl-2 affects cell growth through the mechanism of p21.

Key words: Bcl-2, growth arrest, p21, SC-M1 cells.

INTRODUCTION

Bcl-2 is the first negative regulator of apoptotic cell death to be identified [1–3]. Apoptosis is an active form of cell suicide that is associated with morphological changes such as cell shrinkage, cell membrane blebbing, nuclear fragmentation and DNA degradation [4]. The exogenous expression of the *bcl-2* gene is shown to protect cells from apoptosis induced by p53 overexpression and various stimuli, such as growth-factor withdrawal, irradiation and chemotherapy [1,5–6]. Those cells which survive with Bcl-2 protection against environmental stimuli generally undergo cell-cycle arrest [2,5–6]. There is other recent evidence suggesting that Bcl-2 may also affect growth regulation. For example, it has been shown that Bcl-2 delays the entry into the cell cycle of mitogen-stimulated B and T lymphocytes and delays the serum stimulation-induced entry into S phase of quiescent NIH3T3 fibroblasts [7]. Moreover, certain evidence *in vivo* also indicates the involvement of Bcl-2 in growth regulation. For example, a high concentration of Bcl-2 can be detected in premalignant stomach lesions but not in stomach carcinoma [8]. In addition, expression of Bcl-2 is reported to inversely correlate with the mitotic index of stomach lesions [9,10]. In such situations, it is possible that Bcl-2 might prevent malignant transformation by inhibiting cell growth *in vivo*. These facts indicate that Bcl-2 may inhibit growth when normal cell growth is perturbed.

Retinoic acid (RA)-inhibited growth of SC-M1 cells can be maintained for 70 days by continuous RA exposure, and remains reversible after the removal of RA [11–13]. This provides an excellent system to study mechanisms involved in growth regulation. To further establish its reversible growth inhibitory effect, Bcl-2 was tested on SC-M1 gastric cancer cells. Therefore, in the present study, we investigated whether Bcl-2 could regulate growth of SC-M1 cells in the presence of RA. We found not only that Bcl-2 did indeed accelerate RA-induced growth arrest but also that an enhanced RA-induced p21 [cyclin-dependent kinase inhibitor p21$^{(WAF1/CIP1)}$] expression in Bcl-2 containing cells was observed, suggesting that p21 mediated the early growth arrest of Bcl-2-containing SC-M1 cells. A surprising result of the study was the faster recovery of RA-treated SC-M1/Bcl2 cells from growth arrest after the removal of RA when compared with the recovery of the RA-treated control cells (SC-M1/neo); furthermore, the decrease in *p21* gene expression was faster than that of SC-M1/neo cells. These results indicate that Bcl-2 accelerated both growth arrest and recovery.

EXPERIMENTAL

Cells

SC-M1, a gastric cancer cell line [14] (kindly provided by Dr. Ching-Liang Meng), was cultured in Dulbecco's modified Eagle's medium (DMEM; Gibco Laboratories, Grand Island, NY, U.S.A.) containing 10% (v/v) fetal-bovine serum (FBS, Gibco) and 100 units/ml penicillin and streptomycin. SC-Ml cells were transfected with a pCEP4-based plasmid (Invitrogen, Carlsbad, CA, U.S.A.) encoding human bcl-2 cDNA. After selection with 200 μg/ml hygromycin for 3 weeks, resistant clones were pooled, and named SC-M1/Bcl2.

Abbreviations used DMEM, Dulbecco's modified Eagle's medium, FBS, fetal-bovine serum, p21, cyclin-dependent kinase inhibitor p21$^{(WAF1/CIP1)}$, RA, retinoic acid, m o i., multiplicity of infection

[1] To whom correspondence should be addressed (e-mail yptsao@kimo com tw).

Cell proliferation assay

Cells were plated on to a 6-well plate at a density of 3×10^4 cells per well in DMEM containing 10 % (v/v) FBS and 100 units/ml penicillin and streptomycin. After 24 h, the medium was changed to DMEM with 10 % (v/v) FBS in the presence of 5 μM RA or an equal amount of DMSO. The cell numbers were counted every other day using a haemocytometer. Viability was determined by Trypan Blue exclusion.

RNA isolation and Northern-blot analysis

The single-step method of RNA isolation by acid guanidinium thiocyanate/phenol/chloroform (1:1:0.2, by vol.) extraction was used to obtain total cell RNA. The RNA was separated by electrophoresis on a formaldehyde/1 % agarose denaturing gel and then transferred to a nitrocellulose filter. The filters were then hybridized with probes at 68 °C as follows. The hybridization buffer contained 50 % (v/v) formamide, 5 × Denhardt's solution, 5 × SSPE (where 1 × SSPE is 0.15 M NaCl/10 mM NaH_2PO_4/1 mM EDTA, pH 7.4), 10 % (w/v) dextran sulphate, 0.1 % (w/v) SDS and 200 μg/ml denatured salmon sperm DNA. The probes were p21 cDNA (kindly provided by Dr David Beach, Cold Spring Harbor Laboratory, NY, U.S.A.) and β-actin cDNA labelled with [α-^{32}P]dCTP by nick translation. After hybridization, the filters were washed in 0.1 × SSC (1 × SSC is 0.15 M NaCl/0.015 M sodium citrate) containing 0.1 % (w/v) SDS at 60 °C, and then air-dried and autoradiographed at −70 °C. The intensity of the bands in the autoradiograms was measured by laser densitometry.

Immunoblot

Cellular proteins were extracted into SDS/PAGE sample buffer (New England Biolabs) and boiled for 10 min. The crude protein lysates (150 μg) were separated by SDS/PAGE, transferred to a nitrocellulose filter, reacted with specific primary antibodies and were revealed using secondary antibodies and Western Blue stabilized for alkaline phosphatase (Promega, Madison, WI, U.S.A.). Antibodies recognizing p21 and Bcl-2 were purchased from Pharmingen (San Diego, CA, U.S.A.). The gels were subjected to autoradiography and the intensity of the bands was estimated by laser densitometry.

Flow cytometric analysis of DNA content

Cells were treated with trypsin and resuspended at 5×10^6 cells/ml in citrate buffer [250 mM sucrose/40 mM sodium citrate/5 % (v/v) DMSO, pH 7.6]. A 200 μl sample was added to 1.8 ml of solution A [30 μg/ml trypsin, 3.4 mM sodium citrate, 0.1 % (v/v) Nonidet P40, 1.5 mM spermine and 0.5 mM Tris/HCl, pH 7.6] and incubated for 20 min at room temperature. Following this, 1.5 ml of solution B [500 μg/ml trypsin inhibitor (Sigma), 100 μg/ml ribonuclease A (Sigma), 3.4 mM sodium citrate, 0.1 % Nonidet P40, 1.5 mM spermine and 0.5 mM Tris/HCl, pH 7.6] was added and the solution was incubated for 20 min at room temperature. Finally 1.5 ml of ice-cold solution C (416 μg/ml propidium iodide, 3.4 mM sodium citrate, 0.1 % Nonidet P40, 1.5 mM spermine and 0.5 mM Tris/HCl, pH 7.6) was added and the incubation was continued at 4 °C for 20 min. Flow cytometric analysis was performed using a FACScan (Beckton and Dickinson). Analysis of the percentage of cells in the S phase was performed using CellFIT cell-cycle analysis software (Beckton and Dickinson).

Statistical analysis

The *P* values were calculated by the Wilcoxon rank-sum test. A significant correlation between two parameters was taken at the 95 % confidence limit, where $P < 0.05$.

RESULTS

Establishment of a variant of SC-M1 overproducing Bcl-2

To investigate the effect of Bcl-2 on RA-induced growth arrest in SC-M1 cells, SC-M1/Bcl2 cells were established by transfecting bcl-2 cDNA into SC-M1 cells and then by pooling at least 80 hygromycin-resistant colonies. As a control, vector plasmid (pCEP4; Invitrogen) was transfected into SC-M1 cells to establish SC-M1/neo cells. As shown in Figure 1, high levels of Bcl-2 protein in SC-M1/Bcl2 cells were detected by immunoblotting. This cell line was used to study the effect of Bcl-2 on RA-induced growth arrest, since Bcl-2 levels were not affected by exposure of the cells to 5 μM RA for 2 days. The growth rates of cells revealed that SC-M1/Bcl2 cells proliferated at a similar rate to SC-M1 and SC-M1/neo cells in the absence of RA. The cell growth of SC-M1/Bcl2 cells under the influence of RA was moderately slower than that of SC-M1/neo cells (Figure 2).

Bcl-2 accelerates RA-induced growth arrest of SC-M1 cells

To investigate the effect of Bcl-2 on RA-induced growth arrest, flow cytometric analysis of DNA contents in SC-M1/Bcl2 and SC-M1/neo cells in the presence or absence of RA treatment was performed. As shown in Table 1, the percentage of cells in S phase, which represents the status of cell growth, remained around 26–35 % in both SC-M1/Bcl2 cells and SC-M1/neo cells in the absence of RA treatment during the 6-day culture period. RA exposure reduced the percentage of cells in S phase to 11.2 % in 2 days in SC-M1/Bcl2 cells. However, RA exposure for 4 days

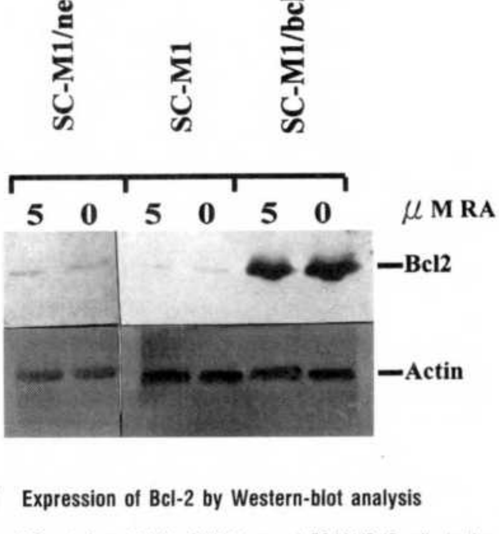

Figure 1 Expression of Bcl-2 by Western-blot analysis

Cell lysates (150 μg) from SC-M1, SC-M1/neo and SC-M1/Bcl2 cells in the presence or absence of 5 μM RA for 2 days were extracted and analysed by SDS/PAGE. Immunoblot analysis was then performed using antibodies recognizing Bcl-2. β-Actin-specific antibodies were used to ensure that equal amounts of protein were present in different lanes. A representative autoradiogram from three independent experiments is shown.

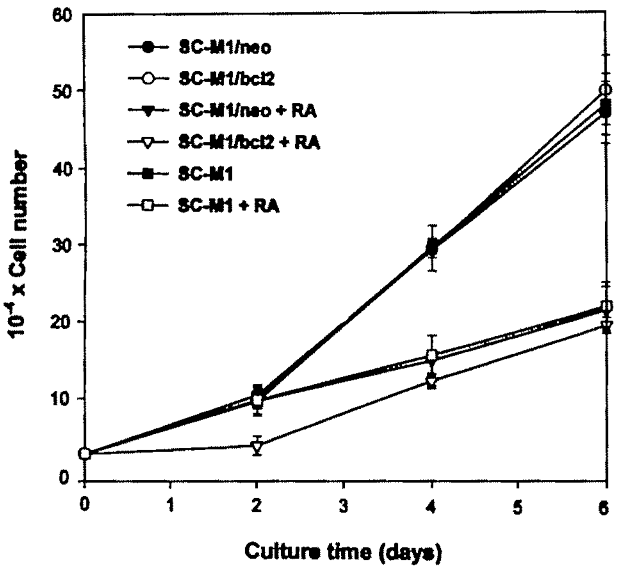

Figure 2 Cell growth of SC-M1, SC-M1/neo and SC-M1/Bcl2 cells in response to RA exposure

Cells (3×10^4) were plated on to a 6-well plate and grown in the presence or absence of 5 μM RA Cell numbers were counted every 2 days using a haemocytometer

was necessary to reduce the percentage of cells in S phase to a similar level (13.4%) in SC-M1/neo cells. The difference in the decrease of the S phase percentage for longer exposure (such as 6 days) of both SC-M1/Bcl2 and SC-M1/neo cells to RA was not significant. In summary, these observations indicate that the response of Bcl-2-containing cells to RA-induced growth arrest is faster than that of SC-M1/neo cells. In addition, since Bcl-2 has an anti-apoptotic effect [1–3], we examined apoptosis of SC-M1/Bcl2 and SC-M1/neo before and after exposure to RA to study what function the anti-apoptotic protein might have in growth arrest regulation. Even with overexpressed exogenous *Bcl-2* gene, the SC-M1/Bcl2 cells had the same ratio of apoptosis as the SC-M1/neo cells (approx. 1%) when measured using the annexin V apoptosis assay. The ratio remained the same in both cell lines when subjected to RA exposure (results not shown).

Table 2 Flow cytometric analysis of DNA content of SC-M1/neo and SC-M1/Bcl2 cells after the removal of RA

Exponential phase SC-M1/neo and SC-M1/Bcl2 cells were cultured in the presence of 5 μM RA for 6 days RA was then removed by washing the cells twice in PBS, and the culture medium was changed At 4, 6 and 8 days after the removal of RA, cells were treated as described in the Experimental section and subjected to flow cytometric analysis of DNA content. The results are the percentage (±S D) of cells in each phase of the cell cycle from three separate experiments.

	Percentage of cells in each phase		
Days after removal of RA	4	6	8
SC-M1/neo cells			
G_0/G_1	87.3±1.1	81.2±1.1	72.1±1.0
S	11.7±0.2	12.3±0.2	18.6±0.3
G_2/M	1.0±0.3	6.5±0.3	9.3±0.5
SC-M1/Bcl2 cells			
G_0/G_1	87.4±1.3	77.3±1.1	67.2±1.1
S	10.6±0.3	22.7±0.4	31.7±1.2
G_2/M	2.0±0.5	0	1.1±0.4

This observation suggests that Bcl-2 does not function as an anti-apoptotic protein in SC-M1 cells in the presence of RA.

Bcl-2 accelerates the reversal of RA-induced growth arrest

One of the possible explanations for the Bcl-2-accelerated RA-induced growth arrest is that Bcl-2 itself may have a growth-suppression effect. The acceleration of growth arrest may represent the synergistic effect of RA and Bcl-2. Under this assumption, Bcl-2 would be expected to slow down the recovery from growth arrest after the removal of RA. SC-M1/neo and SC-M1/Bcl2 cells were exposed to RA for 6 days to achieve complete growth arrest. After the removal of RA cell growth was assayed by monitoring the S-phase population of cells by flow cytometry. Surprisingly, the results showed that Bcl-2-expressing cells (SC-M1/Bcl2) recovered faster than SC-M1/neo cells from growth arrest (Table 2). The percentage of cells in S phase was greater in SC-M1/Bcl2 cells (22.7% at 6 days and 31.7% at 8 days) than in SC-M1/neo cells (12.3% at 6 days and 18.6% at 8 days) after the removal of RA. Since SC-M1/Bcl2 cells recover more quickly from RA-induced growth arrest, Bcl-2 may have a stimulatory effect on growth when RA is removed. These observations indicated the potential role of Bcl-2 as a bi-

Table 1 Flow cytometric analysis of SC-M1/neo cells and SC-M1/Bcl2 cells after RA exposure

Exponential-phase SC-M1/neo and SC-M1/Bcl2 cells were cultured in the presence of 5 μM RA or an equal volume of DMSO (0) for 2, 4 or 6 days respectively Cells were then treated as described in the Experimental section and subjected to flow cytometric analysis of DNA content The results are the percentages (±S D) of cells in each phase of the cell cycle from three separate experiments

	Percentage of cells in each phase					
RA (μM)	0			5		
Culture time (days)	2	4	6	2	4	6
SC-M1/neo cells						
G_0/G_1	62.4±1.2	67.5±1.3	66.3±1.3	75.6±1.2	85.6±1.2	87.2±1.0
S	35.2±1.1	30.4±0.5	25.4±0.2	23.3±0.4	13.4±0.3	8.2±0.3
G_2/M	2.4±0.1	2.1±0.1	8.3±0.5	1.1±0.2	1.0±0.1	4.6±0.2
SC-M1/Bcl2 cells						
G_0/G_1	62.6±1.3	68.6±0.5	69.5±1.3	83.2±1.6	83.5±1.4	87.5±1.1
S	35.1±1.2	30.3±1.0	26.4±0.7	11.2±0.5	10.6±0.4	7.8±0.3
G_2/M	2.3±0.2	1.1±0.1	4.1±0.4	5.6±0.4	5.9±0.5	4.7±0.5

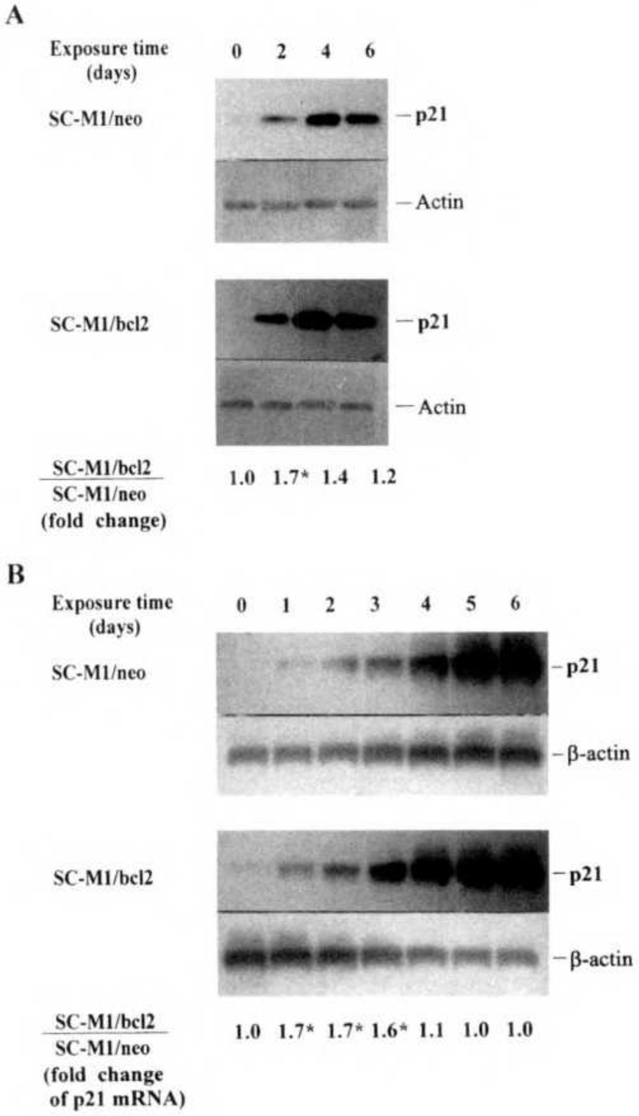

Figure 3 RA treatment increases the concentrations of p21 protein and RNA in SC-M1/Bcl2 cells when compared with SC-M1/neo cells

Exponential-phase growing SC-M1/neo and SC-M1/Bcl2 cells were cultured in the presence of 5 μM RA or an equal volume of DMSO for the indicated times. (**A**) Cell lysates were extracted and separated by SDS/PAGE. Immunoblot analysis was then performed using antibodies recognizing p2l. A representative autoradiogram from four independent experiments is shown. (B) Northern blot analysis. Total cellular RNA was extracted, separated on formaldehyde/agarose (1.0% gel), blotted on to a nitrocellulose filter and hybridized to p21-specific cDNA probes, as described in the Experimental section. The filter was then hybridized to β-actin-specific cDNA probes to ensure that equal amounts of RNA were present in the different lanes. A representative autoradiogram from four independent experiments is shown. *Significant difference between fold change in SC-M1/Bcl2 compared with SC-M1/neo cells at $P < 0.05$ by Wilcoxon rank-sum test.

directional catalyst to accelerate RA-induced growth regulation, both in growth arrest and recovery from growth arrest.

Bcl-2 enhances p21 induction by RA treatment

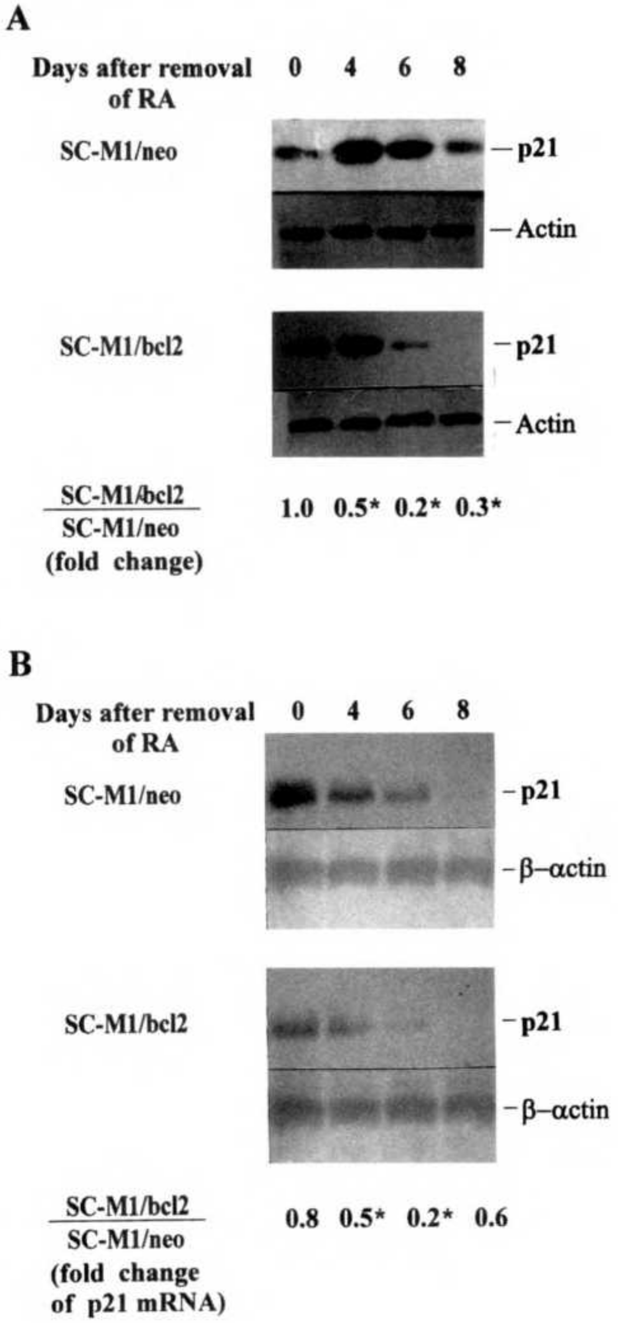

Figure 4 Concentrations of p21 protein and RNA after removal of RA treatment

Exponential-phase growing SC-M1/neo cells and SC-M1/Bcl2 cells were cultured in the presence of 5 μM RA for 6 days. RA was then removed by changing the medium. (**A**) Cell lysates were extracted at the indicated time points and analysed by immunoblotting with antibodies recognizing p2l. A representative autoradiogram from four independent experiments is shown. (**B**) Total cellular RNA was extracted at the indicated time points, separated on formaldehyde/agarose (1.0% gel), blotted on to a nitrocellulose filter and hybridized to a p21-specific cDNA probe, as described in the Experimental section. The filter was then hybridized to a β-actin-specific cDNA probe to ensure that equal amounts of RNA were present in different lanes. A representative autoradiogram from four independent experiments is shown. *Significant difference between fold change in SC-M1/Bcl2 compared with SC-M1/neo cells at $P < 0.05$ by Wilcoxon rank-sum test.

We further studied the mechanism by which Bcl-2 accelerated RA-induced growth arrest. Since p21 is proposed to be involved in this phenomenon [15–18], we investigated whether Bcl-2 overexpression raised the concentration of p21 during RA-induced growth arrest. Immunoblot analysis revealed greater p21 protein concentrations in SC-M1/Bcl2 cells than in SC-M1/neo cells after RA exposure (Figure 3A). The concentrations

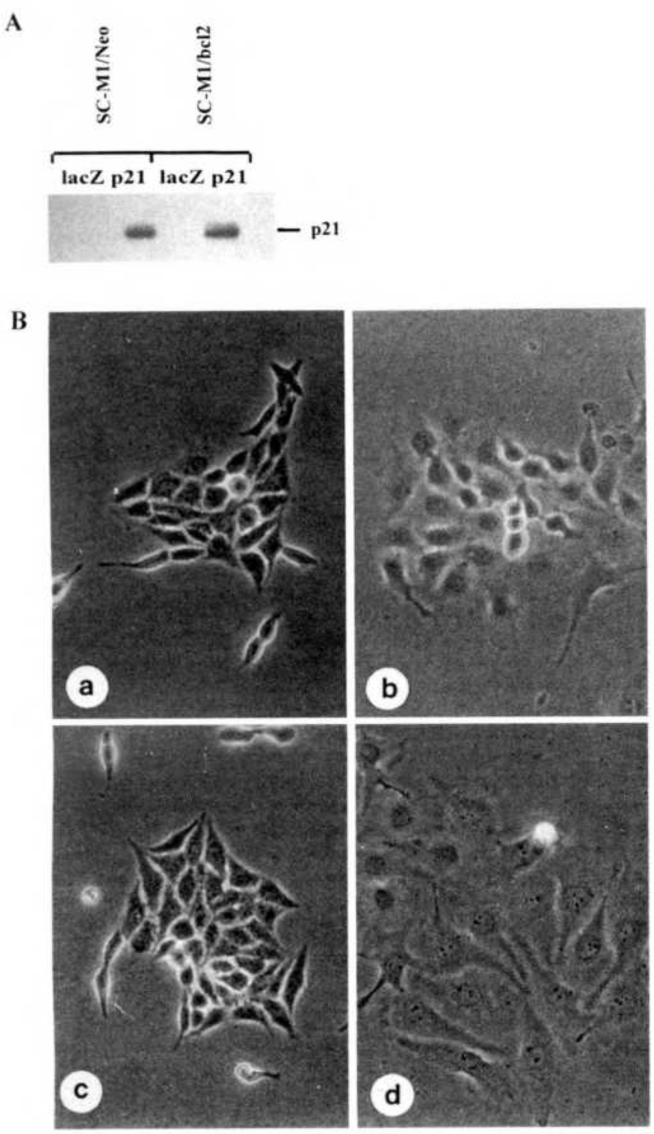

Figure 5 Exogenous p21 induces growth arrest both in SC-M1/neo and SC-M1/Bcl2 cells

Exponential-phase growing SC-M1/neo and SC-M1/Bcl2 cells were infected with recombinant adenovirus encoding *lacZ* and *p21* at m.o.i. of 100. (**A**) Cell lysates (150 μg) were extracted after 48 h and analysed by immunoblotting p21 protein. A representative autoradiogram from three independent experiments is shown. (**B**) Cell morphology of: (a) SC-M1/neo cells infected with recombinant adenovirus encoding *lacZ* for 2 days, (b) SC-M1/neo cells infected with recombinant adenovirus encoding *p21* for 2 days, (c) SC-M1/Bcl2 cells infected with *lacZ*-encoded adenovirus for 2 days, and (d) SC-M1/Bcl2 cells infected with p21-encoded adenovirus for 2 days.

Table 3 Flow cytometric analysis of DNA content of SC-M1/neo and SC-M1/Bcl2 cells infected with adenovirus/lacZ or adenovirus/p21

Exponential phase SC-M1/neo and SC-M1/Bcl2 cells were infected with adenovirus/lacZ or adenovirus/p21 at a m.o.i. of 100 for 48 h. The cells were treated as described in the Experimental section and subjected to flow cytometric analysis of DNA content. The results are the percentages (± S.D.) of cells in each phase of the cell cycle from three separate experiments.

	Percentage of cells in each phase	
	Adenovirus/lacZ	Adenovirus/p21
SC-M1/neo cells		
G_0/G_1	62.8 ± 1.2	80.3 ± 1.5
S	35.6 ± 1.0	18.7 ± 0.7
G_2/M	1.6 ± 0.3	1.0 ± 0.1
SC-M1/Bcl2		
G_0/G_1	68.2 ± 1.4	83.1 ± 1.1
S	29.8 ± 1.2	14.8 ± 0.5
G_2/M	2.0 ± 0.2	2.1 ± 0.4

of p21 protein after exposure to RA for 2, 4 or 6 days in SC-M1/Bcl2 cells were 1.7-, 1.4- and 1.2-fold of those in SC-M1/neo cells respectively. Whereas the comparative levels of p21 protein in SC-M1/Bcl2 increased significantly within 2 days of RA treatment, Northern-blot analysis showed that, during the first 3 days, p21 mRNA levels were also significantly higher in SC-M1/Bcl2 cells (1.7-, 1.7- and 1.6-fold) than in SC-M1/neo cells after exposure to RA, when assessed using Wilcoxon rank-sum test. By day 4 of exposure, the levels of mRNA reached a plateau and the concentrations of p21 mRNA were not significantly different (Figure 3B). Taken together, these results suggest that Bcl-2 may amplify RA-induced *p21* gene induction during growth arrest.

As our previous observations indicated that Bcl-2 accelerated the recovery from growth arrest after the removal of RA (Table 2), we also investigated the p21 levels in SC-M1/neo and SC-M1/Bcl2 cells after the removal of RA using immunoblot and Northern-blot analysis. The levels of p21 protein (Figure 4A) and p21 RNA (Figure 4B) fell more quickly in SC-M1/Bcl2 cells than in SC-M1/neo cells. The concentrations of p21 protein in SC-M1/Bcl2 cells decreased to 0.5-, 0.2- and 0.3-fold of the SC-M1/neo cells after the removal of RA for 4, 6 and 8 days respectively. The difference was significant by Wilcoxon rank-sum test. Similarly, the levels of p21 mRNA also fell more quickly in SC-M1/Bcl2 cells than in SC-M1/neo cells (0.5-, 0.2- and 0.6-fold) (Figure 4B). These results suggest that Bcl-2 may accelerate the recovery of growth arrest by repressing *p21* gene expression after the removal of RA.

p21 is a mediator of RA-induced growth arrest

After documenting the correlation of the effect of Bcl-2 on RA-induced growth arrest and RA-induced *p21* gene expression, the next step was to further establish p21 as the mediator of growth arrest in SC-M1/neo and SC-M1/Bcl2 cells. We tested the capability of p21 to arrest cell growth by overexpressing the exogenous *p21* gene in the two cell lines. SC-M1/neo and SC-M1/Bcl2 cells were transduced by an adenovirus encoding the *p21* gene at 100 multiplicity of infection (m.o.i.) [19]. Figure 5(A) shows high p21 protein expression in cells infected with recombinant adenovirus encoding p21, but not in virus encoded with the *lacZ* gene. Two days after virus p21 infection, both SC-M1/neo (Figure 5B, panel b) and SC-M1/Bcl2 cells (Figure 5B, panel d) acquired the flattened morphological changes showing growth arrest. The same morphological phenomenon occurred when SC-M1/neo cells and SC-M1/Bcl2 cells were exposed to RA (results not shown). Figure 5(B) (panels a and c) show the lack of morphological change in both the SC-M1/neo and the SC-M1/Bcl2 cells when each was infected with an equivalent titre of recombinant adenovirus encoding *lacZ*. As shown in Table 3, flow cytometric analysis of p21 adenovirus-infected cells revealed the depletion of S phase cells 2 days after infection. After adenovirus-p21 infection, the number of S-phase cells in SC-M1/neo cells was reduced to 18.7 % compared with 35.6 % of cells in S phase after infection with adenovirus-lacZ. The ability of exogenous p21 to achieve a similar effect on cell-growth arrest to that of RA, together with the correlation between RA-induced growth arrest and *p21* gene induction, provided some, but not sufficient, evidence for the possible role of p21 as a mediator of the growth arrest induced by RA in both SC-M1/neo and SC-M1/Bcl2 cells.

DISCUSSION

RA is reported to induce cell-growth arrest and cell differentiation in experimental and physiological conditions [20–22]. Indeed, the induction of cell differentiation by RA has been widely used for elucidating the regulating mechanism of cell growth and differentiation. Growth arrest by RA in most research models is irreversible [20–22], this makes the correlation of the biological response with growth regulation or differentiation difficult. However, SC-M1 cells offer a unique system by which RA treatment can induce reversible growth arrest and morphological changes [11–13]. Any biological event can be better correlated with RA-induced growth arrest if it appears with RA treatment and disappears after the removal of RA. In the present study, p21, which correlated well with the reversible cell-growth arrest, may also participate in the growth arrest induced by RA (Figure 4). A supplementary piece of evidence came from the finding that overexpression of p21 by an exogenous *p21* gene delivered by an adenoviral vector led to growth arrest in SC-M1 cells (Table 3).

It was also found that SC-M1/Bcl2 cells, when treated with RA, were arrested in growth 2 days earlier than SC-M1/neo cells (Table 1), indicating that Bcl-2 accelerates RA-induced growth arrest. Further, in addition to this accelerated growth arrest, RA-treated SC-M1/Bcl2 cells also recovered from growth arrest after the removal of RA 2 days faster than SC-M1/neo cells (Table 2). The present report is the first to demonstrate that Bcl-2 accelerates not only growth arrest but also recovery from growth arrest.

In the present study, it was found that Bcl-2 overexpression did not affect cell growth (Figure 2). However, in a previous study, it was stated that the colorectal adenocarcinoma cell line (SW480) was the only cell line among several tested where growth was inhibited by Bcl-2 [23]. This observation was measured by transfecting Bcl-2 cDNA into SW480 cells Colony formation was counted by drug selection. It is not known if growth arrest was the mechanism behind the failure of colony formation. It is, nevertheless, still reasonable to assume that Bcl-2 does not affect the growth of normal cells.

In a search for the mechanism of growth regulation by Bcl-2, in the present study, it was found that the *p21* gene product was an important factor in growth arrest induced by RA, whereas Bcl-2 moderately enhanced the induction of p21 in the presence of RA (Figure 3). This suggests a model where Bcl-2 is involved in RA-induced growth arrest by enhancing the expression of the *p21* gene. It is unlikely that Bcl-2 directly affects *p21* gene expression since Bcl-2 is not a nuclear protein, and has never been reported to be a transcription factor. However, overexpression of Bcl-2 is shown to induce apoptosis-associated changes, such as alteration of the cellular redox state [24–27], change in subcellular calcium ion distribution [28,29], activation of caspases [30] and distribution of the mitochondrial membrane potential [31–33]. These mechanisms may be involved in the regulation of *p21* gene expression resulting from the presence of Bcl-2. Interestingly, the redox state is reported to mediate the regulation of *p21* gene expression [34]. The mechanisms behind the regulation of *p21* gene expression by Bcl-2 are currently being investigated.

From the involvement of Bcl-2 in the growth arrest process, as described above, it is reasonable to conclude that Bcl-2 accelerates RA-induced growth arrest. However, in the present study, by removing RA, we also found that *Bcl-2* transgene cells recovered more quickly from RA-induced growth arrest and regained growth potential faster than the control cells. This suggests that the growth potential of cells can be determined by RA treatment but not by Bcl-2. Our findings that Bcl-2 enhances not only RA-induced growth arrest but also recovery from growth arrest, provide an excellent model with which to study the effects of Bcl-2 on growth regulation. Unravelling the conditions and mechanisms by which Bcl-2 regulates cell growth may advance our knowledge of tumour formation and cancer therapy.

We are grateful to Dr David Beach for providing p21 cDNA, and Mr John Wu, Mr Daniel L Altschuler and Mr Thomas Price for their help in modifying the English of this manuscript. This work was supported by National Science Council Grants, NSC 87-2312-B016-004

REFERENCES

1 Vaux, D L, Cory, S and Adams, J M (1988) Bcl-2 gene promotes haemopoietic cell survival and cooperates with c-myc to immortalize pre-B cells Nature (London) **335**, 440–442
2 Hockenbery, D M, Nunez, G, Milliman, C, Schreiber, R D and Korsmeyer, S J (1990) Bcl-2 is an inner mitochondrial membrane protein that blocks programmed cell death Nature (London) **348**, 334–336
3 Kroemer, G (1997) The proto-oncogene Bcl-2 and its role in regulating apoptosis Nat Med **3**, 614–620
4 Williams, G T. (1991) Programmed cell death Apoptosis and oncogenesis Cell **65**, 1097–1098
5 Miyashita, T and Reed, J C (1995) Tumor suppressor p53 is a direct transcriptional activator of the human bax gene Cell **80**, 293–299
6 Chiou, S K, Rao, L and White, E (1994) Bcl-2 blocks p53-dependent apoptosis Mol Cell Biol **14**, 2556–2563
7 O'Reilly, L A, Huang, D C S and Strasser, A. (1996) The cell death inhibitor Bcl-2 and its homologues influence control of cell cycle entry EMBO J **15**, 6979–6990
8 Nakamura, T, Nomura, S, Sakai, T and Nariya, S. (1997) Expression of bcl-2 oncoprotein in gastrointestinal and uterine carcinomas and their premalignant lesions Hum Pathol **28**, 309–315
9 Uesugi, H., Saegusa, M, Takano, Y and Okayasu, I (1996) Different expression of Bcl-2 protein in gastric adenomas and carcinomas Pathol Int **46**, 274–280
10 Koshida, Y, Saegusa, M and Okayasu, I (1997) Apoptosis, cell proliferation and expression of Bcl-2 and Bax in gastric carcinomas Immunohistochemical and clinicopathological study Br J Cancer **75**, 367–373
11 Shyu, R Y, Jiang, S Y, Huang, S L, Chang, T C, Wu, K L, Roffler, S R and Yeh, M Y. (1995) Growth regulation by all-trans-retinoic acid and retinoic acid receptor messenger ribonucleic acids expression in gastric cancer cells Eur J Cancer **31**, 237–243
12 Jiang, S Y, Shyu, R Y, Chen, H Y, Lee, M M, Wu, K L and Yeh, M Y (1996) *In vitro* and *in vivo* growth inhibition of SC-M1 gastric cancer cells by retinoic acid Oncology **53**, 334–340
13 Chao, T Y., Jiang, S Y, Shyu, R Y, Yeh, M Y and Chu, T M (1997) All-trans retinoic acid decreases susceptibility of a gastric cancer cell line to lymphokine-activated killer cytotoxicity Br J Cancer **75**, 1284–1290
14 Tzeng, C C, Meng, C L, Jin, L and Hsieh, H F (1991) Cytogenetic studies of gastric adenocarcinoma Cancer Genet Cytogenet **55**, 67–71
15 Tsao, Y P., Li, S F, Kuo, S W, Liu, J C and Chen, S L (1996) Reversal of the temperature-shift-induced growth restriction of a temperature-sensitive simian virus 40 T-antigen-transformed human fibroblast cell line by treatment with retinoic acid Biochem J **317**, 707–711
16 Liu, M, Iavarone, A. and Freedman, L P (1996) Transcriptional activation of the human p21(WAF1/CIP1) gene by retinoic acid receptor Correlation with retinoid induction of U937 cell differentiation J Biol Chem **271**, 31723–31728
17 Naka, K, Yokozaki, H, Domen, T, Hayashi, K, Kuniyasu, H, Yasui, W, Lotan, R and Tahara, E (1997) Growth inhibition of cultured human gastric cancer cells by 9-cis-retinoic acid with induction of cdk inhibitor Waf1/Cip1/Sdi1/p21 protein Differentiation **61**, 313–320

18 Hsu, C A, Rishi, A. K., Su-Li, X, Gerald, T M, Dawson, M. I., Schiffer, C, Reichert, U, Shroot, B., Poirer, G C and Fontana, J A (1997) Retinoid induced apoptosis in leukemia cells through a retinoic acid nuclear receptor-independent pathway Blood **89**, 4470–4479

19 Tsao, Y P, Huang, S J., Hsieh, J T, Chang, J L, Pong, R C. and Chen, S L (1999) Adenovirus-mediated p21 (WAF1/SDII/CIP1) gene transfer induces apoptosis of human cervical cancer cell lines J. Virol. **73**, 4983–4990

20 Lotan, R, Lotan, D and Sacks, P G. (1990) Inhibition of tumor cell growth by retinoids Methods Enzymol **190**, 100–110

21 Smith, M. A, Parkison, D R, Cheson, B D and Friedman, M A (1992) Retinoids in cancer therapy J Clin Oncol **10**, 839–864

22 Gudas, L J (1992) Retinoids, retinoid-responsive genes, cell differentiation, and cancer Cell Growth Differ **3**, 655–662

23 Pietenpol, J A, Papadopoulos, N, Markowitz, S., Willson, J K V, Kinzler, K W. and Vogelstein, B (1994) Paradoxical inhibition of solid tumor cell growth by bcl2 Cancer Res **54**, 3714–3717

24 Hockenbery, D M, Oltvai, Z N., Yin, X M, Milliman, C L and Korsmeyer, S J (1993) Bcl-2 functions in an antioxidant pathway to prevent apoptosis Cell **75**, 241–251

25 Kane, D J, Sarafian, T. A, Anton, R, Hahn, H, Gralla, E B, Valentine, J. S, Ord, T and Bredesen, D E (1993) Bcl-2 inhibition of neural death. decreased generation of reactive oxygen species Science **262**, 1274–1277

26 Lawrence, M S, Ho, D Y, Sun, G. H., Steinberg, G K and Sapolsky, R M (1996) Overexpression of Bcl-2 with herpes simplex virus vectors protects CNS neurons against neurological insults *in vitro* and *in vivo* J Neurosci. **16**, 486–496

27 Ellerby, L M, Ellerby, H M, Park, S. M, Holleran, A L, Murphy, A N, Fiskum, G., Kane, D. J, Testa, M P, Kayalar, C and Bredesen, D. E (1996) Shift of the cellular oxidation-reduction potential in neural cells expressing Bcl-2 J Neurochem **67**, 1259–1267

28 Lam, M., Dubyak, G, Chen, L, Nunez, G, Miesfeld, R L and Distelhorst, C. W. (1994) Evidence that BCL-2 represses apoptosis by regulating endoplasmic reticulum-associated Ca_{2+} fluxes Proc Natl. Acad Sci USA **91**, 6569–6573

29 Mann, M C, Fernandez, A, Bick, R J, Brisbay, S, Buja, L M, Snuggs, M, McConkey, D. J., von Eschenbach, A C, Keating, M. J. and McDonnell, T J (1996) Apoptosis suppression by bcl-2 is correlated with the regulation of nuclear and cytosolic Ca_{2}+ Oncogene **12**, 2259–2266

30 Chinnaiyan, A M, Orth, K, O'Rourke, K., Duan, H, Poirier, G G and Dixit, V M (1996) Molecular ordering of the cell death pathway Bcl-2 and Bcl-xL function upstream of the CED-3-like apoptotic proteases J Biol Chem **271**, 4573–4576

31 Kroemer, G, Petit, P., Zamzami, N., Vayssiere, J L and Mignotte, B (1995) The biochemistry of programmed cell death FASEB J. **9**, 1277–1287

32 Yang, J, Liu, X, Bhalla, K., Kim, C N, Ibrado, A M, Cai, J, Peng, T. I, Jones, D P and Wang, X (1997) Prevention of apoptosis by Bcl-2 release of cytochrome c from mitochondria blocked Science **275**, 1129–1132

33 Kluck, R. M, Bossy-Wetzel, E, Green, D R and Newmeyer, D D. (1997) The release of cytochrome c from mitochondria. a primary site for Bcl-2 regulation of apoptosis Science **275**, 1132–1136

34 Esposito, F, Cuccovillo, F, Vanoni, M, Cimino, F, Anderson, C W, Appella, E and Russo, T (1997) Redox-mediated regulation of p21(waf1/cip1) expression involves a post-transcriptional mechanism and activation of the mitogen-activated protein kinase pathway. Eur. J Biochem **245**, 730–737

Received 6 December 1999/14 March 2000, accepted 5 April 2000

Signalling Titles
from Portland Press

Portland Press

The Biology of Nitric Oxide Part 7

Edited by S Moncada, The Wolfson Institute for Biomedical Research, London, UK, LE Gustafsson, Karolinska Institute, Stockholm, Sweden, NP Wiklund, Karolinska Hospital, Stockholm, Sweden and EA Higgs, The Wolfson Institute for Biomedical Research, London, UK

1 85578 142 5 Hardback April 2000 400 pages £110.00

The proceedings of the *Sixth International Meeting on the Biology of Nitric Oxide* held atStockholm, Sweden on 5-8 September 1999.

This book provides an up-to-date overview of the current status of the field with contributions from over 400 specialists covering the following areas:

Molecular Biology, Biochemistry, Physiology, Pathophysiology, Inflammation, Tumours, Apoptosis, Novel Compounds and Clinical Aspects.

Nitric Oxide and the Peripheral Nervous System

Edited by N Toda, Shiga University of Medical Science, Ohtsu, Japan, S Moncada, The Wolfson Institute for Biomedical Research, London, UK, R Furchgott, State University of New York, USA and EA Higgs, The Wolfson Institute for Biomedical Research, London, UK

1 85578 139 5 Hardback June 2000 200 pages £85.00 Provisional

This volume provides an overview of NO in the peripheral nervous system, covering aspects ranging from the molecular biology and distribution of neuronal nitric oxide synthase, through the physiological and pathophysiological roles of NO in various nitrergic systems (systems of nerves whose transmitter function depends on the release of NO). They are of major importance in the regulation of certain genitourinary, gastrointestinal and respiratory functions. In addition, nitrergic nerves mediate neurogenic vasodilation of blood vessels in some vascular beds, notably those in the cerebral circulation.

Potential therapies that may arise from our increasing knowledge of this fascinating field of research are also reviewed.

Landmarks in Intracellular Signalling

Edited by RD Burgoyne and OH Petersen, University of Liverpool, UK

1 85578 101 8 Paperback 1997 278 pages £20.00

The idea behind Landmarks in Intracellular Signalling is to provide full reproductions of a set of key papers which have been chosen as landmark papers in the various aspects of intracelllular signalling. The selected papers have all resulted in significant advances in one or other aspect of intracellular signalling.

Readers of *Landmarks in Intracellular Signalling* will now have easy, ready available access to the original literature from one source. The papers are accompanied by commentaries that describe why the papers were significant, how the work came about and summarize the advances that have been made up to the present time as a consequence of the original paper.

Essays in Biochemistry: Cell Signalling

Edited by DJ Bowles, University of York, UK

1 85578 071 2 Paperback 1997 192 pages £19.00

The subject of this volume of Essays is cell signalling – the molecular events of information transfer, occurring within or between cells, that link external changes to internal responses. A broad range of topics have been chosen, to provide insights on a variety of processes in a range of cells and organisms.

Illustrated through-out with clear diagrams which convey complex information in a more accessible way.

The extensive bibliographies and further reading lists will provide undergraduates and postgraduates with a valuable bridge between textbooks and research papers. Serves as a useful teaching aid for lecturers in biochemistry and molecular biology.

Orders:
www.portlandpress.com/books/orderinfo.htm

***Portland Press, Commerce Way,**
Colchester, CO2 8HP
t: 01206 796351
f: 01206 799331
e: sales@portlandpress.com

Please add £2.50 per book to a maximum of £7.50

In the USA and Canada
Princeton University Press
c/o California/Princeton Fulfillment Services, Inc
1445 Lower Ferry Road,
Ewing, New Jersey 08618
t: 1-800-777-4726
f: 1-800-999-1958
e: orders@cpfs.pupress.princeton.edu

Postage: Please add $3.75 for first book and US$1.00 for each additional book

BWZ/0400/C

Essential Life Sciences Online

Portland Press

Back

Next

.pdf

Home

Biochemical Journal

Chairman of Editorial Board: ***Peter Parker*** *(ICRF, London, UK)*

http://www.BiochemJ.org

The Biochemical Journal is available online offering many additional advantages:

- **New** – Every year in January the online content for the previous years will become free
- Published online one week early
- Electronic multi-media adjuncts
- Medline and Inter-journal linking

Subscription – 2000: Volumes 345–352 (24 issues)
North America: US$1950.00 Rest of World: £1110.00

Biotechnology and Applied Biochemistry

Editor-in-Chief: ***Roger Lundblad*** *(Chapel Hill, USA)*

http://bab.portlandpress.com

In addition to the features of the Biochemical Journal Online, the full text of papers for *Biotechnology & Applied Biochemistry* are now published online as soon as they are ready, several weeks before the printed edition.

It includes scholarly articles and reviews concerning the expression, purification, characterization and application of biological macromolecules in therapeutics and diagnostics.

Subscription – 2000: Volumes 31–32 (6 issues)
North America: US$250.00 Rest of World: £143.00

Clinical Science

Editor-in-Chief: ***Kim Bartlett*** *(Newcastle-upon-Tyne, UK); Associate Editor Americas:* ***Aubrey Taylor*** *(Mobile, USA); Associate Editor Pacific Rim:* ***Stephen Harrap*** *(Melbourne, Australia)*

http://cs.portlandpress.com

Full access to online papers from 1998, abstracts from 1997 plus full text of papers published online as soon as they are ready.

Publishes articles and reviews on all aspects of clinical investigation, including biochemical, physiological, immunological, cellular, molecular biological and other approaches of relevance to disease in man.

Subscription – 2000: Volumes 98–99 (12 issues)
North America: US$525.00 Rest of World: £290.00

Biochemical Society Transactions

http://bst.portlandpress.com

Missed the Biochemical Society Meeting? - Don't Miss the Science

The Biochemical Society's conferences bring together some of the best biochemical and life-science research by international speakers. *Biochemical Society Transactions* contains the scientific reports and poster abstracts from these meetings. The prestigious medal lectures are also published.

New for 2000 full papers will be published online as well as speaker abstracts.

Subscription - 2000: Volume 28 (6 parts)
North America: US$305.00 Rest of World: £178.00

Free to subscribers

Full free online access to the current year of these journals is restricted to institutions that have a subscription to the printed version. Ask your subscribing library to contact us to ensure you have access to papers in these online journals as soon as they are available.

Contact: support@portlandpress.com

Join the email current awareness service for these important journals

Enquiries to:

Portland Press Ltd,
59 Portland Place,
London W1N 3AJ
Tel: +44 020 7580 5530
Fax: +44 020 7323 1136
sales@portlandpress.com
www.portlandpress.com

Portland Press is the not-for-profit subsidiary of the Biochemical Society publishing journals and books in the life sciences.

BVV/0200/S

Printed in Great Britain by the University Press, Cambridge

BIJOAK 348(3) 481–687 2000 • ISSN 0264-6021
Volume 348 • Part 3 • 15 June 2000

BIOCHEMICAL JOURNAL

review

Retinoid-binding proteins: mediators of retinoid action

by N. Noy

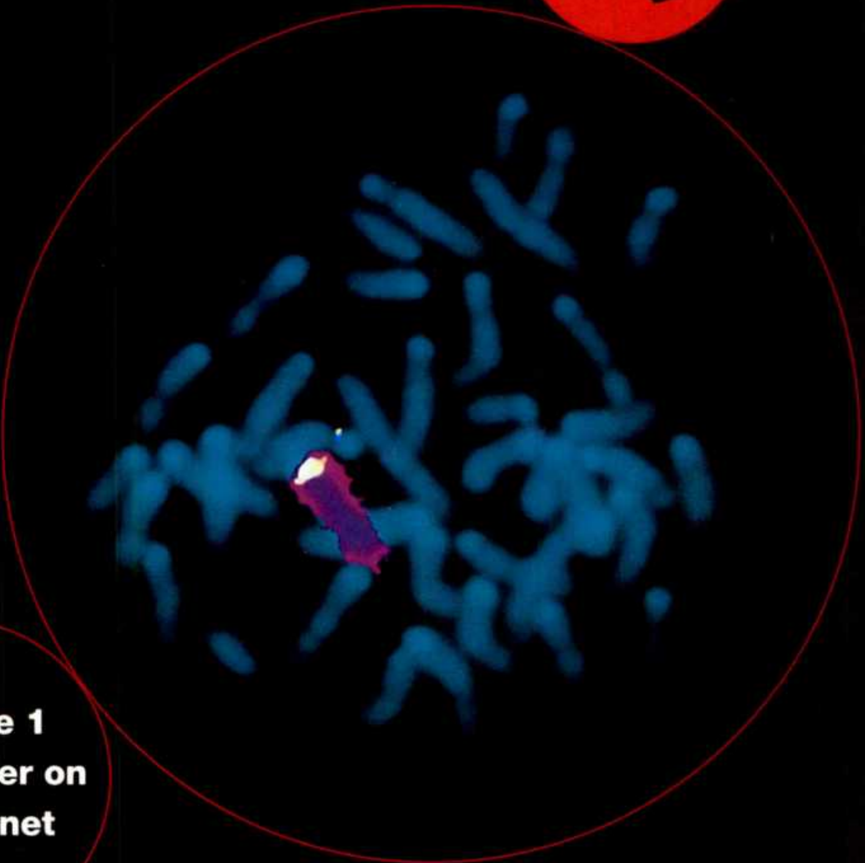

Available 1 week earlier on the Internet

The Biochemical Society, London © 2000

Cell Death Titles

from Portland Press

Portland Press

Mitochondria and Cell Death

Edited by GC Brown, University of Cambridge, UK, D Nicholls, University of Dundee, UK, and C Cooper, University of Essex, UK

This book reviews the involvement of mitochondria in cell death and disease. This is a rapidly expanding field of major importance to both basic biology and medical science. Clear and comprehensive chapters from some of the key researchers in the field cover most aspects of the subject from the molecular to the *in vivo* level. The role of mitochondria in neurodegenerative, inflammatory and ischaemic diseases, as well as necrosis, apoptosis and ageing is reviewed. Each chapter is by a different set of authors describing one aspect of the field. Researchers and postgraduates throughout biology and medical science will want to read this book.

1 85578 125 5 Hardback October 1999 240 pages £65.00

Techniques in Apoptosis: A User's Guide

Edited by TG Cotter, University College Cork, Ireland and SJ Martin, La Jolla Institute for Allergy and Immunology, USA

Cell death/apoptosis is currently an exponentially expanding field of broad research interest. The success of research projects depend on having access to detailed and clearly written accounts of techniques and methodologies used. This is particularly important in a new field. *Techniques in Apoptosis* aims to fill this niche, it differs from recent volumes on apoptosis since its focus will be purely technical in nature.

Each chapter begins with an overview of the methodology to be employed, and goes on to provide detailed experimental protocols for the identification of apoptotic cells from plants to *Drosophila* to man in an easy to-use, step-by-step format. Written by key people in the field, this book is essential reading for all researchers in cell death, from PhD students to senior scientists.

1 85578 129 8 Paperback 1997 300 pages £39.50

Nitric Oxide and the Cell: Proliferation Differentiation and Death

Edited by S Moncada, The Wolfson Institute for Biomedical Research, London, UK, G Nisticò, University of Rome, Italy, G Bagetta, University of Rome, Italy and EA Higgs, The Wolfson Institute for Biomedical Research, London, UK

Proceedings of the II International Paraelios Symosium: Nitric Oxide and the Cell: Proliferation Differentiation and Death, Baia Paraelios, Calabria, Italy, 1996

Nitric Oxide has proven to be a molecule with a wide biological significance. It is involved in myriad actions which range from physiology to pathophysiology. One of the fundamental questions in relation to its biological relevance concerns the paradoxical nature of some of its actions. There is, for example, a whole range of effects related to cytoprotection, cell proliferation, differentiation and cell death. The way in which nitric oxide becomes involved in pathophysiology is slowly being elucidated.

This volume is a summary of the discussions that took place at the Second International Paraelios Symposium on Nitric oxide research. It will make significant contribution to the clarification of this very exciting subject.

"Overall, the book is good if you want to learn details from first principals of the mechanisms of NO activity at the cellular and molecular level. It is well written, well illustrated and easy to read. I would recommend it to both the novice and the established researcher in the NO field. It is a valuable source of new information on NO action and is copiously referenced for those wishing to learn about the background of NO biology."

Immunology News

1 85578 120 4 Hardback 1998 280 pages £80.00

Orders:
www.portlandpress.com/books/orderinfo.htm

***Portland Press, Commerce Way,**
Colchester, CO2 8HP
t: 01206 796351
f: 01206 799331
e: sales@portlandpress.com

USA and Canada:
†California/Princeton
Fulfillment Services Inc.,
1445 Lower Ferry Road,
Ewing, NJ 08618, USA
t: 1 800 777 4726
f: 1 800 999 1958
e: orders@cpfs.pupress.princeton.edu

***Please add £2.50 per book to a maximum of £7.50**

†Please add US$3.75 for first book, US$1.00 for each additional book

BWY/0400/C

27/7/2005

The Biochemical Society, London © 2000

Biochemical Journal

Volume 348, part 3
15 June 2000

First published on the Internet
7 June 2000
http://www.BiochemJ.org

Editorial Board

Chairman
P. J. Parker • London

Deputy Chairmen
G. E. Blair • Leeds
D. N. Brindley • Edmonton
R. A. J. Challiss • Leicester
P. Ferré • Paris
J. T. Gallagher • Manchester
R. A. John • Cardiff
H. Nagase • London
J. D. Pearson • London
M. H. Rider • Bruxelles
S. B. Shears • Research Triangle Park

Reviews Editor
R. D. Burgoyne • Liverpool

Managing Editor
P. J. Starley

Deputy Managing Editor
S. E. Dilley

Senior Staff Editor
S. M. Hobday

Staff Editors
L. Johnson
W. J. Watkins
M. R. Thorne
N. B. Prowse
S. J. Cubie

Editorial Assistant
N. J. Lamb

R. L. P. Adams (Glasgow)
J. W. N. Akkerman (Utrecht)
D. R. Alessi (Dundee)
D. Attaix (Ceyrat)
S. A. Baldwin (Leeds)
F. J. Ballard (Adelaide)
G. J. Barritt (Adelaide)
N. C. Bruce (Cambridge)
A. Clerk (London)
G. M. Cohen (Leicester)
P. Crine (Montreal)
D. Cutler (London)
D. A. Day (Nedlands)
H. Deckmyn (Kortrijk)
K. Docherty (Aberdeen)
B. K. Drøbak (Norwich)
J. M. East (Southampton)
K. R. F. Elliott (Manchester)
B. Engelmann (Munich)
C. Forest (Meudon)
M. J. Fry (Reading)
A. Galione (Oxford)
D. A. F. Gillespie (Glasgow)
S. Goodbourn (London)
G. W. Gould (Glasgow)
S. V. Graham (Glasgow)
S. Gutteridge (Newark, DE)
Y. A. Hannun (Charleston)
P. I. Haris (Leicester)
M. M. Harnett (Glasgow)
J. D. Hayes (Dundee)
P. C. Heinrich (Aachen)
R. Heinrich (Berlin)
B. Henrissat (Marseille)
R. C. Hider (London)
S. High (Manchester)
M. B. Hodgins (Glasgow)
D. Hoekstra (Groningen)
N. M. Hooper (Leeds)
E. F. Hounsell (London)
W. Jessup (Sydney)
J. Johansson (Stockholm)
J. P. Kehrer (Austin)
K. I. Kivirikko (Oulu)
B. L. Knight (London)
R. G. Knowles (Stevenage)
H. Kresse (Münster)
P. W. Kuchel (Sydney)
C. MacKintosh (Dundee)
A. I. Magee (London)
T. J. Mantle (Dublin)
P. Maurel (Montpellier)
A. J. Meijer (Amsterdam)
J. E. Merritt (Welwyn Garden City)
F. Michelangeli (Birmingham)
G. Milligan (Glasgow)
B. P. Morgan (Cardiff)
J. S. Mort (Montreal)
S. E. Moss (London)
K. J. Murray (Harlow)
A. C. Newby (Bristol)
F. Paltauf (Graz)
N. J. Pyne (Glasgow)
C. I. Ragan (Windlesham)
P. R. Rich (London)
N. J. P. Ryba (Bethesda)
G. Salvesen (San Diego)
M. F. Scully (London)
S. Shenolikar (Durham, NC)
A. G. Smith (Cambridge)
M. C. Sugden (London)
P. H. Sugden (London)
R. Sundler (Lund)
J. M. Tavaré (Bristol)
K. F. Tipton (Dublin)
M. A. Titheradge (Brighton)
A. B. Tobin (Leicester)
S. A. Tooze (London)
W. J. van Blitterswijk (Amsterdam)
R. Virden (Newcastle upon Tyne)
H. M. Wallace (Aberdeen)
M. P. Walsh (Calgary)
L. A. Witters (Hanover)
S. J. Yeaman (Newcastle upon Tyne)

- The *Biochemical Journal* (ISSN 0264-6021 for print journal; ISSN 1470-8728 for online journal) is published and distributed by Portland Press Ltd on behalf of the Biochemical Society, and appears twice monthly.
- **Editorial and publishing offices:** *Biochemical Journal*, 59 Portland Place, London W1N 3AJ, U.K.
- Royal Mail International, c/o Yellowstone International, 87 Burlews Court, Hackensack, NJ 07061, U.S.A.
- **Subscriptions department:** Portland Press Ltd, P.O. Box 32, Commerce Way, Colchester CO2 8HP, U.K.

- All rights reserved. Apart from any fair dealing for the purposes of research or private study, or criticism or review, as permitted under the Copyright, Designs and Patents Act, 1988, this publication may be reproduced, stored or transmitted, in any forms or by any means, only with the prior permission in writing of the publishers, or in the case of reprographic reproduction in accordance with the terms of permissions granted by copyright clearing houses such as the Copyright Licensing Agency (U.K.) or the Copyright Clearance Center (U.S.A.). The CCC item-fee code for this publication is 0264-6021/2000/$16.00+0.00. Inquiries concerning reproduction outside those terms should be sent to the publishers at the above-mentioned address.
- Although, at the time of going to press, the information contained in this publication is believed to be correct, neither the authors nor the editors nor the publisher assume any responsibility for any errors or omissions herein contained.

- Periodicals postage paid at Rahway, NJ, and at additional mailing offices.
- **Postmaster:** send address changes to *Biochemical Journal*, c/o Mercury International, 365 Blair Road, Avenel, NJ 07001.
- **Cover illustration:** X-chromosomal location of mouse organic-anion-transporting polypeptide 1 (Oatp1) confirmed by a two-colour FISH analysis [see Hagenbuch et al. (2000) Biochem. J. **345**, 115–120].

Instructions to Authors

● **General policy** The *Biochemical Journal* publishes papers in English in all fields of biochemistry and cellular and molecular biology, provided that they make a sufficient contribution to biochemical knowledge Papers may include new results obtained experimentally, descriptions of new experimental methods of biochemical importance, or new interpretations of existing results Novel theoretical contributions will be considered equally with papers dealing with experimental work. All work presented should have as its aim the development of biochemical concepts rather than the mere recording of facts. Preliminary, confirmatory or inconclusive work will not be published The *Biochemical Journal* will not publish material that has been wholly or largely published elsewhere, even as a preliminary communication or in unrefereed symposium proceedings or on the World Wide Web (WWW), equally, fragmentation of research into the 'least publishable unit' is discouraged

Submission of a paper implies that it has been approved by all the named authors, that all persons entitled to authorship have been so named, that it reports unpublished work that is not under consideration elsewhere, and that if the paper is accepted for publication the authors will transfer to the Biochemical Society the copyright in the paper, which will then not be published elsewhere in the same form, in any language, without the consent of the Society. Authors will be required to sign an undertaking to these effects

Authors may suggest potential reviewers for their papers, but the journal is under no obligation to follow such suggestions. Authors may also specify the names of those they wish to be excluded from the review process, and such wishes are usually respected unless, in the opinion of the journal, such a request unreasonably excludes all the expertise available to it in that scientific area.

To allow the reviewers to assess possible overlap with previous work, all submitted papers must be accompanied by duplicate copies of the author's relevant published work, including that on the WWW, and of all related papers in press or under editorial consideration in this or other journals

The paragraphs below are a summarized version of the journal's complete Instructions to Authors (see http./www BiochemJ org), copies of which are available free of charge from the editorial office

The following types of paper are included in the journal

Research Papers are the normal form of publication, and may be of any length that is justified by their content. However, because of pressure for space in the journal, no paper, whatever its scientific merits, will be accepted if it exceeds the minimum length required for precision in describing the experiments and clarity in interpreting them As a guide, most Research Papers published in the *Biochemical Journal* are of between six and eight printed pages A concise well-written paper tends to be published more rapidly

Research Communications are short (maximum four printed pages) papers bringing particularly novel and significant findings to the attention of the research community It is intended that a decision on acceptance or rejection will be made within 10 working days of receipt, and publication of accepted Communications will follow within 2 months Research Communications receive full but accelerated reviewing The criteria of 'novelty and significance' are strictly enforced, and papers may be rejected solely on the grounds of lack of novelty and significance Communications are not a path to accelerated publication of sound but non-urgent material Authors must include in their letter of submission a brief statement of why they believe their Communication merits accelerated treatment Papers reporting nucleotide sequences only are not acceptable as Research Communications One colour figure will be published free of charge in Research Communications, subsequent figures will cost £300 each

Reviews will usually be solicited, although unsolicited reviews will be considered for publication Prospective writers of reviews should first consult the Reviews Editor, via the editorial office, and should enclose a short (one typed page) summary of the area they propose to cover

● **Procedure for submission** Before preparing papers for the journal, authors should consult a current issue to make themselves familiar with the general format, such as the use of cross-headings, layout of tables and figures and citation of references A full page of text in the *Biochemical Journal* contains approximately 1200 words, when calculating the printed length of papers, allowance must be made for the space occupied by tables and figures and the number of text words reduced accordingly.

The numerical system of references must be used A reference to 'unpublished work' must be accompanied by the names of all persons concerned, a reference to a 'personal communication' must be supported by written permission for the quotation from the person or persons concerned, both of these types of citation are permitted in the text only, not in the list of references

Three copies of the typescript (four copies for Research Communications), with a brief covering letter to which should be attached an additional copy of the synopsis, should be sent to **The Managing Editor, *Biochemical Journal*, 59 Portland Place, London W1N 3AJ, U.K.** (telephone 020 7637 5873; fax 020 7323 1136; from overseas the international code for the U K is 44 and the leading 0 should be omitted, e-mail editorial@portlandpress com)

The typescript should indicate the name, address, telephone number, fax number and e-mail address of the person to whom all correspondence should be addressed The top copy of the typescript should be marked as such and should have attached to it the original figures, for the other copies of the typescript, glossy prints (not photocopies) of the half-tone figures should be provided, but photocopies of line drawings will suffice A short (page-heading) title of not more than 75 characters and a maximum of five key words that do not appear in the title, should be provided

● **Submission by fax** Research Communications that do not contain half-tone or colour figures may be submitted by fax to the number above Only one copy of the typescript need be transmitted The current Instructions to Authors contains full details of this procedure

● **Electronic submission** Manuscripts may be submitted as a **single** Adobe Acrobat PDF file either (i) as a uuencoded attachment to the e-mail address editorial@portlandpress com; or (ii) uploaded to the ftp site ftp portlandpress com in the directory /incoming/BiochemJ [N B. Authors using route (ii) are advised to alert us to any incoming documents via our regular e-mail address.]

● **Colour figures** The first colour figure is published at no charge provided that one author has been a member of the Biochemical Society for at least 2 years and that the use of colour is deemed scientifically necessary by the reviewers Subsequent colour figures in the same paper cost £300 each

● **Multimedia adjuncts** The Biochemical Journal Online is now able to offer authors the opportunity to enhance their papers with multimedia adjuncts (e g time-lapse movies, three-dimensional structures) These will be submitted to peer review alongside the manuscript To submit a paper with a multimedia adjunct, please contact the Managing Editor (editorial@portlandpress com) There is no extra charge associated with the publication of a multimedia adjunct online

● **Use of authors' diskettes** Authors should submit diskettes of revised articles to the editorial office Every effort will be made to use the diskette during typesetting, but this cannot be guaranteed Authors must ensure that files have been updated to incorporate all revisions, and hence that the version on the diskette matches the revised hard copy. Our preferred word-processing format is Word for Windows version 6 Submission of manuscripts in other word-processing formats may lead to delays in processing The diskette should be accompanied by a covering letter specifying manuscript number, operating system and software program Files should be formatted double-spaced with no hyphenation and automatic wordwrap (no hard returns within paragraphs)

Other information

The *Biochemical Journal* is published and distributed by Portland Press Ltd on behalf of the Biochemical Society It is published twice monthly, in 2000 volumes 345–352 (three parts each) will appear The subscription also includes an author and key-word index

● **Subscription rates** Institutional subscription rates for 2000 are shown below Subscribers to the *Biochemical Journal* can subscribe additionally to *Biochemical Society Transactions* and *Biotechnology and Applied Biochemistry* on a joint subscription at a reduced rate Terms are cash with order (US$ in N America, £ sterling for rest of the world, or US$ equivalent at current rate of exchange; subscribers in the EU may pay in £ sterling or Euros), or against pro forma invoice Orders should be sent to the address below, or through your usual agent.

	N America	Rest of world	Euro price
One yr (8 vols)	US$1950	£1110	€1776
Single issues	US$97	£56	€90

Dollar prices include airspeeded delivery Sterling and Euro prices include airspeeded delivery in Europe and delivery by surface mail elsewhere Airspeeded delivery is available to countries other than America and Europe at an additional cost of £50

● **Biochemical Journal Online** Access to the Biochemical Journal Online is restricted to institutions that have a subscription to the print version It will be free to such institutions during 2000. URL· http //www BiochemJ org

● **Microfiche and back issues** Volumes 102–296 of the *Biochemical Journal* are available on microfiche Back issues are also available. Further details may be obtained from the address below.

● **Subscription department**
Portland Press Ltd
P O Box 32, Commerce Way
Colchester CO2 8HP, Essex, U K
(telephone 01206 796351, fax 01206-799331, e-mail sales@portlandpress com)

● **Advertising** Advertising is accepted in the *Biochemical Journal* For information contact the Advertising Department, Portland Press Ltd, 59 Portland Place, London W1N 3AJ (telephone 020 7580 5530, fax 020 7323 1136, e-mail editorial@portlandpress com).

Biochemical Journal
Volume 348, part 3
15 June 2000

First published on the Internet
7 June 2000
http://www.BiochemJ.org

Review

Retinoid-binding proteins: mediators of retinoid action *by* **N. Noy**		**481–495**

Research Papers

Proteins

Defensin-like peptide-2 from platypus venom: member of a class of peptides with a distinct structural fold	A.M. Torres, G.M. de Plater, M. Doverskog, L.C. Birinyi-Strachan, G.M. Nicholson, C.H. Gallagher and P.W. Kuchel	**649–656**

Enzymes

A novel lysine 2,3-aminomutase encoded by the *yodO* gene of *Bacillus subtilis*: characterization and the observation of organic radical intermediates	D. Chen, F.J. Ruzicka and P.A. Frey	**539–549**
Enzymic methylation of arginyl residues in -Gly-Arg-Gly- peptides	Y.-L. Hyun, D.B. Lew, S.H. Park, C.-W. Kim, W.K. Paik and S. Kim	**573–578**
Contrasting effects of N^5-substituted tetrahydrobiopterin derivatives on phenylalanine hydroxylase, dihydropteridine reductase and nitric oxide synthase	E.R. Werner, H.-J. Habisch, A.C.F. Gorren, K. Schmidt, L. Canevari, G. Werner-Felmayer and B. Mayer	**579–583**
Characterization of β-galactosidase mutations $Asp^{332} \rightarrow Asn$ and $Arg^{148} \rightarrow Ser$, and a polymorphism, $Ser^{532} \rightarrow Gly$, in a case of G_{M1} gangliosidosis	S. Zhang, R. Bagshaw, W. Hilson, Y. Oho, A. Hinek, J.T.R. Clarke, A. Hinek and J.W. Callahan	**621–632**
The molecular basis of phosphatidylcholine preference of human group-V phospholipase A_2	K.P. Kim, S.K. Han, M. Hong and W. Cho	**643–647**

Carbohydrates and lipids

Glycosylation-site-selective synthesis of *N*-acetyl-lactosamine repeats in bis-glycosylated human lysozyme	R. Melcher, A. Hillebrand, U. Bahr, B. Schröder, M. Karas and A. Hasilik	**507–515**
Atomic force microscopy of gastric mucin and chitosan mucoadhesive systems	M.P. Deacon, S. McGurk, C.J. Roberts, P.M. Williams, S.J.B. Tendler, M.C. Davies, S.S. (Bob) Davis and S.E. Harding	**557–563**

Gene structure and expression

Multiple conserved segments of E1 small nucleolar RNA are involved in the formation of a ribonucleoprotein particle in frog oocytes	D.D. Ruhl, M.E. Pusateri and G.L. Eliceiri	**517–524**
a new method for the section of protein interactions in mammalian cells	E. Rojo-Niersbach, D. Morley, S. Heck and N. Lehming	**585–590**
Sequence of the 5′-flanking region and promoter activity of the human mucin gene *MUC5B* in different phenotypes of colon cancer cells	I. Van Seuningen, M. Perrais, P. Pigny, N. Porchet and J.-P. Aubert	**675–686**

Regulation of metabolism

Auto-catalysed progression of aneuploidy explains the Hayflick limit of cultured cells, carcinogen-induced tumours in mice, and the age distribution of human cancer	D. Rasnick	**497–506**

Evidence that metformin exerts its anti-diabetic effects through inhibition of complex 1 of the mitochondrial respiratory chain	M R Owen, E Doran and A P Halestrap	**607–614**
Dynamics of haem oxygenase-1 expression and bilirubin production in cellular protection against oxidative stress	J E Clark, R. Foresti, C J Green and R. Motterlini	**615–619**

Membranes and bioenergetics

Determinant of the extracellular location of the N-terminus of human multidrug-resistance-associated protein	J-T Zhang	**597–606**
Activity of phosphatidylinositol transfer protein is sensitive to ethanol and membrane curvature	H Komatsu, B. Bouma, K W A Wirtz, T.F. Taraschi and N Janes	**667–673**

Receptors and signal transduction

Involvement of cytosolic phospholipase A_2, and the subsequent release of arachidonic acid, in signalling by Rac for the generation of intracellular reactive oxygen species in Rat-2 fibroblasts	C-H Woo, Z.-W. Lee, B-C Kim, K-S Ha and J-H Kim	**525–530**
G-protein coupling of μ-opioid receptors (OP_3): elevated basal signalling activity	N T Burford, D. Wang and W Sadée	**531–537**
Ligand binding directly stimulates ubiquitination of the inositol 1,4,5-trisphosphate receptor	C-C Zhu and R J H Wojcikiewicz	**551–556**
Repression of transforming-growth-factor-β-mediated transcription by nuclear factor κB	R P Nagarajan, F. Chen, W Li, E Vig, M A. Harrington, H. Nakshatri and Y. Chen	**591–596**
Modulation of the smooth-muscle L-type Ca^{2+} channel α1 subunit (α1C-b) by the β_2a subunit: a peptide which inhibits binding of β to the I-II linker of α1 induces functional uncoupling	A Hohaus, M. Poteser, C Romanin, N Klugbauer, F Hofmann, I. Morano, H Haase and K Groschner	**657–665**

Cell biology and development

Annexin II is associated with mRNAs which may constitute a distinct subpopulation	A. Vedeler and H Hollås	**565–572**
Possible interference between tissue-non-specific alkaline phosphatase with an $Arg^{54} \rightarrow$ Cys substitution and a counterpart with an $Asp^{277} \rightarrow$ Ala substitution found in a compound heterozygote associated with severe hypophosphatasia	M. Fukushi-Irié, M. Ito, Y. Amaya, N Amizuka, H. Ozawa, S. Omura, Y Ikehara and K Oda	**633–642**

Correction

G_i-mediated translocation of GLUT4 is independent of p85/p110α and p110γ phosphoinositide 3-kinases but might involve the activation of Akt kinase *by* L Wang, H Hayashi, K. Kishi, L. Huang, A. Hagi, K. Tamaoka, P.T. Hawkins and Y. Ebina (volume 345, pages 543–545, 2000)	**687**

Index of Authors

PAGE
Amaya, Y 633
Amizuka, N. 633
Aubert, J.-P 675

Bagshaw, R 621
Bahr, U. 507
Birinyi-Strachan, L C. 649
Bouma, B 667
Burford, N T. 531

Callahan, J W. 621
Canevari, L 579
Chen, D. 539
Chen, F 591
Chen, Y. 591
Cho, W. 643
Clark, J E. 615
Clarke, J T. R. 621

Davies, M. C 557
Davis, S S (Bob) 557
Deacon, M. P 557
de Plater, G M. 649
Doran, E 607
Doverskog, M 649

Ebina, Y. 687
Eliceiri, G L 517

Foresti, R 615
Frey, P. A 539
Fukushi-Irié, M 633

Gallagher, C. H. 649
Gorren, A C. F. 579

PAGE
Green, C. J 615
Groschner, K 657

Ha, K-S. 525
Haase, H 657
Habisch, H-J 579
Hagi, A 687
Halestrap, A P. 607
Han, S K 643
Harding, S E 557
Harrington, M A. 591
Hasilik, A 507
Hawkins, P T 687
Hayashi, H 687
Heck, S. 585
Hillebrand, A 507
Hilson, W. 621
Hinek, Aleksander 621
Hinek, Alina 621
Hofmann, F 657
Hohaus, A 657
Hollås, H. 565
Hong, M 643
Huang, L 687
Hyun, Y-L 573

Ikehara, Y 633
Ito, M 633

Janes, N 667

Karas, M 507
Kim, B.-C. 525
Kim, C.-W. 573
Kim, J.-H. 525

PAGE
Kim, K P 643
Kim, S 573
Kishi, K. 687
Klugbauer, N 657
Komatsu, H 667
Kuchel, P W. 649

Lee, Z.-W 525
Lehming, N. 585
Lew, D. B 573
Li, W 591

Mayer, B 579
McGurk, S 557
Melcher, R 507
Morano, I 657
Morley, D 585
Motterlini, R. 615

Nagarajan, R. P 591
Nakshatri, H. 591
Nicholson, G M. 649
Noy, N 481

Oda, K. 633
Oho, Y. 621
Omura, S. 633
Owen, M R 607
Ozawa, H 633

Paik, W-K 573
Park, S H. 573
Perrais, M 675
Pigny, P 675
Porchet, N 675

PAGE
Poteser, M 657
Pusateri, M E 517

Rasnick, D 497
Roberts, C. J 557
Rojo-Niersbach, E 585
Romanin, C 657
Ruhl, D D. 517
Ruzicka, F. J. 539

Sadée, W 531
Schmidt, K 579
Schröder, B 507

Tamaoka, K 687
Taraschi, T. F 667
Tendler, S J. B 557
Torres, A M 649

Van Seuningen, I. 675
Vedeler, A 565
Vig, E 591

Wang, D. 531
Wang, L 687
Werner, E R 579
Werner-Felmayer, G. 579
Williams, P M. 557
Wirtz, K W A. 667
Wojcikiewicz, R. J. H 551
Woo, C.-H 525

Zhang, J.-T. 597
Zhang, S. 621
Zhu, C-C. 551

Index of Authors
Volume 348, 2000

PAGE
Acosta, M 321
Akahori, M 409
Aledo, J C 257
Alonso, F J 257
Amaya, Y 633
Amizuka, N 633
Annan, R S 263
Ariga, M 409
Arion, D 77
Arnao, M B 321
Arthur, J S C 37
Aubert, J-P 675

Bagshaw, R 621
Bahr, U 507
Baker, J R 465
Bandyopadhyay, A 173
Baranyi, L 151
Barbier-Brygoo, H 291
Barouki, R 235
Baumeister, S 417
Beattie, J H 55
Béliveau, R 273
Bianchi, R 307
Binnyi-Strachan, L C 649
Bishop, A L 241
Blobel, C P 21
Bodin, S 107
Bosco, D 215
Bouma, B 667
Boutabout, M 337
Brachet, P 401
Brand, M D 209
Brinck, J 29
Briskin, M J 29
Broekaert, D 55
Brzozowski, A M 201
Burford, N T 531
Burgaya, F 119
Burger, F 329

Cadenas, S 209
Caldas, C 447
Calero, M 359
Callahan, J W 621
Canevan, L 579
Carde, J-P 291
Chabanon, H 401
Chan, L C 447
Chao, Y-C 473
Chap, H 107
Chen, D 539
Chen, F 591
Chen, S L 263
Chen, S-L 473
Chen, Y 591
Cheniclet, C 291
Cheung, N 447
Chevalier, J 223
Chew, S L 447
Chi, C-W 425
Chittattu, A 183
Cho, W 643
Chou, H-K 473
Christie, G 137
Chung, B-c 439
Chung, S K 447
Clark, A E 83
Clark, J E 615
Clarke, J T R 621
Cohen, G M 93
Colonna, A 315
Costa, A 119
Coulonval, K 351
Creasy, C L 263
Cygler, M 37

Damas, A M 167

PAGE
Dauter, M 201
Davies, G J 201
Davies, M C 557
Davis, J B 137
Davis, S S (Bob) 557
Deacon, M P 557
Dennis, R D 417
de Plater, G M 649
Dickens, M 93
Do, S-H 229
Dombrowski, F 183
Doran, E 343, 607
Doverskog, M 649
Driessen, A J M 367
Dumont, J E 351
Dupret, J-M 159
Dutt, P 37

Ebina, Y 687
Elce, J S 37
Elcein, G L 517
Ellis, E M 389
Erneux, C 107
Eyckerman, S 55
Ezan, P 119

Fein, A 189
Feinstein, M B 189
Ferrara, M 401
Festa, M 315
Foresti, R 615
Forloni, G 307
Fox, S R 145
Frangione, B 359
Frey, P A 539
Fukuma, N 375
Fukushi-Irié, M 633
Furstenberger, G 329

Galbete, J L 307
Gallagher, C H 649
García-Cánovas, F 321
Gelman, M 119
George, A 137
Geyer, R 417
Ghiso, J 359
Gingras, D 273
Girault, J-A 119
Giuriato, S 107
Goodfellow, G H 159
Gorren, A C F 579
Grant, D M 159
Green, C J 615
Grochulski, P 37
Groschner, K 657
Guclu, J 291
Gunaratne, R S 459
Guntaka, R V 297

Ha, K-S 525
Haase, H 657
Habisch, H-J 579
Hagi, A 687
Hakuno, F 409
Halestrap, A P 343, 607
Hall, A 241
Han, S K 643
Harding, S E 557
Harrington, M A 591
Hasilik, A 507
Haussinger, D 183
Hawkins, J 137
Hawkins, P T 687
Hayashi, H 687
Hayes, J D 389
Heck, S 585
Heldin, P 29

PAGE
Hew, C L 439
Hillebrand, A 507
Hills, M J 145
Hilson, W 621
Hinek, Aleksander 621
Hinek, Alina 621
Hiner, A N P 321
Hofmann, F 657
Hohaus, A 657
Holder, A A 459
Hollås, H 565
Holman, G D 83
Hong, M 643
Howard, L 21
Howlett, D R 137
Hsu, C-T 473
Huang, L 687
Hyun, Y-L 573

Ikehara, Y 633
Ireland, L S 389
Ito, M 633
Ito, Y 409
Iynedjian, P B 215

Jacobson, A 29
Janes, N 667
Jennings, K H 137
Jepras, R 137
Jiang, X 113
Johnson, P E 145
Jungermann, K 433

Kamel-Reid, S 63
Kanda, T 71
Karas, M 507
Karran, E H 137
Kassis, S 263
Kaushik, N 77
Kelly, V P 389
Kietzmann, T 433
Kim, B-C 525
Kim, C-W 573
Kim, D H 173
Kim, H-N 229
Kim, J-H 525
Kim, K P 643
Kim, S 573
Kimura, T 71
Kishi, K 687
Klugbauer, N 657
Kobayashi, I 71
Komatsu, H 667
Kon, J 71
Kondo, T 375
Kozma, S C 351
Krieg, P 329
Krones, A 433
Kubitz, R 183
Kuchel, P W 649
Kudlow, J E 281
Kumar, A 359
Kuwabara, A 71

Ladu, M J 359
Lamy, F 351
Lamy, S 273
LaPlante, J M 189
Lee, H-C 425
Lee, J C 263
Lee, K-Y 229
Lee, Z-W 525
Lehming, N 585
Lew, D B 573
Li, W 591
Lichty, B D 63
Lim, H 77
Lin, W-w 439

PAGE
Ling, I T 459
Liu, D 439
Liu, S C H 83
Livi, G P 263
Lloyd Raven, E 321
Lobo, C 257
Lochnit, G 417
Lu, C-Y 425
Lu, X 189
Lunn, C 291

MacFarlane, M 93
Maciewicz, R A 21
Malléa, M 223
Marks, F 329
Márquez, J 257
Matsubara, E 359
Maurel, C 291
Mayer, B 579
McAbee, D D 113
McGurk, S 557
Meda, P 215
Melcher, R 507
Melhuish, T 263
Mima, S 375
Mizushima, T 375
Modena, P 307
Morano, I 657
Morel, Y 235
Morley, D 585
Motterlini, R 615
Muller, J P 367

Nagarajan, R P 591
Nakshatri, H 591
Nambiar, A 297
Nedachi, T 409
Neville, W 137
Nicholson, G M 649
Noy, N 481
Núñez de Castro, I 257

Oda, K 633
Oho, Y 621
Ohta, H 71
Okajima, F 71
Olsen, A 189
Omura, S 633
O'Rourke, F 189
Oudart, H 129
Owen, D E 137
Owen, M R 607
Ozawa, H 633
Ozegowski, J 367

Pachebat, J A 459
Pagès, J-M 223
Paik, W-K 573
Park, S H 573
Parniak, M A 77
Parodi, A J 1
Paterson, A J 281
Payrastre, B 107
Peressini, E 307
Permanne, B 359
Perrais, M 675
Persson, L 401
Phillips, M A 45
Pietropaolo, C 315
Pigny, P 675
Plantavid, M 107
Porchet, N 675
Poteser, M 657
Pritchard, D G 465
Pryor, P R 83
Pusateri, M E 517

Qin, Q 45

PAGE
Raclot, T 129
Rankin, J 15
Rasnick, D 497
Rawsthorne, S 145
Redondo, C 167
Rice, R H 45
Rickhoff, S 417
Roberts, C J 557
Rodríguez-López, J N 321
Rodriguez-Martin, T 307
Rojo-Niersbach, E 585
Romanin, C 657
Roos, M D 281
Rostagno, A 359
Rubinsztein, D C 15
Ruffo, A 315
Ruhl, D D 517
Ruiz-Bellido, M A 257
Ruzicka, F J 539

Sadée, W 531
Saha, N 183
Sajid, M 459
Sakamoto, H 409
Saraiva, M J M 167
Sato, K 71
Schmidt, K 579
Schroder, B 507

PAGE
Schulein, M 201
Sekimizu, K 375
Sham, M H 447
Shin, D -W 173
Slack, B E 381
Sluis-Cremer, N 77
Smith, J D 359
So, C K C 447
So, C W 447
Soboslay, P T 417
Spicer, A P 29
Stein, R C 351
Studler, J -M 119
Su, K 281
Sui, S -F 103
Sum, C 439
Sun, Y -T 103
Swamynathan, S K 297
Swaving, J 367

Takahashi, S -I 409
Tamama, K -i 71
Tamaoka, K 687
Taraschi, T F 667
Tavernier, J 55
Tendler, S J B 557
Tokuda, T. 359
Tolnay, M 151

PAGE
Tomura, H 71
Torres, A M 649
Tosh, D 83
Toutant, M 119
Tripathi, R 459
Tsao, Y -P 473
Tsokos, G C 151
Tsuchiya, T 375

Ui, M 71

Vandekerckhove, J 55
Vandeput, F 351
Van Seuningen, I 675
van Wely, K H M 367
Varrot, A 201
Vedeler, A 565
Verhee, A 55
Vettermann, S 367
Vidal, R 359
Vig, E 591

Waelput, W 55
Wallace, H M 401
Walsh, K B 113
Wang, D 531
Wang, H -W 439
Wang, L 687

PAGE
Wang, S -X 103
Ward, R V 137
Watanabe, T 71
Wei, Y -H 425
Werner, E R 579
Werner-Felmayer, G 579
Wettstein, M 183
Wiedemann, L M 447
Wilhelm, F -X 337
Wilhelm, M 337
Williams, P M 557
Wirtz, K W A 667
Wojcikiewicz, R J H 551
Woo, C -H 525
Woscholski, R 107
Wuhrer, M 417
Wyttenbach, A 15

Yang, J 83
Yang, X 281
Yin, P -H 425

Zhang, J -T 597
Zhang, S 621
Zhu, C -C 551
Zlokovic, B 359

Biochem J (2000) 348, 481–495 (Printed in Great Britain)

REVIEW ARTICLE

Retinoid-binding proteins: mediators of retinoid action

Noa NOY[1]
Division of Nutritional Sciences, Cornell University, Ithaca, NY 14853, U.S.A.

Active vitamin A metabolites, known as retinoids, are essential for multiple physiological processes, ranging from vision to embryonic development. These small hydrophobic compounds associate *in vivo* with soluble proteins that are present in a variety of cells and in particular extracellular compartments, and which bind different types of retinoids with high selectivity and affinity. Traditionally, retinoid-binding proteins were viewed as transport proteins that act by solubilizing and protecting their labile ligands in aqueous spaces. It is becoming increasingly clear, however, that, in addition to this general role, retinoid-binding proteins have diverse and specific functions in regulating the disposition, metabolism and activities of retinoids. Some retinoid-binding proteins appear to act by sequestering their ligands, thereby generating concentration gradients that allow cells to take up retinoids from extracellular pools and metabolic steps to proceed in energetically unfavourable directions. Other retinoid-binding proteins regulate the metabolic fates of their ligands by protecting them from some enzymes while allowing metabolism by others. In these cases, delivery of a bound retinoid from the binding protein to the 'correct' enzyme is likely to be mediated by direct and specific interactions between the two proteins. One retinoid-binding protein was reported to enhance the ability of its ligand to regulate gene transcription by directly delivering this retinoid to the transcription factor that is activated by it. 'Channelling' of retinoids between their corresponding binding protein and a particular protein target thus seems to be a general theme through which some retinoid-binding proteins exert their effects.

Key words: metabolism, retinoids, transport, vitamin A.

INTRODUCTION

Dietary vitamin A gives rise to a variety of active metabolites, collectively known as retinoids. Chemically, retinoids are composed of three distinct structural domains: a β-ionone ring, an isoprenoid tail, and a polar end-group with an oxidation state that may vary: a hydroxyl group in retinols, an aldehyde in retinals, and a carboxylic moiety in retinoic acids (Figure 1). These small lipophilic compounds exhibit multiple and diverse biological activities. One retinoid, 11-*cis*-retinal, is critical for the visual function [1]. Other vitamin A metabolites, i.e. all-*trans*- and 9-*cis*-retinoic acids, are potent regulators of gene transcription, and play important roles in regulating cell proliferation and differentiation [2] Vitamin A-derived *retro*-retinoids were implicated in regulating immune function by controlling lymphocyte survival [3]. The multiple biological actions of retinoids are mediated by two classes of proteins: retinoid receptors and retinoid-binding proteins. Retinoid receptors are ligand-inducible transcription factors that belong to the superfamily of nuclear hormone receptors, and which are activated by stereoisomers of retinoic acid. Discussion of these proteins is beyond the scope of the present review. The term retinoid-binding proteins is used to describe soluble proteins that are found in a variety of tissues and that associate with specific retinoids. The aim of this review is to consider current knowledge on the spectrum of roles that retinoid-binding proteins play in mediating the biological activities of their ligands.

Retinoid-binding proteins

Multiple types of retinoid-binding proteins that associate with different chemical and isomeric forms of retinoids have been identified both intracellularly and in particular extracellular compartments. Hence retinoids are found *in vivo* either associated with cellular membranes or bound to a specific retinoid-binding protein. The parent vitamin A molecule, all-*trans*-retinol, circulates in blood bound to serum retinol-binding protein (RBP). Inside cells, all-*trans*-retinol and its oxidation product, all-*trans*-retinal, are associated with one of the two isoforms of cellular retinol-binding proteins (CRBP-I and CRBP-II). all-*trans*-Retinoic acid is found intracellularly bound to one of the two cellular retinoic acid-binding protein isoforms (CRABP-I and CRABP-II). The visual pigment 11-*cis*-retinal and its precursor, 11-*cis*-retinol, associate in several cell types in the eye with cellular retinal-binding protein (CRALBP). Another ocular protein that can bind retinoids, the interphotoreceptor retinoid-binding protein (IRBP), is present in the extracellular space separating pigment epithelium and photoreceptor cells.

Retinoid-binding proteins are believed to share a common role, in that they act to solubilize and stabilize their hydrophobic and labile ligands in aqueous spaces. However, a growing body of information indicates that, in addition to this general role, specific retinoid-binding proteins have distinct functions in regulation of the transport, metabolism and action of the particular retinoids with which they associate. Of the numerous types of known retinoid-binding proteins, this review considers only those for which such specific functions have been documented (Table 1)

STRUCTURE

With the exception of CRALBP and IRBP, known retinoid-binding proteins belong to two protein families that were

---

Abbreviations used: ARAT, acyl-CoA retinol acyltransferase, CRABP, cellular retinoic acid-binding protein, CRALBP, cellular retinal-binding protein, CRBP, cellular retinol-binding protein, DHA, docosahexaenoic acid, iLBP, intracellular lipid-binding protein, IPM, interphotoreceptor matrix, IRBP, interphotoreceptor retinoid-binding protein, LRAT, lecithin retinol acyltransferase, RAR, retinoic acid receptor, RBP, serum retinol-binding protein The terms retinol, retinal and retinoic acid designate the respective all-*trans*-isomers unless specified otherwise.

[1] e-mail nn14@cornell.edu

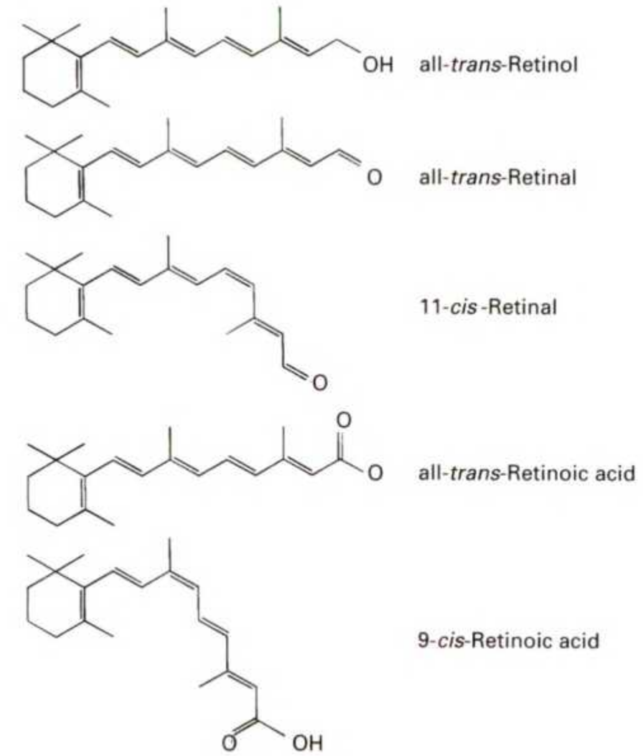

Figure 1 Chemical structures of some biologically active retinoids

Table 1 Characteristics of some retinoid-binding proteins

References: [a] [76] (rat RBP); [b] [57,60,149] (rat CRBP-I); [c] [150] (rat CRBP-II); [d] [101] (human CRABP-I, human CRABP-II); [e] N. Noy and J. C. Saari, unpublished work (bovine CRALBP); [f] [22]; N. Shaw and N. Noy, unpublished work (bovine IRBP).

Protein	Family	Molecular mass (kDa)	Major ligand(s)	K_d (nM)	No. of sites
RBP	Lipocalin	21.0	all-*trans*-Retinol	20^a	1
CRBP-I	iLBP	15.0	all-*trans*-Retinol all-*trans*-Retinal	$< 10^b$ 50^b	1
CRBP-II	iLBP	15.0	all-*trans*-Retinol all-*trans*-Retinal	$\sim 100 \times K_d$ of CRBP-I^c 90^b	1
CRABP-I	iLBP	14.0	all-*trans*-Retinoic acid	0.06^d	1
CRABP-II	iLBP	14.0	all-*trans*-Retinoic acid	0.13^d	1
CRALBP	–	36.0	11-*cis*-Retinol 11-*cis*-Retinal	 $\sim 15^e$	1
IRBP	–	136.0	all-*trans*-Retinol 11-*cis*-Retinal	$50–100^f$ $50–100^f$	3^f

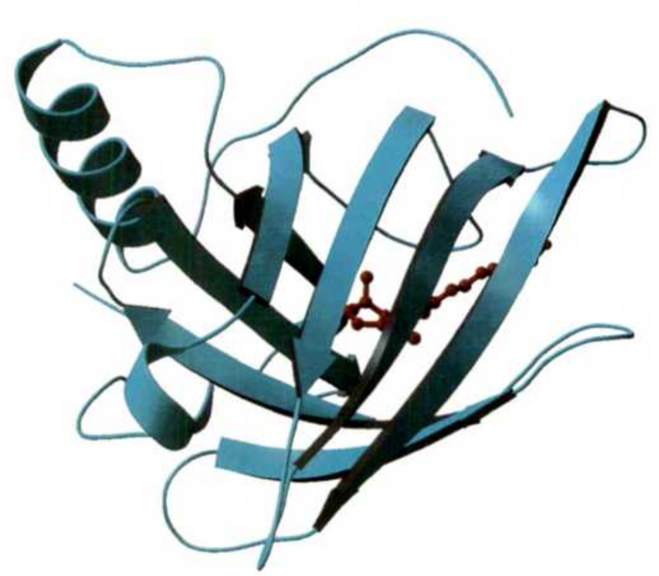

Figure 2 Ribbon drawing of the three-dimensional structure of bovine holo-RBP

Bound retinol is depicted in red. The figure was generated by using the co-ordinates of bovine holo-RBP reported in [148].

originally classified as transport proteins for hydrophobic ligands: the lipocalins and the intracellular lipid-binding proteins (iLBPs). Excellent reviews on the structural relationships between lipocalins and iLBPs have been published [4,5] and these issues are only discussed briefly here.

Lipocalins

Members of the lipocalin family, including the retinoid-binding proteins RBP, epididymal retinoic acid-binding protein and β-lactoglobulin, share a very low sequence identity but display a highly conserved overall fold. They are composed of an eight-stranded antiparallel β-sheet that is folded over itself to form a hydrogen-bonded β-barrel, which constitutes the ligand binding pocket (Figure 2). The *N*-termini of these proteins are folded around the back of the barrel, 'capping' that side of the pocket. In contrast, the front of the β-barrel is open to provide a portal for the ligand. The entrance is flanked by a single loop scaffold. The ligand-binding sites of different lipocalins differ in their structural details, conferring distinct ligand selectivity [4]. In RBP, the β-barrel completely encapsulates the bound retinol, with the β-ionone ring innermost and the hydroxy head-group reaching to the protein surface, where it is co-ordinated to a water molecule at the pocket entrance [6]. The interactions of retinol within RBP are stabilized mainly by hydrophobic interactions of the β-ionone ring and the isoprenoid chain with amino acid residues that line the interior of the pocket, whereas the hydroxyl group does not contribute significantly to ligand–protein interactions [6,7]. In addition to binding their hydrophobic ligands, many lipocalins interact with accessory proteins. RBP is bound in blood to transthyretin, a tetrameric protein with a molecular mass of ~ 55 kDa. This interaction is believed to protect the small RBP molecule from filtration by renal glomeruli, thereby retaining it in blood [8]. The interactions between RBP and transthyretin are mediated through the loop at the entrance of the ligand-binding pocket [9], and also involve amino acid residues at the RBP C-terminus [10].

iLBPs

By sequence identity, CRBPs and CRABPs belong to the family of iLBPs, which also includes the fatty acid-binding proteins. Like lipocalins, iLBPs bind their hydrophobic ligands within an antiparallel β-barrel structure. The β-barrel of iLBPs is constructed of two orthogonal, five-stranded, β-sheets that form a ligand binding pocket, with a helix–turn–helix motif at the entrance to the pocket [11–13] (see Figure 3). A striking difference between the mode by which lipocalins and iLBPs bind their

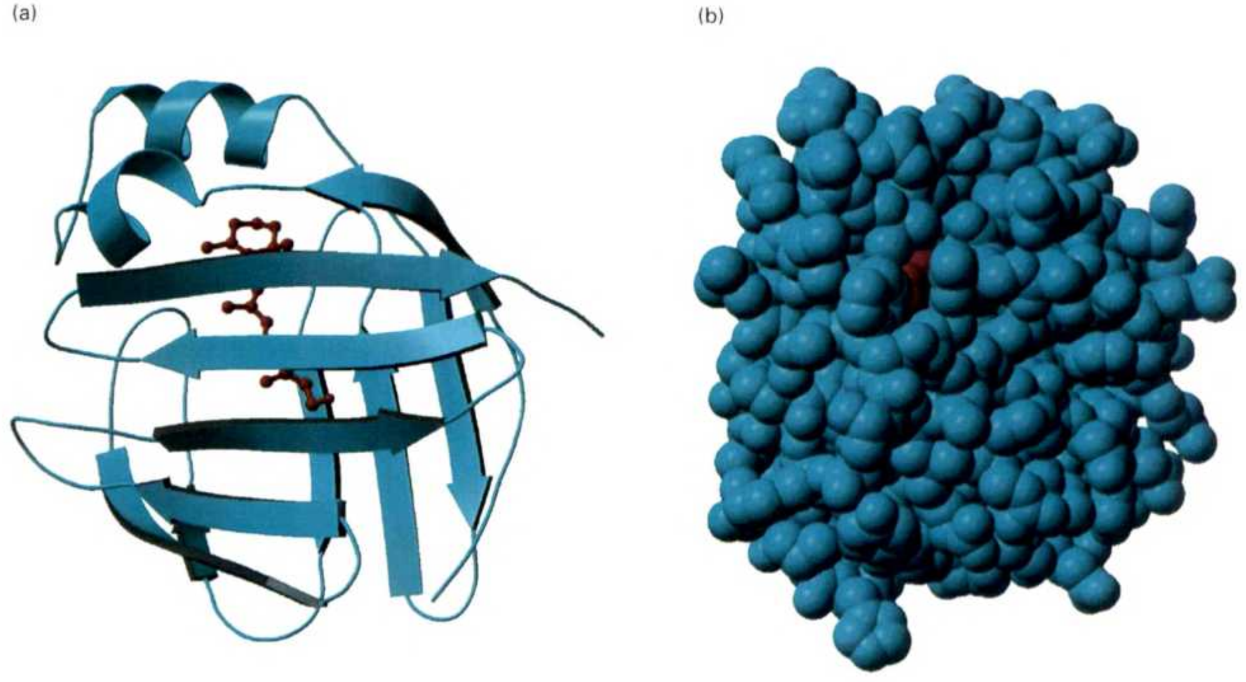

Figure 3 Three-dimensional structure of human holo-CRBP-I

(**a**) Ribbon drawing of the three-dimensional structure of CRBP-I with bound retinol (red). (**b**) Space-filling model of holo-CRBP-I, emphasizing the limited accessibility of bound retinol to the bulk solution. The figures were generated by using the co-ordinates of human holo-CRBP-I reported in [58].

ligands is the reversal of the binding orientation. Thus, in contrast with the orientation of retinol within the RBP binding site, iLBP ligands are oriented such that their polar groups are buried deep in the binding pockets and are co-ordinated to specific polar amino acid residues in this region. In both CRBPs and CRABPs, the β-ionone ring of retinol or retinoic acid is close to the surface of the respective protein, where it fits snugly within the entrance. Similarly to lipocalins, the N-terminus of the iLBP wraps around the back of the barrel, making that side inaccessible to the bulk solution. However, the front of the barrel in CRBPs and CRABPs is flanked by two α-helices that appear to limit access to the binding site [13] (Figure 3). An interesting question that thus arises is how the bound ligand exits the binding pocket to reach its sites of metabolism. Similarly, the closed structure of the binding pocket brings into question the mechanism by which the ligand can gain access to the site. The crystal structures of apo-CRABP-I [14] and -CRABP-II [11] indicate that these proteins crystallize as dimers, and that the pocket entrance is somewhat more open than that observed in the holoprotein. It was thus suggested that dimer formation constitutes a mechanism that allows better accessibility of the binding site. However, recent NMR studies have revealed that apo-CRABP-II is monomeric in solution, and that the entrance to the binding pocket of the apoprotein is greatly enlarged and readily accessible as compared with the holoprotein [12]. Similarly, NMR studies of the solution structure of apo-CRBP-II revealed the presence of an opening that can potentially accommodate initial entry of the polar end of the retinol molecule [15].

Ocular retinoid-binding proteins

The two retinoid-binding proteins that are found specifically in retina and neural tissue, CRALBP and IRBP (Table 1), do not belong to either the lipocalin or the iLBP family, and their structural make-ups are poorly understood. CRALBP is notably similar to two other lipid-binding proteins: tocopherol transfer protein, a liver protein that interacts specifically with the α-conformer of tocopherol [16], and SEC14, which serves as a transfer protein for phosphatidylinositol in yeast [17]. Recent studies have indicated that the retinoid-binding pocket of CRALBP is located at the C-terminus, and have implicated residues Gln^{210} and Lys^{221} in serving to stabilize ligand binding by this protein [18].

IRBP is unique among retinoid-binding proteins in that it contains three binding sites for retinoids as well as one or two binding sites for long-chain fatty acids ([19–22]; N. Shaw and N. Noy, unpublished work). This protein is also unusual in that it can associate with multiple chemical and isomeric forms of retinoids although, in accordance to its proposed role, it displays the highest affinity towards the retinoids that are important in the visual cycle, i.e. 11-*cis*-retinal and all-*trans*-retinol [23]. Bovine IRBP can associate with 2 mol of all-*trans*-retinol or 2 mol of 11-*cis*-retinal per mol of protein. One of the protein's retinoid-binding sites displays a broad ligand selectivity and can accommodate either all-*trans*-retinol or 11-*cis*-retinal with similar affinities [23]. The two additional sites display narrower specificities for retinol and retinal, respectively ([22]; N. Shaw and N. Noy, unpublished work). The thermodynamic characteristics of the interactions of all-*trans*-retinol with IRBP indicate that association of retinol with both of its sites is stabilized mainly by hydrophobic interactions, that neither of the sites requires the hydroxy head-group for binding, and that, nevertheless, the two sites are structurally distinct [24].

The primary sequence of mammalian IRBP reveals four 300-residues-long repeats of homologous stretches. An additional 55-residue extension comprises the C-terminus of the protein [25,26].

It was proposed that conservative hydrophobic sequences located near the C-termini of each of the four repeats may be involved in binding of retinoids and/or fatty acids [26]. In contrast with the mammalian and amphibian proteins, IRBP in teleosts is composed of only two homologous repeats, corresponding to the N-terminal and C-terminal repeats of the mammalian protein [27]. Proteins that share sequence identity with IRBP have also been identified in bacteria and plants. One of these, Tsp, is a periplasmic protease of *Escherichia coli* that has been implicated in playing a role in fatty acid transport [28].

FUNCTIONS

It is becoming increasingly clear that the traditional view that retinoid-binding proteins act mainly as aqueous storage compartments for retinoids is far from being complete. Rather, accumulated evidence indicates that many of these proteins play specific roles in regulating the transport, metabolism and action of their ligands. Retinoid-binding proteins associate with their ligands with affinities in the nanomolar range (Table 1). An important general question that arises regarding their functions is: how do these proteins release the ligands at their sites of metabolism or action? Theoretically, a ligand can move from a donor (the respective binding protein) to an acceptor (the appropriate target) by one of two possible mechanisms. In the first model, the ligand dissociates from the donor, diffuses through the aqueous space, and binds to an acceptor, if such is present (Figure 4a). In this model, the activity of the target will rely on the aqueous pool of the ligand, the transfer process will be driven by concentrations gradients, and its rate will be limited by the rate of dissociation of the donor–ligand complex. Alternatively, a donor may engage in direct interactions with an acceptor, transferring the ligand by 'channelling' between the two proteins (Figure 4b). Such a process will bypass the aqueous space and may result in facilitation of transfer. Available information indicates that, while some retinoid-binding proteins exert their effects simply by binding their ligands and releasing them to the bulk solution, thereby generating concentration gradients, some of these proteins can deliver their ligands to target proteins via direct protein–protein interactions. Direct targets that have been suggested include enzymes that utilize particular retinoids as their substrates, and, in one documented case, a transcription factor that is activated by a retinoid.

Functions of RBP

Retinol is secreted from its storage pools and circulates in blood bound to RBP. The main storage site for vitamin A and, correspondingly, the main site of synthesis of RBP, is the liver, although other tissues (including adipose tissue, kidney, lung, heart, skeletal muscle, spleen, eye and testis) express this protein. Secretion of RBP from the liver is tightly regulated by the availability of retinol. In vitamin A deficiency, RBP secretion is inhibited and the protein accumulates in the endoplasmic

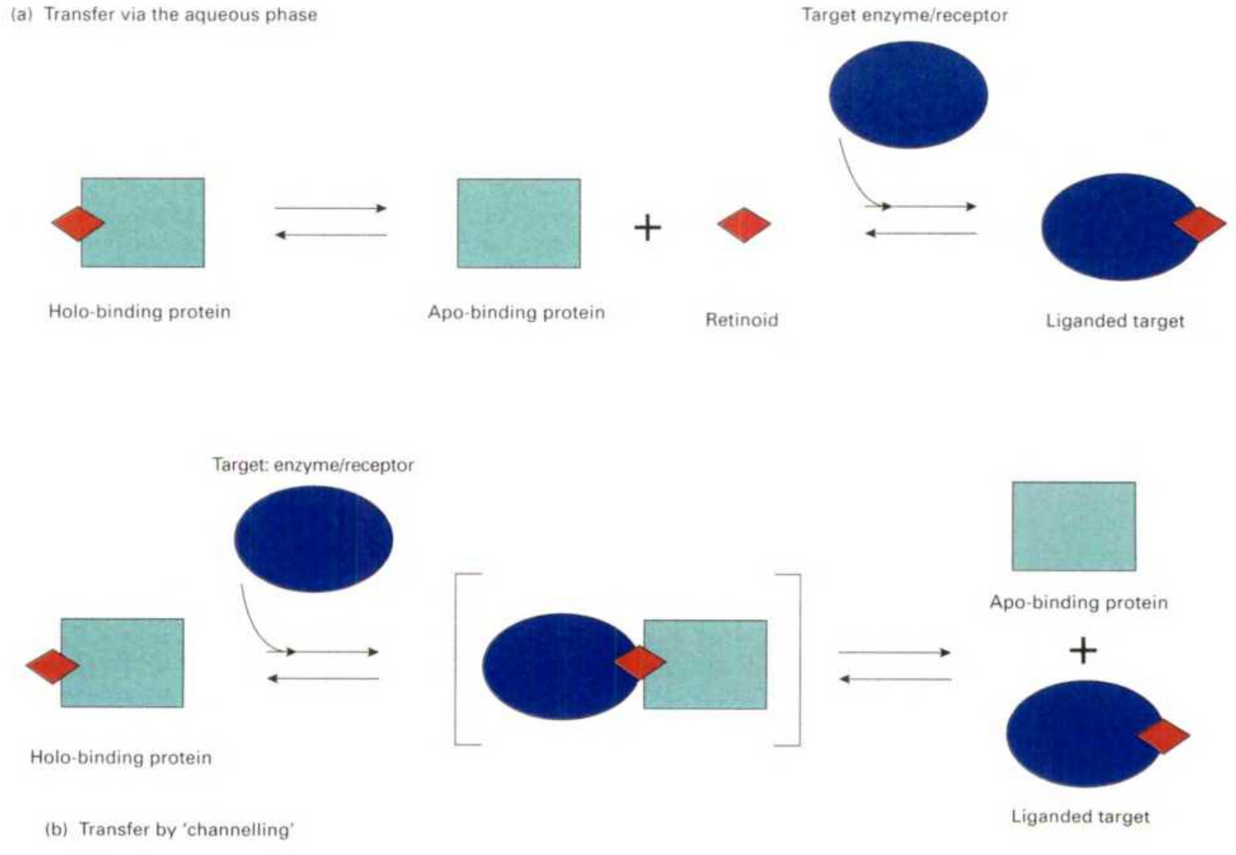

Figure 4 Pathways by which a ligand may transfer from a donor protein to an acceptor

(**a**) Transfer may require dissociation of the donor–ligand complex prior to diffusion of the ligand through the aqueous phase and its association with the acceptor. (**b**) Transfer may be mediated by direct interactions between the donor and the acceptor in a 'channelling' process. This process may result in facilitation of the formation of the acceptor–ligand complex.

reticulum of hepatic parenchymal cells. In the presence of retinol, RBP associates with retinol, moves to the Golgi apparatus and is secreted into blood in the form of the holoprotein [29]. The mechanism by which retinol initiates secretion of RBP from cells is unknown, but appears to be conserved in yeast ectopically expressing RBP [30]. In blood, RBP is bound to transthyretin, which, in addition to associating with RBP, functions as a carrier protein for thyroid hormones. Binding of RBP to transthyretin serves to prevent the loss of the smaller protein from the circulation by filtration in the renal glomeruli. The ternary complex transthyretin–RBP–retinol thus serves to transport retinol in the circulation and to deliver it to target tissues. It has been established that retinol enters most of its target cells (though perhaps not all, see [31,32]) in the form of free retinol, unaccompanied by the binding protein [8,29].

The exact role that RBP plays in regulating vitamin A uptake by extrahepatic cells is controversial, and two alternative views have been presented. On the one hand it has been proposed that a receptor embedded in the plasma membranes of target cells mediates transfer of retinol from RBP, across the membrane and into cytosol, or perhaps directly to the protein that binds retinol in cells, CRBP [33–39]. The function of the 'RBP receptor' has been assigned to a 65 kDa protein (Rpe65) which was originally identified in retinal pigment epithelium cells [36–40]. However, the ability of Rpe65 to act as a plasma membrane receptor for RBP has been questioned in view of its primary sequence, which lacks hydrophobic regions that would allow it to integrate into a membrane, and of immunolocalization studies which localized it intracellularly [41,42]. In addition, a recent study of Rpe65-deficient mice showed that the retinal pigment epithelium of these mice overaccumulates all-*trans*-retinyl esters but contains undetectable levels of 11-*cis*-retinyl esters [43]. These observations suggest that Rpe65 is not essential for uptake of retinol by the pigment epithelium, but rather that it is critical for conversion of all-*trans*-retinoids into the 11-*cis*-isomers in these cells.

An alternative view regarding the mechanism by which retinol leaves RBP in the plasma and enters target cells stemmed from the consideration that, because of the hydrophobic nature of retinol, cellular membranes do not constitute a barrier to it. Indeed, it was shown that retinol spontaneously crosses membranes at rates of the order of ms, that its dissociation from lipid bilayers is characterized by a $t_{\frac{1}{2}}$ of about 1 s, and that it rapidly partitions between proteins and membranes [7,44]. It was shown further that binding to RBP is not required for movement of retinol into or out of cells [45–47]. It was thus proposed that cellular uptake of retinol from RBP in blood occurs spontaneously and simply follows the concentration gradients of free retinol [45,46,48–50]. In support of this model, reported rates of uptake of retinol by several target cells are two to three orders of magnitude lower than the rate of the spontaneous dissociation of retinol from RBP [51]. Thus there does not seem to be a physiological need for facilitating the dissociation of the RBP–retinol complex by a distinct protein entity. These considerations suggest that the cellular uptake of retinol is not limited by events that occur in blood or at the level of the plasma membrane, but by downstream reactions such as the intracellular diffusion of retinol to sites of metabolism, and by subsequent metabolic steps. Accordingly, in most cells the pools of retinol in blood and in cytosol will be near equilibrium, and retinol will be selectively taken up only by cells in which a retinol concentration gradient, directed inwards, can be created. Such a gradient will be generated in cells that actively utilize retinol, or in cells in which CRBP is up-regulated, thereby decreasing the cytosolic concentration of free retinol (reviewed in [8,51]).

Important insights into the biological role of RBP have been obtained recently by studies of mice and humans in which the RBP gene is disrupted. RBP-deficient mice display reduced blood retinol levels and impaired visual function during the first months of life. However, these mice are viable and fertile and, when maintained on a vitamin A-sufficient diet, they acquire normal vision by 5 months of age, even though their blood retinol level remains low [52] A striking phenotype of the RBP-null mice is that they possess larger than normal hepatic vitamin A stores, but are nevertheless dependent on a continuous dietary intake of vitamin A [52]. A recent study of two human siblings that harbour point mutations in their RBP gene and exhibit undetectable plasma RBP levels revealed that these sisters suffer from night blindness and mild retinal dystrophy but do not exhibit other clinical symptoms of vitamin A deficiency [53,54]. Taken together, the observations obtained by examining RBP-deficient mice and humans support the conclusions that RBP is critical for the mobilization of retinol from hepatic storage pools in times of insufficient dietary intake, but that the protein is not essential for the delivery of retinol to tissues. Supply of vitamin A to target tissues in the absence of RBP is likely to be accomplished via newly absorbed retinyl esters, or perhaps β-carotene present in circulating chylomicrons.

Functions of CRBPs

CRBP-I and CRBP-II were the first intracellular retinoid-binding proteins to be discovered. The primary sequences of rat CRBP-I and CRBP-II show 56% identity [55], and each of these proteins is highly conserved among species, exhibiting 91–96% sequence identity among human, rat, mouse, pig and chick (reviewed in [5,56]). Both proteins interact with both all-*trans*-retinol and all-*trans*-retinal. It has been reported that the binding affinity of CRBP-I towards retinol is about 100-fold higher as compared with that of CRBP-II, that the two proteins display a similar binding affinity towards retinal, and that CRBP-II associates with retinol and retinal with similar affinities ([55,57]; see Table 1). The CRBPs belong to the family of iLBPs, and hence bind their ligands within a 10-stranded antiparallel β-barrel with the polar head-group directed innermost. The hydroxy group of retinol within the crystal structure of holo-CRBP is hydrogen-bonded to a Gln residue at the bottom of the barrel [58,59]. CRBP-bound retinol assumes a conformation in which its β-ionone ring is approximately planar in relation to the isoprene chain with the chain fully extended. The planarity of the molecule results in a 25 nm red-shift and in the appearance of fine structure in the absorption spectrum of retinol when bound to either CRBP-I or -II [60,61].

The two isoforms of CRBP display a strikingly different tissue distribution. CRBP-I is expressed in multiple tissues, both in the fetus and in the adult. In the adult, it is particularly abundant in the liver, kidney, lung and reproductive organs, and is also expressed in the choroid plexus in the brain and in pigment epithelium cells in the eye [62–66]. In contrast, in the adult, CRBP-II is restricted to the small intestine, where it is located in mature enterocytes on the villi of the mucosal epithelium [55,67,68]. CRBP-II in the fetus is mainly localized in the intestine, but is also transiently expressed in the liver where, in the rat, it appears several days before birth and disappears shortly after birth [55]. It is also expressed in the yolk sac between embryonic days 10.5 and 15.5 [69].

The high degree of sequence conservation of CRBPs indicate that they play important roles in retinoid biology. The amphipathic nature of retinol results in 'detergent-like' characteristics of the molecule, and its presence indeed affects various aspects of membrane structure and function [70–73]. CRBPs, and especially

CRBP-I with its high affinity for retinol, are believed to sequester this ligand, thereby protecting cells from its membranolytic effects. It has been shown in this regard that the predominant fraction of retinol in the liver is associated with CRBP, with very little of the compound partitioning into cellular membranes [74,75]. Up-regulation of the expression of CRBP is also expected to result in an equilibrium shift, i.e. in a decrease in the intracellular level of free retinol, thereby increasing the flux of retinol from the blood RBP-bound pool into cells [76].

In addition to these roles, the available information implicates CRBPs in regulation of the metabolism of retinol and retinal. A general consideration that should be kept in mind is that all known retinoid-metabolizing enzymes can utilize free retinoids as their substrates. Most of the evidence for the involvement of retinoid-binding proteins in retinoid metabolism thus stems from comparison of the kinetic parameters of key metabolic reactions in the presence and absence of a binding protein. Interpretation of such studies is hampered by the low aqueous solubility of retinoids and by their high affinity for cellular membranes. This caveat is of particular concern when the enzymes under study are integral membrane proteins. Retinoids in such assay mixtures partition between the binding protein, the aqueous space, the membranes and, when present at high concentrations, also between micelles and self-aggregates. Hence, neither the concentrations of retinoids in the different pools nor the potential rate-limiting steps for the observed activities can be readily assessed, complicating kinetic analyses. Nevertheless, accumulated evidence strongly supports the conclusion that some retinoid binding proteins act by allowing access of their ligands to particular enzymes, while restricting access to others.

Multiple enzymic activities that can catalyse metabolic conversions of free retinol and retinal have been reported [77,78]. However, only specific enzymes recognize CRBP-bound retinoids, suggesting that CRBPs limit access of retinoids to some enzymes, while allowing metabolism by others to proceed (reviewed in [5]). Such a role is deemed especially important in view of the need for tight regulation of cellular levels of the active vitamin A metabolite retinoic acid. The notion that a specific process, mediated by protein–protein interactions between CRBP and a target enzyme, may be necessary to allow an enzyme to gain access to bound ligand is also attractive in view of the three-dimensional structure of CRBPs, in which accessibility of bound-retinol to the bulk solution appears to be limited (Figure 3). Available information implicates both CRBP-I and -II in regulating several enzymic activities.

CRBP-I

(a) Regulation of vitamin A storage. The processes by which vitamin A is taken up into the liver, the subsequent metabolism and disposition of retinol in this tissue, and the enzymic steps that have been proposed to be under regulation of CRBP-I are depicted in Scheme 1. In vitamin A sufficiency, retinol accumulates in the liver, where it is stored in the form of retinyl esters. Two distinct enzymic activities that can catalyse the esterification of retinol with long-chain fatty acids to form retinyl esters have been identified: acyl-CoA:retinol acyltransferase (ARAT; EC 2.3.1.76), which is dependent upon the presence of CoA, and lecithin:retinol acyltransferase (LRAT; EC 2.3.1.135), for which the esterification reaction is coupled to hydrolysis of phospholipids [5,8]. It has been demonstrated that, while both enzymes can metabolize free retinol, esterification of CRBP-bound retinol by hepatic microsomal fractions is CoA-independent, implying that CRBP-bound retinol is metabolized by LRAT, but not by ARAT. Furthermore, the inclusion of CRBP-I in LRAT assay mixtures does not seem to significantly alter the observed K_m of the reaction [79]. As the concentration of free retinol is expected to be significantly reduced in the presence of the high-affinity binding protein, these observations were taken to indicate that LRAT can recognize retinol when bound to CRBP-I, suggesting that the substrate is 'channelled' between the binding protein and the enzyme via direct protein–protein interactions [5].

While holo-CRBP-I presents its ligand directly to LRAT, apo-CRBP-I strongly inhibits this reaction. It was reported that a 2-fold excess of CRBP-I over retinol leads to a 80% decrease in LRAT activity. As the magnitude of the decrease could not be accounted for merely by the decrease in the concentration of the free ligand due to the excess binding protein, these data were taken to suggest that apo-CRBP-I is a direct inhibitor of the enzyme [79]. An additional enzymic activity that was reported to be affected by apo-CRBP-I is retinyl ester hydrolase. It was demonstrated that apo-CRBP-I stimulates the hydrolysis of endogenous retinyl esters in liver microsomal fractions in a saturable fashion. The molecular mechanisms underlying this effect have not been clarified [80].

The physiologically relevant scenario that emerges from these observations suggests that, in vitamin A sufficiency, CRBP-I will be largely saturated with retinol and will direct this ligand to storage by delivering it to LRAT. On the other hand, under conditions of vitamin A deficiency, the level of retinol and, consequently, the level of saturation of CRBP-I will decrease, resulting in an elevation in the level of the apoprotein. In turn, apo-CRBP-I will both inhibit retinol esterification and stimulate liberation of retinol from stored retinyl esters, thereby allowing retinol to be released into the circulation [5]. A recent study of mice in which the CRBP-I gene had been disrupted revealed that CRBP-I deficiency is accompanied by a 50% decrease in retinyl ester pools in hepatic stellate cells, although it does not affect the levels of enzymes that catalyse vitamin A metabolism. The decrease was found to stem from decreased retinyl ester synthesis and was accompanied by an accelerated rate of clearance of hepatic retinyl esters, strongly supporting the notion that CRBP-I is essential for maintenance of vitamin A storage [81].

(b) Synthesis of retinoic acid. Retinoic acid is produced from retinol by two enzymic steps. The first step, catalysed by retinol dehydrogenase, results in the formation of retinal, which is then converted, via the action of retinal dehydrogenase, to retinoic acid (Scheme 1) Free retinol can be oxidized by multiple forms of alcohol dehydrogenases with broad substrate specificities that are present in both cytosol and membrane fractions [77,78]. However, only distinct enzymes can gain access to CRBP-I-bound retinol, suggesting that the binding protein delivers its ligand to enzymes in a specific manner which is likely to involve direct protein–protein interactions. As CRBP-I binds not only retinol but also retinal, it was suggested that retinal that is produced following oxidation of retinol also associates with CRBP-I and that the protein-bound retinal serves as a substrate for the subsequent reaction by retinal dehydrogenase. It has been shown in regard to this that CRBP-I-bound retinal is not readily accessible to cytosolic retinal dehydrogenase activity, but is efficiently metabolized to retinoic acid by microsomal enzymes [78,82,83].

Overall, current information implicates CRBP-I in regulating vitamin A storage, as well as in determining the specificity of the two enzymic activities that produce retinoic acid. It is worth noting, however, that while the proposed function for CRBP-I in regulating vitamin A storage has been strongly supported by studies of CRBP-I-null mice, these animals do not display abnormalities related to retinoic acid deficiency, at least under

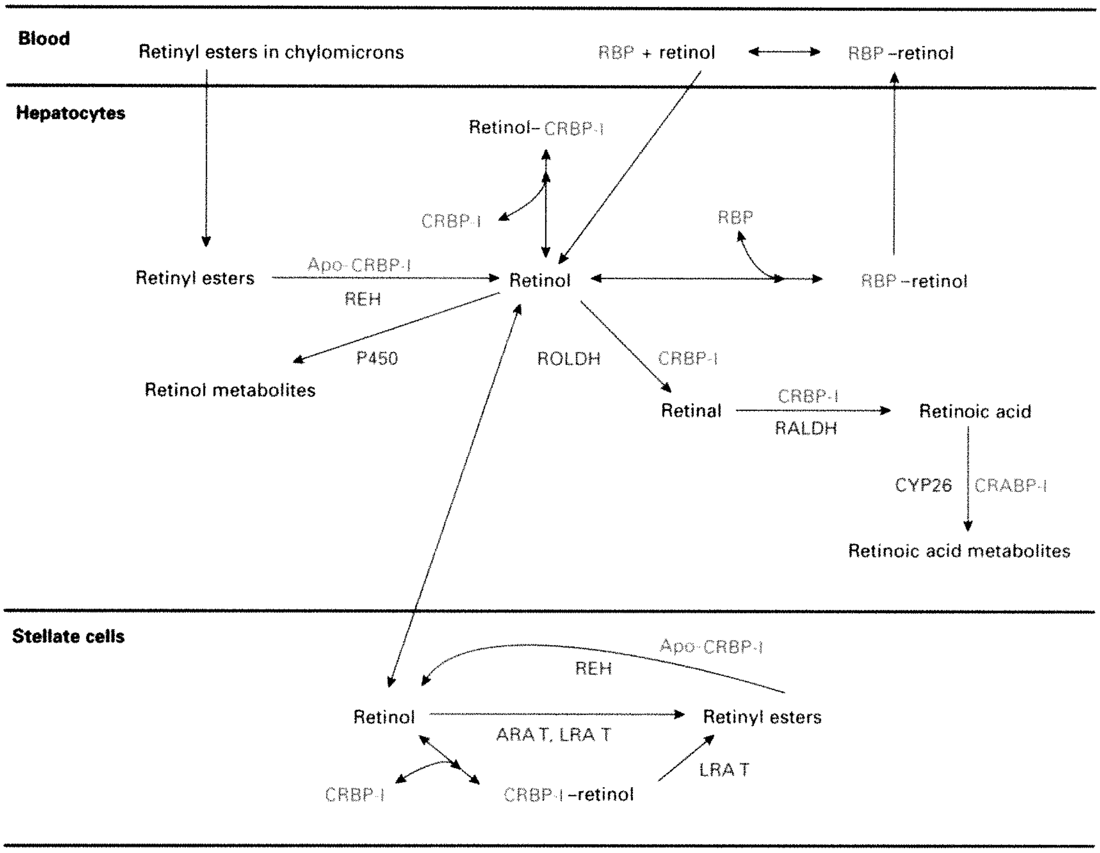

Scheme 1 Proposed involvement of retinoid-binding proteins in modulating the disposition and metabolism of retinoids in the liver

Following uptake of chylomicrons by the hepatocytes, retinyl esters incorporated in these particles are hydrolysed by retinyl ester hydrolase (REH) to yield free retinol. In vitamin A excess, retinol moves to stellate cells, where it is re-esterified by either ARAT or LRAT. In vitamin A deficiency, retinyl esters, stored in lipid droplets in the stellate cells, are hydrolysed by REH. Free retinol thus produced moves back to the hepatocytes, where it complexes with RBP, triggering secretion of holo-RBP into the blood. In the hepatocytes, retinol may be degraded by specific cytochrome P450 enzymes. Alternatively, retinol may be oxidized to retinal and, subsequently, to retinoic acid by processes sequentially catalysed by retinol dehydrogenase (ROLDH) and retinal dehydrogenase (RALDH). Degradation of retinoic acid is catalysed by specific cytochrome P450 enzymes (CYP26). CRBP-I draws retinol from blood into the cell by shifting the equilibrium between plasma and cellular retinol pools. This protein also controls the formation and hydrolysis of retinyl esters: CRBP-I-bound retinol is esterified exclusively by LRAT; apo-CRBP-I was reported to inhibit LRAT and to facilitate REH. It was also reported that CRBP-I directs retinol and retinal to specific ROLDH and RALDH isoforms, while limiting access to others. CRABP-I was shown to enhance retinoic acid degradation. Retinoid-binding proteins are shown in red; enzymic activities are shown in blue. See text for references.

conditions of maternal vitamin A sufficiency [81]. Hence, under these conditions, CRBP-I does not appear to be essential for retinoic acid synthesis during development.

CRBP-II

The exclusive expression of CRBP-II in the absorptive cells of the small intestine, and the high concentration of the protein in this location (comprising up to 1 % of all soluble proteins [5]), suggests that CRBP-II has a role in the initial processing of retinol from food. Vitamin A is present in foods either as β-carotene, derived from plant sources, or as retinyl esters, originating from animal sources. The first step in the metabolism of β-carotene is an oxidative cleavage, generating retinal, which is subsequently reduced to retinol. Retinyl esters are hydrolysed to produce free retinol upon entry into the enterocytes. Retinol, derived either from β-carotene or from dietary retinyl esters, is then esterified and the resulting retinyl esters are packaged into chylomicrons and secreted into blood via the lymphatic system (reviewed in [8]). Similar to CRBP-I, CRBP-II seems to determine the specificity of enzymes that may gain access to retinol and retinal. For example, it has been shown that soluble enzymes present in extracts of intestinal mucosa can reduce free retinal, but not retinal bound to CRBP-II. In contrast, retinal reductase in mucosal microsomal fractions readily produced retinol when presented with CRBP-II-bound retinal [84]. CRBP-II was also reported to block the re-oxidation of retinol to retinal, most likely because protein-bound retinol is not available to enterocyte retinol dehydrogenases [84]. CRBP-II also participates in regulation of the esterification of retinol in the enterocyte. Similar to hepatic ARAT, intestinal ARAT is incapable of processing CRBP-II-bound retinol. In contrast, LRAT catalyses retinol esterification more efficiently when the substrate is presented to the enzyme bound to CRBP as compared with free retinol [79]. Unlike apo-CRBP-I, apo-CRBP-II does not inhibit the activity of LRAT, and thus formation of retinyl esters in the intestine is expected to proceed in times of low intake of vitamin A [79].

Functions of CRABPs

Two binding proteins with a high affinity for all-*trans*-retinoic acid have been identified, CRABP-I and CRABP-II. The two isoforms are highly similar, displaying 74 % sequence identity between human CRABP-I and -II, and are also extremely conserved between species. For example, rat, mouse and bovine

CRABP-I are all identical, and they differ from the human protein by a single amino acid residue [85–90]. In the three-dimensional structure of holo-CRABPs, retinoic acid is buried in the binding pocket such that its carboxy head group interacts with two arginine residues and one tyrosine residue at the bottom of the pocket. The β-ionone ring is twisted into a *cis*-like configuration relative to the isoprene tail, and fits at the entrance to the pocket such that only one edge is accessible to the solvent [13]. Hence, similarly to CRBPs (Figure 3), access to the entrance of the ligand-binding pocket of CRABP appears to be restricted, implying that significant conformational changes are required to allow the ligand to move out of the site.

The two isoforms of CRABP display different patterns of expression across cells and developmental stages. In the adult, CRABP-I is expressed almost ubiquitously [5], while CRABP-II is only expressed in the skin [5], uterus and ovary [66,91], and the choroid plexus [92]. Both CRABPs are widely expressed in the embryo, although they do not usually co-exist in the same cells [93]. The biological functions of CRABPs are not completely understood at present. It was reported that mice in which the genes for either CRABP-I or CRABP-II have been disrupted appear to be essentially normal, except for some defects in limb development [94,95]. It is interesting to note, in regard to these observations, that retinoic acid acts as a morphogen in vertebrate limb development. It was shown, for example, that exogenously generated concentration gradients of retinoic acid across the limb bud in the developing chick induced the formation of additional digits. Furthermore, pattern formation under these circumstances was found to be determined by the shape of the gradient rather than by the actual concentration at the source [96,97]. In view of the noted defects in limb development in CRABP-null mice, CRABPs may be involved in generation of appropriate retinoic acid concentration gradients in the limb bud. However, the molecular mechanisms underlying these effects remain to be clarified.

Similarly to other retinoid binding proteins, it has been proposed that CRABPs serve to solubilize and protect their ligand in the aqueous cytosol, and that they transport retinoic acid between different cellular compartments. It was thus suggested that CRABPs act to deliver their ligand to the nucleus, where it will bind and activate retinoid receptors [98]. In support of this notion, it was demonstrated that both CRABP isoforms are present not only in cytosol but also in the nuclei of cells [99]. The exceptionally high level of conservation of CRABPs across species, and the distinct expression pattern of the two isoforms, imply not only that they play critical roles in retinoic acid biology, but also that the two isoforms serve distinct functions. It was proposed that functional differences between the two isoforms may stem from differences in their binding affinity for retinoic acid [100]. However, the equilibrium dissociation constants of complexes of CRABP-I and -II with retinoic acid differ only by 2-fold ([101], see Table 1) and it is difficult to see how this small difference could account for distinct functions of the two proteins. The question thus remains: what are the different roles that CRABP-I and CRABP-II play in regulating retinoic acid action? Recent studies have begun to shed some light on this question

CRABP-I

CRABP-I has been shown to modulate the activities of enzyme(s) that catalyse the metabolic transformation of retinoic acid. It was reported that, when bound to CRABP-I, retinoic acid serves as a substrate for enzymes in rat testes microsomes, giving rise to the polar metabolites 3,4-didehydro-, 4-hydroxy-, 4-oxo-, 16-hydroxy-4-oxo- and 18-hydroxy-retinoic acids [102]. These metabolites are likely to be products of members of the CYP26 family, cytochromes P450 that specifically metabolize retinoic acid [103–106]. Additionally, it was shown that increased expression of CRABP-I in F9 teratocarcinoma cells enhanced the rate of formation of polar metabolites from retinoic acid [107], and that the sensitivity of F9 cells to retinoic acid-induced differentiation is inversely correlated with the cellular level of CRABP-I [108]. The details of the mechanisms by which CRABP-I regulates the activities of retinoic acid-metabolizing enzyme(s), and the identity of the specific enzyme(s) affected by this binding protein, remain to be clarified. Nevertheless, these observations suggest that CRABP-I acts to dampen cellular responses to retinoic acid, and that this effect reflects the ability of the binding protein to enhance the activity of an enzyme(s) that catalyses the degradation of the hormone.

CRABP-II

Both CRABP-I and -II are present in the nucleus, implying that both proteins may serve to deliver retinoic acid to the transcription factor that is activated by it, namely the retinoic acid receptor (RAR). However, it was recently shown that the mechanisms by which CRABP-I and -II deliver their ligand to RAR are fundamentally different [101]. As discussed above, transfer of retinoic acid from CRABP to RAR may occur either via the aqueous phase (Figure 4a) or by 'channelling' between the two proteins, i.e. through direct protein–protein interactions and in a way that bypasses the bulk solution (Figure 4b). Kinetic studies of the processes through which retinoic acid moves from CRABP-I or CRABP-II to RAR revealed that, while CRABP-I acts as a passive vehicle which binds and releases its ligand according to concentration gradients, CRABP-II delivers retinoic acid to the RAR in a direct collisional process. It was shown further that channelling of retinoic acid between CRABP-II and RAR results in a significant facilitation of the formation of holo-RAR [101]. These observations suggest that, in cells, expression of CRABP-II (but not of CRABP-I) would enhance the transcriptional activity of RAR. This conclusion has been supported by the observation that overexpression of CRABP-II (but not CRABP-I) results in a marked stimulation of transcription of a reporter gene driven by a RAR response element [101,109]. It was also reported that loss of expression of CRABP-II is correlated with resistance of mammary carcinoma cell lines to retinoic acid-induced growth arrest [110], and that expression of a CRABP-II antisense construct in SCC cells results in reduced sensitivity to retinoic acid-induced cell-cycle arrest [111]. Hence expression of CRABP-II appears to play a role in sensitizing cells to retinoic acid. Interestingly, the expression of CRABP-II is associated with cells that synthesize relatively large amounts of retinoic acid [92,112,113], suggesting that cells with an increased physiological requirement for retinoic acid require up-regulation of both the synthesis of the hormone and the level of expression of CRABP-II, allowing for efficient and rapid delivery of retinoic acid to the RAR.

Ocular retinoid-binding proteins

Quantitatively, the main user of vitamin A in the body is the eye, where the vitamin's metabolite 11-*cis*-retinal serves as the chromophore for the visual pigment rhodopsin. Scheme 2 depicts the major steps in the visual cycle through which 11-*cis*-retinal is produced in the eye, provided for regeneration of visual pigments, and replenished following bleaching of rhodopsin that occurs upon light absorption (for a detailed review of the visual cycle,

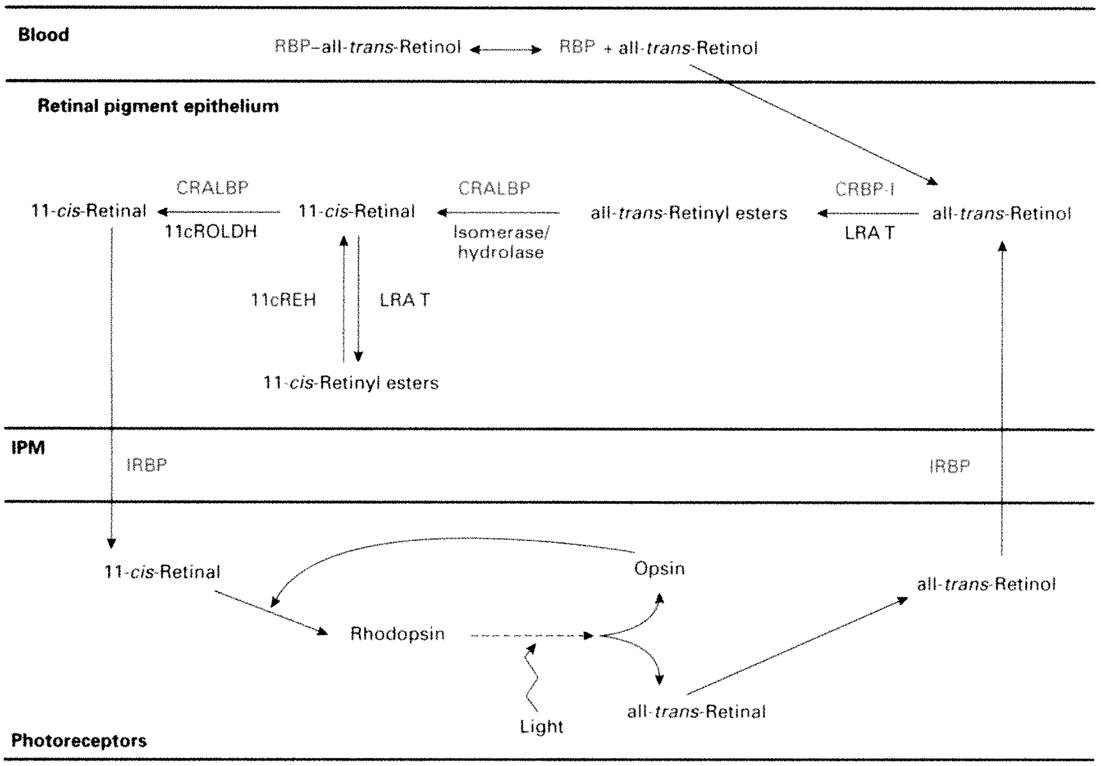

Scheme 2 Proposed involvement of retinoid-binding proteins in the visual cycle

all-*trans*-Retinol enters the eye from blood via retinal pigment epithelium cells, where it is esterified to all-*trans*-retinyl esters by LRAT. An isomerization activity, catalysed by isomerohydrolase [or, perhaps, by sequential catalysis by retinyl ester hydrolase REH and all-*trans*-retinol isomerase], leads to the formation of 11-*cis*-retinol. 11-*cis*-Retinol may either be esterified to form 11-*cis*-retinyl esters and stored, or oxidized by 11-*cis*-retinol dehydrogenase (11cROLDH) to the visual chromophore 11-*cis*-retinal. 11-*cis*-Retinal exits the pigment epithelium, and moves across the IPM to photoreceptor cells, where it binds to opsin to form the visual pigment rhodopsin. Light absorption by rhodopsin results in isomerization of rhodopsin-bound 11-*cis*-retinal, initiating visual signalling. all-*trans*-Retinal thus formed is enzymically reduced to all-*trans*-retinol. all-*trans*-Retinol is then transported back to retinal pigment epithelium for re-isomerization and re-oxidation. Similar to its role in the liver, CRBP-I was reported to deliver all-*trans*-retinol to LRAT of the retinal pigment epithelium. Due to its high affinity for 11-*cis*-retinol, CRALBP enables the all-*trans*- to 11-*cis*-isomerization reaction to occur. CRALBP also enhances the 11-*cis*-ROLDH reaction. This effect is likely to stem from direct interactions between CRALBP and 11-*cis*-ROLDH. Transport of 11-*cis*-retinal and all-*trans*-retinol across the IPM is mediated by IRBP. Retinoid-binding proteins are shown in red; enzymic activities are shown in blue. See text for references.

see [1]). all-*trans*-Retinol, the circulating form of vitamin A, enters the eye via the retinal pigment epithelium, where it is esterified to all-*trans*-retinyl esters. It is generally believed that these esters serve as a substrate for an isomerohydrolase that couples cleavage of the ester bond to isomerization across the retinoid 11–12 double bond, generating 11-*cis*-retinol [114]. Although the details of this model have been questioned by more recent observations [115], it is clear that isomerization occurs at the level of retinol, resulting in the generation of 11-*cis*-retinol. This compound may then be either esterified with long-chain fatty acids to form 11-*cis*-retinyl esters [116,117] or oxidized to the visual chromophore 11-*cis*-retinal [118]. As light sensing and subsequent visual transduction take place not in retinal pigment epithelium but in the outer segments of photoreceptor cells (where rhodopsin is embedded in intracellular membranous discs), regeneration of active visual pigments requires a continuous flux of 11-*cis*-retinal from pigment epithelium to photoreceptor cells. Within the photoreceptors, 11-*cis*-retinal binds to opsin to form active rhodopsin. Following absorption of light by rhodopsin, the visual chromophore is isomerized to all-*trans*-retinal, which is then enzymically reduced to all-*trans*-retinol. As photoreceptor cells do not contain the enzymic machinery necessary for regenerating 11-*cis*-retinal from the parent molecule, all-*trans*-retinol is transported back to the pigment epithelium for re-isomerization and oxidation. Thus the visual cycle critically includes continuous shuttling of retinoids between photoreceptor and pigment epithelium cells via the aqueous space of the interphotoreceptor matrix which separates the two cell types.

RBP, CRBP and CRABP are likely to play similar roles in the eye to those that they fulfil in other tissues. For example, retinol bound to CRBP-I was shown to be an efficient substrate for retinal pigment epithelium LRAT [119]. In addition to these proteins, the eye contains two unique retinoid-binding proteins. These proteins, CRALBP and IRBP, appear to have specific functions in the visual cycle.

Functions of CRALBP

A retinoid-binding protein that displays a high selectivity towards 11-*cis*-retinoids has been identified in retinal pigment epithelium and in the neural retina in the eye, and was termed CRALBP [120,121]. The unique role that 11-*cis*-retinoids play in vision, and the location of CRALBP in the retina, immediately suggested that this protein may be involved in the visual process. Indeed, mutations in the human CRALBP gene can result in recessive retinitis pigmentosa [122]. Interestingly, in addition to its presence in the retinal pigment epithelium and neural retina, CRALBP is also found in the pineal gland [123], ciliary body [124], cornea [125], optic nerve and brain [126]. It was reported that CRALBP isolated from bovine brain, unlike CRALBP derived from the retina, is not associated with any endogenous retinoids [126]. Hence this protein may have other, as yet uncharacterized, functions that are unrelated to the visual process or to its retinoid-binding capabilities [1]. Available information implicates CRALBP in two separate functions in supporting the visual cycle.

Isomerization of all-*trans*-retinoids to 11-*cis*-retinoids

The process by which 11-*cis*-retinoids are generated in retinal pigment epithelium is not completely understood at present. Possible mechanisms include coupling the hydrolysis of all-*trans*-retinyl esters to isomerization, yielding 11-*cis*-retinol [114], or the presence of an enzyme that catalyses the direct isomerization of all-*trans*- to 11-*cis*-retinol [115]. It was recently shown that the formation of 11-*cis*-retinol by isolated retinal pigment epithelium microsomal membranes critically requires the presence of CRALBP [115,127]. It was proposed that CRALBP acts by sequestering 11-*cis*-retinol, thereby driving the energetically unfavourable isomerization reaction by mass action [115]. Alternatively, it was reported that the isomerase is subject to an end-product inhibition by 11-*cis*-retinol, suggesting that CRALBP facilitates the isomerization reaction by binding the product, thereby relieving the inhibition [127]. It was shown further that BSA, a 'non-specific' retinoid-binding protein, can also facilitate the isomerization reaction, albeit at a much higher concentration than the concentration at which CRALBP displays a similar effect [127]. Hence the ability of CRALBP to enable retinol isomerization in the retinal pigment epithelium does not appear to originate from specific interactions between the binding protein and the enzyme, but to stem from the strong binding affinity of the protein for 11-*cis*-retinol.

Regulation of the metabolic fate of 11-*cis*-retinol

11-*cis*-Retinol, generated in the retinal pigment epithelium, is at a metabolic branch point and can be acted upon either by LRAT, which catalyses its esterification to 11-*cis*-retinyl esters, or by 11-*cis*-retinol dehydrogenase, which converts it into 11-*cis*-retinal (Scheme 2). It has been demonstrated that CRALBP governs the partitioning of 11-*cis*-retinol between these alternative metabolic pathways. Hence it was reported that esterification of 11-*cis*-retinol is inhibited, while oxidation of this compound is stimulated, in the presence of CRALBP. The latter effect was shown to be specific to CRALBP and was not manifested when the substrate was presented bound to serum albumin [128]. The inhibition of the LRAT reaction by CRALBP can be readily explained by considering that introduction of a binding protein with a high affinity for 11-*cis*-retinol into reaction mixtures decreases the concentration of free substrate available to the enzyme. The molecular mechanism underlying the ability of CRALBP to stimulate the enzymic oxidation of 11-*cis*-retinol to 11-*cis*-retinal has not been clarified as yet, but is likely to involve protein–protein interactions between CRALBP and 11-*cis*-retinol dehydrogenase, resulting either in 'channelling' of the substrate to the enzyme or in allosteric activation of the enzyme by the binding protein [128].

Functions of IRBP

The regeneration of visual pigments in photoreceptor outer segments relies on the supply of 11-*cis*-retinal from the pigment epithelium; in turn, the maintenance of an adequate pool of 11-*cis*-retinal depends on rapid movement of all-*trans*-retinol, which is generated in photoreceptors following bleaching of rhodopsin, back to the retinal pigment epithelium, where it can be re-isomerized and re-oxidized (Scheme 2). The question thus arises: how do retinoids, compounds that are poorly soluble in water, move across the interphotoreceptor matrix (IPM) at rates that are sufficient for sustaining visual function under light conditions?

The main soluble protein component of the IPM is IRBP, an ~ 140 kDa glycoprotein which is synthesized in photoreceptors and secreted into the IPM, where it binds two classes of ligands: retinoids and long-chain fatty acids. It has been repeatedly suggested that IRBP serves as a carrier for retinoids between photoreceptor and retinal pigment epithelium cells (reviewed in [129]). Such a function for IRBP is implied by the observations that the composition of retinoids that are endogenously associated with the protein is modulated by light [130], and that binding of retinoids to IRBP stabilizes them against degradation [131,132]. It was also reported that IRBP can take up 11-*cis*-retinal from the retinal pigment epithelium and efficiently deliver this chromophore to rod outer segments [133–135]. However, the exact role of IRBP in the transport process remains to be clarified. Theoretically, IRBP could serve simply as a storage compartment for retinoids in the IPM with the ability to bind and release these ligands according to their concentration gradients. Alternatively, the protein could function to specifically target particular retinoids to certain locations in the eye, i.e. to deliver 11-*cis*-retinal to photoreceptors and to transport all-*trans*-retinol to the retinal pigment epithelium. The latter possibility would require the existence of a mechanism that enables IRBP to 'sense' different locations within the IPM.

A potential mechanism that may allow IRBP to target 11-*cis*-retinal to photoreceptor cells has been suggested [22]. IRBP contains three retinoid-binding sites, as well as one or two sites for long-chain fatty acids. One of the retinoid sites can accommodate either all-*trans*-retinol or 11-*cis*-retinal [23]. The two additional sites appear to be selective towards all-*trans*-retinol and 11-*cis*-retinal respectively ([22]; and N. Shaw and N. Noy, unpublished work). It was reported that the long-chain polyunsaturated fatty acid docosahexaenoic acid (DHA), but not more saturated fatty acids, inhibits the ability of IRBP to bind a second molecule of 11-*cis*-retinal. It was further shown that, while DHA facilitates the rate of dissociation of 11-*cis*-retinal from the regulatory site by about an order of magnitude, the fatty acid has little effect on binding of either all-*trans*-retinol or 11-*cis*-retinal in the remaining IRBP retinoid-binding sites [22]. DHA is highly enriched in photoreceptor cells, where it comprises approx. 50% of the acyl chains of phospholipids and, correspondingly, of non-esterified fatty acids [22,136]. Based on the specific effect of DHA on the interactions of IRBP with 11-*cis*-retinal, and considering the concentration gradient of this fatty acid across the IPM, it was suggested that DHA may serve as the 'switch' that allows IRBP to distinguish between different regions of the IPM, and which triggers the release of 11-*cis*-retinal at the correct location. As summarized in Figure 5, this model proposes that while IRBP is in the vicinity of the retinal pigment epithelium, where the concentration of DHA is low, it will possess a high affinity for 11-*cis*-retinal and associate with it. Movement of the protein to the vicinity of photoreceptor cells will expose it to high levels of DHA, resulting in rapid release of 11-*cis*-retinal from the regulated binding site at this location [22].

Despite the body of evidence indicating that IRBP is likely to function in mediating the transport of retinoids across the IPM, it should be noted that it was recently reported that disruption of the IRBP gene in mice does not result in significant decreases in the rates of either the recovery of 11-*cis*-retinal or the regeneration

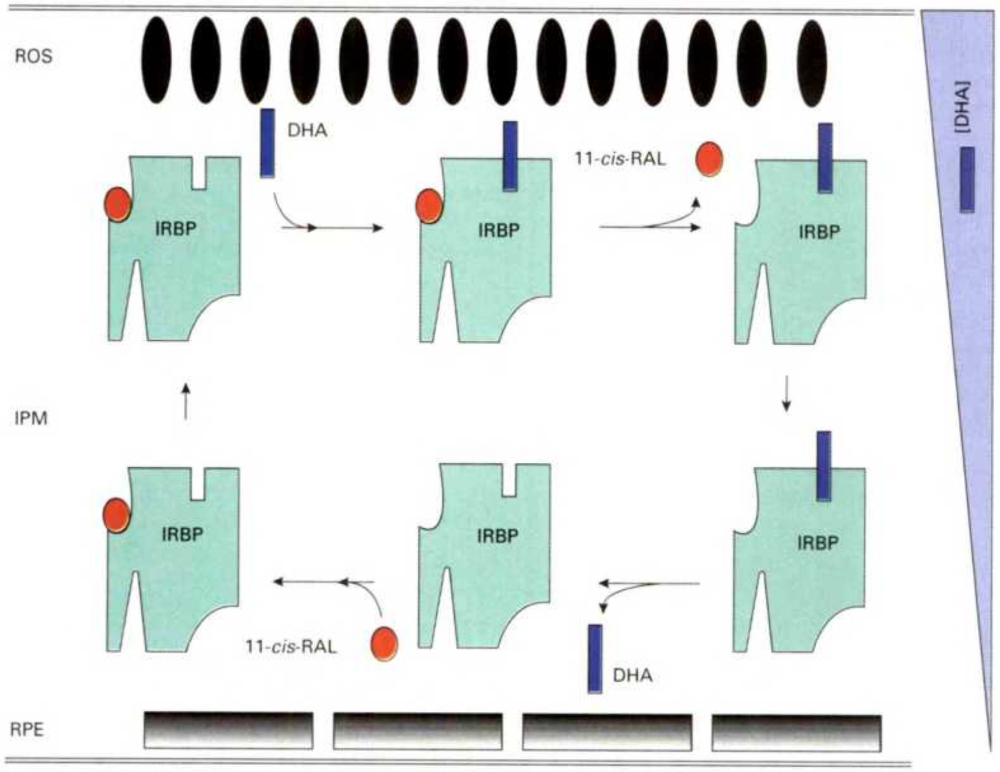

Figure 5 Model for targeting of retinoids by IRBP

The model is based on the findings that: (1) binding of the long chain fatty acid DHA to IRBP switches one of the protein's 11-*cis*-retinal (11-*cis*-RAL) binding sites from a state of a high affinity to a state of low affinity for this ligand, and (2) DHA is highly enriched in photoreceptor cells, resulting in a steep concentration gradient of this fatty acid across IPM. It has been proposed that, because the region of the IPM that is close to the retinal pigment epithelium (RPE) is relatively poor in DHA, IRBP possesses a high affinity for 11-*cis*-retinal at this location. Movement of IRBP, loaded with 11-*cis*-retinal, to the vicinity of photoreceptor cells exposes the protein to a high concentration of DHA. Binding of DHA to IRBP results in the release of 11-*cis*-retinal close to the photoreceptor surface. ROS, rod outer segment.

of rhodopsin following light exposure [137]. Nevertheless, the IRBP-deficient mice displayed progressive photoreceptor degeneration. These observations implicate IRBP in serving a role in photoreceptor survival, but question whether it is essential for a normal rate of visual pigment regeneration [137]. Hence the complete spectrum of the biological functions of IRBP remains ambiguous.

CONCLUSIONS AND PERSPECTIVES

Vitamin A metabolites are essential for numerous biological processes. They are critical for vision, play important roles in regulating proliferation and differentiation in both fetal and adult tissues, and have been implicated in modulating immune function. Retinoids are found *in vivo* primarily bound to various retinoid-binding proteins which utilize diverse mechanisms to modulate the biological activities of their cognate ligands (Table 2). Some retinoid-binding proteins govern the concentrations of retinoids in plasma and in cells, as well as the direction and magnitude of fluxes through which retinoids move between extra- and intra-cellular compartments. Other retinoid-binding proteins appear to act by specifically delivering their ligands to particular targets, such as enzymes or transcription factors. Kinetic evidence suggests that these activities are likely to be mediated by direct protein–protein interactions between the binding protein and the target, resulting in 'channelling' of retinoids to the appropriate metabolic pathway or activity site. However, no molecular-level information on the interactions of retinoid-binding proteins with putative targets has been put forward to date. Progress on this important issue has long been hampered by the lack of availability of retinoid-metabolizing enzymes in pure forms, and hence most of the current information is based on work with crude cellular fractions. Recently the genes for LRAT [138] and for several isoforms of retinol and retinal dehydrogenases [139–147] have been cloned. The availability of these proteins should allow for better clarification of the mechanisms of action of specific retinoid-binding proteins.

Another issue on which virtually no information is currently available relates to the involvement of retinoid-binding proteins in modulating the transport, metabolism and action of bioactive isomers and metabolites of retinoids, such as 9-*cis*-, 13-*cis*- and 4-oxo-retinoids. Future goals also include delineating the structures and obtaining a better understanding of the functions of the less well characterized retinoid-binding proteins IRBP and CRALBP. Particularly intriguing in regard to the latter are the observations that CRALBP is present in areas in the brain that have no known function for the ligands of this protein, i.e. 11-*cis*-retinoids. Studies of retinoid-binding proteins in cultured cells and analyses of transgenic and null animal models for specific retinoid-binding proteins are expected to continue to allow for testing predictions derived from *in vitro* studies, and to provide additional insights into the roles that retinoid binding proteins play in different physiological states.

Table 2 Proposed functions of retinoid-binding proteins

See text for references Abbreviations ROLDH, retinol dehydrogenase; RALDH, retinal dehydrogenase, RPE, retinal pigment epithelium; 11cROLDH, 11-*cis*-retinol dehydrogenase

Protein	Proposed function	Target (proposed mechanism)	Physiological role
RBP	Enable secretion of retinol from the liver	Only holo-RBP is recognized by the secretion machinery in Golgi (?)	Maintenance of plasma retinol homoeostasis
	Carry retinol in blood		
CRBP-I	Draw retinol from blood into cells	(Shift of the intra/extracellular equilibrium of retinol)	Increase of intracellular retinol pools, regulation of vitamin A storage, perhaps involvement in regulating retinoic acid synthesis
	Solubilize retinol and retinal, protect cells from membranolytic retinoid action	(Sequestration)	
	Holo-CRBP-I direct retinol to esterification by LRAT	LRAT (direct interactions)	
	Apo-CRBP-I. inhibit retinol esterification	LRAT (direct interaction)	
	Apo-CRBP-I. stimulate retinyl ester hydrolysis	Retinyl ester hydrolase (product sequestration? direct interactions?)	
	Direct retinol and retinal to specific dehydrogenases	ROLDH/RALDH (direct interactions)	
CRBP-II	Direct retinal to reduction by microsomal enzymes	Microsomal retinal reductase (direct interactions)	Regulation of initial processing and production of retinyl esters from dietary vitamin A in the intestine
	Block re-oxidation of retinol to retinal	(Sequestration of retinol)	
	Direct retinol to esterification by LRAT	LRAT (direct interactions)	
CRABP-I	Enhance conversion of retinoic acid into polar metabolites	CYP26 family members (direct interactions)	Moderation of cellular response to retinoic acid
CRABP-II	'Channel' retinoic acid to RAR	RAR (direct interactions)	Enhancement of cellular response to retinoic acid
CRALBP	Enable isomerization of all-*trans*-retinol to 11-*cis*-retinol	(Sequestration of 11-*cis*-retinol)	Control of generation of 11-*cis*-retinal in RPE
	Enhance oxidation of 11-*cis*-retinol to 11-*cis*-retinal	11cROLDH (direct interactions)	
IRBP	Transport retinoids across the IPM		Regeneration of rhodopsin
	Maintain photoreceptor integrity	?	

I am grateful to Gregory Hoffman for generating the pictures presented in Figures 2 and 3 Work from the author's laboratory is funded by grants from the National Institute of Health (CA68150 and EY09296).

REFERENCES

1 Saari, J. C (1999) Retinoids in mammalian vision In Retinoids. The Biochemical and Molecular Basis of Vitamin A and Retinoid Action, vol. 139 (Nau, H and Blaner, W S, eds), pp 563–588, Springer-Verlag, Berlin

2 Mangelsdorf, D, Umesono, K and Evans, R M (1994) The retinoid receptors In The Retinoids, Biology, Chemistry and Medicine (Sporn, M B, Roberts, A. B and Goodman, D. S, eds), pp 319–350, Raven Press, New York

3 Ross, C A and Hammerling, U G (1994) Retinoids and the immune system In The Retinoids, Biology, Chemistry and Medicine (Sporn, M B, Roberts, A. B. and Goodman, D S, eds), pp 521–544, Raven Press, New York

4 Flower, D R (1996) The lipocalin protein family structure and function Biochem J **318**, 1–14

5 Ong, D E, Newcomer, M E and Chytil, F (1994) Cellular retinoid binding proteins In The Retinoids, Biology, Chemistry and Medicine (Sporn, M B., Roberts, A and Goodman, D S, eds.), pp. 283–318, Raven Press, New York

6 Newcomer, M E, Jones, T A, Aqvist, J, Sundelin, J, Eriksson, U, Rask, L and Peterson, P. A (1984) The three-dimensional structure of retinol-binding protein EMBO J. **3**, 1451–1454

7 Noy, N and Xu, Z J (1990) Thermodynamic parameters of the binding of retinol to binding proteins and to membranes Biochemistry **29**, 3888–3892

8 Vogel, S., Gamble, M V and Blaner, W S (1999) Biosynthesis, absorption, metabolism and transport of retinoids In Retinoids The Biochemical and Molecular Basis of Vitamin A and Retinoid Action, vol 139 (Nau, H. and Blaner, W S., eds), pp 31–96, Springer-Verlag, Berlin

9 Monaco, H L, Mancia, F, Rizzi, M and Coda, A (1994) Crystallization of the macromolecular complex transthyretin–retinol-binding protein J. Mol Biol **244**, 110–113

10 Naylor, H M and Newcomer, M E (1999) The structure of human retinol-binding protein (RBP) with its carrier protein transthyretin reveals an interaction with the carboxy terminus of RBP Biochemistry **38**, 2647–2653

11 Thompson, J R, Bratt, J. M and Banaszak, L J (1995) Crystal structure of cellular retinoic acid binding protein I shows increased access to the binding cavity due to formation of an intermolecular beta-sheet J Mol Biol. **252**, 433–446

12 Wang, L, Li, Y, Abildgaard, F, Markley, J L and Yan, H (1998) NMR solution structure of type II human cellular retinoic acid binding protein implications for ligand binding Biochemistry **37**, 12727–12736

13 Kleywegt, G J., Bergfors, T., Senn, H, Le Motte, P., Gsell, B, Shudo, K and Jones, T A (1994) Crystal structures of cellular retinoic acid binding proteins I and II in complex with all-trans-retinoic acid and a synthetic retinoid Structure **2**, 1241–1258

14 Chen, X., Tordova, M., Gilliland, G L, Wang, L, Li, Y., Yan, H and Ji, X (1998) Crystal structure of apo-cellular retinoic acid-binding protein type II (R111M) suggests a mechanism of ligand entry J Mol Biol **278**, 641–653

15 Lu, J, Lin, C L, Tang, C, Ponder, J W, Kao, J L, Cistola, D P and Li, E (1999) The structure and dynamics of rat apo-cellular retinol-binding protein II in solution. comparison with the X-ray structure J Mol Biol **286**, 1179–1195

16 Sato, Y, Arai, H., Miyata, A, Tokita, S, Yamamoto, K., Tanabe, T and Inoue, K (1993) Primary structure of alpha-tocopherol transfer protein from rat liver Homology with cellular retinaldehyde-binding protein J Biol Chem **268**, 17705–17710

17 Salama, S. R, Cleves, A E, Malehorn, D. E, Whitters, E A and Bankaitis, V. A (1990) Cloning and characterization of *Kluyveromyces lactis* SEC14, a gene whose product stimulates Golgi secretory function in *Saccharomyces cerevisiae* J Bacteriol **172**, 4510–4521

18 Crabb, J W, Nie, Z, Chen, Y, Hulmes, J D, West, K A., Kapron, J. T., Ruuska, S. E, Noy, N and Saari, J C (1998) Cellular retinaldehyde-binding protein ligand interactions. Gln-210 and Lys-221 are in the retinoid binding pocket J Biol Chem **273**, 20712–20720

19 Saari, J. C., Teller, D C, Crabb, J. W and Bredberg, L (1985) Properties of an interphotoreceptor retinoid-binding protein from bovine retina J Biol Chem **260**, 195–201

20 Bazan, N. G., Reddy, T S, Redmond, T M, Wiggert, B and Chader, G J (1985) Endogenous fatty acids are covalently and noncovalently bound to interphotoreceptor retinoid-binding protein in the monkey retina J. Biol Chem **260**, 13677–13680

21 Chen, Y., Saari, J C and Noy, N. (1993) Interactions of all-trans-retinol and long-chain fatty acids with interphotoreceptor retinoid-binding protein Biochemistry **32**, 11311–11318

22 Chen, Y, Houghton, L A, Brenna, J T and Noy, N (1996) Docosahexaenoic acid modulates the interactions of the interphotoreceptor retinoid-binding protein with 11-cis-retinal J Biol Chem **271**, 20507–20515

23 Chen, Y and Noy, N (1994) Retinoid specificity of interphotoreceptor retinoid-binding protein Biochemistry **33**, 10658–10665

24 Tschanz, C. L and Noy, N. (1997) Binding of retinol in both retinoid-binding sites of interphotoreceptor retinoid-binding protein (IRBP) is stabilized mainly by hydrophobic interactions J Biol Chem **272**, 30201–30207

25 Fong, S L and Bridges, C D (1988) Internal quadruplication in the structure of human interstitial retinol-binding protein deduced from its cloned cDNA J Biol Chem **263**, 15330–15334

26 Borst, D E, Redmond, T M., Elser, J. E, Gonda, M A, Wiggert, B., Chader, G J and Nickerson, J M (1989) Interphotoreceptor retinoid-binding protein Gene characterization, protein repeat structure, and its evolution J Biol Chem **264**, 1115–1123

27 Bridges, C D, Liou, G I, Alvarez, R A, Landers, R A, Landry, Jr, A M. and Fong, S L (1986) Distribution of interstitial retinol-binding protein (IRBP) in the vertebrates J Exp Zool. **239**, 335–346

28 Keller, K C and Sauer, R T (1995) Identification of active site residues of the Tsp protease J Biol Chem **270**, 28864–28868

29 Soprano, D R and Blaner, W S (1994) Plasma retinol-binding protein In The Retinoids, Biology, Chemistry, and Medicine (Sporn, M B., Roberts, A and Goodman, D S, eds), pp. 257–282, Raven Press, New York

30 Reppe, S, Smeland, S, Moskaug, J O and Blomhoff, R (1998) Retinol-induced secretion of human retinol-binding protein in yeast FEBS Lett **427**, 213–219

31 Vieira, A V and Schneider, W J (1993) Transport and uptake of retinol during chicken oocyte growth Biochim Biophys Acta **1169**, 250–256

32 Malaba, L, Kindberg, G M, Norum, K R, Berg, T and Blomhoff, R (1993) Receptor-mediated endocytosis of retinol-binding protein by liver parenchymal cells interference by radioactive iodination Biochem J **291**, 187–191

33 Heller, J (1975) Interactions of plasma retinol-binding protein with its receptor Specific binding of bovine and human retinol-binding protein to pigment epithelium cells from bovine eyes J Biol Chem **250**, 3613–3619

34 Rask, L and Peterson, P A (1976) In vitro uptake of vitamin A from the retinol-binding plasma protein to mucosal epithelial cells from the monkey's small intestine J Biol Chem **251**, 6360–6366

35 Rask, L, Geijer, C, Bill, A and Peterson, P A (1980) Vitamin A supply of the cornea Exp Eye Res **31**, 201–211

36 Bavik, C O, Peterson, A and Eriksson, U. (1995) Retinol-binding protein mediates uptake of retinol to cultured human keratinocytes Exp Cell Res **216**, 358–362

37 Bavik, C O, Levy, F, Hellman, U, Wernstedt, C and Eriksson, U (1993) The retinal pigment epithelial membrane receptor for plasma retinol-binding protein Isolation and cDNA cloning of the 63-kDa protein J. Biol Chem **268**, 20540–20546

38 Sivaprasadarao, A, Boudjelal, M and Findlay, J B (1994) Solubilization and purification of the retinol-binding protein receptor from human placental membranes Biochem J **302**, 245–251

39 Sundaram, M, Sivaprasadarao, A, DeSousa, M. M and Findlay, J B (1998) The transfer of retinol from serum retinol-binding protein to cellular retinol-binding protein is mediated by a membrane receptor J. Biol Chem **273**, 3336–3342

40 Ward, S J, Chambon, P, Ong, D E and Bavik, C (1997) A retinol-binding protein receptor-mediated mechanism for uptake of vitamin A to postimplantation rat embryos Biol Reprod **57**, 751–755

41 Hamel, C P, Tsilou, E, Pfeffer, B A, Hooks, J. J, Detrick, B and Redmond, T M (1993) Molecular cloning and expression of RPE65, a novel retinal pigment epithelium-specific microsomal protein that is post-transcriptionally regulated in vitro J Biol Chem **268**, 15751–15757

42 Nicoletti, A, Wong, D J, Kawase, K., Gibson, L H., Yang-Feng, T L, Richards, J E and Thompson, D A (1995) Molecular characterization of the human gene encoding an abundant 61 kDa protein specific to the retinal pigment epithelium Hum Mol Genet. **4**, 641–649

43 Redmond, T M, Yu, S, Lee, E, Bok, D, Hamasaki, D, Chen, N, Goletz, P, Ma, J X, Crouch, R K and Pfeifer, K (1998) Rpe65 is necessary for production of 11-cis-vitamin A in the retinal visual cycle Nat Genet **20**, 344–351

44 Noy, N and Xu, Z J (1990) Kinetic parameters of the interactions of retinol with lipid bilayers Biochemistry **29**, 3883–3888

45 Hodam, J R and Creek, K E (1998) Comparison of the metabolism of retinol delivered to human keratinocytes either bound to serum retinol-binding protein or added directly to the culture medium Exp Cell Res **238**, 257–264

46 Creek, K E, St Hilaire, P and Hodam, J. R. (1993) A comparison of the uptake, metabolism and biologic effects of retinol delivered to human keratinocytes either free or bound to serum retinol-binding protein J Nutr **123**, 356–361

47 van Bennekum, A M., Blaner, W S, Seifert-Bock, I, Moukides, M, Brouwer, A and Hendriks, H. F. (1993) Retinol-uptake from retinol-binding protein (RBP) by liver parenchymal cells in vitro does not specifically depend on its binding to RBP Biochemistry **32**, 1727–1733

48 Fex, G and Johannesson, G. (1988) Retinol transfer across and between phospholipid bilayer membranes Biochim Biophys Acta **944**, 249–255

49 Fex, G and Johannesson, G (1990) Transfer of retinol from retinol-binding protein complex to liposomes and across liposomal membranes Methods Enzymol **189**, 394–402

50 Noy, N and Xu, Z J (1990) Interactions of retinol with binding proteins implications for the mechanism of uptake by cells Biochemistry **29**, 3878–3883

51 Noy, N (1999) Physical-chemical properties and action of retinoids In Retinoids The Biochemical and Molecular Basis of Vitamin A and Retinoid Action, vol 139 (Nau, H and Blaner, W S, eds), pp 3–29, Springer-Verlag, Berlin

52 Quadro, L, Blaner, W S, Salchow, D J, Vogel, S, Piantedosi, R., Gouras, P, Freeman, S, Cosma, M P, Colantuoni, V and Gottesman, M E (1999) Impaired retinal function and vitamin A availability in mice lacking retinol-binding protein EMBO J **18**, 4633–4644

53 Seeliger, M W, Biesalski, H K, Wissinger, B, Gollnick, H, Gielen, S, Frank, J, Beck, S and Zrenner, E (1999) Phenotype in retinol deficiency due to a hereditary defect in retinol binding protein synthesis Invest. Ophthalmol Vis Sci **40**, 3–11

54 Biesalski, H K, Frank, J, Beck, S C., Heinrich, F, Illek, B, Reifen, R., Gollnick, H, Seeliger, M W, Wissinger, B. and Zrenner, E (1999) Biochemical but not clinical vitamin A deficiency results from mutations in the gene for retinol binding protein Am J Clin Nutr. **69**, 931–936

55 Li, E, Demmer, L A, Sweetser, D. A., Ong, D E and Gordon, J I (1986) Rat cellular retinol-binding protein II use of a cloned cDNA to define its primary structure, tissue-specific expression, and developmental regulation Proc Natl Acad. Sci USA **83**, 5779–5783

56 Li, E and Norris, A W (1996) Structure/function of cytoplasmic vitamin A-binding proteins Annu Rev Nutr. **16**, 205–234

57 MacDonald, P N and Ong, D E (1987) Binding specificities of cellular retinol-binding protein and cellular retinol-binding protein, type II J Biol Chem **262**, 10550–10556

58 Cowan, S W., Newcomer, M. E and Jones, T A (1993) Crystallographic studies on a family of cellular lipophilic transport proteins Refinement of P2 myelin protein and the structure determination and refinement of cellular retinol-binding protein in complex with all-trans-retinol. J Mol Biol **230**, 1225–1246

59 Winter, N S, Bratt, J M and Banaszak, L J (1993) Crystal structures of holo and apo-cellular retinol-binding protein II J. Mol Biol **230**, 1247–1259

60 Ong, D E and Chytil, F. (1978) Cellular retinol-binding protein from rat liver Purification and characterization J Biol. Chem **253**, 828–832

61 Ong, D E (1984) A novel retinol-binding protein from rat Purification and partial characterization J Biol Chem **259**, 1476–1482

62 Eriksson, U, Das, K., Busch, C, Nordlinder, H, Rask, L., Sundelin, J., Sallstrom, J and Peterson, P A (1984) Cellular retinol-binding protein Quantitation and distribution J Biol Chem **259**, 13464–13470

63 Kato, M., Kato, K and Goodman, D S (1984) Immunocytochemical studies on the localization of plasma and of cellular retinol-binding proteins and of transthyretin (prealbumin) in rat liver and kidney J Cell Biol **98**, 1696–1704

64 De Leeuw, A M, Gaur, V. P, Saari, J. C and Milam, A H (1990) Immunolocalization of cellular retinol-, retinaldehyde- and retinoic acid-binding proteins in rat retina during pre- and postnatal development J Neurocytol. **19**, 253–264

65 Zetterstrom, R H, Simon, A., Giacobini, M. M, Eriksson, U and Olson, L (1994) Localization of cellular retinoid-binding proteins suggests specific roles for retinoids in the adult central nervous system Neuroscience **62**, 899–918

66 Wardlaw, S A, Bucco, R A, Zheng, W L and Ong, D E (1997) Variable expression of cellular retinol- and cellular retinoic acid-binding proteins in the rat uterus and ovary during the estrous cycle. Biol Reprod **56**, 125–132

67 Crow, J A and Ong, D E (1985) Cell-specific immunohistochemical localization of a cellular retinol-binding protein (type 2) in the small intestine of rat Proc Natl Acad Sci USA. **82**, 4707–4711

68 Schaefer, W H, Kakkad, B, Crow, J A, Blair, I A and Ong, D E (1989) Purification, primary structure characterization, and cellular distribution of two forms of cellular retinol-binding protein, type II from adult rat small intestine J Biol Chem **264**, 4212–4221

69 Sapin, V, Ward, S J, Bronner, S, Chambon, P. and Dolle, P (1997) Differential expression of transcripts encoding retinoid binding proteins and retinoic acid receptors during placentation of the mouse Dev. Dyn **208**, 199–210

70 Wassall, S R, Phelps, T M, Albrecht, M R, Langsford, C A and Stillwell, W. (1988) Electron spin resonance study of the interactions of retinoids with a phospholipid model membrane. Biochim Biophys. Acta **939**, 393–402

71 Dingle, J T and Lucy, J. A (1965) Membrane phenomenons in relation to vitamin A Proc Nutr Soc **24**, 170–172

72 Stillwell, W., Ricketts, M., Hudson, H and Nahmias, S (1982) Effect of retinol and retinoic acid on permeability, electrical resistance and phase transition of lipid bilayers Biochim Biophys Acta **688**, 653–659

73 De Boeck, H and Zidovetzki, R (1988) NMR study of the interaction of retinoids with phospholipid bilayers Biochim Biophys Acta **946**, 244–252

74 Mack, J P., Lui, N. S., Roels, O A. and Anderson, O R (1972) The occurrence of vitamin A in biological membranes Biochim. Biophys. Acta **288**, 203–219

75 Harrison, E H, Blaner, W S, Goodman, D S and Ross, A. C. (1987) Subcellular localization of retinoids, retinoid-binding proteins, and acyl-CoA retinol acyltransferase in rat liver J Lipid Res **28**, 973–981

76 Noy, N. and Blaner, W. S (1991) Interactions of retinol with binding proteins studies with rat cellular retinol-binding protein and with rat retinol-binding protein Biochemistry **30**, 6380–6386

77 Duester, G. (1996) Involvement of alcohol dehydrogenase, short-chain dehydrogenase/reductase, aldehyde dehydrogenase, and cytochrome P450 in the control of retinoid signaling by activation of retinoic acid synthesis. Biochemistry **35**, 12221–12227

78 Napoli, J. L., Posch, K. P., Fiorella, P. D and Boerman, M H (1991) Physiological occurrence, biosynthesis and metabolism of retinoic acid evidence for roles of cellular retinol-binding protein (CRBP) and cellular retinoic acid-binding protein (CRABP) in the pathway of retinoic acid homeostasis Biomed Pharmacother **45**, 131–143

79 Herr, F M. and Ong, D E (1992) Differential interaction of lecithin-retinol acyltransferase with cellular retinol binding proteins Biochemistry **31**, 6748–6755

80 Boerman, M H and Napoli, J. L (1991) Cholate-independent retinyl ester hydrolysis Stimulation by apo-cellular retinol-binding protein. J. Biol Chem **266**, 22273–22278

81 Ghyselinck, N. B., Bavik, C, Sapin, V, Mark, M., Bonnier, D, Hindelang, C, Dierich, A, Nilsson, C. B, Hakansson, H, Sauvant, P et al (1999) Cellular retinol-binding protein I is essential for vitamin A homeostasis EMBO J. **18**, 4903–4914

82 Posch, K C, Boerman, M. H., Burns, R D and Napoli, J L (1991) Holocellular retinol binding protein as a substrate for microsomal retinal synthesis Biochemistry **30**, 6224–6230

83 Boerman, M H and Napoli, J L (1996) Cellular retinol-binding protein-supported retinoic acid synthesis. Relative roles of microsomes and cytosol. J Biol Chem **271**, 5610–5616

84 Kakkad, B P and Ong, D E (1988) Reduction of retinaldehyde bound to cellular retinol-binding protein (type II) by microsomes from rat small intestine. J. Biol Chem **263**, 12916–12919

85 Shubeita, H E, Sambrook, J. F. and McCormick, A M (1987) Molecular cloning and analysis of functional cDNA and genomic clones encoding bovine cellular retinoic acid-binding protein Proc Natl Acad. Sci USA **84**, 5645–5649

86 Nilsson, M H., Spurr, N K, Saksena, P., Busch, C, Nordlinder, H., Peterson, P A, Rask, L and Sundelin, J (1988) Isolation and characterization of a cDNA clone corresponding to bovine cellular retinoic-acid-binding protein and chromosomal localization of the corresponding human gene. Eur J Biochem **173**, 45–51

87 Stoner, C. M and Gudas, L. J. (1989) Mouse cellular retinoic acid binding protein cloning, complementary DNA sequence, and messenger RNA expression during the retinoic acid-induced differentiation of F9 wild type and RA-3-10 mutant teratocarcinoma cells Cancer Res. **49**, 1497–1504

88 Giguere, V, Lyn, S., Yip, P, Siu, C H. and Amin, S (1990) Molecular cloning of cDNA encoding a second cellular retinoic acid-binding protein. Proc Natl Acad Sci. USA **87**, 6233–6237

89 Astrom, A, Tavakkol, A., Pettersson, U, Cromie, M., Elder, J T and Voorhees, J. J. (1991) Molecular cloning of two human cellular retinoic acid-binding proteins (CRABP) Retinoic acid-induced expression of CRABP-II but not CRABP-I in adult human skin in vivo and in skin fibroblasts in vitro J Biol Chem **266**, 17662–17666

90 Eller, M S, Oleksiak, M F., McQuaid, T J, McAfee, S. G. and Gilchrest, B A (1992) The molecular cloning and expression of two CRABP cDNAs from human skin Exp. Cell Res **198**, 328–336

91 Zheng, W. L. and Ong, D E (1998) Spatial and temporal patterns of expression of cellular retinol-binding protein and cellular retinoic acid-binding proteins in rat uterus during early pregnancy. Biol Reprod **58**, 963–970

92 Yamamoto, M, Drager, U C, Ong, D E and McCaffery, P (1998) Retinoid-binding proteins in the cerebellum and choroid plexus and their relationship to regionalized retinoic acid synthesis and degradation Eur J Biochem. **257**, 344–350

93 Maden, M. (1994) In Vitamin A in Health and Disease (Blomhoff, R., ed.), pp 289–322, Marcel Dekker, New York

94 Lampron, C, Rochette-Egly, C, Gorry, P, Dolle, P, Mark, M, Lufkin, T., LeMeur, M and Chambon, P. (1995) Mice deficient in cellular retinoic acid binding protein II (CRABPII) or in both CRABPI and CRABPII are essentially normal. Development **121**, 539–548

95 Fawcett, D., Pasceri, P., Fraser, R, Colbert, M, Rossant, J and Giguere, V. (1995) Postaxial polydactyly in forelimbs of CRABP-II mutant mice. Development **121**, 671–679

96 Eichele, G. (1989) Retinoids and vertebrate limb pattern formation Trends Genet. **5**, 246–251

97 Hoffman, C and Eichele, G (1994) Retinoids in development. In The Retinoids, Biology, Chemistry and Medicine (Sporn, M. B., Roberts, A B and Goodman, D S, eds), pp. 387–441, Raven Press, New York

98 Takase, S, Ong, D E and Chytil, F (1986) Transfer of retinoic acid from its complex with cellular retinoic acid-binding protein to the nucleus. Arch Biochem Biophys **247**, 328–334

99 Gaub, M. P., Lutz, Y., Ghyselinck, N. B, Scheuer, I., Pfister, V., Chambon, P. and Rochette-Egly, C. (1998) Nuclear detection of cellular retinoic acid binding proteins I and II with new antibodies. J. Histochem. Cytochem. **46**, 1103–1111

100 Norris, A W, Cheng, L, Giguere, V., Rosenberger, M and Li, E (1994) Measurement of subnanomolar retinoic acid binding affinities for cellular retinoic acid binding proteins by fluorometric titration. Biochim Biophys Acta **1209**, 10–18

101 Dong, D, Ruuska, S E, Levinthal, D. J. and Noy, N. (1999) Distinct roles for cellular retinoic acid-binding proteins I and II in regulating signaling by retinoic acid J Biol Chem. **274**, 23695–23698

102 Fiorella, P D and Napoli, J L (1991) Expression of cellular retinoic acid binding protein (CRABP) in *Escherichia coli* Characterization and evidence that holo-CRABP is a substrate in retinoic acid metabolism J Biol Chem **266**, 16572–16579

103 Fujii, H, Sato, T., Kaneko, S, Gotoh, O, Fujii-Kuriyama, Y, Osawa, K, Kato, S and Hamada, H (1997) Metabolic inactivation of retinoic acid by a novel P450 differentially expressed in developing mouse embryos EMBO J. **16**, 4163–4173

104 White, J A, Beckett-Jones, B, Guo, Y D, Dilworth, F J., Bonasoro, J, Jones, G and Petkovich, M (1997) cDNA cloning of human retinoic acid-metabolizing enzyme (hP450RAI) identifies a novel family of cytochromes P450 J Biol Chem **272**, 18538–18541

105 White, J. A., Guo, Y D, Baetz, K., Beckett-Jones, B., Bonasoro, J, Hsu, K E, Dilworth, F. J., Jones, G and Petkovich, M (1996) Identification of the retinoic acid-inducible all-trans-retinoic acid 4-hydroxylase J Biol. Chem **271**, 29922–29927

106 Ray, W J, Bain, G, Yao, M and Gottlieb, D. I (1997) CYP26, a novel mammalian cytochrome P450, is induced by retinoic acid and defines a new family. J. Biol Chem **272**, 18702–18708

107 Boylan, J F and Gudas, L J (1992) The level of CRABP-I expression influences the amounts and types of all-trans-retinoic acid metabolites in F9 teratocarcinoma stem cells J Biol Chem **267**, 21486–21491

108 Boylan, J F and Gudas, L J (1991) Overexpression of the cellular retinoic acid binding protein-I (CRABP-I) results in a reduction in differentiation-specific gene expression in F9 teratocarcinoma cells J Cell Biol. **112**, 965–979

109 Delva, L, Bastie, J N, Rochette-Egly, C, Kraiba, R., Balitrand, N, Despouy, G., Chambon, P. and Chomienne, C. (1999) Physical and functional interactions between cellular retinoic acid binding protein II and the retinoic acid-dependent nuclear complex Mol Cell. Biol. **19**, 7158–7167

110 Jing, Y., Waxman, S and Mira-y-Lopez, R (1997) The cellular retinoic acid binding protein II is a positive regulator of retinoic acid signalling in breast cancer cells Cancer Res **57**, 1668–1672

111 Vo, H P and Crowe, D L (1998) Transcriptional regulation of retinoic acid responsive genes by cellular retinoic acid binding protein-II modulates RA mediated tumor cell proliferation and invasion. Anticancer Res **18**, 217–224

112 Bucco, R. A., Zheng, W L, Davis, J. T., Sierra-Rivera, E, Osteen, K. G, Chaudhary, A K and Ong, D. E (1997) Cellular retinoic acid-binding protein(II) presence in rat uterine epithelial cells correlates with their synthesis of retinoic acid Biochemistry **36**, 4009–4014

113 Zheng, W L, Bucco, R. A, Schmitt, M C., Wardlaw, S A and Ong, D E (1996) Localization of cellular retinoic acid-binding protein (CRABP) II and CRABP in developing rat testis Endocrinology **137**, 5028–5035

114 Deigner, P S, Law, W C., Canada, F J and Rando, R. R (1989) Membranes as the energy source in the endergonic transformation of vitamin A to 11-cis-retinol Science **244**, 968–971

115 Stecher, H., Gelb, M H, Saari, J. C. and Palczewski, K (1999) Preferential release of 11-cis-retinol from retinal pigment epithelial cells in the presence of cellular retinaldehyde-binding protein. J. Biol. Chem **274**, 8577–8585

116 Saari, J. C. and Bredberg, D L (1988) CoA- and non-CoA-dependent retinol esterification in retinal pigment epithelium. J. Biol Chem **263**, 8084–8090

117 Saari, J. C. and Bredberg, D L (1989) Lecithin.retinol acyltransferase in retinal pigment epithelial microsomes J Biol Chem **264**, 8636–8640

118 Lion, F, Rotmans, J P, Daemen, F J and Bonting, S L (1975) Biochemical aspects of the visual process. XXVII. Stereospecificity of ocular retinol dehydrogenases and the visual cycle Biochim. Biophys. Acta **384**, 283–292

119 Saari, J C (1994) Retinoids in photosensitive tissues In The Retinoids, Biology, Chemistry and Medicine (Sporn, M B, Roberts, A. B. and Goodman, D. S, eds), pp 351–386, Raven Press, New York

120 Futterman, S, Saari, J C and Blair, S (1977) Occurrence of a binding protein for 11-cis-retinal in retina J Biol Chem **252**, 3267–3271

121 Saari, J. C., Bredberg, L. and Garwin, G. G. (1982) Identification of the endogenous retinoids associated with three cellular retinoid-binding proteins from bovine retina and retinal pigment epithelium J. Biol Chem. **257**, 13329–13333

122 Maw, M. A, Kennedy, B, Knight, A, Bridges, R, Roth, K. E, Mani, E J., Mukkadan, J. K., Nancarrow, D, Crabb, J. W and Denton, M J (1997) Mutation of the gene encoding cellular retinaldehyde-binding protein in autosomal recessive retinitis pigmentosa Nat. Genet **17**, 198–200

123 Bridges, C D., Foster, R. G., Landers, R. A and Fong, S L (1987) Interstitial retinol-binding protein and cellular retinal-binding protein in the mammalian pineal Vision Res. **27**, 2049–2060

124 Martin-Alonso, J. M, Ghosh, S, Hernando, N, Crabb, J W and Coca-Prados, M (1993) Differential expression of the cellular retinaldehyde-binding protein in bovine ciliary epithelium. Exp Eye Res **56**, 659–669

125 Sarthy, V (1996) Cellular retinaldehyde-binding protein localization in cornea Exp Eye Res. **63**, 759–762

126 Saari, J C., Huang, J., Possin, D E, Fariss, R N, Leonard, J., Garwin, G G, Crabb, J W. and Milam, A H (1997) Cellular retinaldehyde-binding protein is expressed by oligodendrocytes in optic nerve and brain Glia **21**, 259–268

127 Winston, A and Rando, R R (1998) Regulation of isomerohydrolase activity in the visual cycle Biochemistry **37**, 2044–2050

128 Saari, J C., Bredberg, D L and Noy, N (1994) Control of substrate flow at a branch in the visual cycle Biochemistry **33**, 3106–3112

129 Pepperberg, D R., Okajima, T L, Wiggert, B., Ripps, H, Crouch, R K. and Chader, G. J (1993) Interphotoreceptor retinoid-binding protein (IRBP) Molecular biology and physiological role in the visual cycle of rhodopsin Mol. Neurobiol **7**, 61–85

130 Adler, A J. and Spencer, S A (1991) Effect of light on endogenous ligands carried by interphotoreceptor retinoid-binding protein Exp Eye Res **53**, 337–346

131 Crouch, R K, Hazard, E. S, Lind, T, Wiggert, B, Chader, G and Corson, D W (1992) Interphotoreceptor retinoid-binding protein and alpha-tocopherol preserve the isomeric and oxidation state of retinol Photochem. Photobiol **56**, 251–255

132 Ho, M T, Massey, J. B, Pownall, H. J, Anderson, R E and Hollyfield, J G. (1989) Mechanism of vitamin A movement between rod outer segments, interphotoreceptor retinoid-binding protein, and liposomes. J. Biol. Chem. **264**, 928–935

133 Jones, G J., Crouch, R. K, Wiggert, B., Cornwall, M C and Chader, G. J (1989) Retinoid requirements for recovery of sensitivity after visual-pigment bleaching in isolated photoreceptors Proc Natl. Acad. Sci U.S.A **86**, 9606–9610

134 Flannery, J. G, O'Day, W, Pfeffer, B. A, Horowitz, J. and Bok, D (1990) Uptake, processing and release of retinoids by cultured human retinal pigment epithelium Exp Eye Res **51**, 717–728

135 Okajima, T. I., Wiggert, B, Chader, G J and Pepperberg, D. R (1994) Retinoid processing in retinal pigment epithelium of toad (*Bufo marinus*). J Biol. Chem. **269**, 21983–21989

136 Chen, H., Wiegand, R. D, Koutz, C A. and Anderson, R. E (1992) Docosahexaenoic acid increases in frog retinal pigment epithelium following rod photoreceptor shedding Exp Eye Res **55**, 93–100

137 Palczewski, K., Van Hooser, J P., Garwin, G G, Chen, J, Liou, G. I. and Saari, J C (1999) Kinetics of visual pigment regeneration in excised mouse eyes and in mice with a targeted disruption of the gene encoding interphotoreceptor retinoid-binding protein or arrestin Biochemistry **38**, 12012–12019

138 Ruiz, A, Winston, A, Lim, Y H, Gilbert, B A, Rando, R R and Bok, D (1999) Molecular and biochemical characterization of lecithin retinol acyltransferase. J Biol Chem **274**, 3834–3841

139 Chai, X, Zhai, Y, Popescu, G and Napoli, J L (1995) Cloning of a cDNA for a second retinol dehydrogenase type II Expression of its mRNA relative to type I J. Biol Chem. **270**, 28408–28412

140 Penzes, P, Wang, X, Sperkova, Z and Napoli, J. L (1997) Cloning of a rat cDNA encoding retinal dehydrogenase isozyme type I and its expression in *E coli.* Gene **191**, 167–172

141 Wang, X, Penzes, P and Napoli, J. L (1996) Cloning of a cDNA encoding an aldehyde dehydrogenase and its expression in *Escherichia coli.* Recognition of retinal as substrate J Biol. Chem. **271**, 16288–16293

142 Chai, X., Zhai, Y. and Napoli, J L (1996) Cloning of a rat cDNA encoding retinol dehydrogenase isozyme type III Gene **169**, 219–222

143 Chai, X., Boerman, M H., Zhai, Y. and Napoli, J L (1995) Cloning of a cDNA for liver microsomal retinol dehydrogenase A tissue-specific, short-chain alcohol dehydrogenase. J Biol. Chem **270**, 3900–3904

144 Jurukovski, V, Markova, N. G., Karaman-Jurukovska, N., Randolph, R K, Su, J, Napoli, J L and Simon, M. (1999) Cloning and characterization of retinol dehydrogenase transcripts expressed in human epidermal keratinocytes. Mol Genet Metab **67**, 62–73

145 Simon, A, Lagercrantz, J, Bajalica-Lagercrantz, S and Eriksson, U. (1996) Primary structure of human 11–cis retinol dehydrogenase and organization and chromosomal localization of the corresponding gene Genomics **36**, 424–430

146 Haeseleer, F, Huang, J, Lebioda, L, Saari, J C and Palczewski, K. (1998) Molecular characterization of a novel short-chain dehydrogenase/reductase that reduces all-trans-retinal J. Biol Chem **273**, 21790–21799

147 Gamble, M. V, Shang, E, Zott, R P., Mertz, J R, Wolgemuth, D J and Blaner, W S (1999) Biochemical properties, tissue expression, and gene structure of a short chain dehydrogenase/reductase able to catalyze cis-retinol oxidation J. Lipid Res. **40**, 2279–2292

148 Zanotti, G., Berni, R and Monaco, H L (1993) Crystal structure of liganded and unliganded forms of bovine plasma retinol-binding protein J. Biol Chem **268**, 10728–10738

149 Levin, M. S., Locke, B, Yang, N. C., Li, E. and Gordon, J. I (1988) Comparison of the ligand binding properties of two homologous rat apocellular retinol-binding proteins expressed in *Escherichia coli* J Biol Chem. **263**, 17715–17723

150 Li, E, Qian, S. J, Winter, N S., d'Avignon, A., Levin, M. S and Gordon, J I (1991) Fluorine nuclear magnetic resonance analysis of the ligand binding properties of two homologous rat cellular retinol-binding proteins expressed in *Escherichia coli* J Biol. Chem. **266**, 3622–3629

Biochem J (2000) 348, 497–506 (Printed in Great Britain)

Auto-catalysed progression of aneuploidy explains the Hayflick limit of cultured cells, carcinogen-induced tumours in mice, and the age distribution of human cancer

David RASNICK[1]

Department of Molecular and Cell Biology, 229 Stanley Hall, University of California at Berkeley, Berkeley, CA 94720, U.S.A.

Evidence continues to accumulate that aneuploidy, an imbalance in the number of chromosomes, is responsible for the characteristic phenotypes of cancer, including the abnormal cellular size and morphology of cancer cells, the appearance of tumour-associated antigens, as well as the high levels of membrane-bound and secreted proteins responsible for invasiveness and loss of contact inhibition. Aneuploidy has also been demonstrated to be the self-perpetuating source of the karyotypic instability of cancer cells. Here it is shown that the auto-catalysed progression of aneuploidy explains the kinetics of the finite lifetime of diploid cells in culture, the time course of the appearance of papillomas and carcinomas in benzo[*a*]pyrene-treated mice, and the age-dependence of human cancers. Modelling studies indicate that the ease of spontaneous transformation of mouse cells in culture may be due to a chaotic progression of aneuploidy. Conversely, the strong preference towards senescence and resistance to transformation of human cells in culture may be the result of a non-chaotic progression of aneuploidy. Finally, a method is proposed for quantifying the aneuploidogenic potencies of carcinogens.

Key words: carcinogenesis, dynamics, metabolic control analysis.

INTRODUCTION

Recently, we have provided experimental and theoretical evidence [1–4] supporting Theodor Boveri's proposal that aneuploidy, an imbalance in the number of chromosomes, is the underlying cause of cancer [5]. Aneuploidy provides a simple and coherent explanation for the fundamental phenotypes of cancer cells, independent of gene mutation. Accordingly, the abnormal cellular size and morphology of cancer cells [6], the appearance of tumour-associated antigens [7,8], the high levels of membrane-bound and secreted proteins [9] responsible for invasiveness and loss of contact inhibition, and even the daunting genetic instability [10,11] that enables cancer cells to evade chemotherapy are all the natural consequence of the massive over- and under-expression of proteins due to aneuploidy [1–3].

Using Metabolic Control Analysis we were able to demonstrate how the fraction of the genome undergoing differential expression, rather than the magnitude of the differential expression, controls phenotypic transformation [3]. In order to transform the robust normal phenotype into cancer the expression of thousands of normal gene products must be increased by an average of 2-fold [3]. The results showed that alterations in a handful of 'gatekeeper' or 'caretaker' genes [12,13] are insufficient for the generation of cancer-specific phenotypes, since their numbers are too few to alter the normal phenotype. Indeed, not one mutant cellular gene, nor even a group of mutants, has ever been shown to transform a normal human or animal cell into a cancer cell [14–18].

We were also able to show that aneuploidy is the self-perpetuating source of the genetic instability of cancer cells [1,3,4]. Aneuploid cells are trapped in an endless cycle of rearranging the genome to produce the most economical production of translation products at the expense of chromosomal balance. The mitotic division of an aneuploid cell is an experiment in evolution that results in the random shuffling and redistribution of the genome. The generations of offspring of aneuploid cells are unlikely to ever have identical genetic compositions [3,19,20]. It is this intrinsic genetic instability of aneuploid cells that fuels the progression to malignancy of cancer cells.

Since a loss of gene dose is more deleterious than a gain [3,21–24], hyperploid cells have a survival advantage over their hypoploid siblings. The survival advantage of hyperploid cells, coupled with the inherent genetic instability of aneuploid cells, fuels the auto-catalysed progression to DNA indices between 1.5 and 2 that are found in most malignant cancers [25].

Here I analyse the time course of the auto-catalysed progression of aneuploidy from its known experimental and unknown spontaneous origins. The results show that the finite *in vitro* lifetime of human diploid cell strains [26,27], the kinetics of tumour formation in benzo[*a*]pyrene-treated mice [28,29] and the age distribution of human cancers [30] can all be explained by the auto-catalysed progression of aneuploidy during cell division.

THE HAYFLICK LIMIT OF MICE AND MEN

Due to the work of Hayflick [26,27], the finite lifetime of diploid cells in culture has become commonly known as the Hayflick limit. After a period of active multiplication, generally less than one year (approx. 50 cell divisions), primary human fetal cells in culture demonstrate an increased generation time, gradual cessation of mitotic activity, accumulation of cellular debris and, ultimately, total degeneration [27]. Only during the degenerative phase (phase III) in cell culture do primary cells lose contact inhibition and become obviously aneuploid [26,27,31]. In contrast to primary, diploid cells derived from an animal or humans, cell lines (immortal cells) are a heterogeneous mix of heteroploid cells.

According to Levan and Biesele [19], the very first mitoses of mouse cells *in vitro* show chromosomal irregularities. A zero level of numerical and structural chromosomal abnormalities '... is possible only with cells *in situ*, and that as soon as they are

---

[1] To whom correspondence should be addressed (e-mail rasnick@mindspring.com)

$$D + \phi \xrightarrow{k} \phi$$

Scheme 1 Kinetic model of an auto-catalysed process

explanted they start mutating... The genetic diversity thus induced in the tissue culture will increase steadily as new aberrations are continuously released by the mitotic mutation process. This situation prevails either until the tissue culture fades out or until some truly superior cells happen to appear...' [19].

In the spirit of Levan and Biesele I propose that the auto-catalysed progression of aneuploidy explains the observed time course of the Hayflick limit, including differences in spontaneous rates of transformation. The simplest kinetic model of an auto-catalysed process is shown in Scheme 1. It is important to point out that Scheme 1 represents an auto-catalysed process, not an auto-catalysed chemical reaction, which would be written as $A+B \rightarrow 2B$ [32]. D and ϕ do not represent chemical species undergoing a chemical reaction and, therefore, do not imply stoichiometry. D is the diploid fraction and ϕ is the aneuploid fraction of an aneuploid cell. D and ϕ can also represent the average diploid and aneuploid fractions, respectively, of a population of cells.

Following an event that produces the initial aneuploidy (i.e. produces $\phi > 0$), the values of D and ϕ tend to change with each mitotic division. We have previously shown that the aneuploid fraction, ϕ, is equivalent to the flux control coefficient of Metabolic Control Analysis and is a measure of the extent to which a given aneuploid segment of the genome controls phenotypic transformation (see Appendix A of [3]).

The rate equation for the increase in the aneuploid fraction, ϕ, in Scheme 1 is given by eqn. (1). Since ϕ appears on both sides of Scheme 1, the growth of the aneuploid fraction, ϕ, is auto-catalysed. In other words, the greater the level of aneuploidy, the faster the growth of the aneuploid fraction ϕ. The constant k in Scheme 1 is a measure of the growth-rate of the aneuploid fraction ϕ

$$\frac{d\phi}{dt} = k\phi D \tag{1}$$

Since the sum of the diploid fraction, D, and the aneuploid fraction, ϕ, always equals 1, the diploid fraction can be expressed in terms of ϕ, i.e. $D = 1-\phi$. Making this substution for D in eqn. (1) gives eqn. (2).

$$\frac{d\phi}{dt} = k\phi(1-\phi) \tag{2}$$

Integrating eqn. (2) yields eqn. (3), which gives the aneuploid fraction, ϕ, as a function of time.

$$\phi_t = \frac{1}{e^{-kt}\left(\frac{1}{\phi_0}-1\right)+1} \tag{3}$$

The constant ϕ_0 is the initial aneuploid fraction of an individual cell, or the average for a population of cells, at time zero, the time when aneuploidy is initiated (e.g. by a carcinogen or cell culturing). The rate constant k has units cell-cycle^{-1} when t is in cell-cycles. Since ϕ_t ranges from 0 to 1 (i.e. 0–100%), eqn. (3) gives the time course for the progression of aneuploidy, and thus the time course of any phenotypic change that depends on it.

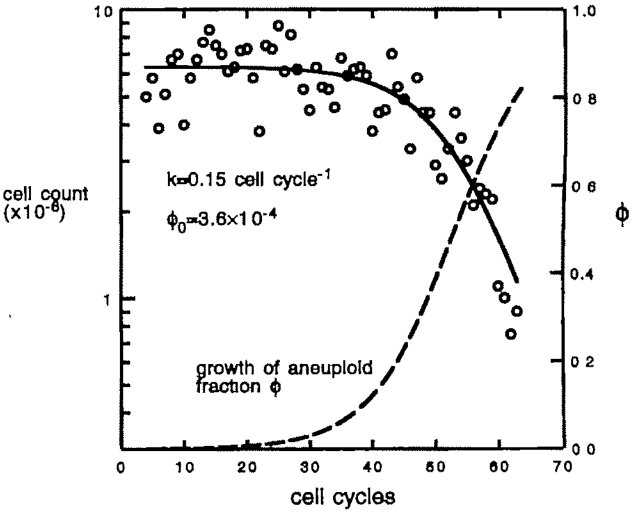

Figure 1 Hayflick limit due to auto-catalysed growth of aneuploidy

Hayflick limit of 63 cell divisions for the human cell strain WI-44. The solid line is the best-fit curve of eqn. (4) to the serial passaging data from Figure 3 of Hayflick [27]. The broken line represents the auto-catalysed progression of the aneuploid fraction, ϕ, for the same data using eqn. (3)

With the growth of aneuploidy there is a corresponding reduction in the diploid fraction, and hence a reduction in the number of dividing cells since aneuploid cells are less viable than diploid cells [3,21–24]. If we assume that cell proliferation is due primarily to diploid cells, then the number of non-transformed dividing cells in culture at time t is proportional to the diploid fraction D_t. Using the relationship $D_t = 1-\phi_t$ and the value of ϕ_t in eqn. (3), one can derive eqn. (4), which shows that the number of dividing cells (N_t) remaining during serial passaging is equal to the number of cells at time zero (N_0) times the diploid fraction at time t [i.e. $N_t = N_0(1-\phi_t)$].

$$N_t = N_0\left(1-\frac{1}{e^{-kt}\left(\frac{1}{\phi_0}-1\right)+1}\right) \tag{4}$$

Figure 1 (solid line) shows that eqn. (4) fits the data from Hayflick's Figure 3 for the serial passaging of the human cell strain WI-44 [27]. The sharp decline in the cell count at around 43 passages (beginning of the degenerative phase III) is mirrored by the steep growth in the aneuploid fraction, ϕ (Figure 1, broken line).

The calculated value $\phi_0 = 0.0004$ (Figure 1) indicates that the average aneuploid fraction at the beginning of the exponential phase (phase II) of cell culture was 0.04%. However, this initial aneuploid fraction is only an estimate since it does not take into account that some aneuploid cells will be viable and divide, albeit at a reduced level. The initial aneuploidy in the WI-44 cells was almost certainly caused by the culturing process itself, especially the mechanical and enzymic treatments used to promote proliferation *in vitro* [19,26,27].

In contrast to cultured cells, the extra copy of chromosome 21 in Down's syndrome individuals is present at fertilization. Trisomy of chromosome 21 represents an aneuploid fraction $\phi = 0.018$ for each cell [3,22,33], which is substantially larger than the initial average value in Figure 1 for normal human explants. As a consequence, one would predict that the Hayflick limit of Down's syndrome cells in culture should be significantly shorter

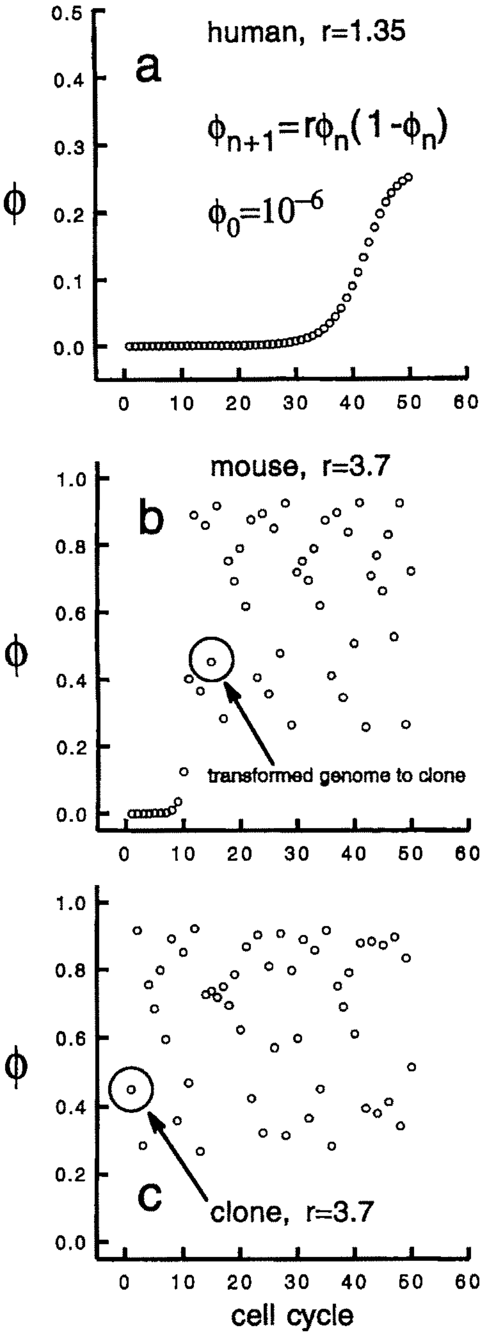

Figure 2 Chaotic growth of aneuploidy drives transformation

The logistic equation, eqn (5), was used to model the auto-catalysed progression of aneuploidy for primary human (**a**) and mouse (**b**) fetal cells in culture. The control parameter $r = 1.35$ and the initial average aneuploid fraction $\phi_0 = 10^{-6}$ (see text for derivation) were used in eqn (5) to model the 50 cell cycle Hayflick limit for primary human fetal cells (**a**). The circles represent the average aneuploid fraction, ϕ, for the population of cells at each cell cycle. In panel (**b**) the same ϕ_0 was used for the mouse fetal cells (see text). Although values of $r > 1.5$ are completely unrealistic for modelling the Hayflick limit of human cells, we could use values of the control parameter greater than 3.57 to model mouse cells. A control parameter greater than 3.57 for the logistic equation [eqn (5)] produces chaotic growth patterns [39]. Therefore, the value $r = 3.7$ produces a chaotic progression of the aneuploid fraction, ϕ, for all cell divisions beyond approx. 12 cycles (**b**). While the aneuploid human cells will probably die out before they can be transformed into an immortal cell line, because so little genome space is being explored, the chaotic redistribution of the mouse genome provides a greater opportunity for the cells to hit upon a genetic combination that leads to transformation and immortalization. (**c**) Shows that when the transforming genome in panel (**b**) (arrow) is cloned, its intrinsic karyotypic instability immediately leads to a heterogeneous population of heteroploid offspring.

than normal cells. A perusal of the literature shows that this prediction is correct. Schneider and Epstein reported in 1972 that, '... Skin fibroblasts derived from patients with Down's syndrome (trisomy-21) have a significantly decreased number of cumulative cell population doublings ... measured from the initial passage to senescence when compared with cultures from karyotypically normal age-matched controls ...' [34]. The Hayflick limit they measured for the Down's syndrome cells was 20% shorter than for normal cells, which represents an approximate 2000-fold reduction in the exponential process of cell doubling.

Recently, Mukherjee and Costello used fluorescence *in situ* hybridization to study the progression of aneuploidy in cultured fibroblasts from patients with three premature aging syndromes: Cockayne, Hutchinson–Gilford, and Werner [35]. '...[T]he interphase aneuploidy levels of all chromosomes under study were significantly higher in cells from the syndromes as compared to those of the normal controls at both earlier and later passages. In general, the interphase aneuploidy levels of each of the chromosomes in both the control and experimental cell cultures increased with *in vitro* proliferation and aging, although to a much lesser extent in the controls ...' [35].

The meticulous studies of Hayflick indicated that, '... the finite lifetime of ... diploid cell strains is an innate characteristic of the cells ...' [26,27]. Furthermore, he argued that, '.. Cells which can be cultivated indefinitely *in vitro* (heteroploid cell lines) can only be compared with continuously cultivable cells *in vivo*, i.e., transplantable tumors. Likewise, diploid cells having a finite lifetime *in vitro* can only be compared with normal cells *in vivo*, i.e., normal somatic cells ...' [27]. Hence, the transformation of mortal (diploid) cells in culture into immortal (aneuploid) cell lines 'can be regarded as oncogenesis *in vitro* ...' [27].

Transformation of cells in culture can also be viewed as evolution *in vitro*. Explanted cells are forced to evolve into viable single cell organisms in the laboratory or perish. Most cultured human cells stop dividing after entering phase III (the degenerative phase) and only rarely undergo spontaneous transformation into immortal (aneuploid) cell lines [27]. In contrast, cultured primary rodent cells frequently undergo spontaneous transformation to become immortal cell lines [19,36]. The 70% shorter Hayflick limit (14 cell divisions) may be a clue as to why primary mouse fetal cells spontaneously transform into immortal cell lines much more readily than human cells [36].

The auto-catalysed genetic instability inherent in aneuploid cells, coupled with the chromosomal heterogeneity of cancer cells, suggests that an underlying chaotic process may be involved in the mitotic division of some aneuploid cells [37]. With this possibility in mind, I suspected that primary mouse cells in culture experience a more chaotic progression of aneuploidy than human cells. A chaotic redistribution of the genome would provide a greater opportunity for aneuploid cells to hit upon a genetic combination that would lead to immortalization and transformation.

While eqn. (2) gives the continuous rate of change of the aneuploid fraction, ϕ, as a function of the instantaneous value of ϕ, the actual change in DNA content of an aneuploid cell is a discrete process that takes place at each cell division. Alternatively, then, the growth of the aneuploid fraction, ϕ, of Scheme 1 can be modelled by eqn. (5), a form of the logistic rate equation that is known to reveal certain chaotic processes [37–39].

$$\phi_{(n+1)} = r\phi_n(1-\phi_n) \qquad (5)$$

The right side of eqn. (5) is formally identical with eqn. (2). However, the left side of eqn. (5) replaces the instantaneous change in ϕ with a discrete value of the aneuploid fraction for each cell division. Eqn. (5) shows that the average aneuploid

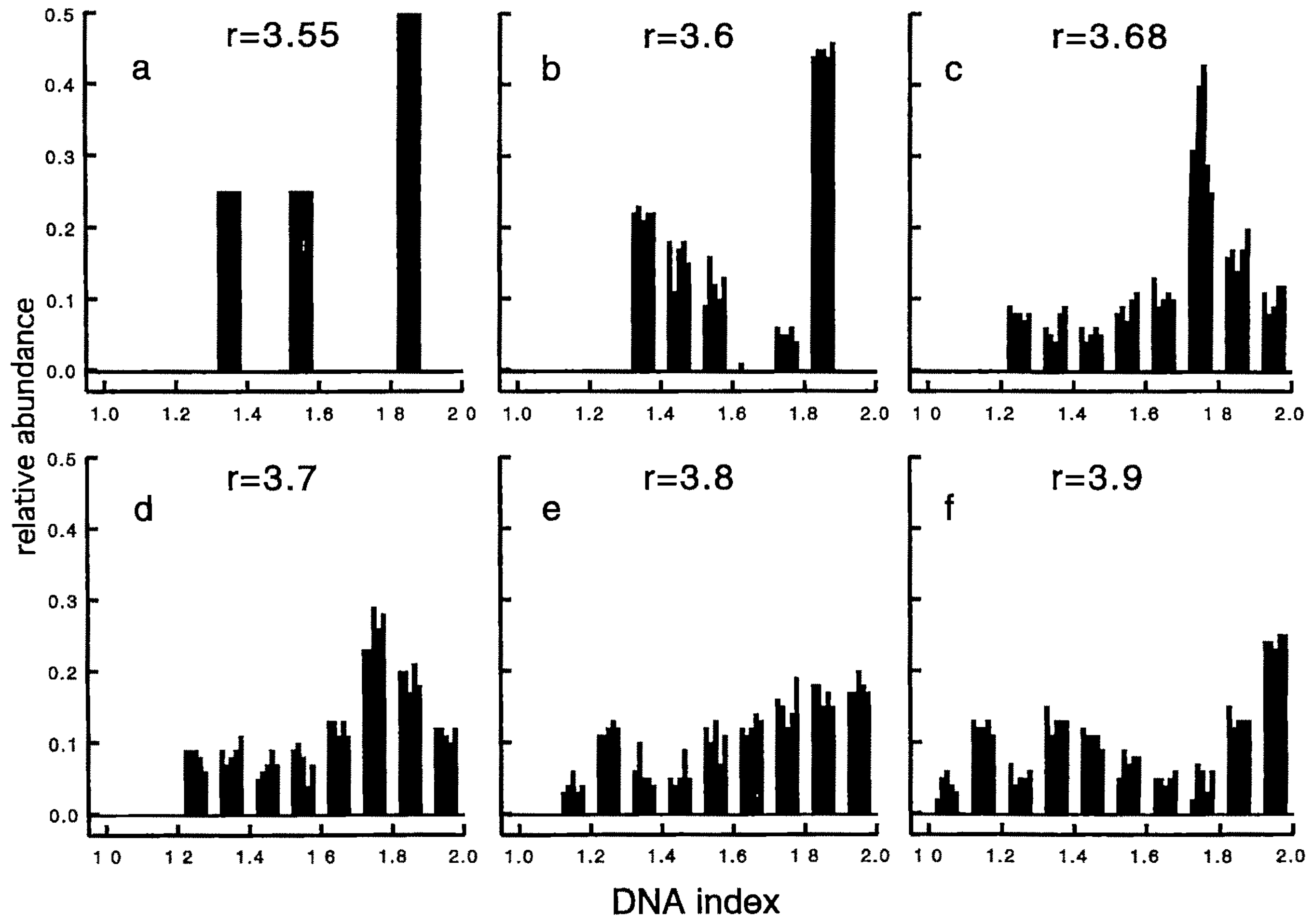

Figure 3 DNA index of cancer cells is due to chaotic growth of aneuploidy

Using the relationship DNA index = $1+\phi$ (see text for details) and the value $n = 1000$ cell cycles, eqn. (5) was used to model the distribution of DNA indices for various values of the control parameter r. In order to capture the long-term average behaviour in the distribution of DNA indices, we used only cell divisions 501–1000. The DNA indices were divided into 10 equal sampling bins centred at DNA index = 1.05, 1.15, 1.25, etc. There were five sampling windows comprising 100 cell divisions each (e.g. 501–600, 601–700, etc.). For each of the five sampling windows, the number of times a value of DNA index fell into a bin was counted. (**a**) A simple distribution of DNA indices for a non-chaotic value of r. (**b–f**) Show that in the chaotic region there is an increasing number of cells with a wider spectrum of DNA indices. (**c** and **d**) Show the DNA indices clustering around a value of 1.75, which compares with DNA indices of 1.7 for cervical cancer [44], 1.7–1.8 for breast cancer [45,46] and 1.6 for liver cancer [47].

fraction of a population of cells at the $n+1$ cell division is determined by the average level of aneuploidy at the nth cell division. The control parameter, r, in eqn. (5) is unitless and is different from the rate constant, k, in eqns. (2) and (3). Since ϕ_1 ranges from 0 to 1 (i.e. 0–100%), eqn. (5) models the discrete growth, including chaotic, of any phenotypic change that depends on the progression of aneuploidy.

Since the non-disjunction frequency of mammalian cells *in situ* is estimated to be 10^{-4} to 10^{-5} per chromosome [40], and since there are 23 and 22 chromosome pairs in normal human and mouse cells, respectively, then the initial aneuploid fraction, ϕ_0, for the explanted cells is no larger than approximately 10^{-6} [i.e. $10^{-4}/(22\text{–}23) \approx 10^{-6}$] Therefore $\phi_0 = 10^{-6}$ was used in eqn. (5) to model the auto-catalysed progression of aneuploidy for human and mouse primary fetal cells in culture (Figure 2).

Several values of the control parameter, r, were tested before finding the value of 1.35 (Figure 2a) that reproduces the 35 cell-divisions of phase II and the sigmoidal growth of the aneuploid fraction, ϕ, of Figure 1 for human cells. Values of the control parameter, r, greater than 1.5 were completely unrealistic since they resulted in phase III starting at approx. 10 cell divisions for the human cells.

In contrast to the human cells, the control parameter, r, had to be increased to at least a value of 2.5 in order to model the Hayflick limit of approx. 14 cell-cycles for primary mouse fetal cells. But what is more interesting, a value of the control parameter greater than 3.57 worked just as well. A value of $r > 3.57$ for the logistic equation [eqn. (5)] results in chaotic growth patterns [39]. Thus the value $r = 3.7$ in Figure 2b produces a chaotic progression of the aneuploid fraction, ϕ, for all cell divisions beyond approx. 12 cycles (Figure 2b).

Figures 2(a) and 2(b) fail to take into account the fact that almost all of the aneuploid cells would lose the gene-shuffling lottery and not become transformed into an immortalized cell line. However, if a transforming genome did happen to appear, for example the hypothetical one circled in Figure 2(b), and was cloned, it would generate from the very first cell division a heterogeneous population of heteroploid offspring as shown in Figure 2(c). Figure 2(c) models exactly the well-known karyotypic instability of cloned transformed cells [1,27,41]. As Hayflick and

Moorhead have said, '–The use of cloning as a means of reducing... variability in heteroploid cell lines is unfortunately limited by the rapid re-emergence of a range of chromosomal types among the progeny of a clone...'[26]. In fact, '...each subpopulation can regenerate the entire range of subpopulations ...' of a heteroploid population of cells [42].

The results of Figure 2 show that it is possible to model the hypothesis that the transformation-prone mouse cells can exhibit a substantially more chaotic pattern of aneuploidy than the transformation-resistant primary human cells in culture. If the results of Figure 2 reflect reality, an interesting question presents itself. What are the biochemical, genetic, or other factors responsible for the dramatically different values of the control parameter, r, that lead to the non-chaotic growth of aneuploidy in human cells on the one hand, and a chaotic progression of aneuploidy in mouse cells on the other? At present we don't know. What is known is that carcinogens initiate aneuploidy and also greatly accelerate its growth [1,2].

THE DNA INDEX OF CANCER CELLS

As discussed above, the DNA index of a population of aneuploid cells tends to increase with each cell division until reaching steady-state values between 1.5 and 2 typical of late-stage cancer [43]. Recently, we have shown that the DNA index $= 1-\phi+\pi\phi$, where π is the segmental ploidy factor (e.g. $\pi = 1.5$ for trisomy) [3]. While there is a limitless number of π values, we have previously shown that $\pi = 2$ is the most economical, hence likely, value of the ploidy factor in cellular transformation [3]. Making this substitution for π gives a DNA index $= 1+\phi$. Exploiting this simple relationship between the DNA index and the aneuploid fraction, ϕ, eqn. (5) can be used to explore the chaotic growth of the DNA index of dividing cells.

Figure 3 shows a series of histograms for the relative abundance of aneuploid cells compared with DNA index for different values of the control parameter r. The most striking feature of Figure 3 is the clustering of cells around certain values of DNA index and the pronounced bias for most cells having hypertriploid to hypotetraploid DNA indices reminiscent of human cancer [43]. Particularly noteworthy is the clustering of cells around a DNA index of 1.75 in Figures 3(c) and 3(d). This value compares with DNA indices of 1.7 for cervical cancer [44], 1.7–1.8 for breast cancer [45,46] and 1.6 for liver cancer [47].

Figure 3(a) shows three populations of cells for $r = 3.55$, a value of the control parameter just below the chaotic region. Two groups of cells are near triploid (DNA index = 1.35 and 1.55) and the largest group is hypotetraploid (DNA index = 1.85). Although the cells in Figure 3(a) have DNA indices typical of cancer, they are unlikely to lead to a transformed, immortalized cell line because so little genome space is being explored. In other words, it is unlikely that dividing cells would happen upon viable transformants in the limited range of DNA indices presented in Figure 3(a).

A chaotic strategy of gene shuffling, on the other hand, is much more likely to lead to successful cancer cells. For example, Figures 3b–3f shows that for $r > 3.57$ (the chaotic region) an increasing number of cells are exploring a wider spectrum of DNA indices, thus increasing their chances of hitting on an aneuploid combination of genes leading to immortalization and transformation.

TUMOUR FORMATION IN CARCINOGEN-TREATED MICE

In a large group of mice, the number of papillomas rises continuously from about five weeks after the first painting with benzo[*a*]pyrene until about a month after painting has been discontinued [28]. Charles and Luce-Clausen have proposed tOhat, '...mutation of some particular gene which is essential to normal differentiation of new skin cells...' is necessary for the production of papillomas in benzo[*a*]pyrene-treated mice [29]. Furthermore, they suggested that papillomas form only after both copies of the hypothetical gene are mutated to the cancerous form. Based on this double-hit scenario, the authors used statistical arguments to derive a model of benzo[*a*]pyrene-induced papilloma formation reproduced here in eqn (6).

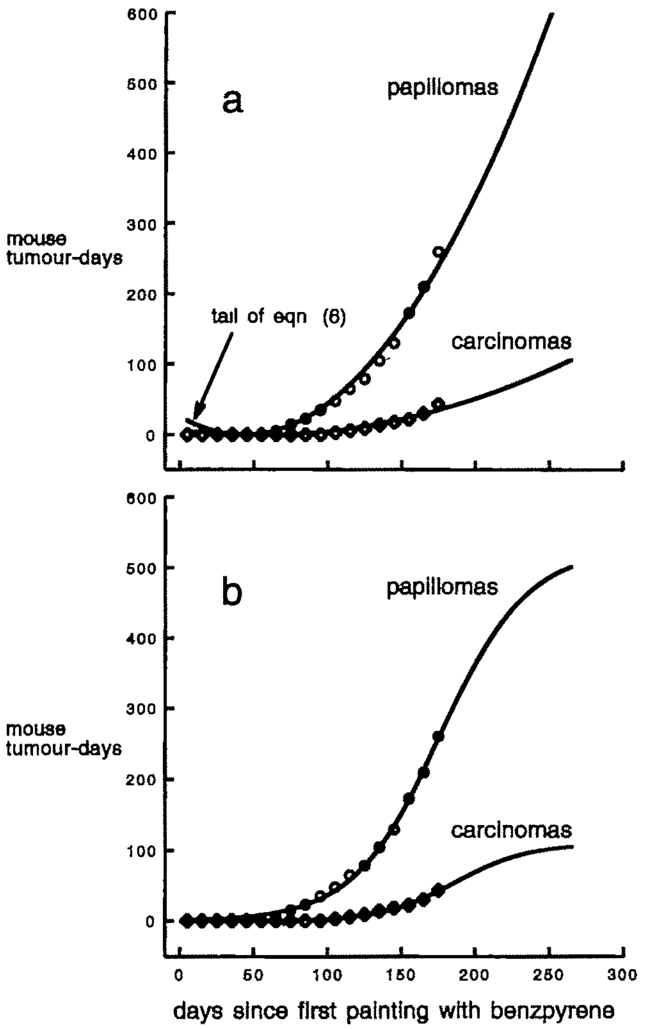

Figure 4 Two models of tumour production in benzo[*a*]pyrene-painted mice

Except for the upward tail of eqn (6) (arrow) near the origin in (**a**), both models, the mutant-gene [eqn. (6)] (**a**) and the auto-catalysed progression of aneuploidy [eqn (7)] (**b**), fit the experimental data of Morton et al reasonably well [28] However, the two models are conceptually quite different The most notable difference is the shape of the growth curves The gene mutation models are all parabolic upwards, hence the upward tail for eqn (6) in (**a**), while the auto-catalysed progression of aneuploidy model is sigmoidal (**b**)

$$n = N\left(\frac{k(t-i)}{c}\right)^2 \qquad (6)$$

The dependent variable, n, is the average number of papillomas per mouse produced at time, t, after the first painting. The value $N = 4\times10^6$ is the average number of stratum germinativum cells (skin cells) painted with benzo[*a*]pyrene per mouse, $c = 3.5$ days is

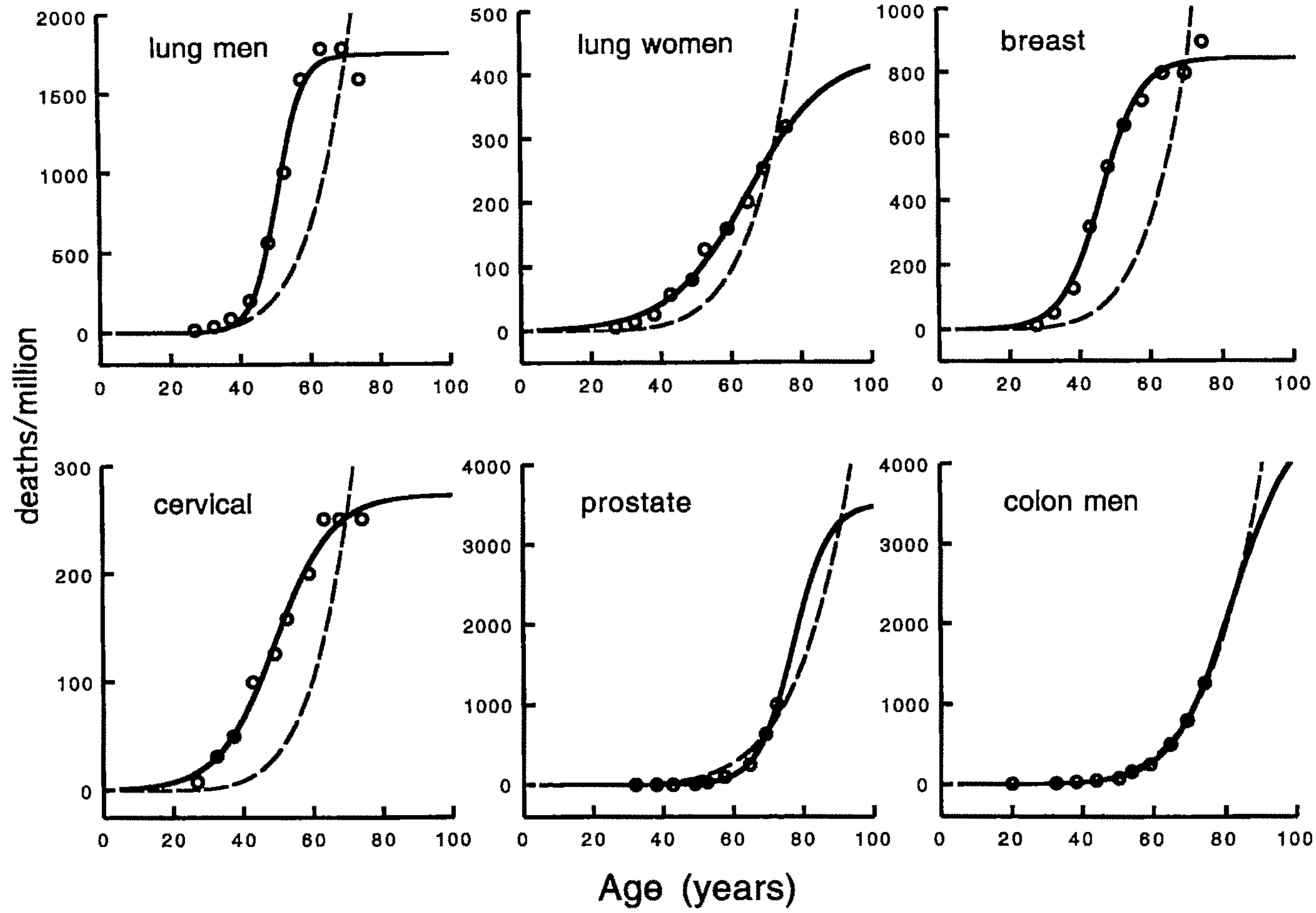

Figure 5 Auto-catalysed growth of aneuploidy explains age distribution of human cancers

The superiority of the sigmoidal curve of eqn. (7) for the auto-catalysed progression of aneuploidy is best demonstrated by comparing it with eqn. (8) for the multi-hit version of the gene mutation theory of human carcinogenesis. Eqn. (7) gives a good fit (solid lines) to the number of deaths per million people for six typical cancers as a function of age [30]. The broken lines show the best-fit curves to the same data for the seven successive mutation model [eqn. (8)]. The only good fit for eqn. (8) is with colon cancer deaths in men.

the interval between paintings, the calculated value $i = 32$ days is the average number of days between the moment a skin cell possesses both copies of the mutated hypothetical proto-cancer gene and the subsequent time when the tissue formed by that cell becomes recognizable as a papilloma, and k is the mutation rate constant.

Figure 4(a) shows the best-fit curves of eqn. (6) to the data of Morton et al. for benzo[*a*]pyrene-induced papillomas and carcinomas in black mice [28]. The calculated mutation rate constants, k, are 2×10^{-4} and 9×10^{-5} for the papilloma and carcinoma data, respectively. This compares with a mutation rate constant of 3×10^{-5} determined by Charles and Luce-Clausen for the same data [29].

If, on the other hand, the production of tumours is due to the auto-catalysed progression of aneuploidy [eqn. (3)] as a result of benzo[*a*]pyrene treatment, then the number (N_t) of papillomas or carcinomas at time t is equal to the plateau number of tumours (N_∞) times the average aneuploid fraction ϕ_t at time t [eqn. (7)].

$$N_t = N_\infty \phi_t \tag{7}$$

Figure 4(b) shows the best-fit curves of eqn. (7) to the data of Morton et al. [28]. Except for the upward tail of eqn. (6) near the origin in Figure 4(a) (arrow), both models, the mutant-gene [eqn. (6)] and the auto-catalysed progression of aneuploidy [eqn. (7)], fit the experimental data of Morton et al. reasonably well. However, the two models are conceptually quite different. The most notable difference is the shape of the growth curves. The gene mutation models are all parabolic upwards [hence the upward tail for eqn. (6) in Figure 4a], while the auto-catalysed progression of aneuploidy model is sigmoidal (Figure 4b).

The gene mutation model, in its various forms, predicts an increasing number of mutations and subsequent cancers over time. Eqn. (6), for example, assumes a specific number of mutations beforehand. In the example considered above, both copies of a hypothetical proto-cancer gene have to be mutated to produce papillomas and carcinomas in benzo[*a*]pyrene-painted mice. The aneuploidy model, on the other hand, makes only one assumption that holds for all cases, which is: the auto-catalysed progression of aneuploidy.

THE AGE DISTRIBUTION OF CANCER IN MAN

The superiority of the sigmoidal curve is best demonstrated by comparing the auto-catalysed progression of aneuploidy with the prevailing multi-hit version of the gene mutation theory of human carcinogenesis. In the 1950s, log–log plots of cancer death-rates compared with age were roughly linear, with slopes of approx. 6 [30]. That meant that cancer death-rates increased proportionally with the sixth power of age. It wasn't long before the sixth-power dependence was interpreted in light of the gene mutation hypothesis of cancer. It was hypothesized that cancer is the end-result of seven successive mutations [48,49]. However, this hypothesis did not lead to the observed result in all circumstances (Figure 5, broken lines). Aware of this shortcoming, Armitage and Doll warned that the successive cellular changes leading to the development of cancer were not necessarily gene mutations [30]. This is an important consideration since carcinogenic and mutagenic activities do not always go hand-in-hand [1,2,16,50]. This insight was short-lived, however. In deriving eqn. (8) to model the incidence-rate of cancer with age, Armitage and Doll assumed that seven mutations lead to cancer, and that the mutations should be specific, discrete, stable and proceed in a unique order [30].

$$\text{Cancer rate}_t = kp_1p_2p_3p_4p_5p_6p_7t^6 \qquad (8)$$

Eqn. (8) shows that the incidence-rate of cancer at age t (assumed to be proportional to death-rate [30]) will be proportional to the product of the probabilities of the occurrences of each of the seven mutations (p_i) and to the sixth power of age, where k is the rate constant. With the exception of colon cancer in men, eqn. (8) is a poor model of the incidence-rate for a number of human cancers (Figure 5, broken lines). In an effort to salvage their model, Armitage and Doll argued that, due to ignorance of the individual mutation probabilities, p_i, they had to combine all the probabilities into one constant. According to the authors, this combined probability was the source of the poor fit between eqn. (8) and the data. They speculated, that if only one knew the individual mutation probabilities or could fashion a suitable weighting scheme to derive the appropriate mean probability, then eqn. (8) should fit the real-world data. Unfortunately, the authors were not able to come up with either. I was also unable to derive a parabolic equation that fits the sigmoidal incidence-rate data of Figure 5.

However, it turns out that eqn. (7), which is based on eqn. (3) for the auto-catalysed progression of aneuploidy, gives a good fit to all the cancer incidence-rate data of Figure 5 (solid lines). In this case, the number of cancer deaths per million persons (N_t) at age t is equal to the plateau number of cancer deaths per million persons (N_∞) times the right side of eqn. (3), which is the average aneuploid fraction, ϕ_t, for a population of cells. The only good fit for eqn. (8) is with the incidence of colon cancer deaths in men, which may be the source of Kinzler and Vogelstein's proposal that seven gene mutations are responsible for colon cancer [49].

The sigmoidal nature of the mortality-rate data is more obvious in Figure 5 than in the log–log plots used by Armitage and Doll. The data points for lung cancer in men and women, as well as breast and cervical cancer in women, span much more of the sigmoidal region of eqn. (7) than do the data for prostate and colon cancer in men (Figure 5). This difference is due to the much later onset of prostate and colon cancer in men than with the other four examples. The inflection points of the sigmoidal curves are a measure of this difference. The inflection points for lung cancer in men and women, and for breast and cervical cancer in women are approx. 50, 60, 45, and 50 years of age respectively (Figure 5). However, the inflection points for prostate and colon cancer in men occur at much older ages: approx. 75 and 80 years, respectively (Figure 5).

QUANTIFYING ANEUPLOIDOGENS

The only variables that a carcinogen, acting as an aneuploidogen, can influence are ϕ_0 and the growth rate constant, k, in eqn. (3) or ϕ_1 and the growth control parameter, r, in eqn (5). If the aneuploidogen is applied only once, it seems reasonable to assume that it will affect only ϕ_0 or ϕ_1 and not k or r. Thus, the effect of a once-only application of an aneuploidogen is to increase the aneuploid fraction at the time it is applied. Under this condition, the growth parameters k and r are intrinsic to the cell and independent of the aneuploidogen. Using eqn. (3), Figure 6 shows how a once-only application of an aneuploidogen affects the progression of the aneuploid fraction, ϕ_t^a, relative to ϕ_t for the untreated normal human cells of Figure 1 (Figure 6a) and for Down's syndrome cells (Figure 6b) respectively.

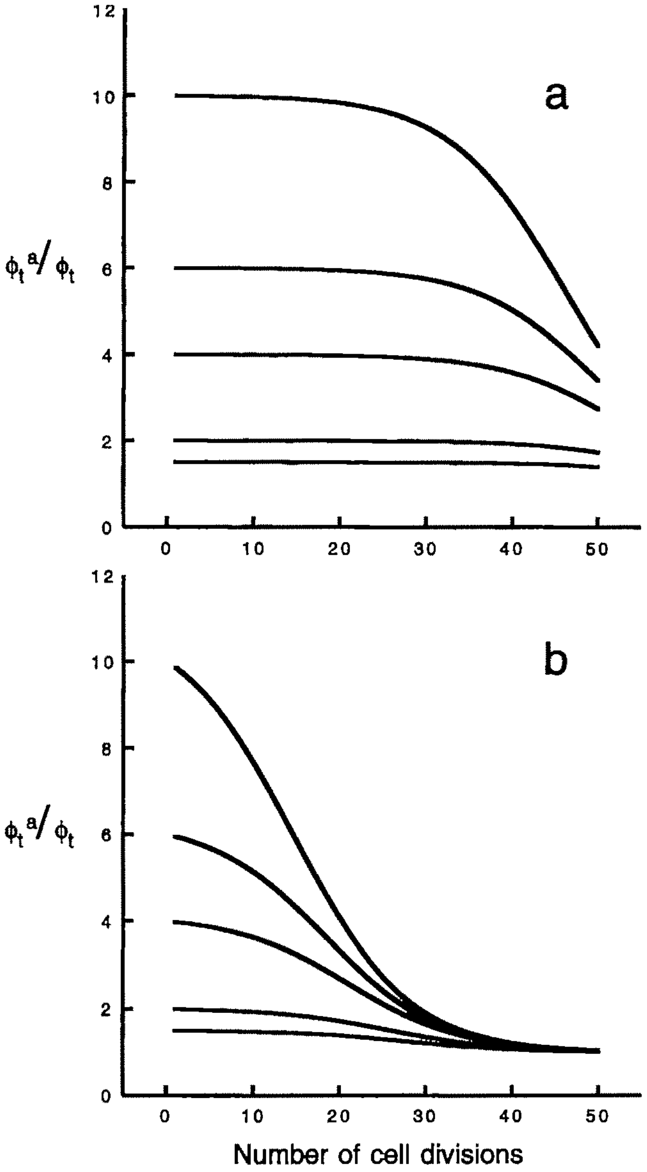

Figure 6 Once-only application of an aneuploidogen

A once-only application of an aneuploidogen affects the progression of the aneuploid fraction, ϕ_t^a, relative to untreated control cells, ϕ_t, for the normal human cells of Figure 1 (**a**) and for Down's syndrome cells (**b**) respectively (α = 1.5, 2, 4, 6, 10, see text) A robust strategy for quantifying aneuploidogenic potencies is a once-only treatment of primary human cells in culture with the test substance followed by periodic measuring of the level of aneuploidy, e g at 10, 15 and 20 cell divisions, and recording the average

On the other hand, if an aneuploidogen is present continuously, then it effectively increases the growth parameters k and r. Again

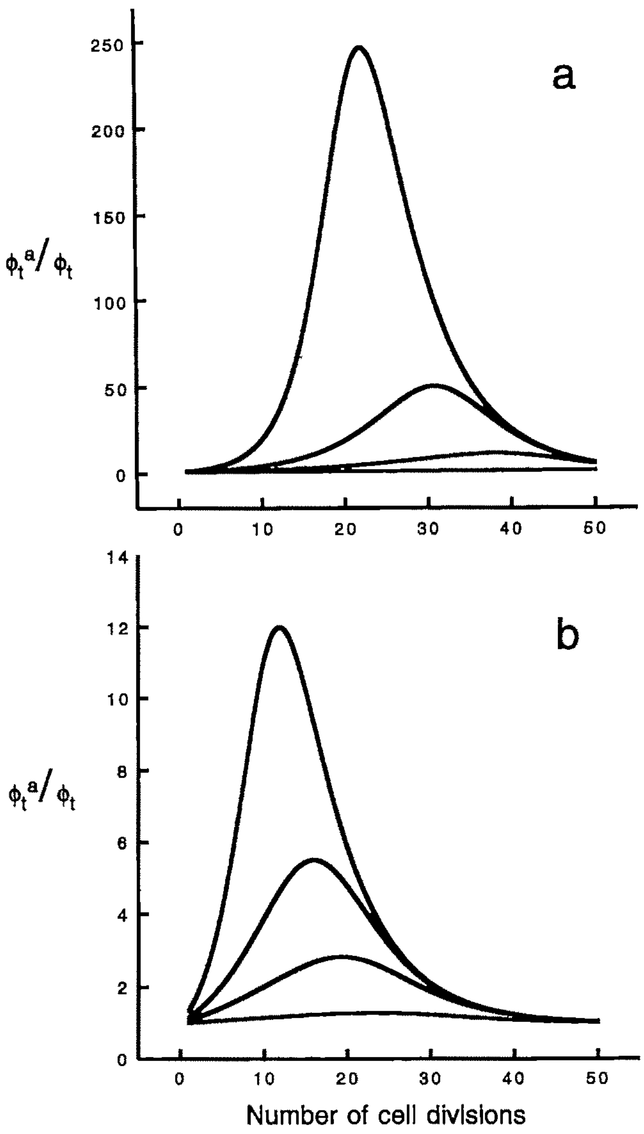

Figure 7 Continuous application of an aneuploidogen

The continuous presence of an aneuploidogen effectively increases the growth parameters k [eqn (3)] and r [eqn (5)], affecting the progression of the aneuploid fraction, ϕ_t^a, relative to untreated control cells, ϕ_t, for the normal human cells of Figure 1 (**a**) and for Down's syndrome cells (**b**) respectively ($k_a = 1.1, 1.5, 2, 3$ times k) While the continuous presence of a carcinogen is efficient at generating aneuploidy and transforming cells, a once-only application is a much better strategy for quantifying aneuploidogenic potencies (Figure 6)

using eqn (3), Figure 7 shows how a continuous application of an aneuploidogen affects the progression of the aneuploid fraction, ϕ_t^a, relative to ϕ_t for the untreated normal human cells of Figure 1 (Figure 7a) and for Down's syndrome cells (Figure 7b) respectively. Figure 7(a) shows that it takes 20–40 cell divisions (depending on the potency or concentration of the drug) for aneuploidogen-treated primary human cells to reach a maximum level of aneuploidy compared with untreated controls. Figure 7(b), as expected, shows that continuously treated Down's syndrome cells should reach a maximum level of aneuploidy sooner than normal cells, i.e. 10–20 cell divisions, depending on the potency or concentration of the drug.

While Figure 7 shows that the continuous presence of a carcinogen is efficient at generating aneuploidy, a once-only application is a much better strategy for quantifying aneuploidogenic potencies (Figure 6). Figure 6(a) shows that compared to untreated human cells in culture, the relative level of aneuploidy, α [eqn. (9)], produced by a once-only application of an aneuploidogen is constant over 25–35 cell divisions.

$$\frac{\phi_t^a}{\phi_t} \approx \frac{\phi_0^a}{\phi_0} = \alpha \tag{9}$$

In contrast, Figure 6(b) shows that for Down's syndrome and other cells, e.g. rodent, which have a high background level of aneuploidy in cell culture, the relative level of carcinogen-induced aneuploidy, α, is approximately constant for only 5–15 cell divisions, depending on the potency of the aneuploidogen. Accordingly, I propose that a robust strategy for quantifying aneuploidogenic potencies is a once-only treatment of primary human cells in culture with the test substance followed by periodic measuring of the relative level of aneuploidy, e.g. at 10, 15 and 20 cell divisions, and recording the average.

DISCUSSION

The fact that euploid cells have a finite lifetime in cell culture has become commonly known as the Hayflick limit [26,27,31]. In the alien environment of cell culture, explanted mammalian diploid cells are forced to reproduce continuously orders of magnitude beyond their *in vivo* existence. Diploid cells *in vitro* respond to the stress of cell culture by altering their genome in order to adapt to life as single-cell organisms or perish. Primary human cells almost never stumble upon the chromosomal alterations needed for unlimited propagation *in vitro* [27].

In contrast with human cells, primary rodent cells forced to endure cell culture often spontaneously hit upon the right combination of aneuploid chromosomes and make the quantum leap to immortalization and thus escape the abyss of the Hayflick limit. The price these cells pay for immortality is perpetual genetic instability due to aneuploidy [1,3]. It may even turn out that genetic instability is necessary for immortality.

In the present study I have proposed that the chaotic growth of aneuploidy is a possible mechanism for the quantum leap to immortalization and transformation. At present it is not known what would lead to the spontaneous chaotic growth of aneuploidy in rodent cells and non-chaotic growth in human cells. It may be that in addition to being aneuploidogens, carcinogens may act to promote the chaotic growth of aneuploidy leading to cancer in humans.

The auto-catalysed progression of aneuploidy during cell division links cancer and the Hayflick limit of cells in culture. The Hayflick limit is due to the production of non-viable aneuploid cells. Transformation and cancer, on the other hand, result from the rare appearance of immortal aneuploid cells. Below I compare the auto-catalysed progression of aneuploidy with the early efforts to model the time course of carcinogenesis.

The early attempts to understand and explain human cancers were largely empirical. For example, in an effort to linearize the strongly non-linear cancer mortality rate data, Armitage and Doll plotted the log of the cancer death rates versus the log of age [30]. Some of the graphs were approximately linear with a slope of 6, to which they and others attributed physiological and biochemical significance. The slope of the log–log plots has been given various interpretations, ranging from indicating that a colony of six or seven cancer cells was a critical size for the propagation of cancer, to that a cancer cell was the end result of seven successive gene mutations. The seven successive gene mutation interpretation has survived to the present [49].

According to the somatic gene mutation hypothesis there are two classes of genes that when mutated lead to cancer. (1) The mutated oncogenes are proposed to actively cause cancer by destabilizing the genome and disrupting hypothetical regulatory networks that maintain homoeostasis. (2) The mutated tumour suppressor genes are proposed to actively protect against and nullify the deleterious effects of mutant oncogenes. In other words, there is a surveillance system of protective genes that actively maintains the euploid state and prevents aneuploidy and cancer. The tumour suppressor gene hypothesis advances the Victorian-like pessimism that an 'unsupervised' euploid cell will follow its natural tendency towards corruption and spontaneously become a cancer cell in the absence of these ever-vigilant guardians of the genome.

A major problem with the somatic gene mutation hypothesis is that to date there is no functional evidence for such genes causing either cancer or, conversely, protecting a cell against aneuploidy and transformation. Furthermore, the somatic gene mutation hypothesis is powerless to explain even the simplest and most glaring facts of carcinogenesis [1–4]. For example, the gene mutation hypothesis cannot explain why a once-only treatment with carcinogens results in tumours only months to years later, long after the inducing carcinogen has reacted with the components of the cell [4,6,51]. The auto-catalysed progression of aneuploidy, on the other hand, readily explains the long latent periods between exposure to a carcinogen and the appearance of cancer (Figures 4 and 5).

The inadequacy of the gene mutation hypothesis to account for phenotypic transformation may be more easily seen with the aid of a metaphor. If the genome is a biological dictionary then the life of a cell is a Shakespearean drama. The most efficient means of rewriting a cell's script, then, would be the wholesale shifting and shuffling of the genes, which aneuploidy accomplishes admirably. Continuing the metaphor, if one were to alter or delete a word here and there in *Hamlet*, for example, such 'point mutations' would be invisible to the vast majority of theatre-goers. The same is true for a multicellular organism, which is at least as resistant to point mutations as a Shakespeare play. On the other hand, without 'mutating' a single word, one could transform the script of *Hamlet* into a legal document, a love letter, a declaration of independence, or more likely gibberish by simply shifting and shuffling, copying and deleting numerous individual words, sentences and whole paragraphs.

In contrast with the somatic gene mutation hypothesis, we have previously proposed that the genetically balanced euploid state is intrinsically stable and not prone to aneuploidy and transformation *in vivo* [1,3]. Aneuploid cells are damaged cells that almost never survive in competition with euploid cells. Nevertheless, there are rare aneuploid cells that win the genetic lottery by evolving into autonomous, single cell organisms that are extremely capable of rewriting their own scripts as evidenced by the extensive genetic instability inherent in these cells.

In spite of the fact that aneuploidy is an efficient mechanism for altering the phenotypes of complex systems, the presence of point mutations in a handful of genes continues to be viewed as a significant, even causal factor in carcinogenesis. However, a more likely reason for the appearance of these point mutations is that they are innocuous, hence readily accommodated during the clonal expansion of barely viable aneuploid cells as they compete with their more viable euploid counterparts. The current emphasis in cancer research on seeking mutant genes in a perpetual background of aneuploidy is a classic example of not seeing the forest for the trees.

Aneuploidy, in contrast to somatic gene mutation, offers a simple and coherent mechanism for the transformation of a range of complex phenotypes [1–4]. The auto-catalysed progression of aneuploidy is sufficient to explain: (1) the time course of primary cells in culture [eqn. (4), Figure 1]; (2) the difference in the spontaneous transformation rates between primary human and mouse cells in culture [eqn. (5), Figure 2]; (3) why the DNA indices of cancer cells are between 1.5 and 2 [eqn. (5), Figure 3]; (4) the time course for the appearance of tumours in carcinogen-treated mice [eqn. (7), Figure 4]; and (5) the age distribution of cancers in man [eqn. (7), Figure 5].

I am grateful to the International Coalition for Medical Justice (Culpeper, VA, U S A), Robert Leppo (philanthropist, San Francisco, CA, U S.A.), the Abraham J. and Phyllis Katz Foundation (New York, NY, U S A), the Nathan Cummings Foundation (San Francisco, CA, U S A), Boveran, Inc (Saratoga, CA, U S A), and a foundation that prefers to be anonymous, for financial support Additional funds were contributed by Carol J Wilhelmy (San Mateo, CA, U.S.A) and other private sources I wish to thank Peter Duesberg (University of California at Berkeley, CA, U S A.), Brian Goodwin (Schumaker College, Devon, U.K.), Ruhong Li (University of California at Berkeley, CA, U S A), Richard Strohman (University of California at Berkeley, CA, U S A), Leonard Hayflick (Sea Ranch, CA, U S A), Harvey Bialy (Guernavaca, Mexico) for many fruitful discussions and valuable criticism, and An Bodhran for years of liquid support and liberating good humour.

REFERENCES

1 Duesberg, P, Rausch, C, Rasnick, D and Hehlmann, R (1998) Genetic instability of cancer cells is proportional to their degree of aneuploidy. Proc Natl Acad Sci U S A **95**, 13692–13697
2 Li, R, Yerganian, G, Duesberg, P, Kraemer, A, Willer, A, Rausch, C and Hehlmann, R (1997) Aneuploidy 100% correlated with chemical transformation of Chinese hamster cells Proc. Natl Acad Sci U S A **94**, 14506–14511
3 Rasnick, D and Duesberg, P. H. (1999) How aneuploidy affects metabolic control and causes cancer Biochem J **340**, 621–630
4 Duesberg, P, Li, R, Rasnick, D, Rausch, C, Willer, A, Kraemer, A, Yerganian, G and Hehlmann, R (2000) Aneuploidy precedes and segregates with chemical carcinogenesis. Cancer Genet Cytogenet, in the press
5 Boveri, T (1914) Zur Frage der Entstehung Maligner Tumoren, Fischer, Jena
6 Pitot, H. C. (1986) The natural history of neoplastic development In Fundamentals of Oncology, pp. 163–200, Marcel Dekker, Inc, New York
7 Basmajian, J V, Desmond-Burke, M, Burnett, G W., Campbell, C C, Cohn, W. E., Corliss, C E, Ferguson, D. J, Frazer, J P, Freedman, B J, Greene, N M et al (1982) Stedman's Medical Dictionary, pp 931, Williams & Wilkins, Baltimore
8 Frati, L, Cortesi, E, Ficorella, C, Manzari, V and Verna, R (1984) Phenotypic and genetic markers of cancer turning point in research In Genetic and Phenotypic Markers of Tumors (Aaronson, S A, Frati, L and Verna, R, eds), pp 1–20, Plenum Press, New York
9 Alderman, E M, Lobb, R. R and Feit, J W (1985) Isolation of tumor-secreted products from human carcinoma cells maintained in a defined protein-free medium Proc Natl Acad Sci U S A **82**, 5771–5775
10 Heppner, G and Miller, F R. (1998) The cellular basis of tumor progression Int Rev. Cytol. **177**, 1–56
11 Nowell, P. C. (1976) The clonal evolution of tumor cell populations Science **194**, 23–28
12 Kinzler, K W and Vogelstein, B (1997) Cancer-susceptibility genes gatekeepers and caretakers Nature (London) **386**, 761,763
13 Tomlinson, I. and W, Bodmer (1999) Selection, the mutation rate and cancer. ensuring that the tail does not wag the dog Nat Med **5**, 11–12
14 Thraves, P, Reynolds, S., Salehi, Z, Kim, W K, Yang, J H., Rhim, J S and Dritschilo, A (1991) Detection of transforming genes from radiation transformed human epidermal keratinocytes by a tumorigenicity assay In Neoplastic Transformation in Human Cell Culture (Rhim, J S and Dritschilo, A, eds), pp 93–101, The Humana Press Inc, Totowa, NJ
15 Lijinsky, W (1989) A view of the relation between carcinogenesis and mutagenesis Environ Mol Mutagen **14**, 78–84
16 Duesberg, P H (1995) Oncogenes and cancer Science **267**, 1407–1408
17 Stanbridge, E J (1990) Human tumor suppressor genes Annu. Rev Genet **24**, 615–657
18 Li, R, Sonik, A, Stindl, R, Rasnick, D and Duesberg, P (2000) Aneuploidy versus gene mutation hypothesis recent study claims mutation, but is found to support aneuploidy. Proc. Natl Acad Sci U S A **97**, 3236–3241
19 Levan, A. and Biesele, J J (1958) Role of chromosomes in cancerogenesis, as studied in serial tissue culture of mammalian cells Ann N Y. Acad. Sci. **71**, 1022–1053

20 Lengauer, C, Kinzler, K. W and Vogelstein, B (1998) Genetic instabilities in human cancers Nature (London) **396**, 643–649

21 Atkin, N B and Baker, M. C (1990) Are human cancers ever diploid – or often trisomic? Conflicting evidence from direct preparations and culture Cytogenet Cell Genet **53**, 58–60

22 Sandler, L and Hecht, F. (1973) Genetic effects of aneuploidy Am. J Hum. Genet **25**, 332–339

23 Lindsley, D L, Sandler, L, Baker, B S, Carpenter, A T C, Denell, R. E., Hall, J C., Jacobs, P A., Miklos, G L. G, Davis, B. K., Gethmann, R C et al (1972) Segmental aneuploidy and the genetic gross structure of the Drosophila genome Genetics **71**, 157–184

24 German, J. (1974) Predisposing to chromosome instability and cancer In Chromosomes and Cancer vol 1 (German, J, ed.), pp 601–617, John Wiley & Sons, New York

25 Wolman, S R (1983) Karyotypic progression in human tumors Cancer Metastasis Rev **2**, 257–293

26 Hayflick, L and Moorhead, P S (1961) The serial cultivation of human diploid cell strains Exp Cell Res. **25**, 585–621

27 Hayflick, L (1965) The limited *in vitro* lifetime of human diploid cell strains. Exp Cell Res. **37**, 614–636

28 Morton, J J, Luce-Clausen, E M and Mahoney, E. B. (1942) Visible light and skin tumors induced with benzpyrene in mice Cancer Res **2**, 256–260

29 Charles, D R and Luce-Clausen, E M. (1942) The kinetics of papilloma formation in benzpyrene-treated mice Cancer Res **2**, 261–263

30 Armitage, P and Doll, R. (1954) The age distribution of cancer and the multi-stage theory of carcinogenesis. Br J Cancer **8**, 1–12

31 Saksela, E and Moorhead, P S (1963) Aneuploidy in the degenerative phase of serial cultivation of human cell strains Proc Natl Acad. Sci U S A **50**, 390–395

32 Steinfeld, J I, Francisco, J S and Hase, W L (1989) Chemical Kinetics and Dynamics, pp 182–182, Prentice Hall, Englewood Cliffs

33 Shapiro, B L (1983) Downs syndrome—a disruption of homeostasis. Am. J Med Genet **14**, 241–269

34 Schneider, E. L and Epstein, C. J (1972) Replication rate and lifespan of cultured fibroblasts in Down's syndrome Proc Soc Exp. Biol. Med **141**, 1092–1094

35 Mukherjee, A B. and Costello, C (1998) Aneuploidy analysis in fibroblasts of human premature aging syndromes by FISH during *in vitro* cellular aging Mech Ageing Dev **103**, 209–222

36 Todaro, G T and Green, H (1963) Quantitative studies of the growth of mouse embryo cells in culture and their development into established lines J Cell Biol **7**, 299–313

37 Posadas, E M, Criley, S R. and Coffey, D. S (1996) Chaotic oscillations in cultured cells rat prostate cancer. Cancer Res. **56**, 3682–3688

38 Alligood, K T, Sauer, T. D and Yorke, J A (1996) One-dimensional maps. In Chaos: An Introduction to Dynamical Systems, (Thomas, F, Banchoff, K D, Gonnet, G., Marsden, J and Wagon, S, eds), pp 1–42, Springer, New York

39 Williams, G P (1997) The parameter as king. In Chaos Theory Tamed, pp. 161–167, Joseph Henry Press, Washington DC

40 Holliday, R (1989) Chromosome error propagation and cancer Trends Genet **5**, 42–45

41 Lengauer, C, Kinzler, K W. and Vogelstein, B (1997) Genetic instability in colorectal cancers Nature (London) **386**, 623–627

42 Kimmel, M and Axelrod, D E (1990) Mathematical models of gene amplification with applications to cellular drug resistance and tumorigenicity Genetics **125**, 633–644

43 Shackney, S E, Berg, G, Simon, S R, Cohen, J., Amina, S, Pommersheim, W, Yakulis, R, Wang, S, Uhl, M., Smith, C A et al (1995) Origins and clinical implications of aneuploidy in early bladder cancer Cytometry **22**, 307–316

44 Reid, R, Fu, Y S, Herschman, B. R, Crum, C. P, Braun, L., Shah, K V., Agronow, S. J. and Stanhope, C R (1984) Genital warts and cervical cancer Am J. Obstet Gynecol **150**, 189–199

45 Shackney, S E, Singh, S G, Yakulis, R, Smith, C. A, Pollice, A A, Petruolo, S, Waggoner, A and Hartsock, R J (1995) Aneuploidy in breast cancer: a fluorescence *in situ* hybridization study Cytometry **22**, 282–291

46 Devilee, P, Thierry, R F, Kievits, T, Kolluri, R., Hopman, A H N, Willard, H F, Pearson, P. L and Cornelisse, C J (1988) Detection of chromosome aneuploidy in interphase nuclei from human primary breast tumors using chromosome-specific repetitive DNA probes Cancer Res **48**, 5825–5830

47 Kato, A, Kubo, K, Kurokawa, F., Okita, K, Oga, A and Murakami, T (1998) Numerical aberrations of chromosomes 16, 17, and 18 in hepatocullular carcinoma Dig. Dis Sci. **43**, 1–7

48 Nordling, C. O (1953) A new theory on the cancer-inducing mechanism. Br. J Cancer **7**, 68–72

49 Kinzler, K and Vogelstein, B. (1996) Lessons from hereditary colorectal cancer Cell **87**, 159–170

50 Duesberg, P. H and Schwartz, J R (1992) Latent viruses and mutated oncogenes: no evidence for pathogenicity. Prog Nucleic Acid Res Mol Biol **43**, 135–204

51 Cairns, J (1978) The epidemiology of cancer In Cancer: Science and Society, pp 35–61, W H Freeman and Company, San Francisco

---

Received 25 November 1999/6 March 2000, accepted 10 April 2000

Biochem. J (2000) 348, 507–515 (Printed in Great Britain)

Glycosylation-site-selective synthesis of *N*-acetyl-lactosamine repeats in bis-glycosylated human lysozyme

Ralph MELCHER*, Alexandra HILLEBRAND*, Ute BAHR†, Bernd SCHRÖDER*, Michael KARAS† and Andrej HASILIK*[1]

*Institut fur Physiologische Chemie, Philipps-Universitat Marburg, D-35033 Marburg, Germany, and †Instrumentelle Analytische Chemie, J W Goethe-Universitat, D-60590 Frankfurt, Germany

---

We have studied the elongation of oligosaccharides containing *N*-acetyl-lactosamine repeats using glycosylated human lysozyme mutants as a model. We reported previously that a combination of glycosylation sites at the 49th (site IV) and 68th (site II) amino acid residues of the protein particularly stimulates the synthesis of *N*-acetyl-lactosamine repeats [Melcher, Grosch, Grosse and Hasilik (1998) Glycoconjugate J. **15**, 987–993]. In the present study we show that it is the carbohydrate attached to site IV that is selectively affected. It contains more *N*-acetyl-lactosamine repeats when site II is glycosylated in the same molecule. As a corollary of the glycosylation at site II, the synthesis of a third antenna at site IV is increased. The triantennary oligosaccharides at site IV contain more *N*-acetyl-lactosamine repeats than the biantennary ones. Thus placing a carbohydrate at site II stimulates the branching and the elongation of the carbohydrate at the other site.

Key words: mutant, oligosaccharide, polylactosamine.

INTRODUCTION

Migration of cells from the vasculature into the surrounding environment is an important step in defense reactions and in the spread of metastases (reviewed in [1,2]). During inflammation, endothelium in the affected tissue becomes activated and interacts with cells bearing cognate structures, such as sialyl Lewis^x substances. These substances bind to selectins, which are exposed on the surface of endothelium and platelets, in a regulated manner. They are found at the non-reducing termini of various glycoconjugates with extensions made of *N*-acetyl-lactosamine repeats. It has been shown in several systems that the synthesis of the repeats depends on the expression of distinct enzymes, including the elongating β-1,3-*N*-acetylglucosaminyltransferase [3–5] and the branching β-1,6-*N*-acetylglucosaminyltransferases [6,7]. Sialyltransferases, meanwhile, act as terminators of elongation [8,9]. *N*-Acetylglucosaminyltransferase V (responsible for the synthesis of the β-1,6-linked branch in complex oligosaccharides) is considered to be an important regulator of the *N*-acetyl-lactosamine repeat synthesis, since branched oligosaccharides are better substrates for elongation than linear ones [6,7]. The branching of complex oligosaccharides and the elongation of the repeats are increased in human neoplastic cells [10]. These modifications support the synthesis of sialyl Lewis^X substances and increase the metastatic potential of cells.

Previously we have described glycosylation of lysozyme mutants at sites referred to as I (Asn^{22}), II (Asn^{68}) and IV (Asn^{49}) [9,11]. We have shown that the processing of the carbohydrates at these sites is similar. Lysozyme glycosylated at site I has been found to contain predominantly biantennary oligosaccharides bearing zero to four *N*-acetyl-lactosamine repeats (in order of decreasing frequency). The size of the oligosaccharides appears to be significantly increased in a mutant bearing carbohydrate simultaneously at sites II and IV, but not in a mutant glycosylated at sites I and IV. In the present study we show that the characteristic modification in molecules glycosylated at sites II and IV particularly affects site IV. Using MS analysis of glycopeptides that were prepared from molecules glycosylated at either site alone or at both sites simultaneously, we conclude that glycosylation at site II strongly affects the processing of the oligosaccharides at site IV. These oligosaccharides become enriched in elongated triantennary oligosaccharides.

MATERIALS AND METHODS

Materials and cells

Human milk lysozyme and rabbit anti-(human lysozyme) serum have been prepared and characterized previously [9,12]. Radioactive methionine/cysteine mixture (Tran^{35}S-label) was purchased from ICN Biomedicals (Eschwege, Germany). Endo-β-*N*-acetylglucosaminidase F2 from *Flavobacterium meningosepticum* and endo-β-galactosidase from *Bacteroides fragilis* were obtained from Boehringer-Mannheim (Mannheim, Germany). Chinese hamster ovary (CHO) cells expressing glycosylated human lysozyme II/IVT have been described previously [11]. The glycosylation sites that are referred to by the symbols II and IVT have been introduced with mutations G68N/P71S and D49N/S51T, respectively. These cells were prepared by stably transfecting CHO cells (CCL61) that were obtained from the American Type Culture Collection (Manassas, VA, U.S.A.).

Cell culture

Cells were grown to confluency in α-minimum essential medium (Life Technologies, Eggenstein, Germany), supplemented with 10 % (v/v) fetal bovine serum (Sigma, Deisenhofen, Germany), 100 units/ml penicillin and 100 μg/ml streptomycin, under air/CO_2 (19:1) at 37 °C

Abbreviations used. CHO, Chinese hamster ovary, MALDI-TOF MS, matrix-assisted laser-desorption ionization–time-of-flight MS

[1] To whom correspondence should be addressed (e-mail hasilik@mailer.uni-marburg.de)

Metabolic labelling, immunoprecipitation and characterization of the labelled lysozyme

Cells grown to early confluency in 3.4 cm diameter dishes were incubated in medium free of methionine and cysteine that was supplemented with 4 MBq of the Tran^{35}S-label for 16 h. Labelled lysozyme was isolated from the medium by immunoprecipitation [9], separated by SDS/PAGE [13] and visualized by PhosphorImager analysis (Molecular Dynamics, Krefeld, Germany). The quantification of the radioactivity associated with lysozyme was evaluated with software provided by the supplier. To characterize the carbohydrate moiety of lysozyme, aliquots of the immunoprecipitates were treated with endo-*N*-acetylglucosaminidase F2 and endo-β-galactosidase [9].

Purification and characterization of lysozyme II/IVT

Recombinant lysozyme II/IVT was produced in cultures of transfected CHO cells and purified from the conditioned medium using immune-affinity and hydroxylapatite chromatography. A previously described procedure [11] was scaled up to obtain 100–200 μg of protein. Briefly, 200 μg of affinity purified rabbit anti-(human lysozyme) antibody was coupled to CNBr-activated Sepharose 4B (Amersham Pharmacia Biotech, Braunschweig, Germany). Medium containing lysozyme was applied to the immunosorbent in a column and the enzyme was eluted with 0.1 M glycine/HCl (pH 2.65)/2 M $MgCl_2$. After concentrating and dialysing the eluate against 10 mM sodium phosphate buffer (pH 6.8), it was applied to a hydroxyapatite column (CHT2-I from Bio-Rad Laboratories GmbH, München, Germany) and this column was eluted with a linear gradient up to 0.5 M sodium phosphate buffer (pH 6.8). Mixtures of glycosylated forms of lysozyme were separated by SDS/PAGE and visualized by staining with silver nitrate [14].

Tryptic digestion, isolation and identification of glycopeptides

Fractions from the hydroxylapatite column, containing mono- and bis-glycosylated lysozyme, were pooled and vacuum-dried. The residues were dissolved in 0.3 ml of 5 M guanidinium chloride. The solution was mixed with 0.1 vol. of 1 M dithiothreitol for 30 min at 37 °C, followed by 0.15 vol. of 2 M iodoacetic acid (that was neutralized with NaOH) for 30 min at 37 °C. The solution was then dialysed against 2 M urea at 4 °C. The resulting solution was subsquently diluted with 1 vol. of H_2O and buffered by adding 0.25 vol. of 0.5 M Tris/HCl (pH 8.5). The carboxymethylated protein was digested with 4 μg of sequencing-grade trypsin (Boehringer Mannheim) at 37 °C for 16 h. The digested mixture was then vacuum-dried and separated by HPLC using a 2 mm × 150 mm C_{18} reverse-phase column (300 Å pore size, 5 μm bead diameter; Delta-Pak from J. T. Baker, Phillipsburg, NJ, U.S.A.). A linear gradient up to 70 % (v/v) acetonitrile over 90 min in 0.5 % trifluoroacetic acid (pH 2.0) was used in a Waters 625LC system with the PDA Waters 996UV detector (Millipore Waters, Eschborn, Germany). Rechromatography was performed at pH 6 in 0.1 % (w/v) ammonium acetate with a linear gradient up to 70 % (v/v) acetonitrile in this buffer over 90 min. For comparative purposes, human milk lysozyme [12] was digested and the peptide fragments were separated as above. The glycopeptides were identified by amino acid sequencing that was performed in a Model 477A amino acid sequencer (Applied Biosystems, Weiterstadt, Germany).

Mass analyses

Mass analyses of the glycopeptides were carried using a matrix-assisted laser-desorption ionization–time-of-flight (MALDI–TOF) [15,16] mass spectrometer (Voyager RP; Perseptive Biosystems, Framingham, MA, U.S.A.). For mass measurements samples were dissolved in a mixture of acetonitrile/0.1 % aqueous trifluoroacetic acid (1 : 1, v/v) at a concentration of approx. 10^{-6} M. Samples (1 μl) were mixed with 1 μl of matrix [2,5-dihydroxybenzoic acid/2-hydroxy-5,5-methoxybenzoic acid; 9 : 1, by vol. (20 g/l of each acid was dissolved in the sample solvent)] directly on the metal sample support and dried in a stream of cold air. Positive ions were analysed in the linear mode. For each spectrum 30–50 single mass scans were accumulated. Mass calibration was performed externally with insulin as the calibrant. Peak intensities were taken as arbitary units for the maximum peak heights evaluated by the instrumental software (Grams/386).

RESULTS

Isolation of glycopeptides from mono- and bis-glycosylated lysozyme

Mutant lysozyme II/IVT with glycosylation sites at Asn^{49} (site IV) and Asn^{68} (site II) was expressed in stably transfected CHO cells. Glycosylation site IV has been engineered in analogy to the single glycosylation signal in lactoglobulin, a similar protein. An additional mutation, S51T, has been introduced to obtain better utilization of the glycosylation signal [11]. The recombinant glycoprotein was purified from conditioned medium using immune-affinity and hydroxyapatite column chromatography. Aliquots of the eluted fractions were analysed by SDS/PAGE. Figure 1 shows that molecules with the highest apparent size and contents of carbohydrate were eluted from the hydroxyapatite column first. The bands representing lysozyme with different contents of carbohydrate were interpreted according to the previously published characterization [11]. Fraction numbers 16–22 and 24–26, which contained the bulk of the bis- and mono-glycosylated molecules, respectively, were pooled and the materials were subjected to tryptic digestion. The apparent cross-contamination of mono- and bis-glycosylated lysozyme in the hydroxyapatite column fractions was considered tolerable for the characterization of the pooled fractions. Owing to a high efficiency of glycosylation of lysozyme II/IVT, the non-glycosylated form of the mutant could not be prepared with a sufficient yield. Therefore, as a control, wild-type human lysozyme was used.

The digested peptide mixtures were separated by reverse-phase HPLC. Novel peaks were expected in the elution profiles of the glycosylated samples when compared to the control. Although, (1) the control differed from the mutant at four amino acid residues that were likely to affect the elution of the fragments, (2) the glycosylation occurred in the neighbourhood of arginine and lysine residues such that it interfered with the tryptic digestion (see below) and (3) the glycosylation was incomplete, a straightforward comparison was possible of the HPLC profiles shown in Figure 2. The glycosylated materials yielded two additional broad peak areas that were not matched in the control and, therefore, tentatively referred to as glycopeptide pools II and IV. The appearance of a broad peak was particularly striking in the tryptic digest of bis-glycosylated lysozyme, in fractions that eluted at the earlier time (pool IV). Material eluting at the later time absorbed light at 295 nm and was referred to as glycopeptide II, since from the primary sequence of lysozyme the fragment bearing glycosylation site II was predicted to contain tryptophan (residue 64). The origin and the nomenclature of the glycopeptides from mono- and bis-glycosylated lysozyme fractions were established after determining the amino acid sequence (see below) and are explained in Figure 3. The glycopeptides were re-

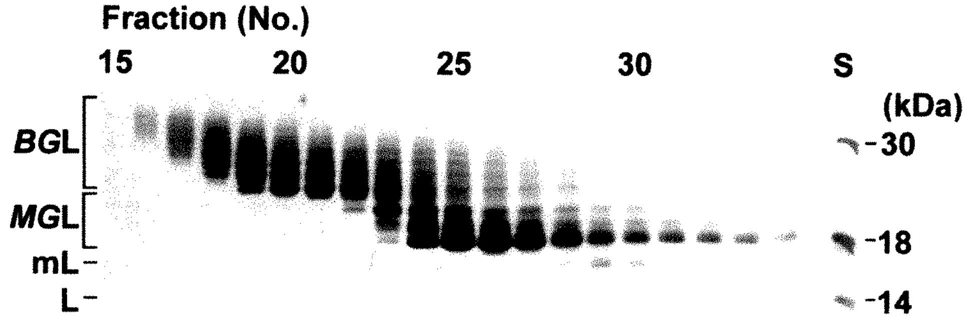

Figure 1 Separation of mono- and bis-glycosylated lysozyme

Lysozyme mutant II/IVT was purified by immune-affinity and hydroxyapatite chromatography. Aliquots of the fractions of the enzyme that were eluted from the hydroxyapatite column were analysed by SDS/PAGE. Protein was stained with silver nitrate. Carbonic anhydrase, trypsin inhibitor and lysozyme (30, 18 and 14 kDa, respectively) were used as standards (S). The positions of lysozyme forms bearing no (L), one mannose-rich (mL), one complex (MGL) or two complex oligosaccharides (BGL) are indicated.

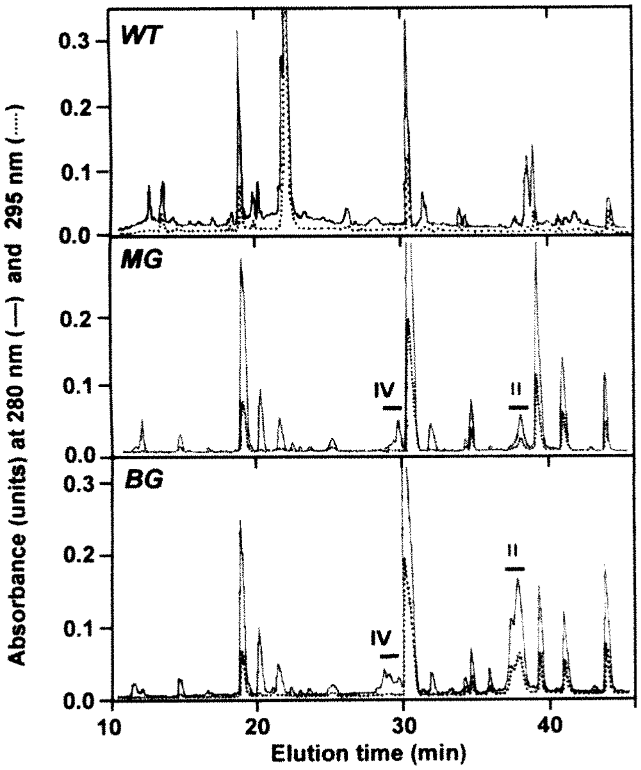

Figure 2 HPLC of tryptic peptides from bis-glycosylated lysozyme

Tryptic peptides were prepared by digesting human milk lysozyme (WT) and bis- (BG) and mono-glycosylated (MG) lysozyme, that corresponded to hydroxylapatite column fractions 16–22 and 24–26, respectively (see Figure 1). The appropriately labelled panels show the separation of the peptides in the three preparations by reverse-phase HPLC. The positions of glycopeptide pools II and IV are indicated. The absorbance at 280 nm and 295 nm is represented by the continuous and dotted lines, respectively.

chromatographed at a higher pH. This resulted in the separation of a few minor contaminants (results not shown). In all these cases the major materials were eluted as rather broad peaks. Glycopeptides comprising the glycosylation site II from either mono- or bis-glycosylated lysozyme yielded two broad peaks in tandem, IIA and IIB. They appeared in similar amounts and were pooled and analysed separately. They were assumed to differ from each other in the length of their peptide moieties (see below). Even when subjected to re-chromatography the glycopeptides eluted as rather broad peaks and the heterogeneity was assumed to be due to carbohydrates. The heterogeneity was prominent in the elution profile of glycopeptide IVBG from bis-glycosylated lysozyme. In this respect glycopeptide IVBG was clearly distinct from all others including the glycopeptide IVMG that originated from mono-glycosylated lysozyme (Figure 2).

By definition, digestion of bis-glycosylated lysozyme yielded two glycopeptides, IIBG and IVTBG, in equimolar amounts. The ratio of their peak areas was 3.3:1 (Figure 2, lower panel). The apparently higher absorbance of the material in peak II fractions was explained by its larger molecular size. From the ratio of 1.4:1 of peak areas of the two glycopeptides in the digest of mono-glycosylated lysozyme (Figure 2, middle panel) it could be concluded that in this mixture molecules glycosylated solely at site II were about half as frequent as those glycosylated solely at site IV. This observation indicated that the two glycosylation sites were utilized independently of each other, since, as reported before [11], in mono-glycosylated lysozyme mutants II and IVT the glycosylation of the former was less frequent.

Identification of the purified glycopeptides

An aliquot of the re-chromatographed pool IVBG was subjected to automated amino acid sequencing. The sequence obtained in 22 cycles was: ATNYNAG-blank-RTTDYGIFQINSR-blank. It was concluded that this peptide contained glycosylation site IV and that the lack of the signal in the eighth cycle was due to glycosylation of asparagine (Asn^{49}) at this position. Thus the glycosylated peptide containing glycosylation site IV comprised 21 amino acid residues (residues 42–62 in lysozyme) and the result of the sequencing confirmed the presence of both mutations (D49N and S51T [11]). It was concluded that the tryptic fragment from pool IVBG was generated by cleavages after Arg^{41} and Arg^{62}. It was assumed that the lack of cleavage at Arg^{50} was due to glycosylation at the adjacent mutated site IV (D49N).

A portion of pool IIBGB was subjected to ten cycles of amino acid sequencing with the following result: YWCND-blank-KTSG. This sequence corresponded to residues 63–72 of human lysozyme, containing the mutations G68N and P71S and, thus,

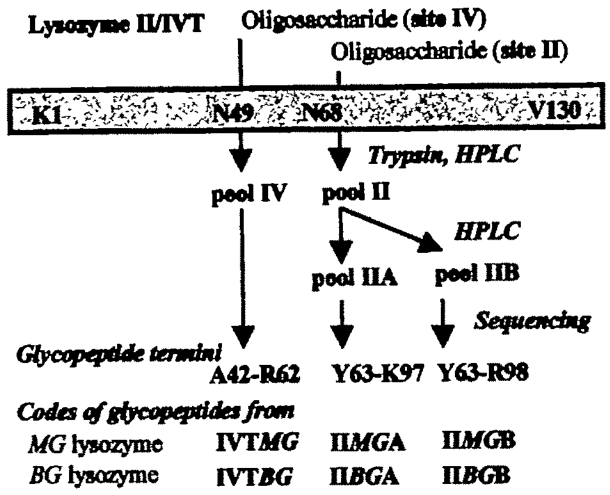

Figure 3 Generation and nomenclature of glycopeptides from glycosylated lysozyme

Glycosylated lysozyme was isolated by immune-affinity chromatography. Mono- and bis-glycosylated lysozyme fractions were separated by hydroxyapatite column chromatography. The glycopeptide codes refer to the origin of two alternative preparations glycopeptides with codes IVTMG, IIMGA, IIMGB were prepared from a tryptic digest of mono-glycosylated (MG) lysozyme Those with codes IVTBG, IIBGA and IIBGB were prepared from bis-glycosylated (BG) lysozyme.

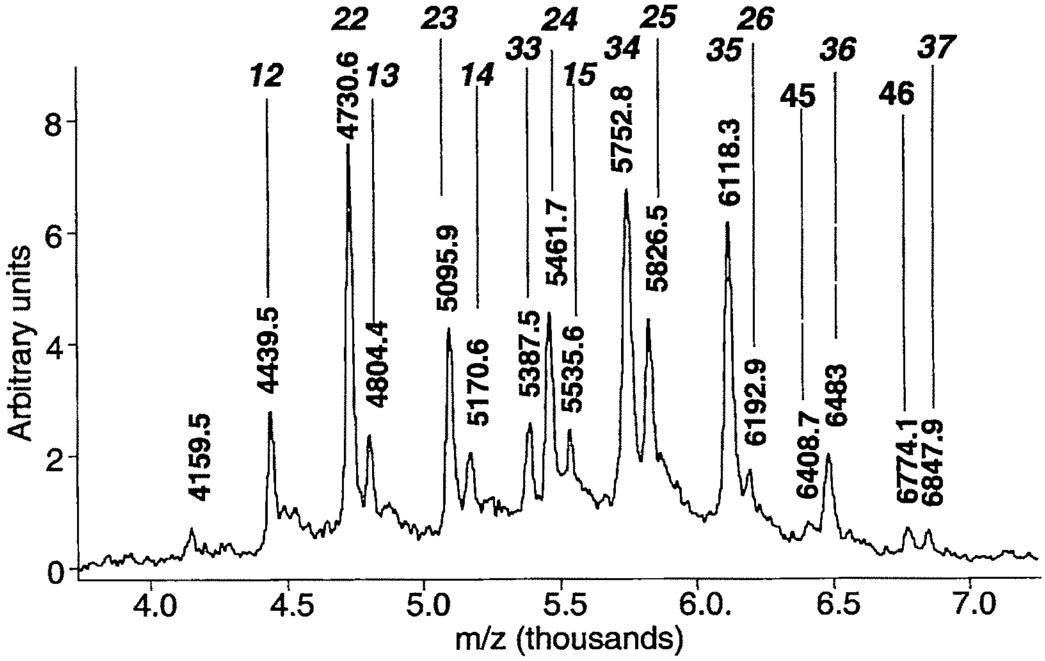

Figure 4 MALDI–TOF mass analysis of tryptic glycopeptide IVBG from glycosylation site IV of bis-glycosylated lysozyme II/IVT molecules

Mass peaks corresponding to glycopeptides bearing mono-, bis- and tris-sialo-oligosaccharides are labelled with numbers that refer to the total content of *N*-acetylneuraminic acid (i e. sialic acid) (the first digit) and *N*-acetyl-lactosamine (the second digit) units Oligosaccharide structure paradigms are shown in Figure 5

to glycosylation site II. The sequence was not interrupted after Lys^{69} probably due to glycosylation at the 68th residue Mass spectra of glycopeptides IIBGA and IIBGB were similar to each other (see below) The mass values of peaks in the former mass spectrum were 156 Da smaller than in the latter mass spectrum. This difference probably resulted from an alternative cleavage by trypsin at the C-terminal side of the glycopeptide. An aliquot of the peptide IIBGB was subjected to amino acid sequencing to examine this possibility. However, after 32 cycles that confirmed the expected sequence of residues 63–94 the signal ceased to be interpretable. No further attempts to elucidate the mass difference were made. Most probably, the glycopeptides from pool II were generated by tryptic cleavage after Arg^{62} and either Lys^{97} or Arg^{98}, and the two alternative fragments were separated during the re-chromatography yielding tandem peaks, IIA and IIB. These optional cleavages are illustrated in Figure 3

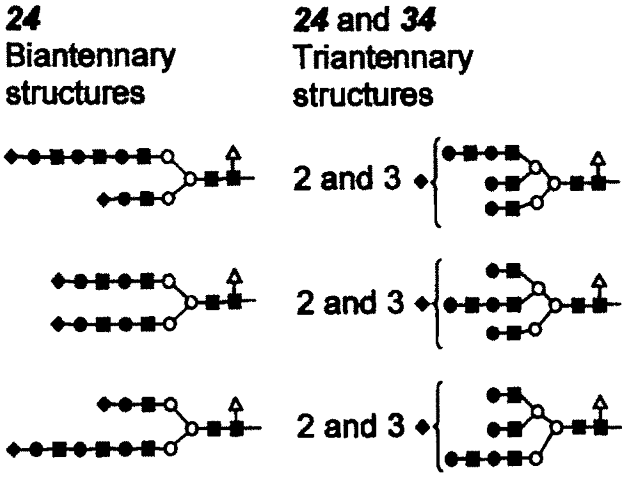

Figure 5 Bi- and tri-antennary isomers of oligosaccharide structures *24* and *34* of glycopeptides from pool IVT*BG*

Glycopeptide masses 5461.7 Da and 5752.8 Da were examined. The calculated masses of the tryptic peptide (2374.6 Da) and of the fucosylated core carbohydrate mannose$_3$-fucose$_1$-*N*-acetylglucosamine$_2$ (1039.1 Da) moieties were subtracted from the examined values. The residual mass values of 2044.7 Da and 2335.8 Da represented the outer chains of the antennae. These values were compatible with four *N*-acetyl-lactosamine units (365.4 Da each) and two or three sialic acid residues (291.3 Da each), respectively. Bi- and tri-antennary structures are shown using the following symbols for sialic acid (◆), galactose (●), *N*-acetylglucosamine (■), mannose (○) and fucose (△) residues. Tetra-antennary isomers are not shown.

Mass analysis of glycopeptides comprising glycosylation sites II and IVT

MALDI–TOF mass analysis of IVTBG, that contained the glycosylation site IVT and was isolated from bis-glycosylated lysozyme, yielded a complex set of mass signals that are shown in Figure 4. The main peak had a protonated mass of 4730.6. This agreed well with the mass of the mutant sequence Ala^{42} through to Arg^{61} (2377.5 Da), combined with that of a biantennary oligosaccharide with two *N*-acetylneuraminic acid, two galactose, three mannose, four *N*-acetylglucosamine and one fucose residues (these residues comprise 2352.2 Da after subtracting the mass of the condensation water), yielding a sum of 4729.7 Da.

The peaks shown in Figure 4 were considered to represent glycopeptides with mono- and bis-sialylated biantennary, bis- and tris-sialylated triantennary and tetrakis-sialylated tetra-antennary oligosaccharides. The peaks were grouped in series that were labelled with two italic numerals. The first numeral was used to indicate the content of sialic acid residues. Within a series the mass values showed an increment that represented the mass of an *N*-acetyl-lactosamine residue. The total number of *N*-acetyl-lactosamine units was represented by the second italic numeral. The mass analysis does not distinguish between biantennary oligosaccharides with *n* lactosamine repeats and triantennary ones with *n* – 1 repeats if the two contained less than three sialic acid residues. Correspondingly, the italic code refers to the contents of the two building blocks and not to the number of the antennae. As an example, in Figure 5 biantennary and triantennary isomeric structures are shown that represent oligosaccharide codes *24* and *34* with four *N*-acetyl-lactosamine units and two or three sialic acid residues, respectively.

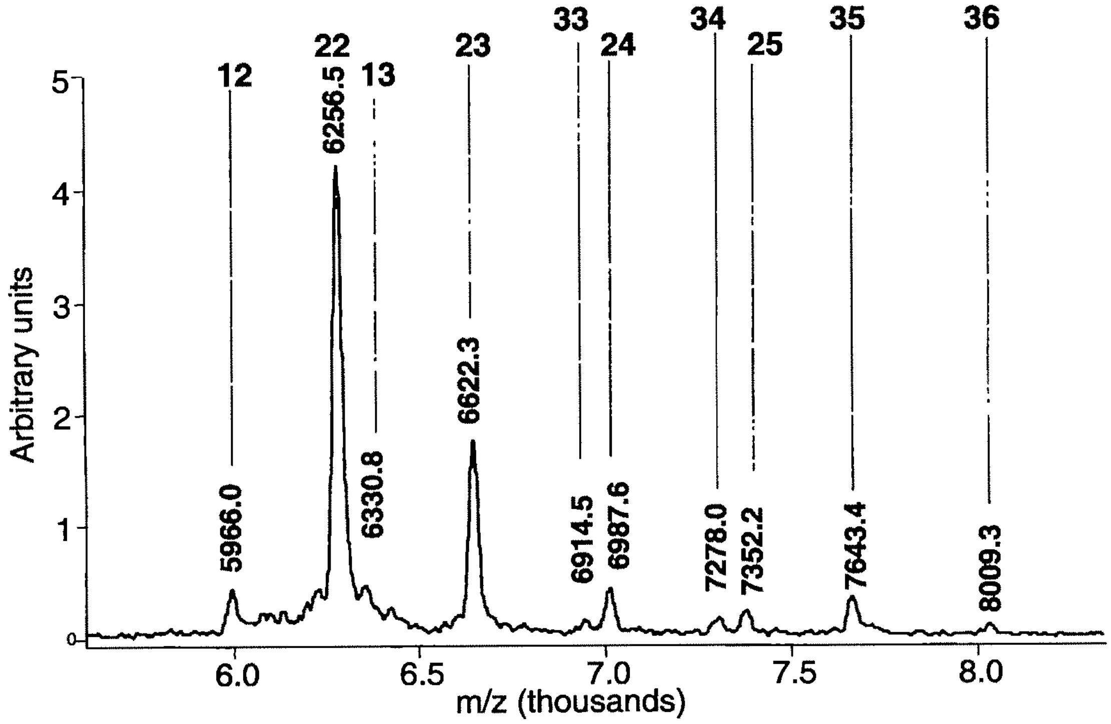

Figure 6 MALDI–TOF mass analysis of tryptic glycopeptide IIBGB from glycosylation site II of bis-glycosylated lysozyme II/IVT molecules

Mass peaks corresponding to glycopeptides with different numbers of *N*-acetylneuraminic acid and of *N*-acetyl-lactosamine units are numbered as explained in the legends of Figure 4 and Table 1

Table 1 MALDI–TOF mass analysis of glycopeptides from mono- and bis-glycosylated lysozyme

In mass spectra of the listed glycopeptides, arbitary units were evaluated that corresponded to calculated masses within 1 Da and represented at least 1% of the total. The calculations were based on carbohydrate structures containing the core unit with one fucose, two *N*-acetylglucosamine and three mannose residues. Further additions were 0–4 *N*-acetylneuraminic acid (sialic acid) residues (this number being represented by the first digit of the code) and 0–6 *N*-acetyl-lactosamine disaccharide units (this number being represented by the second digit of the code). The masses of the peptide moieties were calculated for amino acid sequences Tyr^{63}–Lys^{97} (IIMGA and IIBGA), Tyr^{63}–Arg^{98} (IIBGB) and Ala^{42}–Arg^{62} of the carboxymethylated mutant lysozyme

Structure (code)	Glycopeptides (% of arbitary units)				
	IIMGA	IIBGA	IIBGB	IVTMG	IVTBG
02	14.5			9.9	1.1
03	7.6				
12	41.5	5.1	15.9	18.5	5.1
13	12.9	5.4	7.1	7.7	4.4
14	1.7			2.2	3.8
15					4.8
22	15.8	51.2	48.2	35.6	15.0
23	3.6	21.4	17.9	11.9	8.1
24		5.2	3.7	3.1	8.8
25		2.8	1.1	1.2	8.3
26					3.3
33		1.8		1.4	4.7
34		1.9	1.3	1.7	12.7
35		4.3	3.2	1.3	12.1
36		1.0			3.8
37					1.1
45					1.5
46					1.3

The spectra obtained from glycopeptides of mono-glycosylated lysozyme (IIMGA and IVTMG) and from glycopeptides associated with site II in bis-glycosylated lysozyme (IIBGA and IIBGB) were much simpler than those of IVTBG. The predominant mass values in the former corresponded to mono- and bis-sialylated biantennary oligosaccharides. As an example, a mass spectrum of the glycopeptide IIBGB is shown in Figure 6. In Table 1 the relative abundance of oligosaccharides containing different numbers of sialic acid residues and *N*-acetyl-lactosamine units was estimated from the relative frequency of arbitrary mass units in spectral measurements of the examined glycopeptides. The pattern of oligosaccharides in glycopeptide IIMGB (results not shown) was similar to those of IIBGA, IIBGB and IVTMG. A common feature of oligosaccharides associated with these glycopeptides, in distinction to IVTBG, was the predominance of smaller mass values corresponding to biantennary oligosaccharides with either no or few *N*-acetyl-lactosamine repeats (Table 1).

In the former group of glycopeptides, the mass of the main peak indicated the presence of bis-sialylated biantennary oligosaccharide (code *22*). The amounts of larger oligosaccharides containing more *N*-acetyl-lactosamine units (codes *23–25*) corresponded on average to approx. one third of the bis-sialylated biantennary oligosaccharide without repeats (code *22*). Owing to the limits in quantitative interpretation of mass spectra it should be stressed that the relative contents of the elongated oligosaccharides that could be estimated from spectra of glycopeptides from mono-glycosylated lysozyme (Table 1 and Figure 6) agreed well with the intensity patterns of silver-stained bands of the lysozyme that the glycopeptides originated from (Figure 1) and of the radioactive bands of mono-glycosylated lysozyme containing either glycosylation site that were inspected in this (Figure 7, below) and previous studies [9]. SDS/PAGE of mono-glycosylated lysozyme containing more than two *N*-acetyl-lactosamine units showed that it was nearly completely digested by endo-β-*N*-acetylglucosaminidase F2, indicating that the larger species contained predominantly biantennary oligosaccharides with *N*-acetyl-lactosamine repeats.

A significant portion of all glycopeptides contained incompletely sialylated oligosaccharides. The proportions of partially sialylated forms varied among the different glycopeptides. It was highest in IIMGA and lowest in IIBGA. The incomplete sialylation seemed to be related neither to the origin of the glycopeptides from mono- and bis-glycosylated lysozyme nor the separation in HPLC of site II glycopeptides into fractions A and B. Thus in one case A was less sialylated, while in the other case B was less sialylated. Papac et al. [17] have discussed in detail factors that contribute to loss of sialic acid from glycoconjugates during the preparation and analysis of samples in MALDI–TOF mass determinations. The present measurements were performed in the linear mode that produces spectra without desialylation. However, we could not exclude a loss of sialic acid residues due to interactions with the acidic matrix [17].

From comparisons of mass signal arbitary units in different samples it was apparent that in glycopeptides IVTBG the content of *N*-acetyl-lactosamine repeats and of oligosaccharides with more than two antennae strongly exceeded those in the other glycopeptides (Table 1). These findings confirmed the interpretation of the shape of the HPLC peaks described above.

In glycopeptides IVTBG among the bis-sialylated species (structure codes *22–26* in Table 1) molecules with two and four *N*-acetyl-lactosamine units were the most abundant. We assumed that the amount of the biantennary oligosaccharides with an increasing number of *N*-acetyl-lactosamine units was monotonously decreasing just as in the case of the other glycopeptides shown in Table 1. The relatively high apparent contents of oligosaccharides with 4–6 *N*-acetyl-lactosamine units (structure codes *24–26*) in bis-sialylated glycopeptides IVTBG indicated that these were enriched in triantennary incompletely sialylated forms. Oligosaccharides with the codes *23–26* were likely to contain a decreasing proportion of bis-sialylated biantennary species with 1–4 additional *N*-acetyl-lactosamine repeats and an increasing proportion of bis-sialylated triantennary isomers. Quantitatively, the occurrence of the latter could be related to that of tris-sialylated triantennary oligosaccharides, among which those with one and two repeats (codes *34* and *36*) were the major species (Figure 4). Similarly, oligosaccharides in peaks *12–15* are likely to represent mono-sialylated biantennary forms that have been generated through *in vitro* desialylation [17] of glycopeptides *22–25*.

Characterization of triantennary oligosaccharides in metabolically labelled lysozyme

MS analyses, shown above, indicated that in molecules that were glycosylated at both sites, tris-sialylated oligosaccharides comprising mostly the triantennary species were associated preferentially with the glycosylation site IV. We attempted to estimate the occurence of triantennary and elongated oligosaccharides using metabolic labelling, digestion of glycosylated lysozyme with endo-β-*N*-acetylglucosaminidase F2 that cleaves biantennary, but not triantennary, complex oligosaccharides, and digestion with endo-β-galactosidase that removes antennae containing *N*-acetyl-lactosamine repeats. The interpretation was facilitated by quantitative PhosphorImager analysis (Figure 7). The quantification encompassed all visible bands, however, for the sake of brevity, values of only a few of them will be mentioned. In the control, 67 % of the radioactivity was associated with mono-glycosylated lysozyme bearing complex oligosaccharide side chains (MGL in Figure 7). The most prominent band, lysozyme bearing a single bis-sialylated biantennary oligosaccharide without repeats, represented 40 % of the total radioactivity. Its identity was based on resistance to endo-β-galactosidase (Figure 7) and endo-*N*-acetylglucosaminidase H [18],and sensitivity to endo-β-*N*-acetylglucosaminidase F2 (Figure 7) and sialidase [9]. The bands migrating in SDS/PAGE in the mono-glycosylated lysozyme area, behind the main band, represented 29 % of the total radioactivity. This material was sensitive to endo-β-galactosidase and the cleavage products migrated in front of the main band that was resistant, as expected. In the digested sample, these bands, together, comprised 64 % of the radioactivity, thus resembling the sum of radioactivity associated with the starting components of mono-glycosylated lysozyme. In the sample that had been digested with endo-β-*N*-acetylglucosaminidase F2, little radioactivity was found to migrate immediately behind the main band where the resistant forms of mono-glycosylated lysozyme molecules with elongated triantennary oligosaccharides were expected, thus indicating scarcity of these derivatives in mono-glycosylated lysozyme.

PhosphorImager analysis of the group of bis-glycosylated lysozyme molecules (BGL) comprised 29 % of the total radioactivity in the undigested sample. After removal of the repeats with endo-β-galactosidase these molecules migrated faster and, as expected, their quantity did not change. Due to poor band resolution, it was not possible to distinguish the products of digestion bearing different combinations of bi- and triantennary oligosaccharides with or without removed antennae. Digestion of metabolically labelled lysozyme II/IVT with endo-β-*N*-acetylglucosaminidase F2 was expected to remove one or two biantennary oligosaccharides, thus forming lysozyme with one (L′) or two (L″) fucosyl *N*-acetyglucosamine disaccharide units attached, respectively. As expected from the relative contents of mono- and bis-glycosylated lysozyme the amount of the former product exceeded that of the latter. A small portion of bis-glycosylated lysozyme contained one cleavable biantennary oligosaccharide and one mannose-rich oligosaccharide, as indicated by the appearance of a product (mL′) that migrated behind lysozyme with one mannose-rich oligosaccharide (mL).

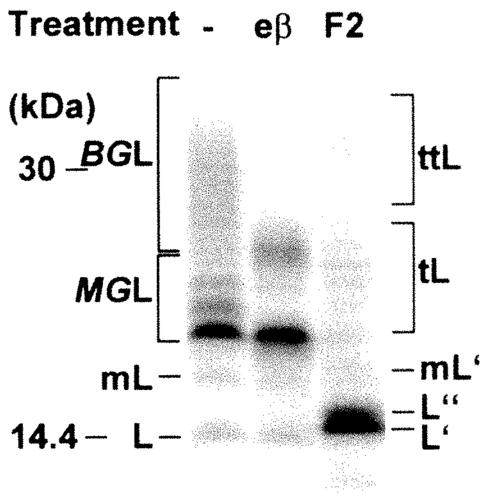

Figure 7 Digestion of biantennary oligosaccharides and of *N*-acetyllactosamine repeats in bis-glycosylated lysozyme with glycosidases

Metabolically labelled II/IVT lysozyme was isolated by immunoprecipitation from secretions of transfected CHO cells. After solubilization, one aliquot was treated with endo-β-*N*-acetylglucosaminidase F2, one with endo-β-galactosidase (eβ) and one remained untreated (—). The radioactivity associated with the different glycosylated forms of lysozyme was analysed by SDS/PAGE, fluorography and PhosphorImaging. Positions of mono-(MGL) and bis-glycosylated lysozyme (BGL), lysozyme bearing mannose-rich (mL), one (tL) or two (ttL) triantennary oligosaccharides, one (L′) or two (L′) fucosyl *N*-acetylglucosamine disaccharides and one fucosyl *N*-acetylglucosamine along with a mannose-rich oligosaccharide (mL′) are indicated.

Portions of the bis-glycosylated molecules were completely or partially resistant to endo-β-*N*-acetylglucosaminidase F2. A minor fraction (2 %) appeared to contain two oligosaccharides even after the digestion (ttL). At least one of these was of complex type and contained *N*-acetyl-lactosamine repeats as indicated by the ladder-like array of the bands. It is possible that the resistance was due to the presence of one mannose-rich and one tri- or tetra-antennary oligosaccharide. The limited amount of this material precluded further analysis. A larger fraction of the resistant molecules (9 % of the total radioactivity) migrated as a group of bands (tL in Figure 7) with apparent sizes intermediate between the typical mono- and bis-glycosylated lysozyme. This material was considered to originate from partially sensitive bis-glycosylated lysozyme, in which one site was sensitive and the other contained larger oligosaccharides resistant to endo-β-*N*-acetylglucosaminidase F2. We assumed that the latter were the source of glycopeptide IVTBG that was the major species containing triantennary and elongated oligosaccharides (Table 1). Similarly to mass analysis of glycopeptide IVTBG, the pattern of bands in the group tL in Figure 7 indicated that triantennary oligosaccharides at site IV in bis-glycosylated lysozyme comprise predominantly structures with one or more *N*-acetyl-lactosamine repeats. Thus the presence of elongated triantennary oligosaccharides in bis-glycosylated lysozyme II/IVT was documented by results from both MALDI–TOF MS (Figure 4 and Table 1) and enzymic digestion (Figure 7). Furthermore, in the pool of bis-glycosylated lysozyme that was isolated by hydroxylapatite column chromatography, shown in Figure 1, the presence of triantennary oligosaccharides was confirmed by digesting this material with endo-β-*N*-acetylglucosaminidase F2, separating the products by SDS/PAGE and visualizing them by silver staining (results not shown). In contrast, in mono-glycosylated lysozyme triantennary oligosaccharides were hardly detectable.

DISCUSSION

The biosynthesis of *N*-acetyl-lactosamine repeats is a complex process and its regulation is poorly understood. Among factors that have been shown to enhance elongation of the repeats are the following: (1) synthesis of the β-1,6-linked third antenna in complex oligosaccharides [6,7]; (2) cell differentiation correlating with an increase in the activity of *N*-acetylglucosaminyltransferase involved in elongation [4,5]; (3) slow transport through the Golgi apparatus in cells cultured at a decreased temperature [3]; (4) a lack of sialylation of complex oligosaccharides [9]. Furthermore, increased synthesis of *N*-acetyl-lactosamine repeats is known to correlate with neoplastic transformation [6]. To our knowledge, the present data show for the first time that elongation of *N*-acetyl-lactosamine repeats at a particular carbohydrate attachment site is dependent on the presence of another oligosaccharide. In mutant lysozyme, glycosylation at Asn^{68} (site II) enhances the synthesis of *N*-acetyl-lactosamine repeats at Asn^{49} (site IV). This enhancement results at least in part from an increase in the synthesis of the third antenna that is the preferred site of elongation. The triantennary oligosaccharides in bis-glycosylated lysozyme contain mostly one or two repeats. Owing to the biological significance of the repeats as a scaffold in the synthesis of sialyl Lewis^x substances it should be of interest to determine the three-dimensional structures of natural Lewis^x-bearing molecules and examine these for the presence of multiple carbohydrate residues that might be spaced similarly to glycosylation sites II and IV in the mutant lysozyme.

Carlsson and Fukuda [19] have reported that in lamp proteins *N*-acetyl-lactosamine repeats are confined to particular glycosylation sites and suggested that their synthesis might depend on the accessibility of the sites, as well as on the three-dimensional structure surrounding them. Our results with an engineered glycoprotein that is not related to lamp proteins extend the ideas of these authors and suggest that the synthesis of the repeats may be independent of any protein signal. As observed in bis-glycosylated lysozyme the processing signal seems to be associated with a carbohydrate rather than protein. Furthermore, the effect depends on the location of this carbohydrate. Thus as reported previously [11], in bis-glycosylated lysozyme the characteristic processing at site IV is observed if a second carbohydrate is located at site II (Asn^{68}), but not at site I (Asn^{22}).

Our findings are based on the separation of glycopeptides representing glycosylation sites II and IV from both mono- and bis-glycosylated lysozyme and their mass spectral analysis. We are aware that quantitative evaluation of arbitary units in mass spectra must be interpreted with caution. For this reason we should point out that in mono-glycosylated lysozyme, with predominantly biantennary oligosaccharides, the relative proportions of molecules with increasing numbers of *N*-acetyl-lactosamine repeats, as observed in either silver-stained gels (Figure 1) or PhosphorImaged metabolically labelled lysozyme (Figure 7) are similar to those found in MALDI–TOF spectra of corresponding glycopeptides (Table 1). It has been shown that during MALDI–TOF sample preparation and/or measurement a partial desialylation of oligosaccharides may occur [17]. We have observed previously that in CHO cells oligosaccharides in mono-glycosylated lysozyme appear to be nearly completely sialylated [9]. Therefore we assume that the contents of completely sialylated bi- and triantennary oligosaccharides at site IVT in bis-glycosylated lysozyme may be higher than can be anticipated from the present mass spectrum results. Although mass spectral analysis indicates how many *N*-acetyl-lactosamine units are present it does not differentiate between isomers. However, from mass values the minimum number of sialic acids and, thus of antennae, can be estimated. Our finding on the increase in branching of the oligosaccharides at site IV in lysozyme II/IVT is based on the increase in both the contents of tris-sialylated oligosacharides and the resistance of oligosaccharides towards endo-β-*N*-acetylglucosaminidase F2.

Two or more β-1,3-*N*-acetylglucosaminyltransferases are likely to participate in the synthesis of the elongating units in *N*-linked oligosaccharides. The known candidates are the elongating β-1,3-*N*-acetylglucosaminyltransferase [20] and a novel β-1,3-*N*-acetylglucosaminyltransferase that is related to β-1,3-galactosyltransferases [21]. In complex oligosaccharides elongation proceeds preferentially at the β-1,6-linked antenna [22] and the synthesis of this antenna in glycoproteins is increased in metastatic tumour cells [23]. This so-called Warren–Glick phenomenon has been explained by a cancer-related increase in the activity of *N*-acetylglucosaminyltransferase V [24,25]. Our results suggest that this enzyme may preferentially modify particular carbohydrate side chains in the context of an additional glycosylation. In lysozyme II/IVT the modification of the oligosaccharide at the glycosylation site IV appears to result from the presence of carbohydrate at glycosylation site II. Thus a question may be raised whether isolated β-1,6-*N*-acetylglucosaminyltransferase V can be activated by oligosaccharides that are attached to the substrate protein near the acceptor carbohydrate. This enzyme has been the subject of numerous enzymological studies [26–31]. However, to our knowledge its activation by carbohydrate side chains has yet to be examined.

This work was supported by the Deutsche Forschungsgemeinschaft, SFB 286, the Alexander von Humboldt-Stiftung (to A H) and the Fonds der Chemischen Industrie We thank Gertraud Jarosch for excellent technical help, Evelin Heinemann for secretarial assistance and Barbara Schedding for amino acid sequence analyses.

REFERENCES

1 Ley, K (1996) Molecular mechanisms of leukocyte recruitment in the inflammatory process Cardiovasc Res **32**, 733–742
2 McEver, R. P (1997) Selectin-carbohydrate interactions during inflammation and metastasis Glycoconjugate J **14**, 585–591
3 Wang, W-C , Lee, N., Aoki, D , Fukuda, M N and Fukuda, M (1991) The poly-*N*-acetyl-lactosamines attached to lysosomal membrane glycoproteins are increased by the prolonged association with the Golgi complex J Biol Chem **266**, 23185–23190
4 Lee, N , Wang, W-C. and Fukuda, M (1990) Granulocytic differentiation of HL-60 cells is associated with increase of poly-*N*-acetyl-lactosamine in Asn-linked oligosaccharides attached to human lysosomal membrane glycoproteins J Biol Chem **265**, 20476–20487
5 Radons, J , Faber, V , Buhrmester, H , Volker, W , Horejsi, V and Hasilik, A. (1992) Stimulation of the biosynthesis of lactosamine repeats in glycoproteins in differentiating U937 cells and its suppression in the presence of NH_4Cl Eur J Cell Biol. **57**, 184–192
6 Yousefi, S , Higgins, E , Daoling, Z , Pollex-Kruger, A., Hindsgaul, O and Dennis, J. W. (1991) Increased UDP-GlcNAc Gal beta-1,3-GalNAc-R (GlcNAc to GalNAc) beta-1,6-*N*-acetylglucosaminyltransferase activity in metastatic murine tumor cell lines. Control of polylactosamine synthesis J Biol Chem. **166**, 1772–1782
7 Koenderman, H L , Koppen, P L and van den Eijnden, D. H (1987) Biosynthesis of polylactosaminoglycans. Novikoff ascites tumor cells contain two UDP-GlcNAc·beta-galactoside beta-1–6-*N*-acetylglucosaminyltransferase activities Eur J Biochem **166**, 199–208
8 Capon, C., Laboisse, C L , Wieruszenski, J-N , Maoret, J J , Augeron, C and Fournet, B (1992) Oligosaccharide structures of mucins secreted by the human colonic cancer cell line CL16E. J. Biol Chem **267**, 19248–19257
9 Hummel, M , Hedrich, H C and Hasilik, A (1997) Elongation of *N*-acetyl-lactosamine repeats in biantennary oligosaccharides Eur J Biochem **245**, 428–433
10 Fernandes, B , Sagman, U , Auger, M., Demetrio, M and Dennis, I W (1991) Beta-1,6-branched oligosaccharides as a marker of tumor progression in human breast and colon neoplasia Cancer Res **51**, 718–723
11 Melcher, R , Grosch, H-W , Grosse, O and Hasilik, A (1998) Increased elongation of *N*-acetyl-lactosamine repeats in doubly glycosylated lysozyme with a particular spacing of the glycosylation sites Glycoconjugate J **15**, 987–993
12 Gupta, D. K , Theisen, N , von Figura, K and Hasilik, A (1985) Comparison of biosynthesis and transport of lysozyme and cathepsin D in U937 monocytes. Biochim. Biophys Acta, **847**, 217–222
13 Laemmli, U K (1970) Cleavage of structural proteins during the assembly of the head of bacteriophage T4 Nature (London) **227**, 680–685
14 Heukeshoven, J and Dernick, R (1988) Improved silver staining procedure for fast staining in PhastSystem Development Unit I Staining of sodium dodecyl sulfate gels Electrophoresis **9**, 28–32
15 Beavis, R C and Chait, B T (1996) Matrix-assisted laser desorption ionization mass-spectrometry of proteins Methods Enzymol **270**, 519–551
16 Tsarbopoulos A , Bahr U , Pramanik B N and Karas M (1997) Glycoprotein analysis by delayed extraction and post-source decay MALDI TOF MS Int J Mass Spectrom Ion Processes **169/170**, 251–261
17 Papac, D. I., Wong, A. and Jones, A J S (1996) Analysis of acidic oligosaccharides and glycopeptides by matrix-assisted laser desorption/ionization time-of-flight mass spectrometry Anal. Chem **68**, 3215–3223
18 Horst, M , Harth, N and Hasilik, A (1990) Biosynthesis of glycosylated human lysozyme mutants J Biol Chem **266**, 13914–13919
19 Carlsson, S R and Fukuda, M. (1990) The polylactosaminoglycans of human lysosomal membrane glycoproteins lamp-1 and lamp-2. Localization on the peptide backbones J Biol. Chem. **265**, 20488–20495

20 Sasaki, K., Kurata-Miura, K., Ujita, M., Angata, K., Nakagawa, S., Sekine, S., Nishi, T. and Fukuda, M. (1997) Expression cloning of cDNA encoding a human β-1,3-*N*-acetylglucosaminyltransferase that is essential for poly-*N*-acetyl-lactosamine synthesis. Proc. Natl. Acad. Sci. U.S.A. **94**, 14294–14299

21 Zhou, D., Dinter, A., Gallego, R. G., Kamerling, J. P., Vliegenthart, J. F. G., Berger, E. G. and Hennet, T. (1999) A β-1,3-*N*-acetylglucosaminyltransferase with poly-*N*-acetyl-lactosamine synthase activity is structurally related to β-1,3-galactosyltransferases. Proc. Natl. Acad. Sci. U.S.A. **96**, 406–411

22 van den Eijnden, D. H., Koenderman, A. H. and Schiphorst, W. E. (1988) Biosynthesis of blood group i-active polylactosaminoglycans. Partial purification and properties of an UDP-GlcNAc *N*-acetyl-lactosaminide beta-1,3-*N*-acetylglucosaminyltransferase from Novikoff tumor cell ascites fluid. J. Biol. Chem. **263**, 12461–12471

23 Dennis, J. W., Laferte, S., Waghorne, C., Breitman, M. L. and Kerbel, R. S. (1987) Beta-1,6 branching of Asn-linked oligosaccharides is directly associated with metastasis. Science **236**, 582–585

24 Kobata, A. (1989) Altered glycosylation of surface glycoproteins in tumor cells and its clinical application. Pigm. Cell Res. **2**, 304–308

25 Dennis, J. W., Granovsky, M. and Warren, C. E. (1999) Glycoprotein glycosylation and cancer progression. Biochim. Biophys. Acta **1473**, 21–34

26 Kanie, O., Crawley, S. C., Palcic, M. M. and Hindsgaul, O. (1993) Acceptor-substrate recognition by *N*-acetylglucosaminyltransferase-V: critical role of the 4″-hydroxyl group in beta-D-Glcp*N*Ac-(1 → 2)-alpha-D-Manp(1 → 6)-beta-D- Glcp-OR. Carbohydr. Res. **243**, 139–164

27 Khan, S. H., Crawley, S. C., Kanie, O. and Hindsgaul, O. (1993) A trisaccharide acceptor analog for N-acetylglucosaminyltransferase V which binds to the enzyme but sterically precludes the transfer reaction. J. Biol. Chem. **268**, 2468–2473

28 Gu, J., Nishikawa, A., Tsuruoka, N., Ohno, M., Yamaguchi, N., Kangawa, K. and Taniguchi, N. (1993) Purification and characterization of UDP-*N*-acetylglucosamine: alpha-6-D-mannoside beta-1,6 *N*-acetylglucosaminyl- transferase (*N*-acetylglucosaminyltransferase V) from a human lung cancer cell line. J. Biochem. (Tokyo) **113**, 614–619

29 Do, K. Y., Fregien, N., Pierce, M. and Cummings, R. D. (1994) Modification of glycoproteins by *N*-acetylglucosaminyltransferase V is greatly influenced by accessibility of the enzyme to oligosaccharide acceptors. J. Biol. Chem. **269**, 23456–23464

30 Brockhausen, I., Reck, F., Kuhns, W., Khan, S., Matta, K. L., Meinjohanns, E., Paulsen, H., Shah, R. N., Baker, M. A. and Schachter, H. (1995) Substrate specificity and inhibition of UDP-GlcNAc: GlcNAc beta 1,2 Man alpha 1,6R beta 1,6-*N*-acetylglucosaminyltransferase V using synthetic substrate analogues. Glycoconjugate J. **12**, 371–379

31 Zhang, N., Peng, K. C., Chen, L., Puett, D. and Pierce, M. (1997) Circular dichroic spectroscopy of *N*-acetylglucosaminyltransferase V and its substrate interactions. J. Biol. Chem. **272**, 4225–4229

Received 17 September 1999/6 March 2000; accepted 7 April 2000

Biochem J (2000) **348**, 517–524 (Printed in Great Britain)

Multiple conserved segments of E1 small nucleolar RNA are involved in the formation of a ribonucleoprotein particle in frog oocytes

Donald D. RUHL, Mary Ellen PUSATERI and George L. ELICEIRI[1]

Department of Pathology, Saint Louis University School of Medicine, 1402 South Grand Boulevard, St. Louis, MO 63104-1028, U.S.A

E1/U17 small nucleolar RNA (snoRNA) is a box H/ACA snoRNA. To identify E1 RNA elements required for its assembly into a ribonucleoprotein (RNP) particle, we have made substitution mutations in evolutionarily conserved sequences and structures of frog E1 RNA. After E1 RNA was injected into the nucleus of frog oocytes, assembly of this exogenous RNA into an RNP was monitored by non-denaturing gel electrophoresis. Unexpectedly, nucleotide substitutions in many phylogenetically conserved segments of E1 RNA produced RNPs with abnormal gel-electrophoresis patterns. These RNA segments were at least nine conserved sequences and an apparently conserved structure. In another region needed for RNP formation, the requirement may be sequence(s) and/or structure. Base substitutions in each of these and in one additional conserved E1 RNA segment reduced the stability of this snoRNA in frog oocytes. Nucleolar localization was assayed by fluorescence microscopy after injection of fluorescein-labelled RNA. The H box (ANANNA) and the ACA box are both needed for efficient nucleolar localization of frog E1 RNA.

Key words: nucleolar localization, snoRNA element, snoRNA stability, snoRNP asssembly, *Xenopus laevis*.

INTRODUCTION

There are many small nucleolar RNAs (snoRNAs) in the eukaryotic cell that function in the maturation of ribosomal RNA (reviewed in [1–4]). Most snoRNAs belong to one of two families. Box C/D snoRNAs have conserved sequence elements named box C (UGAUGA) and box D (CUGA) [1,5]. Some box C/D snoRNAs function in pre-rRNA cleavage processing; most guide 2-*O*-ribose methylation of pre-rRNA [6,7]. In the second family, box H/ACA snoRNAs have the conserved motif ACA and box H (ANANNA) [8,9]. Some box H/ACA snoRNAs have roles in pre-rRNA cleavage; most direct pseudouridine synthesis in pre-rRNA [10,11]. E1/U17 is an H/ACA snoRNA [12–16]. E1 RNA differs from most H/ACA snoRNAs in several aspects. First, it is required for the accumulation of mature 18 S rRNA [17]. Secondly, an rRNA 'pseudouridylation pocket', present in all the rRNA pseudouridylation guide snoRNAs, has not been found in E1 RNA [11]. (An rRNA pseudouridylation pocket consists of two sequences, one on each side of an internal loop structure of a snoRNA, that are complementary to two pre-rRNA sequences that flank a pseudouridylation site [11].) Thirdly, E1 RNA interacts directly (psoralen-photo-crosslinks) *in vivo* with two segments of pre-rRNA [13] which do not have any pseudouridylation sites that could be potentially guided by E1 RNA through the base-pairing mechanism of the known rRNA pseudouridylation guide snoRNAs.

Assembly into its ribonucleoprotein (RNP), usually its functional form, is an important process in the life cycle of most RNA species. Identification of the necessary RNA *cis*-acting elements is a valuable step towards studying RNP biogenesis For each box C/D snoRNA species studied thus far, few RNA elements required for RNP assembly have been identified [18,19], and less is known about these elements in box H/ACA snoRNAs. We set out to identify the E1 RNA *cis*-acting elements needed for formation of its RNP. In the present study, an unexpectedly high number of phylogenetically conserved segments of E1 RNA was found to be involved in the formation of its RNP *in vivo*.

EXPERIMENTAL

Synthesis of mutants

Sequence *f* of *Xenopus laevis* E1 RNA was used, since it is expressed [16] and functional [17]. Site-specific base-substitution mutants were made by PCR-based *in vitro* mutagenesis. In the conserved sequences, nucleotide substitutions were G to C, C to G, A to U and U to A. In segments where sequence phylogeny indicated that the structure was conserved but the sequence was not [20], base substitutions were designed to prevent base pairing to the putative partner nucleotide on the opposite strand. For example, substitution was to G when the apparent base-pairing partner was a G, etc. The RNA sequence of the segment substituted in each mutant is shown in Table 1. A bacteriophage T7 RNA polymerase promoter was added to each product during PCR amplification so that each mutant RNA was made directly from a PCR product. Internal snoRNA mutations were made by a modification of the method for 'megaprimer' PCR-based mutagenesis [21]. The mutants were sequenced after the last PCR amplification. Their sequencing ladders were sufficiently clean, so that it was not necessary to clone the final PCR products.

Synthesis of RNA

Uncapped RNAs were synthesized *in vitro* with bacteriophage T7 RNA polymerase, using PCR products as templates. The synthetic (wild-type and mutant) E1 RNAs had the same 3′ end as natural E1 RNA, and two extra G residues at the 5′ terminus. The final concentrations of the four nucleotides were 0.5 mM to synthesize unlabelled RNA. To make ^{32}P-labelled RNA, [α-^{32}P]UTP was added and the final concentration of UTP was 25 μM. Fluorescein-labelled RNA was made using 12 μM fluorescein-UTP and 38 μM UTP. After PAGE, the level of fluorescein incorporation was quantified by scanning with 450-nm excitation light in a Storm 860 scanner (Molecular

---

Abbreviations used snoRNA, small nucleolar RNA, RNP, ribonucleoprotein, snoRNP, small nucleolar RNP

[1] To whom correspondence should be addressed (e-mail eliceirι@slu edu)

Table 1 RNA sequences of the segments substituted in each E1 RNA mutant

Nucleotide positions correspond to those shown in Figure 2(A). Upper-case letters in the sequences denote substituted nucleotides, lower-case letters are unchanged bases.

Mutant number	Nucleotide positions	RNA sequence
1	2–7	GGUUGC
2	7–13	CACCUuU
3	15–22	GAcUACUC
4	20–22	CUC
5	27–29	GAG
6	35–43	CCGAGACAG
7	47–51	CACCG
8	56–61	CCCUCG
9	67–69	GGA
10	85–87	CAU
11	91–93	GGG
12	97–99	GGU
13	109–114	UgUacU
14	114–117	UUCG
15	153–155	GAC
16	153–158	GACGUA
17	157–164	UAUAAGGAU
18	168–171	GAAG
19	173–176	GUgU
20	196–199	CCUC
21	202–210	UUUGGUACG
22	216–218	UGU

Dynamics, Sunnyvale, CA, U.S.A.). To measure the amount of RNA made, the gel was then stained with SYTO 61 (Molecular Probes, Eugene, OR, U.S.A.) and the gel was scanned with 635-nm excitation light in the same apparatus.

RNA stability *in vivo*

Isolation of *X. laevis* oocytes, nuclear injections (9 or 18 nl per oocyte), and oocyte incubations were as described earlier [22]. ^{32}P-Labelled wild-type or mutant E1 RNA was mixed with ^{32}P-labelled yeast tRNA. Each mixture had Blue Dextran at a final concentration of 20 mg/ml, to verify which injections had reached the nucleus [23]. Some aliquots of each mixture were injected into oocytes and other aliquots were loaded on to electrophoresis gels. Oocytes were incubated for 20 h at 18 °C, and then their nuclei were isolated manually in oil [24]. Only oocytes with blue nuclei were analysed. RNA was extracted from whole oocytes with proteinase K, phenol and chloroform, and was fractionated by 10% PAGE in the presence of 7 M urea. Incorporation of ^{32}P was quantified by PhosphorImaging, using the scanner mentioned above.

Formation of RNA–protein complexes *in vivo*

A mixture of ^{32}P-labelled RNA and Blue Dextran, with and without a 10- or 100-fold molar excess of competitor unlabelled RNA, was injected into the nuclei of frog oocytes. After 4 or 20 h of incubation at 18 °C, nuclei were isolated. Each blue nucleus was mixed with 10 μl of 50 mM Tris/50 mM boric acid/1 mM EDTA, and broken up by pipetting briefly with a pipettor disposable tip. The nuclear contents were kept on ice and were loaded on to electrophoresis gels as quickly as possible. Non-denaturing 5% PAGE was in 50 mM Tris/50 mM boric acid/1 mM EDTA, at 4 °C.

Nucleolar localization of RNA

Fluorescein-labelled, wild-type or mutant E1 RNA (0.2 ng per oocyte), mixed with ^{32}P-labelled, wild-type frog E1 RNA (0.02 ng per oocyte), was injected into the nucleus of oocytes. The nucleus was isolated after 2 h of oocyte incubation. The nuclear contents of each oocyte were dispersed on a glass slide as described in [25]. The amount of ^{32}P in each nuclear-contents spread was quantified by PhosphorImaging to monitor the extent of injection delivery into the nucleus. Only the nuclear spreads with high levels of ^{32}P were analysed further. The nuclear contents were visualized by fluorescence microscopy [26] and phase microscopy.

RESULTS

RNP formation *in vivo*

The presence of endogenous E1 RNA in a small nucleolar RNP (snoRNP) particle *in vivo* has been observed by glycerol-gradient sedimentation [13]. In previous studies, the formation of RNPs

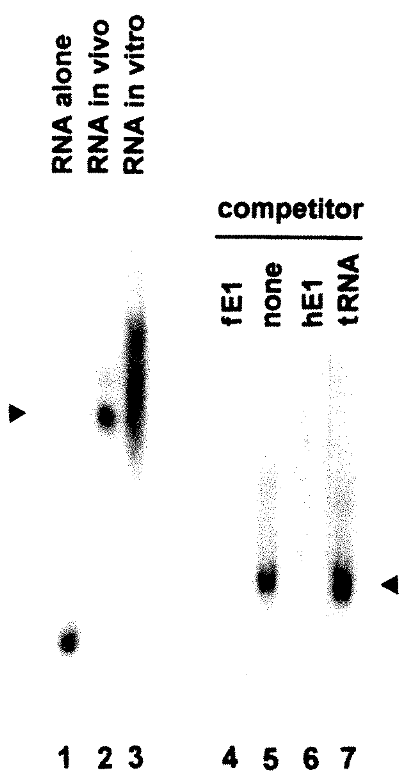

Figure 1 Exogenous E1 RNA assembles into a specific RNP *in vivo*

A mixture of ^{32}P-labelled, wild-type frog E1 RNA and Blue Dextran was injected into the nuclei of frog oocytes, followed by 4 h of oocyte incubation. Nuclei were isolated and, if blue (indicating that the injection had reached the nucleus), their contents were fractionated by non-denaturing PAGE (lane 2). As a control, E1 RNA was loaded directly on to the same gel (lane 1). As another control, E1 RNA was mixed with the contents of a nucleus from a non-injected oocyte (same amount of E1 RNA, nuclear contents and buffer, and buffer composition as in lane 1) and loaded directly on to the gel (lane 3). Frog oocytes were injected into the nucleus with ^{32}P-labelled, frog E1 RNA alone (lane 5), and mixtures of this RNA with a 10-fold excess of unlabelled frog E1 RNA (fE1, lane 4), a 10-fold excess of unlabelled human E1 RNA (hE1, lane 6), and a 100-fold excess of unlabelled tRNA (lane 7). The migration of the RNP formed *in vivo* is indicated by the arrowheads. Lanes 4–7 and 1–3 are from long and short electrophoretic runs, respectively.

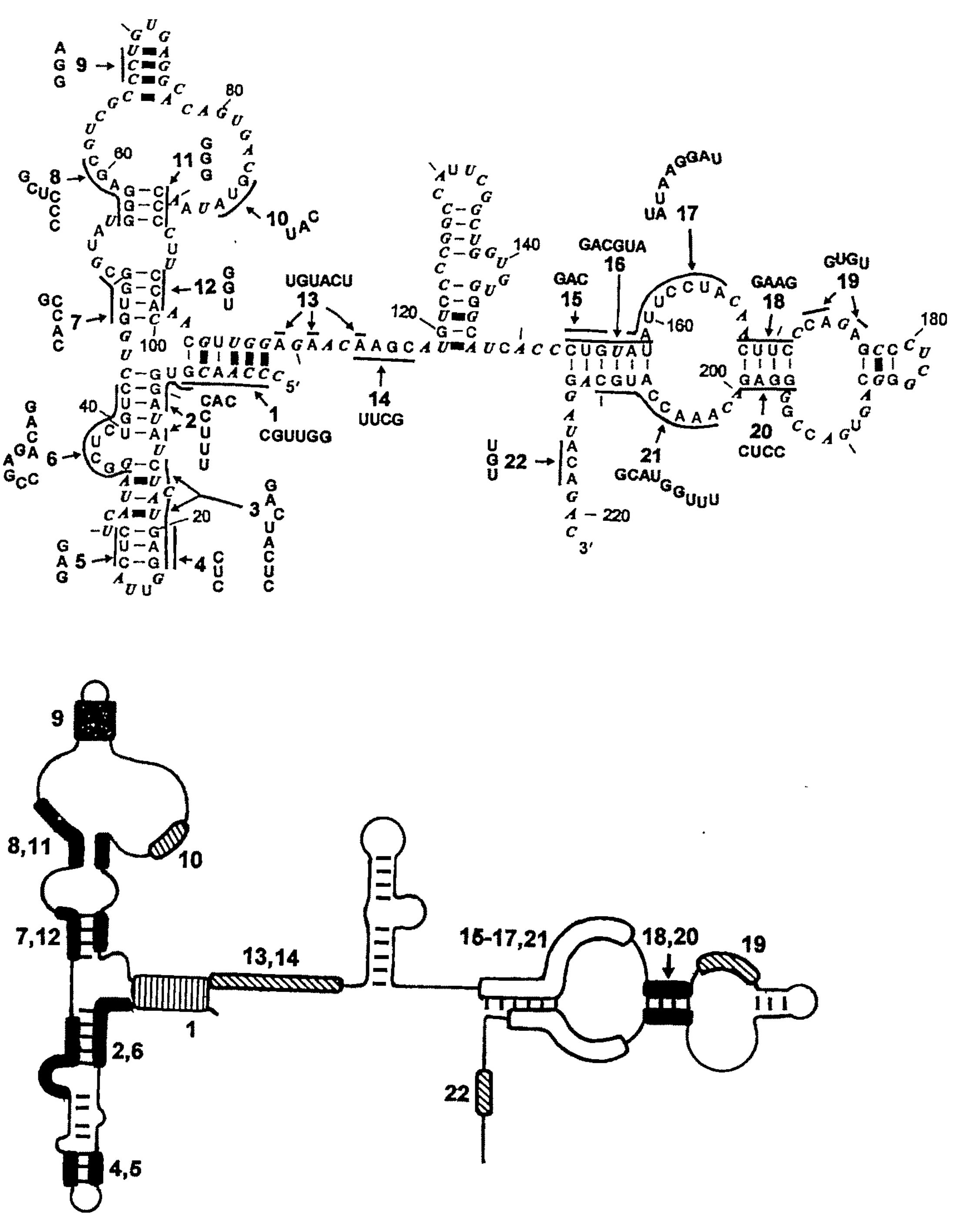

Figure 2 Substitution mutants of frog E1 RNA (top panel) and summary of segments conserved in E1 RNA that are involved in the RNP formation and/or stability *in vivo* of E1 RNA (bottom panel)

(Top panel) Vertebrate E1 RNA consensus sequence and consensus secondary structure are based on comparative sequence phylogeny, including co-variation analysis [20]. Nucleotides conserved in E1 RNA are in standard print. Non-conserved nucleotides of sequence *I* of *X. laevis* E1 RNA [16] are in italics. The 22 mutants were as long as the wild-type sequence. A number both identifies each mutant and the segment substituted in that mutant. The substituted segment of each mutant is indicated, both by a line next to each changed nucleotide and by showing the sequence of the segment substituted in each mutant, next to the wild-type full-length sequence. Sequence co-variations [20] are indicated by black rectangles. (Bottom panel) Conserved segments that are involved in E1 RNP formation and snoRNA stability *in vivo* are apparently (i) sequences in four regions (hatched boxes), (ii) one sequence in each of five regions, plus either the other sequence or the structure in that region (black boxes), (iii) a structure (grey box) and (iv) sequence(s) and/or structure in one region (white boxes). An additional conserved segment whose mutation decreases E1 RNA stability is apparently a structure (box with vertical lines). For simplicity, these segments are labelled with the same numbering as the mutants (see top panel).

was analysed by immunoprecipitation. Immunoprecipitation would fail to detect (i) RNA elements needed for those interactions with proteins that are not required, directly or indirectly, for association of the RNA of interest with the protein targeted by the antibody, and (ii) RNA elements needed only for RNP conformation. In addition, there are no known antibodies that

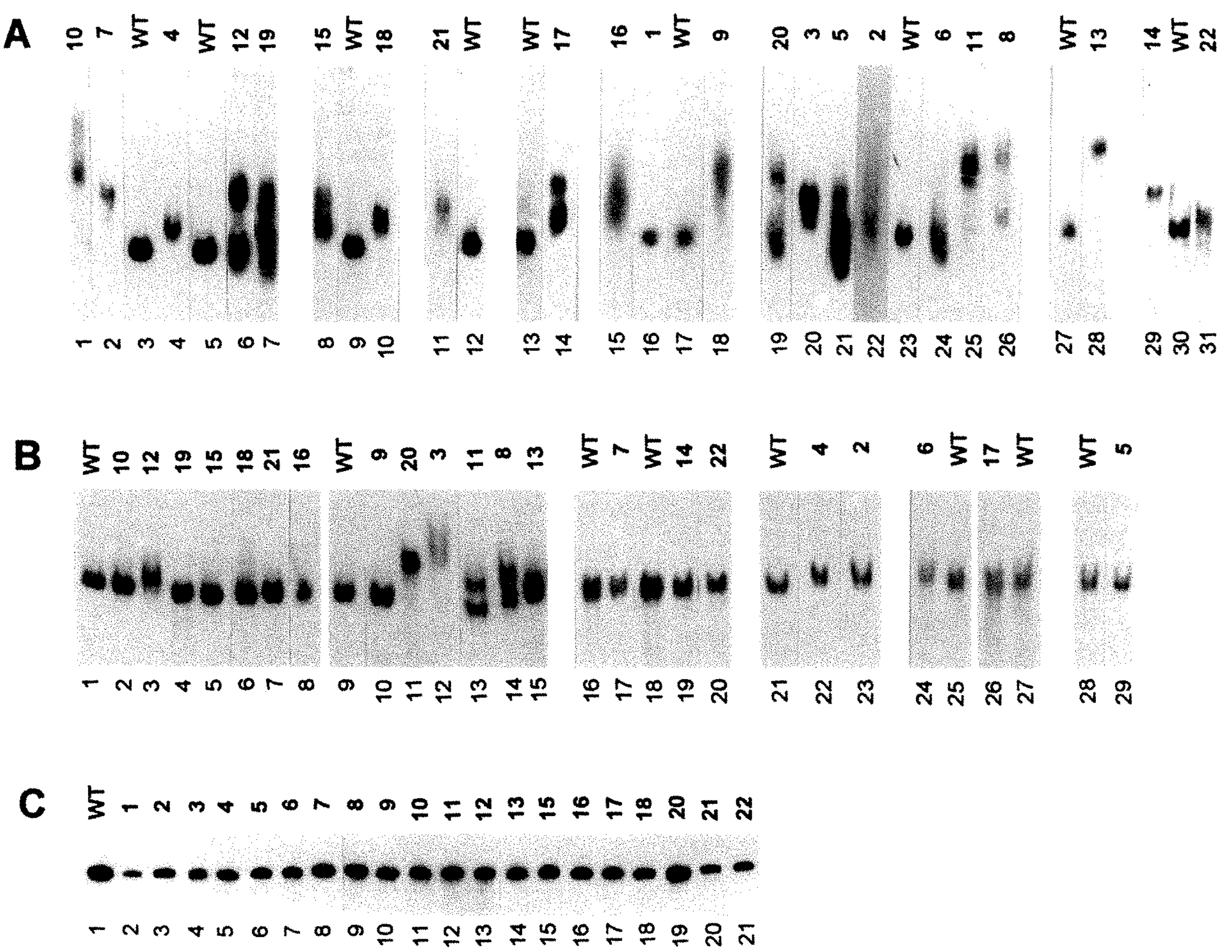

Figure 3 RNP assembly of different E1 RNA mutants *in vivo*

(**A**) ^{32}P-Labelled, wild-type E1 RNA (WT) or mutant E1 RNA (numbered above each lane as in Figure 2, top panel), mixed with Blue Dextran, was injected into the nuclei of frog oocytes that were then incubated for 4 h (lanes 1–7 and 11–28) or 20 h (lanes 8–10 and 29–31). The nucleus of each oocyte was isolated and, if blue, its contents were fractionated by non-denaturing PAGE. Gaps between lanes indicate separate electrophoreses. (**B**) Non-denaturing PAGE of wild-type and mutant E1 RNAs that had been synthesized *in vitro* and deproteinized, without injection into oocytes. (**C**) Same as (**B**), but analysed on denaturing (7 M urea) 10% PAGE.

recognize only the E1 snoRNP. It appeared that the non-denaturing gel electrophoresis typically used for gel mobility-shift analysis would be a more general assay to monitor RNP formation in whole cells. Potentially it could detect (i) the failure of the RNA to associate with any of the protein components of the RNP, and (ii) changes in RNP conformation. We chose to do this assay *in vivo* rather than *in vitro* because E1 RNA function, including snoRNA 'add-back' experiments, can be monitored in whole cells [17] but not in cell-free systems ([27], but see [27a]). We injected uncapped RNAs because natural (endogenous) E1 RNA is not capped and is metabolically long lived, and uncapped, synthetic, wild-type E1 RNA is also long lived *in vivo* (see below). After being injected into frog oocytes, *in vitro*-synthesized, wild-type E1 RNA assembled into an RNP, since its electrophoretic mobility was much lower than that of free E1 RNA (Figure 1, lanes 1 and 2). This particle, made of exogenous RNA and endogenous proteins, is functional, since it reverses a blockage in pre-rRNA processing in E1-depleted oocytes and this reversal is RNA-sequence-specific [17]. In contrast, naked E1 RNA does not reverse blocked pre-rRNA processing *in vitro* ([27], but see [27a]). E1 RNA, mixed with the contents of an isolated oocyte nucleus, generated a smear on gel electrophoresis (Figure 1, lanes 2 and 3), indicating that the RNP assembly of injected E1 RNA requires incubation *in vivo*. This smear could not be caused by testing overly concentrated RNA because that sample had the same RNA concentration as the samples in the other lanes, and the smear was reproducible. Exogenous E1 RNA assembles into an RNA-sequence-specific RNP particle, since this assembly was blocked by an excess of frog E1 RNA, but not tRNA (Figure 1, lanes 4, 5 and 7). For higher resolution, these were long electrophoretic runs in which free E1 RNA ran off the gel. However, these results represent competition because they were very reproducible. This RNP assembly depends on conserved segments of E1 RNA, since human E1 RNA competed with frog E1 RNA (Figure 1, lanes 5 and 6). This suggests that at least some of the proteins that bind E1 RNA specifically do so by recognizing conserved segments of this snoRNA. The high mobility of this RNP particle in 5% PAGE indicates that this complex is small, as expected from the sedimentation rate of the endogenous E1 snoRNP [13]. This RNP is nucleolar, since the injected E1 RNA localized in nucleoli (see below).

Evolutionarily conserved E1 RNA sequences and secondary structures were identified before, based on comparative sequence phylogeny, including co-variation analysis [20]. To identify the

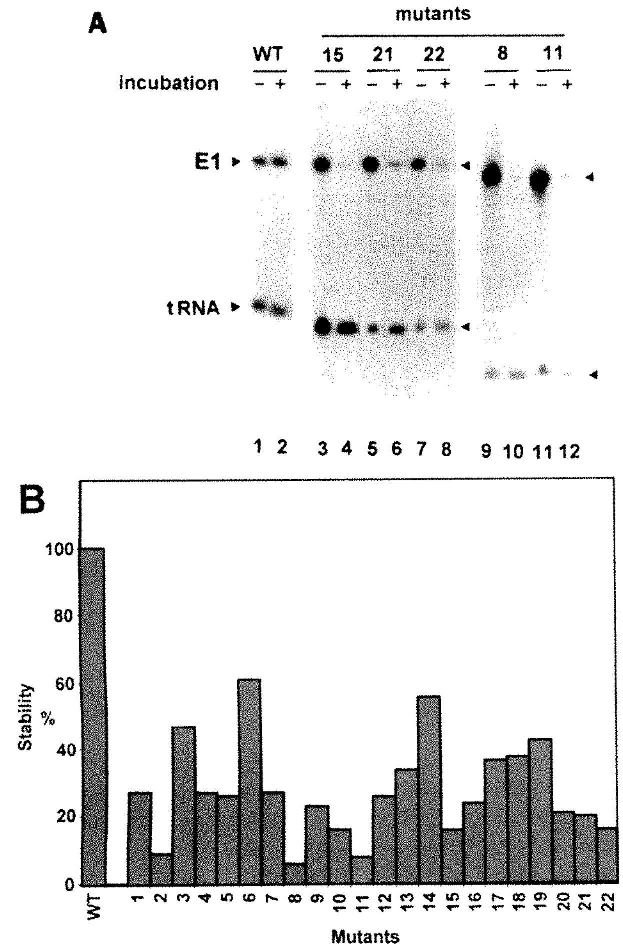

Figure 4 Stability of E1 RNA mutants *in vivo*

(**A**) Stability of some E1 RNA mutants, relative to tRNA. A mixture of ^{32}P-labelled tRNA, Blue Dextran and ^{32}P-labelled wild-type (WT) or mutant (numbered as in Figure 2, top panel) E1 RNA was injected into the nuclei of oocytes that were then incubated for 20 h. Only oocytes whose nuclei were blue (indicating a successful nuclear injection) were harvested. RNA extracted from whole oocytes was analysed by denaturing 10% PAGE, and then exposed to X-ray film. RNA mixtures before injection (–) and after oocyte incubation (+) are shown. Gaps between lanes indicate separate electrophoreses. (**B**) Stability of E1 RNA mutants, relative to (tRNA and then to) wild-type E1 RNA. After oocyte injection and incubation, and gel electrophoresis as in (**A**), the radioactive bands were quantified by PhosphorImaging. In each sample, the amount of radiolabelled E1 RNA was normalized by the level of radioactive tRNA. Then, the remaining amount of each mutant E1 RNA was corrected in reference to the remaining level of wild-type E1 RNA (WT).

E1 RNA segments involved in RNP formation, we made a series of base-substitution mutants of frog E1 RNA, in phylogenetically conserved sequences and secondary structures (Figure 2, top panel). Surprisingly, base substitutions in many conserved segments of E1 RNA resulted in abnormal RNP PAGE patterns (Figure 3A). The RNP smears were not caused by snoRNA degradation, since we verified that each of the E1 RNA mutants still migrated electrophoretically as a narrow, single RNA band after these oocyte incubations (results not shown). (A number both identifies each mutant and the segment substituted in that mutant.) The PAGE pattern differences between each mutant E1 RNA and wild-type E1 RNA, including the RNP smears, could not be caused by differences in the amount of E1 RNA injected per oocyte, or by differences in the amount of nuclear contents loaded per gel lane, because of the following. First, we injected the same amount of mutant E1 RNA and wild-type E1 RNA per oocyte, and monitored delivery into the nucleus by co-injecting Blue Dextran with each sample. Secondly, the PAGE pattern differences between each E1 RNA mutant and wild-type E1 RNA, including the RNP smears, were seen in multiple oocytes that were analysed individually. Thirdly, we saw the same PAGE patterns when loading either most of the nuclear contents of one oocyte per gel lane or one-tenth or less than that amount from the same oocyte per gel lane. In the examples shown in Figure 3(A), four mutants and their wild-type controls are shown after 20 h of post-injection oocyte incubation, and the other mutants and their wild-type controls are shown after 4 h of oocyte incubation. The differences in PAGE mobility between the RNP of each mutant snoRNA and the RNP of the wild-type snoRNA were seen both after 4 h and after 20 h of post-injection oocyte incubation. The differences in signal intensity among gel lanes do not necessarily represent recovery variations. Instead, these differences were caused (i) by loading on gels the contents of various percentages of one oocyte nucleus, to have wild-type controls in many sections of some gels, and (ii) by showing autoradiographs from different times of X-ray film exposure, to make the differences in electrophoretic migration patterns as visible as possible.

Deproteinized molecules of most mutant E1 RNAs migrated with or very close to wild-type, naked E1 RNA in non-denaturing PAGE; the exceptions were mutants 3, 8, 11 and 20 (Figure 3B). However, in these gels, the mobilities of deproteinized molecules of mutants 8, 11 and 20 relative to wild-type snoRNA (Figure 3B) were substantially different from the relative migrations of the corresponding RNPs (Figure 3A). Therefore, for 20 of these mutants the abnormal RNP PAGE patterns do not simply reflect a corresponding difference in migration of naked RNA. We cannot draw conclusions about mutant 3, since its mobility relative to wild-type was similar in RNPs (Figure 3A) and isolated RNA (Figure 3B). Deproteinized molecules of all these mutant snoRNAs co-migrated, as single bands, with wild-type E1 RNA in denaturing PAGE (Figure 3C). Only mutants 8 and 11 showed double bands of naked E1 RNA in non-denaturing PAGE (Figure 3B). Interestingly, segments 8 and 11 are on opposite strands of the same double helix in the phylogeny-based model of E1 RNA secondary structure (Figure 2, top panel) [20]. These results suggest that this double helix exists.

With regard to segments 10, 13, 14, 19 and 22, (i) they are evolutionarily conserved sequences in E1 RNA, (ii) they are in single-stranded regions in the phylogeny-based model of E1 RNA secondary structure (Figure 2, top panel) [20], and (iii) substitution of their nucleotides produced abnormal RNP patterns (Figure 3A). This suggests that, in these segments, their sequences are needed for E1 RNP formation. Segments 7 and 12 (i) are evolutionarily conserved sequences in E1 RNA, (ii) are on opposite strands of the same double helix in the phylogeny-based model of E1 RNA secondary structure (Figure 2, top panel) [20], and (iii) substitution of their bases generated abnormal RNP PAGE patterns that differed from each other (Figure 3A). If this double helix were the only requirement from this region for E1 RNP formation, mutants 7 and 12 would be expected to have the same RNP PAGE pattern. Therefore, these results suggest that E1 RNP formation requires both (i) the sequence of one of these two segments; and (ii) either the sequence of the other segment or this double helix. These observations, and therefore these conclusions, about the pair of segments 7 and 12 also apply to the four pairs of evolutionarily conserved segments 2 and 6, 4 and 5, 8 and 11, and 18 and 20 (Figures 2, top panel, and 3A).

Mutant 9 has an abnormal RNP PAGE pattern (Figure 3A). In segment 9, RNA structure appears to be involved in E1 RNP

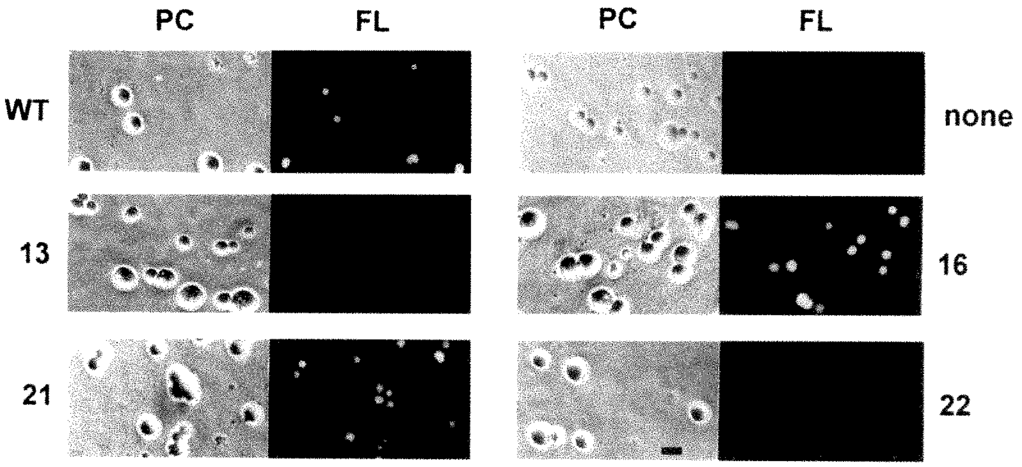

Figure 5 Nucleolar localization of exogenous wild-type and mutant E1 RNAs

Frog oocytes were injected into the nucleus with mixtures of ^{32}P-labelled, wild-type E1 RNA and a fluorescein-labelled RNA. In the examples shown, the fluorescein-labelled RNA was wild-type frog E1 RNA (WT), and E1 mutants 13, 16, 21 and 22. Some oocytes were not injected (none). After 2 h of oocyte incubation, nuclei were isolated and their contents were spread on glass slides. The level of ^{32}P in the nuclear contents (extent of nuclear injection) was quantified by PhosphorImaging. The nuclear contents were then photographed under phase microscopy (PC) and fluorescence microscopy (FL). Scale bar, 10 μm.

formation, because (i) segment 9 has been shown to be in a double helix, since this section has had multiple base co-variations during evolution; and (ii) this segment does not have any conserved nucleotides (Figure 2, top panel) [20]. Segments 15–17 are base-paired to segment 21 in the phylogeny-based model of E1 RNA secondary structure (Figure 2, top panel) [20]. Mutants 15–17 and 21 each resulted in similarly abnormal RNP PAGE patterns (Figure 3A). Therefore, RNA sequence(s) and/or structure may be involved in these phenotypes. It might not be only RNA structure, since the RNP PAGE patterns of mutants 15–17 and 21 did not appear identical (Figure 3A). When mutated, not all conserved segments generated abnormal RNP PAGE patterns. For example, substitution of segment 1 produced an RNP that co-migrated electrophoretically with the RNP of wild-type E1 RNA (Figure 3A).

snoRNA stability *in vivo*

Metabolic stability is an important aspect of the life cycle of any RNA molecule. A few elements needed for snoRNA stability *in vivo* have been identified in box C/D snoRNAs [18,26,28–31]. Information about E1 RNA segments involved in snoRNA stability *in vivo* was also of interest both to correlate it with the preceding results on E1 RNP formation and to plan the search for E1 RNA nucleolar-localization elements (see below). The effect of the mutations shown in Figure 2 (top panel) on the metabolic stability of E1 RNA was tested next. We injected RNAs that were not capped because uncapped, *in vitro*-synthesized, wild-type E1 RNA is long lived *in vivo* (Figure 4A) and natural E1 RNA is not capped. A mixture of radioactive tRNA and wild-type or mutant E1 RNA was injected into oocytes, which were then incubated for 20 h. Base substitutions in all the regions of E1 RNA that produced abnormal RNP PAGE patterns also decreased the stability of this snoRNA *in vivo* (Figure 4B). RNA sequence is apparently involved in segment 2, since (i) mutant 6 was substantially more stable (Figure 4B), and segments 2 and 6 are on opposite strands of the same double helix in the phylogeny-based model of E1 RNA secondary structure and (ii) the six nucleotides in segment 2 are evolutionarily conserved in E1 RNA (Figure 2, top panel) [20]. In addition, mutant 1 was unstable in oocytes (Figure 4B), although its RNP PAGE pattern was apparently normal. In segment 1, RNA structure is apparently involved, because (i) at least four out of the six nucleotides in segment 1 are not evolutionarily conserved in E1 RNA, and (ii) segment 1 has been shown to be in a double helix, since this section has had multiple base co-variations during evolution (Figure 2, top panel) [20]. The instability of the mutants was not caused specifically by lacking a 5′ end cap, since the injected wild-type E1 RNA was also uncapped but was long lived *in vivo*.

snoRNA nucleolar localization

snoRNAs require nucleolar-localization elements, when nascent, to be transported from the nucleoplasm to the nucleolus, and when mature, to remain in the nucleolus between mitoses. The nucleolar-localization elements of box C/D snoRNAs have been identified [26,30–33]. For cellular-localization experiments, oocytes were incubated for 2 h after injection, since the levels of many of these mutants dropped appreciably after 20 h of oocyte incubation (Figure 4B). Fluorescein-labelled, wild-type E1 RNA injected into the nucleus migrated to nucleoli; the intensity of this signal can be compared with non-injected oocytes (Figure 5). Oocytes injected with fluorescein-labelled tRNA gave low background fluorescence images similar to those of non-injected oocytes (results not shown). The prominent structures in Figure 5 are the large nucleoli of *Xenopus laevis* oocytes, since the nuclei of these cells do not have any other structures of this size, morphology and abundance [34].

Mutants 13 and 22 (substituted in boxes H and ACA, respectively) localized poorly to nucleoli (Figure 5). These results were not due to instability of these mutants. After 2 h of oocyte incubation, in stability-quantification experiments similar to those in Figure 4(B), we measured similar stabilities in mutants 13 and 22 and in mutants that localized efficiently in the nucleolus (results not shown). Mutants 16 and 21 are shown as examples of those positive controls (Figure 5). These data were not caused by low injection delivery into the nucleus, since each sample was co-injected with ^{32}P-labelled, wild-type E1 RNA, and nuclear delivery was quantified by PhosphorImaging.

DISCUSSION

Unexpectedly, we have identified 11 evolutionarily conserved regions in U17 RNA that are needed for U17 RNP formation *in vivo*. Similar results have not been reported in other H/ACA snoRNPs, any other snoRNPs, or apparently any other RNP. Figure 2 (bottom panel) summarizes the conserved sequences and structures of E1 RNA whose base substitution interfered with the RNP formation and/or metabolic stability of this snoRNA. At least some of the abnormal RNP PAGE patterns are expected to be caused by the failure of proteins to bind E1 RNA, which in some cases might be coupled to changes in RNP shape. Others might result instead from an alteration in the conformation of the RNP, preserving the number of bound polypeptides. Among the regions of E1 RNA that affected RNP formation, ten were detected by substitution of only three nucleotides each. The location of several of these three-base substitutions in E1 RNA suggests that they would not have major global effects on the conformation of E1 RNA. For example, three-base substitutions in four single-stranded segments (numbers 10, 13, 19 and 22) generated four different abnormal RNP PAGE patterns. Indeed, most of the 22 mutations had no detectable effect on the conformation of naked E1 RNA (Figure 3B). Many of the abnormal RNP PAGE patterns differed from each other, implying diverse changes in the RNP. The different RNP PAGE patterns generated by base substitutions in various conserved E1 RNA segments suggest that, in many E1 RNA elements, each element plays a different role in RNP formation. These different PAGE patterns, and the separation of these conserved E1 RNA regions by evolutionarily non-conserved sections, suggest that many of these segments are separate elements.

Most of the abnormal E1 RNP PAGE patterns were two bands or a smear (Figure 3A). This did not reflect an *in vivo*-induced change in the RNA, since after oocyte incubation each mutant E1 RNA, deproteinized, co-migrated with wild-type E1 RNA as a single, narrow band in denaturing PAGE (results not shown). In some of these cases, failure to bind a protein might generate two or more forms of the RNP. Except for the H and ACA boxes, the other snoRNA segments needed for E1 RNP formation and/or snoRNA metabolic stability are specific for E1 RNA, rather than generic for the box H/ACA snoRNA family [4,20]. It is likely that disruptions of RNP formation at various E1 RNA segments may then decrease E1 RNA stability *in vivo*, since both were abnormal after mutating each of 11 regions of this snoRNA. In contrast, segment 1 is involved in snoRNA stability but apparently is not essential for E1 RNP formation.

The H and ACA boxes, and the proximal stem structures in the 5′ and 3′ hairpins, are essential for accumulation of some H/ACA snoRNAs (yeast snR5, snR11 and snR36, and human U64) in experiments that could not distinguish RNA biosynthesis from RNA stability [8,9,35]. Our results indicate that RNA stability is affected in those segments, since the following frog E1 RNA mutants were very unstable: 13 (substituted in box H); 22 (changed in box ACA); 1 (mutated in the 5′-terminal stem); and 21 (altered in the 3′-terminal stem) These are among the most unstable E1 RNA mutants in frog oocytes (Figure 4). We also detected segments of the snoRNA involved in RNA stability that had not been detected before. There are several differences between the work in [8,9,35] and ours. Those studies (i) did not mutate some of the snoRNA segments that we mutated, (ii) did not monitor RNA stability itself, but assayed for RNA accumulation, the sum of RNA biosynthesis and RNA stability (then, a role of a given RNA segment in RNA biosynthesis might mask an additional participation of the same RNA region in RNA stability), (iii) focused primarily on yeast snoRNAs, and there are differences between yeast RNAs and their vertebrate orthologues and (iv) dealt with H/ACA snoRNA species other than E1 RNA, and there are differences among various members of a given snoRNA family [26,28,30,31,33].

Many snoRNA segments are involved in the stability of E1 RNA *in vivo* (this study), but few snoRNA stability elements have been reported for box C/D snoRNAs [18,26,28–31]. Another factor for this apparent difference might be various differences in experimental design in each study. We (i) incubated oocytes for 20 h after snoRNA injection, which makes it easier to detect decreased RNA stability, (ii) injected all snoRNA mutants into the nucleus (snoRNAs tend to migrate poorly from cytoplasm to nucleus; they might have abnormal stabilities in their non-physiological subcellular compartment), (iii) co-injected each E1 RNA mutant with a long-lived, heterologous RNA and (iv) mutated every evolutionarily conserved sequence and structure of the snoRNA.

While this manuscript was being revised, it was reported that (i) the nucleolar localization of human U67 and E1 H/ACA snoRNAs was fully eliminated when either only box H or only box ACA was mutated [36], (ii) in apparent contrast, the nucleolar localization of frog E1 RNA decreased partially when either only box H or only box ACA was mutated, and that it was completely abolished when both boxes were mutated simultaneously [37], (iii) disruption of the base of the 3′ hairpin decreased the nucleolar localization of human U65 H/ACA snoRNA [36] and (iv) box H and box ACA are elements for frog E1 RNA stability *in vivo* [37]. In the present work, substitution of either box H alone or box ACA alone resulted in a marked decrease in nucleolar localization of frog E1 RNA. We did not detect less nucleolar localization of frog E1 RNA after disruption of the base of the 3′ hairpin (mutants 16 and 21, Figure 5). We found that mutation of many additional individual conserved segments of frog E1 RNA lowered its stability *in vivo*. Some of the apparent differences in results might be related to the fact that the E1 RNA molecules tested were not capped in the present work and in [36], but were 5′-end-capped in [37] (natural E1 RNA is not capped). For example, a 5′-end-cap-binding protein (for other RNA species) might increase the stability of wild-type and mutant E1 RNAs, and might make it difficult to detect some snoRNA stability elements. There are also apparent differences in the nucleolar-localization element requirements of various snoRNA species that are members of the same snoRNA family [26,28,30,31,33].

In other small RNAs, very few *cis*-acting elements are known to be required for RNP assembly or RNA metabolic stability. The present study shows that for E1 RNA, the formation of the RNP and the stability of the RNA *in vivo* depend on a much larger number of phylogenetically conserved snoRNA segments. In view of this surprising complexity, it will be interesting to identify the proteins whose specific interactions with these snoRNA elements are necessary for E1 RNP formation.

We thank Rani Tanam and Jennifer Wu for preparing some of the mutants, Francesco Amaldi and Glauco Tocchini-Valentini for DNA clones, James W Brown for the folded RNA structure, Sascha Lange, Wayne Speckmann and Joseph G. Gall for advice on methods, and Jan Ryerse, Clifford Bellone and Peter Zassenhaus for the use of equipment We also thank Joyce Weber for photography and Anne Chau for assistance. This work was supported by grant R01 GM56301 from the National Institute of General Medical Sciences

REFERENCES

1 Maxwell, E. S and Fournier, M J. (1995) The small nucleolar RNAs Annu. Rev Biochem **35**, 897–934

2 Tollervey, D and Kiss, T (1997) Function and synthesis of small nucleolar RNAs· Curr Opin. Cell Biol **9**, 337–342

3 Weinstein, L B and Steitz, J A (1999) Guided tours from precursor snoRNA to functional snoRNP Curr. Opin Cell Biol **11**, 378–384

4 Eliceiri, G L (1999) Small nucleolar RNAs Cell Mol Life Sci **56**, 22–31

5 Tyc, K and Steitz, J A (1989) U3, U8 and U13 comprise a new class of mammalian snRNPs localized in the cell nucleus EMBO J **8**, 3113–3119

6 Kiss-László, Z , Henry, Y , Bachellerie, J.-P , Caizergues-Ferrer, M and Kiss, T (1996) Site-specific ribose methylation of preribosomal RNA a novel function for small nucleolar RNAs Cell **85**, 1077–1088

7 Tycowski, K T , Smith, C M , Shu, M-D and Steitz, J A (1996) A small nucleolar RNA requirement for site-specific ribose methylation of rRNA in *Xenopus* Proc Natl Acad Sci U S A. **93**, 14480–14485

8 Balakin, A G., Smith, L and Fournier, M J (1996) The RNA world of the nucleolus· two major families of small RNAs defined by different box elements with related functions Cell **86**, 823–834

9 Ganot, P , Caizergues-Ferrer, M and Kiss, T (1997) The family of Box ACA small nucleolar RNAs is defined by an evolutionarily conserved secondary structure and ubiquitous sequence elements essential for RNA accumulation Genes Dev **11**, 941–956

10 Ni, J , Tien, A L and Fournier, M. J (1997) Small nucleolar RNAs direct site-specific synthesis of pseudouridine in ribosomal RNA Cell **89**, 565–573

11 Ganot, P , Bortolin, M-L and Kiss, T (1997) Site-specific pseudouridine formation in preribosomal RNA is guided by small nucleolar RNAs Cell **89**, 799–809

12 Ruff, E A , Rimoldi, O J , Raghu, B and Eliceiri, G. L (1993) Three small nucleolar RNAs of unique nucleotide sequences Proc Natl Acad Sci U.S A **90**, 635–638

13 Rimoldi, O J., Raghu, B , Nag, M K. and Eliceiri, G L (1993) Three new small nucleolar RNAs that are psoralen crosslinked *in vivo* to unique regions of pre-rRNA Mol Cell Biol **13**, 4382–4390

14 Kiss, T and Filipowicz, W (1993) Small nucleolar RNAs encoded by introns of the human cell cycle regulatory gene RCC1 EMBO J **12**, 2913–2920

15 Nag, M. K , Thai, T , Ruff, E A., Selvamurugan, N , Kunnimalaiyaan, M and Eliceiri, G L (1993) Genes for E1, E2 and E3 small nucleolar RNAs Proc. Natl Acad Sci U S A **90**, 9001–9005

16 Cecconi, F., Mariottini, P , Loreni, F , Pierandrei-Amaldi, P , Campioni, N and Amaldi, F (1994) $U17^{XS8}$, a small nucleolar RNA with a 12 nt complementarity to 18S rRNA and coded by a sequence repeated in the six introns of *Xenopus laevis* ribosomal protein S8 gene Nucleic Acids Res. **22**, 732–741

17 Mishra, R. K and Eliceiri, G. L (1997) Three small nucleolar RNAs that are involved in ribosomal RNA precursor processing. Proc Natl. Acad. Sci U S A **94**, 4972–4977

18 Peculis, B A and Steitz, J A (1994) Sequence and structural elements critical for U8 snRNP function in *Xenopus* oocytes are evolutionarily conserved Genes Dev **8**, 2241–2255

19 Watkins, N J., Newman, D R , Kuhn, J. F and Maxwell, E S. (1998) *In vitro* assembly of the mouse U14 snoRNP core complex and identification of a 65-kDa box C/D-binding protein RNA **4**, 582–593

20 Selvamurugan, N , Joost, O H., Haas, E S , Brown, J W , Galvin, N J and Eliceiri, G L (1997) Intracellular localization and unique conserved sequences of three small nucleolar RNAs. Nucleic Acids Res **25**, 1591–1596

21 Datta, A K (1995) Efficient amplification using 'megaprimer' by asymmetric polymerase chain reaction. Nucleic Acids Res **23**, 4530–4531

22 Eliceiri, G L (1999) Reversible depletion of specific RNAs by antisense oligodeoxynucleotide-targeted degradation in frog oocytes Methods Enzymol **313**, 436–442

23 Jarmolowski, A , Boelens, W C , Izaurralde, E and Mattaj, I W. (1994) Nuclear export of different classes of RNA is mediated by specific factors. J Cell Biol. **124**, 627–635

24 Lund, E. and Paine, P L (1990) Nonaqueous isolation of transcriptionally active nuclei from *Xenopus* oocytes Methods Enzymol. **181**, 36–43

25 Gall, J. G , Murphy, C , Callan, H G and Wu, Z (1991) Lampbrush chromosomes Methods Cell Biol **36**, 149–166

26 Lange, T S , Borovjagin, A , Maxwell, E S and Gerbi, S A (1998) Conserved boxes C and D are essential nucleolar localization elements of U14 and U8 snoRNAs EMBO J **17**, 3176–3187

27 Enright, C. A , Maxwell, E S , Eliceiri, G L and Sollner-Webb, B (1996) 5 ETS rRNA processing facilitated by four small RNAs U14, E3, U17 and U3 RNA **2**, 1094–1099

27a Erratum (1996) RNA **2**, 1318

28 Terns, M P , Grimm, C , Lund, E and Dahlberg, J E (1995) A common maturation pathway for small nucleolar RNAs EMBO J **14**, 4860–4871

29 Caffarelli, E., Fatica, A , Prislei, S., De Gregorio, E , Fragapane, P and Bozzoni, I (1996) Processing of the intron-encoded U16 and U18 snoRNAs the conserved C and D boxes control both the processing reaction and stability of the mature snoRNA EMBO J **15**, 1121–1131

30 Lange, T S , Borovjagin, A and Gerbi, S A (1998) Nucleolar localization elements in U8 snoRNA differ from sequences required for rRNA processing RNA **4**, 789–800

31 Lange, T S , Ezrokhi, M , Borovjagin, A V , Rivera-León, R , North, M T and Gerbi, S. A (1998) Nucleolar localization elements of *Xenopus laevis* U3 small nucleolar RNA. Mol Biol Cell **9**, 2973–2985

32 Samarsky, D A , Fournier, M J , Singer, R H and Bertrand, E (1998) The snoRNA box C/D motif directs nucleolar targeting and also couples snoRNA synthesis and localization EMBO J **17**, 3747–3757

33 Narayanan, A , Speckmann, W., Terns, R and Terns, M P (1999) Role of the C/D motif in localization of small nucleolar RNAs to coiled bodies and nucleoli Mol. Biol. Cell **10**, 2131–2147

34 Gall, J. G , Tsvetkov, A , Wu, Z and Murphy, C. (1995) Is the sphere organelle/coiled body a universal nuclear component? Dev. Genet **16**, 25–35

35 Bortolin, M-L., Ganot, P and Kiss, T (1999) Elements essential for accumulation and function of small nucleolar RNAs directing site-specific pseudouridylation of ribosomal RNAs EMBO J **18**, 457–469

36 Narayanan, A , Lukowiak, A , Jády, B E , Dragon, F , Kiss, T., Terns, R. M and Terns, M P (1999) Nucleolar localization signals of Box H/ACA small nucleolar RNAs EMBO J **18**, 5120–5130

37 Lange, T S , Ezrokhi, M., Amaldi, F and Gerbi, S A (1999) Box H and box ACA are nucleolar localization elements of U17 small nuclear RNA Mol Biol Cell **10**, 3877–3890

Received 12 January 2000/28 March 2000, accepted 12 April 2000

Biochem. J (2000) 348, 525–530 (Printed in Great Britain)

Involvement of cytosolic phospholipase A_2, and the subsequent release of arachidonic acid, in signalling by Rac for the generation of intracellular reactive oxygen species in Rat-2 fibroblasts

Chang-Hoon WOO*, Zee-Won LEE†, Byung-Chul KIM*, Kwon-Soo HA† and Jae-Hong KIM*[1]

*Department of Life Science, Kwang-Ju Institute of Science and Technology (K-JIST), 1-Oryong-dong, Buk-gu, Kwang-Ju, 500-712, Korea, and †Biomolecule Analysis Group, Korea Basic Science Institute, 52 Ueon-dong, Yoosung-gu, Taejon, 305-333, Korea

Although there have been a number of recent studies on the role of Rac in the generation of reactive oxygen species (ROS), details of the signalling pathway remain unclear. In the present study we analysed the extent to which the activation of cytosolic phospholipase A_2 and the resultant release of arachidonic acid (AA) are involved in the Rac-mediated generation of ROS. Transfection of Rat-2 cells with RacV12, a constitutively active form of Rac1, induced elevated levels of ROS, as reflected by increased H_2O_2-sensitive fluorescence of 2′,7′-dichlorofluorescein. These effects could be blocked by inhibiting phospholipase A_2 or 5-lipoxygenase but not by inhibiting cyclo-oxygenase. The application of exogenous AA increased levels of ROS but the effect was dependent on the further metabolism of AA to leukotrienes $C_4/D_4/E_4$ by 5-lipoxygenase. Indeed, the exogenous application of a mixture of leukotrienes $C_4/D_4/E_4$ elicited transient elevations in the levels of ROS that were blocked by catalase. These findings indicate that phospholipase A_2 and subsequent AA metabolism by 5-lipoxygenase act as downstream mediators in a Rac signalling pathway leading to the generation of ROS.

Key words: hydrogen peroxide, leukotrienes, 5-lipoxygenase, signal transduction.

INTRODUCTION

Rac, a member of the Rho family of small GTPases, mediates such cellular functions as the reorganization of the actin cytoskeleton, cell growth and transformation, cell motility and migration, and response to stress [1–6]. In addition, Rac was recently shown to serve as a regulator of the intracellular redox state of non-phagocytic cells [7–10]. Therefore, after ligand-evoked activation, Rac might function to regulate the levels of reactive oxygen species (ROS) such as superoxide ($O_2^{\cdot -}$) and H_2O_2. For example, Rac1 seems to mediate increases in intracellular ROS in NIH 3T3 cells exposed to tumour necrosis factor α or interleukin 1β [9]. However, the downstream pathway leading from Rac1 activity to ROS generation remains poorly characterized, especially in fibroblasts.

It has been shown that, when activated, Rac in turn activates cytosolic phospholipase A_2 (cPLA$_2$), and there is a resultant release of arachidonic acid (AA), a principal product of cPLA$_2$ activity [11,12]. This makes it likely that cPLA$_2$ is a major downstream mediator of Rac signalling. For instance, Rac-induced release of AA has been shown to be a component of the biochemical pathways by which Rac stimulates both Ca^{2+} influx and Rho-dependent cytoskeletal organization in fibroblasts [11]. In addition, we observed that in response to tumour necrosis factor α or exogenously applied ceramide (a proposed lipid second messenger generated by sphingomyelin hydrolysis in response to various stresses and proinflammatory cytokines [13,14]), a Rac–cPLA$_2$–AA cascade mediates *c-fos* serum response element (SRE) activation and nuclear signalling [15,16].

To improve our understanding of the molecular mechanism responsible, in the present study we assessed the respective roles of cPLA$_2$, AA and 5-lipoxygenase (5-LO) in the Rac-mediated generation of ROS. Here we show that cPLA$_2$ and subsequent AA metabolism by 5-LO are involved in a Rac signalling pathway leading to the generation of ROS.

MATERIALS AND METHODS

Chemicals and plasmids

2′,7′-Dichlorofluorescein diacetate (DCFDA) was obtained from Molecular Probes (Eugene, OR, U.S.A.); AA, MK-886, indomethacin, AA-861 and arachidonyltrifluoromethyl ketone (AACOCF$_3$) were from Biomol (Plymouth Meeting, PA, U.S.A.); leukotrienes and *N*-acetylcysteine were from Sigma Chemical Co. (St. Louis, MO, U.S.A.); anti-cPLA$_2$ antibody was from Santa Cruz (Santa Cruz, CA, U.S.A.); and Dulbecco's modified Eagle's medium (DMEM), Phenol Red-free DMEM, non-essential amino acids and fetal bovine serum (FBS) were from Gibco-BRL (Gaithersburg, MD, U.S.A.). All other chemicals were from standard sources and were of molecular biology grade or higher. pEXV, a Myc-tagged expression vector, and pEXV-RacV12, an expression vector encoding RacV12 (a constitutively activated form of Rac1), were gifts from Dr Alan Hall (University College London, London, U.K.).

Cell culture, transfections and luciferase assay

Rat-2 fibroblasts were obtained from the American Type Culture Collection (A. T. C. C., Manassas, VA, U.S.A.) (CRL 1764) and maintained in DMEM supplemented with 0.1 mM non-essential amino acids, 10% (v/v) FBS and penicillin (50 i.u./ml)/streptomycin (50 μg/ml) (Gibco-BRL) at 37 °C under a humidified air/CO_2 (19:1) atmosphere. Rat2-RacV12 cells were prepared by transfecting Rat-2 cells with pEXV-RacV12 and a

---

Abbreviations used: AA, arachidonic acid; AACOCF$_3$, arachidonyltrifluoromethyl ketone; cPLA$_2$, cytosolic phospholipase A_2; DCF, 2′,7′-dichlorofluorescein; DCFDA, 2′,7′-dichlorofluorescein diacetate; DMEM, Dulbecco's modified Eagle's medium; FBS, fetal bovine serum; 5-LO, 5-lipoxygenase; ROS, reactive oxygen species; SRE, serum response element.

[1] To whom correspondence should be addressed (e-mail jkim@eunhasu.kjist.ac.kr).

neomycin resistance vector (pSV-Neo), after which clones were selected for 2 weeks in the presence of G418 antibiotic (0.4 mg/ml), as described previously [17]. Expression of RacV12 protein by the transfectants was confirmed by Western blot analysis with an anti-Myc epitope antibody as a probe. As a control, Rat-2 cells were transfected with the empty pEXV vector along with the neomycin resistance vector.

Transient transfection was performed by plating approx. 5×10^5 cells in 100 mm dishes for 24 h and then adding calcium phosphate/DNA precipitates prepared with 20 μg of DNA per dish. To control for variations in cell number and transfection efficiency, all clones were co-transfected with 1 μg of pCMV-βGAL, a eukaryotic expression vector containing the *Escherichia coli* β-galactosidase (*lacZ*) structural gene under the transcriptional control of the CMV promoter. In each transfection, the quantity of DNA used was held constant at 20 μg by the addition of sonicated calf thymus DNA (Sigma). After incubation for 6 h with the calcium phosphate/DNA precipitates, the cells were rinsed twice with PBS before incubation in fresh DMEM supplemented with 0.5 % (v/v) FBS. Each dish of cells was then rinsed twice with PBS and lysed in 0.2 ml of lysis solution [0.2 M Tris/HCl (pH 7.6)/0.1 % (v/v) Triton X-100], after which the lysed cells were scraped and centrifuged for 1 min. Supernatants were assayed for protein concentration and β-galactosidase activity. Luciferase activity was assayed with 10 μl of extract in accordance with the manufacturer's protocol (Promega Luciferase Assay System; Promega, Madison, WI, U.S.A.) and counted for 10 s in a Beckman liquid-scintillation spectrometer, using the tritium channel with the coincidence circuit disconnected. Transfection experiments were performed in triplicate with two independently isolated sets of cells; the results were averaged [16].

$cPLA_2$ translocation by RacV12 transfection

Rat-2 cells transiently transfected with pEXV-RacV12 were serum-starved for 24 h in DMEM containing 0.5 % (v/v) FBS. The medium was then removed and the cells were washed twice with ice-cold PBS, scraped, harvested by microcentrifugation and resuspended in 0.2 ml of buffer A [137 mM NaCl/8.1 mM Na_2HPO_4/2.7 mM KCl/1.5 mM KH_2PO_4/2.5 mM EDTA/1 mM dithiothreitol/0.1 mM PMSF/10 μg/ml leupeptin (pH 7.5)]. The resuspended cells were then mechanically lysed on ice by trituration with a 21.1-gauge needle. To prepare cytosolic and total particulate fractions, the lysates were first centrifuged at 100000 ***g*** for 1 h. The supernatants (cytosolic fraction) were then precipitated with 5 vol. of acetone, incubated for 5 min on ice and centrifuged at 14000 rev./min for 20 min at 4 °C. The resultant pellet was resuspended in buffer A containing 1 % (v/v) Triton X-100. The particulate fractions, which contained the membrane fraction, were washed twice and resuspended in 50 μl of buffer A containing 1 % (v/v) Triton X-100. The protein in each fraction was quantified with a Bradford procedure with 1 μl of extract, 799 μl of water and 200 μl of Bio-Rad Dye Reagent. Aliquots of protein sample (20 μl containing approx. 40 μg of protein) were then loaded on polyacrylamide gels for subsequent immunoblot assay for $cPLA_2$.

Leukotriene $C_4/D_4/E_4$ assays

Cells were seeded at 3×10^5 per 60 mm dish in DMEM containing 10 % (v/v) FBS for 24 h. Cells were then rinsed twice with cold PBS and mixed with 4 vol. of ethanol and left at 4 °C for 30 min. The resulting precipitate was removed by centrifugation at 15000 ***g*** (10000 rev./min) for 30 min at 4 °C. The ethanolic supernatant containing leukotrienes was collected. The ethanol was then removed by evaporation under vacuum and the samples were stored under argon at −50 °C before assay for the leukotriene $C_4/D_4/E_4$ levels as described in the Leukotriene $C_4/D_4/E_4$ enzyme immunoassay system (RPN 224; Amersham Pharmacia Biotech).

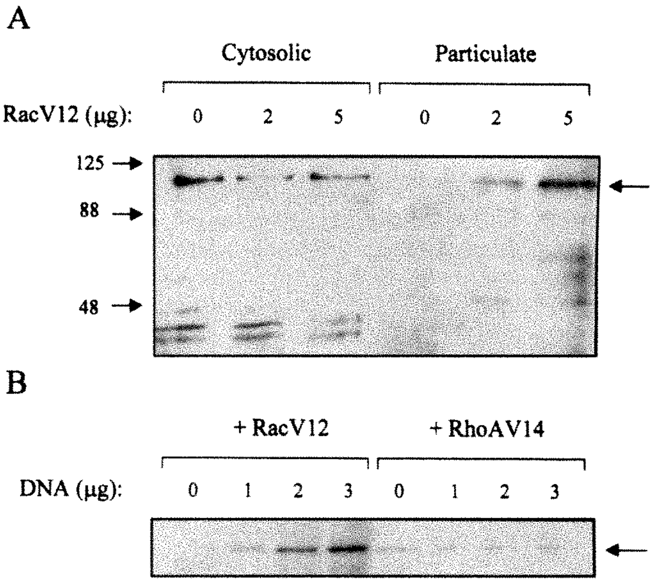

Figure 1 $cPLA_2$ translocation evoked by transfection with RacV12

(**A**) Western blot illustrating the shift in the anti-$cPLA_2$-reactive band (arrowed at the right) from the cytosolic fraction to the particulate fraction in Rat-2 cells transiently transfected with 0, 2 or 5 μg of the RacV12 expression vector, pEXV-RacV12. The quantity of transfected vector was kept constant by adding decreasing amounts of pEXV. Cells were then serum-starved for 24 h in DMEM containing 0.5% (v/v) FBS, after which the cytosolic and particulate fractions were prepared as described in the Materials and methods section. The positions of molecular mass markers are indicated (in kDa) at the left. (**B**) Western blot performed as described for (**A**) and showing the effect of transiently transfecting Rat-2 cells with 0, 1, 2 or 3 μg of pEXV-RacV12 or pEXV-RhoV14 (a RhoV14 expression vector encoding a constitutively activated form of RhoA) on $cPLA_2$ translocation to the particulate fraction. Note that, transfection with RacV12 but not RhoAV14 evoked $cPLA_2$ translocation (arrowed at the right). Results are representative of three independent experiments.

Measurement of intracellular H_2O_2

Intracellular H_2O_2 was measured as a function of 2′,7′-dichlorofluorescein (DCF) fluorescence by using the procedures of Ohba et al. [18]. In brief, cells were grown on coverslips for 2 days and then serum-starved in DMEM containing 0.5 % (v/v) FBS for an additional 2 days. The cells were then stabilized in serum-free DMEM without Phenol Red for at least 30 min before exposure to agonists (AA or leukotrienes) for the indicated durations. When the effects of inhibitors were being assessed, cells were pretreated with the respective inhibitor for 30 min. To measure intracellular H_2O_2, cells were then incubated for 10 min with the H_2O_2-sensitive fluorophore DCFDA (5 μg/ml), which, when taken up, fluorescently labels intracellular H_2O_2 with DCF. The cells were then immediately observed under a laser-scanning confocal microscope (Carl Zeiss LSM 410). DCF-labelled H_2O_2 was excited by a 488 nm argon laser, and the evoked emission was filtered with a 515 nm long-pass filter. DCF fluorescence was measured in 30 randomly selected cells. Values are means ± S.D. for DCF fluorescence intensity in three independent experiments.

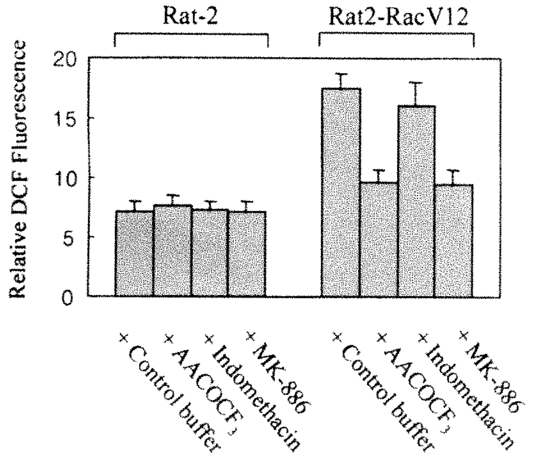

Figure 2 Role of cPLA$_2$ in RacV12-mediated generation of ROS

Serum-starved Rat-2 and Rat2-RacV12 stable cells were pretreated for 30 min with control buffer, AACOCF$_3$ (10 μM), indomethacin (10 μM) or MK886 (50 nM) before the measurement of levels of fluorescence. The relative intensities of H_2O_2-sensitive DCF fluorescence (arbitrary units), which served as an index of the levels of ROS, were measured in DCFDA-loaded cells. Results are means ± S.D. (*n* = 30 cells).

RESULTS

Rac-induced translocation of cPLA$_2$

We have previously shown that transiently transfecting cells with the constitutively active RacV12 induced a dose-dependent release of AA that was completely abolished by pretreatment by mepacrine, a potent inhibitor of PLA$_2$ [12]. In the present study the activation of cPLA$_2$ by Rac was further characterized in Rat-2 fibroblasts by examining the effect of RacV12 expression on cPLA$_2$ translocation [19,20] (Figure 1). Transient transfection of Rat-2 fibroblasts with 0, 2 or 5 μg of pEXV-RacV12 elicited rapid and dose-dependent translocation of cPLA$_2$ (molecular mass approx. 100 kDa) from the cytosolic fraction to the particulate fraction (Figure 1A). As an example, transfection with 5 μg of pEXV-RacV12 elicited an approx. 4.8-fold increase in the size of the particulate cPLA$_2$ fraction and a concomitant decline in the cytosolic fraction, which is indicative of the activation of cPLA$_2$ by RacV12. In contrast, there was no detectable translocation in response to transfection of pEXV-RhoV14 (0, 1, 2 and 3 μg), an expression vector encoding a constitutively activated form of RhoA (Figure 1B). These results are therefore in good agreement with the proposed role of cPLA$_2$ as one of the signalling mediators downstream of Rac.

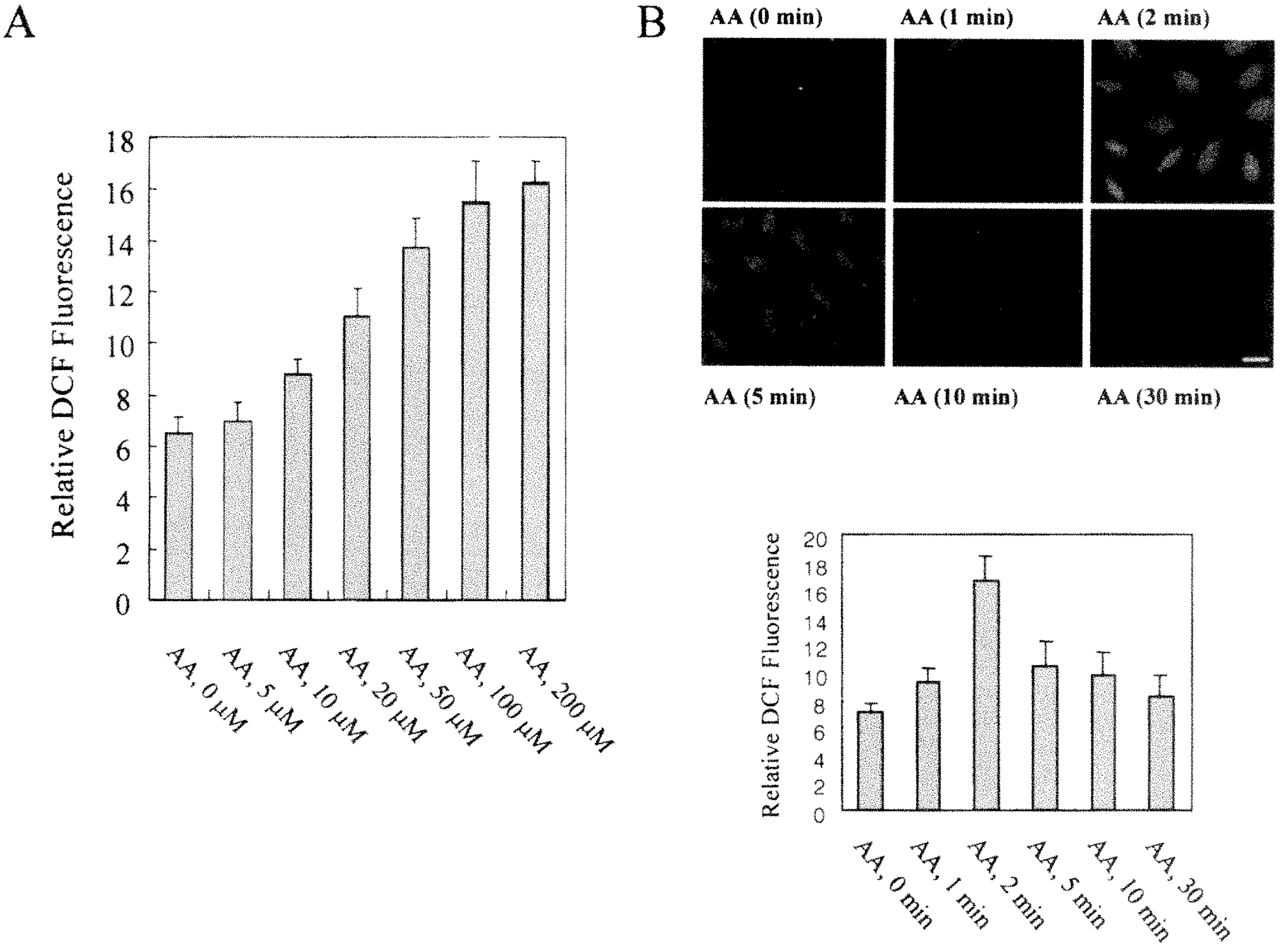

Figure 3 Activation of ROS by exogenous AA in a dose- and time-dependent manner

Rat-2 cells were serum-starved for 2 days and then stimulated with either AA at the indicated doses (0, 5, 10, 20, 50, 100 and 200 μM) for 2 min (**A**) or AA (100 μM) for the indicated durations (0, 1, 2, 5, 10 and 30 min) (**B**). DFC fluorescence intensities reflecting the relative levels of ROS (arbitrary units) were imaged with a confocal laser scanning fluorescence microscope and quantified. Results are means ± S.D. (*n* = 30 cells). Scale bar, 30 μm.

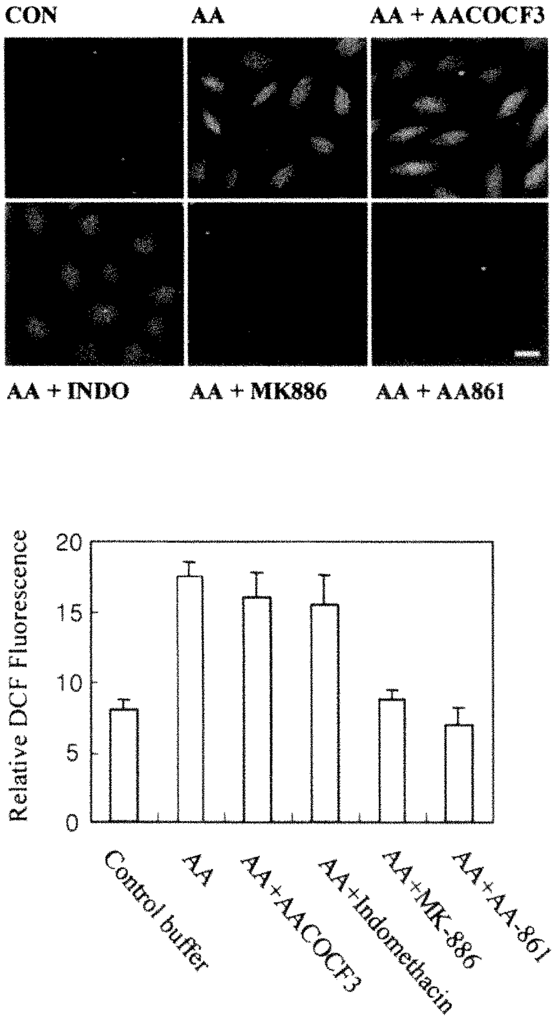

Figure 4 Effect of MK-886 and AA-861 on the AA-induced generation of ROS

Serum-starved Rat-2 cells were exposed to 100 μM AA for 2 min in the presence or absence of AACOCF$_3$ (10 μM), indomethacin (10 μM), AA-861 (1 μM) and/or MK-886 (50 nM), as indicated. Inhibitors were added 30 min before the addition of AA. DFC fluorescence was imaged and quantified as in Figure 3. Scale bar, 30 μm. Results are means ± S.D. ($n = 30$ cells).

Effect of cPLA$_2$ inhibition on the generation of ROS in RacV12 cells

One potential mechanism by which Rac might regulate the generation of ROS is via the cPLA$_2$–AA cascade. Therefore, by analysing images of H_2O_2-sensitive DCF fluorescence, we assessed the extent to which pretreatment with specific inhibitors of cPLA$_2$ or AA metabolism attenuate Rac-mediated ROS generation. In comparison with Rat-2 controls, Rat2-RacV12 cells, stably expressing RacV12, showed significantly increased basal DCF fluorescence (Figure 2). Pretreatment with 10 μM AACOCF$_3$, a specific cPLA$_2$ inhibitor, almost completely blocked ROS generation in Rat2-RacV12 cells (more than 90% inhibition). Similar effects were exerted by MK-886, a specific 5-LO inhibitor, suggesting that cPLA$_2$ activity and the subsequent metabolism of AA by 5-LO are involved in the Rac signalling leading to ROS generation. In contrast, levels of ROS were unaffected by 10 μM indomethacin, a non-specific cyclooxygenase inhibitor. Consistent with these results was the observation that Rat2-RacV12 cells generated a significantly enhanced level of leukotrienes, products of 5-LO, in comparison with control Rat-2 cells. For example, the level of leukotrienes $C_4/D_4/E_4$ generated in RacV12 cells was approx. 2-fold higher than that in control cells (Table 1).

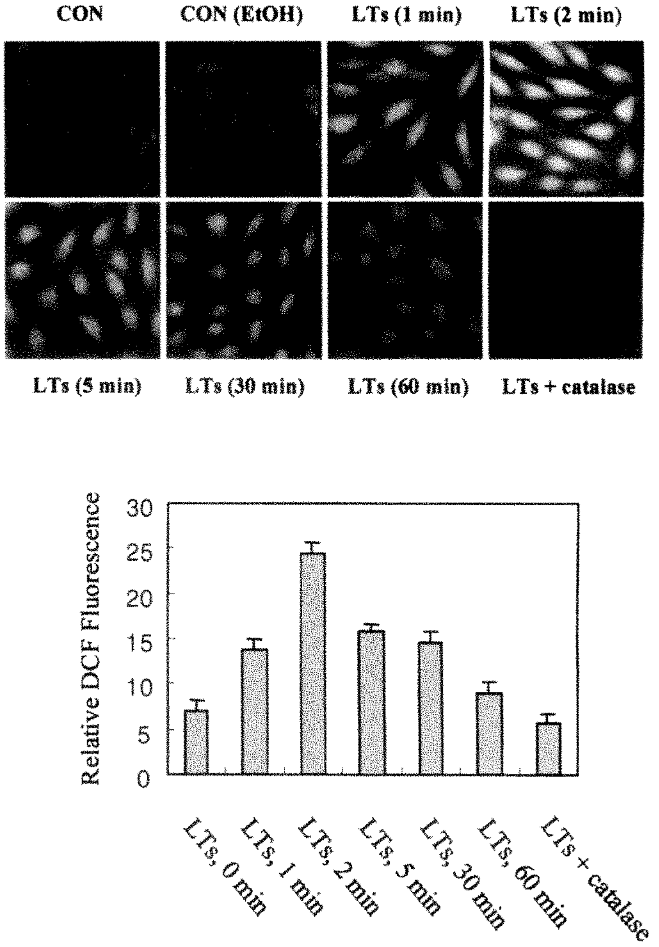

Figure 5 Application of exogenous leukotrienes induces the generation of ROS

Serum-starved Rat-2 cells were exposed to mixture of leukotrienes $C_4/D_4/E_4$ (LTs; 200 nM mixture) for the indicated durations (0, 1, 2, 5, 30 and 60 min). In some cases, cells were exposed to the mixture of leukotrienes for 2 min in the presence of catalase (10 units). DCF fluorescence was imaged and quantified as in Figure 3. Results are means ± S.D. ($n = 30$ cells).

Table 1 Enhanced generation of leukotrienes $C_4/D_4/E_4$ by RacV12

Rat-2, Rat2-RacN17 (stable cells expressing RacN17, a dominant-negative mutant of Rac1 [17]) and Rat2-RacV12 cells were grown for 24 h in DMEM containing 10% (v/v) FBS and then harvested for the analysis of intracellular levels of leukotrienes $C_4/D_4/E_4$ mixture as described in the Materials and methods section. Results are averages of three independent experiments.

Cell type	Concentration of leukotrienes $C_4/D_4/E_4$ (pg/ml)
Rat-2	16 ± 4
Rat2-RacN17	12 ± 5
Rat2-RacV12	32 ± 3

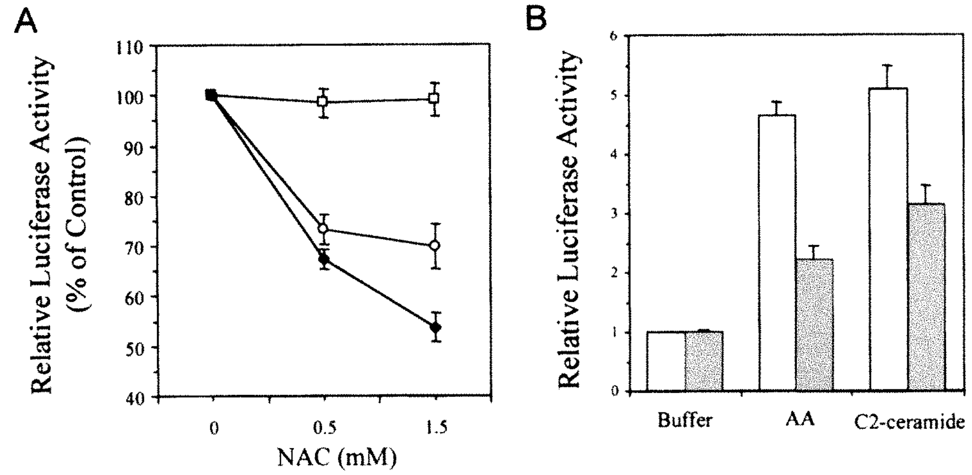

Figure 6 Essential role of ROS in the activation of SRE by C2-ceramide and AA

(**A**) Rat-2 cells were transiently transfected with 3 μg of pSRE-Luc reporter plasmid and then serum-starved for 36 h. Thereafter, cells were incubated for 30 min with the indicated concentrations of *N*-acetylcysteine (NAC) (0.5 and 1.5 mM) prior to incubation for 1 h with buffer (control) (□), C2-ceramide (5 μM) (○) or AA (100 μM) (◆). Cells were then harvested and relative luciferase activity was assessed. Results are expressed as percentages of control. The results shown are representative of at least three independent transfections. (**B**) Rat-2 cells were transiently co-transfected with 3 μg of pRc (vector) (open bars) or pRc-superoxide dismutase (SOD) (filled bars) along with 3 μg of pSRE-Luc reporter plasmid. DNA sample size was held at 20 μg by the addition of calf thymus carrier DNA. Transfectants were serum-starved for 36 h then incubated with buffer (control), AA (100 μM) or C2-ceramide (5 μM) for 1 h after which they were harvested and relative luciferase activity was assessed. Results are expressed as percentages of control. The results shown are representative of at least three independent transfections.

Application of exogenous AA generates ROS via 5-LO-dependent pathway

The foregoing results encouraged us to examine in more detail the role of cPLA$_2$ in the Rac-mediated generation of ROS. To do this, we first tested whether exogenous AA could stimulate ROS generation. After serum starvation for 48 h DCDFA-loaded Rat-2 cells were exposed to AA at the indicated doses (0, 5, 10, 20, 50, 100 and 200 μM) and for the indicated durations (0, 1, 2, 5, 10 and 30 min). Consistent with the proposed role of cPLA$_2$ as a downstream mediator of Rac in ROS generation, the application of exogenous AA significantly increased DCF fluorescence intensities in dose- and time-dependent ways, reflecting increases in the levels of ROS (Figure 3). For example, maximum ROS generation (approx. 2.4-fold increase over control) was observed within 2 min of exposure; levels declined thereafter.

The aforementioned effect of MK-886 in Rat2-RacV12 cells suggests that 5-LO activity is required for Rac-mediated ROS generation. To investigate the role of 5-LO further, we tested the effect of MK-886 and AA-861, two unrelated inhibitors of 5-LO, on ROS generation elicited by AA. As shown in Figure 4, each of the inhibitors almost entirely abolished the AA-induced generation of ROS (more than 90% inhibition). In contrast, neither AACOCF$_3$ nor indomethacin affected AA-induced ROS generation.

Exogenous leukotrienes C$_4$/D$_4$/E$_4$ stimulate ROS generation

To demonstrate further the involvement of 5-LO in ROS generation, we then assessed the effect of leukotrienes C$_4$/D$_4$/E$_4$, products of AA metabolism by 5-LO, on levels of ROS. As shown in Figure 5, the exogenous application of a mixture of leukotrienes C$_4$/D$_4$/E$_4$ (200 nM) to DCFDA-loaded Rat-2 cells induced an approx. 3.5-fold increase in the levels of ROS within 2 min. Leukotriene-evoked ROS generation was not inhibited by pretreatment with either MK-886 or AA-861 (results not shown), although the addition of catalase (10 units), an oxygen radical scavenger, completely abolished the response. Thus 5-LO, but not cyclo-oxygenase, seems to have a critical role in mediating ROS generation via the Rac–AA cascade.

DISCUSSION

In the present study, the crucial role played by the cPLA$_2$–AA-linked cascade in the signalling cascade leading from Rac activation to the generation of ROS was demonstrated by using three approaches: first, pretreatment with AACOCF$_3$ was shown to block RacV12-induced ROS generation (Figure 2); secondly, exogenous AA was shown to increase levels of ROS significantly within 2 min of application (Figure 3); and thirdly, the metabolism of AA by 5-LO, yielding leukotrienes C$_4$/D$_4$/E$_4$, was also shown to be essential for the generation of ROS (Figure 4). The role of 5-LO in mediating ROS generation was further demonstrated by a significant increase in the ROS level after the direct addition of leukotrienes C$_4$/D$_4$/E$_4$ to the cells (Figure 5). Our proposed mode of Rac activation of ROS via the 'cPLA$_2$–AA' signalling cascade seems very similar to that of c-*fos* SRE activation [12]. In c-*fos* SRE activation by Rac, essential roles of cPLA$_2$ activation and subsequent AA production have already been demonstrated [12]. Additionally, in a previous study we reported that 5-LO has a critical role as a downstream mediator of 'Rac–cPLA$_2$–AA' signalling to stimulate c-*fos* SRE [12]. Thus, the cPLA$_2$–AA signalling cascade is apparently common to the Rac-mediated regulation of both ROS and SRE. To study whether there is any signalling link between ROS generation and c-*fos* SRE activation, we have tested whether ROS generation is necessary for SRE activation by AA or C2-ceramide, which has previously been shown to activate SRE via the Rac–cPLA$_2$-dependent pathway [16]. As shown in Figure 6(A), pretreatment with 0.5 mM *N*-acetylcysteine, a free-radical scavenger, significantly inhibited the SRE stimulation by C2-ceramide or exogenous AA. In addition, co-transfection with an expression plasmid of superoxide dismutase markedly diminished the activation of SRE by these agonists (Figure 6B). Together, these results suggest that the ROS generated via the Rac–cPLA$_2$–AA-linked cascade is crucial for the nuclear signalling cascade leading to c-*fos* SRE activation, in response to various agonists acting through Rac. Recently, Shin et al. [21] reported that AA-induced stress-activated protein kinase ('SAPK') activation and ROS generation were partly prevented by RacN17, thus indicating that AA might act upstream of Rac for the generation of ROS. Their results are quite in contrast with previous reports of ours and others [11,12,15,16]; the reason for this discrepancy is not clear. Interestingly, we could not reproduce the results as published [21] and we therefore suspect that the experimental conditions might have been different, or there could have been a positive feedback loop regulation by AA acting on Rac, as claimed by the same authors [21]. However, we predict that the role of feedback regulation would be minimal even if there were any. In any event, our present findings make us confident that cPLA$_2$ is essential for generating ROS in response to Rac activation. In support of our observation, there is an increasing amount of previous evidence supporting a signalling link between ROS and cPLA$_2$-mediated AA metabolism [22–25]. In summary, the results presented are indicative of the crucial role of cPLA$_2$ in the regulation of the Rac-mediated generation of ROS. Although we do not know the details of the downstream mediators of cPLA$_2$ in a Rac signalling pathway leading to the generation of ROS, our findings indicate that AA and subsequent AA metabolism by 5-LO are involved. Further studies should provide additional information about the specific steps linking 5-LO-catalysed leukotriene synthesis with ROS generation.

We thank Dr A Hall (University College London, London, U K.) for providing us with pEXV, pEXV-RacV12 and pEXV-RhoV14 plasmids This work was supported by a grant of Molecular Medicine Research Group (02-03-A-05) from the Ministry of Science and Technology, a research grant of Regional University's Specialization from the Government Ministry of Education, and a grant (1999-2-207-004-5) from the Interdisciplinary Research Program of KOSEF

Received 27 May 1999/8 February 2000, accepted 15 March 2000

REFERENCES

1 Aspenstorm, P (1999) Exp Cell Res **246**, 20–25
2 van Aelst, L and D'Souza-Schorey, C (1997) Genes Dev **11**, 2295–2322
3 Nobes, C. D. and Hall, A (1995) Cell **81**, 53–62
4 Olson, M F, Ashworth, A and Hall, A (1995) Science **269**, 1270–1272
5 Qui, R-G, Chen, J, Kim, D, McCormick, F and Symons, M (1995) Nature (London) **374**, 457–459
6 Hall, A. (1998) Science **279**, 509–514
7 Cool, R H, Merten, E, Theiss, C and Acker, H (1998) Biochem J **332**, 5–8
8 Kim, K S, Takeda, K, Sethi, R, Pracyk, J B, Tanaka, K, Zhou, Y F, Yu, Z X., Ferrans, V J, Bruder, J T, Kovesdi, I et al (1998) J Clin Invest **101**, 1821–1826
9 Sundaresan, M, Yu, Z X, Ferrans, V J, Sulciner, D J, Gutkind, J S, Irani, K, Goldschmidt-Clermonst, P. J and Finkel, T (1996) Biochem J **318**, 379–382
10 Sulciner, D J, Irani, K, Yu, Z X, Ferrans, V J, Goldschmidt-Clermont, P and Finkel, T (1996) Mol Cell Biol **16**, 7115–7121
11 Peppelenbosch, M P, Qiu, R G, de Vries-Smits, A. M M, Tertoolen, L G J, de Laat, S W, McCormick, F., Hall, A, Symons, M H and Bos, J L (1995) Cell **81**, 849–856
12 Kim, B C and Kim, J H (1997) Biochem J **326**, 333–337
13 Hannun, Y A. (1994) J Biol Chem **269**, 3125–3128
14 Verheij, M, Bose, R, Lin, X H, Yao, B, Jarvis, W D, Grant, S, Birrer, M J, Szabo, E, Zon, L I, Kyriakis, J M. et al (1996) Nature (London) **380**, 75–79
15 Kim, B C, Lee, M N, Kim, J. Y., Lee, S S, Cjang, J D, Kim, S S., Lee, S. Y. and Kim, J H (1999) J Biol Chem **274**, 24372–24377
16 Kim, B. C and Kim, J H (1998) Biochem J **330**, 1009–1014
17 Kim, B C, Yi, Y. J, Yi, S J, Shin, I C, Ha, K S, Jhun, B H, Hwang, S B. and Kim, J H (1998) Molecules Cells **8**, 90–95
18 Ohba, M, Shibanuma, M, Kuroki, T and Nose, K (1994) J Cell Biol **26**, 1079–1088
19 Schievella, A R, Regier, M K., Smith, W L and Lin, L-L (1996) J Biol Chem **270**, 30749–30754
20 Schonhardt, T. and Ferber, E. (1987) Biochem Biophys Res Commun **149**, 769–775
21 Shin, E A, Kim, K H, Han, S I, Ha, K S, Kim, J H, Kang, K I, Kim, H D and Kang, H S (1999) FEBS Lett **452**, 355–359
22 Cui, X. L and Douglas, J G (1997) Proc Natl Acad Sci U S A **94**, 3771–3776
23 Goldman, R, Ferber, E and Zor, U (1992) FEBS Lett **309**, 190–192
24 Zor, U, Ferber, E, Gergely, P, Szucs, K, Dombradi, V and Goldman, R (1993) Biochem J **295**, 879–888
25 Tang, D G, Chen, Y Q and Honn, K V (1996) Proc Natl Acad Sci U S A. **93**, 5241–5246

Biochem J (2000) 348, 531–537 (Printed in Great Britain) 531

G-protein coupling of μ-opioid receptors (OP$_3$): elevated basal signalling activity

Neil T. BURFORD, Danxin WANG and Wolfgang SADÉE[1]

Department of Biopharmaceutical Sciences and Pharmaceutical Chemistry, School of Pharmacy, Box 0446, University of California, San Francisco, CA 94143-0446, U.S.A

To determine μ-opioid receptor (OP$_3$) signalling activity, guanosine 5′-[γ-[^{35}S]thio]triphosphate (GTP[^{35}S]) binding to G-proteins was measured in the membranes of human embryonic kidney cells (HEK-293) transfected with μ-opioid receptor (HEK-μ). GTP[^{35}S] binding to HEK-μ membranes was significantly elevated compared with HEK-293 control membranes (without OP$_3$), and this was abolished by pertussis-toxin pretreatment. The irreversible antagonist β-chlornaltrexamine (β-CNA) dose-dependently decreased elevated basal G-protein coupling of HEK-μ to control levels in cells devoid of OP$_3$. This characterizes β-CNA as an inverse OP$_3$ agonist. Immunoprecipitation of solubilized G-proteins with G$_{13}\alpha$ antisera demonstrated that basal GTP[^{35}S] binding to G$_{13}\alpha$ was also substantially elevated in HEK-μ membranes over the control, whereas G$_{13}\alpha$ protein levels were unchanged. Basal GTP[^{35}S] binding to G$_{11}\alpha$/G$_{12}\alpha$ and G$_o\alpha$ was also increased twofold in HEK-μ membranes over the control. Morphine further increased coupling to each of these Gα proteins with similar potency, but not to G$_q$/$_{11}\alpha$ or G$_s\alpha$. These results indicate that the wild-type OP$_3$ can couple constitutively to endogenously expressed G$_{13}\alpha$, G$_{11}\alpha$/G$_{12}\alpha$ and G$_o\alpha$ subunits of G-proteins in HEK-293 cells.

Key words: β-chlornaltrexamine, G-protein α-subunits, immunoprecipitation, morphine, guanosine 5′-[γ-[^{35}S]thio]triphosphate binding.

INTRODUCTION

Opioid receptors (μ, δ and κ; MOR, DOR and KOR; or, more recently, OP$_3$, OP$_1$ and OP$_2$) are members of the superfamily of G-protein-coupled receptors (e.g. [1–4]). Opioid-receptor activation leads to inhibition of adenylate cyclase [5,6], stimulation of potassium-channel conductance [7,8] and inhibition of calcium-channel conductance [9], mediated by pertussis-toxin (PTX)-sensitive G-proteins [10,11]. Receptor activation causes exchange of GDP for GTP on the α-subunit of heterotrimeric G-proteins; Gα–GTP can then dissociate from $\beta\gamma$ subunits and both Gα–GTP and G$\beta\gamma$ subunits can modulate effector activity [12,13]. An intrinsic GTPase activity of Gα then hydrolyses GTP to GDP, and Gα–GDP and G$\beta\gamma$ reassociate. Activation of G-proteins can be measured using radiolabelled, poorly hydrolysed analogues of GTP {5′-[γ-[^{35}S]thio]triphosphate (GTP[^{35}S]) and 5′-[α-^{32}P]triphosphate ([α-^{32}P]GTP) azidoanilide} [14–17]. These analogues remain bound to Gα subunits and their accumulation can be measured.

Many G-protein-coupled receptors appear to activate G-proteins spontaneously (in the absence of agonist) [18–20]. Constitutive activity of wild-type β-adrenergic [20], 5-hydroxytryptamine ('serotonin') [21], bradykinin [22], δ-opioid receptor [23] and muscarinic [24] receptors has been reported. Constitutive activation of μ-opioid receptor (OP$_3$) following chronic treatment with opiates has been hypothesized to account for part of the regulatory mechanism underlying narcotic tolerance and dependence [25,26], but clear evidence of the existence of constitutive activity of OP$_3$ receptors has not been forthcoming. The present study addresses the hypothesis that the OP$_3$ indeed displays basal signalling activity in the absence of agonist. This was measured with the use of a GTP[^{35}S] binding assay, using cell membranes expressing the OP$_3$. Moreover, GTP[^{35}S] binding was determined to individual Gα proteins immunoprecipitated with Gα-selective antisera [27]. Here we demonstrate enhanced basal activation of the OP$_3$ to specific endogenously expressed Gα proteins.

EXPERIMENTAL

Materials

GTP[^{35}S] and the G-protein antisera [G$_{11}\alpha$/G$_{12}\alpha$ (AS/7), G$_{13}\alpha$ (EC/2), G$_o\alpha$ (GC/2), G$_q\alpha$/G$_{11}\alpha$ (QL) and G$_s\alpha$ (RM/1)] were from New England Nuclear (Boston, MA, U.S.A.). Protein G–Sepharose was from Pharmacia Biotech (Sweden). Normal rabbit serum and Nonidet P40 (NP40) were from Calbiochem (La Jolla, CA, U.S.A.). Morphine sulphate was from the National Institute on Drug Abuse, NIH, Bethesda, MD, U.S.A. β-Chlornaltrexamine dihydrochloride (β-CNA) was from Research Biochemicals International (Natick, MA, U.S.A.). SDS/PAGE and immunoblotting reagents were from Bio-Rad. (Hercules, CA, U.S.A.). All other reagents were from Fisher Scientific (Fair Lawn, NJ, U.S.A.).

Cell culture and membrane preparation

Human embryonic kidney (HEK) 293 cells transfected either with cDNA encoding recombinant rat OP$_3$ (HEK-μ) [28] (expressing $\approx$ 4 pmol of [^{3}H]diprenorphine sites/mg of membrane protein) or with pRC vector alone (without OP$_3$ cDNA, HEK-vec) were grown to confluence in T-175 cm^2 tissue-culture flasks containing 30 ml of media (a 1:1 mix of Dulbecco's modified Eagle's medium and Ham's F-12 medium, supplemented with

---

Abbreviations used. OP$_3$, μ-opioid receptor, HEK-μ, human embryonic kidney cells (HEK 293) transfected with μ-opioid receptor, HEK-vec, HEK 293 cells transfected with vector alone (without μ-opioid-receptor cDNA); β-CNA, β-chlornaltrexamine, PTX, pertussis toxin, GTP[^{35}S], guanosine 5′-[γ-[^{35}S]thio]triphosphate, NP40, Nonidet P40, DAMGO, [D-Ala^2,MePhe^4,Gly(ol)^5]enkephalin

[1] To whom correspondence should be addressed (e-mail sadee@cgl ucsf edu)

10 % (v/v) foetal-bovine serum and 200 μg/ml G418). Cells were washed three times with PBS, homogenized in 30 ml of buffer containing 10 mM Hepes, pH 7.4, and 10 mM EDTA, and then centrifuged at 30000 **g** for 10 min at 4 °C. The pellets were resuspended in 1 ml of 10 mM Hepes (pH 7.4)/0.1 mM EDTA, divided into portions and stored at -80 °C.

GTP[^{35}S] binding assay

The procedure for measuring GTP[^{35}S] binding to cell membrane homogenates (total GTP[^{35}S] binding) was described previously [27]. Aliquots of frozen cell membranes were diluted in assay buffer (10 mM Hepes/10 mM MgCl$_2$/100 mM NaCl, pH 7.4) to yield final protein concentrations of 10–35 μg/50 μl. Membranes were then incubated with GTP[^{35}S] (0.4 nM for total G-protein binding, 1 nM for individual Gα-subunit binding) at 30 °C for the indicated time periods. In experiments measuring total GTP[^{35}S] binding, the membrane pellets obtained after centrifugation were washed twice with 0.5 ml of assay buffer and radioactivity measured by liquid-scintillation counting. GTP[^{35}S] binding to individual Gα subunits was determined as described in [27]. Briefly, after washing twice with assay buffer, membranes were solubilized and precleared with 100 μl of buffer containing 50 mM Tris/HCl, pH 7.4, 1 % NP40, 100 mM NaCl, 1 mM EDTA, 0.1 % SDS and 15 μl of normal rabbit serum at 4 °C for 2 h, then spun at 13000 **g** for 10 min at 4 °C. The supernatants were transferred to a set of new tubes and after addition of 40 μl of 20 % slurry Protein G beads and 15 μl of anti-Gα antiserum (1:20 dilution), incubated at 4 °C for another 12 h. Then the beads were spun down and washed twice with PBS at 4 °C and radioactivity measured by scintillation counting. For inverse-agonist experiments, membranes (10 μg) were incubated with different concentrations of β-CNA in 50 mM Hepes (pH 7.4)/100 mM NaCl/10 mM EDTA/5 mM MaCl$_2$/1 mM DTT/10 μM GDP/0.1 % BSA at 30 °C for 20 min, then the reactions were stopped by filtration. The filters were washed twice with 50 mM Tris/HCl (pH 7.4)/50 mM NaCl, and radioactivities were counted.

SDS/PAGE and Western-blot analysis

Cell membranes (5–40 μg) were separated by SDS/PAGE (10 % polyacrylamide gel) as described by Laemmli [29]. Separated proteins were electrophoretically transferred to PVDF membrane (0.2 μm) [30]. The membrane was blocked in 5 % non-fat dried milk in TBST [Tris-buffered saline (20 mM Tris/HCl (pH 7.6)/137 mM NaCl)/0.05 % Tween-20] for 2 h at room temperature with agitation, followed by 2 h incubation in the presence of the primary antibody G$_{13}\alpha$ antisera (1:1000 dilution). After washing in TBST, a secondary antibody [goat anti-rabbit IgG conjugated to alkaline phosphatase (1:2000 dilution)] was added for 2 h at room temperature, followed by development with AP Development Buffer (Bio-Rad).

Data analysis

Results expressed as means $\pm$ S.E.M. for at least three experiments, each performed in duplicate. Curve fits of dose–response curves were analysed, and EC$_{50}$ values were obtained using KaleidaGraph. Statistical analysis was performed by Student's *t* test or ANOVA. Western blots were scanned and analysed using Adobe Photoshop and NIH-image.

RESULTS

GTP[^{35}S] binding to HEK-vec and HEK-μ membranes

Total GTP[^{35}S] binding was determined in HEK-vec and HEK-μ membrane preparations. Expression of OP$_3$ in HEK-cell membranes resulted in a significant increase (20–25 %) in basal levels of GTP[^{35}S] binding compared with HEK-vec membranes (Figure 1), in both the absence and presence of 1 μM GDP, after a 5 min incubation at 30 °C. Addition of a maximally effective concentration of the full agonist morphine (10 μM) to HEK-μ membranes resulted in a 85 % increase in GTP[^{35}S] binding compared with HEK-vec basal activity, in both the absence and presence of GDP (EC$_{50}$ values for morphine were 1.7 nM in the absence of GDP and 7.4 nM in the presence of GDP respectively; results not shown). Thus about 25 % of the overall response attributable to OP$_3$ appears to be accounted for by basal receptor activity in the absence of agonist. In contrast, morphine had no significant effect on GTP[^{35}S] binding to HEK-vec membranes (results not shown). PTX pretreatment (100 ng/ml for 16 h) of HEK-vec cells had no significant effect on basal GTP[^{35}S] binding under the assay conditions. The lack of a demonstrable effect of PTX on basal GTP[^{35}S] binding in non-transfected cell membranes is probably a result of the rather small amount of membrane protein per sample incubation (12 μg of protein in this experiment) when compared with previous studies. In contrast, PTX pretreatment abolished the enhanced basal GTP[^{35}S] binding in HEK-μ membranes, in both the absence and presence of GDP. Moreover, PTX treatment suppressed morphine-stimulated GTP[^{35}S] binding (> 90 %) (results not shown), demonstrating that G$_i$/G$_o$ type-α subunits were indeed inactivated. These results indicate the presence of substantial basal signalling activity of OP$_3$ to PTX-sensitive G-proteins. Basal activity was detectable regardless of the presence of GDP

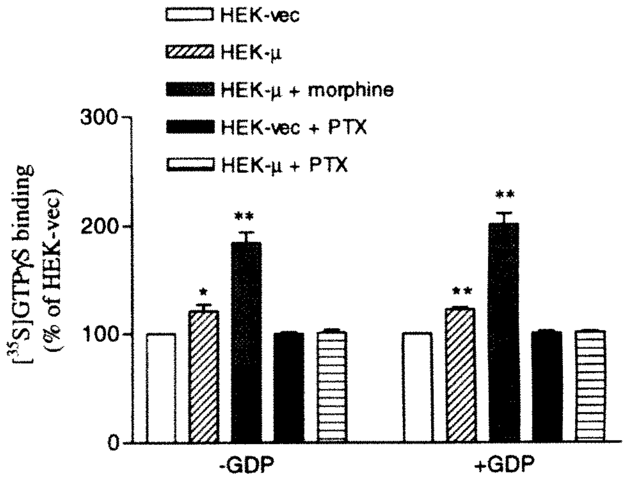

Figure 1 Effect of PTX and GDP on basal and agonist-mediated GTP[^{35}S] binding to membranes of HEK-vec and HEK-μ cells

GTP[^{35}S] ('[^{35}S]GTPγS' in this and subsequent Figures) binding experiments were conducted as described in the Experimental section either with no drug added or in the presence of 10 μM morphine, in membranes (12 μg/tube) of HEK-vec and HEK-μ cells. Experiments were terminated after a 5 min incubation at 30 °C. Basal activity was also determined in membranes after PTX pretreatment of the intact cells (100 ng/ml for 16 h). Similar measurements were determined both in the absence and presence of GDP (1 μM). Data are expressed as a percentage (mean $\pm$ S.E.M.) of the response in HEK-vec membranes. The 100% value represents approx. 4000–6000 d.p.m.; statistical significance versus HEK-vec: $^*P < 0.05$; $^{**}P < 0.01$; ANOVA; $n = 4$–2.

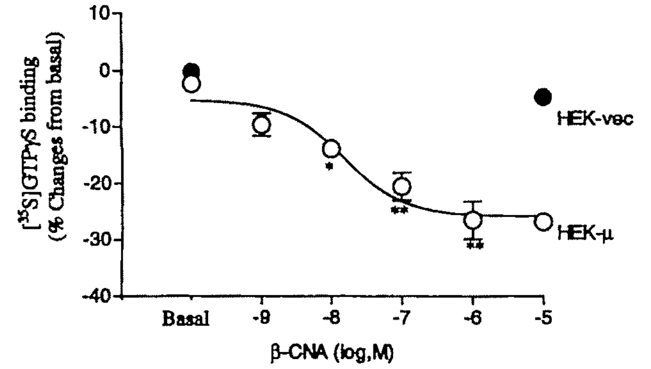

Figure 2 Dose–response curve of β-CNA effect on basal GTP[^{35}S] binding to HEK-μ membranes

Different concentrations of β-CNA were incubated with HEK-μ membranes at 30 °C for 20 min followed by filtration as described in the Experimental section Results are means ± S.E.M., $n = 3$ Statistical significance versus basal $^{*}P < 0.05$, $^{**}P < 0.01$, ANOVA; 10 μM β-CNA has no effect on HEK-vec membrane (●)

(Figure 1), which tends to suppress weak basal G-protein-coupled-receptor signalling.

β-CNA decreases basal GTP[^{35}S] binding of HEK-μ

Under the assay conditions described here, the irreversible OP_3 antagonist β-CNA dose-dependently reduced basal GTP[^{35}S] binding of HEK-μ, but not HEK-vec (Figure 2). The EC_{50} value for β-CNA is 52 ± 1.8 nM. β-CNA was the most effective inverse agonist among a panel of known opioid antagonists tested (D. Wang and W. Sadee, unpublished work). This result confirms the presence of basal G-protein coupling of OP_3. It remains to be resolved whether β-CNA acts as a non-covalent competitive or an irreversible ligand, or both, over the 20 min incubation period.

Basal GTP[^{35}S] binding after immunoprecipitation with $G_{i3}\alpha$ antisera in HEK-μ compared with HEK-vec membranes

We have previously shown that OP_3-mediated GTP[^{35}S] binding following immunoprecipitation with specific G-protein antisera is most pronounced using $G_{i3}\alpha$ antisera, in HEK-μ cell membranes [27]. This antiserum was therefore used to determine basal and agonist-stimulated GTP[^{35}S] binding following immunoprecipitation. Comparisons of maximal agonist (morphine)-stimulated GTP[^{35}S] binding between total GTP[^{35}S] binding to HEK-μ membranes and GTP[^{35}S] binding following solubilization and immunoprecipitation with $G_{i3}\alpha$ antisera (1:200 dilution), showed that approx. 6% of the total pool of labelled G-proteins were immunoprecipitated as GTP[^{35}S] binding to $G_{i3}\alpha$. A larger percentage recovery could be achieved with increasing concentrations of antisera. However, the concentration of antisera used was minimized to reduce the expense of the experiments while still providing a good signal-to-noise ratio and level of reproducibility. Under these assay conditions, recovery levels were nearly identical between different experiments and therefore suitable for quantitative analysis. Further, immunoprecipitation of $G_{i3}\alpha$ reduced the background level of GTP[^{35}S] binding compared with whole membranes, thereby enhancing the signal-to-noise ratio of the measurements.

In the absence of opioid receptor ligands, HEK-μ membranes produced a 142 ± 25% (three independent experiments) greater GTP[^{35}S] binding compared with HEK-vec membranes, after immunoprecipitation with $G_{i3}\alpha$ antisera, following a 30 min incubation (Figure 3). PTX pretreatment of HEK-μ cells decreased basal GTP[^{35}S] binding to a level indistinguishable from that observed with PTX-pretreated HEK-vec membranes ($P > 0.05$) (Figure 3) This result indicates that the enhanced GTP[^{35}S] binding activity of HEK-μ cells results largely from basal μ-opioid receptor signalling. A small decrease in GTP[^{35}S] binding caused by PTX pretreatment of HEK-vec membranes further suggests the presence of detectable basal $G_{i3}\alpha$ activity unrelated to OP_3.

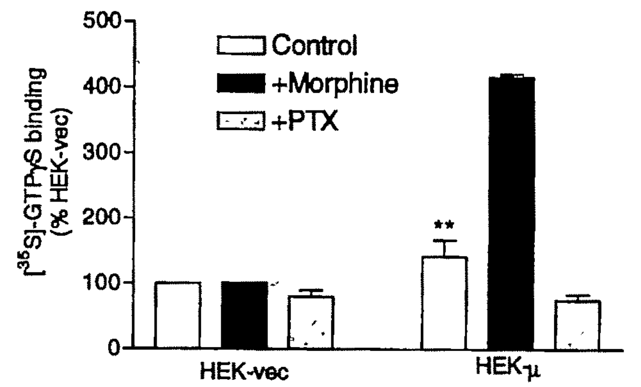

Figure 3 Basal GTP[^{35}S] binding to HEK-vec and HEK-μ membranes after immunoprecipitation with $G_{i3}\alpha$ antisera

Comparisons of the basal GTP[^{35}S] binding to $G_{i3}\alpha$ proteins were conducted in membranes from HEK-vec and HEK-μ (30 μg/tube) before and after pretreatment with PTX (100 ng/ml for 16 h), after a 30 min time period, without added GDP Data are expressed as a percentage (mean ± S.E.M., $n = 3$) of the HEK-vec basal response in the absence of PTX pretreatment (1355 ± 35 d.p.m.) Statistical significance versus HEK-vec control $^{**}P < 0.01$, ANOVA

Western-blot analysis of the content of $G_{i3}\alpha$ in membranes from HEK-vec and HEK-μ

The $G_{i3}\alpha$ expression level was determined by quantitative Western-blot analysis. The $G_{i3}\alpha$ antiserum used revealed the presence of a single immunoreactive band consistent with $G_{i3}\alpha$ protein. The results show that HEK-μ and HEK-vec membranes contain the same level of $G_{i3}\alpha$ (results not shown). Therefore, the difference in GTP[^{35}S] binding between HEK-μ and HEK-vec is not due to different levels of $G_{i3}\alpha$ in these two cell clones, but rather appears to result from an enhanced activation of $G_{i3}\alpha$ proteins in HEK cell membranes expressing OP_3.

Comparisons of basal GTP[^{35}S] binding activity between HEK-μ and HEK-vec after immunoprecipitation with various G-protein antisera

Basal GTP[^{35}S] binding between HEK-μ and HEK-vec was compared after immunoprecipitation with the selective G-protein antisera (Figure 4). Basal activity in HEK-μ membranes was approx. 2-fold greater than in HEK-vec after immunoprecipitation with $G_{i1}\alpha/G_{i2}\alpha$, $G_o\alpha$ and $G_{i3}\alpha$ antisera. Basal activity was not significantly different between these two cell clones after immunoprecipitation with $G_s\alpha$ antisera, whereas immunoprecipitation with $G_q\alpha/G_{11}\alpha$ antisera resulted in a reduction (by 36%) in basal GTP[^{35}S] binding in HEK-μ compared with HEK-vec membranes. To test the selectivity of the $G_s\alpha$ and $G_q\alpha/G_{11}\alpha$ antisera, we determined their ability to detect activation of these Gα subunits by their cognate receptors Agonist stimulation (1 mM carbachol and 1 μM α-melanocyte-stimu-

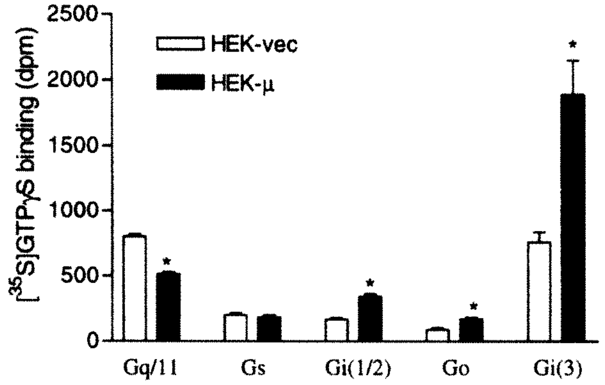

Figure 4 Comparisons of basal GTP[^{35}S] binding between HEK-vec and HEK-μ cell membranes after immunoprecipitation with various G-protein antisera

Experiments were carried out in the presence of equal protein concentrations of either HEK-vec or HEK-μ cell membranes for 30 min. Samples were immunoprecipitated with different G-protein antisera (1:200 dilution), and basal GTP[^{35}S] binding was compared. Data are expressed as the means ± S.E.M. for three experiments each performed in duplicate. Statistical significance versus HEK-vec: $^{*}P < 0.05$, Student's t test.

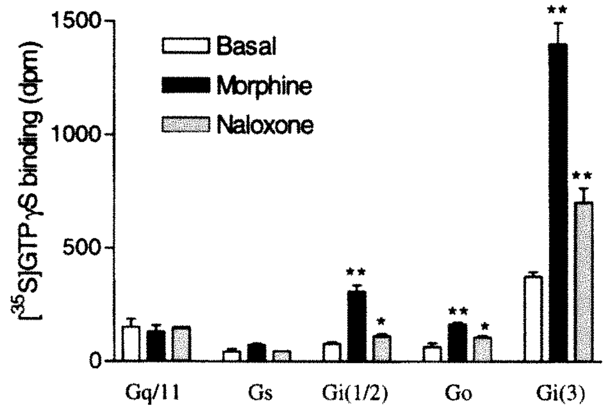

Figure 5 Morphine- and naloxone-stimulated GTP[^{35}S] binding to specific G-proteins in HEK-μ membranes

GTP[^{35}S] binding experiments were conducted in HEK-μ membranes in the absence or presence of morphine (10 μM) or naloxone (10 μM) for 1 min. Samples were then solubilized and immunoprecipitated with various G-protein antisera (1:200 final dilution). Data are means ± S.E.M. for three experiments each performed in duplicate. Statistical significances versus basal: $^{*}P < 0.05$, $^{**}P < 0.01$, ANOVA.

lating hormone) expressing m1 muscarinic receptors (HEK-m1, expressing 2 pmol of receptor/mg of protein) or melanocortin receptors (HEK-mc4) increased GTP[^{35}S] binding more than tenfold above basal activity, measured with $G_q\alpha/G_{11}\alpha$ and $G_s\alpha$ antisera respectively (results not shown). Basal signalling was minimal or undetectable. This demonstrated that coupling to $G_q\alpha/G_{11}\alpha$ and $G_s\alpha$ can be detected sensitively under these assay conditions. Muscarinic wild-type receptor also activated $G_{i3}\alpha$ upon carbachol stimulation (results not shown); however, in contrast with OP_3, no basal signalling activity of $Gi_3\alpha$ (102 ± 5 % versus vector membranes) was detectable. Our analysis may not be indicative of the absolute levels of $G\alpha$ coupling by OP_3 among individual $G_i\alpha$ and $G_o\alpha$ subunits, since we have not determined overall recovery for each separately.

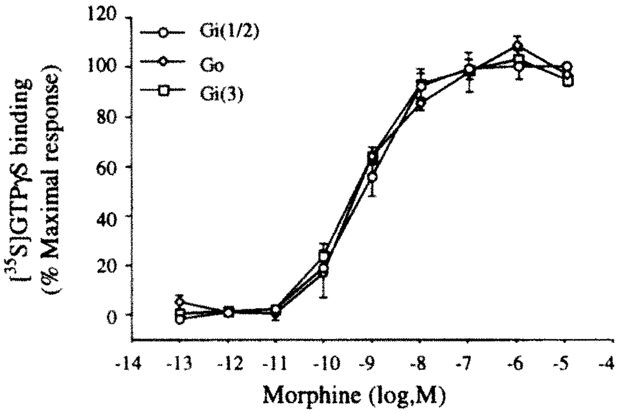

Figure 6 Dose-response curves for morphine-stimulated GTP[^{35}S] binding in HEK-μ membranes after immunoprecipitation with various G-protein antisera

GTP[^{35}S] binding dose–response curves to morphine after 1 min incubation were determined in HEK-μ membranes. Samples were then immunoprecipitated with either $G_{i1}\alpha/G_{i2}\alpha$, $G_o\alpha$ or $G_{i3}\alpha$ antisera (1:200 dilution). Data are represented as means ± S.E.M. for three experiments each performed in duplicate (see also Table 1).

Morphine- and naloxone-stimulated GTP[^{35}S] binding in HEK-μ membranes after immunoprecipitation with various G-protein antisera

Using the initial rates of GTP[^{35}S] binding in the first 1 min of incubation, morphine produced a robust response of 3.9-fold, 2.5-fold and 3.7-fold above basal GTP[^{35}S] binding to G-proteins immunoprecipitated with $G_{i1}\alpha/G_{i2}\alpha$, $G_o\alpha$ and $G_{i3}\alpha$ antisera respectively (see also [27]; Figure 5). As described above, no stimulation was detectable with $G_q\alpha/G_{11}\alpha$ and $G_s\alpha$ antisera after 1 min (Figure 5) or 90 min incubation (results not shown), even though coupling to these subunits can be sensitively measured in our assay. Although naloxone is considered an antagonist, it also produced a small stimulation of GTP[^{35}S] binding under the assay condition used (1.4-fold, 1.6-fold and 1.9-fold above basal for $G_{i1}\alpha/G_{i2}\alpha$, $G_o\alpha$ and $G_{i3}\alpha$ respectively) (Figure 5).

Neither morphine nor naloxone induced detectable GTP[^{35}S] binding above basal levels in HEK-vec after immunoprecipitation with $G_{i3}\alpha$ antisera. PTX pretreatment of cells (100 ng/ml for 16 h) abolished both morphine- and naloxone-stimulated GTP[^{35}S] binding at $G_{i1}\alpha/G_{i2}\alpha$, $G_o\alpha$ and $G_{i3}\alpha$ (results not shown).

Dose–response curves for morphine and naloxone at specific G-proteins in HEK-μ membranes

Dose–response curves were obtained at optimal time periods of incubation (highest signal-to-noise ratio) for morphine (1 min) and naloxone (30 min) in HEK-μ membranes. In this experiment, morphine produced a dose-dependent increase in GTP[^{35}S] binding above basal levels after immunoprecipitation with $G_{i1}\alpha/G_{i2}\alpha$, $G_o\alpha$ and $G_{i3}\alpha$ antisera, reaching a maximal increase above basal of 3.1-, 3.0- and 5.2-fold respectively (Figure 6 and Table 1). In each case, the EC_{50} for morphine ranged from 0.4 to 0.7 nM, with no significant difference between each of the G-protein subtypes studied.

Naloxone also produced a small dose-dependent increase in GTP[^{35}S] binding above basal levels after immunoprecipitation with $G_{i1}\alpha/G_{i2}\alpha$, $G_o\alpha$ and $G_{i3}\alpha$ antisera, reaching a maximal increase above basal of 1.3-, 1.6- and 1.8-fold respectively (Table 1; data obtained with no GDP added). The EC_{50} for naloxone

Table 1 Basal, morphine (after 1 min incubation) and naloxone (after 30 min stimulation)-stimulated GTP[^{35}S] binding to HEK-μ membranes after immunoprecipitation with G protein antisera

Data represent means ± S.E.M. for three experiments each performed in duplicate

	Stimulation (d.p.m.)		
	Basal	Maximal	EC_{50} (log M)
Morphine (1 min)			
$G_{11}\alpha/G_{12}\alpha$	134±5	410±29	−9.15±0.11
$G_o\alpha$	147±12	442±47	−9.25±0.16
$G_{i3}\alpha$	525±17	2708±368	−9.33±0.03
Naloxone (30 min)			
$G_{11}\alpha/G_{12}\alpha$	448±25	598±53	−9.27±0.41
$G_o\alpha$	407±13	640±42	−9.14±0.37
$G_{i3}\alpha$	3042±70	5329±176	−9.33±0.04

was similar to that of morphine, ranging from 0.4 to 0.7 nM, and no significant differences were noted for EC_{50} values at the individual Gα subunits.

Time course of GTP[^{35}S] binding

Time-course studies were performed for GTP[^{35}S] incorporation into membranes of HEK-vec and HEK-μ cells. Shown in Figure 7 are time courses for basal OP_3 activity (above HEK-vec control) and morphine (10 μM)- and naloxone (10 μM)-stimulated GTP[^{35}S] binding. Experiments including GDP (10 μM) gave qualitatively similar time courses, except for a greatly attenuated naloxone response (results not shown). Basal OP_3 stimulation of total GTP[^{35}S] incorporation into membranes was significantly elevated over the control in all but one time point in this experiment (Figure 7A). Morphine induced a rapid increase in total GTP[^{35}S] binding to HEK-μ membranes, which peaked at 15 min and then declined somewhat. In contrast, naloxone stimulated a steady increase over the basal level, with no apparent decline at longer incubation times. As a result, naloxone stimulated more GTP[^{35}S] binding than morphine over longer incubation periods (Figure 7A). Similar results were obtained following solubilization of the membranes and immunoprecipitation with $G_{i3}\alpha$ antiserum (Figure 7B). Basal activity and naloxone-induced activity were more prominent because of reduced background GTP[^{35}S] binding after immunoprecipitation. Morphine again caused a rapid initial surge in GTP[^{35}S] binding, followed by a slow decline (Figure 7B).

The necessity of using early time points to distinguish between agonist and basal binding of guanine nucleotides has been observed previously. [D-Ala^2,MePhe^4,Gly(ol)^5]enkephalin (DAMGO)-stimulated elevation of [α-^{32}P]GTP azidoanilide into $G_{i3}\alpha$ in SH-SY5Y cell membranes was maximally elevated above basal at 1.5 min and was no longer significantly different from basal levels after 6 min [31]. Similarly, dopamine-induced binding of [α-^{32}P]GTP in rat brain membranes could only be observed at early incubations (3 min, 30 °C) [32].

The gradual loss of GTP[^{35}S] binding to $G_{i3}\alpha$ upon morphine incubations exceeding 5–15 min suggests that additional processes occur, such as morphine-induced desensitization of the OP_3, GTP[^{35}S] dissociation from $G_{i3}\alpha$, or $G_{i3}\alpha$ dissociation from the membrane during incubation with morphine. To investigate whether activated G-proteins could be detected in the supernatant rather than the membrane pellet, supernatants were immunoprecipitated with $G_{i3}\alpha$ antisera. No increase in GTP[^{35}S] binding was observed in the supernatant after 1 min compared with basal conditions. However, an increase in both morphine- and naloxone-induced GTP[^{35}S] binding to $G_{i3}\alpha$ above basal was detected after 30 min (966 and 662 d.p.m. respectively, $n = 2$), suggesting that some of the activated G-proteins may leave the membrane environment upon extended stimulation with agonist. However, this result only partially accounts for the loss of GTP[^{35}S] binding after the initial morphine-induced peak. Clearly, an additional unknown process appears to occur with morphine, but not as a result of basal and naloxone-induced activity.

Incubation of HEK-μ membranes with morphine (1 μM) and naloxone (10 μM) together resulted in a time course similar to that of naloxone alone (results not shown). Therefore naloxone can inhibit the initial large morphine-induced GTP[^{35}S] binding at 1 min.

Similar time-course profiles were observed in HEK-μ membranes using $G_{11}\alpha/G_{12}\alpha$ antisera and $G_o\alpha$ antisera (results not shown), although basal coupling and drug treatments produced lower levels of GTP[^{35}S] binding than those observed after immunoprecipitation with $G_{i3}\alpha$ antisera (see Figure 4). In each case, morphine-induced GTP[^{35}S] binding was maximal after

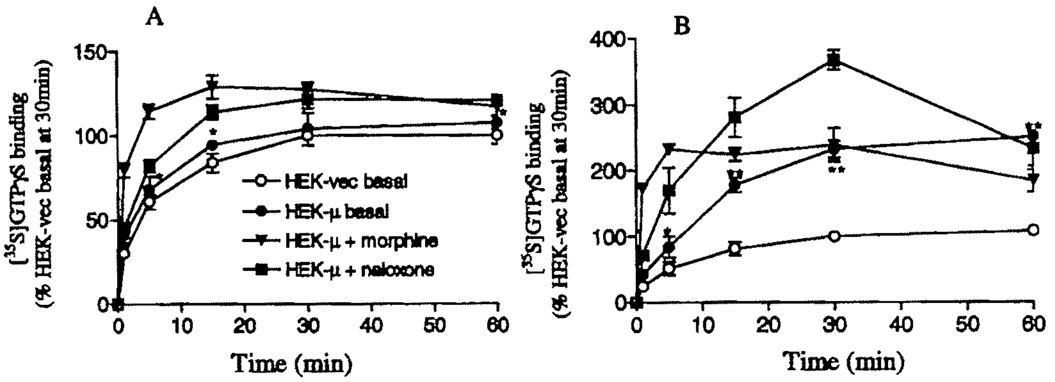

Figure 7 Time course of GTP[^{35}S] binding in HEK-μ membranes and following solubilization and immunoprecipitation with $G_{i3}\alpha$ antisera

GTP[^{35}S] binding experiments were conducted either with no drug added, in the presence of morphine (10 μM) or in the presence of naloxone (10 μM) for the times indicated. Total GTP[^{35}S] binding to HEK-μ membranes (**A**) and GTP[^{35}S] binding following solubilization and immunoprecipitation with $G_{i3}\alpha$ antisera (1:200 final dilution) in HEK-μ membranes (**B**), were determined. Data are represented as means ± S.E.M. for three experiments each performed in duplicate. Statistical significance versus HEK-vec basal: $^{*}P < 0.05$, $^{**}P < 0.01$, ANOVA.

1 min. Similar time-course profiles of agonist-induced GTP[^{35}S] binding to HEK-μ membranes after immunoprecipitation with $G_{i3}\alpha$ antisera were observed with lower concentrations of morphine (100 nM) and with the agonists DAMGO and endomorphin I [27].

DISCUSSION

The present study demonstrates that OP_3 expression in HEK cell membranes enhances basal G-protein activation, indicative of constitutive OP_3 activity. Enhanced basal activity was observed both with total GTP[^{35}S] binding to the entire pool of G-proteins in HEK-μ membranes (Figure 1) and after immunoprecipitation with $G_i\alpha$ antisera, particularly $G_{i3}\alpha$ (Figure 3). Basal OP_3 activity was blocked by PTX pretreatment of HEK-μ cells. This result indicates that basal signalling occurs at PTX-sensitive G-proteins, as observed for agonist-stimulated OP_3 activity. The ability of β-CNA to decrease basal GTP[^{35}S] binding of HEK-μ membrane comfirmed the presence of substantial basal OP_3 activity.

Basal activity at $G_{i3}\alpha$ in HEK-δ cell membranes was also detectable under the same assay conditions (results not shown). Basal activity had been reported previously for the δ-opioid receptor (OP_1) [23]. Further, no basal activity was observed in HEK-m1 cell membranes (expressing m1 muscarinic receptors). Therefore, under the assay conditions used, another highly expressed receptor type failed to show any constitutive signalling activity. These comparisons support the view that basal activity detected with OP_3 might be relevant physiologically.

Enhanced basal GTP[^{35}S] binding to $G_{i3}\alpha$ expressed in HEK-μ cell membranes could have been accounted for by an increase in endogenously expressed $G_{i3}\alpha$ levels as a result of OP_3 transfection. However, Western-blot analysis of HEK-μ and HEK-vec membranes showed no significant difference in the levels of $G_{i3}\alpha$ expressed between the two cell clones. This indicates that OP_3 expressed in HEK-μ membranes is capable of constitutively activating endogenous $G_{i3}\alpha$ proteins Basal activation of $G_{i1}\alpha/G_{i2}\alpha$ and $G_o\alpha$ was also elevated by approx. 2-fold in HEK-μ compared with HEK-vec membranes. By contrast, basal activation of $G_s\alpha$ remained unchanged between the two cell clones, and basal activation of $G_q\alpha/G_{11}\alpha$ was reduced in HEK-μ compared with HEK-vec membranes. Possibly, OP_3 expression could have affected the level of $G_q\alpha/G_{11}\alpha$ expression, $\beta\gamma$ subunits liberated from G_i/G_o could have scavenged $G_q\alpha/G_{11}\alpha$, or OP_3 could have inhibited basal GTP binding (for a discussion on possible inhibitory receptor action, see [33,34]).

Analysis of basal and agonist-dependent G-protein coupling is sensitive to the experimental conditions used. Previous studies investigating GTP[^{35}S] binding without immunoprecipitation have required the presence of excess GDP to dampen basal activity so that agonist-stimulated GTP[^{35}S] binding could be observed above background [14–16]. In the present study we have shown that basal OP_3 activity and agonist-stimulated GTP[^{35}S] binding to HEK-μ membranes are detectable in both the presence and absence of GDP, both in total binding experiments and after immunoprecipitation with $G_{i3}\alpha$ antisera Therefore basal OP_3 activity was robust under several conditions, even in the presence of GDP, which is known to suppress basal signalling.

The presence of basal receptor activity prompted us to search for inverse OP_3 agonists. The GTP[^{35}S] binding assay described here provides a screen for identifying inverse agonists at OP_3. Inverse agonists have previously been described for OP_1 [24,36]. Further screening of known OP_3 antagonists {naltrexone, diprenorphine, CTAP [H-D-Phe-Cys-Tyr-D-Trp-Arg-Thr-Pen-Thr-NH_2(cyclic)], β-funaltrexamine, β-CNA} revealed β-CNA as a full inverse agonist. Relative efficacies of these compounds will be reported separately. Dependent upon the incubation conditions, naloxone either had little or no effect or displayed low partial-agonist activity. Since the addition of GDP largely suppressed naloxone-stimulated GTP[^{35}S] binding, it appears that naloxone has at best very low efficacy as an agonist [35]. Yet, a partial agonist effect of naloxone is consistent with our previous observations that naloxone decreases cAMP levels in untreated SH-SY5Y cells [26] and HEK-μ cells [36]. Since SH-SY5Y cells express relatively low levels of OP_3 [37], it appears that the partial agonist properties of naloxone may not necessarily require high levels of OP_3 expression. Thus the partial agonist activity of naloxone may account for the 'morphine-like' effects of naloxone seen in early studies [38]. We are currently studying the behaviour of naloxone after morphine pretreatment – resulting in an apparent shift toward inverse agonism in morphine-dependent tissues [26].

Dose–response curves at optimal time points for morphine (after 1 min) and naloxone (after 30 min) produced similar EC_{50} values for activation of $G_{i1}\alpha/G_{i2}\alpha$, $G_o\alpha$ and $G_{i3}\alpha$, suggesting that both morphine and naloxone activated each of these G-proteins with equal potency. Previous studies have suggested that different G-proteins can be activated with different potencies by OP_3 agonists in Chinese-hamster ovary cell membranes [39] This was not found in the present study in HEK cell membranes, which agrees with studies on δ- and κ-opioid receptors, suggesting that commonly used agonists of these receptors can activate multiple G-protein subtypes with similar potency [10,11,40]. These discrepant results might be resolved if one considers the different experimental conditions.

In conclusion, this study supports the hypothesis that OP_3 receptors are constitutively active. It remains to be seen how such basal activity affects signalling pathways in intact cells. We have previously proposed that constitutive activation of OP_3 following chronic agonist treatment played a role in narcotic tolerance and dependence [26]. We are currently investigating the effect of chronic opiate treatment on OP_3 coupling to G-proteins, including possible changes in basal activation of these G-proteins.

This study was supported by the National Institute on Drug Abuse, Bethesda, MD, U.S A (grant DA 04166)

REFERENCES

1 Evans, C J., Keith, Jr, D E, Morrison, H, Magendzo, K and Edwards, R H (1992) Cloning of a δ opioid receptor by functional expression (see comments) Science **258**, 1952–1955

2 Kieffer, B L, Befort, K, Gaveriaux-Ruff, C and Hirth, C G (1992) The δ-opioid receptor isolation of a cDNA by expression cloning and pharmacological characterization and Proc Natl. Acad Sci U S A **89**, 12048–12052 (but see [2a])

2a Kieffer, B L, Befort, K, Gaveriaux-Ruff, C and Hirth, C G (1994) Erratum Proc Natl Acad Sci U S A **91**, 1193

3 Chen, Y, Mestek, A, Liu, J, Hurley, J A and Yu, L (1993) Molecular cloning and functional expression of a μ-opioid receptor from rat brain Mol Pharmacol **44**, 8–12

4 Chen, Y, Mestek, A, Liu, J and Yu, L (1993) Molecular cloning of a rat κ-opioid receptor reveals sequence similarities to the μ-opioid and δ-opioid receptors Biochem. J **295**, 625–628

5 Kazmi, S M and Mishra, R K (1987) Comparative pharmacological properties and functional coupling of μ and δ opioid receptor sites in human neuroblastoma SH-SY5Y cells Mol Pharmacol **32**, 109–118

6 Yu, V C and Sadée, W (1988) Efficacy and tolerance of narcotic analgesics at the μ opioid receptor in differentiated human neuroblastoma cells J Pharmacol Exp Ther **245**, 350–355

7 North, R A., Williams, J T, Surprenant, A and Christie, M J (1987) μ and δ receptors belong to a family of receptors that are coupled to potassium channels Proc Natl Acad Sci U S A **84**, 5487–5491

8 Williams, J T, North, R A and Tokimasa, T. (1988) Inward rectification of resting and opiate-activated potassium currents in rat locus coeruleus neurons. J. Neurosci. **8**, 4299–4306

9 Hescheler, J., Rosenthal, W, Trautwein, W and Schultz, G (1987) The GTP-binding protein, G_o, regulates neuronal calcium channels. Nature (London) **325**, 445–447

10 Prather, P L, Loh, H. H and Law, P Y (1994) Interaction of δ-opioid receptors with multiple G-proteins – a non-relationship between agonist potency to inhibit adenylyl cyclase and to activate G-proteins Mol Pharmacol **45**, 997–1003

11 Prather, P L, McGinn, T M, Erickson, L J, Evans, C J, Loh, H. H and Law, P Y (1994) Ability of δ-opioid receptors to interact with multiple G-proteins is independent of receptor density J Biol Chem **269**, 21293–21302

12 Birnbaumer, L, Abramowitz, J and Brown, A M (1990) Receptor–effector coupling by G-proteins Biochim Biophys Acta **1031**, 163–224

13 Clapham, D E and Neer, E J (1997) G-protein $\beta\gamma$ subunits Annu Rev Pharmacol. Toxicol **37**, 167–203

14 Hilf, G, Gierschik, P and Jakobs, K H (1989) Muscarinic acetylcholine receptor-stimulated binding of guanosine 5′-*O*-(3-thiotriphosphate) to guanine-nucleotide-binding proteins in cardiac membranes Eur J Biochem **186**, 725–731

15 Lazareno, S, Farries, T. and Birdsall, N J M (1993) Pharmacological characterization of guanine nucleotide exchange reactions in membranes from CHO cells stably transfected with human muscarinic receptors M1–M4 Life Sci **52**, 449–456

16 Traynor, J R and Nahorski, S R (1995) Modulation by μ-opioid agonists of guanosine-5′-*O*-(3-[^{35}S]thio)triphosphate binding to membranes from human neuroblastoma Sh-Sy5y cells Mol Pharmacol **47**, 848–854

17 Offermans, S, Schafer, R, Hoffmann, B, Bombien, E, Spicher, K, Hinsch, K D, Schultz, G and Rosenthal, W (1990) Agonist-sensitive binding of a photoreactive GTP analog to a G-protein α-subunit in membranes of HL-60 cells. FEBS Lett **260**, 14–18

18 Lefkowitz, R J., Cotecchia, S., Samama, P and Costa, T (1993) Constitutive activity of receptors coupled to guanine nucleotide regulatory proteins Trends Pharmacol Sci **14**, 303–307 .

19 Leff, P (1995) Inverse agonism – theory and practice Trends Pharmacol Sci. **16**, 256–256

20 Chidiac, P, Hebert, T E, Valiquette, M, Dennis, M and Bouvier, M (1994) Inverse agonist activity of β-adrenergic antagonists Mol Pharmacol **45**, 490–499

21 Barker, E L, Westphal, R S, Schmidt, D and Sandersbush, E (1994) Constitutively active 5-hydroxytryptamine (2c) receptors reveal novel inverse agonist activity of receptor ligands J Biol Chem **269**, 11687–11690

22 Leeblundberg, L M F, Mathis, S A and Herzig, M C S (1994) Antagonists of bradykinin that stabilize a G-protein-uncoupled state of the B2 receptor act as inverse agonists in rat myometrial cells J Biol Chem **269**, 25970–25973

23 Costa, T and Herz, A (1989) Antagonists with negative intrinsic activity at δ opioid receptors coupled to GTP-binding proteins Proc Natl Acad Sci U S A **86**, 7321–7325

24 Jakubik, J, Bacakova, L, Elfakahany, E E and Tucek, S (1995) Constitutive activity of the M(1)M(4) subtypes of muscarinic receptors in transfected CHO cells and of muscarinic receptors in the heart cells revealed by negative antagonists, FEBS Lett **377**, 275–279

Received 6 January 2000/21 February 2000, accepted 17 March 2000

25 Sadee, W, Wang, Z, Arden, J R and Segredo, V (1994) Constitutive activation of the μ-opioid receptor a novel paradigm for receptor regulation in narcotic analgesia, tolerance and dependence. Analgesia **1**, 11–14

26 Wang, Z, Bilsky, E J, Porreca, F and Sadee, W (1994) Constitutive μ opioid receptor activation as a regulatory mechanism underlying narcotic tolerance and dependence Life Sci **54**, PL339–PL350

27 Burford, N T, Tolbert, L M and Sadee, W (1998) Specific G-protein activation and μ-opioid receptor internalization caused by morphine, DAMGO and endomorphin I Eur J Pharmacol **342**, 123–126

28 Segredo, V, Burford, N T, Lameh, J and Sadee, W. (1997) A constitutively internalizing and recycling mutant of the μ-opioid receptor J Neurochem **68**, 2395–2404

29 Laemmli, U K (1970) Cleavage of structural proteins during the assembly of the head of bacteriophage T4 Nature (London) **227**, 680–685

30 Towbin, H, Staehelin, T and Gordon, J (1979) Electrophoretic transfer of proteins from polyacrylamide gels to nitrocellulose sheets procedure and some applications Proc Natl Acad. Sci U S A **76**, 4350–4354

31 Laugwitz, K L, Offermanns, S, Spicher, K and Schultz, G (1993) μ and δ Opioid receptors differentially couple to G-protein subtypes in membranes of human neuroblastoma Sh-Sy5y cells. Neuron **10**, 233–242

32 Friedman, E., Butkerait, P and Wang, H Y (1993) Analysis of receptor-stimulated and basal guanine nucleotide binding to membrane G-proteins by sodium dodecyl sulfate polyacrylamide gel electrophoresis Anal Biochem. **214**, 171–178

33 Ueda, H, Uno, S, Harada, J, Kobayashi, I, Katada, T, Ui, M and Satoh, M. (1990) Evidence for receptor-mediated inhibition of intrinsic activity of GTP-binding protein, G_i1 and G_i2, but not G_o in reconstitution experiments FEBS Lett. **266**, 178–182

34 Misawa, H, Ueda, H, Katada, T, Ui, M and Satoh, M. (1995) A subtype of opioid κ-receptor is coupled to inhibition of G_i1-mediated phospholipase C activity in the guinea pig cerebellum FEBS Lett **361**, 106–110

35 Selley, D E, Sim, L J, Xiao, R. Y, Liu, Q X and Childers, S. R (1997) μ-opioid receptor-stimulated guanosine-5′-*O*-(γ-thio)-triphosphate binding in rat thalamus and cultured cell lines Signal transduction mechanisms underlying agonist efficacy Mol Pharmacol **51**, 87–96

36 Arden, J R., Segredo, F, Wang, Z J, Lameh, J and Sadee, W (1995) Phosphorylation and agonist-specific intracellular trafficking of an epitope-tagged μ-opioid receptor expressed in hek 293 cells J Neurochem **65**, 1636–1645

37 Yu, V C, Eiger, S., Duan, D. S., Lameh, J and Sadée, W. (1990) Regulation of cyclic AMP by the μ-opioid receptor in human neuroblastoma SH-SY5Y cells J Neurochem **55**, 1390–1396

38 Sawynok, J, Pinsky, C and LaBella, F S. (1979) On the specificity of naloxone as an opiate antagonist Life Sci **25**, 1621–1632

39 Chakrabarti, S, Prather, P L, Yu, L, Law, P Y and Loh, H H (1995) Expression of the μ-opioid receptor in CHO cells – ability of μ-opioid ligands to promote α-azidoanilido [^{32}P]GTP labelling of multiple G-protein α subunits J Neurochem **64**, 2534–2543

40 Roerig, S C, Loh, H H and Law, P Y (1992) Identification of three separate guanine nucleotide-binding proteins that interact with the δ-opioid receptor in NG108-NG115 neuroblastoma × glioma hybrid cells Mol Pharmacol **41**, 822–831

Biochem. J. (2000) 348, 539–549 (Printed in Great Britain)

A novel lysine 2,3-aminomutase encoded by the *yodO* gene of *Bacillus subtilis*: characterization and the observation of organic radical intermediates

Dawei CHEN, Frank J. RUZICKA and Perry A. FREY[1]

Department of Biochemistry, College of Agricultural and Life Sciences, University of Wisconsin-Madison, 1710 University Avenue, Madison, WI 53705, U.S.A.

The *yodO* gene product of *Bacillus subtilis* has been cloned and overexpressed in *Escherichia coli* and purified. The nucleotide sequence encodes a protein of 471 amino acids with a calculated molecular mass of 54071 Da. The translated amino acid sequence is more than 60 % identical to that of the lysine 2,3-aminomutase from *Clostridium subterminale* SB4. Analytical HPLC gel-permeation chromatography leads to an estimate of an overall molecular mass of 224000 ± 21000 Da, which corresponds to a tetrameric protein. The purified protein contains iron, sulphide and pyridoxal 5′-phosphate (PLP) and displays an optical absorption band extending to 700 nm, suggesting the presence of an iron-sulphide cluster. After reductive incubation with L-cysteine anaerobically, the protein catalyses the transformation of L-lysine into β-lysine in the presence of *S*-adenosylmethionine (AdoMet) and sodium dithionite. The K_m value for L-lysine is estimated to be 8.0 ± 2.2 mM. The iron-sulphur centre is stable in air, allowing aerobic purification. EPR spectroscopy at 10 K of the purified enzyme revealed an EPR signal similar to that of the $[4Fe\text{-}4S]^{3+}$ cluster observed in the clostridial lysine 2,3-aminomutase. Incubation with cysteine under anaerobic conditions converts the iron-sulphur centre into the EPR-silent $[4Fe\text{-}4S]^{2+}$. Unlike the clostridial enzyme, the fully reduced $[4Fe\text{-}4S]^{+}$ could not be characterized by further reduction with dithionite in the presence of AdoMet, although both dithionite and AdoMet were required to activate the enzyme. Upon addition of L-lysine, dithionite and AdoMet to the reduced enzyme and freezing the solution to 77 K, the EPR spectrum revealed the presence of an organic free-radical signal ($g = 2.0023$), which displayed multiple hyperfine transitions very similar to the spectrum of the β-lysine-related radical in the mechanism of the clostridial lysine 2,3-aminomutase. Experiments with isotopically substituted L-lysine and lysine analogues verified the association of spin density with the carbon skeleton of lysine. The data indicate that the protein encoded by the *yodO* gene of *B. subtilis* is a novel lysine 2,3-aminomutase. The *E. coli* homologue of clostridial lysine 2,3-aminomutase was also expressed in *E. coli* and purified. This protein contained iron and sulphide but not PLP, it did not display lysine 2,3-aminomutase activity, and addition of PLP did not induce 2,3-aminomutase activity.

Key words: *S*-adenosylmethionine, cysteine, EPR spectroscopy, iron-sulphur cluster, pyridoxal phosphate.

INTRODUCTION

Lysine 2,3-aminomutase catalyses the interconversion of L-lysine and L-β-lysine, which involves migration of the α-amino group to the β-carbon with the concomitant transfer of the β-hydrogen to the α-carbon. This enzyme plays a role in the utilization of lysine for growth of the anaerobe *Clostridium subterminale* SB4 [1–3]. β-Lysine is also a precursor in the biosynthesis of antibiotics, such as viomycin and streptothricin, in *Streptomyces* [4,5]. Therefore, enzymes that convert α-amino acids into β-amino acids are potentially useful for production in the pharmaceutical industry. Lysine 2,3-aminomutase from *C. subterminale* SB4 is the only well-characterized amino acid 2,3-aminomutase [6–8].

The reaction catalysed by lysine 2,3-aminomutase is analogous to the adenosylcobalamin-dependent rearrangements, in which hydrogen transfer is mediated by the adenosyl moiety of the coenzyme. Unlike adenosylcobalamin-dependent enzymes, clostridial lysine 2,3-aminomutase is not adenosylcobalamin-dependent, but contains [4Fe-4S] clusters and pyridoxal 5′-phosphate (PLP) and is activated by *S*-adenosylmethionine (AdoMet). AdoMet and [4Fe-4S] clusters are thought to function in place of adenosylcobalamin in providing for the transient and reversible formation of the 5′-deoxyadenosyl radical. A radical rearrangement mechanism has been proposed for the clostridial enzyme [9–11], in which the 5′-deoxyadenosyl radical initiates the rearrangement by abstracting a hydrogen atom from C-3 of L-lysine to form the substrate-based free radical **1** (Scheme 1). PLP facilitates the rearrangement by forming an aldimine linkage to the migrating nitrogen [12,13] and allowing the transformation of radical **1** into the product-related radical **3**, presumably through the intermediate formation of **2**.

Based on the amino acid sequence of lysine 2,3-aminomutase from *C. subterminale* SB4, seven homologous proteins have been identified in the prokaryotic database [14]. The amino acid sequences of these proteins share 32–72 % identities with *C. subterminale* lysine 2,3-aminomutase. The *Bacillus subtilis* protein encoded by the *yodO* gene [15] is 62 % identical, and the *Escherichia coli* protein is 32 % identical. A prominence that is similar in all of these proteins is the cysteine motif that is thought to be the iron binding site. This is shown in Figure 1(A), in which appears the striking and unique presence of at least three conserved arginine residues in all eight motifs. The sequences are shown top to bottom in order of decreasing overall identity to *C. subterminale* lysine 2,3-aminomutase. The eight homologous proteins may be differentiated by their ability to bind PLP, as suggested in Figure 1(B). The upper group of four, including the *B. subtilis* protein, incorporate a putative PLP-binding motif,

---

Abbreviations: PLP, pyridoxal 5′-phosphate; AdoMet, *S*-adenosylmethionine; AdoHCys, *S*-adenosylhomocysteine; IPTG, isopropyl β-D-thiogalactoside; DTT, dithiothreitol.

[1] To whom correspondence should be addressed (e-mail frey@biochem.wisc.edu).

Scheme 1

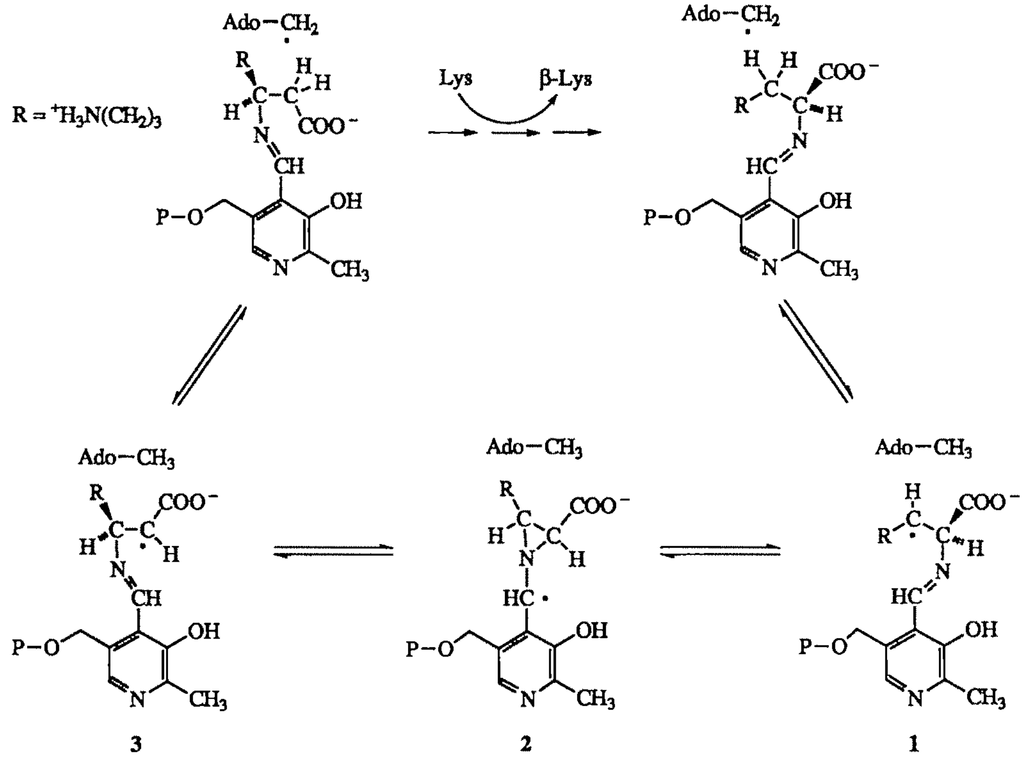

Scheme 1 The proposed mechanism of clostridial lysine 2,3-aminomutase

which is similar to that associated with serine and threonine dehydratases. The lower group of five homologues, including the *E. coli* protein, lacks this motif.

Here we report the identification of the protein encoded by the *yodO* gene of *B. subtilis* as a lysine 2,3-aminomutase, as well as the characterization of this new member of the lysine aminomutase family. Like the clostridial enzyme, but unlike adenosylcobalamin-dependent enzymes, the *B. subtilis* lysine 2,3-aminomutase contains iron, inorganic sulphide and PLP and is activated by AdoMet. Similarities with the clostridial enzyme notwithstanding, the *B. subtilis* lysine 2,3-aminomutase exhibits distinctive physical, chemical and mechanistic properties. Of particular interest is its remarkable stability in air, which facilitates mechanistic studies and makes it potentially useful for applications in the synthesis of pharmaceutical agents with antibiotic properties. We also show that the homologous protein from *E. coli* lacks PLP and is not a lysine 2,3-aminomutase.

MATERIALS AND METHODS

Materials

B. subtilis strain A.T.C.C 27505 was obtained from the American Type Culture Collection. L-[3,3,4,4,5,5,6,6-$^{2}H_{8}$]Lysine (99% enrichment) was obtained from CDN Isotopes (Pointe-Claire, Quebec, Canada). AdoMet, *S*-adenosylhomocysteine (AdoHCys), PLP and 4-thia-L-lysine were from Sigma. AdoMet was purified by chromatography using a 2 cm × 20 cm column of CM-cellulose before use. All other compounds were used directly without further purification.

Cloning of *B. subtilis yodO*

The *yodO* gene was isolated from *B. subtilis* chromosomal DNA by PCR. Primers were prepared that produced a 1.4-kb insert containing *Nde*I and *Xho*I restriction sites necessary for cloning into pET 23a(+) plasmid vector under the control of the T7 promoter. The PCR primers used were. (+) strand, 5′-TATACATATGAAAAACAAATGGTATAAACCGAAACGGCATTGGAAGG-3′, and (−) strand, 5′-TAGACTCGAGTCATGAAGAATCCCCTCCGCATTCAGTCTCTTTCTG-3′. Chromosomal DNA from *B. subtilis* (Ehrenberg) Cohn (A.T.C.C. 15818) was prepared using the Qiagen Genomic Tip 500/G from cells grown in nutrient broth (Difco #3). The PCR reaction mixture (100 μl total volume) contained: *B. subtilis* chromosomal DNA, 0.5 μg; *Pfu* DNA polymerase reaction buffer (Stratagene, La Jolla, CA, U.S.A.); dNTPs, 0.2 mM each; oligonucleotide primers, 0.2 μM each; and Turbo *Pfu* DNA polymerase, 5 units. Samples were subjected to 30 cycles of 1 min at 96 °C, 1 min at 60 °C and 3 min at 72 °C. After thermocycling, DNA formed during the PCR process was purified by 2% agarose gel electrophoresis in 0.04 M Tris/acetate, pH 8.0, with 1 mM EDTA. Following identification and excision of the appropriately sized (≈ 1.4 kb) ethidium bromide-stained band, DNA was extracted from the agarose, ethanol-precipitated and resuspended in 0.01 M Tris/HCl/EDTA (TE) buffer, pH 8. The purified PCR product was blunt-end ligated to pCR-Script Amp cloning vector (Stratagene) using 0.3 pmol of insert/0.005 pmol of vector according to the manufacturer's specification. The ligated DNA was used to transform XL1-MRF′ *E. coli* cells, which were subsequently plated on Luria–Bertani/carbenicillin (100 μg/ml)/

A.

138 CSMYCRHCTRRRF 150	*C. subterminale* KAM
CSMYCRHCTRRRF	*P. gingivalis*
134 CSMYCRYCTRRRF 146	*B. subtilis* KAM
CASYCRYCTRSRI	*D. radiodurans*
CAVYCRHCMRKRI	*A. aeolicus*
CFSHCRYCFRRGF	*T. pallidum*
CAVNCRYCFRRHF	*H. influenzae*
CAVNCRYCFRRHF	*E. coli*

B.

293 LVKIRV 298	*C. subterminale* KAM
LVKMRV	*P. gingivalis*
288 LVKIRV 293	*B. subtilis* KAM
LVKIRV	*D. radiodurans*
LLRIKV	*A. aeolicus*
LTCLGV	*T. pallidum*
LFQTGI	*H. influenzae*
LFDAGV	*E. coli*
SFKIRG	Rat liver serine dehydratase
SFKLRG	Yeast threonine dehydratase
SFKIRG	*E. coli* L-threonine dehydratase
SIKARG	*E. coli* D-threonine dehydratase

Figure 1 Amino acid sequences of iron- and PLP-binding motifs in clostridial lysine 2,3-aminomutase and its homologues

(A) Iron-binding motifs of *C. subterminale* lysine 2,3-aminomutase and its homologues. The cysteine residues that are proposed to bind the iron sulphide cluster are shown in bold. Note the presence of at least three conserved arginine residues. **(B)** Putative PLP-binding motif of *C. subterminale* lysine 2,3-aminomutase and the corresponding sequences in its homologues. Note that the upper four homologous proteins, including the *B. subtilis* protein, retain the KXR motif of the PLP-binding sites in four serine and threonine dehydratases, which are also shown. This motif is absent in the lower five homologous proteins, including that from *E. coli*. *P. gingivalis*, *Porphyromonas gingivalis*, *D. radiodurans*, *Deinococcus radiodurans*, *A. aeolicus*, *Aquifex aeolicus*, *T. pallidum*, *Treponema pallidum*; *H. influenzae*, *Haemophilus influenzae*

isopropyl β-D-thiogalactoside (IPTG)/X-Gal plates and cultured overnight. White colonies were chosen for subcloning into pET23a(+).

Plasmid DNA (10 μg) was double-digested with *Nde*I/*Xho*I, and the *yodO* fragment gel-purified as before. pET-23a(+) (10 μg) was similarly digested with *Nde*I/*Xho*I, dephosphorylated with 1 unit of calf-intestine alkaline phosphatase for 30 min at 37 °C, gel-purified and ethanol precipitated. *yodO* and cut pET-23a(+) were ligated with T4 DNA ligase overnight at 14 °C. Competent *E. coli* cells (DH5α, Life Technologies) were transformed and cells plated on Luria–Bertani/carbenicillin plates. Plasmid DNAs from individual colonies were sequenced to confirm the construct. For expression of *B. subtilis yodO* gene in *E. coli*, pAF-98/*yodO* was transformed into competent BL21(DE3) *E. coli* cells (Novagen). For transformation, 20 ml of competent cells were transformed with 0.1 μg of plasmid DNA. The sequence was verified in its entirety by DNA sequencing using the automated ABI Prism Dye Terminator Cycle Sequencing procedure (University of Wisconsin Biotechnology Center, Madison, WI, U.S.A.).

Cloning of *E. coli* unknown gene (P39280)

The *E. coli* gene P39280 of unknown function was isolated from *E. coli* chromosomal DNA (JM109) by PCR according to the procedure described above. The PCR primers used were: (+) strand, 5′-ATGGCGCATATTGTAACCCTAAATAC-3′, and (−) strand, 5′-TTACTGCTGGCGTAGCTGGAGATC-3′. DNA from PCR was cloned into pET-23a(+) vector at the *Nde*I/*Xho*I restriction sites. The final plasmid construct was transformed into *E. coli* BLR(DE3) plysS cells (Novagen) for protein expression.

Expression of recombinant lysine 2,3-aminomutase (*yodO*) and unidentified *E. coli* gene

E. coli strain BL21(DE3) carrying the expression vector pAF-98/*yodO* was grown aerobically at 37 °C in shake flasks containing Terrific Broth medium plus 100 μg/ml ampicillin and 0.5 mM IPTG. High-level expression of the active enzyme was achieved when cells were grown into the stationary phase. The unknown *E. coli* gene product was expressed in cells grown anaerobically in a 15-l fermentor following sparging with nitrogen. The cells were cultured in 2 × YT medium (16 g/l bacto-tryptone, 10 g/l bacto-yeast extract and 5 g/l NaCl in distilled water) supplemented with 50 mM $FeSO_4$, 50 mM sodium sulphide, 100 μg/ml ampicillin and 30 μg/ml chloramphenicol. When the cell density had reached D_{600} of 0.6, IPTG (1 mM) was added and the culture continued for an additional 3 h. In both cases, cells were harvested by centrifugation, frozen in liquid nitrogen, and stored at −70 °C.

Protein purification

In the purification of the recombinant *B. subtilis yodO* gene product (lysine 2,3-aminomutase), all steps were carried out at 4 °C unless otherwise stated. The harvested cells were lysed by sonication. Cell debris, large ribosomal protein and RNA were removed by ultracentrifugation for 45 min at 46000 revs./min (174000 *g*) using a Beckman 55 2Ti rotor. Streptomycin sulphate was added slowly to the supernatant to a concentration of 0.1 %, and precipitated nucleic acids were removed by centrifugation at 39000 *g*. Ammonium sulphate was added slowly to 40 % saturation, the precipitated protein was removed by centrifugation, ammonium sulphate was added to 55 % saturation, and the suspension was centrifuged at 27000 *g*. The pellet was redissolved in a minimum volume of 100 mM Hepps buffer at pH 8.0 containing 50 μM lysine and 25 μM PLP, loaded on to a 120 cm × 2.5 cm Sephacryl S-300 column (Pharmacia), and eluted with the same buffer containing 20 mM NaCl. Fractions displaying absorbance at 410 nm were pooled and loaded on to a 2.5 cm × 30 cm DEAE-Sephacel column (Pharmacia), which was eluted with a linear gradient formed from 1 l of the Sephacryl elution buffer and 1 l of the same buffer containing 500 mM NaCl. Fractions displaying absorbance at 410 nm were pooled and concentrated using an Amicon concentrator. The purified enzyme was stored at −70 °C after being frozen in liquid nitrogen. Anaerobic purifications were carried out at room temperature in a Coy anaerobic chamber except for preparative centrifugations, in which centrifuge bottles filled and sealed in the anaerobic chamber were removed for centrifugation and later returned to the chamber before being opened.

The recombinant gene product from the expression of the *E. coli* unknown gene was purified by methods described previously for the purification of clostridial lysine 2,3-aminomutase [16,17].

Protein and cofactor analysis

The purity of *Bacillus* lysine 2,3-aminomutase was judged by inspection of Coomassie Brilliant Blue-stained gels from SDS/PAGE and the chromatogram of analytical HPLC gel filtration of the protein. Routine measurements of enzyme concentrations were performed using the BCA protein assay reagent (Pierce). The N-terminal amino acid sequence of the purified protein was determined at the Macromolecular Structure Facility of Michigan State University (East Lansing, MI, U.S.A.). The subunit molecular mass was measured by electrospray ionization MS to an accuracy of ±0.02% at the Biotechnology Center of the University of Wisconsin-Madison.

Metal content of the purified enzyme was analysed by inductively coupled plasma-emission spectroscopy (Soil Science Lab, University of Wisconsin-Madison). The total enzyme-bound PLP was measured spectrophotometrically for solutions of known enzyme concentrations using the phenylhydrazine method [18]. Analyses for inorganic sulphide was carried out by the method of Beinert [19].

Enzyme activation and assay

Enzyme was pre-incubated in 100 mM Hepps buffer at pH 8.0 with 8.0 mM L-cysteine in the presence or absence of 0.5 mM PLP and/or 1.0 mM ferrous ammonium sulphate at 37 °C for 3 h in a Coy anaerobic chamber before assaying for activity. Enzyme activity was assayed according to the procedure of Chirpich et al [2] as modified by Ballinger et al. [6], in which 1 unit of activity was defined as the amount of enzyme required to produce 1.0 μmol of β-lysine$\cdot$min^{-1} under standard conditions. Owing to its low activity relative to the clostridial lysine 2,3-aminomutase, the activity of the *Bacillus* enzyme is expressed in m-units. In a typical radiochemical assay, the reductively pre-incubated lysine 2,3-aminomutase was further diluted before mixing with L-[U-^{14}C]lysine, sodium dithionite and AdoMet to give final concentrations of 44 mM L-[U-^{14}C]lysine, 3.5 mM dithionite and 80 μM AdoMet in 100 mM Hepps buffer at pH 8.0. When PLP and/or Fe(II) were included in the pre-activation mixture, the final concentrations of PLP and Fe(II) in the assay mixtures were 45 and 90 μM, respectively. Reactions were quenched at different time intervals with 0.5 M formic acid. Radiolabelled α- and β-lysine were separated by paper electrophoresis, and the radioactivity was measured by scintillation counting as described in [2,6]. HPLC assays of the reaction were carried out by derivatizing an aliquot of the reaction mixture with phenylisothiocyanate before chromatography and comparison with standards as described in [20,21].

Steady-state kinetic parameters of the recombinant lysine 2,3-aminomutase from *Bacillus* were estimated after reductive incubation in the presence of cysteine, PLP and ferrous ammonium sulphate. Initial rates for the conversion of lysine into β-lysine were measured at 37 °C under the conditions described above for assaying the enzyme, except that the concentration of lysine was varied from 2.4 to 48 mM. Kinetic constants and their associated errors were determined by fitting rate data to the Michaelis–Menten equation using the weighted linear-regression analysis described by Wilkinson [30].

EPR spectroscopy

In preparation of EPR samples, the enzyme was incubated (4:1) with the activation buffer, consisting of 200 mM Hepps buffer at pH 8.0, 40 mM cysteine, 2.5 mM PLP and 5.0 mM ammonium iron (II) sulphate at 37 °C for 3 h. Enzyme concentrations in the activation mixture for EPR samples are ≈ 200 μM. For a multiple-sample experiment, a reductively pre-incubated enzyme mixture was prepared for all samples. For each sample, an aliquot of reductively pre-incubated enzyme was mixed with Hepps buffer at pH 8.0, substrate, dithionite and AdoMet in a microcentrifuge tube to give a final volume of 250 μl and transferred to a 3-mm (inner diameter) quartz EPR tube. The concentrations of Hepps, lysine, dithionite and AdoMet in a typical EPR sample were 200 mM, 67.2 mM, 2.5 mM and 2.0 mM, respectively. Components excluded in controls were replaced with 200 mM Hepps buffer (pH 8.0). The EPR sample tubes were then frozen in liquid nitrogen within 4–5 min. For studying the correlation of enzyme activity and spin concentrations, ^{14}C-labelled L-lysine was used and an aliquot was withdrawn for radiochemical assays before the sample was frozen in the EPR tube.

EPR spectra were recorded at X-band on a Varian E3 spectrometer. A standard liquid nitrogen immersion dewar was used. Low-temperature X-band EPR spectra were acquired on a Varian E Line spectrometer equipped with a Varian E102 microwave bridge. An Oxford Instruments ESR-900 continuous-flow helium cryostat Oxford Instruments 3120 temperature controller were used. Both the spectrometers were connected with an IBM AT microcomputer for data acquisition and analysis. Spin concentrations were determined by integration of spectra, using a Cu-EDTA standard as a reference [22]. All spectra were obtained as averages of three 4-min scans.

RESULTS

Characterization of the *yodO* gene product

By making use of two primers complementary to the nucleotide sequences at the 5′ and 3′ termini of the *yodO* gene, a 1.4-kb DNA fragment was amplified by PCR from the genomic *Bacillus* DNA and cloned into an expression vector pET-23a(+). A base change was made in the upstream primer so that the leucine, encoded by the first codon of the open reading frame, was changed to methionine. The cloned DNA fragment encodes a peptide of 471 amino acid residues with a calculated molecular mass of 54071 Da. The amino acid sequence predicted from the cloned DNA displays 62% sequence identity to that of the clostridial lysine 2,3-aminomutase.

The protein was expressed in *E. coli* and purified to apparent homogeneity, as judged by SDS/PAGE and HPLC molecular-filtration chromatography. The purification steps and associated data on yield and purity are set forth in Table 1. N-terminal amino acid sequence analysis generated the sequence MKNKWYKPKR, which confirmed that the purified protein is the *yodO* gene product As shown in Figure 1(A), the sequences contain three conserved cysteine residues, a motif for metal ligands often found in iron-sulphur-cluster-containing enzymes [23]. Also of interest is a putative consensus sequence for PLP binding found in some PLP-containing proteins [24] (Figure 1B).

Calibrated molecular-filtration analysis of protein samples under non-denaturing conditions led to an estimated molecular mass of 224000±21000 Da. The purified protein could be dissolved in 90% formic acid to disrupt non-covalent interactions, and subsequent analysis by electrospray ionization MS gave a molecular mass of 54061±10 Da. The value matches the calculated mass of 54071 Da based on the nucleotide sequence of the gene. The gel-permeation and mass-spectrometric results suggest a homotetrameric quaternary structure for the protein, in contrast to the hexameric structure of the clostridial enzyme.

The dashed line in Figure 2 is the UV-visible absorption spectrum of the purified protein. The spectrum consists of the protein band at 280 nm, a band at 420 nm and a long-wavelength tail extending to 700 nm. The 420-nm band is attributed mainly to the iron-sulphur centre, although PLP may make a minor contribution at this wavelength. A similar 420-nm band is observed in the homologous, PLP-free *E. coli* protein, which is discussed in a later section.

The *yodO* gene product was analysed for transition metal ions, inorganic sulphide and PLP, with the results shown in Table 2. The *B. subtilis* yodO protein contains iron, inorganic sulphide

Table 1 Purification of recombinant *Bacillus* lysine 2,3-aminomutase

Details of the purification procedure are given in the Materials and methods section

Step	Total protein (mg)	Total activity (m-units)	Specific activity (m-units·mg^{-1})	Yield (%)	Purification (fold)
Streptomycin fraction	1850	184	99	100	1.0
$(NH_4)_2SO_4$ fraction	690	153	222	83	2.2
Sephacryl S-300	338	107	317	58	3.2
DEAE-Sephacel	109	68	623	37	6.3

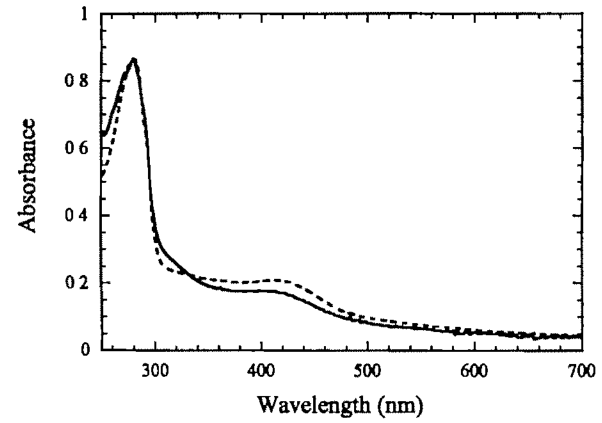

Figure 2 UV-visible absorption spectra of clostridial lysine 2,3-aminomutase homologues

Dashed line the spectrum of the *B subtilis* protein obtained in 50 mM Hepps buffer at pH 8.0 in the presence of 1 mM DTT and 0.05 mM lysine Solid line: the spectrum of the *E coli* P39280 gene product Note that both the *B subtilis* and *E coli* proteins display the 420-nm band and the long-wavelength tail characteristic of iron sulphide proteins.

and PLP. The sulphide and iron are stoichiometrically comparable and correspond to ≈ 8 Fe and 8 S^{2-} per tetramer, and the PLP analysis indicates four PLP per tetramer. The data are consistent with the presence of either two [4Fe-4S] clusters or four [2Fe-2S] clusters per tetramer.

Biochemical activity of the *yodO* gene product

The cofactor content and high degree of identity in primary structure with the clostridial lysine 2,3-aminomutase suggest that the *yodO* protein is an amino acid aminomutase. Such activity was sought using L-arginine, L-ornithine, L-phenylalanine, L-leucine and L-isoleucine as substrates in addition to L-lysine. Under assay conditions similar to those used for the clostridial lysine 2,3-aminomutase [6], we found the yodO protein to be a lysine 2,3-aminomutase, and none of the other amino acids were accepted as substrates. Like the clostridial enzyme, a pre-incubation process is required to activate the enzyme. However, unlike the clostridial enzyme, which displays full activity after reductive pre-incubation with dihydrolipoate or dithiothreitol (DTT) in the presence of Fe(II), the *B. subtilis* enzyme requires the presence of L-cysteine instead of dihydrolipoate or DTT to achieve maximum activity, and added Fe(II) is not necessary. Table 3 summarizes various conditions used to activate the enzyme and the activities measured in each case. The complete reductive incubation mixture contained 8.0 mM cysteine, 1.0 mM

Table 3 Effect of various reductive incubation mixtures on lysine 2,3-aminomutase activity

Reductive incubation was in 50 mM Hepps buffer at pH 8.0 and at 37 °C for 3 h in a Coy anaerobic chamber. Concentrations of reactants were cysteine, 8 mM, Fe(II), 1.0 mM, PLP, 0.5 mM, DTT, 35 mM, mercaptoethanol, 70 mM, dihydrolipoate, 20 mM, and lysine 2,3-aminomutase, 20–30 μM. Activities were measured in 0.2 M Hepps buffer at pH 8.0 with 44 mM L-lysine, 3.5 mM dithionite and 35 μM AdoMet at 37 °C, means ± S.D. are shown.

Experiment	Reductive incubation mix	Activity measured (m-units mg^{-1})
1	Complete [cysteine, Fe(II), PLP]	660 ± 51
2	− Reductive incubation	38 ± 6
3	− Fe(II)	640 ± 58
4	− PLP	580 ± 34
5	− Cysteine	215 ± 15
6	− Cysteine, + DTT	190 ± 17
7	− Cysteine, + mercaptoethanol	210 ± 9
8	− Cysteine, + dihydrolipoate	177 ± 12
9	Complete + DTT	417 ± 20

Table 2 Transition-metal ions, sulphide and PLP in *Bacillus* lysine 2,3-aminomutase (in mol per mol of tetrameric enzyme)

Iron was measured by inductively coupled plasma-emission spectroscopy, sulphide was measured by the method of Beinert [19], and PLP was measured by the phenylhydrazine method of Wada and Snell [18] Means ± S.D. are shown.

Ion	Enzyme preparation...	A	B	C	D
Iron		6.64 ± 0.74	7.67 ± 0.61	8.40 ± 0.87	–
Cobalt		0.12 ± 0.04	0.05 ± 0.04	0.03 ± 0.03	–
Copper		0.06 ± 0.01	0.04 ± 0.01	0.04 ± 0.01	–
Zinc		1.78 ± 0.09	0.98 ± 0.07	0.77 ± 0.08	–
Sulphide		–	–	7.31 ± 0.56	8.41 ± 0.62
PLP		–	3.60 ± 0.25	3.87 ± 0.31	4.20 ± 0.32

Table 4 Effect of AdoMet, L-methionine and 5′-deoxyadenosine on activity

Enzyme was reductively incubated in 50 mM Hepps buffer with 8 mM L-cysteine at pH 8.0 and 37 °C for 3 h inside a Coy anaerobic chamber. Concentrations of components were, where applicable: enzyme, 1.5–2.0 μM; lysine, 44 mM, dithionite, 3.5 mM, AdoMet, 80 μM, L-methionine, 3.6 mM, and 5′-deoxyadenosine, 3.6 mM. Means ± S.D. are shown

Experiment	Reaction mixture	Activity measured (m-units mg^{-1})
1	Complete (activated enzyme, dithionite, AdoMet)	620 ± 50
2	+ L-Methionine	600 ± 73
3	+ 5′-Deoxyadenosine	450 ± 24
4	+ L-Methionine + 5′-deoxyadenosine	420 ± 18
5	− AdoMet	4.9 ± 0.4
6	− AdoMet, + L-methionine	3.5 ± 0.3
7	− AdoMet, + 5′-deoxyadenosine	7.9 ± 0.3
8	− AdoMet, + L-methionine + 5′-deoxyadenosine	8.2 ± 0.4

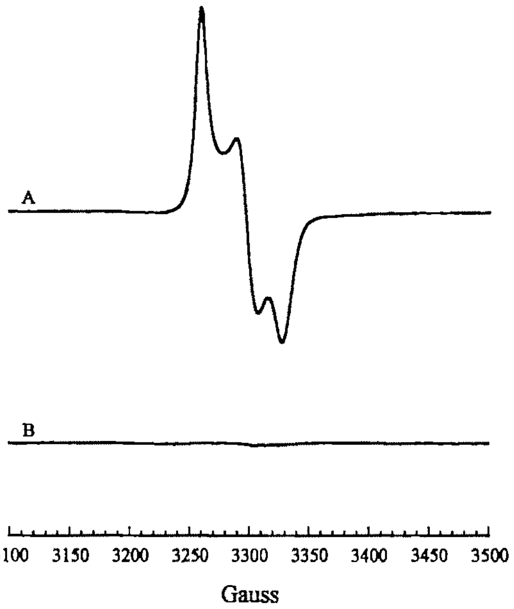

Figure 3 Low-temperature X-band EPR spectra of *B. subtilis* lysine 2,3-aminomutase

Spectra were acquired at 10 K and normalized to 60 mM aminomutase (tetramer). Spectra were recorded at 9.24 GHz, with modulation amplitude of 5 G at 1 mW power. The receiver gain was 2.5×10^3. (**A**) Spectrum of the purified enzyme in 100 mM Hepps buffer at pH 8.0. The specific activity of the enzyme was 520 m-units · mg^{-1}. (**B**) Spectrum of activated enzyme. The enzyme was activated by incubation in 50 mM Hepps buffer at pH 8.0 with 8.0 mM cysteine, 1.0 mM Fe (II) and 0.5 mM PLP in an anaerobic chamber for 4 h at 37 °C. The receiver gain was 2.5×10^3.

Fe(II) and 0.5 mM PLP. Incubation of the purified enzyme in this mixture increases the activity more than 17-fold (Table 3, experiment 1), as compared with the enzyme sample assayed in the absence of reductive incubation (Table 3, experiment 2). Omitting Fe(II) or PLP in the pre-activation has little or no effect on activity (Table 3, experiments 3 and 4), showing that the iron and PLP intrinsic to the protein (Table 2) correspond to the full complement of these cofactors. Omitting cysteine from the activation mixture leads to dramatically less activity (Table 3, experiment 5). DTT, 2-mercaptoethanol or dihydrolipoate cannot substitute for cysteine (Table 3, experiments 6–8). In fact, DTT is inhibitory when cysteine is present (Table 3, experiment 9).

The reductively pre-incubated enzyme catalyses the conversion of L-lysine into β-lysine only when sodium dithionite and AdoMet are added. Omission of either dithionite or AdoMet leads to a very low residual activity. The apparent K_m value for L-lysine was estimated to be 8.0 ± 2.2 mM.

The specific activity of a typical enzyme preparation was ≈ 620 ± 50 m-units · mg^{-1} when the standard pre-activation process (Table 3, exp. 1) was used. This activity is about 1.7 % that of the clostridial enzyme [11]. Enzyme samples purified under anaerobic conditions exhibited similar activities, and an anaerobically purified enzyme prepared from anaerobically grown *E. coli* cells also failed to display a higher activity. Unlike the clostridial enzyme, which is extremely oxygen-sensitive, the *B. subtilis* enzyme purified aerobically displays full activity after reductive pre-incubation, indicating a remarkable stability of the enzyme in air.

Effects of L-methionine and 5′-deoxyadenosine on activity

As discussed above, the reductively pre-incubated enzyme requires AdoMet and dithionite for activity (Table 4, experiment 1). In the case of the clostridial enzyme, dithionite reduces the iron-sulphur cluster [11], and AdoMet participates directly in hydrogen transfer [12]. AdoMet is transiently cleaved to L-methionine and 5′-deoxyadenosine in the course of catalysis [12]. Under the complete assay conditions, the presence of L-methionine in the assay mixture does not affect enzyme activity (Table 4, experiment 2). However, added 5′-deoxyadenosine significantly inhibits the enzyme (Table 4, experiment 3). This inhibition is presumably caused by competitive binding of 5′-deoxyadenosine to the AdoMet-binding site. The presence of both Met and 5′-deoxyadenosine causes the same inhibition as 5′-deoxyadenosine alone (Table 4, experiment 4).

When assayed in the absence of added AdoMet, the reductively pre-incubated enzyme displays a low activity of ≈ 5 m-units · mg^{-1} (Table 4, experiment 5). This basal activity is observed routinely and may be due to the fact that a small fraction of the purified enzyme contains bound AdoMet. The basal activity was stimulated by the addition of 5′-deoxyadenosine or of both 5′-deoxyadenosine and methionine (Table 4, experiments 7 and 8). Methionine alone is slightly inhibitory (Table 4, experiment 6).

Spectroscopic evidence of [Fe-S] cluster

The presence of equimolar amounts of iron and sulphide, as well as the long-wavelength absorbances in the UV-visible spectrum of the enzyme, indicates the presence of iron-sulphur cluster. To examine this issue, the X-band EPR spectra of various enzyme samples were obtained at 10 K. As shown in Figure 3(A), the purified enzyme displays an EPR signal at 10 K with an average g value of 2.01. The spectrum is similar to one observed in the clostridial enzyme [25] and assigned as a species of $[4Fe\text{-}4S]^{3+}$ [11]. The measured spin concentration ranges from 15 to 25 % of the enzyme concentration, differing from preparation to preparation. Addition of dithionite directly to the sample does not cause any noticeable change to the spectrum, however, reductive pre-incubation with cysteine converts the enzyme into an EPR-silent form (Figure 3B), presumably due to reduction of the cluster from $[4Fe\text{-}4S]^{3+}$ to $[4Fe\text{-}4S]^{2+}$.

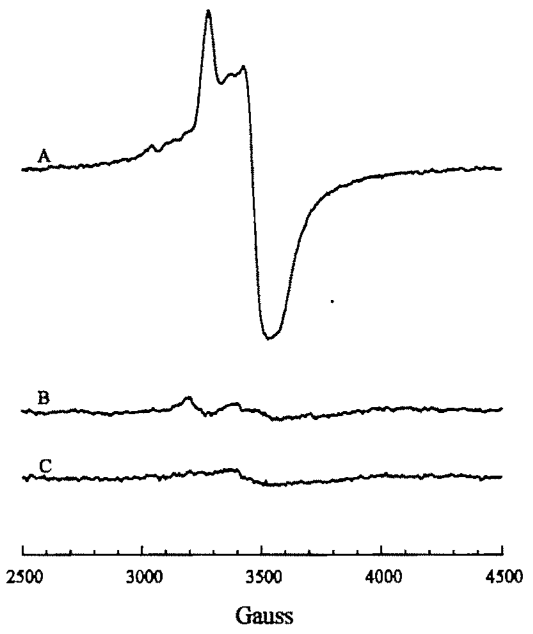

Figure 4 A comparison of AdoMet-dependent reduction of the iron-sulphur clusters in *Clostridium* and *B. subtilis* lysine 2,3-aminomutases

Shown are X-band EPR spectra acquired at 10 K. (**A**) 40 μM *Clostridium* enzyme plus 1.8 mM AdoMet and 4.0 mM dithionite, (**B**) 60 μM *B. subtilis* enzyme plus 1.8 mM AdoMet and 4.0 mM dithionite, (**C**) 60 μM *B. subtilis* enzyme plus 1.8 mM AdoHCys and 4 mM dithionite. Enzyme samples were subjected to reductive activation with dihydrolipoate for the *Clostridium* enzyme and with cysteine for the *B. subtilis* enzyme before being further treated with dithionite and AdoMet or dithionite and AdoHCys. Spectra were recorded at 9.244 GHz, with a modulation of 8.0 G and 1.0 mW power. Receiver gains were 5.0×10^3 for all samples. Spectra shown are averages of three 4-min scans with a time constant of 1.0 s.

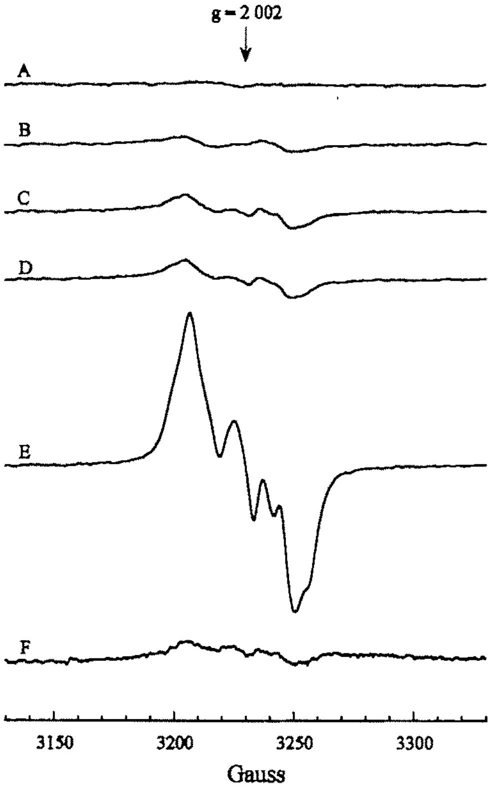

Figure 5 EPR spectra of organic radicals associated with *B. subtilis* lysine 2,3-aminomutase

All samples contained ≈ 60 μM enzyme (tetramer concentration) and in 100 mM Hepps buffer at pH 8.0 and 77 K. Spectra: (**A**) activated enzyme, (**B**) activated enzyme plus 67.2 mM lysine, (**C**) activated enzyme plus 67.2 mM lysine and 2.0 mM AdoMet, (**D**) activated enzyme plus 67.2 mM lysine and 2.5 mM dithionite, (**E**) activated enzyme plus 67.2 mM lysine, 2.0 mM AdoMet and 2.5 mM dithionite; (**F**) purified enzyme. Instrument settings: scan range, 200 G; centre field, 3300 G; microwave frequency, 9.093 GHz, modulation amplitude, 3.2 G, microwave power, 5.0 mW, receiver gain, 1.0×10^5

In the case of the clostridial enzyme, the $[4Fe\text{-}4S]^{2+}$ cluster of the reductively pre-incubated enzyme can be further reduced to $[4Fe\text{-}4S]^{+}$ by dithionite in the presence of AdoMet or AdoHCys, with the concomitant appearance of a strong EPR signal of average $g = 1.85$ [11], as shown in Figure 4(A). In contrast, mixing the reductively pre-incubated *B. subtilis* enzyme with dithionite and AdoMet or AdoHCys elicits only weak, broad EPR signals (Figures 4B and 4C), which may represent a very low concentration of $[4Fe\text{-}4S]^{+}$. Like the clostridial enzyme, the reductively pre-incubated *B. subtilis* enzyme requires a strong one-electron reducing agent such as dithionite for activity, indicating that a further reduction of the enzyme is needed. Therefore, in both enzymes, the reduction of the cluster to the $[4Fe\text{-}4S]^{+}$ state seems to be a prerequisite for initiating the rearrangement reaction. The very low accumulation of the $[4Fe\text{-}4S]^{+}$ species in the *B. subtilis* enzyme may represent less stabilization of the reduced state by the protein environment relative to the 2+ state and may suggest a lower reduction potential for the $[4Fe\text{-}4S]^{2+}/[4Fe\text{-}4S]^{1+}$ couple in the *B. subtilis* relative to the clostridial enzyme.

EPR spectra of substrate-based free radicals

The presence of PLP together with the requirement for AdoMet suggests that the *B. subtilis* enzyme functions by a radical rearrangement mechanism similar to that proposed for the *Clostridium* enzyme (Scheme 1). To determine whether organic radicals could be observed, various enzyme–cofactor–substrate mixtures were examined by EPR at 77 K. Samples of the complete reaction mixture, including reductively pre-incubated *B. subtilis* enzyme, L-lysine, dithionite and AdoMet, reproducibly exhibit an EPR signal centred at $g = 2.002$ (Figure 5E). The g value of 2.002 and the partially resolved hyperfine structure indicate that the EPR signals are derived from an organic free radical. Indeed, the spectral envelope is very similar to that of the α-radical form of the β-lysine-PLP external aldimine (radical **3** in Scheme 1) observed in the steady state of the reaction of the clostridial lysine 2,3-aminomutase [6]. The spectral similarities suggest that the hyperfine coupling constants for the radical are similar in the *B. subtilis* and clostridial enzymes.

A series of control experiments show that the EPR signal is associated with enzyme activity and not with a by-product of the reductive pre-incubation. The spectrum does not appear in samples containing only the reductively pre-incubated enzyme (Figure 5A). Very weak signals were observed in samples lacking AdoMet and dithionite (Figure 5B), samples lacking dithionite alone (Figure 5C) and samples lacking AdoMet alone (Figure 5D). The presence of weak EPR signals in these control samples is attributed to the presence of a low concentration of lysine added as an enzyme stabilizer to buffers used in purification. Mixing the purified enzyme with lysine, dithionite and AdoMet does not produce the EPR signal either (Figure 5F). These observations are consistent with activity assays and indicate that the appearance of a strong EPR signal and a high activity of β-

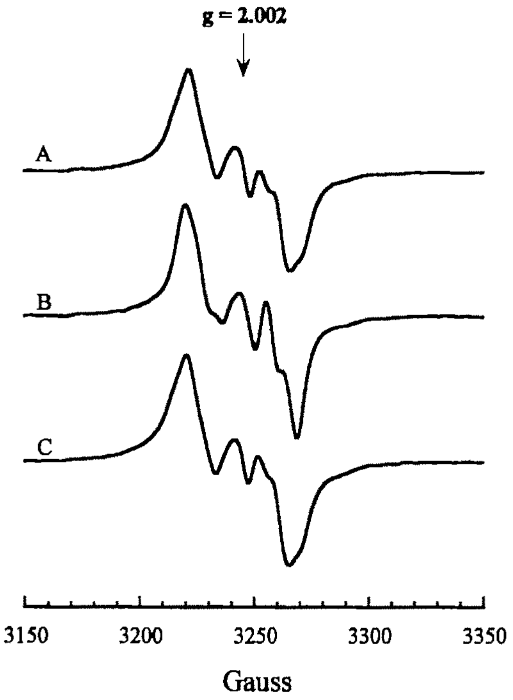

Figure 6 Effects of deuterium-labelled substrate on the EPR spectrum

All samples were prepared as described in Figure 5 except for the listed isotopic substitutions. Spectra (**A**) reaction with L-lysine, (**B**) reaction with L-[3,3,4,4,5,5,6,6-$^2H_8$]lysine (99% enrichment), (**C**) reaction with L-lysine in 75% ^2H_2O Instrument settings were identical to those listed in Figure 5 except the centre field was 3250 G

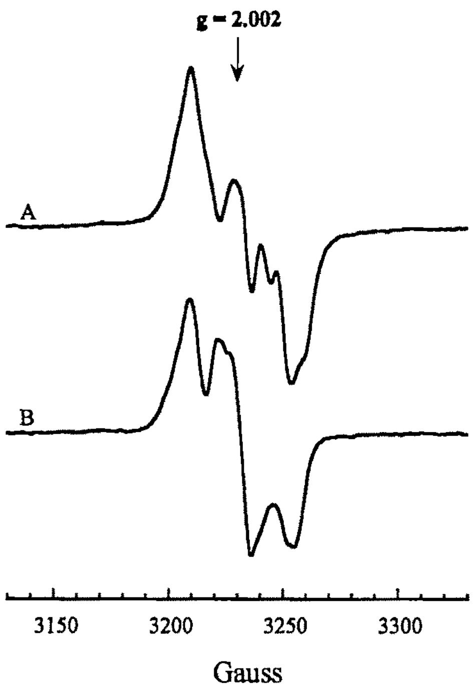

Figure 7 Effect of substrate analogue on the EPR spectrum

Activated *B subtilis* lysine 2,3-aminomutase was mixed with either lysine or 4-thialysine in EPR tubes and then frozen in liquid nitrogen within 3 min (**A**) The reaction mixture contained 50 mM activated enzyme, 67.2 mM lysine, 2.5 mM sodium dithionite and 2.0 mM AdoMet in 100 mM Hepps buffer at pH 8.0, (**B**) the reaction mixture contained 67.2 mM 4-thialysine in place of lysine in the same reaction mixture The spectra were obtained at 77 K. Instrument settings microwave frequency, 9.093 GHz, modulation amplitude, 1.6 G, microwave power, 5 mW, receiver gain, 1.0×10^5

lysine formation require the fulfilment of the same conditions; that is, reductively pre-incubated enzyme and the presence of substrate, a strong one-electron reducing agent and AdoMet.

The EPR spectrum obtained from a reaction mixture with L-[3,3,4,4,5,5,6,6-$^2H_8$]lysine (Figure 6B) exhibits small but definite differences compared with that of unlabelled lysine (Figure 6A). These spectra show that one or more protons at C-3–C-6 of the lysine are coupled to the radical centre, most probably the C-3-proton as found for the corresponding radical in the clostridial enzyme [6]. The persistence of the predominant splitting pattern in the deuterated sample shows that protons from C-3 to C-6 of lysine are only weakly coupled to the unpaired electron spin and are not responsible for the major hyperfine splitting pattern in the spectrum. The effect of deuterium substitution in the solvent was also examined. The spectrum resulting from a reaction in 75% ^2H_2O is shown in Figure 6(C). The absence of any change in the splitting pattern indicates that solvent-exchangeable hydrogens are not strongly coupled to the radical.

4-Thialysine is an alternative substrate for clostridial lysine 2,3-aminomutase [26]. Upon mixing 4-thialysine with the reductively pre-incubated *B. subtilis* lysine 2,3-aminomutase in the presence of dithionite and AdoMet, an EPR signal centred at $g = 2.002$ was observed (Figure 7B). The signal is similar to that of the β-radical of 4-thialysine observed in the clostridial enzyme [26]. The similarities in the hyperfine structures of the spectra of organic free radicals derived from lysine and 4-thialysine bound to the *B. subtilis* lysine 2,3-aminomutase to those observed with the clostridial enzyme confirm that the reaction mechanisms are the same, and the conformations of the α- and β-substrate-based radicals are the same in the two enzymes.

Dependence of spin concentration on enzyme activity

The unpaired spin concentration at the $g = 2.0$ region depends on the concentration of the active enzyme, as shown in Figure 8. In preparing EPR samples, high concentrations of enzymes were used in both the pre-activation process and the filling of EPR sample tubes (see the Materials and methods section). In assays at high enzyme concentrations, the measured specific activities are severalfold lower than when the enzyme is assayed under standard conditions of low concentration (see Figure 8 and compare data in Table 3). An inverse correlation between enzyme concentration and specific activity at high enzyme concentrations was observed reproducibly (results not shown). However, the concentration of the unpaired electron spin was well correlated with the enzymic activities of the samples. The data indicate further that the observed radical is associated with enzyme that is actively turning over the substrate and that the radical is a genuine intermediate.

The product of the unknown *E. coli* gene P39280

In the absence of knowledge about the dioxygen-sensitivity of the unknown *E. coli* gene product, the protein was expressed in *E. coli* cells grown anaerobically. SDS/PAGE of cellular extracts demonstrated a very high level of expression of this gene in its natural host. No lysine 2,3-aminomutase activity could be detected, either in cellular extracts or in the purified protein, with

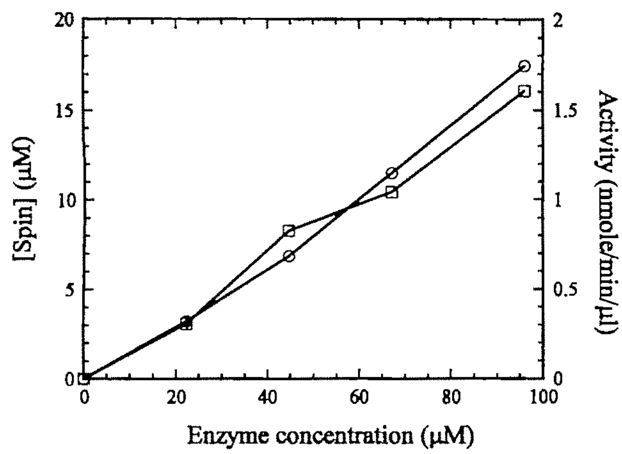

Figure 8 Correlation of spin with enzyme concentration and activity

All samples contained 100 mM Hepps buffer at pH 8.0, 67.2 mM lysine, 2.5 mM sodium dithionite and 2.0 mM AdoMet, in addition to components carried over from the pre-activation incubation along with the enzyme. Activity was measured by radiochemical assay of the same activated enzyme at concentrations identical to those used to generate EPR samples. □, Specific enzymic activity, ○, spin concentration

or without reductive pre-incubation. This suggested a different and still unknown biological activity for this protein. The solid line in Figure 2 is the UV-visible absorption spectrum of the P39280 gene product. It includes a band at 420 nm and a long-wavelength tail, indicative of an iron sulphide cluster. Analysis for iron and sulphide confirmed their presence in equimolar amounts corresponding to about 3.0 mol per mol of subunits. This is in accord with the presence of the cysteine motif in the amino acid sequence (Figure 1A). The spectrum was similar to that of lysine 2,3-aminomutase but slightly less intense in the region of 400–430 nm, perhaps because of the absence of PLP. It was concluded that the *E. coli* protein of unknown function was not a lysine 2,3-aminomutase.

DISCUSSION

Oxygen insensitivity and low activity of *B. subtilis* lysine 2,3-aminomutase

Lysine 2,3-aminomutase from *C. subterminale* SB4 is extremely oxygen sensitive. Purification of the clostridial enzyme must be carried out under strictly anaerobic conditions to ensure maximal activity because exposure to dioxygen leads to irreversible destruction of the iron-sulphur cluster. In contrast, the *B. subtilis* lysine 2,3-aminomutase can be expressed and purified under aerobic conditions without loss of activity or iron-sulphur clusters. The purified enzyme must still be reductively pre-incubated with L-cysteine under anaerobic conditions to display its maximum activity, but the iron-sulphur cluster is not irreversibly oxidized by dioxygen. Dioxygen insensitivity is a potential advantage for future mechanistic studies of the *B. subtilis* enzyme and for its practical use in the production of L-β-lysine.

Although the activity of the *B. subtilis* enzyme is $\approx 1.7\,\%$ that of the clostridial enzyme, the spin concentration associated with the radical intermediate under steady-state conditions is 20–25 % of the tetrameric enzyme concentration, comparable with the observed spin intensity for the clostridial enzyme [6]. Furthermore, a very small deuterium kinetic isotope effect of $k_H/k_D \approx 1.2$ was observed with L-[3,3,4,4,5,5,6,6-$^2H_8$]lysine in the reaction of the *B. subtilis* enzyme, whereas an isotope effect of 3.0 was observed for the clostridial enzyme [10]. The high spin concentration generated during turnover and the low primary kinetic isotope effect in the reaction of the *B. subtilis* enzyme suggest that there is a slow step after the hydrogen-abstraction step, presumably the release of β-lysine.

The catalytically functional states of the iron-sulphur cluster

A strong, one-electron reducing agent such as dithionite is needed for activity in both the clostridial and the *B. subtilis* lysine 2,3-aminomutase-catalysed reactions. The strong reducing agent activates clostridial enzyme by reducing the iron-sulphur cluster from the EPR-silent [4Fe-4S]$^{2+}$ to the fully reduced [4Fe-4S]$^{+}$, which displays a low-temperature EPR spectrum centred at 1.85 *g*. The reduction requires the presence of AdoMet or AdoHCys, indicating that the binding of AdoMet to the enzyme makes the reduction potential of the iron-sulphur cluster less negative [11]. The E-[4Fe-4S]$^{+}$/AdoMet is postulated to be in equilibrium with a low concentration of a radical-initiating form that contains the 5′-deoxyadenosyl radical and may be designated as E-[4Fe-4S]$^{2+}$/Met/Ado$^{\bullet}$. The radical rearrangement is initiated by action of the 5′-deoxyadenosyl radical in abstracting a hydrogen atom from C-3 of lysine, which is bound as its external aldimine with PLP (Scheme 1).

Although the *B. subtilis* enzyme also requires a strong reducing agent for activity, dithionite is less effective in reducing the iron-sulphur cluster to [4Fe-4S]$^{+}$ than in the case of the clostridial enzyme. Only a weak broad EPR signal centred at $g = 1.9$ could be detected in the presence of AdoMet or AdoHCys, whereas a strong EPR signal is observed with the clostridial enzyme under the same conditions (Figure 4). However, the low *g* value (1.9) and the breadth of the *B. subtilis* signal are characteristic of [4Fe-4S]$^{+}$ clusters. The fact that a strong reducing agent such as dithionite is required for activity by both enzymes suggests that [4Fe-4S]$^{+}$ is also the active state in the *B. subtilis* enzyme. The low concentration of the reduced form in the *B. subtilis* enzyme, with dithionite as the reducing agent, may mean that the reduction potential for [4Fe-4S]$^{2+}$ + e^{-} → [4Fe-4S]$^{+}$ is more negative than in the case of the clostridial enzyme. The low concentration of [4Fe-4S]$^{+}$ in the *B. subtilis* lysine 2,3-aminomutase may contribute to its low activity relative to the clostridial enzyme.

On reductive pre-incubation

Although the purified *B. subtilis* lysine 2,3-aminomutase displays a trace of activity, reductive pre-incubation with L-cysteine increases it more than 15-fold. The increase is not directly correlated with the amount of the [4Fe-4S]$^{3+}$ state in the purified enzyme, indicating that L-cysteine does more than simply reduce the iron-sulphur cluster to [4Fe-4S]$^{2+}$. The requirement for L-cysteine in the pre-activation mixture suggests that cysteine may act as both a reducing agent and an activator in helping to position the iron-sulphur clusters in a reactive state. A possible function of L-cysteine is to remove inhibitory ligands adventitiously bound to the active site, perhaps to the iron-sulphur cluster, during cell growth and enzyme purification.

Effect of 5′-deoxyadenosine on activity

The data in the last four lines of Table 4 show that, in the absence of added AdoMet, 5′-deoxyadenosine significantly activates the enzyme. Under these conditions, 5′-deoxyadenosine is postulated to activate by increasing the amount of endogenous AdoMet. This could occur if part of the AdoMet sites were non-productively occupied by methionine in a poised state from which 5′-deoxyadenosine had escaped. Reduction of the iron-sulphur cluster by dithionite in the presence of exogenous 5′-deoxyadenosine could lead to the formation of AdoMet, thereby activating those sites. The modest extent of activation by 5′-deoxyadenosine in Table 4 indicates that only a small percentage of the active sites could exist in such a poised state.

Significance of lysine 2,3-aminomutase associated with the *yod* operon

The *yodO* gene lies between *yodP* and *yozE* within a gene cluster of the *Bacillus* genome [15]. This cluster includes *yodT*, *yodS*, *yodR*, *argE*, *yodP*, *yodO* and *yozE* in an orientation in which *yodT* is transcribed first and *yozE* is last. The products of *yozE* and *yodP* are not similar to other known proteins. The *argE* gene encodes acetylornithine deacetylase for arginine biosynthesis, while the products of *yodR*, *yodS* and *yodT* are similar to butyrate:acetoacetate-CoA transferase, 3-oxoadipate-CoA transferase and adenosylmethionine:8-amino-7-oxononanoate aminotransferase, respectively. From this information, and our observation that the *yodO* protein does not accept either arginine or ornithine as aminomutase substrates, the relationship between the *Bacillus* lysine 2,3-aminomutase and other proteins encoded by this cluster cannot be ascertained at the present time.

The homologous product of *E. coli* gene P39280

The biological function of the *E. coli* gene product is unknown. Although it shares significant sequence identity with the clostridial and *B. subtilis* lysine 2,3-aminomutases (30%), residues that may be important for PLP binding, including a lysine residue, are absent, and PLP cannot be detected in the purified protein. Therefore, despite being homologous to lysine 2,3-aminomutase, the *E. coli* protein cannot be an aminomutase.

The gene is located in the *E. coli* genome adjacent to *efp*, encoding elongation factor P involved in the control of protein synthesis [27], and downstream from *groES* and *groEL* (*mopA*), genes which code for chaperonin proteins [28,29]. The fact that these genes do not code for enzymes directly or indirectly involved in lysine metabolism further supports a different biological role for this protein.

Other homologues of lysine 2,3-aminomutase

Among the seven homologues of *C. subterminale* lysine 2,3-aminomutase in Figure 1, two in addition to the *Bacillus yodO*-product are likely to be lysine 2,3-aminomutases. All of the homologues contain the cysteine motif (Figure 1A), but only the upper four contain the PLP-binding motif (Figure 1B). Those that include the PLP-binding motif are likely to be lysine 2,3-aminomutases. In particular, the homologous protein in *P. gingivalis* is 72% identical to *C. subterminale* lysine 2,3-aminomutase. The lower three homologues, including the *E. coli* protein, lack the PLP-binding motif and are unlikely to be lysine 2,3-aminomutases. The homologous protein in *A. aeolicus* includes a sequence that is similar to and aligned with the PLP motif in the other proteins, but with lysine and arginine in reversed positions. This protein cannot be assigned with confidence as a lysine 2,3-aminomutase, although the possibility should be regarded as open.

We thank Professor George H Reed for generously allowing us to use his EPR equipment We are also grateful to Mr Olafur Th. Magnusson for numerous valuable discussions. This research was supported by grant no. DK 28607 from the National Institute of Diabetes and Digestive and Kidney Diseases of the United States Public Health Service.

REFERENCES

1 Costilow, R N, Rochovansky, O M and Barker, H A (1966) Isolation and identification of β-lysine as an intermediate in lysine fermentation. J Biol Chem **241**, 1573–1578

2 Chirpich, T P, Zappia, V, Costilow, R N and Barker, H A (1970) Lysine 2,3-aminomutase Purification and properties of a pyridoxal phosphate and *S*-adenosylmethionine-activated enzyme J Biol Chem **245**, 1778–1789

3 Stadtman, T C (1973) Lysine metabolism by Clostridia. Adv Enzymol Relat. Areas Mol Biol **38**, 413–448

4 Charter, II, J H, Du Bus, R H, Dyer, J R, Floyd, J C, Rice, K C and Shaw, P. D (1974) Biosynthesis of viomycin II Origin of β-lysine and viomycidine Biochemistry **13**, 1227–1233

5 Thiruvengadam, T K, Gould, S. J., Aberhart, J D. and Lin, H J (1983) Biosynthesis of streptothricin F 5 Formation of β-lysine by *Streptomyces* L-1689–23 J Am Chem Soc **105**, 5470–5476

6 Ballinger, M D, Reed, G H and Frey, P. A. (1992) An organic radical in the lysine 2,3-aminomutase Biochemistry **31**, 949–953

7 Ballinger, M D, Frey, P A and Reed, G. H (1992) Structure of a substrate radical intermediate in the reaction of lysine 2,3-aminomutase Biochemistry **31**, 10782–10788

8 Reed, G H and Ballinger, M D (1995) Characterization of a radical intermediate in the lysine 2,3-aminomutase reaction Methods Enzymol **258**, 362–379

9 Moss, M and Frey P A (1987) The role of *S*-adenosylmethionine in the lysine 2,3-aminomutase reaction J Biol Chem **262**, 14859–14862

10 Baraniak, J, Moss, M. L and Frey, P A (1989) Lysine 2,3-aminomutase Support for a mechanism of hydrogen transfer involving *S*-adenosylmethionine J Biol Chem **264**, 1357–1360

11 Lieder, K. W, Booker, S., Ruzicka, F J, Beinert, H, Reed, G H and Frey, P A (1998) *S*-adenosylmethionine-dependent reaction of lysine 2,3-aminomutase and observation of the catalytically functional iron-sulfur centers by electron paramagnetic resonance. Biochemistry **37**, 2578–2585

12 Frey, P A (1993) Lysine 2,3-aminomutase is *S*-adenosylmethionine a poor man's adenosylcobalamin? FASEB J **7**, 662–670

13 Ballinger, M D, Frey, P A and Reed, G H (1995) Pulsed electron paramagnetic resonance studies of the lysine 2,3-aminomutase substrate radical: evidence for participation of pyridoxal 5′-phosphate in a radical rearrangement Biochemistry **34**, 10086–10093

14 Ruzicka, F J., Lieder, K W and Frey, P A (2000) Lysine 2,3-aminomutase from *Clostridium subterminale* SB4 mass spectral characterization of cyanogen bromide-treated peptides and cloning, sequencing, and expression of the gene *kam*A in *Escherichia coli* J Bacteriol **184**, 469–476

15 Kunst, F, Ogasawara, N, Moszer, I, Albertini, A M., Alloni, G, Azevedo, V, Bertero, M G, Bessières, P, Bolotin, A., Borchert, S et al (1997) The complete genome sequence of the Gram-positive bacterium *Bacillus subtilis* Nature (London) **390**, 249–256

16 Moss, M. L and Frey, P A. (1990) Activation of lysine 2,3-aminomutase by *S*-adenosylmethionine J Biol Chem **265**, 18112–18115

17 Petrovich, R M, Ruzicka, F J, Reed, G. H and Frey, P. A (1991) Metal cofactors of lysine 2,3-aminomutase J Biol Chem **266**, 7656–7660

18 Wada, H. and Snell, E E (1961) The enzymatic oxidation of pyridoxine and pyridoxamine phosphates J Biol. Chem **236**, 2089–2095

19 Beinert, H. (1983) Semi-micro methods for analysis of labile sulfide and of labile sulfide plus sulfane sulfur in unusually stable iron-sulfur proteins Anal Biochem **131**, 373–378

20 Heinrikson, R L and Meredich, S C (1984) Amino acid analysis by reverse-phase high-performance liquid chromatography precolumn derivatization with phenylisothiocyanate Anal Biochem **136**, 65–74

21 Ebert, R F. (1986) Amino acid analysis by HPLC: optimized conditions for chromatography of phenylthiocarbamyl derivatives Anal Biochem **154**, 431–435

22 Palmer, G (1973) Electron paramagnetic resonance Methods Enzymol **10**, 594–609

23 Flint, D H and Allen, R M (1996) Iron-sulfur proteins with nonredox functions Chem. Rev **96**, 2315–2334

24 Ogawa, H, Konishi, K and Fujioka, M (1989) The peptide sequences near the bound pyridoxal phosphate are conserved in serine dehydratase from rat liver, and threonine dehydratases from yeast and *Escherichia coli* Biochim Biophys Acta **996**, 139–141

25 Petrovich, R. M, Ruzicka, F. J, Reed, G H and Frey, P A (1992) Characterization of iron-sulfur clusters in lysine 2,3-aminomutase by electron paramagnetic resonance spectroscopy Biochemistry **31**, 10774–10781

26 Wu, W, Lieder, K W, Reed, G H and Frey, P A (1995) Observation of a second substrate radical intermediate in the reaction of lysine 2,3-aminomutase a radical centered on the *β*-carbon of the alternative substrate, 4-thia-L-lysine Biochemistry **34**, 10532–10537

27 Aoki, H, Dekany, K, Adams, S L and Ganoza, M C. (1997) The gene encoding the elongation factor P protein is essential for viability and is required for protein synthesis J. Biol. Chem **272**, 32254–32259

28 Ben-Zvi, A P, Chatellier, J, Fersht, A R and Goloubinoff, P (1998) Minimal and optimal mechanisms for GroE-mediated protein folding Proc Natl. Acad Sci U.S A **95**, 15275–15280

29 Ranson, N A, White, H E and Saibil, H. R (1998) Chaperonins Biochem J **333**, 233–242

30 Wilkinson, G N (1961) Statistical estimations in enzyme kinetics Biochem J **80**, 324–332

Received 13 December 1999/2 March 2000, accepted 29 March 2000

Biochem J (2000) 348, 551–556 (Printed in Great Britain)

Ligand binding directly stimulates ubiquitination of the inositol 1,4,5-trisphosphate receptor

Chang-Cheng ZHU[1] and Richard J. H. WOJCIKIEWICZ[2]

Department of Pharmacology, College of Medicine, SUNY Upstate Medical University, 750 East Adams Street, Syracuse, NY 13210-2339, U.S.A

Down-regulation of the Ins(1,4,5)P_3 receptor is an adaptive response to the activation of certain phosphoinositidase C-linked cell-surface receptors. It is manifested as a profound decline in cellular Ins(1,4,5)P_3 receptor content, occurs with a half-time of 0.5–2 h and is due to accelerated proteolysis. It has been shown that this process is mediated by the ubiquitin/proteasome pathway and is therefore initiated by Ins(1,4,5)P_3 receptor ubiquitination. To investigate the role of ligand binding in Ins(1,4,5)P_3 receptor ubiquitination, we expressed 'exogenous' wild-type and ligand-binding-defective mutant type I Ins(1,4,5)P_3 receptors in human neuroblastoma SH-SY5Y cells, in which muscarinic receptor activation elicits Ins(1,4,5)P_3 receptor down-regulation. We found (1) that exogenous wild-type Ins(1,4,5)P_3 receptors are efficiently ubiquitinated in response to muscarinic receptor stimulation, (2) that exogenous ligand binding-defective mutant Ins(1,4,5)P_3 receptors are resistant to ubiquitination, (3) that this resistance is not caused by the removal of potential ubiquitin-conjugating sites in the mutated region, and (4) that in heterotetramers of exogenous mutant receptors and 'endogenous' receptors, only the latter are targeted for ubiquitination. These results indicate that the binding of Ins(1,4,5)P_3 directly stimulates ubiquitination of the Ins(1,4,5)P_3 receptor and that the targeting of Ins(1,4,5)P_3 receptors for ubiquitination is a highly specific process. We therefore propose that an Ins(1,4,5)P_3-binding-induced conformational change in the receptor exposes a degradation signal that leads to ubiquitination.

Key words: degradation signal, muscarinic, neuroblastoma, ubiquitin.

INTRODUCTION

Ins(1,4,5)P_3 receptors [Ins(1,4,5)P_3Rs] form tetrameric, Ins(1,4,5)P_3-gated Ca^{2+} channels in endoplasmic reticulum membranes, and have a pivotal role in intracellular signalling [1–4]. By governing the release of Ca^{2+} stored in the endoplasmic reticulum, they allow extracellular ligands that activate phosphoinositidase C and elevate Ins(1,4,5)P_3 concentrations to increase cytoplasmic Ca^{2+} concentration [1–4]. Three Ins(1,4,5)P_3R types, termed I, II and III, have been defined [4–8]. These proteins share moderate (60–70%) amino acid sequence identity and the same general structure [4–8], and can combine to form either homotetramers or heterotetramers [9–11].

Persistent phosphoinositidase C activation can cause Ins(1,4,5)P_3R down-regulation [12–18]; Ins(1,4,5)P_3Rs therefore represent a novel locus for the desensitization of phosphoinositidase C-mediated signalling. This down-regulation decreases the sensitivity of Ca^{2+} stores to Ins(1,4,5)P_3 [12,18], is due to accelerated receptor proteolysis [14,15], has a half-time of 0.5–2 h [14–18], can decrease Ins(1,4,5)P_3R levels by as much as 90% [14,15], is evident with all three receptor types [15,17,18], and occurs in a variety of cells *in vitro* [14–18] and *in vivo* [19]. Although the mechanism of Ins(1,4,5)P_3R proteolysis has yet to be defined, it might be executed through the ubiquitin/proteasome pathway [17–20], a pathway crucial to basal and regulated degradation of many cytosolic, nuclear, and membrane proteins [21–25].

The first step in the ubiquitin/proteasome pathway is the conjugation of ubiquitin, a 76-residue protein, to one or more lysine residues in the substrate destined for degradation [21–25]. This ubiquitination is sequentially catalysed by a ubiquitin-activating enzyme (E1), a ubiquitin-conjugating enzyme (E2, or Ubc) and a ubiquitin ligase (E3) [21–25]. Because the newly attached ubiquitin can also be ubiquitinated, targeted proteins become tagged with ubiquitin chains [21–25]. Polyubiquitinated proteins are then recognized and degraded by the proteasome, a 26 S multi-subunit protease [26,27]. Thus ubiquitin conjugation has a central role, and seems to be the rate-limiting step, in directing proteins towards proteasomal degradation [21,26]. Several mechanisms [28–31] have been proposed as the stimulus or 'degradation signal' for ubiquitination but no information is yet available on what activates Ins(1,4,5)P_3R ubiquitination, other than indirect evidence that Ins(1,4,5)P_3 is the trigger; this comes from studies showing that Ins(1,4,5)P_3R ubiquitination is seen only with those agonists that persistently elevate Ins(1,4,5)P_3 concentration [20].

Here we describe studies aimed at defining the event that initiates Ins(1,4,5)P_3R ubiquitination. We have focused on the ubiquitination of wild-type and ligand-binding-defective mutant Ins(1,4,5)P_3Rs stably expressed in human neuroblastoma SH-SY5Y cells. This has allowed us to establish that ligand binding is the stimulus for Ins(1,4,5)P_3 receptor ubiquitination.

EXPERIMENTAL

Cell culture and cell lines

SH-SY5Y cells were grown as monolayers as previously described [15,32]. The generation and maintenance of *S*Ins(1,4,5)P_3RHA and *S*ΔIns(1,4,5)P_3RHA cells, which are transfected SH-SY5Y cells stably expressing haemagglutinin (HA) epitope-tagged mouse cerebellum wild-type type I receptor [Ins(1,4,5)P_3RHA] and binding-defective mutant type I

Abbreviations used: ALLN, *N*-acetyl-Leu-Leu-norleucinal; HA, haemagglutinin; Ins(1,4,5)P_3R, wild-type mouse type I Ins(1,4,5)P_3 receptor; Ins(1,4,5)P_3RHA, HA epitope-tagged Ins(1,4,5)P_3R; ΔIns(1,4,5)P_3RHA, HA epitope-tagged binding-defective Ins(1,4,5)P_3 mouse type I Ins(1,4,5)P_3 receptor; K350RIns(1,4,5)P_3RHA, Ins(1,4,5)P_3RHA with a substitution of arginine for Lys-350.

[1] Present address: Department of Pharmacology and Physiology, University of Rochester Medical Center, Rochester, NY 14642, U.S.A.

[2] To whom correspondence should be addressed (e-mail wojcikir@mail.upstate.edu).

receptor [ΔIns(1,4,5)P_3RHA] respectively, have been described [32]. The HA epitope tag (YPYDVPDYA) was introduced at the receptor C-terminus [32]; the binding-defective mutant receptor lacked 37 residues (316–352) in the ligand-binding domain [33]. Culture medium was changed every 3 days and was replaced 1 day before experiments.

To replace Lys-350 (K350) with arginine (R) in Ins(1,4,5)P_3RHA, pcWIHA, which carries the cDNA insert encoding Ins(1,4,5)P_3RHA [32], was mutated; A^{1377} was changed to G in the codon for K350 (A^{1376}AA^{1378}) by PCR-based site-directed mutagenesis. In brief, primers P1 (5′-ATGTCGTAACAACTCCGCCCCATTG-3′) and P2 (5′-CCAGAGAGTATACCATTCTTTCTTGCGCGTTTC-3′) were used to amplify the region between nt 743 of the vector [32] and 1394 of the insert, and primers P3 (5′-GAAACGCGCAAGAAAGAATGGTATACTCTCTGG-3′) and P4 (5′-CTGCTTCTGCATGAAGCCAAACTGC-3′) were used to amplify the region between nt 1362 and 2080 of the insert. Thus mismatched nucleotides (underlined in P2 and P3) were introduced into the 1589 bp and 718 bp fragments produced. These two fragments were then fused via their overlapping regions through denaturing, annealing and DNA polymerization [32], yielding a 2135 bp sequence. After amplification with P1 and P4, the fusion product was digested with *Kpn*I (New England Biolabs) and was substituted for the corresponding region of pcWIHA, yielding pcK350RWIHA, encoding K350RIns(1,4,5)P_3RHA. The mutation and sequences derived from amplification were validated by DNA sequencing. Stable transfection of SH-SY5Y cells [32] with pcK350RWIHA was performed with LipofectAMINE (Life Technologies).

Measurement of Ins(1,4,5)P_3R ubiquitination

Cells were grown in dishes 10 cm in diameter to confluence and, before exposure to agonist, were preincubated for 2 h with *N*-acetyl-Leu-Leu-norleucinal (ALLN), a potent proteasome inhibitor [34] that leads to the accumulation of ubiquitinated proteins within cells [17,20]. Agonist-stimulated or control cells were then disrupted for 20 min in ice-cold lysis buffer [150 mM NaCl/50 mM Tris base/1 mM EDTA/1 % (v/v) Triton X-100/0.2 mM PMSF/1 mM dithiothreitol/10 μM leupeptin/10 μM pepstatin/0.2 μM soybean trypsin inhibitor (pH 8.0); 1 ml per dish of cells] and were centrifuged (14000 ***g*** for 10 min at 4 °C). Supernatants were then incubated for 2 h at 4 °C with either 100 μl of CT1 {an affinity-purified rabbit polyclonal antibody against the type I Ins(1,4,5)P_3R [15]} or 2 μl of HA11 (a mouse monoclonal antibody against the HA epitope [32]) and then for a further 2 h at 4 °C with 10 mg of Protein A-conjugated Sepharose CL-4B beads. The immunoprecipitates were then washed four times with 1 ml of lysis buffer and were finally resuspended in 80 μl of gel-loading buffer [100 mM Tris/HCl (pH 6.8)/200 mM dithiothreitol/4 % (w/v) SDS/0.2 % Bromophenol Blue/20 % (v/v) glycerol]. Samples and prestained molecular mass markers were then separated by SDS/PAGE [5 % (w/v) gel], transferred to nitrocellulose membranes and probed with CT1, HA11 or polyclonal anti-ubiquitin as described [20]. Immunoreactivity was detected by enhanced chemiluminescence (Pierce) and X-ray film [15,20], and was quantified with Quantity One software (Bio-Rad), using the range in which band intensity was linearly related to the quantity of ubiquitinated receptors loaded. Molecular mass values and quantified chemiluminescence are expressed as means ($n = 3$) or means ± S.E.M. ($n = 3$).

To measure selectively the ubiquitination of HA-tagged Ins(1,4,5)P_3Rs, a two-step immunoprecipitation procedure [20] was performed to concentrate ubiquitinated species. In brief, in step 1, HA11-derived immunoprecipitates were prepared, washed three times with 1 ml of 150 mM NaCl/50 mM Tris base (pH 8.0)/1 mM EDTA/0.2 % (v/v) Triton X-100 and heated for 3 min at 100 °C in 100 μl of 150 mM NaCl/50 mM Tris base (pH 8.0)/1 mM EDTA/20 mM dithiothreitol/1 % (w/v) BSA/1 % (w/v) SDS. This denatured the immunoprecipitated proteins, causing disassembly of the immune complex and dissociation of Ins(1,4,5)P_3R tetramers [20]. The samples were then centrifuged (500 ***g*** for 1 min at 20 °C) and supernatants were collected and diluted with 0.9 ml of ice-cold lysis buffer. In step 2, half of the diluted supernatants were incubated with 1.5 μl of monoclonal anti-ubiquitin for 2 h and then with Protein A beads for 2 h at 4 °C to precipitate ubiquitinated receptors; the remainder, which served as a control, was processed identically, except that monoclonal anti-ubiquitin was omitted. After four washes with 1 ml of lysis buffer, the beads were resuspended in 80 μl of gel-loading buffer and were probed in immunoblots with CT1, HA11 and polyclonal anti-ubiquitin.

Materials

Sources of materials for cell culture, immunoprecipitation, immunoblotting, transfection, and PCR were as defined previously [15,20,32].

RESULTS

Ins(1,4,5)P_3R ubiquitination in human neuroblastoma SH-SY5Y cells

Before transfection of Ins(1,4,5)P_3R cDNA species, we sought to determine whether 'endogenous' Ins(1,4,5)P_3Rs in SH-SY5Y cells, which are predominantly (more than 99 %) type I [15], are ubiquitinated and whether ubiquitination of these receptors is

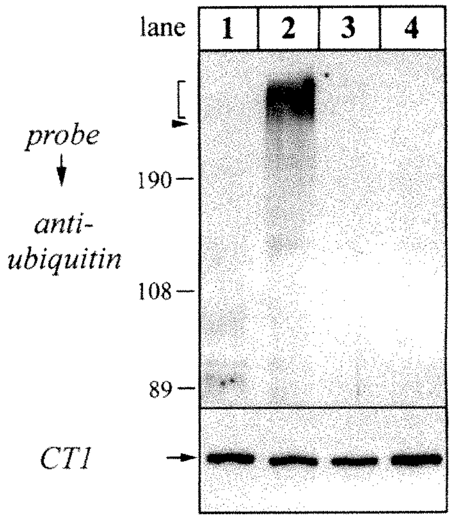

Figure 1 Ins(1,4,5)P_3R ubiquitination is stimulated by muscarinic receptor activation

SH-SY5Y cell monolayers were preincubated with ALLN (20 μg/ml) for 2 h and then exposed for 1 h to vehicle (lane 1), 1 mM carbachol (lane 2), 10 μM atropine (lane 3) or 1 mM carbachol plus 10 μM atropine (lane 4). Ins(1,4,5)P_3Rs were then immunoprecipitated with CT1, resolved by SDS/PAGE [5% (w/v) gel] and probed in immunoblots with either polyclonal anti-ubiquitin (upper panel) or CT1 (lower panel). The migration positions of molecular mass markers (in kDa) (lines), type I Ins(1,4,5)P_3Rs (arrow) and ubiquitinated Ins(1,4,5)P_3Rs (square bracket) are indicated. The arrowhead indicates the position to which unmodified type I Ins(1,4,5)P_3Rs migrated. The images shown (the lower panel being only the approx. 190–380 kDa region of a gel) are representative of three independent experiments.

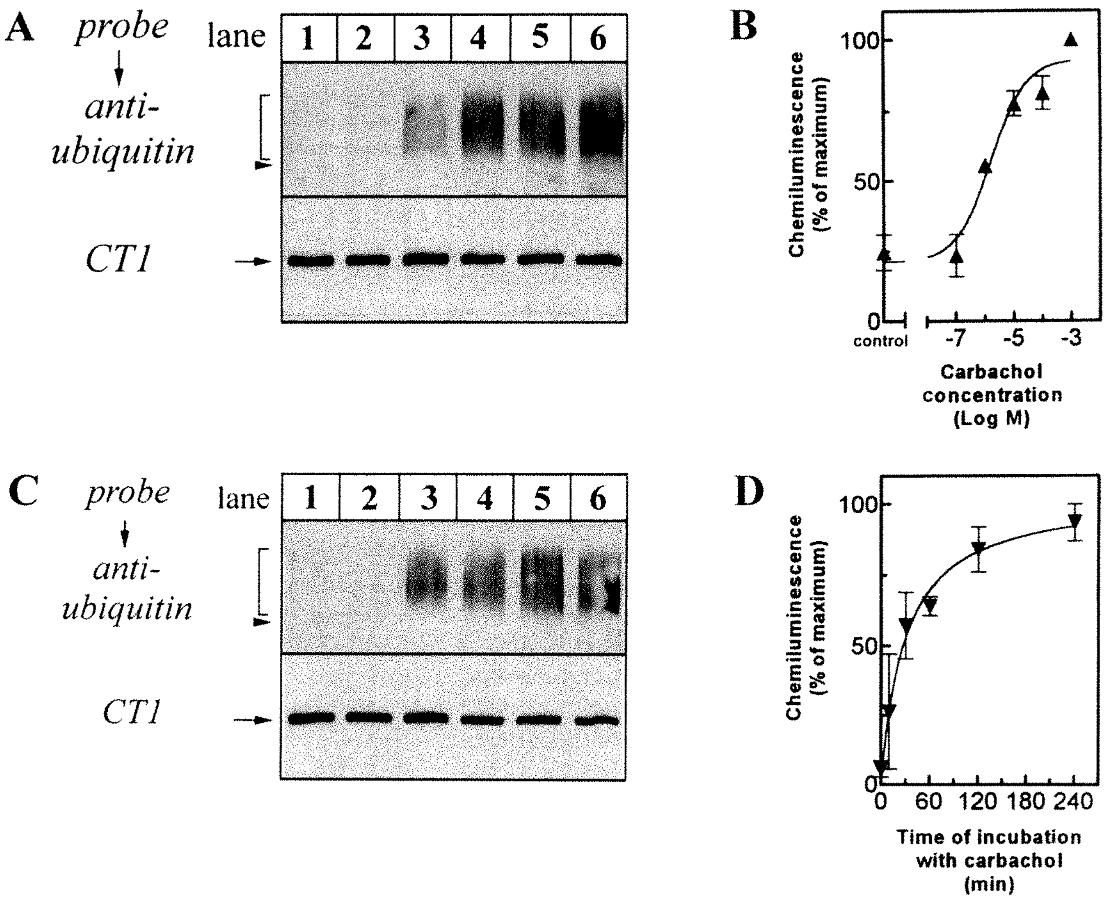

Figure 2 Concentration- and time-dependence of Ins(1,4,5)P_3R ubiquitination

SH-SY5Y cell monolayers were preincubated with ALLN (20 μg/ml) for 2 h and then exposed for 1 h to 0, 0.1, 1, 10, 100 or 1000 μM carbachol (**A**, lanes 1–6) or to 10 μM carbachol for 0, 10, 30, 60, 120 or 240 min (**C**, lanes 1–6). Ins(1,4,5)P_3Rs were then immunopurified, probed and labelled as in Figure 1. The images shown (upper panels, approx. 190–420 kDa; lower panels, approx. 190–380 kDa) are representative of three independent experiments. (**B**, **D**) Quantified ubiquitin immunoreactivity is also expressed as a percentage of maximal chemiluminescence.

correlated with the characteristics of muscarinic agonist (carbachol)-induced Ins(1,4,5)P_3R down-regulation described previously for this cell type [13–16]. Figure 1 shows that carbachol does indeed cause the association of ubiquitin immunoreactivity with immunoprecipitated type I receptors. The apparent molecular mass of the ubiquitinated species ranged from 285 to 383 kDa, was centred on 323±6 kDa (Figure 1, upper panel, lane 2), and was considerably greater than that of unmodified type I Ins(1,4,5)P_3Rs (approx. 260 kDa). This observation indicates that carbachol stimulates Ins(1,4,5)P_3R polyubiquitination, and agrees with findings from agonist-stimulated WB rat liver epithelial cells [17], AR4-2J rat pancreatoma cells, INS-1 rat insulinoma cells and neonatal rat cerebellar granule cells [20], in which polyubiquitinated Ins(1,4,5)P_3Rs migrated similarly. Ins(1,4,5)P_3R down-regulation was not substantial in these experiments (Figure 1, lower panel, compare lanes 1 and 2), because the proteasome inhibitor ALLN was included in incubations. However, despite this blockade and the accumulation of ubiquitinated species, we were unable to detect CT1 immunoreactivity in the area in which ubiquitinated Ins(1,4,5)P_3Rs migrated (Figure 1, lower panel, lane 2), indicating that the steady-state level of ubiquitinated Ins(1,4,5)P_3Rs in stimulated cells remained low. This was consistent with findings in other cell types [17,20] and might reflect the activity of de-ubiquitinating enzymes [20] or feedback inhibition of Ins(1,4,5)P_3R ubiquitination by accumulating ubiquitinated species; it was not due to masking of the CT1 epitope by ubiquitin [20]. Figure 1 (upper panel, lane 4) also shows that the effects of carbachol were muscarinic-receptor-mediated, because atropine, a specific muscarinic receptor antagonist, totally blocked the appearance of ubiquitin immunoreactivity.

Analysis of the concentration dependence (Figures 2A and 2B) and the time course (Figures 2C and 2D) of ubiquitination revealed that the response had an EC_{50} of approx. 1 μM carbachol and a half-time of approx. 30 min. These results are similar to those for the carbachol-induced down-regulation of the type I Ins(1,4,5)P_3R in this cell type, which were approx. 0.1 μM and approx. 1 h respectively [14]; the discrepancies might reflect the inclusion of ALLN in the present study. Thus Ins(1,4,5)P_3R ubiquitination in SH-SY5Y cells occurs with characteristics consistent with its having a role in mediating Ins(1,4,5)P_3R down-regulation.

Ins(1,4,5)P_3R ubiquitination in SH-SY5Y cells transfected with Ins(1,4,5)P_3R cDNA species

To define whether Ins(1,4,5)P_3 binding is important in initiating Ins(1,4,5)P_3R ubiquitination, we generated *S*Ins(1,4,5)P_3RHA

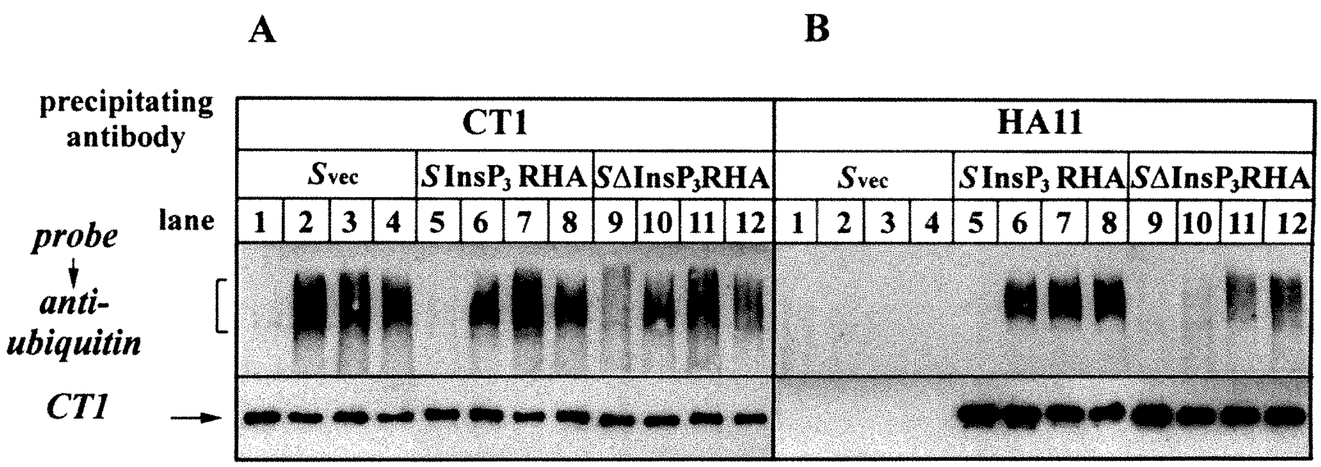

Figure 3 Ins(1,4,5)P_3R ubiquitination in cells expressing exogenous Ins(1,4,5)P_3Rs

$S_{\rm vec}$ (lanes 1–4), *S*Ins(1,4,5)P_3RHA (lanes 5–8), and *S*ΔIns(1,4,5)P_3RHA (lanes 9–12) cell monolayers were pretreated with ALLN (20 μg/ml) for 2 h and then exposed to 1 mM carbachol for 0 h (lanes 1, 5, 9), 0.5 h (lanes 2, 6, 10), 2 h (lanes 3, 7, 11) or 4 h (lanes 4, 8, 12). Ins(1,4,5)P_3Rs were then immunoprecipitated with either CT1 (**A**) or HA11 (**B**), resolved by SDS/PAGE [5% (w/v) gel] and probed in immunoblots with polyclonal anti-ubiquitin (upper panels) or CT1 (lower panels). The migration positions of type I Ins(1,4,5)P_3Rs (arrow) and ubiquitinated Ins(1,4,5)P_3Rs (square bracket) are indicated. The images shown (upper panels, approx. 190–420 kDa; lower panels, approx. 220–320 kDa) are representative of three independent experiments.

and *S*ΔIns(1,4,5)P_3RHA, SH-SY5Y cell lines that stably expressed HA-tagged wild-type and binding-defective mutant Ins(1,4,5)P_3Rs respectively, at levels 2–4-fold those of endogenous type I receptors [32]. Previous work with these cells had shown (1) that the endogenous and 'exogenous' HA-tagged Ins(1,4,5)P_3Rs assemble into heteromers and form functional Ins(1,4,5)P_3-sensitive Ca^{2+} channels, (2) that carbachol-induced Ins(1,4,5)P_3 generation and Ca^{2+} mobilization in intact cells are essentially unaffected by the expression of either Ins(1,4,5)P_3RHA or ΔIns(1,4,5)P_3RHA, and (3) that CT1 recognizes and immunoprecipitates both [32].

Figure 3 depicts the ubiquitination of Ins(1,4,5)P_3Rs in *S*Ins(1,4,5)P_3RHA and *S*ΔIns(1,4,5)P_3RHA cells and in control cells ($S_{\rm vec}$, SH-SY5Y cells transfected with empty vector [32]). To facilitate the comparison of the efficiencies of receptor ubiquitination, differences between the cell lines in receptor expression levels were compensated for by the loading of approximately equal amounts of immunopurified receptors for each cell line under control conditions (Figure 3A, lower panel, lanes 1, 5 and 9, and Figure 3B, lower panel, lanes 5 and 9). Consistent with SH-SY5Y cells (Figure 1) was the observation that carbachol stimulated the polyubiquitination of CT1-immunoprecipitatable Ins(1,4,5)P_3Rs in the three cell lines (Figure 3A, upper panel). Little difference in the time course and the extent of receptor ubiquitination was seen between $S_{\rm vec}$ and *S*Ins(1,4,5)P_3RHA (lanes 1–4 and 5–8) cells, whereas ubiquitination was somewhat attenuated in *S*ΔIns(1,4,5)P_3RHA cells (lanes 9–12). These results suggest that, whereas Ins(1,4,5)P_3RHA ubiquitination proceeds normally, ΔIns(1,4,5)P_3RHA might be resistant to ubiquitination.

Note that the ubiquitin immunoreactivity detected in Figure 3(A) was derived from both endogenous and exogenous Ins(1,4,5)P_3Rs, because CT_1 interacts with both [32]. To examine more selectively the ubiquitination of exogenous Ins(1,4,5)P_3Rs, we also used HA11, which interacts only with HA-tagged receptors [32], as an immunoprecipitating agent. Owing to receptor heteromerization, however, a minor proportion of the receptors recovered will be co-immunoprecipitating endogenous receptors [32]. Figure 3(B) shows that HA11 did not immunoprecipitate material from $S_{\rm vec}$ cells (lanes 1–4), as expected, and that HA11-immunopurified receptors from *S*Ins(1,4,5)P_3RHA cells cross-reacted with anti-ubiquitin in a similar fashion to CT1-immunopurified endogenous receptors (compare Figure 3B, upper panel, lanes 5–8, with Figure 3A, upper panel, lanes 1–4), suggesting again that Ins(1,4,5)P_3RHA is ubiquitinated normally. Strikingly, a parallel analysis of *S*ΔIns(1,4,5)P_3RHA cells yielded much less ubiquitin immunoreactivity (Figure 3B, lanes 9–12), indicating that ΔIns(1,4,5)P_3RHA ubiquitination was severely impaired; the residual ubiquitin immunoreactivity (lanes 9–12) might have originated from ubiquitinated endogenous Ins(1,4,5)P_3Rs that co-immunoprecipitated with ΔIns(1,4,5)P_3RHA [32]. It is therefore plausible that ΔIns(1,4,5)P_3RHA is totally resistant to ubiquitination.

To confirm or refute this suggestion, equal quantities of HA11-immunopurified receptor complexes from stimulated *S*Ins(1,4,5)P_3RHA and *S*ΔIns(1,4,5)P_3RHA cells (obtained as in Figure 3B) were disrupted by being heated in the presence of 1 % (w/v) SDS, and then ubiquitinated receptors were isolated by immunoprecipitation. Figure 4(A) (lower panel, lane 1) shows, as expected, that receptors so isolated from *S*Ins(1,4,5)P_3RHA cells cross-reacted strongly with polyclonal anti-ubiquitin. Furthermore, and in contrast with the findings in Figures 1, 2 and 3, these receptors were now also recognized by CT1 (Figure 4A, lane 1, top panel), apparently because of the enrichment of ubiquitinated species [20]. Importantly, HA11 also recognized these receptors (Figure 4A, middle panel, lane 1), confirming that ubiquitin was conjugated to Ins(1,4,5)P_3RHA. Note also that immunoreactive bands were not detectable in control samples from this cell type (Figure 4A, middle panel, lane 3). When the same procedure was applied to *S*ΔIns(1,4,5)P_3RHA cells, only weak immunoreactivity to either anti-ubiquitin (Figure 4A, bottom panel, lane 2) or CT1 (top panel, lane 2) was identified and, strikingly, specific immunoreactivity against HA11 in the region corresponding to ubiquitinated receptors was not detected (middle panel, lane 2), indicating that ΔIns(1,4,5)P_3RHA was totally resistant to ubiquitination. Note that a background of non-specific immunoreactivity is present in both lanes 1 and 2 of Figure 4(A) (middle panel), apparently because, in this case,

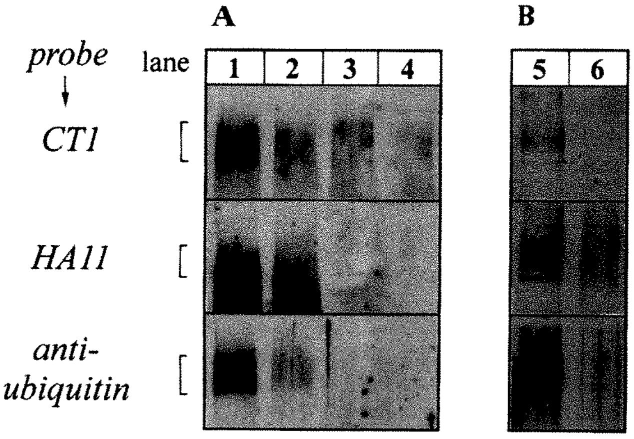

Figure 4 Ubiquitination of exogenous Ins(1,4,5)P_3Rs

SIns(1,4,5)P_3RHA (lanes 1 and 3), ***S***ΔIns(1,4,5)P_3RHA (lanes 2 and 4) and **S**K350RIns-(1,4,5)P_3RHA (lanes 5 and 6) cell monolayers were pretreated with ALLN (20 μg/ml) for 2 h and then exposed to 1 mM carbachol for 1 h. Ins(1,4,5)P_3Rs were then immunoprecipitated with HA11 and disrupted by being boiled in the presence of 1% (w/v) SDS. The dissociated receptors were then immunoprecipitated with monoclonal anti-ubiquitin to concentrate ubiquitinated receptors (lanes 1, 2 and 5). As controls, duplicate samples were processed identically except that monoclonal anti-ubiquitin was omitted (lanes 3, 4 and 6). After separation by SDS/PAGE [5% (w/v) gel], samples were probed with CT1 (top panel), HA11 (middle panel) or polyclonal anti-ubiquitin (bottom panel). The migration positions of ubiquitinated Ins(1,4,5)P_3Rs are denoted by square brackets. Images (approx. 220–420 kDa) shown are representative of three (**A**) or two (**B**) independent experiments.

HA11 was used both as the immunoprecipitating antibody and the probing antibody; the band corresponding to ubiquitinated receptors in lane 1 is superimposed on this background. The lack of immunoreactivity to HA11 (Figure 4A, middle panel, lane 2) also indicates that the weak immunoreactivity to anti-ubiquitin and CT1 was derived from ubiquitinated co-immunoprecipitating endogenous receptors [32], and that the low level of ubiquitin immunoreactivity seen in Figure 3(B) (upper panel, lanes 10–12) had the same origin. Remarkably, therefore, these results also reveal that individual subunits in a tetrameric channel can be differentially targeted for ubiquitination.

Mutation of K350 does not affect Ins(1,4,5)P_3R ubiquitination

Although the total resistance of ΔIns(1,4,5)P_3RHA to ubiquitination (Figure 4A) most probably reflects its inability to bind Ins(1,4,5)P_3, the possibility also exists that the 316–352 deletion in ΔIns(1,4,5)P_3RHA might have removed lysine residues that were ubiquitin conjugation sites. Indeed, the deletion did remove one lysine residue, K350. Therefore, to define the importance of K350 to receptor ubiquitination, we replaced it with arginine, to which ubiquitin cannot be conjugated, and stably expressed this mutant [K350RIns(1,4,5)P_3RHA] in SH-SY5Y cells.

Figure 4(B) (lane 5) shows that in response to carbachol, immunopurified K350RIns(1,4,5)P_3RHA was recognized by CT1, HA11 and anti-ubiquitin, indicating that it was ubiquitinated and that the loss of K350 could not account for the resistance of ΔIns(1,4,5)P_3RHA to ubiquitination. Consistent with this observation was our finding that carbachol caused Ins(1,4,5)P_3R down-regulation in *S*K350RIns(1,4,5)P_3RHA cells (results not shown) to an extent indistinguishable from that seen in *S*Ins(1,4,5)P_3RHA cells [32], indicating that the K350R mutation did not affect Ins(1,4,5)P_3R down-regulation.

DISCUSSION

In the present study we have demonstrated (1) that muscarinic receptor stimulation activates type I Ins(1,4,5)P_3R ubiquitination in SH-SY5Y cells and that this correlates well with the characteristics of Ins(1,4,5)P_3R down-regulation in this cell type, (2) that ligand-binding-defective mutant Ins(1,4,5)P_3Rs are resistant to ubiquitination, (3) that K350, which is missing from the mutant Ins(1,4,5)P_3Rs, is not required for Ins(1,4,5)P_3R ubiquitination, and (4) that individual Ins(1,4,5)P_3R subunits in a tetrameric channel are differentially targeted for ubiquitination (only those subunits with ligand-binding activity are ubiquitinated). We therefore conclude that Ins(1,4,5)P_3 binding is directly responsible for initiating Ins(1,4,5)P_3R ubiquitination and that the targeting of Ins(1,4,5)P_3Rs for ubiquitination is a highly specific process. Importantly, these results can account for our previous findings [32] that ΔIns(1,4,5)P_3RHA is resistant to carbachol-initiated down-regulation and strengthen the causal link between ubiquitination and receptor degradation. They also agree with findings [32] that only the endogenous Ins(1,4,5)P_3Rs in ΔIns(1,4,5)P_3RHA-containing heterotetramers are degraded in response to carbachol.

This selectivity argues against the suggestion [16] that mobilized Ca^{2+} might stimulate Ins(1,4,5)P_3R degradation, perhaps by activating ubiquitination, a possibility given credence by observations that domains of high Ca^{2+} concentration exist near the mouth of open Ins(1,4,5)P_3R channels [2]. If this were so, then ubiquitination and degradation of all subunits in a tetramer should be accelerated simultaneously whether or not they bound Ins(1,4,5)P_3, because they would all be exposed to the high Ca^{2+} concentrations.

Rather, our results point to two possible mechanisms by which Ins(1,4,5)P_3 binding could initiate Ins(1,4,5)P_3R ubiquitination. First, ubiquitination could result from a modification of interactions between tetramerized receptor subunits. The degradation signal that mediates ubiquitination in each subunit could be shielded by other subunits of the tetrameric complex; Ins(1,4,5)P_3-induced subunit reorganization could expose this region. This type of mechanism has been observed for the yeast transcription factors α2 and a1, both of which, when expressed alone, are short-lived proteins that are degraded through the ubiquitin/proteasome pathway [35,36]. However, when co-expressed they heterodimerize, their degradation signals become masked, and they are stable [35,36]. Although theoretically possible, it is, however, hard to envisage how only the degradation signal of endogenous receptors, and not mutant receptors, could be exposed after Ins(1,4,5)P_3-driven conformational changes to a tetramer. Second, and perhaps more likely, is the possibility that conformational changes within individual subunits account for receptor ubiquitination. In this model, the degradation signal of each receptor subunit is buried intramolecularly and exposure of this signal is triggered by Ins(1,4,5)P_3-binding-induced conformational changes. Thus ligand-occupied endogenous Ins(1,4,5)P_3Rs in ΔIns(1,4,5)P_3RHA-containing channels are ubiquitinated, whereas ΔIns(1,4,5)P_3RHA subunits are not. This mechanism would be analogous to the ubiquitin-dependent destruction of misfolded proteins in the endoplasmic reticulum, in which the exposure of normally buried hydrophobic motifs seems to have a role [28,37]; Ins(1,4,5)P_3-induced conformational changes might similarly cause the exposure of hydrophobic regions.

It is important to consider that these models are valid only if the 316–352 deletion has not removed a ubiquitin conjugation site or the putative degradation signal. K350, which is conserved in types I, II and III receptors [4–8], is indeed removed by this deletion; however, Ins(1,4,5)P_3Rs with a substitution of arginine for K350 are ubiquitinated and down-regulated normally, indicating that K350 is not required for Ins(1,4,5)P_3R ubiquitination. Furthermore, region 316–352 is not compatible with known degradation signals; this sequence is highly hydrophilic [5], whereas degradation signals are often stretches of hydrophobic residues [31,35]. In addition, as all three Ins(1,4,5)P_3Rs are ubiquitinated in response to phosphoinositidase C activation [17–20], it would be expected that the 316–352 region would be highly conserved between receptors if it were the degradation signal. This, however, is not so: the 316–352 region is poorly conserved in types I, II and III receptors (only 16 % similarity in this region).

Taken together, our results show that Ins(1,4,5)P_3 binding initiates Ins(1,4,5)P_3R ubiquitination, possibly by causing a conformational change that exposes a degradation signal. The ubiquitinated receptors are then translocated to proteasomes for degradation. To define the putative degradation signal and the enzymes that mediate Ins(1,4,5)P_3R ubiquitination is a challenging goal for future studies.

We thank Dr Jon Oberdorf, Dr Mary Lou Vallano, Dr Barry E. Knox and Mr Jack M. Webster for many helpful discussions, and Dr T Furuichi and Dr K Mikoshiba for providing the mouse type I Ins(1,4,5)P_3 cDNA from which the constructs used in this study were generated This work was supported by a grant from NIH (DK49194) and a grant-in-aid from the American Heart Association (NY State Affiliate)

REFERENCES

1 Berridge, M J. (1993) Nature (London) **361**, 315–325
2 Clapham, D E (1995) Cell **80**, 259–268
3 Berridge, M J, Bootman, M D and Lipp, P (1998) Nature (London) **395**, 645–648
4 Patel, S, Joseph, S K and Thomas, A P (1999) Cell Calcium **25**, 247–264
5 Furuichi, T, Yoshikawa, S., Miyawaki, A, Wada, K, Maeda, N and Mikoshiba, K (1989) Nature (London) **342**, 32–38
6 Mignery, G A, Newton, C L, Archer, III, B T and Sudhof, T C (1990) J Biol Chem. **265**, 12679–12685
7 Sudhof, T C, Newton, C L, Archer, III, B T, Ushkaryov, Y A and Mignery, G A (1991) EMBO J **10**, 3199–3206
8 Blondel, O, Takeda, J., Janssen, H, Seino, S and Bell, G I. (1993) J Biol Chem **268**, 11356–11363
9 Wojcikiewicz, R J H and He, Y (1995) Biochem Biophys Res Commun **213**, 334–341
10 Joseph, S K, Lin, C, Pierson, S., Thomas, A P and Maranto, A R (1995) J Biol Chem **270**, 23310–23316
11 Morikawa, T, Miyawaki, A, Sugiyama, T, Yoneshima, H, Yamamoto-Hino, M, Furuichi, T, Saruta, T, Hasegawa, M and Mikoshiba, K (1995) J. Biol Chem **270**, 14700–14704
12 Wojcikiewicz, R J H and Nahorski, S R (1991) J Biol Chem **266**, 22234–22241
13 Wojcikiewicz, R J. H., Nakade, S., Mikoshiba, K. and Nahorski, S R (1992) J Neurochem **59**, 383–386
14 Wojcikiewicz, R J H, Furuichi, T, Nakade, S, Mikoshiba, K and Nahorski, S R (1994) J Biol Chem **269**, 7963–7969
15 Wojcikiewicz, R J. H (1995) J Biol Chem **270**, 11678–11683
16 Wojcikiewicz, R J H and Oberdorf, J A (1996) J Biol Chem **271**, 16652–16655
17 Bokkala, S and Joseph, S K (1997) J Biol Chem. **272**, 12454–12461
18 Sipma, H, Deelman, L., Smedt, H D, Missiaen, L, Parys, J B, Vanlingen, S., Henning, R H and Casteels, R (1998) Cell Calcium **23**, 11–21
19 Wojcikiewicz, R J H, Ernst, S A and Yule, D. I (1999) Gastroenterology **116**, 1194–1201
20 Oberdorf, J, Webster, J M, Zhu, C-C, Luo, S. and Wojcikiewicz, R J H (1999) Biochem. J **339**, 453–461
21 Hershko, A and Ciechanover, A (1998) Annu Rev. Biochem **67**, 425–479
22 Bonifacino, J. S and Weissman, A M (1999) Annu Rev Cell Dev Biol **14**, 19–57
23 Hochstrasser, M (1996) Annu. Rev Genet **30**, 405–439
24 Hochstrasser, M (1995) Curr. Opin Cell Biol **7**, 215–223
25 Hicke, L (1999) Trends Cell Biol **9**, 107–112
26 Baumeister, W, Walz, J, Zuhl, F. and Seemuller, E. (1998) Cell **92**, 367–380
27 Ciechanover, A (1998) EMBO J **17**, 7151–7160
28 Laney, J D and Hochstrasser, M (1999) Cell **97**, 427–430
29 Varshavsky, A (1997) Trends Biochem Sci **22**, 383–387
30 Brown, K., Gerstberger, S, Carlson, L, Franzoso, G. and Siebenlist, U (1995) Science **267**, 1485–1488
31 Gilon, T, Chomsky, O. and Kulka, R G (1998) EMBO J. **17**, 2759–2766
32 Zhu, C-C, Furuichi, T, Mikoshiba, K and Wojcikiewicz, R J H (1999) J Biol Chem **274**, 3476–3484
33 Miyawaki, A, Furuichi, T., Ryou, Y, Yoshikawa, S, Nakagawa, T, Saitoh, T and Mikoshiba, K (1991) Proc Natl Acad. Sci USA **88**, 4911–4915
34 Mellgren, R L (1997) J Biol Chem **272**, 29899–29903
35 Johnson, P R, Swanson, R, Rakhilina, L and Hochstrasser, M. (1998) Cell **94**, 217–227
36 Chen, P, Johnson, P, Sommer, T, Jentsch, S and Hochstrasser, M (1993) Cell **74**, 357–369
37 Kopito, R. R (1997) Cell **88**, 427–430

Received 15 October 1999/24 January 2000, accepted 15 March 2000

Biochem J (2000) 348, 557–563 (Printed in Great Britain)

Atomic force microscopy of gastric mucin and chitosan mucoadhesive systems

Matthew P. DEACON*†, Simon McGURK†, Clive J. ROBERTS†, Phillip M. WILLIAMS†, Saul J. B. TENDLER†, Martyn C. DAVIES†, S. S. (Bob) DAVIS† and Stephen E. HARDING*[1]

*University of Nottingham, NCMH Physical Biochemistry Laboratory, School of Biosciences, Sutton Bonington LE12 5RD, U.K., and †University of Nottingham, School of Pharmacy, University Park, Nottingham NG7 2RD, U.K.

Atomic force microscopy has been utilized to probe, at a molecular level, the interaction between purified pig gastric mucin (PGM) and a mucoadhesive cationic polymer, chitosan (sea cure 210+); with a low degree (approx. 11 %) of acetylation. Images were produced detailing the structures of both PGM and chitosan in 0.1 M acetate buffer (pH 4.5), followed by the complex of the two structures in the same buffer. PGM in 0.1 M acetate buffer revealed long linear filamentous structures, consistent with earlier electron microscopy and scanning tunnelling micoscopy studies. The chitosan molecules also adopted a linear conformation in the same buffer, although with a smaller average length and diameter. They appeared to adopt a stiff-coil conformation consistent with earlier hydrodynamic measurements The complexes formed after mixing PGM and chitosan together revealed large aggregates. In 0.1 M ionic strength buffer they were of the order of 0.7 μm in diameter, consistent with previous electron microscopy studies. The effect of ionic strength of the buffer on the structure of the complex was also studied and, together with molecular hydrodynamic data, demonstrates that the interaction is principally electrostatic in nature.

Key words: electrostatic complex, interaction, ionic strength.

INTRODUCTION

The last two decades have seen major inroads into our understanding of the molecular architecture of the mucosal layers, which line the gasterointestinal, tracheobronchial, reproductive and ocular systems [1–5]. These advances have been paralleled with increasing efforts by the pharmaceutical industries to develop more efficient ways of delivering drugs. Many of these delivery routes, particularly those through the nasal, ocular, reproductive and gastrointestinal systems, involve contact with mucosal surfaces. The gastrointestinal route has been particularly popular among medical staff and patients alike Although convenient, unfortunately, this route can be very inefficient for a number of reasons, including too rapid transit of the drug-containing delivery system (powder, tablet, suspension, capsule etc.) past the optimum site for absorption, which is normally the small intestine, and, to a lesser degree the stomach and colon. Resolution of this problem would be particularly important in the case of controlled-release drug delivery systems, designed to deliver drugs over extended periods of time (12–24 h). An ideal oral sustained-release dosage form should be comparable to an intravenous infusion, which continuously supplies the amount of drug needed to maintain constant plasma levels once a steady-state has been reached [6].

Attempts are being made to develop mucoadhesive polymer carrier systems for drugs that interact with the mucosal surface in a favourable way. Prime targets have been the gastrointestinal tract and also the ocular surface to (1) retard the natural clearing action of the body, slowing down the transit through the optimal sites of absorption in the stomach, intestine and colon [7] and (2) slow down the washing away action on the surface of the eye [8], respectively. In order to develop the most efficient systems, a sensible approach is to take advantage of the considerable advances in our knowledge of the structure and molecular biology of the principal macromolecular component of mucus, which largely dictates the physical properties of mucus. This is the mucus glycoprotein, or 'mucin', a large [approx. (5–50) thousand kDa] linear polypeptide decked with O-linked carbohydrate side chains, with the carbohydrate forming the bulk of the molecule (approx. 80 %).

The mucoadhesive potential of a range of polymeric substances has already been examined by molecular hydrodynamics, electron microscopy and scanning tunnelling microscopy (see [7] and references therein). One of the most promising substances appears to be derived from the insoluble polysaccharide, chitin [β-(1 → 4)-linked poly-*N*-acetylglucosamine] The derivative is the soluble cationic polymer chitosan, formed from partial deacetylation of the chitin. Interactions with mucin appear to be both electrostatic, via NH_3^+ groups on the chitosan with either COO^- or SO_3^- groups on the mucin carbohydrate side chains, and/or hydrophobic, via $-CH_3$ groups on acetylated chitosan residues with $-CH_3$ groups on mucin side chains [depending on the degree of acetylation of the chitosan, local solvent conditions (pH, ionic strength) and the degree of sulphonation and sialic acid content of the mucin]. These molecular studies have been supported by macroscopic studies involving mechanical measurements based around the tensiometry principle on whole mucus [9].

We now seek to take advantage of the development of the powerful imaging potential of atomic force microscopy (AFM) [10] to (1) examine the structure of a gastrointestinal mucin, pig gastric mucin (PGM), (2) examine the structure of a chitosan with a low degree of acetylation (i e. 11 %) and (3) investigate the interaction of these molecules, already established by molecular hydrodynamic, electron microscopy and scanning tunnelling microscopy probes.

AFM does not require invasive and destructive sample preparation before analysis, unlike most electron microscopic procedures [11], and facilitates the imaging of samples under ambient

---

Abbreviations used AFM, atomic force microscopy, PGM, pig gastric mucin, APTES, aminopropyl-triethoxysilane, RMS, root-mean-square, SC210+, sea cure +210, z, vertical displacement

[1] To whom correspondence should be addressed (e-mail Steve Harding@nottingham ac uk)

temperatures and liquid environments. A recent study [12] has successfully demonstrated the virtue of this approach to the study of ocular mucins. We now focus on gastrointestinal mucin and its mucoadhesive properties with this methodology.

MATERIALS AND METHODS

Materials

PGM (sample MD [13]), was purified and isolated according to the modified procedure described in [14]. The purified mucin preparations were gently defrosted and dialysed into buffer overnight at 4 °C before use. Their molecular integrity (molecular mass distribution) was checked by size-exclusion chromatography coupled to multi-angle laser light scattering ('SEC-MALLS'), as first applied to mucins by Jumel et al. [15]. Sea cure +210 (SC210+), a glutamate salt of chitosan (Pro-Nova Ltd., Drammen, Norway), was used. This is a preparation with a degree of acetylation of 11 %, which has previously been well-characterized in our laboratory [16].

Sample preparation for AFM

Freshly cleaved mica (Agar Scientific, Essex, U.K.) was silanized with aminopropyl-triethoxysilane (APTES). The mica pieces were placed into a glass Petri-dish and three drops of APTES solution were placed on the inner side of the cover. The Petri-dish was then sealed with Parafilm and the sheets were left for 2 h at room temperature. Mucin, chitosan and mixture solutions prepared in 0.1 M sodium acetate buffer, pH 4.5 containing 0.1 M NaCl, [13] were pipetted (20 μl) into an eppendorf. Glycerol solution [15–25 % (v/v)] was then added to a volume of 0.5 ml and left for 30 min. The mica sheets were subsequently coated with the sample solution for 30 s, rinsed with deionized water and then dried with argon. AFM investigation was performed immediately after sample preparation.

AFM

All imaging was performed in air with a Nanoscope IIIa (Digital Instruments, Santa Barbara, CA, U.S.A.). TappingMode™ was employed with a probe constructed from silicon with a length and resonant frequency of 125 μm and 307–375 kHz, respectively (Digital Instruments, Santa Barbara, U.S.A.). All measurements made on the images of structures such as root-mean-square (RMS) 'roughness', vertical displacement (z) and size (width and diameter) were made utilizing the operating software provided with the Nanoscope IIIa AFM. Simultaneously with topographic imaging, phase data were recorded. Such data can reveal contrast based upon adhesion or viscoelastic heterogeneity in a sample surface [17].

RESULTS AND DISCUSSION

Control surfaces

In order to reveal both the thin filamentous nature of the gastric mucin structure previously shown with transmission electron

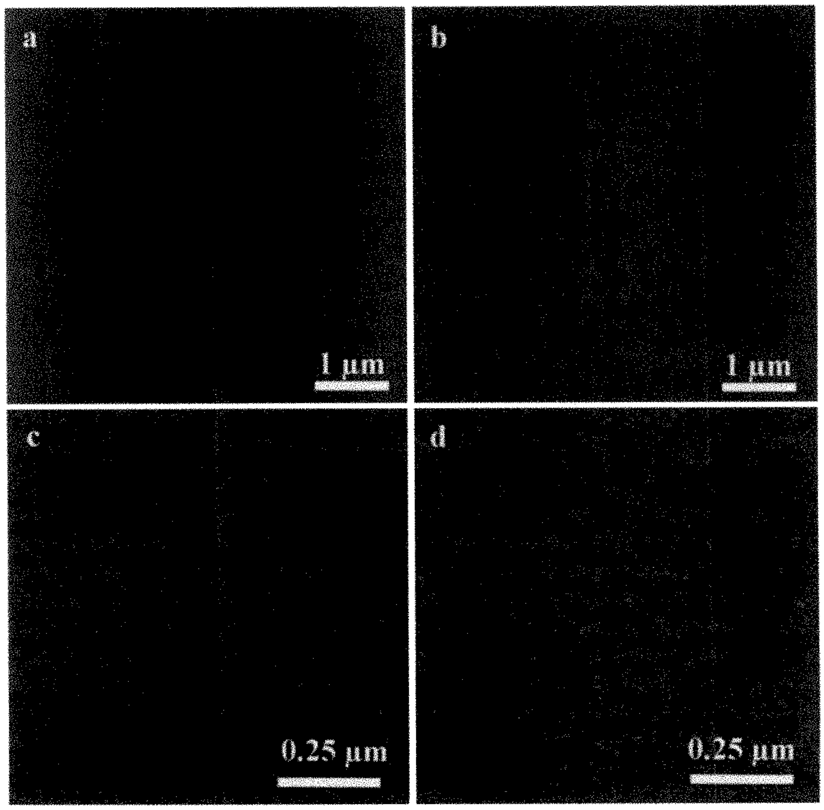

Figure 1 AFM of the substrate mica and APTES-coated mica

Mica (topography) (**a**), mica (phase) (**b**), APTES-coated mica (topography) (**c**) and APTES-coated mica (phase) (**d**).

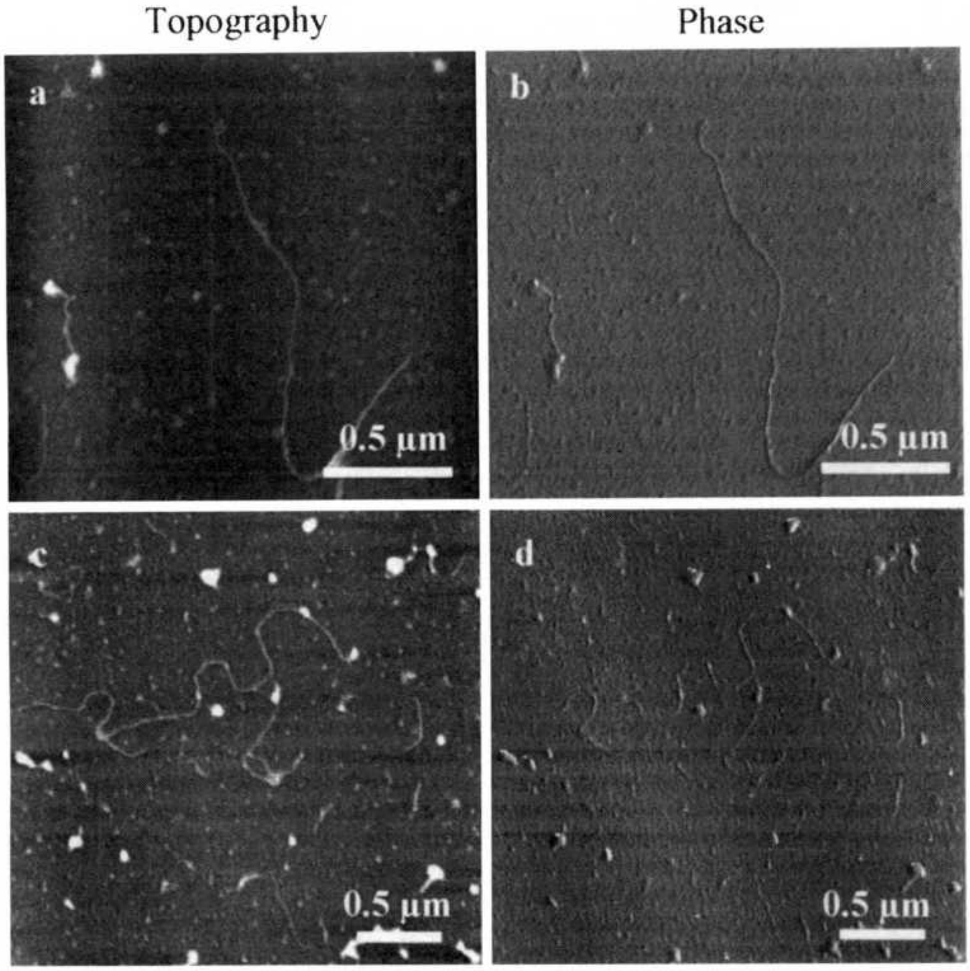

Figure 2 AFM images of purified PGM in 0.1 M ionic strength sodium acetate buffer

Topography images (**a** and **c**) and phase images (**b** and **d**).

[18–20] and scanning tunnelling microscopy [21], together with the previously unvisualized characteristics of chitosan, an extremely flat sample substrate is required. To this end, mica was chosen for this study. Figures 1(a) and 1(b) show an AFM image (topography and phase, respectively) of a clean mica surface. It is evident from this figure that the surface of this sample substrate is flat and featureless with a RMS roughness of 0.11 nm and a 'total z movement' of 0.9 nm (vertical distance moved by the z-piezoelectric scanner in AFM). Hence any further adsorbed material in future sample preparations should be apparent against such a background. Figures 1(c) and 1(d) show topography and phase AFM images, respectively, of the mica sheet that had been treated with APTES. As before, the sample substrate surface was flat and featureless with an RMS roughness of 0.14 nm and total z movement of 1.03 nm. APTES treatment was necessary to attach amino groups to the surface of the mica, to enhance the attraction of the large mucin structures. This attraction has been attributed to a charge interaction between the positive amino groups and the sialic acid or sulphate residues on the mucosal glycoproteins. Structural studies have indicated that the negative charge on PGM is thought to be attributed mostly to the amount of sulphated O-linked oligosaccharide residues in the glycosylated region and not to the amount of sialic acid present [22].

PGM glycoprotein

With the previous imaging studies on PGMs by transmission electron microscopy [18–20], to facilitate visualization it had been necessary to coat the substrate with a thin layer of conductive material, and the mucins themselves were sprayed onto the surface of this substrate. The advantage of AFM over this is that the mucins may be adsorbed directly from solution and do not require further sample treatment prior to visualization.

Figure 2 shows both topography and phase images of PGM adsorbed from solution onto the APTES-treated mica surface. The images were selected at random and are representative of a large library of images, which portray similar structural information and surface coverage. The PGM appears as long filamentous strands, which is in good agreement with previous studies using electron and scanning tunnelling microscopy [18–21], and consistent with the swollen coil array/linear random coil model for mucins [4,23]. The characteristic flattened areas along the backbone seen earlier from electron microscopy for PGM and earlier for bronchial mucins [23] were notably absent. These flattened areas were considered to correspond to the areas of high glycosylation along the polypeptide chain, the flattening

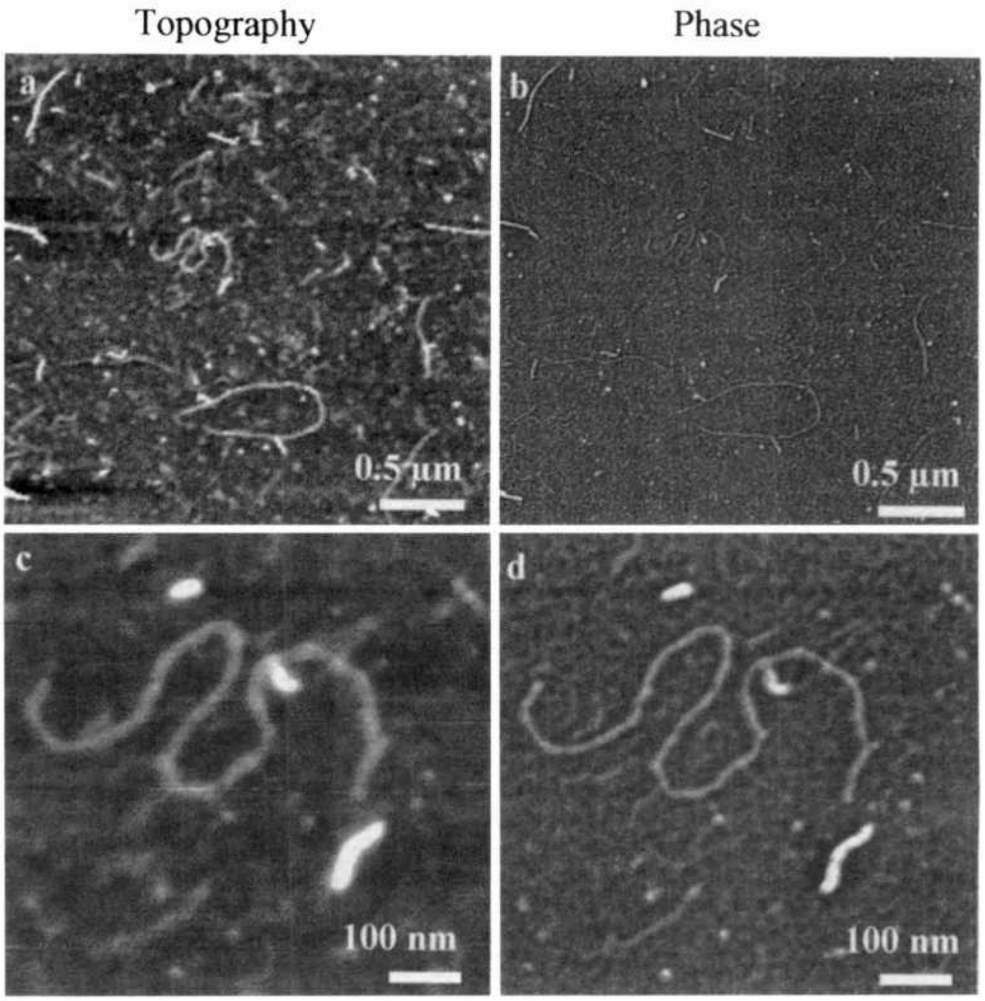

Figure 3 AFM images of chitosan SC210+ in 0.1 M ionic strength sodium acetate buffer

Topography (**a**), phase (**b**), topography (close up) (**c**) and phase (close up) (**d**).

caused by the effect of the vacuation on areas of very high hydration [23]. The molecule would not have been subject to these effects for AFM visualization, and therefore it is not surprising that these regions were not evident from AFM.

From the AFM images of Figure 2 and similar, the average length of the PGM molecules was determined to be approximately 2.00 ± 0.55 μm, which agrees with studies performed with transmission electron microscopy and sedimentation equilibrium experiments [3,4]. However, occasionally some PGM filaments were seen to possess a maximum length of nearly 4 μm and a minimum of 0.5 μm, reflecting the polydisperse nature of the material. The diameters of the filaments were approximately constant, at 16 nm.

Chitosan SC210+

Figure 3 illustrates AFM images of the chitosan (SC210+) molecules. It is possible to see from the larger 0.5 μm image (Figures 3a and 3b) that the structure is extremely polydisperse, with the polysaccharide chain lengths varying extensively. The average length of the polysaccharide was approx. 0.70 ± 0.27 μm, which is smaller than the average backbone length for the PGM. The widths of these polymer chains were very consistent, being approx. 11 nm, which is smaller than for the PGM. This is consistent with the absence of side chain branches in the chitin/chitosan structure. Figures 3(c) and 3(d), which appear to represent a single chitosan chain, reveal that there are no obvious structural features to distinguish this from the mucin glycoprotein. However, the molecules appear to adopt a stiff-coil conformation, consistent with these molecules being Zone B (rigid rod) or Zone C (semi-flexible coil) structures [24,25] depending on the chain length, the shorter chains being more rigid.

Immobilization strategy

The immobilization strategy chosen for this study was aimed at immobilizing the much larger of the two molecules, namely the mucin. A positive surface potential was created to attract the somewhat negatively-charged mucin glycoproteins. Naturally one would not expect any charge attraction between the positively-charged chitosan molecule and the positively-charged surface. However, such observations have been made in the extensive studies of DNA by AFM, whereby negatively-charged DNA is immobilized onto negatively-charged bare mica using $MgCl_2$ or similar buffers [26,27]. The Mg^{2+} ions shield the repulsion that would otherwise occur between the DNA and the mica. Interestingly it has been noted by Bezanilla et al. [26] that

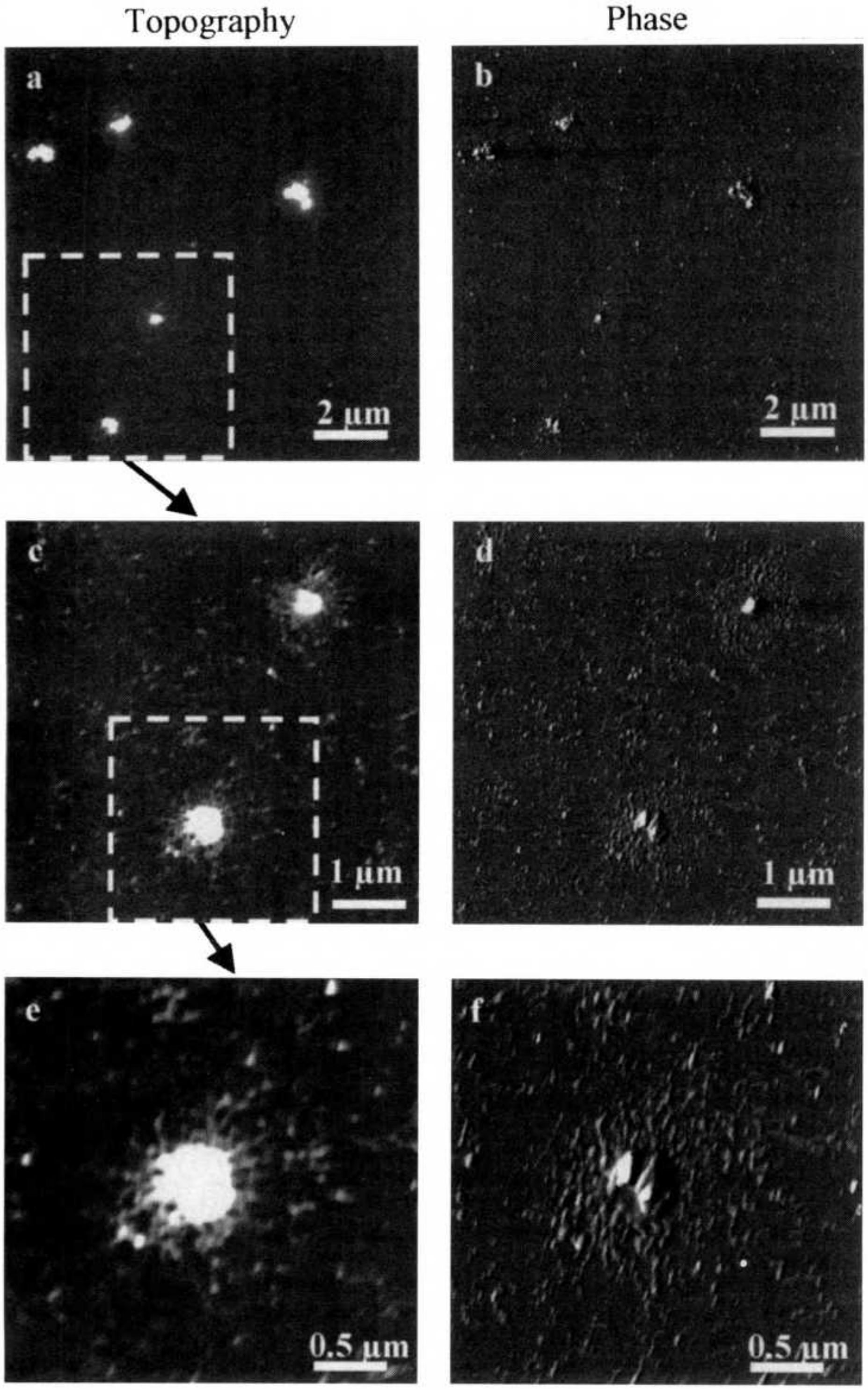

Figure 4 AFM images of PGM complexed with chitosan SC210+ in 0.1 M ionic strength sodium acetate buffer at different degrees of magnification

Figures (**a**, **c** and **e**) were recorded using the topography mode. Figures (**b**, **d** and **f**) were obtained in the phase mode, giving much crisper images.

a lack of DNA adhesion occurs as ionic strength increases, suggesting that the DNA prefers to remain in solution as the ionic strength increases. In a similar fashion we also observed a lack of chitosan adhesion when using higher ionic strength solutions (results not shown).

It is also worth noting that at the lower ionic concentrations employed (0.1 M) the counterion concentration appears insufficient to suppress the repulsive forces between the positively-charged deacetylated units situated along the polymer backbone, which keep the polymer in the extended linear arrangement

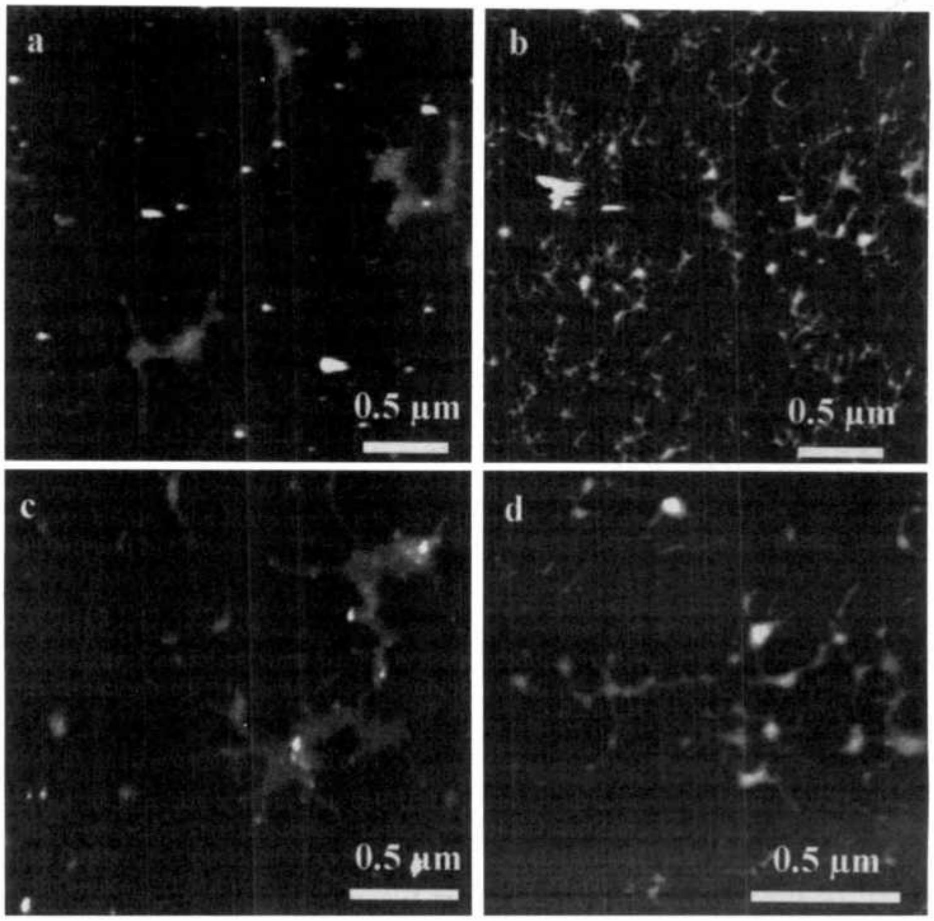

Figure 5 AFM topography images of PGM and PGM complexed with chitosan SC210+ in 0.2 M and 0.3 M ionic strength sodium acetate buffer

PGM at 0.2 M (**a**), PGM–SC210+ complex at 0.2 M (**b**), PGM at 0.3 M (**c**) and PGM–SC210+ complex at 0.3 M (**d**).

observed. As the ionic concentration is increased this repulsion effect is reduced resulting in a more coiled arrangement of the polymer [28]. This may also contribute to the lack of chitosan visualized on the surface at the elevated ionic concentrations.

Complexes of PGM and chitosan at 0.1 M ionic strength

As has been previously indicated [7,19,20,29] a significant interaction has been shown between the purified PGM and this form of chitosan on the basis of molecular hydrodynamics, electron microscopy and scanning tunnelling microscopy, consistent with macroscopic tensiometry studies [9]. Figure 4 illustrates the complex formed between the chitosan and mucin structures when mixed together in solution and then immobilized to the APTES-coated substrate. Instead of the characteristic filamentous nature of both the chitosan and PGM (Figures 2 and 3, respectively) large clump-like aggregates were observed, consistent with the electron microscopy observations of Fiebrig et al. [19,20]. The average diameter of these aggregates, determined by taking two diameter measurements (x and y) on a large number of aggregates (20) was approx. 0.70 ± 0.18 μm (some complexes were seen with radial diameters of approx. 0.3 μm and some as large as approx. 1.2 μm). Surrounding these aggregates was a tangled arrangement of filaments that seemed to emanate from the central aggregate. The diameter of these filaments was approx. 16 nm. This suggests that these filaments were strands of PGM radiating from the complex.

Complexes of PGM and chitosan at 0.2 M and 0.3 M ionic strength

Earlier hydrodynamic studies [13,29] have shown a clear effect on mucin–chitosan complexes by increasing the ionic strength. Figure 5 shows the characteristic mucin (Figures 5a and 5c) and complex (Figures 5b and 5d) structures at 0.2 M and 0.3 M ionic strength, respectively. It is apparent that the structure of the mucin at 0.2 M and 0.3 M ionic strength is quite different to that at 0.1 M ionic strength. At 0.2 M (Figure 5a) the long filamentous structure seen at 0.1 M is no longer present. It was difficult to measure the average length of the mucins at this molar concentration as the structures seemed to be formed from a number of mucin filaments. However, where an individual filament was evident, the average width was equivalent to that in the 0.1 M solution, i.e. approx. 16 nm. This apparent mucin self-interaction effect became more pronounced at the higher 0.3 M ionic strength, shown in Figure 5(c). At this ionic strength there seemed to be many filaments interacting to form more complex aggregates of mucin. The only mucins available for analysis of dimensions were those which emanated from the complex. The average diameter was again 16 nm, but the average length was impossible to determine due to the extent of interaction. If the number of mucin strands which emanate from the mucin complex are counted it shows that, on average, over many complexes imaged, at 0.2 M there are 3–4 mucin strands and at 0.3 M there are 10–11 mucin strands interacting to form the complex. Clearly, increasing the ionic strength seems to promote self-association among the mucin molecules. Ionic strengths < approx. 0.2 M (including physiological conditions) appear to be insufficient to suppress charge repulsion effects on the charged mucin side chains, hence the mucins remain unassociated.

The images presented in Figures 5(b) and 5(d) are the structures of the complexes from the mucin/chitosan mixtures at 0.2 M and 0.3 M ionic strength, respectively. These also display some differences from the structures observed at 0.1 M (Figure 4). While there still appears to be some degree of complex formation between the mucin and chitosan, the size of the complexes is greatly reduced. At 0.1 M large aggregates formed that had an average diameter of 0.7 μm, while at 0.2 M and 0.3 M the smaller aggregate structures visualized had an average diameter of approx. 150 nm (visualized in the same way as those structures at 0.1 M). Noticeably there is a greater number of these 'mucoadhesive complexes' at 0.1 M ionic strength, suggesting a reduction in interaction between the mucin and chitosan as the ionic strength increases beyond physiologically relevant conditions, and consistent with what was observed earlier by molecular hydrodynamics [7,29]. Charge suppression clearly reduces the amount of electrostatic interaction. Although the higher ionic strengths do not represent physiological conditions, the experiments across the range of ionic strengths do appear to demonstrate that it is indeed electrostatic interactions that are important for (1) keeping mucins apart through inter-chain repulsion and (2) promoting mucoadhesive interaction at low (physiological) ionic strength conditions.

Conclusions

There now exists irrefutable evidence that chitosans interact with mucins. The findings in the present study, based on AFM imaging, clearly support the earlier molecular data based on molecular hydrodynamics, electron microscopy and scanning tunnelling microscopy [7]. Molecular imaging, which 'visualizes' macromolecules, coupled with molecular hydrodynamics, which refers to macromolecules in their 'natural physiological state' unperturbed by sample preparation protocols, is clearly a powerful combination for the study of this and other heterogeneous molecular systems. The main contribution towards the interaction is clearly electrostatic, with some hydrophobic contribution [7]. The AFM data also support the macroscopic tensiometric measurements [9]. This demonstration should assist with the design of more efficient gastrointestinal drug delivery systems [30,31].

M P D was in receipt of a BBSRC CASE studentship with Optokem Ltd. (Mold, U K)

Received 2 December 1999/18 February 2000, accepted 27 March 2000

REFERENCES

1 Allen, A, Pain, R. H and Robson, T H. (1976) Nature **264**, 88–89

2 Creeth, J. M (1977) Mod Probl Paediatr. **19**, 34–35

3 Harding, S E (1989) Adv Carbohydr Chem Biochem. **47**, 345–381

4 Sheehan, J. K and Carlstedt, I (1989) in Dynamic Properties of Biomolecular Assemblies (Harding, S E and Rowe, A J, eds), pp 256–275, Royal Society of Chemistry, Cambridge, U.K

5 Gum, J. R (1995) Biochem Soc Trans **23**, 795–799

6 Forster, H and Lippold, B C (1982) Pharmaceutica Acta Helvetica **57**, 345–349

7 Harding, S E, Davis, S S, Deacon, M P and Fiebrig, I. (1999) Biotechnol Gen Eng. Rev. **16**, 41–86

8 Greaves, J L and Wilson, C G (1993) Adv. Drug Delivery Rev **11**, 349–383

9 Lehr, C-M, Bouwstra, J A., Schacht, E H. and Junginger, H E (1992) Int J Pharm **78**, 43–48

10 Binnig, G., Quate, C F. and Gerber, C H (1986) Phys Rev Lett **56**, 930–933

11 Kirby, A R, Gunning, A P and Morris, V J (1995) Trends Food Sci Technol **6**, 359–365

12 McMaster, T J, Berry, M, Corfield, A P and Miles, M J (1999) Biophys. J **77**, 533–541

13 Deacon, M P, Davis, S S, White, R J, Nordman, H, Carlstedt, I, Errington, N, Rowe, A J and Harding, S E (1999) Carbohydr Polym **38**, 235–238

14 Hutton, D A, Pearson, J P, Allen, A. and Foster, S N E (1990) Clin Sci **78**, 265–271

15 Jumel, K., Fiebrig, I and Harding, S E (1996) Int J Biol Macromol **18**, 133–134

16 Errington, N, Harding, S. E, Vårum, K M and Illum, L (1993) Int J Biol. Macromol **15**, 113–117

17 Chen, X, Daview, M C, Roberts, C J, Tendler, S J B, Williams, P. M, Davies, J, Dawkes, A. C and Edwards, J C (1998) Ultramicroscopy **75**, 171–181

18 Sheehan, J K, Oates, K and Carlstedt, I (1986) Biochem J **239**, 147–153

19 Fiebrig, I, Harding, S. E, Rowe, A J, Hyman, S. C. and Davis, S S (1995) Carbohydr Polym **28**, 239–244

20 Fiebrig, I, Vårum, K M, Harding, S E, Davis, S S and Stokke, B T (1997) Carbohydr Polym. **33**, 91–99

21 Roberts, C J, Shivji, A, Davies, M C, Davis, S S., Fiebrig, I, Harding, S E, Tendler, S J B and Williams, P M (1995) Protein Pept Lett **2**, 409–414

22 Nordman, H., Davies, J R, Herrman, A, Karlsson, N G, Hansson, G C and Carlstedt, I (1997) Biochem J **326**, 903–910

23 Harding, S E, Rowe, A. J. and Creeth, J M (1983) Biochem J **209**, 893–896

24 Pavlov, G M, Rowe, A J and Harding, S E (1997) Trends Anal Chem **16**, 401–405

25 Tombs, M P and Harding, S. E (1998) In An Introduction to Polysaccharide Biotechnology, pp 144–147, Taylor & Francis, London.

26 Bezanilla, M., Bustamante, C J and Hansma, H G (1993) Scanning Microsc **7**, 1145–1148

27 Rabke, C E, Wenzler, L A and Bebbe, Jr, T P (1994) Scanning Microsc **8**, 471–480

28 Skaugrud, O, Hagen, A, Borgesen, B. and Dornishm, M (1999) Biotechnol Gen Eng. Rev **16**, 23–40

29 Fiebrig, I, Harding, S E and Davis, S S (1994) Prog Colloid Polym Sci **93**, 66–73

30 Fiebrig, I, Harding, S E and Davis, S S (1995) In Biopolymer Mixtures (Harding, S E, Hill, S E and Mitchell, J R, eds), pp 373–419, Nottingham University Press, Nottingham

31 Mathiowitz, E, Chickering, III, D E and Lehr, C-M. (1999) Bioadhesive Drug Delivery Systems Fundamentals, Novel Approaches and Development, Marcel Dekker, New York

UV cross-linking

RNA–protein cross-linking of the B fraction was carried out using UV irradiation (254 nm) during a 10-min incubation at 0 °C in a 1-ml cuvette at a protein concentration of 3–4 mg/ml.

RNA-binding assays

Aliquots (3 μl) containing 0.75, 1.5 and 3.0 μg of annexin II complex isolated from Krebs II ascites cells or pig microvillar epithelium were spotted on to nitrocellulose membranes and allowed to air-dry. Protein concentration in each spot was adjusted to 3.0 μg with BSA. The membranes were blocked overnight at 4 °C in binding buffer (10 mM triethanolamine, pH 7.4, 50 mM KCl, 1 mM dithiothreitol, 2 mM $MgSO_4$, 1 mM $CaCl_2$ and 500 μg/ml yeast tRNA). A sample of ^{32}P-labelled RNA corresponding to 50000 c.p.m. was added and the membranes were incubated for 30 min at room temperature in binding buffer containing 20 units/ml RNasin (Promega). Radiolabelled total RNA from each polysome population was isolated as described above and mRNA and rRNA were further purified using magnetic oligo(dT_{25}) beads (Dynal A. S.) as described by the supplier. After incubation with RNA, the membranes were washed for 4 × 15 min at room temperature in binding buffer without yeast tRNA. The binding of RNA was quantified and visualized using a Canberra Packard Instant Imager™.

RESULTS

The presence of annexin II in cytoskeleton-bound polysomes

We have demonstrated previously that polysomes from different cell types can be fractionated into three different populations, corresponding to 'free' (or loosely cytoskeleton-associated), cytoskeleton-bound and membrane-bound polysomes [8]. These fractions are referred to as A, B and C, respectively, and the polysomes purified from each fraction similarly A, B and C polysomes. These polysomes are enriched in different mRNA species [8–11,26], and also differ in their complement of poly(A)$^+$-binding proteins [10]. Short-term stimulation of cells with insulin increases the amount of cytoskeleton-bound B polysomes in Krebs II ascites cells [33].

Analysis of the protein composition of the different fractions, obtained from Krebs II ascites cells, revealed an approx. 36-kDa protein as one of the most abundant proteins in the B fraction [9], suggesting a structural protein. Since the B fraction is also enriched in actin [8] and the 36-kDa protein could be released by EGTA, it was of interest to see if it might be a member of the annexin family of Ca^{2+}-binding proteins. The three fractions, as well as the isolated polysomes, were subjected to immunoblotting using a peptide antibody raised against a conserved motif present in repeat 2 of the annexins [31]. As shown in Figure 1, the antibody recognized a protein of about 36 kDa that was enriched in the B fraction and, most interestingly, was found associated with the purified B polysomes. The immunoreactive 36-kDa protein was also recovered in the C fraction, but it was absent in C polysomes. In addition, the antibody detected weakly two additional proteins in the 50–55-kDa range in the B and C polysomes (Figure 1).

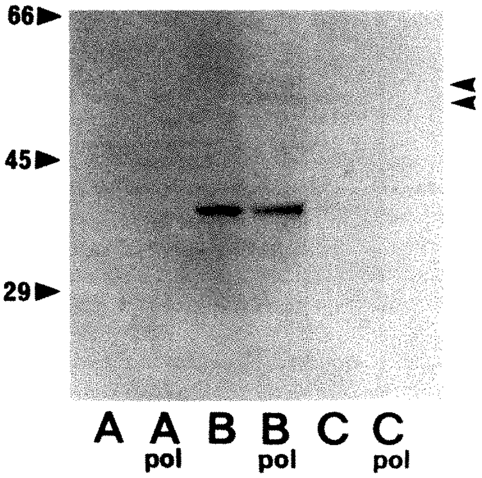

Figure 1 Identification of annexins in the fractions (A, B and C) isolated from Krebs II ascites cells and the respective polysomal subfractions

The three fractions were prepared and the corresponding polysomes (pol) were isolated as described in Materials and methods section. Proteins (40 μg/lane) were separated by SDS/PAGE (10% gels), transferred to nitrocellulose filters, and probed with antibodies against the consensus sequence 2 present in all annexins (CP-2). The positions of the prestained molecular-mass markers (29, 45 and 66 kDa) are indicated. Note the enrichment of the 36-kDa annexin in the B fraction and B polysomes. The arrows indicate two additional annexins in the 50–55-kDa range.

To show that the enrichment of the 36-kDa annexin in the B fraction was not unique to the Krebs II ascites cells, similar fractions were prepared from two other cell lines, MPC-11 and L-929 [2,34]. These are transformed mouse cell lines that grow both in suspension and as monolayers, but display different organization of the cytoskeleton since the MPC-11 cells are known to lack vimentin filaments [35]. The different fractions (A, B and C) were again analysed by immunoblotting, in this case employing an affinity-purified antibody against the 36-kDa annexin II since it has the expected size and is known to bind actin [22,23]. The results showed that the 36-kDa protein that was also found enriched in the B fractions derived from MPC-11 and L-929 cells appears to be annexin II (Figure 2). Furthermore, the relative amounts of annexin II recovered in the B and C fractions of L-929 cells appeared to depend on culture conditions, as more annexin II, like actin (results not shown), was present in the C fraction isolated from monolayer L-929 cells. In the corresponding suspension cells, both annexin II (Figure 2) and actin (results not shown) were more concentrated in the B fraction containing the cytoskeleton-bound polysomes. In gen-

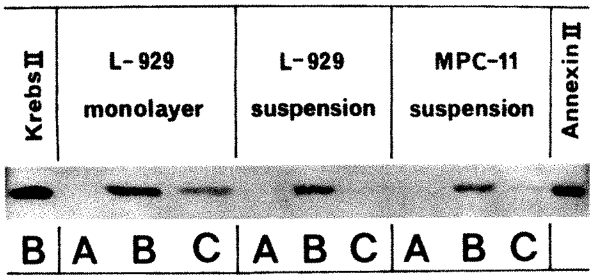

Figure 2 Distribution of the 36-kDa annexin II in the A, B and C fractions isolated from MPC-11 cells and from L-929 cells, grown either as monolayers or in suspension

Proteins (40 μg/lane) were separated by SDS/PAGE (10% gels), transferred to nitrocellulose filters, and immunostained with affinity-purified antibodies against annexin II. The lanes to the left and right contained the B fraction from Krebs II ascites cells and purified annexin II, respectively. Note the enrichment of annexin II in the B fractions and the increased recovery of the protein in the C fraction from monolayer L-929 cells, as compared with the suspension cells.

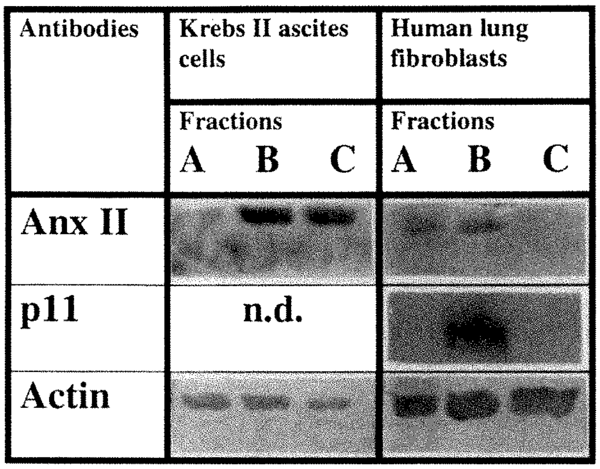

Figure 3 Distributions of annexin II (Anx II), p11 and actin in A, B and C fractions isolated from Krebs II ascites cells and human lung fibroblasts

Proteins (40 μg/lane) from the different fractions (A, B or C) were separated by SDS/PAGE (10% gels), transferred to nitrocellulose filters, and analysed by immunoblotting using antibodies against annexin II, p11 or actin antibodies as described in the Materials and methods section. n.d., not determined.

eral, we observed that the relative amounts of annexin II in the B and C fractions varied to some extent, possibly due to heterogeneity of the cells based on the cell cycle. Despite these variations, annexin II reproducibly was only found associated with one population of polysomes, namely the B polysomes.

The distributions of actin, annexin II and p11, the intracellular protein ligand of annexin II [12], in the A, B and C fractions derived from Krebs II ascites and human lung fibroblasts are shown in Figure 3. The human fibroblasts were chosen to provide an untransformed control cell type and to facilitate the detection of p11, since the available antibody only recognizes the human or bovine protein. A marked difference in the distribution of annexin II was observed in lung fibroblasts, as compared with Krebs II ascites cells. Namely, in addition to the B fraction, a considerable pool of annexin II was also found in the 'soluble' A fraction, whereas no annexin II was detectable in the C fraction. In contrast, p11 was only detected in the B fraction, suggesting that the A fraction contains the soluble monomeric annexin II, while the B fraction contains the annexin II–p11 complex, i.e. the form that is thought to be associated with membranes and/or the cortical cytoskeleton [36–38]. All fractions isolated from human lung fibroblasts contained a substantial amount of actin and the apparent ratio of annexin II to actin was much lower in these cells as compared with the transformed Krebs II ascites cells.

Binding *in vitro* of cytoskeleton-bound B polysomes to annexin II after freezing

In the course of these experiments we observed that freezing in liquid nitrogen and thawing of the B fraction before isolation of B polysomes resulted in the loss of annexin II associated with those polysomes (Figure 4, lanes 1 and 2). This made it possible to carry out binding experiments *in vitro* in which the annexin II-depleted polysomes were incubated in the presence of calcium and an annexin II-enriched extract prepared from Krebs II ascites cells (Figure 4, lane 4). Subsequently, the polysomes were re-purified by centrifugation through a sucrose cushion. As shown in Figure 4 (lane 3), the binding of annexin II to B polysomes could be reconstituted *in vitro*. The contribution of annexin II in polysomes present in the annexin II-enriched extract was negligible, as shown in Figure 4, lanes 5–7.

More detailed binding experiments were performed either by incubating a constant amount of B annexin II-depleted polysomes in the presence of increasing amounts of the annexin II-enriched extract, or vice versa, followed by isolation of the polysomes as above and quantification of bound annexin II by immunoblotting. The use of both the annexin II antibody and ^{125}I-Protein A in excess ensured linearity of annexin II detection. The binding curves (Figures 5I and 5II) show that in both cases the association between annexin II and B polysomes increased linearly. Also, at higher concentrations of the variable component, saturation of binding was observed. The binding curve in Figure 5(I) shows a decrease in annexin II binding when the incubation was carried out in the presence of high concentrations of the annexin II-enriched extract. This is probably caused by the formation of annexin II-containing aggregates that do not pellet together with the polysomes.

Evidence for direct association of annexin II with mRNA

To further analyse the nature of the association between annexin II and B polysomes, the B fraction isolated from the Krebs II ascites cells was used in UV-cross-linking experiments. During the UV treatment the amount of aggregation that can occur during or shortly after cross-linking was followed and the duration of the UV irradiation was restricted to avoid the run-off of ribosomes. Polysome profiles were recorded from both control and UV-cross-linked B fractions to make sure that UV-induced aggregation, which would have caused the polysomes to behave abnormally in the sucrose gradients, had not occurred (Figure 6I).

Krebs II ascites cells contain a high level of endogenous RNAses which, during the long procedure used for isolation of polysome subfractions, can cleave the covalently cross-linked RNA to fragments consisting of only a few nucleotides. Interestingly, UV cross-linking caused a slight decrease in the mobility of annexin II (Figure 6II, see particularly the second lane from left), which could be due to binding of the protein to such short RNA fragments. To further assess whether covalent binding of annexin II to RNA had indeed occurred as a result of UV cross-linking, control and UV-treated B fractions were treated with EGTA, which releases the protein from cytoskeletal and/or membrane fractions [22]. Actin was included in the analysis since it associates with annexin II *in vitro* [22,23] and co-purifies with the cytoskeleton-bound polysomes [8] but is not known to bind directly to RNA. Figure 6(II) shows that EGTA efficiently released annexin II from the control B polysomes, whereas in the UV-treated B polysomes the protein became partly resistant to the treatment. In contrast, EGTA treatment did not seem to significantly affect the amount of actin in either the UV-irradiated or control polysomes as judged by Western blotting which, however, provides only a semi-quantitative measure.

As another approach to study the possible interaction between annexin II and RNA, we examined the binding of ^{32}P-labelled total RNA isolated from Krebs II ascites cells to B polysomal proteins (Figure 7I, lane 1), or a mixture of Ca^{2+}-binding proteins, enriched in annexin II, that could be released by EGTA (Figure 7I, lane 3), on a NorthWestern blot. Both preparations were observed to contain an approx. 36-kDa protein that bound the RNA probe, and displayed the same mobility as immunologically detected annexin II from the same blot (Figure 7II), suggesting direct binding of RNA to annexin II.

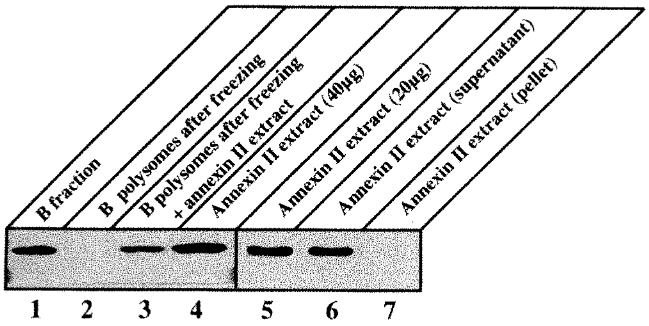
B fraction
B polysomes after freezing
B polysomes after freezing + annexin II extract
Annexin II extract (40µg)
Annexin II extract (20µg)
Annexin II extract (supernatant)
Annexin II extract (pellet)
1
2
3
4
5
6
7

Figure 4 Annexin II reassociates with annexin II-depleted B polysomes *in vitro*

The B fraction (lane 1) was prepared from Krebs II ascites cells and, following one freeze-and-thaw cycle, the B polysomes were isolated. These annexin II-depleted B polysomes (lane 2) were then incubated with a protein extract (a dialysed EGTA extract) enriched in annexin II (lane 4) in the presence of 2 mM calcium and, following incubation, polysomes were re-isolated by centrifugation through at sucrose cushion (lane 3). The annexin II-enriched extract (lane 5) was subjected to high-speed centrifugation used to purify polysomes (see the Materials and methods section), resulting in a supernatant (lane 6) and a pellet (lane 7). Subsequently, 40 µg of protein/lane (lanes 1–4) and 20 µg/lane of annexin II-enriched extract (lane 5) and equivalent volumes of the supernatant (lane 6) and the pellet (lane 7) were loaded on the gel. Proteins were separated by SDS/PAGE (10% gels), transferred to nitrocellulose, and immunostained with affinity-purified polyclonal antibodies (lanes 1–4) or monoclonal antibodies (lanes 5–7) against annexin II.

However, the detection of binding of radiolabelled RNA to the 36-kDa protein on NorthWestern blots (Figure 7) required very long exposure times, suggesting that this putative annexin II in its denatured form may be a rather poor substrate for binding

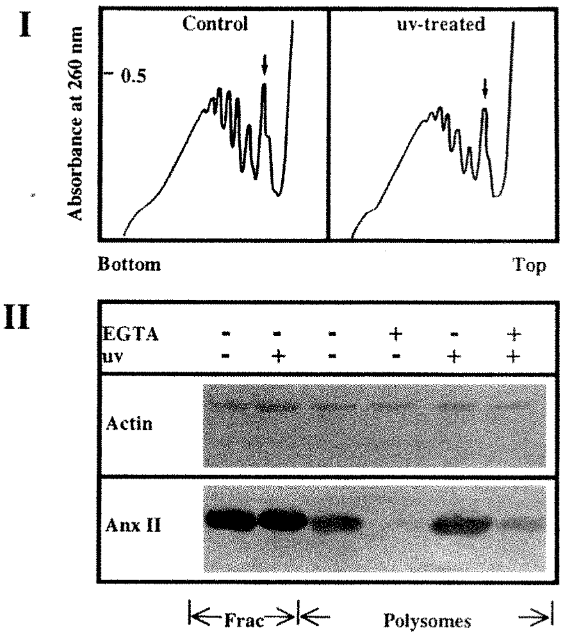

Figure 6 The effect of UV cross-linking and EGTA treatment on the association of annexin II with the B polysomes of Krebs II ascites cells

(**I**) Sedimentation profiles of polysomes from control and UV-treated B fractions. Arrows indicate the 80 S monosomal peak. (**II**) The detection of actin and annexin II in control and UV-irradiated B fractions (Frac) and the corresponding polysomes that were further incubated in the presence or absence of EGTA. Proteins (40 µg/lane) were separated by SDS/PAGE (10% gels), transferred to nitrocellulose filters, and analysed by immunoblotting using antibodies against actin and annexin II as indicated in the Figure. Note that in response to UV cross-linking part of annexin II in the polysomes becomes resistant to release by EGTA.

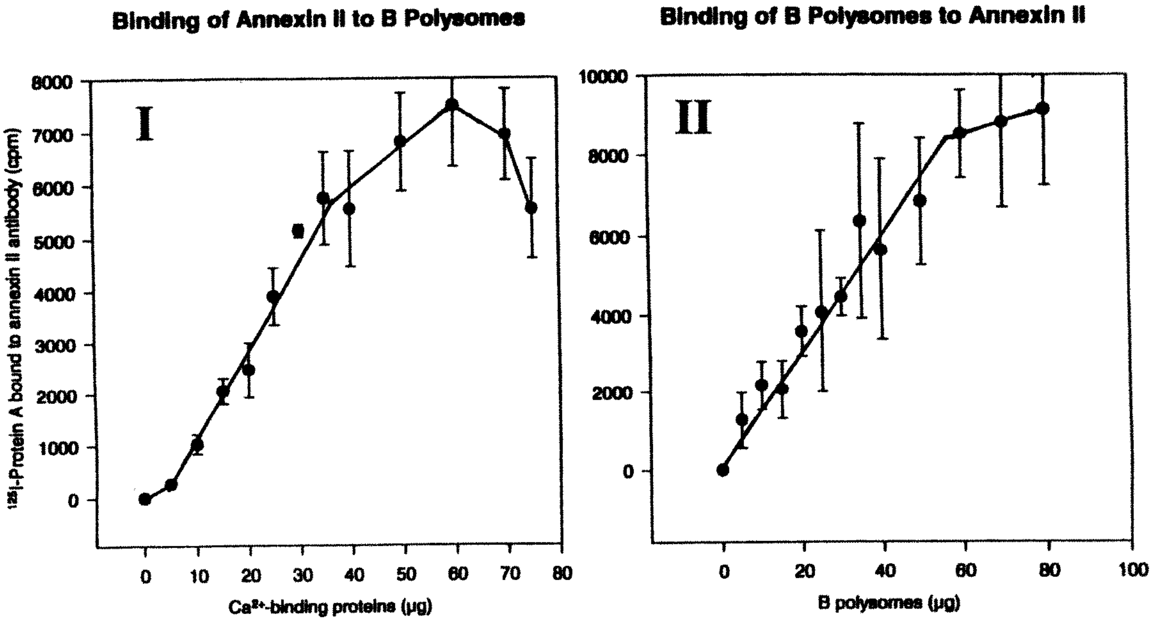

Figure 5 Assays *in vitro* show linear and saturable binding between annexin II and B polysomes

B polysomes and the dialysed EGTA-released protein extract, enriched in annexin II, were prepared from Krebs II ascites cells. In the binding assays, the concentration of either B polysomes (**I**), or the protein extract (**II**), was kept constant (40 µg/assay). Incubations were carried out in a total volume of 100 µl in 130 mM KCl buffer supplemented with 2 mM calcium. Subsequently the polysomes were re-isolated, and solubilized in SDS sample buffer. The proteins were separated by SDS/PAGE (10% gels), transferred to nitrocellulose, and immunostained with affinity-purified antibodies against annexin II, followed by detection of bound annexin II antibodies using ^{125}I-Protein A. Quantification was performed using a Canberra Packard Instant Imager™. The data points show the average of three experiments, and the standard deviations are indicated.

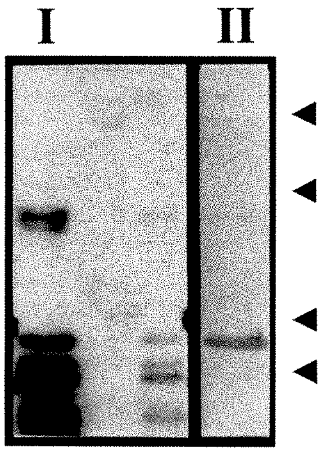

Figure 7 The binding of ^{32}P-labelled total RNA to a protein identified as annexin II by immunodetection

(**I**) B polysomes (lane 1), a post-polysomal supernatant (the proteins were precipitated by chloroform/methanol; lane 2), and an extract of Ca^{2+}-binding proteins (lane 3) were prepared from Krebs II ascites cells. Proteins (40 μg/ml) were separated by SDS/PAGE (10% gels), transferred to nitrocellulose filters, and probed with total ^{32}P-labelled RNA (isolated from Krebs II ascites cells) on a NorthWestern blot. (**II**) Immunostaining of B polysomal proteins with an affinity-purified antibody against annexin II (lane 4). Lane 4 was excised from and, following immunostaining, realigned with the same filter that was used for the NorthWestern blot. The arrowheads on the right indicate the positions of molecular-mass markers (34, 37, 50 and 67 kDa).

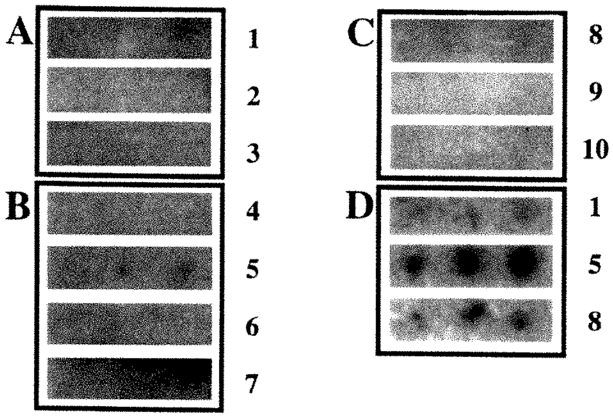

Figure 8 The binding of ^{32}P-labelled total, ribosomal and messenger RNAs, isolated from the A, B and C polysomes of Krebs II ascites cells, to purified annexin II

The annexin II_2p11_2 complex was isolated from Krebs II ascites cells (**A**, **B** and **C**) or porcine microvillar epithelium (**D**). Then, 0.75, 1.5 or 3.0 μg of the purified protein was spotted on to nitrocellulose membranes and the total protein concentration in each spot was adjusted to 3.0 μg with BSA. Binding assays involving total RNA (rows 3, 7 and 10), mRNA (rows 1, 4, 5 and 8) or rRNA (rows 2, 6 and 9), isolated from A polysomes (**A**), B polysomes (**B**) and C polysomes (**C**), were performed as described in the Materials and methods section. mRNA was isolated from A (**D**, row 1), B (**D**, row 5) or C polysomes (**D**, row 8). Binding of mRNA isolated from the B fraction was also performed in the presence of EGTA (**B**, row 4). The bound radiolabelled RNA was visualized using an Canberra Packard Instant Imager™.

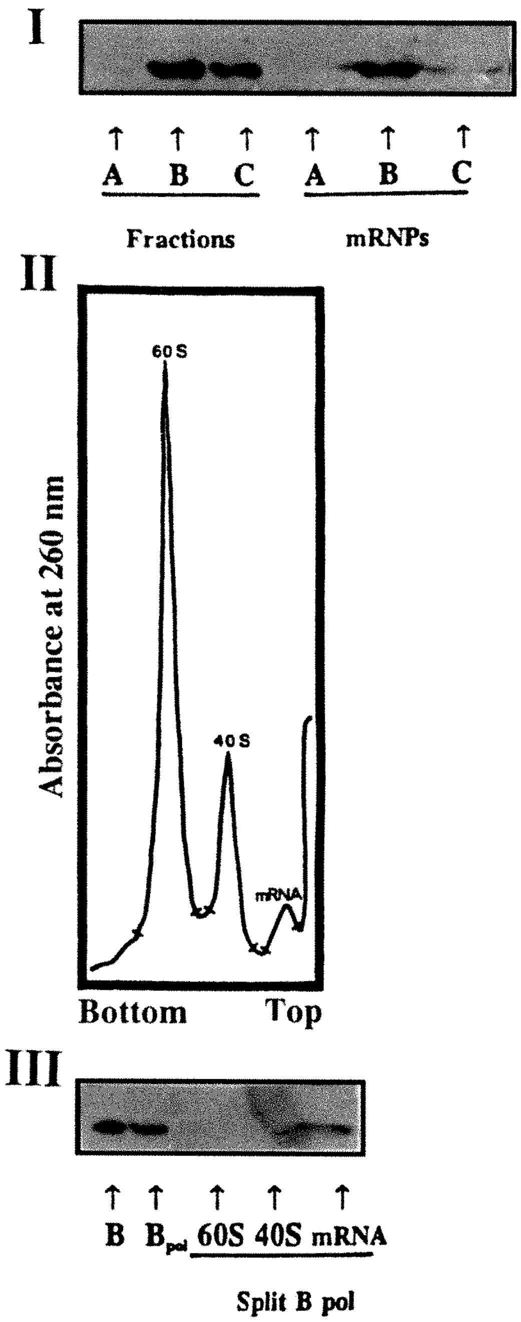

Figure 9 Annexin II in the B fraction associates with both mRNAs and inactive mRNPs

(**I**) The distribution of annexin II in the A, B and C fractions of Krebs II ascites cells and inactive mRNP complexes, isolated from the respective post-polysomal supernatants using poly(A)$^+$ magnetic beads. (**II**) Sedimentation profile after splitting of the cytoskeleton-bound B polysomes, isolated from a UV-treated B fraction, by TPCK into ribosomal subunits and mRNAs. (**III**) Detection by immunoblotting, of annexin II in the B fraction (B). B polysomes (B_{pol}), and the 60 S and 40 S ribosomal subunits, as well as the mRNA-containing peak. The contents of the collected peaks (indicated in **II**) were pelleted by centrifugation. Proteins (40 μg/lane) were separated by SDS/PAGE (10% gels), transferred to nitrocellulose filters, and immunostained with affinity-purified antibodies against annexin II.

of RNA. Therefore, to demonstrate directly the binding of RNA to the native protein, the annexin II–p11 complex was purified from both Krebs II ascites and porcine intestinal epithelial cells, immobilized on nitrocellulose membranes, and incubated with ^{32}P-labelled RNA. The presence of a high molar excess of yeast tRNA had no effect on RNA binding. Thus immobilized annexin II was tested for its possible binding specificity to rRNA (Figure 8, rows 2, 6 and 9) or mRNA (Figures 8A–8C, rows 1, 4, 5 and

8; in row 4 the binding was performed in the presence of EGTA). Interestingly, weak, but specific binding of mRNA isolated from B polysomes to the annexin II complex could be detected (Figure 8B, row 5), whereas mRNAs isolated from A (Figure 8A, row 1) or C polysomes (Figure 8B, row 8), as well as rRNA (Figure 8, rows 2, 6 and 9) showed negligible binding. Also, the association of B mRNAs with the protein, observed in this assay, was calcium-dependent as EGTA abolished the binding (Figure 8B, row 4). Binding of total RNA isolated from the respective polysomes to immobilized annexin II (Figure 8, rows 3, 7 and 10) was also included as a further test of specificity. Since rRNA constitutes about 98–99 % of total RNA [39], no binding of total RNA to the annexin II–p11 complex was observed in this case.

Finally, we also examined the binding of mRNAs obtained from the three polysome populations of Krebs II ascites cells to the annexin II–p11 complex, purified from porcine intestine microvillar epithelium using a well-established procedure [22], and observed that this annexin II complex bound selectively B mRNA, and with a much higher affinity than the protein isolated from the transformed Krebs II ascites cells (Figure 8D, row 5).

Annexin II is associated with both active and inactive mRNAs

The results obtained from the above *in vitro* studies suggest that annexin II binds to mRNA. To obtain further evidence for this conclusion, polysomes were sub-fractionated to separate the mRNAs from ribosomal subunits. In addition, inactive mRNAs (non-polysomal) present as mRNP complexes were isolated from the post-polysomal A, B and C supernatants using oligo(dT) magnetic beads. Routine procedures for splitting the polysomes/ribosomes with puromycin or TPCK, and their separation on sucrose gradients into 60 S, 40 S and mRNA-containing peaks, require both high salt and the presence of 10 mM EDTA in the buffer [40]. Since both conditions release annexin II, UV cross-linking of the polysomes was performed before their splitting with TPCK and sub-fractionation on sucrose gradients (Figure 9II). Subsequently, the 60 S, 40 S and the top mRNA peaks were pooled and analysed for their content of annexin II. As shown in Figures 9(I) and 9(III), respectively, annexin II was observed to associate with the B mRNP complexes and, in addition, was only found in the distinct peak, obtained after the splitting of the B polysomes, which contained the mRNAs (Figure 9II).

DISCUSSION

Earlier studies involving sucrose-gradient sedimentation analysis and immunoprecipitation have shown the association of annexin II with small RNA particles (RNPs), isolated both from transformed and non-transformed chick embryo fibroblasts [25]. Here we show that annexin II is enriched in a fraction that can be prepared from a number of cell types and contains cytoskeleton-bound polysomes. Further purification of the polysomes from this B fraction resulted in the presence of annexin II in these polysomes, whereas the protein was not found associated with polysomes purified from the two other fractions studied (A and C). Our results demonstrate further that two additional proteins, which can be classified as annexins by immunological criteria, are present in the different polysomal fractions. The characteristics of the polysome-associated annexin II are not known, but the observation that it could be co-purified with B polysomes even in the absence of externally added calcium (results not shown) would indicate that the calcium requirement for binding is in the lower concentration range, but is required for association of annexin II with mRNA (Figure 8).

The presence of annexin II in the B fraction is presumably caused by its binding to actin, an interaction that has been well established *in vitro* [22,23]. An increased annexin II-to-actin ratio was observed in all the transformed cell lines examined (Krebs II, L-929, MPC-11), as compared with the non-transformed human lung fibroblasts (Figure 3). The results obtained with L-929 cells, grown either in suspension or as monolayers, showing the partial shift of both annexin II and actin to the C fraction in the monolayer cells also argues in favour of their association. Further, the release of annexin II to the B fraction by increasing the salt concentration from 25 to 130 mM KCl is indeed reminiscent of the binding of F-actin to annexin VI, which is optimal at 10–30 mM KCl [41]. Krebs II ascites cells, an aggressive transformed cell line, contain elevated levels of annexin II as compared with the L-929 and MPC-11 cells and, in particular, the human lung fibroblasts. Malignant transformation of different cell lines has previously been shown to involve an increased expression of annexin II, both at the mRNA and protein levels, as well as an increase in its phosphorylation [42].

Not only was annexin II present in the purified cytoskeleton-bound polysomes, but it could also reassociate with annexin II-depleted cytoskeleton-bound polysomes *in vitro*, and remained associated to these polysomes after a new purification of these polysomes by centrifugation through a sucrose cushion, indicating that the association of the protein with these polysomes is specific. Also, the isolation of polysomes as such did not cause trapping of annexin II since no annexin II was found in the polysomes purified from the fractions after freezing and thawing (Figure 4, lane 2), even though the corresponding fraction contained substantial amounts of the protein (Figure 4, lane 1).

A number of additional experiments, including UV cross-linking in combination with fractionation of ribosomes, North-Western blotting and binding of ^{32}P-labelled RNA to annexin II immobilized on nitrocellulose, further indicate that annexin II binds directly to the mRNA moiety of the cytoskeleton-bound polysomes. In particular, immobilization of the native annexin II complex on nitrocellulose followed by incubation with ^{32}P-labelled RNA resulted in a weak but specific binding of mRNAs isolated from B polysomes when compared with rRNA and the other two populations of mRNAs isolated from the A or C polysomes (Figure 8). Using an identical binding assay, but with the annexin II complex isolated from porcine intestinal microvillar epithelium, the preference of annexin II to bind mRNAs isolated from B polysomes was even more evident and the binding was of much higher affinity. The reason for this is not clear but it could be caused by different post-translational modifications of the two preparations. rRNA did not bind to the annexin II complex isolated from porcine intestinal microvillar epithelium (results not shown). Since a high molar excess of tRNA was present during binding, we conclude that a specific population of mRNAs appears to bind selectively to annexin II. Our data are also in accordance with earlier studies suggesting that annexin II associates with RNA [24,25] in the form of small RNPs [25]. However, in the latter case the apparent binding of annexin II to less complex RNA species could have been caused by mRNA degradation.

Further, UV irradiation of the B fraction resulted in covalent binding of annexin II to RNA, as demonstrated by the finding that UV-generated RNA–protein cross-links rendered part of the protein resistant to EGTA-mediated release. In contrast, if the treatment was carried out in the presence of EGTA, no cross-linking of annexin II to B polysomes was observed (A. Vedeler and H. Hollås, unpublished work). L5 is a ribosomal protein of the 60 S subunit [43] and UV cross-linking did not result in an increased recovery of this protein, as measured by immunodetection, in the polysomes (results not shown). Since this protein is an intrinsic member of the 60 S ribosomal subunit, this suggests that UV-induced cross-linking of annexin II to mRNA is not an artefact.

Using affinity purification of mRNA on poly(A)$^+$ magnetic beads, annexin II was only found in association with the mRNA moiety of cytoskeleton-bound polysomes and mRNPs present in the cytoskeletal fraction. Whereas the association of polysomes with actin filaments and microtubules appears to represent a rather non-specific and more general type of attachment [9], our data indicate that the mRNAs that bind annexin II could constitute a distinct subpopulation.

There was no enrichment of annexin II in the B polysomes relative to the fraction itself, suggesting that the annexin II that associates with polysomes could represent a distinct post-translational modification or isoform of the protein (see below) not involved in endocytosis or exocytosis. It is noteworthy that several annexin II variants or isoforms have been described [44]. The data shown in Figure 9 also show that annexin II binds to the mRNA moiety of mRNPs and polysomes and thus an enrichment of annexin II in polysomes would not be expected as the mRNA-binding proteins, not taking into account initiation, elongation and termination factors, constitute only a minor part of the proteins present in polysomes.

It is possible that the annexin II, which associates with cytoskeleton-bound polysomes, represents a distinct variant/isoform that is different from the one(s) that bind to membranes. This is currently being investigated to confirm this suggestion. Earlier findings showing that only about 3 % of total cellular phospholipids are recovered in the B fraction [9] together with no immunological detection of rab4 protein in this fraction (results not shown), support the conclusion that the B fraction is not significantly contaminated by early endosomal membranes.

By calculating the amount of annexin II in B polysomes by Western blotting using the ECL detection method and an annexin II standard curve, one arrives at an estimate of 3 ± 1 annexin II molecules per ribosome. This calculation is based on the assumption that the protein content of polysomes is about 50 % of the total ribosomal mass, not taking into account the mRNAs. Although this is a rough estimate, it is in the same order of magnitude as obtained for Y-box proteins (reviewed in [45]). These phosphoproteins function both as DNA- (role in transcription) as well as RNA-binding proteins and have been proposed to be involved in mRNA packaging and to bundle actin.

In conclusion, the present biochemical analysis shows that annexin II may be associated with a specific population of mRNAs and strongly suggests that the binding involves its direct interaction with mRNA. Thus annexin II seems to be involved in association with both vesicles and mRNA. In this regard it is very interesting that one of the protein ligands of testis and brain RNA-binding protein is the transitional endoplasmic reticulum ATPase [46] involved in the ATP-dependent fusion of vesicles in transport from endoplasmic reticulum to Golgi.

Our data also indicate that annexin II binds to both translationally active and inactive mRNAs and that this binding may be regulated by calcium. Studies to identify specific mRNAs belonging to the subpopulation of polysomes with which annexin II interacts, as well as the specific sequences that are involved in this association, are in progress.

We would like to express special gratitude to Dr Volker Gerke for his generous gift of antibodies, for numerous discussions and constructive suggestions during the various phases of this work as well as for critical comments on the manuscript. In addition, we are grateful to Dr Jaakko Saraste and Dr Robert Kretsinger for critically reading the manuscript and giving valuable comments. Dr Bruno Goud and Dr Joachim Stahl are appreciated for their generous gifts of rab4p and L5 antibodies, respectively. Finally, Dr Torgeir Flatmark is thanked for discussions concerning the binding experiments This work was supported in part by the Norwegian Cancer Society.

REFERENCES

1 St Johnston, D (1995) Cell **81**, 161–170
2 Pryme, I F, Johannessen, A and Vedeler, A (1995) Adv Mol Cell Biol **12**, 41–74
3 Oleynikov, Y and Singer, R H (1998) Trends Cell Biol **8**, 381–383
4 Hazelrigg, T (1998) Cell **95**, 451–460
5 Jansen, R P (1999) FASEB J **13**, 455–466
6 Takizawa, P. A, Sil, A, Swedlow, J R, Herskowitz, I. and Vale, R D (1997) Nature (London) **389**, 90–93
7 Nasmyth, K and Jansen, R P (1997) Curr Opin Cell Biol **9**, 396–400
8 Vedeler, A, Pryme, I. F and Hesketh, J E (1991) Mol Cell Biochem **100**, 183–193
9 Vedeler, A., Pryme, I. F and Hesketh, J E. (1991) Biochem Soc Trans. **19**, 1108–1111
10 Moss, R, Pryme, I F and Vedeler, A (1994) Mol Cell Biochem **131**, 131–139
11 Hesketh, J E, Campbell, G P and Whitelaw, P F (1991) Biochem J **274**, 607–609
12 Raynal, P and Pollard, H B (1994) Biochim Biophys Acta **1197**, 63–93
13 Waisman, D M (1995) Mol Cell Biochem **149–150**, 301–322
14 Gerke, V and Moss, S.E (1997) Biochim Biophys Acta **1357**, 129–154
15 Glenney, J. R, Boudreau, M, Galyean, R, Hunter, T and Tack, B (1986) J Biol Chem. **261**, 10485–10488
16 Becker, T, Weber, K. and Johnsson, N (1990) EMBO J **9**, 4207–4213
17 Jost, M and Gerke, V (1996) Biochim Biophys Acta **1313**, 283–289
18 Donelly, S R and Moss, S E (1997) Cell Mol Life Sci **53**, 533–538
19 Boyko, V, Mudrak, O, Svetlova, M, Negishi, Y, Ariga, H and Tomilin, N. (1994) FEBS Lett **345**, 139–142
20 Vishwanatha, J K and Kumble, S (1993) J Cell Sci **105**, 533–540
21 Siever, D A and Erickson, H P (1997) Int J Biochem Cell Biol **29**, 1219–1223
22 Gerke, V and Weber, K (1984) EMBO J **3**, 227–233
23 Ikebuchi, N. W and Waisman, D M (1990) J Biol Chem **265**, 3392–3400
24 Glenney, Jr., J. R (1986) Exp Cell Res **162**, 183–190
25 Arrigo, A P, Darlix, J. L and Spahr, P F. (1983) EMBO J **2**, 309–315
26 Johannessen, A J, Pryme, I F. and Vedeler, A (1995) Mol Cell Biochem **142**, 107–115
27 Pong, S S, Nuss, D L and Koch, G. (1975) J Biol Chem **10**, 240–245
28 Bradford, M M (1976) Anal Biochem **72**, 248–254
29 Laemmli, U K (1970) Nature (London) **227**, 680–685
30 Towbin, M, Staehelin, T and Gordon, J (1979) Proc Natl Acad Sci U S A **76**, 4350–4354
31 Gerke, V. (1989) FEBS Lett **258**, 259–262
32 Chomczynski, P and Sacchi, N (1987) Anal Biochem **162**, 156–159
33 Vedeler, A, Pryme, I F and Hesketh, J E (1990) Cell Biol Int Reports **14**, 211–218
34 Moss, R, Pryme, I F and Vedeler, A (1993) Cell Biol Int **17**, 1065–1073
35 Traub, U E., Nelson, W J and Traub, P (1983) J Cell Sci **62**, 129–147
36 Zokas, L and Glenney, J R (1987) J Cell Biol **105**, 2111–2121
37 Thiel, C., Osborn, M and Gerke, V (1992) J Cell Sci **103**, 733–742
38 Harder, T and Gerke, V (1993) J Cell Biol **123**, 1119–1132
39 Sambrook, J, Fritsch, E F and Maniatis, T (1989) in Molecular Cloning: a Laboratory Manual, 2nd edn, chapter 7, Cold Spring Harbor Press, Cold Spring Harbor
40 Adelman, M. R., Sabatini, D D and Blobel, G (1973) J Cell Biol **56**, 206–229
41 Hosoya, H, Kobayashi, R, Tsukita, S and Matsumura, F (1992) Cell Motil Cytoskel. **22**, 200–210
42 Vishwanatha, J, Chiang, Y, Kumble, K D., Hollingsworth, M A and Pour, P M (1993) Carcinogenesis **14**, 2575–2579
43 Kargel, H J, Stahl, J, Gross, B, Knespel, S, Bielka, H and Saarma, M (1987) FEBS Lett **220**, 126–128
44 Ma, A S P, Bell, D. J., Mittal, A A and Harrison, H H (1994) J Cell Sci **107**, 1973–1984
45 Matsumoto, K and Wolffe, A P (1998) Trends Cell Biol **8**, 318–323
46 Wu, X-Q, Lefrancois, S, Morales, C R and Hecht, N B (1999) Biochemistry **38**, 11261–11270

Received 5 November 1999/8 March 2000, accepted 30 March 2000

Biochem J (2000) 348, 573–578 (Printed in Great Britain)

Enzymic methylation of arginyl residues in -Gly-Arg-Gly- peptides

Young-Lan HYUN*, D. Betty LEW†, Seung Hee PARK‡, Chan-Wha KIM*, Woon Ki PAIK§ and Sangduk KIM*[1]

*Graduate School of Biotechnology, Korea University, 136, 5-ka Anam-dong, Sungbuk-ku, Seoul, 136-701 Korea, †Department of Pediatrics, College of Medicine, University of Tennessee, 50 North Dunlap Street, Room 401, Memphis, TN 38103, U S A, ‡Kung-Gi Research Center, Sung Kyun Kwan University, 300 Tchuntchun-dong, Changan-ku, Suwon, 440-746, Korea, and §Department of Biochemistry, School of Medicine, Ajou University, Wontchun-dong, San-5, Paldal-ku, Suwon, 442-749, Korea

N^G-Methylation of arginine residues in many nucleic-acid-binding proteins are formed post-translationally, catalysed by *S*-adenosylmethionine: protein-arginine *N*-methyltransferase in their glycine-rich and arginine-rich motifs. The amino acid sequences of the stimulator of HIV-1 TAR (Tat-responsive element) RNA-binding protein (SRB) and fibronectin also show the presence of the internal -Gly-Arg-Gly- (-GRG-) sequence, which is potentially methylatable by the methyltransferase. To investigate the sequence requirement for methylation of these proteins, several synthetic oligopeptides with different chain lengths and sequences similar to the -GRG- regions of SRB and fibronectin were synthesized. Whereas the heptapeptide AGGRGKG (residues 16–22 in SRB) served as the methyl acceptor for the methyltransferase with a K_m of 50 μM, the 19-mer peptide (residues 10–28 in SRB) was methylated with a K_m of 8.3 μM, indicating that a greater peptide chain length yields a better methyl acceptor. Product analysis of the methylated [*methyl*-^{14}C]SRB-peptide by HPLC indicated the formation of N^G-monomethylarginine and N^G,N^G-dimethyl(asymmetric)-arginine. Synthetic peptides containing the cell attachment sequence [Arg-Gly-Asp ('RGD')] in fibronectin, GRGDSPK, GGRGDSPK and GGGRGDSPK, were also studied; whereas GRGDSPK was a poor methyl acceptor, the longer peptides were better methyl acceptors. To provide an understanding of the effect of methylation on fibronectin peptide, arginine-unmethylated and methylated GGRGDSPK were compared for their effect on the mitogenesis induced by β-hexosaminidase A and an agonistic antibody (mAb$_{16}$) in bovine tracheal smooth-muscle cells; whereas the former inhibited 35–67 % of mitogenesis at a concentration of 5–10 μM, the latter did not block mitogenesis. This lack of inhibition by the insertion of a methyl group on the arginyl residue of the cell attachment sequence might be due to the hindrance of the binding of fibronectin peptide to integrins.

Key words: *S*-adenosylmethionine, fibronectin-peptide, N^G-methylarginine, protein methylase I, RNA-binding protein.

INTRODUCTION

The methylation of protein-bound amino acid side chains is one of several post-translational modifications catalysed by highly specific methyltransferases [1,2]. Among these, protein methylase I (*S*-adenosylmethionine: protein arginine N-methyltransferase, EC 2.1.1.23) [also referred to as protein methylase I (PMI), and protein-arginine methyltransferase (PRMT1, RMT1 and HMT1)] catalyses transfer of the methyl group from *S*-adenosyl-L-methionine (AdoMet) to the guanidino nitrogen of specific arginine residues in polypeptide substrates, yielding N^G-mono-methylarginine, N^G,N^G-dimethyl(asymmetric)arginine and N^G,N'^G-dimethyl(symmetric)arginine with the release of *S*-adenosyl-L-homocysteine, the demethylated AdoMet [1,3].

Two subclasses of protein methylase I have been identified and purified to near homogeneity from calf brain and rat liver: myelin-basic-protein-specific methylase I and nuclear protein/histone-specific protein methylase I, both exhibiting distinct substrate specificities towards the respective methyl acceptor protein [4,5] Rajpurohit et al. [5] have demonstrated that the nuclear protein/histone-specific protein methylase I methylates most efficiently arginine residues within the Arg-Gly-Gly (RGG) motif of the recombinant heterogeneous ribonucleoprotein particle (hnRNP) A1 protein. Earlier, the presence of N^G,N^G-dimethyl(asymmetric)arginine at residue 193 of helix-unwinding protein 1 ('UP1', the N-terminal proteolytic fragment of hnRNP A1 protein) [6] was reported. More recently, three additional N^G,N^G-dimethyl(asymmetric)arginine residues in the RGG motif (residues 205, 217 and 224) of hnRNP protein A1 isolated from HeLa nuclei have also been identified [7]. Thus hnRNP A1 protein is one of the most highly arginine-dimethylated proteins in nature.

The RGG motif occurs in several nucleic-acid-binding proteins and is known to be a conserved domain consisting of clusters of glycine and N^G,N^G-dimethyl(asymmetric)arginine residues interspersed with phenylalanine, often spanning over 10–20 chain lengths [8–10]. Compilation of several nucleic-acid-binding proteins, such as nucleolin and fibrillarin from different species, indicated a common sequence alignment within the methylatable site of the RGG motif [7]. In addition, further examination of the sequences around the N^G-methylated arginines indicated -GRG- as the preferred sequence for methylation, although the $n-1$ position of the Arg residue could be replaced by a few selected amino acids other than Gly [7]. This feature is in good agreement with the previous studies performed with several synthetic oligopeptides as the methyl acceptor for protein methylase I [11,12]. In an effort to extend these studies, we examined the primary sequences of several proteins and found the stimulator of HIV-1 Tat-responsive element (TAR) RNA-binding protein (SRB) [13] and fibronectin [14] to contain the -GRG- sequence.

The SRB protein is one of the three transactivators to regulate HIV-1 gene expression, consisting of 539 residues (accession number U38846) and containing a -GRG- sequence at residue 18–20 in the N-terminus [13]. One-quarter of the N-terminal amino acid sequence showed a high degree of similarity to a member of the chaperonin family of proteins as well as the P-loop

---

Abbreviations used AdoMet, *S*-adenosyl-L-methionine, Hex, hexosaminidase, hnRNP, heterogeneous nuclear ribonucleoprotein particle, SRB, stimulator of HIV-1 TAR RNA-binding protein; TAR, Tat-responsive element

[1] To whom correspondence should be addressed (e-mail sdkim@kuccnx korea ac kr).

motif, a glycine-rich region capable of binding to ATP or GTP [13]. Fibronectin is one of the integrin families mediating cell adhesion in communicating with a receptor at the cell surface [15]; the attachment sequence is known to be the common tripeptide Arg-Gly-Asp (RGD) [14,16]. Therefore the fibronectin peptides containing RGD have often been used in many experimental systems [14,17,18].

In the present study we synthesized several oligopeptides that were identical or similar to the GRG-containing region of SRB and fibronectin peptides, and used them as substrates *in vitro* for the purified rat liver protein methylase I. In addition, the chemically synthesized fibronectin peptide containing the N^G-methylated and unmethylated arginine residues were compared for their effect on cell-surface receptor-mediated DNA synthesis and cell proliferation in tracheal smooth-muscle cells.

EXPERIMENTAL

Materials

Ado[*methyl*-^{14}C]Met (specific radioactivity 46.8–53.0 mCi/mmol), Ado[*methyl*-^{3}H]Met (75.0 Ci/mmol) and [^{3}H]thymidine (5 Ci/mmol) were purchased from Amersham Life Science. N^G,N^G-Dimethylarginine, Sephadex G-10 and histone (type II-AS) were from Sigma (St Louis, MO, U.S.A.). Fetal bovine serum was purchased from Hyclone Lab (Logan, UT, U.S.A.). The synthetic oligopeptides containing the -GRG- sequence with variable chain lengths (Table 1) were synthesized at the W. M. Keck Foundation Biotechnology Resource Laboratory of Yale University (New Haven, CT, U.S.A.). All other chemicals were of the reagent grade available from various commercial sources.

Purification of protein methylase I

The purification of protein methylase I from rat liver was performed essentially by the same method as described previously [19]. In brief, rat liver was homogenized in 4 vol. of 5 mM sodium phosphate, pH 7.4, containing 5 mM EDTA and 0.25 M sucrose, and the homogenate was centrifuged at 105000 ***g*** for 60 min. The supernatant was mixed with an equal volume of 10 mM Mops (pH 7.4)/2 mM EDTA/0.5 mM PMSF/10 mM 2-mercaptoethanol and chromatographed on DE-52 followed by Sephadex G-200. The purified enzyme transferred 28.4 pmol of methyl groups/min per mg of protein, with histone as the methyl acceptor substrate under the assay conditions.

Assay for protein methylase I

The enzymic activity for protein methylase I was determined as described previously [4,19]. A total 0.125 ml reaction mixture containing 0.1 M potassium phosphate buffer, pH 7.6, 0.5 mg of histone (type II-AS) and 0.04 mM Ado[*methyl*-^{3}H]Met (500 d.p.m./pmol) was incubated in the presence of rat liver methylase preparation (approx. 100 μg) at 37 °C for 30 min, unless otherwise specified. The reaction was terminated by the addition of 15% (w/v) trichloroacetic acid and the resulting precipitates were repeatedly washed as described [4].

Table 1 List of synthetic oligopeptides used for methylation reactions

Single-letter amino acid abbreviations are used The underlined bold letter **R** is the potential methyl-acceptor residue Abbreviation FN, fibronectin

Peptide	Sequence	Comments	Reference
SRB P-1	HN$_2$-AGG**R**GKG-CO$_2$H	Residues 16–22 in SRB	[13]
SRB P-2	Acetyl-AGG**R**GKG-amide	Residues 16–22 in SRB (N-terminus and C-terminus blocked)	
SRB P-3	HN$_2$-GATAGAAGG**R**GKGA YQDRD-CO$_2$H	Residues 10–28 in SRB	[13]
FN P-1	NH$_2$-G**R**GDSPK-CO$_2$H	Cell attachment sequence	[16]
FN P-2	NH$_2$-GG**R**GDSPK-CO$_2$H		
FN P-2	NH$_2$-GGG**R**GDSPK-CO$_2$H		

Protein concentration was estimated by the Coomassie Blue method of Bradford [20], as modified by Pierce Chemical Co., with BSA as the standard.

Enzymic methylation of synthetic oligopeptides

Because the synthetic oligopeptides employed in the present study were not precipitable by trichloroacetic acid, the gel-filtration method described previously was employed [11]. Different amounts of each peptide substrate were incubated in a total 0.125 ml reaction mixture as described above, but with 0.04 mM Ado[*methyl*-^{14}C]Met (103–117 d.p.m./pmol, as indicated in the respective tables) in the presence of various concentrations of the rat liver methylase I (47–174 μg) at 37 °C for 12–60 min as indicated. The reaction was terminated by adjusting the pH of the mixture to 4.0 with 0.2 M sodium citrate and heated at 100 °C for 30 min. This treatment cleaves unreacted Ado[*methyl*-^{14}C]Met, resulting in 5′-[*methyl*-^{14}C]methylthioadenosine, thus enabling the [*methyl*-^{14}C]-peptide to be separated easily from the unreacted Ado[*methyl*-^{14}C]Met by subsequent molecular sieve chromatography. The total reaction mixture was applied to a column of Sephadex G-10 (0.5 cm × 110 cm) that had been pre-equilibrated with 0.01 M HCl; it was then eluted with the same solvent, collecting fractions of 0.5 ml. The aliquots of each of the fractions were counted for the radioactivity incorporated, and other aliquots were used for ninhydrin reaction to assess the peptide elution profile. A typical chromatographic profile is shown in Figure 1 below. To obtain K_m values for SRB peptides, the methylation reactions were performed with variable concentrations of peptide at a fixed concentration of 0.04 mM Ado[*methyl*-^{14}C]Met

HPLC analysis of methylated amino acids

The *methyl*-^{14}C-labelled oligopeptide, purified by Sephadex G-10 chromatography, was filtered through a Centricon-10 (Amicon Co.) to remove the enzyme protein from the *methyl*-^{14}C-labelled peptide. The filtrate was subjected to hydrolysis in 6 M HCl at 110 °C for 24 h. The hydrolysate was washed with distilled water repeatedly to remove HCl completely; 10 μl of redrying agent [triethylamine/ethanol/water (2:2:1, by vol.)] was added to the hydrolysate. After drying under vacuum, 50 μl of derivatizing agent [ethanol/triethylamine/water/phenylisothiocyanate (7:1:1.1, by vol.)] were added to the mixture and left to react for 20 min at room temperature The mixture was again dried completely and dissolved in 100 μl of solvent A [2.5% (v/v) acetonitrile in 70 mM sodium phosphate buffer, pH 6.5]. The derivatized sample was then injected onto a C_{18} reverse-phase column (Shodex C_{18}, 5 μm spherical particles, 4.6 mm internal diam. × 25 cm) equilibrated in solvent A at 43 °C, and eluted at a flow rate of 1.2 ml/min for 10 min and then with solvent B [15% (v/v) methanol in 45% (v/v) acetonitrile] with the use of the following gradient (v/v): 0–10 min, 0% B; 10–40 min, 5% B; 40–55 min, 5% B; 55–65 min, 5–15% B; 65–69 min, 15–30% B. The eluate was monitored at 254 nm and 1 min fractions were collected.

Airway smooth-muscle cell culture

Primary cultures of bovine tracheal smooth-muscle cells were prepared from bovine trachealis muscle, as described previously [21]. Direct immunofluorescence staining of the cells with an FITC-conjugated monoclonal antibody against smooth-muscle isoactin (Sigma) demonstrated that cultures consisted of a homogeneous population of smooth-muscle cells [22]. Cells at passage 1–7 were used for experiments.

Assessment of proliferation

DNA synthesis rates were assessed by measuring [^{3}H]thymidine incorporation as follows: cells were seeded in microtitre wells (25000 cells per well) and allowed to grow to confluence. The medium was replaced with medium M199 (Cellgro; Mediatech, Washington, DC, U.S.A.) containing 0.4% (v/v) fetal bovine serum. After a 48 h starvation, the inhibitors to be tested were added 30 min before stimulation of the cells. Without a change of medium, purified hexosaminidase A (Hex A) or vehicle (PBS) was added [21]. In some experiments, an agonistic antibody (mAb$_{15}$; [23]) directed to the extracellular domain of human macrophage mannose receptors was used to stimulate cells. [^{3}H]Thymidine (0.5 μCi per well) was added to the cells 20 h after the stimulation; cells were harvested 18 h later. Radioactivity was quantified in a liquid-scintillation counter. Experiments were performed in quadruplicate and were repeated three times.

Parallel experiments were set up to assess cell counts and cytotoxicity by tetrazolium salt reduction with the use of a 3-[4,5-dimethylthiozol-2-yl]-2,5-diphenyl tetrazolium bromide (5 mg/ml; Millipore-filtered) (MTT) colorimetric assay, as described previously [21]. MTT dissolved in PBS was added to the adherent cells in microtitre wells (20 μl per well) at the end of the experimental period. After incubation for 4 h at 37 °C, medium was removed from the microtitre wells and acidified with 0.04 M HCl; 2-propane/propan-2-ol was then added to wells (200 μl per well). The plates were left at room temperature for 30 min and then read on an ELISA reader (EL340 Microplate; Bio-Tek Instruments, Winooski, VT, U.S.A.) at 570 nm. Cell numbers were derived from a standard curve generated from known cell numbers.

RESULTS

Enzymic methylation of oligopeptides derived from SRB

Previous studies had indicated that the arginine residue in -GRG- in polypeptide sequences was the most methylatable by protein methylase I; SRB was found to contain this tripeptide sequence (residues 18–20). Therefore, to investigate the methylation of SRB peptides, SRB P-1 (7-mer), SRB P-2 (7-mer with blocked N-terminus and C-terminus) and SRB P-3 (19-mer) were synthesized chemically. All three peptides served as methyl acceptors for the rat liver cytosolic protein methylase I (Table 2). However, the 19-mer was the best methyl acceptor, even though only less than one-third the amount of the 7-mer peptides was used for methylation. To examine whether free amino and carboxy groups in the peptide exerted any effect on methyl acceptability, the N-terminus and C-terminus were blocked with an acetyl and an amide group respectively; the blocked 7-mer (SRB P-2) was 14% less effective as a methyl acceptor than the unblocked (SRB P-1).

The K_m values for 7-mer and 19-mer peptides were then compared (Table 3). SRB P-3 (the 19-mer) showed a much lower K_m value than the 7-mer peptides (8.3 μM compared with 50.0 and 52.6 μM), indicating clearly that the longer peptide had a

Table 2 Methyl-acceptability of peptides derived from the SRB protein by rat liver protein methylase I

The methylation reaction was performed in a total reaction mixture of 0.125 ml containing 0.125 M potassium phosphate, pH 7.6, 0.04 mM Ado[*methyl*-^{14}C]-Met (103 d.p.m./pmol), 174 μg of protein methylase I and the indicated amounts of substrate at 37 °C for 12 min. The mixture was then adjusted to pH 4.0 and boiled for 30 min to terminate the reaction, methyl incorporation into the peptides was estimated with a Sephadex G-10 column as described in the Experimental section. *The methyl incorporations into hnRNP protein A1 and histone II-AS were quantified by the trichloroacetic acid precipitation method.

			Incorporation of *methyl*-^{14}C	
Substrate	Molecular mass (Da)	Amount used (nmol)	(d.p.m.)	(mol%)
SRB P-1	602	229	5060	0.021
SRB P-2	643	298	4410	0.014
SRB P-3	1820	68.0	5800	0.083
hnRNP protein A1*	34000	1.5	5340	3.453
Histone II-AS*	12000–14000	23.8	2980	0.121

Table 3 Kinetic constants for SRB peptides by rat liver protein methylase I

The experimental conditions were the same as those described in Table 2, except that variable concentrations of substrate peptides were used in the presence of a fixed amount of 0.04 mM Ado[*methyl*-^{14}C]Met

Substrate	K_m (μM)	V_{max} (pmol of [*methyl*-^{14}C]/min per mg)
SRB P-1	50.0	3.03
SRB P-2	52.6	2.63
SRB P-3	8.3	3.39
hnRNP protein A1	0.5*, 0.19†	151†
Histone II-AS	21.0†	25.5†

* From [19].
† From [5]

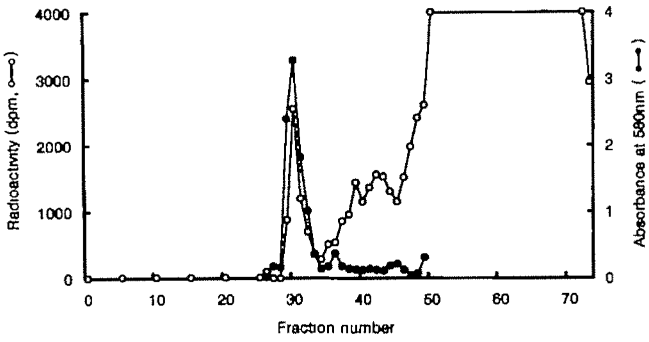

Figure 1 Sephadex G-10 chromatography of *methyl*-^{14}C-labelled SRB-P3

SRB-P3 (39.6 μg) was methylated in a standard reaction mixture with Ado[*methyl*-^{14}C]Met in the presence of protein methylase I for 60 min. After incubation, the mixture was adjusted to pH 4.0 and heated at 100 °C for 30 min to destroy unreacted AdoMet. The mixture was then chromatographed on a Sephadex G-10 column (0.5 cm × 110 cm) and 0.5 ml fractions were collected. Aliquots (0.05 ml) from each fraction were counted for radioactivity; other aliquots were analysed by ninhydrin reaction to obtain a peptide elution profile. The sum of the total radioactivities eluted in fractions 30–33 was taken as the total enzyme activity. Symbols: ●, ninhydrin at 580 nm, ○, radioactivity incorporated

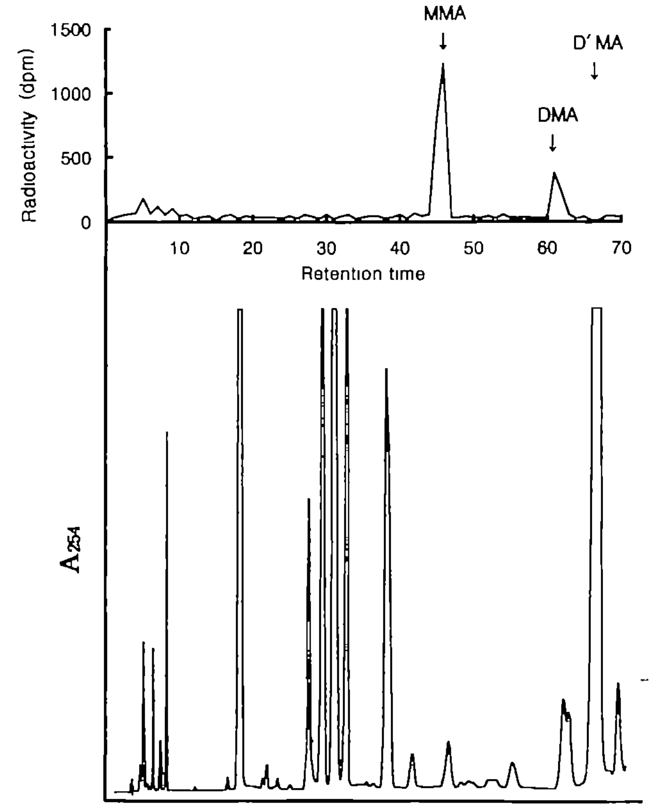

Figure 2 HPLC analysis of [*methyl*-^{14}C]SRB P-2

Details of the methylation and derivatization reactions are described in the Experimental section The *methyl*-^{14}C-labelled SRB P-2 was hydrolysed in 6 M HCl at 110 °C for 24 h and the hydrolysate was prepared for HPLC analysis The sample (37 nmol of [*methyl*-^{14}C]SRB P-2) was injected on a C_{18} reverse-phase column and analysed for methylated amino acids as described in the Experimental section Abbreviations MMA, N^{G}-monomethylarginine, DMA, N^{G},N^{G}-dimethyl(asymmetric)arginine, D′MA, N^{G},N'^{G}-dimethyl(symmetric)arginine

Table 4 Methyl-acceptability of fibronectin peptides by rat liver protein methylase I

The experimental conditions were the same as those described in Table 2, except that incubation was performed for 60 min at 37 °C, with 47 μg of protein methylase I The specific radioactivity of the Ado[*methyl*-^{14}C]Met was 117 d.p m /pmol For histone II-AS the trichloroacetic acid precipitation method was used.

Substrate	Molecular mass (Da)	Amount used (nmol)	Incorporation of *methyl*-^{14}C (d p m)
FN P-1	717	1390	174
FN P-2	774	1290	1750
FN P-3	831	1200	2970
Histone II-AS	12000–14000	76 9	9340

Table 5 Effect of arginine-methylated and unmethylated fibronectin peptides on mitogenesis induced by β-Hex A and mannose receptor agonist antibody in bovine tracheal smooth-muscle cells

Quiescent cells [starved in medium containing 0 4% (v/v) FBS] in microtitre wells were pretreated with one of the peptides [GGRGDSPK or GGR(CH$_3$)GDSPK, in which R(CH$_3$) indicates N^{G},N^{G}-dimethyl(asymmetric)arginine] at a concentration of 5–10 μM dissolved in medium M199 for 30 min before the addition to the cells of Hex A (50 nM), vehicle for Hex A (PBS), mAb$_{15}$ (25 nM) or non-immune mouse IgG$_1$ Parallel experiments were performed as described above. Viable cell numbers were obtained by MTT assay at the end of a 48 h experimental period as described in the Experimental section Results are means ± S E M ($n = 3$ three separate experiments of quadruplicate cultures from different cell populations each from a different animal) Single-letter amino acid abbreviations are used

			Inhibition (%)	
Agonist	Fibronectin peptide	Concentration (μM)	DNA synthesis	Cell number
Hex A	None	0	0	0
	GGRGDSPK	5	39 ± 2	35 ± 5
	GGRGDSPK	10	62 ± 7	51 ± 5
	GGR(CH$_3$)GDSPK	5	0	0
	GGR(CH$_3$)GDSPK	10	0	0
mAb$_{15}$	None			0
	GGRGDSPK	5	36 ± 5	36 ± 6
	GGRGDSPK	10	67 ± 8	48 ± 3
	GGR(CH$_3$)GDSPK	5	0	0
	GGR(CH$_3$)GDSPK	10	0	0

higher affinity for the enzyme. It has also been previously reported that the K_m of hnRNP A1 protein was 0.5 μM; this high affinity was most probably due to the protein chain length as well as the presence of four methylatable arginine residues in A1 protein

Identification of enzymically methylated [*methyl*-^{14}C]SRB P-2

To identify the enzymic product, the *methyl*-^{14}C-labelled SRB P-2 purified on a Sephadex G-10 column (Figure 1) was concentrated and subjected to hydrolysis with HCl. The hydrolysate was then analysed by HPLC for *methyl*-^{14}C-labelled amino acids. As shown in Figure 2, two radioactive peaks, N^{G}-monomethylarginine (78.6%) and N^{G},N^{G}-dimethylarginine (21.4%), migrated together with respective authentic arginine derivatives, with retention times of 46 and 66 min, respectively, indicating that the enzymic products were indeed due to the protein arginine N-methyltransferase. No other methylated basic amino acids were seen.

Enzymic methylation of fibronectin peptide and its analogues

Several synthetic oligopeptides similar to the sequence of the cell attachment domain in fibronectin were examined as substrates for protein methylase I. As shown in Table 4, the synthetic heptapeptide Gly-Arg-Gly-Asp-Ser-Pro-Lys (FN P-1) showed negligible substrate capability. However, when the N-terminal glycine residue of FN P-1 was extended with extra glycine residues, the methyl acceptability increased in proportion to the number of residues added, indicating that the number of glycine residues at the N-terminus of the GRG motif was an important factor in increasing the methyl acceptability of the fibronectin peptide. However, because of very low methyl incorporation in these peptides, K_m values were not determined.

Effect of arginine methylation of the fibronectin peptides on their β-Hex-induced DNA synthesis

It has been known that lysosomal hydrolases, such as human Hex A and the agonist antibody against the macrophage mannose receptor, induce DNA synthesis and cell proliferation in the mannose-receptor-mediated mitogenesis of bovine tracheal smooth-muscle cells [22,23]. To investigate the effect of methylation of the arginine residue in the cell attachment peptide, two analogues of fibronectin peptide (FN P-2; GRGDSPK) were synthesized chemically, one with arginine and the other with N^{G},N^{G}-dimethyl(asymmetric)arginine. As shown in Table 5, the fibronectin peptide (FN P-2) containing an arginine residue inhibited the synthesis of DNA induced by both the ligand (Hex A) and an agonistic antibody (mAb_{15}), as well as cell division, in a concentration-dependent manner (35–67% inhibition, 5–10 μM). In contrast, FN P-2, containing dimethylarginine, inhibited neither of the agonist-induced mitogeneses.

DISCUSSION

N^G-Methylated arginine residues in protein are formed post-translationally in polypeptides only when the amino acid sequence and chain length are specifically recognized by protein arginine N-methyltransferase [1,2]. Previous studies indicated that the -GRG- motif within the methyl acceptor oligopeptides was the most favourable local sequence for methylation by the methyltransferase [7,11,12]. In extending the above observations in the present study, we chemically synthesized several oligopeptides with overlapping local sequences of SRB and fibronectin for methylation *in vitro*, because these proteins contain a -GRG- sequence and are biologically important.

SRB protein is an RNA-binding protein that acts as one of the cofactors in the regulation of HIV-1 gene expression. The regulation of the HIV-1 gene is dependent on a number of *cis*-acting regulatory elements in the long terminal repeat [24,25]; a double-stranded RNA structure transcribed from the HIV-1 long terminal repeat, known as TAR, is critical for increasing gene expression in response to the Tat transactivator protein [26]. Two cellular factors, RNA polymerase II and TRP-185, bind specifically to TAR RNA in the presence of cellular factors [13]. Three cellular proteins have been identified in the cofactor fraction: elongation factor 1-α, the polypyrimidine-tract-binding proteins and SRB. SRB has a high degree of similarity to a variety of cellular proteins known as chaperonins [13]. The primary structure of SRB contains a GRG motif at the N-terminus (residues 18–20). As shown in Table 2, comparing the methyl acceptability of the synthetic 7-mer (SRB P-1; residues 16–22) and 19-mer (SRB P-3, residues 10–28), it is clear that the longer peptide showed a much better substrate activity, with a lower K_m value, than the 7-mer peptide. These findings were predictable because our previous study had indicated that a hexapeptide was the minimum chain length for methylation; a tetrapeptide was completely inert as a substrate for myelin-basic-protein-specific protein methylase I (EC 2.1.1.126) [11]. When the N-terminus and the C-terminus of the 7-mer (SRB P-2) were blocked, an approx. 15% decrease in methyl acceptability was observed in comparison with the unblocked 7-mer (SRB P-1), indicating that the charge status of the N-terminus and the C-terminus of peptide did not greatly affect the methylation; rather, the chain length of the substrate was significant. It would constitute a great challenge to study whether the whole molecule of SRB protein has methyl-accepting activity and what effect methylation has on RNA-binding activity. Unfortunately, however, unmethylated SRB protein is not available at present. Nevertheless, when the arginine residue in the RGG motif was N^G-methylated (1.4 mol%), the binding activity of hnRNP A1 protein towards RNA was depressed [27]. Because the methylation would be expected to block hydrogen-bonding interactions between the phosphoryl group of RNA and the N^G-guanidino nitrogen that allows a single essential arginine residue in Tat protein to recognize the TAR RNA target [28], methylation might be expected to have a far-reaching effect on the regulation of HIV gene expression.

In general, enzymic post-synthetic modification of protein *in vitro* is not a stoichiometric reaction and often yields a fractional modification, thereby resulting in microheterogeneity on gel electrophoresis of the reaction product. Fractional modification was more obvious when peptide substrates were employed. To overcome this drawback, we chemically synthesized an analogue of the 8-mer cell-attachment peptide (GGRGDSPK; FN P-2) containing N^G,N^G-dimethyl-(asymmetric)-L-arginine in the place of L-arginine and studied its effect on the tracheal smooth-muscle cells in culture. As shown in Table 5, the arginine-unmethylated fibronectin peptide (FN P-2) inhibited an agonistic antibody of DNA synthesis induced by mannose receptor and Hex, as well as cell proliferation, in proportion to the concentration of peptide, whereas the methylated peptide did not block under the identical conditions. On activation of the receptors for Hex A in tracheal smooth-muscle cells, $\alpha_5\beta_1$ integrins rapidly associate directly with the receptor [29]. The present results further support the notion that the fibronectin peptide inhibits mannose-receptor-mediated signalling pathways and mitogenesis indirectly by binding the integrins. This in turn might inhibit the interaction between integrins and the mannose receptors in tracheal smooth-muscle cells.

Fibronectin interacts with extracellular matrix macromolecules and with receptors at the surface of most eukaryotic cells [15]; the interaction of fibronectin with cells results in the attachment and spreading of those cells on a surface covered with fibronectin. It has been known that the RGD sequence is required for the recognition of fibronectin in cells [14]. These sequences have also been identified in cell recognition sites of vitronectin, fibrinogen, von Willebrand factor, type I collagen and osteopontin, each of which can bind to one or more integrins [30,31]. The results presented here, that N^G-methylated arginine in fibronectin peptide abolished the inhibitory effect of fibronectin peptide on mannose-receptor-mediated reactions, suggest that the post-translational methylation of arginine in fibronectin-like proteins is involved in the regulation of the interactions of the RGD sequence with cells.

We thank Dr Kenneth R Williams (Yale University, New Haven, CT, U S A.) for his generous gift of the synthetic peptides used in this study This work was supported by a research grant from the Graduate School of Biotechnology, Korea University (to S.K), and from the National Institutes of Health (HL56812) (to D.B.L).

REFERENCES

1 Paik, W K. and Kim, S (1980) in Protein Methylation (Paik, W K and Kim, S , eds), pp. 8–25, John Wiley and Sons, New York
2 Kim, S , Park, G H. and Paik, W K (1998) Amino Acids **15**, 291–306
3 Kim, S., Ghosh, S. K and Chanderkar, L P. (1990) in Protein Methylation (Paik, W. K and Kim, S , eds), pp 75–95, CRC Press, Boca Raton, FL
4 Ghosh, S K , Paik, W K and Kim, S (1988) J Biol Chem **263**, 19024–19033
5 Rajpurohit, R , Lee, S O , Park, J O., Paik, W K and Kim, S (1994) J Biol Chem. **269**, 1075–1082
6 Williams, K R., Stone, K L, LoPresti, M B , Merrill, B. M. and Plank, S R (1985) Proc Natl Acad Sci U.S A **82**, 5666–5670
7 Kim, S , Merrill, B M , Rajpurohit, R , Kumar, A , Stone, K L , Papov, V V., Schneiders, J M , Szer, W., Wilson, S H , Paik, W K and Williams, K R (1997) Biochemistry **36**, 5185–5192
8 Lischwe, M A (1990) in Protein Methylation (Paik, W K and Kim, S , eds), pp 97–103, CRC Press, Boca Raton, FL
9 Lischwe, M. A , Cook, R G , Ahn, Y S , Yeoman, L C. and Busch, H (1985) Biochemistry **24**, 6025–6028
10 Lischwe, M A , Ochs, R. L., Reddy, R , Cook, R G , Yeoman, L C , Tan, E M , Reichlin, M and Busch, H (1985) J Biol. Chem. **260**, 14304–14310
11 Ghosh, S K , Syed, S K , Jung, S , Paik, W K and Kim, S (1990) Biochim Biophys Acta **1039**, 142–148
12 Rawal, N , Rajpurohit, R., Lischewe, M , Williams, K R., Paik, W K and Kim, S (1995) Biochim Biophys Acta **1248**, 11–18
13 Wu-Baer, F , Lane, W S and Gaynor, R B (1996) J Biol Chem **271**, 4201–4208
14 Pierschbacher, M D and Rouslahti, E. (1984) Proc Natl Acad Sci U S A **81**, 5985–5988
15 Hynes, R O and Yamada, K (1982) J Cell Biol **95**, 369–377

16 Pytela, R., Pierschbacher, M. D., Ginsberg, M. H., Plow, E. F. and Ruoslahti, E. (1986) Science **231**, 1559–1562
17 Hautanen, A., Gailit, J., Mann, D. M. and Ruoslahti, E. (1989) J. Biol. Chem. **264**, 1437–1442
18 Schebuski, R. J., Ramjit, D. R., Bencen, G. H. and Polokoff, M. A. (1989) J. Biol. Chem. **264**, 21550–21556
19 Rawal, N., Rajpurohit, R., Paik, W. K. and Kim, S. (1994) Biochem. J. **300**, 483–489
20 Bradford, M. M. (1976) Anal. Biochem. **72**, 248–254
21 Lew, D. B., Dempsey, B. K., Zhao, Y., Muthalif, M., Fatima, S. and Malik, K. U. (1999) Am. J. Respir. Cell Mol. Biol. **21**, 111–118
22 Lew, D. B. and Rattazzi, M. C. (1991) J. Clin. Invest. **88**, 1969–1975
23 Lew, D. B., Songu-Mize, E., Pontow, S. E., Stahl, P. D. and Rattazzi, M. C. (1994) J. Clin. Invest. **94**, 1855–1863
24 Gaynor, R. (1992) AIDS **6**, 347–363
25 Cullen, B. R. (1995) AIDS **9**, S19–32
26 Feng, S. and Holland, E. C. (1988) Nature (London) **334**, 165–167
27 Rajpurohit, R., Paik, W. K. and Kim, S. (1994) Biochem. J. **304**, 903–909
28 Calnan, B. J., Tidor, B., Biancalana, S., Hudson, D. and Frankel, A. D. (1991) Science **252**, 1167–1171
29 Lew, D. B., Dempsey, B. K. and Malik, K. U. (1998) Pediatr. Res. **43**, 8A (abstract)
30 Ruoslahti, E. and Pierschbacher, M. D. (1987) Science **238**, 491–497
31 Hynes, R. O. (1987) Cell **48**, 549–554

Received 17 November 1999/16 February 2000; accepted 30 March 2000

Contrasting effects of N^5-substituted tetrahydrobiopterin derivatives on phenylalanine hydroxylase, dihydropteridine reductase and nitric oxide synthase

Ernst R. WERNER*[1], Hans-Jörg HABISCH†, Antonius C. F. GORREN†, Kurt SCHMIDT†, Laura CANEVARI‡, Gabriele WERNER-FELMAYER* and Bernd MAYER†

*Institute for Medical Chemistry and Biochemistry of the University of Innsbruck, Fritz-Pregl-Str 3, A-6020 Innsbruck, Austria, †Institute for Pharmacology and Toxicology, University of Graz, Universitätsplatz 2, A-8010 Graz, Austria, and ‡Department of Biochemistry, Institute of Neurology, Queen Square, London WC1N 3BG, U.K

Tetrahydrobiopterin [(6*R*)-5,6,7,8-tetrahydro-L-biopterin, H_4 biopterin] is one of several cofactors of nitric oxide synthases (EC 1.14.13.39). Here we compared the action of N^5-substituted derivatives on recombinant rat neuronal nitric oxide synthase with their effects on dihydropteridine reductase (EC 1.6.99.7) and phenylalanine hydroxylase (EC 1.14.16.1), the well-studied classical H_4biopterin-dependent reactions. H_4biopterin substituted at N^5 with methyl, hydroxymethyl, formyl and acetyl groups were used. Substitution at N^5 occurs at a position critical to the redox cycle of the cofactor in phenylalanine hydroxylase/dihydropteridine reductase. We also included $N^{2'}$-methyl H_4biopterin, a derivative substituted at a position not directly involved in redox cycling, as a control. As compared with N^5-methyl H_4biopterin, N^5-formyl H_4biopterin bound with twice the capacity but stimulated nitric oxide synthase to a lesser extent. Depending on the substituent used, N^5-substituted derivatives were redox-active: N^5-methyl- and N^5-hydroxylmethyl H_4biopterin, but not N^5-formyl- and N^5-acetyl H_4biopterin, reduced 2,6-dichlorophenol indophenol. N^5-Substituted H_4biopterin derivatives were not oxidized to products serving as substrates for dihydropteridine reductase and, depending on the substituent, were competitive inhibitors of phenylalanine hydroxylase· N^5-methyl- and N^5-hydroxymethyl H_4biopterin inhibited phenylalanine hydroxylase, whereas N^5-formyl- and N^5-acetyl H_4 biopterin had no effect. Our data demonstrate differences in the mechanism of stimulation of phenylalanine hydroxylase and nitric oxide synthase by H_4biopterin. They are compatible with a novel, non-classical, redox-active contribution of H_4biopterin to the catalysis of the nitric oxide synthase reaction

Key words: biopterin, inhibition, reaction mechanism, redox cycling, stimulation.

INTRODUCTION

The role of tetrahydrobiopterin [(6*R*)-5,6,7,8-tetrahydro-L-biopterin, H_4biopterin] in nitric oxide synthase (NOS; EC 1.14.13.39) has attracted attention due to its differences to the well-known function of this pteridine in the phenylalanine hydroxylase reaction [1], and due to the prospects of using this knowledge for inhibitor design. In contrast to phenylalanine hydroxylase (EC 1.14.16.1), NOS is stimulated by much lower concentrations of the cofactor and exhibits a much higher selectivity for the (6*R*) 6-(L-erythro-1,2-dihydroxypropyl) side chain [2,3]. In common with phenylalanine hydroxylase, only tetrahydro- but no dihydroderivatives of pteridines stimulate the reaction [4,5]. In addition to increasing NOS activity, H_4biopterin promotes dimerization of the enzyme [6–8], stimulates the shift of the haem iron from low spin to high spin [9,10], and increases the affinity of the enzyme for the substrate L-arginine [4]. However, these allosteric effects alone are insufficient to explain the role of H_4biopterin in the NOS reaction, since the 4-amino analogue exerts all of these allosteric effects without stimulating the enzyme's activity [10,11]. Experimental results hint at a redox-active role of H_4biopterin in the NOS reaction: the decay of the ferrous oxygen complex of the neuronal NOS (nNOS) oxygenase domain is accelerated by H_4biopterin [12]. Low-temperature UV spectra of nNOS suggest a reductive activation of the ferrous oxygen complex by H_4biopterin [13].

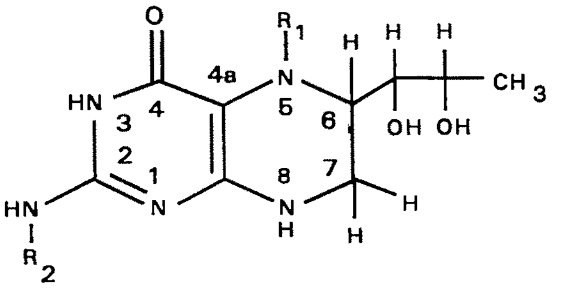

Figure 1 Structural formula of H_4biopterin derivatives used in this study

N^5-substituted derivatives, R_1 = methyl, hydroxymethyl, formyl or acetyl, and R_2 = H $N^{2'}$-Methyl H_4biopterin, R_1 = H and R_2 = methyl H_4biopterin (R_1 = R_2 = H) leaves the phenylalanine hydroxylase reaction as 4*a*-hydroxy derivative. This 4*a*-hydroxy group together with the hydrogen atom (R_1) at N^5 is then cleaved off as water to yield the quinonoid 6,7-[8H]dihydrobiopterin, which is the substrate of the dihydropteridine reductase reaction [1]

Abbreviations used H_4biopterin, (6*R*)-5,6,7,8-tetrahydro-L-biopterin, DCPIP, 2,6-dichlorophenol indophenol, NOS, nitric oxide synthase, nNOS, neuronal NOS

[1] To whom correspondence should be addressed (e-mail ernst r werner@uibk ac at)

We have shown recently that the N^{5}-methyl derivative of H_4biopterin stimulates nNOS, although it does not react with molecular oxygen [14]. Here we compare the action of a series of N^{5}-substituted H_4biopterin derivatives (Figure 1) on phenylalanine hydroxylase, dihydropteridine reductase (EC 1.6.99 7) and nNOS. Substitution at N^{5} occurs at a position critical to the redox cycle of the cofactor in phenylalanine hydroxylase/dihydropteridine reductase. As a control, we included $N^{2'}$-methyl H_4biopterin (Figure 1), a derivative substituted at a position not directly involved in redox cycling. We show that N^{5}-substituted derivatives do not support the dihydropteridine reductase reaction and are inhibitors of phenylalanine hydroxylase. The nNOS stimulatory potential of N^{5}-substituted H_4biopterin derivatives correlates with their reductive potential, but not with their affinity to nNOS. Our data are compatible with a novel, non-classical, redox-active role of the pterin cofactor in the NOS reaction.

EXPERIMENTAL

Materials

All pteridine derivatives were obtained from Dr Schircks Laboratories, Jona, Switzerland. H_4biopterin content of the novel N^{5}- and $N^{2'}$-substituted H_4biopterin derivatives was checked by HPLC with electrochemical detection as described in [15]. All N^{5}-derivatives and the $N^{2'}$-methyl derivative had no detectable H_4biopterin (< 0.0033 %), except for N^{5}-hydroxymethyl H_4biopterin, which contained 1.1 % H_4biopterin. [3′-^{3}H]-H_4biopterin (14 Ci/mmol) was enzymically prepared from [8,5′-^{3}H]GTP as detailed elsewhere [16]. L-[2,3,4,5-^{3}H]Arginine (57 Ci/mmol) was from Amersham Pharmacia Biotech (Uppsala, Sweden). H_4biopterin-free rat nNOS was prepared from baculovirus-infected insect cells treated with 2,4-diamino-6-hydroxypyrimidine as described in [17]. Sheep liver dihydropteridine reductase (100 units/mg) and rat liver phenylalanine hydroxylase (0.069 units/mg) were obtained from Sigma (St.Louis, MO, U.S.A.). All other chemicals were from Sigma or Merck (Darmstadt, Germany).

Determination of phenylalanine hydroxylase activity

Phenylalanine hydroxylase was incubated under conditions modified from [18] and the amount of tyrosine formed was determined by HPLC with fluorescence detection. Briefly, phenylalanine hydroxylase (60 μg/ml) was preincubated with 200 μM phenylalanine for 10 min at 37 °C, and the reaction was started by addition of a mixture of H_4biopterin derivative (10 μM–1 mM) and 10^{4} units/ml catalase (Serva, Heidelberg, Germany). After a further 20 min at 37 °C, the reaction was stopped by addition of 10 μl of 1 M HCl. Then, 10 μl were injected on to an RP-18 column (125 × 4 mm, Lichrosphere, 5 μm particle size; Merck) and eluted with 75 mM KH_2PO_4 buffer containing 20 % (v/v) acetonitrile, 10 % (v/v) methanol, 0.44 g/l SDS and 1.5 μM EDTA, pH 3.1 (adjusted with 1 M trichloroacetic acid) at a flow rate of 0.8 ml/min. Tyrosine was detected by fluorescence (excitation 285 nm, emission 325 nm) with a detection limit of 2.5 pmol.

Assay for dihydropteridine reductase

Two assays were used. (i) A method based on oxidation of the H_4biopterin derivative by peroxidase/hydrogen peroxide and monitoring of the consumed NADH was updated from [19]. In 200 μl of 50 mM Tris/HCl, pH 7.2, the following components were incubated at 37 °C for 5 min: hydrogen peroxide (0.003 %), peroxidase (1 unit, Sigma), H_4biopterin derivative (1–35 μM), NADH (150 μM) and dihydropteridine reductase (2 μg/ml). The reaction was started by addition of dihydropteridine reductase and the consumption of NADH was monitored by UV absorption at 340 nm in a microplate reader (Anthos 2001, Anthos, Salzburg, Austria). (ii) The second method used to determine dihydropteridine reductase monitors the consumption of 2,6-dichlorophenol indophenol (DCPIP) [3], which is used to oxidize the tetrahydropterin to the 'quinonoid' 6,7-[8H]dihydrobiopterin. In a total volume of 200 μl, 2 μg/ml dihydropteridine reductase are incubated with 0.1–3.4 μM H_4biopterin in the presence of 150 μM NADH and 150 μM DCPIP for 5 min at 37 °C. The reaction is started by addition of DCPIP, and the consumption of the dye is quantified by measurement of the absorption at 620 nm in a microplate reader (Anthos)

Measurement of NOS activity

NOS activity was determined by quantification of [^{3}H]citrulline from L-[2,3,4,5-^{3}H]arginine as described in [20]. Incubations were performed in 0.1 ml of 50 mM triethanolamine/HCl, pH 7.4, containing 0.1–0.2 μg of purified, recombinant H_4biopterin-free nNOS [17], 0.1 mM [2,3,4,5-^{3}H]L-arginine (≈ 60000 c.p.m.), 0.5 mM $CaCl_2$, 10 μg/ml calmodulin, 0.2 mM NADPH, 5 μM FAD, 5 μM FMN, 0.2 mM CHAPS and 10^{-8}–10^{-3} M H_4 biopterin derivative. In some experiments, 5 μM haemoglobin was added to scavenge NO to inactivate feedback inhibition, since NO rather than peroxynitrite is the product of the NOS reaction with N^{5}-methyl H_4biopterin [14].

Binding of H_4biopterin derivatives to nNOS

Purified, H_4biopterin-free rat nNOS was incubated for 10 min at 37 °C with 10 nM [3′-^{3}H]H_4biopterin (14 nCi), 0.1 mM L-arginine and 10^{-8}–10^{-3} M H_4biopterin derivative in 0.1 ml of triethanolamine/HCl buffer, pH 7.4, followed by rapid vacuum filtration using the MultiScreen Assay System from Millipore. Determination of the radioactivity retained on the filters by liquid scintillation counting was performed as in [3].

Reduction of DCPIP by H_4biopterin derivatives

At room temperature in volumes of 200 μl, H_4biopterin derivatives (150 μM) or water were mixed with DCPIP (150 μM) at the following pH values in the following buffer systems (100 mM each): pH 7.2 (K_2HPO_4/KH_2PO_4), pH 6.0 (K_2HPO_4/KH_2PO_4); pH 4.5 (acetic acid/sodium acetate) and pH 3.0 (KH_2PO_4/H_3PO_4). Within 2 min, the absorbance at 620 nm (pH 7.2 and 6.0) and at 540 nm (pH 4.5 and 3 0) was measured with a microplate reader, and the absorbance of the wells containing no H_4biopterin derivative was set to 100 %. Stopped-flow experiments to analyse the kinetics of reduction of DCPIP by the H_4biopterin derivatives were performed with a Biosequential SX-17 MV ASVD apparatus (Applied Photophysics, Leatherhead, U.K.). Solutions of pteridines and DCPIP, 100 μl each, were mixed at 25 °C and the decrease of UV absorption at 600 nm was monitored up to 30 s. The final reaction mixture consisted of 0 2 M K_2HPO_4/HCl buffer (pH 6.0), 150 μM H_4biopterin derivative and 25 μM DCPIP. Six independent experiments yielded the means ± S.E.M. mentioned in the Results section. All values shown are means ± S.E.M. of three independent experiments unless indicated otherwise.

RESULTS

Depending on the nature of the N^5-substituent, N^5-substituted H_4biopterin derivatives are still capable of donating electrons. This is exemplified by the equilibrium concentrations of DCPIP in reaction mixtures with the H_4biopterin derivatives (Figure 2). Whereas H_4biopterin and its $N^{2'}$-methyl derivative reduced DCPIP at all investigated pH values to 100 %, N^5-substituted derivatives showed declining reductive potential in the order of the N^5-substituent hydrogen > methyl > hydroxymethyl. N^5-formyl and N^5-acetyl derivatives were not capable of reducing DCPIP in the investigated pH range (Figure 2). A similar ranking was observed by studying the kinetics of the reaction of DCPIP with the H_4biopterin derivatives: Second-order rate constants declined from $170 \pm 4\ \text{mM}^{-1} \cdot \text{s}^{-1}$ for the N^5-substituent hydrogen, to $1.3 \pm 0.3\ \text{mM}^{-1} \cdot \text{s}^{-1}$ for the N^5-methyl, and $6.0 \pm 0.3\ \text{mM}^{-1} \cdot \text{s}^{-1}$ for the N^5-hydroxymethyl derivative. N^5-formyl and N^5-acetyl H_4biopterin did not react at all. The $N^{2'}$-methyl derivative, in contrast, reduced DCPIP with a second-order rate constant of $200 \pm 7\ \text{mM}^{-1} \cdot \text{s}^{-1}$, which is as fast as the parent compound H_4biopterin.

Substitution of H_4biopterin at $N^{2'}$ with a methyl group did not affect the ability of the compound to serve as substrate for the dihydropteridine reductase reaction (Figure 3). N^5-substitution, however, completely blocked the ability of the compounds to serve as substrates for dihydropteridine reductase regardless of the nature of the N^5-substituent [Figure 3, assay (i)]. When given at a 10-fold excess (35 µM) together with H_4biopterin (3.5 µM), none of the N^5-substituted H_4biopterin derivatives inhibited the dihydropteridine reductase reaction [assay (ii), not shown].

When the derivatives were tested for their ability to serve as substrates for the phenylalanine hydroxylase reaction, only $N^{2'}$-methyl H_4biopterin could act as cofactor for the enzyme instead of H_4biopterin (Figure 4). Whereas the K_m of $N^{2'}$-methyl H_4biopterin (25.2 ± 7.4 µM) was comparable with that of H_4biopterin (17.4 ± 1.2 µM), only 24.6 ± 2.8 % of the V_{max} of H_4biopterin was achieved. When given together with H_4biopterin, N^5-formyl H_4biopterin as well as the N^5-acetyl derivative had no effect on phenylalanine hydroxylase activity. N^5-methyl H_4biopterin ($K_i = 23.1 \pm 5.4$ µM) and N^5-hydroxymethyl H_4biopterin ($K_i = 237 \pm 70$ µM), in contrast, inhibited phenylalanine hydroxylase activity competitively with H_4biopterin.

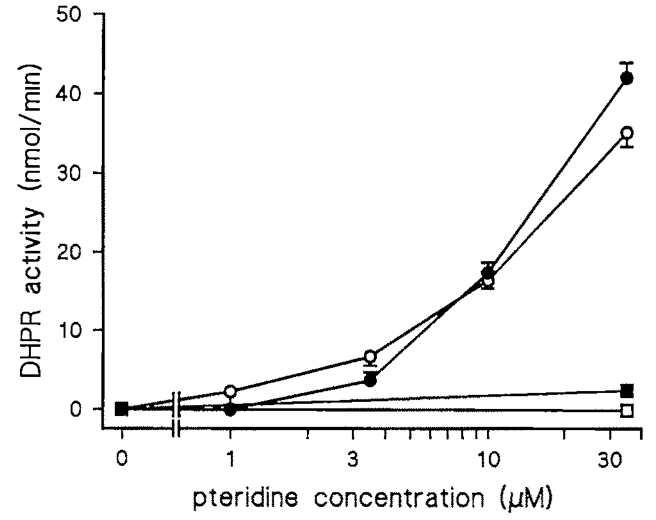

Figure 3 Ability of H_4biopterin derivatives to provide substrates to the dihydropteridine reductase reaction

Pteridines were used in the indicated concentrations in the assay for dihydropteridine reductase, which used hydrogen peroxide/peroxidase to oxidize the pterins and monitor the consumption of NADH at 340 nm (assay I, see the Experimental section) Results show means ± S D of four parallel incubations ○, H_4biopterin, ●, $N^{2'}$-methyl H_4biopterin; ■, N^5-hydroxymethyl H_4biopterin; ☐ (= no stimulation), N^5-methyl H_4biopterin, N^5-formyl H_4biopterin and N^5-acetyl H_4biopterin.

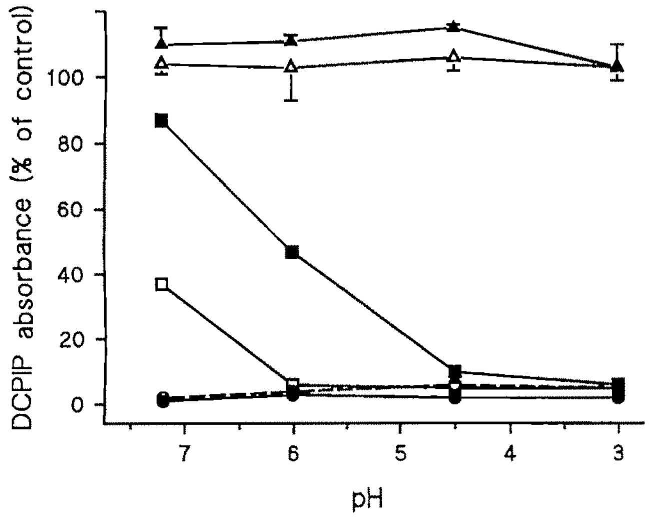

Figure 2 Reduction of DCPIP by H_4biopterin derivatives as a function of pH

Pteridine derivatives (final concentration 150 µM) were mixed with DCPIP (final concentration 150 µM) at room temperature, and the absorbance determined at 620 and 540 nm within 2 min The control was the absorption of DCPIP mixed with water instead of H_4biopterin-derivative-containing solution Values shown are means ± S D of 8 determinations ○, H_4biopterin, ●, $N^{2'}$-methyl H_4biopterin, ☐, N^5-methyl H_4biopterin; ■, N^5-hydroxymethyl H_4biopterin; △, N^5-formyl H_4biopterin, ▲, N^5-acetyl H_4biopterin

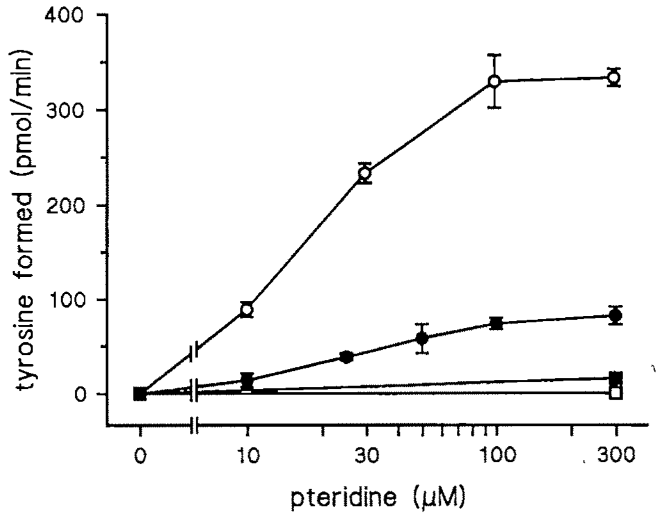

Figure 4 Stimulation of phenylalanine hydroxylase by H_4biopterin derivatives

Phenylalanine hydroxylase was incubated with the indicated concentrations of H_4biopterin derivatives and the formation of tyrosine from phenylalanine measured by HPLC with fluorescence detection Values shown are means ± S D of three parallel incubations ○, H_4biopterin, ●, $N^{2'}$-methyl H_4biopterin, ■, N^5-hydroxymethyl H_4biopterin, ☐ (= no stimulation), N^5-methyl H_4biopterin, N^5-formyl H_4biopterin and N^5-acetyl H_4biopterin.

Table 1 Binding and stimulatory characteristics of H_4biopterin derivatives on recombinant, H_4biopterin-free rat nNOS

H_4biopterin-free, recombinant nNOS was prepared as described in [17]. Binding of H_4biopterin derivatives to the enzyme was assayed by replacement of enzyme-bound [3′-^{3}H]H_4biopterin according to [3]. NOS activities were determined by measurement of [2,3,4,5-^{3}H]citrulline formed from L-[2,3,4,5-^{3}H]arginine in the presence of haemoglobin to avoid feedback inhibition by nitric oxide, which is the product of the NOS reaction in the presence of N^5-methyl H_4biopterin [14]. Values are means ± S.E.M. of three experiments. %V_{max} shows V_{max} as a percentage of that of the parent compound, H_4biopterin (= 100%).

Derivative	Binding to nNOS (K_d or K_i, μM)	Stimulation of nNOS (EC_{50}, μM)	Stimulation of nNOS (%V_{max})
H_4biopterin	0.26 ± 0.01	0.041 ± 0.015	100 ± 13
$N^{2'}$-Methyl H_4biopterin	15 ± 6	48 ± 14	62 ± 10
N^5-Methyl H_4biopterin	5.6 ± 1.2	7.0 ± 1.8	108 ± 15
N^5-Formyl H_4biopterin	2.5 ± 0.2	3.2 ± 1.7	47 ± 10
N^5-Acetyl H_4biopterin	130 ± 55	None	None

Table 1 compares binding and stimulation of H_4biopterin-free rat nNOS by H_4biopterin and its derivatives studied in this work. Substitution at $N^{2'}$ with a methyl group greatly reduced the affinity of H_4biopterin to the enzyme, and stimulation required a concentration of the pterin derivative three orders of magnitude higher. Substitution at N^5 with acetyl led to a complete loss in stimulation of nNOS, and binding was very poor (Table 1). Substitution at N^5 with methyl yielded a compound that could bind to nNOS and lead to full stimulation of the enzyme, albeit with a 170-fold higher EC_{50} compared with the parent compound. This is consistent with the more than two orders of magnitude lower affinity for the N^5-methyl derivative (Table 1). N^5-formyl H_4biopterin exhibits twice the affinity to nNOS as N^5-methyl H_4biopterin. Consistent with this, only about half of the concentration of N^5-formyl H_4biopterin as compared with N^5-methyl H_4biopterin is required for half-maximal stimulation of nNOS. The V_{max} reached with N^5-formyl H_4biopterin, however, is less than 50% when compared with N^5-methyl H_4biopterin or H_4biopterin (Table 1). N^5-Hydroxymethyl H_4biopterin bound with a K_i of 1.5 ± 0.7 μM, and stimulated the enzyme with an EC_{50} of 6.3 ± 1.9 μM to 84 ± 19% of the V_{max} observed with H_4biopterin. Since the 1.1% H_4biopterin contained in this preparation could contribute strongly to these observed values, they were omitted from the Table and not considered for further interpretation.

DISCUSSION

The role of H_4biopterin in the NOS reaction has fascinated researchers since its detection about 10 years ago [2,21,22]. A straightforward approach has been to assume that the first step of the NOS reaction, the hydroxylation of L-arginine, depends on H_4biopterin by a mechanism comparable with the phenylalanine hydroxylase reaction [23]. Several pieces of experimental evidence have made it more and more difficult to maintain this hypothesis. H_4biopterin was not required in stoichiometric amounts compared with product formation [24,25], and recycling of H_4biopterin was not observed [25]. In addition, the second step of the NOS reaction, the conversion of N^G-hydroxy-L-arginine to citrulline and NO, was found to require H_4biopterin [26] and is inhibited by the 4-amino analogue of the pterin cofactor [11]. Further, as shown in the present study, N^5-methyl H_4biopterin stimulates the NOS reaction, even though it is an inhibitor of the phenylalanine hydroxylase reaction and cannot be oxidized to products serving as substrate for the dihydropteridine reductase reaction. This demonstrates that the mechanisms of stimulation of phenylalanine hydroxylase and NOS by H_4biopterin may be fundamentally different. A comparison of data on NOS stimulation and binding of N^5-substituted H_4biopterin derivatives reveals a striking discrepancy between binding and stimulatory capacity: N^5-formyl H_4biopterin binds with twice the affinity compared with N^5-methyl H_4biopterin. Nevertheless, only N^5-methyl H_4biopterin yields a V_{max} comparable with H_4biopterin. The V_{max} obtained with N^5-formyl H_4biopterin is less than half of the V_{max} of the former two compounds. An explanation for this difference could be the different redox potentials of the two H_4biopterin derivatives, N^5-methyl and N^5-formyl H_4biopterin. Whereas cyclic voltammograms of the two compounds have a similar shape, the reductive potential of the N^5-formyl derivative is weaker by 0.53 V (A. C. F. Gorren, A. Kungl, K. Schmidt, E. R. Werner and B. Mayer, unpublished work). The N^5-formyl derivative, therefore, can no longer react with DCPIP. If a reductive potential is relevant for NOS catalysis by the pterin, this difference might explain the lower V_{max} for the N^5-formyl derivative. This interpretation is compatible with previous suggestions [13,27,28] that H_4biopterin may stimulate the NOS reaction by donating electrons in an unconventional way, thus coupling NADPH oxidation to NO and citrulline formation [29]. Detection of a trihydrobiopterin radical in the inducible-NOS oxygenase domain [30] impressively supports these suggestions.

The behaviour of $N^{2'}$-methyl H_4biopterin is difficult to interpret. Although the redox properties of this derivative are indistinguishable from the H_4biopterin parent compound, the V_{max} reached for stimulation of NOS is only 60% of V_{max} reached with H_4biopterin. The rather poor affinity of this compound to NOS may prevent saturation from being reached. Alternatively, the $N^{2'}$-methyl substitution may interfere with a potential interaction of the pterin with the haem in NOS. Crystal structures of NOS oxygenase domains containing pterin [28,31,32] suggest N^3 as a potential candidate for mediating an electronic interaction. Methyl at $N^{2'}$ might interfere with this interaction. Remarkably, calculated electronic structures of tetrahydropteridines [33] show that the two stimulators of NOS, H_4biopterin and its N^5-methyl derivative, share comparable potentials around N^3. In contrast, the 4-amino analogue of H_4biopterin, which inhibits NOS, has a totally different electronic structure at N^3.

The nature of the oxidation products of N^5-substituted H_4biopterin derivatives are not known thus far. As we show here, these oxidation products cannot serve as substrates in the dihydropteridine reductase reaction. Since H_4biopterin is not consumed in the NOS reaction in stoichiometric amounts [24,25], NOS must also have a means of restoring the cofactor with the electron(s) it has donated to the reaction, if the assumption of single electron donation by the pterin [13,27,28] is correct. Our results suggest clearly that this potential recycling in NOS may occur by a mechanism different to the dihydropteridine reductase reaction.

We are indebted to Eva Pitters and Bettina Fritz for expert technical assistance. Financial support by the Austrian Research Funds 'zur Foerderung der wissenschaftlichen Forschung' projects 13793-MOB (to E.R.W.), 13013-MED and 13586-MED (to B.M.) is gratefully acknowledged.

REFERENCES

1 Kaufman, S. (1993) New tetrahydrobiopterin-dependent systems. Annu. Rev. Nutr. **13**, 261–286

2 Kwon, N. S., Nathan, C. F. and Stuehr, D. J. (1989) Reduced biopterin as a cofactor in the generation of nitrogen oxides by murine macrophages. J. Biol. Chem. **264**, 20496–20501

3 Werner, E. R., Pitters, E., Schmidt, K., Wachter, H., Werner-Felmayer, G. and Mayer, B. (1996) Identification of the 4-amino analogue of tetrahydrobiopterin as a dihydropteridine reductase inhibitor and a potent pteridine antagonist of rat neuronal nitric oxide synthase. Biochem. J. **320**, 193–196

4 Klatt, P., Schmid, M., Leopold, E., Schmidt, K., Werner, E. R. and Mayer, B. (1994) The pteridine binding site of brain nitric oxide synthase – tetrahydrobiopterin binding kinetics, specificity, and allosteric interaction with the substrate domain. J. Biol. Chem. **269**, 13861–13866

5 Presta, A., Siddhanta, U., Wu, C. Q., Sennequier, N., Huang, L. X., Abu-Soud, H. M., Erzurum, S. and Stuehr, D. J. (1998) Comparative functioning of dihydro- and tetrahydropterins in supporting electron transfer, catalysis, and subunit dimerization in inducible nitric oxide synthase. Biochemistry **37**, 298–310

6 Baek, K. J., Thiel, B. A., Lucas, S. and Stuehr, D. J. (1993) Macrophage nitric oxide synthase subunits – purification, characterization, and role of prosthetic groups and substrate in regulating their association into a dimeric enzyme. J. Biol. Chem. **268**, 21120–21129

7 Klatt, P., Schmidt, K., Lehner, D., Glatter, O., Bachinger, H. P. and Mayer, B. (1995) Structural analysis of porcine brain nitric oxide synthase reveals a role for tetrahydrobiopterin and L-arginine in the formation of an SDS-resistant dimer. EMBO J. **14**, 3687–3695

8 List, B. M., Klosch, B., Volker, C., Gorren, A. C., Sessa, W. C., Werner, E. R., Kukovetz, W. R., Schmidt, K. and Mayer, B. (1997) Characterization of bovine endothelial nitric oxide synthase as a homodimer with down-regulated uncoupled NADPH oxidase activity: tetrahydrobiopterin binding kinetics and role of haem in dimerization. Biochem. J. **323**, 159–165

9 Wang, J., Stuehr, D. J. and Rousseau, D. L. (1995) Tetrahydrobiopterin-deficient nitric oxide synthase has a modified heme environment and forms a cytochrome P-420 analogue. Biochemistry **34**, 7080–7087

10 Mayer, B., Wu, C., Gorren, A. C. F., Pfeiffer, S., Schmidt, K., Clark, P., Stuehr, D. J. and Werner, E. R. (1997) Tetrahydrobiopterin binding to macrophage inducible nitric oxide synthase expressed in *Escherichia coli*. Heme spin shift and dimer stabilization by the potent pterin antagonist 4-amino tetrahydrobiopterin. Biochemistry **36**, 8422–8427

11 Pfeiffer, S., Gorren, A. C. F., Pitters, E., Schmidt, K., Werner, E. R. and Mayer, B. (1997) Allosteric modulation of rat brain nitric oxide synthase by the pterin-site enzyme inhibitor 4-amino tetrahydrobiopterin. Biochem. J. **328**, 349–352

12 Abu-Soud, H. M., Gachhui, R., Raushel, F. M. and Stuehr, D. J. (1997) The ferrous-dioxy complex of neuronal nitric oxide synthase – divergent effects of L-arginine and tetrahydrobiopterin on its stability. J. Biol. Chem. **272**, 17349–17353

13 Bec, N., Gorren, A. C. F., Voelker, C., Mayer, B. and Lange, R. (1998) Reaction of neuronal nitric-oxide synthase with oxygen at low temperature. Evidence for reductive activation of the oxy-ferrous complex by tetrahydrobiopterin. J. Biol. Chem. **273**, 13502–13508

14 Riethmuller, C., Gorren, A. C. F., Pitters, E., Hemmens, B., Habisch, H. J., Heales, S. J. R., Schmidt, K., Werner, E. R. and Mayer, B. (1999) Activation of neuronal nitric oxide synthase by the 5-methyl analog of tetrahydrobiopterin. J. Biol. Chem. **274**, 16047–16051

15 Hyland, K. (1985) Estimation of tetrahydro, dihydro and fully oxidised pterins by high-performance liquid chromatography using sequential electrochemical and fluorometric detection. J. Chromatogr. **343**, 35–41

16 Werner, E. R., Schmid, M., Werner-Felmayer, G., Mayer, B. and Wachter, H. (1994) Synthesis and characterization of ^{3}H-labelled tetrahydrobiopterin. Biochem. J. **304**, 189–193

17 List, B. M., Klatt, P., Werner, E. R., Schmidt, K. and Mayer, B. (1996) Overexpression of neuronal nitric oxide synthase in insect cells reveals requirement of haem for tetrahydrobiopterin binding. Biochem. J. **315**, 57–63

18 Kaufman, S. (1987) Phenylalanine 4-monooxygenase from rat liver. Methods Enzymol. **142**, 3–17

19 Craine, J. E., Hall, E. S. and Kaufman, S. (1972) The isolation and characterization of dihydropteridine reductase from sheep liver. J. Biol. Chem. **247**, 6082–6091

20 Mayer, B., Klatt, P., Werner, E. R. and Schmidt, K. (1994) Molecular mechanisms of inhibition of porcine brain nitric oxide synthase by the antinociceptive drug 7-nitro-indazole. Neuropharmacology **33**, 1253–1259

21 Tayeh, M. A. and Marletta, M. A. (1989) Macrophage oxidation of L-arginine to nitric oxide, nitrite, and nitrate. Tetrahydrobiopterin is required as a cofactor. J. Biol. Chem. **264**, 19654–19658

22 Mayer, B., John, M. and Bohme, E. (1990) Purification of a Ca^{2+}/calmodulin-dependent nitric oxide synthase from porcine cerebellum. Cofactor-role of tetrahydrobiopterin. FEBS Lett. **277**, 215–219

23 Marletta, M. A. (1989) Nitric oxide: biosynthesis and biological significance. Trends Biochem. Sci. **14**, 488–492

24 Mayer, B., John, M., Heinzel, B., Werner, E. R., Wachter, H., Schultz, G. and Bohme, E. (1991) Brain nitric oxide synthase is a biopterin- and flavin-containing multi-functional oxido-reductase. FEBS Lett. **288**, 187–191

25 Giovanelli, J., Campos, K. L. and Kaufman, S. (1991) Tetrahydrobiopterin, a cofactor for rat cerebellar nitric oxide synthase, does not function as a reactant in the oxygenation of arginine. Proc. Natl. Acad. Sci. U.S.A. **88**, 7091–7095

26 Stuehr, D. J., Kwon, N. S., Nathan, C. F., Griffith, O. W., Feldman, P. L. and Wiseman, J. (1991) N omega-hydroxy-L-arginine is an intermediate in the biosynthesis of nitric oxide from L-arginine. J. Biol. Chem. **266**, 6259–6263

27 Marletta, M. A., Hurshman, A. R. and Rusche, K. M. (1998) Catalysis by nitric oxide synthase. Curr. Opin. Chem. Biol. **2**, 656–663

28 Raman, C. S., Li, H., Martasek, P., Kral, V., Masters, B. S. and Poulos, T. (1998) Crystal structure of constitutive endothelial nitric oxide synthase: a paradigm for pterin function involving a novel metal center. Cell **95**, 939–950

29 Pfeiffer, S., Mayer, B. and Hemmens, B. (1999) Chemical puzzles posed by a biological messenger. Angew. Chem. Int. Ed. **38**, 1714–1731

30 Hurshman, A. R., Krebs, C., Edmondson, D. E., Huynh, B. H. and Marletta, M. A. (1999) Formation of a pterin radical in the reaction of the heme domain of inducible nitric oxide synthase with oxygen. Biochemistry **38**, 15689–15696

31 Crane, B. R., Arvai, A. S., Ghosh, D. K., Wu, C., Getzoff, E. D., Stuehr, D. J. and Tainer, J. A. (1998) Structure of nitric oxide synthase dimer with pterin and substrate. Science **279**, 2121–2126

32 Fischmann, T. O., Hruza, A., Niu, X. D., Fossetta, J. D., Lunn, C. A., Dolphin, E., Prongay, A. J., Reichert, P., Lundell, D. J., Narula, S. K. and Weber, P. C. (1999) Structural characterization of nitric oxide synthase isoforms reveals striking active-site conservation. Nat. Struct. Biol. **6**, 233–242

33 Reibnegger, G., Pauschenwein, J. and Werner, E. R. (1999) Electronic structure of tetrahydropteridine derivatives. Pteridines **10**, 91–94

Received 16 November 1999/8 March 2000; accepted 30 March 2000

Biochem. J. (2000) 348, 585–590 (Printed in Great Britain)

A new method for the selection of protein interactions in mammalian cells

Eileen ROJO-NIERSBACH, Debra MORLEY, Stephanie HECK, and Norbert LEHMING[1]
Max-Delbruck-Laboratorium in der Max-Planck-Gesellschaft, Carl-von-Linné-Weg 10, 50829 Koln, Germany

In the present study we present a new method that allows for the selection of protein interactions in mammalian cells. We have used this system to verify two interactions previously characterized *in vitro*. (1) The interaction between human TATA-binding protein 1 and nuclear factor κB and (2) the association of *Homo sapiens* nuclear autoantigen SP100B with human heterochromatin protein 1α, a protein implicated in chromatin remodelling. We observe for the first time that these interactions also occur *in vivo*. One protein was fused to the N-terminal half of ubiquitin, while the interacting partner was fused to the C-terminal half of ubiquitin, that was itself linked to guanine phosphoryltransferase 2 (gpt2) modified to begin with an arginine residue. Upon interaction of both proteins, ubiquitin is reconstituted, and its association with the Rgpt2 reporter is subsequently cleaved off by ubiquitin-processing enzymes. The presence of arginine in the *Rgpt2* gene product leads to the degradation of the product by the N-end rule pathway. In the human fibroblast cell line HT1080HPRT⁻ (that is deficient in the enzyme for hypoxanthine-guanine phosphoribosyltransferase) cells in which interaction between both proteins of interest occurs can then be selected for by hypoxanthine/aminopterin/thymine medium and counterselected against by 6-thioguanine medium. This method provides a suitable alternative to the yeast two-hybrid system and is generally applicable.

Key words: *Homo sapiens* nuclear autoantigen 100B, human heterochromatin protein 1α, human TATA-binding protein 1, nuclear factor κB, transcription.

INTRODUCTION

Protein interactions are necessary for all biological processes. These interactions can be studied with purified proteins *in vitro*, but these studies must be validated for their biological significance inside the living cell. For example, the yeast two-hybrid assay can be used to functionally analyse protein interactions *in vivo*. This assay was first described for *Saccharomyces cerevisiae* [1,2] and has since been adapted to monitor protein interactions in tissue culture cells [3]. However, the assay is based on a transcriptional readout; as a consequence, the analysis of transcription factors is limited. For example, transcriptional repressors may interfere with the signal, while transcriptional activators may produce a signal in the absence of an interacting protein. Also, the interaction must take place inside the nucleus, thereby excluding, for example, the analysis of membrane proteins in their native environment. An alternative system based on cell proliferation has been described for *S. cerevisiae* [4], and this system has recently been adapted for mammalian cells [5]. This system allows transcription factors to be tested; however, membrane proteins cannot be studied. Additionally, it is only possible to monitor protein interactions, because a selection method has not yet been described.

The split-ubiquitin assay is an alternative to the standard yeast two-hybrid system [6]. Ubiquitin is split into N-terminal and C-terminal halves (N_{ub} and C_{ub}, respectively), and each half is fused to either protein of interest. If the two proteins interact inside the living cell, the two halves of ubiquitin are brought into close contact; hence, this complemented ubiquitin is recognized by the ubiquitin-specific proteases (UBPs). The fusion containing C_{ub} is cleaved, resulting in a protein product of reduced size. Since ubiquitin proteases are present in the cytosol and in the nucleus [7,8], the assay is not limited to interactions reconstituted in the nucleus of the cell. The split-ubiquitin assay was first described for *S. cerevisiae*, and the analysis was performed with Western-blots [9]. Recently, a selection in *S. cerevisiae* based on the split-ubiquitin assay has been published [10]. One protein is fused to N_{ub}, while a second protein is fused to C_{ub} followed by orotidine-5′-phosphate decarboxylase (ura3) with an arginine at position 1. As shown by the N-end rule [11], which correlates the *in vivo* half-life of a protein with the nature of its N-terminal residue, introduction of this arginine residue promotes the rapid degradation of the *Rura3* gene product. If the two proteins of interest interact inside the living cell, ubiquitin is reconstituted and the C_{ub} fusion protein is cleaved from the *Rura3* gene product. Upon its cleavage from the C_{ub} fusion protein, the Rura3 reporter is degraded; as a result, the yeast cells become phenotypically uracil-deficient. 5-Fluoroorotic acid (FOA) can be used to select for uracil-deficient *S. cerevisiae* cells; therefore, the protein interactions inside the living cells can be selected for (with uracil-depleted medium) and counterselected against (with medium containing FOA).

We utilize this system to verify protein–protein interactions implicated in the transcriptional regulation of human genes. Previously, it has been demonstrated that human TATA-binding protein 1 (hTBP1) interacts with the C-terminal activation domain (amino acids 305–551) of nuclear factor κB (NF-κB), known as p65C, *in vitro* [12], and that co-transfection of hTBP1 with NF-κB augments transcription [13]. In *S. cerevisiae* it has recently been demonstrated that the occupancy of TBP on the TATA-box is increased in response to transcriptional activators [14,15]. Even though the presence of other factors, like transcription factor IIB, on active promoters is increased as well, the binding of TBP to the TATA-box is considered to be a crucial

---

Abbreviations used: C_{ub}, C-terminal half of ubiquitin, DMEM, Dulbecco's modified Eagle's medium, FCS, fetal calf serum, FOA, 5-fluoroorotic acid, gpt2, guanine phosphoryltransferase 2, HA, haemagglutinin, HAT, hypoxanthine/aminopterin/thymidine, hHP1α, human heterochromatin protein 1α, HPRT, hypoxanthine-guanine phosphoribosyltransferase, hSP100B, *Homo sapiens* nuclear autoantigen 100B; hTBP1, human TATA-binding protein 1, N_{ub}, N-terminal half of ubiquitin, NF-κB, nuclear factor κB, p65C, C-terminal activation domain of NF-κB, 6TG, 6-thioguanine, UBPs, ubiquitin-specific proteases, ura3, orotidine-5′-phosphate decarboxylase

[1] To whom correspondence should be addressed (e-mail lehming@mpiz-koeln.mpg.de)

step for transcriptional activation, and direct binding of TBP to activation domains could explain transcriptional activation by a simple recruitment model [16].

Likewise, it has been shown that *Homo sapiens* nuclear autoantigen (hSP100B), a splice variant of the nuclear dot protein hSP100A, binds to the repressing non-histone chromosomal protein, human heterochromatin protein 1α (hHP1α), *in vitro* [17]. hHP1α, in the context of the Gal4 DNA-binding domain, has also been demonstrated to repress transcription of a promoter containing Gal4-DNA binding sites in mammalian cells, and its ability to repress depends on DNA binding [17]. This result suggests that the interaction between hSP100B and hHP1α may be functionally relevant to the ability of hHP1α to repress transcription.

In the present study we have developed a split-ubiquitin system that allows for the selection of protein interactions inside the living human cell. Using this system we demonstrate for the first time *in vivo* two previously characterized interactions, one between hTBP1 and human NF-κB and the other between hSP100B and hHP1α.

MATERIALS AND METHODS

Standard protocols [18] were used for all procedures, unless otherwise indicated.

Cell lines and *Escherichia coli* strains

The human fibroblast cell line HT1080HPRT$^-$, which is deficient in the enzyme for hypoxanthine-guanine phosphoribosyltransferase (HPRT) was obtained from Sandra Pellegrini (Department of Immunology, Institut Pasteur, Paris, France) [19]. Stable cell lines were made by lipofectamine transfections (Life Technologies, Eggenstein-Leopoldshafen, Germany) according to the manufacturer's protocol. Cell lines containing the C_{ub} fusion vectors were selected for by resistance to zeocin (Invitrogen, Leek, The Netherlands), while those containing the N_{ub} fusion vectors were selected for by resistance to G418 (PAA Laboratories, Cölbe, Germany).

Plasmids

The N_{ub} fusion vector was created by inserting a *Hin*dIII/*Eco*RI-restricted PCR fragment containing N_{ub} into pcDNA3 (Invitrogen), and the C_{ub} fusion vector was created by placing a *Xho*I/*Apa*I-cut PCR fragment containing a fusion of C_{ub} with guanine phosphoryltransferase 2 (gpt2), modified to begin with an arginine residue, into pcDNA3 + zeocin (Invitrogen). PCR fragments containing the cDNAs of hTBP1 and p65C were cut with *Xho*I/*Xba*I and *Eco*RI/*Xho*I, respectively, and inserted into the two vectors to create the N_{ub}–hTBP1 and p65C–C_{ub}–Rgpt2 fusions. Likewise, cDNAs of hHP1α and hSP100B, generated via PCR and cut with *Eco*RI/*Sal*I, were subcloned into the same vectors to create the respective N_{ub}–hHP1α and hSP100B–C_{ub}–Rgpt2 fusions. The following primers were used: N_{ub}, 5′-GCCAAGCTTATGCAGATTTTCGTCAAGAC-3′ and 5′-GGCGAATTCAGCGTAATCTGGAACATC-3′; C_{ub}Rgpt2, 5′-GCCCTCGAGCGGTATCCCCTCCAGATCAA-3′ and 5′-GCCGGGCCCTTAGCGACCGGAGATT-3′; hTBP1, 5′-GGCCTCGAGTATGGATCAGAACAACAGCCT-3′ and 5′-GGCTCTAGATTACGTCTTCCTGAATC-3′; p65C, 5′-GCCGAATTCATGGTGACATATGAGACCTTCA-3′ and 5′-CTCGAGCTGATCTGACTCAGCAGGGC-3′; hHP1α, 5′-GCCGAATTCATGGGAAAGAAAACCAAGCG-3′ and 5′-GCCGTCGACGCGCTCTTTGCTGTTTCTTTCTC-3′; hSP100B, 5′-GCCGAATTCATGGCAGGTGGGGGCGGCGAA-3′ and 5′-GGCGTCGACTTTTCCAAAGTAGAATTGTTTT-3′.

Selections

HT1080HPRT$^-$ cells were grown in Dulbecco's modified Eagle's medium (DMEM), supplemented with 10% (v/v) fetal calf serum (FCS). Zeocin (80 mg/l) was added to select for the C_{ub} fusions and G418 (400 mg/l) was added to select for the N_{ub} fusions. Single colonies were picked and several stable cell lines were analysed for each construct. Hypoxanthine/aminopterin/thymidine (HAT) medium was made according to the manufacturer's protocol (Roche, Mannheim, Germany), as well as 6-thioguanine (6TG) medium (15 mg/l) (Sigma, Deisenhofen, Germany).

Western-blots

Proteins were separated by SDS/PAGE and transferred to nitrocellulose membranes (Sartorius, Göttingen, Germany) by semi-dry blotting (Pharmacia, Freiburg, Germany). The membranes were probed with anti-haemagglutinin (HA) antibody (BabCO, Freiburg, Germany). Secondary horseradish peroxidase-coupled anti-mouse antibody (Bio-Rad, München, Germany) was used to detect the proteins with the help of the ECL$^\bullet$ system (Amersham International, Braunschweig, Germany).

RESULTS

The split-ubiquitin assay was originally developed for *S. cerevisiae*, utilizing the *ura3* gene for selection (absence of uracil) and counterselection (presence of FOA) of protein interactions inside the living cell. The readout in this assay configuration is based on proteolytic degradation and not on transcription; therefore, it can be used to analyse transcription factors, among others. In order to adapt this elegant system for mammalian cells we used the human fibroblast cell line HT1080HPRT$^-$ [19]. This cell line is deficient in the enzyme for HPRT, and thus is sensitive to medium containing HAT, but is resistant to medium containing 6TG. This deficiency can be complemented with the *E. coli* gene for gpt2. In order to test if Rgpt2 was a substrate of the N-end rule, we produced two stable cell lines: one expressing gpt2 as a fusion to the full-length ubiquitin with a glycine in position 1 after cleavage and one with an arginine in this position. Both fusions containing full-length ubiquitin were rapidly cleaved into ubiquitin and the corresponding gpt2 protein by the UBPs. If Rgpt2 was a good substrate for the N-end rule in mammalian cells, the HT1080HPRT$^-$ cells carrying ubiquitin–Rgpt2 should have been HAT-sensitive and 6TG-resistant, whereas the cells

Table 1 Rgpt2 is rapidly degraded in human fibroblast cells

The parental cell line HT1080HPRT$^-$ is sensitive to zeocin and HAT but resistant to 6TG. A stable cell line, created with the help of the zeocin marker, that expresses a fusion of ubiquitin to gpt2 with a glycine in position 1 (ubiquitin–Ggpt2) is resistant to zeocin and HAT but sensitive to 6TG. If the glycine is replaced by an arginine (ubiquitin–Rgpt2) the cell line becomes resistant to zeocin and 6TG but sensitive to HAT.

HT1080HPRT$^-$	zeocin	HAT	6TG
–	sensitive	sensitive	resistant
+ ubiquitin–Ggpt2	resistant	resistant	sensitive
+ ubiquitin–Rgpt2	resistant	sensitive	resistant

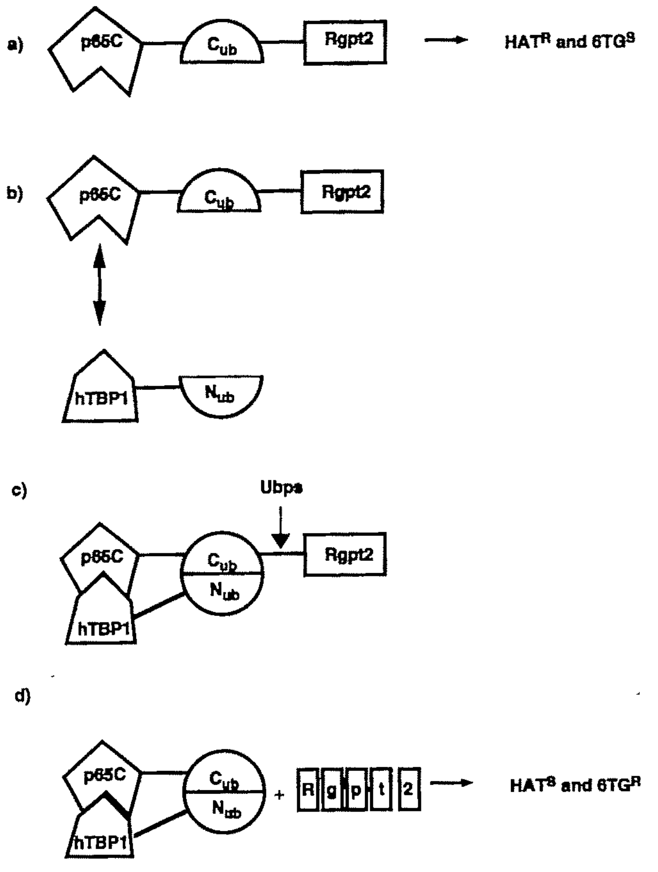

Figure 1 Schematic representation of the mammalian split-ubiquitin assay

(**a**) An HT1080HPRT⁻ cell line expressing p65C–C_{ub}–Rgpt2 is HAT-resistant (HAT^R) and 6TG-sensitive ($6TG^S$) (**b** and **c**) If N_{ub}–hTBP1 is co-expressed, hTBP1 and p65C bind each other inside the living cell As a result of this, ubiquitin is reconstituted and the p65C–C_{ub}–Rgpt2 fusion protein is cleaved behind C_{ub} (**d**) The cleavage product Rgpt2 is subject to rapid degradation by the enzymes of the N-end rule, leading to HAT-sensitivity and 6TG-resistance

carrying ubiquitin-Ggpt2 should have been HAT-resistant and 6TG-sensitive. As shown in Table 1 this prediction was confirmed. This demonstrated that the fusion protein was cleaved and that the cleavage product with the glycine was stable whereas the cleavage product with the arginine was degraded, following the N-end rule.

Next, we split ubiquitin in half and fused N_{ub} to hTBP1, and C_{ub} to the activation domain of human NF-κB, p65C, and Rgpt2. A cell line expressing p65C–C_{ub}–Rgpt2 alone should be HAT-resistant and 6TG-sensitive (Figure 1a). If hTBP1 and p65C interact *in vivo*, co-expression of N_{ub}–hTBP1 should lead to a reversal of the phenotype, for hTBP1 should bind the activation domain of NF-κB, which brings N_{ub} and C_{ub} in close contact (Figure 1b). The reconstituted ubiquitin will be recognized by the UBPs and Rgpt2 will subsequently be released from C_{ub} (Figure 1c). As a consequence, Rgpt2 will be rapidly degraded, and the cell will become HAT-sensitive and 6TG-resistant (Figure 1d). A stable cell line expressing the p65C–C_{ub}–Rgpt2 fusion was made by selecting the cells in zeocin, whose resistance marker was also present on the plasmid encoding the p65C fusion protein. This cell line was HAT-resistant and 6TG-sensitive, demonstrating that the fusion protein was enzymically active. Three independent stable cell lines were made from this one, co-expressing N_{ub} alone by selecting for the neomycin marker present on the N_{ub}-expression plasmid. In all cases, the cell lines were still HAT-resistant and 6TG-sensitive (Figure 2, first column). However, when three independent stable cell lines were made co-expressing an N_{ub}–hTBP1 fusion with p65C–C_{ub}–Rgpt2, all cell lines became HAT-sensitive and 6TG-resistant (Figure 2, second column), demonstrating that hTBP1 interacts with p65C inside the living human cell.

We also utilized this system to verify the interaction between hSP100B and hHP1α inside the living cell [17,20]. In this instance, hHP1α was fused to N_{ub}, while hSP100B was fused to C_{ub}–Rgpt2. Consistent with the *in vitro* interaction previously observed between hSP100B and hHP1α [17], co-expression of these fusion proteins in our HT1080HPRT⁻ cell line resulted in a HAT-sensitive and 6TG-resistant phenotype (Figure 3). In conclusion, this result shows that these proteins associate with each other *in vivo*.

A Western-blot was performed with cell lines, expressing p65C–C_{ub}–Rgpt2 together with N_{ub} or with N_{ub}–hTBP1, grown in nonselective medium (Figure 4). Epitopes for the HA tag were present in all of the fusion proteins. The p65C–C_{ub}–Rgpt2 band was readily detected when N_{ub} was present (lane 2). On the other hand, of the two cell lines co-expressing N_{ub}–hTBP1 tested, both showed a reduction of this band, indicative of Rgpt2 protein degradation (lanes 3 and 4). For cell line number 2, which showed good expression of N_{ub}–hTBP1, the p65C–C_{ub}–Rgpt2 band was no longer detectable. For cell line number 1, where the N_{ub}–hTBP1 expression was barely visible, the p65C–C_{ub}–Rgpt2 band was reduced but still detectable. Therefore the amount of N_{ub}–hTBP1 protein produced by the cell lines correlated with the degree of reduction of the p65C–C_{ub}–Rgpt2 band. In conclusion, our results show that the Western-blot represents an independent method by which one can confirm protein interactions *in vivo*.

DISCUSSION

In the present study, we have successfully adapted the split-ubiquitin system for mammalian cells. We have used this assay to demonstrate that certain protein–protein interactions (between hTBP1 and NF-κB and between hSP100B and hHP1α) previously characterized *in vitro* also occur inside the living cell. We utilized a C_{ub}–Rgpt2 fusion protein and a human fibroblast cell line which is HPRT-deficient. A stable cell line expressing a fusion of p65C [21] or hSP100B to C_{ub}, followed by Rgpt2, is HAT-resistant and 6TG-sensitive. Co-expression of a fusion of hTBP1 or hHP1α, respectively, to N_{ub} results in a cell line that is HAT-sensitive and 6TG-resistant. This demonstrates that the system can be used to select for and to counterselect against protein interactions inside living human cells. The ubiquitin-processing machinery seems to be equally distributed in the cytosol of the cell [7], including the nucleus [8]; as a consequence, the assay is not limited to interactions that can be reconstituted in the nucleus of the cell. Also, the readout is based on proteolytic stability; hence transcription factors can be analysed [22]. We envisage this system being used in the following applications. (1) Two human proteins known to interact *in vitro* can be tested for interaction inside living human cells, as shown in the present study. (2) Libraries expressing altered forms of the proteins can be screened for mutants deficient in interaction. We propose to mutate the protein fused to C_{ub}–Rgpt2, for the subsequent selection would demand a functionally active gpt2 protein; as a consequence, mutations leading to stop codons or frame shifts would not be selected for. (3) Cells expressing the two proteins of interest can be mutated and mutant cell lines, in which the two proteins no longer interact, can be selected for in HAT-medium.

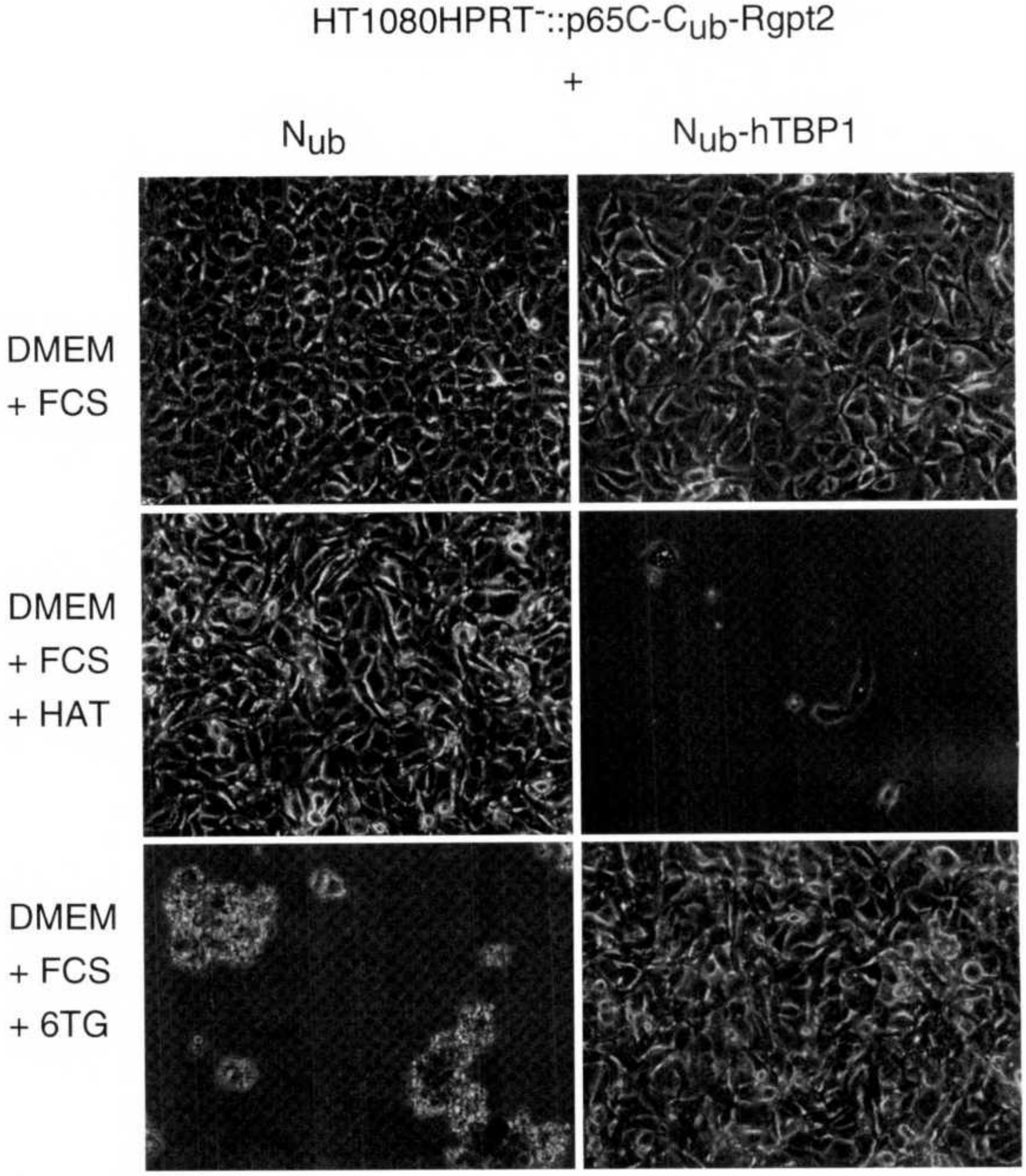

Figure 2 hTBP1 interacts with p65C *in vivo*

Left column: An HT1080HPRT$^-$ cell line co-expressing p65C–C_{ub}–Rgpt2 and N_{ub} was grown in DMEM/10% FCS (first line), in DMEM/10% FCS/HAT (second line), or in DMEM/10% FCS/6TG (third line). Right column: HT1080HPRT$^-$ cell line co-expressing p65C–C_{ub}–Rgpt2 and N_{ub}–hTBP1 grown in different selection media as described above.

Since the cell lines are diploid the mutations are likely to be dominant and the genes can be cloned from cDNA expression libraries made from these mutant cell lines. If the two interacting proteins are part of a complex, for example it should be possible to clone the other components of the complex by this method. Also, the mutant cell lines can be used to analyse the function of the proteins of interest. (4) It is possible to perform competition screens in mammalian cells. In this scenario a cell line expressing the two proteins of interest as N_{ub} and C_{ub} fusions is transformed with a library expressing human cDNAs from a strong promoter. The cell line is originally HAT-sensitive because of the interaction of the two proteins. If a third protein competes with this interaction by binding to one or both proteins, the clone expressing this protein can be isolated by its ability to confer HAT-resistance to the cell line. (5) It is possible to test the effects of drugs on specific protein interactions in human cells. (6) A library expressing fusions of N_{ub} to human cDNAs can be screened to find new partners for human proteins of interest.

Transcriptional regulation of human genes depends on a network of protein–protein interactions which occur between DNA-binding proteins and components of the transcriptional machinery. In the case of transcriptional activators, they regulate eukaryotic genes by simultaneously binding to enhancer sequences and targeting factors of the RNA polymerase II

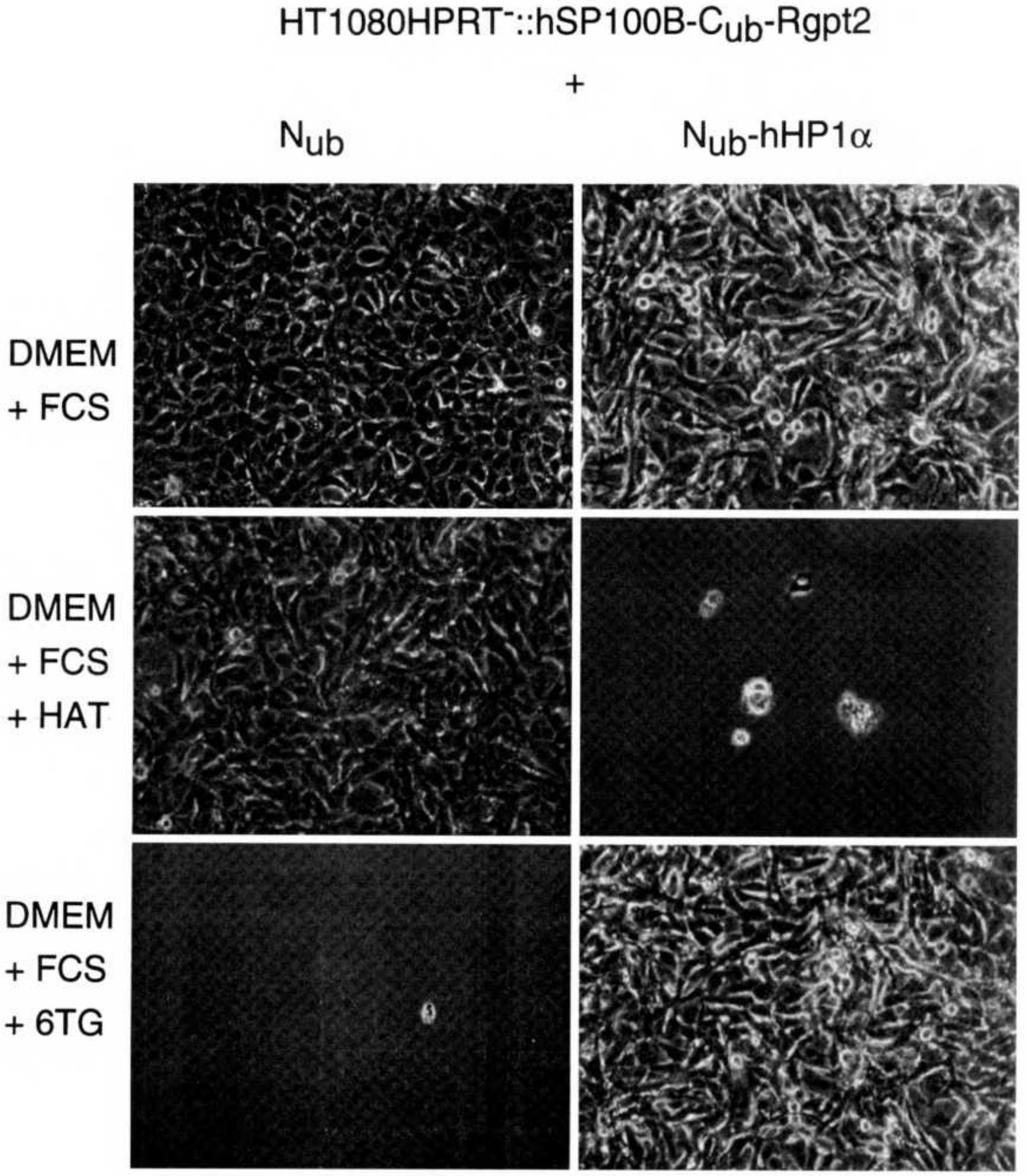

Figure 3 hSP100B interacts with hHP1α *in vivo*

Left column: The HT1080HPRT$^-$ cell line co-expressing hSP100B–C_{ub}–Rgpt2 and N_{ub} was grown in DMEM/10% FCS (first line), in DMEM/10% FCS/HAT (second line) or in DMEM/10% FCS/6TG (third line). Right column: HT1080HPRT$^-$ line co-expressing hSP100B–C_{ub}–Rgpt2 and N_{ub}–hHP1α grown in different selection media as described above.

transcription complex [23]. Direct protein interaction between the activating region of the activator and the TBP has been proposed as an important step in transcriptional activation [24]. This proposition was confirmed by studies of activator mutants which showed a correlation between the strength of protein interactions *in vitro* and the activation capacity *in vivo* [25]. Also, artificial recruitment by fusing DNA-binding domains to components of the holoenzyme [26] results in transcriptional activation [27,28]. Recently two studies demonstrated that binding of TBP to the TATA-box is greatly enhanced upon activator binding in *S. cerevisiae* [14,15]. For human cells, we propose that NF-κB binds the NF-κB binding sites present in many promoters, interacts with and thus recruits the TBP to the TATA-box, where it is needed to start transcription.

Likewise, protein–protein interaction has also been suggested to play an essential role in transcriptional repression [29]. An important class of repressors have also been shown to bind to specific promoter elements and concurrently interact with various targets (e.g. basal transcription factors, activator/coactivator proteins and co-repressors) to inhibit transcription. With regards to the hSP100B-hHP1α interaction, previous studies have suggested that this interaction may be relevant in the ability of hHP1α to repress transcription when tethered to DNA in human cells [17]. Other nuclear bodies, such as promyelocytic leukaemia

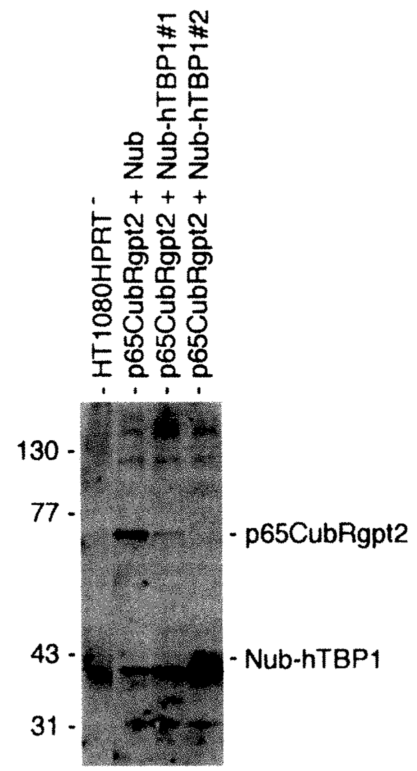

Figure 4 Western-blot confirming the *in vivo* interaction between p65C and hTBP1

Stable cell lines expressing the indicated fusions were grown in nonselective medium to show that the expression of the bands were observed in all control and experimental cell lines under identical conditions. The appearance of the N_{ub}–hTBP1 band correlates with the disappearance of the p65C–C_{ub}–Rgpt2 band. The protein band directly below that of N_{ub}–hTBP1 is a non-specific band cross-reacting with the anti-HA antibody. The Western-blot for the hSP100B-hHP1α interaction is not shown, because hSP100B–C_{ub}–Rgpt2 was barely detectable with the anti-HA antibody. #1, cell line number 1; #2, cell line number 2.

protein ('PML') and hSP100A, a splice variant of hSP100B, have been demonstrated to be upregulated in the presence of interferons, which are important growth and tumour-suppressive cytokines [30,31]. It is tempting to speculate that the interaction between hSP100B and hHP1α may be important in maintaining the physical and functional integrity of a transcriptional repressor complex. Further research is needed to examine which genes may be negatively regulated by this complex.

We thank Nils Johnsson for providing reagents and information prior to publication, as well as helpful discussions and suggestions, Mark Ptashne and Benno Müller-Hill for critical reading of the manuscript, Sandra Pellegrini for providing the HT1080HPRT⁻ cell line, Julia Fleck for technical help and Matthias Godde for help with the pictures of the human cells. This work was supported by grants from the Bundesministerium für Forschung und Bildung and the Max-Planck-Gesellschaft to N.L.

REFERENCES

1 Ma, J. and Ptashne, M. (1988) Converting a eukaryotic transcriptional inhibitor into an activator. Cell **55**, 443–446

2 Fields, S. and Song, O. (1989) A novel genetic system to detect protein-protein interactions. Nature (London) **340**, 245–246

3 Luo, Y., Batalao, A., Zhou, H. and Zhu, L. (1997) Mammalian two-hybrid system: a complementary approach to the yeast two-hybrid system. BioTechniques **22**, 350–352

4 Aronheim, A., Zandi, E., Hennemann, H., Elledge, S. J. and Karin, M. (1997) Isolation of an AP-1 repressor by a novel method for detecting protein-protein interactions. Mol. Cell. Biol. **17**, 3094–3102

5 Maroun, M. and Aronheim, A. (1999) A novel *in vivo* assay for the analysis of protein-protein interaction. Nucleic Acids Res. **27**, e4

6 Johnsson, N. and Varshavsky, A. (1994) Split ubiquitin as a sensor of protein interactions *in vivo*. Proc. Natl. Acad. Sci. U.S.A. **91**, 10340–10344

7 Varshavsky, A. (1997) The ubiquitin system. Trends Biochem. Sci. **22**, 383–387

8 Byrd, C., Turner, G. C. and Varshavsky, A. (1998) The N-end rule pathway controls the import of peptides through degradation of a transcriptional repressor. EMBO J. **17**, 269–277

9 Dünnwald, M., Varshavsky, A. and Johnsson, N. (1999) Detection of transient *in vivo* interactions between substrate and transporter during protein translocation into the endoplasmic reticulum. Mol. Biol. Cell **10**, 329–344

10 Wittke, S., Lewke, N., Müller, S. and Johnsson, N. (1999) Probing the molecular environment of membrane proteins in vivo. Mol. Biol. Cell **10**, 2519–2530

11 Varshavsky, A. (1996) The N-end rule: functions, mysteries, uses. Proc. Natl. Acad. Sci. U.S.A. **93**, 12142–12149

12 Kerr, L. D., Ransone, L. J., Wamsley, P., Schmitt, M. J., Boyer, T. G., Zhou, Q., Berk, A. J. and Verma, I. M. (1993) Association between proto-oncoprotein Rel and TATA-binding protein mediates transcriptional activation by NF-kappa B. Nature (London) **365**, 412–419

13 Schmitz, M. L., Stelzer, G., Altmann, H., Meisterernst, M. and Baeuerle, P. A. (1995) Interaction of the COOH-terminal transactivation domain of p65 NF-kappa B with TATA-binding protein, transcription factor IIB, and coactivators. J. Biol. Chem. **270**, 7219–7226

14 Li, X. Y., Virbasius, A., Zhu, X. and Green, M. R. (1999) Enhancement of TBP binding by activators and general transcription factors. Nature (London) **399**, 605–609

15 Kuras, L. and Struhl, K. (1999) Binding of TBP to promoters *in vivo* is stimulated by activators and requires Pol II holoenzyme. Nature (London) **399**, 609–613

16 Ptashne, M. and Gann, A. (1997) Transcriptional activation by recruitment. Nature (London) **386**, 569–577

17 Lehming, N., Le Saux, A., Schüller, J. and Ptashne, M. (1998) Chromatin components as part of a putative transcriptional repressing complex. Proc. Natl. Acad. Sci. U.S.A. **95**, 7322–6

18 Ausubel, F., Brent, R., Kingston, R. E., Moore, D. D., Seidman, J. G., Smith, J. A. and Struhl, K. (1987) Current protocols in molecular biology, John Wiley & Sons, Inc., New York

19 Pellegrini, S., John, J., Shearer, M., Kerr, I. M. and Stark, G. R. (1989) Use of a selectable marker regulated by alpha interferon to obtain mutations in the signaling pathway. Mol. Cell. Biol. **9**, 4605–4612

20 Seeler, J. S., Marchio, A., Sitterlin, D., Transy, C. and Dejean, A. (1998) Interaction of SP100 with HP1 proteins: a link between the promyelocytic leukemia-associated nuclear bodies and the chromatin compartment. Proc. Natl. Acad. Sci. U.S.A. **95**, 7316–7321

21 Moore, P. A., Ruben, S. M. and Rosen, C. A. (1993) Conservation of transcriptional activation functions of the NF-kappa B p50 and p65 subunits in mammalian cells and *Saccharomyces cerevisiae*. Mol. Cell. Biol. **13**, 1666–1674

22 Wellhausen, A. and Lehming, N. (1999) Analysis of the *in vivo* interaction between a basic repressor and an acidic activator. FEBS Lett. **453**, 299–304

23 Ptashne, M. (1988) How eukaryotic transcriptional activators work. Nature (London) **335**, 683–689

24 Stargell, L. A. and Struhl, K. (1996) Mechanisms of transcriptional activation *in vivo*: two steps forward. Trends Genet. **12**, 311–315

25 Wu, Y., Reece, R. J. and Ptashne, M. (1996) Quantitation of putative activator-target affinities predicts transcriptional activating potentials. EMBO J. **15**, 3951–3963

26 Koleske, A. J. and Young, R. A. (1995) The RNA polymerase II holoenzyme and its implications for gene regulation. Trends Biochem. Sci. **20**, 113–116

27 Barberis, A., Pearlberg, J., Simkovich, N., Farrell, S., Reinagel, P., Bamdad, C., Sigal, G. and Ptashne, M. (1995) Contact with a component of the polymerase II holoenzyme suffices for gene activation. Cell **81**, 359–368

28 Gaudreau, L., Keaveney, M., Nevado, J., Zaman, Z., Bryant, G. O., Struhl, K. and Ptashne, M. (1999) Transcriptional activation by artificial recruitment in yeast is influenced by promoter architecture and downstream sequences. Proc. Natl. Acad. Sci. U.S.A. **96**, 2668–2673

29 Hanna-Rose, W. and Hansen, U. (1996) Active repression mechanisms of eukaryotic transcription repressors. Trends Genet. **12**, 229–234

30 Lavau, C., Marchio, A., Fagioli, M., Jansen, J., Falini, B., Lebon, P., Grosveld, F., Pandolfi, P. P., Pelicci, P. G. and Dejean, A. (1995) The acute promyelocytic leukaemia-associated PML gene is induced by interferon. Oncogene **11**, 871–876

31 Guldner, H. H., Szostecki, C., Grotzinger, T. and Will, H. (1992) IFN enhance expression of Sp100, an autoantigen in primary biliary cirrhosis. J. Immunol. **149**, 4067–4073

Received 10 January 2000/16 March 2000; accepted 28 March 2000

Biochem J (2000) 348, 591–596 (Printed in Great Britain)

Repression of transforming-growth-factor-β-mediated transcription by nuclear factor κB

Raman P. NAGARAJAN*, Feifei CHEN*, Wei LI*, Eva VIG†, Maureen A. HARRINGTON†, Harikrishna NAKSHATRI†
and Yan CHEN*†[1]
*Department of Medical and Molecular Genetics, Indiana University School of Medicine, 975 West Walnut Street IB130, Indianapolis, IN 46202, U.S.A., and
†Walther Oncology Center, Indiana University School of Medicine, Indianapolis, IN 46202, U.S.A.

Activation of transforming growth factor-β (TGF-β) and activin receptors leads to phosphorylation of Sma- and Mad-related protein 2 (Smad2) and Smad3, which function as transcription factors to regulate gene expression. Smad7 is a regulatory protein which is able to inhibit TGF-β and activin signalling in a negative-feedback loop, mediated by a direct regulation by Smad3 and Smad4 via a Smad-binding element (SBE) in the Smad7 promoter. Interestingly, we found that the Smad7 promoter was also regulated by nuclear factor κB (NF-κB), a transcription factor which plays an important role in inflammation and the immune response. Expression of NF-κB p65 subunit was able to inhibit the Smad7 promoter activity, and this inhibition could be reversed by co-expression of IκB, an inhibitor of NF-κB. In addition, the inhibitory activity of p65 was observed in a minimal promoter that contained only the Smad7 SBE and a TATA box, without any consensus NF-κB binding site. This inhibitory effect appeared to be common to other TGF-β- and activin-responsive promoters, since p65 also inhibited the forkhead-activin-signal-transducer-2-mediated activation of a *Xenopus* Mix.2 promoter, as well as the Smad3-mediated activation of 3TP-lux which contains PMA-responsive elements and a plasminogen-activator-inhibitor-1 promoter. Activation of endogenous NF-κB by tumour necrosis factor-α (TNF-α) was also able to inhibit the Smad7 promoter in human embryonic kidney 293 cells. In human hepatoma HepG2 cells, TNF-α was able to inhibit TGF-β- and activin-mediated transcriptional activation. Furthermore, overexpression of the transcription co-activator p300 could abrogate the inhibitory effect of NF-κB on the Smad7 promoter. Taken together, these data have indicated a novel mode of crosstalk between the Smad and the NF-κB signalling cascades at the transcriptional level by competing for a limiting pool of transcription co-activators.

Key words: activin, p300, signal transduction, Smad7, transcription factor.

INTRODUCTION

Sma- and Mad-related proteins (Smads) are a family of proteins which mediate signalling for the transforming growth factor-β (TGF-β) superfamily of cytokines, including TGF-β, activin, bone morphogenetic proteins, and many others [1,2]. Structural and functional characterization of Smad proteins has allowed their categorization into three groups: pathway-specific, common mediator and inhibitory. Smads 1–3, 5 and 8 are pathway-specific Smads which are phosphorylated by the type I receptors of the TGF-β superfamily [1,2]. Upon phosphorylation, the pathway-specific Smads form hetero-oligomeric complexes with Smad4, the common mediator Smad. These complexes then migrate to the nucleus, and regulate gene transcription through either direct DNA binding, via the MH1 domain of the Smad proteins, or association with other specific transcription factors, such as *Xenopus* FAST-1 (forkhead activin signal transducer-1) or mouse FAST-2 [3–6]. The MH2 domain of Smad proteins contains a transactivating activity that is mediated by interaction with two closely related proteins, CREB-binding protein (CBP) and p300, which function as transcriptional co-activators that link specific transcription factors with the basal transcriptional machinery [7–9]. On the other hand, Smad6 and Smad7 constitute the third group of Smads, the inhibitory Smads. These two proteins inhibit TGF-β, activin and bone-morphogenetic-protein signalling by interacting with the type I receptors of the TGF-β superfamily, or competing for the complex formation between pathway-specific Smads and Smad4 [1,2].

Nuclear factor κB (NF-κB) is a transcription factor which controls expression of a wide range of genes [10,11]. It is mainly involved in cellular functions in immunological and inflammatory responses, as well as control of cell growth and apoptosis. For example, NF-κB is involved in the cellular response initiated by different proinflammatory cytokines, including interleukins and tumour necrosis factor-α (TNF-α) [12]. In mammalian cells, NF-κB exists in the cytoplasm as a homodimer or heterodimer composed of variable subunits: p50, p52, p65(RelA), c-Rel, and RelB; although the major form of NF-κB exists as a heterodimer between p50 and p65 [10,11]. Three of these subunits, p65, RelB and c-Rel, contain a C-terminal transactivation domain, and all five subunits have an N-terminal Rel homology domain, which mediates DNA binding, dimerization, and interaction with an inhibitor of NF-κB (IκB). The interaction of NF-κB with IκB masks a nuclear localization sequence of NF-κB, and this interaction sequesters NF-κB in the cytoplasm. Activation of NF-κB is initiated when IκB is phosphorylated and degraded in response to inflammatory cytokines, such as TNF-α, UV radiation, viral infection, potent oxidants, or other substances [10,11].

Abbreviation used: CA-ALK, constitutively active activin-receptor-like kinase; CBP, CREB-binding protein, CMV, cytomegalovirus, FAST, forkhead activin signal transducer, HEK-293 cells, human embryonic kidney 293 cells; NF-κB, nuclear factor κB, IκB, inhibitor of NF-κB, SBE, Smad binding element, Smad, Sma- and Mad-related protein; TGF-β, transforming growth factor-β, TNF-α, tumour necrosis factor-α

[1] To whom correspondence should be addressed (e-mail ychen3@iupui.edu)

These stimuli release NF-κB and enable it to translocate into the nucleus, where it regulates transcription of target genes. Similar to other transcription factors including Smads, the transactivating activity of NF-κB is mediated by an interaction with the common transcription co-activators CBP and p300 which contain an intrinsic acetyltransferase activity [13–15]. Upon activation by associating with other DNA-binding transcription factors, CBP/p300 bridge those transcription factors to the basic transcription apparatus, alter the conformation of the chromatin, and initiate stimulation of transcription.

The TGF-β and NF-κB signalling pathways may crosstalk with each other. For example, TNF-α and TGF-β1 can synergistically enhance expression of type VII collagen gene that forms part of the extracellular matrix [16]. On the other hand, treatment of B-cell lymphomas with TGF-β1 can antagonize the activity of NF-κB by elevating IκB transcription, leading to accelerated apoptosis by attenuating the NF-κB-mediated repression of c-*myc* transcription [17]. Conversely, NF-κB can block TGF-β1-induced apoptosis of hepatocytes [18]. These observations indicate that there exists an intrinsic interaction between these two signalling pathways that might be dependent on the cellular context, as well as the nature of gene expression.

We recently reported characterization of the mouse Smad7 promoter [19]. We have found that Smad7 transcription is regulated by TGF-β signalling through direct binding of Smad3 and Smad4 with a Smad-binding element (SBE) present in Smad7 promoter [19]. This observation, in conjunction with recent studies demonstrating an upregulation of Smad7 mRNA upon TGF-β or activin treatment in the cells [20,21], suggests that Smad7 participates in a negative-feedback loop which regulates the length and intensity of the TGF-β and activin signalling. Using the Smad7 promoter and other TGF-β-responsive promoters as model systems, we investigated the functional interaction between TGF-β and NF-κB signalling pathways at the molecular level; and unveiled a novel crosstalk between them at the transcriptional level.

MATERIALS AND METHODS

Cell culture and cell transfection

The human embryonic kidney 293 cells (HEK-293 cells) and the human hepatoma HepG2 cells were cultured in Dulbecco's modified Eagle's medium, containing 10% fetal bovine serum supplemented with penicillin and streptomycin. Transient cell transfection was performed by calcium phosphate method for HEK-293 cells, and DEAE-dextran method for human hepatoma HepG2 cells [19].

Plasmids

The rat Smad3, the constitutively active activin-receptor-like kinase TGF-β type I receptors (CA-ALK-5), the mouse FAST-2, and the Smad7 promoter constructs have been described previously by us [6,19]. To generate the minimal Smad7 promoter containing the SBE of the Smad7 promoter, an E1B TATA box (5′-TATATAAT-3′) in adenovirus type 5 [22] was first engineered into the pGL2-basic vector (Promega). Subsequently, two tandem repeats of the SBE (5′-TCGACAGGGTGTCTAGACGGCC-ACG-3′) of the Smad7 promoter were subcloned immediately 5′ to the TATA box. The human NF-κB p65 subunit, p50 subunit, and IκB have been described previously [23,24] The promoter construct containing three tandem repeats of HIV NF-κB binding sites (NF-κB3-luc) has been described previously [25,26]. The *Mix.2* AR3-lux containing three tandem repeats of activin-responsive elements has been described in [6,27]. The 3TP-lux promoter reporter containing three repeats of PMA-responsive elements and a portion of plasminogen activator inhibitor-1 promoter was originally described by Wrana et al. [28].

Promoter assay

For the promoter assay, about 5×10^4 cells per well in six-well plates were transfected with different combinations of plasmid DNA. An empty vector pcDNA3 (Invitrogen) was used to make up to 5 μg of total DNA for each transfection. The p cytomegalovirus (pCMV)-β-galactosidase plasmid was co-transfected with other plasmids as an internal control for the transfection efficiency The cells were harvested at 48 h after transfection by lysis with 400 μl of Nonidet P40 lysis buffer [29]. In TNF-α-treated-groups, cells were treated with TNF-α (2 or 20 ng/ml) for 16 h before harvest. A 20 μl aliquot of the lysate was used in the β-galactosidase assay as reported previously [30], and 10μl of the lysate was used in the luciferase assay with a Promega luciferase assay kit, and counted for 10 s in a FB12 luminometer (Zylux) with the data represented as the relative light unit per second.

RESULTS AND DISCUSSION

Inhibition of Smad7 promoter by NF-κB

Our initial characterization with the mouse Smad7 promoter indicated the presence of a putative NF-κB regulatory site at the position of +34bp to +41bp, relative to the major transcription initiation site [19]. To determine whether NF-κB indeed played a role in regulating the transcription of the *Smad7* gene, we tested the effect of expression of NF-κB p65 subunit on the Smad7 promoter activity. We used three different promoter constructs containing different lengths of the Smad7 promoter fused to a luciferase reporter gene [19]. When transfected into HEK-293 cells, all three promoter constructs gave rise to a high level of basal transactivating activity. As shown in Figure 1(A), the largest reporter construct, spanning −2.2 kb to +112 bp of the Smad7 promoter, exhibited the highest level of basal promoter activity. The second (−408 to +112 bp) and the third (−408 to −124 bp) promoters showed a little lower basal activity. Interestingly, co-expression of p65 with each of these reporters greatly reduced the basal transcription of the Smad7 promoter. In p65 co-transfected cells, the basal luciferase activity was reduced to approx. 10–15% of the control level for all three Smad7 promoter constructs. This finding was somewhat unexpected, because the putative NF-κB binding site in the Smad7 promoter was not covered by the third reporter that spans −408 bp to −124 bp of the promoter. Therefore these data not only indicated that NF-κB was able to inhibit the basal Smad7 transcription, but also suggested that this inhibition was unlikely to be caused by the interaction of NF-κB with the putative NF-κB consensus site in the region of +34 bp to +41 bp.

In mammalian cells, the predominant form of NF-κB is composed of a heterodimer of p65 and p50 [10,11]. When p50 alone was transfected in HEK-293 cells, it had no effect on the basal transcription of Smad7 promoter (results not shown). However, co-expression of p50 with p65 gave the similar level of inhibition as p65 expression alone (Figure 1B). Because p65, but not p50, contains the transactivating domain in the NF-κB family of transcription factors, this finding suggested that the inhibitory effect might be linked to the presence of the transactivating activity of NF-κB. In order to further test if the inhibitory effect of NF-κB p65 on Smad7 promoter was specific, we determined whether or not IκB was able to reverse the p65

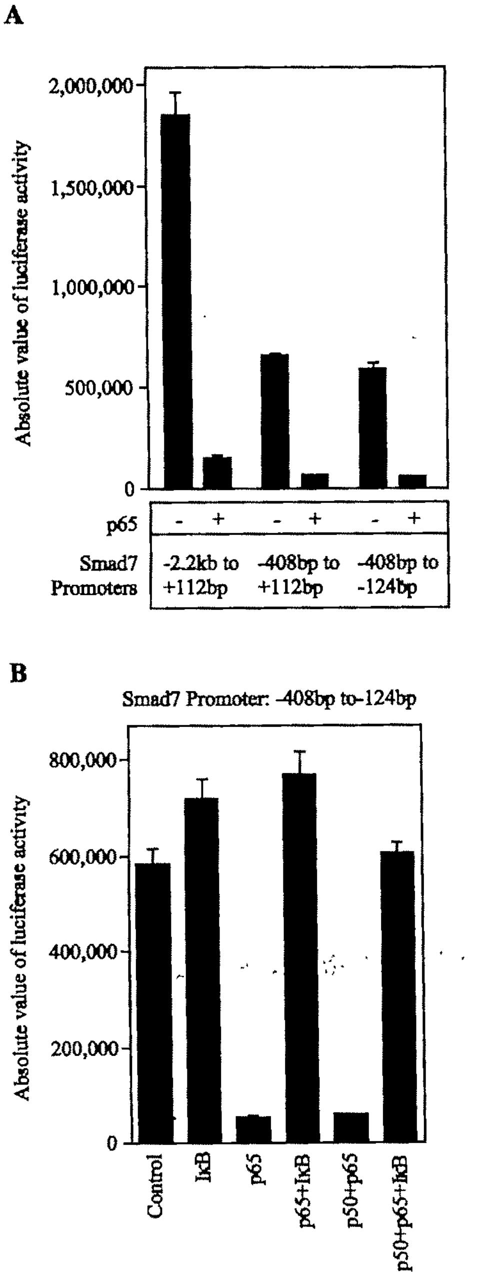

Figure 1 Repression of Smad7 promoter by NF-κB

(**A**) Effect of NF-κB p65 on different lengths of Smad7 promoter. HEK-293 cells were transiently transfected with Smad7 promoter constructs (0.5 μg), pCMV-β-gal (0.5 μg) and p65 (2 μg) as indicated. The absolute change of luciferase activity is shown as means ± S.D. (**B**) IκB reverses the repression effect of p65. HEK-293 cells were transiently transfected with Smad7 promoter −408 to −124 construct (0.5 μg), pCMV-β-gal (0.5 μg), p50 (1 μg), p65 (1 μg) and IκB (2 μg) as indicated. The change of luciferase activity shown as means ± S.D. was derived by comparing to the value of the vector-transfected cells and normalized by β-galactosidase activity.

effect. IκB is a specific inhibitor of NF-κB through masking of the nuclear translocation site of NF-κB. When IκB was co-expressed with p65, or p65 plus p50, it was able to completely abrogate the inhibitory effect of NF-κB on the Smad7 promoter. These data, therefore, provided further evidence that the inhibitory effect that we observed with Smad7- promoter was specifically caused by p65.

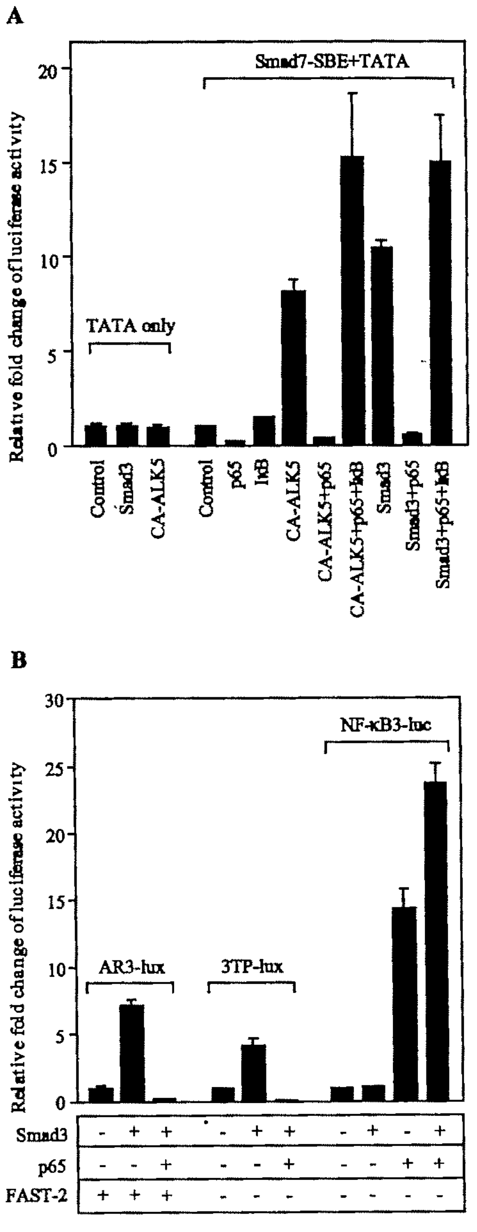

Figure 2 Effect of p65 on multiple TGF-β-responsive promoters

(**A**) Repression of the SBE of the Smad7 promoter by p65. HEK-293 cells were transiently transfected with pCMV-β-gal (0.5 μg), a control promoter containing only the TATA-box (0.5 μg), a promoter containing two tandem repeats of the SBE and one TATA-box (0.5 μg), p65 (1 μg), IκB (2 μg), Smad3 (1 μg), and the constitutively active ALK-5 (1 μg) as indicated. The fold change of luciferase activity as compared to the vector-transfected cells (set to 1) is shown as means ± S.D. after being normalized by β-galactosidase activity. (**B**) p65 inhibited transcription of other TGF-β-responsive promoters. A similar experiment as above was performed by transfection with AR3-lux (0.5 μg), 3TP-lux (0.5 μg) or the HIV NF-κB3-luc reporter (0.5 μg) instead. The mouse FAST-2 (1 μg) was co-transfected with AR3-lux.

NF-κB represses the SBE of the Smad7 promoter

As we have shown before, Smad7 promoter contains a consensus SBE that is able to associate with Smad3 and Smad4. To further determine the regulatory role of NF-κB on the Smad7 promoter, we generated a luciferase reporter that contained two tandem repeats of this SBE and an E1B TATA box [22]. When the control reporter only containing the TATA-box and the SBE-containing reporter were transfected into HEK-293 cells, both of them gave rise to a very low basal transactivation, as compared with the longer Smad7 promoter constructs used in Figure 1. However, expression of either CA-ALK-5 or Smad3 was able to significantly stimulate the SBE-containing reporter, but not the TATA-only reporter (Figure 2A) These data provided further evidence that the regulatory function of TGF-β and activin signalling through Smad proteins on Smad7 transcription was mediated by this particular SBE present in the Smad7 promoter

We next determined the effect of p65 on this shorter form of Smad7 promoter. When p65 was co-transfected with the SBE-containing reporter, it could completely reverse the stimulatory effect of either CA-ALK-5 or Smad3 on the reporter (Figure 2A). These data indicated that the inhibitory activity of p65 could overcome the stimulatory effect of CA-ALK-5 or Smad3 on the SBE of the Smad7 promoter. In addition, we also found that IκB was able to reverse the p65 effect, further indicating that the inhibitory effect of NF-κB on the SBE was mediated by p65. It is noteworthy that IκB appeared to augment the stimulatory effect of CA-ALK5 or Smad3 on the SBE transcription. This might be caused by the possibility that the overexpressed IκB was able to inhibit endogenous p65 and therefore relieve the basal inhibitory effect of the endogenous p65 on the Smad-mediated transcription.

NF-κB was able to inhibit other TGF-β-regulated promoters

Our experiments so far have indicated that NF-κB plays a unique regulatory role on the Smad7 promoter. Is this regulatory function only specific for Smad7 promoter, or common to other promoters that are regulated by TGF-β signalling? To address this issue, we tested two other promoters regulated by TGF-β and activin signalling. AR3-lux is a luciferase reporter that contains three tandem repeats of the activin-responsive elements which are regulated by the FAST group of transcription factors when complexed with Smad proteins following activation of TGF-β or activin signalling [3,31]. Previous studies, as well as our own observations, have indicated that a mouse FAST homologue, FAST-2, was able to stimulate AR3-lux following activation of TGF-β or activin signalling [5,6]. 3TP-lux is another reporter that has been commonly used as an indicator of TGF-β or activin signalling. This reporter contains three tandem repeats of PMA-responsive elements fused with the promoter of plasminogen activator inhibitor-1 [28]. Numerous studies have indicated that 3TP-lux could be activated by TGF-β or activin signalling, possibly through binding of Smad proteins with a CAGA motif in the plasminogen activator inhibitor-1 promoter [32], or interaction of Smads with activator protein-1 that binds PMA-responsive elements [33]. As shown in Figure 2(B), expression of Smad3 in HEK-293 cells was able to stimulate AR3-lux in the presence of the mouse FAST-2. Similarly, Smad3 was also able to elevate the transcription of 3TP-lux. However, the stimulatory effect of Smad3 on both of these promoters was largely abrogated by co-expression of p65. These data clearly indicated that p65 has an inhibitory effect on different types of promoters that are regulated by TGF-β or activin signalling. To prove that p65 was indeed functionally expressed in our experimental system, we tested the effect of p65 on another reporter construct that contains three tandem repeats of NF-κB binding element present in the long terminal repeat of the HIV genome [25,34]. As shown in Figure 2(B), p65 was able to strongly stimulate this promoter, indicating that p65 was indeed expressed and functioning in these cells. Interestingly, Smad3 expression appeared to further augment the stimulatory effect of p65 on this promoter. This is consistent with a recent report demonstrating that TGF-β is able to stimulate HIV enhancer through the NF-κB binding element [35].

Inhibition of TGF-β-mediated transcription by TNF-α

NF-κB is mainly involved in cellular response to inflammatory and immunological stimuli. One of the prototypic pathways in which NF-κB plays a pivotal role is TNF-α signalling [12]. Activation of TNF receptors by TNF-α is followed by activation of a whole array of signalling pathways, including activation of NF-κB through phosphorylation and degradation of IκB. To see if the regulatory role of NF-κB we observed here is of any biological significance, we determined whether endogenous NF-κB could mimic the inhibitory effect of ectopically expressed p65 following TNF-α treatment. To test this possibility, we expressed Smad3 in HEK-293 cells, followed by treatment with different amounts of TNF-α. We observed that TNF-α treatment could significantly inhibit Smad3-induced stimulation of the Smad7 SBE reporter in a dose-dependent manner, and that this effect could be reversed with IκB expression (Figure 3A). HEK-293 cells do express TNF-α receptors, and this TNF-α effect was presumably due to the activation of endogenous NF-κB, since this repression could be reversed by IκB. Taken together, these results indicated that activation of endogenous NF-κB by biological stimuli may impose an inhibitory effect on the TGF-β/activin-responsive Smad7 promoter in HEK-293 cells. It is interesting to note here that the inhibitory effect of TNF-α on Smad3 activation of the Smad7 promoter was unlikely due to an inhibition of the Smad3 expression by p65. Western-blotting analysis showed that the Smad3 protein level was higher in the cells when it was co-expressed with p65 than in cells which were transfected with Smad3 alone (results not shown). This was probably due to the presence of the NF-κB binding site in the CMV promoter that drove the ectopic expression of Smad3.

To further delineate the biological significance of our observation that p65 was able to inhibit TGF-β-mediated transcription, we examined the effect of TNF-α treatment on TGF-β- and activin-induced transcription of the AR3-lux reporter derived from the *Xenopus Mix.2* promoter in human hepatoma HepG2 cells. This experiment excluded the use of exogenously expressed p65 or Smad proteins in the experimental system. As shown in Figure 3(B), TGF-β and activin treatment were able to stimulate the AR3-lux transcription by approx. 140- and 20-fold respectively. Furthermore, co-treatment with TNF-α was able to inhibit the TGF-β- and activin-mediated transactivation. These data would indicate that the TNF-α signalling pathway is able to inhibit the transactivating activity of endogenous Smad proteins following stimulation by TGF-β or activin.

Overexpression of p300 overcomes the inhibitory effect of p65

What is the molecular mechanism underlying the inhibitory effect of NF-κB on TGF-β/activin-regulated promoters? Our findings that p65 could inhibit different types of TGF-β or activin-responsive promoters indicted that this effect is unlikely due to the binding of p65 with a specific sequence element in these promoters, since none of these promoters including the Smad7 SBE, the FAST-binding activin-responsive element, and the 3TP-lux, contain the consensus NF-κB binding element [36]. On the other hand, recent studies have indicated that the MH2 domain of Smad proteins was able to bind the general transcription co-activators CBP and p300 at the C-terminal region to mediate their transactivating activity [7–9]. Interestingly, NF-κB is also able to bind the N-terminal and C-terminal regions of

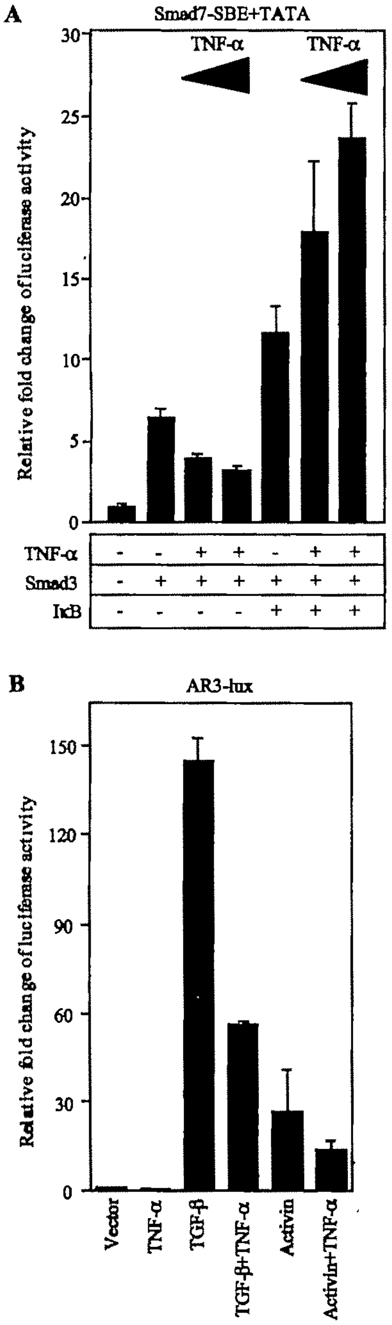

Figure 3 TNF-α inhibited TGF-β-mediated transcription

(A) TNF-α inhibited SBE transcription of the Smad7 promoter. HEK-293 cells were transiently transfected with the SBE-containing Smad7 minimal promoter (0.5 μg), pCMV-β-gal (0.5 μg), Smad3 (1 μg) and IκB (2 μg) as indicated. The cells were treated with TNF-α 16 h before the luciferase and β-galactosidase assays. The fold change of luciferase activity is shown as means ± S.D after normalization with a β-galactosidase assay. (B) TNF-α inhibited TGF-β- and activin-mediated transcription of AR3-lux derived from *Xenopus Mix.2* promoter. Human hepatoma HepG2 cells cells were transfected with AR3-lux (0.5 μg), mouse FAST-2 (1 μg) and pCMV-β-gal (0.5 μg). The cells were treated with TGF-β1 (1 ng/ml), activin (10 ng/ml) or TNF-α (20 ng/ml) for 16 h before luciferase assay. The fold change of luciferase activity normalized by β-galactosidase assay is shown as means ± S.D.

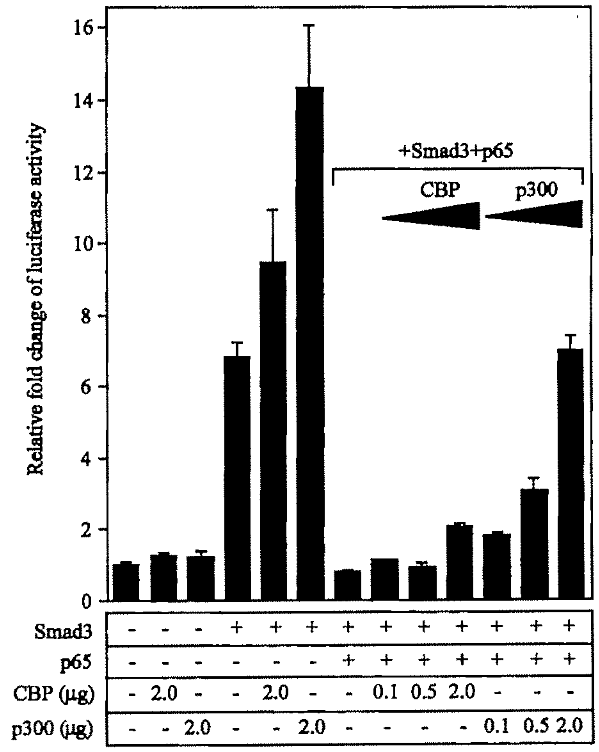

Figure 4 Overexpression of p300 overcame the NF-κB-mediated repression

HEK-293 cells were transiently transfected with the SBE-containing Smad7 minimal promoter (0.5 μg), pCMV-β-gal (0.5 μg), Smad3 (1 μg), p65 (1 μg) and different amounts of CBP or p300 as indicated. The fold change of luciferase activity was shown as means ± S.D after normalization with β-galactosidase activity.

CBP/p300 [13–15]. There have been some observations demonstrating that NF-κB is able to repress the transactivating activity of other transcription factors through sequestration of a limiting pool of CBP/p300. For example, NF-κB and p53 signalling pathways mutually repress each other's transactivating activity by competing for CBP/p300 [37]. NF-κB can also repress STAT2-mediated HIV transcription through a similar mechanism [38].

To test if such a transcriptional sequestration of CBP/p300 may underlie the inhibitory effect of NF-κB on TGF-β/activin- or Smad-mediated transcriptional activation, we determined the effect of overexpression of CBP or p300 in our experimental system. As shown in Figure 4, Smad3 expression was able to stimulate the SBE-containing promoter, and the Smad3 effect was inhibited by co-expressed p65. Both CBP and p300 were able to enhance the stimulation of the promoter by Smad3, consistent with previous reports that CBP and p300 are required for the transactivating activity of Smad proteins [7–9]. Interestingly, expression of p300 was indeed able to abrogate the inhibitory effect of p65 on Smad3-activated Smad7 SBE activation in a dose-dependent manner. CBP could also reverse part of the inhibitory activity of p65, although to a lesser degree. Taken together, these data indicated that p65 may inhibit the Smad-mediated transcriptional control by competing for a limiting pool of CBP/p300. When NF-κB is overexpressed or activated, it may preferentially bind CBP or p300 and limit the amount of these transcription co-activators available to Smad proteins that are activated by TGF-β or activin signalling.

In conclusion, our results have indicated that the NF-κB-mediated repression of gene expression via sequestration of the common transcription co-activators may play a role in the transcriptional regulation by Smad proteins. However, it is noteworthy that NF-κB may repress or stimulate Smad-mediated transcription depending on the promoter configuration. We hypothesize that, in Smad-regulated promoters without NF-κB binding sites, NF-κB may repress gene expression by sequestration of CBP/p300, as exemplified in the present study. On the other hand, if the promoters in which Smad-binding element is in close proximity with NF-κB binding site, NF-κB may cooperate with Smad proteins to transactivate the target genes, as observed in the transcriptional regulation of the type VII collagen promoter [16]. In certain cell types, TNF-α treatment was able to increase the mRNA level of Smad7, leading to inhibition of TGF-β signalling [39]. How Smad7 transcription is modulated by NF-κB might be dependent on the cellular context as well as the configuration of the Smad7 promoter. TNF-α may inhibit the TGF-β-mediated transcription by either an upregulation of the inhibitory Smad or a p65-mediated competition for the common transcription co-activators.

We wish to thank M Whitman for the pAR3-Lux, R. Janknecht for the CBP and p300 clones, W. C. Greene for NF-κB p50 and p65 expression plasmids and D. J. McKean for the HIV NF-κB luciferase reporter. We thank O N Ozes for critical comments This work was supported by the Foundation for Medical Research, Inc. from Indiana University School of Medicine, and a Grant-in-Aid and a Scientist Development Award from the American Heart Association to Y C.

REFERENCES

1 Massague, J (1998) TGF-beta signal transduction. Annu Rev Biochem **67**, 753–791
2 Heldin, C H, Miyazono, K and ten Dijke, P (1997) TGF-beta signalling from cell membrane to nucleus through SMAD proteins Nature (London) **390**, 465–471
3 Chen, X, Rubock, M J and Whitman, M (1996) A transcriptional partner for MAD proteins in TGF-beta signalling Nature (London) **383**, 691–696
4 Labbe, E, Silvestri, C, Hoodless, P. A, Wrana, J L and Attisano, L (1998) Smad2 and Smad3 positively and negatively regulate TGF beta-dependent transcription through the forkhead DNA-binding protein FAST2 Mol Cell **2**, 109–120
5 Liu, B, Dou, C L, Prabhu, L and Lai, E (1999) FAST-2 is a mammalian winged-helix protein which mediates transforming growth factor beta signals Mol Cell Biol **19**, 424–430
6 Nagarajan, R P., Liu, J and Chen, Y. (1999) Smad3 inhibits transforming growth factor-beta and activin signaling by competing with smad4 for FAST-2 binding J Biol Chem. **274**, 31229–31235
7 Janknecht, R, Wells, N J and Hunter, T (1998) TGF-beta-stimulated cooperation of smad proteins with the coactivators CBP/p300 Genes Dev **12**, 2114–2119
8 Feng, X H, Zhang, Y, Wu, R Y and Derynck, R (1998) The tumor suppressor Smad4/DPC4 and transcriptional adaptor CBP/p300 are coactivators for smad3 in TGF-beta-induced transcriptional activation Genes Dev **12**, 2153–2163
9 Pouponnot, C., Jayaraman, L and Massague, J. (1998) Physical and functional interaction of SMADs and p300/CBP J Biol Chem **273**, 22865–22868
10 Baeuerle, P A and Baltimore, D (1996) NF-kappa B ten years after Cell **87**, 13–20
11 Baldwin, Jr, A. S (1996) The NF-kappa B and I kappa B proteins new discoveries and insights Annu Rev Immunol **14**, 649–683
12 Wallach, D, Varfolomeev, E E, Malinin, N L, Goltsev, Y V, Kovalenko, A V and Boldin, M P (1999) Tumor necrosis factor receptor and Fas signaling mechanisms Annu Rev Immunol **17**, 331–367
13 Gerritsen, M E, Williams, A J, Neish, A. S, Moore, S, Shi, Y and Collins, T (1997) CREB-binding protein/p300 are transcriptional coactivators of p65 Proc Natl Acad Sci U S A **94**, 2927–2932
14 Perkins, N D, Felzien, L K, Betts, J C, Leung, K, Beach, D H and Nabel, G J (1997) Regulation of NF-kappaB by cyclin-dependent kinases associated with the p300 coactivator Science **275**, 523–527
15 Vanden Berghe, W, De Bosscher, K, Boone, E, Plaisance, S and Haegeman, G (1999) The nuclear factor-kappaB engages CBP/p300 and histone acetyltransferase activity for transcriptional activation of the interleukin-6 gene promoter J Biol Chem **274**, 32091–32098
16 Kon, A, Vindevoghel, L, Kouba, D. J, Fujimura, Y., Uitto, J. and Mauviel, A. (1999) Cooperation between SMAD and NF-kappaB in growth factor regulated type VII collagen gene expression Oncogene **18**, 1837–1844
17 Arsura, M, Wu, M and Sonenshein, G E (1996) TGF beta 1 inhibits NF-kappa B/Rel activity inducing apoptosis of B cells transcriptional activation of I kappa B alpha Immunity **5**, 31–40
18 Arsura, M, FitzGerald, M J, Fausto, N and Sonenshein, G E (1997) Nuclear factor-kappaB/Rel blocks transforming growth factor beta1-induced apoptosis of murine hepatocyte cell lines Cell Growth Differ **8**, 1049–1059
19 Nagarajan, R P, Zhang, J, Li, W and Chen, Y (1999) Regulation of smad7 promoter by direct association with smad3 and smad4 J Biol Chem **274**, 33412–33418
20 Nakao, A, Afrakhte, M, Moren, A, Nakayama, T., Christian, J L, Heuchel, R., Itoh, S, Kawabata, M, Heldin, N E, Heldin, C H and ten Dijke, P (1997) Identification of Smad7, a TGFbeta-inducible antagonist of TGF-beta signalling Nature (London) **389**, 631–635
21 Ishisaki, A, Yamato, K., Nakao, A, Nonaka, K, Ohguchi, M, ten Dijke, P. and Nishihara, T (1998) Smad7 is an activin-inducible inhibitor of activin-induced growth arrest and apoptosis in mouse B cells J Biol Chem **273**, 24293–24296
22 Parks, C L, Banerjee, S and Spector, D J (1988) Organization of the transcriptional control region of the E1b gene of adenovirus type 5 J Virol **62**, 54–67
23 Stein, B, Baldwin, Jr, A S, Ballard, D W, Greene, W. C, Angel, P and Herrlich, P (1993) Cross-coupling of the NF-kappa B p65 and Fos/Jun transcription factors produces potentiated biological function EMBO J **12**, 3879–3891
24 Nakshatri, H, Bhat-Nakshatri, P, Martin, D. A, Goulet, Jr, R J and Sledge, Jr, G W (1997) Constitutive activation of NF-kappaB during progression of breast cancer to hormone-independent growth Mol Cell Biol **17**, 3629–3639
25 Hedin, K E, Bell, M P., Kalli, K R, Huntoon, C J, Sharp, B M and McKean, D J (1997) Delta-opioid receptors expressed by Jurkat T cells enhance IL-2 secretion by increasing AP-1 complexes and activity of the NF-AT/AP-1- binding promoter element J Immunol **159**, 5431–5440
26 Vig, E, Green, M, Liu, Y, Donner, D B, Mukaida, N, Goebl, M G and Harrington, M A (1999) Modulation of tumor necrosis factor and interleukin-1-dependent NF-kappaB activity by mPLK/IRAK J Biol Chem **274**, 13077–13084
27 Huang, H C, Murtaugh, L C, Vize, P D and Whitman, M (1995) Identification of a potential regulator of early transcriptional responses to mesoderm inducers in the frog embryo EMBO J **14**, 5965–5973
28 Wrana, J L, Attisano, L, Carcamo, J, Zentella, A, Doody, J, Laiho, M, Wang, X F and Massague, J (1992) TGF beta signals through a heteromeric protein kinase receptor complex Cell **71**, 1003–1014
29 Lagna, G, Hata, A, Hemmati-Brivanlou, A and Massague, J (1996) Partnership between DPC4 and SMAD proteins in TGF-beta signalling pathways Nature (London) **383**, 832–836
30 Chen, Y, Lebrun, J J and Vale, W (1996) Regulation of transforming growth factor beta- and activin-induced transcription by mammalian Mad proteins Proc Natl Acad Sci. U S A **93**, 12992–12997
31 Chen, X, Weisberg, E, Fridmacher, V, Watanabe, M, Naco, G and Whitman, M (1997) Smad4 and FAST-1 in the assembly of activin-responsive factor Nature (London) **389**, 85–89
32 Dennler, S, Itoh, S, Vivien, D, ten Dijke, P, Huet, S. and Gauthier, J M (1998) Direct binding of Smad3 and Smad4 to critical TGF beta-inducible elements in the promoter of human plasminogen activator inhibitor-type 1 gene EMBO J **17**, 3091–3100
33 Zhang, Y, Feng, X H and Derynck, R (1998) Smad3 and Smad4 cooperate with c-Jun/c-Fos to mediate TGF-beta-induced transcription Nature (London) **394**, 909–913
34 Nabel, G and Baltimore, D (1987) An inducible transcription factor activates expression of human immunodeficiency virus in T cells Nature (London) **326**, 711–713
35 Li, J M, Shen, X, Hu, P P and Wang, X F (1998) Transforming growth factor beta stimulates the human immunodeficiency virus 1 enhancer and requires NF-kappaB activity Mol Cell Biol **18**, 110–121
36 Zabel, U, Schreck, R and Baeuerle, P A. (1991) DNA binding of purified transcription factor NF-kappa B Affinity, specificity, Zn^{2+} dependence, and differential half-site recognition J Biol Chem **266**, 252–260
37 Webster, G A and Perkins, N D (1999) Transcriptional cross talk between NF-kappaB and p53 Mol. Cell Biol **19**, 3485–3495
38 Hottiger, M O, Felzien, L K and Nabel, G J (1998) Modulation of cytokine-induced HIV gene expression by competitive binding of transcription factors to the coactivator p300 EMBO J **17**, 3124–3134
39 Bitzer, M, von Gersdorff, G, Liang, D, Dominguez-Rosales, A, Beg, A. A, Rojkind, M and Bottinger, E P (2000) A mechanism of suppression of TGF-beta/SMAD signaling by NF-kappaB/RelA Genes Dev **14**, 187–197

Received 7 March 2000/3 April 2000, accepted 18 April 2000

Biochem. J (2000) 348, 597–606 (Printed in Great Britain)

Determinant of the extracellular location of the N-terminus of human multidrug-resistance-associated protein

Jian-Ting ZHANG[1]

Department of Pharmacology and Toxicology, IU Cancer Center, R4-Room 166, Indiana University School of Medicine, 1044 W Walnut St, Indianapolis, IN 46202, U.S A

Multidrug-resistance-associated protein (MRP) is a member of the ATP-binding cassette (ABC) membrane-transport superfamily and is responsible for multidrug resistance in cancer cells. Distinct from other members of the ABC superfamily, MRP has three membrane-spanning domains (MSDs) and the N-terminus is located extracellularly. It has been shown that the first MSD (MSD1) with an extracellular N-terminus is important for MRP function. To address what ensures the generation of this structural organization of MRP and to understand in general the molecular mechanism of membrane folding of polytopic proteins with extracellular N-termini, the biogenesis of MSD1 in human MRP1 was examined using an *in vitro* expression system. Surprisingly, the second transmembrane segment (TM2) in MSD1 was found to play a critical role in the correct membrane translocation and folding of MSD1 in human MRP1. TM2 not only plays an essential role to ensure the N-terminus-outside/C-terminus-inside orientation of TM1 with an extracellular N-terminus, it can also translocate into membranes post-translationally in a signal-recognition particle and ribosome-dependent manner to provide an additional insurance for correct folding of MSD1 in MRP. These findings suggest that TM2 in a polytopic membrane protein with an extracellular N-terminus may play a critical role in controlling correct membrane translocation and folding of the protein in general.

Key words: membrane targeting, MRP, ribosome, signal sequence, topogenesis.

INTRODUCTION

The early steps in biogenesis of membrane proteins closely resemble the biogenesis of secretory proteins in the endoplasmic reticulum (ER). A signal sequence in membrane proteins, as in secretory proteins, is responsible for the membrane targeting to the ER whereas topogenic sequences (including the signal sequence) will determine how the protein is folded in the membrane [1]. Membrane targeting and translocation of a nascent membrane protein also involves many cytoplasmic and translocation-machinery proteins on the ER [2].

Most polytopic (spanning membranes twice or more) and bitopic (spanning membranes once) membrane proteins in eukaryotic cells are thought to acquire their final membrane orientations during or immediately after synthesis on the ER [3–6]. Topogenic sequences involved in signal, signal anchorage and stop-transfer activities have been identified in eukaryotic polytopic membrane proteins [7–11]. A polytopic topology was thought to be generated by a sequential translocation and membrane integration of independent topogenic sequences [1,6,9,12,13]. However, for polytopic proteins with an extracellular N-terminus it remains unknown what determines the generation of the extracellular location of the N-terminus.

Multidrug resistance in cancer cells is a major problem in successful chemotherapy. One of the known causes for multidrug resistance is the elevated expression of plasma-membrane proteins that efflux anti-cancer drugs. Two major proteins have been found which have a drug-efflux function: P-glycoprotein (Pgp) [14,15] and multidrug-resistance-associated protein (MRP) [16,17]. Both Pgp and MRP are polytopic membrane proteins and belong to the same ATP-binding cassette (ABC) transport superfamily [18].

The topological folding of Pgp has been mapped and more than one topology was found [19–22]. Although it remains controversial, the observed alternative topologies may be very important for Pgp-mediated drug transport. Recently, the topology of MRP has also been studied. Surprisingly, MRP was found to have three rather than two membrane-spanning domains (MSDs) and its N-terminus was found in the extracellular space [23–25] (see also Figure 1A). This observation is different from the prediction and also contradicts the traditional view of two MSDs with N-termini located in the cytoplasm for most other ABC transporters. This peculiar feature may underlie a unique property in MRP-mediated drug transport. A recent study on the functional importance of the additional MSD (or MSD1) showed that truncation of the extracellular N-terminus with the first transmembrane (TM) segment, TM1, eliminated MRP function [26], although more recent studies showed that the loop linking MSD1 and MSD2 was essential for MRP function [27,28].

In this study, I determined the biogenesis of MSD1 of human MRP1 and examined what controls the generation of the extracellular N-terminus of MRP in the biogenesis process. I found that (i) both TM1 and the second TM segment, TM2, had *de novo* activity to initiate signal-recognition-particle (SRP)-dependent membrane translocation; (ii) the orientation of TM1 was determined by charged amino acids flanking TM1 and by the strong N-terminus-inside/C-terminus-outside (N_{in}-C_{out}) membrane-translocation activity of TM2; (iii) TM2 could initiate

---

Abbreviations used ABC, ATP-binding cassette, MRP, multidrug-resistance-associated protein, MSD, membrane-spanning domain, ER, endoplasmic reticulum; Pgp, P-glycoprotein, TM, transmembrane, RRL, rabbit reticulocyte lysate, WGE, wheat germ extract, WGR, wheat germ ribosome, SRP, signal-recognition particle, RM, microsome membranes, KRM, SRP-stripped RM, NEM, *N*-ethylmaleimide, NRM, NEM-treated RM, PNGase F, peptide N-glycosidase F, N_{in}-C_{out}, N-terminus inside/C-terminus outside, N_{out}-C_{in}, N-terminus outside/C-terminus inside; CFTR, cystic fibrosis transmembrane conductance regulator

[1] E-mail jianzhan@iupui edu

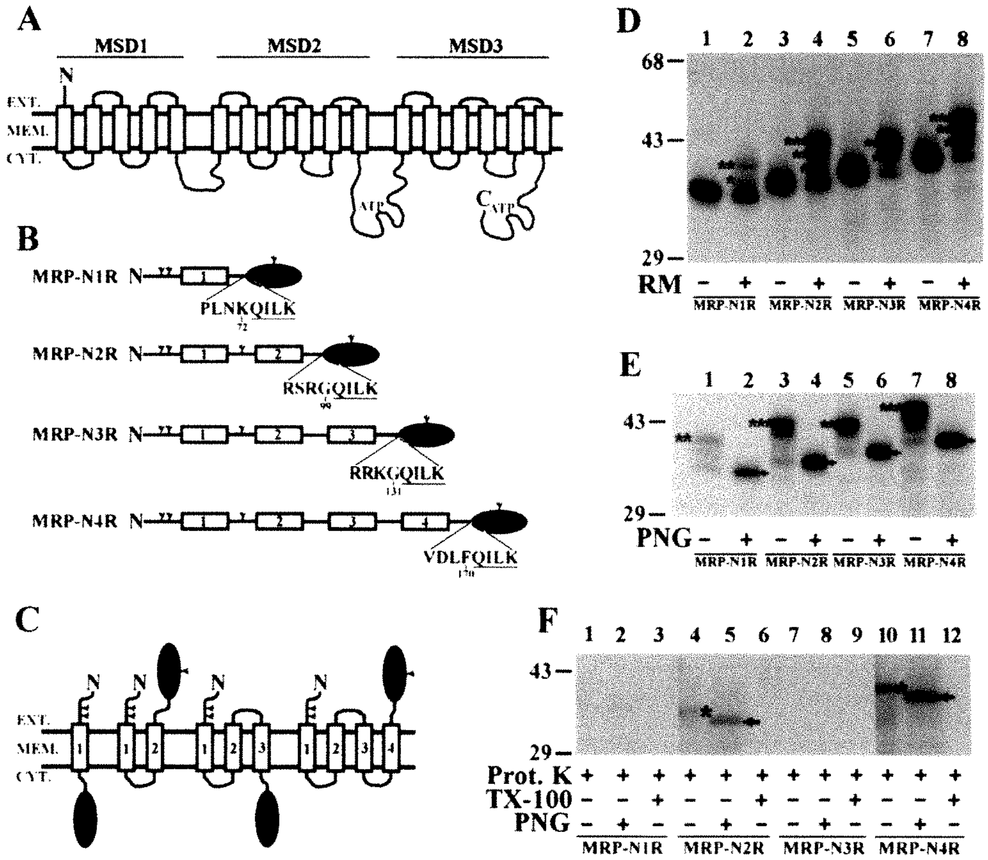

Figure 1 Translation and topology of MRP-N1R, MRP-N2R, MRP-N3R and MRP-N4R

(**A**) Schematic diagram of human MRP topology. The topological structure shown here is from Bakos et al. [23]. CYT, cytoplasm; EXT, extracellular; MEM, membrane. TM segments are denoted by open boxes. (**B**) Schematic diagram of MRP-N1R–MRP-N4R constructs. TM segments are denoted by numbered boxes. The glycosylation reporter is shown as a black ellipse. The potential glycosylation sites are indicated by branched symbols. The amino acid sequence of the fusion site is shown with the glycosylation reporter sequence underlined. (**C**) Predicted membrane orientation of MRP-N1R–MRP-N4R proteins. Glycosylations are indicated by branched symbols. Note the membrane orientation and glycosylation status of the glycosylation reporter in each construct. (**D**) Fluorography of truncated MRP translation products. Translations were performed in RRL in the absence (lanes 1, 3, 5 and 7) or presence (lanes 2, 4, 6 and 8) of RM. The number of asterisks denotes the number of oligosaccharide chains attached to the protein product. (**E**) Endoglycosidase PNGase F (PNG) treatment of truncated MRP translation products. Translation products produced in the presence of RM were treated by PNGase F (lanes 2, 4, 6 and 8). Samples in lanes 1, 3, 5 and 7 are control reactions without PNGase F. ← and * indicate deglycosylated and glycosylated proteins respectively. (**F**) Proteinase K digestion of truncated MRP translation products. Translation products generated in the presence of RM were treated by proteinase K in the absence (lanes 1, 2, 4, 5, 7, 8, 10 and 11) or presence of Triton X-100 (TX-100; lanes 3, 6, 9 and 12). Samples in lanes 2, 5, 8 and 11 were further treated with PNGase F.

post-translational membrane translocation to ensure correct membrane folding of MSD1; (iv) the membrane translocation of TM2, TM3 and TM4 appeared to follow the sequential membrane-translocation model independent of TM1; and (v) truncation of the extracellular N-terminal sequence including TM1 did not affect the membrane translocation and folding of MSD1.

EXPERIMENTAL PROCEDURES

Materials

Human MRP1 cDNA [29] was obtained from Dr Piet Borst (Netherlands Cancer Institute, Amsterdam, The Netherlands). pGEM-4z plasmid, SP6 RNA polymerase, RNasin, ribonucleotides, RQ1 DNase, rabbit reticulocyte lysate (RRL) and pGEM-T Easy vector were obtained from Promega. Dog pancreatic microsomal membranes were prepared as described previously [30]. [^{35}S]Methionine and Amplify were purchased from New England Nuclear and Amersham, respectively. m^{7}G(5′)ppp(5′)G cap analogue (diguanosine triphosphate) was obtained from Pharmacia. Peptide N-glycosidase F (PNGase F) and restriction enzymes were obtained from Boehringer Mannheim, New England Biolabs or Promega. All other chemicals were obtained from Sigma or Fisher Scientific.

Construction of human MRP1 cDNA with a glycosylation reporter gene and site-directed mutagenesis

PCR was used to engineer fusion constructs and mutations as described previously [31]. Briefly, cDNAs encoding TM1, TM1–TM2, TM1–TM3 and TM1–TM4 of human MRP1 were amplified by PCR using a sense primer 5′-GTCGTGATGGCGCTCCGGGG-3′ (for all constructs), and antisense primers 5′-CTTCAAGATCTGTTTGTTGAGAGG-3′ (for TM1), 5′-CTTCAAGATCTGGCCCCGACTTCT-3′ (for TM1–TM2), 5′-CTTCAAGATCTGTCCCTTCCTCCT-3′ (for TM1–TM3), and 5′-CTTCAAGATCTGAAACAGGTCCAC-3′ (for TM1–TM4). The sense primer contained a Kozak initiation codon ATG (underlined) and antisense primers contained a *Bgl*II digestion sequence AGATCT (underlined). The PCR products were cloned into pGEM-T Easy vectors. The cDNA inserts in pGEM-T Easy vectors were then released by *Eco*RI and *Bgl*II digestion and ligated into an *Eco*RI/*Bgl*II-linearized pGEM 4z vector containing a glycosylation reporter gene. The glycosylation reporter was derived from an ATP-binding domain of Pgp and has been used successfully in our previous studies [32–35]. These fusion DNA constructs were named MRP-N1R, MRP-N2R, MRP-N3R and MRP-N4R, respectively.

Truncations at the N-terminus of MRP1 were engineered using MRP-N1R, MRP-N2R and MRP-N3R DNA as templates for PCR. To remove the N-terminal sequence, a sense primer, 5′-GAATACGAATTCGTCGTGATGTGGAATGTCACGTGG-3′ (MRPTNE) or 5′-GAATACGAATTCGTCGTGATGCGAGGCTACATTCAG-3′ (MRPTTM1), and a T7 vector primer were used. Both MRPTNE and MRPTTM1 primers contained an *Eco*RI site (GAATTC) and a translation-initiation codon (ATG; both underlined). The PCR products were digested with *Eco*RI and *Hin*dIII and cloned into an *Eco*RI/*Hin*dIII-linearized pGEM-4z vector. The truncated DNA constructs were named MRP-N1ΔNE, MRP-N2ΔNE, MRP-N2ΔNTM1 and MRP-N3ΔNTM1.

To mutate Asp^{10}, Asp^{13} and Asp^{17} to Arg, an antisense oligonucleotide containing these mutations 5′-GACATTCCAGCGCCAGAGCGGGCGGGAGCCCCGGGCGCTGCA-3′ (MRPN$_{\text{mut}}$) was synthesized. The three codons underlined are the mutated sequences. The first PCR reaction was performed using MRPN$_{\text{mut}}$ and SP6 vector primers on MRP-N1R DNA template. The PCR products were then isolated and used as a primer, together with T7 vector primer, to perform PCR on the remaining sequence of MRP-N1R. The final PCR products were digested with *Eco*RI and *Bgl*II and cloned into the *Eco*RI/*Bgl*II-linearized pGEM-4z vector containing a glycosylation reporter gene as described above. The mutant DNA construct was named MRP-N1RN$_{\text{mut}}$. To engineer these mutations into MRP-N2R, MRP-N3R and MRP-N4R, a cassette containing the mutations was released from MRP-N1RN$_{\text{mut}}$ using *Eco*RI and *Dra*III digestion and then used to replace the wild-type sequence in MRP-N2R, MRP-N3R and MRP-N4R DNA. The mutant DNAs were named MRP-N2RN$_{\text{mut}}$, MRP-N3RN$_{\text{mut}}$ and MRP-N4RN$_{\text{mut}}$. All DNA constructs were sequenced to confirm the correct fusion, truncation and mutation.

Transcription and translation *in vitro*

Transcription *in vitro* was performed as described previously [19]. Cell-free translations in RRL or wheat germ extract (WGE), proteolysis/membrane-protection assay, limited endoglycosidase treatment, isolation of membrane fractions by centrifugation as well as analysis using SDS/PAGE and fluorography, were performed as described previously [19]. Treatment of microsome membranes (RM) with *N*-ethylmaleimide (NEM) and salt were performed as described previously by Gilmore et al. [36] and Walter and Blobel [37], respectively. For the post-translational membrane-translocation experiment, translation was performed without RM for 1 h and terminated by addition of puromycin to a final concentration of 20 μM and incubation for 20 min, then followed by incubation with RM for 30 min. All incubations were at 30 °C. Translation using pre-mixed RRL and WGE were performed as described previously [38]. Translation in RRL in the presence of wheat germ ribosome (WGR) and purification of WGR were done in the same way as described by Wang et al. [39]. The fluorograph images were digitized using a HP ScanJet 6100C and Adobe Photoshop 4.0.

RESULTS

Topology of MSD1 in ER membranes

MRP differs from other ABC transporters by having three MSDs with an extracellular N-terminus (Figure 1A). To understand the importance of the additional MSD (MSD1) in biogenesis of human MRP1, the TM segments in MSD1 were first tested for their membrane-translocation properties. To achieve this goal, a glycosylation reporter was engineered at the C-terminal side of each of the four TM segments of MSD1. These constructs (named MRP-N1R, MRP-N2R, MRP-N3R and MRP-N4R) are shown schematically in Figure 1(B). Figure 1(C) shows the predicted topology of these constructs. Note that the two potential glycosylation sites at the N-terminus are attached with oligosaccharide chains in all constructs whereas the potential site in the C-terminal glycosylation reporter is glycosylated only in MRP-N2R and MRP-N4R (Figure 1C).

As shown in Figure 1(D), translation of MRP-N1R, MRP-N2R, MRP-N3R and MRP-N4R transcripts in RRL in the absence of dog pancreatic RM generated products with incremental increases in size, as expected (Figure 1D, lanes 1, 3, 5 and 7). In the presence of RM, products with higher molecular masses were generated from all constructs (as indicated by asterisks in Figure 1D, lanes 2, 4, 6 and 8). The increased size in the presence of RM was due to glycosylation, as demonstrated by endoglycosidase (PNGase F) treatment, which reduced their sizes to the same level as the ones produced in the absence of RM (see Figure 1E). Therefore, the nascent protein containing one, two, three and four TM segments of MSD1 actively translocated into membranes and were modified by glycosylation. However, it is noteworthy that the membrane translocation by MRP-N1R was less than that by other constructs (compare lane 2 with lanes 4, 6 and 8, Figure 1D)

To determine the membrane orientation of the N- and C-termini of these proteins, the glycosylation status was examined. As indicated by the number of asterisks in Figure 1(D), MRP-N1R and MRP-N3R both had a maximum of two high-mannose chains whereas MRP-N2R and MRP-N4R had a maximum of three high-mannose chains attached. The glycosylation status was also independently demonstrated using limited deglycosylation studies (J.-T. Zhang, unpublished work). Thus, MRP-N1R, MRP-N2R, MRP-N3R and MRP-N4R all had their N-termini located in the RM lumen and glycosylated with a maximum of two high-mannose chains (Figure 1C). MRP-N2R and MRP-N4R proteins, in addition, also had their C-terminal glycosylation reporter located in the RM lumen and attached with an additional oligosaccharide chain (Figure 1C). The orientation of the C-terminal glycosylation reporter in these proteins was demonstrated further by proteolysis/membrane-protection assay. As shown in Figure 1(F), no protease-resistant glycosylation reporter was observed from proteinase K digestion of membrane-associated MRP-N1R (Figure 1F, lanes 1–3) or MRP-N3R (Figure 1F, lanes 7–9), suggesting the cytoplasmic location of the C-terminal glycosylation reporter of these proteins. On the other hand, peptide fragments corresponding to the glycosylation reporter were produced from proteinase K digestion of MRP-N2R (Figure 1F, lane 4) and MRP-N4R (Figure 1F, lane 10). The protected fragments from MRP-N2R and MRP-N4R were also sensitive to PNGase F treatment (Figure 1F, lanes 5 and 11). The protected fragments were digested away if membranes were first permeabilized with Triton X-100 (Figure 1F, lanes 6 and 12). These results indicate that the glycosylation reporters of MRP-N2R and MRP-N4R were glycosylated and located in the RM lumen. Therefore, the N-terminus of human MRP1 was in the extracellular space and the

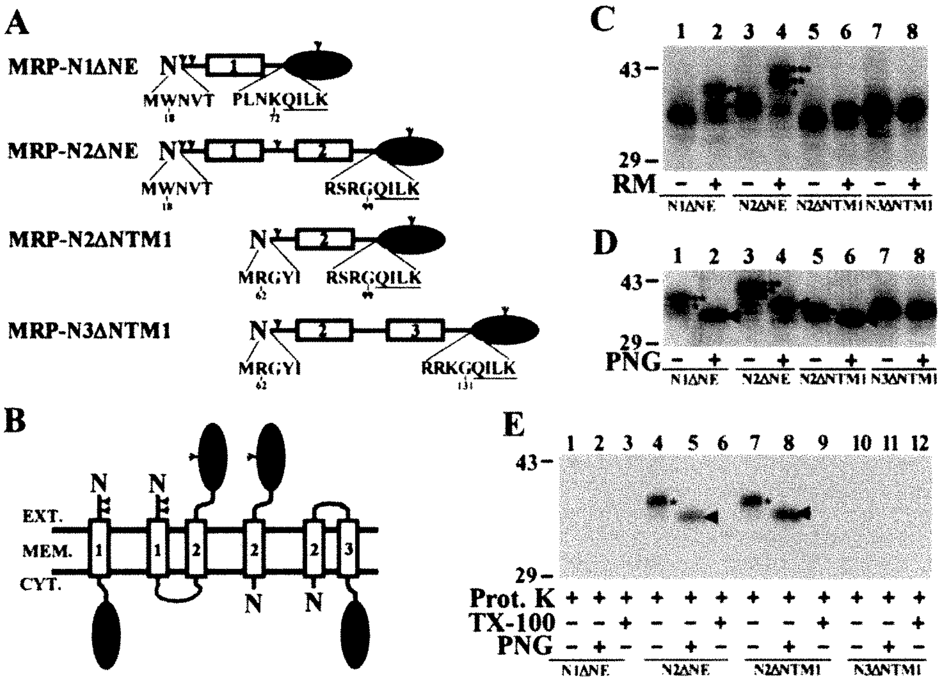

Figure 2 Translation and topology of deletion mutants MRP-N1ΔNE, MRP-N2ΔNE, MRP-N2ΔNTM1 and MRP-N3ΔNTM1

(**A**) Schematic diagram of MRP-N1ΔNE, MRP-N2ΔNE, MRP-N2ΔNTM1 and MRP-N3ΔNTM1 deletion constructs. The symbols used are the same as in Figure 1(B). (**B**) Membrane orientation of deletion-mutant proteins. The symbols are the same as in Figure 1(C). (**C**) Fluorography of translation products of deletion mutants. Translations were performed in RRL in the absence (lanes 1, 3, 5 and 7) or presence (lanes 2, 4, 6 and 8) of RM. The number of asterisks indicates the number of oligosaccharide chains attached with the translation product. (**D**) Endoglycosidase PNGase F (PNG) treatment of translation products. Deletion-mutant products translated in the presence of RM were treated by PNGase F (lanes 2, 4, 6 and 8). Samples in lanes 1, 3, 5 and 7 are control reactions without PNGase F. ← and * indicate deglycosylated and glycosylated proteins respectively. (**E**) Proteinase K digestion of translation products. Deletion-mutant products translated in the presence of RM were treated by proteinase K in the absence (lanes 1, 2, 4, 5, 7, 8, 10 and 11) or presence of Triton X-100 (lanes 3, 6, 9 and 12). Samples in lanes 2, 5, 8 and 11 were further treated with PNGase F.

topology of MSD1 of human MRP1 in ER membranes was the same as in plasma membranes, as shown previously [23–25].

Effect of N-terminal truncation on the orientation of MSD1

Previously, it was shown that the N-terminal sequence may be important for MRP function and that deletion of TM1 inhibited MRP function [26]. It has also been suggested in previous studies that the N-terminal sequence is important for the biogenesis of polytopic membrane proteins [34,40]. To determine whether truncation of the N-terminal sequence affects the topogenesis of MSD1, the first 17 amino acids at the N-terminal end of MRP-glycosylation reporter fusion proteins were deleted and a new start codon was engineered (see Figure 2A). The two potential N-linked glycosylation sites at the N-terminus, however, remain intact. The effect of this deletion on TM1 and TM2 biogenesis was tested. As shown in Figure 2(C), translation of the N-terminally truncated MRP-N1R and MRP-N2R (named MRP-N1ΔNE and MRP-N2ΔNE, respectively) generated proteins of predicted size in the absence of RM (Figure 2C, lanes 1 and 3). In the presence of RM, proteins with maximum of two and three oligosaccharide chains were produced for MRP-N1ΔNE and MRP-N2ΔNE, respectively (indicated by asterisks, Figure 2C, lanes 2 and 4), suggesting that the N-termini of both MRP-N1ΔNE and MRP-N2ΔNE were glycosylated whereas only the C-terminus of MRP-N2ΔNE was glycosylated. The glycosylation status of these two proteins was confirmed by endoglycosidase treatment (Figure 2D, lanes 1–4) and the membrane orientation of the glycosylation reporter was confirmed by proteinase K digestion (Figure 2E, lanes 1–6). Thus the truncated MRP-N1ΔNE and MRP-N2ΔNE proteins had the same topology as their corresponding wild-type proteins (compare Figure 2B with Figure 1B).

The above study suggested that removal of the N-terminal 17 amino acids did not affect either TM1 or TM2 membrane translocation and orientation. However, in the previous functional study by Gao et al. [26], the N-terminal 66 amino acids of MRP1 were deleted to create an inactive protein. To determine whether a large truncation affects the membrane orientation of MSD1, the N-terminal 61 amino acids were deleted to create MRP-N2ΔNTM1 and MRP-N3ΔNTM1. Translation of MRP-N2ΔNTM1 in the presence of RM generated a protein with a single oligosaccharide chain compared with the translation in the absence of RM (Figure 2C, compare lanes 5 and 6), suggesting the lumenal location of the glycosylation reporter (Figure 2B). This was confirmed by a reduction of ≈ 2–3 kDa in size with endoglycosidase treatment (Figure 2D, lanes 5 and 6) and by protection of the glycosylated reporter from proteinase K digestion (Figure 2E, lanes 7–9). Translation of MRP-N3ΔNTM1 generated proteins of the same sizes in the absence and presence of RM (compare lanes 7 and 8, Figure 2C), suggesting that no oligosaccharide was added to the nascent protein. This observation was further confirmed by endoglycosidase treatment that did not change the size of the protein (Figure 2D, lanes 7 and 8). Thus the glycosylation reporter of MRP-N3ΔNTM1 was located in the cytoplasm (Figure 2B). This

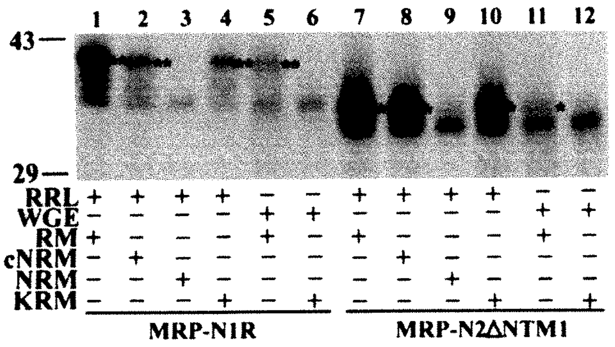
1 2 3 4 5 6 7 8 9 10 11 12
43—
29—
RRL + + + + − − + + + + − −
WGE − − − − + + − − − − + +
RM + − − − + − + − − − + −
cNRM − + − − − − − + − − − −
NRM − − + − − − − − + − − −
KRM − − − + − + − − − + − +
MRP-N1R
MRP-N2ΔNTM1

Figure 3 SRP and docking-protein dependence of the membrane translocation of MRP TM1 and TM2

MRP-N1R and MRP-N2ΔNTM1 were translated in RRL (lanes 1–4 and 7–10) or WGE (lanes 5, 6, 11 and 12) supplemented with normal RM (lanes 1, 5, 7 and 11), NEM-treated RM (NRM; lanes 3 and 9), control RM treated without NEM (cNRM; lanes 2 and 8) and SRP-stripped RM (KRM; lanes 4, 6, 10 and 12). The translocated and glycosylated proteins are indicated by asterisks.

conclusion was supported by proteinase K digestion, which did not generate any membrane-protected glycosylation reporter from MRP-N3ΔNTM1 (Figure 2E, lanes 10–12). Therefore, truncation of N-terminal sequences up to 61 amino acids did not affect the biogenesis of MSD1 of human MRP1.

SRP and SRP-receptor-dependent membrane translocation of MSD1

The above studies also suggested that TM2, in the absence of TM1 (MRP-N2ΔNTM1 construct), could initiate *de novo* N_{in}-C_{out} membrane targeting and translocation while TM1 initiated N-terminus-outside/C-terminus-inside (N_{out}-C_{in}) membrane translocation. To determine whether the membrane targeting and translocation of TM1 and TM2 in MSD1 is dependent on SRPs, translations of MRP-N1R and MRP-N2ΔNTM1 were performed in WGE in conjunction with normal microsomes (RM) and SRP-stripped RM (KRM), depleted of SRP by high-salt wash [37]. In contrast to RRL, WGE does not contain endogenous functional SRP [30]. As shown in Figure 3, fully glycosylated MRP-N1R and MRP-N2ΔNTM1 were generated in the presence of RM both in RRL (Figure 3, lanes 1 and 7) and WGE (Figure 3, lanes 5 and 11), although the production of these proteins in WGE was lower than in RRL because of the existence of a lower level of SRP in WGE brought in by RM. In the presence of KRM the glycosylated proteins were not generated in WGE (Figure 3, lanes 6 and 12), whereas they were still produced in RRL (Figure 3, lanes 4 and 10). Mock treatment of RM without high salt did not affect membrane translocation in WGE (results not shown). Thus the *de novo* membrane targeting and translocation of TM1 (in MRP-N1R) and TM2 (in MRP-N2ΔNTM1) is SRP-dependent.

The dependency of membrane translocation on SRP receptor was demonstrated by producing no glycosylated proteins in RRL supplemented with microsomes (NEM-treated RM, NRM) that had been treated with 2 mM NEM to inactivate SRP receptors (Figure 3, lanes 3 and 9), as demonstrated previously [36].

Determinant of the extracellular location of the N-terminus of MSD1

The amino acid sequence surrounding TM1 was examined in order to investigate what determines the N_{out}-C_{in} membrane orientation of TM1, which results in an extracellular N-terminus. The result showed that the domain at the N-terminal side of TM1 was clearly less positive (with a total net charge of −2) than the domain at the C-terminal side of TM1 (with a total net charge of +3; Figure 4A). Thus it is possible that the membrane orientation of TM1 is determined by the 'positive-inside' rule [41]. To test this hypothesis, three negative charges (Asp^{10}, Asp^{13} and Asp^{17}) at the N-terminus of TM1 were mutated to positive charges (Arg^{10}, Arg^{13} and Arg^{17}, respectively; Figure 4B). The

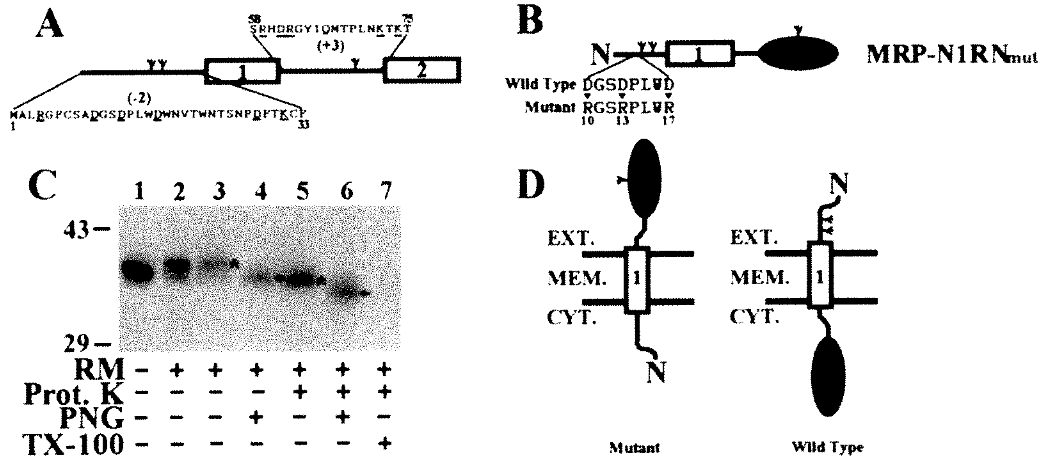

Figure 4 Translation and topology of $MRP\text{-}N1RN_{mut}$

(**A**) Charge distribution surrounding TM1. The symbols used are the same as in Figure 1(B). Charged amino acids are underlined. (**B**) Mutations at the N-terminus of TM1. Aspartic acids at positions 10, 13 and 17 were changed to arginine in MRP-N1R by site-directed mutagenesis. (**C**) Translation of $MRP\text{-}N1RN_{mut}$. Translations were performed in RRL in the absence (lane 1) or presence (lanes 2–7) of RM. The products translated in the presence of RM were further treated by PNGase F (PNG; lane 4) or by proteinase K (Prot. K; lane 5). Lane 3 is a control reaction for PNGase F digestion. Lanes 6 and 7 are proteinase K digestion followed by PNGase F treatment and in combination with Triton X-100 (TX-100), respectively. ← and * indicate deglycosylated and glycosylated proteins, respectively. (**D**) Membrane orientation of mutant and wild-type MRP-N1R.

mutant MRP-TM1R was named MRP-N1RN$_{\text{mut}}$ and had a net charge of +4 at the N-terminal domain of TM1. When MRP-N1RN$_{\text{mut}}$ was translated in the presence of RM, a protein with one oligosaccharide chain was produced in comparison with the translation in the absence of RM (compare lanes 1 and 2, Figure 4C). This observation was confirmed by endoglycosidase treatment that reduced ≈ 2–3 kDa of the protein to the size of the protein translated in the absence of RM (compare lanes 3 and 4, Figure 4C). Proteinase K digestion of the membrane-associated MRP-N1RN$_{\text{mut}}$ generated a protected glycosylation reporter which was glycosylated (compare lanes 5 and 6, Figure 4C). The protected fragments were digested away when membranes were first permeabilized with Triton X-100 (Figure 4C, lane 7). However, in our control digestion using wild-type MRP-N1R, no protected glycosylation reporter was found (results not shown, but see Figure 1F). These results suggest that the glycosylation reporter of MRP-N1RN$_{\text{mut}}$ was located in RM lumen, an orientation opposite to the wild-type MRP-N1R (Figure 4D). Thus, N$_{\text{out}}$-C$_{\text{in}}$ orientation of TM1 is determined by the charged amino acids flanking TM1 and mutation of these charges can invert the membrane orientation of TM1 in MRP-N1R (Figure 1D). It should be noted that the mutations at the N-terminus completely inverted the orientation of TM1 in the presence of the glycosylation reporter, indicating that the reporter domain did not affect the membrane translocation and orientation of TM1.

To determine if the same mutations would still affect the membrane topology of TM1 in the presence of other TM segments, TM2–TM4, Asp^{10}, Asp^{13} and Asp^{17} were all mutated to Arg to create MRP-N2RN$_{\text{mut}}$, MRP-N3RN$_{\text{mut}}$ and MRP-N4RN$_{\text{mut}}$, respectively. The membrane orientations of these mutant proteins were then determined. As shown in Figure 5(A), translation of MRP-N2RN$_{\text{mut}}$, MRP-N3RN$_{\text{mut}}$ and MRP-N4RN$_{\text{mut}}$ in the presence of RM generated proteins with a maximum of three, two and three oligosaccharide chains attached (as indicated by the numbers of asterisks), respectively. This was demonstrated by comparison of the products generated in the absence and presence of RM (compare lanes 1, 4 and 7 with lanes 2, 5 and 8, respectively, Figure 5A) and by endoglycosidase treatment (lanes 3, 6 and 9, Figure 5A). Proteinase K digestion in combination with PNGase F treatment of the membrane-associated products showed that both MRP-N2RN$_{\text{mut}}$ and MRP-N4RN$_{\text{mut}}$ proteins had their C-terminal glycosylation reporters protected by RM (Figure 5B, lanes 1, 2, 7 and 8), indicating the RM-lumen location of the glycosylation reporter. MRP-N3RN$_{\text{mut}}$, on the other hand, did not have its C-terminal glycosylation reporter protected by RM (Figure 5B, lanes 4–6), indicating a cytoplasmic location of the glycosylation reporter. These results suggest that the N-terminus be glycosylated and located in the RM lumen for all MRP-N2RN$_{\text{mut}}$, MRP-N3RN$_{\text{mut}}$ and MRP-N4RN$_{\text{mut}}$ and that the C-terminal glycosylation reporter be located in the RM lumen only for MRP-N2RN$_{\text{mut}}$ and MRP-N4RN$_{\text{mut}}$. Thus, the topology of MRP-N2RN$_{\text{mut}}$, MRP-N3RN$_{\text{mut}}$ and MRP-N4RN$_{\text{mut}}$ in RM was the same as that of the wild-type MRP-N2R, MRP-N3R and MRP-N4R, respectively (see Figure 1B). That is, the mutations did not invert the orientation of TM1 in MRP-N2RN$_{\text{mut}}$, MRP-N3RN$_{\text{mut}}$ and MRP-N4RN$_{\text{mut}}$. This observation is surprisingly interesting because mutations of Asp^{10}, Asp^{13} and Asp^{17} to Arg could invert the TM1 orientation in the absence of other TMs following TM1 (MRP-N1RN$_{\text{mut}}$) but not in the presence of these TMs (MRP-N2RN$_{\text{mut}}$, MRP-N3RN$_{\text{mut}}$ and MRP-N4RN$_{\text{mut}}$). The inverted orientation of TM1 by mutations had apparently been corrected by the existence of a minimum sequence of TM2 plus its flanking residues. Therefore, TM2 appeared to play a very important role in helping MSD1 of human MRP1 fold correctly and could correct the mutation-caused inversion of the TM1 orientation in membranes. However, it should be noted that replacing the glycosylation reporter domain of MRP-N1R with TM2 might have also altered the charges at the C-terminal side of TM1, which in turn affected the folding of TM1. Nevertheless, replacing the glycosylation reporter of MRP-N1R with TM2 (MRP-N2R) in the wild-type sequence did not affect the membrane orientation of TM1 and it only affected the mutated sequence. This observation suggests that TM2 is very important for TM1 membrane translocation and orientation.

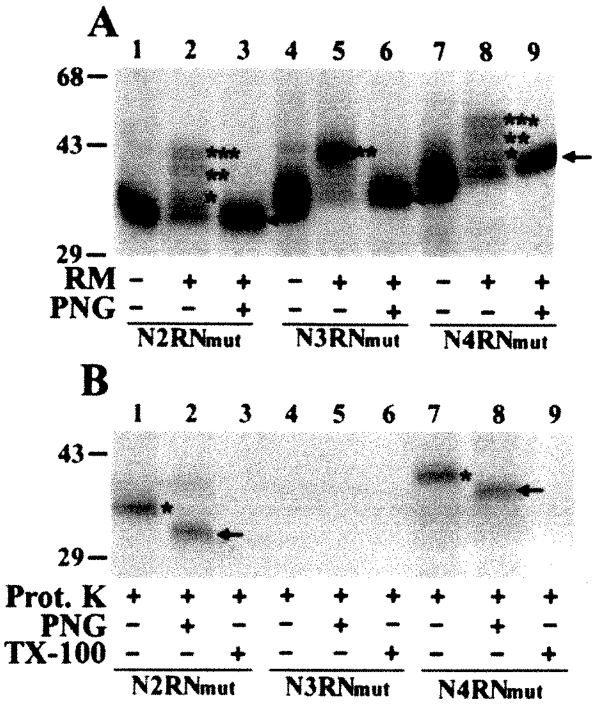

Figure 5 Translation and topology of MRP-N2RN$_{\text{mut}}$, MRP-N3RN$_{\text{mut}}$ and MRP-N4RN$_{\text{mut}}$

(**A**) Translation and endoglycosidase treatment of MRP-N2RN$_{\text{mut}}$–MRP-N4RN$_{\text{mut}}$. Translations were performed in RRL in the absence (lanes 1, 4 and 7) or presence (lanes 2, 3, 5, 6, 8 and 9) of RM. Endoglycosidase PNGase F (PNG) treatment was performed with the products translated in the presence of RM (lanes 3, 6 and 9). The number of asterisks denotes the number of oligosaccharide chains attached to the protein product. ← indicates deglycosylated proteins. (**B**) Proteinase K digestion of MRP-N2RN$_{\text{mut}}$–MRP-N4RN$_{\text{mut}}$. Membrane-associated MRP-N2RN$_{\text{mut}}$–MRP-N4RN$_{\text{mut}}$ were treated with proteinase K (Prot. K), followed by PNGase F digestion (lanes 2, 5 and 8), or in combination with Triton X-100 (TX-100; lanes 3, 6 and 9). ← and * indicate deglycosylated and glycosylated fragments, respectively.

Post-translational membrane translocation of MSD1

In a previous study on cystic fibrosis transmembrane conductance regulator (CFTR), Lu et al. [42] found that TM2 of CFTR has an ability to translocate into membranes post-translationally as a redundant mechanism to ensure correct membrane insertion of CFTR. In the current study, TM2 of human MRP1 was found to have an ability to initiate membrane translocation in an SRP-dependent manner and that TM2 could correct the mutation-induced inversion of TM1 orientation. This suggests that TM2 plays a very important role in regulating the topogenesis of MSD1. To determine whether TM2 of human MRP1 also has post-translational membrane targeting and translocation activity to provide an additional insurance for correct folding of MSD1 in case TM1 fails to initiate membrane translocation correctly, a

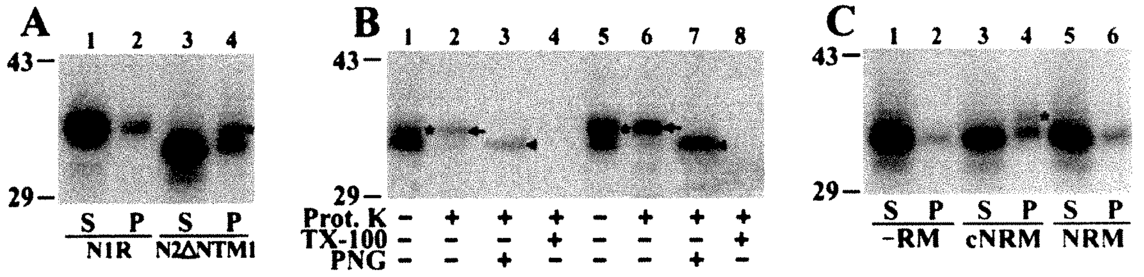

Figure 6 Post-translational membrane translocation of MRP TM2

(**A**) Post-translational membrane translocation. MRP-N1R and MRP-N2ΔNTM1 were translated in RRL in the absence of RM and terminated by addition of puromycin followed by addition of RM and incubation. Membranes (P, lanes 2 and 4) were then separated from soluble (S, lanes 1 and 3) fractions by centrifugation and analysed by SDS/PAGE. The glycosylated protein is indicated by asterisks. (**B**) Proteinase K (Prot. K) digestion of post-translationally translocated MRP-N2ΔNTM1. Membrane-associated MRP-N2ΔNTM1 from post-translational translocation (lanes 1–4) or co-translational translocation (lanes 5–8) were treated with proteinase K (lanes 2–4 and 6–8), followed by PNGase F (PNG) digestion (lanes 3 and 7), or in combination with Triton X-100 (TX-100; lanes 4 and 8). ◀ and * indicate deglycosylated and glycosylated fragments, respectively; ← indicates the protein resistant to proteinase K digestion. (**C**) SRP-dependence of post-translational translocation. MRP-N2ΔNTM1 was translated in RRL in the absence (lanes 1 and 2) or presence of control NRM (cNRM; lanes 3 and 4) and NRM (lanes 5 and 6). The insoluble fraction was then isolated by centrifugation and analysed by SDS/PAGE. The glycosylated protein is indicated by the asterisk.

post-translational membrane-translocation experiment was performed. RM was added to a translation of MRP-N2ΔNTM1 after the translation was completed and terminated by addition of puromycin and then membrane fractions were isolated by centrifugation for analysis by SDS/PAGE. Extended incubation in the presence of puromycin did not generate more translation products, indicating that the translation was fully stopped (results not shown). As shown in Figure 6(A), a glycosylated protein (indicated by an asterisk) was generated from MRP-N2ΔNTM1 and it was associated with the membrane pellet (compare lanes 3 and 4, Figure 6A), whereas no glycosylated protein was found from MRP-N1R (compare lanes 1 and 2, Figure 6A). This observation suggests that TM2 in MRP-N2ΔNTM1 can target and translocate into membranes after the translation is terminated, whereas TM1 in MRP-N1R cannot target and translocate into membranes post-translationally.

To confirm the post-translational membrane translocation of MRP-N2ΔNTM1, membrane-associated nascent MRP-N2ΔNTM1 was treated with proteinase K. As shown in Figure 6(B), the glycosylated protein was resistant to protease digestion (Figure 6B, lane 2) and its size was reduced by endoglycosidase treatment (Figure 6B, lane 3). This observation is the same as that for co-translationally translocated MRP-N2ΔNTM1 (Figure 6B, lanes 6 and 7). Thus the post-translationally translocated MRP-N2ΔNTM1 had the same orientation as the co-translationally translocated MRP-N2ΔNTM1. Note that the only difference between the co-translational and post-translational targeting and translocation of MRP-N2ΔNTM1 was that the efficiency of this process was lower by post-translational than co-translational mechanism (compare the amount of glycosylated protein indicated by an asterisk in Figure 6B, lanes 1 and 5).

To determine whether the post-translational membrane targeting and translocation of TM2 is also SRP- and SRP-receptor-dependent, NRM was added to the translation after terminating the translation with puromycin. As shown in Figure 6(C), the glycosylated protein in the membrane pellet was not observed in the presence of NRM (compare lanes 5 and 6, Figure 6C), whereas it was produced in the presence of control RM treated without NEM (compare lanes 3 and 4, Figure 6C). This observation was confirmed by proteinase K digestion that did not produce membrane-protected glycosylation reporter from the translation in the presence of NRM (results not shown). Thus the post-translational membrane targeting and translocation of TM2 was also by the SRP and its receptor-dependent mechanism. Note that the unglycosylated band found in the pellet appears to represent background since it was also observed when no membranes were added to the translation (Figure 6C, lane 2).

Ribosomal role in membrane translocation of MSD1

In previous studies, it has been reported that ribosomes are important for the membrane targeting and translocation of polytopic membrane proteins [39]. Because TM2 of human MRP1 is a very important element in the topogenesis of MSD1, MRP-N2R was translated in both RRL or WGE to determine whether the membrane translocation and orientation of MRP-N2R is different between these two different systems. Surprisingly, MRP-N2R did not generate the fully glycosylated protein in WGE as compared with the translation in RRL (compare lanes 1 and 2, Figure 7A). Only proteins with two oligosaccharide chains and the unglycosylated peptide backbone were produced in WGE. This suggests that, in WGE, TM1 of MRP-N2R may initiate the membrane targeting and translocation with the N_{out}-C_{in} orientation. However, TM2 of MRP-N2R may be unable to initiate the N_{in}-C_{out} membrane translocation. Thus only the two potential sites at the N-terminus were glycosylated while the C-terminal glycosylation reporter was located in cytoplasm. This was supported by proteinase K treatment of MRP-N2R translated in WGE that did not generate any glycosylated or unglycosylated and membrane-protected glycosylation reporter fragments (compare lanes 1–4 with lanes 5–8, Figure 7C).

A lack of SRP in WGE was unlikely to be responsible for the failure of membrane translocation of TM2 in MRP-N2R, because supplementation of RM would provide enough SRP to support the membrane translocation of TM2 in WGE (see Figure 3). To support this argument, translations of MRP-N2R in pre-mixed RRL and WGE were performed. As shown in Figure 7(D), MRP-N2R containing three oligosaccharide chains (indicated by three asterisks) was produced in RRL (Figure 7D, lane 1) but not in WGE (Figure 7D, lane 9). In the mixture of different ratios of RRL and WGE, production of fully glycosylated MRP-N2R (with three oligosaccharide chains) in the presence of up to 50 % RRL (Figure 7B, lane 5) was not recovered to the same extent as in RRL alone (Figure 7B, lane 1). Thus lacking SRP in WGE was not responsible for the failure of TM2 membrane trans-

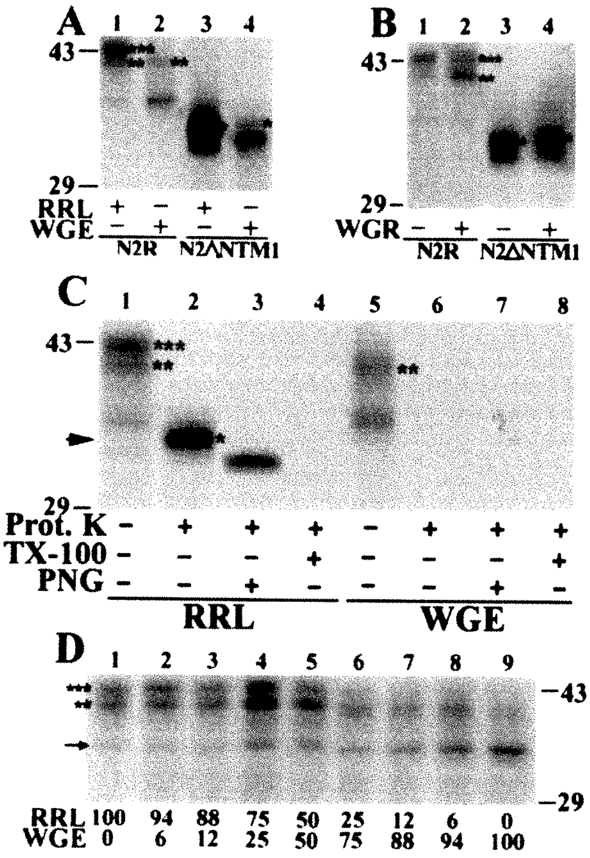

Figure 7 Ribosomal dependence of the membrane translocation of MRP TM2

(**A**) MRP-N2R and MRP-N2ΔNTM1 were translated in RRL or WGE and membrane fractions were isolated and analysed by SDS/PAGE. (**B**) Translation of MRP-N2R in RRL and WGE translation systems that were pre-mixed prior to translation. (**C**) Proteinase K (Prot. K) digestion of MRP-N2R translated in WGE. Membrane-associated MRP-N2R translated in RRL (lanes 1–4) or WGE (lanes 5–8) were treated with proteinase K (lanes 2–4 and 6–8), followed by PNGase F (PNG) digestion (lanes 3 and 7), or in combination with Triton X-100 (TX-100; lanes 4 and 8). The arrowhead indicates the membrane-protected glycosylation reporter. (**D**) Effect of WGR on membrane translocation of TM2 in MRP-N2R and MRP-N2ΔNTM1. MRP-N2R and MRP-NΔNTM1 in RRL were translated in the absence or presence of WGR and membrane fractions where then isolated and analysed by SDS/PAGE. The numbers below the panel denote the percentages (in volume) of RRL and WGE. The glycosylated proteins are indicated by the asterisks. The arrow indicates the unglycosylated protein.

location in WGE because addition of a small fraction of RRL should supply enough SRP to support fully the membrane translocation of TM2. Therefore, factors other than lacking SRP in WGE may be responsible for the failure of membrane translocation of TM2 of MRP-N2R.

One possible cause for generating the fully glycosylated MRP-N2R in WGE is that WGR may function differently in folding the nascent protein than RRL ribosome and that TM2 translated by WGR may not re-initiate membrane translocation after TM1 was translocated into membranes. To test this hypothesis, WGR were isolated from WGE and added to the RRL translation system to determine if WGR could compete with RRL ribosomes to increase the production of MRP-N2R with two oligosaccharide chains. As shown in Figure 7(B), the amount of proteins with two oligosaccharide chains (indicated by two asterisks) was clearly increased by addition of WGR (compare lanes 1 and 2, Figure 7B). This observation indicates that the TM2 of MRP-N2R did not translocate into membranes efficiently in the presence of WGR. Thus the difference in ribosomes between RRL and WGE translation systems may be the cause for the difference in topogenesis of TM2 of MRP-N2R. WGR could probably not help TM2 of MRP-N2R target and translocate into membranes. These observations indicate that the membrane targeting and translocation of MRP TM2 in the presence of TM1 was regulated by ribosomes that may involve a re-targeting process (see the Discussion).

It should be noted, however, that a glycosylated protein was generated from MRP-N2ΔNTM1 (lacking TM1) in WGE (Figure 7A, lane 4). This observation suggests that TM2 in the absence of TM1 can target and translocate into RM with a N_{in}-C_{out} orientation in WGE, albeit at a much lower level than that in RRL (compare lanes 3 and 4, Figure 7A). This is in contrast to the observation that TM2 of MRP-N2R (in the presence of TM1) in WGE could not target and translocate into membranes with a N_{in}-C_{out} orientation (Figure 7A, lane 2). This difference may have been due to the possibility that the TM2-initiated membrane targeting and translocation in the absence of TM1 was ribosome-independent whereas in the presence of TM1 it was ribosome-dependent. To test this hypothesis, WGR was supplemented into the RRL translation system and production of the glycosylated MRP-N2ΔNTM1 was compared with that generated in the RRL alone. As shown in Figure 7(B), addition of WGR did not increase or decrease significantly the generation of the glycosylated MRP-N2ΔNTM1 proteins (compare lanes 3 and 4, Figure 7B). Thus membrane targeting and translocation of TM2 in the absence of TM1 was not ribosome-dependent. The lower level of membrane targeting and translocation of TM2 in MRP-N2ΔNTM1 (in the absence of TM1) in WGE as compared with that in RRL (Figure 7A, lanes 3 and 4) was due to the low level of SRP associated with RM in WGE (see Figure 3 and the Discussion).

DISCUSSION

The domain structure of MRP is different from other ABC transporters such as Pgp. While Pgp consists of two domains with each containing a MSD followed by an ATP-binding site, MRP has an additional MSD (MSD1). This additional MSD is at the N-terminal end of the protein and has an extracellular N-terminus. In this study, the controlling elements for the extracellular location of the N-terminus and the biogenesis of MSD1 were investigated. Both the membrane-targeting and -translocation properties of TM2 and the charged residues flanking TM1 were found to be important factors in generating the unique structure of human MRP1. The MSD1 of human MRP1 was also used as a model to investigate how the sequential membrane-translocation theory applies to a polytopic protein that has an extracellular N-terminus. The results showed that except TM1 the membrane translocation of MSD1 was sequential and independent of TM1. That is, TM2 initiated a N_{in}-C_{out} membrane-translocation event that was stopped by TM3. TM4 initiated the second event to be stopped by TM5.

TM1 alone could also function as a signal-anchor sequence in an SRP-dependent manner and resulted in an N_{out}-C_{in} orientation. The N_{out}-C_{in} orientation of TM1 appeared to be determined by charged amino acids surrounding TM1 and this observation was consistent with the 'positive-inside' rule [41]. However, the membrane translocation and orientation of TM2 also determined the membrane orientation of TM1. In the presence of TM2, the effect of charges on the membrane orientation of TM1 became obsolete. That is, the inversion of TM1 orientation induced by charge mutations could be corrected by the N_{in}-C_{out} membrane translocation of TM2. Thus the extracellular location of the N-terminus was secured by two factors: charged amino acids flanking TM1 and N_{in}-C_{out} membrane translocation of TM2. Interestingly, a recent study on a polytopic membrane protein with an extracellular N-terminus also showed that TM2 was required for the extracellular location of the N-terminus when mutation was engineered into the protein [43]. The fact that TM2 determined the N_{out}-C_{in} orientation of TM1 in MRP and could correct mutation-induced inversion of TM1 orientation may be a general mechanism for generating a polytopic topology with an extracellular N-terminus. Thus, the 'positive-inside' rule may not apply to the first TM segment with an extracellular N-terminus in a polytopic membrane protein. It is not known how TM2 forced TM1 of MRP to translocate into membranes in an N_{out}-C_{in} orientation, notwithstanding that the mutated charges flanking TM1 favoured the opposite TM1 orientation. It became even more difficult to comprehend whether the membrane targeting and translocation of TM1 and TM2 involve two separate ribosome-targeting processes (see below). Clearly, further studies are needed to determine the molecular mechanism of TM2 control of TM1 biogenesis in MRP.

TM2 not only can correct mutation-induced inversion in TM1 orientation, it may also play an important role in MSD1 biogenesis. First, TM2 has a strong *de novo* activity to initiate N_{in}-C_{out} membrane targeting and translocation in an SRP-dependent manner. The membrane targeting and translocation of TM2 does not need its preceding or following TMs (TM1 and TM3). It should be noted that the membrane translocation of TM2 might not need SRP if TM1 translocates into membranes correctly as reported previously for an artificial protein [6]. Should TM1 fail to correctly target and translocate into membranes, the SRP-dependent strong *de novo* membrane-insertion activity of TM2 may come into effect. Secondly, TM2 has an ability to target and translocate into membranes post-translationally. This ability of TM2 may render an additional mechanism to ensure the correct membrane folding of MRP Should TM2 fail to translocate into membranes co-translationally, it may initiate N_{in}-C_{out} membrane targeting and translocation post-translationally. Therefore, TM2 appears to play a critical role in correct membrane targeting and translocation of MRP MSD1.

A recent study [42] showed that post-translational translocation of TM2 of human CFTR provided a redundant mechanism to ensure correct membrane folding for CFTR. If TM1 of CFTR fails to translocate into membranes, topogenic information encoded in TM2 provides a second chance for the nascent chain to acquire its correct topology. It is interesting to note that TM1 of CFTR had insufficient activity to initiate membrane translocation, the same as TM1 of human MRP1. This observation argues for the importance of the alternative mechanism provided by TM2 to ensure correct topogenesis of the nascent CFTR and MRP. Based on the observation with TM2 of human CFTR and MRP1, a tentative speculation would be that post-translational membrane targeting and translocation by TM2 provide a general redundant mechanism to ensure correct membrane translocation and folding for polytopic proteins in eukaryotes.

Post-translational membrane translocation has been reported for other eukaryotic membrane proteins such as connexin 26 [44], yeast prepro-α-factor [37,45] and glucose transporter [46]. The post-translational translocation of these proteins has been shown to be dependent on ATP binding [44] and hydrolysis [47,48] and on nascent-chain-attached ribosomes [49] Currently, it is not clear whether the post-translational membrane translocation of MRP-N2ΔNTM1 also requires ATP binding and hydrolysis. Although the post-translational translocation of MRP-N2ΔNTM1 was performed after puromycin pre-treatment, which presumably released ribosome from nascent chains, it cannot be ruled out that nascent-chain-attached ribosomes were still involved in the post-translational translocation of MRP-N2ΔNTM1.

The results from the comparison of translations in RRL and WGE systems suggested that the membrane targeting and translocation of TM2 in the presence of TM1 depended on the types of ribosome used. WGR appeared unable to help TM2 target and translocate into membranes once TM1 was membrane translocated. This observation suggests that there may be a ribosome re-targeting process involved in TM2 membrane translocation following TM1 membrane translocation. A similar observation has been made about the role of ribosomes in the membrane translocation of Pgp sequences [39,50,51]. It is therefore possible that following the membrane translocation of TM1, ribosomes release from the protein-conducting channel and re-dock back when TM2 emerges from the ribosome. However, WGR may lack proteins that help them to re-dock on to dog pancreatic RM. Thus TM2 failed to translocate into membranes co-translationally and remained in the cytoplasm of WGE. It is unknown why TM2 did not use its post-translational activity to initiate the membrane translocation after failing to translocate into membranes co-translationally in WGE. However, it is possible that the post-translational membrane targeting and translocation of TM2 requires SRP (Figure 6B), and WGE does not have SRP. Thus WGE could not support post-translational membrane translocation of TM2. This was supported by an observation that no post-translationally translocated MRP-N2ΔNTM1 was found in WGE (J.-T. Zhang, unpublished work).

Although, in this study, TM2 was shown to play a very important role in ensuring the correct folding of MSD1 *in vitro*, it cannot be ruled out that TM2 may not do so *in vivo*. However, the topology of MSD1 obtained in this study is the same as the one generated using the full-length molecule in *in vivo* systems. This suggests that the *in vitro* system faithfully translated and folded truncated MRP1 and it is probably in accord with the *in vivo* system. Furthermore, the study by Lu et al. [42] showed both *in vitro* and *in vivo* that isolated TM2 of CFTR provides a redundant mechanism for correct folding of CFTR. Thus the use of truncated molecules in an *in vitro* system in this study should reflect the natural process of human MRP1 biogenesis *in vivo*. Moreover, because of the limitation of available techniques it is almost necessary to dissect and examine each domain separately to understand the detailed biogenesis process of a large and complex membrane protein such as human MRP1.

I thank Dr Piet Borst for the generous gift of human MRP cDNA, Dr Ernest Han and Ms Roxana Pincheira for their valuable suggestions during the course of this study, and Dr David Ohannesian for his critical comments on this manuscript This work was supported by the National Institutes of Health grants CA64539 and GM59475 J.-T. Z. is a recipient of a Career Investigator Award from the American Lung Association

REFERENCES

1 Blobel, G (1980) Proc Natl Acad Sci U S A **77**, 1496–1500
2 Corsi, A K and Schekman, R (1996) J Biol Chem **271**, 30299–30302
3 Goldman, B M. and Blobel, G (1981) J. Cell Biol **90**, 236–242
4 Braell, W A and Lodish, H F (1982) Cell **28**, 23–31
5 Brown, D A and Simoni, R D (1984) Proc Natl Acad Sci U S A **81**, 1674–1678
6 Wessels, H P and Spiess, M (1988) Cell **55**, 61–70
7 Friedlander, M. and Blobel, G (1985) Nature (London) **318**, 338–343
8 Audigier, Y, Friedlander, M and Blobel, G (1987) Proc Natl Acad Sci U S A **84**, 5783–5787
9 Lipp, J, Flint, N, Haeuptle, M T and Dobberstein, B (1989) J Cell Biol **109**, 2013–2022

10 Chavez, R A and Hall, Z W. (1991) J. Biol. Chem **266**, 15532–15538

11 Silve, S, Volland, C, Garnier, C, Jund, R, Chevallier, M R. and Haguenauer-Tsapis, R. (1991) Mol Cell Biol **11**, 1114–1124

12 Hartmann, E, Rapoport, T A and Lodish, H. F (1989) Proc Natl Acad Sci. U S.A. **86**, 5786–5790

13 Skach, W R and Lingappa, V R (1993) In Mechanisms of Intracellular Trafficking and Processing of Proproteins (Peng Loh, Y, ed.), pp 19–77, CRC Press, Boca Raton

14 Gottesman, M M., Hrycyna, C A, Schoenlein, P. V, Germann, U A. and Pastan, I. (1995) Annu. Rev Genet **29**, 607–649

15 Ling, V (1997) Cancer Chemother. Pharmacol **40**, S3–S8

16 Cole, S. P., Bhardwaj, G, Gerlach, J, Mackie, J, Grant, C. E, Almquist, K. C, Stewart, A. J., Kurz, E. U, Duncan, A M and Deeley, R G (1992) Science **258**, 1650–1654

17 Borst, P, Kool, M and Evers, R (1997) Semin Cancer Biol **8**, 205–213

18 Higgins, C F (1992) Annu. Rev Cell Biol. **8**, 67–113

19 Zhang, J T and Ling, V. (1991) J Biol Chem. **266**, 18224–18232

20 Bibi, E. and Beja, O (1994) J Biol Chem **269**, 19910–19915

21 Skach, W R, Calayag, M. C and Lingappa, V R (1993) J Biol Chem **268**, 6903–6908

22 Zhang, M, Wang, G, Shapiro, A and Zhang, J T (1996) Biochemistry **35**, 9728–9736

23 Bakos, E, Hegedus, T, Hollo, Z, Welker, E., Tusnady, G E, Zaman, G J, Flens, M J, Varadi, A and Sarkadi, B (1996) J Biol. Chem **271**, 12322–12326

24 Hipfner, D R, Almquist, K C, Leslie, E M., Gerlach, J. H, Grant, C. E, Deeley, R. G and Cole, S P (1997) J Biol. Chem **272**, 23623–23630

25 Kast, C and Gros, P (1997) J Biol Chem **272**, 26479–26487

26 Gao, M., Yamazaki, M, Loe, D. W., Westlake, C. J, Grant, C. E, Cole, S P C. and Deeley, R G. (1998) J Biol. Chem **273**, 10733–10740

27 Bakos, E, Evers, R, Szakacs, G, Tusnady, G, Welker, E, Szabo, K, de Haas, M, van Deemter, L, Borst, P, Varadi, A and Sarkadi, B (1998) J Biol Chem **273**, 32167–32175

28 Hipfner, D. R, Deeley, R G and Cole, S. P C (1999) Biochim Biophys Acta **1461**, 359–376

29 Zaman, G J., Flens, M J., van Leusden, M R, de Haas, M, Mulder, H. S, Lankelma, J, Pinedo, H M., Scheper, R. J, Baas, F, Broxterman, H J et al (1994) Proc. Natl. Acad Sci U S A. **91**, 8822–8826

30 Walter, P and Blobel, G (1983) Methods Enzymol **96**, 84–93

31 Zhang, J T, Lee, C H, Duthie, M and Ling, V. (1995) J Biol Chem **270**, 1742–1746

32 Zhang, J T, Duthie, M and Ling, V (1993) J Biol Chem **268**, 15101–15110

33 Chen, M and Zhang, J T. (1996) Mol Membr Biol **13**, 33–40

34 Zhang, J. T (1996) Mol Biol Cell **7**, 1709–1721

35 Zhang, J T, Chen, M, Han, E and Wang, C (1998) Mol Biol. Cell **9**, 853–863

36 Gilmore, R, Blobel, G and Walter, P (1982) J Cell Biol **95**, 463–469

37 Walter, P and Blobel, G (1981) J. Cell Biol **91**, 551–556

38 Zhang, J T and Ling, V (1995) Biochemistry **34**, 9159–9165

39 Wang, C, Chen, M, Han, E and Zhang, J T (1997) Biochemistry **36**, 11437–11443

40 Chen, M. and Zhang, J T. (1999) Biochemistry **38**, 5471–5477

41 von Heijne, G. (1986) EMBO J **5**, 3021–3027

42 Lu, Y, Xiong, X, Helm, A., Kimani, K., Bragin, A and Skach, W R (1998) J Biol Chem **273**, 568–576

43 Monne, M, Gafvelin, G, Nilsson, R. and von Heijne, G (1999) Eur J Biochem **263**, 264–269

44 Zhang, J. T., Chen, M., Foote, C and Nicholson, B. J (1996) Mol Biol Cell **7**, 471–482

45 Rothblatt, J. A and Meyer, D. I (1986) Cell **44**, 619–628

46 Mueckler, M and Lodish, H F (1986) Cell **44**, 629–637

47 Mueckler, M and Lodish, H F (1986) Nature (London) **322**, 549–552

48 Hansen, W, Garcia, P. D and Walter, P (1986) Cell **45**, 397–406

49 Garcia, P. D and Walter, P (1988) J Cell Biol. **106**, 1043–1048

50 Borel, A. C and Simon, S M (1996) Biochemistry **35**, 10587–10594

51 Borel, A C and Simon, S M. (1996) Cell **85**, 379–389

Received 8 December 1999/2 March 2000, accepted 29 March 2000

Evidence that metformin exerts its anti-diabetic effects through inhibition of complex 1 of the mitochondrial respiratory chain

Mark R. OWEN, Elena DORAN and Andrew P. HALESTRAP[1]
Department of Biochemistry, School of Medical Sciences, University of Bristol, Bristol BS8 1TD, U.K.

Although metformin is widely used for the treatment of non-insulin-dependent diabetes, its mode of action remains unclear. Here we provide evidence that its primary site of action is through a direct inhibition of complex 1 of the respiratory chain. Metformin (50 μM) inhibited mitochondrial oxidation of glutamate+malate in hepatoma cells by 13 and 30% after 24 and 60 h exposure respectively, but succinate oxidation was unaffected. Metformin also caused time-dependent inhibition of complex 1 in isolated mitochondria, whereas in sub-mitochondrial particles inhibition was immediate but required very high metformin concentrations ($K_{0.5}$, 79 mM). These data are compatible with the slow membrane-potential-driven accumulation of the positively charged drug within the mitochondrial matrix leading to inhibition of complex 1. Metformin inhibition of gluconeogenesis from L-lactate in isolated rat hepatocytes was also time- and concentration-dependent, and accompanied by changes in metabolite levels similar to those induced by other inhibitors of gluconeogenesis acting on complex 1. Freeze-clamped livers from metformin-treated rats exhibited similar changes in metabolite concentrations. We conclude that the drug's pharmacological effects are mediated, at least in part, through a time-dependent, self-limiting inhibition of the respiratory chain that restrains hepatic gluconeogenesis while increasing glucose utilization in peripheral tissues. Lactic acidosis, an occasional side effect, can also be explained in this way.

Key words: gluconeogenesis, glucose utilization, lactic acidosis, mitochondria, NIDDM.

INTRODUCTION

The biguanide, metformin (N^1,N^1-dimethylbiguanide), is used extensively to treat non-insulin-dependent diabetes mellitus (NIDDM), yet its primary locus of action remains uncertain. Major effects of the drug in humans are to decrease hepatic glucose output, especially gluconeogenesis from L-lactate, and to increase both glycolytic lactate production by the intestine and insulin-dependent peripheral glucose utilization [1–3]. The latter process is associated with increased plasma-membrane expression of glucose-transporter isoforms GLUT1 and GLUT4 [4–7].

Early studies showed that some alkylguanidines, which are related to the biguanides, can inhibit the oxidation of glutamate+malate but not succinate by isolated energized liver mitochondria, although their exact locus and mode of action was not elucidated [8,9]. Although direct effects of phenformin and metformin on the respiratory chain of isolated mitochondria have not been reported, mitochondria isolated from the livers of guinea pigs treated with phenformin were shown to exhibit decreased rates of 2-oxoglutarate oxidation but not succinate oxidation [10]. Thus it was suggested by some workers that biguanides might inhibit hepatic gluconeogenesis through inhibition of mitochondrial respiration and ATP production [8,9,11,12]. However, direct measurements of tissue ATP content did not support this view [13] and most workers now regard the effects of metformin on mitochondria as being responsible only for side effects of the drug, such as occasional lactic acidosis.

We decided to re-examine the possibility that inhibition of mitochondrial respiration might be a primary site of action of metformin, since previous work from this laboratory has demonstrated that the respiratory chain has a high flux-control coefficient for gluconeogenesis. Indeed, we showed that a modest inhibition of respiration by the mild respiratory-chain inhibitors 3-(3,4-dichlorophenyl)-1,1-dimethylurea (DCMU) or amytal caused a substantial inhibition of gluconeogenesis without significant changes in total tissue ATP content [14,15]. Furthermore, activation of the respiratory chain by glucagon is thought to play an important role in the stimulation of gluconeogenesis by this hormone [14]. Thus a drug that produces mild inhibition of the respiratory chain could be an effective hypoglycaemic agent. In this paper we provide strong evidence that this is the case for metformin and phenformin that directly inhibit complex 1 of the respiratory chain in a time-dependent, self-limiting manner. We propose that this inhibition restrains hepatic gluconeogenesis while increasing glucose utilization in peripheral tissues and may also explain why lactic acidosis is an occasional side effect of treatment [3]. After completion of this work, a study by El-Mir et al. [16] also demonstrated inhibition of complex 1 in hepatocytes and perfused livers by high concentrations (1–10 mM) of metformin, but proposed that this effect was exerted indirectly by some unidentified signalling pathway.

EXPERIMENTAL

Animals, chemicals, drugs and reagents

Male Wistar rats (250–300 g in weight) were used for preparation of both hepatocytes and liver mitochondria, and for studies *in vivo*.

Metformin, phenformin and antibiotics were obtained from Sigma (Poole, Dorset, U.K.). Cell-culture media were from Gibco-BRL (Paisley, U.K.). The sources of all other chemicals and biochemicals were as given previously [14,15].

Preparation and incubation of isolated mitochondria and sub-mitochondrial particles (SMPs)

Isolated rat liver mitochondria were prepared from 24-h-starved rats and further purified by Percoll gradient centrifugation to remove microsomal and plasma-membrane contamination as

---

Abbreviations used DCMU, 3-(3,4-dichlorophenyl)-1,1-dimethylurea, SMP, sub-mitochondrial particle

[1] To whom correspondence should be addressed (e-mail A.Halestrap@Bristol.ac.uk)

described previously [15]. Heart mitochondria were prepared from fed rats using a similar procedure but incorporating protease treatment before homogenization [17]. SMPs were prepared by sonication of either heart or liver mitochondria as described elsewhere [18]. Respiration by isolated mitochondria (1 mg of protein/ml) was studied at 30 °C using an oxygen electrode [17,19]. The medium contained 125 mM KCl, 20 mM Mops, 10 mM Tris, 0.5 mM EGTA, 2 mM potassium phosphate and 2 mM $MgCl_2$ (pH 7.2). The substrate was either 5 mM L-glutamate + 1 mM L-malate or 5 mM succinate + 1 μM rotenone, and respiration was stimulated by additions of 0.4 mM ADP (state 3). Oxidation of NADH by SMPs (75 μg of protein/ml) was measured at 30 °C in the same buffer containing 0.15 mM NADH; the decrease in [NADH] was measured continuously at 340 nm in a split-beam spectrophotometer.

Culture, permeabilization and measurement of mitochondrial respiration in rat hepatoma cells

Rat hepatoma cells (H4IIE) were grown under air/CO_2 (19:1) in Ham's F-12 medium, supplemented with 5% foetal bovine serum, 2 mM L-glutamine and 2 mM penicillin/streptomycin and were maintained in logarithmic phase throughout. Metformin (final concentration 50 or 100 μM from a 25 mM stock solution in water) was added to cells for 24 or 60 h prior to harvesting, with water alone added to controls. Once harvested, cells were washed twice with media containing 150 mM NaCl, 5 mM KCl, 10 mM glucose and 10 mM Tris, pH 7.4, and then suspended in ice-cold medium containing 210 mM mannitol, 70 mM sucrose, 10 mM glucose, 5 mM Hepes and 5 mg/ml defatted BSA, pH 7.2. Cells were then permeabilized according to Bogucka et al. [20]. Digitonin (0.2 mg/ml, final concentration) was added for 1–2 min at 0 °C until > 90% of the cells became permeable to Trypan Blue. The reaction was stopped by adding 2 vol. of the mannitol/sucrose medium and the cells sedimented at 3000 *g* for 3 min before resuspending in the mannitol/sucrose medium at 8–12 mg of protein/ml. Respiration was measured in a Clark-type oxygen electrode as described above.

Preparation and incubation of isolated hepatocytes

Hepatocytes were isolated from 24-h-starved rats by collagenase digestion as described previously [14,15] and incubated at 5 mg of protein/ml in bicarbonate-buffered saline medium containing 10 mM L-lactate, 1 mM pyruvate, 0.3 μM glucagon and 20 mg/ml defatted BSA, with a gas phase of O_2/CO_2 (19:1). Glucagon was added to provide conditions of stimulated gluconeogenesis and fatty acid oxidation such as occur in diabetes. Measurements of the rates of gluconeogenesis and metabolite concentrations were performed as described previously [15].

Metformin treatment of rats and measurement of metabolites in freeze-clamped livers

Oral intubation was used to deliver doses (1 ml) of either metformin (50 or 150 mg/ml in water) or water alone directly into the stomachs of male Wistar rats (250–300 g in weight). Animals were treated once each day for 5 days. They were allowed free access to water at all times, but food was removed 24 h before the final treatment. The treatments were carried out according to Home Office regulations and did not cause the animals any visible distress or significantly affect mean body weight. It should be noted that the doses of metformin used in the present study are typical of those shown by many workers to be required for the demonstration of therapeutic effects in rats and mice [21–25]. Following the final treatment (4 h), animals were anaesthetized and their livers rapidly removed and divided to provide material for both the preparation of mitochondria (as described above) and for freeze-clamping. Freeze-clamped material was ground in a pestle and mortar pre-cooled with liquid nitrogen. The ground material (1 g) was mixed with ice-cold perchloric acid [4 ml of 5% (w/v)] and homogenized using a Polytron blender (15 s at setting 3). Precipitated protein was removed by centrifugation and aliquots of the acid supernatant neutralized and assayed for various metabolites as described previously [15].

Statistics

The significance of differences between control and experimental groups were performed using a two-tailed Student's *t* test.

RESULTS

Inhibition of mitochondrial respiration by metformin in permeabilized rat hepatoma cells

Rat hepatoma cells were cultured with 50 and 100 μM metformin for either 24 or 60 h and then, following digitonin permeabilization, the rates of their ADP-stimulated mitochondrial respiration were measured. Data are shown in Figure 1. No effect of metformin on succinate oxidation was observed, whereas rates of glutamate + malate oxidation were reduced significantly. Metformin (50 μM) caused 12.6 ± 4.3 and 29.4 ± 7.7% inhibition after 24 and 60 h, respectively, whereas for 100 μM metformin the inhibition was 25.8 ± 3.4 and 37.1 ± 10.0%, respectively. Control ratios (the ratio of respiration rates in the presence and absence of ADP) were 3.5 ± 0.24 for glutamate + -

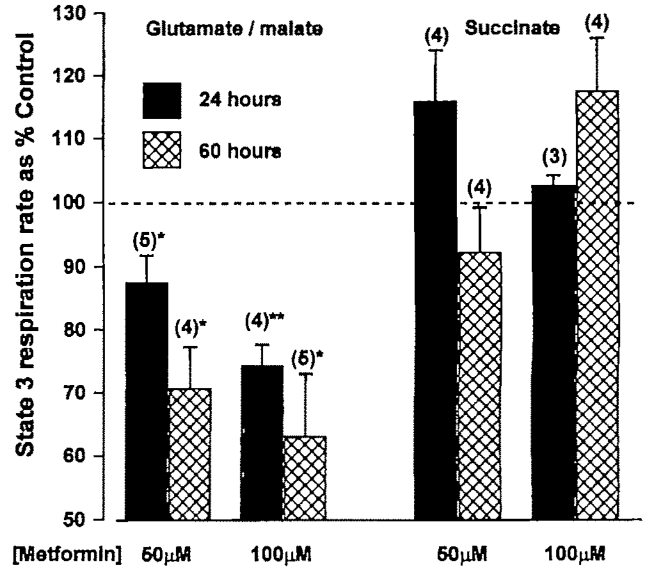

Figure 1 Inhibition by metformin of mitochondrial respiration in permeabilized rat hepatoma cells

Rat hepatoma (H4IIE) cells were cultured for 24 or 60 h in the presence or absence of metformin at 50 or 100 μM, before digitonin permeabilization and measurement of respiration as described in the Experimental section. Rates of ADP-stimulated respiration in the presence of metformin are expressed as a percentage of control rates (no metformin) and as means ± S.E.M. of the number of observations on separate cell preparations indicated in parentheses. Absolute rates of ADP-stimulated respiration in the absence of metformin were 16.8 ± 0.3 nmol of O atoms/min per mg of cell protein for glutamate + malate ($n = 18$) and for succinate oxidation 15.8 ± 0.43 ($n = 15$). The statistical significance of the effect of metformin treatment was determined by a paired Student's *t* test ($^{*}P < 0.05$, $^{**}P < 0.01$).

malate and 2.5±0.16 for succinate and were not significantly changed by metformin treatment. These data are consistent with a time-dependent inhibition of complex 1 and this was investigated further using isolated rat liver mitochondria.

Metformin and phenformin inhibit complex 1 in isolated mitochondria and SMPs

Preliminary experiments showed that addition of metformin to rat liver mitochondria oxidizing 5 mM L-glutamate + 1 mM L-malate in the presence of ADP gave no inhibition over a period of 5 min at 30 °C, even at concentrations as high as 10 mM. However, the data from the hepatoma cells suggested that the inhibition by metformin may take a long time to develop, perhaps indicating a very slow permeation of the drug into the mitochondria. We found that incubation of isolated mitochondria at physiological temperatures for periods longer than 10 min is not possible without considerable loss of mitochondrial integrity. Thus we decided to incubate at low temperature even though this might further reduce the rate of metformin permeation. We show in Figure 2(a) that incubation of mitochondria at 8 °C with 10 mM metformin produced progressive inhibition of the ADP-stimulated oxidation of glutamate + malate, but not of succinate, and even after 6 h inhibition was still increasing. The concentration dependence of this inhibition (after 255 min of pre-incubation at 8 °C) is shown in Figure 2(b), but it is important to note that much greater inhibition would be predicted if incubation with the inhibitor could have been continued for longer. Thus the true $K_{0.5}$ value for metformin will be substantially lower than indicated by the data shown. In contrast, the phenyl and ethyl groups on phenformin (N^1,N^1-phenylethylbiguanide) make it a more lipophilic drug that can permeate biological membranes readily, and this is reflected in the ability of this drug to exert its maximum inhibitory effect on glutamate + malate oxidation within 5 min at 30 °C. The concentration dependence of this inhibition is shown in Figure 2(b) and yields a $K_{0.5}$ value of 50 μM. Again, no effect of the drug on succinate oxidation was observed, implying that inhibition of respiration was occurring, either at the level of the dehydrogenases producing NADH, as has been suggested by others [9,10], or at complex 1 of the respiratory chain.

In order to discriminate between these possibilities, SMPs were used. These particles have the matrix surface of the respiratory chain accessible to the medium and unlike mitochondria they can oxidize added NADH directly. Furthermore, there is no permeability barrier to restrict access of metformin and phenformin to the matrix surface of the respiratory chain. Indeed, we found that NADH oxidation by SMPs was inhibited immediately upon addition of either drug with $K_{0.5}$ values of 79 and 2.2 mM, respectively (Figure 2c). Exposure of the SMPs to the drug for longer time periods did not increase the inhibition observed (results not shown). We have confirmed that inhibition of complex 1 is not confined to liver mitochondria by demonstrating that there was no difference in the sensitivity to metformin inhibition of respiration by SMPs from liver (Figure 2c, closed symbols) and heart (Figure 2c, open symbols). It is clear that the concentrations of the two drugs required to inhibit respiration in SMPs are substantially higher than for mito-

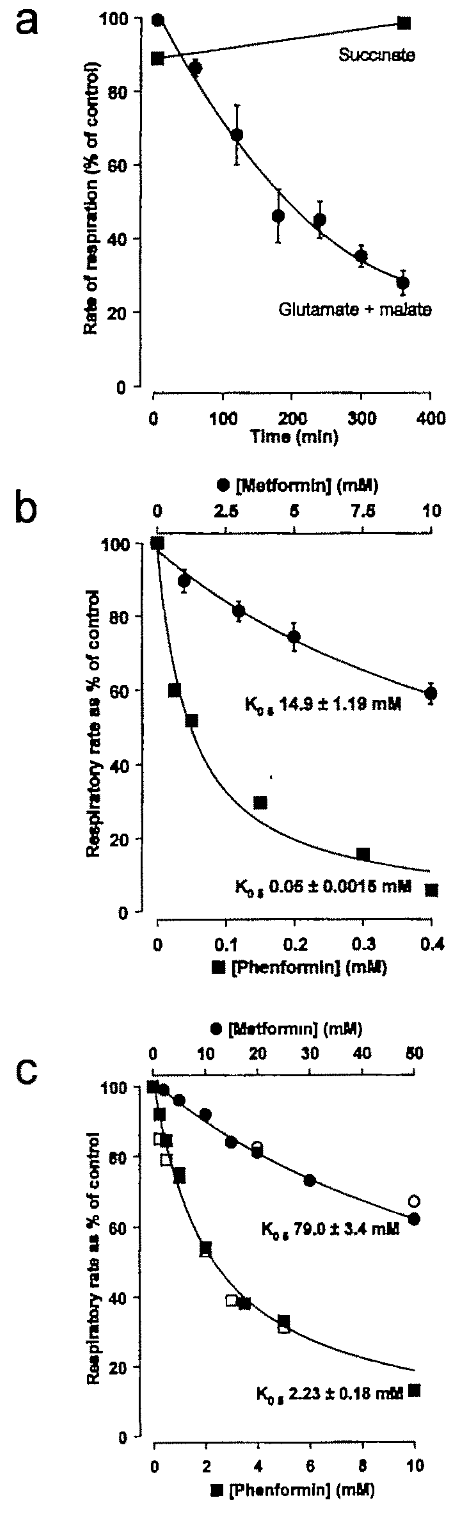

Figure 2 Metformin and phenformin inhibit NADH-dependent respiration by isolated mitochondria and SMPs

(a) Rat liver mitochondria (40 mg/ml) were incubated with gentle orbital shaking at 8 °C in isolation medium containing 10 mM metformin for the times shown. The rate of ADP-stimulated respiration in the presence of glutamate + malate or succinate + rotenone was then determined. (b) The inhibition following pre-incubation for 255 min with metformin at the concentrations shown is compared with that produced by phenformin following pre-incubation for 5 min. Data are expressed as a percentage of the control rate (incubated for the same time without drug). (c) The concentration dependence of the inhibition by phenformin and metformin of NADH oxidation by SMPs is shown. In (a) and (b) data for metformin are given as means ± S.E.M. of three separate mitochondrial preparations whereas for phenformin a single experiment is shown. In (c) the open and closed symbols represent preparations of SMPs from heart and liver mitochondria respectively. The $K_{0.5}$ values were derived by non-linear least-squares regression analysis using the equation v% = 100/(1 + I/$K_{0.5}$), where I is the concentration of inhibitor and v% is the rate of respiration in the presence of the drug as a percentage of the rate in its absence.

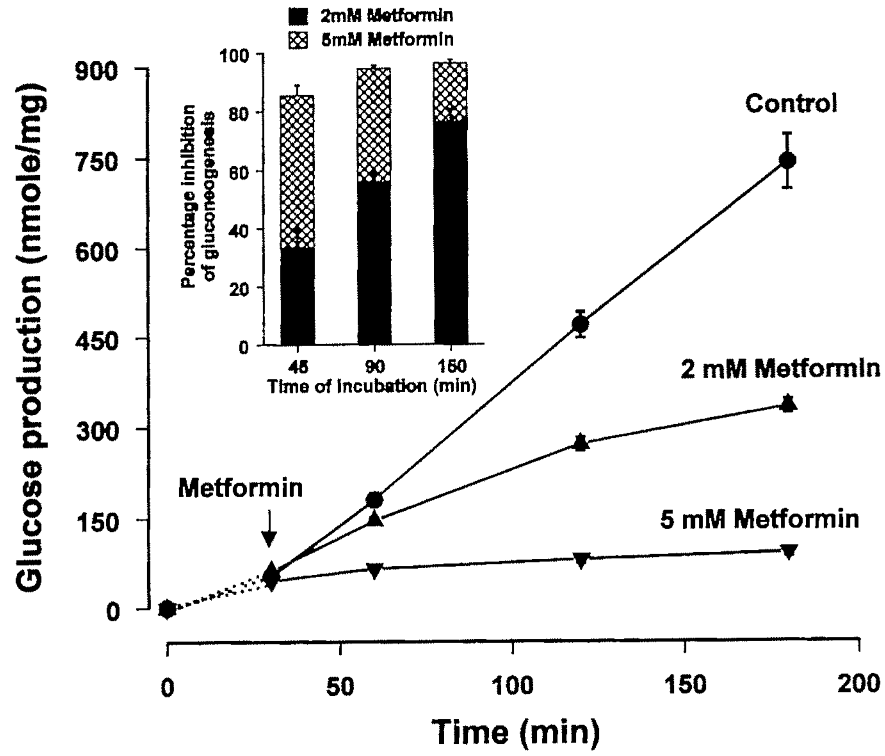

Figure 3 Inhibition of gluconeogenesis by metformin in isolated rat hepatocytes

Glucose production was determined after incubation of hepatocytes from 24-h-starved rats for the time shown in the presence of 10 mM L-lactate, 1 mM pyruvate, 20 mg/ml defatted BSA and 0.3 μM glucagon. Metformin at the concentrations shown was added as indicated by the arrow. The inset shows the progressive inhibition of gluconeogenesis caused by incubation with two concentrations of metformin for the times indicated.

chondria. This is most readily explained by a membrane-potential-driven accumulation of the positively charged drug within the mitochondria (see the Discussion section).

Changes in hepatocyte metabolite concentrations associated with the inhibition of gluconeogenesis by metformin

The data of Figure 3 show that metformin inhibits gluconeogenesis from L-lactate in isolated hepatocytes in a time- and concentration-dependent fashion. This is consistent with the time-dependent accumulation of the drug within the mitochondria and subsequent inhibition of the respiratory chain described above. After 2.5 h of incubation with 5 mM metformin inhibition of gluconeogenesis was almost total, whereas inhibition by 2 mM metformin had reached only 75 %, but was still increasing. Although it is probable that inhibition of gluconeogenesis could have been obtained at substantially lower concentrations of metformin if hepatocytes had been incubated with the drug for longer, this was not a viable option. Control rates of gluconeogenesis were found to decline substantially when incubations were continued for long periods, implying that the integrity of the hepatocytes was not maintained.

In Figure 4 we report changes in the total hepatocyte content of some key metabolites of the gluconeogenic pathway following incubation with 2 mM metformin for 3 h. The concentrations of 2- and 3-phosphoglycerate and phosphoenolpyruvate increased by 411 and 336 % respectively, whereas the concentrations of glucose 6-phosphate and fructose 6-phosphate decreased by about 50 %. In addition, increases in the ratios of β-hydroxybutyrate/acetoacetate (349 %) and L-lactate/pyruvate (266 %) were found. These changes were all very similar to those we observed previously in isolated hepatocytes treated with the mild respiratory-chain inhibitors DCMU and amytal [14,15,26] and by others using phenformin [11]. Although previous work has demonstrated inhibition of gluconeogenesis by metformin in isolated rat hepatocytes [27,28] and perfused livers [29,30], detailed determination of the changes in metabolite concentrations were not made.

Effects of oral treatment of rats with metformin on hepatic metabolite concentrations

In order to demonstrate that metformin may act to inhibit gluconeogenesis *in vivo* through the same mechanism as observed in isolated hepatocytes, 250–300-g rats were treated by oral intubation for a period of 5 days with either 50 or 150 mg of metformin given once daily. It is recognized that even the lower dose (150–200 mg/kg) is some 4–5 times greater than the maximal daily dose of about 3 g used in humans [2,3]. However, it is well established that these relatively high doses of metformin are necessary for the drug to reach plasma concentrations in rats similar to those found in humans and to exert its hypoglycaemic effects in diabetic rats [21–25]. Wilcock and Bailey [25] have shown that in mice treated with 50 mg/kg metformin, portal and inferior vena cava concentrations of the drug peaked at 52 and 29 μM, respectively, there being no significant differences between control and diabetic mice. However, these values declined to < 2 % after 24 h. Thus the concentrations used in our studies probably are similar to those found therapeutically in humans. The species difference in drug dosage required may

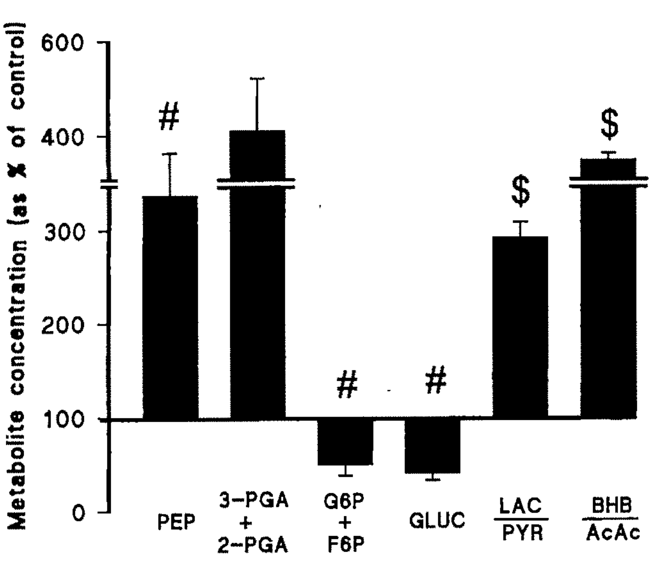

Figure 4 Changes in key metabolite concentrations and ratios after incubation of hepatocytes with 2 mM metformin for 3 h

Following incubation, hepatocytes were separated from the medium by centrifugation through oil into perchloric acid and metabolites measured in the neutralized extracts and supernantants [9] Data in the presence of metformin are expressed as a percentage of the control value in the absence of metformin and as means ± S E M of values for three separate cell preparations Control values were similar to those reported previously [9] The statistical significance of the effects of metformin were determined by a paired Student's *t* test (#$P < 0.05$, \$$P < 0.01$) PEP, phosphoenolpyruvate, 2- and 3-PGA, 2- and 3-phosphoglycerate, G6P, glucose 6-phosphate, F6P, fructose 6-phosphate; GLUC, glucose, LAC/PYR, L-lactate/pyruvate; BHB/AcAc, β-hydroxybutyrate/acetoacetate

reflect a difference in the intestinal absorption and renal clearance of the drug [21–25].

After the final drug administration (4 h), livers were removed, freeze-clamped and extracted with perchloric acid for analysis of metabolites. The changes in glycolytic metabolite concentrations are shown in Figure 5 and are very similar to those found in isolated liver cells (Figure 4). Thus increased concentrations of 2- and 3-phosphoglycerate (257 and 332 % at 50 and 150 mg of metformin respectively) and phosphoenolpyruvate (309 and 535 %) and decreased concentrations of glucose 6-phosphate (60 and 61 %) and fructose 6-phosphate (63 and 33 %) were observed, whereas the ratios of both β-hydroxybutyrate/acetoacetate (233 and 403 %) and L-lactate/pyruvate (153 and 204 %) increased. Total cell concentrations of ATP, ADP and AMP showed no changes at either concentration of metformin. Control values for ATP, ADP and AMP (expressed as nmol/mg of protein, mean ± S.E.M., for four separate rat livers) were 8 81 ± 0.21, 4.97 ± 0.30 and 2.27 ± 0.19 respectively, whereas the values after metformin treatment at 50 mg daily were 8.57 ± 0.76, 5.05 ± 0.26 and 2.68 ± 0.17 respectively, and after metformin treatment at 150 mg daily were 9.00 ± 0.21, 5.09 ± 0.13 and 2.44 ± 0.01 respectively.

These values represent total tissue concentrations of the adenine nucleotides whereas metabolic control is exerted through the free metabolite concentrations. Thus in Figure 5 we also present data for the ratio for the free concentrations of ATP and ADP calculated from metabolite concentrations and the equilibrium constants of the reactions catalysed by lactate dehydrogenase, phosphoglyceraldehyde dehydrogenase and phosphoglycerate kinase [15]. The assumptions behind the use of these calculations have been verified in rat liver [31] and we have confirmed that 10 mM metformin does not inhibit any of the enzymes involved in these equilibria (results not shown). The calculated ATP/ADP ratio shows a substantial drop in the livers of the metformin-treated animals, values after treatment with 50 and 150 mg of metformin being 32 and 20 % of control values respectively. The data for oxaloacetate concentrations (83 and 82 %) shown in Figure 5 are also calculated values, based on the measured malate concentrations and the β-hydroxybutyrate/acetoacetate ratios [15].

DISCUSSION

Metformin is slowly accumulated within mitochondria and directly inhibits complex 1

Comparison of the time and concentration dependence of complex-1 inhibition by metformin in mitochondria and SMPs suggest that there is a slow permeation of the drug across the mitochondrial inner membrane where it inhibits complex 1 directly. As would be predicted, phenformin, a more hydrophobic, lipid-soluble molecule, which binds more tightly to mitochondrial membranes [1–3], inhibited much more rapidly in intact mitochondria even at micromolar concentrations. The positive charge on metformin and phenformin could account for their accumulation within the matrix of energized mitochondria driven by the membrane potential ($\Delta\psi$). Such energy-dependent accumulation of biguanides within the matrix has been shown to occur experimentally [9] and is similar to that observed for some other positively charged hydrophobic inhibitors of complex 1 such as phenylpyridine analogues [32]. Indeed, the $K_{0.5}$ values for the inhibition of complex 1 by these compounds in energized mitochondria are 30–100-fold lower than with SMPs, a similar difference to that seen with phenformin in the present experiments (Figures 2b and 2c). A recent paper by El-Mir et al. [16] also demonstrated a specific time-dependent inhibition of complex 1 by 1–10 mM metformin in hepatocytes. These authors confirmed that these effects of metformin could not be demonstrated when the drug was added directly to mitochondria or permeabilized heptocytes, but was maintained after permeabilization of hepatocytes and when mitochondria were prepared from livers perfused with 10 mM metformin. However, they concluded from these data that the effect was indirect, through an unidentified signalling pathway. Our data suggest that there is no need to invoke such an indirect mechanism.

Inhibition of complex 1 by metformin can occur at drug concentrations found in treated patients

Thermodynamic considerations predict that with a $\Delta\psi$ of -180 mV, metformin should accumulate 1000-fold within the mitochondrial matrix. This would give a $K_{0.5}$ value with respect to extra-mitochondrial metformin of about 80 μM at equilibrium and is consistent with the 29 and 37 % inhibition of ADP-stimulated glutamate + malate oxidation observed in mitochondria from cultured rat hepatoma cells exposed for 60 h to 50 and 100 μM metformin respectively (Figure 1).

The plasma concentrations of metformin found in patients are about 10–20 μM [1–3]. However, the liver receives the majority of its blood via the portal vein, which may contain concentrations of metformin substantially higher than those present in the general circulation [25]. Thus significant inhibition of the respiratory chain of liver mitochondria in patients treated with metformin would be predicted. The observed inhibition of gluconeogenesis and pattern of hepatic metabolites in metformin-

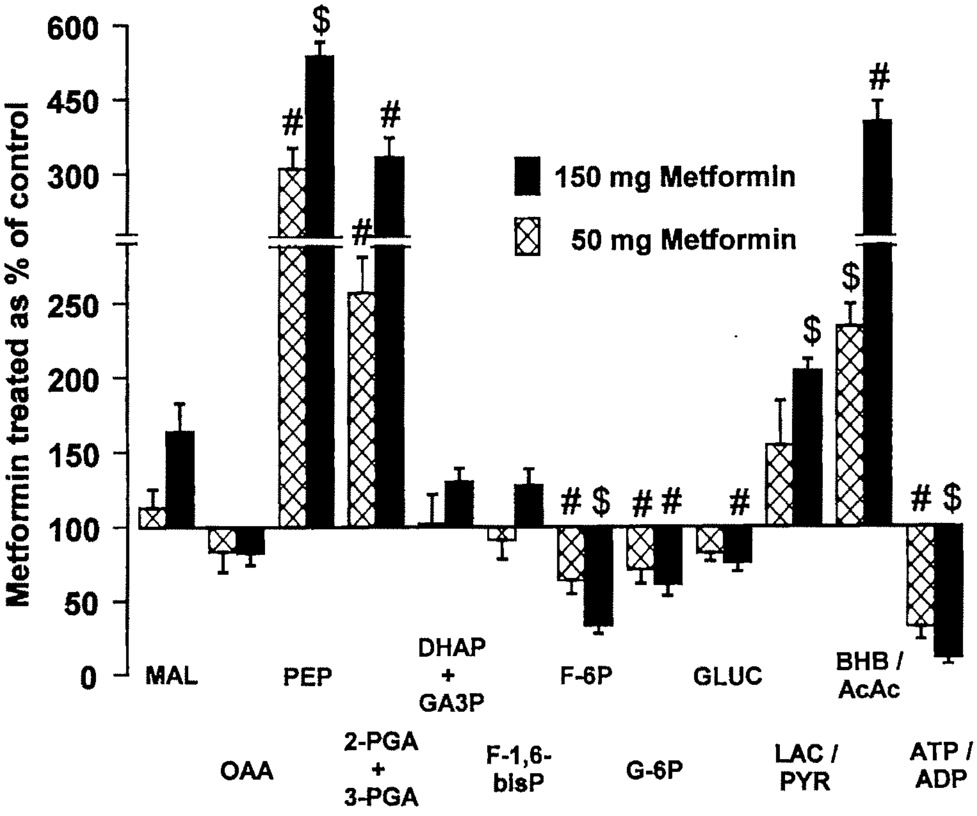

Control metabolite concentrations (nmoles/mg protein) or ratios

MAL	2940 ± 150	DHAP + GA3P	49 ± 2	Glucose	26510 ± 2190
OAA	11.6 ± 1.0	F-1,6-bisP	20 ± 1	LAC/PYR	35.5 ± 3.8
PEP	75 ± 30	F-6P	158 ± 13	BHB/AcAc	0.28 ± 0.044
2/3-PGA	610 ± 140	G-6P	377 ± 57	ATP/ADP	2.60 ± 0.49

Figure 6 The effect of treatment of rats with metformin on the metabolite concentrations of their freeze-clamped livers

Treatment of rats with metformin (50 or 150 mg per rat) was performed daily for 5 days as described in the Experimental section. Control animals were given an equivalent volume of water. Metabolite concentrations for control livers ($n = 4$) are given in the table below, the values for ATP/ADP are the free cytosolic values calculated from the other metabolite levels as described in the text. The bar graph shows changes in metabolite concentrations and ratios induced by drug treatment ($n = 4$) expressed as percentages of the mean control values. The error bars represent the S.E.M. calculated from the ratios of the means and S.E.M. of the control and experimental data. The statistical significance of the effects of metformin were determined by an unpaired two-tailed Student's *t* test (#$P < 0.05$, \$$P < 0.01$). MAL, malate; OAA, oxaloacetate, PEP, phosphoenolpyruvate, 2- and 3-PGA, 2- and 3-phosphoglycerate, DHAP, dihydroxyacetone phosphate, GA3P, glyceraldehyde 3-phosphate, F-1,6-bisP, fructose 1,6-bisphosphate, G-6P, glucose 6-phosphate; F-6P, fructose 6-phosphate, GLUC, glucose, LAC/PYR, L-lactate/pyruvate, BHB/AcAc, β-hydroxybutyrate/acetoacetate

treated rats provide further evidence that this is the case. Furthermore, in the case of phenformin, it has been shown by others that treatment of guinea pigs with 30 mg/kg of the drug leads to impaired oxidation of 2-oxoglutarate by subsequently isolated liver mitochondria [10]. We attempted similar experiments with control and metformin-treated rats (50 mg daily for 5 days) and determined rates of ADP-stimulated respiration by their liver mitochondria. To correct for non-specific effects on mitochondrial respiratory-chain activity, rates of respiration were expressed relative to the rate of ascorbate oxidation in the presence of *N,N,N′,N′*-tetramethyl-*p*-phenylenediamine (which only utilizes cytochrome *c* and complex 4 of the respiratory chain). With glutamate+malate as respiratory substrate, the control and metformin ratios (expressed as means ± S.E.M. for five preparations of liver mitochondria from separate rats) were 0.86 ± 0.03 and 0.79 ± 0.09 respectively. In two rats treated with 150 mg for 5 days the ratios were 0.67 and 0.81. More substantial inhibition (about 50 %) was observed by El-Mir et al. [16] after subcutaneous injection of rats with 600 mg/kg metformin or treatment of the perfused liver with 10 mM metformin for 30 min.

At first sight our own data may seem to indicate that little inhibition of complex 1 is occurring *in vivo* despite the changes in liver metabolite concentrations occurring that are characteristic of such inhibition. However, an alternative explanation is that the drug was lost from the mitochondria during their isolation, and previous data from this laboratory support this view. We have shown that during the standard isolation procedure, rat liver mitochondria become permeant to small hydrophilic compounds such as mannitol, which do not normally cross the inner membrane, even though they remain impermeant to sucrose [33]. In order to confirm that the permeability of the mitochondrial

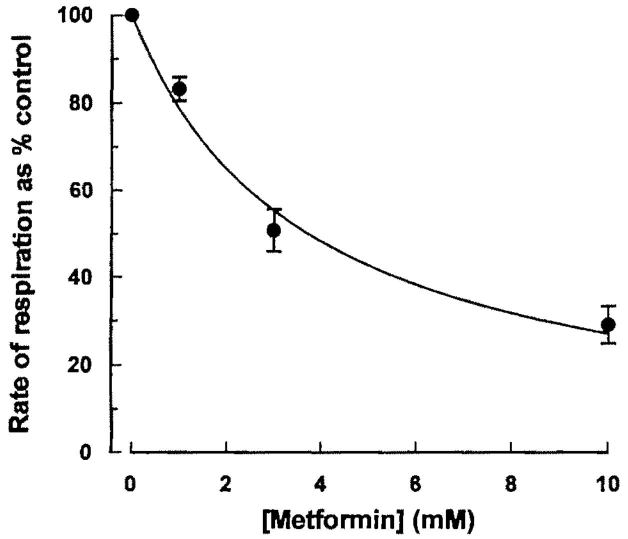

Figure 6 Isolation of liver mitochondria in the presence of metformin enhances the ability of the drug to inhibit NADH-dependent respiration

Rats livers were divided into four equal portions and each homogenized in standard sucrose isolation medium supplemented with 0, 1, 3 or 10 mM metformin as indicated Isolation of mitochondria was performed as usual but metformin-supplemented buffers were used throughout State-3 rates of respiration were then determined in the presence of glutamate + malate as substrate and metformin at the same concentration used for mitochondrial isolation. Each data point represents the mean ± S E.M of four separate mitochondrial preparations

inner membrane to metformin also increases during mitochondrial isolation, rat livers were divided into four equal portions and each homogenized in normal sucrose media containing 0, 1, 3 or 10 mM metformin. Mitochondria were then isolated at 4 °C by the standard procedure using buffers supplemented with the same concentrations of metformin This process takes about 90 min and yet the inhibition of glutamate + malate-dependent respiration by the metformin under these conditions (Figure 6) was considerably greater than that observed when isolated mitochondria were incubated at 8 °C for 4–5 h (Figure 2). This confirms that there is an increase in membrane permeability to metformin during mitochondrial preparation Although the mechanism responsible is uncertain (see [33]) our data imply that a significant amount of the metformin accumulated *in vivo* will be lost during mitochondrial preparation. Thus the 10 % decrease in respiration rates that we observed following metformin treatment may reflect a substantially greater inhibition *in vivo*.

Inhibition of complex 1 by metformin can account for inhibition of gluconeogenesis

Our data demonstrate clearly that metformin produces a time- and concentration-dependent inhibition of gluconeogenesis in isolated hepatocytes, consistent with its progressive inhibition of the respiratory chain. It was not possible to reach a steady state of inhibition over the short time frame of these experiments, but longer incubations were not desirable since the control rates of gluconeogenesis could not be maintained. For this reason higher doses of metformin had to be used than occur *in vivo*. Nevertheless, the changes in intracellular metabolites seen in the hepatocytes (Figure 4) were the same as those determined in metformin-treated rats (Figure 5). They were also identical to those we have shown previously to accompany the action of other inhibitors of the respiratory chain and oxidative phosphorylation such as amytal, DCMU, oligomycin and atractyloside at sub-maximal doses [14,15]. These reagents also cause inhibition of gluconeogenesis without a significant decrease in total tissue ATP concentration, although decreases in the free ATP/ADP ratio do occur [15]. In these earlier experiments we performed a detailed analysis of the relationship between inhibition of complex 1 and inhibition of gluconeogenesis. We showed that 50 and 80 % inhibition of respiration led to 20 and 60 % inhibition of gluconeogenesis, respectively [14]. After a 30-min exposure of hepatocytes to 1 and 5 mM metformin, El-Mir et al. directly determined 25 and 60 % inhibition of complex 1 [16]. This would be predicted to give about 10 and 40 % inhibition of gluconeogenesis respectively, which is quite consistent with the inhibition we observed in our experiments (Figure 4). El-Mir et al. [16] also demonstrated increases in lactate/pyruvate and β-hydroxybutyrate/acetoacetate ratios in response to metformin, just as we did, but unlike us they detected a decrease in the ATP/ADP ratio determined from total adenine nucleotides. This probably reflects their use of 10 mM metformin as opposed to the 2 mM used in the present studies. Our previous work with respiratory-chain inhibitors demonstrated that decreases in both cytosolic and mitochondrial ATP/ADP ratios are observed as inhibition of the respiratory chain increases beyond 50 % [14,15].

Changes in the free ATP/ADP ratios cannot be measured directly since much of the ADP is believed to be bound and so masks significant changes in free [ADP], which is probably nearly two orders of magnitude less than the total [ADP] [34]. However, the calculated ATP/ADP ratio in the livers of metformin-treated rats was decreased substantially (Figure 5) and this is reflected in an increase in the 2-phosphoglycerate, 3-phosphoglycerate and phosphoenolpyruvate concentrations. We have demonstrated previously that the decrease in ATP/ADP ratio inhibits gluconeogenesis by inhibiting pyruvate carboxylase, an effect that may be reinforced by an increase in the cytosolic NADH/NAD$^+$ ratio and consequent decrease in cytosolic and mitochondrial pyruvate concentrations [14,15]. This is reflected by the modest decrease in calculated oxaloacetate concentrations (Figure 5 and [15]) and has been demonstrated directly by others using ^{13}C-tracer measurements [30]. In addition to an inhibition of pyruvate carboxylase, a stimulation of pyruvate kinase flux will occur as a result of the increased phosphoeneolpyruvate concentrations [14,15], an effect confirmed directly by others [27]. Together, these two effects will lead to an inhibition of gluconeogenesis, which may be further enhanced by the decrease in hexose phosphate concentrations leading to reduced flux through glucose-6-phosphatase.

Inhibition of complex 1 may explain other effects of metformin

Inhibition of complex 1 can also account directly for the modest inhibition of fatty acid oxidation that occurs following metformin treatment [1–3]. In addition, many other known effects of metformin treatment such as increased peripheral glucose metabolism and the stimulation of glycolytic lactate production by the intestine [1–3] would be predicted to occur as secondary consequences of respiratory-chain inhibition. The latter effect can be explained by a more extensive inhibition of mitochondrial respiration in the cells of the intestinal mucosa since these cells will be exposed to a higher local concentration of metformin in the intestinal lumen. The increase in insulin-dependent glucose utilization by peripheral tissues, including muscle and adipose tissue, that occurs following metformin treatment [2,3] is associated with increased expression of the plasma-membrane glucose transporters GLUT1 and GLUT4 [4–7]. It is known that in many cells modest inhibition of the respiratory chain up-regulates the expression of glucose transporters and glycolytic enzymes [35,36] and causes glycolytic glucose utilization to be stimulated. Thus it would be predicted that modest inhibition of the respiratory chain by metformin would elicit the same response.

It might also be predicted that an increase in blood lactate would occur as a result of the increased glycolytic activity, and an increase is usually observed in patients treated with metformin [2,3,12,25,37,38]. The effect is usually small, probably reflecting the ability of other tissues such as heart and red muscle to oxidize excess lactic acid. However, an occasional side effect of metformin treatment is lactic acidosis [3], which would be predicted if inhibition of the respiratory chain by the drug treatment became excessive. This side effect is more common with phenformin [2,3,37,38], consistent with its more potent effects on the respiratory chain (Figure 2). Metformin probably avoids this complication because its inhibition may become self-limiting. As the matrix concentration of the drug increases, progressive inhibition of the respiratory chain will lead to a drop in membrane potential, which will prevent further accumulation of the drug.

This work was funded by the British Diabetic Association. We thank Professor R M. Denton for helpful discussions

REFERENCES

1 Schafer, G (1983) Biguanides: a review of history, pharmacodynamics and therapy. Diabete Metabolisme (Paris) **9**, 148–163
2 Hermann, L S and Melander, A (1997) Biguanides basic aspects and clinical uses, in International Textbook of Diabetes, 2nd edn. (Alberti, K. G M M., Zimmet, P., DeFronzo, R A and Keen, H, eds), pp. 841–864, John Wiley, Chichester
3 Bailey, C J. and Turner, R C (1996) Metformin New Eng. J Med. **334**, 574–579
4 Hundal, H S, Ramlal, T, Reyes, R, Leiter, L A and Klip, A. (1992) Cellular mechanism of metformin action involves glucose transporter translocation from an intracellular pool to the plasma membrane in l6 muscle cells Endocrinology **131**, 1165–1173
5 Hamann, A, Benecke, H, Greten, H and Matthaei, S. (1993) Metformin increases glucose transporter protein and gene expression in human fibroblasts. Biochem Biophys Res Commun **196**, 382–387
6 Matthaei, S., Hamann, A, Klein, H H., Benecke, H., Kreymann, G, Flier, J S. and Greten, H (1991) Association of metformin's effect to increase insulin-stimulated glucose transport with potentiation of insulin-induced translocation of glucose transporters from intracellular pool to plasma membrane in rat adipocytes Diabetes **40**, 850–857
7 Fischer, Y., Thomas, J, Rosen, P and Kammermeier, H (1995) Action of metformin on glucose transport and glucose transporter GLUT1 and GLUT4 in heart muscle cells from healthy and diabetic rats Endocrinology **136**, 412–420
8 Chappell, J B (1963) The effect of alkylguanidines on mitochondrial metabolism J Biol. Chem **238**, 410–417
9 Davidoff, F (1971) Effects of guanidine derivatives on mitochondrial function III The mechanism of phenylethylbiguanide accumulation and its relationship to *in vitro* respiratory inhibition J Biol Chem. **246**, 4017–4027
10 Gettings, S D, Reeve, J E and King, L J (1988) Possible role of intracellular Ca^{2+} in the toxicity of phenformin Biochem Pharmacol **37**, 281–289
11 Cook, D E, Blair, J. B. and Lardy, H A (1973) Mode of action of hypoglycemic agents V Studies with phenylethylbiguanide in isolated perfused rat liver J Biol. Chem **248**, 5272–5277
12 Evans, P F, King, L J, Park, D V, Margetts, G and Jones, W E (1983) The mechanism of action of phenformin in starved rats Biochem Pharmacol. **32**, 3459–3463
13 Toews, C J, Keyner, J L, Connon, J. J and Chill, G F J (1970) The effect of phenformin on gluconeogenesis in isolated perfused rat liver Diabetes **19**, 368 (abstract)
14 Pryor, H J, Smyth, J E, Quinlan, P T and Halestrap, A P (1987) Evidence that the flux control coefficient of the respiratory chain is high during gluconeogenesis from lactate in hepatocytes from starved rats Biochem J **247**, 449–457
15 Owen, M R. and Halestrap, A. P (1993) The mechanisms by which mild respiratory chain inhibitors inhibit hepatic gluconeogenesis. Biochim. Biophys. Acta **1142**, 11–22
16 El-Mir, M. Y., Nogueira, V., Fontaine, E., Averet, N, Rigoulet, M. and Leverve, X. J. (2000) Dimethylbiguanide inhibits cell respiration via an indirect effect targeted on the respiratory chain complex I. J. Biol Chem **275**, 223–8
17 Halestrap, A. P. (1987) The regulation of the oxidation of fatty acids and other substrates in rat heart mitochondria by changes in matrix volume induced by osmotic strength, valinomycin and Ca^{2+}. Biochem. J. **244**, 159–164
18 Titheradge, M. A, Binder, S. B., Yamazaki, R. K. and Haynes, R. C. (1978) Glucagon treatment stimulates the metabolism of hepatic submitochondrial particles. J. Biol Chem. **253**, 3357–3360
19 Halestrap, A. P and Dunlop, J. L (1986) Intramitochondrial regulation of fatty acid β-oxidation occurs between flavoprotein and ubiquinone A role for changes in matrix volume Biochem J **239**, 559–565
20 Bogucka, K., Wroniszewska, A., Bednarek, M., Duszynski, J. and Wojtczak, L. (1992) Energetics of Ehrlich ascites mitochondria: membrane potential of isolated mitochondria within digitonin-permeabilized cells. Biochim. Biophys. Acta **1015**, 503–509
21 Penicaud, L, Hitier, Y., Ferre, P. and Girard, J (1989) Hypoglycemic effect of metformin in genetically obese (fa/fa) rats results from an increased utilization of blood glucose by intestine. Biochem. J **262**, 881–885
22 Wilcock, C. and Bailey, C. J. (1990) Sites of metformin-stimulated glucose metabolism Biochem. Pharmacol. **39**, 1831–1834
23 Verma, S. and McNeill, J. H. (1994) Metformin improves cardiac function in isolated streptozotocin-diabetic rat hearts Am. J Physiol **266**, H714–H719
24 Rouru, J., Koulu, M, Peltonen, J., Santti, E, Hanninen, V, Pesonen, U. and Huupponen, R (1995) Effects of metformin treatment on glucose transporter proteins in subcellular fractions of skeletal muscle in fa/fa Zucker rats Br. J Pharmacol **115**, 1182–1187
25 Wilcock, C. and Bailey, C J (1994) Accumulation of metformin by tissues of the normal and diabetic mouse. Xenobiotica **24**, 49–57
26 Owen, M. R (1993) The mechanisms by which mild respiratory chain inhibitors regulate hepatic gluconeogenesis Ph D Thesis, University of Bristol
27 Argaud, D, Roth, H, Wiernsperger, N and Leverve, X. M (1993) Metformin decreases gluconeogenesis by enhancing the pyruvate kinase flux in isolated rat hepatocytes Eur J. Biochem. **213**, 1341–1348
28 Wollen, N and Bailey, C J (1988) Inhibition of hepatic gluconeogenesis by metformin Biochem Pharmacol. **37**, 4353–4358
29 Radziuk, J, Zhang, Z., Wiernsperger, N and Pye, S (1997) Effects of metformin on lactate uptake and gluconeogenesis in the perfused rat liver Diabetes **46**, 1406–1413
30 Large, V and Beylot, M (1999) Modifications of citric acid cycle activity and gluconeogenesis in streptozotocin-induced diabetes and effects of metformin Diabetes **48**, 1251–1257
31 Akerboom, T P M, van der Meer, R and Tager, J M. (1979) Techniques for the investigation of intracellular compartmentation, in Techniques in Metabolic Research, vol B205 (Kornberg, H L, Metcalfe, J. C, Northcote, D H, Pogson, C I and Tipton, K. F, eds.), pp 1–33, Elsevier/North-Holland Scientific Publishers, Shannon
32 Gluck, M R, Youngster, S K, Ramsay, R R, Singer, T P and Nicklas, W J (1994) Studies on the characterization of the inhibitory mechanism of 4′-alkylated 1-methyl-4-phenylpyridinium and phenylpyridine analogues in mitochondria and electron transport particles J Neurochem **63**, 655–661
33 Whipps, D E. and Halestrap, A. P. (1984) Rat liver mitochondria prepared in mannitol media demonstrate increased mitochondrial volumes compared with mitochondria prepared in sucrose media Relationship to the effect of glucagon on mitochondrial function Biochem J **221**, 147–152
34 Monkofer-Zwez, S and Walter, P (1989) Binding of ADP to rat liver cytosolic proteins and its influence on the ratio of free ATP/free ADP Biochem J. **259**, 117–124
35 Ebert, B L, Firth, J D and Ratcliffe, P J (1995) Hypoxia and mitochondrial inhibitors regulate expression of glucose transporter-1 via distinct *cis*-acting sequences J Biol Chem **270**, 29083–29089
36 Wheeler, T. J, Fell, R D and Hauck, M. A (1994) Translocation of two glucose transporters in heart effects of rotenone, uncouplers, workload, palmitate, insulin and anoxia. Biochim Biophys Acta **1196**, 191–200
37 Perriello, G, Misericordia, P, Volpi, E, Santucci, A, Santucci, C, Ferrannini, E, Ventura, M M., Santeusanio, F, Brunetti, P and Bolli, G B (1994) Acute antihyperglycemic mechanisms of metformin in NIDDM – evidence for suppression of lipid oxidation and hepatic glucose production Diabetes **43**, 920–928
38 Gan, S C, Barr, J, Arieff, A I and Pearl, R G (1992) Biguanide-associated lactic acidosis – case report and review of the literature Arch Internal Med. **152**, 2333–2336

Received 3 February 2000/30 March 2000; accepted 7 April 2000

Dynamics of haem oxygenase-1 expression and bilirubin production in cellular protection against oxidative stress

James E. CLARK*†, Roberta FORESTI†, Colin J. GREEN*† and Roberto MOTTERLINI†[1]

*Vascular Biology Unit, RAFT Institute of Plastic Surgery, Leopold Muller Building, Mount Vernon Hospital, Northwood, Middlesex HA6 2RN, U K and
†Department of Surgical Research, Northwick Park Institute for Medical Research, Harrow, Middlesex HA1 3UJ, U K

The inducible isoform of haem oxygenase (HO-1) has been proposed as an effective system to counteract oxidant-induced cell injury. In several circumstances, this cytoprotective effect has been attributed to increased generation of the antioxidant bilirubin during haem degradation by HO-1. However, a direct implication for HO-1-derived bilirubin in protection against oxidative stress remains to be established. In the present study, we examined the dynamics of HO-1 expression and bilirubin production after stimulation of vascular smooth-muscle cells with hemin, a potent inducer of the HO-1 gene. We found that hemin-mediated increase in HO-1 protein expression and haem oxygenase activity is associated with augmented bilirubin levels. The majority of bilirubin production occurred early after exposure of cells to hemin. Hemin pre-treatment also resulted in high resistance to cell injury caused by an oxidant-generating system. Interestingly, this protective effect was manifest only when cells were actively producing bilirubin as a consequence of increased haem availability and utilization by HO-1. Tin protoporphyrin IX, an inhibitor of haem oxygenase activity, significantly reduced bilirubin generation and reversed cellular protection afforded by hemin treatment. Furthermore, addition of bilirubin to the culture medium markedly reduced the cytotoxicity produced by oxidants. Our findings provide direct evidence that bilirubin generated after up-regulation of the HO-1 pathway is cytoprotective against oxidative stress.

Key words: carbon monoxide, glucose oxidase, hydrogen peroxide , smooth-muscle cells, tin protoporphyrin IX.

INTRODUCTION

Oxidative stress is the result of excessive production of oxidant species and/or depletion of intracellular antioxidant defences, leading to an imbalance in the redox status of the cell. Because of its anatomical location, the vascular tissue is particularly exposed to oxidative stress-mediated injury and vascular wall dysfunction is associated with the pathology of a number of common cardiovascular diseases. Similarly to other cellular systems, endothelium and smooth muscle possess the intrinsic ability to induce a series of protective enzymes once the production of oxidants overcomes the primary endogenous defences [1].

In recent years, the inducible isoform of haem oxygenase (HO-1) has been suggested to function as an effective system to counteract the oxidative threat [2]. Haem oxygenase is the rate-limiting enzyme in haem degradation to CO, iron and biliverdin, the latter being converted into bilirubin by biliverdin reductase [3]. The proposed antioxidant role for HO-1 is based on some crucial experimental observations: (i) HO-1 gene expression is extremely sensitive to up-regulation by oxidative stress in a variety of mammalian tissues [2,4–6]; (ii) induction of HO-1 protein or transfection of cells with the HO-1 gene protect tissues against oxidant-mediated injury [7–10]; and (iii) HO-1 knockout mice exhibit reduced stress defences when exposed to oxidative challenge [11]. Since biliverdin and bilirubin have been shown to possess potent antioxidant properties [12] and up-regulation of HO-1 is usually accompanied by increased levels of ferritin, a protein which sequesters intracellular catalytic iron [13], HO-1 appears to be an excellent candidate for cytoprotection. Stocker and co-workers [12] originally showed that micromolar concentrations of bilirubin efficiently scavenge peroxyl radicals *in vitro* and that, at low oxygen tension, the antioxidant activity of bilirubin surpasses that of α-tocopherol, the best-known antioxidant against lipid peroxidation [12]. In previous studies we have reported that exogenously applied bilirubin attenuates hydrogen peroxide-induced damage in vascular endothelial cells [14]. More recently, we have implicated HO-1-derived bilirubin in reduction of endothelial apoptosis mediated by peroxynitrite [15] and amelioration of post-ischaemic myocardial dysfunction in the isolated perfused rat heart [16]. Doré and co-workers [17] have also demonstrated that enhanced bilirubin production following activation of haem oxygenase-2 (HO-2), the constitutive isoform of haem oxygenase, is protective against the neurotoxicity elicited by hydrogen peroxide [17]. However, further studies on the physiological importance of bilirubin generated by HO-1 are required to fully account for the cytoprotection conferred by HO-1 induction.

Here we examined the dynamics of HO-1 expression and bilirubin production after stimulation of vascular smooth-muscle cells with hemin, a potent inducer of the HO-1 gene. The response to an oxidant-generating system was then evaluated in control cells and cells producing increased amounts of bilirubin.

EXPERIMENTAL PROCEDURES

Materials

Bovine vascular smooth-muscle cells were obtained from the Corell Cell Repository (Camden, NJ, U.S.A.) and grown in Dulbecco's minimal essential medium (MEM) supplemented with 20 % fetal calf serum, 2 × MEM vitamins, 2 × MEM non-essential and essential amino acids, penicillin (100 units/ml) and streptomycin (0.1 mg/ml). Hemin and tin protoporphyrin IX (SnPPIX) were from Porphyrin Products (Logan, UT, U.S.A.). All other chemicals were obtained from Sigma (Poole, Dorset, U.K.)

Abbreviations used HO-1, haem oxygenase-1; SnPPIX, tin protoporphyrin IX, GOX, glucose oxidase

[1] To whom correspondence should be addressed (e-mail r motterlini@ic ac uk)

Western-blot analysis for HO-1 expression and haem oxygenase activity

Confluent cells were exposed to increasing concentrations of hemin (50–400 μM) for 2 h followed by incubation with medium alone for various times. At the end of the incubation, cells were collected and analysed for HO-1 protein expression and haem oxygenase activity. Western-blot technique was performed using specific antibodies against rat HO-1 [18,19] and haem oxygenase activity was determined spectrophotometrically as described previously [18].

Determination of bilirubin in cell-culture medium

Haem oxygenase-derived bilirubin was determined as described recently by Turcanu and co-workers [20]. Cells were pre-treated with hemin (100 and 200 μM) for 2 h and exposed to medium ~~alone or medium~~ containing an inhibitor of haem oxygenase activity (SnPPIX, 40 μM) for an additional 4 or 22 h. Each culture supernatant (500 μl) was then collected in a tube and 250 mg of barium chloride was added. After vortexing, 0.75 ml of benzene was added and the tubes mixed again. The benzene phase containing the extracted bilirubin was separated from the aqueous phase by centrifugation for 30 min at 13000 g. Bilirubin was determined spectrophotometrically as a difference in absorbance between 450 and 600 nm ($\epsilon_{450} = 27.3\ \text{mM}^{-1}\cdot\text{cm}^{-1}$).

Cytotoxicity assay

Cells were pre-treated with hemin (25–400 μM) for 2 h followed by 4 or 22 h incubation with medium alone or medium containing SnPPIX (40 μM). In another set of experiments, different concentrations of exogenous bilirubin were applied to cells for 2 h. At the end of the incubation, cells were washed and exposed for 2 h to fresh culture medium containing various concentrations (10–120 m-units/ml) of glucose oxidase (GOX), an enzyme that catalyses the conversion of D-glucose to D-gluconolactone, producing hydrogen peroxide at constant rate. This oxidant-generating system has been used previously in cell culture *in vitro* to promote oxidative injury [21]. Cell viability was assessed using a colorimetric assay kit from Promega (Madison, WI, U.S.A.) according to manufacturers' instructions.

Statistical analysis

Results were expressed as means ± S.E.M. of six independent experiments per group. Statistical analysis was performed using ANOVA combined with Student's two-tailed t test. Differences among the groups were considered significant at $P < 0.05$.

RESULTS AND DISCUSSION

Vascular smooth-muscle cells exposed to hemin for 2 h exhibited considerable changes in HO-1 expression and haem oxygenase activity in a time- and concentration-dependent manner. Maximal protein levels and activity were detected 4 h after treatment with hemin at 100 μM (Figure 1). Although HO-1 protein expression was more prominent at 200 μM compared with 100 μM hemin, haem oxygenase activity peaked at 100 μM and started to decrease at higher concentrations of hemin. This effect is presumably a consequence of the cytotoxic nature of the hemin moiety. In fact, by virtue of its iron content, hemin can act as a promoter of reactive-oxygen-species formation and thus mediate cell injury [8,22,23]. This concept is also sustained by our findings showing that at 200 μM hemin-stimulated cells started to exhibit increased levels of inducible heat-shock protein 70 (hsp70; Figure 1C), a chaperone involved in refolding of damaged and denatured proteins. It is interesting to note that HO-1 expression and haem oxygenase activity were considerably diminished 22 h after exposure to hemin at all concentrations used (Figure 1A), indicating a gradual return of cells to basal conditions after the initial response to hemin.

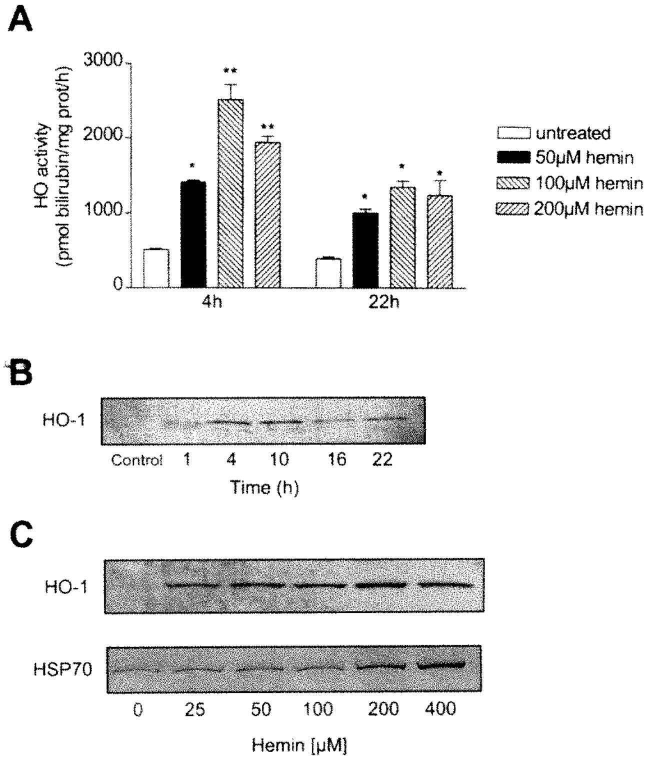

Figure 1 Effect of hemin on haem oxygenase activity, and HO-1 and hsp70 protein expression in vascular smooth-muscle cells

(**A**) Cells were exposed to hemin (0–200 μM) for 2 h and haem oxygenase activity was measured at 4 and 22 h after hemin treatment as reported in the Experimental procedures section. Each bar represents the mean ± S.E.M. of six experiments performed independently. *$P < 0.05$ versus untreated; **$P < 0.01$ versus untreated. (**B**) HO-1 protein expression in smooth-muscle cells was detected by Western blotting at different time points after treatment with 100 μM hemin. (**C**) HO-1 and hsp70 protein expression were determined 4 h after exposure of cells to various concentrations of hemin (0–400 μM).

Increased HO-1 expression following treatment of cells with hemin was accompanied by augmented bilirubin production, as shown in Table 1. However, and in accordance with the haem oxygenase activity results, we observed that the majority of the bile pigment (86 and 68 %) was generated within the first 4 h after exposure to 100 and 200 μM hemin, respectively. Notably, after this initial period of incubation, cells treated with 100 μM hemin did not exhibit a significant further elevation in bilirubin levels. This suggests that most of the hemin taken up by cells is consumed by haem oxygenase in a relatively short period of time and that the tetrapyrrole ring subsequently becomes the limiting factor in the generation of bilirubin despite HO-1 protein expression remaining elevated. This hypothesis is substantiated by the fact that smooth-muscle cells exposed to higher concentrations of hemin (200 μM) continued to release bilirubin into the medium during both the earlier and later times of incubation.

Having established that HO-1 up-regulation is accompanied by increased bilirubin production, we wanted to verify whether this inducible pathway could provide protection against oxidative

Table 1 Production of bilirubin in control and hemin-treated cells

Cells were exposed for 2 h to medium alone (control) or medium supplemented with hemin (100 or 200 μM). Bilirubin released into the culture medium was measured 4 or 22 h after hemin treatment, as described in the Experimental procedures section Bilirubin was also measured in the medium of cells treated with 100 μM hemin for 2 h followed by incubation with 40 μM SnPPIX for 4 h Results represent the means ± S E M of six experiments for each group *$P < 0\,05$ versus control; †$P < 0\,05$ versus 4 h

	Bilirubin (nM/well)	
	4 h	22 h
Control	375 ± 38	311 ± 33
100 μM Hemin	540 ± 33*	622 ± 111*
100 μM Hemin + 40 μM SnPPIX	302 ± 35	–
200 μM Hemin	769 ± 54*	1117 ± 174*†

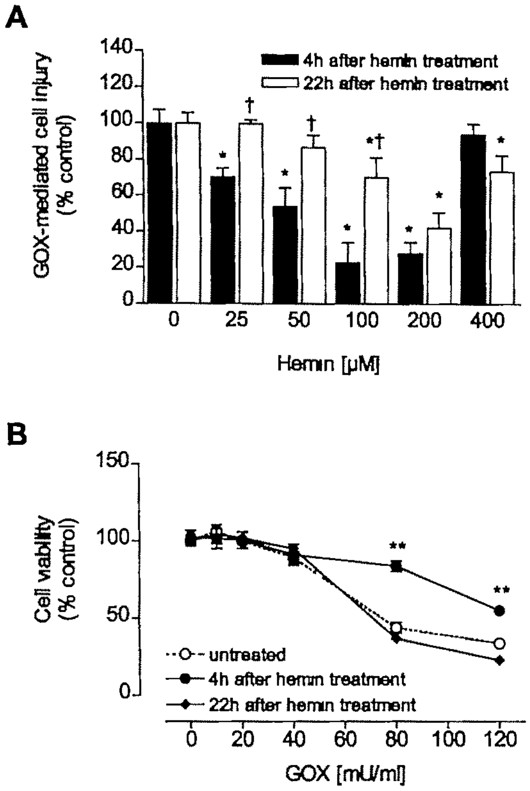

Figure 2 Effect of hemin pre-treatment on GOX-mediated cell injury

(**A**) Cells were pre-treated for 2 h with increasing concentrations of hemin (0–400 μM) and were then incubated with fresh medium for 4 or 22 h prior to exposure to 80 m-units/ml GOX for 2 h Cell injury was assessed as reported in the Experimental procedures section (**B**) Cells were pre-treated for 2 h with 100 μM hemin, incubated with fresh medium for 4 or 22 h and then exposed to increasing concentrations of GOX (20–120 m-units/ml) for 2 h Control experiments (untreated) were performed by exposing cells to medium alone prior to GOX challenge Each bar represents the mean ± S.E.M of six experiments performed independently *$P < 0\,05$ versus 0 μM hemin, †$P < 0\,05$ versus 4 h, **$P < 0\,01$ versus untreated

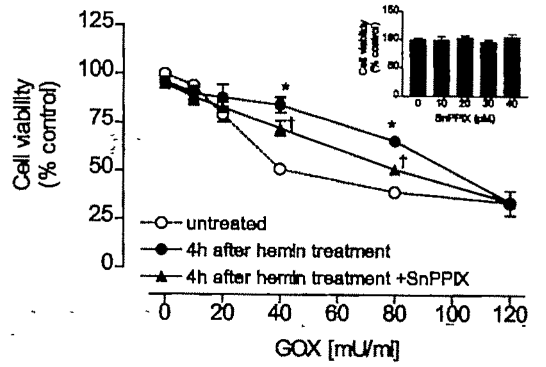

Figure 3 SnPPIX attenuates hemin-mediated cytoprotection against oxidative stress

Cells were pre-treated with 100 μM.hemin for 2 h and then incubated for 4 h in medium alone or medium containing 40 μM SnPPIX After incubation, cells were exposed to increasing concentrations of GOX for 2 h and cell viability was assessed as described in the Experimental procedures section Control experiments (untreated) were performed by exposing cells to medium alone prior to GOX challenge Inset, effect of various concentrations of SnPPIX on cell viability. Cells were incubated for 4 h with 0–40 μM SnPPIX and cell viability was assessed. Results represent the means ± S E M. of six experiments for each group *$P < 0.05$ versus untreated; †$P < 0\,05$ versus hemin treatment

stress. Several previous reports have revealed a direct correlation between HO-1 induction and high resistance to oxidant-mediated damage [5,9,24,25]. This cytoprotective effect has always been attributed to augmented levels of the antioxidants biliverdin and bilirubin although actual measurements of any of these HO-1 products were lacking. We believe this is an important point to address because (i) up-regulation of the HO-1 gene does not necessarily imply up-regulation of the products and (ii) specific investigations on the availability of haem as a substrate for increased HO-1 expression have yet to be performed. In the present study, cells exposed to an oxidant-generating system (GOX, 80 m-units/ml) for 2 h showed a considerable decrease in viability (Figure 2). In contrast, pre-treatment with hemin resulted in a concentration-dependent reduction in GOX-mediated cell injury. Highest protection was seen 4 h after treatment with 100 μM hemin, the concentration that resulted in maximal HO activity. A similar decrease in cell injury was also observed with 200 μM hemin. Significantly less protection was found 22 h following exposure to hemin ($P < 0.05$ versus 4 h); however, pre-treatment with 200 μM hemin still resulted in considerable reduction of cell damage caused by oxidative stress. These data are best explained when considering the experimental protocol employed. Following exposure of smooth-muscle cells to hemin (4 or 22 h), the medium was replaced with fresh medium containing GOX for 2 h prior to assessment of cell viability. Therefore, the medium in which bilirubin accumulated was removed before the addition of GOX. In view of this finding and the bilirubin data presented in Table 1, cytoprotection afforded 4 h after treatment with 100 μM hemin was probably a result of endogenous bilirubin actively generated by HO-1 at the time of oxidant challenge. Accordingly, production of less bilirubin can account for the decreased ability of hemin (100 μM) pre-treatment to protect cells at 22 h. Also at 22 h, the effect of 200 μM hemin could reflect sustained bilirubin generation over a longer period of time with a possible contribution of other inducible defensive systems such as hsp70.

Injury following exposure to increasing concentrations of GOX (10–120 m-units/ml) was also significantly diminished in cells pre-treated with 100 μM hemin; once again this protection was evident at 4 but not at 22 h (Figure 2B) and is consistent with the dynamics of HO-1 expression, haem oxygenase activity and bilirubin production in relation to haem availability. A direct contribution of the haem oxygenase/bilirubin pathway in minimizing oxidative damage was ascertained in our study by using

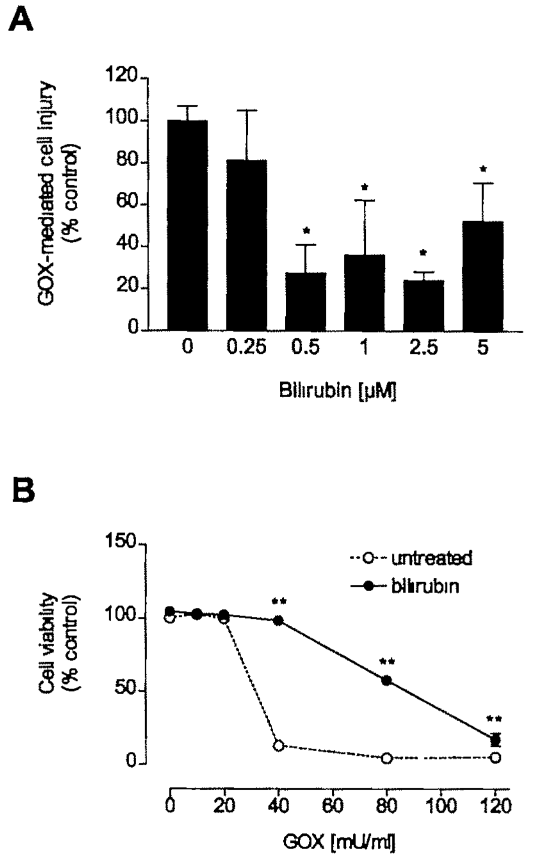

Figure 4 Effect of exogenous bilirubin on GOX-mediated cell injury in smooth-muscle cells

(**A**) Cells were incubated for 2 h with increasing concentrations of bilirubin (0–5 μM) and cell injury was assessed 2 h after exposure to 80 m-units/ml GOX (**B**) Cells were incubated for 2 h with medium alone (untreated) or medium containing bilirubin (1 μM) and cell viability was assessed 2 h after exposure to increasing concentrations of GOX (0–120 m-units/ml). $^{*}P < 0.05$ versus 0 μM bilirubin; $^{**}P < 0\,05$ versus untreated.

an inhibitor of its activity, SnPPIX. As shown in Table 1 and Figure 3, SnPPIX (40 μM) reduced bilirubin formation (302 ± 35 nM/well) to levels comparable with the control (375 ± 38 nM/well) and attenuated the cytoprotection conferred by hemin treatment against GOX-induced cell injury. It is important to note that SnPPIX itself did not cause any evident cytotoxic effect at the concentrations tested (Figure 3, inset). The participation of additional defence mechanisms cannot be excluded since SnPPIX did not completely reverse the protective effect mediated by hemin. To confirm the important role of bilirubin in protection against oxidative stress, cells were incubated with various concentrations of the bile pigment prior to GOX challenge. A marked decrease in cell damage was observed with bilirubin at 0.5 μM and above (Figure 4A). Similarly, 1 μM bilirubin significantly reduced the toxic actions of increasing concentrations of GOX (Figure 4B). Although our data are in agreement with recent published observations by Doré and co-workers in cultured neurons [17], the concentrations of bilirubin that provided cytoprotection in the present work were higher. However, differences in cell types and experimental conditions used can explain differences in results. For instance, we found that perfusion of isolated rat hearts with serum-free buffer containing bilirubin at concentrations as low as 100 nM reduces infarct size and improves myocardial function following ischaemia–reperfusion [16].

Thus, this study demonstrates that increased bilirubin as a consequence of HO-1 induction contributes to cytoprotection of smooth-muscle cells against oxidant-mediated damage. In addition, our results show how the dynamics of haem oxygenase activity and bilirubin production determine the adaptive response of cells to oxidative stress. The important issues concerning the availability of haem as a substrate for augmented HO-1 levels and the generation of bilirubin in sufficient amounts to provide resistance to stressful stimuli were also raised. The present findings strongly support a role for bilirubin derived from HO-1 in cytoprotection; nevertheless, the participation of the other products of haem degradation by HO-1 is attainable since CO, biliverdin and iron have all been shown to modulate biological processes [12,13,26–28]. Accordingly, Otterbein and co-workers have reported recently that exposure of rats to low concentrations of CO increases tolerance to hyperoxic lung injury [29]. The fact that bilirubin can counteract oxidative injury caused by hydrogen peroxide [14,17], peroxynitrite [15,30] and peroxyl radicals [12] indicates a wide spectrum of antioxidant activities for this bile pigment. It is tempting to suggest that these properties of bilirubin can be extended to nitric oxide and other reactive nitrogen species [31,32].

This work was supported by grants from the National Heart Research Fund, Leeds, U K (to R M.) and the British Heart Foundation (PG99-005, to R.M)

REFERENCES

1 Benjamin, I J and McMillan, D R (1998) Stress (heat shock) proteins Molecular chaperones in cardiovascular biology and disease. Circ Res **83**, 117–132
2 Maines, M D. (1997) The heme oxygenase system: a regulator of second messenger gases Annu Rev Pharmacol Toxicol. **37**, 517–554
3 Tenhunen, R, Marver, H. S and Schmid, R (1969) Microsomal heme oxygenase Characterization of the enzyme J Biol Chem **244**, 6388–6394
4 Abraham, N. G, Drummond, G S, Lutton, J D and Kappas, A. (1996) The biological significance and physiological role of heme oxygenase Cell. Physiol Biochem **6**, 129–168
5 Applegate, L. A, Luscher, P. and Tyrrell, R M (1991) Induction of heme oxygenase. a general response to oxidant stress in cultured mammalian cells Cancer Res **51**, 974–978
6 Stocker, R. (1990) Induction of heme oxygenase as a defense against oxidative stress. Free Radical Res Commun **9**, 101–112
7 Nath, K. A, Balla, G, Vercellotti, G M, Balla, J, Jacob, H S, Levitt, M D and Rosenberg, M E (1992) Induction of heme oxygenase is a rapid, protective response in rhabdomyolysis in the rat J. Clin Invest **90**, 267–270
8 Balla, J, Jacob, H S, Balla, G, Nath, K, Eaton, J. W and Vercellotti, G M (1993) Endothelial-cell heme uptake from heme proteins Induction of sensitization and desensitization to oxidant damage Proc Natl Acad. Sci U S A **90**, 9285–9289
9 Choi, A M K. and Alam, J. (1996) Heme oxygenase-1 function, regulation, and implication of a novel stress-inducible protein in oxidant-induced lung injury Am J Respir Cell Mol Biol **15**, 9–19
10 Abraham, N G., Lavrovsky, Y, Schwartzman, M L., Stoltz, R A, Lever, R D, Gerritsen, M E, Shibahara, S and Kappas, A. (1995) Transfection of the human heme oxygenase gene into rabbit coronary microvessel endothelial cells protective effect against heme and hemoglobin toxicity Proc Natl Acad Sci U S A **92**, 6798–6802
11 Poss, K D and Tonegawa, S (1997) Reduced stress defense in heme oxygenase 1-deficient cells Proc Natl Acad. Sci U S A **94**, 10925–10930
12 Stocker, R, Yamamoto, Y., McDonagh, A F, Glazer, A N and Ames, B. N (1987) Bilirubin is an antioxidant of possible physiological importance Science **235**, 1043–1046
13 Balla, G., Jacob, H S, Balla, J, Rosenberg, M, Nath, K, Apple, F, Eaton, J W and Vercellotti, G M (1992) Ferritin a cytoprotective antioxidant stratagem of endothelium. J Biol Chem **267**, 18148–18153
14 Motterlini, R., Foresti, R, Intaglietta, M and Winslow, R. M (1996) NO-mediated activation of heme oxygenase endogenous cytoprotection against oxidative stress to endothelium Am J Physiol. Heart Circ Physiol **270**, H107–H114

15 Foresti, R., Sarathchandra, P., Clark, J. E., Green, C. J. and Motterlini, R. (1999) Peroxynitrite induces haem oxygenase-1 in vascular endothelial cells: a link to apoptosis. Biochem. J. **339**, 729–736

16 Clark, J. E., Foresti, R., Sarathchandra, P., Kaur, H., Green, C. J. and Motterlini, R. (2000) Heme oxygenase-1-derived bilirubin ameliorates post-ischemic myocardial dysfunction. Am. J. Physiol. Heart Circ. Physiol. **278**, H643–H651

17 Doré, S., Takahashi, M., Ferris, C. D., Hester, L. D., Guastella, D. and Snyder, S. H. (1999) Bilirubin, formed by activation of heme oxygenase-2, protects neurons against oxidative stress injury. Proc. Natl. Acad. Sci. U.S.A. **96**, 2445–2450

18 Foresti, R., Clark, J. E., Green, C. J. and Motterlini, R. (1997) Thiol compounds interact with nitric oxide in regulating heme oxygenase-1 induction in endothelial cells. Involvement of superoxide and peroxynitrite anions. J. Biol. Chem. **272**, 18411–18417

19 Clark, J. E., Green, C. J. and Motterlini, R. (1997) Involvement of the heme oxygenase-carbon monoxide pathway in keratinocyte proliferation. Biochem. Biophys. Res. Commun. **241**, 215–220

20 Turcanu, V., Dhouib, M. and Poindron, P. (1998) Determination of heme oxygenase activity in murine macrophages for studying oxidative stress inhibitors. Anal. Biochem. **263**, 251–253

21 Chang, J., Rao, N. V., Markewitz, B. A., Hoidal, J. R. and Michael, J. R. (1996) Nitric oxide donor prevents hydrogen peroxide mediated endothelial cell injury. Am. J. Physiol. Lung Physiol. **270**, L931–L940

22 Balla, G., Vercellotti, G. M., Eaton, J. W. and Jacob, H. S. (1990) Iron loading of endothelial cells augments oxidant damage. J. Lab. Clin. Med. **116**, 546–554

23 Vesely, M. J. J., Exon, D. J., Clark, J. E., Foresti, R., Green, C. J. and Motterlini, R. (1998) Heme oxygenase-1 induction in skeletal muscle cells. hemin and sodium nitroprusside are regulators *in vitro*. Am. J. Physiol. Cell Physiol. **275**, C1087–C1094

24 Vogt, B. A., Alam, J., Croatt, A. J., Vercellotti, G. M. and Nath, K. A. (1995) Acquired resistance to acute oxidative stress. Possible role of heme oxygenase and ferritin. Lab. Invest. **72**, 474–483

25 Ishikawa, K., Navab, M., Leitinger, N., Fogelman, A. M. and Lusis, A. J. (1997) Induction of heme oxygenase-1 inhibits the monocyte transmigration induced by mildly oxidized LDL. J. Clin. Invest. **100**, 1209–1216

26 Motterlini, R., Gonzales, A., Foresti, R., Clark, J. E., Green, C. J. and Winslow, R. M. (1998) Heme oxygenase-1-derived carbon monoxide contributes to the suppression of acute hypertensive responses *in vivo*. Circ. Res. **83**, 568–577

27 Sammut, I. A., Foresti, R., Clark, J. E., Exon, D. J., Vesely, M. J. J., Sarathchandra, P., Green, C. J. and Motterlini, R. (1998) Carbon monoxide is a major contributor to the regulation of vascular tone in aortas expressing high levels of haem oxygenase-1. Br. J. Pharmacol. **125**, 1437–1444

28 Mcphee, F., Caldera, P. S., Bemis, G. W., McDonagh, A. F., Kuntz, I. D. and Craik, C. S. (1996) Bile pigments as HIV-1 protease inhibitors and their effects on HIV-1 viral maturation and infectivity *in vitro*. Biochem. J. **320**, 681–686

29 Otterbein, L. E., Mantell, L. L. and Choi, A. M. K. (1999) Carbon monoxide provides protection against hyperoxic lung injury. Am. J. Physiol. Lung Physiol. **276**, L688–L694

30 Minetti, M., Mallozzi, C., Di Stasi, A. M. M. and Pietraforte, D. (1998) Bilirubin is an effective antioxidant of peroxynitrite-mediated protein oxidation in human blood plasma. Arch. Biochem. Biophys. **352**, 165–174

31 Foresti, R. and Motterlini, R. (1999) The heme oxygenase pathway and its interaction with nitric oxide in the control of cellular homeostasis. Free Radical Res. **31**, 459–475

32 Kaur, H., Green, C. J. and Motterlini, R. (1999) Interaction of bilirubin and biliverdin with reactive nitrogen species. Free Radical Biol. Med. **27**, S78

Received 16 February 2000/15 March 2000, accepted 7 April 2000

Biochem J (2000) 348, 621–632 (Printed in Great Britain)

Characterization of β-galactosidase mutations Asp^{332} → Asn and Arg^{148} → Ser, and a polymorphism, Ser^{532} → Gly, in a case of G_{M1} gangliosidosis

Sunqu ZHANG*, Richard BAGSHAW*, William HILSON*, Yuko OHO*, Alina HINEK*, Joe T. R. CLARKE†‡,
Aleksander HINEK§ and John W. CALLAHAN‡§‖[1]

*Research Institute, The Hospital for Sick Children, 555 University Avenue, Toronto, ON, Canada M5G 1X8, †Department of Medical Genetics, University of Toronto, Toronto, ON, Canada M5G 1X8, ‡Department of Pediatrics, University of Toronto, Toronto, ON, Canada M5G 1X8, §Department of Laboratory Medicine and Pathobiology, University of Toronto, Toronto, ON, Canada M5G 1X8, and ‖Department of Biochemistry, University of Toronto, Toronto, ON, Canada M5G 1X8

We have identified and characterized three missense mutations in a patient with type 1 G_{M1} gangliosidosis, namely a substitution of G for A at nucleotide position 1044 (G1044 → A; in exon 10) on one allele, which converts Asp^{332} into asparagine, and both a mutation (C492 → A in exon 4, leading to the amino acid change of Arg^{148} → Ser) and a polymorphism (A1644 → G in exon 15, leading to a change of Ser^{532} → Gly) on the other allele. This patient had less than 1 % residual β-galactosidase activity and minimally detectable levels of immunoreactive β-galactosidase protein in fibroblasts. To account for the above findings, a series of expression and immunolocalization studies were undertaken to assess the impact of each mutation. Transient overexpression in COS-1 cells of cDNAs encoding Asp^{332}Asn, Arg^{148}Ser and Ser^{532}Gly mutant β-galactosidases produced abundant amounts of precursor β-galactosidase, with activities of 0, 84 and 81 % compared with the cDNA clone for wild-type β-galactosidase (GP8). Since the level of vector-driven expression is much less in Chinese hamster ovary (CHO) cells than in COS-1 cells, and we knew that exogenous β-galactosidase undergoes lysosomal processing when expressed in these cells, transient expression studies were performed of Arg^{148}Ser and Ser^{532}Gly, which yielded active forms of the enzyme. In this case, the Arg^{148}Ser and Ser^{532}Gly products gave rise to 11 % and 86 % of the control activity respectively. These results were not unexpected, since the Arg^{148}Ser mutation introduced a major conformational change into the protein, and we anticipated that it would be degraded in the endoplasmic reticulum (ER), whereas the polymorphism was expected to produce near-normal activity. To examine the effect of the Asp^{332}Asn mutation on the catalytic activity, we isolated CHO clones permanently transfected with the Asp^{332}Asn and Asp^{332}Glu constructs, purified the enzymes by substrate-analogue-affinity chromatography, and determined their kinetic parameters. The V_{max} values of both mutant recombinant enzymes were markedly reduced (less than 0.9 % of the control), and the K_m values were unchanged compared with the corresponding wild-type enzyme isolated at the same time. Both the Arg^{148}Ser β-galactosidase in CHO cells and Asp^{332}Asn β-galactosidases (in COS-1 and CHO cells) produced abundant immunoreaction in the perinuclear area, consistent with localization in the ER. A low amount was detected in lysosomes. Incubation of patient fibroblasts in the presence of leupeptin, which reduces the rate of degradation of lysosomal β-galactosidase by thiol proteases, had no effect on residual enzyme activity, and immunostaining was again detected largely in the perinuclear area (localized to the ER) with much lower amounts in the lysosomes. In summary, the Arg^{148}Ser mutation has no effect on catalytic activity, whereas the Asp^{332}Asn mutation seriously reduces catalytic activity, suggesting that Asp^{332} might play a role in the active site. Immunofluorescence studies indicate the expressed mutant proteins with Arg^{148}Ser and Asp^{332}Asn mutations are held up in the ER, where they are probably degraded, resulting in only minimum amounts of the enzyme becoming localized in the lysosomes. These results are completely consistent with findings in the cultured fibroblasts. Our results imply that most of the missense mutations described in G_{M1} gangliosidosis to date have little effect on catalytic activity, but do affect protein conformation such that the resulting protein cannot be transported out of the ER and fails to arrive in the lysosome. This accounts for the minimal amounts of enzyme protein and activity seen in most G_{M1} gangliosidosis patient fibroblasts.

Key words: active site, gene expression, immunofluorescence, polymorphisms, protein folding.

INTRODUCTION

A deficiency of human lysosomal β-galactosidase activity is the primary defect in patients with the autosomal recessive storage diseases, G_{M1} gangliosidosis, and Morquio disease, type B [1]. In G_{M1} gangliosidosis, G_{M1} ganglioside accumulates in the neurons of the central nervous system. G_{M1} patients have a marked deficiency (0–3 % of normal) of lysosomal β-galactosidase activity [2], accounting for the neuronal and visceral organ storage of galactose-terminal substances. Morquio disease type B patients are neurologically normal, do not store G_{M1} ganglioside, but display severe skeletal dysostosis multiplex because of an accumulation of keratan sulphate, a glycosaminoglycan, characterized by poly(galactose-N-acetylglucosamine)-repeating units

---

Abbreviations used: CAT, chloramphenicol acetyltransferase, CHO, chinese hamster ovary, COS-1, African green monkey kidney cells, ER, endoplasmic reticulum, GP8, cDNA clone for wild-type β-galactosidase, poly(A)$^+$, polyadenylated; SSCP, single-strand conformation polymorphism, SSPE, sodium chloride–sodium phosphate–EDTA

[1] To whom correspondence should be addressed, at the Research Institute, Room 9144, The Hospital for Sick Children, Toronto, ON, Canada (e-mail jwc@sickkids.on.ca)

with sulphate attached at the 6-position of both sugars. While Morquio type B patients have been reported to have a higher residual activity (activity 5–10 % of normal) of lysosomal β-galactosidase [3,4] than do G_{M1} gangliosidosis patients (0–3 %), why this should lead solely to the storage of keratan sulphate, and not the other natural substrates of the enzyme, is at present poorly understood.

The β-galactosidase gene, residing on chromosome 3p21.33, encodes a 677-amino-acid prepropolypeptide, from which a 23-amino-acid N-terminal signal sequence is removed on entry into the ER to generate a propolypeptide precursor of 654 residues [5,6]. When N-glycosylated at most, if not all, of its seven candidate sites, the nascent chain migrates as an 84-kDa propolypeptide and, after obtaining its mannose-phosphate lysosomal tag (whereby the mass as determined by SDS/PAGE increases to 88 kDa), is then rapidly transported to the endosomal–lysosomal compartment [7], where it is proteolytically processed to the mature 64-kDa form of the enzyme. We have previously shown that purified lysosomal β-galactosidase undergoes rapid and irreversible inactivation by 2,4-dinitrophenyl-2-fluoro-2-deoxy-β-D-galactopyranoside, a potent mechanism-based suicide substrate [7]. These results indicate that lysosomal β-galactosidase cleaves substrates by a Koshland double-displacement mechanism, involving two acidic residues; one residue, the catalytic nucleophile, forms a galactosylated-enzyme intermediate. The second acidic residue, the acid-base catalyst, donates a proton for cleavage of the galactosyl amino-acid bond, and extracts a proton from water, allowing attack by the hydroxy ion with release of free β-D-galactose and restoring the enzyme to an active state. Using electrospray ionization mass spectrometry after proteolytic digestion and HPLC separation of peptides, we identified the galactosylated nucleophile as being Glu^{268} [8]. Glu^{268} is conserved in the mouse, dog and all other members of Family 35 β-galactosidases defined to date, which includes a variety of plant species (tomato, asparagus, cauliflower, apple, *Aspergillus* and others) [8]. The second acidic residue in the mechanism remains to be identified. The majority of the mutations in the β-galactosidase gene are of the missense type, which are spread uniformly throughout the gene and give rise to G_{M1} gangliosidosis [1]. No mutation involving Glu^{268} has been described to date, but one mutation in particular, Trp^{273}Leu, located only five residues from Glu^{268}, has been found regularly in patients with Morquio disease type B [1].

Studies assessing mutations in the β-galactosidase gene for their impact on the expression of the protein in fibroblasts from G_{M1} gangliosidosis patients have been hampered by the general lack of well-characterized antibodies. Although β-galactosidase exits the ER–Golgi compartment and might be secreted from cells as a fully active precursor [7], its stability upon arrival in the lysosome and its productive processing to the mature enzyme are critically dependent on it forming a complex with two other independently synthesized and targeted hydrolases, namely protective protein/Cathepsin A and neuraminidase [9,10]. This renders studies on the impact of mutations more difficult to assess, because the products must survive both the ER 'quality-control' system and a unique lysosomal-processing system [11,12]. In the present work, we have identified Arg^{148}Ser and Asp^{332}Asn mutations in a patient with type 1 G_{M1} gangliosidosis. The Asp^{332}Asn mutation results in a catalytically defective enzyme, as judged from expression studies, where conversion of Asp^{332} into Asn^{332} or into Glu^{332} resulted in markedly reduced catalytic activities in the enzymes, suggesting that Asp^{332} serves as an acidic active site residue. In addition, the Asp^{332}Asn mutant localizes in the ER, suggesting it is also transport-defective. The Arg^{148}Ser mutation was found on the same allele as a Ser^{532}Gly mutation, which has been shown to be a common polymorphism. Arg^{148}Ser and Ser^{532}Gly were transiently expressed in both COS-1 and CHO cells, and show that the enzyme containing the Arg^{148}Ser mutation, although catalytically active, is localized and degraded in the endoplasmic reticulum (ER), whereas the common Ser^{532}Gly polymorphism results in an active enzyme. A preliminary report on this work has appeared in abstract form [13].

EXPERIMENTAL

Patient information

The proband, case 1, was born by Caesarean section to non-consanguineous parents after a normal pregnancy. Developmental delay, hypotonia, cherry red spots, kyphoscoliosis and hepatosplenomegaly were noted at 6 months of age. He died at 3 years. The urinary oligosaccharide pattern and the level of residual enzyme activity measured with synthetic substrate were typical for G_{M1} gangliosidosis. Fibroblasts from case 2 (patient 1 of [14]) were referred to us by Dr C. A. Rupar and Dr B. Gordon (Children's Psychiatric Research Institute, London, ON, Canada). Cultured fetal fibroblasts (case 3) were available from a case detected prenatally (courtesy of Dr Don Whelan; McMaster University, Hamilton,). These fibroblast strains were established for diagnostic studies, which were subject to informed consent. Cells from a fourth case [case 4; from NIGMS Human Genetic Mutant Cell Repository (GM05652A)] displayed no detectable acid β-galactosidase activity, and normal levels of β-hexosaminidase, β-glucuronidase and neuraminidase were found. Cells from a case of Morquio disease type B, also from the NIGMS Human Genetic Mutant Cell Repository (GM01602), gave a residual activity < 5 % of control values. In general, skin fibroblasts were grown in α-MEM with penicillin (100 units/ml) and streptomycin (100 mg/ml), supplemented with 10 % (v/v) fetal-calf serum at 37 °C in an air/CO_2 (19:1) atmosphere until confluent. These cell cultures were free from mycoplasma contamination, as analysed by a PCR-based method. Origin-defective simian-virus-40-transformed African green monkey kidney cells (COS-1) and Chinese hamster ovary cells (CHO) were obtained from the American Type Culture Collection (Rockville, MD, U.S.A.)

Northern blot analysis

Extraction of polyadenylated [poly(A)$^+$] mRNA from five 100-mm plates of confluent fibroblasts was performed by following the Oligotex® direct mRNA kit (Qiagen, Chatsworth, CA, U.S.A.)-guanidinium isothiocyanate method [15]. Samples of poly(A)$^+$ RNA (30 or 50 μg) were heat-denatured at 65 °C for 30 min, quickly loaded on to a 1 % (w/v) agarose gel, and after electrophoresis were transferred to a nitrocellulose blot. A *Sal*I-digested fragment of the full-length β-galactosidase cDNA (called GP8, described in [16], and kindly supplied by Professor Y. Suzuki, International University of Health and Welfare Kita Kanemaru, Otawara, Japan) was used as the β-galactosidase probe, whereas a Cox6a cDNA fragment (derived from cytochrome oxidase protein, 6a) was used as an internal control. Both were labelled with ^{32}P using the random-primer-labelling system (Life Technologies, Rockville, MD, U.S.A.). Prehybridization of the membrane was performed at 42 °C in 50 % (v/v) formamide, 5 × sodium chloride–sodium phosphate–EDTA (SSPE), 0.1 % (w/v) SDS, 5 × Denhardt's solution (where 1 × Denhardt's solution is 0.02 % Ficoll 400/0.02 % polyvinylpyrrolidone/0.002 % BSA), 200 mg/ml denatured salmon-sperm DNA and 10 % (w/v) dextran sulphate. The RNA was hybridized overnight at 42 °C with the labelled probes, and washed twice in 6 × SSPE/0.1 % (w/v) SDS at room temperature for 20 min, followed by two washes in 1 × SSPE/ 0.1 % (w/v) SDS at 55 °C for 30 min. The blot was air-dried, and then exposed overnight at −70 °C to Kodak XAR-5 film for developing.

Isolation of genomic DNA

Genomic DNA was isolated from harvested cultured skin fibroblasts by freeze–thawing (ten times) the cells suspended in lysis buffer (100 mM NaCl, 10 mM Tris/HCl, pH 8, 25 mM EDTA, pH 8, 0.5 % SDS, 0.1 mg/ml proteinase K) in a dry ice/ethanol bath [17]. An equal volume of phenol/chloroform was added, and DNA was precipitated by adding 0.5 vol. of 7.5 M ammonium acetate and 2 vols. of 100 % ethanol. The DNA pellet was rinsed with 70 % ethanol, and dissolved in TE buffer (10 mM Tris/HCl, 0.1 mM EDTA, pH 8).

PCR analysis

Exons 2–16 were amplified from 500 ng of patient or normal genomic DNA as described by the procedure by Saiki et al. [18]. The primers used to amplify the appropriate exons of the β-galactosidase gene and those used for site-directed mutagenesis are on the basis of the published intron–exon junction sequences [19]. DNA-amplification reactions were performed in a total volume of 100 μl, containing 100 ng of each primer, 10 units of *Taq* polymerase (Promega, Madison, WI, U.S.A.) and 0.5 mM each of dCTP, dGTP, dTTP and dATP, in 10 mM Tris/HCl, pH 8.3/50 mM KCl/1.5 mM $MgCl_2$. The reaction conditions used for PCR were 30 cycles comprising 1 min at 94 °C (denaturation), 70 s at 56 °C (annealing) and 1 min at 72 °C (extension), using the RoboCycler 40 (Stratagene, La Jolla, CA, U.S.A.) thermal cycler. PCR products were run on a 1 % agarose gel to check for insertions or deletions, before single-strand conformation polymorphism (SSCP) analysis was performed.

SSCP analysis

SSCP analysis was performed at either room temperature or 4 °C with 6 % (w/v) polyacrylamide gels in 0.5 × TBE running buffer (where 1 × TBE is 45 mM Tris/borate/1 mM EDTA) containing 5 % (v/v) glycerol (40 W), as described in refs. [20] and [21]. The gels were fixed in 50 % (v/v) methanol and 10 % (v/v) acetic acid solution for 1 h, and then were washed three times in distilled water for 15 min, followed by staining in a solution containing equal volumes of 0.5 M sodium carbonate and 10 mM silver nitrate/25 mM ammonium nitrate/3.5 mM tungstosilicic acid/ 0.8 % (v/v) formalin for 10–30 min. The reaction was stopped by the addition of 10 % acetic acid.

DNA sequencing

PCR products were sequenced directly, or after ligating them into the TOPO TA cloning kit vector (Invitrogen, Carlsbad, CA, U.S.A.) following the manufacturer's instructions. Non-radiolabelled PCR products were run on a 1 % agarose gel, excised, and then purified using the Glassmax DNA isolation system (Gibco BRL, Burlington, ON, Canada). Direct sequencing was performed using 100 ng of purified PCR product, 100 ng of primers, [α-^{35}S]dATP and the Sequenase kit (United States Biochemical, Cleveland, OH, U.S.A.), as recommended by the manufacturer.

Restriction enzyme analyses

*Dde*I

To examine the C → A transversion in codon 148 (Arg^{148}Ser), a 10-μl sample containing the 139-bp PCR product from exon 4 (primer sequences are shown in Table 1) was digested with 10 units of *Dde*I for 1 h at 37 °C, run on a 10 % polyacrylamide gel and silver-stained.

*Bsr*G1

For the Asp^{332}Asn mutation, PCR reactions included the upstream primer (5′-AGCACAGCCCACCATGTAC-3′, where the underlined bases are mismatched), along with the usual downstream primer for exon 10 (Table 1) at 64 °C. In the presence of the G1044 → A transition, a *Bsr*GI site is created in the amplified product (125 bp), where digestion with the enzyme results in release of 17- and 108-bp fragments.

*Hpa*II

For the Ser^{532}Gly polymorphic mutation, part of exon 15 was amplified (Table 1) using genomic DNA and a specifically constructed upstream primer (5′-GGGCTGGGGACACCGTGCC-3)′ where C corresponds to a mispairing with the normal sequence, whereby, in the presence of the A → G transition, a *Hpa*II restriction site is created.

Construction in β-galactosidase of missense mutations found in G_{M1} gangliosidosis

Fragment-replacement mutagenesis was used to introduce the following mutations into wild-type β-galactosidase GP8. The Asp^{332}Asn, Arg^{148}Ser and Ser^{532}Gly mutations were then examined by transient expression in COS-1 and CHO cells. Wild-type β-galactosidase cDNA (GP8-pGEM) was used as the template, and primers are given in Table 1(B).

Arg^{148}Ser mutation

The 558-bp fragment containing the CGC → AGC change, with a 5′ *Sal*I site and a 3′ *Pvu*II site, was completely sequenced and then subcloned into these sites in the wild-type GP8 cDNA in pGEM-3Z.

Asp^{332}Asn and Asp^{332}Glu mutations

The initial 255-bp fragment with a 5′ *Eco*RI and a 3′ *Dra*III site, containing the GAC → AAC or GAC → GAG changes leading to the amino acid mutations of Asp^{332} → Asn or Asp^{332} → Glu respectively (205 bp after digestion with these enzymes), was purified, sequenced and subcloned into β-galactosidase GP8-pGEM-3Z.

Ser^{532}Gly mutation

The 505-bp fragment with 5′ and 3′ *Bam*HI sites containing the AGT → GGT change was purified, sequenced and subcloned into GP8-pGEM-3Z. For COS-1 cell expression, the wild-type and mutated forms of GP8 were inserted into the *Xho*I site of pSVL vector using T4 DNA ligase (1 unit/μg DNA for 12 h at 12 °C). For CHO cell expression, the wild-type and mutated forms of GP8 were inserted into pRc/RSV at the *Hin*dIII site, as

Table 1 Primers for the amplification of exons 4, 10, and 15 in β-galactosidase (a), and those for site-directed mutagenesis of specific residues in exons 4, 10 and 15 (b)

(a) In all cases, the melting temperature (T_m) was 60 °C (b) The nucleotide changes are underlined.

(a)

Exon	Upstream (5′ → 3′)	Downstream (5′ → 3′)	Product size (bp)
4	CGGAACAGACATTATAATGGC	GCTTTTATAAATCTTCTCAAGAC	139
10	TGGCACATTTTTGTCTTCTAG	GCACCCACCACAGCTCATA	165
15	CAGCTCACTGTGCTCTGTTT	GAATTCAAACCCTTCCCATGA	315

(b)

Location of mutation (codon affected)	cDNA primer position	Oligonucleotides used (5′ → 3′)	cDNA codon change	Mutation introduced
Exon 4 (Arg^{148})	Upstream	CGTCGACGGGGCGCCGA		
	Middle	CTATTCTTCTCAGCTCCTCCG	CGC → AGC	Arg^{148}Ser
	Downstream	ACTTGTCCACAGCTGCCAGG		
Exon 10 (Asp^{332})	Upstream	GCAGCTACTTTGCCTGTGATTT		
	Middle	GGGGCATCATAGTTGTAGCTG	GAC → AAC	Asp^{332}Asn
	Downstream	AACATATGCTCGATCGTGGAC		
Exon 10 (Asp^{332})	Upstream	GCAGCTACTTTGCCTGTGATTT		
	Middle	GGGGCATCATACTCGTAGCTGG	GAC → GAG	Asp^{332}Glu
	Downstream	AACATATGCTCGATCGTGGAC		
Exon 15(Ser^{532})	Upstream	AATAACCCTCACTAAAG		
	Middle	GACGGTGGCCACCATGATG	AGT → GGT	Ser^{532}Gly
	Downstream	AATACGACTCACTATAG		

described in detail previously [7]. All plasmids were examined for the correct orientation of inserts.

DNA transfection

CHO cells were transfected using the liposome-mediated (Lipofectin®) method, while the COS-1 cells were transfected using the adenovirus-mediated method.

Lipofectin® transfection

CHO cells were transfected with the pRc/RSV-GP8-Arg^{148}Ser, -Asp^{332}Asn, -Asp^{332}Glu and -Ser^{532}Gly constructs, and with wild-type GP8. CHO cells were grown until they had reached 80–85 % confluency. Of each construct, 20 μg was transfected separately with the Lipofectin® reagent (Gibco BRL), as described by Felgner et al [22]. After a 4-h incubation at 37 °C, medium was added and the cells were incubated for an additional 48–72 h before harvesting. CHO clones permanently transfected with pRc/RSV-GP8-Asp^{332}Asn and -Asp^{332}Glu were isolated as described previously [7].

Adenovirus-mediated transfection

COS-1 cells were grown to 80 %–85 % confluency for transfection [23] The growth medium was removed, and the cells were washed twice with 10 ml of PBS. Aliquots (1 ml) of diluted adenovirus-lysed HEK-293 cell media and 8 μg of pSVL-GP8-Arg^{148}Ser, -Asp^{332}Asn and -Ser^{532}Gly constructs, together with wild-type GP8 and DEAE-dextran (at a final concentration of 80 mg/ml), were added to the diluted adenovirus media. The DNA/adenovirus/DEAE-dextran mixture was added dropwise to the COS-1 cells, and incubated at 37 °C for 2 h. A chloramphenicol acetyltransferase (CAT) construct was included to check for transfection efficiency After the transfection incubation, the cells were washed once with 10 ml of PBS containing 10 % (v/v) DMSO, twice with 10 ml of PBS, and grown in 10 ml of medium for 2–3 days.

Enzyme purification, protein analysis and enzyme assays

Harvested cultured-skin fibroblasts and transfected cells were resuspended in 0.25 M Tris/HCl, pH 7.8, containing the protease inhibitors PMSF (1 mM) and leupeptin (10 mg/ml), subjected to ten freeze–thaw cycles, and soluble lysates were collected for enzyme and protein analyses. Recombinant Asp^{332}Asn and Asp^{332}Glu enzymes were purified from the medium above the CHO cells, as described previously [7,24]. To assess the amount of endogenous CHO enzyme in these preparations, we subjected the same volume of medium conditioned with non-transfected CHO cells to this isolation procedure. Protein content was determined either in duplicate or triplicate [25] with BSA (0.5 mg/ml) used as the standard. Enzyme activity was measured in duplicate by adding a 60-μl aliquot of enzyme solution to 190 μl of 0.6 mM artificial substrate, 4-methylumbelliferyl-β-D-galactopyranoside (Sigma, St. Louis, MO, U.S.A.) in 50 mM citrate/100 mM phosphate buffer, pH 4.3 [7,24]. For measurement of the kinetic constants, the volume of substrate used was increased to 240 μl, to which was added a 10-μl aliquot of enzyme diluted into the above buffer containing BSA (0.1 mg/ml). After incubation at 37 °C for 30 min, all reactions were stopped by adding 2 ml of 0 1 M 2-methylpropan-1-ol buffer, pH 10, and the fluorescence was determined with an excitation wavelength of 365 nm and an emission wavelength of 450 nm with a Perkin–Elmer (model 650-40) spectrofluorimeter (Norwalk, CT, U.S.A.). A known amount of 4-methylumbelliferone (Eastman Kodak Company, Rochester, NY, U.S.A.) in 0.1 M 2-methylpropan-1-ol, pH 10, was used as a standard. Transfection efficiency was monitored by the CAT activity using the phase-extraction system [26].

Western blot analysis

Cells were harvested by scraping in PBS, and lysed by sonication, as described previously [9]. Fibroblast protein (30 μg) and 20 μg of total COS-1 and CHO cellular protein were analysed using SDS/PAGE. Samples were reduced by boiling for 5 min in 62.5 mM Tris/HCl/3 % (w/v) SDS/10 mM dithiothreitol, and then loaded on to an 8 % Bio-Rad (Mississauga, ON, Canada) Mini-Gel SDS/PAGE system, run as described by Laemmli [27]. Proteins were transferred overnight to nitrocellulose, and the resultant Western blot was probed using a 1 : 1500 dilution of our well-characterized rabbit IgG (P-Gal) raised against purified human β-galactosidase precursor, as described previously [7,9]. Immunoblots were developed using the enhanced chemiluminescence system (ECL®) Western Blot (Amersham, Oakville, ON, Canada).

Immunolocalization of β-galactosidase in intracellular compartments

Patient 1 and control fibroblasts were incubated for 48 h in α-MEM medium with 10 % (v/v) fetal-bovine serum at 37 °C in an air/CO_2 (19 : 1) mixture, to which 20 μM leupeptin was added. We have previously shown in normal and galactosialidosis fibroblasts that leupeptin reduces the lysosomal degradation of β-galactosidase, resulting in a prolonged half-life and an increased level of the enzyme activity, without affecting the correct processing of the enzyme to its mature form [9]. Leupeptin-treated fibroblasts were analysed for protein by Western blot analysis, for enzyme activity and for immunolocalization of β-galactosidase. Immunolocalization of β-galactosidase was performed in non-transfected and permanently transfected CHO cells with the wild-type β-galactosidase, $Asp^{332}Asn$ and $Asp^{332}Glu$ constructs. Cells were grown in α-MEM medium with 10 % (v/v) fetal-bovine serum at 37 °C in air/CO_2 (19 : 1) on glass cover slips and, after 48 h, the cells were fixed and gently permeabilized with 100 % cold methanol at −20 °C for 30 min. The fixed cells were then washed in PBS, blocked with 1 % BSA, and incubated for 1 h with rabbit IgG raised against purified human β-galactosidase precursor, as described above (diluted 1 : 200). The secondary antibody, a green fluorescein-labelled goat-(anti-rabbit) IgG (Fab2), diluted 1 : 100, was then added for 1 h, either alone or in combination with a 1 : 10000 dilution of propidium iodide (which, in addition to nuclear DNA, also stains cytoplasmic RNA and RNA bound to the rough ER), thereby marking the position of the ER by the location of red fluorescence. The cells were then washed three times with PBS and mounted with elvanol. In control cultures, the preimmune rabbit IgG was substituted for the primary antibody.

The slides were analysed, and the proportion of immunoreactive protein present in the ER or the endosome/lysosome was determined using a fluorescent microscope (Olympus Vanox-AH-3; magnification × 800) and two narrow-band filters to detect the green and red fluorescence separately. An additional broad-spectrum filter was also used for the simultaneous detection of the green fluorescein-tagged P-gal antibody and the nucleic acids labelled with red propidium iodide fluorescence. In this setting, the overlapping of the red and green fluorescence in the cytoplasm gave rise to a yellow fluorescence, which indicated the co-localization of β-galactosidase with the ER. Multiple images of the same cell obtained with all of the abovementioned filters were captured with a charge-coupled-device (CCD) camera (Optronics, Galeta, CA, U.S.A.), stored in a MacIntosh 9500 computer, and quantitatively analysed using the Image Pro Plus program (Media Cybernetics, Silver Spring, MD, U.S.A.), according to the manufacturer's instructions. In each of the three experimental groups (wild-type, $Asp^{332}Asn$ and $Asp^{332}Glu$), images of 50 cells were analysed, and results were statistically evaluated to give quantitative measurements of the percentage of the area occupied by the anti-(β-galactosidase) reactive ligands that reside in the ER (green and red fluorescence overlapped), and in the endosomal and lysosomal compartments (green fluorescence alone). Cultures of COS-1 cells transiently transfected with wild-type and $Asp^{332}Asn$ constructs, maintained in small dishes with coverslips, were fixed as described above. Separate coverslips were incubated for 1 h with PBS-diluted primary antibody (2 μg/μl) followed by a 1-h incubation with the appropriate fluorescein (FITC)-conjugated goat-(anti-rabbit) or goat-(anti-mouse) secondary antibodies. An additional 10-min incubation with propidium iodide (0.1 μg/ml) ensured the nuclear counterstaining. The coverslips were mounted on glass slides with elvanol, and analysed using an Olympus Vanox AH-3 fluorescence microscope.

RESULTS

Level of β-galactosidase protein

Western blot analysis of cultured skin fibroblasts showed that the patient (Figure 1, lane 3), like most other G_{M1} patients (two examples are shown in Figure 1, lanes 4 and 5) we have examined to date, has barely detectable amounts of the 64 kDa mature form of the enzyme (the normal amount is shown in lane 2). The 84 kDa precursor, which we have previously shown [9] amounts to approx. 20 % or less of the total β-galactosidase in fibroblasts, is proportionately lower in abundance in all the G_{M1} cell strains examined compared with normal cells. The Morquio type B strain (lane 6), which has approx. 5 % residual β-galactosidase activity, has proportionately decreased amounts of the 84 kDa precursor and the 64 kDa mature form. Northern blot analysis showed that the abundance and size of the mRNAs were normal for case 1, as in all the other cases examined (results not shown).

Identification of the mutations

SSCP analysis was used to screen for mutations in exons 2–16 using intron/exon primers, as described by Morreau et al. [19].

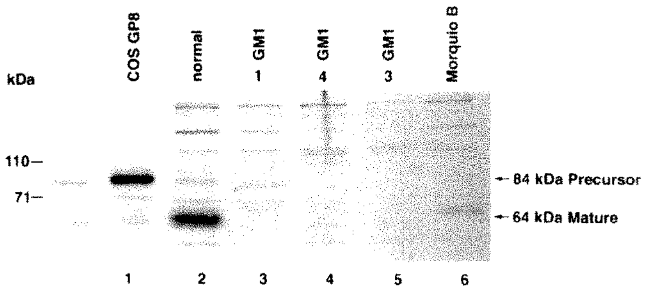

Figure 1 Western blot of fibroblast cell lysates from three G_{M1}-gangliosidosis and one Morquio type B patients

Of total cellular protein, 30 μg was analysed by SDS/PAGE and probed using an antibody that cross-reacts with the 84 kDa precursor and 64 kDa mature forms of β-galactosidase. Lane 1 (positive control) corresponds to wild-type β-galactosidase transiently expressed in COS-1 cells, and demonstrates the location of the 84 kDa precursor. Lane 2 is from a normal fibroblast control, showing the small amount of precursor and the abundant 64 kDa mature form of β-galactosidase. Lane 3 shows the index case, case 1, where very little precursor and no mature protein is visible. This is comparable with other G_{M1}-gangliosidosis patients, such as cases 3 and 4 (lanes 5 and lane 4 respectively), where no precursor and no mature protein is visible. For comparison, lane 6 corresponds to a fibroblast lysate from Morquio type B (case 5, positive control) where reduced amounts of precursor and mature enzyme are visible.

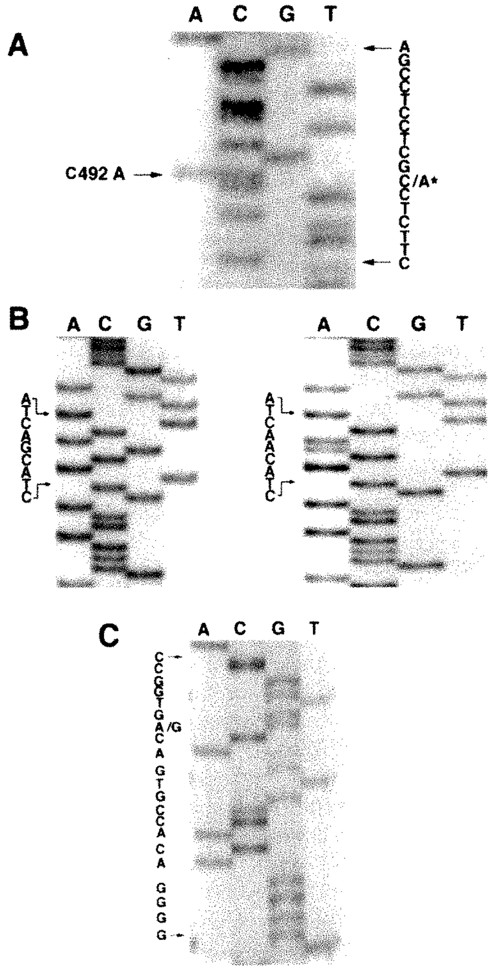
A
A C G T
C492 A
A G C C T C C T C G C/A* C C T C T T C
B
A C G T
A T C A G C A T C
A C G T
A T C A A C A T C
C
A C G T
C C G G T G A/G C A G T G C C A C A G G G G

Figure 2 Sequencing analysis showing three different mutations in the β-galactosidase gene in G_{M1}-gangliosidosis cases

All of the sequencing used PCR-amplified genomic DNA as template. (**A**) The C492 → A transversion mutation is shown, leading to an Arg^{148}Ser amino acid substitution found in case 1, where the presence of both C and A indicates heterozygosity at this position. (**B**) The PCR products were subcloned as described. Only the area containing the mutation is shown. The left panel shows the normal sequence found on the one allele in case 1, whereas the right panel shows the G1044 → A change in case 1, which converts Asp^{332} into Asn. (**C**) The A1644 → G change shown here was from case 4, who was homozygous for this mutation and for Arg^{351} 'Stop' (result not shown). Cases 1 and 3 were heterozygous for the A1644 → G mutation.

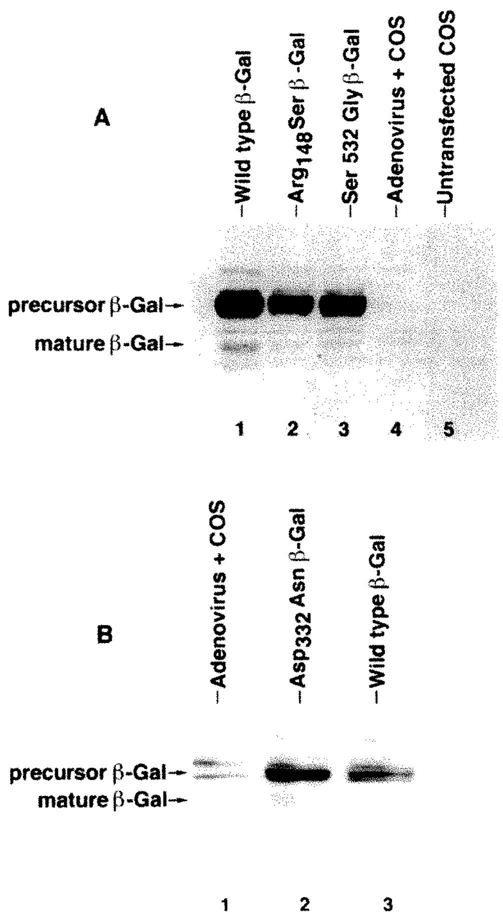

Figure 3 Western blot analysis of transfected COS-1 cells

(**A**) COS-1 cells were transfected with wild-type pSVL-GP8 cDNA (lane 1), pSVL-GP8-Arg^{148}Ser cDNA (lane 2) and pSVL-GP8-Ser^{532}Gly cDNA (lane 3), and processed as described in the Materials and methods section. No cross-reacting material (lanes 4 and 5) was detected in the mock-adenovirus-transfected or the untransfected COS-1 cells. (**B**) COS-1 cells were mock-adenovirus-transfected (lane 1) or transfected with pSVL-GP8-Asp^{332}Asn (lane 2) or wild-type pSVL-GP8 cDNA (lane 3). β-Gal, β-galactosidase.

A 139-bp PCR product, obtained from amplification of exon 4, produced an SSCP-mobility shift in DNA from case 1, but not in cases 2, 3 and 4 (results not shown). Direct sequencing of this product from case 1 identified a C492 → A transversion (Figure 2A), which resulted in an Arg^{148}Ser substitution. This mutation creates a *Dde*I site (generating fragments of 82 bp and 57 bp from the 139-bp product), which was used to analyse all the other G_{M1} cases used in this study. The C492 → A transversion mutation was identified on one allele in a second case of infantile G_{M1} gangliosidosis (case 2), described previously [14]. The mutation on the second allele in case 2, G1445 → A, converts Arg 482 into His, and has been described previously [16]. The C492 → A (Arg^{148}Ser) mutation was not detected in 50 unrelated normal individuals, indicating that it was unlikely to be a common polymorphism. On SSCP analysis of the proband exon 10 (Table 1), a band shift was noted, and a G1044 → A mutation (which converts Asp ^{332} into Asn) was detected on sequencing both the direct and subcloned PCR products (Figure 2B). To examine the occurrence of this mutation in the population, we constructed an oligonucleotide 5′-A_{1025}GCACAGCCCACCATGTAC$_{1043}$-3′ (where TG are mismatched nucleotides) which, in the presence of the G1044 → A mutation, creates a unique *Bsr*GI restriction site (*Bsr*GI cleavage of the 125-bp product generates 108-bp and 17-bp products). This mutation was not detected in 50 unrelated individuals, indicating it is unlikely to represent a polymorphic change. Upon amplification of exon 15, the 191-bp PCR product undergoes an SSCP shift that was seen in cases 1, 3 and 4. Both the proband and case 3 were heterozygous for this change, whereas case 4 was homozygous. This SSCP shift indicated the presence of a third mutation in case 1, identified as an A1644 → G change converting Ser ^{532} into Gly (Figure 2C), and is judged to be a common polymorphism, since it was detected in 5 out of the 20 normal individuals tested. Its occurrence is easily detected using *Hpa*II restriction-enzyme digestion, since the 191-bp PCR product is cleaved into 119-bp and a 72-bp fragments when the mutation is absent, and 119-bp and 53-bp products when the A1644 → G change is present. The disease-associated C492 → A (Arg^{148}Ser) and the polymorphic A1644 → G (Ser^{532}Gly)

Table 2 β-Galactosidase activity associated with mutations as measured in transiently transfected COS-1 cell lysates

The activities are representative average values from replicate plates, and were corrected for transfection efficiency using the CAT assay. The activity in mock-transfected COS-1 cells was the separately determined baseline value in each experiment, and this value was subtracted from all values in that experiment. This experiment was performed independently three times. –, not determined.

	β-Galactosidase activity (nmol/h per mg of protein)	% of wild-type
COS + adenovirus	272	–
Wild-type GP8-β-gal pSVL	720	100
$Arg^{148}Ser$ β-gal pSVL	601	83.5
$Ser^{532}Gly$ β-gal pSVL	583	81.0
$Asp^{332}Asn$ β-gal pSVL	256	0

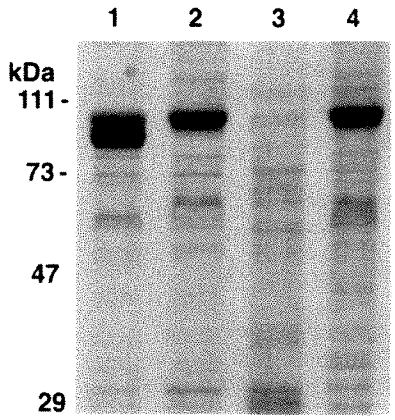

Figure 4 SDS/PAGE of purified $Asp^{332}Asn$- and $Asp^{332}Glu$-β-galactosidase

Wild-type and mutant β-galactosidases were purified from medium conditioned with CHO cells permanently transfected with wild-type β-galactosidase or the respective recombinant β-galactosidases. The enzymes were purified on the substrate analogue-affinity column, as described in the Materials and methods section. Lanes 1–4 respectively were loaded with 5 μg of the purified wild-type enzyme (lane 1), the purified $Asp^{332}Glu$ enzyme (lane 2) and the $Asp^{332}Asn$ enzyme (lane 4); lane 3 contains 5 μg of protein purified from medium above untransfected CHO cells. The molecular-mass standards are indicated. The proteins were detected by Coomassie Blue staining.

mutations were found in the mother of the proband, and the exon 10 G1044 → A, $Asp^{332}Asn$ change was found in the father (results not shown). Interestingly, case 2, the second patient in which we found the C492 → A, $Arg^{148}Ser$ mutation in exon 4, was also polymorphic for A1644 → G, $Ser^{532}Gly$. However, this appears to be a fortuitous association, because the case 4 cell line was found to be homozygous for both a new nonsense mutation and for A1644 → G, $Ser^{532}Gly$ (S. Zhang, R. Bagshaw and J. W. Callahan, unpublished work).

Expression of mutated β-galactosidase in COS-1 and CHO cells

We examined expression of these mutations in both COS-1 and CHO cells. In general, COS-1 cells amplify the transfected cDNA, and high levels of mRNA encoding the transfected gene are transcribed. In this instance, abundant β-galactosidase protein was produced (Figure 3). Therefore expression in this system allows us to differentiate between mutations that affect the active site, and those that do not. When expressed in COS-1 cells, all of these constructs yielded high levels of the 84 kDa precursor, with small amounts processed to the 64 kDa mature form of the enzyme, as judged by Western blot analysis (Figure 3). Both the $Arg^{148}Ser$ and the $Ser^{532}Gly$ β-galactosidases showed substantial levels of enzyme activity, whereas the $Asp^{332}Asn$ β-galactosidase gave < 1 % residual activity, suggesting that the $Asp^{332}Asn$ mutation affected the active site of the enzyme (Table 2). As the COS-1 β-galactosidase is only weakly cross-reactive with our antibody, only small amounts of cross-reacting material (Figure 3) were detected in the untransfected and the mock-adenovirus-transfected host cells. We then performed transient expression in CHO cells where, because only a minor degree of amplification of the cDNA occurs, considerably less mRNA would be transcribed compared with COS-1 cells resulting in less directed β-galactosidase synthesis by these cells. In this case, the ER 'quality-control' system would be expected to function normally, and we would be better able to discriminate between mutations that affected folding and those that did not. In addition, CHO cells process human β-galactosidase to generate both the mature enzyme and its degradation products [7,9]. When the effect of the $Arg^{148}Ser$ and $Ser^{532}Gly$ mutations were compared with the GP8 wild-type control using transient transfections in CHO cells, we found markedly reduced levels of activity attributable to the $Arg^{148}Ser$ mutant enzyme (Table 3), while the levels of activity produced from the polymorphic $Ser^{532}Gly$ form were virtually indistinguishable from those of the GP8 wild-type control. Taken together, these expression data suggest the $Arg^{148}Ser$ mutant β-galactosidase, while catalytically active (as judged from the COS-1 expression), is largely degraded (presumably in the ER, as shown in Figure 5A below). This

Table 3 β-Galactosidase activity measured in transfected CHO cell lysates

Enzyme activity was measured in duplicate from each of two separate dishes for each experiment, as described in the Materials and methods section. Corrected specific activities are values obtained after subtraction of the CAT controls. Exper, experiment; –, not applicable.

	Specific activity (nmol/h per mg of protein)					
	Uncorrected		Corrected		% of corrected wild-type control	
Transfectant	Exper 1	Exper 2	Exper 1	Exper 2	Exper 1	Exper 2
Mock	641	548	–	–	–	–
CAT	755	576	–	–	–	–
Wild-type GP8	1122	1165	367	589	100	100
GP8-$Arg^{148}Ser$	786	658	31	82	8.4	13.9
GP8-$Ser^{532}Gly$	1030	1147	275	571	74.9	96.9

Table 4 Kinetic constants of wild-type and mutant β-galactosidases

The recombinant precursor proteins were purified on the substrate-analogue affinity column and concentrated as described in the Materials and methods section. Total activity represents the units of activity from 600 ml of conditioned medium bound to and eluted from the 1-ml affinity column. Eight substrate concentrations in the range 0.15–0.55 mM were used to derive kinetic constants by curve-fitting to a rectangular hyperbola using the SigmaPlot for Windows program, version 4.0 (Jandell Scientific). All values are the means ± S.D. for at least three determinations. –, not determined.

Form of the enzyme	Total activity (μmol/h)	Specific activity (μmol/h per mg of protein)	K_m (mM)	V_{max} (μmol/h per mg of protein)
Human placenta, mature*	–	500	0.43	660
Wild type, precursor†	–	827 ± 338	0.29	989
Wild type, precursor, the present study	1027.0	379 ± 105	0.36 ± 0.23	490 ± 172
Asp^{332}Asn, precursor, the present study	3.53	1.03 ± 0.61	0.35 ± 0.02	1.82 ± 0.05
Asp^{332}Glu, precursor, the present study	5.26	2.94, 3.10	0.32 ± 0.03	4.44 ± 0.20
Non-transfected medium, the present study	3.75	1.89	0.15 ± 0.08	2.26 ± 0.28

*, Taken from [24]; †, see [7,8].

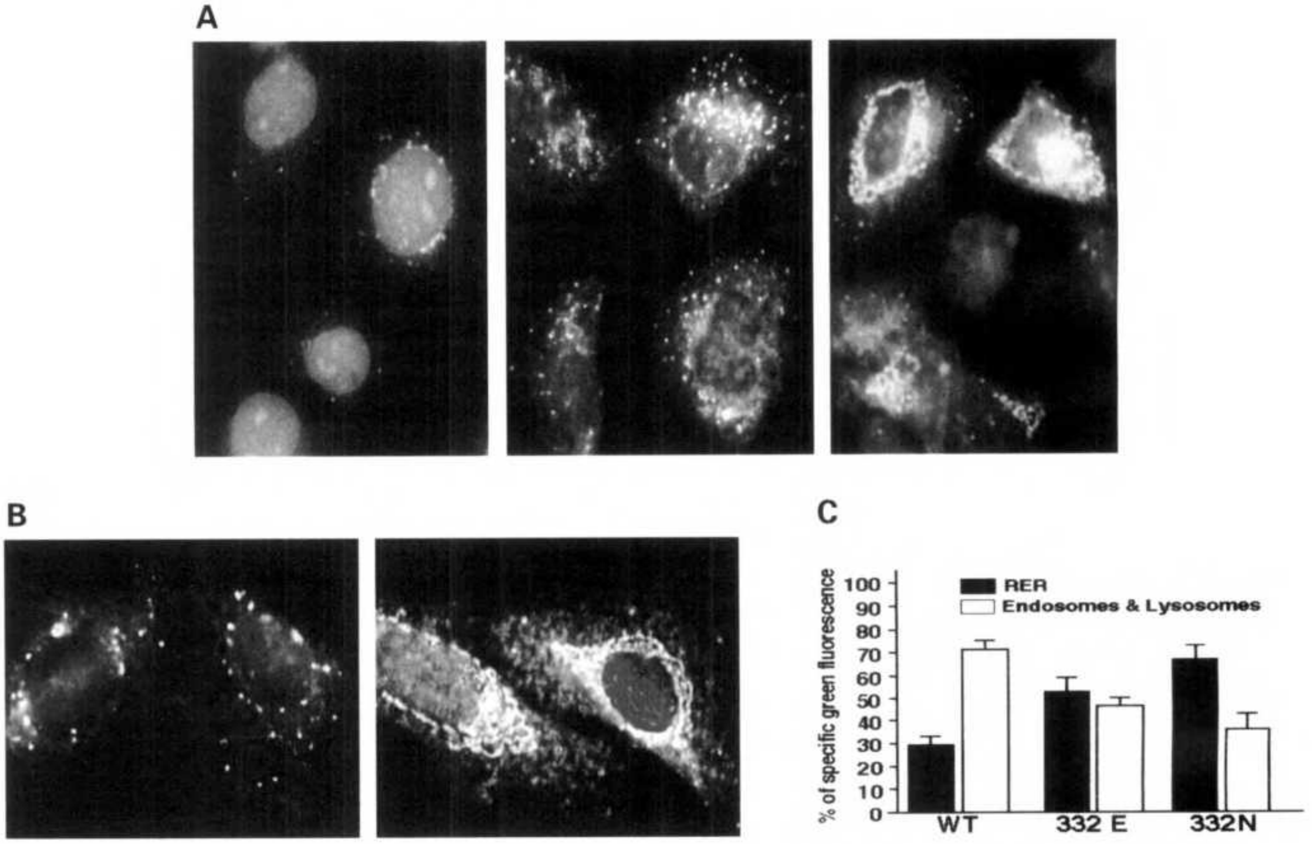

Figure 5 Immunofluorescence detection of β-galactosidase

(**A**) COS-1 cells were transiently transfected with vector alone (left panel), with wild-type pSVL-GP8-β-galactosidase (centre panel) or with pSVL-GP8-Asp^{332}Asn (right panel). Nuclei were stained with propidium iodide. Very little β-galactosidase is detected with the P-Gal antibody in the mock-transfected cell (left panel). With wild-type pSVL-GP8 β-galactosidase (centre panel) immunostaining is detected in punctate organelles distributed throughout the cytoplasm, whereas with pSVL-GP8-Asp^{332}Asn β-galactosidase (right panel), immunostaining is localized primarily to the cisternae of the ER, with a small but discernible reaction detected in lysosomes. (**B**) When CHO cells were transiently transfected with the mutant construct, pRc/RSV-GP8-Arg^{148}Ser β-galactosidase (right panel), strong immunostaining is found in cisternae and in the perinuclear area suggesting localization of the enzyme primarily in the ER, whereas with vector pRc/RSV alone (left panel) a lower level of immunostaining was seen and, as expected, the endogenous host cell enzyme was localized primarily in the lysosomes (left panel). (**C**) shows the immunolocalization of β-galactosidase in permanently transfected CHO cells by graphical representation of the percentage of the various β-galactosidases [wild-type GP-8 (WT), Asp^{332}Asn (332N) or Asp^{332}Glu (332E)] localized in the endosome–lysosome compartment or the ER. The bars represent the S.D. of each value obtained from the analyses of 50 cells per experimental group.

would then account in part for the lack of detectable β-galactosidase, cross-reacting material in fibroblasts from this patient.

Since the naturally occurring Asp^{332}Asn mutation, when expressed in COS-1, resulted in ample amounts of protein, but negligible catalytic activity, it was of interest to examine in

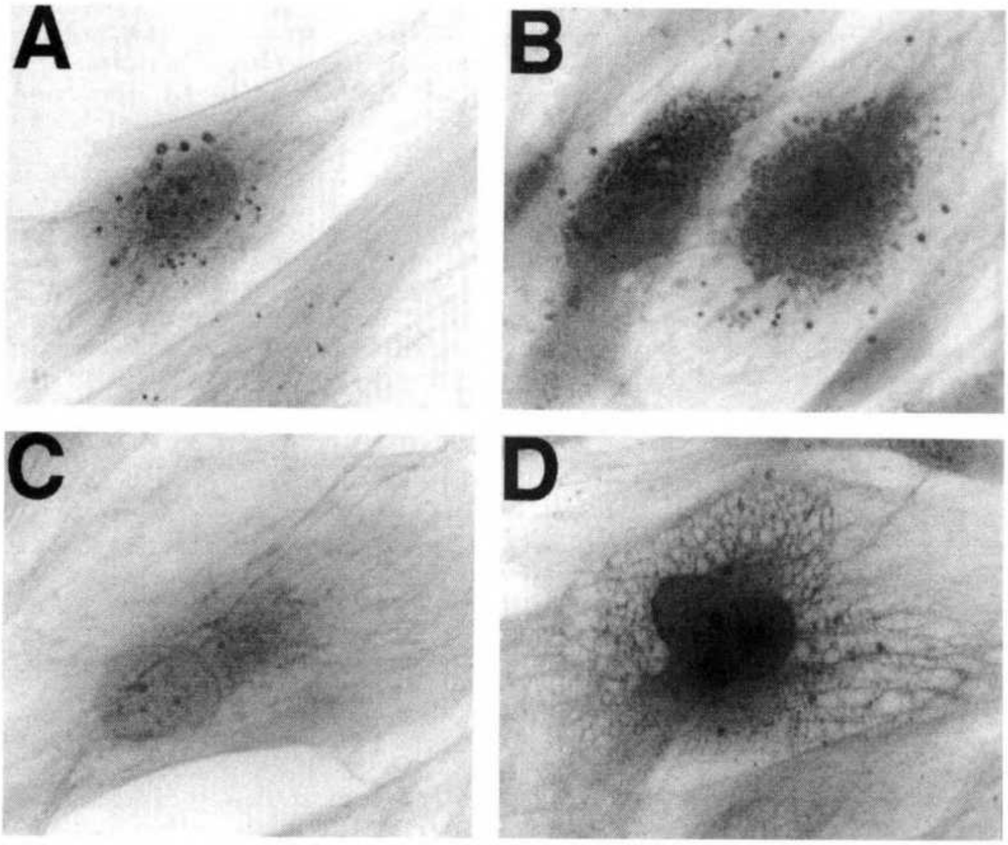

Figure 6 Immunofluorescence detection of β-galactosidase in fibroblasts incubated in the presence of leupeptin

Control (**A** and **B**) and patient's (**C** and **D**) fibroblasts were incubated for 48 h in the absence (**A** and **C**) or presence (**B** and **D**) of leupeptin (20 μM). As expected, the specific activity of β-galactosidase increased in the control cells (from 681 nmol/h per mg of protein to 994 nmol/h per mg of protein), and the enzyme was immunolocalized almost exclusively in lysosomes. In the patient's fibroblasts there was no change in the enzyme activity (undetectable in the presence or absence of leupeptin), the level of immunodetectable enzyme remained much lower than in normal cells, and was found primarily in the perinuclear area and the cisternae of the ER (**C** and **D**), with some found additionally in lysosomes (with leupeptin; **D**).

greater detail a possible role for Asp^{332} in the active site. To do this we converted Asp^{332} into both Asn^{332} and Glu^{332}, and isolated permanently transfected CHO cell clones expressing high levels of these enzymes. We have used a similar approach to successfully purify and characterize the normal β-galactosidase precursor [7,8]. Mutant $Asp^{332}Asn$, $Asp^{332}Glu$, and wild-type β-galactosidases were purified to apparent homogeneity (Figure 4, lanes 1, 2 and 4) in a single step from the CHO cell medium on the phenylthio-β-D-galactoside–Sepharose substrate-analogue affinity column, under the standard conditions described previously [8,24]. As a control, a corresponding amount of medium conditioned with non-transfected CHO cells was run to account for any host contribution to the protein (Figure 4, lane 3) and activity (Table 4). We then determined kinetic constants for the mutant enzymes (Table 4). The 'V measured against S' plots followed Michaelis–Menten kinetics at two enzyme concentrations up to the highest limit of substrate solubility, and the calculated K_m values were the same as those obtained for the wild-type control. Although the V_{max} values alone were substantially lowered, the value for $Asp^{332}Glu$ β-galactosidase was twice that of the $Asp^{332}Asn$ β-galactosidase, a result that reinforces a putative role for Asp^{332} in the active site of the enzyme.

Immunofluorescence localization of mutant β-galactosidases

On the basis of the above results, the residual activity in the patient's cells should be no less than 50% (activity from $Arg^{148}Ser$) if all the enzyme synthesized were to arrive in the lysosome, with subsequent stabilization there. However, as shown in Figure 1, the patient's fibroblasts consistently displayed negligible amounts of β-galactosidase activity or cross-reacting material, suggesting that the bulk of the synthesized enzyme either does not reach this compartment or is rapidly degraded upon its arrival. The $Arg^{148}Ser$ mutation replaces a bulky, positively charged residue with a smaller and less polar one, and a Garnier plot predicts a change in the conformation of the protein, i.e. the resulting protein is at least partially misfolded and, on the basis of studies with other lysosomal hydrolases [28], might be degraded in the ER. However, the $Asp^{332}Asn$ mutation does not alter the Garnier plot, suggesting only a minor effect on folding. To address these questions, we used immunofluorescence to examine the localization of the individual mutant enzymes. For the $Arg^{148}Ser$ mutant, the bulk of the protein was found in the perinuclear network (Figure 5B), consistent with its localization in the ER, with a barely discernible reaction in lysosomes. The $Asp^{332}Asn$ β-galactosidase was also found principally in the perinuclear area in the transiently transfected COS-1 cells. Lysosome localization was more discernible, although still significantly lower than normal (Figure 5A). The bulk of the wild-type control enzyme was found in the endosome–lysosome compartment, as expected (Figure 5A and 5C). In the permanently transfected CHO cells (Figure 5C), the bulk (approx. 70%) of the wild-type immunoreaction was localized to the endosome–lysosome compartment, with 30% detected in the ER (Figure 5C). In contrast, about 65% of the Asp^{332}Asn β-galactosidase and 50% of the Asp^{332}Glu β-galactosidase were found in the ER. Since it could be argued that stability of mutant human β-galactosidase in these hosts might be compromised by the absence of protective protein/Cathepsin A and neuraminidase, key members of a complex found in lysosomes that affect the stability and processing of β-galactosidase, we examined the immunolocalization of the enzyme in the patient's fibroblasts in the presence and absence of leupeptin. This potent inhibitor of lysosomal thiol proteases has no effect on conversion of β-galactosidase from the precursor into the mature form or its ability to form the complex, but does slow its rate of degradation [9]. Furthermore, since the Arg^{148}Ser mutation results in an active enzyme, we postulated that slowing its degradation might foster its stabilization via complex formation and result in a significant increase in activity in the cells. However, in the presence of leupeptin, the level of β-galactosidase activity remained negligible in the patient's cells, and only a small but detectable increase was noted in the amount of precursor on the basis of the result of a Western blot (results not shown). Although the intensity of immunostaining in the patient's cells (Figures 6C and 6D) was significantly less than in the control (Figures 6A and 6B), an increased cell immunoreactivity of the patient was detectable in the presence of leupeptin, and was localized to both the ER and the endosomal–lysosomal compartment (Figure 6D). These findings are in complete accordance with our immunolocalization (Figure 5), and other expression, studies (Tables 2 and 3).

DISCUSSION

Although our studies focus on the mutations and their impact on the fate of the resulting protein from case 1, G_{M1} gangliosidosis cases 2 and 3, used as positive controls in this study, and indeed in all of the cases we have studied to date (at least 10) where mutations are of the missense type, also have little or no precursor or mature β-galactosidase protein. The reasons for this are readily apparent from the expression and immunofluorescence studies included in the present report, and are able to be generalized, at least in part. Transient expression of the Arg^{148}Ser and the Asp^{332}Asn mutations in COS-1 and CHO cells results in proteins that are largely confined to the perinuclear area of the cell, specifically the ER, presumably because they are not folded to the lowest energy state compatible with its complex quality-control system, and are subsequently degraded there. A small fraction of the enzyme survives, and reaches the lysosome. This alone might account for the low levels of enzyme protein and minimal enzyme activity in the fibroblasts. Of the approximately 29 missense mutations in the β-galactosidase gene that have been reported, few have been studied by expression in host cells where assays such as Western-blotting or immunofluorescence were included (reviewed in [10]). Consequently, details on the impact of many of these mutations on the active site or intra-organellar transit of β-galactosidase must be inferred with little information known directly about how these mutations affect folding of the enzyme in the ER. However, recently Bradford et al. [29] expressed a Cys^{91}Thr mutation in the gene for *N*-acetylgalactosamine 4-sulphatase, the enzyme deficient in Maroteaux–Lamy disease (MPS VI), and found that, although the enzyme was synthesized normally and was active, it was nonetheless rapidly degraded in an early-ER compartment. Their data are in agreement with the present findings.

Transient overexpression in COS-1 cells allowed us to readily discriminate mutations affecting catalytic activity from those that did not, because in both instances the high levels of protein produced forced the folding of the enzyme generating substantial amounts of active (as in the case of Arg^{148}Ser) or inactive (as with Asp^{332}Asn) enzyme However, in the CHO cells, the vector-directed rate of synthesis of the recombinant enzymes is much lower than in COS-1 cells, and does not exceed the quality-control system of the ER in this cell type [30–32]. Consequently, because of the predicted alteration in the folding arising from the Arg^{148}Ser mutation, and consistent with our fibroblast results, total activity resulting from this construct was much lower in CHO cells (11% of normal) compared with COS-1 cells. In the case of the Asp^{332}Asn mutation, although the Garnier plot does not predict a major alteration in conformation, a significant proportion of the enzyme nevertheless was localized to the ER, reinforcing the view that the ER quality-control system is exquisitely sensitive, even to slightly misfolded proteins. Taken together, these results indicate that both the Asp^{332}Asn and the Arg^{148}Ser mutations alter the conformation sufficiently such that the newly synthesized enzyme precursor cannot readily exit the ER, and a substantial proportion is degraded there. We have previously shown in both normal and galactosialidosis-affected fibroblasts that treatment with leupeptin results in increased levels of precursor and mature lysosomal forms of β-galactosidase by decreasing their rate of degradation [9] Since there was no measurable enhancement of β-galactosidase activity in fibroblasts from the proband under these conditions, this suggests that little of the enzyme synthesized actually reaches this organelle, thus supporting the conclusion that the mutations in this patient result in degradation of the enzyme in a pre-lysosomal compartment, i.e the ER. Earlier studies predicted that secretory and plasma membrane proteins that were not folded absolutely correctly were retained and degraded in the ER [33,34]. Another example is provided by Tay–Sachs disease, caused by mutations affecting the α-subunit of hexosaminidase A, where of the 87 missense mutations described to date only α-Arg^{178}His results in near-normal amounts of cross-reacting material in lysosomes of fibroblasts [35].

Our identification of Glu^{268} as the catalytic nucleophile in human β-galactosidase [8], confirming the catalytic mechanism as a Koshland double-displacement reaction [7], means that substrate hydrolysis occurs via a nucleophilic attack, with formation of an α-linked galactosyl-Glu^{268} intermediate. In this mechanism, which is comparable with that established for *Escherichia coli* β-galactosidase [36], the degalactosylation reaction requires a second acidic amino acid, the acid/base catalyst, for the release of the galactosyl moiety, accompanied by the addition of water and retention of the β-configuration [7,8]. Purified Asp^{332}Asn β-galactosidase and Asp^{332}Glu β-galactosidase mutant enzymes display at least a 270-fold and 110-fold lower level of catalytic activity, respectively, compared with the wild-type precursor. The fact that both the mutant enzymes result in major decremental effects on the V_{max} parameter, but not on the K_m value, in the presence of a significant amount of expressed protein provide suggestive evidence that Asp^{332} has a role in the active site. Because the host CHO enzyme cannot be easily separated from the expressed human enzymes under the affinity-column conditions, at least a portion of the residual activity must be attributed to the CHO enzyme. Whether Asp^{332}

might serve as the second residue in the catalytic mechanism cannot be ascribed with certainty until the contaminating host cell enzyme is decreased to a minimum and the roles of the only other strictly conserved acidic residues (such as Glu^{129}, Glu^{186}, Glu^{188} and Glu^{339}) have been defined. We now have preliminary evidence that conversion of Glu^{339} has no effect on enzyme activity, and we have found that introducing a hexahistidine epitope tag at the C-terminal end of the protein has no effect on enzyme activity (S. Zhang and J. W. Callahan, unpublished observations), thus offering a solution to these problems. It is noteworthy that Asp^{332} resides in an 11-amino-acid motif (-Thr^{329} to Glu^{339}-), where the five-member sequence containing Asp^{332} (-Thr^{329}Ser^{330}Tyr^{331}Asp^{332}Tyr^{333}-) and Glu^{339} are absolutely conserved in all species in the family (Family 35, as defined by Henrissat [37–40]), which also includes mouse [41], dog [42] and a series of plant β-galactosidases (asparagus, apple, *Aspergillus* and other plants) [8]. Of the many missense mutations defined to date (reviewed in [10]), only Asp^{491}Asn, recently identified by Giuliani and co-workers [43], and Glu^{632}Gly, identified by Boustany et al. [44], involve acidic residues. Asp^{491} is not conserved in these β-galactosidases, and resides outside the major conserved domains in the protein, while Glu^{632}Gly occurs in the C-terminal region of the protein, a part of the enzyme that is removed during intra-lysosomal processing to the mature enzyme and is therefore unlikely to play any role in the catalytic mechanism. In summary, we have defined new mutations in the β-galactosidase gene in a single case of G$_{M1}$ gangliosidosis, and have shown that, by expressing them in different host cells, it is possible to discriminate those that have effects primarily on the catalytic activity from those that have an effect on enzyme folding in the ER. We also show in the case of Asp^{332}Asn that a single mutation can affect both the enzyme's ability to be transported out of the ER and its catalytic activity.

We are indebted to Dr Don Mahuran for helpful discussions during the course of this work and for a critical reading of the manuscript, and to Marie-Anne Skomorowski and Irene Warren for technical support This work was supported by the Research Institute, The Hospital for Sick Children, and by the Medical Research Council of Canada (grant MT 13719)

REFERENCES

1 Suzuki, Y, Sakuraba, H and Oshima, A (1995) β-Galactosidase deficiency (β-Galactosidosis) GM1 gangliosidosis and Morquio B disease. In Metabolic Basis of Inherited Disease, vol. 2 (Scriver, C R., Beaudet, A, Sly, W S and Valle, D., eds) pp 2785–2823, McGraw–Hill, New York

2 Mutoh, T, Naoi, M, Nagatsu, T, Takahashi, A, Matsuoka, Y, Hashizume, Y and Fujiki, N (1988) Purification and characterization of human liver β-galactosidase from a patient with the adult form of GM1 gangliosidosis and a normal control Biochim Biophys Acta **964**, 244–253

3 Koto, A., Horwitz, A. L, Suzuki, K, Tiffany, C. W and Suzuki, K. (1978) The Morquio syndrome: neuropathology and biochemistry Ann Neurol **4**, 26–36

4 Paschke, E and Kresse, H (1982) Morquio disease, type B activation of GM1 gangliosidase by GM1 activator protein Biochem Biophys Res. Commun **109**, 568–575

5 Sips, J H, Wit-Verbeek, H A, De Wit, J., Westerveld, A and Galjaard, H (1985) The chromosomal localization of human β-galactosidase revisited: a locus for β-galactosidase on human chromosome 3 and for its protective protein on human chromosome 22 Hum Genet **69**, 340–344

6 Morreau, H., Galjart, N J, Gillemans, N., Willemsen, R., van der Horst, G. T J and D'Azzo, A (1989) Alternative splicing of β-galactosidase mRNA generates the classic lysosomal enzyme and a β-galactosidase-related protein J Biol Chem **264**, 20655–20663

7 Zhang, S, McCarter, J D, Okamura-Oho, Y, Yaghi, F, Hinek, A, Withers, S G and Callahan, J W (1994) Kinetic mechanism and characterization of human β-galactosidase precursor secreted by permanently transfected Chinese hamster ovary cells Biochem J **304**, 281–288

8 McCarter, J D, Burgoyne, D L, Miao, S., Zhang, S, Callahan, J W and Withers, S G (1997) Identification of Glu-268 as the catalytic nucleophile of human lysosomal β-galactosidase precursor by mass spectrometry J Biol Chem **272**, 396–400

9 Okamura-Oho, Y, Zhang, S Q., Hilson, W., Hinek, A and Callahan, J W (1996) Early proteolytic cleavage with loss of a C-terminal fragment underlies altered processing of the β-galactosidase precursor in galactosialidosis Biochem J **313**, 787–794

10 Callahan, J W. (1999) Molecular basis of GM1 gangliosidosis and Morquio disease, type B Structure–function studies of lysosomal β-galactosidase and the non-lysosomal β-galactosidase-like protein Biochim Biophys. Acta **1455**, 85–103

11 Kim, P S and Arvan, P (1998) Endocrinopathies in the family of endoplasmic reticulum storage diseases disorders of protein trafficking and the role of ER molecular chaperones Endocrine Rev **19**, 173–202

12 D'Azzo, A, Andria, G, Strisciuglio, P and Galjaard, H (1995) Galactosialidosis In Metabolic Basis of Inherited Disease, vol 2 (Scriver, C R., Beaudet, A, Sly, W S and Valle, D, eds), pp 2825–2837, McGraw–Hill, New York

13 Hilson, W. L, Okamura-Oho, Y, Zhang, S, Clarke, J T R, Whelan, D, Mahuran, D J and Callahan, J W (1995) Expression studies of two missense mutations in β-galactosidase that result in GM1 gangliosidosis Am. J Hum Genet **57**, A180

14 Rosenberg, H, Frewen, C, Li, M D, Gordon, B L, Jung, J H, Finlay, J P, Roy, P L, Grover, D and Spence, M W (1985) Cardiac involvement in diseases characterized by β-galactosidase deficiency J Pediatr. (St Louis) **106**, 78–80

15 Chomczynski, P and Sacchi, N. (1987) Single step method of RNA isolation by acid guanidinium thiocyanate-phenol-chloroform extraction Anal Biochem **162**, 156–159

16 Oshima, A, Tsuji, A, Nagao, Y, Sakuraba, H and Suzuki, Y (1988) Cloning, sequencing and expression of cDNA for human β-galactosidase. Biochem Biophys Res Commun **157**, 238–244

17 Gross-Bellard, M, Oudet, P and Chambon, O (1973) Isolation of high molecular weight DNA from mammalian cells Eur J. Biochem. **36**, 32–38

18 Saiki, R K, Scharf, S., Faloona, F, Mullis, K. B, Horn, G T, Erlich, H A and Arnheim, N. (1985) Enzymatic amplification of β-globin genomic sequences and restriction site analysis for diagnosis of sickle cell anaemia Science **230**, 1350–1354

19 Morreau, H, Bonten, E, Zhou, X Y and D'Azzo, A (1991) Organization of the gene encoding human lysosomal β-galactosidase. DNA Cell. Biol **10**, 495–504

20 Orita, M., Suzuki, Y., Sekiya, T. and Hayashi, K (1989) Rapid and sensitive detection of point mutations and DNA polymorphisms using the polymerase chain reaction Genomics **5**, 874–879

21 Spinardi, L, Mazars, R and Theillet, C (1991) Protocols for an improved detection of point mutations by SSCP Nucleic Acids Res **19**, 4009

22 Felgner, P. L, Gadek, T R, Holm, M, Roman, R, Chan, H W, Wenz, M, Northrop, J P, Ringold, G M. and Danielsen, M (1987) Lipofectin a highly efficient, lipid-mediated DNA/transfection procedure Proc Natl Acad Sci U S A **84**, 7413–7417

23 Kaufman, R J (1990) Overview of vectors used for expression in mammalian cells Methods Enzymol **185**, 487–511

24 Hubbes, M, D'Agrosa, R M and Callahan, J W (1992) Human placental β-galactosidase characterization of the dimer and complex forms of the enzyme Biochem J. **285**, 827–831

25 Bradford, M (1976) A rapid and sensitive method for the quantitation of microgram quantities of protein utilizing the principle of protein-dye binding Anal Biochem **72**, 248–254

26 Kingston, R E and Sheen, J. (1990) A simple phase extraction assay for CAT activity In Current Protocols in Molecular Biology, chapter 9 6 6–9 6 7, Greene Publishing and Wiley-Interscience, New York

27 Laemmli, U K (1970) Cleavage of structural proteins during the assembly of the head of bacteriophage T4 Nature (London) **227**, 680–685

28 Hou, Y, McInnes, B, Hinek, A, Karpati, G. and Mahuran, D (1998) A Pro504 → Ser substitution in the β-subunit of β-hexosaminidase A inhibits α-subunit hydrolysis of GM2 ganglioside, resulting in chronic Sandhoff disease J Biol Chem **273**, 21386–21392

29 Bradford, T M, Gething, M-J, Davey, R, Hopwood, J J and Brooks, D A (1999) Processing of normal lysosomal and mutant N-acetylgalactosamine 4-sulfatase BiP (immunoglobulin heavy-chain binding protein) may interact with critical protein contact sites Biochem J **341**, 193–201

30 Lodish, H F (1988) Transport of secretory and membrane glycoproteins from the rough endoplasmic reticulum to the Golgi J. Biol Chem **263**, 2107–2110

31 Brooks, D A (1997) Protein processing a role in the pathophysiology of genetic disease FEBS Lett **409**, 115–120

32 Wang, C C and Tsou, C L (1998) Enzymes as chaperones and chaperones as enzymes FEBS Lett **425**, 382–384

33 Hurtley, S M and Helenius, A (1989) Protein oligomerization in the endoplasmic reticulum Annu Rev Cell Biol **5**, 277–307

34 Pelham, H R B (1989) Control of protein exit from the endoplasmic reticulum Annu Rev Cell Biol **5**, 1–23

35 Mahuran, D J. (1999) Biochemical consequences of mutations causing the GM2 gangliosidoses Biochim Biophys Acta **1455**, 105–138

36 Jacobson, R H, Zhang, X-J., DuBose, R F and Matthews, B. W (1994) Three dimensional structure of β-galactosidase from *E coli* Nature (London) **369**, 761–766
37 Henrissat, B (1991) A classification of glycosyl hydrolases based on amino acid sequence similarities Biochem J **280**, 309–316
38 Henrissat, B and Bairoch, A (1993) New families in the classification of glycosyl hydrolases based on amino acid sequence similarities Biochem J **293**, 781–788
39 Henrissat, B and Romeu, A (1995) Families, superfamilies and subfamilies of glycosyl hydrolases. Biochem J **311**, 350–351
40 Henrissat, B (1998) Glycosidase families. Biochem Soc. Trans **26**, 153–156
41 Nanba, E and Suzuki, K (1990) Molecular cloning of mouse acid β-galactosidase cDNA sequence, expression of catalytic activity and comparison with the human enzyme Biochem Biophys Res Commun **173**, 141–148
42 Ahern-Rindell, A J., Kretz, K A. and O'Brien, J S (1996) Comparison of the canine and human acid β-galactosidase gene. Am J. Med Genet **63**, 340–345
43 Silva, C M D, Severini, M H., Sopelsa, A, Coelho, J. C, Zaha, A, D'Azzo, A. and Giuliani, R (1999) Six novel β-galactosidase gene mutations in Brazilian patients with GM1 gangliosidosis Hum Mutat **13**, 401–409
44 Boustany, R M, Qian, W H and Suzuki, K (1993) Mutations in acid β-galactosidase cause GM1-gangliosidosis in American patients. Am J Hum Genet **53**, 881–888

Received 6 December 1999/13 March 2000, accepted 5 April 2000

Biochem J (2000) 348, 633–642 (Printed in Great Britain)

Possible interference between tissue-non-specific alkaline phosphatase with an Arg^{54} → Cys substitution and a counterpart with an Asp^{277} → Ala substitution found in a compound heterozygote associated with severe hypophosphatasia

M. FUKUSHI-IRIÉ[*], M. ITO[*], Y. AMAYA[*], N. AMIZUKA[†], H. OZAWA[†], S. OMURA[‡], Y. IKEHARA[§] and K. ODA[*1]

[*]Department of Oral Biochemistry, Faculty of Dentistry, Niigata University, Gakkocho-dori, Niigata 951-8514, Japan, [†]Department of Oral Anatomy, Faculty of Dentistry, Niigata University, Gakkocho-dori, 951-8514 Niigata, Japan, [‡]The Kitasato Institution, Shirokane, Minato-ku, 108-8642 Tokyo, Japan, and [§]Department of Biochemistry, Fukuoka University School of Medicine, Nanakuma, Jonan-ku, 814-0180 Fukuoka, Japan

Tissue-non-specific alkaline phosphatase (TNSALP) with an Arg^{54} → Cys (R54C) or an Asp^{277} → Ala (D277A) substitution was found in a patient with hypophosphatasia [Henthorn, Raducha, Fedde, Lafferty and Whyte (1992) Proc. Natl. Acad. Sci. U.S.A. **89**, 9924–9928]. To examine effects of these missense mutations on properties of TNSALP, the TNSALP mutants were expressed ectopically in COS-1 cells. The wild-type TNSALP was synthesized as a 66-kDa endo-β-N-acetylglucosaminidase H (Endo H)-sensitive form, and processed to an 80-kDa mature form, which is anchored to the plasma membrane via glycosylphosphatidylinositol (GPI). Although the mutant proteins were found to be modified by GPI, digestion with phosphatidylinositol-specific phospholipase C, cell-surface biotinylation and immunofluorescence observation demonstrated that the cell-surface appearance of TNSALP (R54C) and TNSALP (D277A) was either almost totally or partially retarded respectively. The 66-kDa Endo H-sensitive band was the only form, and was rapidly degraded in the cells expressing TNSALP (R54C). In contrast with cells expressing TNSALP (R54C), where alkaline phosphatase activity was negligible, significant enzyme activity was detected and, furthermore, the 80-kDa mature form appeared on the surface of the cells expressing TNSALP (D277A). Analysis by sedimentation on sucrose gradients showed that a considerable fraction of newly synthesized TNSALP (R54C) and TNSALP (D277A) formed large aggregates, indicating improper folding and incorrect oligomerization of the mutant enzymes. When co-expressed with TNSALP (R54C), the level of the 80-kDa mature form of TNSALP (D277A) was decreased dramatically, with a concomitant reduction in enzyme activity in the co-transfected cell. These findings suggest that TNSALP (R54C) interferes with folding and assembly of TNSALP (D277A) *in trans* when expressed in the same cell, thus probably explaining why a compound heterozygote for these mutant alleles developed severe hypophosphatasia.

Key words: autosomal recessive, degradation, glycosylphosphatidylinositol, missense mutation.

INTRODUCTION

Hypophosphatasia is an inborn error of metabolism characterized by defective mineralization of hard tissues and reduced levels of alkaline phosphatase activity in tissues and serum [1–3]. Mutations in the tissue-non-specific alkaline phosphatase (TNSALP) gene cause hypophosphatasia, pointing towards the involvement of TNSALP in mineralization of bone and teeth, although the precise role that TNSALP plays in mineralization remains elusive. The physiological substrate(s) of TNSALP is/are also still obscure; however, inorganic pyrophosphate, phosphoethanolamine and 5′-pyridoxal phosphate are potential candidates, since levels of these compounds were reported to be increased in both serum and urine of patients with hypophosphatasia. This was supported further by the finding that the levels of these phospho-compounds were elevated in serum and urine of TNSALP-deficient mice [4]. TNSALP-deficient mice did not develop typical skeletal hypomineralization symptomatic of the severe form of hypophosphatasia; however, it seems likely that mouse TNSALP is involved at least in the maintenance of mineralized bone and teeth, and in development of neural tubes [4,5].

The intracellular transport of proteins, which are ferried to their final destinations via vesicular transport, depends on proper folding and correct oligomeric assembly in the endoplasmic reticulum (ER). Many disease-causing mutations are known to impair intracellular transport of proteins by disturbing their folding and assembly [6,7]. Mutated proteins, which fail to acquire transport-competence, are often retained and eventually degraded in the ER [8,9]. Even if misfolded and incorrectly assembled proteins manage to exit from the ER, they are recycled back to the ER from the intermediate compartment and/or the *cis*-Golgi, ensuring that only correctly folded and oligomerized proteins transverse the Golgi stacks and reach the *trans*-Golgi network, where proteins are believed to be sorted for their final destinations.

Abbreviations used: DMEM, Dulbecco's modified Eagle's medium, Endo H, endo-β-N-acetylglucosaminidase H; ER, endoplasmic reticulum, GPI, glycosylphosphatidylinositol, MEM, minimum essential medium, MG132, benzyloxycarbonyl-L-leucyl-L-leucyl-L-leucinal, PI-PLC, phosphatidylinositol-specific phospholipase C; PNGase F, peptide N-glycosidase F, TM, tunicamycin; TNSALP, tissue non-specific alkaline phosphatase, WT, wild-type

[1] To whom correspondence should be addressed (e-mail oda@dent.niigata-u.ac.jp)

Recently, there have been an increasing number of reports on the mutation of the TNSALP gene associated with hypophosphatasia [10–19]. Most of the mutations are missense mutations, whereas deletion mutations and mutations in the non-coding region, which might affect splicing and promoter activity, have also been reported. By studying missense mutations associated with hypophosphatasia, it is possible to elucidate how each amino acid change affects the structure and function of TNSALP, leading to an understanding of the mechanism whereby the mutations cause hypophosphatasia. During the course of our studies on biosynthesis of TNSALP mutants to define their molecular defects, we found that TNSALPs with either an Ala^{162} → Thr substitution (A162T) or a Gly^{317} → Asp substitution (G317D), which were reported in patients who were homozygous for either of these hypophosphatasia alleles, aggregated in an early stage of the secretory pathway and, consequently, the TNSALP mutants largely failed to reach the cell surface, where they are thought to act as a glycosylphosphatidylinositol (GPI)-anchored ectoenzyme [20,21]. In the present study, we examined TNSALP (R54C) and TNSALP (D277A), both of which were found in a patient who developed severe hypophosphatasia. When separately expressed, TNSALP (R54C) was degraded in the cell, whereas TNSALP (D277A) partially appeared as a functional enzyme on the surface of cells expressing this mutant. However, the assembly and subsequent processing of TNSALP (D277A) were found to be markedly impaired, and the resultant alkaline phosphatase activity was reduced in cells co-transfected with cDNAs for TNSALP (R54C) and TNSALP (D277A), thus suggesting that the former exerts *trans*-negative effects on the latter.

MATERIALS AND METHODS

Materials

Express ^{35}S^{35} protein-labelling mix (> 1000 Ci/mmol) was obtained from Dupont-New England Nuclear (Boston, MA, U.S.A.), and [1-^{3}H]ethanolamine hydrochloride (12.0 Ci/mmol), ^{14}C-methylated proteins, Protein A–Sepharose CL-4B and the Thermo Sequenase fluorescence labelled-primer cycle-sequencing kit were from Amersham Pharmacia Biotech (Arlington Heights, IL, U.S.A.). Lipofectamine Plus Reagent was from Gibco–BRL (Gaithersburg, MD, U.S.A.), immobilized streptavidin was from Pierce (Rockford, IL, U.S.A.); aprotinin, baker's yeast alcohol dehydrogenase, BSA, Fast Blue RR salt, naphthol AS-BI phosphate and saponin (Quillaja Bark) were from Sigma Chemical Co. (St. Louis, MO, U.S.A.); Pansorbin was from Calbiochem–Novabiochem (La Jolla, CA, U.S.A.); rhodamine-conjugated goat anti-(rabbit IgG) was from Cappel Laboratories (Malvern, PA, U.S.A.); Peptide: *N*-glycosidase F (PNGase F), various DNA-modifying enzymes and restriction endonucleases were from New England Biolabs, Inc. (Beverly, MA, U.S.A.) and Takara Shuzo (Kyoto, Japan), antipain, chymostatin, elastatinal, leupeptin, pepstatin A and benzyloxycarbonyl-L-leucyl-L-leucyl-L-leucinal (MG132) were from the Protein Research Foundation (Osaka, Japan); phosphatidylinositol-specific phospholipase C (PI-PLC) was from Funakoshi Co. (Tokyo, Japan); bovine liver catalase and tunicamycin (TM) were from Wako Pure Chemical Co. (Tokyo, Japan); sulphosuccinimidyl-*N*-(D-biotinyl)-6-aminohexanoate was from Dojindo Laboratories (Kumamoto, Japan); and endo-*β*-*N*-acetylglucosaminidase H (*Streptomyces griseus*; Endo H) was from Seikagaku Kogyo (Tokyo, Japan). Lactacystin was purified as described previously [22]; antiserum against rat TNSALP or recombinant human TNSALP was raised in rabbits, also as described previously [23,24]. COS-1 cells were cultured in Dulbecco's modified Eagle's minimum essential medium (DMEM) supplemented with 10 % (v/v) fetal-bovine serum [20].

Plasmids and transfection

Construction of pSG5-TNSALP (Stratagene, San Diego, CA, U.S.A.) encoding a full-length cDNA for wild-type (WT) human TNSALP was as described previously [20]. Point mutations were introduced at desired sites using a Takara Mutan K kit (Takara Shuzo, Kyoto, Japan). Oligonucleotides used were. 5′-CGGCTGCCTGCATCCTCA-3′ for the C387T (R54C) mutation, and 5′-GCCAGGGGCCATGCAGTA-3′ for A1057C (D277A). Mutations were verified by restriction-enzyme digestion, and nucleotide sequences of mutation sites were determined further by the dideoxynucleotide chain-termination method using a Thermo Sequenase fluorescence-labelled-primer cycle-sequencing kit with 7-deaza-dGTP. pSG5-TNSALP(A162T) encoding TNSALP with an Ala^{162} → Thr substitution [10], which was found in a patient who was homozygous for this mutation, was constructed as described previously [20]. For transfection, plasmids were prepared using a plasmid Midi kit (Qiagen, Hilden, Germany). Cells were transfected using Lipofectamine Plus, essentially as described in the manufacturer's protocol. COS-1 cells [$(1.0–1.4) \times 10^{5}$] were inoculated into 35-mm dishes approx. 24 h before transfection. Unless otherwise stated, 1 μg of each plasmid was used for a single transfection experiment. After 3 h of incubation with Lipofectamine–plasmid complex, the medium was replaced with 2 ml of DMEM supplemented with 10 % (v/v) fetal-bovine serum, and the cells were incubated further for 24 h before use.

Metabolic labelling and immunoprecipitation

For pulse–chase experiments, cells were preincubated for 0.5–1 h in methionine-free minimum essential medium (MEM), and labelled with 50–100 μCi of [^{35}S]methionine for 0.5 h in fresh methionine-free MEM. After a pulse period, cells were washed and chased in MEM as described previously [20,21]. Where indicated, cells were preincubated for 1 h in the presence of 2 μg/ml of TM, and labelled with [^{35}S]methionine while in its presence. For specific labelling of the GPI-anchor moiety of TNSALP, cells were pre-incubated in MEM for 1 h and then labelled with 300 μCi of [^{3}H]ethanolamine in MEM for 6 h. To prevent degradation of TNSALP mutants, lactacystin (10 μM) was included throughout the course of the experiment. The medium was removed, and cells were washed with cold PBS and lysed in 0.5 ml of lysis buffer [1 % (w/v) Triton X-100/0.5 % (w/v) sodium deoxycholate/0.05 % (w/v) SDS in PBS], as described previously [20]. A protease inhibitor cocktail (antipain, aprotinin, chymostatin, elastatinal, leupeptin and pepstatin A) was added to cell lysates and media (10 μg of each/ml). The lysates were incubated for 20 min at 37 °C to extract TNSALP. The lysates and media were centrifuged at 15000 *g* for 10 min to remove insoluble materials and incubated with 20–40 μl of a 10 % suspension of Pansorbin (fixed *Staphylococcus aureus* cells) for 30 min. The precleared supernatants were mixed with 50 μl of powdered skimmed milk (5 % in PBS) and incubated with 3–4 μl of anti-TNSALP serum for 3–16 h. The immune complexes were collected on 30–40 μl of Protein A–Sepharose (50 % suspension in PBS) by shaking for 1 h, washed once with the lysis buffer, and then washed extensively as described before [20]. The immune complexes/Protein A beads were either used for digestion with Endo H or PNGase F or directly boiled in Laemmli's sample buffer [25] in the absence or presence of 2-mercaptoethanol, and then analysed by SDS/PAGE [9 % (w/v) gels]. Gels were fixed and processed for fluorography as described previously [20].

Sucrose-density-gradient centrifugation

Metabolically labelled cells were lysed as described above and incubated at 37 °C for 20 min. The clarified cell lysates were loaded on to continuous sucrose-density gradients [5 ml, 5–35 % (w/w) sucrose in 10 mM Tris/HCl, pH 7.5, containing 150 mM NaCl and 0.2 % (v/v) Triton X-100] and centrifuged for 18 h at 4 °C in an MLS-50 Rotor (Beckman Coulter, Fullerton, CA, U.S.A.) at 45000 rev./min (163000 *g*). Twelve fractions of 0.4 ml were collected from the top. Of each fraction, 50 µl was used for the alkaline phosphatase assay; 300 µl of each fraction was diluted 3-fold with the lysis buffer and subjected to immunoisolation.

Enzyme digestions

For PI-PLC digestion, metabolically labelled cells were washed three times with MEM and subsequently incubated with 0.2 unit of PI-PLC in 0.7 ml of MEM for 1 h in a CO_2 incubator [20]. Media were harvested and centrifuged at 5000 *g* for 5 min to remove detached cells. The resultant supernatants were subjected to immunoisolation as described above. For digestion with Endo H, immune complexes collected on Protein A beads were washed once with distilled water, divided into two equal parts, and then suspended in 50 µl of 50 mM acetate buffer, pH 5.5, in the presence of the protease inhibitor cocktail. Enzyme digestions were performed in the absence or presence of 0.2 unit/ml Endo H at 37 °C for 16 h. Then, immune complex/Protein A beads were washed once with distilled water and boiled in Laemmli's sample buffer [25]. For PNGase F digestion, immune complexes/Protein A beads were boiled in PBS containing 1 % (w/v) SDS for 3 min, and centrifuged. Then the resultant supernatants were diluted 10-fold with 1 % Nonidet P-40 and incubated in the absence or presence of 1000 units/ml of PNGase F at 37 °C for 16 h, as described previously [20,24].

Cell-surface biotinylation

Biotinylation was performed essentially as described previously [20]. Metabolically labelled cells were washed three times with 20 mM Hepes buffer, pH 7.3, containing 150 mM NaCl and incubated on ice with 0.5 mg/ml of sulphosuccinimidylbiotin in the same buffer for 15 min. This step was repeated once more. After the biotinylation reagent was removed, the cells were incubated further with the same buffer containing 20 mM glycine on ice for 10 min. Cells were washed with PBS and lysed in 0.5 ml of the lysis buffer containing the protease inhibitor cocktail. The lysates were warmed at 37 °C for 20 min and centrifuged at 15000 *g* for 10 min. The resultant supernatants were subjected to immunoisolation as described above. The immune complexes/Protein A–Sepharose were then divided into two equal parts: one was directly boiled in Laemmli's sample buffer, whereas the other was boiled in 50 µl of PBS containing 1 % SDS and centrifuged. The resultant supernatant was adjusted to final concentrations of 1 % Nonidet P40 and 0.05 % SDS, and incubated further with 40 µl of streptavidin beads (50 % slurry) at 4 °C overnight. The biotinylated TNSALP/streptavidin beads were washed extensively, and then boiled in Laemmli's sample buffer [25].

Determinations of protein and alkaline phosphatase activity

Cells were homogenized in 50 mM Tris/HCl, pH 7.5, using a small glass homogenizer with a Teflon pestle. Aliquots were used for the determination of enzyme activity and protein concentration. Alkaline phosphatase was assayed using *p*-nitrophenyl phosphate as a substrate [26] (1 unit of activity is defined as nmol of substrate hydrolysed per min at 37 °C). Protein was assayed using a Bio-Rad protein assay kit (Hercules, CA, U.S.A.) with BSA as a standard.

Immunofluorescence

COS-1 cells grown on cover slips in a 35-mm dish were transfected with 1.0 µg of plasmid as described above. After 24 h, the cells were fixed with 4 % (w/v) paraformaldehyde in PBS for 20 min at room temperature. The cells were incubated further with PBS in the absence or presence of 0.1 % (w/v) saponin for 20 min on ice. Then intact cells and permeabilized cells were incubated with PBS containing 5 % skimmed milk in the absence or presence of 0.1 % saponin at 4 °C overnight. The cells were incubated first with anti-TNSALP serum, and then with rhodamine-conjugated goat anti-rabbit IgG. The cover slip was washed with PBS, mounted on a slide glass with 50 % (w/v) glycerol in distilled water, and subjected to microscopic observations.

Enzyme histochemistry

COS-1 cells expressing TNSALP mutants on cover slips were stained for alkaline phosphatase activity according to the method of Burstone [27]. Cells were fixed with 4 % (w/v) paraformaldehyde in PBS for 30 min on ice and washed three times with 0.1 M Tris/HCl, pH 8.5. Then the cells were incubated with a mixture of 3 mg of naphthol AS-PI as a substrate and 18 mg of Fast Blue RR salt dissolved in 30 ml of 0.1 M Tris/HCl (pH 8.5) at room temperature for 5 min. The cells were counterstained with Methyl Green.

RESULTS

Enzyme activities of COS-1 cells expressing TNSALP mutants

COS-1 cells do not express a significant amount of endogenous TNSALP, allowing us to analyse molecular properties of TNSALP mutants that are expressed ectopically in the cells [20]. To examine effects of amino acid substitutions on the catalytic properties of TNSALP, COS-1 cells transiently expressing either the WT or two mutants, TNSALP (R54C) or TNSALP (D277A), were homogenized and assayed for alkaline phosphatase activity. For comparison, TNSALP (A162T) was also expressed in COS-1 cells and assayed for enzyme activity. TNSALP (A162T) was found in a patient who was homozygous for this mutation [10]. As shown in Table 1, TNSALP (WT) showed the highest specific activity among the four TNSALPs. In contrast, the enzyme activity level of cells expressing TNSALP (R54C) was found to be the same as that of untransfected COS-1 cells, suggesting that this mutant is synthesized in a non-active

Table 1 Enzyme activity of cells expressing TNSALP mutants

COS-1 cells expressing the WT TNSALP or the TNSALP mutants were homogenized and assayed for alkaline phosphatase activity, as described in the Materials and methods section. Values are averages of two experiments. n.d., not determined.

Plasmid	Enzyme activity (nmol/min per mg of protein)	K_m ($\times 10^{-4}$ M)
None	30	n.d.
TNSALP (WT)	3080	2.3
TNSALP (R54C)	35	n.d.
TNSALP (D277A)	1075	3.5
TNSALP (A162T)	749	1.3

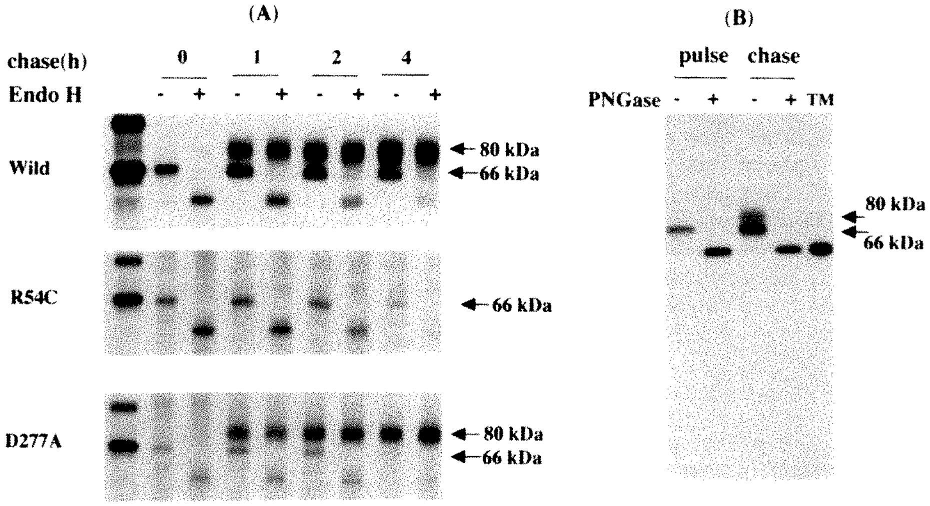

Figure 1 Acquisition of Endo-H resistance of the TNSALP mutant

(**A**) Cells transfected with the cDNA encoding TNSALP (WT) (Wild), TNSALP (R54C) or TNSALP (D277A) were pulse-labelled with [^{35}S]methionine for 0.5 h and chased for 1 h, 2 h or 4 h. Cell lysates were subjected to immunoisolation and the immune complexes were incubated in the absence (−) or presence (+) of Endo H. Each sample was analysed by SDS/PAGE/fluorography. The furthermost lane on the left shows ^{14}C-methylated protein markers: 97.4-kDa and 66-kDa, from the top of the gel. (**B**) Cells transfected with the cDNA for TNSALP (WT) were pulsed-labelled with [^{35}S]methionine for 0.5 h and chased for 1 h in the absence or presence of TM. Cell lysates were subjected to immunoisolation and the immune complexes were incubated in the absence (−) or presence (+) of PNGase F. Each sample was analysed by SDS/PAGE/fluorography.

form. The specific activity of cells expressing TNSALP (D277A) was roughly one-third of that of cells expressing the WT. We also confirmed that TNSALP (A162T) exhibited a low but significant enzyme activity, as reported previously [20]. K_m values of TNSALP (D277A) and TNSALP (A162T) determined by the Lineweaver–Burk method were similar to that of TNSALP (WT), indicating that replacement of aspartate at position 277 or alanine at position 162 with alanine or threonine respectively does not significantly affect the substrate affinity of TNSALP.

Intracellular transport of TNSALP mutants

To examine effects of amino acid substitution on biosynthesis of TNSALP, COS-1 cells transiently expressing either TNSALP (WT), TNSALP (R54C) or TNSALP (D277A) were metabolically labelled with [^{35}S]methionine for 0.5 h and chased for up to 4 h. TNSALP were immunoprecipitated, further incubated in the absence or presence of Endo H and analysed by SDS/PAGE, followed by fluorography. We reported previously that at least three of five potential N-linked glycosylation sites of the WT human TNSALP are N-glycosylated when it is expressed in COS-1 cells [20]. TNSALP (WT) was synthesized as a 66-kDa Endo H-sensitive form, and became an 80-kDa Endo H-resistant mature form along with chase times (Figure 1A). Upon digestion with PNGase F, which cleaves the linkage between the innermost *N*-acetylglucosamine and asparagine residue of high-mannose, hybrid and complex oligosaccharides from N-linked glycoproteins, the 66-kDa and 80-kDa forms migrated to the same position (Figure 1B), indicating that the size difference was due to modification of N-linked sugar chains. In contrast, TNSALP (R54C) remained Endo H-sensitive, and the 80-kDa mature form was barely detectable throughout the chase time (Figure 1A), pointing towards a block in transport of this mutant from the ER to the Golgi, where N-linked oligosaccharides of glycoproteins become Endo H-resistant. It is evident that TNSALP (D277A) was processed to give rise to the 80-kDa mature form at almost the same rate as was the WT enzyme (Figure 1A). It is noteworthy that the intensity of the 66-kDa form of both TNSALP (R54C) and TNSALP (D277A) declined progressively as the chase time increased, reflecting its degradation within the cell. Lactacystin and MG132, as proteasome inhibitors, strongly inhibited the degradation of the 66-kDa form (results not shown), as reported in the case of TNSALP (G3217D) [21].

Cell-surface appearance of TNSALP mutants

TNSALP (WT) is anchored to the cell surface via GPI, and is believed to function as an ectoenzyme. To examine whether the TNSALP mutants are expressed on the cell surface via GPI, COS-1 cells expressing either the WT or the mutants proteins were incubated with PI-PLC, which renders membrane-bound GPI-anchored proteins released from the cell surface [28,29]. Upon incubation with PI-PLC, both TNSALP (WT) and TNSALP (D277A) were recovered in the medium, whereas TNSALP (R54C) was not detected in the medium (Figure 2A), indicating that TNSALP (WT) and TNSALP (D277A), but not TNSALP (R54C), are exposed on the cell surface via GPI. We then asked whether the disappearance of TNSALP (R54C) on the cell surface is due to failure in terms of the modification by GPI. Under conditions where GPI attachment is in some way inhibited, precursor proteins of GPI-anchored proteins are known to be retained and subsequently degraded in the ER/pre-Golgi compartment [30–33]. The transfected cells were metabolically labelled with [^{3}H]ethanolamine, a component of GPI, before cell lysis and TNSALP immunoprecipitation, as shown in Figure 2(B). In this experiment, lactacystin was included throughout to inhibit the degradation of the TNSALP mutants. Not only the 80-kDa mature forms of TNSALP (WT) and TNSALP (D277A), which were sensitive to PI-PLC digestion (Figure 2A), but also the 66-kDa form of TNSALP (R54C) were labelled by [^{3}H]ethanolamine, indicating that TNSALP (R54C) is modified by GPI, like TNSALP (WT) and TNSALP (D277A). Another TNSALP mutant with an Ala^{162} → Thr substitution, which showed a lower specific activity relative to TNSALP (D277A)

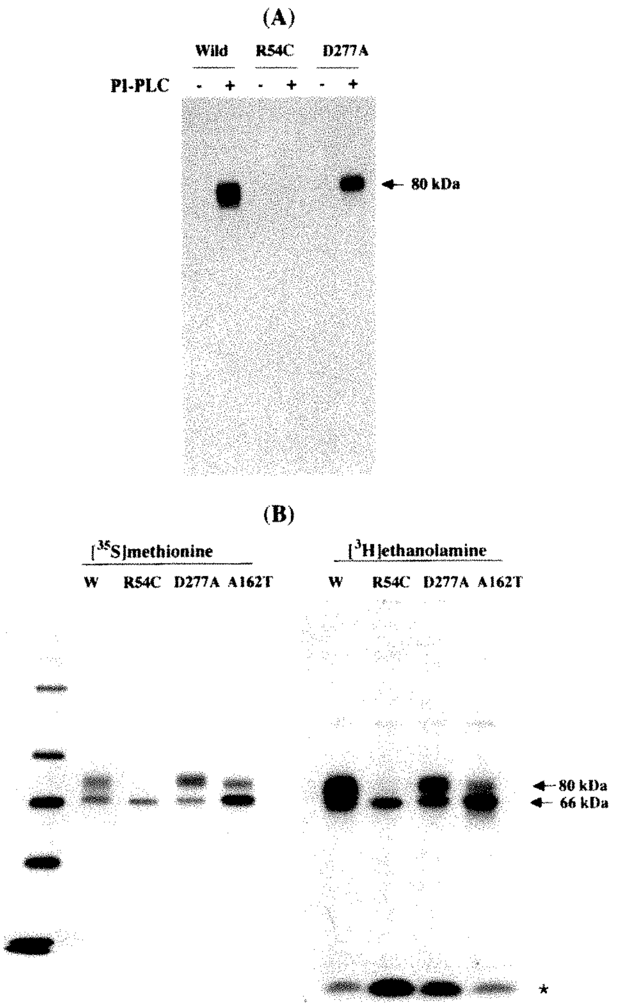

Figure 2 Modification of TNSALP mutants by GPI

(**A**) Cells transfected with the cDNA encoding TNSALP (WT) ('Wild'), TNSALP (R54C) or TNSALP (D277A) were labelled with [^{35}S]methionine for 3 h. The cells were washed and incubated further in the absence (−) or presence (+) of PI-PLC, as described in the Materials and methods section. Media were subjected to immunoisolation and analysed by SDS/PAGE/fluorography. (**B**) Cells transfected with the cDNA encoding TNSALP (WT) (W), TNSALP (R54C), TNSALP (D277A) or TNSALP (A162T) were labelled with 50 μCi of [^{35}S]methionine or 300 μCi of [^{3}H]ethanolamine for 6 h. Lactacystin (10 μM) was included throughout the experiments to prevent the degradation of the TNSALP mutants. Cell lysates were subjected to immunoisolation and analysed by SDS/PAGE/fluorography. The left lane shows ^{14}C-methylated protein markers (from the top of the gel, 200, 97.4, 66, 46, 30 and 14.3 kDa). The bands marked by an asterisk presumably represent phosphatidylethanolamine. The samples were run on the same gel; the left half of the gel was exposed for 2 weeks, while the other half was exposed for a month.

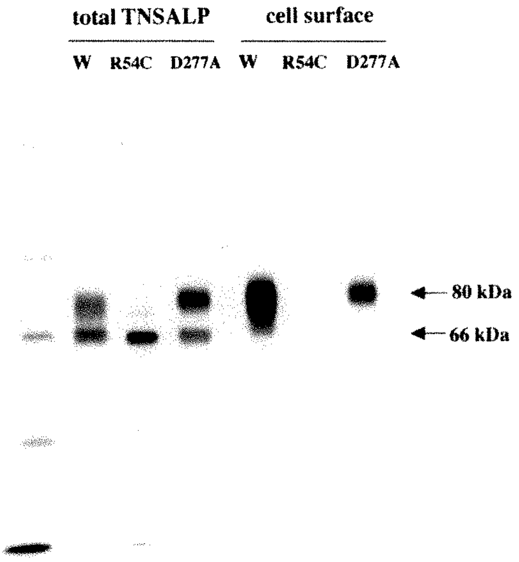

Figure 3 Cell surface biotinylation

Cells transfected with the cDNA encoding TNSALP (WT) (W), TNSALP (R54C) or TNSALP (D277A) were labelled with [^{35}S]methionine for 6 h. The cells were incubated further with biotin succinimidyl ester on ice, as described in the Materials and methods section. Cell lysates were subjected to immunoisolation. The immune complexes were divided into two equal parts: one part was directly analysed by SDS/PAGE, whereas the other was boiled and incubated further with streptavidin beads before analysis. Left lane: the same ^{14}C-methylated protein markers as shown in Figure 2(B).

(Table 1), was also intensely labelled with [^{3}H]ethanolamine in the presence of lactacystin, whereas this mutant was only weakly labelled in its absence [20].

Cell-surface expression of the TNSALP mutants was studied further by labelling transfected cells with biotin (Figure 3). Metabolically labelled cells were first incubated with biotin succinimidyl ester, which reacts with exposed lysine residues on proteins on the cell surface, then cellular TNSALP was immunoprecipitated with anti-TNSALP antibody. Subsequently, biotinylated TNSALP was separated from intracellular TNSALP using a streptavidin resin. In good agreement with the result of PI-PLC digestion (Figure 2A), the 80-kDa form of both TNSALP (WT) and TNSALP (D277A) were labelled with biotin, although TNSALP (D277A) was expressed on the cell surface to a considerably lesser extent than was TNSALP (WT). In contrast, the 66-kDa form of TNSALP (R54C) was not reactive to streptavidin, confirming that TNSALP (R54C) failed to reach the cell surface.

Immunofluorescence observation showed that TNSALP (WT) and TNSALP (D277A) were localized on the surface of transfected cells, while the surface of the cells expressing TNSALP (R54C) were largely devoid of immunofluorescence (Figure 4). When cells were permeabilized, TNSALP (R54C) was found to be accumulated in the intracellular reticular network resembling the ER. Occasionally, we encountered a cell expressing TNSALP (R54C) on the cell surface under a microscope (results not shown). It is probable that the number of cells subjected to the cell-surface staining was too small to be detectable by means of biochemical methods.

Co-transfection with the cDNA constructs for TNSALP mutants

Purified TNSALPs have been reported to exist as a homodimer [23,34–36], although a tetrameric structure was also proposed for a membrane-bound form of TNSALP [35]. Cells expressing TNSALP mutants were metabolically labelled with [^{35}S]-methionine, and TNSALP mutants were immunoprecipitated. The immunoprecipitates were then analysed by SDS/PAGE under reducing or non-reducing conditions (Figure 5A). Irrespective of the absence or presence of a reductant, most TNSALP (WT) migrated as the 66- or 80-kDa monomeric form

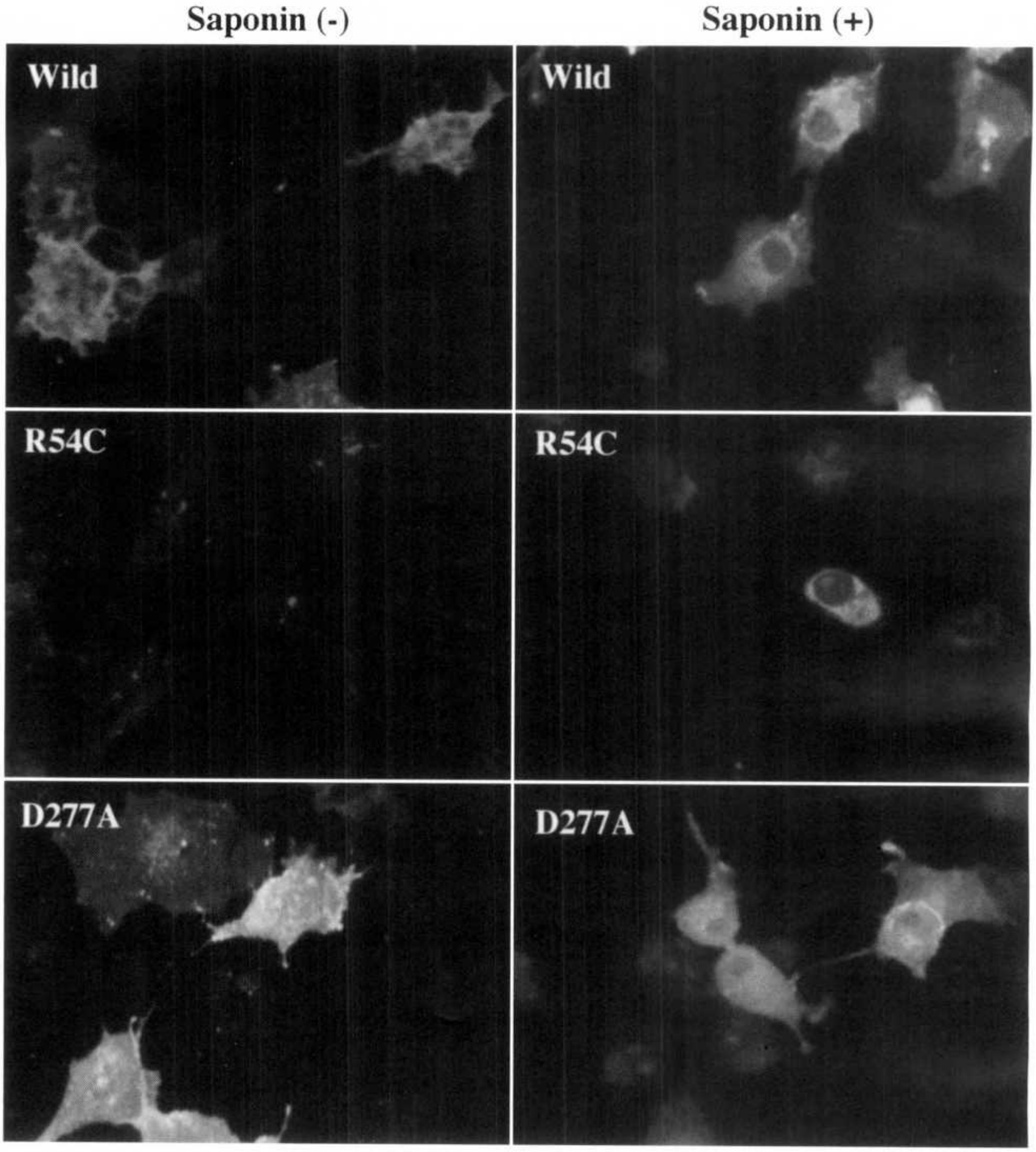

Figure 4 Immunofluorescence of the cells expressing the TNSALP mutants

Cells transfected with the cDNA encoding TNSALP (WT) ('Wild'), TNSALP (R54C) or TNSALP (D277A) were fixed, incubated in the absence or presence of saponin and then stained by an indirect immunofluorescence technique, as described in the Materials and methods section.

on an SDS/polyacrylamide gel (Figure 5A), indicating that the oligomeric structure of the WT TNSALP is held non-covalently. A small amount of aggregate on the top of the gel was probably due to overexpression of the enzyme. Compared with the WT, a significantly large amount of aggregate was found in the cells expressing TNSALP (R54C). This was confirmed further by sedimentation-velocity experiments using sucrose-density gradients, as described below in Figure 6. Thus a portion of newly synthesized TNSALP (R54C) formed disulphide-bonded high-molecular-mass aggregates. Although TNSALP (D277A) is able to fold and assembles properly, as shown by its enzyme activity (Table 1) and the appearance of the 80-kDa mature form on the cell surface of the transfected cells (Figures 1–3), a considerable fraction of newly synthesized TNSALP (D277A) was also found to aggregate, as found for TNSALP (R54C) (Figure 5A). This probably explains why the extent of the cell-

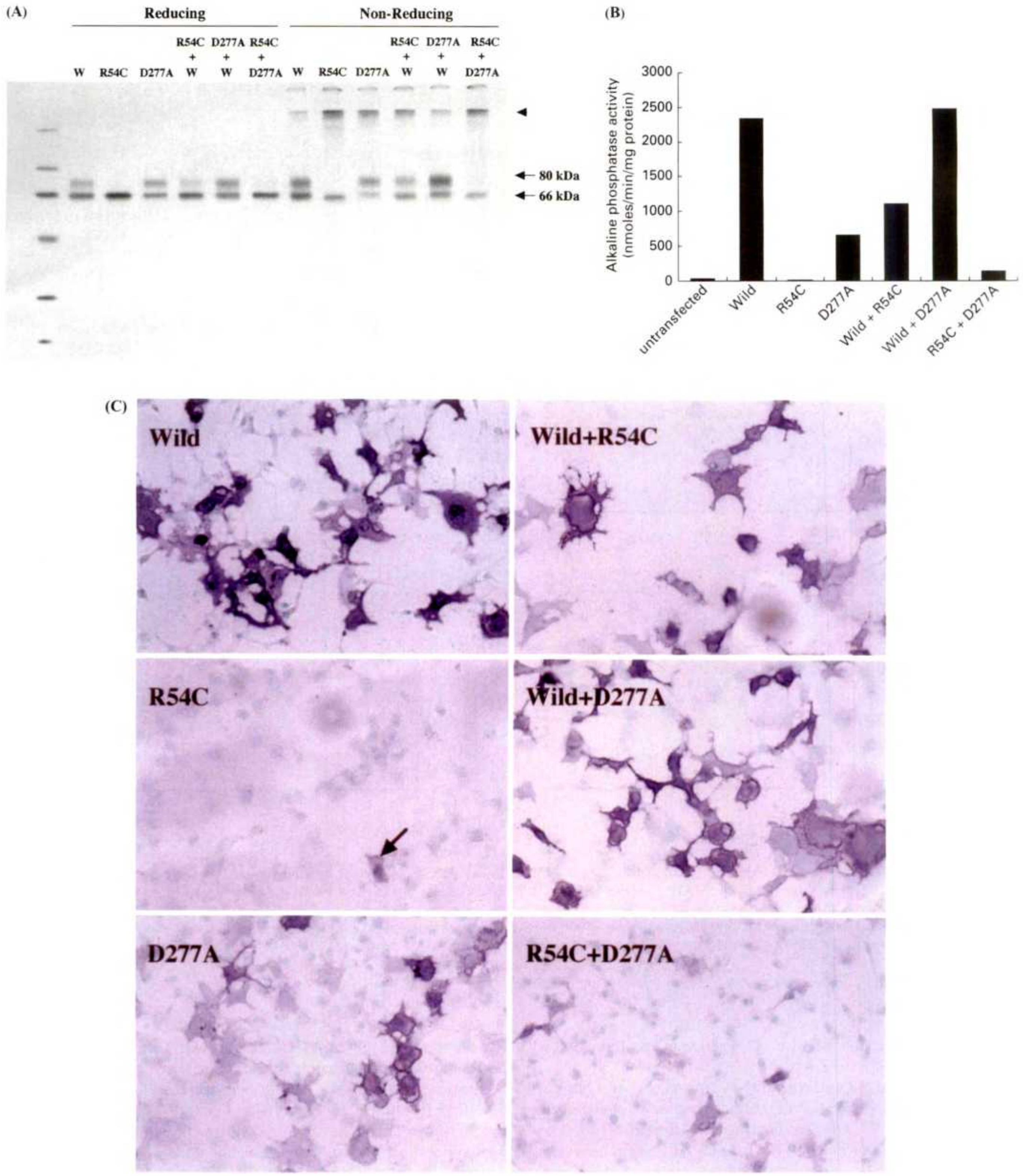

Figure 5 Co-transfection with the cDNAs for the TNSALP mutants

COS-1 cells were transfected with the cDNA encoding the WT TNSALP (W), TNSALP (R54C) or TNSALP (D277A), separately or in combination. (**A**) Cells were labelled with [^{35}S]methionine for 3 h. Cell lysates were subjected to immunoisolation and the immune complexes were analysed by SDS/PAGE under reducing or non-reducing conditions, followed by fluorography. When the cells were transfected with the cDNA separately, 1 μg of plasmid was routinely used, whereas for cells that were co-transfected with two different cDNAs, 0.5 μg of plasmid was used. Left lane: the same ^{14}C-methylated protein markers as shown in Figure 2(B). An arrowhead indicates the position of the top of the resolving gel. (**B**) The transfected cells were homogenized and assayed for alkaline phosphatase activity. (**C**) The transfected cells were stained for alkaline phosphatase for 5 min at room temperature, as described in the Materials and methods section. The arrow indicates a single cell showing alkaline phosphatase activity.

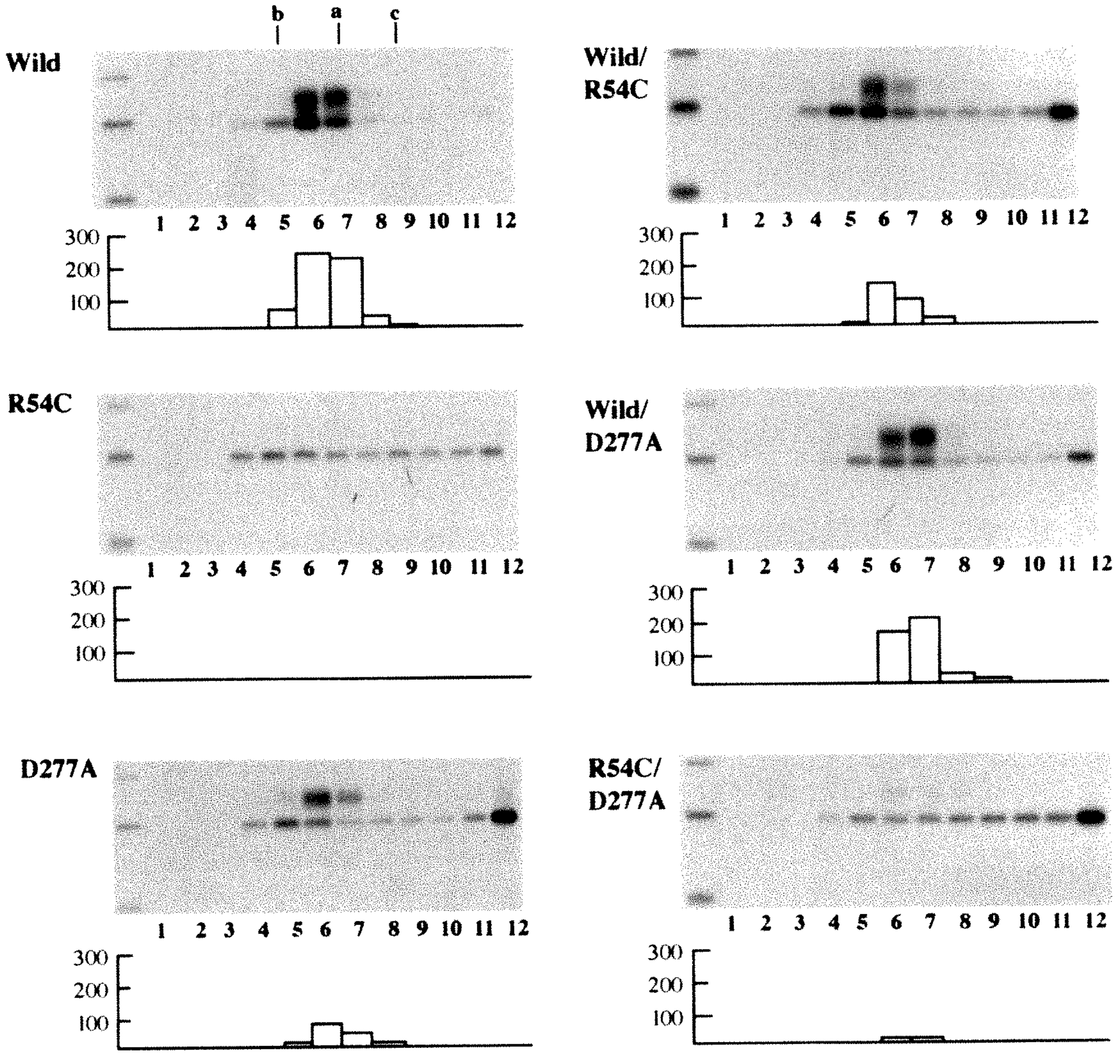

Figure 6 Sucrose-density-gradient centrifugation

COS-1 cells were transfected with the cDNA encoding TNSALP (WT) ('Wild'), TNSALP (R54C) or TNSALP (D277A), separately or in combination. Cells were pulsed-labelled with [^{35}S]methionine for 0.5 h and chased for 2 h. To prevent the degradation of TNSALP mutants, MG132 (50 μM) was included throughout the course of the experiments. Cell lysates were prepared and loaded on to a 5–35% sucrose gradient and centrifuged, as described in the Materials and methods section. Twelve fractions were collected from the top (fraction 1) and used for enzyme assays (lower panels of gel/histogram pairings: ordinate, alkaline phosphatase activity expressed as units/ml) and immunoprecipitation (upper panels). The left lane of each gel contains ^{14}C-methylated protein markers (from the top of the gel, 97.4, 66 and 46 kDa). BSA (**b**; 68 kDa), alcohol dehydrogenase (**a**; 141 kDa) and catalase (**c**; 250 kDa) were loaded on to a separate gradient as molecular-mass markers.

surface appearance of TNSALP (D277A) was less than that of TNSALP (WT) (Figures 2 and 3).

When co-transfected with the cDNA constructs for TNSALP (WT) and TNSALP (R54C) (Figure 5A), the 80-kDa mature form appeared in the cells, indicating that the latter does not seriously perturb maturation of the former. Although the level of alkaline phosphatase activity was lower than that of cells transfected by TNSALP (WT) alone (Figure 5B), this is because only half the amount of the WT plasmid (0.5 μg) was used in the co-transfection experiments. Similarly, the 80-kDa mature form was detected in cells co-transfected with the cDNA constructs for TNSALP (WT) and TNSALP (D277A) (Figure 5A). These findings agree with the notion that these mutation are inherited in a recessive manner [12]. In contrast, there was a marked decrease in the intensity of the 80-kDa mature form of TNSALP (D277A) in cells co-transfected with the cDNA constructs for the two mutants (Figure 5A). Consistent with the decrease in the 80-kDa mature form, alkaline phosphatase activity was also strongly suppressed in cells co-transfected with the cDNAs for the two TNSALP mutants (Figure 5B).

Cytohistochemical staining confirmed the presence of a strong alkaline phosphatase activity on the surface of cells transfected with cDNA for TNSALP (WT) or TNSALP (D277A) (Figure 5C). In contrast, cells transfected with cDNA for TNSALP (R54C) were almost deficient in positive staining, although we occasionally detected cells expressing alkaline phosphatase (Figure 5C, arrow). The strong-activity staining was also observed in the cells co-transfected with the cDNAs for the WT and either TNSALP (R54C) or TNSALP (D277A). Much weaker staining, however, was observed in cells co-transfected with the two mutant cDNAs compared with cells transfected with the cDNAs for TNSALP (WT) and TNSALP (R54C). A diminished cell-surface appearance of TNSALP (D277A) in the co-transfected cells with the cDNAs for the mutants was supported further by cell-surface biotinylation (results not shown). Taken together, when co-transfected in the cells, TNSALP (R54C) exerts a *trans*-negative effect on TNSALP (D277A), resulting in a marked reduction of the functional enzyme on the cell surface.

Analysis by sedimentation on sucrose gradient

To examine directly the oligomeric structure of TNSALP molecules in transfected cells, metabolically labelled cells were solubilized and proteins were separated by centrifugation on a 5–35% sucrose gradient. MG132 was included throughout the pulse–chase experiments to block the degradation of the mutants. The gradient was fractionated and TNSALP was immunoprecipitated, before analysis with SDS/PAGE (Figure 6). TNSALP (WT) appeared in a peak at a position expected for the dimeric form of the 66- or 80-kDa protein The distribution of alkaline phosphatase activity correlated well with that of the 80-kDa form of TNSALP. Consistent with Figure 5(a), only the 66-kDa form was detected in the cells expressing TNSALP (R54C) and a considerable proportion of newly synthesized TNSALP (R54C) formed high-molecular-mass aggregates (fractions 10–12). Although TNSALP (D277A) gave a similar sedimentation pattern to that of TNSALP (WT), obviously the proportion of aggregates was increased. The active 80-kDa form of the enzyme appeared in the cells co-transfected with the cDNAs for TNSALP (WT) and TNSALP (R54C) or TNSALP (D277A), confirming that the mutants do not seriously impair the oligomeric assembly of the wild-type enzyme. In contrast, there was a marked decrease in the level of the 80-kDa form of TNSALP (D277A) and a concomitant increase in the aggregates in the cells co-transfected with the cDNAs for TNSALP (R54C) and TNSALP (D277A) (compare Wild/R54C with R54C/D277A, top right and bottom right panels of Figure 5C), strongly suggesting that the former interferes with folding and assembly of the latter.

DISCUSSION

Folding of a protein is thought to be primarily dictated by its amino acid sequence. Thus it is not surprising that replacement of a single amino acid with another could influence to varying degrees the formation of the functional three-dimensional structure of a protein by altering folding and assembly pathway in the ER [6,7].

Both TNSALP (R54C) and TNSALP (D277A) were reported in a hypophosphatasia patient who was a compound heterozygote for these alleles. Arg^{54} is evolutionarily conserved, while Asp^{277} is present in all four human alkaline phosphatase isoenzymes, but not in *Escherichia coli* alkaline phosphatase [37–41]. TNSALP (WT) was synthesized as the 66-kDa Endo H-sensitive form, and underwent processing of N-linked oligosaccharide chains to become the 80-kDa Endo H-resistant form, which was anchored to the cell surface via GPI. In contrast, TNSALP (R54C) remained Endo H-sensitive, formed high-molecular-mass aggregates and was finally degraded in the cell (probably in the ER), reflecting the fact that the replacement of arginine at position 54 with cysteine causes a major effect on protein folding and subunit assembly, such that this mutant failed to acquire transport-competence and formed aberrant disulphide-bonded aggregates. It remains to be determined whether the substituted cysteine residue is directly involved in the formation of interchain disulphide linkages. The aggregation and degradation of the mutant was not due to a defect in GPI-anchor attachment, since the 66-kDa form of the TNSALP mutant was found to be labelled with [^{3}H]ethanolamine. As a result, the cells expressing TNSALP (R54C) showed only negligible enzyme activity.

Although a considerable fraction of newly synthesized TNSALP (D277A) formed aggregates, as in the case of TNSALP (R54C), this mutant also gave rise to the 80-kDa form expressed on the cell surface. Once the mutant succeeded in acquiring a transport-competence structure, the mutant moved to the Golgi at almost the same rate as the WT enzyme, as evidenced by acquisition of Endo H, and exhibited a significant alkaline phosphatase activity. Since the K_m value of TNSALP (D277A) is similar to that of the WT enzyme, the amino acid substitution at position 277 does not appear to grossly change the enzyme structure required for catalytic activity. Thus it is likely that the mutation reduces the probability that TNSALP (D277A) assumes a transport-competent structure, although the precise order of subunit folding and assembly remains unknown. In this context, we cannot exclude the possibility that TNSALP (R54C) also acquires transport-competence and is expressed on the cell surface, albeit at a much reduced level compared with TNSALP (D277A). Cytohistochemically, we detected a few cells exhibiting alkaline phosphatase activity in a large number of cells transfected with the cDNA for TNSALP (R54C), raising the possibility that, once properly folded and correctly oligomerized, an Arg^{54} → Cys substitution also does not strongly distort the catalytic domain of TNSALP.

When cells were co-transfected with the cDNA constructs for TNSALP (WT) in combination with either TNSALP (R54C) or TNSALP (D277A), the 80-kDa mature form appeared in the cells, indicating that neither of the mutants seriously perturb the intracellular transport of TNSALP (WT). In contrast, when cells were co-transfected with the cDNAs for the two mutants, the 80-kDa mature form of TNSALP (D277A) almost disappeared, resulting in a decrease of the enzyme activity. These findings strongly suggest that, when expressed in the same cell, TNSALP (R54C) interferes *in trans* with folding and assembly of TNSALP (D277A), thus reducing the conversion rate of TNSALP (D277A) into a transport-competent structure. Taken together, these results suggest that the suppression of alkaline phosphatase activity of TNSALP (D277A) by TNSALP (R54C) provides the molecular basis for lethal hypophosphatasia, found in a patient bearing these two hypophosphatasia alleles.

The possibility exists that low but significant levels of alkaline phosphatase activity detected in the co-transfected cells with the cDNAs for two mutants are ascribed to cells expressing only TNSALP (D277A), since the present experiments were performed on cells transiently expressing the two mutants. Although we have succeeded in cloning CHO cells stably expressing TNSALP (WT), several attempts to establish CHO clones stably expressing TNSALP (R54C) have so far failed, possibly because of the cytotoxity of the aggregates of TNSALP (R54C), which probably overwhelm the capacity of the lactacystin-sensitive degradation pathway in an early stage of the secretory pathway. We are currently establishing cell lines that express the mutant protein only in response to an external stimulus.

Recently, two groups have reported that TNSALP with substitutions of Phe^{301} → Leu and Leu^{272} → Phe exhibit a level of activity of 70% and 50% of the WT enzyme respectively upon their expression in cells [18,42]. However, it has not been determined whether the decrease in enzyme activity of cells expressing these TNSALP mutants is due to a quantifiable or a qualitative defect in TNSALP biosynthesis. So far we have analysed four naturally occurring missense mutations: TNSALP (R54C), TNSALP (D277A), TNSALP (A162T) and TNSALP (G317D), all of which were found in patients diagnosed with lethal hypophosphatasia (perinatal and infantile hypophosphatasia) [20,21]. Interestingly, the phenotypes exhibited by these mutants are more or less similar. These amino acid changes seem to retard the folding of the enzyme into its normal conformation, resulting in the formation of the aggregates. An amino acid change could destabilize folding intermediates and alter the equilibrium between a proper conformation and aggregates in favour of formation of the aggregates. According to this hypothesis, the equilibrium constants might be different depending upon the site of mutations and the nature of the substituted amino acid. Consequently, the ratio of native enzyme to aggregates varies from one missense mutation to another [TNSALP (WT) > TNSALP (D277A) > TNSALP (A162) > TNSALP (R54C) = TNSALP (G317D)]. These TNSALP mutants were known to be inherited in a recessive manner. Consistent with this, TNSALP (R54C) or TNSALP (D277A) does not seem to significantly affect the folding and assembly of WT enzyme when expressed in the same cell. However, the co-transfection experiments strongly suggested that TNSALP (R54C) interferes *in trans* with the folding of TNSALP (D277A). Although the molecular mechanism underlying this interference event remains unknown, it is possible that unfolded intermediates of TNSALP (R54C) associate with those of TNSALP (D277A), causing a shift of the equilibrium to rapid aggregate formation of the latter. With respect to inheritance, some mild forms of hypophosphatasia are reported to be autosomally dominantly inherited [43]. If these diseases are caused by mutations in the coding region of the TNSALP gene, it will be interesting to examine how the mutants exert dominant-negative effects on the WT enzyme when expressed in the same cell.

We thank Dr Y. Misumi (Fukuoka University, Japan) for kindly providing competent cells. This work was supported in part by a grant from Research Fellowships of the Japan Society for Young Scientists (to M F.-I.) and a Grant-in-Aid for Scientific Research from the Ministry of Education, Science, Sports and Culture of Japan (to K O.)

REFERENCES

1 Harris, H. (1989) Clin. Chim. Acta **186**, 133–150
2 Whyte, M. P (1994) Endocrine Rev. **15**, 439–461
3 Whyte, M P., Walkenhorst, D A , Fedde, K. N , Henthorn, P S and Hill, C S (1996) J Clin Endocrinol Metab. **83**, 3936–3942
4 Waymire, K G , Mahuren, J D , Jaje, J M , Guilarte, T R , Coburn, S P. and MacGregor, G R. (1995) Nat Genet **11**, 45–51
5 Narisawa, S , Frohlander, N and Millán, J. L (1997) Dev Dyn **208**, 432–446
6 Amara, J F , Cheng, S H and Smith, A E. (1992) Trends Cell Biol **2**, 145–149
7 Thomas, P J , Qu, B -H and Pederson, P L (1995) Trends Biochem Sci **20**, 456–459
8 Helenius, A , Marquardt, T and Braakman, I (1992) Trends Cell Biol. **2**, 227–231
9 Bergeron, J J M , Brenner, M B , Thomas, D. Y and Williams, D. B (1994) Trends Biochem Sci **19**, 124–128
10 Weiss, M J , Cole, D E C , Ray, K , Whyte, M P , Lafferty, M A , Mulivor, R A and Harris, H (1988) Proc Natl Acad. Sci U S A **85**, 7666–7669
11 Weiss, M J , Ray, K , Fallon, M D , Whyte, M. P , Fedde, K N , Lafferty, M A , Mulivor, R A and Harris, H (1989) Am J Genet **44**, 686–694
12 Henthorn, P S , Raducha, M., Fedde, K N., Lafferty, M A and Whyte, M. P (1992) Proc. Natl. Acad Sci U S A **89**, 9924–9928
13 Greenberg, C. R , Taylor, C L. D , Haworth, J C , Seargeant, L E , Philipps, S , Triggs-Raine, B and Chodirker, B N (1993) Genomics **17**, 215–217
14 Orimo, H., Hayashi, Z , Watanabe, A , Hirayama, T and Shimada, T (1994) Hum Mol Genet **3**, 1683–1684
15 Ozono, K , Yamagata, M , Michigami, T , Nakajima, S., Sakai, N , Cai, G , Satomura, K , Yasui, N , Okada, S and Nakayama, M (1996) J Clin Endocrinol Metab. **81**, 4458–4461
16 Orimo, H , Goseki-Sone, M., Sato, S and Shimada, T (1997) Genomics **442**, 364–366
17 Goseki-Sone, M., Orimo, H , Iimura, T , Takagi, Y , Watanabe, H , Taketa, K , Sato, S , Mayanagi, H , Shimada, T and Oida, S (1998) Hum Mutat , suppl 1, S263–S267
18 Sugimoto, N , Iwamoto, S., Hoshino, Y and Kajii, E (1998) J Hum Genet **43**, 160–164
19 Mornet, E , Taillandier, A , Peyramaure, S , Kaper, F., Muller, F , Brenner, R , Bussiere, P , Freisinger, P., Godard, J , Le Merrer, M et al (1998) Eur J Hum Genet **6**, 308–314
20 Shibata, H , Fukushi, M , Igarash, A , Misumi, Y , Ikehara, Y , Ohashi, Y and Oda, K. (1998) J Biochem (Tokyo) **123**, 968–977
21 Fukushi, M , Amizuka, N , Hoshi, K , Ozawa, H , Kumagai, H , Omura, S., Misumi, Y , Ikehara, Y and Oda, K (1998) Biochem Biophys Res Commun **246**, 613–618
22 Omura, S , Matsuzaki, K , Fujimoto, T , Kosuge, K , Furuya, T., Fujita, S and Nakagawa, A. (1991) J Antibiotics **44**, 117–118
23 Miki, A , Tanaka, Y , Ogata, S and Ikehara, Y (1986) Eur J. Biochem **160**, 41–48
24 Oda, K , Amaya, Y., Fukushi-Irié, M , Kinameri, Y , Ohsuye, K , Kubota, I , Fujimura, S and Kobayashi, J (1999) J Biochem (Tokyo) **126**, 694–699
25 Laemmli, U K (1970) Nature (London) **227**, 680–685
26 Ikehara, Y , Mansho, K , Takahashi, K and Kato, K (1978) J Biochem (Tokyo) **83**, 1471–1483
27 Burstone, M. S (1962) in Enzyme Histochemistry and Its Application on the Study of Neoplasms, (Burstone, M S , ed), pp 275–276, Academic Press, New York
28 Ikezawa, H , Yamanegi, M , Taguchi, R , Miyashita, T and Ohyabu, T. (1976) Biochim Biophys Acta **450**, 154–164
29 Low, M G and Finean, J. B (1977) Biochem J **167**, 281–284
30 Field, M. C , Moran, P , Wenlu, L , Keller, G -A and Caras, I W (1994) J Biol Chem **269**, 10830–10837
31 Oda, K , Ikehara, Y. and Omura, S (1996) Biochem Biophys Res Commun **219**, 800–805
32 Oda, K., Wada, I , Takami, N , Fujiwara, T , Misumi, Y. and Ikehara, Y (1996) Biochem. J **316**, 623–630
33 Wibourne, B , Nesbeth, D N , Wainwright, L J and Field, M C (1998) Biochem J. **332**, 111–118
34 Ohkubo, A , Langerman, N and Kaplan, M. M (1974) J. Biol. Chem **249**, 7174–7180
35 Oida, S., Sone, M. and Sasaki, S. (1984) Anal. Biochem **140**, 117–120
36 Hawrylak, K and Stinson, R A (1988) J Biol. Chem **263**, 14368–14373
37 Weiss, M. J , Henthorn, P S , Lafferty, M A , Slaughter, C , Raducha, M and Harris, H (1986) Proc Natl Acad Sci U S A **83**, 7182–7186
38 Millán, J L (1986) J Biol Chem. **261**, 3112–3115
39 Henthorn, P S , Raducha, M , Edwards, Y H , Weiss, M , Slaughter, C , Lafferty, M A and Harris, H (1987) Proc Natl Acad Sci U S.A **84**, 1234–1238
40 Millán, J L and Manes, T (1988) Proc Natl. Acad. Sci U S A **85**, 3024–3028
41 Kishi, F , Matsuura, S and Kajii, T. (1989) Nucleic Acids Res **17**, 2129
42 Cai, G , Michigami, T , Yamamoto, T , Yasui, N , Satomura, K , Yamagata, M., Shima, M , Nakajima, S , Mushiake, S., Okada, S. and Ozono, K (1998) J Clin Endocrinol Metab **83**, 3936–3942
43 Whyte, M P., Landt, M., Ryan, L M , Mulivor, R A , Henthorn, P S , Fedde, K N., Mahuren, J D and Coburn, S P (1995) J Clin Invest **95**, 1440–1445

Received 13 September 1999/4 February 2000, accepted 29 March 2000

Biochem J (2000) 348, 643–647 (Printed in Great Britain)

The molecular basis of phosphatidylcholine preference of human group-V phospholipase A_2

Kwang Pyo KIM, Sang Kyou HAN, Mihae HONG and Wonhwa CHO[1]

Department of Chemistry (M/C 111), University of Illinois at Chicago, 845 West Taylor Street, Chicago, IL 60607-7061, U.S.A.

Human group-V phospholipase A_2 (hVPLA$_2$) is a secretory phospholipase A_2 (PLA$_2$) that is involved in eicosanoid formation in such inflammatory cells as macrophages and mast cells. We showed that hVPLA$_2$ can bind phosphatidylcholine membranes and hydrolyse phosphatidylcholine molecules much more efficiently than human group-IIa PLA$_2$, which accounts for its high activity on the outer plasma membrane of mammalian cells. To understand the molecular basis of the high phosphatidylcholine specificity of hVPLA$_2$, we mutated several residues (Gly-53, Glu-56 and Glu-57) that might be involved in interaction with an active-site-bound phospholipid molecule. Phospholipid head-group specificities of mutants determined using polymerized mixed-liposome substrates indicate that a small glycine residue in position 53 is important for accommodating a bulky choline head group. Also, results indicated that two anionic residues, Glu-56 and Glu-57, favourably interact with cationic head groups of phosphatidylcholine and phosphatidylethanolamine. Together, these steric and electrostatic properties of the active site of hVPLA$_2$ allow for effective binding and hydrolysis of a bulky cationic choline head group of phosphatidylcholine, which is unique among mammalian secretory PLA$_2$s.

Key words: head-group specificity, interfacial catalysis, pro-inflammatory enzyme, secretory PLA$_2$, substrate specificity.

INTRODUCTION

Phospholipases A_2 (PLA$_2$) are a large family of ubiquitous enzymes that are found both intra- and extracellularly in mammalian tissues. Mammalian secretory PLA$_2$s (sPLA$_2$s) are homologous proteins that are divided in a number of groups, Ib, IIa, IIc, IId, IIe, IIf, V and X, on the basis of minor structural differences [1]. All these sPLA$_2$s share the same catalytic mechanism in which Ca^{2+} plays an essential catalytic role [2,3]. Intracellular PLA$_2$s, including group-IV cytosolic PLA$_2$ [4] and group-VI Ca^{2+}-independent PLA$_2$ [5], share no structural homology with sPLA$_2$s and have distinct catalytic mechanisms. Recent cell studies have indicated that both sPLA$_2$s and cytosolic PLA$_2$ are involved in eicosanoid production [6,7]. The critical involvement of cytosolic PLA$_2$ was demonstrated by recent gene-knock-out studies [8,9]. However, the nature of pro-inflammatory sPLA$_2$ is not fully understood. Group-IIa sPLA$_2$ has long been implicated in inflammation, based on findings that it is synthesized and secreted by a variety of cells in response to inflammatory cytokines and that it is found in fluids from inflammatory exudation [10,11]. Also, group-V sPLA$_2$ has been shown to be involved in eicosanoid formation from murine macrophages and mast cells [12,13]. Recently, we showed that human group-V PLA$_2$ (hVPLA$_2$) can bind zwitterionic phosphatidylcholine (PC) membranes and hydrolyse PC molecules much more efficiently than human group-IIa PLA$_2$ (hIIaPLA$_2$). This suggested that hVPLA$_2$ is better suited than hIIaPLA$_2$ for acting on the outer plasma membranes of mammalian cells that are composed largely of zwitterionic PC and sphingomyelin [14]. Our subsequent cell studies demonstrated that exogenous hVPLA$_2$ has much greater activity than hIIaPLA$_2$ with respect to releasing fatty acids and eliciting eicosanoid formation from various mammalian cells [15]. We also showed that a single tryptophan residue (Trp-31) located on the putative interfacial binding surface is essential for its high affinity for PC membranes [15]. In this study, we performed a structure–function analysis on the putative substrate-binding site of hVPLA$_2$ to identify the residues essential for its unique ability to bind and hydrolyse PC molecules.

EXPERIMENTAL

Materials

1-Hexadecanoyl-2-(1-pyrenyldecanoyl)-*sn*-glycero-3-phosphocholine (pyrene-PC), -ethanolamine (pyrene-PE) and -glycerol (pyrene-PG) were purchased from Molecular Probes (Eugene, OR, U.S.A.). 1-Hexadecanoyl-2-(1-pyrenyldecanoyl)-*sn*-glycero-3-phosphoserine (pyrene-PS) was prepared by the phospholipase D-catalysed transphosphatidylation of pyrene-PC and purified as described by Comfurius and Zwaal [16]. 1,2-*bis* [12-(Lipoyloxy)dodecanoyl]-*sn*-glycero-3-phosphoglycerol (BLPG) was prepared as described elsewhere [17,18]. Polymerized mixed liposomes were prepared by polymerizing large unilamellar liposomes (100 nm in diameter) prepared by extrusion as described in [17,18]. Phospholipid concentrations were determined by phosphate analysis [19]. Fatty acid-free BSA was from Bayer (Kankakee, IL, U.S.A.). All restriction enzymes, T4 ligase, T4 polynucleotide kinase and isopropyl β-D-thiogalactoside were obtained from Boehringer Mannheim. Oligonucleotides were purchased from Integrated DNA Technologies (Coralville, IA, U.S.A.) and used without further purification.

Mutagenesis and protein expression

The mutagenesis of hVPLA$_2$ was performed using a Sculptor *in vitro* mutagenesis kit from Amersham Pharmacia Biotech and a phagemid DNA prepared from the pSK vector in the presence of

---

Abbreviations used BLPG, 1,2-*bis*[12-(lipoyloxy)dodecanoyl]-*sn*-glycero-3-phosphoglycerol, PLA$_2$, phospholipase A_2; sPLA$_2$, secretory PLA$_2$, hIIaPLA$_2$, human group-IIa PLA$_2$, hVPLA$_2$, human group-V PLA$_2$, PC, phosphatidylcholine, PE, phosphatidylethanolamine, PG, phosphatidylglycerol, PS, phosphatidylserine, pyrene-PC, 1-hexadecanoyl-2-(1-pyrenyldecanoyl)-*sn*-glycero-3-phosphocholine, pyrene-PE, 1-hexadecanoyl-2-(1-pyrenyldecanoyl)-*sn*-glycero-3-phosphoethanolamine, pyrene-PG, 1-hexadecanoyl-2-(1-pyrenyldecanoyl)-*sn*-glycero-3-phosphoglycerol, pyrene-PS, 1-hexadecanoyl-2-(1-pyrenyldecanoyl)-*sn*-glycero-3-phosphoserine

[1] To whom correspondence should be addressed (e-mail wcho@uic.edu)

helper phage R408 as described previously [20]. Proteins were expressed in *Escherichia coli*, refolded and purified to near homogeneity (> 90 % pure) as described previously [15] and stored as lyophilized powder at −20 °C.

Kinetic measurements

The PLA_2-catalysed hydrolysis of polymerized mixed liposomes was carried out at 37 °C in 2 ml of 10 mM Hepes buffer, pH 7.4, containing 0.1 μM pyrene-labelled phospholipids (1 mol %) in 9.9 μM BLPG, 2 μM BSA, 0.16 M NaCl and 10 mM $CaCl_2$ [17,21]. The progress of hydrolysis was monitored as an increase in fluorescence emission at 378 nm using a Hitachi F4500 fluorescence spectrometer with the excitation wavelength set at 345 nm. Spectral band width was set at 5 nm for both excitation and emission. Values of k_{cat}^*/K_m^* were determined from reaction progress curves as described previously [22].

RESULTS

Molecular cloning of group-V PLA_2s from different species showed that these enzymes, although homologous to group-IIa PLA_2s, have some unique variations in amino acid sequence [23]. Structure–function studies on several $sPLA_2$s have shown that residues 53–58, which are located in the C-terminal end of a long α-helix, are involved in interaction with the phospholipid head group [24–28]. As illustrated in Figure 1, $hVPLA_2$ has two noticeable amino acid substitutions in this substrate-binding site when compared with $hIIaPLA_2$; a small Gly-53 and an anionic Glu-57 in place of Lys residues. Mouse group-V PLA_2 also contains Gly-53 and Glu-57. We reasoned that these residues are responsible for the unique activity of $hVPLA_2$ to effectively hydrolyse a bulky cationic PC head group. To test this notion, we mutated Gly-53 and Glu-57 of $hVPLA_2$ to Lys (G53K and E57K respectively). We also mutated Gly-53 to Glu (G53D) because some $sPLA_2$s have Glu in position 53 [29]. Finally, Glu-56 was mutated to Lys (E56K) to see if this residue is involved in interaction with cationic PC and phosphatidylethanolamine (PE) head groups, as seen with $hIIaPLA_2$ [26]. Initial attempts to prepare these mutants were hampered by extremely low refolding efficiency of their solubilized inclusion bodies. To overcome this difficulty, we used W79A of $hVPLA_2$, which was shown to be as active as and much more stable than the wild type [15], as a template for mutant preparation (e.g. G53K/W79A). All the double mutants produced were expressed in high yields as inclusion bodies and their refolding yields were uniformly high (i.e. > 2 mg/l of culture after purification).

	51									60		69
$hIbPLA_2$	C	Y	D	Q	A	K	K	L	D	S	C	Y
$hIIaPLA_2$	C	Y	K	R	L	E	K	R	-	G	C	K
$hVPLA_2$	C	Y	**G**	R	L	**E**	**E**	K	-	G	C	**R**
$mVPLA_2$	C	Y	G	Q	L	E	E	K	-	G	C	R
$hXPLA_2$	C	Y	T	R	A	E	E	A	-	G	C	K
AppD49	C	Y	G	-	-	-	K	V	T	G	C	K

Figure 1 Partial amino acid sequences of selected $sPLA_2$s, including human group-Ib pancreatic PLA_2 ($hIbPLA_2$), $hIIaPLA_2$, $hVPLA_2$, mouse group-V PLA_2 ($mVPLA_2$) and human group-X PLA_2 ($hXPLA_2$), and an Asp-49 PLA_2 from *Agkistrodon piscivorus piscivorus* (App-D49)

Amino acid sequences between two conserved cysteines (Cys-51 and Cys-61) and in position 69 are shown. Mutated residues of $hVPLA_2$ are shown in bold type.

Table 1 Phospholipid head-group specificity of $hVPLA_2$ and mutants

See the Experimental section for experimental conditions and methods for calculating rate constants. Values of k_{cat}^*/K_m^* represent means ± S.D. from triplicate determinations. PG, phosphatidylglycerol.

	$k_{cat}^*/K_m^* \times 10^6$ (M^{-1} s^{-1})					
Enzyme	Pyrene-PC	Pyrene-PE	Pyrene-PG	Pyrene-PS	PC/PG	PC/PE
$hVPLA_2$ (W79A)	6.5±1.5	4.8±1.0	9.5±1.5	2.4±0.6	0.7	1.4
G53K/W79A	1.2±0.5	4.9±1.5	11.5±2.5	1.8±0.6	0.1	0.2
G53D/W79A	3.6±1.0	4.6±1.5	9.1±1.0	1.2±0.5	0.4	0.8
E56K/W79A	2.6±0.8	1.5±0.3	1.7±0.8	1.1±0.4	1.5	1.7
E57K/W79A	2.0±1.0	1.8±1.0	10.0±3.0	1.7±0.3	0.2	1.1
R69K/W79A	5.0±2.0	5.0±1.2	4.2±2.0	0.5±0.2	1.2	1.0
R69Y/W79A	7.5±4.0	7.5±3.0	6.5±4.0	0.6±0.3	1.2	1.0
$hIIaPLA_2$*	0.2±0.1	2.0±0.3	28.0±4.0	1.9±0.4	< 0.01	0.09

* From [26]

We then measured the phospholipid head-group specificities of the mutants with polymerized mixed liposomes. In the polymerized mixed-liposome system, it is possible to accurately determine the head-group specificity of PLA_2 by varying the head-group structure of hydrolysable pyrene-phospholipids in an inert polymerized matrix [17,21]. Two zwitterionic phospholipids, pyrene-PC and pyrene-PE, and two anionic phospholipids, pyrene-PG and pyrene-PS, were used as inserts in the BLPG polymerized matrix. The anionic BLPG was used as a polymerized matrix because $hVPLA_2$, albeit active on zwitterionic membranes, still prefers anionic membranes to zwitterionic ones [15]. Values of k_{cat}^*/K_m^* determined for the mutants and various polymerized mixed liposomes are summarized in Table 1. Note that the differences in k_{cat}^*/K_m^* values between wild-type and mutant enzymes were in general modest and in some cases fell within the range of experimental error. Thus a direct comparison was made between wild type and mutants for a particular substrate only when the difference was large enough to be statistically significant. First of all, the phospholipid head-group specificity of W79A was essentially identical with that of wild type [14], i.e. pyrene-PG > pyrene-PC > pyrene-PE > pyrene-PS, thereby validating the use of this mutant as a wild-type substitute. When compared with W79A, G53K/W79A showed a 5.4-fold lower activity on pyrene-PC but comparable activities on all other pyrene lipids, including zwitterionic pyrene-PE. This suggested that the effect of mutation is largely steric and not electrostatic. This notion is supported by the similar activities of G53D/W79A, i.e. 1.8-fold lower activity on pyrene-PC and no significant effects on other pyrene lipids. A smaller decrease in activity on pyrene-PC for this mutation might simply reflect the size difference between Asp and Lys. The mutation of Glu-57 to Lys reduced the activity of W79A towards pyrene-PC and pyrene-PE by factors of 3.3 and 2.7, respectively, supporting the notion that this residue interacts favourably with a cationic head group. On the other hand, the activities on pyrene-PG and pyrene-PS were changed less significantly. A slight decrease in pyrene-PS activity might indicate that Glu-57 also interacts favourably with the ammonium group of pyrene-PS. Similarly, E56K/W79A exhibited lower activities on pyrene-PC, -PE and -

PS. Interestingly, however, this mutant also showed much reduced activity on pyrene-PG. This is in contrast with the effect of the same mutation on hIIaPLA$_2$, which reduced its pyrene-PC and pyrene-PE activities but not pyrene-PG activity. Presumably, the side-chain orientation of Glu-56 and its interaction mode with the phospholipid head group are different in the two enzymes.

As shown in Table 1, hVPLA$_2$ is significantly less active than hIIPLA$_2$ on pyrene-PG. Interestingly, hVPLA$_2$ has Arg in position 69 that is normally occupied by Lys for group-II PLA$_2$s [3] and the K69R mutation of hIIPLA$_2$ resulted in a 5-fold drop in pyrene-PG activity [26]. We thus measured the effects of mutation of Arg-69 of hVPLA$_2$ to either Lys or Tyr (R69K and R69Y) to test if the presence of Arg-69 in place of Lys is responsible for its low activity on pyrene-PG. Unexpectedly, however, both mutations modestly affected the activities of W79A on pyrene-PC, pyrene-PE and pyrene-PG but significantly decreased the activity on pyrene-PS ($\approx$ 4-fold). Thus it appears that Arg-69 is involved in specific interactions with the phosphatidylserine (PS) head group.

DISCUSSION

We showed previously that hVPLA$_2$ can bind zwitterionic PC membrane surfaces and hydrolyse a PC molecule much more effectively than other human sPLA$_2$s [14]. We subsequently demonstrated that Trp-31 in its putative interfacial binding surface is largely responsible for its high affinity for PC membranes [14]. The present structure–function study of hVPLA$_2$ identifies Gly-53 as an important determinant of its unique PC activity. As shown in Figure 1, hVPLA$_2$ is the only known human sPLA$_2$ with Gly in position 53. The model structure of a hVPLA$_2$–PC analogue complex, built on the basis of the structure of a hIIaPLA$_2$–PE analogue complex [30], is shown in Figure 2. X-ray structures of phospholipids show that the polar head group of PC ($\approx$ 350 Å^3) is much larger than that of PE ($\approx$ 250 Å^3) [31]. A model building also indicates that the PC head group is considerably larger than those of phosphatidylglycerol (PG) and PS (results not shown). Figure 2 suggests that the room provided by a small glycine side chain in position 53 of hVPLA$_2$ is essential for the binding of the PC head group to its active site. In fact, this strategy has been widely adapted by snake-venom PLA$_2$s (group IIa) acting on PC membranes. For instance, we showed previously that a PLA$_2$ from the venom of *Agkistrodon piscivorus piscivorus* contains Gly-53 and, consequently, hydrolyses pyrene-PC as well as pyrene-PE and pyrene-PG in polymerized mixed liposomes [20]. Since all human sPLA$_2$s, except for group-Ib pancreatic sPLA$_2$, are released to the extracellular space as fully active enzymes, it might be important for the purpose of regulation and cell protection to keep the activities of

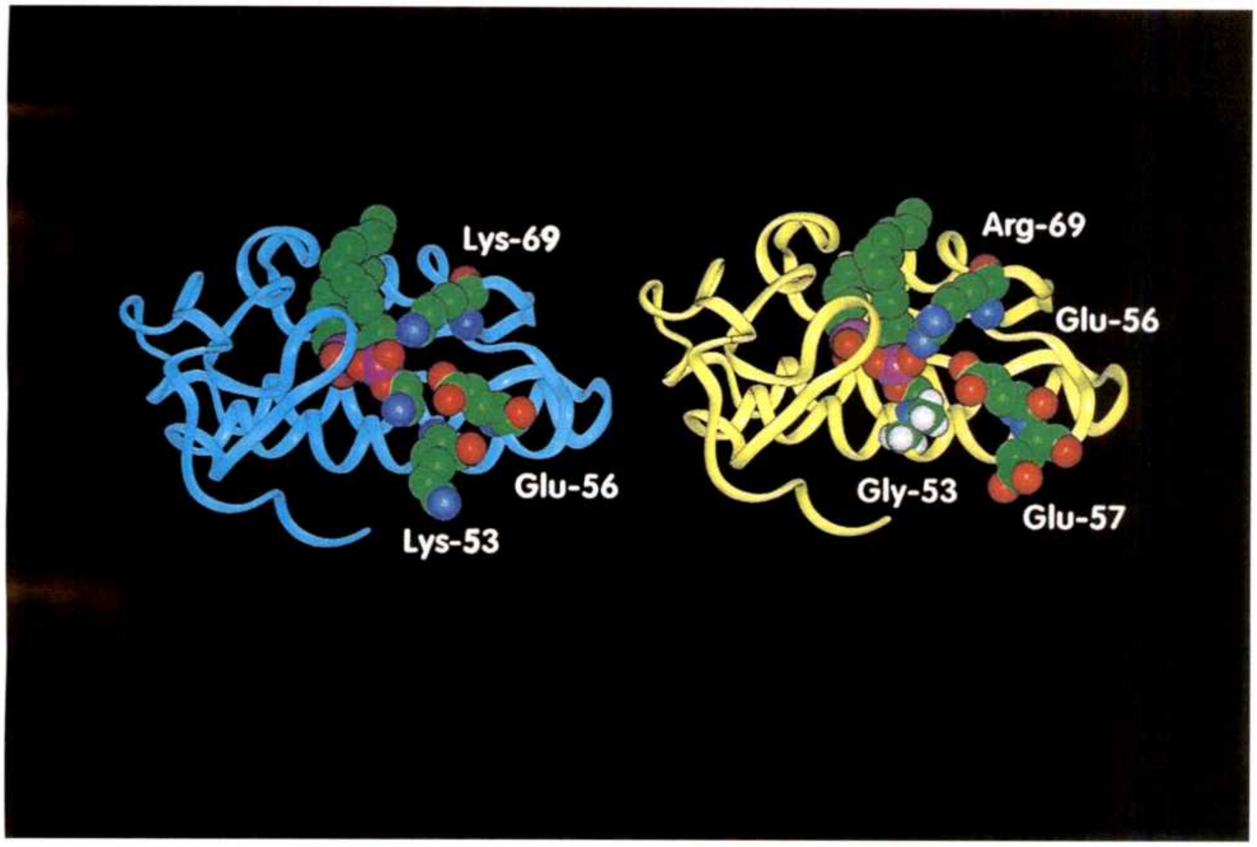

Figure 2 A model structure of a hVPLA$_2$–inhibitor complex

The model structure of hVPLA$_2$ shown in ribbon diagram (yellow) is built on the backbone of hIIaPLA$_2$ (blue) in a complex with the transition-state analogue inhibitor, L-1-*O*-octyl-2-heptylphosphonyl-*sn*-glycero-3-phosphoethanolamine [30]. All side chains were substituted for by hVPLA$_2$ residues using a program, Biopolymer (Molecular Simulation). Then, a PC analogue of the transition-state inhibitor was built on to its backbone using a program, Discover (Molecular Simulation), and docked into the active site of hVPLA$_2$ to a position that corresponds to that of L-1-*O*-octyl-2-heptylphosphonyl-*sn*-glycero-3-phosphoethanolamine in the active site of hIIaPLA$_2$. Energy minimization was not performed. The inhibitors and side chains of mutated residues are shown in space-filling representation. Carbon atoms are shown in green, nitrogen in blue, oxygen in red, phosphorus in pink and hydrogens of the PC head group in white.

sPLA$_2$s on the outer plasma membranes (i.e. PC activity) in check. The fact that hVPLA$_2$ has evolved to possess this activity thus points to its direct involvement in interaction with the outer plasma membranes of inflammatory cells to elicit inflammatory responses.

hVPLA$_2$ and hIIaPLA$_2$ are distinct from group-IIa snake-venom PLA$_2$s in that the former have an extended sequence (residues 54–58) that is deleted in the latter. The extension forms part of an elongated α-helix in hIIaPLA$_2$ and the side chain of Glu-56 makes direct contact with the ethanolamine head group of an active-site-bound PE analogue (see Figure 2). In the extended sequence, hVPLA$_2$ contains Glu-57 as well as Glu-56. Due to the presence of Gly in position 53 that is known to break the α-helix, it is unlikely that the extension will be part of the α-helix in hVPLA$_2$. Thus, residues 53–58 of hVPLA$_2$ and hIIaPLA$_2$ are expected to have different side-chain orientations with respect to an active site-bound phospholipid. This in turn might account for the fact that neither G53D or G53K showed appreciable effects on the activities of hVPLA$_2$ on any pyrene lipid but pyrene-PC. For hIIaPLA$_2$ [32] and other sPLA$_2$s [25,27], mutations of the residue in position 53 exhibited significant effects on the head-group specificity. Also, differential effects of the E56K mutation on the substrate specificity of hVPLA$_2$ and hIIaPLA$_2$ can be explained in terms of the structural differences. For hIIaPLA$_2$, E56K mutation selectively reduced the enzyme activity on pyrene-PC and pyrene-PE without affecting the activity on pyrene-PG, and enhanced the activity on pyrene-PS [26]. In contrast, the same mutation decreased the activities of hVPLA$_2$ on all pyrene lipids, with the largest activity drop seen with pyrene-PG. However, the effects of E57K mutation on hVPLA$_2$ activities are in line with the effects of K57E mutation on hIIPLA$_2$ activities [26]. A full explanation for these findings would require the tertiary structural information on a hVPLA$_2$–inhibitor complex. Evidently, however, these results indicate that Glu-56 and Glu-57 in the substrate-binding pocket interact favourably with zwitterionic substrates, PC and PE, thereby enhancing its activity on these substrates versus anionic ones.

Mammalian group-V PLA$_2$s uniquely contain Arg in position 69 that is occupied by Lys in most group-II PLA$_2$s and invariably by Tyr in group-I PLA$_2$s [3]. X-ray structures of enzyme–inhibitor complexes showed that either Tyr or Lys in position 69 forms a hydrogen bond with pro-S non-bridging oxygen of *sn*-3 phosphate [30,33] Our previous study on *A. p. piscivorus* PLA$_2$ showed that a K69Y mutation selectively reduced the enzyme activity on pyrene-PG without interfering with PC and PE activities, suggesting that Lys-69 of group-II PLA$_2$s might be important for their anionic head-group specificity [20]. Similar but less pronounced effects were observed with the K69Y mutation of hIIaPLA$_2$ [26]. Interestingly, the K69R mutation of hIIaPLA$_2$ uniformly ($\approx$ 5-fold) reduced the activities on all pyrene lipids, suggesting the specific nature of the Lys-69-*sn*-3 phosphate hydrogen bond. This, in conjunction with the finding that hVPLA$_2$ is about 5-fold less active than hIIPLA$_2$ on pyrene-PG, implies that one might be able to improve the activity of hVPLA$_2$ on anionic phospholipids by R69K mutation. Our results indicate otherwise. The R69K mutation selectively reduced the activities on anionic phospholipids, pyrene-PS in particular. This suggests that Arg-69 of hVPLA$_2$ is involved in specific interactions with PS (and PG) head groups that cannot be fully simulated by Lys. Slight increases in PC and PE activities by R69Y mutation also suggest that Tyr is slightly more effective than Arg in forming a hydrogen bond with the *sn*-3 phosphate in hVPLA$_2$. Again, the lower activities of R69Y on pyrene-PG and pyrene-PS suggest that Tyr cannot replace the role of Arg in interactions with anionic lipid head groups. Together, these results underscore the complex nature of the structural determinants of phospholipid head-group specificity of sPLA$_2$s. Whatever the origin of lower activity of hVPLA$_2$ on PG substrates might be, it would not compromise pro-inflammatory actions of hVPLA$_2$ since PG is only a minor component of mammalian plasma membranes. However, hVPLA$_2$ might have significantly lower activity on PG-rich bacterial cell membranes than hIIaPLA$_2$, which has been shown to have potent bactericidal activities [34].

This work was supported in part by a Biomedical Science Grant from the Arthritis Foundation and a National Institutes of Health grant (GM52598) W C. is an Established Investigator of the American Heart Association

REFERENCES

1 Dennis, E. A (1997) The growing phospholipase A_2 superfamily of signal transduction enzymes Trends Biochem Sci **22**, 1–2

2 Scott, D L, White, S P, Otwinowski, Z, Gelb, M H and Sigler, P B (1990) Interfacial catalysis: the mechanism of phospholipase A_2 Science **250**, 1541–1546

3 Scott, D L. and Sigler, P B (1994) Structure and catalytic mechanism of secretory phospholipase A_2 Adv Prot Chem **45**, 53–88

4 Leslie, C C (1997) Properties and regulation of cytosolic phospholipase A_2 J Biol Chem **272**, 16709–16712

5 Balsinde, J and Dennis, E A (1997) Function and inhibition of intracellular calcium-independent phospholipase A_2 J Biol Chem **272**, 16069–16072

6 Balsinde, J., Balboa, M A and Dennis, E A (1998) Functional coupling between secretory phospholipase A_2 and cyclooxygenase-2 and its regulation by cytosolic group IV phospholipase A_2 Proc Natl Acad Sci U S A **95**, 7951–7956

7 Murakami, M, Shimbara, S, Kambe, T, Kuwata, H, Winstead, M V, Tischfield, J A and Kudo, I (1998) The functions of five distinct mammalian phospholipase A_2s in regulating arachidonic acid release Type IIa and type V secretory phospholipase A_2s are functionally redundant and act in concert with cytosolic phospholipase A_2 J Biol Chem **273**, 14411–14423

8 Bonventre, J V, Huang, Z, Taheri, M R, O'Leary, E, Li, E, Moskowitz, M A and Sapirstein, A. (1997) Reduced fertility and postischaemic brain injury in mice deficient in cytosolic phospholipase A_2 Nature (London) **390**, 622–625

9 Uozumi, N, Kume, K, Nagase, T, Nakatani, N, Ishii, S, Tashiro, F, Komagata, Y, Maki, K, Ikuta, K, Ouchi, Y, Miyazaki, J. and Shimizu, T (1997) Role of cytosolic phospholipase A_2 in allergic response and parturition Nature (London) **390**, 618–622

10 Vadas, P, Stefanski, E and Pruzanski, W. (1985) Characterization of extracellular phospholipase A_2 in rheumatoid synovial fluid Life Sci **36**, 579–587

11 Vadas, P and Pruzanski, W (1986) Role of secretory phospholipases A_2 in the pathobiology of disease Lab Invest **55**, 391–404

12 Balboa, M A, Balsinde, J., Winstead, M V, Tischfield, J. A and Dennis, E A. (1996) Novel group V phospholipase A_2 involved in arachidonic acid mobilization in murine P388D1 macrophages J. Biol Chem **271**, 32381–32384

13 Reddy, S T and Herschman, H R (1996) Transcellular prostaglandin production following mast cell activation is mediated by proximal secretory phospholipase A_2 and distal prostaglandin synthase 1. J Biol Chem **271**, 186–191

14 Han, S-K., Yoon, E T and Cho, W. (1998) Bacterial expression and characterization of human secretory class V phospholipase A_2 Biochem J **331**, 353–357

15 Han, S K, Kim, K P, Koduri, R, Bittova, L, Munoz, N M, Leff, A R, Wilton, D C, Gelb, M H and Cho, W. (1999) Roles of Trp31 in high membrane binding and proinflammatory activity of human group V phospholipase A_2 J Biol Chem **274**, 11881–11888

16 Comfurius, P and Zwaal, R F. A (1977) The enzymatic synthesis of phosphatidylserine and purification by CM-cellulose column chromatography Biochim Biophys Acta **488**, 36–42

17 Wu, S-K and Cho, W (1993) Use of polymerized liposomes to study interactions of phospholipase A_2 with biological membranes Biochemistry **32**, 13902–13908

18 Cho, W, Wu, S K, Yoon, E and Lichtenbergova, L (1999) Fluorometric phospholipase assays based on polymerized liposome substrates Methods Mol Biol **109**, 7–17

19 Kates, M (1986) in Techniques of Lipidology, 2nd edn, pp 114–115, Elsevier, Amsterdam

20 Han, S-K, Yoon, E T, Scott, D L, Sigler, P B and Cho, W. (1997) Structural aspects of interfacial adsorption: a crystallographic and site-directed mutagenesis study of the phospholipase A_2 from the venom of *Agkistrodon piscivorus piscivorus* J Biol Chem **272**, 3573–3582

21 Wu, S-K and Cho, W (1994) A continuous fluorometric assay for phospholipases using polymerized mixed liposomes Anal. Biochem. **221**, 152–159

22 Snitko, Y, Koduri, R, Han, S-K, Othman, R, Baker, S F, Molini, B. J, Wilton, D. C, Gelb, M H and Cho, W (1997) Mapping the interfacial binding surface of human secretory class II phospholipase A_2 Biochemistry **36**, 14325–14333

23 Chen, J., Engle, S J., Seilhamer, J. J and Tischfield, J. A (1994) Cloning and recombinant expression of a novel human low molecular weight Ca^{2+}-dependent phospholipase A_2 J Biol. Chem **269**, 2365–2368

24 Lugtigheid, R B., Otten-Kuipers, M A, Verheij, H. M and De Haas, G H. (1993) Arginine 53 is involved in head-group specificity of the active site of porcine pancreatic phospholipase A_2 Eur J Biochem **213**, 517–522

25 Dua, R, Wu, S K and Cho, W (1995) A structure-function study of bovine pancreatic phospholipase A_2 using polymerized mixed liposomes J Biol Chem **270**, 263–268

26 Snitko, Y, Yoon, E T and Cho, W (1997) High specificity of human secretory class II phospholipase A_2 for phosphatidic acid Biochem J **321**, 737–741

27 Snitko, Y, Han, S K, Lee, B I and Cho, W (1999) Differential interfacial and substrate binding modes of mammalian pancreatic phospholipases A_2 a comparison among human, bovine, and porcine enzymes Biochemistry **38**, 7803–7810

28 Lee, B. I., Dua, R and Cho, W. (1999) A structural determinant of the unique interfacial binding mode of bovine pancreatic phospholipase A_2 Biochemistry **38**, 7811–7818

29 Han, S-K, Lee, B-I and Cho, W. (1997) Bacterial expression and characterization of human pancreatic phospholipase A_2 Biochim Biophys Acta **1346**, 185–192

30 Scott, D L, White, S. P, Browning, J L, Rosa, J J., Gelb, M H. and Sigler, P B (1991) Structure of free and inhibited human secretory phospholipase A_2 from inflammatory exudate Science **254**, 1007–1010

31 Hauser, H, Pascher, I, Pearson, R H. and Sundell, S (1981) Preferred conformation and molecular packing of phosphatidylethanolamine and phosphatidylcholine Biochim. Biophys. Acta **650**, 21–51

32 Koduri, R, Baker, S F, Snitko, Y., Han, S-K., Cho, W, Wilton, D C. and Gelb, M. H (1998) Action of human group IIa secreted phospholipase A_2 on cell membranes vesicle but not heparinoid binding determines rate of fatty acid release. J Biol. Chem **273**, 32142–32153

33 White, S T, Scott, D L, Otwinowski, Z, Gelb, M H and Sigler, P B. (1990) Crystal structure of cobra-venom phospholipase A_2 in a complex with a transition-state analogue. Science **250**, 1560–1563

34 Weinrauch, Y, Abad, C, Liang, N. S, Lowry, S F and Weiss, J. (1998) Mobilization of potent plasma bactericidal activity during systemic bacterial challenge Role of group IIA phospholipase A_2. J. Clin Invest **102**, 633–638

Received 14 December 1999/18 March 2000, accepted 3 April 2000

Defensin-like peptide-2 from platypus venom: member of a class of peptides with a distinct structural fold

Allan M. TORRES*, Greg M. DE PLATER†, Magnus DOVERSKOG‡, Liesl C. BIRINYI-STRACHAN§, Graham M. NICHOLSON§, Clifford H. GALLAGHER|| and Philip W. KUCHEL*[1]

*Department of Biochemistry, University of Sydney, NSW 2006, Australia, †Centre for Molecular Structure and Function, The John Curtin School of Medical Research, Australian National University, Canberra ACT 2601, Australia, ‡Department of Biotechnology, KTH, S-100 44, Stockholm, Sweden, §Department of Health Sciences, University of Technology, Sydney NSW 2007, Australia, and ||Taronga Zoo, Mosman, NSW 2088, Australia

The venom of the male Australian duck-billed platypus contains a family of four polypeptides of appox. 5 kDa, which are referred to as defensin-like peptides (DLPs). They are unique in that their amino acid sequences have no significant similarities to those of any known peptides; however, the tertiary structure of one of them, DLP-1, has recently been shown to be similar to β-defensin-12 and to the sodium neurotoxin peptide ShI (*Stichodactyla helianthus* neurotoxin I). Although DLPs are the major peptides in the platypus venom, little is known about their biological roles. In this study, we determined the three-dimensional structure of DLP-2 by NMR spectroscopy, with the aim of gaining insights into the natural function of the DLPs in platypus venom. The DLP-2 structure was found to incorporate a short helix that spans residues 9–12, and an antiparallel β-sheet defined by residues 15–18 and 37–40. The overall fold and cysteine-pairing pattern of DLP-2 were found to be similar to those of DLP-1, and hence β-defensin-12; however, the sequence similarities between the three molecules are relatively small. The distinct structural fold of the DLP-1, DLP-2, and β-defensin-12 is based upon several key residues that include six cysteines. DLP-3 and DLP-4 are also likely to be folded similarly since they have high sequence similarity with DLP-2. The DLPs, and β-defensin-12 may thus be grouped together into a class of polypeptide molecules which have a common or very similar global fold. The fact that the DLPs did not display antimicrobial, myotoxic, or cell-growth-promoting activities implies that the nature of the side chains in this group of peptides is likely to play an important role in defining the biological function(s).

Key words: β-defensin-12, disulphide pairing pattern, NMR spectroscopy, peptide fold.

INTRODUCTION

The male duck-billed platypus, *Ornithorhynchus anatinus*, is peculiar amongst mammals in having a functional venomous spur on each hind limb [1,2]. Knowledge of the evolutionary origin and the natural function of the platypus venom apparatus is limited [1–6]. There have been many hypotheses drawn about the function of the spurs, and the prevailing view is that the apparatus is used as both an offensive and a defensive weapon [7]. The spurs are used offensively against other male platypuses to assert dominance, especially during the mating season [3,8]. It has also been observed that platypuses use the spurs to ward off potential enemies such as dogs and humans. Human envenomation is not rare and has been described as causing excruciating pain followed by profound swelling of local tissue [6].

Platypus venom contains several protein components with a wide range of sizes from 4–6 kDa [9–13] (Figure 1). Two of these components, namely the 4.2 kDa C-type natriuretic peptide (OvCNP) [10–12] and the 13 kDa nerve growth factor protein (OvNGF) [11], have some similarities to proteins from other sources. The OvCNP causes relaxation of the rat uterus, histamine release in the mast cell, and tissue oedema, while OvNGF has been implicated in the pain-producing activity of the venom.

Besides the above two proteins, there are several protein components which are unique in that their primary structures do not share strong resemblance with any proteins listed in the SwissProt database [9–11]. Many of these proteins are in fact present in much larger amounts than the OvCNP and OvNGF proteins. Among these is a group of four peptides of approx. 5 kDa which are referred to as defensin-like peptides (DLPs) [9] (Figures 1 and 2). These peptides are named as such because the three-dimensional fold of one of its member peptides, DLP-1, has a strong similarity to β-defensin-12 [14,15], although the amino acid sequence similarity is weak. Unlike β-defensin-12, DLP-1 does not show any apparent antimicrobial activity, and its role in the venom is still unknown. Detailed analysis of the DLP-1 and β-defensin-12 structures reveals that although their secondary and tertiary structures are similar, the locations of the hydrophobic and hydrophilic cationic residues, which are known to be important in the activity in β-defensin-12, are significantly different in the two molecules [9].

Four DLPs have been identified in platypus venom thus far. DLP-2 was found to have 36% sequence identity with DLP-1. Despite this low similarity, it was hypothesized that the two peptides would be folded in the same fashion because, in both molecules, six disulphide residues are spaced similarly in the sequence, and important amino acid stretches such as 14–17 and 37–40, which incorporate most of the antiparallel β-strands in DLP-1, are also present in DLP-2. It is interesting to note that five out of the six cysteine residues of DLP-1 and DLP-2 can be

---

Abbreviations used: DLP, defensin-like peptide, DQF, double-quantum-filtered, NOE, nuclear Overhauser enhancement, RMSD, root-mean-square deviation, 2D, two-dimensional, OvCNP, *Ornithorhynchus* venom C-type natriuretic peptide, OvNGF, *Ornithorhynchus* venom nerve growth factor

[1] To whom correspondence should be addressed (e-mail p.kuchel@biochem.usyd.edu.au)

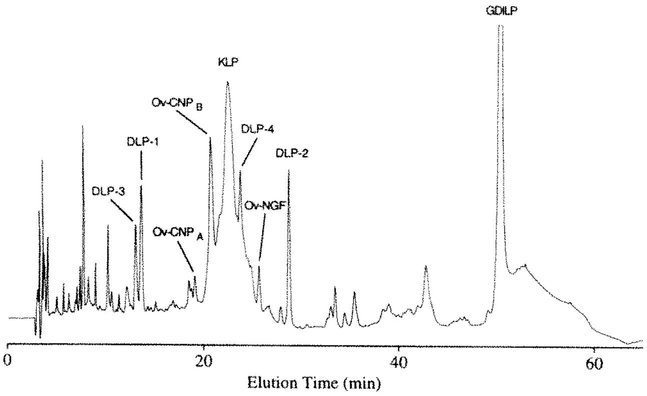

Figure 1 Reverse-phase HPLC chromatogram of complete platypus venom

Peaks of components that eluted before DLP-3 were identified as non-proteinaceous. Abbreviations: KLP, Kunitz-type protease inhibitor-like protein; GDILP, guanosine diphosphate-dissociation inhibitor-like protein.

readily aligned with those of β-defensin-12. However, the sequence similarity of the two DLPs with β-defensin-12 are small, being 28 % for DLP-1 and 21 % for DLP-2.

The other two DLPs in platypus venom are more closely related to DLP-2 than to DLP-1. DLP-4 is the most recently identified peptide and it has an identical amino acid sequence and the same molecular mass as DLP-2, but it elutes with a different retention time in reverse-phase HPLC experiments. On the other hand, DLP-3 is shorter than DLP-2 with a few amino acid deletions and substitutions. It is interesting in that it has only two pairs of cysteine residues instead of three. Since the identification of the protein components in the venom is far from complete, it is possible that other DLP peptides will be discovered in the venom.

In this study, we first report the determination of the solution structure of DLP-2, a 42 residue peptide which has some sequence similarities to DLP-1 and β-defensin-12. The obtained structure was then analysed and compared with the structures of these two peptides. We also used the results to speculate on the tertiary structures of DLP-3 and DLP-4. It is expected that this study will help illuminate the role of DLPs in platypus venom.

MATERIALS AND METHODS

Separation, identification and purification

Venom components were fractionated using reverse-phase HPLC on a GBC system (Melbourne, Vic., Australia) with LC 1110 pumps controlled by a DP 800 workstation. Details of this procedure are described elsewhere [9]. DLP-4 was sequenced by Edman degradation using an Applied Biosystems 494 Procise HT and cLC pulsed-liquid protein sequenators, and its molecular mass was determined using a VG Analytical TOFSPEC matrix-assisted laser-desorption ionization–time-of-flight mass spectrometry instrument and a saturated solution of α-cyano-4-hydroxycinnamic acid (in 40 % CH_3CN/0.1 % trifluoroacetic acid) as matrix.

The DLP-2 used in the NMR experiments was isolated from whole crude venom and venom gland extracts. Several reverse-phase HPLC experiments were performed in order to obtain sufficient DLP-2 for the NMR analysis. HPLC fractions containing DLP-2 were pooled, freeze-dried, and subsequently purified by centrifugal membrane-filtration using an Amicon YM-10 tube (Millipore). NMR samples contained approx. 1.0 mM DLP-2 in 0.35 ml total volume at pH 3.6.

NMR spectroscopy

NMR experiments were performed with the sample at either 10 °C or 25 °C on a Bruker AVANCE-600 DRX spectrometer (Karlsruhe, Germany) using a 5 mm ^1H inverse probe. All two-dimensional (2D) NMR spectra were acquired in the phase-sensitive mode using time-proportional phase detection [16]. Homonuclear 2D spectra that were recorded included: double-quantum filtered (DQF) COSY [17], with the phase-cycle modified for fast recycle times [18]; TOCSY [19], with MLEV spin-lock periods of 30 ms, 70 ms and 90 ms; and NOESY [20], with mixing times of 200 ms, 250 ms and 300 ms. Solvent suppression in TOCSY and one NOESY experiment was achieved by using the WATERGATE [21] pulse sequence, while that in DQF and other NOESY experiments was achieved by low-power irradiation at the water resonance frequency during the relaxation delay in the transients (1.3–1.4 s) and during the mixing period in NOESY experiments. ^1H–^2H exchange experiments were carried out by reconstituting the freeze-dried sample with ^2H_2O, acquiring a series of one-dimensional experiments for 30 min, and then acquiring a short-time 2D NOESY spectrum. Slowly exchanging amide protons were interpreted as being hydrogen-bond donors. Spectra were processed using XWIN-NMR software (Bruker).

Structure calculations

All 2D spectra were analysed using the XEASY program [22]. Distance constraints were derived from NOESY spectra recorded at 25 °C with a mixing time of 300 ms. This ultimately yielded

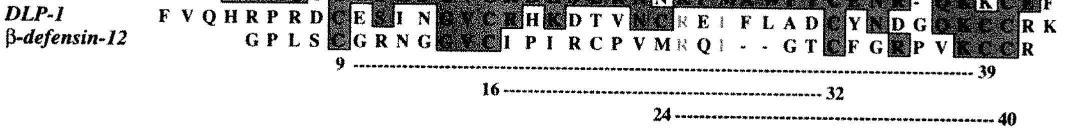
10
20
30
40
DLP-2/DLP-4 I M F F E M Q A C W S H S G V C R D K S E R N C K P M A W T Y C E N R N Q K C C E Y
DLP-3 F E M Q Y C W S H S G V C R D K S E R N N K P M A W T Y C E N R - Q K K C E F
DLP-1 F V Q H R P R D C E S I N G V C R H K D T V N C K E I F L A D C Y N D G Q K C C R K
β-defensin-12 G P L S C G R N G G V C I P I R C P V M K Q I - - G T C F G R P V K C C R
9
39
16
32
24
40

Figure 2 Primary structures of DLPs and β-defensin-12

The amino acid sequences are aligned to show maximum correspondence between them. Similarities are shown relative to DLP-2 and DLP-4; identical residues are boxed and conservative substitutions are faint. The disulphide-bonding pattern determined for DLP-2 from the NMR data is shown below the numbered sequences (dashed lines). The secondary structure of DLP-2, as determined in the current study, is shown above the sequences (helix denoted as cylinder and β-strand denoted as arrow). The diagram was drawn using ALSCRIPT [42].

699 non-redundant inter-proton distance constraints, which were automatically assigned upper-distance limits based on the corresponding cross-peak intensities or volumes. To allow for conformational averaging and errors in volume integration, a correction of 0.3 Å (0.03 nm) was added to all upper-distance bounds.

Twenty four ϕ dihedral angle constraints were derived from $^3J_{NH\alpha}$ coupling constants obtained by inverse Fourier transformation of in-phase multiplets from 2D NOESY spectra, using the program INFIT [23]. The ϕ angles were constrained to -60 ± 30 ° for $^3J_{NH\alpha} < 5$ Hz; -60 ± 40 ° for $^3J_{NH\alpha}$ 5–6 Hz; -120 ± 30 ° for $^3J_{NH\alpha}$ 8–9 Hz; and -120 ± 20 ° for $^3J_{NH\alpha}$ 9 Hz. Hydrogen-bond constraints were deduced from ^{1}H–^{2}H exchange experiments and the preliminary calculated structures. The latter constraints were introduced only in the final stages of the structure calculations and were given upper distance-limits of 2.2 Å for NH_i to O_j and 3.2 Å for N_i to O_j. The disulphide linkages were deduced from preliminary structures by measuring distances between sulphur atoms and checking the orientation of the cysteine side chains.

The torsion-angle dynamics program, DYANA [24], was used at all stages of the structure calculations prior to refinement. The NOAH protocol [25,26] was used in calculating preliminary structures and in assigning non-intra-residue and non-sequential NOESY cross-peaks. After obtaining the majority of the NOESY assignments, a standard simulated annealing procedure was applied. In the final structure calculations, 4800 DYANA structures were generated from random starting conformations. The 'best' 120 structures, with the lowest NOE violations, were then refined by simulated annealing with X-PLOR [27]. The simplified all-hydrogen force field was used, and the covalent geometry was constrained using the standard X-PLOR parameters. Interatomic distances and dihedral angles were constrained by experimental energy terms ($k_{noe} = 50$ kcal·mol^{-1}·Å^{-2}, $k_{cdihed} = 200$ kcal·mol^{-1}·rad^{-2}), which remained constant throughout the calculations. Initial atomic velocities were set from the Maxwell distribution at 1000 K, in which all non-bonded interactions were ignored, allowing the atoms to pass through each other (repel = 0.9, $C_{rep} = 0.005$ kcal·mol^{-1}·Å^{-2}). Simulated annealing was then performed by gradually 'cooling' the system to 100 K over 20 ps of simulated time, during which C_{rep} was increased linearly to 4 kcal·mol^{-1}·Å^{-2} while 'repel' was decreased to 0.75. Restrained gradient-minimization of 40 cycles was performed in the final stage of the protocol.

The coordinates for the ensemble of 20 structures have been deposited with the Brookhaven Protein Data Bank with accession code 1D6B.

RESULTS AND DISCUSSION

Structure determination by NMR

Standard procedures were implemented in assigning NMR resonances [28]. The amide-proton signals of DLP-2 at 298 K and pH 3.6 were generally well resolved, making the resonance assignment process straightforward. Most of the signals from the backbone amide protons were intense, except for those of Ser^{12} and Tyr^{31} that were also broad. Spectra were also obtained at 283 K to aid in resolving several overlapping peaks and in confirming other resonance assignments.

Preliminary structure calculations were performed with DYANA [24] implementing the NOAH automatic structure calculation scheme [25,26]. This protocol led to a moderately well-defined global fold with identification of approx. 90 % of all NOESY cross peaks. The validity of the assignments obtained by NOAH were checked, and further NOESY cross-peak assignments were manually performed by analysing the 2D data and the calculated medium resolution structures.

Although no disulphide bonds were included during the early stages of the calculations, the resulting medium-resolution structures did show the defined cysteine pairing configurations of DLP-2 to be Cys^9-Cys^{39}, Cys^{16}-Cys^{32} and Cys^{24}-Cys^{40}. Direct NOE cross-peaks, which were evident between the Hβ of the six cysteine residues, assisted considerably in orientating the cysteine side chains in the calculation, allowing the cysteine pairs to be identified with ease.

After using the NOAH protocol, the standard simulated-annealing procedure in DYANA was used to improve the 'quality' of the structures; thus an iterative cycle of calculation, structure analysis, and constraint revision was performed. The hydrogen-bonding pairs were deduced only during the later stages of the calculations, and were included as conformational constraints.

A total of 715 non-redundant inter-proton distance constraints, 24 dihedral-angle constraints, and 16 hydrogen-bond constraints, were used to obtain the final DLP-2 structure. The NOE distance constraints consisted of 172 long-range, 95 medium-range, 190 sequential, and 242 intraresidue constraints. In the final round of calculations, 120 out of 4800 structures that had been generated in DYANA were refined using the simulated annealing protocol in X-PLOR [27]. The 'best' 20 X-PLOR structures with the lowest total 'energies' were used as representatives of the DLP-2 solution structure. None of these structures had NOE violations greater than 0.2 Å, or dihedral-angle violations greater than 2 °. Table 1 contains a summary of the structural characteristics of the ensemble of 20 DLP-2 structures.

Description of the structure of DLP-2

The DLP-2 structure incorporates a poorly defined N-terminal region of up to five residues, as indicated by the low backbone angular order parameters for ϕ and ψ angles, and high root-mean-square difference(s) (RMSD) from the mean structure. The well-defined region of the molecule, which encompasses residues 6–42, had angular parameters (S) greater than 0.86 in all cases, and the mean global backbone RMSD, with respect to the mean structure, was 0.46 ± 0.13 Å. In contrast, the mean global backbone RMSD was 1.28 ± 0.35 Å when the backbone of the whole molecule was considered. Figure 3 shows the ensemble of 20 calculated structures superimposed over the backbone of the 'well-defined' region (residues 6–42). Some parts of the well-defined region are clearly seen in Figure 3 to be better defined than other parts, for example residues 14–19, 25–27, and 37–42.

PROMOTIF analysis [29] of the ensemble of 20 DLP-2 structures revealed that the main secondary structural elements in DLP-2 consist of a helical conformation over residues 9–12, and an antiparallel β-sheet over residues 15–18 and 37–40 (Figure 4A). Thus the DLP-2 structure begins with a flexible five-residue N-terminus. Residues 7–8 are situated close to residues 30–31, with the backbone NH of Gln^7 forming a hydrogen bond with the carbonyl of Tyr^{31}. This configuration almost creates a small parallel β-sheet in this part of the molecule. In nine out of the 20 calculated structures, residues 9–12 formed a short α-helix; in one structure this formed a 3_{10} helix, while in 10 of the structures this region incorporated a series of three β-turns situated at residues 8–11, 9–12, and 10–13. The dearth of medium-range cross-peaks in the NOESY spectrum was responsible for the lack of consistent definition in this part of the molecule. Residues 13–14 connected this helix-like configuration to the first strand of

Table 1 Structural statistics for the ensemble of 20 DLP-2 structures

Values given as means ± S.D.

(a)

	Distance restraints
Intraresidue (|i–j| = 0)	242
Sequential (|i–j| = 1)	190
Medium-range (|i–j| ≤ 5)	95
Long-range (|i–j| > 5)	172
Hydrogen bonds	16
Total	715
	Dihedral-angle restraints
ϕ	24

(b)

	Mean RMSD
From experimental restraints	
NOE (Å)	0.013 ± 0.001
Dihedrals (deg.)	0.08 ± 0.05
From idealised covalent geometry*	
Bonds (Å)	0.00137 ± 0.00008
Angles (deg.)	0.307 ± 0.003
Impropers (deg.)	0.106 ± 0.006

(c)

	Mean energies (kcal · mol^{-1})
E_{NOE}†	6.44 ± 0.95
E_{cdih}†	0.01 ± 0.02
E_{vdW}	0.08 ± 0.08
E_{bond}	1.29 ± 0.16
$E_{improper}$	0.66 ± 0.08
E_{angle}	17.59 ± 0.30
E_{total}	26.07 ± 1.23

(d)

	Ramachandran plot analysis (PROCHECK [43])
Most favoured region	49.9 ± 4.7
Additionally allowed region	40.4 ± 5.9
Generously allowed region	9.1 ± 4.4
Disallowed region	0.6 ± 1.1

(e)

	Atomic RMSD (Å)‡	
	Versus mean	Pairwise
Backbone atoms (6–42)	0.46 ± 0.13	0.65 ± 0.18
Heavy atoms (6–42)	1.00 ± 0.12	1.41 ± 0.21

* Idealized geometry as defined by the CHARMM force field within X-PLOR.

† Final values of the square-well NOE and dihedral-angle potentials calculated with force constants of 50 kcal · mol^{-1} · Å^{-2} and 200 kcal · mol^{-1} · Å^{-2} respectively.

‡ Atomic differences given as average RMSD against mean coordinate structure (mean) and average RMSD of all pairwise structures (pairwise). Values given as means ± S.D.

the antiparallel β-sheet, as defined by residues 15–18. The ϕ dihedral angle of residue 13 had a characteristic positive value near 90 °, suggesting a reverse turn [30]. The helix axis was seen to be almost parallel to the second β-strand.

The presence of an antiparallel β-sheet formed by residues 15–18 and 37–40 is consistent with the results of the ^{1}H–^{2}H exchange experiment which provided evidence of the hydrogen-bonded pairs as follows: NH Val^{15}-CO Cys^{40}, NH Cys^{40}-CO Val^{15}, NH Arg^{17}-CO Lys^{38}, and NH Lys^{38}-CO Arg^{17}. The antiparallel β-sheet appeared to be twisted and connected by a large loop defined by residues 19–36 that surrounds the second β-strand formed by residues 37–40. This gives the impression that the second strand (or the C-terminus) is trapped in the middle of the molecule, surrounded by the first strand on one side and by the large loop on the other (Figure 4B). The loop defined by residues 19–36 incorporates four β-turns, 18–21 (type I), 21–24 (type IV), 27–30 (type IV), and 34–37 (type IV). The turn at residues 27–30 forms a distinct bulge on the loop. The C-terminus is bent near residue 41 and points towards the first β-strand.

The disulphide conformation of Cys^9-Cys^{39} was right-handed in 19 out of 20 of the calculated structures, with a χ_{ss} value of 86 ± 4 °, while that of Cys^{24}-Cys^{40} was left handed in 14 out of the 20 structures with a χ_{ss} value of -72 ± 7 °. The conformation of the Cys^{16}-Cys^{32} disulphide bond was poorly defined, although direct NOE interactions between the Hβ of the cysteine pairs were observed experimentally, so they were included as constraints in the structure calculations. The DLP-2 molecule has a large hydrophobic region that spans most of the N-terminus and the bulge on the large loop. Hydrophobic residues in this region include Ile^1, Met^2, Phe^3, Phe^4, Ala^8, Cys^9, Trp^{10}, Pro^{26}, Met^{27}, Ala^{28}, Trp^{29}, and Cys^{39}. With the exception of Cys^9 and Cys^{39}, which are buried in the interior of the molecule, all these hydrophobic residues have their side chains orientated towards the surface of the molecule, thus exposing them to the solvent.

Two highly charged regions exist in the calculated DLP-2 structures; these are situated near or within the β-turns along the large loop. The first region, which includes Arg^{17}, Asp^{18}, Lys^{19}, Glu^{21}, and Arg^{22}, is relatively large and encompasses part of the first β-strand and two β-turns (residues 18–21 and 21–24). The second region is located at the end of the large loop and encompasses one β-turn (residues 34–37) and incorporates Glu^{33}, Arg^{35}, and Lys^{38}. Both of these charged regions of DLP-2 are very hydrophilic since they also include polar residues such as Asn, Gln, and Ser. The region defined by residues 10–13, 29–31, and 41–42 are moderately hydrophilic.

Comparison of DLP-2 with β-defensin-12

The superposition of the backbone atoms of residues 7–42 in DLP-1 and DLP-2 (Figure 5A) yielded an RMSD value of 1.1 Å, clearly showing that the tertiary structures of the two molecules are very similar, notwithstanding the fact that their sequence similarity is only 36 %. This similarity of folding is manifest in the disulphide-bond pairing patterns of Cys^9-Cys^{39}, Cys^{16}-Cys^{32}, and Cys^{24}-Cys^{40} that are identical in the two DLPs. Moreover, the N-termini of DLP-1 and DLP-2 are both flexible, while the C-termini that incorporate residues 40–42 are bent in the same manner.

The secondary structural elements found in DLP-2 are similar to those in DLP-1 (Figure 5B); the helix, antiparallel β-sheets, and β-turns that are present in DLP-1 [9] were also evident in DLP-2. A subtle difference is that the helix in many of the calculated DLP-2 structures was an α-helix, spanning residues 9–12, while in DLP-1 it is a 3_{10} helix that spans residues 10–12. This may not be a 'real' difference since this region of the molecule was not as clearly defined in the calculated structures of DLP-2 as it was in DLP-1. The similarity in the secondary structures of DLP-1 and DLP-2 is also manifest in the results

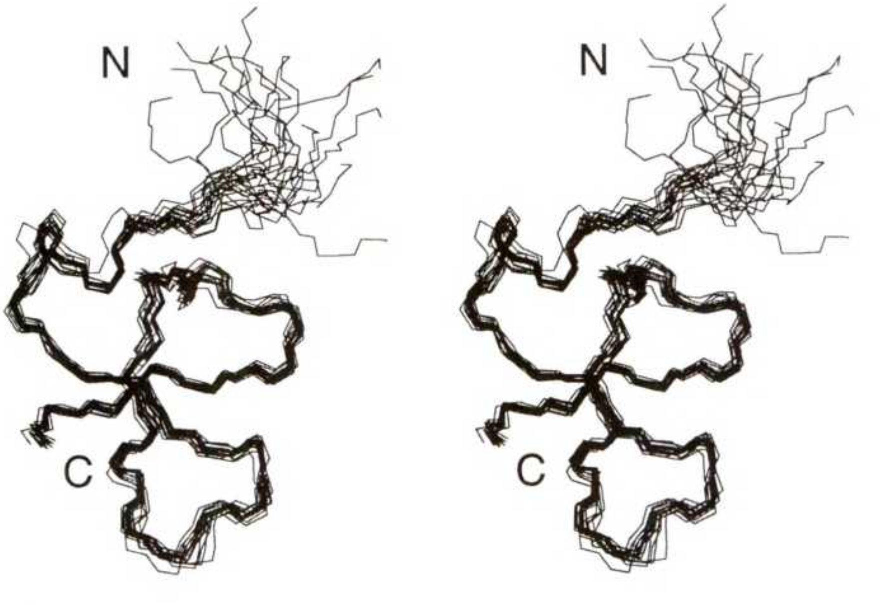

Figure 3 Ensemble of 20 DLP-2 structures

Stereo view of the ensemble of 20 DLP-2 structures superimposed to show the best fit over the backbone atoms of residues 6–42 of the mean-coordinate structure. Only the N, C, and Cα atoms of the backbone are displayed.

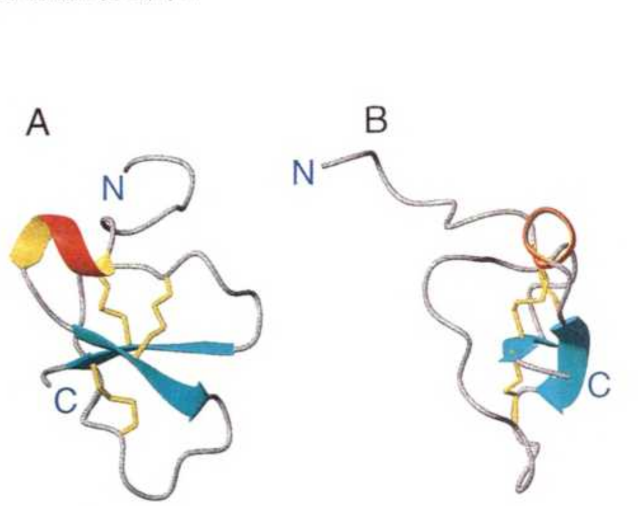

Figure 4 Schematic drawing of DLP-2 structure

Schematic drawing of DLP-2 showing the locations of the disulphide bonds (yellow), β-strands (cyan), and α-helix (red and yellow). The two Figures are related by approx. 90 ° rotation about the 'virtual' vertical axis. The program MOLMOL [44] was used to generate the Figures.

of ^1H–^2H exchange experiments that showed a similar pattern of exchange rates for the amide protons.

The major difference between the structural features of DLP-1 and DLP-2 was only revealed when the nature of the side chains on the different regions of the molecules were emphasized. Specifically, in DLP-2 the N-terminus up to residue 6 is highly hydrophobic, while in DLP-1 only the first two residues are hydrophobic. The surface region which encompasses residues 8, 10 and 31 in DLP-2 is moderately hydrophobic, but it is highly basic in DLP-1. DLP-2 has a large continuous hydrophobic surface region incorporating the N-terminus up to residue 11 and the hydrophobic bulge in the large loop, but these features are not evident in DLP-1. These differences between DLP-1 and DLP-2 are illustrated in the surface representation of the two molecules in Figure 6.

Despite a sequence similarity of only 21 %, DLP-2 and β-defensin-12 have similar global folds (Figures 5C and 5D). As with DLP-1, the two antiparallel β-strands of DLP-2 closely match those of β-defensin-12, but the latter is longer by one residue. Furthermore, part of the large loop in DLP-2 can be superimposed well on the third antiparallel β-strand that contains the β-bulge in β-defensin-12. However, a computer-based structure comparison using the DALI algorithm [31] showed that the degree of 'structural similarity' between DLP-2 and β-defensin-12 is less than that between DLP-1 and β-defensin-12 [9].

Structural implications

Considering the fact that DLP-2, DLP-1, and β-defensin-12 are folded similarly, it is reasonable to postulate that the unique fold shared by these peptides is due to the conserved residues in their amino acid sequences. As mentioned above, there are only a few of these equivalent residues; they are Cys^9, Gly^{14}, Val^{15}, Cys^{16}, Cys^{32}, Lys^{38}, Cys^{39}, and Cys^{40} in all three molecules, and Lys^{25} and Met^{27} in DLP-2, which are conservatively substituted as Arg and Ile, in DLP-1 and β-defensin-12 respectively. It is clear that the cysteine residues that are paired in the order 1–5, 2–4, and 3–6 in all three molecules play a crucial role in achieving and/or maintaining the distinct tertiary structure. Also, most of the conserved residues (including the cysteines) are involved in hydrogen bonding with other residues.

It was shown previously that the disulphide-connectivity pattern of 1–5, 2–4, and 3–6 of the DLPs is also found in other toxic peptides, such as the sea anemone peptides ShI, ATX-II and AP-A [32–34], and the rattle snake myotoxin *a* [35,36]. The global fold of DLP-1 was shown, using the DALI algorithm, to have some weak similarities to ShI. Superposition of the structurally equivalent backbone atoms showed that the β-strands

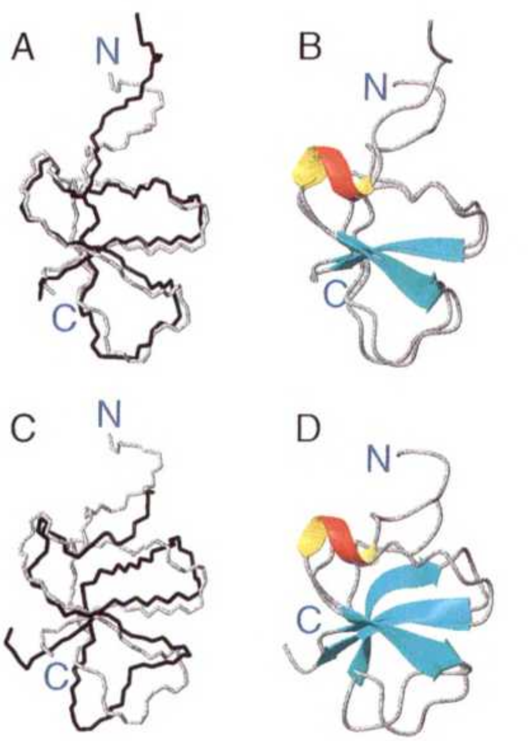

Figure 5 Comparison of DLP-2, DLP-1 and β-defensin-12 structures

(**A**) DLP-2 and DLP-1 structures superimposed over N, C, and Cα atoms of the backbone of residues 7–42. DLP-2 and DLP-1 residues are shown in light grey and black respectively. (**B**) Same as diagram in (**A**) except drawn in MOLMOL [44]. (**C**) DLP-2 and β-defensin-12 structures superimposed over N, C, and Cα atoms of the backbone of residues 8–23, 24–27, and 30–41 of DLP-2, and residues 4–19, 21–24, and 25–36 of β-defensin-12. DLP-2 and β-defensin-12 residues are shown in light grey and black respectively. (**D**) Same as diagram in (**C**) except drawn in MOLMOL [44].

in the antiparallel β-sheet in both molecules coincide well, although the primary structures are significantly different. This finding, together with the similarity to DLP-2, underscores the importance of the cysteine-pairing pattern as an indicator of the specific tertiary structure.

Possible structures of DLP-3 and DLP-4

Due to the high level of sequence similarity between DLP-2, DLP-3, and DLP-4, it is likely that they are all folded in a similar manner. One possible difference between the folds of DLP-2 and DLP-4, which are isomers, is that their cysteines are paired in different ways. This is plausible because the six cysteines are relatively close to each other and in particular the last two cysteines of DPL-2 and DLP-4 are adjacent in the sequence, thus enabling interchange of the disulphide bonds without significantly altering the main part of the tertiary structure. The latter exchange phenomenon is exemplified by β-defensin-12 and NP-2, which have similar global folds but their disulphide pairings are quite different, being 1–5, 2–4 and 3–6 in β-defensin-12 and 1–6, 2–4, 3–5 in NP-2 [15]. Disulphide-pairing patterns such as 1–4, 2–5, 3–6, are also conceivable in the DLPs: the first cysteine is relatively close to the fourth one situated in the large loop, while the second cysteine that is located on the first β-strand is also near the fifth cysteine that is located in the adjacent second β-strand. Although some of these disulphide-pairing patterns are possible, the fact that the 1–5, 2–4, and 3–6 pattern is found in DLP-1, DLP-2, β-defensin-12, ShI, and myotoxin *a* implies that it is probably more stable than other possible combinations.

DLP-3 lacks the third and the fifth cysteines that correspond to Cys^{24} and Cys^{39} in DLP-2 (Figure 2). Since the disulphide-pairing pattern in DLP-2 is 1–5, 2–4, and 3–6, this implies that the four cysteines in DLP-3 could be paired differently from those in DLP-2. Assuming that the global folds of DLP-2 and DLP-3 are similar, the likely disulphide pairing in DLP-3 is therefore 1–6 and 2–4, which is similar to that in NP-2. However, it is important also to consider the fact that DLP-3 lacks the residue corresponding to Asn^{36} in DLP-2, so that the sixth cysteine may be the one that is actually missing and not the fifth. This line of reasoning leads to the proposal that the cysteine pairing is 1–5 and 2–4.

Roles of DLPs in the platypus venom

As mentioned in the Introduction, the platypus venom is not likely to be used to capture prey since its venom apparatus is absent from the female and it is situated on the hind legs away from the mouth. Also, because of its relatively low toxicity, compared to the snake venoms, platypus venom most probably is used to incapacitate and ward off enemies without necessarily inflicting permanent harm to them. Therefore it is unlikely that platypus venom includes highly toxic components like those in the snake venoms; the latter are clearly used to capture prey and include α- and β-neurotoxins, and proteases and phospholipases which aid in the pre-digestion of the prey.

The discovery of OvCNP and OvNGF in platypus venom provided important clues on the basis of action of the venom, as these peptides have significant sequence similarities to those found in other biological systems. Natriuretic peptides exist in tissues such as mammalian heart, brain, and endothelium, where they are involved in reducing blood pressure; and it has recently been discovered in the venom of green mamba snake (*Dedroaspis anguisceps*) [37]. The NGF, on the other hand, exists in mouse submaxillary glands and is also prevalent in the venom of a wide variety of snake venoms. However, it is worth emphasizing that the distinctly different location of the venom glands suggests an evolutionary/embryological relationship that is not straightforward, or that the peptide composition of the secreted solution may be the result of common evolution in various exocrine glands.

The existence of numerous protein and non-protein components is not peculiar to platypus venom. Snake venoms are also complex, but what makes the platypus venom unique is the presence of many novel components, such as the DLPs, whose physiological actions are unknown at present. We have performed various assays to assess the antimicrobial [9], myotoxic [38], haemolytic [39], and cell-promoting activities [40] of DLPs, however all of these tests gave negative results.

Determining the roles of the components has proven difficult, and this may be partly due to the activity being affected by the presence of other components, similar to some lipases which require a co-lipase for their activity to be manifest. Specifically, a venom component may act synergistically with others so that it may be inactive during a pharmacological/physiological assay when present alone. Note also that the platypus lives in an isolated environment in eastern Australia and therefore encounters very few species of animals its own size during its lifetime. Thus common biological assays may not be applicable to the platypus venom since the cells that are routinely used are obtained from tissues of species that may never be encountered by a platypus.

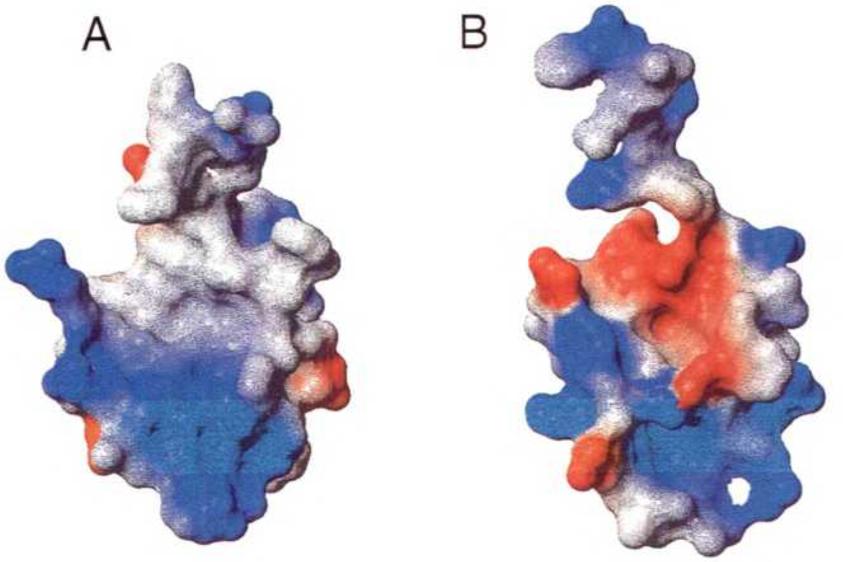

Figure 6 Comparison of DLP-2 and DLP-1 molecular surfaces

Molecular forms of DLP-2 (**A**) and DLP-1 (**B**) showing the charge distributions of one of their corresponding surfaces. Surfaces with positive and negative electrostatic potentials were drawn in blue and red respectively. These Figures were created using the standard charge settings in MOLMOL [44].

One possible role of the DLPs in the venom is that they may act synergistically with OvNGF to produce the pain that is such a prominent symptom of platypus envenomation. It has been speculated that NGF in some snake venoms potentiates the effect of other toxins by stimulating various cells of its victim, thus rendering the victim more susceptible to the toxins. Human NGF causes hyperalgaesia and not pain itself [41]; hyperalgaesia is also found with platypus envenomation. The suggestion that OvNGF causes pain is based on experiments using composite protein fractions of the venom. Since DLPs are abundant in platypus venom and DLP-3 co-elutes with OvNGF in reverse-phase HPLC, there is a distinct possibility that DLPs were present in all the samples of OvNGF that were used in experiments which elicited hyperalgaesia.

Conclusion

Unlike the situation with most snake venoms, the existing knowledge on the nature of platypus venom is far from complete. Platypus venom has been shown to contain numerous novel peptides and proteins whose structures and functions require further investigation before a definitive understanding of the pharmacology of this mixture is arrived at. The biological roles of the constituents have been elusive partly due to complications introduced by 'synergistic effects' in the assays used, and partly because the constituents are unique and absent in the venoms of other animals.

The present study of the tertiary fold of DLP-2 is a step towards understanding the biological function of the DLPs which are the major peptides in platypus venom. The work not only revealed structural information on the DLPs but also provided useful data on the structures of β-defensin-12. The distinct fold shared by DLP-1, DLP-2, and β-defensin-12 can be attributed to a small number of amino acid residues in the sequence that appear to determine and maintain the form of the structural fold. These important residues include six cysteines that are paired in the order 1–5, 2–4, and 3–6. The distinct structural scaffold of the DLPs is a configuration that has evolved to yield a small compact molecule. The findings presented here introduce a structural peptide core that could support different functional groups and hence display different pharmacological/physiological activities.

This work was supported by a grant from Australian Research Council to P. W. K. We thank Dr Bill Bubb and Dr Bob Chapman for help with the NMR spectrometer, and Mr Bill Lowe for expert technical assistance.

REFERENCES

1 Calaby, J. H. (1968) in Venomous Animals and Their Venoms, vol. 1 (Bucherl, W., Buckley, E. E. and Deulofeu, V., eds.), pp. 15–29, Academic Press, New York
2 Sutherland, S. K. (1983) Australian Animal Toxins: The Creatures, Their Toxins and Care of The Poisoned Patient, Oxford University Press, Melbourne
3 Burell, H. (1927) The Platypus, Angus & Robertson, Sydney
4 Edstrom, A. (1992) Venomous and Poisonous Animals, Krieger Publishing Company, Florida
5 Grant, T. (1995) The Platypus, a Unique Mammal, New South Wales University Press, Kensington, NSW
6 Fenner, P. J., Williamson, J. A. and Myers, D. (1992) Platypus envenomation—a painful experience. Med. J. Aust. **157**, 829–832
7 Wood-Jones, F. (1923) The Mammals of South Australia, Part 1, Government Printer, Adelaide
8 Martin, C. J. and Tidswell, F. (1895) Observations of the femoral gland of Ornithorhynchus and its secretion: together with an experimental enquiry concerning its supposed toxic action. Proc. Linn. Soc. NSW **9**, 471–500
9 Torres, A. M., Wang, X, Fletcher, J. I., Alewood, D., Alewood, P. F., Smith, R., Simpson, R. J., Nicholson, G. M., Sutherland, S. K., Gallagher, C. H. et al. (1999) Solution structure of a defensin-like peptide from platypus venom. Biochem. J. **341**, 785–794
10 De Plater, G., Martin, R. L. and Milburn, P. J. (1995) A pharmacological and biochemical investigation of the venom from the platypus (Ornithorhynchus anatinus). Toxicon **33**, 157–169
11 De Plater G. (1998) Fractionation, Primary Structural Characterisation and Biological Activities of Polypeptides from the Venom of the Platypus (Ornithorhynchus anatinus). Ph.D. Thesis, Australian National University, Canberra, Australia
12 De Plater, G., Martin, R. L. and Milburn, P. J. (1998) The natriuretic peptide (OVCNP-39) from platypus (Ornithorhynchus anatinus) venom relaxes the isolated rat uterus and promotes oedema and mast cell histamine release. Toxicon **36**, 847–857

13 Temple-Smith, P. D (1973) Seasonal Breeding Biology of the Platypus, Ornithorhynchus anatinus with Special Reference to the Male Ph.D. Thesis, Australian National University, Canberra, Australia

14 Selsted, M E, Tang, Y Q, Morris, W L, McGuire, P A, Novotny, M J, Smith, W, Henschen, A H and Cullor, J S (1993) Purification, primary structures, and antibacterial activities of β-defensins, a new family of antibacterial peptides from bovine neutrophils J Biol Chem **228**, 6641–6648

15 Zimmermann, G R., Legault, P, Selsted, M E. and Pardi, A (1995) Solution structure of bovine neutrophil β-defensin-12 the peptide fold of the β-defensins is identical to that of the classical defensins. Biochemistry **34**, 13663–13671

16 Marion, D and Wuthrich, K (1983) Application of phase-sensitive two-dimensional correlated spectroscopy (COSY) for measurements of ^{1}H-^{1}H spin-spin coupling constants in proteins. Biochem Biophys Res Commun **113**, 967–974

17 Rance, M, Sørensen, O W, Bodenhausen, G, Wagner, G, Ernst, R. R and Wuthrich, K (1983) Improved spectral resolution in COSY ^{1}H NMR spectra of proteins via double quantum filtering Biochem Biophys. Res Commun **117**, 479–485

18 Derome, A E and Williamson, M P. (1990) Rapid-pulsing artefacts in double-quantum-filtered COSY J Magn Reson. **88**, 177–185

19 Bax, A and Davis, D G (1985) MLEV-17 based two-dimensional homonuclear magnetisation transfer spectroscopy J. Magn Reson **65**, 355–360

20 Kumar, A, Ernst, R. R and Wuthrich, K. (1980) A two-dimensional nuclear Overhauser enhancement (2D nOe) experiment for elucidation of complete proton-proton cross-relaxation networks in biological macromolecules Biochem Biophys Res Commun **95**, 1–6

21 Piotto, M, Saudek, V and Sklenář, V (1992) Gradient-tailored excitation for single-quantum NMR spectroscopy of aqueous solutions J Biomol NMR **2**, 661–665

22 Bartels, C, Xia, T, Billeter, M, Guntert, P and Wuthrich, K (1995) The program XEASY for computer-supported NMR spectral analysis of biological macromolecules J Biomol NMR **5**, 1–10

23 Szyperski, T, Guntert, P, Otting, G and Wuthrich, K (1992) Determination of scalar coupling constants by inverse Fourier transformation of in-phase multiplets J. Magn Reson **99**, 552–560

24 Guntert, P, Mumenthaler, C and Wuthrich, K. (1997) Torsion angle dynamics for NMR structure calculation with the new program DYANA J Mol Biol. **273**, 283–298

25 Mumenthaler, C and Braun, W (1995) Automated assignment of simulated and experimental NOESY spectra of proteins by feedback filtering and self-correcting distance geometry J Mol Biol **254**, 465–480

26 Mumenthaler, C., Guntert, P, Braun, W and Wuthrich, K (1997) Automated combined assignment of NOESY spectra and three-dimensional structure determination. J. Biomol NMR **10**, 351–362

27 Brunger, A T (1992) X-PLOR Version 3 1 A System for X-ray Crystallography and NMR, Yale University, New Haven, CT

Received 7 February 2000/24 March 2000, accepted 11 April 2000

28 Wuthrich, K (1986) NMR of Proteins and Nucleic Acids, John Wiley and Sons, New York

29 Hutchinson, E G and Thorton, J M (1996) PROMOTIF—a program to identify and analyze structural motifs in proteins Protein Sci **5**, 212–220

30 Ludvigsen, S and Poulsen, F M (1992) Positive ϕ-angles in proteins by nuclear magnetic resonance spectroscopy J Biomol NMR **2**, 227–233

31 Holm, L and Sander, C (1993) Protein structure alignment of distance matrices J Mol Biol **233**, 123–138

32 Fogh, R H, Kem, W R and Norton, R S (1990) Solution structure of neurotoxin I from the sea anemone Stichodactyla helianthus A nuclear magnetic resonance, distance geometry, and restrained molecular dynamics study J Biol Chem **265**, 13016–13028

33 Wilcox, G R, Fogh, R. H and Norton, R S (1993) Refined structure in solution of the sea anemone neurotoxin ShI J Biol Chem **267**, 24707–24719

34 Gould, A L, Mabbutt, B C, Llewellyn, L E, Goss, N H and Norton, R S (1992) Linear and cyclic peptide analogues of the polypeptide cardiac stimulant, anthopleurin-A, ^{1}H-NMR and biological studies Eur J Biochem **206**, 641–651

35 Fox, J W, Elzinga, M and Tu, A T (1979) Amino acid sequence and disulfide bond assignment of myotoxin *a* isolated from the venom of prairie rattlesnake (Crotalus viridis viridis) Biochemistry **18**, 678–684

36 Mebs, D and Ownby, C L (1990) Myotoxic components of snake venoms their biochemical and biological activities Pharmacol Ther **48**, 223–236

37 Schweitz, H., Vigne, P, Moinier, D, Frelin, C. and Lazdunski, M (1992) A new member of natriuretic peptide family is present in the venom of the green mamba (Dendroaspis angusticeps) J Biol Chem **267**, 13928–13932

38 Barfaraz, A and Harvey, A L (1994) The use of the chick biventer cervicis preparation to assess the protective activity of six international reference antivenoms on the neuromuscular effects of snake venoms in vitro Toxicon **32**, 267–272

39 Kellaway, C H and LeMessurier, D H (1935) The venom of the platypus (Ornithorhynchus anatinus) Aust J Exp Biol Med Sci **13**, 205–221

40 Doverskog, M, Han, L and Haggstrom, L (1998) Cystine/cysteine metabolism in cultured Sf9 cells influence of cell physiology on biosynthesis, amino acid uptake and growth Cytotechnology **26**, 91–102

41 Dyck, P J, Peroutka, S, Rasks, C, Burton, E, Baker, M K, Lehman, K A, Gillen, D A, Hokanson, J. L and O'Brien, P C (1997) Intradermal recombinant human nerve growth factor induces pressure allodynia and lowered heat-pain threshold in humans Neurology, **48**, 501–505

42 Barton, G J (1993) ALSCRIPT A tool to format multiple sequence alignments Protein Eng **6**, 37–40

43 Laskowski, R A, MacArthur, M W, Moss, D.S and Thorton, J M (1993) PROCHECK a program to check the stereochemical quality of protein structure coordinates J Appl Crystallogr **26**, 283–292

44 Koradi, R, Billeter, M and Wuthrich, K (1996) MOLMOL a program for display and analysis of macromolecular structures J Mol Graphics **14**, 51–55

Biochem J. (2000) 348, 657–665 (Printed in Great Britain)

Modulation of the smooth-muscle L-type Ca^{2+} channel $\alpha1$ subunit (α1C-b) by the β2a subunit: a peptide which inhibits binding of β to the I–II linker of $\alpha1$ induces functional uncoupling

Annette HOHAUS*, Michael POTESER†, Christoph ROMANIN‡, Norbert KLUGBAUER§, Franz HOFMANN§, Ingo MORANO*, Hannelore HAASE* and Klaus GROSCHNER†[1]

*Max-Delbruck-Centrum fur Molekulare Medizin, D-13092 Berlin, Germany, †Institut fur Pharmakologie und Toxikologie, Karl-Franzens-Universitat Graz, Universitatsplatz 2, A-8010 Graz, Austria, ‡Institut fur Biophysik, Johannes-Kepler-Universitat Linz, A-4040 Linz, Austria, and §Institut fur Pharmakologie und Toxikologie, Technische Universitat Munchen, D-80802 Munchen, Germany

---

Modulation of the smooth-muscle Ca^{2+} channel α1C-b subunit by the auxiliary β2a subunit was studied in the HEK 293 (cell line from human embryonic kidney cells) expression system. In addition, we tested whether the α1–β interaction in functional channels is sensitive to an 18-amino-acid synthetic peptide that corresponds to the sequence of the defined major interaction domain in the cytoplasmic I–II linker of α1C (AID-peptide). Ca^{2+} channels derived by co-expression of α1C-b and β2a subunits exhibited an about 3-fold higher open probability (P_o) than α1C-b channels. High-P_o gating of α1C-b·β2a channels was associated with the occurrence of long-lasting channel openings [mean open time (τ) > 10 ms] which were rarely observed in α1C-b channels. Modulation of fast gating by the β2a subunit persisted in the cell-free, inside-out recording configuration. Biochemical experiments showed that the AID-peptide binds with appreciable affinity to β2 subunits of native Ca^{2+} channels. Binding of the β2 protein to immobilized AID-peptide was specifically inhibited (K_i of 100 nM) by preincubation with free (uncoupled) AID-peptide, but not by a corresponding scrambled peptide. Administration of the AID-peptide (10 μM) to the cytoplasmic side of inside-out patches induced a substantial reduction of P_o of α1C-b·β2a channels. The scrambled control peptide failed to affect α1C-b·β2a channels, and the AID-peptide (10 μM) did not modify α1C-b channel function in the absence of expressed β2a subunit. Our results demonstrate that the β2a subunit controls fast gating of α1C-b channels, and suggest the α1–β interaction domain in the cytoplasmic I–II linker of α1C (AID) as a possible target of modulation of the channel. Moreover, our data are consistent with a model of α1–β interaction that is based on multiple interaction sites, including AID as a determinant of the affinity of the α1–β interaction.

INTRODUCTION

Gating as well as regulation of class C high-voltage-activated Ca^{2+} channels is for a large part determined by the interaction between α1 and β subunits [1–6].

In tissues of the cardiovascular system, L-type channels are formed by one out of two splice variants of α1C (a and b [7,8]) that are preferentially associated with β subunits of the β2 and β3 [9–11] isoform. A significant fraction of the L-type channels in various smooth-muscle tissues appear to be comprised of α1C-b and β2, and the subunit composition is considered essential for fine tuning of channel function [11]. Divergent modulatory effects have been observed with different β subunits, with β2a being an effective modulator of channel inactivation and open probability (P_o) [6,9,12]. So far, the susceptibility of the two class-C α1 splice variants to modulation by β2 species has not been compared in detail. A structure involved in the α1–β interaction has been located in the cytoplasmic loop between domains I and II of the α1 subunit [13,14]. Recent data support the view that modulation of the gating behaviour of the α1 subunit by β proteins involves multiple interaction sites [12]. Moreover, Shistik et al. [5] suggested the N-terminal tail of α1C as a crucial determinant of β subunit-dependent control of Ca^{2+} channel gating. Since the cardiac- and the smooth-muscle splice variants of α1C differ substantially in the N-terminal sequence, divergent modulation of these splice variants by β subunits may be anticipated. Modulation by β2a of the cardiac isoform of α1C-a has recently been characterized at the single-channel level [6], but so far a study on functional modulation of the smooth-muscle α1C-b isoform is lacking. The present study was designed to analyse the effects of β2a on the gating properties of α1C-b channels in intact cells as well as in excised inside-out patches. Cell-free, inside-out recording of Ca^{2+} channel activity was used to test for a role of the interaction domain in the I–II linker of α1C-b by disruption of the α1–β interaction in this motif using an 18-amino-acid synthetic peptide (QQLEEDLKGYLDWITQAE) that corresponds to the sequence of the proposed α1-β interaction domain in the I–II linker of class C α1 subunits. Our results demonstrate that fast gating of the smooth-muscle isoform of α1C is modulated by the β2a in a manner similar to α1C-a. Moreover, we report for the first time that the α1–β interaction within a functional Ca^{2+} channel is reversed by a synthetic peptide that interferes with binding of β to the I–II linker of the Ca^{2+} channel α1C subunit.

EXPERIMENTAL

Materials

The α1C–β interaction (AID) peptide as well as a corresponding control peptide of random amino acid sequence (scrambled peptide) was synthesized and purified by BioSyntan (Berlin,

---

Abbreviations used AID, α1C-β interaction domain in the cytoplasmic I-II linker of the Ca^{2+} channel α1C subunit, HEK 293, cell line from human embryonic kidney cells, P_o, open probability; τ, mean open time

[1] To whom correspondence should be sent (e-mail klaus groschner@kfunigraz ac at)

Germany). The 18-amino-acid AID-peptide (QQLEEDLKGYLDWITQAE) comprised the sequence 477–494 of the smooth-muscle α1C splice variant [7] designated as α1C-b. This sequence is identical with amino acids 458–475 of the cardiac Ca^{2+} channel α1 sequence ([13]; designated as α1C-a). The AID-peptide corresponds to the conserved sequence of the α1–β interaction domain (QQ-E-L-GY-WI--E) within the I–II linker of α1 subunits reported by Pragnell et al. [14]. The sequence of the scrambled peptide was TDIQDEGALWEQYLQKEL. Tissue-culture medium was from Gibco BRL (Vienna, Austria); the dihydropyridine-Ca^{2+} channel activator S(−)-BayK 8644 was from Research Biochemicals Incorporated (Natick, MA, U.S.A.), and all other chemicals were from Sigma Chemical Co. (Vienna, Austria).

Cell culture and transfection

HEK 293 (human embryonic kidney cells) were stably transfected with the coding region of the α1C-b subunit (HEKα1C-b) as described in [16]. To study the function of channels comprised of α1C-b [7] and β2a [9] subunits, HEKα1C-b were transiently transfected with β2a subunit as described in [17]. Expression of CD8 antigen and binding of CD8-antibody-coated beads was used as a marker to identify cells which were successfully transfected. HEK293 cells were cultured in Dulbecco's modified Eagle's medium that was supplemented with 10% (v/v) foetal-calf serum and contained 0.178 g/litre geneticin.

Measurement of single-channel currents

Ba^{2+} currents through single Ca^{2+} channels were recorded in the membrane of intact cells (cell-attached configuration) and in inside-out patches. Cell potentials were set to approximately zero by use of a high-K^+ low-Cl^- extracellular solution that contained (in mM): 110 potassium aspartate, 20 KCl, 2 $MgCl_2$, 20 Hepes, 2 EGTA; the pH was adjusted to 7.3 with N-methyl-D-glucamine, and pCa was adjusted to 7.5 using a Ca^{2+}-sensitive electrode. Patch pipettes were fabricated from borosilicate glass (Clark Electromedical Instruments, Pangbourne, Reading, Berks., U.K.), and had resistances of 5–10 MΩ. The pipette solution contained (in mM): 10 $BaCl_2$, 100 NaCl, 30 tetraethylammonium chloride and 15 Hepes, pH adjusted to 7.4. S(−)-BayK 8644 (1.0 μM) was included in the pipette solution to facilitate stabilization of channel activity in inside-out patches as well as in intact cells. To prevent run-down of channel activity in inside-out experiments, 2 mM ATP/Na_2 and 1 unit/ml calpastatin were added to the bath solution before patch excision [18]. Exchange of bath solutions and administration of the α1–β interaction peptide (10 μM) or a scrambled control peptide was performed during constant-flow perfusion. All experiments were performed at room temperature.

Voltage clamp and current amplification was performed with a List (Darmstadt, Germany) EPC/7 patch-clamp amplifier. Current records were filtered at 1 kHz (−3 dB) and digitized at a rate of 5 kHz. Experiments were controlled using pClamp software (Axon Instruments, Foster City, CA, U.S.A.). For idealization of current records, custom-made level-detection software was employed [19]. Ca^{2+} channel activity was calculated as the mean number of open channels (NP_o) during depolarizing pulses, and the gating properties of single channels were analysed in terms of channel availability (P_s), i.e. the probability that a channel will open upon depolarization, as well as the open probability (P_o) of available channels as described previously [20,21].

Events were compiled in open-time histograms constructed with variable bins (logarithmic scale) and fitted with multiple exponential functions.

Ca^{2+} channel preparations

Cardiac homogenate and cytoplasmic proteins were prepared from adult Wistar rats (strain Schö:Wist) and used as a source of native Ca^{2+} channel β2 subunits. Frozen cardiac tissue was homogenized as in [22] using a Polytron PT homogenizer and buffer A, consisting of 5 mM histidine/HCl, pH 7.4, 120 mM KCl, 50 mM $Na_4P_2O_7$, 25 mM NaF, 10 mM EDTA, 0.2 mM dithiothreitol, 0.1 mM PMSF, 1 μM pepstatin A, 17 μg/ml calpain I and 7 μg/ml calpain II. The cytoplasmic fraction was prepared by high-speed centrifugation of the homogenate proteins at 100000 **g** for 2 h. Homogenate proteins were solubilized with 1% digitonin as described in [23].

Affinity binding of β2 subunits to immobilized α1C–β interaction peptide

To achieve covalent binding of the α1C–β interaction peptide (AID-peptide) to agarose beads, the AID-peptide was synthesized with a N-terminal monochloroacetylglycyl extension. The peptide was immobilized to ω-aminohexyl-agarose for 3 h at a peptide concentration of 6 mg/ml of packed gel via activation of the ω-amino groups as previously described [24]. *In vitro* binding assays were performed by incubation of solubilized rat heart homogenate proteins (0.5 mg) or cytosolic proteins (0.5 mg) with 10 μl of beads in buffer A (supplemented with 0.1% digitonin) for 2 h at 4 °C on a rotating wheel. The beads were extensively washed with digitonin-containing buffer A, extracted with SDS-sample buffer, and the eluted proteins separated on 7% (w/v) polyacrylamide gels. Competition experiments were done by incubation of cardiac β2 protein samples with either free AID-peptide or scrambled peptide overnight at 4 °C prior to binding on to AID-affinity beads.

SDS/PAGE and Western-blot analysis

Protein samples were subjected to SDS/PAGE and Western-blot analysis according to standard protocols. Briefly, the blots were incubated with the affinity-purified, β2 isoform-specific antibody (directed against the C-terminal β2 epitope EWNRDVYIRQ) at a concentration of 1 μg IgG/ml for 90 min and with the secondary peroxidase-conjugated antibody (anti-rabbit IgG; BioGenes, Berlin, Germany; diluted 1:10000) for 60 min at room temperature as described in [22]. Immunoreactive β2 protein bands were revealed by enhanced chemiluminescence reaction kit (ECL®, Amersham) using a X-ray film. The antibody recognized the 85-kDa β2 subunit expressed in brain [25], cardiac [25,26] and smooth muscle [10]. For comparison, the β3-isoform-specific antibody was employed. It stained an approx.-60-kDa protein [22,25]. ECL® signals were evaluated by computer-assisted scanner densitometry (ScanPack; Biometra, Goettingen, Germany). Densitometric analysis of the bands was within the linear range of immunoreaction.

Statistics

Averaged results are given as means ± S.E.M. for the indicated number of experiments. Two-tailed *t* tests were used for statistical comparisons, using either the unpaired or paired format. Differences were considered statistically significant at $P < 0.05$.

RESULTS

The β2a subunit promotes high P_0 gating and induces ultralong openings of α1C-b

Figure 1 shows representative single-channel recordings obtained with α1C-b and α1C-b·β2a channels in the cell-attached recording configuration. Multiple channels were detected in the majority of experiments in cells co-expressing α1C-b and β2a subunits. The observed functional channels/patch were in the range of 2–6 in cells co-expressing α1C-b and β2a, but 1–3 in cells expressing α1C-b only. Gating properties were analysed with a recently developed method [20] for the analysis of multichannel

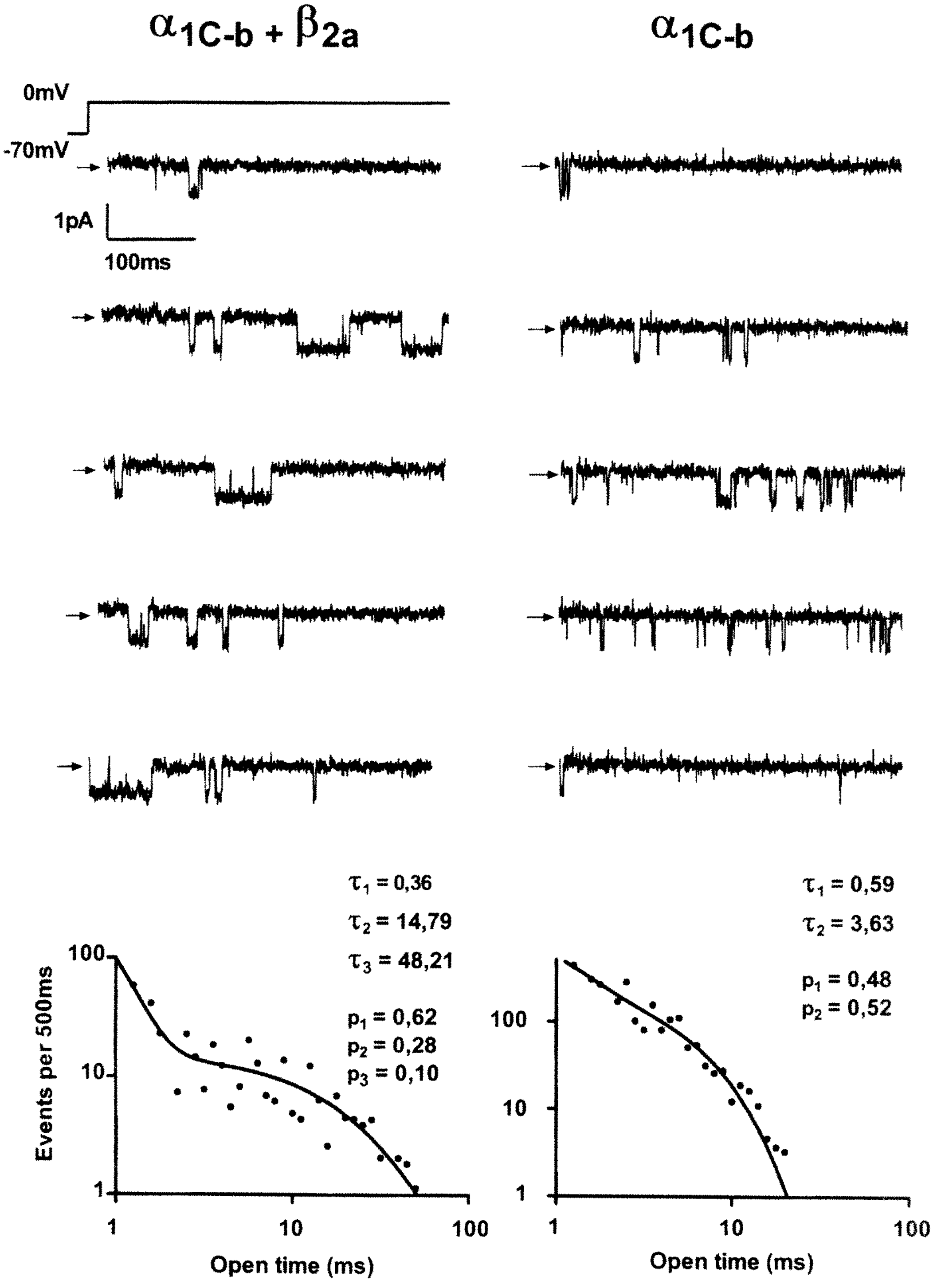

Figure 1 β**2a subunit increases the fraction of long-lasting openings of** α**1C-b channels in cell-attached patches**

Top: individual current responses recorded during depolarizing voltage pulses. Bottom: open dwell-time histograms calculated from the experiments shown above. Dwell-time histograms were fitted with exponential functions (continuous lines) using Marquardt-least-squares or maximum-likelihood method. Time constants (τ_1, τ_2) and percentual fractions of dwell times (p_1, p_2) are given.

Table 1 Effects of β2a on gating of α1C-b channels

Values are means ± S E M for the indicated number of experiments *Denotes statistically significant difference versus channels derived by expression of α1C-b only n d , not detectable

	P_o (%)	P_s (%)	Mean open time (ms)	Proportion of long openings ($\tau > 10$ms) (%)
Cell-attached				
α1C-b ($n = 5$–7)	3 3±0 7	42 2±8 2	2 3±0 3	n d
α1Cb β2a ($n = 10$)	11 1±1 9*	48 3±2 2	9 3±2 2*	35 0±11 4
Inside-out				
α1C-b ($n = 8$)	3 6±1 0	50 1±2 2	3 5±0 4	6 0±4 55
α1C-b·β2a ($n = 8$–10)	7 3±0 7*	56 9±2 5	6 2±1 0*	15 1±5 16

patches that allows for calculation P_o as a parameter of fast gating, and availability (P_s) as a parameter that characterizes the slow gating between available and unavailable states of the Ca^{2+} channels. This analysis revealed that co-expression of the β2a subunit increased not only the mean number of functional channels in the patches of membrane, but, in addition, clearly increased P_o of individual channels (Table 1). In contrast, availability (P_s) of Ca^{2+} channels was not significantly affected by expression of the β2a subunit. Channels comprising both α1C-b and β2a subunits exhibited a fast gating pattern strikingly different from that of channels derived by expression of the α1C-b subunit alone In experiments with single-channel patches, or when mostly the opening of a single channel was recorded, open time distributions were analysed. As illustrated in Figure 1, the elevated level of P_o in α1Cb β2a channels was associated with a significantly increased mean open time and promotion of long-lasting channel openings. Open time distributions obtained with α1C-b·β2a channels were best fitted by two, or in most cases, by three exponentials with an ultra-long-lived open state exhibiting a mean open time (τ) > 10 ms. The mean proportion of such ultra-long-lasting openings amounted to 35±11.2% (Table 1). In cells expressing only the α1C-b subunit, open time distributions were best fitted with two exponential components Openings with $\tau > 10$ ms were not statistically resolved in the open-time histograms.

When the expressed Ca^{2+} channels were studied in the excised inside-out configuration, differences in the gating pattern of channels comprised of α1C-b plus β2a versus α1C-b alone were again detectable (Figure 2) The most striking discrepancy concerned P_o, which was significantly (about 2-fold) higher in α1C-b β2a channels (Table 1). In inside-out recordings, ultra-long-lasting openings ($\tau > 10$ ms) were detectable in the open-time distributions of both α1C-b·β2a and, albeit less frequently, also in α1C-b channels (Table 1). Single-channel amplitude, P_o and P_s of channels did not change significantly with time in inside-out recordings (results not shown). Thus the functional α1–β interaction was fairly stable in excised inside-out patches, as expected from the reported high-affinity interaction between α1 and β subunits [15]. To further investigate the properties of the α1–β interaction, we performed experiments with a synthetic peptide that corresponds to the sequence of the conserved α1–β interaction domain within the I–II linker of α1C. This peptide is expected to bind to Ca^{2+}-channel β subunits and to inhibit the interaction of β with AID under equilibrium binding conditions in a competitive manner Where the stable interaction between α1 and β is based exclusively on a single high-affinity interaction site within AID, this peptide is not expected to promote dissociation of β from AID in inside-out experiments By contrast, where the α1–β interaction involves multiple interaction sites, the AID peptide may promote dissociation by a step-by-step binding mechanism involving the formation of an unstable ternary complex.

A synthetic peptide corresponding to a sequence of the I–II linker of α1C binds to the β2 subunit and is able to disrupt α1–β interactions

As an initial step we characterized the 18-amino-acid synthetic AID-peptide in terms of its ability to bind to β2 subunits by an *in vitro* affinity-bead assay. The AID-peptide was covalently coupled to an agarose-gel matrix and incubated with the Ca^{2+}-channel β2 subunit solubilized from rat cardiac tissue homogenates. Western-blot analysis with the β2-isoform-specific antibody showed that the β2 subunit was recovered by affinity beads, but not by the agarose-gel matrix (Figure 3, +/− coupled peptide). Moreover, β2 protein binding to affinity beads was entirely prevented by preincubation with 10 μM AID-peptide (Figure 3, free peptide) By contrast, inclusion of the scrambled peptide (up to 20 μM) did not interfere with β2 binding under the same conditions (Figure 3). In addition to the 85 kDa β2 subunit, a minor protein migrating at approx. 60 kDa was specifically recovered by AID-affinity beads too. Because of similarities in apparent molecular mass with the β3 subunit [22], we tested the possibility of whether AID beads precipitate the β3 subunit from heart homogenates. However, no β3 subunit was detected by the β3-isoform-specific antibody (results not shown). Thus the 60 kDa protein is considered to be a β2 subunit isoform which was also observed following protein kinase A-mediated phosphorylation [27,28]

Binding affinity of the major 85 kDa β2 subunit was further assessed by competition experiments. Cytosolic proteins from rat heart were incubated with increasing concentrations of the AID-peptide (1 nM to 10 μM) prior to binding on affinity beads Densitometric evaluation of β2 protein binding demonstrated that preincubation with the 18-amino-acid synthetic peptide prevented the association of native β2 subunits with affinity beads with a K_i of 100 nM (Figure 4).

Administration of the AID-peptide to the cytoplasmic face of α1C-b·β2a channels results in rapid removal of β-induced channel modulation

To investigate the functional role of the α1–β interaction that takes place within the I–II linker of α1C, we studied the effect of the AID-peptide on gating of α1C-b·β2a channels in the inside-out recording configuration. The peptide was administered at a concentration (10 μM) that was sufficient to completely inhibit α1-β interaction in *in vitro* affinity-bead assay. In five out of six experiments a substantial change in the gating properties was obtained during exposure of the cytoplasmic face of inside-out patches to AID-peptide. A typical experiment is illustrated in Figure 5(A) Channel activity ($N \times P_o$) declined rapidly (within 2–5 min) in the presence of the AID-peptide, whereas $N \times P_o$ of α1C-b·β2a channels remained fairly constant within 20–30 min in control experiments (Figure 5, insert) The mean P_o of α1C-b·β2a channels was decreased significantly from 9 3±1.5% to 6.3±1.4% ($N = 6$) by the AID-peptide. The reduction in channel activity was associated with a decrease of the mean open time and a reduction of the proportion of ultra-long-lasting channel opening (Figure 5B) A peptide-induced decrease in

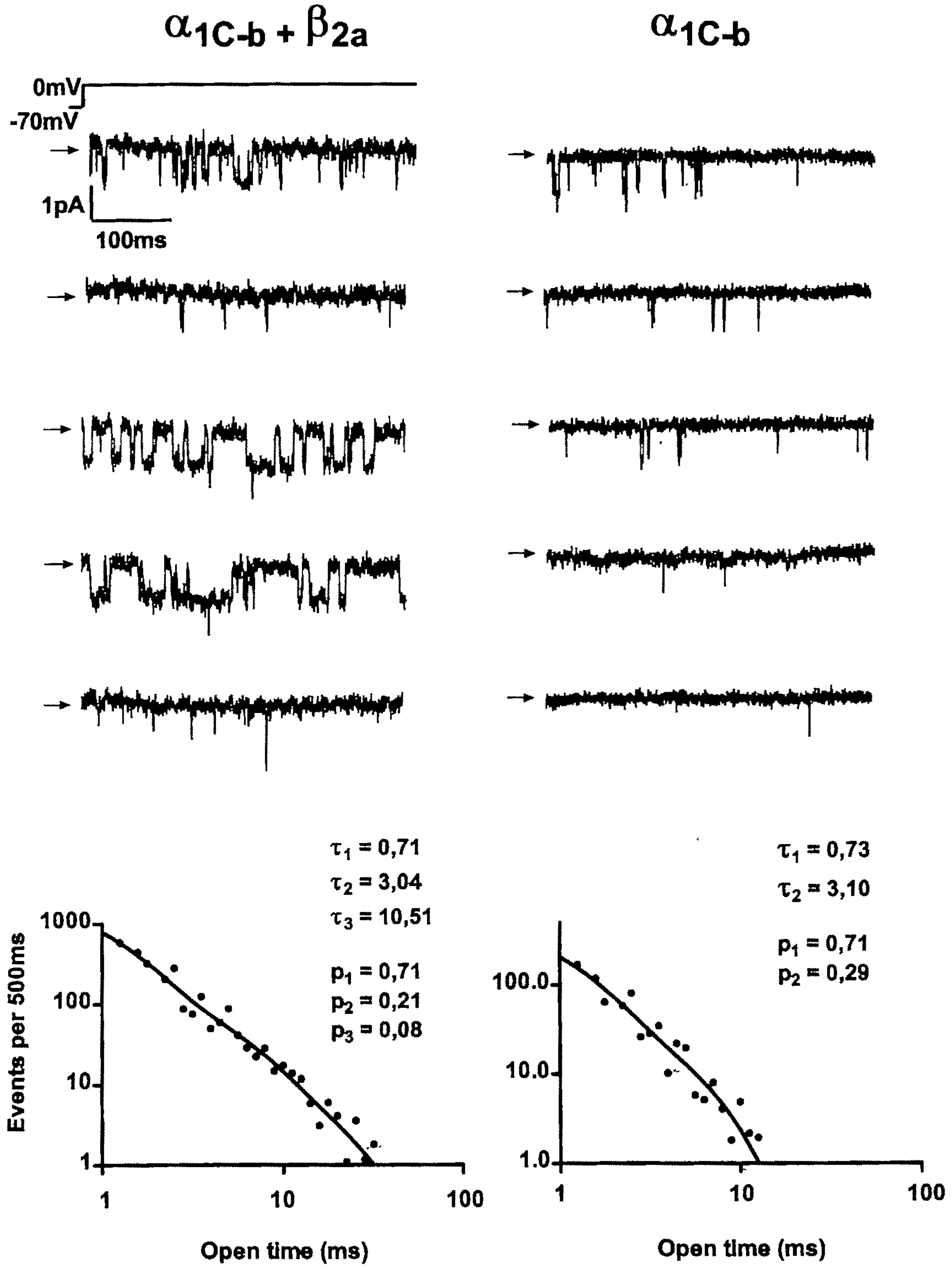

Figure 2 **β2a subunit increases the fraction of long-lasting openings of α1C-b channels in excised patches**

Top individual current responses recorded during depolarizing voltage pulses Bottom open dwell-time histograms calculated from the experiments shown above Dwell-time histograms were fitted with exponential functions (solid lines) using Marquardt-least-squares or maximum-likelihood method Time constants (τ_1, τ_2) and percentual fractions (ρ_1, ρ_2) are of dwell times are shown

mean open times was clearly observed in the experiments which allowed for analysis of open time distributions ($N = 2$). The peptide decreased P_o, but did not affect availability of either α1C-b·β2a or α1C-b channels. Thus peptide-induced changes in gating behaviour were consistent with removal of β-induced channel modulation To further test the hypothesis that the observed effect of the AID-peptide was related to β-induced channel modulation, we performed control experiments with a scrambled control peptide and tested whether the AID-peptide would inhibit channels derived by expression of α1C-b only

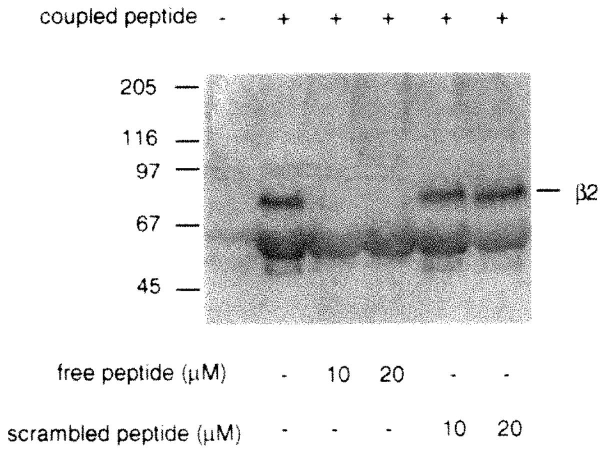
coupled peptide - + + + + +
205
116
97
67
45
β2
free peptide (μM) - 10 20 - -
scrambled peptide (μM) - - - 10 20

Figure 3 Native β2 subunit binds to the 18-amino-acid synthetic peptide resembling the α1C interaction site within the I–II linker (AID)

Affinity beads were produced by covalent coupling of the AID-peptide to ω-aminohexyl agarose (above gel photograph, −/+ coupled peptide). The AID-affinity beads were incubated with rat heart homogenate proteins (0.5 mg) in the absence or presence of either the AID-peptide (free peptide) or the control peptide (scrambled peptide) as indicated (below gel photograph). Binding of the β2 subunit was revealed by subsequent SDS/PAGE and immunoreaction with the β2- isoform-specific antibody.

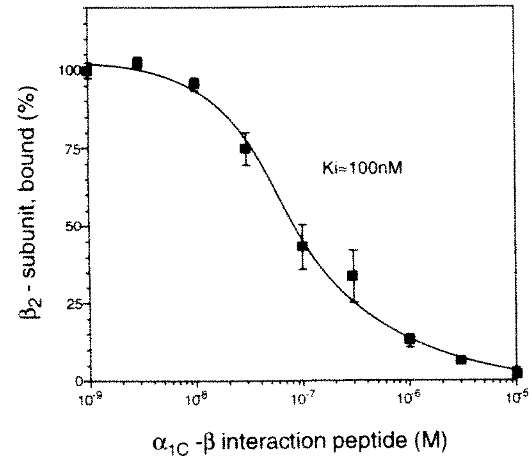

Figure 4 Displacement of the β2 subunit from AID-affinity beads by the α1C–β interaction peptide

Rat heart proteins (0.5 mg) of the cytoplasmic fraction were incubated with increasing concentrations (1 nM–10 μM) of the synthetic 18-amino-acid α1C–β interaction peptide (AID-peptide) prior to binding on to AID-affinity beads. The amount of the β2 subunit bound to the beads was estimated by densitometric evaluation of immunoblots.

Administration of a control (scrambled) peptide (10 μM) did not affect channel activity of α1C-b·β2a channels in inside-out patches ($N = 2$), and the AID-peptide failed to modulate the function of α1C-b in the absence of expressed β2a proteins ($N = 3$).

DISCUSSION

The present study demonstrates that the smooth-muscle isoform of the Ca^{2+}-channel α1 subunit is susceptible to modulation by the β2a subunit. Moreover, we provide, for the first time, evidence for the principle reversibility of β modulation in a functional Ca^{2+} channel. We report on uncoupling of Ca^{2+} channel α1 and β subunits in cell-free patches by a peptide that interferes with binding of β to the conserved domain in the I–II linker of α1.

Control of fast gating of the smooth-muscle splice variant of α1C by the β2 subunit

Ca^{2+}-channel β subunits have been shown to potentiate Ca^{2+} currents in various expression systems [1,4,6,12,29]. This potentiation of the Ca^{2+} current is in part due to an increase in the number of channel complexes in the plasma membrane. In addition to this effect of β subunits on subcellular localization and targeting of the channel complex, evidence for an allosteric, β-induced modification of channels have been presented [1,4,6,12]. Here we demonstrate a substantial modification of the fast gating of the b- splice variant of the class C Ca^{2+} channel α1 subunit by a β2 subunit (β2a). These Ca^{2+}-channel subunits are expressed in cardiac and smooth muscle [8,10,11,25], and recent experimental evidence supports the view that complexes consisting of α1C-b and β2a contribute to the formation of L-type channels in various smooth-muscle tissues [11]. Co-expression of the β2a subunit increased P_o of α1C-b channels approx. 2-fold, due to promotion of long-lasting channel openings. This observation is consistent with the results of a previous study on the modulation by β2 of the myocardial (a-) splice variant of α1C [6]. Despite a high degree of homology, a- and b- splice variants of α1C were reported to differ in their pharmacological properties [30,31]. Since the structural difference between a- and b- splice variants of α1C resides for a large part in the N-terminal sequence, which has recently been suggested as a critical determinant of α1-β interaction [5], a differential modulation by β subunits of the cardiac- and smooth-muscle splice variant of α1C may be anticipated. Nonetheless, we observed a β2-induced modulation of fast gating behaviour of the smooth-muscle splice variant α1C-b that is reminiscent of the modulation reported for α1C-a channels [6]. The functional effect of β2a on both splice variants appears similar, in that frequent occupation of a long-lived open state was observed. Both the results reported by Costantin et al. [6], as well as our present results, were obtained in the presence of the Ca^{2+} channel agonist BayK 8644, which may to some extent interfere with the β-induced modulation of channel function. Nonetheless, β-induced prolongation of mean open time has been reported recently for α1C-a channels to occur also in the absence of BayK 8644 [12]. It has been suggested that a long-lived open state exists also in the absence of exogenously expressed β2 subunit, and that the auxiliary subunit promotes the occupation of this existing open state [6]. Consistently, we observed occasional ultra-long openings in α1C-b channels. Our results demonstrate that the β2a subunit is able to modify fast gating of the smooth muscle (b-) splice variant of α1C in a manner similar to that of the cardiac a-form, despite the structural difference in the N-terminus. Thus our results demonstrate that modulation by β2a of both class C splice variants are similar and argue against a crucial role of the N-terminal tail in fast-gating modulation by the β2 subunit.

Role of the I–II linker of α1 in functional coupling between α1 and β subunits

The interaction between α1 and β proteins involves a conserved motif in the intracellular I–II connecting loop of α1 [14]. A recent

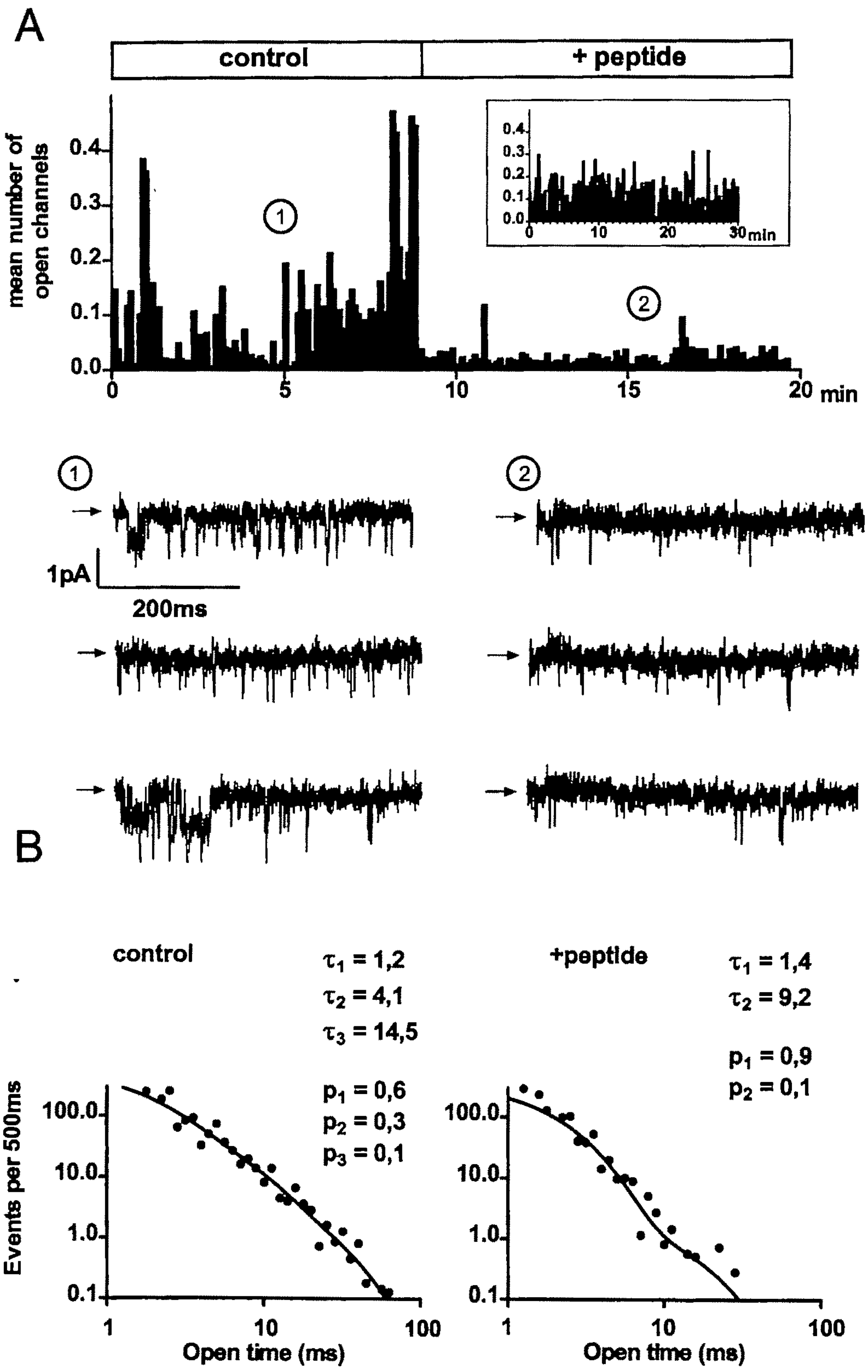

Figure 5 Synthetic α1C–β interaction peptide decreases channel activity and the proportion of long-lasting channel openings in excised patches

(A) The upper panel shows the time course of Ca^{2+}-channel activity in an excised patch Administration of 10 μM α1C–β interaction peptide is indicated The insert illustrates the stability of inside-out patches during control perfusion of the cytoplasmic side The lower panel shows individual current responses during depolarizing voltage pulses before and after administration of α_{1C}–β interaction peptide (B) Dwell-time histograms derived from the experiment shown in (A) Dwell-time histograms were fitted to exponential functions (continuous lines) using Marquardt-least-squares or maximum-likelihood method Time constants (τ_1, τ_2) and percentual fractions (p_1, p_2) of dwell times are given study demonstrates that binding of β subunits to this motif is essential for membrane targeting of the $\alpha 1$–β complex [32]. The role of this $\alpha 1$–β interaction domain and of other hypothetical interaction sites in functional modulation of $\alpha 1$ by β subunits is still an open question. In the present study we employed a synthetic peptide corresponding to a partial sequence of the I–II linker of $\alpha 1$ (AID-peptide) as a tool to disrupt the $\alpha 1$–β interaction. *In vitro* binding experiments confirmed that this peptide exhibits a reasonable affinity to cardiac $\beta 2$ subunits to serve this purpose. Administration of the AID-peptide to the cytoplasmic side of inside-out patches resulted in a significant change in fast gating of $\alpha 1$C-b·$\beta 2$a channels in that the P_o of the channels declined rapidly. This decrease in P_o was associated with prevention of entry into the ultra-long open state, i.e. a modulation consistent with elimination of the functional modulation of $\alpha 1$C-b by the $\beta 2$a subunit. The peptide did not exert any effect on the function of $\alpha 1$C-b when expressed alone, excluding a direct inhibitory effect of the peptide on the $\alpha 1$ subunit. It appears thus reasonable to conclude that the employed AID-peptide inhibits Ca^{2+}-channel activity due to functional uncoupling of $\alpha 1$C-b and $\beta 2$a proteins. In the absence of AID-peptide, gating of $\alpha 1$C-b·$\beta 2$a channels was fairly stable in inside-out recordings up to 30 min, despite complete wash-out of any free cytosolic β proteins, indicating a tight high-affinity binding of the β subunit to $\alpha 1$. Such a high affinity $\alpha 1$–β interaction has previously been demonstrated in *in vitro* binding experiments [15]. The observed rapid elimination of the typical β-induced gating behaviour upon addition of excess of the AID-peptide was interpreted in terms of an increased dissociation rate constant of the $\alpha 1$–β complex and thus in terms of a decrease in $\alpha 1$–β binding affinity by the peptide The basis of this conclusion is that it appears reasonable to assume that free β subunit is rapidly removed by perfusion of the cytoplasmic face of inside-out patches, as the $\beta 2$a subunit employed in the present study lacks structures for membrane anchoring [9]. Consistently, removal of the AID-peptide after elimination of β modulation did not result in recovery of high P_o gating of the channels (A. Hohaus and K. Groschner, unpublished work), indicating that reassociation of $\alpha 1$ and β is effectively prevented in the inside-out configuration. The observed AID-peptide-induced functional uncoupling of the subunits is therefore likely to reflect an increased dissociation rate of the $\alpha 1$–β complex. Such a change in dissociation rate cannot be explained by a classical competitive interaction at a single interaction site according to the principal concepts of receptor–ligand interactions [33–35]. Hence the AID-peptide-induced reduction of the stability of $\alpha 1$–β complexes is consistent with the hypothesis of multiple $\alpha 1$–β interaction sites Formation of a ternary complex comprised of $\alpha 1$, $\beta 2$a and the AID-peptide is required to explain the observed uncoupling of $\alpha 1$–β interaction in inside-out patches. Such a ternary complex involving multiple $\alpha 1$–β attachment sites is likely to exhibit low stability, resulting in rapid dissociation and washout of AID-peptide-bound β subunit. This concept implies that, despite the high affinity of $\alpha 1$–β interactions observed *in vitro*, an exchange of β subunits via a step-by-step binding mechanism is in principle possible in functional channels *in vivo*. On the basis of our present experiments we cannot distinguish whether suggested multiple attachment points are located within the same channel domain, i.e the I–II linker, or whether attachment sites are located outside of this classical AID. Interaction domains in $\alpha 1$C outside of the classical AID have so far not been detected, and recent experimental evidence argues against an interaction of β subunits with the cytoplasmic N- and C-termini of $\alpha 1$C [5]. Nonetheless, a recent study shows that mutation of a single amino acid residue in AID of $\alpha 1$C-a (Y467S, i.e. $Tyr^{467} \rightarrow Ser$) is sufficient to disturb the effect of $\beta 2$ on membrane targeting of the channels, but not to affect the allosteric modulation of channel function [12]. These findings were also interpreted in terms of multiple interaction sites between $\alpha 1$ and β subunits and in terms of the existence of one low-affinity site that contributes to functional coupling. A functionally relevant low-affinity interaction may well take place in $\alpha 1$Y467S channels which exhibit none or weak AID interaction, as long as a sufficient concentration of cytosolic β proteins is maintained Such low-affinity interaction may well explain the β-modulation of $\alpha 1$Y467S channels observed in intact HEK 293 cells [12] In the present inside-out experiments, disruption of the AID interaction resulted in rapid loss of β-modulation. These data suggest that the $\alpha 1$–β interaction in AID is essential for stabilization of the subunit complex. It remains to be clarified to what extent the AID interaction contributes to functional coupling between α and β subunits.

Our results provide, for the first time, evidence for principal reversibility of Ca^{2+}-channel modulation by β subunits and suggest disruption of $\alpha 1$–β interaction or exchange of β subunits as a possible mechanism of channel regulation.

This work was supported by the Fonds zur Forderung der Wissenschaftlichen Forschung (SFB Biomembranes F715) and P12667 to K G., P12728 and NB 7000 to C R, as well as the Deutsche Forschungsgemeinschaft (Ha-1779/3-2 to H H) We thank Dr J. Striessnig, Dr H G Knaus, and Dr F Brunner for helpful discussions, and Mrs Ingrid Hauser for excellent technical assistance.

REFERENCES

1 Neely, A, Wei, X, Olcese, R, Birnbaumer, L and Stefani, E (1993) Science **262**, 575–578

2 Neely, A, Olcese, R, Baldelli, P, Wei, X, Birnbaumer, L and Stefani, E (1995) Am J Physiol **268**, C 732–740

3 Schuhmann, K., Voelker, C, Hofer, G F, Pflügelmeier, H, Klugbauer, N, Hofmann, F, Romanin, C and Groschner, K (1997) FEBS Lett **408**, 75–80

4 Yamaguchi, H, Hara, M, Strobeck, M, Fukasawa, K, Schwartz, A and Varadi, G (1998) J Biol Chem **273**, 19348–19356

5 Shistik, E, Ivanina, T, Blumenstein, Y and Dascal, N (1998) J Biol Chem **273**, 17901–17909

6 Costantin, J, Noceti, F, Qin, N, Wei, X, Birnbaumer, L and Stefani, E (1998) J Physiol (London) **507**, 93–103

7 Biel, M, Ruth, P, Bosse, E, Hullin, R, Stuehmer, W, Flockerzi, V and Hofmann, F (1990) FEBS Lett **269**, 409–412

8 Biel, M, Hullin, R, Freundner, S., Singer, D, Dascal, N., Flockerzi, V and Hofmann, F (1991) Eur J Biochem **200**, 81–88

9 Hullin, R, Singer-Lahat, D, Freichel, M, Biel, M, Dascal, N, Hofmann, F and Flockerzi, V (1992) EMBO J **11**, 885–890

10 Gollasch, M, Haase, H, Ried, C, Lindschau, C, Miethke, A, Morano, I, Luft, F C and Haller, H (1998) FASEB J **12**, 593–601

11 Reimer, D, Huber, I G, Garcia, M L, Haase, H and Striessnig, J (2000) FEBS Lett **467**, 65–69

12 Gerster, U, Neuhuber, B, Groschner, K, Striessnig, J and Flucher, B E (1999) J Physiol (London) **517**, 355–368

13 Mikami, A, Imoto, K, Tanabe, T, Niidome, T, Mori, Y, Takeshima, H, Narumiya, S. and Numa, S (1989) Nature (London) **340**, 230–233

14 Pragnell, M, De Waard, M, Mori, Y, Tanabe, T, Snutch, T P and Campbell, K P (1994) Nature (London) **368**, 67–70

15 De Waard, M, Witcher, D R, Pragnell, M, Liu, H. and Campbell, K P (1995) J Biol Chem **270**, 12056–12064

16 Zong, X, Schreieck, J, Mehrke, G, Welling, A, Schuster, A, Bosse, E, Flockerzi, V and Hofmann, F (1995) Pflugers Arch **430**, 340–347

17 Kingston, R E (1994) in Introduction of DNA into Mammalian Cells (Ausubel, F M, Brent, R, Kingston, R, Morre, D D, Seidmann, J G, Smith, J A and Struhl, K, eds), pp. 905–919, John Wiley & Sons, Inc, New York

18 Romanin, C, Grosswagen, P and Schindler, H (1991) Pflugers Arch **418**, 86–92

19 Pastushenko, V P and Schindler, H (1997) Philos Trans. R Soc London B Biol Sci **352**, 39–51

20 Baumgartner, W, Hohenthanner, K, Hofer, G F, Groschner, K and Romanin, C (1997) Biophys J **72**, 1143–1152

21 Schuhmann, K., Romanin, C, Baumgartner, W and Groschner, K (1997) J Gen Physiol **110**, 503–513

22 Haase, H, Kresse, A, Hohaus, A, Schulte, H D., Maier, Osterziel, M K J., Lange, P E and Morano, I (1996) J Mol Med **74**, 99–104

23 Haase, H, Striessnig, J, Holtzhauer, M, Vetter, R and Glossmann, H (1991) Eur J Pharmacol. **207**, 51–59

24 Calovini, T, Haase, H and Morano, I (1995) J. Cell. Biochem **59**, 69–78

25 Pichler, M., Cassidy, T N, Reimer, D., Haase, H, Kraus, R., Ostler, D and Striessnig, J (1997) J. Biol Chem **272**, 13877–13882

26 Haase, H, Pfitzmaier, B, McEnery, M and Morano, I (2000) J Cell Biochem **76**, 695–703

27 Haase, H, Karczewski, P, Beckert, R and Krause, E G (1993) FEBS Lett **335**, 217–222

28 Haase, H., Podzuweit, T, Lutsch, U., Hohaus, A, Kostka, S, Lindschau, C., Kott, M, Kraft, R and Morano, I. (1999) FASEB J **13**, 2161–2172

29 Perez-Reyes, E, Castellano, A, Kim, H S, Bertrand, P, Baggstrom, E., Lacerda, A E, Wei, X and Birnbaumer, L (1992) J Biol. Chem **267**, 1792–1797

30 Welling, A, Ludwig, A, Zimmer, S, Klugbauer, N, Flockerzi, V and Hofmann, F (1997) Circ Res **81**, 526–532

31 Morel, N, Buryi, V, Feron, O, Gomez, J-P, Christen, M-O and Godfraind, T (1998) Br J Pharmacol **125**, 1005–1012

32 Gao, T, Chien, J and Hosey, M M (1999) J Biol Chem **274**, 2137–2144

33 DeLean, A. and Rodbard, D. (1979) in The Receptors A Comprehensive Treatise, vol 1 (O'Brian, R D, ed), Plenum Press, New York

34 Trifiletti, R R, Lo, M M S and Snyder, S H (1984) Mol Pharmacol **26**, 228–240

35 Groschner, K, Ulle, P and Kukovetz, K. (1989) Eur J Pharmacol **159**, 125–131

Received 16 November 1999/15 March 2000, accepted 7 April 2000

Activity of phosphatidylinositol transfer protein is sensitive to ethanol and membrane curvature

Hiroaki KOMATSU*, Barend BOUMA†, Karel W. A. WIRTZ‡, Theodore F. TARASCHI* and Nathan JANES*[1]

*Department of Pathology, Anatomy, and Cell Biology, Jefferson Medical College of Thomas Jefferson University, 1020 Locust Street, Philadelphia, PA 19107, U.S.A., †Bijvoet Center for Biomolecular Research, Department of Crystal and Structural Chemistry, Utrecht University, Padualaan 8, 3584 CH Utrecht, The Netherlands, and ‡Center for Biomembranes and Lipid Enzymology, Department Biochemistry of Lipids, Utrecht University, P O Box 80 054, 3508 TB Utrecht, The Netherlands

Phosphatidylinositol transfer protein (PITP) is critical for many cellular signalling and trafficking events that are influenced by ethanol. The influence of ethanol and membrane curvature on the activity of recombinant mouse PITP-α *in vitro* is evaluated by monitoring the transfer of phosphatidylinositol (PtdIns) from rat hepatic microsomes to unilamellar vesicles. Acute exposure to pharmacological levels of ethanol enhanced the function of PITP. Chloroform shared a similar ability to enhance function when both drug concentrations were normalized to their respective octanol/water partition coefficients, indicating that the effect is not unique to ethanol and might be common to hydrophobic solutes. Neither the PITP activity nor its ethanol enhancement was altered by using thermally pretreated (denatured) or protease-treated microsomes, indicating that the native microsomal protein structure was unlikely to be a determinant of transfer. Kinetic analyses indicated that ethanol acted by increasing the PITP-mediated flux of PtdIns from both microsomal and liposomal surfaces. The activity of PITP was strongly dependent on the lipid structure, with a steep dependence on the expressed curvature of the membrane. Activity was greatest for small, highly curved sonicated vesicles and decreased markedly for large, locally planar unilamellar vesicles. Ethanol enhanced PITP-mediated PtdIns transfer to all vesicles, but its effect was much smaller than the enhancement due to curvature, which is consistent with ethanol's comparatively modest ability to perturb membrane lipids. The ethanol efficacy observed is as pronounced as any previously described lipid-mediated ethanol action. In addition, these observations raise the possibility that PITP specifically delivers PtdIns to metabolically active membrane domains of convex curvature and/or low surface densities of lipid.

Key words: anaesthetic, membrane curvature, membrane fluidity, polyphosphoinositide signalling, signal transduction.

INTRODUCTION

Alcohol abuse is linked to numerous disorders in many organs, including the liver, brain, heart, skeletal muscle and pancreas [1]. Ethanol administered acutely and chronically is known to interfere with polyphosphoinositide signalling pathways [2,3]. The acute administration of ethanol is known to disorder or fluidize membranes. Chronic exposure to ethanol induces an adaptive change in membrane properties known as membrane tolerance that is manifested by a resistance to the disordering effects of ethanol [4]. The resistance to disordering was retained in liposomes prepared from the phospholipid extracts [5] Of the microsomal phospholipid fractions, the ability to resist the disordering effects of ethanol was accentuated in the phosphatidylinositol fraction [5,6].

In intact hepatocytes, ethanol and other short-chain alcohols activated the polyphosphoinositide-specific phospholipase C and initiated the polyphosphoinositide signal transduction cascade [2,3]. In permeabilized hepatocytes (under conditions in which hormonal stimulation was abolished), ethanol was ineffective in activating G-protein-mediated phospholipase Cβ [7]. In platelets the activation of the G-protein-mediated phospholipase Cβ was sensitive to the degree of permeabilization [8]. These studies raised the possibility that a cytosolic cofactor might be an important element in the response to ethanol. It was shown subsequently that controlled permeabilization of HL60 cells permitted the release of endogenous phosphatidylinositol transfer protein (PITP) while maintaining polyphosphoinositide-specific phospholipase Cβ levels, but that PITP was critical for activation of the signal transduction cascade [9]. These results suggested that PITP might be the cofactor required for activation by ethanol. Unlike most receptor-mediated agonist activators of the signal cascade, ethanol elevated levels of the phosphorylated PtdIns products PtdIns4P and PtdIns(4,5)P_2 [10]. The addition of PITP to unstimulated erythrocyte ghosts also elevated PtdIns4P and PtdIns(4,5)P_2 levels [11]. Furthermore, it has long been known that the total phospholipid transfer between liver organelles *in vitro* was diminished by chronic treatment with ethanol *in vivo* [12].

PITPs are cytosolic proteins originally identified by their ability to induce PtdIns transfer (reviewed in [13]). They are ubiquitous in mammalian cells. Mammalian PITP has critical roles in cellular growth [14], in polyphosphoinositide signalling [9,13], in constitutive and regulated vesicular trafficking among intracellular organelles [15,16] and in secretory trafficking pathways [17]. Its activity is strongly dependent on the physicochemical status of the membrane, the structure and charge of polar head groups, acyl-chain composition and acyl-chain order or fluidity [18]. Kinetic models supported a Ping Pong Bi Bi mechanism of lipid transfer for PITP [19,20]. Immediately downstream in distinct pathways are kinases (phosphoinositide 3-kinase and phosphoinositide 4-kinase) whose activities also are strongly dependent on lipid structure [21].

The central location of PITP in these manifestations of exposure to ethanol and the known sensitivity of PITP activity to membrane structure and order led us to investigate whether the

---

Abbreviations used LUV, large unilamellar vesicle, PITP, phosphatidylinositol transfer protein, POPC, 1-palmitoyl-2-oleoyl-3-*sn*-phosphatidylcholine, SUV, small unilamellar vesicle

[1] To whom correspondence should be addressed (e-mail nathan janes@mail tju edu)

activity of PITP was altered by ethanol. In the present study, the activity of recombinant mouse PITP-α was assayed *in vitro* by monitoring the transfer of radiolabelled PtdIns from rat hepatic microsomes to unilamellar vesicles in the presence of ethanol. Chloroform was examined to gauge whether the response was specific to ethanol or whether it might be shared by other membrane-fluidizing agents. Thermally pretreated microsomes and protease-treated microsomes were examined to assess the role of membrane proteins in PtdIns transfer. Several sizes of vesicle were employed to assess the effect of membrane curvature on transfer and the effect of ethanol. To evaluate the action of ethanol mechanistically, the donor and acceptor membrane concentrations were varied and the initial transfer rates were evaluated by using non-linear kinetic analyses [19].

MATERIALS AND METHODS

Materials

Cholesteryl [1-^{14}C]oleate and *myo*-[2-^{3}H]inositol were purchased from American Radiolabeled Chemicals (St Louis, MO, U.S.A.). 1-Palmitoyl-2-oleoyl-3-*sn*-phosphatidylcholine (POPC) and phosphatidylinositol sodium salt from bovine liver were obtained from Avanti Polar Lipids (Alabaster, AL, U.S.A). Proteinase K (*Tritirachium album*, 10 units/mg) was obtained from Sigma (St. Louis, MO, U.S.A.) and used as supplied. All other chemicals were purchased from Sigma or Fisher Scientific (Pittsburgh, PA, U.S.A.). Recombinant mouse PITP-α was prepared from inclusion bodies after expression of the cDNA in *Escherichia coli* [22] and was stored at −80 °C before use.

Preparation of donor microsomes and acceptor liposomes

Microsomes were isolated from rat liver by the method of Helmkamp et al. [23] Microsomal PtdIns was radiolabelled by head-group exchange of inositol by using *myo*-[2-^{3}H]inositol, as described previously [23,24]. Heat-treated microsomes were incubated in boiling water for 5 min under argon [25].

Protease treatment of microsomes (4.4 mg of protein/ml) was done with proteinase K (1 mg/ml) for 20 min at 37 °C. The reaction was stopped with 5 mM PMSF [added in a methanol vehicle, 1% (v/v) final concentration]; 5 vol. of SET buffer (0.25 M sucrose/1 mM EDTA/10 mM Tris/HCl, adjusted to pH 7.4 with HCl) was added and the membranes were centrifuged at 100000 g for 1 5 h. The pellet was resuspended and washed twice in 6.25 vol. of SET buffer, and finally resuspended in the original volume of SET buffer and stored at −20 °C. The microsomal protein content was decreased by 42%.

Lipids were dried to a thin film under a stream of N_2. The lipid film was evacuated overnight [to less than 5 mtorr (667 mPa)]. The dried lipid film was hydrated at 4 °C with SET buffer. Small unilamellar vesicles (SUVs) were obtained by sonication at 4 °C for 15 min under N_2 with a W-225 probe-type sonicator (Heat System, Farmingdale, NY, U S.A.) at a continuous power of 40 W. The sonicated solutions were centrifuged for 10 min at 3000 g to remove titanium particles and any multilamellar vesicles. Large unilamellar vesicles (LUVs) were prepared with a freeze–thaw (five cycles) and extrusion protocol [26] that employed a lipid extruder (Avestin, Ottawa, Ontario, Canada) at ambient temperature. The LUVs were extruded by using five passes through two stacked polycarbonate filters of 0.1 or 0.2 μm pore size; these were designated LUV_{100} and LUV_{200} respectively.

Assay of phosphatidylinositol transfer

PITP transfer activity was assayed by established methods [23]. In brief, the transfer of radiolabelled [^{3}H]PtdIns from microsomes to liposomes composed of POPC and bovine liver PtdIns (98:2 molar ratio) and a trace (less than 0.01 mol%) of cholesteryl [1-^{14}C]oleate was monitored. An aliquot of PITP was added to mixtures of the donor microsomes and acceptor liposomes in SET buffer for a total volume of 250 μl The reaction was incubated at 37 °C for 5 min unless specified otherwise. After the incubation, the samples were immersed in ice and 50 μl of acetate buffer [0.2 M sodium acetate/0.25 M sucrose (pH 5), 4 °C] was added immediately and mixed to aggregate the microsomal particles. After mixing, the samples were centrifuged at 15000 g for 20 min at 4 °C to pellet the microsomes. Samples (200 μl) of the supernatant were transferred to scintillation vials containing 0.9 ml of water and 9 ml of Bio-Safe II scintillation cocktail (Research Products International Corp., Mount Prospect, IL, U.S.A.) and analysed for ^{3}H and ^{14}C radioactivities. The radiolabels were counted in a Packard Tri-Carb model 1900CA liquid-scintillation analyser (Packard Instrument Co., Downers Grove, IL, U.S.A.) equipped with a ^{133}Ba external γ-ray source, with the use of a dual-window analysis (0–9.1 and 9.1–156 keV). Typical counting times were 5 min.

Loss of liposomes from the supernatant due to co-precipitation with the microsomal fraction (less than 20%) was quantified by measuring the activity of cholesteryl [1-^{14}C]oleate. All calculated transfer rates accounted for loss from the liposomal fraction. Control experiments were performed without PITP to quantify spontaneous transfer. The background from spontaneous transfer was subtracted to yield PITP-mediated transfer rates. At the 5 min time point, spontaneous transfer rates were as follows (expressed as percentages of the total outer-leaflet microsomal [^{3}H]PtdIns; $n \geq 3$; mean ± S.D.): microsomes → SUV, $1.47 \pm 0.25\%$; thermally pretreated microsomes → SUV, $1.77 \pm 0.35\%$; microsomes → LUV_{100}, $1\ 13 \pm 0.06\%$; microsomes → LUV_{200}, $0.95 \pm 0.20\%$. Ethanol did not significantly alter these spontaneous transfer rates.

Kinetic treatment

The initial rate (V_0) at which PITP catalyses the PtdIns exchange between membranes was expressed by the following theoretical rate equation proposed by Van den Besselaar et al. [19] for the shuttle or Ping Pong Bi Bi mechanism relevant to PITP:

$$V_0 = \frac{k_1[\mathrm{PtdIns}]_M k_2[\mathrm{PtdIns}]_L[\mathrm{PITP}]}{(k_1[\mathrm{PtdIns}]_M + k_2[\mathrm{PtdIns}]_L)(1 + K_1[\mathrm{PtdIns}]_M + K_2[\mathrm{PtdIns}]_L)} \tag{1}$$

where k_1 and k_2 are rate constants of association of PITP to microsomes and to liposomes respectively, and K_1 and K_2 are the binding constants of PITP to microsomes and to liposomes respectively. Our application focused on PtdIns transfer and neglected the lower phosphatidylcholine transfer capabilities of PITP. Consequently the rates are meant to be descriptive from a mechanistic standpoint, with the differences being more significant than absolute values V_0 is dependent on the amounts of PtdIns, $[\mathrm{PtdIns}]_M$ and $[\mathrm{PtdIns}]_L$, present in the outer leaflet of the microsomal and liposomal membranes respectively [19]. The initial $[\mathrm{PtdIns}]_M$ and $[\mathrm{PtdIns}]_L$ were determined as follows. Rat hepatic microsomal membranes contain 8.5 mol% PtdIns of the total phospholipid [6]. The concentration of phospholipids in the microsome was 0.374 mg/mg of protein [27]. In microsomal membranes, PtdIns is distributed symmetrically [28]; the outer leaflet therefore contained half of the microsomal PtdIns. In curved liposomes the leaflets are not equally populated, so that packing and mean headgroup areas vary with liposome size. In sonicated vesicles, approx. 70 % of the phospholipids are in the outer leaflet [29]. The transbilayer distribution of phospholipids in SUVs depends on packing and electrostatic factors [30], resulting in a PtdIns distribution that closely resembles the inside-to-outside ratio of phosphatidylcholine [31]. The units of the fitted parameters are as follows. The association rate constant k_1 is expressed as μmol of PtdIns transferred/μmol of PtdIns in the microsomal outer leaflet per μM PITP. The association rate constant k_2 is expressed similarly, with the liposomal outer leaflet PtdIns concentration replacing that of the microsomes. Both expressions reduce to units of $\mu M^{-1} \cdot min^{-1}$. The dissociation rate constants k_{-1} and k_{-2} are expressed in units of min^{-1}. The initial velocities are expressed in units of μmol of PtdIns transferred/min per μmol of PITP.

RESULTS

Effects of ethanol on PITP activity

The dependence of the initial PtdIns transfer velocity on PITP concentration is shown in Figure 1(A) for PtdIns transfer between donor microsomes and acceptor SUVs at 37 °C. The initial transfer rate (V_0) is expressed as the percentage of the total outer-leaflet microsomal [^{3}H]PtdIns pool that was transferred to the acceptor liposomes. The PtdIns transfer rates were taken from the 5 min time point, which was well within the linear range of transfer, as shown in the time course (inset) for 0.017 μM PITP. Background transfer levels in the absence of PITP were small for this microsome/SUV assay and also for the microsome/LUV assay discussed below, as summarized in the Materials and methods section.

The presence of ethanol accelerated the PtdIns transfer mediated by PITP as shown in Figure 1(B) for the 0.017 μM PITP situation in Figure 1(A). The inset shows the time course of the ethanol enhancement, which confirmed that the 5 min point was also within the linear regime when ethanol was present. To represent more accurately the consistency of the ethanol effect, the ethanol enhancement was plotted as the increase in the rate of PITP-mediated PtdIns transfer caused by the presence of ethanol Shown on the right-hand axis is the ethanol-induced increase in PITP activity. Transfer in the absence of PITP was not altered by ethanol (results not shown). The ethanol concentrations examined comprise the pharmacologically relevant range for rats; the range for humans is half as much [32]. The ethanol concentrations used here were well below those (more than 7 M) known to compromise liposomal integrity [33].

To assess whether the enhancement was specific to ethanol or a general response to organic solvents (i.e. a common property of anaesthetics or membrane perturbants), the effect of chloroform on PtdIns transfer is shown in Figure 1(C). Chloroform accelerated PtdIns transfer, but at much lower concentrations than was observed for ethanol. The chloroform and ethanol concentration axes shown in Figure 1(C) were matched by normalization to the respective octanol/water partition coefficients (P_{oct}) [34]. The total chloroform concentrations are shown. Aqueous concentrations were estimated to be approx. 5 % less. For reference to a common biological endpoint, the arrows reflect the respective narcotic concentrations in amphibians [35]. Plotted as normalized concentrations, their efficacies are similar. Similar efficacies at concentrations normalized to P_{oct} suggest a hydrophobic mechanism of action [34].

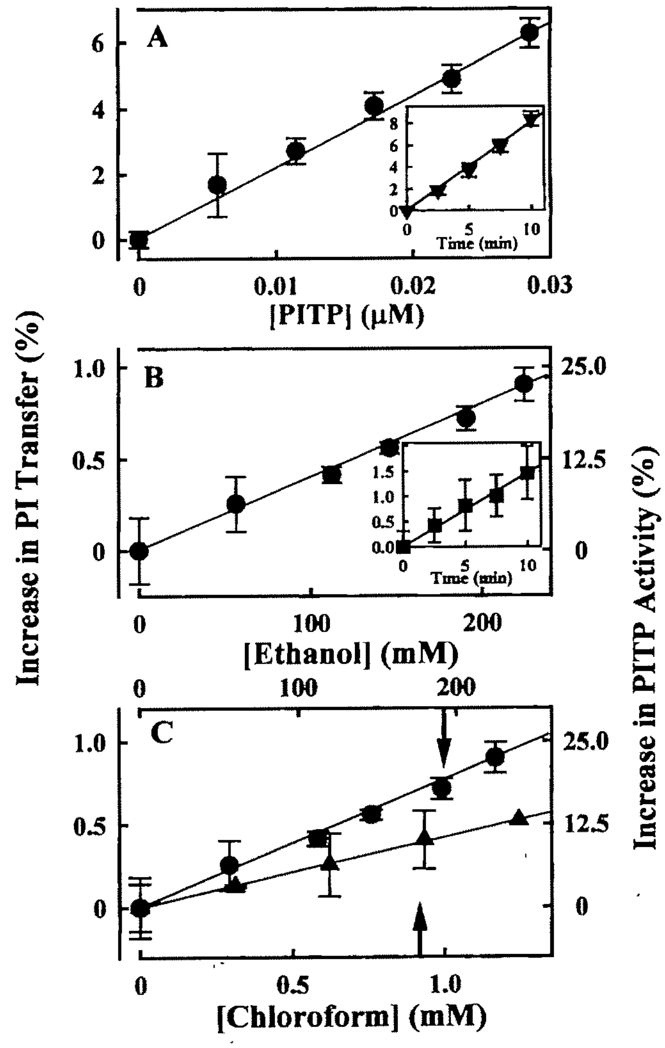

Figure 1 Activity of PITP and the effects of chloroform and ethanol

The ability of PITP to transfer PtdIns *in vitro* from donor microsomes (80 μg/ml protein) to acceptor liposomes (SUVs; 0 4 mg/ml) and the ability of ethanol and chloroform to accelerate PtdIns transfer are shown (**A**) The PITP dose–response curve for PITP-mediated PtdIns transfer after a 5 min incubation at 37 °C is shown ($n = 4$–6) The inset shows the time course of increases in PtdIns transfer for 0.017 μM PITP ($n = 6$). (**B**) The enhancement of PITP-mediated (0 017 μM PITP) PtdIns transfer by ethanol after a 5 min incubation at 37 °C is presented as the increase in transfer caused by the presence of ethanol ($n = 3$–16) The inset shows the time course of increases in PtdIns transfer caused by ethanol (225 mM) for 0 017 μM PITP ($n = 6$) (**C**) Comparison of the enhancement of PITP-mediated PtdIns transfer by ethanol (●, $n = 3$–16) and by chloroform (▲, $n = 3$, except at 1 24 mM, for which $n = 1$) at 0.017 μM PITP. The right-hand axes in (**B**) and (**C**) show the percentage increase in the PITP activity caused by ethanol or chloroform The concentrations of chloroform and ethanol were matched using their respective octanol/water partition coefficients [34]. The arrows represent the reported biological endpoint for narcosis in amphibians [35]. The data were fitted by linear regression, error bars show S D Abbreviation PI, PtdIns

Influence of microsomal membrane proteins on PITP activity

To address whether microsomal proteins participated in the transfer process or influenced the sensitivity to ethanol, the assay was conducted with microsomes that had been briefly incubated in boiling water (5 min) before the assay or had been subjected to protease pretreatment. The thermal treatment had previously been shown to abolish the ability of microsomes to bind ethanol saturably [25]. The protease treatment decreased the microsomal

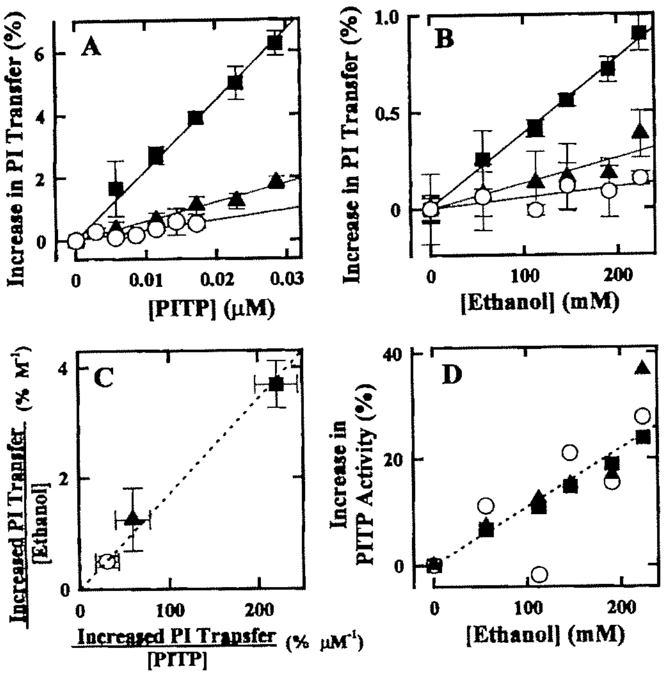

Figure 2 Effect of membrane curvature on PtdIns transfer and its enhancement by ethanol

(A) The increase in PITP-mediated PtdIns transfer as a function of PITP concentration is shown for highly curved sonicated vesicles (■) and for more planar extruded vesicles LUV$_{100}$ (▲) and LUV$_{200}$ (○). (B) The effect of ethanol on PtdIns transfer for the liposomes shown in (A) is presented as the increase in transfer caused by the presence of ethanol (C) The slope from (A) plotted against the slope from (B) (D) The increase in PITP activity induced by ethanol for each vesicle size All conditions were as described in the legend to Figure 1 (sonicated vesicles, $n = 3$–16, LUV$_{100}$ and LUV$_{200}$, $n = 3$, error bars show S.D) Abbreviation PI, PtdIns

protein content by 42%. Neither thermal pretreatment nor protease pretreatment of the donor microsomes affected the PITP-mediated PtdIns transfer or its ethanol enhancement (results not shown). This result was consistent with the microsomal proteins neither being involved in the transfer process nor being the source of the hydrophobic site that was responsible for the response to ethanol.

Effects of liposomal size/curvature on PITP activity and its ethanol enhancement

Figure 2 presents the effects of liposomal size on PtdIns transfer in the absence and the presence of ethanol. PITP-mediated PtdIns transfer was sharply diminished with the increased size of the acceptor vesicles (Figure 2A). The most planar acceptor membranes exhibited the slowest rates of transfer; conversely, the most curved membranes exhibited the fastest rates of transfer. The relative rates were as follows: SUV, 7.1; LUV$_{100}$, 1.9; LUV$_{200}$, 1.0. The dose response to ethanol mirrored that of PITP concentration, as shown in Figure 2(B). The ethanol-induced increase in PITP-mediated PtdIns transfer was least for the most planar membranes and greatest for the most curved membranes. However, when the decreased activity of PITP in the larger vesicles was accounted for, the enhancement of PITP activity by ethanol was independent of vesicle size. The slopes in Figures 2(A) and 2(B) are plotted in Figure 2(C) to indicate that changes in the degree of curvature exerted similar effects on the dose–response curves of both PITP and ethanol. Similarly, when the influence of ethanol was expressed in terms of its ability to enhance the PITP activity, no dependence on curvature could be discerned (Figure 2D). The effect of ethanol was applicable to membranes of all degrees of expressed curvature.

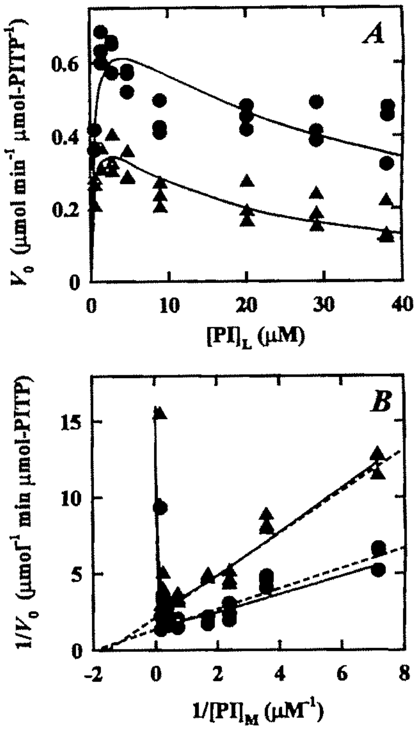

Figure 3 Kinetic analysis of PtdIns transfer

The initial velocities of PtdIns transfer were obtained for a variety of microsome and sonicated liposome (SUV) concentrations and fitted to the kinetic model of eqn (1) with the parameters shown in Table 1 Shown are two representative slices of these data and the corresponding fits in the absence (▲) and the presence (●) of 225 mM ethanol (A) The slice shown demonstrates the dependence of the initial transfer rate on the liposome concentration at constant microsome concentration (1.49 μM outer-leaflet microsomal PtdIns) (B) A second slice through the data set is presented in double-reciprocal format for constant liposome concentration (0.952 μM outer-leaflet liposomal PtdIns) and various microsome concentrations Solid lines represent kinetic fits from eqn (1), dotted lines represent regression analyses of the linear regime of the data sets In both panels the liposome and microsome concentrations were expressed in terms of the concentration of PtdIns on the outer leaflet of the liposome or microsome (see the text) Abbreviation PI, PtdIns

Kinetic analysis of the ethanol enhancement

A kinetic analysis of PtdIns transfer was undertaken to provide a mechanistic description of the enhancement by ethanol. Initial transfer velocities were obtained as a function of donor and acceptor membrane concentrations. A three-dimensional nonlinear regression analysis of the initial velocities to the theoretical rate equation [eqn (1)] was performed. A representative slice through the data set is shown in Figure 3(A) for a constant microsome concentration and various liposome concentrations in the presence and the absence of ethanol. The sharp enhancement by ethanol is evident, and the fit to eqn. (1) was reasonable.

The fitted parameters (k_1, k_2, K_1 and K_2) are summarized in Table 1. Parameters k_{-1} and k_{-2}, the dissociation rate constants

Table 1 Effects of ethanol on kinetic parameters

k_1, k_2, K_1 and K_2 were obtained from non-linear regression analysis based on 63 values (n) for outer-leaflet concentrations $[\text{PtdIns}]_M = 0.14$–$5.9\ \mu M$ and $[\text{PtdIns}]_L = 0.20$–$38\ \mu M$, at $0.034\ \mu M$ [PITP]. k_{-1} and k_{-2} were calculated from $k_{-1} = k_1/K_1$ and $k_{-2} = k_2/K_2$. r^2 is the correlation coefficient of the regression analysis. Results are presented as means ± S.E.M.

Ethanol (mM)	k_1 ($\mu M^{-1}\cdot min^{-1}$)	k_{-1} (min^{-1})	k_2 ($\mu M^{-1}\cdot min^{-1}$)	k_{-2} (min^{-1})	K_1 (μM^{-1})	K_2 (μM^{-1})	n	r^2
0	23 ± 3	23	78 ± 28	487	1.0 ± 0.3	0.16 ± 0.04	63	0.81
225	52 ± 11	32	200 ± 81	1834	1.7 ± 0.6	0.11 ± 0.03	63	0.74

of PITP from microsomes or SUVs respectively, were calculated from the following relations: $k_{-1} = k_1/K_1$ and $k_{-2} = k_2/K_2$ [19]. Ethanol (225 mM) approximately doubled the association and dissociation rate constants, indicating that it lowered the activation barrier to the PITP-mediated insertion and desorption of PtdIns. In contrast, the binding of PITP to the membranes was largely unaffected.

A second slice through the data set is presented in Figure 3(B) in the double-reciprocal format occasionally used to assess the activities of phospholipid transfer proteins [20]. In the slice shown, the microsome concentration was varied at a constant liposome concentration. The solid lines represent the fits from eqn. (1) that were shown in Figure 3(A) and compiled in Table 1. The upturn at high membrane concentrations is characteristic of phospholipid transfer proteins and was reproduced by the kinetic model. This effect arises largely from a diminution of the aqueous PITP concentration owing to binding at the microsomal membrane surface; an analogous decrease in the initial transfer velocity at high liposome concentrations is apparent in Figure 3(A). The dotted lines show a regression analysis of the linear portion of the curve. K_m was not significantly altered (0.66 ± 0.10 to 0.55 ± 0.15 μM for outer-leaflet microsomal PtdIns in the absence and the presence of ethanol respectively). Ethanol enhanced V_{max} (0.46 ± 0.05 to 0.80 ± 0.15 μmol/min per μmol of PITP in the absence and the presence of ethanol respectively).

DISCUSSION

Ethanol and PITP

The activity of PITP is very sensitive to the physical character of membranes. Acyl-chain order and surface charge greatly influence the activity of PITP [18], with PtdIns transfer being enhanced at more disordered or fluidized membranes [18]. Here we have illustrated the steep functional dependence on lipid structure by showing that the activity of PITP is strongly dependent on the expressed curvature of the acceptor vesicles. Steep functional dependences on expressed curvature have previously been reported for phosphatidylcholine transfer protein [36,37], phosphoinositide 4-kinase and phosphoinositide 3-kinase [21]. Ethanol enhanced the activity of PITP by increasing the PITP-mediated flux of PtdIns at the membrane surface. This ability to enhance PITP activity was not unique to ethanol: chloroform also enhanced PITP activity. Chloroform shares ethanol's ability to disorder or fluidize membranes. Their abilities to disorder membranes are correlated with their respective octanol/water partition coefficients [38]. Similarly, their abilities to enhance PITP transfer are correlated with their octanol/water partition coefficients. This result suggests that an enhancement of PITP activity could be a general consequence shared by membrane-fluidizing agents. However, membrane fluidity is only one of many biochemical processes involving hydrophobic sites that are correlated with octanol/water partitioning [39]. To investigate the role of microsomal proteins in the activity of PITP or its ethanol enhancement, transfer from thermally pretreated microsomes was monitored. We have shown previously that brief thermal pretreatment abolished the saturable binding of ethanol in microsomes [25]. Thermal pretreatment of the donor microsomes did not alter the activity of PITP and did not alter the enhancement by ethanol. Similar results were obtained with protease-treated microsomes. It is therefore unlikely that microsomal proteins or hydrophobic regions within them have a direct role in PITP transfer.

The activity of PITP depends inversely on the size of the liposomes. Smaller vesicles exhibit greater local convex curvature, greater headgroup areas and smaller cohesive forces in the outer leaflet in comparison with larger, more planar vesicles [40]. Similarly, ethanol and chloroform are membrane perturbants that fluidize membranes, increase headgroup areas and decrease cohesive forces between membrane lipids. PITP is very sensitive to the cohesive forces in membranes: a correlation between cohesive forces and phospholipid extraction has been postulated [41]. Ethanol enhanced the spontaneous desorption of fluorescent phospholipid analogues from lipid bilayers owing to its ability to decrease the cohesive forces between phospholipids in membranes [42]. The kinetic analysis supported this reasoning by showing that ethanol increased the successful insertion/desorption rates without significantly affecting PITP binding. The potential importance of the cohesive forces or membrane surface tension on PITP activity can be understood from the phospholipid exchange mechanism formulated from the recent crystal structure of the non-homologous yeast PITP [43]. The yeast PITP contained an unusual surface helix that was proposed to act like a swinging door, swinging into the membrane to sweep open a cavity and deposit the incoming phospholipid, then swinging back to abstract the outgoing phospholipid. The model was so disruptive to the membrane phospholipids that the authors termed it the 'bulldozer model'. Thus phospholipid exchange might be influenced by lateral cohesive forces between the membrane lipids that, in turn, were altered by curvature, chloroform or ethanol.

A dynamic viewpoint gives rise to a subtly different, but complementary, physical interpretation of ethanol's actions. Alcohols and other non-polar solutes are known to induce fluctuations in the shape of membranes by locally reducing the bending modulus (membrane stiffness) [44,45]. Consequently the alcohol-containing membranes are more malleable and more prone to local deformations, which would reduce the energy barriers to transfer.

The reasoning for a lipid-mediated pathway of ethanol action is based on a comparison of the effects of membrane structure on PITP activity and the known effects of ethanol on membrane structure, with the locus being the cohesiveness of the membrane lipids. An alternative explanation is that ethanol or chloroform binds to the hydrophobic acyl-chain-binding sites of PITP to enhance transfer. If this were true, we would expect transfer to be diminished, not enhanced. When alcohols and anaesthetics bind to hydrophobic clefts meant to dock with hydrophobic substrates, they interfere with or weaken substrate binding [46]. However, it is the competition between the association energy of the PtdIns–PITP complex and the association energy of the bilayer lipids (cohesiveness) that determines the transfer rate (for constant electrostatic factors) [41]. When the binding strength is much greater than the lipid cohesiveness, the surface flux is high. It is thought that the extraction/desorption step of the transfer process is rate-limiting, owing to the difficulty of overcoming the cohesive forces in the membrane, as is necessary for lipid extraction. If ethanol were to act by binding to the hydrophobic cleft, it would weaken the strength of the PtdIns–PITP complex and decrease the speed of transfer.

Implications for ethanol action

Historically, explanations for the common actions of organic solvents (anaesthetics) have fluctuated between protein, lipid and interface theories. More recently, opinion has shifted from lipid theories to protein theories as evidence has accumulated that clearly implicate hydrophobic regions of proteins as common targets of alcohols and anaesthetics [25,47]. This has led some to question whether any of the functional effects of alcohols and anaesthetics are mediated by membrane lipids [47]. Persuasive evidence for lipid-mediated actions of ethanol has been presented but is limited [48–50]. The sensitivity to ethanol described here for PITP rivals or exceeds that of any previously described lipid-mediated action of ethanol. Ethanol is best viewed as a very promiscuous molecule that acts on the hydrophobic regions of all biomaterials.

PITP might be a prototypical example for proteins that are sensitive to ethanol's effects on bulk lipids. Foremost, its function is exquisitely sensitive to membrane structure. By comparison, its sensitivity to ethanol is modest, being consistent with the modest lipid perturbations exerted by pharmacological concentrations of alcohols and anaesthetics [4]. A steep functional dependence on lipid structure and a comparatively modest functional dependence on alcohol are likely to be common features of proteins influenced by ethanol's effects on membrane lipids. Thus a strong sensitivity of proteins to lipid structure is likely to be a prerequisite for mechanisms of ethanol action mediated by bulk lipids.

Membrane curvature and PITP

It is a puzzle why PITP is critical to many biochemical processes. Membranous PtdIns stores are known not to be depleted significantly in processes that require PITP [9,11]. PITP seems to deliver PtdIns to metabolically active sites in the membrane, rather than passively maintaining the membrane's overall PtdIns content. The marked sensitivity of PITP to membrane structure provides a plausible mechanism for the ability of PITP to direct the delivery of PtdIns to metabolically active membrane domains. Transfer to membrane regions of convex curvature or low lipid surface density, as shown above, is markedly enhanced in comparison with transfer to planar regions. Because phosphoinositide 3-kinase and phosphoinositide 4-kinase also are much more active at convex surfaces [21], the potential exists for exponential increases in the production of PtdIns3*P* and PtdIns4*P* at curved membrane regions

We thank Jan B. Hoek and George M. Helmkamp Jr for valuable discussions. This work was supported by National Institutes of Health grants AA00163, AA07186 and AA07463, and by the Alcoholic Beverage Medical Research Foundation.

REFERENCES

1 Lieber, C S (1992) Medical and Nutritional Complications of Alcoholism, Plenum Medical Book Company, New York

2 Hoek, J B and Rubin, E (1990) Alcohol and membrane-associated signal transduction Alcohol Alcohol **25**, 143–156

3 Hoek, J. B., Thomas, A P, Rooney, T A, Higashi, K and Rubin, E (1992) Ethanol and signal transduction in the liver FASEB J **6**, 2386–2396

4 Taraschi, T. F. and Rubin, E (1985) Biology of disease Effects of ethanol on the chemical and structural properties of biologic membranes. Lab. Invest **52**, 120–131

5 Taraschi, T F, Ellingson, J S., Wu, A, Zimmerman, R and Rubin, E (1986) Phosphatidylinositol from ethanol-fed rats confers membrane tolerance to ethanol Proc. Natl. Acad Sci U.S A **83**, 9398–9402

6 Ellingson, J S, Janes, N, Taraschi, T F and Rubin, E (1991) The effect of chronic ethanol consumption on the fatty acid composition of phosphatidylinositol in rat liver microsomes as determined by gas chromatography and ^{1}H-NMR Biochim Biophys Acta **1082**, 199–205

7 Rubin, R, Thomas, A P and Hoek, J B (1987) Ethanol does not stimulate guanine nucleotide-induced activation of phospholipase C in permeabilized hepatocytes Arch Biochem Biophys. **256**, 29–38

8 Rubin, R and Hoek, J B (1988) Alcohol-induced stimulation of phospholipase C in human platelets requires G-protein activation Biochem J **254**, 147–153

9 Cunningham, E, Thomas, G M H, Ball, A, Hiles, I and Cockcroft, S (1995) Phosphatidylinositol transfer protein dictates the rate of inositol trisphosphate production by promoting the synthesis of PIP$_2$ Curr Biol **5**, 775–783

10 Higashi, K. and Hoek, J. B. (1991) Ethanol causes desensitization of receptor-mediated phospholipase C activation in isolated hepatocytes J Biol Chem **266**, 2178–2190

11 Currie, R A, MacLeod, B M. G and Downes, C P. (1997) The lipid transfer activity of phosphatidylinositol transfer protein is sufficient to account for enhanced phospholipase C activity in turkey erythrocyte ghosts Curr Biol **7**, 184–190

12 Kamath, S A and Rubin, E (1974) Alterations in the rate of phospholipid exchange between cell membranes Lab Invest **30**, 500–504

13 Wirtz, K W A (1997) Phospholipid transfer proteins revisited Biochem J **324**, 353–360

14 Snoek, G T., Berrie, C P, Geijtenbeek, T B H, van der Helm, H A, Cadeé, J A. Iurisci, C, Corda, D and Wirtz, K. W. A (1999) Overexpression of phosphatidylinositol transfer protein α in NIH3T3 cells activates a phospholipase A J Biol Chem **274**, 35393–35399

15 Tuscher, O, Lorra, C, Bouma, B., Wirtz, K W A and Huttner, W B (1997) Cooperativity of phosphatidylinositol transfer protein and phospholipase D in secretory vesicle formation from the TGN – phosphoinositides as a common denominator? FEBS Lett **419**, 271–275

16 Jones, S M., Alb, Jr, J G, Phillips, S E, Bankaitis, V A and Howell, K E (1998) A phosphatidylinositol 3-kinase and phosphatidylinositol transfer protein act synergistically in formation of constitutive transport vesicles from the trans-golgi network J Biol Chem **273**, 10349–10354

17 Ohashi, M., Jan de Vries, K, Frank, R, Snoek, G, Bankaitis, V, Wirtz, K W A and Huttner, W B (1995) A role for phosphatidylinositol transfer protein in secretory vesicle formation Nature (London) **377**, 544–547

18 Helmkamp, Jr, G M (1985) Phosphatidylinositol transfer proteins structure, catalytic activity, and physiological function Chem. Phys Lipids **38**, 3–16

19 Van den Besselaar, A M H P, Helmkamp, Jr, G M and Wirtz, K W. A (1975) Kinetic model of the protein-mediated phosphatidylcholine exchange between single bilayer liposomes Biochemistry **14**, 1852–1858

20 Yoshimura, T, Welti, R and Helmkamp, Jr, G M (1988) General kinetic model for protein-mediated phospholipid transfer between membranes Arch. Biochem. Biophys **266**, 299–312

21 Hubner, S, Couvillon, A. D, Kas, J A, Bankaitis, V A, Vegners, R, Carpenter, C L and Janmey, P. A (1998) Enhancement of phosphoinositide 3-kinase (PI 3-kinase) activity by membrane curvature and inositol-phospholipid-binding peptides Eur. J. Biochem **258**, 846–853

22 Geijtenbeek, T. B H, de Groot, E, van Baal, J, Brunink, F, Westerman, J, Snoek, G T and Wirtz, K W A (1994) Characterization of mouse phosphatidylinositol transfer protein expressed in *Escherichia coli*. Biochim Biophys Acta **1213**, 309–318

23 Helmkamp, Jr, G M, Harvey, M. S, Wirtz, K W A and van Deenen, L L M (1974) Phospholipid exchange between membranes Purification of bovine brain proteins that preferentially catalyze the transfer of phosphatidylinositol J Biol Chem **249**, 6382–6389

24 Thomas, G M H, Cunningham, E and Cockcroft, S (1994) Purification of phosphatidylinositol transfer protein from brain cytosol for reconstituting G-protein-regulated phosphoinositide-specific phospholipase C-β isozymes Methods Enzymol **238**, 168–181

25 Channareddy, S., Jose, S. S., Eryomin, V. A., Rubin, E., Taraschi, T. F. and Janes, N. (1996) Saturable ethanol binding in rat liver microsomes. J. Biol. Chem. **271**, 17625–17628

26 Mayer, L. D., Hope, M. J. and Cullis, P. R. (1986) Vesicles of variable sizes produced by a rapid extrusion procedure. Biochim. Biophys. Acta **858**, 161–168

27 White, D. A. (1973) The phospholipid composition of mammalian tissues. In Form and Function of Phospholipids (Ansell, C., Hawthorne, J. and Sauson, R., eds), pp. 441–482, Elsevier, Amsterdam

28 Higgins, J. A., Hitchin, B. W. and Low, M. G. (1989) Phosphatidylinositol-specific phospholipase C of *Bacillus thuringiensis* as a probe for the distribution of phosphatidylinositol in hepatocyte membranes. Biochem. J. **259**, 913–916

29 Victorov, A. V., Janes, N., Moehren, G., Rubin, E., Taraschi, T. F. and Hoek, J. B. (1994) Rapid transbilayer movement of phosphatidylethanol in unilamellar phosphatidylcholine vesicles. J. Am. Chem. Soc. **116**, 4050–4052

30 Victorov, A. V., Janes, N., Taraschi, T. F. and Hoek, J. B. (1997) Packing constraints and electrostatic surface potentials determine transmembrane asymmetry of phosphatidylethanol. Biophys. J. **72**, 2588–2598

31 Low, M. G. and Zilversmit, D. B. (1980) Phosphatidylinositol distribution and translocation in sonicated vesicles. A study with exchange protein and phospholipase C. Biochim. Biophys. Acta **596**, 223–234

32 Wallgren, H. and Barry, III, H. (1970) Actions of Alcohol, Elsevier Publishing Company, New York

33 Vierl, U., Löbbecke, L., Nagel, N. and Cevc, G. (1994) Solute effects on the colloidal and phase behavior of lipid bilayer membranes: ethanol-dipalmitoylphosphatidylcholine mixtures. Biophys. J. **67**, 1067–1079

34 Hansch, C. and Leo, A. (1979) Substituent Constants for Correlation Analysis in Chemistry and Biology, John Wiley and Sons, New York

35 Firestone, L. L., Miller, J. C. and Miller, K. W. (1986) Tables of physical and pharmacological properties of anesthetics. In Molecular and Cellular Mechanisms of Anesthetics (Roth, S. H. and Miller, K. W., eds), pp. 455–470, Plenum Publishing Corp., New York

36 Berkhout, T. A., van den Bergh, C., Mos, H., de Kruijff, B. and Wirtz, K. W. A. (1984) Regulation of the activity of phosphatidylcholine transfer protein by vesicle phosphatidic acid and membrane curvature: a fluorescence study using 2-parinaroylphosphatidylcholine. Biochemistry **23**, 6894–6900

37 Wirtz, K. W. A., Vriend, G. and Westerman, J. (1979) Kinetic analysis of the interaction of the phosphatidylcholine exchange protein with unilamellar vesicles and multilamellar liposomes. Eur. J. Biochem. **94**, 215–221

38 Janoff, A. S. and Miller, K. W. (1982) A critical assessment of the lipid theories of general anesthetic action. In Biological Membranes (Chapman, D., ed.), vol 4, pp. 417–476, Academic Press, New York

39 Hansch, C. and Dunn, III, W. J. (1972) Linear relationships between lipophilic character and biological activity of drugs. J. Pharmacol. Sci. **61**, 1–19

40 Beschiaschvili, G. and Seelig, J. (1992) Peptide binding to lipid bilayers. Nonclassical hydrophobic effect and membrane-induced pK shifts. Biochemistry **31**, 10044–10053

41 Wirtz, K. W. A. (1991) Phospholipid transfer proteins. Annu. Rev. Biochem. **115**, 981–984

42 Slater, S. J., Ho, C., Taddeo, F. J., Kelly, M. B. and Stubbs, C. D. (1993) Contribution of hydrogen bonding to lipid–lipid interactions in membranes and the role of lipid order: effects of cholesterol, increased phospholipid unsaturation, and ethanol. Biochemistry **32**, 3714–3721

43 Sha, B., Phillips, S.E., Bankaitis, V. A. and Luo, M. (1998) Crystal structure of the *Saccharomyces cerevisiae* phosphatidylinositol-transfer protein. Nature (London) **391**, 506–510

44 Safinya, C. R., Sirota, E. B., Roux, D. and Smith, G. S. (1989) Universality in interacting membranes: the effect of cosurfactants on the interfacial rigidity. Phys. Rev. Lett. **62**, 1134–1137

45 Häckl, W., Seifert, U. and Sackmann, E. (1997) Effects of fully and partially solubilized amphiphiles on bilayer bending stiffness and temperature dependence of the effective tension of giant vesicles. J. Phys. II **7**, 1141–1157

46 Franks, N. P. and Lieb, W. R. (1984) Do general anaesthetics act by competitive binding to specific receptors? Nature (London) **310**, 599–601

47 Franks, N. P. and Lieb, W. R. (1994) Molecular and cellular mechanisms of general anaesthesia. Nature (London) **367**, 607–614

48 Mitchell, D. C., Lawrence, J. T. R. and Litman, B. J. (1996) Primary alcohols modulate the activation of the G protein-coupled receptor rhodopsin by a lipid-mediated mechanism. J. Biol. Chem. **271**, 19033–19036

49 Pflugmacher, D. and Sandermann, Jr, H. (1998) The lipid/protein interface as a target site for general anesthetics: a multiple-site kinetic analysis of synaptosomal Ca^{2+}-ATPase. Biochim. Biophys. Acta **1415**, 174–180

50 Sze, P. Y. and Iqbal, Z. (1994) Ethanol modulates [^{125}I]calmodulin binding to synaptic plasma membranes from rat brain. J. Pharmacol. Exp. Ther. **268**, 1183–1189

Received 2 November 1999/14 March 2000; accepted 11 April 2000

Biochem. J. (2000) **348**, 675–686 (Printed in Great Britain)

Sequence of the 5′-flanking region and promoter activity of the human mucin gene *MUC5B* in different phenotypes of colon cancer cells

Isabelle VAN SEUNINGEN*[1], Michaël PERRAIS*, Pascal PIGNY*†, Nicole PORCHET*‡ and Jean-Pierre AUBERT*‡

*Unité INSERM 377, Place de Verdun, 59045 Lille Cedex, France, †Laboratoire de Biochimie Endocrinienne de l'Hôpital C. Huriez, CHRU, 59037 Lille Cedex, France, and ‡Laboratoire de Biochimie et de Biologie Moléculaire de l'Hôpital C. Huriez, CHRU, 59037 Lille Cedex, France

Control of gene expression in intestinal cells is poorly understood. Molecular mechanisms that regulate transcription of cellular genes are the foundation for understanding developmental and differentiation events. Mucin gene expression has been shown to be altered in many intestinal diseases and especially cancers of the gastrointestinal tract. Towards understanding the transcriptional regulation of a member of the 11p15.5 human mucin gene cluster, we have characterized 3.55 kb of the 5′-flanking region of the human mucin gene *MUC5B*, including the promoter, the first two exons and the first intron. We report here the promoter activity of successively 5′-truncated sections of 956 bases of this region by fusing it to the coding region of a luciferase reporter gene. The transcription start site was determined by primer-extension analysis. The region upstream of the transcription start site is characterized by the presence of a TATA box at bases $-32/-26$, DNA-binding elements for transcription factors c-Myc, N-Myc, Sp1 and nuclear factor κB as well as putative activator protein (AP)-1-, cAMP-response-element-binding protein (CREB)-, hepatocyte nuclear factor (HNF)-1-, HNF-3-, TGT3-, gut-enriched Krüppel factor (GKLF)-, thyroid transcription factor (TTF)-1- and glucocorticoid receptor element (GRE)-binding sites. Intron 1 of *MUC5B* was also characterized, it is 2511 nucleotides long and contains a DNA segment of 259 bp in which are clustered eight tandemly repeated GA boxes and a CACCC box that bind Sp1. AP-2α and GATA-1 nuclear factors were also shown to bind to their respective cognate elements in intron 1. In transfection studies the *MUC5B* promoter showed a cell-specific activity as it is very active in mucus-secreting LS174T cells, whereas it is inactive in Caco-2 enterocytes and HT-29 STD (standard) undifferentiated cells. Within the promoter, maximal transcription activity was found in a segment covering the first 223 bp upstream of the transcription start site. Finally, in co-transfection experiments a transactivating effect of Sp1 on to *MUC5B* promoter was seen in LS174T and Caco-2 cells.

Key words: differentiation, LS174T, Myc, Sp1, transcription.

INTRODUCTION

Human mucins are the main glycoprotein component of epithelial secretions and play important roles in maintaining mucosae integrity. So far, eight genes have been described [1] and among them *MUC6-MUC2-MUC5AC-MUC5B* are clustered on human chromosome 11p15.5 [2]. Previous studies have demonstrated that the expression of these four genes is tissue- and cell-specific, and that their expression is dysregulated during the pathogenesis of several diseases [3]. These results suggest that mucin gene expression is tightly regulated. *MUC5B* is mainly expressed in normal bronchus, submaxillary glands, endocervix, pancreas [4] and gall bladder [5,6]. Interestingly enough, *MUC5B* has been shown to be highly expressed in colon cancer [3] and especially in the mucus-secreting colon cancer cell lines HT-29 MTX (methotrexate) [7] and LS174T [6].

The *MUC5B* gene is 39.09 kb in length, contains 49 exons and encodes a 5701-amino-acid polypeptide with an M_r of approx. 627000. *MUC5B* shows extensive similarity in its 5′ and 3′ regions to the other genes of the cluster *MUC2*, *MUC5AC* and *MUC6* [8–11]. Regarding *MUC5B* regulation, we showed previously that intron G, now called intron 37 (30 kb downstream of the ATG), contains eight repeats of a perfect Sp1 (GGGCGG)-binding site [9]. It binds Sp1 and a 42-kDa nuclear factor called NF1-MUC5B specific to the mucus-secreting colon cancer cell line HT-29 MTX [12].

Regarding the other 11p15.5 mucin genes, promoter sequences and transcriptional regulation are known for *MUC2* and *MUC5AC*. *MUC2* a prominent mucin gene expressed in the colon, has a TATA and a CCAAT box as well as predicted binding sites for many transcription factors [13,14]. Transfection studies carried out in colon cancer cell lines (HT-29, LS174T) showed that a region in the promoter of *MUC2* that extends 848 bp upstream of the ATG confers maximal transcriptional activity [13]. Gum et al. showed that a short segment including bases $-91/-73$ relative to the start site was essential for basal promoter activity in several colon cancer cell lines [14]. By the means of transgenesis, the same group showed that *cis*-elements necessary for *MUC2* goblet-cell-specific expression are present within the *MUC2* promoter [15]. More recently, it was shown that Sp1 regulates rat *muc2* gene transcription in lung cells [16]. Li et al. showed that *Pseudomonas aeruginosa* lipopolysaccharide activates a c-Src-Ras-MEK 1/2-pp90rsk signalling pathway that leads to activation of nuclear factor κB (NF-κB; p65/p50) [17]. Activated NF-κB binds to κB sites in the 5′ proximal region of the gene and induces *MUC2* transcription [18,19].

MUC5AC is highly expressed in airway epithelial cells and in the stomach. A TATA box is located at $-23/-29$ of the transcription start site and putative binding sites for Sp1, activator protein (AP)-2, glucocorticoid receptor element (GRE), NF-κB as well as a CACCC box were found within the promoter [20]. *MUC5AC* transcription is activated when bronchial ex-

---

Abbreviations used: GAPDH, glyceraldehyde-3-phosphate dehydrogenase; MTX, methotrexate; STD, standard; RT, reverse transcriptase; NF-κB, nuclear factor κB; AP, activator protein; UTR, untranslated region; GRE, glucocorticoid receptor element; HNF, hepatocyte nuclear factor; GKLF, gut-enriched Krüppel factor; TTF, thyroid transcription factor.

[1] To whom correspondence should be addressed (e-mail vanseuni@lille.inserm.fr).

The nucleotide sequences reported here have been submitted to GenBank under the accession numbers AJ011582 and AJ012453.

plants, airway epithelial cells (NCIH292) or colon cancer cells (HM3) are exposed to *P. aeruginosa* or its exoproducts in cell-free supernatants. Both *MUC2* and *MUC5AC* are up-regulated by other Gram-positive and Gram-negative organisms [20]. These results suggest that the pathology of cystic fibrosis bacterial infection increases *MUC2* and *MUC5AC* mucin mRNA production.

In this report, we present the genomic sequence of 3.55 kb of the *MUC5B* 5′-flanking region that includes the promoter and the first intron The promoter and first intron were characterized and several important *cis*-elements that bind nuclear factors (Sp1, N-Myc, NF-κB, TGT3, AP-2α and GATA-1) were identified. *MUC5B* transcriptional activity was studied in colon cancer cell lines that are undifferentiated [HT-29 STD (standard)] or that either differentiate in mucus-secreting cells (LS174T) or in enterocytes (Caco-2). It appears that *MUC5B* expression shows cell-specificity and is the highest in mucus-secreting colon cancer cell line LS174T. The roles of the structural and functional properties of the *MUC5B* promoter in *MUC5B* gene transcription are discussed.

MATERIALS AND METHODS

Cloning

Inserts were prepared using the restriction map of two cosmid clones called ELO9 [21] and BEN1 [8], which cover the 5′ proximal region of *MUC5B*. Gel-purified fragments (Qiaquick gel extraction kit, Qiagen) were subcloned into the promoterless pGL3 Basic vector (Promega). Internal deletion mutants were generated by PCR using pairs of primers bearing specific restriction sites at their 5′ and 3′ ends. PCR products were digested, gel-purified and subcloned into the pGL3 vector that has previously been cut with the same restriction enzymes. All clones were sequenced on both strands on an automatic LI-COR sequencer (ScienceTec, France) using infrared-labelled RV3 and GL2 primers (Promega). Plasmids used for transfection studies were prepared using the Endofree plasmid Mega kit (Qiagen).

Cell culture

The LS174T cell line was cultured in a 37 °C incubator with 5 % CO$_2$ in Dulbecco's modified Eagle's minimal essential medium supplemented with non-essential amino acids and 10 % foetal calf serum (Boehringer Mannheim). Other human colon adenocarcinoma cell lines were cultured in a 37 °C incubator with 10 % CO$_2$ in Dulbecco's modified Eagle's medium supplemented with either 10 % (HT-29 STD, HT-29 MTX) or 20 % (Caco-2) foetal calf serum. All cell lines were a kind gift from Dr A. Zweibaum (Unité INSERM N°178, Villejuif, France).

Reverse transcriptase PCR (RT-PCR)

Total RNAs from colon cancer cells were prepared using the RNeasy midi-kit from Qiagen. Cells were harvested at 70 % confluence and 1.5 μg of total RNA was used to prepare cDNA (Advantage® RT-for-PCR kit, Clontech). PCR was then performed on 5 μl of cDNA using specific pairs of primers for *MUC2* and *MUC5B* mucin genes (M.-P. Buisine, N Moniaux, S. Nollet, E. Destailleur, I. Van Seuningen, A. Laine, N. Porchet and J.-P. Aubert, unpublished work): *MUC2* forward primer, 5′-CTGCACCAAGACCGTCCTCATG-3′, *MUC2* reverse primer, 5′-GCAAGGACTGAACAAAGACTCAGAC-3′ (positions nt 15291–15312 and nt 15667–15691, accession number L21998 [22]); *MUC5B* forward primer, 5′-CTGCGAGACCGAGGTCAACATC-3′; *MUC5B* reverse primer, 5′-TGGGCAGCAGGAGCACGGAG-3′ (positions nt 9057–9078 and nt 10108–10127, accession number Y09788 [9]). Single-stranded oligonucleotides were synthesized by MWG-Biotech, Ebersberg, Germany Glyceraldehyde-3-phosphate dehydrogenase (GAPDH) was used as an internal control. PCR reactions were carried out in 50-μl final solutions [5 μl of Perkin-Elmer buffer, 5 μl of 25 mM MgCl$_2$, 5 μl of 2.5 mM dNTPs, 10 pmol of each primer, 2 units of *Taq* polymerase (Ampli Taq Gold, Perkin Elmer)]. Cycling conditions were as follows: (i) denaturation, 96 °C, 10 min for one cycle, (ii) denaturation, 96 °C, 30 s; annealing, 60 °C, 30 s; and extension, 72 °C, 1 min for 30 cycles and (iii) final extension, 72 °C, 15 min. PCR products were analysed on 2 % E-gels run in 1 × Tris/borate/EDTA buffer (Invitrogen). Mixed ladder was purchased from Invitrogen. Expected sizes of PCR products were 401 bp for *MUC2* and 415 bp for *MUC5B*.

Table 1 Sequences of the pairs of oligonucleotides used in PCR to produce deletion mutants in the *MUC5B* 5′-flanking region (see Figure 1)

*Kpn*I (GGTACC), *Sac*I (GAGCTC) and *Mlu*I (ACGCGT) sites were added at the ends of the primers to direct subcloning (underlined). Positions of the DNA fragments in *MUC5B* 5′-flanking region relative to the transcription start site are indicated S, sense, AS, antisense

pGL3 deletion mutant	Position of the DNA fragment	Orientation	Oligonucleotides used for PCR (5′ → 3′)
1916	−956/+57	S	CGCGGTACCGAGGTATTGCAGCGC
		AS	CGCACGCGTCCTGGGGGCTGGCAC
1896	−956/−1	S	CGCGGTACCGAGGTATTGCAGCGC
		AS	CGCACGCGTTGCTTGCTCCCCTGGGGGC
1597	−223/+57	S	CGCGAGCTCTCCCTTCCGATTCTCAGA
		AS	CGCACGCGTCCTGGGGGCTGGCAC
1596	−223/−1	S	CGCGAGCTCTCCCTTCCGATTCTCAGA
		AS	CGCACGCGTTGCTTGCTCCCCTGGGGGC
1895	−956/−223	S	CGCGGTACCGAGGTATTGCAGCGC
		AS	CGCACGCGTAGAGAAGGGCCTACCCCA
1595	−446/−223	S	CGCGAGCTCCAGCCTCGTGGGCCCTCC
		AS	CGCACGCGTAGAGAAGGGCCTACCCCA
1598	−956/−441	S	CGCGGTACCGAGGTATTGCAGCGC
		AS	CGCGAGCTCAGGCATGCACATGGC

Primer extension

Primer-extension reactions were performed using 25 μg of total RNA isolated from LS174T and HT-29 MTX cell lines. Primers were end-labelled with [γ-^{32}P]dATP. Exon 1 reverse primer, 5′-TGCCTGCGGCACCACGAGCATG-3′ (see Figure 2B below) was annealed to RNA at 62 °C for 20 min followed by a 10 min incubation at room temperature. Extension was performed as described in the Promega primer-extension kit using 200 units of Moloney-murine-leukaemia virus (MMLV) RT (Advantage® RT-for-PCR kit, Clontech) for 45 min at 42 °C Reactions were stopped by adding 20 μl of loading buffer (98 % formamide/10 mM EDTA/0.1 % xylene cyanol/0.1 % Bromophenol Blue). ϕX174 DNA/*Hin*fI dephosphorylated markers were radiolabelled with [γ-^{32}P]dATP just before use (Promega). Manual sequencing of fragment 1429 (DNA fragment of *MUC5B* promoter region) was performed using the T7 Sequenase version 2.0 kit (Amersham). Samples were denatured for 10 min at 90 °C before loading on a 6 % sequencing gel (Sequagel-6, National Diagnostic). The gel was then vacuum-dried and autoradiographed for 3–4 days at −80 °C.

Oligonucleotides and DNA fragments

Oligonucleotides used for PCR are shown in Table 1. Those used for gel-shift assays are indicated in Table 2. They were synthesized

Table 2 Sequences of the sense oligonucleotides used for gel-shift-assay experiments

Mutated bases are in bold. Antisense complementary oligonucleotides were also synthesized and annealed to the sense oligonucleotides to produce double-stranded DNA.

Oligonucleotide (sense orientation)	Sequence (5′ → 3′)
c-Myc/N-Myc/Max site/promoter	GAGAGCAAACACACGTGGCTGGAG
CACCC/Sp1 site/promoter	CTGCTGGGGGTGGGGGCGTCCTGG
NF-κB site/promoter	CAGAGGCTGGGATTCCCTTCCAGC
CCAAT site/promoter	GGCTGGCATTGGACAAGCGCACGT
TGT3 site/promoter	GAGGACCCCGGGCAGGTCCAGGAC
CACCC box/intron 1	TTAGGGGACACACCCCAAAGT
GA box/intron 1	GCAGGGGAGGGGCTGCCTGGG
Mutated GA box no. 1	GCA**TTA**GAGGGGCTGCCTGGG
Mutated GA box no. 2	GCAGGG**ATT**GGGCTGCCTGGG
Mutated GA box no. 3	GCAGGGGAG**CTA**CTGCCTGGG
Sp1 site/intron 1	CCCTTGGGGCGGCCAACGCCT
AP-2 site/intron 1	ACGTCCTGTGGCCGGGGGAAGGCA
GATA-1 site/intron 1	ACGGAGCAGATAACCAAGGGC
NF-κB site/intron 1	GCAGGGGGCTTCCCCCAGTGG

by MWG-Biotech. Annealed oligonucleotides were radiolabelled using T4 polynucleotide kinase (Promega) and [γ-^{32}P]dATP. Radiolabelled probes were separated from free nucleotides on Sephadex G-25 columns (Boehringer Mannheim). DNA fragment 1472 was produced by PCR (forward primer, 5′-CGCGAGCTCGATAACCAAGGGCAGTCA-3′; reverse primer, 5′-CGCACGCGTTCCACCCCGACCCACAGC-3′) and cloned into the pGL3 vector. This fragment contains the eight GA boxes found in intron 1. The fragment was cut out of the vector by *Sac*I–*Mlu*I double digestion, gel-purified and labelled with [α-^{32}P]dCTP at the 3′ end by a fill-in reaction using the Klenow fragment (Boehringer Mannheim).

Transfections

Cells from the human colon adenocarcinoma cell lines HT-29 STD (parental undifferentiated cell line), Caco-2 (enterocytes) and LS174T (goblet cells, mucus-secreting) were electroporated using Gene Pulser II apparatus (Bio-Rad) on day 7 (70 % confluence). Before electroporation, 25 μg of plasmid were added to the cells. In co-transfection experiments, 20 μg of pGL3 deletion mutant and 5 μg of pCMV-Sp1 or pCMV-Sp3 were used. After a 10-min incubation at room temperature, transfected cells were plated and incubated for 48 h at 37 °C. Total cell extracts were prepared using 1 × Reagent Lysis Buffer (Promega) as described in the manufacturer's instruction manual. Results were corrected for transfection efficiency by co-transfecting 2 μg of pSV-βGal vector (Promega). β-Galactosidase activity was measured in 96-well plates as described in the manufacturer's instruction manual using 50 μl of cell extracts (Promega). Luciferase activity was measured on a Berthold 5901 luminometer on 100 μl of cell extracts using luciferase assay reagent (Promega). The luciferase activity is expressed as fold induction of the test plasmid activity compared with that of the corresponding control vector (pGL3 control, Promega) after correction for transfection efficiency by dividing by β-galactosidase activity. Each plasmid was assayed in duplicate in at least three separate experiments. pCMV4, pCMV4-Sp1 and pCMV4-Sp3 vectors were a kind gift from Dr J. M. Horowitz (North Carolina State University, Raleigh, NC, U.S.A.).

Nuclear-extract preparation

Nuclear extracts from cell lines of interest were prepared as described in [23], and kept at −80 °C until use. Protein content (5 μl of cell extracts) was measured using the bicinchoninic acid method in 96-well plates, as described in the manufacturer's instruction manual (Pierce).

Gel-shift assays

Nuclear proteins (5 μg) were pre-incubated for 20 min on ice in 20 μl of binding buffer with 2 μg of poly dI-dC (Sigma) and 1 μg of sonicated salmon sperm DNA. Radiolabelled DNA probe was added (120000 c.p.m./reaction) and the reaction left for another 20 min on ice. For super-shift analyses, 1 μl of the antibody of interest (anti-Sp1, anti-AP2α, anti-GATA-1, anti-c-Myc, anti-N-Myc, anti-Max, anti-c-Fos, anti-NF-κB p50 and anti-NF-κB p65, Santa Cruz Laboratories) was added to the proteins and left for 1 h on ice before adding the radiolabelled probe. Negative controls were carried out using 1 μl of irrelevant antibody in the reaction mixture. Competitions were performed with 50-, 150- and 300-fold excesses of unlabelled oligonucleotide in the reaction mixture before adding the radiolabelled probe. Commercial Sp1 oligonucleotide and Hela-cell nuclear extract used as positive controls were from Promega. The reactions were stopped by adding 2 μl of loading buffer, loaded on to a 4 % non-denaturing polyacrylamide gel (for oligonucleotides) and electrophoresis conditions were as described in [24]. Gels were pre-run for 30 min at 200 V before loading the samples and running the electrophoresis at 200 V for 2–3 h in 0.5 × Tris/borate/EDTA buffer at 4 °C. For DNA probes longer than 250 bp (1472), 6 % gels were run as described in [25], with slight modifications: the pre-run was 1 h and 15 min long and electrophoresis was run for 4 h and 15 min at 4 °C. Gels were then vacuum-dried and autoradiographed overnight at −80 °C.

Southwestern- and immuno-blotting

Nuclear proteins (25 μg) were resolved by SDS/PAGE (10 % gel) and then electrotransferred on to a nitrocellulose membrane (pore size 0.22 μm, Schleicher and Schuell). Proteins were submitted to a denaturation/renaturation cycle as described by Jackson [26] before radiolabelled probe (1 × 10^6 c.p.m./ml of buffer) was added to the mixture and left for 30 min at room temperature. When necessary, unlabelled competitor (150-fold excess) was pre-incubated with the membrane before adding the radiolabelled probe. The membrane was then washed and autoradiographed overnight at −80 °C. The radiolabelled probe was washed off by incubating the membrane twice for 5 min in boiling 0.1 × SSC/0.1 % SDS solution (where 1 × SSC is 0.15 M NaCl/0.015 M sodium citrate) and rinsed once with 3 × SSC. Immunostaining was then performed using the anti-Sp1 antibody PEP2 (Santa Cruz Laboratories) at a 1:1000 dilution. Alkaline phosphatase-conjugated goat anti-rabbit antibody (Promega) was used at a 1:4725 dilution. Protein bands were developed using Nitro Blue Tetrazolium chloride and 5-bromo-4-chloro-3-indolylphosphate *p*-toluidine salt (Life Technologies) as chromogenic substrates for alkaline phosphatase. Prestained protein molecular-mass standards were from Life Technologies.

DNA sequence and transcription-factor-binding site analyses

DNA sequences were analysed using PC-GENE software and the TRANSFAC database [27] was used to define potential transcription-factor-binding sites within the clones of interest. The search was conducted using MatInspector V2.2 software [27].

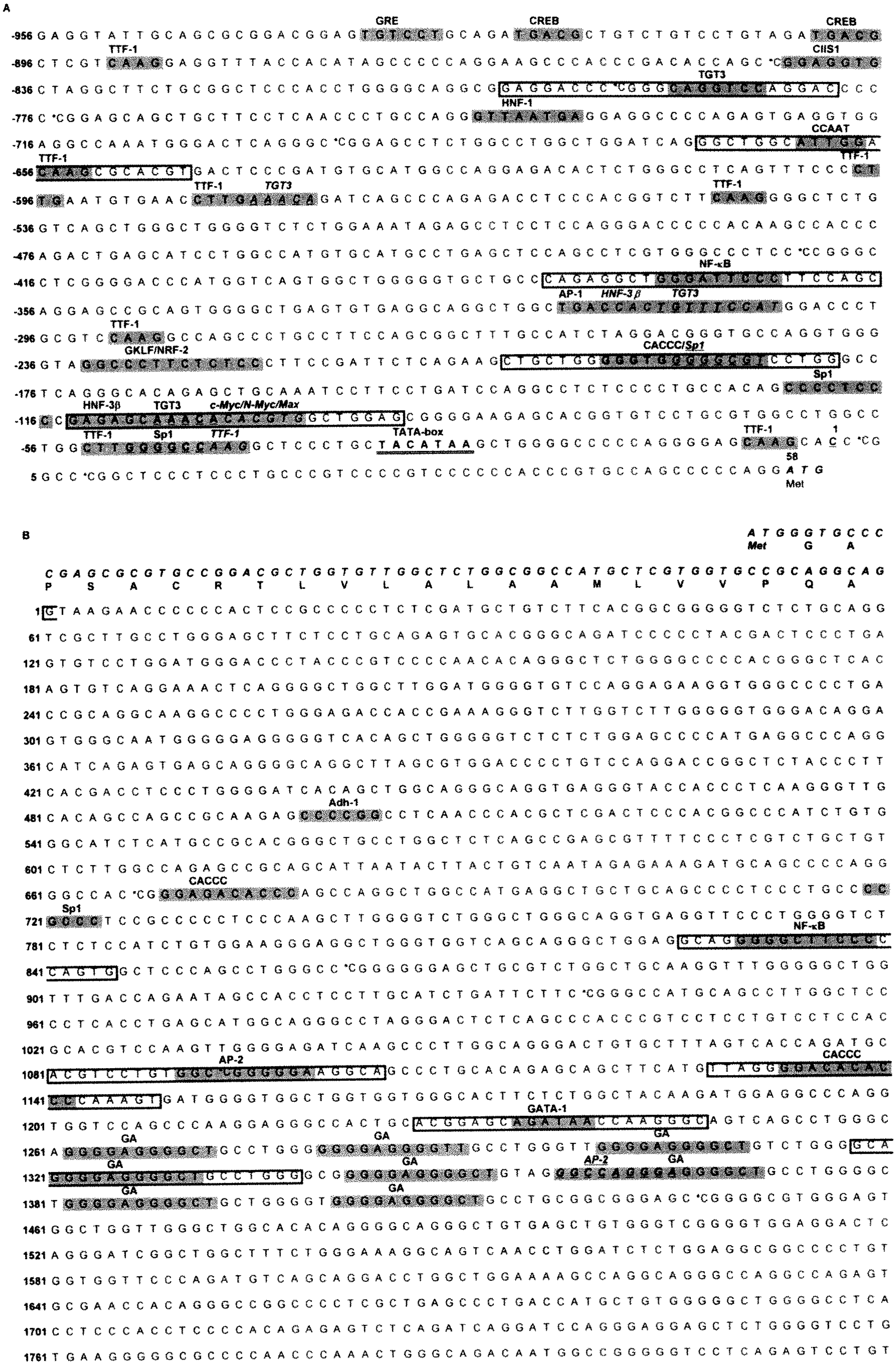

Figure 1 For legend see opposite.

```
1821 G G G T T G G A G C T G C C T C C T C C C A G C C T C C A T G G G G T T G G T G G G T G A G G C C T T G C C *C G G A G G
                                                                 Sp1
1881 C G G T G G T C A G C C T G G G G G A C C T T G G G C G G C C A T C C C A G T A T C A A C G G C C A C A C A G C T T G C
1941 G C G G C C C A G A G T C C T G C C C C C A G C C T G C C C C A C T C G C C C T G A C T T A G G A T C T A G T T C G A A
2001 A C T G G T T C T G T G T T T A G G T T T C T G C T A A G T C A C G C C T G G A A G G C T C C A A G T G T G T C C T C C
2061 T A A C A A A G C T G G T C T T T G T C C T T C T C C A A G G G A T G T G T G G G A T G G G G C G A A A T C C C C C C T
            Sp1
2121 T G G G G C G G C C A A C G C C T T T T C C T G A T T C C A T T T T C T C C C C C A T C C C T T G A G A A G G A G G C A
2181 C C A T C C C C G C C T G T C A G T C G G G G A C A G G G C A G G C C G T G C T G G G G G C A G C T C A G G G C T C C C
2241 T G C T G G A A G C T T C C A T C C C G C A G G C T T T C C A T A G C A T T G A G C A G G A G C *C G G A G G C A T C T G
2301 C G G C T G A C G G T T G G G G T G G C C T G A G C G G C T G G G G A G G A G T C C *C G G C C T T G G C C A C A G T G T
2361 G T C G T G A G G G T G A A C C T G C A G G G C A T G G A G A C C G C C A C C A A G G A C C C C A C A T G C G C G T G C
2421 C G C A C C A G G G A T G T G G C C A G G T C C G T G G T T G G G T T T C G G C T G G C A G C C A C A T C T A G T T C C
2481 T C A C T G G A C T C C C C A T T C C C T C T T C C C A C A G]A G A C C C A G G G C C C T G T G G A G C C G A G C T G G
                                                              E     T     Q     G     P     V     E     P     S     W

     G G G A A T G C A G G G C A C A C C A T G G A T G G C G G T
       G     N     A     G     H     T     M     D     G     G
```

Figure 1 DNA sequence of the human *MUC5B* promoter (A) and intron 1 (B)

(**A**) The TATA-like box (TACATAA) at −32/−26 is double-underlined and potential binding sites for known transcription factors are in grey. The transcription start site is designated as +1 and first ATG is bold and italicized. *Hpa*II (C*Cgg) potential methylation sites are also indicated. (**B**) DNA and peptide sequences of exon 1 and exon 2 surrounding intron 1 are bold and italicized. Square brackets indicate the beginning and end of intron 1 sequence. DNA sequences used for binding assays are boxed.

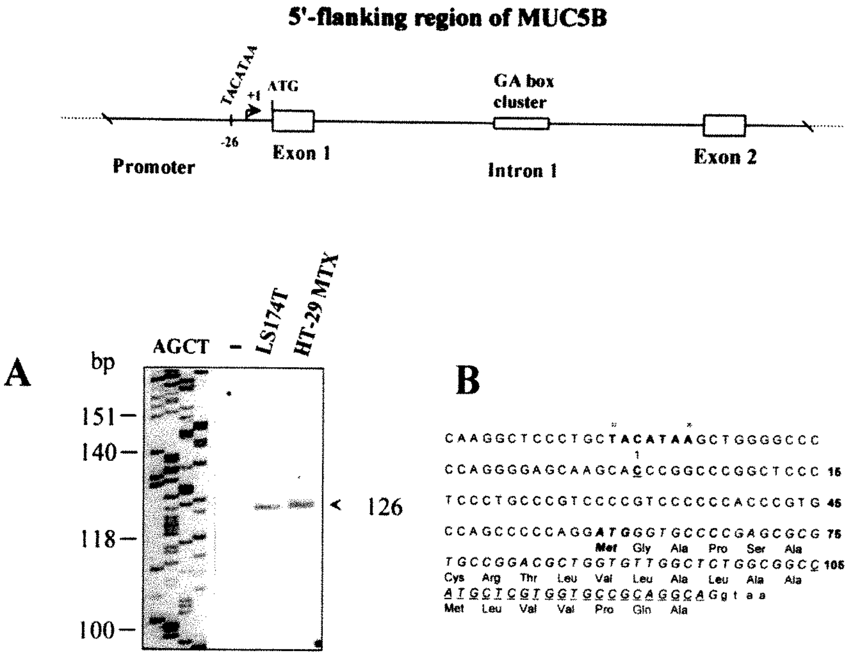

```
CAAGGCTCCCTGCTACATAAGCTGGGGCCC
               1
CCAGGGGAGCAAGCAGCCGGCCCGGCTCCC 16
TCCCTGCCCGTCCCCGTCCCCCCACCCGTG 46
CCAGCCCCCAGGATGGGTGCCCCGAGCGCG 76
            Met Gly Ala Pro Ser Ala
TGCCGGACGCTGGTGTTGGCTCTGGCGGCC 106
Cys Arg Thr Leu Val Leu Ala Leu Ala Ala
ATGCTCGTGGTGCCGCAGGCAGgtaa
Met Leu Val Val Pro Gln Ala
```

Figure 2 Transcription start site of human *MUC5B* mucin gene

Schematic representation of the 5′-flanking region of *MUC5B*. The bent arrow indicates the transcription start-site position (upper panel). (**A**) Primer-extension reactions were performed on 25 μg of total RNA from LS174T and HT-29 MTX cell lines. A product of 126 bp was produced when using the exon 1 reverse primer. φX174 DNA/*Hin*fI dephosphorylated markers previously radiolabelled and denatured are shown on the left. (**B**) DNA sequence surrounding the transcription start site. The reverse exon 1 oligonucleotide used for primer-extension experiments was designed from the underlined sequence.

RESULTS

DNA sequence and characterization of *MUC5B* 5′-flanking region

Two genomic clones, ELO9 and BEN1, which we previously isolated to study *MUC5B* and *MUC5AC* gene organization [9,21], were used in this work to characterize the 5′-flanking region of *MUC5B*. Here, we report the genomic sequence obtained and an analysis of transcriptional activity of the 5′-flanking region including 956 bases of DNA sequence located upstream of the transcriptional start site as well as 2637 bases downstream that include the first two exons and the first intron. Between the transcription start site and the ATG codon coding for the first methionine lies the 5′ untranslated region (UTR) of 56 nucleotides (Figure 1A). The first exon encodes the first 23 amino acids (MGAPSACRTLVLALAAMLVVPQA) and is separated from exon 2, which is composed of 19 amino acids

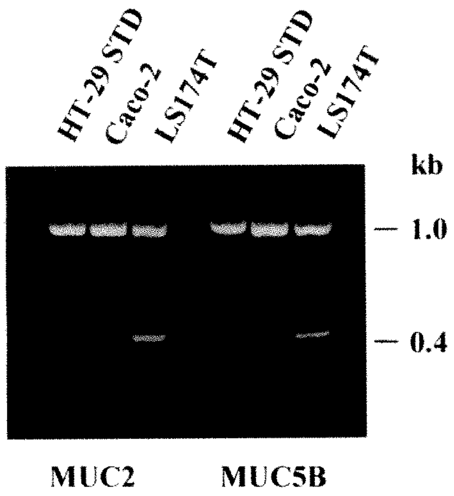

Figure 3 Mucin gene-expression profiles in colon cancer cells by RT-PCR

RT-PCR was performed on total RNA extracted from cells at day 7. Specific oligonucleotides for *MUC2* and *MUC5B* generate 401- and 415-bp PCR products, respectively. The *GAPDH* PCR product is 980 bp long. PCR products were separated on a 2% agarose gel. Molecular-mass markers are shown on the right.

(ETQGPVEPSWGNAGHTMDG), by an intron of 2511 nucleotides (Figure 1B).

Analysis of the DNA sequence using PC-GENE software and the TRANSFAC database [27] showed that the 5′-flanking region upstream of the transcription start site contained a TATA-box-like sequence TACATAA located at bases −32/−26 upstream of the transcription start site (Figure 1A). In the close vicinity to the TATA-box-like sequence were found potential binding sites for c-Myc/N-Myc/Max transcription factors (consensus CACGTG), Sp1 and numerous GC and CACCC boxes. It is of interest to note that GC and CACCC boxes are always clustered. Further upstream, putative binding sites were found for AP-1, NF-κB, CCAAT, cAMP-response-element-binding protein (CREB) and GRE transcription factors as well as for a silencer called CIIS1. A striking feature was the presence, throughout the 5′-flanking region upstream of the TATA box, of numerous putative binding sites for transcription factors known to be involved in intestinal [hepatocyte nuclear factor (HNF)-1, HNF-3, TGT3, gut-enriched Krüppel factor (GKLF)] or respiratory [HNF-3, thyroid transcription factor (TTF)-1] cell differentiation. Numerous *Hpa*II sites that could be potential methylation sites were found, two of them being located in the 5′-UTR region.

In the first intron (Figure 1B), a high amount of GC boxes, Sp1 binding sites and CACCC boxes were present. More

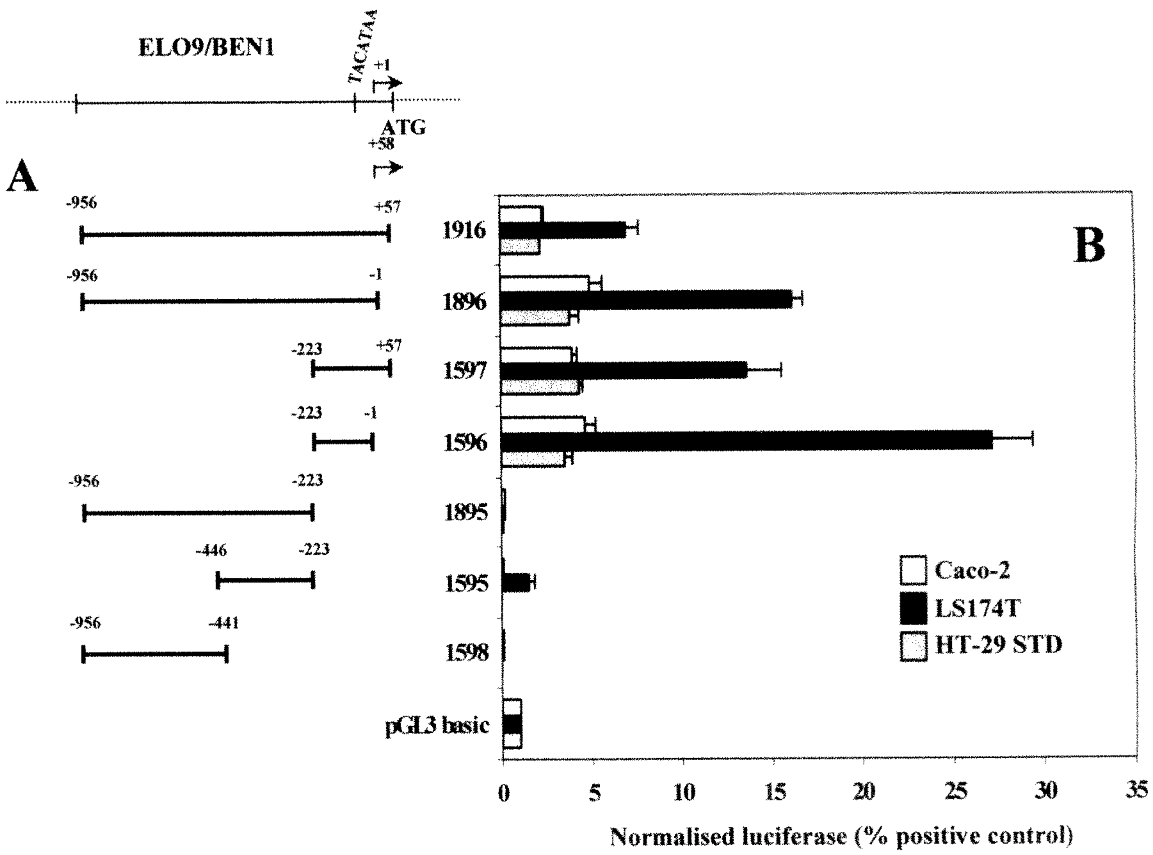

Figure 4 Position and transcriptional activity of the pGL3 deletion mutants in *MUC5B* promoter

(**A**) Schematic representation of the localization of the different pGL3 deletion mutants covering 1013 nucleotides upstream of exon 1. Numbering refers to the transcription start site designated +1. The TATA-box location in fragments 1916, 1896, 1597 and 1596 is indicated. (**B**) Transcriptional activity of the deletion mutants was studied in enterocytic Caco-2 (white bars), in mucus-secreting LS174T (black bars) and in undifferentiated HT-29 STD (grey bars) colon cancer cell lines. The background activity of pGL3 Basic promoterless vector used to subclone *MUC5B* fragments is shown. The results are means ± S.D. and represent more than three different experiments performed in duplicate for each fragment.

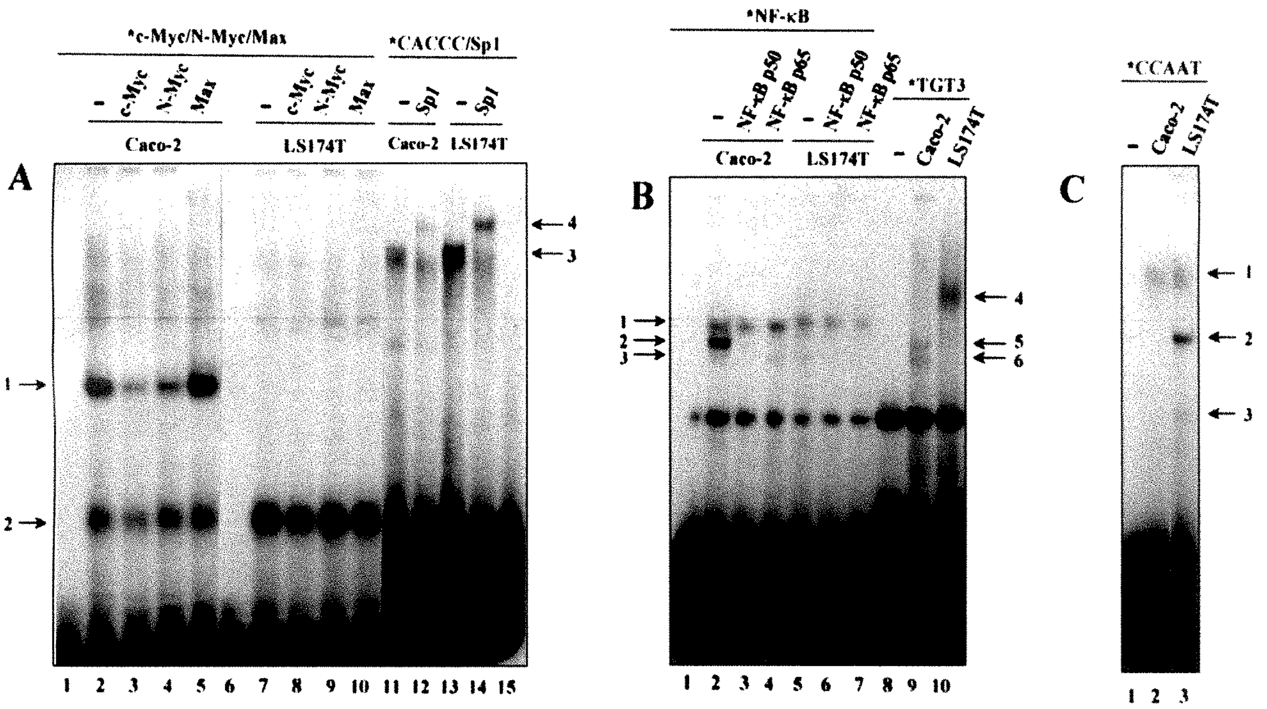

Figure 5 Binding of nuclear factors to the promoter of *MUC5B*

Autoradiograms of the gel-shift assays in which 5 μg of LS174T or Caco-2 nuclear extracts were incubated with double-stranded radiolabelled oligonucleotides representative of the c-Myc/N-Myc/Max (−108/−98, **A**, lanes 2–5 and 7–10), CACCC/Sp1 (−196/−185, **A**, lanes 11–14), NF-κB (−372/−364, **B**, lanes 2–7), TGT3 (−791/−785, **B**, lanes 9 and 10) and CCAAT (−662/−658, **C**, lanes 2 and 3) binding sites found in the *MUC5B* promoter. (**A**) No proteins added (lanes 1, 6 and 15). Nuclear extracts were either incubated in the absence (− ; lanes 2, 7, 11 and 13) or the presence (lanes 3–5, 8–10, 12 and 14) of 1 μl of the antibody of interest. (**B**) No proteins added (lanes 1 and 8). Nuclear extracts were either incubated in the absence (− ; lanes 2, 5, 9 and 10) or the presence (lanes 3, 4, 6 and 7) of 1 μl of the antibody of interest. There was no antibody added in lanes 9 and 10. (**C**) No proteins added (lane 1). The CCAAT radiolabelled probe was incubated with Caco-2 (lane 2) or LS174T (lane 3) nuclear extracts. DNA–protein complexes are indicated by the numbers on each side of the autoradiograms.

importantly, in the central part of the intron were found clustered a CACCC box followed by an array of eight GA boxes repeated in tandem containing the consensus sequence GGGGAGGGGCT, each separated by 8–10 bp. Other putative sites for known transcription factors are shown in Figure 1(B) and include three canonical Sp1 binding sites, two AP-2 sites, one NF-κB site, one GATA-1 site and one Adh-1 site.

Characterization of the *MUC5B* transcription start site

Primer-extension reactions were performed using RNAs from the two mucus-secreting colon cancer cell lines LS174T and HT-29 MTX to identify the transcription start site in the *MUC5B* 5′-flanking region. These two cell lines were chosen as they both express *MUC5B*. The result, shown in Figure 2(A), indicates that the reactions carried out with reverse primer E1 localized in exon 1 (sequence underlined in Figure 2B) produced one extension product of the same size (126 bp) in both cell lines. In the sequence, the start site matches a cytosine residue that we numbered +1. The 5′-UTR region is 56 nucleotides long (Figure 2B).

MUC5B gene expression in LS174T, Caco-2 and HT-29 STD colon cancer cells

To investigate the cell-specific expression of *MUC5B*, three colon cancer cell lines showing different phenotypes were chosen: the mucus-secreting LS174T, the Caco-2 enterocyte and the undifferentiated HT-29 STD cell lines. *MUC2* expression was studied in parallel as a positive control of RT-PCR as it is the main mucin expressed in colon. *MUC5B* (415-bp PCR product) and *MUC2* (401-bp PCR product) mRNA expression was studied by RT-PCR from 70% confluent cells in order to correlate RT-PCR results with transfection experiments. As shown in Figure 3, undifferentiated cell line HT-29 STD slightly expresses *MUC2* and *MUC5B* mRNAs. Caco-2 cells that spontaneously differentiate in enterocytes also show a very low expression of the two genes. Overall, in these two cell lines, mucin gene expression remains very discrete when compared with the GAPDH internal control. On the other hand, *MUC2* and *MUC5B* are highly expressed in the mucus-secreting cell line LS174T. The level of expression of both genes is maximal after cells have differentiated into mucus-secreting cells. Moreover, one can notice that *MUC2* and *MUC5B* follow the same pattern of expression in the three colon cancer cell lines studied.

Promoter activity of the *MUC5B* 5′-flanking region

In order to identify DNA sequences involved in *MUC5B* transcriptional regulation, constructs were generated in the promoterless pGL3 Basic vector and analysed for transcriptional activity after cell electroporation. Insert sequences were confirmed by infrared sequencing of both strands and aligned with ELO9 and BEN1 sequences.

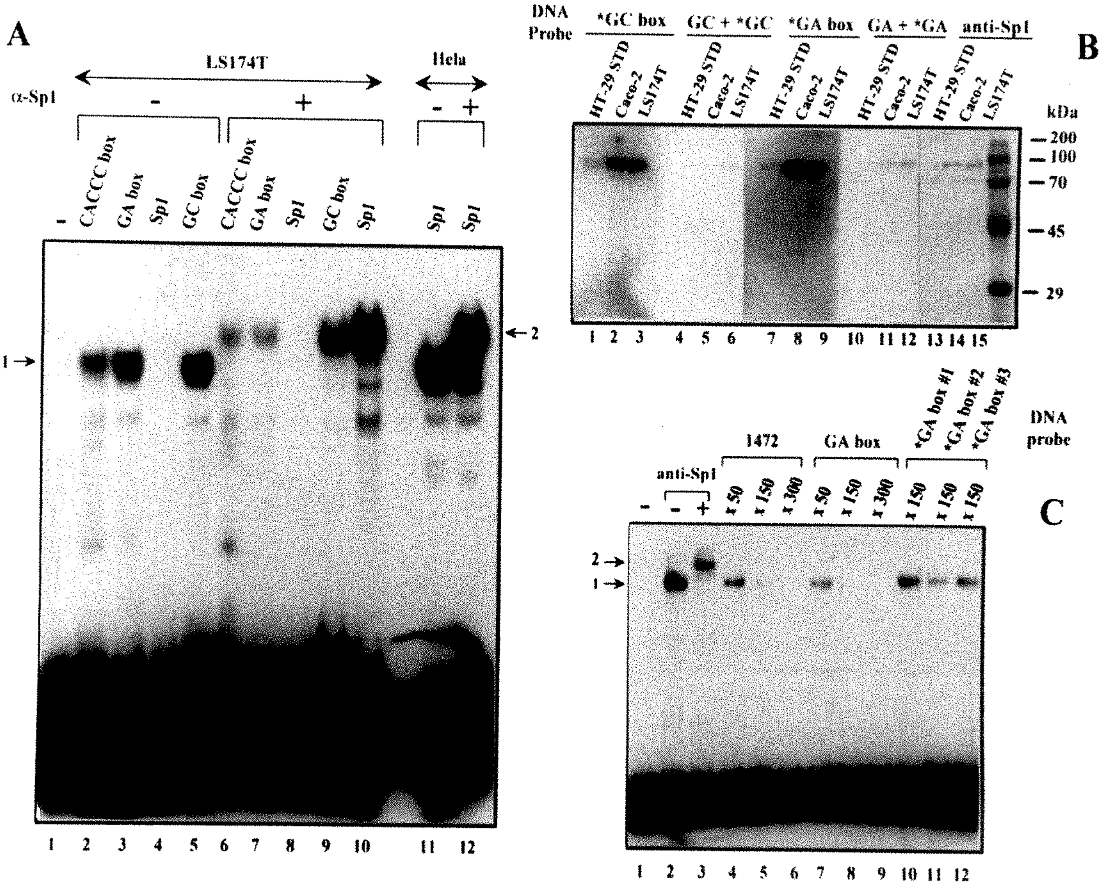

Figure 6 Sp1 binds to the eight clustered GA boxes and the CACCC box found in intron 1

(**A**) Autoradiogram of the gel-shift assay in which 5 μg of LS174T nuclear extracts were incubated with double-stranded oligonucleotides representative of the CACCC (lane 2), GA (lane 3), Sp1 (lane 4) boxes found in *MUC5B* intron 1 and with the GC box located in intron 37 [12] (lane 5). Super-shift analyses were performed by adding an antibody directed against Sp1 (lanes 6–10 and 12). A positive control was included by performing shift analysis with a commercial Sp1 oligonucleotide mixed with LS174T extracts (lane 10) and Hela cell extracts (lane 11). Sp1 super-shift is shown with Hela cells in lane 12. Arrow 1 indicates the position of the DNA–protein complex and the arrow 2 the position of the super-shifted complex when the antibody of interest was added. (**B**) Autoradiogram of the Southwestern blot of 25 μg of nuclear proteins from Caco-2 (lanes 2, 5, 8, 11 and 14), LS174T (lanes 3, 6, 9, 12 and 15) and HT-29 STD (lanes 1, 4, 7, 10 and 13) cells incubated with the GC- (lanes 1–6) and GA- (lanes 7–12) box radiolabelled probes. 'Cold' competition with a 150-fold excess of GC (lanes 4–6) and GA (lanes 10–12) boxes. Sp1 immunostaining of the same blot with a commercial antibody directed against Sp1 (PEP2; lane 13–15). (**C**) Autoradiogram of the gel-shift assay with 1472 as the probe with 5 μg of LS174T nuclear proteins. No extracts (lane 1), proteins and 1472 probe (lane 2), super-shift with anti-Sp1 antibody (lane 3). Competition with unlabelled 1472 DNA, molar ratios of × 50 (lane 4), × 150 (lane 5) and × 300 (lane 6). Competition with unlabelled GA-box oligonucleotide, molar ratios of × 50 (lane 7), × 150 (lane 8) and × 300 (lane 9). Competition with unlabelled mutated GA-box oligonucleotides with molar ratio × 150, *GA box no. 1 (lane 10), *GA box no. 2 (lane 11) and *GA box no. 3 (lane 12). Arrow 1 indicates the position of the DNA–protein complex and arrow 2 the position of the super-shifted complex when the anti-Sp1 antibody was added.

Transfection experiments on deletion fragments of the *MUC5B* promoter were carried out in Caco-2, LS174T and HT-29 STD cell lines. Seven fragments were generated that cover 956 nucleotides upstream of the transcription start site (Figure 4A). The fragments 1916, 1896, 1597 and 1596 contain the TATA-box-like sequence (TACATAA), the three Sp1-binding sites and the CACCC box. In fragments 1916 and 1597, the 5′-UTR region was included. In LS174T cells, the *MUC5B* 5′-flanking region shows a highly active promoter activity. In these cells, the fragment 1896 that covers the whole region shows a lower luciferase activity when compared with the region restricted to the first 223 nucleotides upstream of the transcription start site (1596; Figure 4B). Interestingly enough, when the 5′-UTR region was included in the fragments corresponding to the whole region (1916) or to the 223 first bases (1597), luciferase activity dropped by approx. 2-fold. This result indicates that the 5′-UTR region of *MUC5B* plays a role in regulating promoter activity. In conclusion, the first 223 bp (fragment 1596) adjoining the transcription start site suffice to drive basal promoter activity of the luciferase reporter gene. Three other deletion mutants were then constructed to identify a potential inhibitory domain in the promoter that would explain the low luciferase activity of the fragment 1896. Fragment 1895 covers the upstream 734 bases (−956/−223) and fragments 1595 and 1598 include bases −446/−223 and −956/−441, respectively. Experiments show that in all cell lines 1595 has no activity whereas fragments 1895 and 1598 act as inhibitory domains. Thus this result confirms the fact that inhibitory factors bind to *cis*-elements present in the −956/−441 region of the promoter. Finally, *MUC5B* promoter activity is minimal in Caco-2 and HT-29 STD cell lines when compared with that in LS174T cells.

Binding studies of *MUC5B* promoter with nuclear proteins

In order to characterize *cis*-elements and *trans*-nuclear factors that could account for *MUC5B* transcription regulation in colon

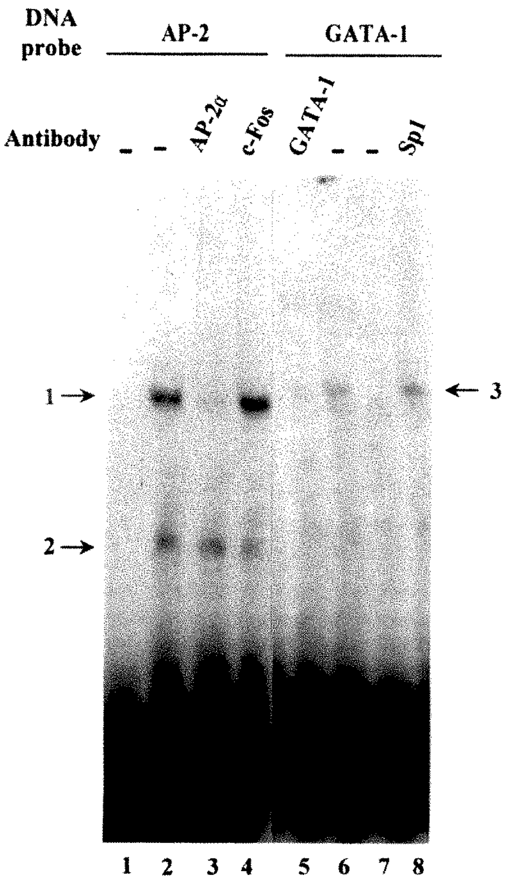

Figure 7 AP-2α and GATA-1 transcription factors bind to the first intron of *MUC5B*

Autoradiogram of the gel-shift assay in which radiolabelled oligonucleotides including the AP-2- (lanes 1–4) and GATA-1- (lanes 5–8) binding sites found in intron 1 were incubated with 5 μg of Caco-2 nuclear extracts in the absence (lanes 2 and 6) or presence (lanes 3–5 and 8) of 1 μl of specific antibody as indicated. Radiolabelled probe alone (lanes 1 and 7).

cancer cells, electrophoretic mobility-shift assays were carried out with double-stranded DNA probes containing binding sites for specific nuclear factors (Figure 5). In Figure 5(A), two retarded bands (lanes 1 and 2) were obtained when Caco-2 nuclear extracts were incubated with the double-stranded oligonucleotide comprising the c-Myc/N-Myc/Max putative binding site (Figure 5A, lane 2). Addition of c-Myc or N-Myc antibodies prior to the radiolabelled probe dramatically reduced the intensity of complex no. 1 but had no effect on complex no. 2 (Figure 5A, lanes 3 and 4). On the other hand, addition of the Max antibody had no effect (Figure 5A, lane 5). Complex no. 1 was not visualized in LS174T cells (Figure 5A, lanes 7–10). Sp1 binds to the CACCC box in both cell lines (complex no. 3) as addition of Sp1 antibody resulted in a totally super-shifted complex (band no. 4, Figure 5A, lanes 11–14).

In Figure 5(B) is shown the binding of NF-κB (lanes 1–7). When Caco-2 nuclear proteins were incubated with the double-stranded oligonucleotide containing the putative NF-κB binding site (Figure 5B, lane 2), three retarded bands were visualized on the autoradiogram (bands 1–3). When incubated with LS174T nuclear proteins (Figure 5B, lane 5) only bands 1 and 3 could be seen. Upon addition of the specific NF-κB p50 antibody (Figure 5B, lane 3), complexes 2 and 3 were abolished. With the antibody directed against the NF-κB p65 subunit, only complex 2 disappeared. Complex 1 is therefore due to an interaction with another nuclear protein since the addition of these two antibodies did not have any effect on the shifted band. Binding studies with the TGT3 putative binding site (Figure 5B, lanes 8–10) resulted in two high-mobility retarded bands with Caco-2 nuclear proteins (Figure 5B, lane 9, complexes 5 and 6) but only one low-mobility-shifted band with LS174T nuclear extracts (Figure 5B, lane 10, complex 4).

In Figure 5(C), studies with the CCAAT DNA probe showed one retarded band with Caco-2 nuclear extracts (lane 2, complex 1). Two more retarded bands with a higher mobility (complexes 2 and 3) were visualized when incubated with LS174T nuclear extracts (lane 3).

Binding studies of *MUC5B* first intron with nuclear proteins

Given that first introns have been shown to play roles in the regulation of tissue-specific intestinal genes, we investigated whether such potential DNA-binding *cis*-elements could be found in *MUC5B*'s rather large (2.5 kb) first intron. A highly striking feature was the presence of eight clustered GA boxes repeated in tandem located near to a CACCC box. All these *cis*-elements represent potential binding sites for the ubiquitous nuclear factor Sp1. Gel-shift-assay experiments were performed with nuclear extracts from the three cell lines of interest. As they gave the same results only those with LS174T nuclear proteins are shown. When we used double-stranded DNA representative of the CACCC box one low-mobility retarded band was visualized (complex 1, Figure 6A, lane 2) that was totally super-shifted when an anti-Sp1 antibody was added in the reaction mixture (Figure 6A, lane 6). The same result was obtained with the double-stranded oligonucleotide containing the GA-box consensus sequence GGGGAGGGGCT (Figure 6A, lanes 3 and 7). A similar experiment conducted with an oligonucleotide containing an Sp1 found in the 3′ region of the intron did not produce any retarded bands (Figure 6A, lanes 4 and 8).

In order to confirm the binding of Sp1 to the GA boxes, Southwestern- and immuno-blotting studies were performed (Figure 6B). The nuclear protein recognized by the radioactive GA-box DNA probe shows an M_r of around 95000 in the three cell lines (Figure 6B, lanes 7–9). When 'cold' competition was performed with a 150-fold excess of the unlabelled GA-box DNA probe the signal was almost totally abolished, demonstrating the specificity of the interaction (Figure 6B, lanes 10–12). As a positive control for Sp1 binding, the blot was then probed with a DNA probe representative of one of the Sp1-binding sites present in *MUC5B* promoter (see Figure 5A, lanes 11–14). The same band was visualized (Figure 6B, lanes 1–3) and 'cold' competition also resulted in the loss of the signal (Figure 6B, lanes 4–6). The same blot was then probed with the anti-Sp1 antibody (Figure 6B, lanes 13–15). The band visualized after immunostaining could be superimposed on the radioactive band obtained from the Southwestern-blotting study, confirming the fact that Sp1 binds to the GA box. We can conclude from these results that the Sp1 nuclear factor engages with the CACCC and GA boxes found in *MUC5B* intron 1. It is likely that the other seven GA boxes that contain the same consensus sequence GGGGAGGGCT also interact with Sp1.

To verify this hypothesis, gel-shift experiments were performed using the fragment 1472 that contains the eight GA boxes as the DNA probe. Figure 6(C) shows that the shifted band obtained when 1472 was incubated with nuclear proteins from LS174T

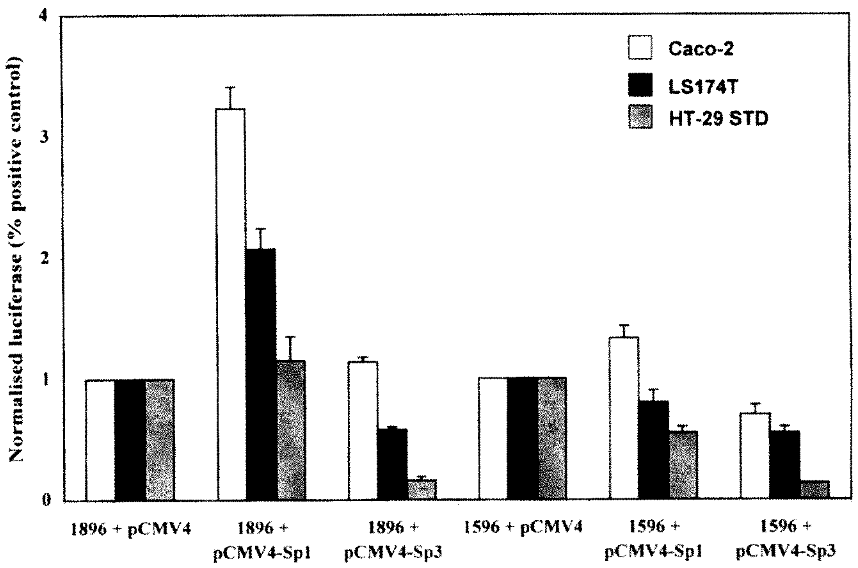

Figure 8 Sp1 and Sp3 effects on *MUC5B* promoter activity

Co-transfections were performed in enterocyte Caco-2, mucus-secreting LS174T and undifferentiated HT-29 STD colon cancer cell lines. pGL3 deletion mutants (20 μg) 1596 or 1896 were co-transfected with 5 μg of pCMV4 expression vector either empty (pCMV4) or carrying the coding sequence of Sp1 (pCMV4-Sp1) or Sp3 (pCMV4-Sp3) transcription factors. The results are means ± S.D. and represent more than three different experiments performed in duplicate for each fragment.

cells (Figure 6C, lane 2, complex 1) was completely super-shifted when the anti-Sp1 antibody was added to the reaction mixture (Figure 6C, lane 3, complex 2). The shift was shown to be specific by performing competition experiments with unlabelled DNA fragment 1472 (Figure 6C, lanes 4–6) or unlabelled GA box oligonucleotide (Figure 6C, lanes 7–9) as competitors. The shift is almost totally inhibited when competitors are added at a molar ratio of 150 (Figure 6C, lanes 5 and 8) and totally disappears at a ratio of 300 (Figure 6C, lanes 6 and 9). Using mutated oligonucleotides with a modified GA-box sequence (see Table 2) only produced a partial inhibition of the retarded band (Figure 6C, lanes 10–12).

Among the other predicted binding sites present in intron 1, we studied NF-κB, AP-2 and GATA-1 binding (Figure 7). Two shifted bands were obtained when Caco-2 nuclear proteins were incubated with the AP-2 oligonucleotide (Figure 7, lane 2). Of these two bands, the upper one disappeared upon addition of the anti-AP-2α antibody (Figure 7, lane 3). The specificity of the binding was confirmed by the absence of any effect when an irrelevant anti-c-Fos antibody was used (Figure 7, lane 4). Complex 1 was not seen in LS174T cells (results not shown). When we used the double-stranded GATA oligonucleotide, one shifted band (complex 3) was visualized with Caco-2 nuclear proteins (Figure 7, lane 6). The intensity of the shifted band decreased substantially when an anti-GATA-1 antibody was added to the reaction mixture (Figure 7, lane 5), whereas there was no effect with the anti-Sp1 antibody (Figure 7, lane 8). No shift was visualized with the NF-κB oligonucleotide in either cell line (results not shown).

Sp1 transactivation of the *MUC5B* promoter

In order to demonstrate the active participation of Sp1 in *MUC5B* promoter activity, co-transfection experiments were performed in the three cell lines of interest. Sp3, another member of the Sp family known to compete with Sp1 for the same binding sites, was also studied (Figure 8). Co-transfection of Sp1 with fragment 1896 (−956/−1) led to an increase in luciferase activity in LS174T and Caco-2 cells (2- and 3.5-fold, respectively), whereas co-transfection with Sp3 led to a slight decrease of activity in LS174T cells and had no effect in Caco-2 cells. When the same experiments were conducted with the fragment 1596 (−223/−1), no significant effect was observed in either cell line. In HT-29 STD cells, co-transfection with Sp1 had no effect, whereas co-transfection with Sp3 dramatically decreased the luciferase activity of both fragments by about 5-fold.

DISCUSSION

Molecular mechanisms involved in the control of gene expression in intestinal cells are still poorly understood. An understanding of the regulatory network of nuclear proteins that direct transcriptional initiation of genes will provide insight into the mechanisms of normal intestinal development and differentiation as well as disease processes such as neoplasia [28]. Since mucins are the main components of human epithelial secretions, responsible for the mucus rheology and physical properties, and since mucin genes display altered expression in neoplastic and pre-neoplastic processes affecting the colon [3,29], it is essential to understand the molecular mechanisms that prevail to their expression. Thus characterization of the promoter regions as well as the nuclear factors involved in the regulation of mucin gene expression is necessary.

In order to identify regulatory regions involved in *MUC5B* transcription, the *MUC5B* promoter region as well as the first intron have been sequenced and analysed. Transcriptional activity was studied in three colon cancer cell lines and transcription-factor binding to *cis*-elements present in either the promoter or the first intron were identified. The 5′-flanking region upstream of the transcriptional start site revealed the presence of a TATA-like sequence TACATAA at −26/−32, which is a characteristic of tissue-specific genes. The *MUC5B* promoter contains a high number of GC and CACCC boxes that are known to bind Sp1. In this study, Sp1 binding was demonstrated to occur in this region in the three cell lines. Involvement of Sp1 in regulation of mucin genes has already been shown for *MUC1* [30] and *MUC2* [13,14]. Also in this study, the transactivating effect of Sp1 on the *MUC5B* promoter was shown to be effective on the whole promoter region but not on the fragment containing the first 223 nucleotides adjacent to the TATA box. This result may be explained by the fact that other transcription factors or epigenetic mechanisms like methylation are required to mediate Sp1 activity. In the *MUC5B* promoter, Sp1 binding sites were often found to be nearby binding sites for other specific factors. This phenomenon usually indicates that the clustered factors act in conjunction with each other to modulate transcription [31]. Among the other factors, NF-κB may be a good candidate as it has already been shown to increase *MUC2*-promoter activity in epithelial cells via an Src-dependent pathway in response to bacterial exoproducts [18]. The *MUC5B* promoter contains a κB element that binds NF-κB in Caco-2 cells. In these cells, N-Myc, c-Myc as well as AP-2 and GATA factors may also control regulation of *MUC5B* since these factors were shown in this report to bind to the *MUC5B* promoter and first intron, respectively.

The first intron of *MUC5B*, whose sequence is described for the first time in this report, is very large (2.5 kb) and contains a striking feature, a central domain of 259 bp, which contains eight GA boxes repeated in tandem. Sp1 was shown to bind throughout this domain suggesting that this domain may serve as a docking platform for Sp1. Such repetitive sequences located in introns of 5′-flanking regions have already been described for human immunoglobin heavy chain, insulin and serotonin transporter genes. However, this type of sequence remains relatively rare in the human genome [32]. They are usually rich in GC and GA residues and induce looping of DNA, and therefore their presence is often associated with a role in regulating gene transcription [32]. Such a role may thus be played by the first intron of *MUC5B*.

MUC5B-promoter activity was studied in three intestinal cancer cell lines showing different phenotypes in order to address cell-specific activity. The cells were either undifferentiated (HT-29 STD), differentiated in enterocytes (Caco-2) or mucus-secreting (LS174T). Clearly, the *MUC5B* promoter is not active in undifferentiated and enterocyte colon cancer cells. It is however very active in LS174T mucus-secreting cells. This result confirmed our RT-PCR results in which *MUC5B* mRNA expression was important in LS174T cells and almost absent from HT-29 STD and Caco-2 cells. Our results regarding *MUC2* and *MUC5B* expression in LS174T cells are in good agreement with those published by Van Klinken et al. [33]. A recent study by these authors also showed that *MUC2* and *MUC5B* were expressed in the same subset of colonic cells, that is goblet cells in the crypt base; co-localized expression was also shown in the small granules within goblet cells [6]. Why the cell needs to express several mucin genes simultaneously is another issue that will have to be addressed. Furthermore, knowledge of the mechanisms that control transcription of the four human mucin genes, *MUC6*, *MUC2*, *MUC5AC* and *MUC5B*, clustered on the chromosome 11 will certainly help in understanding the role of some regulatory factors in intestinal diseases in which altered expression of mucin genes has already been demonstrated [34].

Numerous putative binding sites for transcription factors involved in intestinal (HNF-1, HNF-3, three consensus binding sites for TGT3, GKLF) or respiratory (10 consensus binding sites for TTF-1) cell differentiation were found throughout the *MUC5B* promoter. *In situ* hybridization studies performed in our laboratory showing early expression of human mucin genes during embryonic and foetal development in intestine and respiratory tracts suggest the involvement of these genes during ontogenesis [35,36]. Identification of silencers is also important to elucidate *MUC5B* down-regulation in certain cells. A putative binding site for such a factor, called CIIS1 [37], was found in the *MUC5B* promoter in fragments that showed inhibitory activity (1895 and 1598).

In conclusion, we have characterized the 5′-flanking region of *MUC5B* and shown that promoter activity was the highest in mucus-secreting cells. Important features and *cis*-elements that bind specific transcription factors were identified in the promoter (TATA box, Sp1, NF-κB, c-Myc and N-Myc) and the first intron (Sp1, GATA-1 and AP-2α) of *MUC5B* that might account for the cell-specific expression pattern of that gene. We also showed that Sp1 is involved in the regulation of *MUC5B* promoter activity. Experiments are now in progress to identify transcription factors and cell-signalling pathways responsible for the altered expression of *MUC5B* in intestinal diseases. Of particular interest will be the deciphering of the molecular mechanisms implicating the *MUC5B* gene in gastrointestinal cell differentiation. Moreover, experiments are now in progress to determine the influence of intron 1 and of intron 37, which has already been shown to bind Sp1 and NF1-MUC5B nuclear factors [12], on *MUC5B* promoter activity.

We are indebted to Danièle Petitprez, Pascal Mathon, Marie-Paule Delescaut and Isabelle Clavereau for their excellent technical help. We thank Dr J. M. Horowitz for the kind gift of pCMV4, pCMV4-Sp1 and pCMV4-Sp3 vectors. We thank the members of our E.U. consortium CEEBMH4-3222 for stimulating discussions. This work was supported by grants from l'Association de Recherche contre le Cancer and le Comité du Nord de la Ligue Nationale contre le Cancer.

REFERENCES

1 Gendler, S. J. and Spicer, A. P. (1995) Annu. Rev. Physiol. **57**, 607–634

2 Pigny, P., Guyonnet-Dupérat, V., Hill, A. S., Pratt, W. S., Galiegue-Zoutina, S., Collyn D'Hooge, M., Laine, A., Van Seuningen, I., Degand, P., Gum, J. R., Kim, Y. S., Swallow, D. M., Aubert, J.-P. and Porchet, N. (1996) Genomics **38**, 340–352

3 Lesuffleur, T., Zweibaum, A. and Real, F. X. (1994) Crit. Rev. Hematol. Oncol. **17**, 153–180

4 Aubert, J.-P., Porchet, N., Crépin, M., Duterque-Coquillaud, M., Vergnes, G., Mazzuca, M., Debuire, B., Petitprez, D. and Degand, P. (1991) Am. J. Respir. Cell Mol. Biol. **5**, 178–185

5 Vandenhaute, B., Buisine, M.-P., Debailleul, V., Clément, B., Moniaux, N., Dieu, M.-C., Degand, P., Porchet, N. and Aubert, J.-P. (1997) J. Hepatol. **27**, 1057–1066

6 Van Klinken, B. J.-W., Dekker, J., Van Gool, S. A., Van Marle, J., Büller, H. A. and Einerhand, A. W. C. (1998) Am. J. Physiol. **274**, G871–G878

7 Lesuffleur, T., Roche, F., Hill, A. S., Lacasa, M., Fox, M., Swallow, D. M., Zweibaum, A. and Real, F. X. (1995) J. Biol. Chem. **270**, 13665–13673

8 Desseyn, J.-L., Guyonnet-Dupérat, V., Porchet, N., Aubert, J.-P. and Laine, A. (1997) J. Biol. Chem. **272**, 3168–3178

9 Desseyn, J.-L., Aubert, J.-P., Van Seuningen, I., Porchet, N. and Laine, A. (1997) J. Biol. Chem. **272**, 16873–16883

10 Desseyn, J.-L., Buisine, M.-P., Porchet, N., Aubert, J.-P. and Laine, A. (1998) J. Biol. Chem. **273**, 30157–30164

11 Offner, G., Nunes, D. P., Keates, A. C., Afdhal, N. H. and Troxler, R. F. (1998) Biochem. Biophys. Res. Commun. **251**, 350–355

12 Pigny, P., Van Seuningen, I., Desseyn, J.-L., Nollet, S., Porchet, N., Laine, A. and Aubert, J.-P. (1996) Biochem. Biophys. Res. Commun. **220**, 186–191

13 Velcich, A., Palumbo, L., Selleri, L., Evans, G. and Augenlicht, L. (1997) J. Biol. Chem. **272**, 7968–7976

14 Gum, J. R., Hicks, J. W. and Kim, Y. S. (1997) Biochem. J. **325**, 259–267

15 Gum, J. R., Hicks, J. W., Gillepsie, A.-M., Carlson, E. J., Komuves, L., Karnik, S., Hong, J. C., Epstein, C. J. and Kim, Y. S. (1999) Am. J. Physiol. **276**, G666–G676

16 Nogami, H., Ohmori, H., Li, J.-D., Gallup, M., Gum, J., Kim, Y. and Basbaum, C. (1997) Gene **198**, 191–201

17 Li, J.-D., Dohrman, A. F., Gallup, M., Miyata, S., Gum, J. R., Kim, Y. S., Nadel, J. A., Prince, A. and Basbaum, C. (1997) Proc. Natl. Acad. Sci. U.S.A. **94**, 967–972

18 Li, J.-D., Feng, W., Gallup, M., Kim, J.-H., Gum, J., Kim, Y. and Basbaum, C. (1998) Proc. Natl. Acad. Sci. U.S.A. **95**, 5718–5723

19 Li, D., Gallup, M., Fan, N., Szymkowski, D. E. and Basbaum, C. (1998) J. Biol. Chem. **273**, 6812–6820

20 Dohrman, A., Miyata, S., Gallup, M., Li, J.-D., Chapelin, C., Coste, A., Escudier, E., Nadel, J. and Basbaum, C. (1998) Biochim. Biophys. Acta **1406**, 251–259
21 Buisine, M.-P., Desseyn, J.-L., Porchet, N., Degand, P., Laine, A. and Aubert, J.-P. (1998) Biochem. J. **332**, 1–10
22 Gum, J. R., Hicks, J. W., Toribara, N. W., Siddiki, B. and Kim, Y. S. (1994) J. Biol. Chem. **269**, 2440–2446
23 Van Seuningen, I., Ostrowski, J., Bustelo, X. R., Sleath, P. and Bomsztyk, K. (1995) J. Biol. Chem. **270**, 26976–26985
24 Vindevoghel, L., Chung, K.-Y., Davis, A., Kouba, D., Kivirikko, S., Alder, H., Uitto, J. and Mauviel, A. (1997) J. Biol. Chem. **272**, 10196–10204
25 Taylor, J. D., Badcoe, I. G., Clarke, A. R. and Halford, S. E. (1991) Biochemistry **30**, 8743–8753
26 Jackson, S. P. (1993) in Gene Transcription, a Practical Approach (Hames, D. and Higgins, S. J., eds.), pp. 189–242, IRL Press, Oxford
27 Quandt, K., Frech, K., Karas, H., Wingender, E. and Werner, T. (1995) Nucleic Acid Res. **23**, 4878–4884
28 Traber, P. G. (1998) Phil. Trans. R. Soc. Lond. Ser. B **353**, 911–914
29 Buisine, M.-P., Janin, A., Maunoury, V., Audié, J.-P., Delescaut, M.-P., Copin, M.-C., Colombel, J.-F., Degand, P., Aubert, J.-P. and Porchet, N. (1996) Gastroenterology **110**, 84–91
30 Kovarik, A., Lu, P. J., Peat, N., Morris, J. and Taylor-Papadimitriou, J. (1996) J. Biol. Chem. **271**, 18140–18147
31 Kadonaga, J. T., Carner, K. R., Marsiarz, F. R. and Tjian, R. (1987) Cell **51**, 1079–1090
32 Nakamura, Y., Koyama, K. and Matsushima, M. (1998) J. Hum. Genet. **43**, 149–152
33 Van Klinken, B. J. W. E., Oussoren, E., Weeninck, J. J., Strous, G. J., Buller, H. A., Dekker, J. and Einerhand, A. W. C. (1996) Glycoconj. J. **13**, 757–768
34 Lesuffleur, T., Porchet, N., Aubert, J.-P., Swallow, D., Gum, J. R., Kim, Y. S., Real, F. X. and Zweibaum, A. (1993) J. Cell Sci. **106**, 771–783
35 Buisine, M.-P., Devisme, L., Savidge, T. C., Gespach, C., Gosselin, B., Porchet, N. and Aubert, J.-P. (1998) Gut **43**, 519–524
36 Buisine, M.-P., Devisme, L., Copin, M.-C., Durand-Réville, M., Gosselin, B., Aubert, J.-P. and Porchet, N. (1999) Am. J. Respir. Cell Mol. Biol. **20**, 209–218
37 Savagner, P., Miyashita, T. and Yamada, Y. (1990) J. Biol. Chem. **265**, 6669–6674

Received 7 February 2000; accepted 12 April 2000

CORRECTION

G_i-mediated translocation of GLUT4 is independent of p85/p110α and p110γ phosphoinositide 3-kinases but might involve the activation of Akt kinase

L. WANG, H. HAYASHI, K. KISHI, L. HUANG, A. HAGI, K. TAMAOKA, P. T. HAWKINS and Y. EBINA

Volume 345 (2000), pp. 543–555

On p. 549, the subheading in the right-hand column should read:

G_i-mediated GLUT4myc translocation was not accompanied by an increase in p85/p110α or p110γ PI-3K activity

Signalling Titles
from Portland Press

Portland Press

The Biology of Nitric Oxide Part 7

Edited by S Moncada, The Wolfson Institute for Biomedical Research, London, UK, LE Gustafsson, Karolinska Institute, Stockholm, Sweden, NP Wiklund, Karolinska Hospital, Stockholm, Sweden and EA Higgs, The Wolfson Institute for Biomedical Research, London, UK

1 85578 142 5 Hardback April 2000 400 pages £110.00

The proceedings of the *Sixth International Meeting on the Biology of Nitric Oxide* held atStockholm, Sweden on 5-8 September 1999.

This book provides an up-to-date overview of the current status of the field with contributions from over 400 specialists covering the following areas:

Molecular Biology, Biochemistry, Physiology, Pathophysiology, Inflammation, Tumours, Apoptosis, Novel Compounds and Clinical Aspects.

Nitric Oxide and the Peripheral Nervous System

Edited by N Toda, Shiga University of Medical Science, Ohtsu, Japan, S Moncada, The Wolfson Institute for Biomedical Research, London, UK, R Furchgott, State University of New York, USA and EA Higgs, The Wolfson Institute for Biomedical Research, London, UK

1 85578 139 5 Hardback June 2000 200 pages £85.00 Provisional

This volume provides an overview of NO in the peripheral nervous system, covering aspects ranging from the molecular biology and distribution of neuronal nitric oxide synthase, through the physiological and pathophysiological roles of NO in various nitrergic systems (systems of nerves whose transmitter function depends on the release of NO). They are of major importance in the regulation of certain genitourinary, gastrointestinal and respiratory functions. In addition, nitrergic nerves mediate neurogenic vasodilation of blood vessels in some vascular beds, notably those in the cerebral circulation.

Potential therapies that may arise from our increasing knowledge of this fascinating field of research are also reviewed.

Landmarks in Intracellular Signalling

Edited by RD Burgoyne and OH Petersen, University of Liverpool, UK

1 85578 101 8 Paperback 1997 278 pages £20.00

The idea behind Landmarks in Intracellular Signalling is to provide full reproductions of a set of key papers which have been chosen as landmark papers in the various aspects of intracelllular signalling. The selected papers have all resulted in significant advances in one or other aspect of intracellular signalling.

Readers of *Landmarks in Intracellular Signalling* will now have easy, ready available access to the original literature from one source. The papers are accompanied by commentaries that describe why the papers were significant, how the work came about and summarize the advances that have been made up to the present time as a consequence of the original paper.

Essays in Biochemistry: Cell Signalling

Edited by DJ Bowles, University of York, UK

1 85578 071 2 Paperback 1997 192 pages £19.00

The subject of this volume of Essays is cell signalling – the molecular events of information transfer, occurring within or between cells, that link external changes to internal responses. A broad range of topics have been chosen, to provide insights on a variety of processes in a range of cells and organisms.

Illustrated through-out with clear diagrams which convey complex information in a more accessible way.

The extensive bibliographies and further reading lists will provide undergraduates and postgraduates with a valuable bridge between textbooks and research papers. Serves as a useful teaching aid for lecturers in biochemistry and molecular biology.

Orders:
www.portlandpress.com/books/orderinfo.htm

***Portland Press, Commerce Way,**
Colchester, CO2 8HP
t: 01206 796351
f: 01206 799331
e: sales@portlandpress.com

Please add £2.50 per book to a maximum of £7.50

In the USA and Canada
Princeton University Press
c/o California/Princeton Fulfillment Services, Inc
1445 Lower Ferry Road,
Ewing, New Jersey 08618
t: 1-800-777-4726
f: 1-800-999-1958
e: orders@cpfs.pupress.princeton.edu

Postage: Please add $3.75 for first book and US$1.00 for each additional book

BWZ/0400/C

Essential Life Sciences Online

Portland Press

Biochemical Journal

Chairman of Editorial Board: ***Peter Parker*** *(ICRF, London, UK)*

http://www.BiochemJ.org

The Biochemical Journal is available online offering many additional advantages:

- **New** – Every year in January the online content for the previous years will become free • Published online one week early • Electronic multi-media adjuncts • Medline and Inter-journal linking

Subscription – 2000: Volumes 345–352 (24 issues)
North America: US$1950.00 Rest of World: £1110.00

Biotechnology and Applied Biochemistry

Editor-in-Chief: ***Roger Lundblad*** *(Chapel Hill, USA)*

http://bab.portlandpress.com

In addition to the features of the Biochemical Journal Online, the full text of papers for *Biotechnology & Applied Biochemistry* are now published online as soon as they are ready, several weeks before the printed edition.

It includes scholarly articles and reviews concerning the expression, purification, characterization and application of biological macromolecules in therapeutics and diagnostics.

Subscription – 2000: Volumes 31–32 (6 issues)
North America: US$250.00 Rest of World: £143.00

Clinical Science

Editor-in-Chief: ***Kim Bartlett*** *(Newcastle-upon-Tyne, UK); Associate Editor Americas:* ***Aubrey Taylor*** *(Mobile, USA); Associate Editor Pacific Rim:* ***Stephen Harrap*** *(Melbourne, Australia)*

http://cs.portlandpress.com

Full access to online papers from 1998, abstracts from 1997 plus full text of papers published online as soon as they are ready.

Publishes articles and reviews on all aspects of clinical investigation, including biochemical, physiological, immunological, cellular, molecular biological and other approaches of relevance to disease in man.

Subscription – 2000: Volumes 98–99 (12 issues)
North America: US$525.00 Rest of World: £290.00

Biochemical Society Transactions

http://bst.portlandpress.com

Missed the Biochemical Society Meeting? - Don't Miss the Science

The Biochemical Society's conferences bring together some of the best biochemical and life-science research by international speakers. *Biochemical Society Transactions* contains the scientific reports and poster abstracts from these meetings. The prestigious medal lectures are also published.

New for 2000 full papers will be published online as well as speaker abstracts.

Subscription - 2000: Volume 28 (6 parts)
North America: US$305.00 Rest of World: £178.00

Free to subscribers

Full free online access to the current year of these journals is restricted to institutions that have a subscription to the printed version. Ask your subscribing library to contact us to ensure you have access to papers in these online journals as soon as they are available.

Contact: support@portlandpress.com

Back

Next

.pdf

Home

Join the email current awareness service for these important journals

Enquiries to:

Portland Press Ltd,
59 Portland Place,
London W1N 3AJ
Tel: +44 020 7580 5530
Fax: +44 020 7323 1136
sales@portlandpress.com
www.portlandpress.com

Portland Press is the not-for-profit subsidiary of the Biochemical Society publishing journals and books in the life sciences.

BVV/0200/S

Printed in Great Britain by the University Press, Cambridge